The Synthesis and Biological Evaluation of PROTACs Targeting the Transcriptional Coactivators CREBBP and p300



Katrina Harriet Andrews
St Peter's College, University of Oxford

Thesis submitted for the degree of:
Doctor of Philosophy in Chemical Biology
Trinity Term 2023

Under the supervision of:
Prof Stuart J. Conway (University of Oxford)
Dr John Harling (GlaxoSmithKline)

Abstract

CREBBP and p300 are multidomain paralogues involved in numerous cellular pathways, including epigenetic regulation and the mediation of target gene expression. They share high sequence and structure homologies and perform distinct, but overlapping, cellular functions. Mutations in both CREBBP and p300 have been implicated in a range of cancers and in Rubinstein-Taybi syndrome.

The work in this dissertation describes the synthesis and biological evaluation of proteolysis targeting chimeras (PROTACs) and hydrophobic tags (HyTs) targeting CREBBP and p300 for proteasomal degradation. Such molecules enable the overall cellular functions of the proteins to be studied and provide starting points for therapeutic development.

PROTACs and HyTs are bifunctional molecules comprising a POI ligand and an E3 ubiquitin ligase ligand, joined by a linker. PROTACs were designed to recruit the E3 ligases VHL and cereblon, while HyTs used an adamantane group for non-specific E3 ligase recruitment. Initially, PROTACs and HyTs used the CREBBP/p300 ligand **(*R*)-OXFBD05** and four PEG linker lengths were evaluated. The resultant compounds had low synthetic throughput, lacked potency, had poor physicochemical properties, and the VHL-targeting PROTACs and the HyTs exhibited off-target cytotoxicity. HyTs were abandoned and the next series of PROTACs was designed to enhance synthetic throughput and physicochemical properties.

CREBBP/p300 bromodomain ligands were functionalised with amine groups to enable one-step derivatisation to the final PROTACs in amide coupling reactions. Three CREBBP and p300 ligands were investigated based on **(*R*)-OXFBD05** and **Inobrodib**, and a variety of linker lengths, linker composition, and E3 ligase ligands were used. A total of 42 novel PROTACs were synthesised and their ability to degrade CREBBP and p300 was assessed using an optimised capillary electrophoresis immunoassay. PROTAC **144** is a potent degrader of both CREBBP and p300 and subsequent investigation into the mechanism of action confirmed protein degradation was using the proteasomal degradation pathway.

Table of Contents

Abstract i

Acknowledgements vi

Abbreviations ix

Chapter 1 – Introduction 1

1.1 – Proteolysis targeting chimeras (PROTACs) 1

1.1.1 – PROTAC Mechanism of Action 1

1.1.2 – PROTAC Ligands 3

1.1.3 – The Challenges of PROTAC Property Space 4

1.1.4 – Impact of PROTAC Structure on Potencies and Selectivities 4

1.1.5 – The Effects of Linker Structure on PROTAC Function 9

1.2 – Targeting CREBBP and p300 for Proteasomal Degradation 11

1.2.1 – CREBBP and p300 Structures and Cellular Functions 11

1.2.2 – Why Target CREBBP and p300 for Proteasomal Degradation? 14

1.2.3 –Targeting a PROTAC to CREBBP and p300 by Binding the Bromodomain 16

1.2.4 – Current CREBBP and p300-Targeting PROTACs 19

1.3 – Thesis Aims 23

Chapter 2 – The Rational Design and Evaluation of PROTACs Using the CREBBP and p300 Bromodomain Ligand **(*R*)-OXFBD05** 25

2.1 – Investigation into the Modification of CREBBP and p300 Bromodomain Ligand **(*R*)-OXFBD05** to Attach a Linker for PROTAC Development 25

2.1.1 – Structure Activity Relationship Exploration Ligand **(*R*)-OXFBD05** 25

2.1.2 – Investigation into the Effect of Alkyl Linker Length on **(*R*)-OXFBD05** Analogue Binding Affinities for the CREBBP Bromodomain 33

2.2 – Synthesis of the Initial Series of **(*R*)-OXFBD05**-Based PROTACs 37

2.2.1 – Attachment of a Linker to CREBBP and p300 Bromodomain Ligand **(*R*)-OXFBD05** 37

2.2.2 – Synthesis of the Initial Series of **(*R*)-OXFBD05**-Based PROTACs and HyTs 43

2.3 – Assessment of the Abilities of the **(*R*)-OXFBD05**-Based PROTACs **31** – **38** to Induce the Degradation of CREBBP and p300 46

2.3.1 – Western Blot Assay and Antibody Validation using siRNA-Mediated Knockdown 46

2.3.2 – Measuring the Abilities of PROTACs **31** – **38** and HyTs **65** – **68** to Induce the Degradation of CREBBP and/or p300 50

2.4 – The Rational Design of PROTACs and HyTs Using the CREBBP and p300 Bromodomain Ligand **(*R*)-OXFBD05** Conclusions 56

Chapter 3 – Higher Throughput Synthesis of PROTACs Using CREBBP and p300 Bromodomain Ligands 59

3.1 – Design of Novel Amine Terminal CREBBP and p300 Ligands to Facilitate Higher Throughput PROTAC Synthesis 59
3.1.1 – Modification of CREBBP and p300 Bromodomain Ligand **(*R*)-OXFBD05** with a Piperidine Ring for PROTAC Synthesis 59
3.1.2 – Modification of CREBBP and p300 Bromodomain Ligand **Inobrodib** with a Piperidine Ring for PROTAC Synthesis 62
3.1.3 – Modification of **Inobrodib** with an (*S*)-Methyl Ethyl Piperazine Group for PROTAC Synthesis 64
3.2 – Synthesis of Novel Amine Terminal CREBBP and p300 Ligands 67
3.2.1 – Synthesis of Piperidine Modified **(*R*)-OXFBD05** Ligand **86** 67
3.2.2 – Synthesis of Piperidine-Modified **Inobrodib** Ligand **87** 71
3.2.3 – Attempted Synthesis of (*S*)-Methyl Ethyl Piperazine-Modified **Inobrodib** Ligand **88** 74
3.2.4 – Synthesis of Ethyl Piperazine-Modified **Inobrodib** Ligand **106** 79
3.3 – Higher Throughput PROTAC Synthesis Using Amide Coupling Reactions 82
3.3.1 – Amide Coupling Arrays 82
3.3.2 – Synthesis of PROTACs Using Piperidine-Modified **(*R*)-OXFBD05** Ligand **86** 83
3.3.3 – Synthesis of PROTACs Using Piperidine-Modified **Inobrodib** Ligand **86** 87
3.3.4 – Synthesis of PROTACs Using Ethyl Piperazine-Modified **Inobrodib** Ligand **106** 89
3.3 – Higher Throughput PROTAC Synthesis Conclusions 93
Chapter 4 – Optimisation of a Higher Throughput *in vitro* Assay for Assessing the Abilities of the Amide-Series of PROTACs to Induce the Degradation of CREBBP and/or p300 94
4.1 – Immunoassay Design 94
4.1.1 – Capillary Electrophoresis Immunoassay 94
4.1.2 – Immunoassay Parameter Optimisation 97
4.2 – Capillary Electrophoresis Immunoassay Validation Using **dCBP-1** 106
Chapter 5 – Assessment of the Abilities of the Amide Series of PROTACs to Degrade CREBBP and p300 Using the Higher Throughput Screening Assay 110
5.1 – Assessment of Abilities of Piperidine-**(*R*)-OXFBD05**-Derived PROTACs to Degrade CREBBP and/or p300 110
5.1.1 – Capillary Electrophoresis Immunoassay Results for PROTACs **112** – **122** 110
5.1.2 – Discussion of Immunoassay Results for PROTACs **112** – **122** 112
5.2 – Assessment of Abilities of Ethyl Piperazine-**Inobrodib**-Derived PROTACs to Degrade CREBBP and/or p300 118
5.2.1 – Capillary Electrophoresis Immunoassay Results for PROTACs **147** – **157**, **160** – **164**, and **168** – **170** 118
5.2.2 – Discussion of Immunoassay Results for PROTACs **149** – **157**, **160** – **162**, **164**, and **168** – **170** 121

5.3 – Assessment of Abilities of Piperidine-**Inobrodib**-Derived PROTACs to Degrade CREBBP and/or p300 125
5.3.1 – Capillary Electrophoresis Immunoassay Results for PROTACs **134** – **146** 125
5.2.2 – Discussion of Immunoassay Results for PROTACs **134** – **146** 129
5.4 – Higher Throughput *in vitro* Testing of CREBBP and p300-Targeting PROTACs Conclusions 134
Chapter 6 – Validation of the Ability of PROTAC **144** to Induce the Proteasomal Degradation of CREBBP and p300 137
6.1 – PROTAC **144** Activity Validation and Mechanism of Action Assay 137
6.1.1 –Larger Scale Cellular Assays and Western Blotting 137
6.1.2 – The Ability of PROTAC **144** to Induce the Degradation of CREBBP and/or p300 in the Larger Scale Cellular Assays 139
6.1.3 – PROTAC **144** CREBBP/p300 and E3 Ubiquitin Ligase Target Engagement Assay Results 140
6.1.4 – Investigation into the PROTAC **144**-Induced CREBBP and p300 Degradation Pathway Assay Results 141
6.2 –PROTAC **144**-Induced Proteasomal Degradation of CREBBP and p300 Investigation Conclusions 143
Chapter 7 – Conclusions and Future Work 144
7.1 – Conclusions 144
7.2 – Future Work 147
7.2.1 – Further Investigation into the Role of Cereblon on PROTAC **144** Activity 147
7.2.2 – Further Investigation into Optimal Conditions for CREBBP and p300 Degradation using PROTAC **144** 147
7.2.3 – Investigation into PROTAC **144** Stability 148
7.2.4 –Investigation into the Consequences of PROTAC **144**-Induced CREBBP and p300 Degradation 150
7.2.5 – PROTAC **144** SAR Investigation 150
Chapter 8 – Experimental 152
8.1 – Biochemical and Biophysical Methods 152
8.1.1 Biological reagents and pH measurements 152
8.1.2 Protein Expression and Purification 152
8.1.3 Isothermal Calorimetry 155
8.1.4 *In Vitro* Assays 155
8.2 – General Synthetic Methods 163
8.3 – Synthesis 168
8.3.1 – Synthesis of Compounds in Chapter 2 168
8.3.2 – Synthesis of Compounds in Chapter 3 233

Bibliography 304
Appendices 323
Chapter 1 Appendices 323
Human CREBBP Protein Sequence: 323
Human p300 Protein Sequence: 324
Chapter 2 Appendices 325
Chapter 3 Appendices 339
Chapter 4 Appendices 341
Chapter 5 Appendices 345
Chapter 6 Appendices 346
NMR Spectra of Novel Compounds 348

Acknowledgements

I would like to begin by thanking Professor Stuart J Conway for his supervision. I appreciate all of the support and encouragement you have offered me over the past four and a half years, and I have learnt so much as a result. I am grateful to have had Dr John Harling as my industrial supervisor over the course of my DPhil. Your insights into the project have been invaluable and I am particularly thankful to you for organising a 4 month placement at GSK.

The work described in this dissertation would not have been possible without the efforts of others. I would like to thank Dr James Clayton, Dr Mustafa Moroglu, and Dr Margarida Espadinha for your contributions towards the early stages of the project. I am also grateful to have worked closely with Dr Pascal Heitel on the synthesis and evaluation of the initial series of PROTACs, and I thank Jenni Cryan for her guidance in the biological work performed at GSK. For proof-reading chapters of this dissertation, I would like to thank Prof Stuart J Conway, Dr Adam Thomas, Alistair Boyd, Dr Glen Brodie, Harriet Haysom, and Dr Marta Serafini. Thank you to Prof Akane Kawamura and Nina Stamps for your organisation of the Oxford-GSK-Crick Chemical Biology CDT and to BBSRC and GSK for funding my studies. I am grateful to the Russel Group for use of their tissue culture facilities, the Schofield Group for access to various pieces of lab equipment, and the Vincent Group for use of their high pressure reactor. I would also like to thank the facilities teams in the CRL.

Though lab members have changed over the many years of my DPhil, the Conway Group has always been an enjoyable and supportive environment to work in. I would like to thank all of the group members, past and present, for creating this working atmosphere. Mus – I can't think of a better person to have started me off in the group. Your excitement for the project was infectious and I learnt so much from being in the lab with you. I appreciate all the support and kindness you've offered me over the course of my DPhil, even after you'd moved on from the group, and I'm really grateful to have spent part of my final year working down the corridor from you at GSK. Pascal – I'm really glad to have been able to work with you on this project and I would like to thank you for your patience and willingness to teach. Thank you for all of your painful western blot optimisation, which I could then take advantage of. This project really would have come to a standstill without you. Antoine – merci for humouring my

bad French and for always encouraging me to dance along to the music playing in the lab. Debs – it was lovely starting with you in G12 and thank you for being a model for hard work whilst remaining cheerful. Glen – thank you for being handy with a fire extinguisher and for being such fun to work with. I've enjoyed having you in the group and being able to chat across the desk. Maria – it was a pleasure to have worked with you, even when you were down the corridor. Marta – thank you for being so lovely to work with and for helping me to strive for non-wonky westerns. Adam – thank you for always bringing good energy into the lab and for being so helpful over the years. Coco – thank you for your help with protein expression and purification and for being so welcoming when I started in the group. Holly – you've been so supportive over my time in Oxford, and I really appreciate it. Thank you for being so kind and friendly. Jess – thank you for being such a positive person to be around, it was great to have had you in the group when I first joined. Darius – I'm glad to have gone through pretty much the whole of my DPhil with you! I've enjoyed spending time together in and out of the lab and would like to thank you for your support over the years. Jenny – thank you for being such a lovely person to work with and be around. I especially enjoyed our New York and California trip together! Patrick – it's been great working with you and being able to discuss all things cereblon, as well as other topics of conversation. Bernie –thank you for keeping me going with cake and for all the conversations at our desks. Alistair – it's been great working on CREBBP together! Thank you for your high energy and kindness. Harriet – thank you for being my Great Chemistry Bake Off co-organiser and for helping to make it a surprising success. I've really enjoyed working together and I apologise for my lack of compound numbering in the chapter you proof-read. Sophie – it was fun to have you in the lab before you moved to oncology. Michael – thank you for being a calming influence in the lab, it's been really lovely working with you. Keefe – thank you for always being keen to go to Horsebox for a coffee. Ceri – it's been really lovely getting to know you and thank you for always being so friendly. Ada – thank you for having great taste in music and for being such a joy to be around. Maxim – it was great having you in the group and I'd like to thank you for your chemical knowledge and interesting stories. Dan – it was great supervising you for your Part II and I wish you all the best with your PhD. Sam – it was also lovely to supervise your Part II even though it got cut short.

I would also like to thank Afjal, Darren, Tracey, James, Max, Rebecca, Hiffy, and Carla from the Modalities group at GSK for helping me in the lab and for making my time on placement so enjoyable. In particular I would like to thank Jenni Cryan for teaching me how to use the Sally Sue and for saving me from having to screen all my final compounds using western blotting. I learnt a lot of new skills under your guidance, and I really enjoyed our time spent together.

Outside of the lab, I am lucky to have lived with a wonderful group of housemates and I thank you for making Bartlemas Road my home over the past four years. Thank you to everyone for listening to my lab stories and for cheering me on. I would also like to thank Madeline and the friends I met in Nottingham nearly 10 years ago for your support and for offering fun escapes from the lab. There are times where I relied heavily on you, and I am thankful that you were always there for me. Finally, thank you to my family for always being on the end of a phone when I've needed you and for your continual support throughout my life.

Abbreviations

Alloc	*N*-Allyloxycarbonyl
Ar	Aromatic group
AT	Acetyltransferase
Aq.	Aqueous
BCP	Bromodomain containing proteins
BET	Bromodomain and extraterminal
BPin	Pinacolborane
br	Broad
BRD	Bromodomain
Boc	*tert*-Butyloxycarbonyl protecting group
cAMP	Cyclic adenosine monophosphate
Cpd.	Compound
CBP	cAMP response element-binding protein binding protein
COSY	Correlation spectroscopy
CREB	cAMP response element-binding protein
CREBBP	cAMP response element-binding protein binding protein
CV	Column volume
d	Doublet
DBU	1,8-Diazabicyclo(5.4.0)undec-7-ene
DHBD	4,5-dihydrobenzodiazepinone
DIPEA	*N,N*-Diisopropylethylamine
DMAP	4-Dimethylaminopyridine
DMEM	Dulbecco's Modified Eagle Medium
DMF	Dimethylformamide
DMSO	Dimethylsulfoxide
Dppf	1,1'-Bis(diphenylphosphino)ferrocene
EDTA	Ethylenediaminetetraacetic acid
ESI	Electrospray ionisation
FBS	Fetal bovine serum
Fmoc	Fluorenylmethyloxycarbonyl protecting group
GSK	GlaxoSmithKline

Gt	Goat
h	Hour(s)
HATU	1-[Bis(dimethylamino)methylene]-1*H*-1,2,3-triazolo[*4,5-b*]pyridinium 3-oxid hexafluorophosphate
H-bond	Hydrogen bond
HEK	Human embryonic kidney
HMBC	Heteronuclear Multiple Bond Correlation
HPLC	High-performance liquid chromatography
HRMS	High resolution mass spectrometry
HRP	Horseradish peroxidase
HSQC	Heteronuclear single quantum coherence
HyT	Hydrophobic tag
IgG	Immunoglobulin G
IMAC	Immobilised metal affinity chromatography
Int.	Intermediate
IR	Infrared
ITC	Isothermal titration calorimetry
KAc	Acetylated lysine
KAT	Lysine acetyltransferase
KIX	Kinase-inducible domain interacting
LG	Leaving group
LRMS	Low resolution mass spectrometry
M	Molar
m	Medium
m	Multiplet
mAb	Monoclonal antibody
MDAP	Mass directed auto purification
min	Minute(s)
mp	Melting point
MS	Mass spectrometry
MW	Molecular weight
n.b.	No detectable binding
NCBD	Nuclear coactivator binding domain

NIS	*N*-Iodosuccinimide
NMP	*N*-Methyl-2-pyrrolidone
NMR	Nuclear magnetic resonance spectroscopy
NRID	Nuclear receptor interaction domain
ns	Not statistically significant
p300	Adenovirus E1A-associated 300-kD protein
PBS	Phosphate buffer saline
PCR	Polymerase chain reaction
PEG	Polyethylene glycol
PFI	Property forecast index
PG	Protecting group
PHD	Plant homeodomain
POI	Protein of interest
PPI	Protein-protein interaction
ppm	parts per million
PROTACs	Proteolysis targeting chimeras
PVDF	Polyvinylidene difluoride
Rb	Rabbit
Ref.	Reference
R_f	Retention factor
RING	Really interesting new gene
RIPA	Radioimmunoprecipitation assay
RISC	RNA-induced silencing complex
RNA	Ribonucleic acid
rt	Room temperature
s	Singlet
s	Strong
Sat.	Saturated
SAR	Structure-activity relationship
SDS-PAGE	Sodium dodecyl-sulfate polyacrylamide gel electrophoresis
SEC	Size-exclusion chromatography
sec	Second(s)

siRNA	Small interfering RNA
S_NAr	Nucleophilic aromatic substitution
SPE	Solid phase extraction
SPR	Surface plasmon resonance
t	Triplet
^{t}Bu	*tert*-Butyl
TAZ	Transcriptional adaptor zinc-binding
TBAI	Tetrabutylammonium iodide
TFA	Trifluoroacetic acid
THF	Tetrahydrofuran
THP	Tetrahydropyran
THQ	Tetrahydroquinoline
TLC	Thin-layer chromatography
t_R	Retention time
UPS	Ubiquitin- proteasome system
UTB	Urea-Tris-Bicine
UV	Ultraviolet
UV/Vis	Ultraviolet–visible
VHL	Von Hippel Lindau
w	Weak

Chapter 1 – Introduction

1.1 – Proteolysis targeting chimeras (PROTACs)

1.1.1 – PROTAC Mechanism of Action

Proteolysis targeting chimeras (PROTACs) are bifunctional molecules that cause a protein of interest (POI) to be degraded by redirecting the cellular ubiquitin-proteasome system (UPS) (Figure 1).[1,2] This chemical knockdown removes the full-length POI from the cell, making PROTACs important chemical tools for understanding overall protein cellular functions. Additionally, PROTACs are emerging as therapeutic agents for the treatment of diseases, ranging different cancers and autoimmune diseases, with at least 15 examples in clinical trials.[3]

The UPS is a native process used by eukaryotic cells for the removal of proteins, utilising the 26S proteasome and three additional classes of enzyme: an E1 ubiquitin-activating enzyme, an E2 ubiquitin-conjugating enzyme, and an E3 ubiquitin ligase enzyme (Figure 1a).[4,5] First, an E1 ubiquitin-activating enzyme adenylates the *C*-terminus of ubiquitin, promoting a thioesterification reaction with a cysteine residue in the E1 active site. The ubiquitin is then transferred from the monoubiquitinated E1 complex to a cysteine residue in the active site of an E2 ubiquitin-conjugating enzyme in a transthioesterification reaction, forming a monoubiquitinated E2 complex. Multiple monoubiquitinated E2 complexes can then post-translationally modify the protein being targeted for degradation with a polyubiquitin chain. The polyubiquitination process is regulated by the E3 enzyme, which first complexes with the target protein, then iteratively recruits monoubiquitinated E2 complexes, and mediates the transfer of the ubiquitin onto the POI. The first ubiquitin is coupled to a surface lysine residue on the target protein, then subsequent ubiquitin proteins are added to a protein-bound ubiquitin lysine residue. The polyubiquitinated protein is recognised by the 26S proteasome, which degrades the full-length protein into a mixture of shorter peptide sequences by the processes of unfolding, translocation, deubiquitination, and peptide bond cleavage.

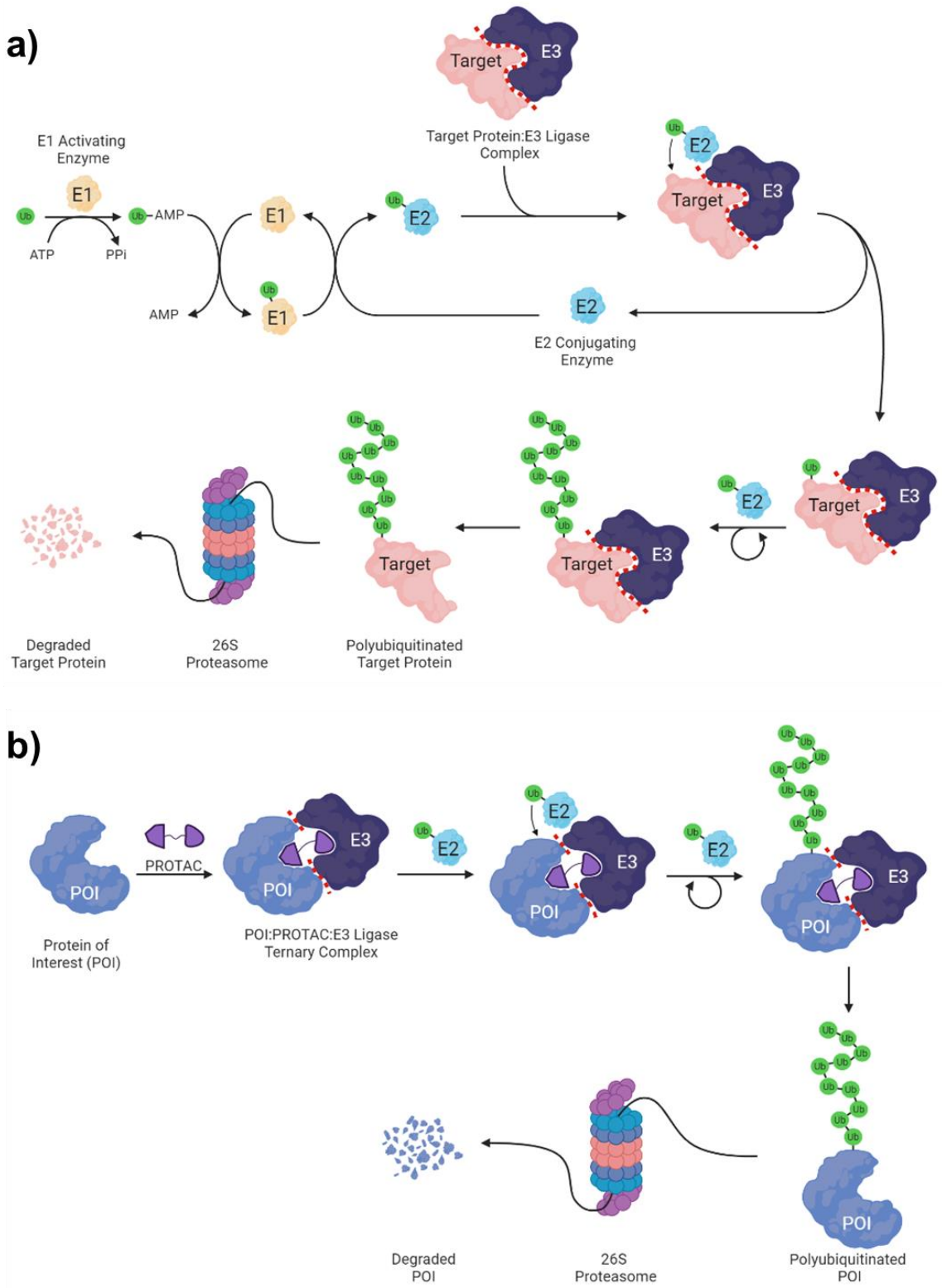

Figure 1. a) The native cellular degradation of a target protein (pink) by the ubiquitin proteasome system. An E1 ubiquitin-activating enzyme (yellow) activates a ubiquitin protein (green) by adenylation before a cysteine in the E1 active site binds the ubiquitin in a thioesterification reaction. The ubiquitin then transfers from the E1 ubiquitin-activating enzyme to an E2 ubiquitin-conjugating enzyme (cyan) in a transthioesterification reaction with a cysteine in the E2 active site. An E3 ubiquitin ligase enzyme (dark blue) mediates the transfer of the ubiquitin from the E2 ubiquitin-conjugating enzyme onto a surface lysine residue of the protein being targeted for degradation. The E3 recruits further monoubiquitinated E2 enzymes to transfer ubiquitin onto the target protein in an iterative cycle to build a polyubiquitin chain. The post-translationally modified target protein can then be recognised by the 26S proteasome (multicoloured) which unfolds the protein and breaks it down into small peptides. This process removes a full protein from the cell. Protein-protein interactions (PPIs) are highlighted as red dashed lines. **b)** PROTAC-mediated degradation of a POI using the UPS. A heterobifunctional PROTAC (purple) binds to the POI (light blue)

and an E3 ubiquitin ligase (dark blue), forming a ternary complex that is further stabilised by cooperative PPIs (red dashed lines). This ternary complex can into the UPS, where the E3 ubiquitin ligase sequentially recruits E2 ubiquitin-conjugating enzymes (cyan) that have been monoubiquitinated (green) to mediate the transfer of the ubiquitin onto the POI. The polyubiquitinated POI can then be recognised, and subsequently degraded by the 26S proteasome (multicoloured). Figure created using BioRender online software (www.biorender.com).[1,2,4,5]

PROTACs comprise a POI ligand joined by a linker to an E3 ubiquitin ligase ligand. They are able to artificially induce proteasomal degradation of a POI by hijacking the UPS through the formation a POI:PROTAC:E3 ligase ternary complex (Figure 1b).[1,2] In this complex, the bound POI and E3 ubiquitin ligase enzyme are held in close proximity by the PROTAC, enabling the E3-mediated modification of the POI with a polyubiquitin chain from sequential monoubiquitinated E2 enzymes. The polyubiquitinated POI can then be recognised and subsequently degraded by the 26S proteasome. PROTACs have an event-driven modality, where a binding event leads to protein degradation, unlike inhibitors which are occupancy-driven and must remain bound to the protein. This enables one PROTAC molecule to potentially mediate multiple POI ubiquitination cycles, and sub-stoichiometric amounts of PROTAC can be sufficient for effective POI degradation.[6]

1.1.2 – PROTAC Ligands

PROTACs are heterobifunctional molecules that comprise a ligand for the POI being targeted for degradation, an E3 ubiquitin ligase ligand and a linker.[2] There are over 600 human genes encoding E3 ubiquitin ligase enzymes, yet, only a small number have been exploited for use in PROTACs.[7] Two of the most commonly recruited E3 ubiquitin ligase substrate adapters are Von Hippel Lindau (VHL) protein and cereblon, due to the development high affinity ligands that have been well validated for use in PROTACs (Figure 2).[8–10]

PROTACs have been designed to bind, and subsequently degrade, a variety of POIs in the cell including kinases, bromodomain containing proteins (BCPs), and transcription factors.[6] As PROTACs function by an event-driven modality, only transient PROTAC-POI binding is required, and PROTACs have been reported that cause potent POI degradation despite having a low PROTAC-POI binding affinity.[6,8]

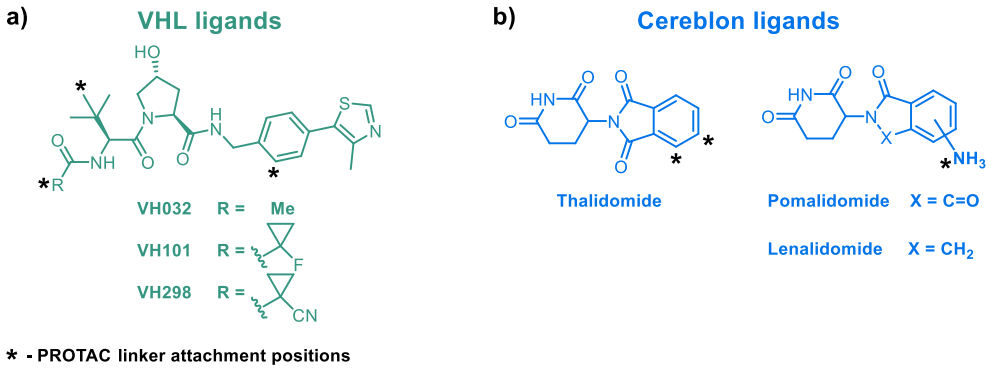

Figure 2. Structures of ligands commonly used by PROTACs to bind the E3 ubiquitin ligase enzymes VHL and cereblon. Positions that can be modified to attach a linker for PROTAC synthesis denoted by *. **a)** Structures of ligands VH032, VH101, and VH298 used by PROTACs to target VHL.[11–14] **b)** Structures of ligands thalidomide, pomalidomide, and lenalidomide used by PROTACs to target cereblon.[15,16]

1.1.3 – The Challenges of PROTAC Property Space

The nature of the large, flexible structures of PROTACs means that they commonly suffer from poor physicochemical properties, resulting in low compound solubilities and permeabilities.[17] The high lipophilicities of PROTACs can present challenges for their use in cellular assays such as, poor solubilities in aqueous solutions at physiological pH and non-specific binding to plastic labware, which can act to reduce the effect concentration of the PROTAC available in the cell to induce protein degradation.[18] However, Atilaw, *et al*. use NMR spectroscopy to show that a PROTAC with a flexible PEG linker was able to adopt different conformations depending on the polarity of its environment.[19] They hypothesise that PROTAC solubility could be promoted in the cytosol by exposing hydrophilic regions and, conversely, permeability could be promoted by conformational changes to shield the hydrophilic regions. This makes it difficult to predict optimal PROTAC properties, but designing PROTACs to have low lipophilicities could help to improve the chances of achieving aqueous (pH 7.4) solubility.[18,20,21]

1.1.4 – Impact of PROTAC Structure on Potencies and Selectivities

PROTAC potencies and selectivities do not directly correlate to the affinities of the constituent ligands for their target proteins, but instead derive from the stability of the formed POI:PROTAC:E3 ligase ternary complex.[8,11,22,23] For example, Bondeson *et al.* developed a VHL-targeting PROTAC (**V-1**) and a cereblon-targeting targeting PROTAC (**C-1**) using the promiscuous kinase ligand **foretinib**, where

both PROTACs exhibited superior degradation selectivity than the binding profile of the parent kinase ligand (Figure 3).[8] For each PROTAC, only a portion of the 54 foretinib-binding kinases were degraded, with distinct but overlapping degradation profiles, which did not correlate to binding affinities of the PROTACs for the kinase proteins. The lack of binding affinity to potency correlation is exemplified by the VHL-targeting PROTAC (**V-1**), which degraded kinase p38α with a high potency (DC_{50} = 210 nM), despite having a low PROTAC-kinase binding affinity (K_d = 11,000 nM). However, the **V-1** did not degrade kinase Axl which has a high PROTAC-kinase binding affinity (K_d = 26 nM). The influence of ternary complex formation on degradation was further investigated by Bondeson *et al.* by an enrichment assay between whole cell lysate and immobilised VHL in the presence of the **V-1**.[8] The assay showed a high correlation between the proteins being recruited to VHL by the PROTAC and those that were degraded in the cellular assay, indicating that ternary complex formation is the driving force for protein degradation.

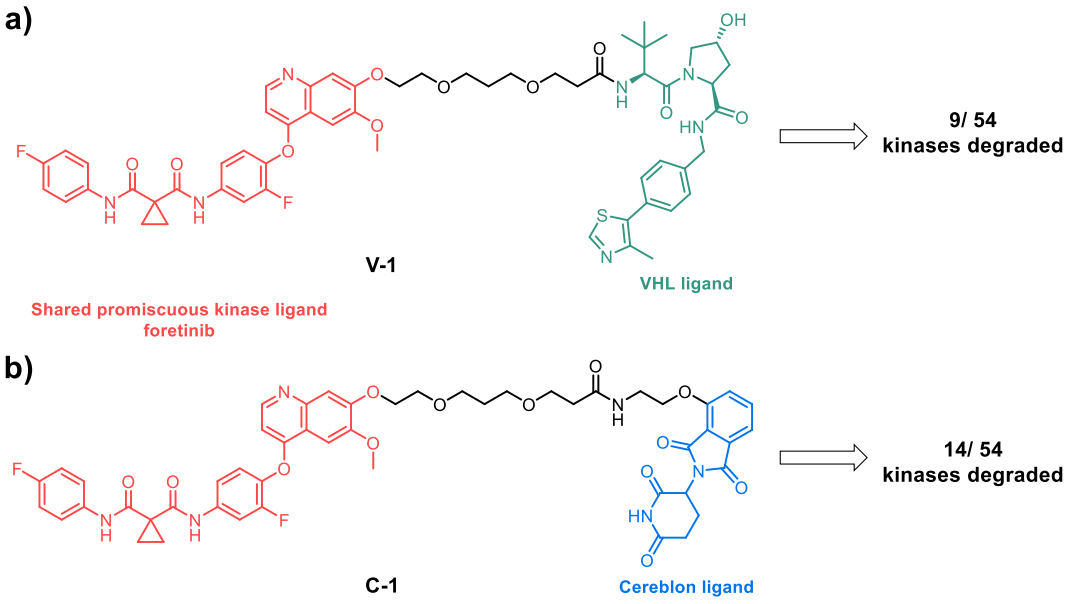

Figure 3. Examples of PROTACs comprising a promiscuous POI ligand that show a more selective protein degradation profile than the binding profile of the POI ligand.[8,24] Two PROTACs (**V-1** and **C-1**) were synthesised using the multi-kinase inhibitor foretinib (red), and different E3 ubiquitin ligase ligands that either recruit VHL using the ligand VH032 (teal), or cereblon using the ligand thalidomide (blue).[15,25] Each induced the degradation of a portion of the POI ligand binding partners showing greater selectivity than that of the parent ligand. Additionally, each PROTAC degraded an overlapping but distinct set of kinases, displaying different selectivity between the PROTACs. Six kinases were degraded by both PROTACs. Protein degradation did not correlate to the binding affinity of the kinase to each PROTAC but was, instead, influenced by POI:PROTAC:E3 ligase ternary complex formation as indicated by an enrichment assay.[8] **a)** Structure of the VHL-targeting PROTAC *V-1* which causes the degradation of nine kinases of the 54 examined. **b)** Structure of the cereblon-targeting PROTAC *C-1* which causes the degradation of 14 kinases of the 54 examined.

The importance of PROTAC design in guiding degradation profiles is further evident for PROTACs **dBET1**, **MZ1**, and **AZ1** (Figure 4).[11,22,23] Each of these PROTACs target the bromodomain and extraterminal (BET) family of BCPs using the pan-BET ligand **JQ1**, but comprise of different E3 ligase ligands and linkers. These distinct PROTAC structures result in different degradation profiles where **dBET1** non-specifically degrades all of the BET family of BCPs, **MZ1** preferentially degrades BRD4, and **AZ1** selectively degrades BRD4.

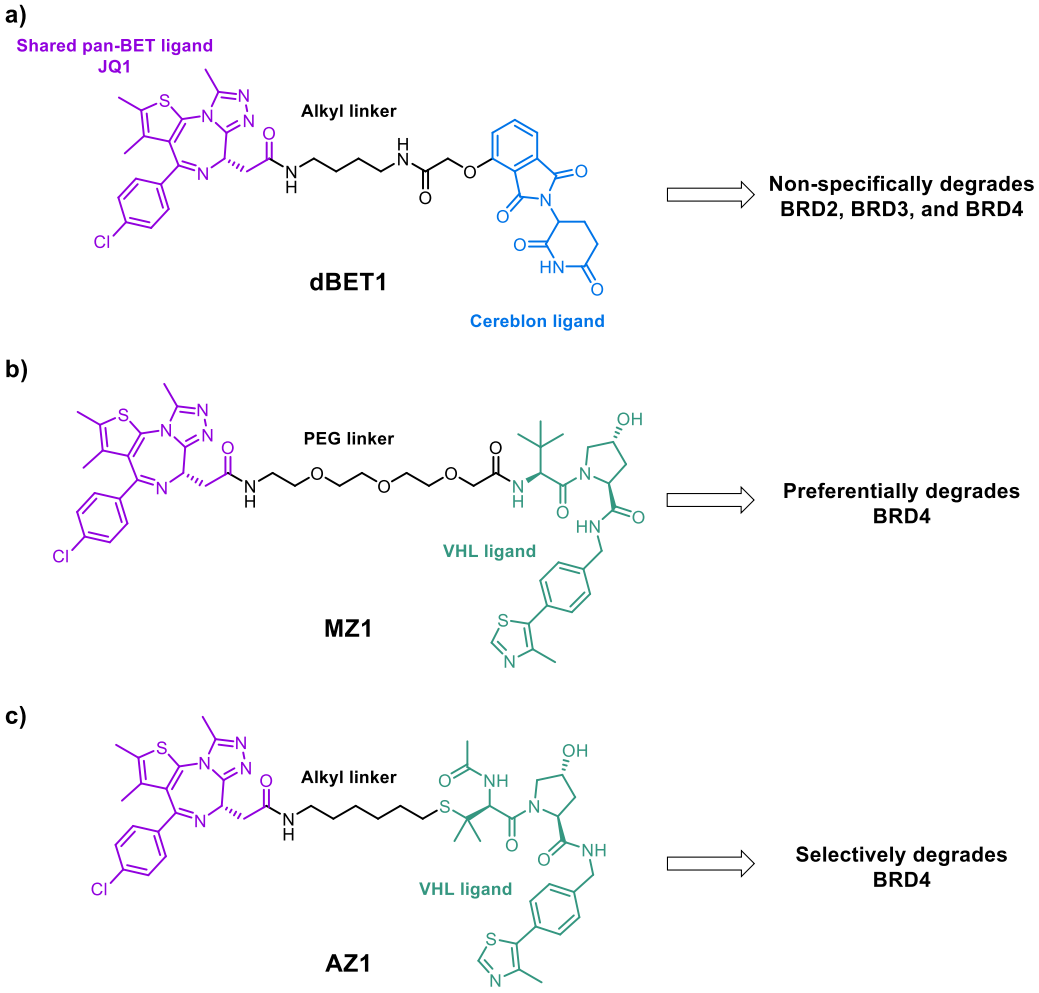

Figure 4. Examples of three PROTACs that target the BET family of BCPs using the same pan-BET ligand, JQ1 (purple), but show different degradation profiles in the cell.[11,22] **a)** Structure of **dBET1**. **dBET1** binds the E3 ubiquitin ligase cereblon using the ligand thalidomide (blue) which is attached to **JQ1** via an alkyl linker (black) and non-specifically degrades all paralogues of the BET family of BCPs.[15,22] **b)** Structure of **MZ1**. **MZ1** binds the E3 ubiquitin ligase VHL using the ligand **VH032** (teal), which is linked to JQ1 via a polyethylene glycol (PEG) linker (black) and preferentially degrades BRD4 over the other membered of the BET family of BCPs.[11,25] **c)** Structure of **AZI**. **AZ1** binds the E3 ubiquitin ligase VHL using the ligand **VH032** (teal), which is linked to **JQ1** via an alkyl linker (black) from a different position on the ligand than in **MZ1**. **AZ1** selectively degrades BRD4 over the other membered of the BET family of BCPs.[23]

An X-ray crystal structure of the BRD4(2):**MZ1**:VHL ternary complex (PDB: 5T35) demonstrates that, in addition to the expected ligand-protein binding interactions, the ternary complex is further stabilised

by electrostatic and hydrophobic interactions between the three ternary complex components (Figure 5).[23] The structure shows hydrophobic interactions formed between the protein surfaces that involve BRD4 residues W374, L385, and A384; and VHL residues P71, I109, H110, and Y112 (Figure 5c). Additionally, there are five interprotein H-bonds with one between BRD4 residue E438 and VHL residue R69, and four between BRD4 residues D381 and E383 with VHL residue R108, as well as an electrostatic attraction between VHL residue R107 and BRD4 residue E383 (Figure 5d–e). There is a further stabilising PROTAC-protein H-bond formed between and ether of the **MZ1** PEG linker and BRD4 residue H437 (Figure 5d). Collectively, these interactions stabilise the BRD4(2):**MZ1**:VHL ternary complex, and it was hypothesised the preferential degradation of BRD4 was the result of this ternary complex being more stable than the POI:**MZ1**:VHL ternary complexes for the other paralogue binders. To assess the strength of the cooperative interactions formed within the different POI:**MZ1**:VHL ternary complexes of the paralogue binders, isothermal titration calorimetry (ITC) was used to measure the heat release of adding VHL to the different POI:**MZ1** binary complexes, where greater heat release correlates to stronger cooperative interactions.[23] The strongest cooperative interactions were measured when VHL was added to the BRD4(2):**MZ1** binary complex, supporting the hypothesis that ternary complex stability directs **MZ1** selectivity.

This X-ray crystal structure (PDB: 5T35) was then used to guide the optimisation of **MZ1** to **AZ1** to enhance the selectivity of the PROTAC further towards BRD4 degradation. This was achieved by modifying the PEG4 linker to a shorter alkyl linker and modifying the linker attachment position on the **VH032** VHL ligand (Figure 5b–c).[11,23]

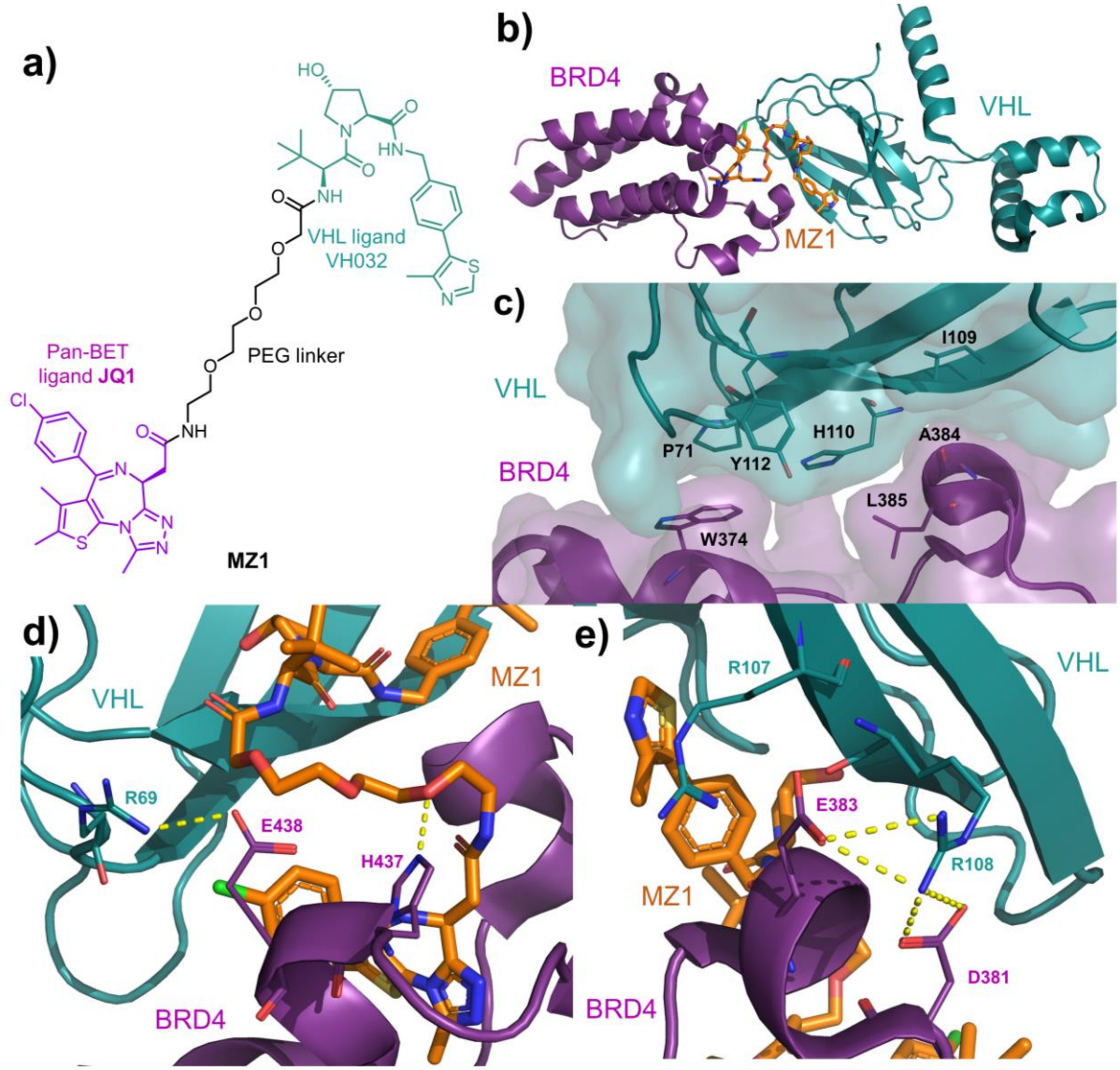

Figure 5. MZ1 comprises the pan-BET ligand **JQ1** and binds all of the BET family of BCPs but preferentially degrades BRD4.[11] It is rationalised that the formed BRD4(2):**MZ1**:VHL ternary complex is the most stable ternary complex of the BCP binders, and that this directs the PROTAC selectivity. An X-ray crystal structure of the BRD4(2):**MZ1**:VHL ternary complex shows stabilising interactions not only between the BRD4(2) and VHL proteins, but also between BRD4(2) and **MZ1** (PDB: 5T35).[23] These interactions include both electrostatic interactions and hydrophobic effects. **a)** Chemical structure of BRD4-degrading PROTAC **MZ1**. **MZ1** comprises the pan-BET ligand **JQ1** which non-specifically binds the BET family of BCPs (purple), the VHL-targeting ligand **VH032** (teal), and a PEG linker (black). **b)** X-ray crystal structure of the ternary complex formed between BRD4(2) (purple), VHL (teal), and **MZ1** (orange). c) Expanded BRD4(2):**MZ1**:VHL ternary complex X-ray crystal structure displaying the formed hydrophobic interactions between the BRD4 bromodomain (purple) residues W374, A384, and L385; and VHL (teal) residues P71, I109, H110, and Y112 (interacting residues shown as wire lines). **MZ1** structure hidden for clarity. **d)** Expanded region of the BRD4(2):**MZ1**:VHL ternary complex X-ray crystal structure displaying key interprotein H-bond between BRD4(2) (purple) residue E438 and VHL (teal) residue R69 and the protein-PROTAC H-bond between BRD4(2) residue H437 and PEG linker of **MZ1** (orange). Key interacting residues shown as wire lines, H-bonds shown as yellow dashed lines. **e)** Expanded region of the BRD4(2):**MZ1**:VHL ternary complex X-ray crystal structure displaying four interprotein H-bonds between VHL residue R108 and BRD4(2) residues D381 and E383. Key interacting residues shown as wire lines, H-bonds are shown as yellow dashed lines.

1.1.5 – The Effects of Linker Structure on PROTAC Function

Modifications to the linker region of a PROTAC, alone, can improve degradation activity.[26,27] For example, a study by Farnaby *et al.* found that the potency of a duel SMARCA2 and SMARCA4 was enhanced by replacement of a flexible polyethylene glycol (PEG) group in PROTAC **ACBI** with a rigid benzene ring in PROTAC **ACBI1** (Figure 6).[26] DC_{50} values for SMARCA2 and SMARCA4 were decreased from 300 nM and 250 nM, respectively, to 6 nM and 11 nM, respectively. The subsequent ternary complex is stabilised by a π-π stacking interaction between the linker phenyl group and residue Y98 on the VHL surface. Additionally, the decreased linker flexibility will reduce the entropy loss from ternary complex formation, which could drive ternary complex occupancy time to enhance POI degradation.[28]

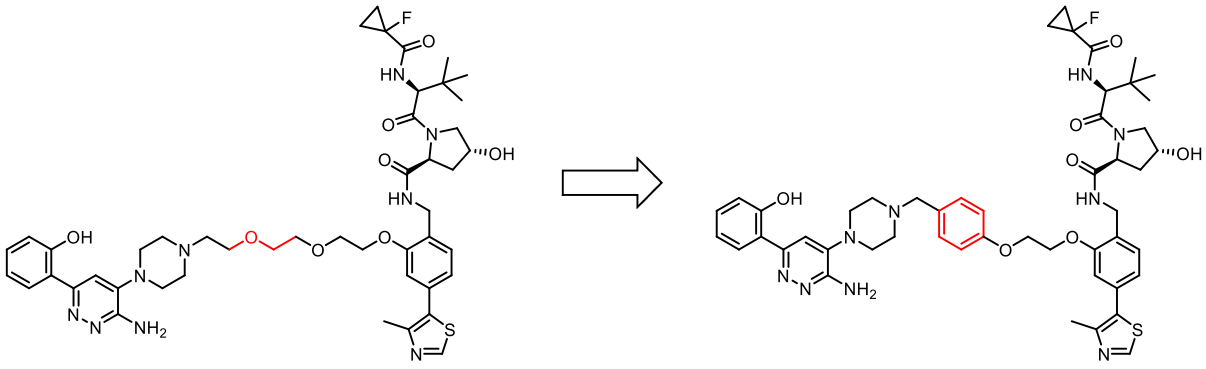

Figure 6. Optimisation of duel SMARCA2- and SMARCA4-targeting PROTAC **ACBI** to **ACBI1** which has a greater potency. Addition of a rigid benzene ring to the flexible PEG linker (highlighted in red) acted to increase linker rigidity and induce stabilising π-π stacking with the protein surface.[26]

In another example of PROTAC linker optimisation, Nunes *et al.* discovered that the conversion of a flexible, lipophilic alkyl linker in PROTAC **dIRAK4-1** to one comprising a spirocyclic group and a pyrimidine in **dIRAK4-2**, enhanced PROTAC potency with a reduction in the DC_{50} value for target protein IRAK4 from 259 nM to 151 nM (Figure 7).[27] Similar to **ACBI1**, this modification will rigidify the linker region and reduce the entropic cost of PROTAC binding, which could act to enhance ternary complex stability and subsequent POI degradation. Additionally, this modification reduced the lipophilicity of the PROTAC, with a decrease in the calculated log of the distribution coefficient at pH 7.4 ($clogD_{pH7.4}$) from 6.44 to 4.97.[27] These data suggest that **dIRAK4-2** would have a greater

solubility than **dIRAK-1** in the *in vitro* assays, and this could promote the effective concentration of the PROTAC available in the cell to bind its target proteins and induce IRAK4 degradation.

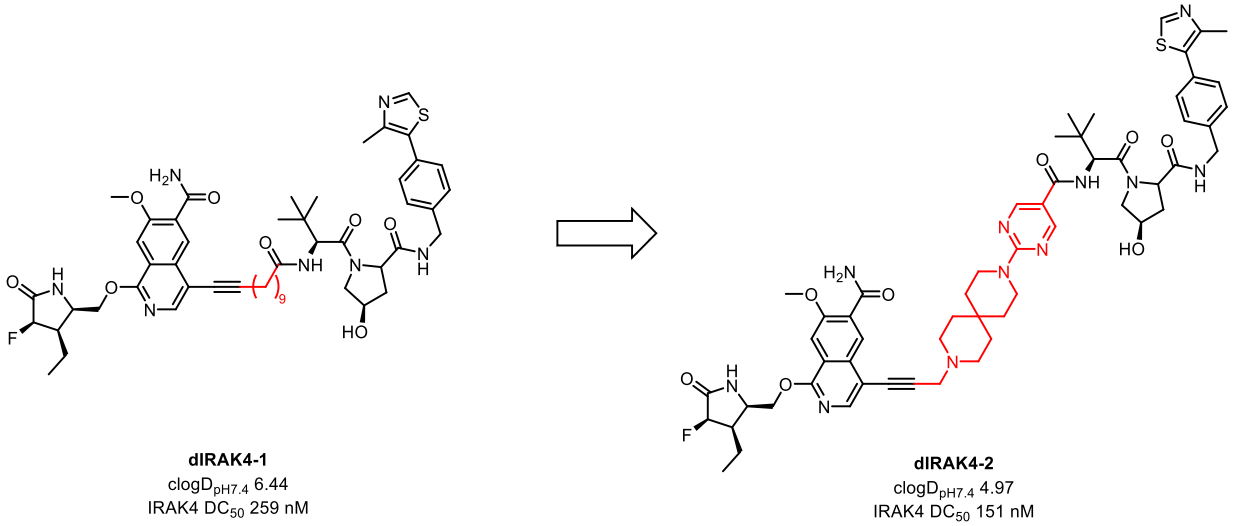

Figure 7. Optimisation of IRAK4-targeting PROTAC **dIRAK4-1** to **dIRAK4-2** to enhance hydrophobicity and potency. Optimisation from a flexible, lipophilic alkyl linker to a rigid linker (highlighted in red) led to a reduction in clogD$_{pH7.4}$ and DC$_{50}$ values for the optimised PROTAC.[27]

1.2 – Targeting CREBBP and p300 for Proteasomal Degradation

1.2.1 – CREBBP and p300 Structures and Cellular Functions

1.2.1.1 – CREBBP and p300 Protein Structures

cAMP response element-binding protein (CREB) binding protein (CREBBP) and adenovirus E1A-associated 300-kD protein (p300) were discovered independently due to their abilities to bind the transcription factors CREB and adenovirus E1A, respectively.[29,30] Investigation into protein structures and functions identified CREBBP and p300 as closely related paralogues that share high sequence and structure homologies. Each protein comprises at least 10 conserved domains including the bromodomain,[31] lysine acetyltransferase (KAT) domain,[32] two transcriptional adaptor zinc-binding (TAZ) domains (TAZ1 and TAZ2),[33,34] really interesting new gene (RING) finger domain,[35,36] plant homeodomain (PHD) finger domain,[35,36] ZZ-type zinc finger domain,[37] kinase-inducible domain interacting (KIX) domain,[38] nuclear receptor interaction domain (NRID),[39] and nuclear coactivator binding domain (NCBD)[40] (Figure 8a–b).

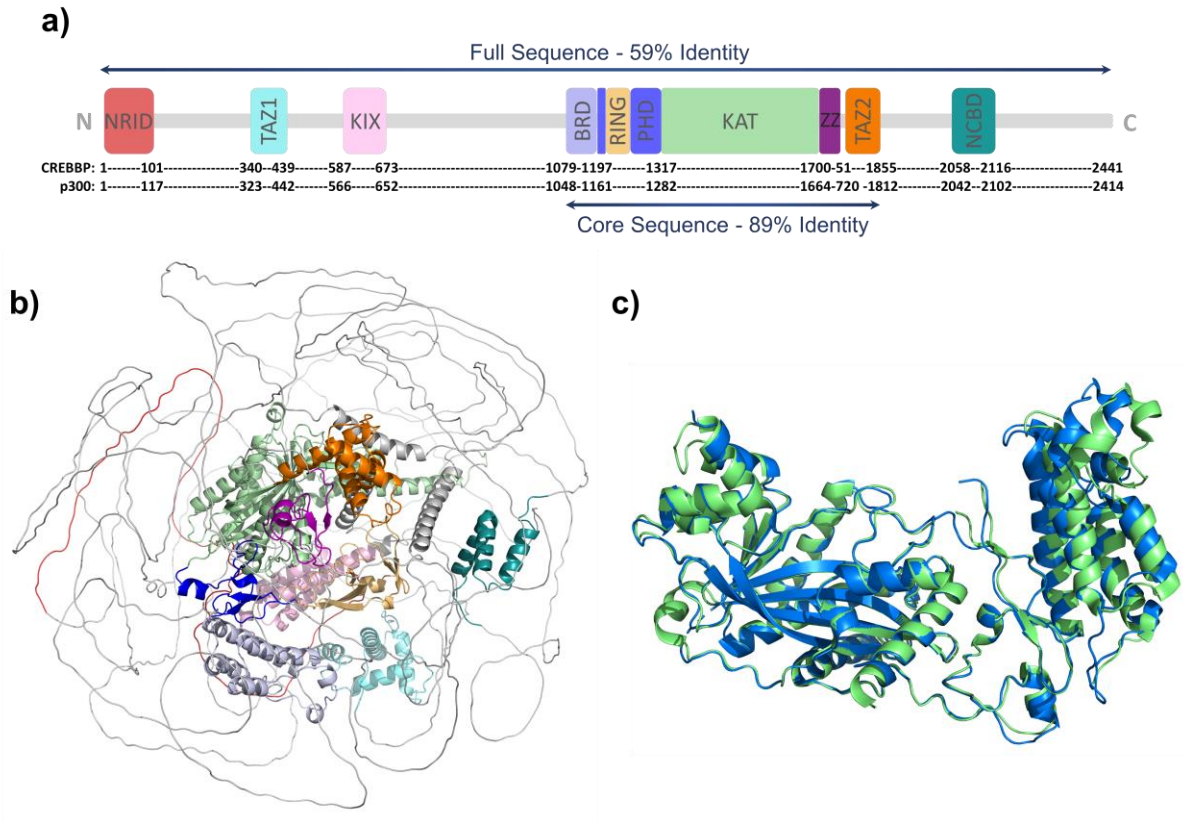

Figure 8. Structures of the paralogues CREBBP and p300. **a)** Representation of the primary structures of CREBBP and p300 highlighting the domain regions and sequence identities of the full protein lengths and of the catalytic core regions. CREBBP sequence: NRID (red)- residues 1 – 101,[41] TAZ1 domain (light cyan)- residues 340 – 439,[33] KIX domain (pink)- residues 587 – 673,[42] bromodomain (light purple)- 1079 – 1197,[43] PHD (dark blue) and RING domain (yellow)- residues

1197 – 1317,[35] HAT domain (light green)- residues 1317 – 1700,[35] ZZ domain (purple)- residues 1700 – 1751,[35] TAZ2 domain (orange)- residues 1764 – 1855,[44] NCBD (dark cyan)- residues 2058 – 2116,[45] overall sequence obtained from UniProt.[46,47] p300 sequence: NRID (red)- residues 1 – 117,[41] TAZ 1 domain (light cyan)- 323 – 424,[33] KIX domain (pink)- 566 – 652,[42] bromodomain (light purple)- 1048 – 1161,[48] PHD (dark blue) and RING domain (yellow)- residues 1161 – 1285,[35] HAT domain (light green)- residues 1285 – 1664,[35] ZZ domain (purple)- 1664 – 1720,[49] TAZ2 domain (orange)-1723 – 1812,[50] NCBD (dark cyan)- residues 2042 – 2102,[45] overall sequence obtained from UniProt.[47,51] Sequence identities calculated using Protein BLAST® software.[52,53] **b)** Tertiary structure of CREBBP predicted by the AlphaFold Protein Structure Database.[54–56] Domains are highlighted as for Figure 1a. Image created using PyMOL. **c)** Overlay of the X-ray crystal structures for the catalytic core regions of CREBBP (blue, PDB: 5U7G)[35] and p300 (green, PDB: 4BHW)[57] showing a high degree of spatial overlap. For clarity, only the domains present in both X-ray crystal structures (bromodomains, PHD domains, and KAT domains) are shown.

CREBBP and p300 share the greatest sequence and structure homologies between their domains, while protein variation primarily occurs within the disordered regions.[58] Alignment of human CREBBP and p300 primary structures (see Appendix for protein sequences, sequence data obtained from UniProt)[47] using Protein BLAST® online software, calculated the full protein sequences share 59% identity, and that this increases to 89% sequence identity for the catalytic core regions (CREBBP residues 1079 – 1855, p300 residues 1048 – 1812) (Figure **8**a).[52,53] Additionally, overlaying the X-ray crystal structures of the catalytic core regions of CREBBP (PDB: 5U7G)[35] and p300 (PDB: 4BHW)[57] shows a high structural overlap between the two proteins (Figure 8c).

1.2.1.2 – CREBBP and p300 Cellular Functions

CREBBP and p300 are transcriptional coactivators and are fundamental for the regulation of numerous cellular pathways because of the activities of their domains, summarised in Table 1. One, key function of CREBBP and p300 is the epigenetic regulation of protein expression through the acetylation of lysine residues on histone tails.[59] This acts to neutralise the positive charge of the histone lysine residues at physiological pH, decreasing histone electrostatic attraction to anionic DNA, which destabilises the chromatin structure and promotes protein transcription. The KAT domain mediates this process by catalysing the transfer of acetyl groups from acetyl-coenzyme A onto lysine residues, and is regulated by the bromodomain, which binds to acetylated lysine (KAc) residues to anchor the protein to chromatin.[59,60] CREBBP and p300-mediated protein acetylation is not limited to histones and ~5300 members of the CREBBP and p300 acetylome have been identified, including over 200 transcription factors, chromatin remodelling proteins, and transcriptional coactivators.[61,62] CREBBP and p300 also

mediate protein-protein-interactions (PPIs), with around 400 identified interacting protein partners in their interactome.[63,64] These PPIs act to form larger protein complexes and to activate multiple transcription factors and nuclear receptors to promote the downstream transcription of their target genes.

Table 1. Summary of the shared cellular functions of the individual domains of CREBBP and p300 with examples of their known interactomes.

Domain	Function	Known Interactome	Ref.
NRID	Activation of nuclear receptors to promote target gene expression	Retinoic acid receptor, retinoid X receptor, glucocorticoid receptor, thyroid hormone receptor, and estrogen receptor	39,41
TAZ1	Activation of transcription factors to promote target gene expression	HIF-1α, NF-κB, STAT2, p73, Ets1, and CITED2	65–73
KIX	Activation of transcription factors to promote target gene expression	CREB, p53, c-Myb, BRCA1, mixed lineage leukaemia protein, c-Jun, FOXO3a, and the sterol regulatory element binding protein family	38,74–81
Bromodomain	Regulatory domain which binds acetylated lysine residues to form larger protein complexes, epigenetic reader domain	H3K56Ac, H4K20Ac, H4K12AcK16Ac, p53-K382Ac, MyoD-K99Ac, MyoD-K102Ac	82–87
PHD	Non-canonical structure. Cellular function poorly understood but is believed to regulate protein KAT activity	CREBBP/p300 KAT domain	57,88
RING	Non-canonical structure. Cellular function poorly understood but is believed to regulate protein KAT activity	CREBBP/p300 KAT domain	57,89
KAT	Catalytic domain mediating the acetylation of lysine residues, epigenetic writer domain	Multiple positions on H2A.Z, H3, and H4 tails >200 transcription factors, chromatin remodelling proteins, and transcriptional coactivators	61,62,90–92
ZZ	Epigenetic reader domain	$H3K4Me_{n=1–3}$, $H3K9Me_{n=1–3}$, H3K4Ac, H3K9Ac, H3K14Ac, H3K18Ac	49
TAZ2	Activation of transcription factors to promote target gene expression	E1A, p53, C/EBP family members, E2A, MEF2, STAT1, B-Myb	44,50,69,93–97
NCBD	Activation of transcription factors to promote target gene expression	P53, p160 coactivator family, IRF-3	40,45,98,99

Due to the high sequence and structure homologies of CREBBP and p300, it was initially believed that the paralogues were functionally redundant, but there is increasing evidence that the proteins have overlapping but distinct functions. For example, siRNA-mediated knockdown of CREBBP and p300 followed by reverse-transcription PCR showed the paralogues to be involved in the regulation of both

overlapping and distinct genes and that the regulation of some genes requires the double knockdown of both proteins.[100] Furthermore, *in vivo* experiments have shown both shared and independent phenotypes arising from CREBBP or p300 heterogeneous knockout. Both $CREBBP^{+/-}$ and $p300^{+/-}$ knockout cause cases of embryonically lethal neural tube defects, however, $CREBBP^{+/-}$ mice exhibited splenomegaly and hematopoietic differentiation defects, while $p300^{+/-}$ mice exhibited exencephaly and heart defects.[101,102] Furthermore, heterogeneous knockout of CREBBP or p300 acetyltransferase (AT) activity showed that the $p300^{+/AT}$ mutation causes a greater impact on development of the cardiovascular system, the lungs, and the small intestine.[103]

1.2.2 – Why Target CREBBP and p300 for Proteasomal Degradation?

CREBBP and p300 are involved in many, complex cellular pathways and so obtaining a variety of high-quality chemical probes is imperative for enhancing our mechanistic understanding of their functions.[104] It is difficult to investigate the individual functions of CREBBP and p300 chemically, as chemical probes interact with both proteins due to the high sequence and structure homologies of the shared domains. High-affinity chemical probes have been developed to elucidate the combined functions of the CREBBP and p300 KAT domains and bromodomains.[104] However, the NRID, TAZ1, KIX, TAZ2, and NCBD domains lack well defined small molecule binding sites making the development of high affinity, selective chemical probes difficult, and the functions of these domains remains underexplored.[33,65,104–108] No chemical probes investigating the functions of the ZZ domain, PHD domain or RING domain have been reported in the literature thus far and their cellular functions remain elusive.

The development of PROTACs for CREBBP and p300 will enable overall cellular functions to be investigated by examining the consequences of inducible protein degradation. Furthermore, the ability of PROTACs to bind multiple protein paralogues, but preferentially degrade one protein (discussed in Section 1.1.4) means that it might be possible to develop a CREBBP or p300-selective PROTAC. Such a chemical probe would enable the specific cellular function of CREBBP or p300 to be investigated by studying the effects of selectively degrading CREBBP over p300 or *vice versa*.

In addition to use as chemical probes, CREBBP and/ or p300-degrading PROTAC could be developed into therapeutic agents. CRREBBP and p300 are implicated in numerous cancer types, including leukaemias and solid tumours, which can result from the paralogues interacting with oncogenes to promote tumorigenesis, or be due to activating and deactivating CREBBP/p300 mutations.[109–111] Already there is therapeutic interest in inhibiting the bromodomain of CREBBP and p300, with ongoing clinic trials into the use of two CREBBP and p300 bromodomain inhibitors (**Inobrodib** and **NEO2734**) as chemotherapeutics for the treatment of acute myeloid leukaemia, multiple myeloma, and advanced solid tumours.[112–114] The PROTAC-induced degradation of CREBBP and/or p300 will likely result in a different phenotypic effect compared to single domain inhibition, and this could offer superior therapeutic value. A study by Burslem *et al.* has shown that PROTAC-induced kinase degradation (PROTAC structures not reported) afforded more favourable cellular effects than inhibition of kinase activity alone, using the corresponding small-molecule inhibitor.[115] These benefits included lower compound concentrations required for the inhibition of downstream cellular pathways, longer sustained cellular effects (even after compound washout), and the ability to degrade kinases that were mutationally activated.

There is also the potential that a CREBBP or p300 selective PROTAC could provide a means to selectively target cancer tissue over healthy cells, where the cancer has a loss-of-function mutation in CREBBP or p300, by using synthetic lethality.[116,117] Due to the overlapping cellular functions shared by the paralogues (discussed in Section 1.2.1.2) it is possible that the cellular activity of one paralogue may compensate for the loss of the other paralogue.[118] Using a cancer with loss-of-function of p300 as an example, treatment with a CREBBP-selective PROTAC would leave the cancer cells with neither functioning paralogue, causing cell death due to dysregulation of transcription. The CREBBP-selective PROTAC would also cause the degradation of CREBBP in normal cells, however, these cells will possess a functioning p300 protein, which may compensate for the loss of CREBBP, and the cells will survive.

1.2.3 –Targeting a PROTAC to CREBBP and p300 by Binding the Bromodomain

PROTACs have been reported that degrade the BET family of BCPs using ligands for the bromodomain, suggesting this is a promising route for CREBBP and p300 PROTAC development.[11,22,23,119,120] Bromodomains are regulatory domains that bind KAc residues on a protein to form a larger protein complex.[82] There are 46 BCPs within the human proteome with 61 distinct bromodomain structures, and the bromodomains of the BET family of BCPs are some of the most closely related to those of CREBBP and p300.[31,121–123]

Primary structures vary across bromodomains, but they each form a highly conserved, hydrophobic KAc binding pocket made up of a four-helix bundle (helices αA, αB, αC, and αZ) connected by two loops (ZA and BC loops) (Figure 9a).[122,123] Structural and sequence diversity across bromodomains primarily occurs in the loops and at the *C*- and *N*-terminal regions, with variations in structure and electrostatic potentials contributing towards binding specificity.[122,123] Additionally, the majority of bromodomains contain five conserved water molecules at the base of the KAc binding pocket, and it has been hypothesised that the dynamics of these water molecules play a role in bromodomain specificity.[121,124]

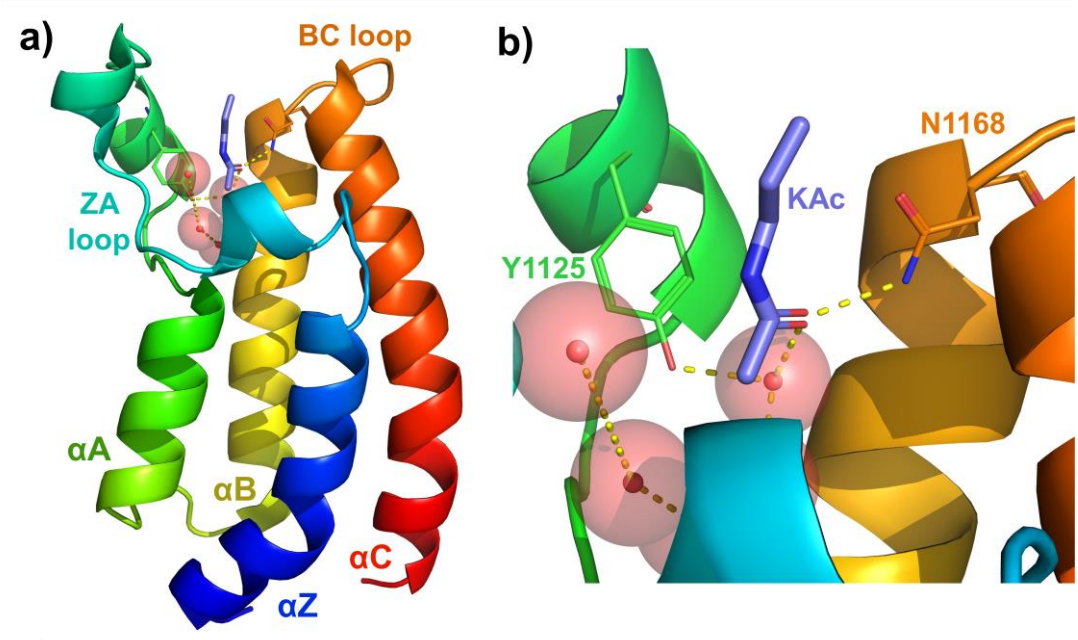

Figure 9. X-Ray crystal structure of the CREBBP bromodomain (multicoloured) bound to a KAc residue (purple) which is the native bromodomain substrate (PDB: 3P1C).[122] Bromodomain structures are highly conserved across BCPs and comprise a four-helix bundle (helices αA (green), αB (yellow), αC (red), and αZ (dark blue)) connected by two loops (ZA (cyan) and BC (orange) loops).[121–123] The majority of bromodomains have five conserved water molecules in the KAc binding pocket (red spheres).[121,124] Bromodomain-KAc binding is stabilised by an H-bond between the KAc residue and an asparagine residue in the bromodomain BC loop, and by a water-mediated H-bond between

the KAc residue and a tyrosine residue in the bromodomain ZA loop. H-bond interactions are depicted as yellow dashed lines. **a)** Overall X-ray crystal structure of the CREBBP bromodomain-KAc complex indicating the αA, αB, αC, and αZ helices and the ZA and BC loops. **b)** An expanded region of the X-ray crystal structure of the CREBBP bromodomain-KAc complex to highlight the stabilising H-bonds formed between the bound KAc residues and residues N1168 and Y1125 (water-mediated) of the CREBBP bromodomain. These residues are highly conserved across most BCPs.[121–123]

The bromodomains of CREBBP and p300 share a 97% sequence identity in humans (calculated using Protein BLAST® online software, CREBBP residues 1079 – 1197,[43] p300 residues 1048 – 1161,[48] see Appendix for protein sequences) and only differ by two amino acid residues (CREBBP residues: N1131 and R1177, and p300 residues: S1095 and Y1141).[52,53] The bromodomain-KAc complex is stabilised by an H-bond interaction between the KAc *N*-acetyl carboxy group with an asparagine residue in the bromodomain BC loop (Figure 9b). This asparagine residue is highly conserved across bromodomains and, when not present, is most commonly exchanged for another H-bond forming residue, such as threonine and tyrosine.[84,122] Additional complex stabilisation is obtained through a water-mediated hydrogen bond between the KAc *N*-acetyl carboxyl group with a tyrosine residue in the ZA loop (Figure 9b). This tyrosine residue is conserved across all but two bromodomains.[122,125]

Multiple, high affinity probes that are selective for the bromodomains of CREBBP and p300 have been developed, including within the Conway group (Figure 10).[43,125–132] Each of these compounds contain a chemical group that mimics KAc residues by formation of electrostatic interactions with the conserved asparagine and tyrosine residues in the KAc binding pocket. To develop any of the CREBBP and p300 bromodomain inhibitors into a PROTAC, they must be modified to enable attachment of the linker but not in such a way that would destroy protein binding.

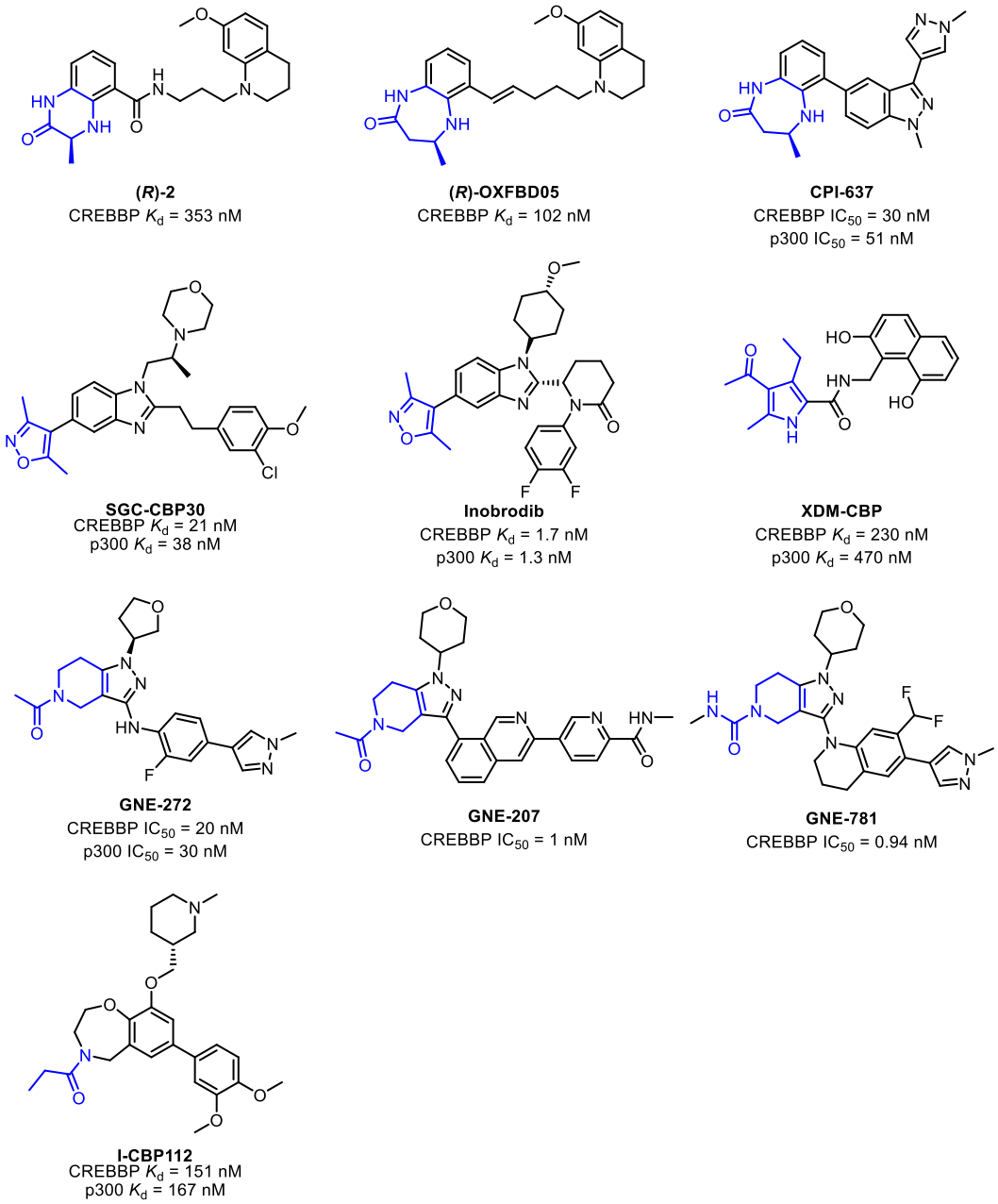

Figure 10. Structures of published inhibitors of the bromodomains of CREBBP and p300. Each compound comprises a KAc mimetic group (blue) that can form H-bond interactions in the KAc binding pocket.[43,125–132] Due to the high homologies of the CREBBP and p300 bromodomains, there is a trend in this field to assess binding affinity against the CREBBP bromodomain with the assumption that compounds with have equivalent affinities for the p300 bromodomain. K_d values were each obtained using isothermal titration calorimetry, IC_{50} values were each obtained using time-resolved fluorescence energy transfer (TR-FRET).

1.2.4 – Current CREBBP and p300-Targeting PROTACs

Since the start of the body of work described in this dissertation, three CREBBP and p300-degrading PROTACs have been reported in the literature (Figure 11).[133–135] All of these compounds target cereblon using a thalidomide-derivative ligand, two bind to the CREBBP and p300 bromodomain while the other binds to the KAT domain, and each comprise a different linker structure.

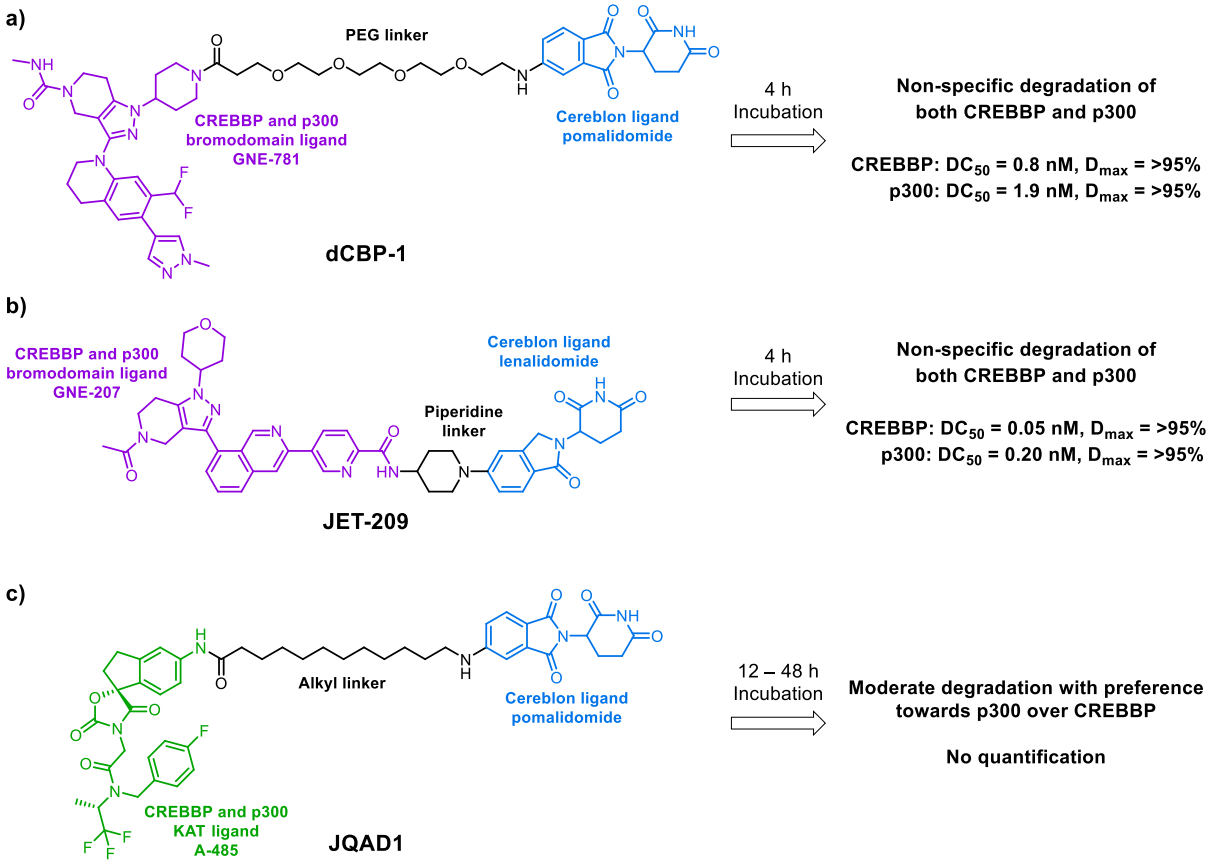

Figure 11. Structure and activities of previously reported CREBBP and p300-degrading PROTACs.[133–135] **a) dCBP-1** is a potent PROTAC that degrades both CREBBP and p300 over short incubation times.[133,134] **dCBP-1** comprises the CREBBP and p300 bromodomain inhibitor **GNE-781** which is joined by a PEG4 linker to the cereblon binder **pomalidomide**.[15,132] DC_{50} values calculated for 4 h dCBP-1 incubation in RS4;11.[134] **b) JET-209** is a potent PROTAC that degrades both CREBBP and p300 over short incubation times.[134] **JET-209** comprises the CREBBP and p300 bromodomain inhibitor **GNE-207** which is joined by piperidine group to the cereblon binder **lenalidomide**.[15,131] DC_{50} values calculated for 4 h **JET-209** incubation in RS4;11.[134] **c) JQAD** induces the moderate degradation of both CREBBP and p300 with preferential degradation of p300.[134] **JQAD** comprises the CREBBP and p300 KAT inhibitor **A-485** which is joined by an alkyl linker to the cereblon binder **pomalidomide**.[15,136]

dCBP-1 was the first reported CREBBP and p300-degrading PROTAC and comprises the high affinity CREBBP and p300 bromodomain inhibitor **GNE-781** (CREBBP IC_{50} = 0.9 nM, p300 IC_{50} = 1.2 nM) which is linked to the cereblon ligand **pomalidomide** by a PEG4 linker (Figure 11a).[132,133] **dCBP-1**

exhibits the potent, non-specific degradation of both CREBBP and p300 in HAP1 and multiple myeloma cancer cell lines over short timepoints (≤6 h) using 10 – 1000 nM dCBP-1.[133] Later studies by Thomas *et al.* quantified the potency of **dCBP-1** in RS4;11 cells following 4 h PROTAC incubation, and measured DC_{50} values of 0.8 nM and 1.9 nM for CREBBP and p300, respectively, and D_{max} of >95% for each paralogue.[134] *In vitro* studies have shown **dCBP-1**-induced CREBBP and p300 degradation caused greater cellular effects than small-molecule inhibition of the bromodomain or KAT domain.[133] These effects included the dysregulation of downstream proteins, downregulation of acetylation on H3-K27, and antiproliferative activity.

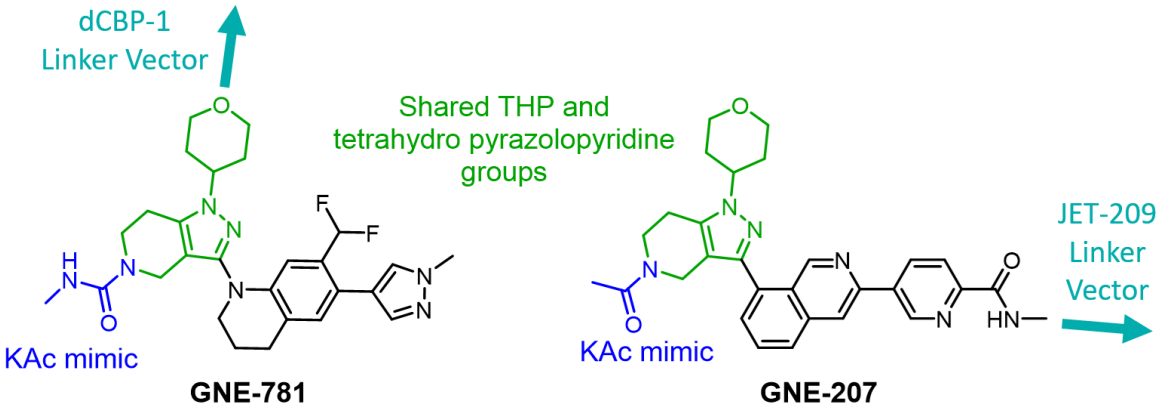

Figure 12. Structures of CREBBP and p300 bromodomain inhibitors **GNE-781** and **GNE-207** which are used as the POI ligand for the PROTACs **dCBP-1** and **JET-209**, respectively.[131–134] **GNE-781** and **GNE-207** share a scaffold comprising a tetrahydropyran (THP) and tetrahydro pyrazolopyridine group (green) and use similar KAc mimetic structures (blue), **GNE-781** uses a urea while **GNE-207** uses an amide) to bind the KAc binding pocket of the bromodomain. The PROTACs **dCBP-1** and **JET-209** attach a linker to their respective ligands at distinct positions (teal arrows).[133,134] This would suggest that the PROTACs use different exit vectors from the bromodomain binding site.

JET-209 was recently published and targets the CREBBP and p300 bromodomain using high affinity inhibitor **GNE-207** (CREBBP IC_{50} = 1.0 nM).[131] **GNE-207** is structurally similar to the ligand used by **dCBP-1** (**GNE-781**), however, the PROTAC linkers are attached at distinct positions (Figure 11b, Figure 12).[131,134] There is no X-ray crystal structure of **GNE-207** bound to the bromodomain of CREBBP or p300, so direct comparison of the PROTAC ligand-bromodomain binding is not possible, but it is likely **dCBP-1** and **JET-209** access different bromodomain exit vectors based on the linker attachment positions (Figure 12). Additionally, the two PROTACs differ in their cereblon ligand (**dCBP-1** uses **pomalidomide** while **JET-209** uses **lenalidomide**) and their linker compositions (Figure 11b). **JET-209** causes the non-specific degradation of CREBBP and p300 in RS4;11 cells with a greater

potency than **dCBP-1** (4 h PROTAC incubation gave DC_{50} values of 0.05 nM and 0.2 nM for CREBBP and p300, respectively) and an equivalent D_{max} of >95% for each paralogue.[134] **JET-209** was shown to induce greater effects in various leukaemia cell lines than observed by bromodomain or KAT domain inhibition with greater downregulation of the oncogenes *MYC* and *MYB*, decrease in cell proliferation, and increase in cell cycle arrest. Additionally, treatment of mouse RS4;11 xenograft models with **JET-209** showed a greater reduction in tumour growth than observed with bromodomain inhibition (68% reduction with **JET-209**, 34% reduction with **GNE-207**), however, higher doses led to mouse weight loss, suggesting toxicity. Analysis of the CREBBP and p300 levels in the xenograft RS4;11 cells following treatment with **JET-209** after 3 h and 6 h, showed the almost complete loss of both proteins. The protein levels then recovered to the control level after 24 h, after which time **JET-209** could also not be detected. These data could suggest that the PROTAC is either being degraded or metabolised, but it is difficult to discern as *in vitro* data is not given for timepoints longer than 4 h.[131]

Unlike **dCBP-1** and **JET-209**, **JQAD1** targets CREBBP and p300 by binding the KAT domain using the high affinity inhibitor **A-485** (CREBBP IC_{50} = 9.8 nM, p300 IC_{50} = 2.6 nM), which is attached to the cereblon ligand **pomalidomide** by an alkyl linker (Figure 11c).[135,137] It is claimed that **JQAD1** induces the selective degradation of p300 over CREBBP, however, protein levels have not been quantified, and the reported western blots show only moderate protein degradation with potentially some preferential degradation of p300 over CREBBP, which decreases over longer timepoints.[135]

The quick succession of **dCBP-1**, **JQAD1**, and **JET-209** (published in 2021, 2022, and 2023, respectively) highlights the high interest in designing PROTACs to degrade CREBBP and p300.[133–135] To gain meaningful understanding into the consequences of degrading these proteins in the cell, and to validate CREBBP and/ or p300 degradation as clinical targets, access to multiple, structurally diverse PROTAC chemical probes is required.[138,139]

Although **dCBP-1** and **JET-209** show a high potency for degrading CREBBP and p300 in the cell, degradation data are only available for short timepoints, and **JET-209** showed protein recovery and no detectable compound in mouse xenograft cells 24 h after dosing. siRNAs can mediate the specific knockdown of either CREBBP or p300, and are effective up to 96 h after transfection, making them

more desirable for examining individual CREBBP and p300 function *in vitro* over longer timepoints, at present.[100] Therefore, PROTACs need to be developed that induce the sustained knockdown of CREBBP and/or p300 in the cell for use as both chemical probes and as therapeutics.

PROTAC potency and selectively derives from interactions formed between the components of the POI:PROTAC:E3 ligase ternary complex (discussed in Section 1.1.4), making it difficult to predict which PROTAC structures will induce POI degradation.[140] Therefore, the synthesis of multiple PROTACs is required to tune PROTAC selectively towards CREBBP over p300 or *vice versa*. Additionally, the greater structural diversity between these compounds, the more information about the PROTAC structure-activity relationship (SAR) can be gained.

1.3 – Thesis Aims

For the above reasons, more PROTACs targeting CREBBP and p300 for degradation are required. The aim of this thesis is to contribute towards the efforts of synthesising potent PROTACs for CREBBP and p300, that can induce the sustained knockdown of these proteins, and potentially gain selectivity for the degradation of one paralogue over the other. The work described explores the development of different CREBBP and p300 bromodomain ligands into bifunctional PROTAC molecules, investigating different exit vectors from the bromodomain binding site. Additionally, the recruitment of two different E3 ubiquitin ligase enzymes is examined, and a variety of PROTAC linker structures will be used. Once synthesised, the ability of these novel PROTACs to degrade CREBBP and p300 will be evaluated in cells over longer timepoints with the aim of identifying long-acting compounds.

Results from the PROTACs evaluated in this work could then be used in collaboration with **dCBP-1** and **JET-209** to gain better understanding of the SAR of PROTACs which target CREBBP and p300 for degradation by binding their bromodomains. This could aid in the design the next generation of PROTACs targeting these proteins, to help develop chemical probes to understand CREBBP and p300 overall cellular functions, and work towards clinical development.

To achieve these aims we will:

- Rationally design a series of PROTACs using the CREBBP and p300 bromodomain ligand **(*R*)-OXFBD05**. These compounds will explore different linker lengths and will recruit two different E3 ubiquitin ligase enzymes with the aim of forming a stable POI:PROTAC:E3 ligase ternary complex.
- Evaluate the ability of the PROTACs to degrade CREBBP and/or p300 using western blot assays and to use the results to design the next generation of PROTACs.
- Synthesise a large range of structurally diverse PROTACs using three different CREBBP/p300 bromodomain ligands, different linker lengths, different linker rigidities, and different E3 ubiquitin ligase enzymes.
- Develop a higher throughput immunoassay for measuring the abilities of the PROTACs to degrade CREBBP and/or p300.

- Validate the activity of any CREBBP and p300-degrading PROTACs as on-target effects in follow up western blot assays.

Chapter 2 – The Rational Design and Evaluation of PROTACs Using the CREBBP and p300 Bromodomain Ligand **(*R*)-OXFBD05**

2.1 – Investigation into the Modification of CREBBP and p300 Bromodomain Ligand **(*R*)-OXFBD05** to Attach a Linker for PROTAC Development

2.1.1 – Structure Activity Relationship Exploration Ligand **(*R*)-OXFBD05**

2.1.1.1 – Structure of the Ligand-Protein Complex to Guide Linker Attachment

The Conway group recently published a series of inhibitors for the bromodomains of CREBBP and p300.[43] **(*R*)-OXFBD05** (Figure 13a) exhibited the greatest protein binding affinity, with CREBBP K_d = 102 nM (ITC), 200 nM (BromoScan); and p300 K_d = 240 nM (BromoScan) and a >100 fold selectivity over the closely related BCP, BRD4(1). This bromodomain inhibitor was selected as the CREBBP and p300 ligand for PROTAC development as its synthesis and structure activity relationship (SAR) was already well understood within the group. It also has the benefit that the (*S*)-enantiomer does not bind to the CREBBP/ p300 bromodomain, enabling synthesis of negative control compounds which will not bind the POI.

To utilise **(*R*)-OXFBD05** as the POI ligand in PROTAC design, we first wanted to understand how the position and functionality of an attached linker would affect the bromodomain binding affinity. Crystallisation of **(*R*)-OXFBD05** with the CREBBP bromodomain, for X-ray crystallography, resulted in a complex structure with seven bromodomain-ligand complexes in the unit cell (PDB: 6YIJ).[43] The structure displays dimerisation of the bromodomain-ligand complex where the tetrahydroquinoline (THQ) groups of **(*R*)-OXFBD05** form bridging interactions with the R1173 residue of the paired bromodomain (Figure 13b). Size-exclusion chromatography (SEC) experiments indicated that this dimerization was not occurring in solution and was, instead, a crystallographic artefact. Using a monomeric binding model, molecular dynamic simulations predicted that **(*R*)-OXFBD05** would bind in a similar mode to its amide bioisostere **1**, for which there is a monomeric X-ray crystal structure (PDB: 6YIM) (Figure 13c).[43] In this ligand-bromodomain complex, the 4,5-dihydrobenzodiazepinone (DHBD) moiety of **1** acts as the KAc mimic and binds to the deep KAc binding pocket in the protein, where the DHBD amide bond forms two H-bonds with residue N1168 and one water-mediated H-bond

with residue Y1125. The THQ moiety of **1** binds to an induced-fit pocket on the protein surface, created through a cation-π interaction with R1173 that alters in the surface structure of the protein upon ligand binding.[43,125]

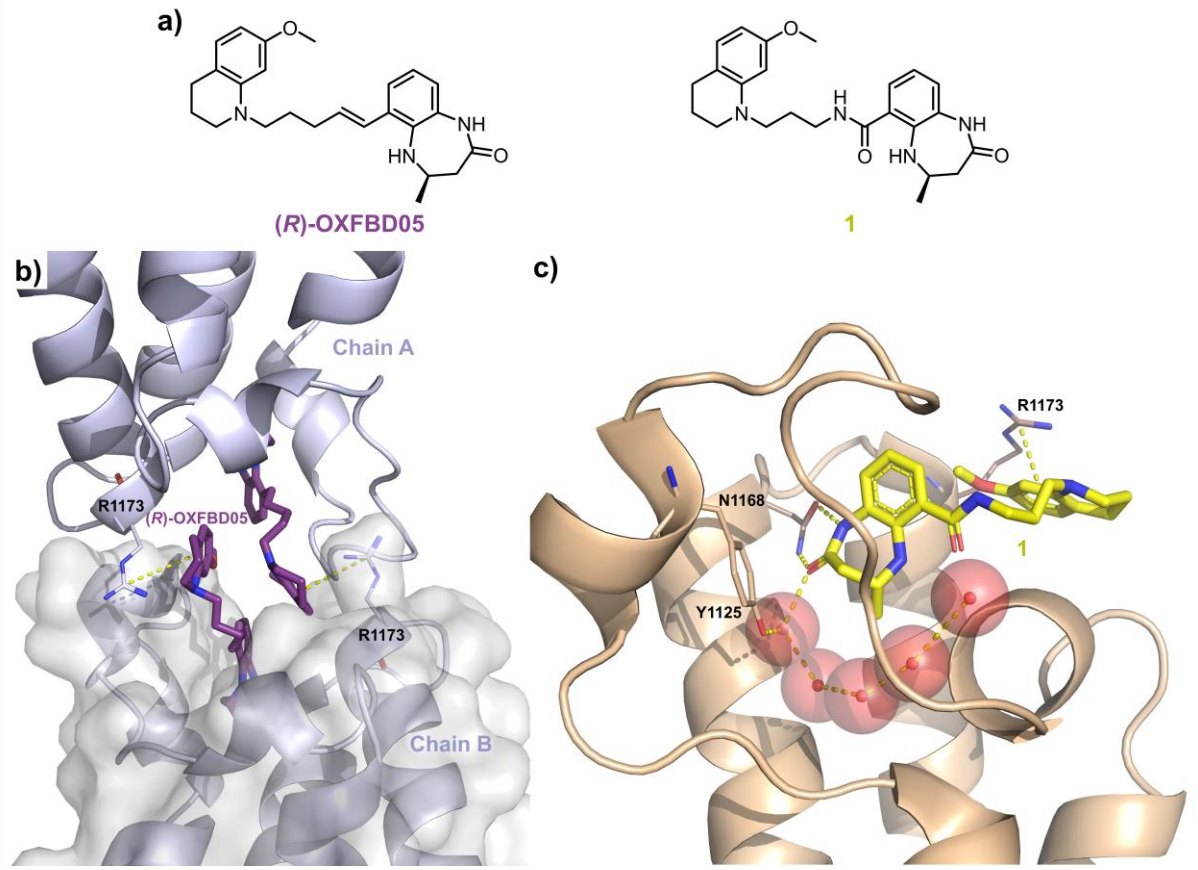

Figure 13. a) Structures of CREBBP and p300 bromodomain ligands **(*R*)-OXFBD05** and **1**. **b)** X-Ray crystal structure of the dimeric ligand-protein complex between **(*R*)-OXFBD05** (dark purple) and the CREBBP bromdomain (light purple) (PDB: 6YIJ).[43] For each **(*R*)-OXFBD05** compound, the DHBD-moiety of binds the KAc binding pocked of one bromodomain and the THQ moiety forms a cation-π interaction with residue R1173 of the other bromodomain in the dimer. The protein surface of one bromodomain is shown (grey) for clarity. Binding site protein residues are depicted as wire lines and electrostatic interactions are depicted as yellow dotted lines. **c)** X-Ray crystal structure of inhibitor **1** (yellow) bound to the bromodomain of CREBBP (beige) (PDB: 6YIM).[43] The DHBD-moiety of binds the KAc binding site of the protein and forms two H-bonds with reside N1168 and one water induced H-bond with residue Y1125. The THQ moiety of the ligand binds to an induced-fit pocket formed through a cation-π interaction with residue R1173. Binding site protein residues are depicted as wire lines, water molecules are depicted as red spheres, and interactions are shown as yellow dotted lines.

The X-ray crystal structure of ligand **1** bound to the CREBBP bromodomain was used to determine positions of attaching a linker to **(*R*)-OXFBD05** by identifying solvent exposed regions (Figure 14). The aromatic moiety of the DHBD group and the methoxy group of the THQ group point out of their respective binding pockets and a small library of compounds was designed to investigate the SAR of **(*R*)-OXFBD05** at these positions. Different functional groups, such as amide bonds and triazoles, were introduced to probe potential methods linker attachment (Figure 14).

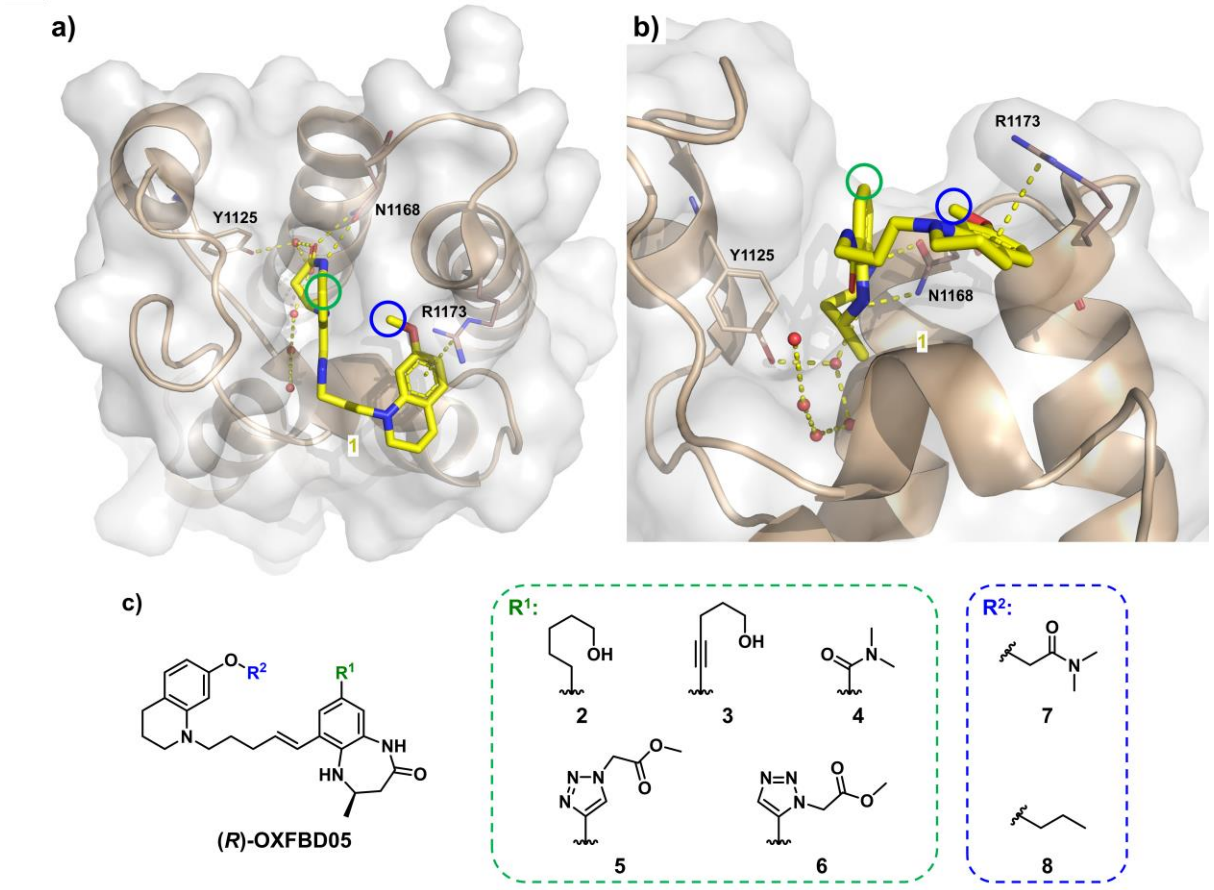

Figure 14. Rational design of CREBBP and p300-targeting PROTACs from **(*R*)-OXFBD05** using the X-Ray crystal structure of ligand **1** bound to the bromodomain of CREBBP as a guide. **a)** and **b)** X-Ray crystal structure of ligand **1** (yellow) bound to the bromodomain of CREBBP (cartoon: beige, surface: grey) (PDB: 6YIM).[43] The aromatic moitey of the DHBD group (circled in green) and the methoxy moitey of the THQ group (circled in blue) were identified as being solvent exposed and as promosing positions for linker attachment. Binding site protein residues are shown as lines, and interactions are shown as yellow dotted lines. **c)** Compounds **2** – **8** were designed to probe the SAR of **(*R*)-OXFBD05** at these positions. The solvent exposed postions of **(*R*)-OXFBD05** were modified with a variety of functional groups which could represent different methods of linker attachment. Compounds **2** – **6** (green dashed box) investigate attachment to the DHBD group of **(*R*)-OXFBD05**, while compounds **7** and **8** (blue dashed box) investigate attachment to the THQ group.

2.1.1.2 – Synthesis of Analogues to Investigate the SAR of CREBBP and p300 Bromodomain Ligand (R)-OXFBD05

(*R*)-OXFBD05 was resynthesised, according to the literature procedure, for use as a positive control in binding affinity assays (Scheme 1).[43] **(*R*)-OXFBD05** was synthesised in two parts, which were then coupled together in the final step using a Suzuki-Miyaura reaction, in a 58% yield. THQ-containing boronic acid pinacol ester intermediate **13** was synthesised from commercially available 7-hydroxy-3,4-dihydroquinolin-2(1*H*)-one. First, the phenol was methylated using methyl iodide, then the amide group was reduced to a secondary aniline using $LiAlH_4$, in yields of 76% and 91%, respectively, to afford **10**. The alkyl chain was then introduced in a substitution reaction, using the corresponding

mesylate, giving a mixture of desired product **12** (51% isolated yield) and the starting THQ intermediate **10**, which was recycled for further alkylations. The boronic acid pinacol ester could then be stereoselectively introduced to give the (*E*)-alkene **13** using HBPin and Schwartz's reagent, as the catalyst, in a 57% yield. To synthesise DHBD-containing intermediate **17**, first (*R*)-β-amino acid **14** was synthesised using a stereoselective conjugate-addition, developed by Davies, *et al.*, between commercially available (*R*)-*N*-benzyl-1-phenylethan-1-amine and *tert*-butyl crotonate in a yield of 49%.[141] The benzylic groups on the amine were removed using hydrogenolysis, catalysed by palladium hydroxide on carbon, to give **15** in a 89% yield.[141] The aromatic group was then introduced in an S_NAr reaction, with commercially available 1-bromo-2-fluoro-3-nitrobenzene, to give **16** in a yield of 99%. Finally, the 7-membered ring was formed by first deprotecting the *tert*-butyl group using TFA, and then heating under reflux in acetic acid with Fe(0) to simultaneously reduce the nitro group and induce acid-catalysed, intramolecular nucleophilic attack of the carboxylic acid by the aniline. This provided the DHBD-containing intermediate **17** in a yield of 78% over the two steps.

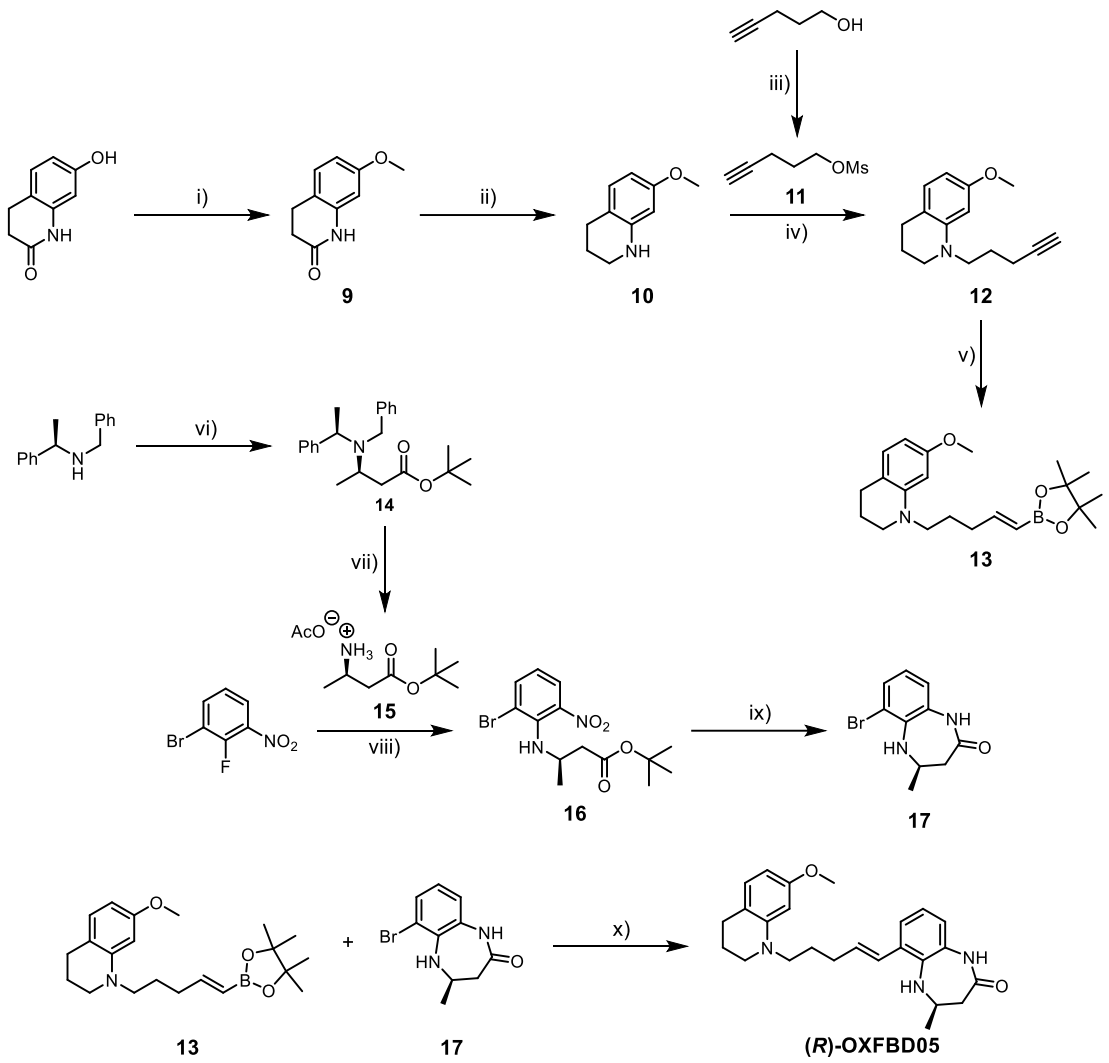

Scheme 1. Synthesis of **(*R*)-OXFBD05**. *Reagents and conditions*: i) MeI, K_2CO_3, DMF, 60 °C, 18 h, 76%; ii) $LiAlH_4$, THF, 0 °C – rt, 3 h, 91%; iii) MsCl, NEt_3, CH_2Cl_2, 0 °C – rt, 1.5 h, 89%; iv) KI, DIPEA, DMF, 100 °C, 1 h, 51%; v) HBPin, $ZrClCp_2H$, NEt_3, 60 °C, 18 h, 57%; vi) *n*-BuLi, *tert*-butyl crotonate THF, −78 °C, 3 h, 49%; vii) H_2, $Pd(OH)_2/C$, MeOH, AcOH, H_2O, rt, 15 h, 89%; viii) DIPEA, DMF, 80 °C, 14 h, 99%; ix) step 1: TFA, CH_2Cl_2, 0 °C – rt, 3 h; step 2: Fe(0), AcOH, 120 °C, 13 h, 78% (two steps); x) $Pd(PPh_3)_3Cl$, K_2CO_3, 1,4-dioxane, H_2O, 100 °C, 24 h, 58%.

A synthetic pathway developed by Dr Mustafa Moroglu (unpublished) was used to synthesise intermediate **2** (Scheme 2). Electrophilic aromatic substitution using *N*-iodosuccinimide was exploited for the regioselective addition of an iodo group to the 5-position of commercially available 1-bromo-2-fluoro-3-nitrobenzene, affording compound **18** in an 85% yield, and limited formation of side-products due to over-iodination was observed. The (*R*)-β-amino acid intermediate **15** was then introduced in a nucleophilic aromatic substitution reaction to afford **19** in a 93% yield. The alkyl chain was coupled in a Sonogashira reaction using commercially available 4-pentyn-1-ol, which gave intermediate **20** in a 77% yield, with preferential reaction with the iodide over the bromide residue of intermediate **19**. The

alkyne was reduced using hydrogenation with Wilkinson's catalyst, which did not cause debromination of the aromatic ring, giving **21** in a yield of 83%. Then, a similar route was followed as for **(*R*)-OXFBD05**, in which the 7-membered ring was formed by deprotection of the *tert*-butyl group using TFA, followed by nitro reduction and cyclisation, using Fe(0) in acetic acid. However, this reaction created a side-product where the terminal alcohol of the alkyl-chain was acetylated, but this could be easily hydrolysed using lithium hydroxide, and intermediate **22** was obtained in a 92% yield over three steps. Finally, **(*R*)-OXFBD05** analogue **2** was formed in a Suzuki-Miyaura coupling reaction between DHBD-containing intermediate **22** and THQ-containing intermediate **13** in a 79% yield.

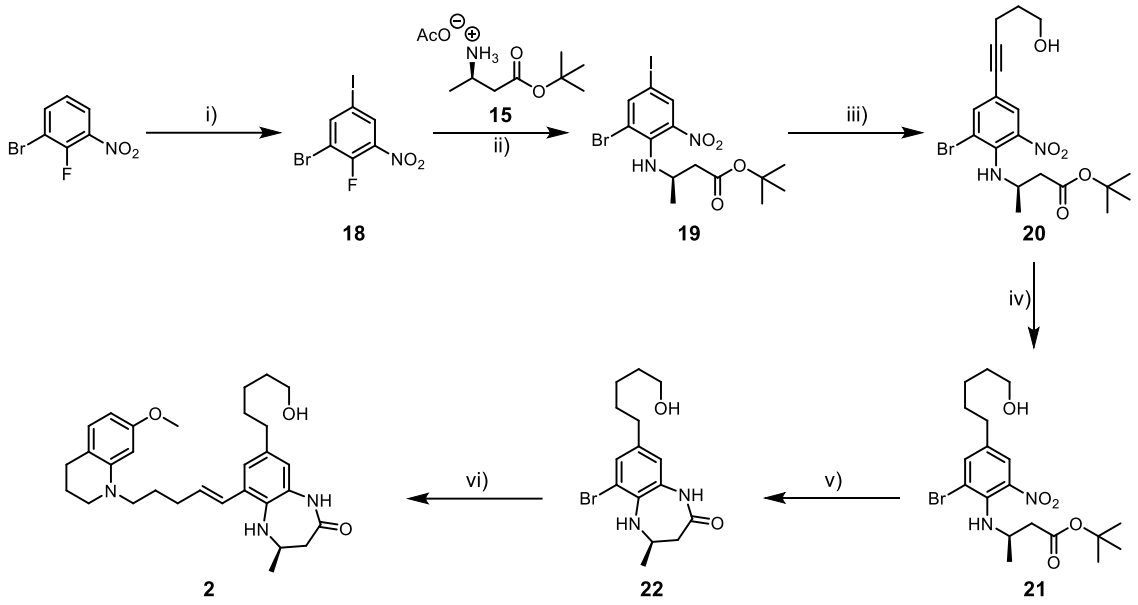

Scheme 2. Synthesis of analogue **2**. *Reagents and conditions:* i) NIS, H_2SO_4, rt, 16 h, 85%; ii) Cs_2CO_3, toluene, 85 ºC, 17 h, 93%; ii) 4-Pentyn-1-ol, $Pd(PPh_3)_2Cl_2$, CuI, NEt_3, THF, rt, 3.5 h, 77%; iv) H_2, $Rh(PPh_3)_3Cl$, toluene, 60 ºC, 11 h, 83%; v) step 1: TFA, CH_2Cl_2, rt, 2 h; step 2: Fe(0), AcOH, 100 ºC 3.5 h; step 3: LiOH, THF, MeOH, H_2O, rt, 3 h, 92% (three steps); vi) 7-Methoxy-1-[(4*E*)-5-(4,4,5,5-tetramethyl-1,3,2-dioxaborolan-2-yl)pent-4-en-1-yl]-1,2,3,4-tetrahydroquinoline (**13**), $Pd(PPh_3)_2Cl_2$, K_2CO_3, 1,4-dioxane, H_2O, 100 ºC, 16 h, 79%.

To synthesise **(*R*)-OXFBD05** analogue **3**, the direct cyclisation of open-ring intermediate **20** was initially investigated using the same conditions as for previous reactions (Scheme 3a). However, multiple products formed during whilst heating the reaction under reflux in acetic acid, and desired intermediate **23** was not isolated. Instead, the 7-membered ring was formed before introduction of the alkyne (Scheme 3b). First, intermediate **19** was cyclised, using the same conditions as previously, to afford the iodo-DHBD intermediate **24** in 94% yield over two steps. The alkyne was then introduced in a Sonogashira coupling, to form intermediate **23** in a 14% yield. The alkynyl-DHBD intermediate **23**

and THQ-containing intermediate **13** were then coupled using a Suzuki-Miyaura reaction to give **3** in a 59% yield. Though lower yielding, derivatisation of the DHBD-group uses a later stage intermediate than the route used for **2** synthesis and, this case, prevented the need for a hydrolysis reaction because the terminal alcohol was introduced after the acidic cyclisation reaction. Therefore, this route is preferable for the synthesis of future analogues based on the structures of compounds **2** and **3**.

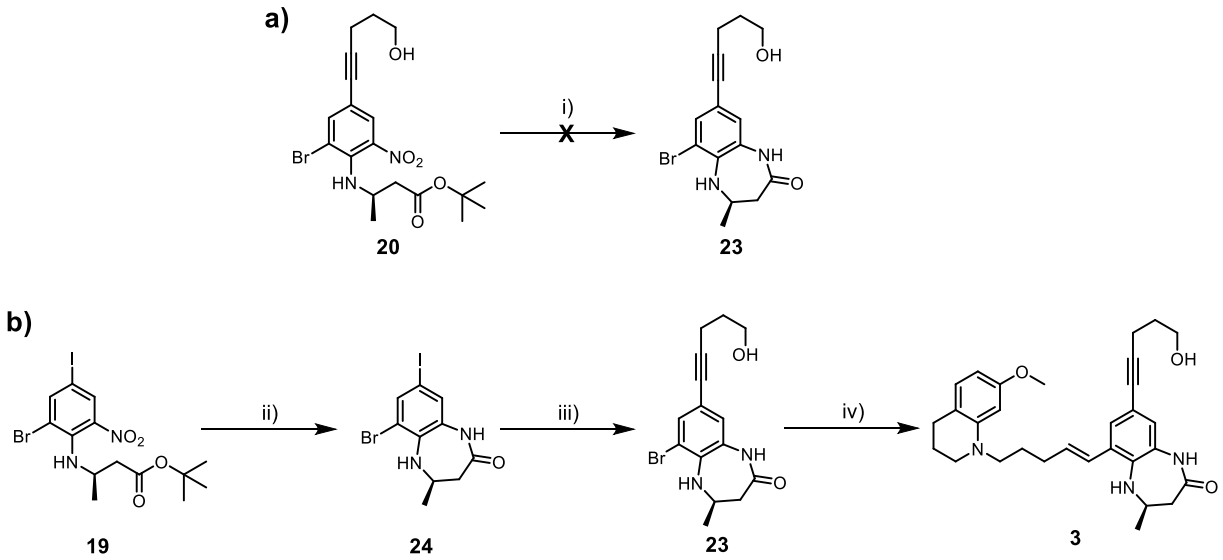

Scheme 3. a) Attempted cyslisation of **20** to form **23**. **b)** Synthesis of analogue **3**. *Reagents and conditions:* i) Step 1: TFA, CH_2Cl_2, rt, 1 h; step 2: Fe, AcOH, 100 ºC; ii) step 1: TFA, CH_2Cl_2, rt, 45 min; step 2: Fe(0), AcOH, 100 ºC, 4 h, 94%; iii) $Pd(PPh_3)_2Cl_2$, CuI, NEt_3, DMF, 40 ºC, 19 h, 14%; iv) 7-Methoxy-1-[(4*E*)-5-(4,4,5,5-tetramethyl-1,3,2-dioxaborolan-2-yl)pent-4-en-1-yl]-1,2,3,4-tetrahydroquinoline (**13**), $Pd(PPh_3)_2Cl_2$, K_2CO_3, H_2O, 1,4-dioxane, 100 ºC, 16 h, 59%.

(*R*)-OXFBD05 analogues **4 – 8** were synthesised by either Dr Mustafa Moroglu or Dr Margarida Espadinha.

*2.1.1.3 – Assessment of the Binding Affinities of Analogues Probing the SAR of **(R)-OXFBD05** for the CREBBP Bromodomain*

To determine the binding affinities of compounds **2 – 8**, the bromodomain of CREBBP was expressed and purified in collaboration with Dr Corentine Laurin, Dr Mustafa Moroglu, and Dr Margarida Espadinha (Appendix Figure 1). All compounds were tested for CREBBP bromodomain binding affinity using isothermal titration calorimetry (ITC) (Table 2, Appendix Figure 2, Appendix Figure 3). ITC was performed either by Dr Mustafa Moroglu, in collaboration with Dr Mustafa Moroglu, or independently.

Table 2. Binding affinities of compounds **(*R*)-OXFBD05**, and analogues **2 – 8** for the CREBBP bromodomain. K_d values were obtained using ITC. Darker green indicates higher ligand binding affinity to the bromodomain. Cpd. = compound, n.b. = no detectable binding. Compounds **4 – 8** were synthesised by Dr Mustafa Moroglu or Dr Margarida Espadinha.

Cpd.	Structure	K_d (nM)
(*R*)-OXFBD05	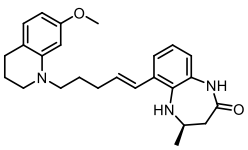	102
2	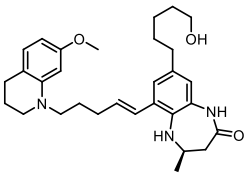	538
3	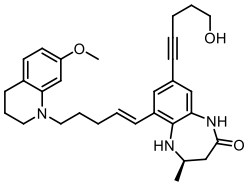	1460
4	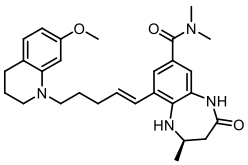	1300

Cpd.	Structure	K_d (nM)
5	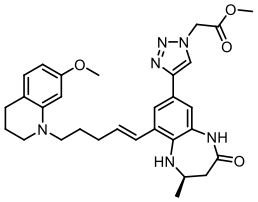	1310
6	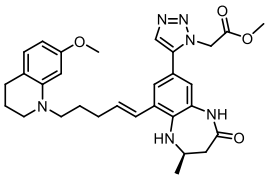	1260
7	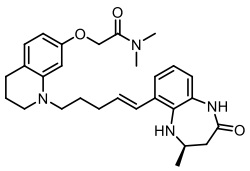	n.b.
8	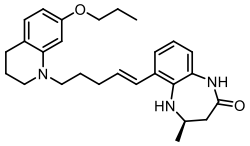	1450

The results from ITC analysis are shown in Table 2. The addition of rigid, electron rich moieties adjacent to the DHBD-group in analogues **3** – **6** reduced ligand binding affinities for the CREBBP bromodomain to the micromolar range. Similarly, modifications to the ether of the THQ group proved detrimental to binding affinity. Elongation to a propyl ether in analogue **8** reduced binding affinity to 1450 nM, and addition of an amide group in analogue **7** resulted in no detectable binding being observed. Consequently, these positions and methods were deemed unsuitable for PROTAC development. Addition of a flexible alkyl chain to the DHBD-group in analogue **2**, however, retained a high binding affinity for the CREBBP bromodomain with K_d = 538 nM. Thus, addition of flexible linkers to the DHBD-group of **(*R*)-OXFBD05** looked like a promising avenue for developing PROTACs.

2.1.2 – Investigation into the Effect of Alkyl Linker Length on **(*R*)-OXFBD05** Analogue Binding Affinities for the CREBBP Bromodomain

*2.1.2.1 – Synthesis of Alkyl Analogues of **(R)-OXFBD05***

The length of the alkyl chain was then investigated by synthesising analogues **25** and **26**, which comprise an *n*-propanol and an *n*-decanol group, respectively. These analogues were produced using similar route to the initial alkyl-analogue **2**, except the Sonogashira coupling was performed on the later stage, 7-membered ring intermediate **24** to streamline the synthesis (Scheme 4), as discussed in Section *2.1.1.2*. Sonogashira couplings between the DHBD-containing intermediate **24** and the relevant alkynes gave intermediates **27** and **28** gave yields of 62% and 96%, respectively. Reduction of the alkyne was achieved using hydrogenation with Wilkinson's catalyst to afford **29** and **30**, in yields of 65% and 63%, respectively. The final alkyl-**(*R*)-OXFBD05** analogues **25** and **26** were produced using Suzuki-Miyaura couplings with THQ-containing intermediate **13** in yields of 46% and 47%, respectively.

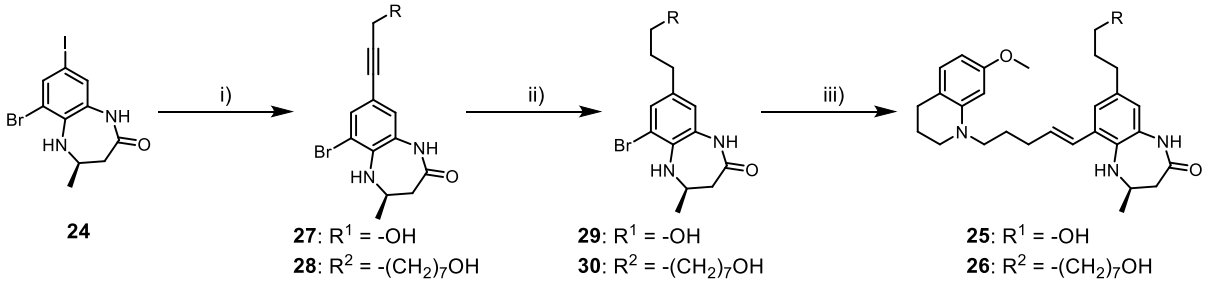

Scheme 4. Synthesis of alkly-OXFBD05 analogues **25** and **26**. *Reagents and conditions*: i) General procedure: alcohol, $Pd(PPh_3)_2Cl_2$, CuI, NEt_3, DMF, rt; R^1: Propargyl alcohol, 18 h, 62%; R^2: 9-Decyn-1-ol, 20 h, 96%; ii) General procedure: H_2, $Rh(PPh_3)_3Cl$, toluene, 60 ºC; R^1: 6 h, 65%; R^2: 3.5 h, 63%; iii) General procedure: 7-Methoxy-1-[(4*E*)-5-(4,4,5,5-tetramethyl-1,3,2-dioxaborolan-2-yl)pent-4-en-1-yl]-1,2,3,4-tetrahydroquinoline (**13**), $Pd(PPh_3)_2Cl_2$, K_2CO_3, 1,4-dioxane, H_2O, 100 ºC; R^1: 17 h, 46%; R^2: 17 h, 47%.

2.1.2.2 – ITC Binding Affinity Results and Predicted Compound Physicochemical Properties

The **(*R*)-OXFBD05** analogues **25** and **26** were tested for CREBBP affinity using ITC (Table 3, Appendix Figure 4, Appendix Figure 5). Analogue **25**, with the shortest alkyl chain, showed comparable binding to **(*R*)-OXFBD05** while analogue **26**, with the longest alkyl chain, exhibited no detectible binding. These compounds would be expected to bind to the protein in the same conformation as

compound **2**, which has K_d = 538 nM, so the trend of decreasing binding affinity with increasing alkyl chain length was surprising.

Table 3. Ligand binding affinities for the CREBBP bromodomain, $clogD_{pH7.4}$, and Property Forecast Index (PFI) values of **(*R*)-OXFBD05** and analogues **2**, **25**, and **26**. Compound **25** has comparable binding affinity, $clogD_{pH7.4}$, and PFI values as the parent ligand **(*R*)-OXFBD05**, however, as the alkyl linker length increases in compounds **2** and **26**, the binding affinity for the CREBBP bromodomain decreases. This trend appears to correlate with the increasing lipophilicities of the compounds, where predicted aqueous solubility (pH 7.4) decreases with increasing alkyl linker length. Binding affinity K_d values were obtained using ITC. Darker green indicates higher binidng affinity of the compound to the CREBBP bromodomain, n.b. = no detectable binding. $clogD_{pH7.4}$ values were calculated using Chemicalize (http://www.chemicalize.com) and are coloured according to compound aqueous solubility observations by Hill and Young, where $2 < x \leq 4$ predicts moderate solubility (yellow) and $x > 4$ predicts poor solubility (red), darker colour indicates higher value within category.[20] The Property Forecast Index (PFI) is a measurement developed by GSK for predicting aqueous solubility (PFI = $clogD_{pH7.4}$ + #Ar rings).[21] PFI values are coloured according to compound aqueous solubility observations by Tinworth and Young, where $4 < x \leq 8$ predicts moderate solubility (yellow) and $x > 8$ predicts poor solubility (red), darker colour indicates higher value within category.[21]

Cpd.	Structure	K_d (nM)	$clogD_{pH7.4}$	PFI
(*R*)-OXFBD05	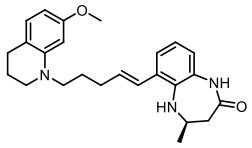	102	4.54	6.54
25	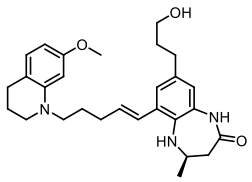	111	4.50	6.50
2	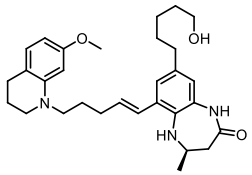	538	5.39	7.39
26	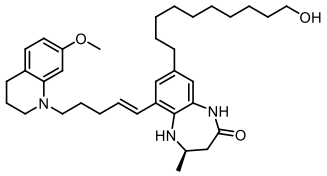	n.b.	7.61	9.61

ITC experiments take place in aqueous HEPES buffer at pH 7.4 and the binding affinity trend was believed to be related to compound solubility. To confirm this, $clogD_{pH7.4}$ and Property Forecast Index (PFI) values were calculated for these compounds to examine the impact of predicted compound solubility (aqueous, pH 7.4) on the binding affinity measurements (Table 3).[20] Using analysis by Hill and Young, $logD_{pH7.4}$ values of $x \leq 2$ predict good solubility, $2 < x \leq 4$ predict moderate solubility, and $x > 4$ predict poor solubility.[20] $clogD_{pH7.4}$ (calculated using Chemicalize online software) for

(*R*)-OXFBD05 and *n*-propanol-containing analogue **25**, gives equivalent values of 4.54 and 4.50, respectively. The equivalent $clogD_{pH7.4}$ values are in accordance with their comparable CREBBP bromodomain binding affinities of 102 nM and 111 nM, respectively, and suggests that modification of **(*R*)-OXFBD05** with the propanol group does not affect CREBBP and p300 binding. As the alkyl length increases, the $clogD_{pH7.4}$ values also increase, where *n*-pentanol-containing compound **2** has $clogD_{pH7.4} = 5.39$ and *n*-decanol-containing compound **26** has $clogD_{pH7.4} = 7.61$. The decreasing $clogD_{pH7.4}$ values correspond to the decrease in bromodomain binding affinity to $K_d = 538$ nM for compound **2** and no binding being detected for compound **26**. However, each compound would be predicted to be poorly soluble PFI takes compound aromaticity into account (PFI = $logD_{pH7.4}$ + number of aromatic rings), and was developed by GSK due to the observed trend that compound aqueous (pH 7.4) solubility decreased as the number of aromatic rings increased.[20,21,142,143] Analysis of the measured aqueous (pH 7.4) solubilities of ~20000 proprietary compounds by Hill and Young, showed PFI to be a better predictor of solubility than $clog_{pH7.4}$, particularly for poorly soluble compounds, and found that aromatic rings had a greater impact on decreasing solubility than just their added hydrophobicity.[20] Each of the compounds **(*R*)-OXFBD05**, **2**, **25**, and **26** have two aromatic rings, meaning their PFI value increase in accordance with the $clogD_{pH7.4}$ values (Table 3), however, analysis by Tinworth and Young, show different ranges for predicted aqueous (pH 7.4) solubilities where PFI values of $x \leq 4$ predict good solubility, $4 < x \leq 8$ predict moderate solubility, and $x > 8$ predict poor solubility.[21] This indicates that **(*R*)-OXFBD05**, **2**, and **25** will have a moderate solubility, while **26** will be poorly soluble. Overall, the $clogD_{pH7.4}$ and PFI values indicate that the decrease in CREBBP bromodomain binding affinities is due to a decreasing solubility in the ITC assay, as opposed to differences in ligand-protein binding. As ligand solubility decreases, the effective concentration in the assay would be expected to decrease, and less compound will be available in solution to bind to the protein, giving a lower K_d readout. Similar binding affinity to lipophilicity trends were not observed for the previously tested **(*R*)-OXFBD05** analogues **3 – 8** indicating that the changes in CREBBP bromodomain binding affinities were the result of less favourable ligand-protein interactions (Appendix Table 1).

This work demonstrates that care should be taken with the physicochemical properties of the final PROTAC compounds, as poor aqueous solubility at physiological pH may impact the effective concentrations of PROTAC in *in vitro* assays. **(*R*)-OXFBD05** already has a calculated $clogD_{pH7.4}$ of 4.54 and PFI of 6.54, so its development into large PROTACs will likely produce compounds with high lipophilicities, which is a challenge commonly associated with PROTAC development (discussed in Section 1.1.5).

2.2 – Synthesis of the Initial Series of **(*R*)-OXFBD05**-Based PROTACs

2.2.1 – Attachment of a Linker to CREBBP and p300 Bromodomain Ligand **(*R*)-OXFBD05**

2.2.1.1 – Linker and E3 Ligase Ligand Selection

The SAR studies in Section 2.1 indicate that addition of a flexible chain to the DHBD-group of **(*R*)-OXFBD05** should not impact ligand binding to the CREBBP and p300 bromodomains and presents a promising route for attaching a linker in the development of PROTACs. Therefore, it was decided to synthesise the initial series of PROTAC molecules by attaching flexible PEG linkers attached to this position (Figure 15). PEG linkers not only mimic the flexible *n*-propanol group of compound **25**, but allow linker length, which is important for ternary complex formation, to be readily assessed by varying the number of PEG groups in the chain. These linkers also exhibit superior hydrophilicity compared with alkyl linkers, which otherwise have a similar capability of assessing optimal linker length.[28,144] The initial series of compounds will examine four PEG linker lengths, then if an optimal linker length is identified, the linker structure could be investigated in subsequent PROTAC molecules. As discussed in Section 1.1.5, the ability of a PROTAC to degrade its POI can be enhanced by increasing linker rigidity, which can also help to reduce compound lipophilicity.[26,27]

Due to their prevalence in the literature (discussed in Section 1.1.2), initial PROTACs will target the E3 ligases cereblon and VHL using the ligands **pomalidomide** and **VH032**, respectively (Figure 15).[15,25]

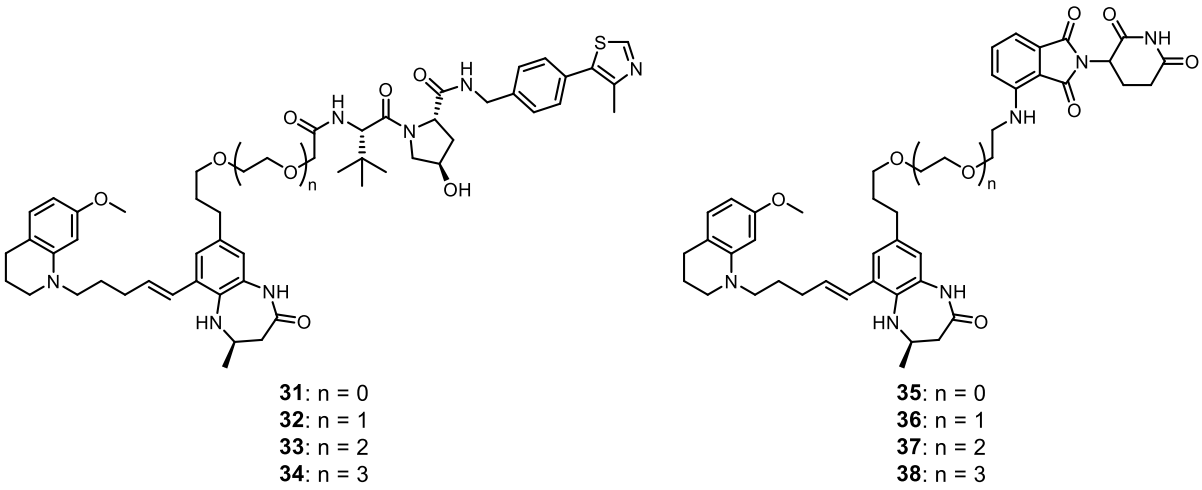

Figure 15. Structures of the initial series of VHL-targeting PROTACs **31** – **34** and cereblon-targeting PROTACs **35** – **38**. Bromodomain ligand **(*R*)-OXFBD05** is used to target CREBBP and p300, while ligands **VH032** and **pomalidomide** are used to target the E3 ubiquitin ligases cereblon and VHL, respectively.[15,25] Four different PEG linker lengths were used for each PROTAC series to probe the effect of linker length on ternary complex formation and protein degration.

2.2.1.2 – Initial PROTAC Synthetic Strategy

To avoid a linear synthesis and to enhance overall yields, the initial strategy was to synthesise the final PROTACs in two halves, then to couple them in alkylation reactions (Scheme 5). The CREBBP and p300 bromodomain ligand **25** could be activated by mesylation and then reacted with the E3 ligase ligand with different length PEG linkers.

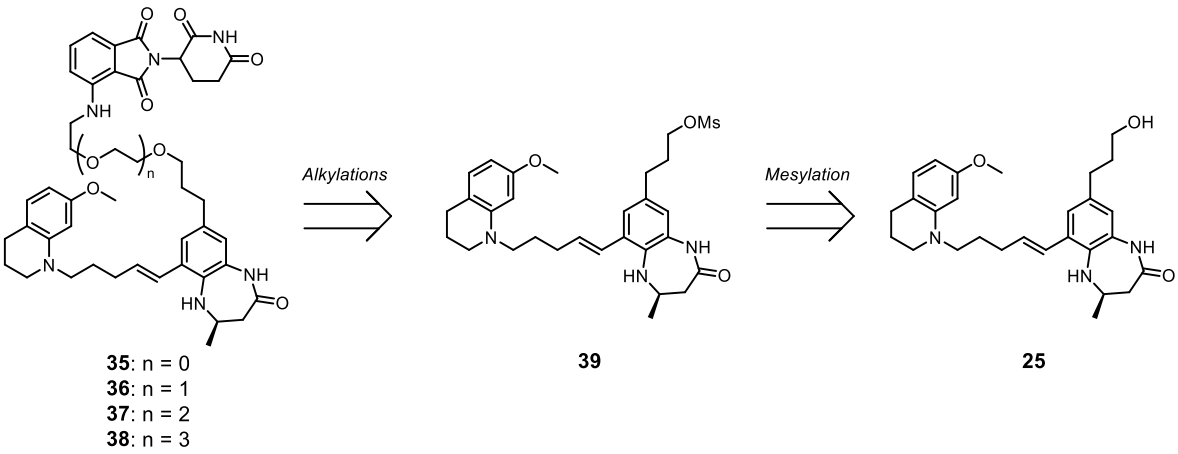

Scheme 5. Proposed retrosynthesis of PROTAC PROTACs **35** – **38** from **(*R*)-OXFBD05** analogue **25.** Final PROTACs could be synthesised by mesylating **25** and then performing alkylating with alcohol terminal E3 ligase ligand-linker compounds.

This proposed pathway was initially investigated using with bromodomain ligand **25** and 2-(2,6-dioxopiperidin-3-yl)-4-[(5-hydroxypentyl)amino]-2,3-dihydro-1*H*-isoindole-1,3-dione (**41**) using excess sodium hydride as the base for the reaction (Scheme 6). However, the alkylation reaction proceeded slowly, with remaining starting materials after stirring at room temperature for 20 h and the formation of multiple side-products was detected using TLC. Following quenching, both the organic and aqueous phases contained a complex mixture of products in TLC analysis, which was likely due, in part, to the known instability of thalidomide derivatives to basic aqueous solutions.[145] A product with the correct molecular weight was isolated, however, it transpired that this was not the desired PROTAC, but compound **42** resulting from nucleophilic attack of the mesylate by the imide nitrogen of **41** instead of the alcohol (Scheme 6). This was evident through analysis of the 2D NMR spectra of the isolated product (Appendix Figure 6).

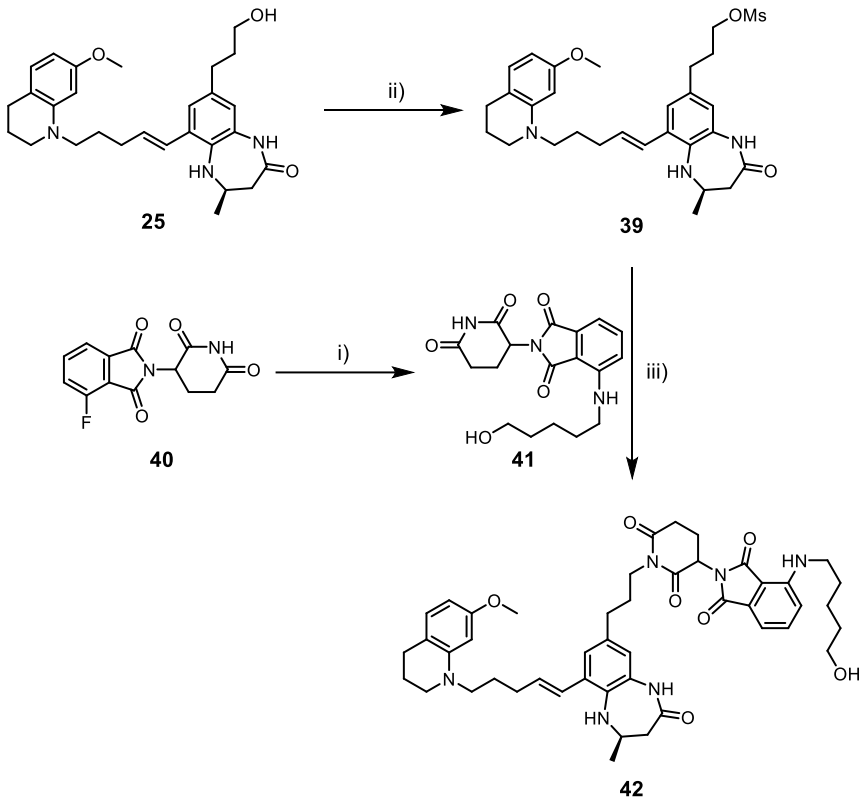

Scheme 6. Synthesis of undesired product **42**. *Reagents and conditions*: i) 3-Fluorophthalic anhydride, 3-aminopiperidine-2,6-dione hydrochloride, NaOAc, AcOH, reflux, 4 h, 85%; ii) MsCl, DIPEA, anhydrous CH_2Cl_2, 0 ºC, 3 h; ii) NaH, anhydrous DMF, 0 ºC – rt, 20 h, 9% (two steps).

The order of this synthetic route could be swapped so that the E3 ligase-ligand compound is mesylated and the free alcohol of bromodomain ligand **25** performs the nucleophilic attack. None-the-less, alcohols remain poor nucleophiles meaning a strong base would be required. There are multiple positions on the compounds that could be deprotonated, likely resulting in a similar mixture of products, so this approach was not pursued further.

Protection of the imide nitrogen was investigated to prevent the imide nitrogen from participating in alkylation reactions (Scheme 7). 4-Fluorothalidomide (**40**) was protected with a Boc group using Boc-anhydride to afford compound **43** in a 70% yield. However, the subsequent S_NAr reaction to attach a linker gave no remaining starting material (**43**) and a complex mixture of products, even at the decreased temperature of 50 °C after 10 min. As a result, an alternative linker attachment strategy was required.

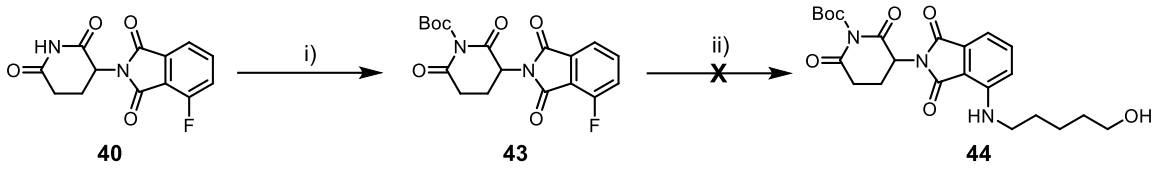

Scheme 7. Boc protection of 4-fluorothalidomide **40** and attempted S_NAr to add an alkyl linker to afford **44**. *Reagents and conditions*: i) Boc_2O, DMAP, 1,4-dioxane, 0 ºC – rt, 1.5 h, 70%; ii) Conditions I: 5-Amino-1-pentanol, DIPEA, NMP, 90 ºC, 30 min; conditions II: 5-Amino-1-pentanol, DIPEA, NMP, 50 ºC, 10 min.

*2.2.1.3 – Synthesis of **(R)-OXFBD05**-PEG Linker Compounds **61** – **64***

To overcome the issues describes above, it was decided to install the full length PEG linkers to the CREBBP and p300 bromodomain ligand then couple the E3 ligase ligand in the final step using similar methodology to that employed for the synthesis of compound **25**, described in Section 2.1.2.1 (

Scheme 8). This route is disadvantageous because the linker must be added to the early stage intermediate 24, increasing the number of steps to obtain the final compounds. This is because the (*R*)-OXFBD05 ligand contains an *E*-alkene which is necessary for its binding affinity for the CREBBP and p300 bromodomain and for selectivity against the BET family of bromodomain containing proteins.[43] If the linker were added later in the synthesis, reduction of the linker alkyne group would also reduce this essential double bond in the bromodomain ligand.

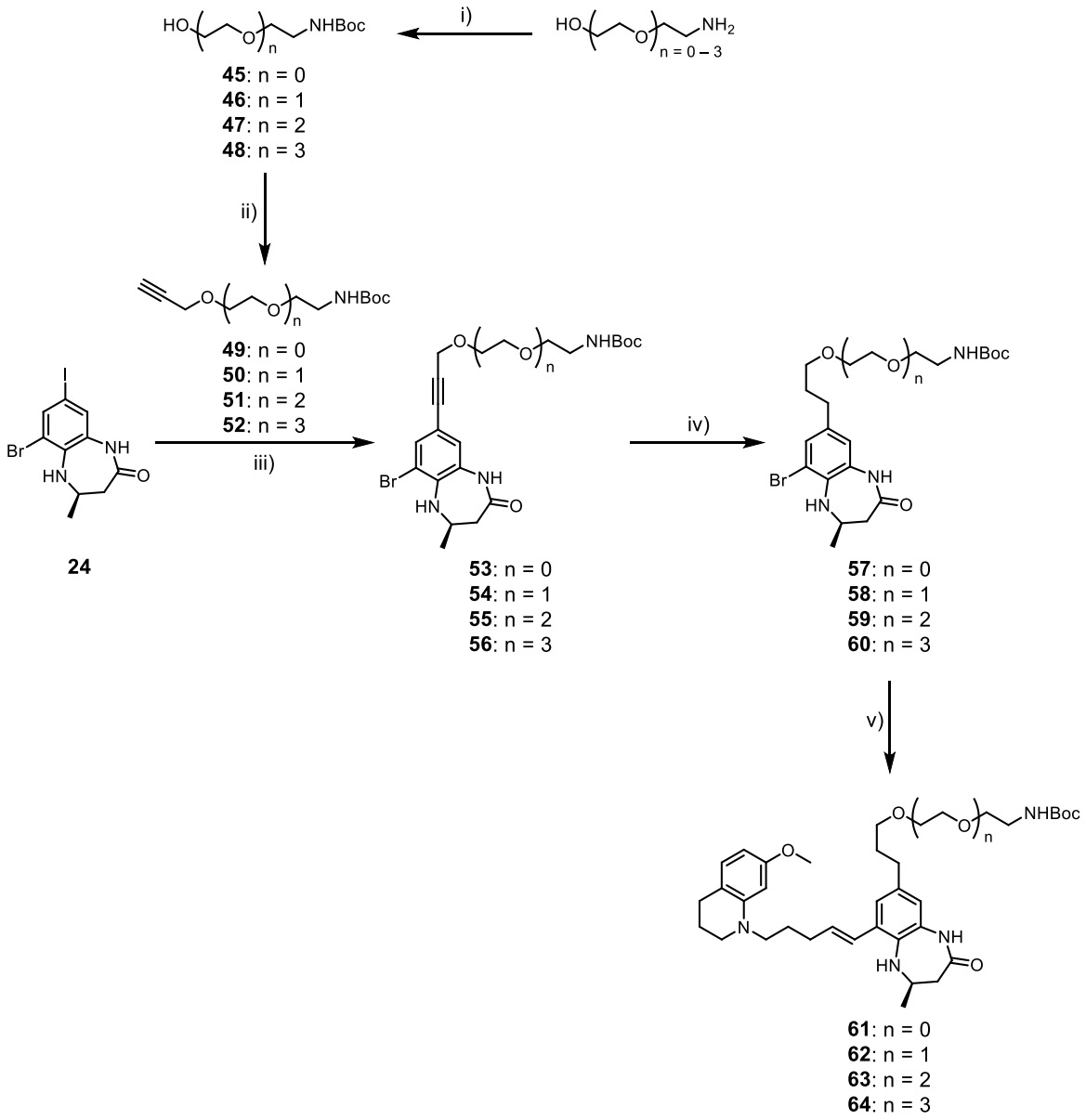

Scheme 8. Synthesis of compounds **61** – **64**. *Reagents and conditions*: i) General procedure: Boc_2O, anhydrous CH_2Cl_2, 0 ºC– rt; n = 0: 3 h, 99%; n = 1: 18 h, 79%; n = 2: 18 h, 89%; n = 3 27 h, 99%; ii) General procedure: propargyl bromide 80% *w/w* in toluene, sodium hydride 60% *w/w* in mineral oil, TBAI, anhydrous THF, 0 ºC – rt/ 50 ºC; n = 0: 5 h, 54%; n = 1: 0 ºC – rt, 24 h, 54%; n = 2: 0 ºC – rt, 24 h, 42%; n = 3: 0 – 50 ºC 5 h, 63%; iii) General procedure: $Pd(PPh_3)_2Cl_2$, CuI, NEt_3, DMF, rt; n = 0: 16 h, 78%; n = 1: 16 h, 83%; n = 2: 16 h, 98%; n = 3: 16 h, 9%; iv) General procedure: H_2, $Rh(PPh_3)_3Cl$, toluene, 60 ºC; n = 0: 20 h, 58%; n = 1: 20 h, 39%; n = 2: 7 h, 67%; n = 3: 20 h, 92%; v) General procedure: 7-methoxy-1-[(4*E*)-5-(4,4,5,5-tetramethyl-1,3,2-dioxaborolan-2-yl)pent-4-en-1-yl]-1,2,3,4-tetrahydroquinoline (**13**), $Pd(dppf)Cl_2$, K_2CO_3, 1,4-dioxane, H_2O, 100 ºC; n = 0: 16 h, 65%; n = 1: 26 h, 78%; n = 2: 16 h, 77%; n = 3: 26 h, 58%.

Four PEG linkers (**49** – **52**) were functionalised with a terminal amine, to facilitate S_NAr coupling to an E3 ligase ligand, and an alkyne, to enable Sonogashira coupling to the CREBBP and p300 bromodomain ligand. First commercially available PEG linkers were Boc-protected using Boc-anhydride to afford compounds **45** – **48** in 79 – 99% yields, then the alkyne moiety was installed in an alkylation reaction with propargyl bromide to afford compounds **49** – **52** in yields of 42 – 63%. The linkers were introduced

onto the bromodomain ligand using Sonogashira couplings with DHBD intermediate **24**, using $Pd(PPh_3)_2Cl_2$ as the catalyst, giving compounds **53** – **56**. The products were isolated with a large range in yields resulting from coelution of $OPPh_3$, a by-product from the reaction catalyst, with the desired product during purification of the PEG3 intermediate **56**, which was isolated in a 9% yield. Meanwhile, intermediates **53** – **55** did not encounter this purification issue and were obtained in yields of 78 – 98%. The linker alkyne was then reduced via hydrogenation using Wilkinson's catalyst, similarly, with a large range in yields of 39 – 92% due to coelution of $OPPh_3$ with the products during purification. In this instance, the highest polarity PEG3 intermediate **60** was obtained in a 92% yield, while PEG1 intermediate **58** had the greatest coelution with $OPPh_3$ and was obtained in a 39% yield. The final compounds **35** – **38** were synthesised using Suzuki-Miyaura couplings with intermediate **13**. However, the previously used $Pd(PPh_3)_2Cl_2$ catalyst was changed for $Pd(dppf)Cl_2$, which contains a bidentate phosphine ligand, with the aim of avoiding $OPPh_3$ contamination of the desired products. This afforded the **(*R*)-OXFBD05**-linker compounds **61** – **64** in yields of 58 – 78% and no $OPPh_3$ contamination was observed. Despite the greater synthetic demand of this route, the terminal amine means that compounds **61** – **64** can be easily functionalised with a variety of different ligands, making them valuable intermediates for future investigations.

2.2.2 – Synthesis of the Initial Series of **(*R*)-OXFBD05**-Based PROTACs and HyTs

*2.2.2.1 – Synthesis of Cereblon-Targeting PROTACs **35** – **38***

PROTACs **35** – **38** were synthesised using pomalidomide as the ligand for the E3 ubiquitin ligase cereblon. First the **(*R*)-OXFBD05**-linker compounds **61** – **64** were Boc-deprotected, then S_NAr reactions were performed with 4-fluorothalidomide (**40**) to give the PROTAC compounds in yields of 10 – 26%, which are comparable to yields obtained in the literature.[146]

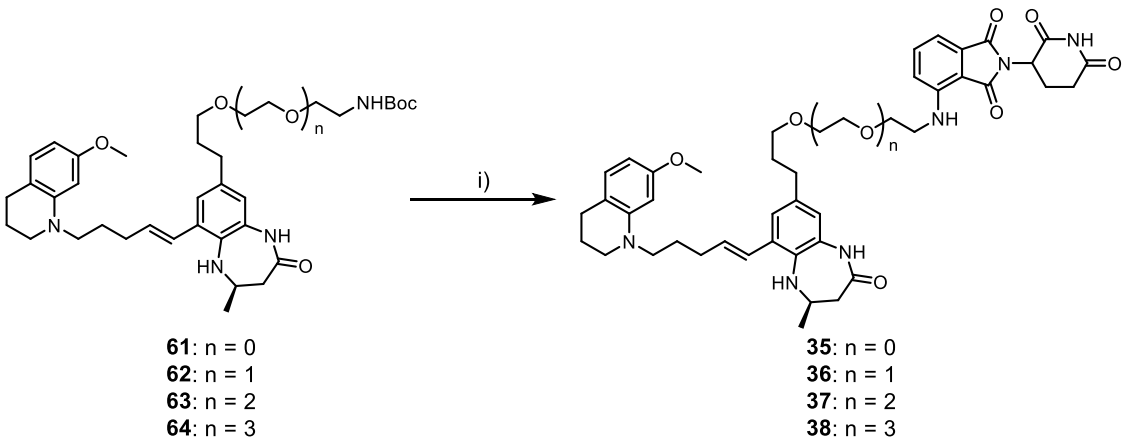

Scheme 9. Synthesis of cereblon-targeting PROTACs **35** – **38**. *Reagents and conditions*: i) General procedure: step 1: 4 M HCl in 1,4-dioxane, CH_2Cl_2, 0 ºC – rt; step 2: 2-(2,6-dioxopiperidin-3-yl)-4-fluoro-2,3-dihydro-1*H*-isoindole-1,3-dione (**40**), DIPEA, DMF, 90 ºC; n = 0: step 1: 1 h; step 2: 4 h, 26% (two steps); n = 1: step 1: 2 h; step 2: 2 h, 10% (two steps); n = 2: step 1: 1.5 h; step 2: 3.5 h, 21% (two steps); n = 3: step 1: 2 h; step 2: 3 h, 13% (two steps).

*2.2.2.2 – Synthesis of Hydrophobic Tag-Containing Compounds **65** – **68***

Given the ability of the **(*R*)-OXFBD05**-linker compounds **61** – **64** to be functionalised with a variety of different groups, it was decided to synthesise a series of hydrophobic tags (HyTs). This was achieved by the addition of lipophilic adamantane groups using amide coupling reaction to afford HyTs **65** – **68** (Scheme 10). HyTs function in a similar manner to PROTACs but use a lipophilic group to non-specifically recruit an E3 ubiquitin ligase enzyme to induce polyubiquitination of the POI (Appendix Figure 7).[6,147,148]

Compounds **61** – **64** were Boc-deprotected, using 4 M HCl in 1,4-dioxane, then the crude amines were reacted with 1-adamantaneacetic acid in amide coupling reactions using HATU as the activating reagent. The final HyTs **65** – **68** were obtained in yields of 22 – 74%, where the high lipophilicity of PEG3 HyT **68** caused purification difficulties leading to a lower yield.

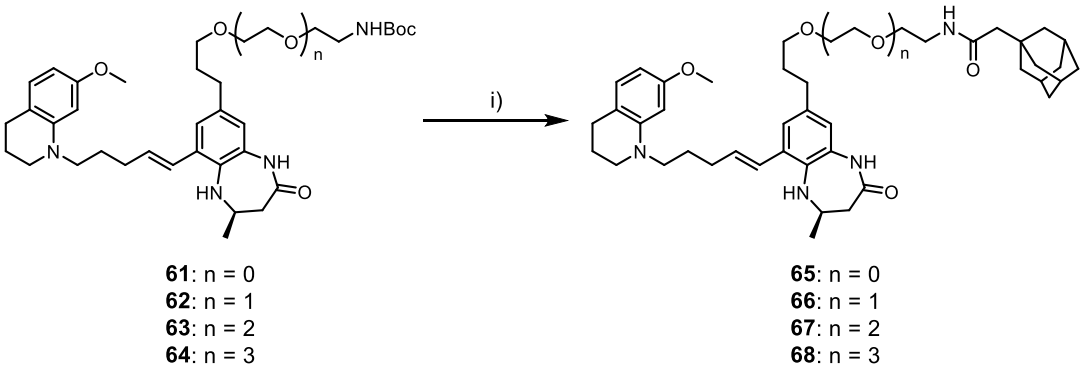

Scheme 10. Synthesis of hydrophobic tag-containing compounds **65** – **68**. *Reagents and conditions*: i) General procedure: step 1: 4 M HCl in 1,4-dioxane, CH_2Cl_2, 0 ºC – rt; step 2: 1-adamantaneacetic acid, HATU, DIPEA, DMF, 90 ºC; n = 0: step 1: 1 h; step 2: 3 h, 59% (two steps); n = 1: step 1: 2 h; step 2: 13 h, 74% (two steps); n = 2: step 1: 1.5 h; step 2: 3 h, 57% (two steps); n = 3: step 1: 2 h; step 2: 20 h, 22% (two steps).

*2.2.2.3 – Synthesis of VHL Targeting PROTACs **31** – **34***

The VHL-targeting PROTACs **31** – **34** were synthesised by Dr Pascal Heitel. Dr Heitel persevered in attempts to make PROTACs **31** – **34** directly from ligand **25** with little success. Attempts to activate ligand **25**, using mesylation or various halogenation reactions, then alkylation reactions with alcohols resulted in little to no yield of the desired product. Instead, **(*R*)-OXFBD05**-linker compounds **69** – **72** were synthesised using a similar synthetic route as was developed in *2.2.1.3*, but instead using carboxylic acid terminal linkers (Scheme 11). The VHL ligand was then introduced in the final step using amide coupling reactions to afford the final PROTACs (**31** – **34**) in yields of 39 – 70%.

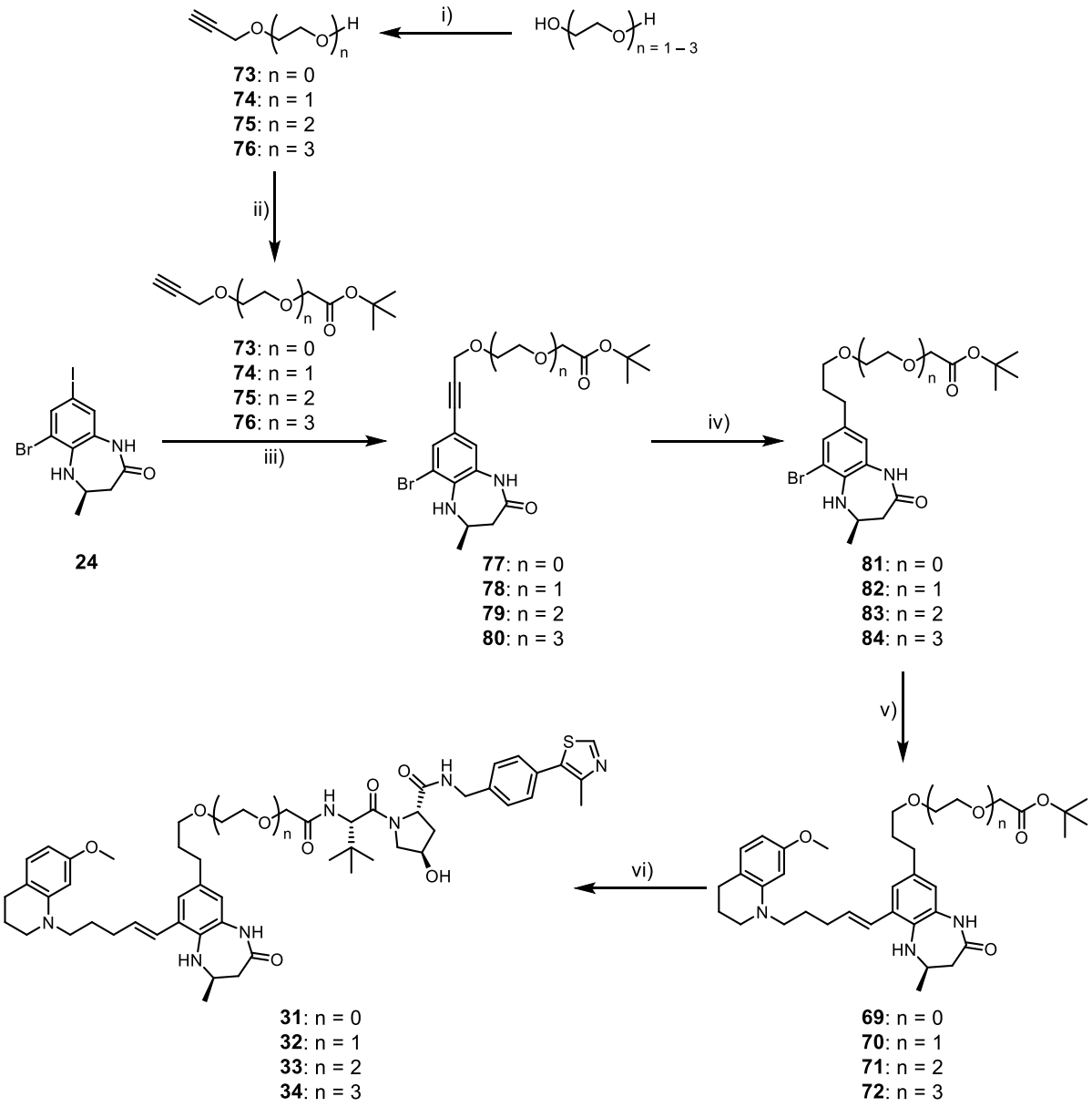

Scheme 11. Synthesis of VHL-targeting -PROTACs **31 – 34** conducted by Dr Pascal Heitel. *Reagents and conditions*: i) General procedure: propargyl bromide 80% *w/w* in toluene, sodium hydride 60% *w/w* in mineral oil, anhydrous THF, 0 ºC – 40 ºC; n = 1: 1 h, 58%; n = 2: 3 h, 88%; n = 3: 3 h, 76%; ii) n = 0: *tert*-butyl bromoacetate, sodium hydride 60% *w/w* in mineral oil, anhydrous THF, 0 ºC – 40 ºC, 1.5 h, 52%; General procedure: *tert*-butyl bromoacetate, TBAB, 37% *w/v* aq. NaOH, CH_2Cl_2, rt; n = 1: 48 h, 87%; n = 2: 22 h, 75%; n = 3: 16 h, 72%; iii) General procedure: $Pd(PPh_3)_2Cl_2$, CuI, anhydrous NEt_3, anhydrous THF; n = 0: 5 h, 85%; n = 1: 4 h, 86%; n = 2: 14 h, 75%, n = 3: 28 h, 69%; iv) General procedure: $Rh(PPh_3)_3Cl$, H_2, toluene, 60 °C; n = 0: 15 h, 72%; n = 1: 14 h, 68%; n = 2: 16 h, 58%; n = 3: 13 h, 73%; v) General procedure: $Pd(PPh_3)_2Cl_2$, K_2CO_3, 1,4-dioxane, H_2O, 80 °C; n = 0: 2 h, 92%; n = 1: 21 h, 50%; n = 2: 18 h, 46%; n = 3: 2 h, 65%; vi) General procedure: step 1: TFA, CH_2Cl_2, rt; step 2: (2*S*,4*R*)-1-[(2*S*)-2-amino-3,3-dimethylbutanoyl]-4-hydroxy-*N*-{[4-(4-methyl-1,3-thiazol-5-yl)phenyl]methyl}pyrrolidine-2-carboxamide, HATU, DIPEA, DMF, rt; n = 0: step 1: 3 h; step 2: 2 h, 47% (two steps); n = 1: step 1: 2 h; step 2: 18 h, 70% (two steps); n = 2: step 1: 3 h; step 2: 18 h, 54% (two steps); n = 3: step 1: 2 h; step 2: 18 h, 39% (two steps).

2.3 – Assessment of the Abilities of the **(*R*)-OXFBD05**-Based PROTACs **31** – **38** to Induce the Degradation of CREBBP and p300

2.3.1 – Western Blot Assay and Antibody Validation using siRNA-Mediated Knockdown

2.3.1.1 – siRNA-Mediated CREBBP and p300 Knockdown Assay Setup

A western blotting protocol for measuring the relative cellular levels of CREBBP and p300 was optimised by Dr Pascal Heitel. As CREBBP and p300 are closely related paralogues, they share similar molecular weights (CREBBP MW: 265.44 kDa, p300 MW: 264.25)[46,51,149], and their protein bands appear at equivalent positions on western blots. Therefore, it was important to ensure that the primary antibodies used were specific to each protein over the other to avoid cross-interference. This was achieved by performing siRNA-mediated knockdown of each protein in HeLa cells and then assessing the relative protein levels using the western blotting protocol.

Each siRNA reagent comprises a pool of four individual siRNAs that target different positions of the target mRNA sequence. This acts to lower the effective concentration of each siRNA sequence to decrease the probability of off-target effects.[150] Additionally, each siRNA sequence is chemically modified to enhance the specificity of the siRNA sense strand and to prevent undesired interactions between the siRNA sense strand and RISC.[151–153] A pool of four siRNAs targeting non-human, firefly luciferase mRNA was used as a negative control in these assays. Firefly luciferase mRNA is commonly targeted as a negative control in literature siRNA knockdown experiments because it is not natively expressed in human cells.[154–156]

Cells were treated with either the transfection reagent as a control, CREBBP-targeting siRNAs, p300-targeting siRNAs, a 1:1 mixture of CREBBP-targeting and p300-targeting siRNAs, or non-targeting siRNAs over a period of 24 h, 48 h, and 72 h. Individual western blots were performed to measure the relative levels of each paralogue (Figure 16 and Figure 17) using the same prepared sample of denatured cell lysate. This eliminated the need for a membrane stripping protocol, which can interfere with accurate protein quantification due to incomplete or over stripping of the membrane.[157] Each experiment was performed as three biological repeats, western blot band intensities analysed using Image Lab (Bio-Rad) software, and the data were quantified using Excel where CREBBP/p300 bands

were normalised against the corresponding β-actin loading control then relative to the vehicle (lipofectamine) treated cells (Appendix Table 2, Appendix Table 3).

2.3.1.2 – siRNA-Mediated Knockdown Effect on CREBBP Cellular Levels

Each siRNA-mediated knockdown *in vitro* assay was measured for relative CREBBP levels as described above (Figure 16, quantification calculations available in Appendix Table 2, western blots of the three biological repeats shown in Appendix Figure 8). Treatment with the CREBBP-targeting siRNAs caused a reduction of CREBBP levels by around 80% for all time points. The remaining 20% detected protein could be explained by either incomplete knock down of the target-protein by the siRNAs, or that the CREBBP-targeting primary antibody in the western blot assay is non-specifically binding p300, whose levels should not have been knocked down in this case. Slightly higher levels of CREBBP, approximately 25%, were detected in cells treated with the 1:1 mixture of CREBBP-targeting and p300-targeting siRNAs for all time points. This indicates that the remaining CREBBP expression is a result on incomplete protein knockdown and not due to non-specific primary antibody binding. A reduction in CREBBP levels to 50% was observed for the non-targeting siRNA control when tested at 24 h which could represent non-specific siRNA effects because they should not impact CREBBP transcription.[158] The CREBBP levels then recover for non-targeting siRNA treated cells following 48 h and 72 h incubation times. Therefore, the relative CREBBP levels at these timepoints are likely to be on-target effects.

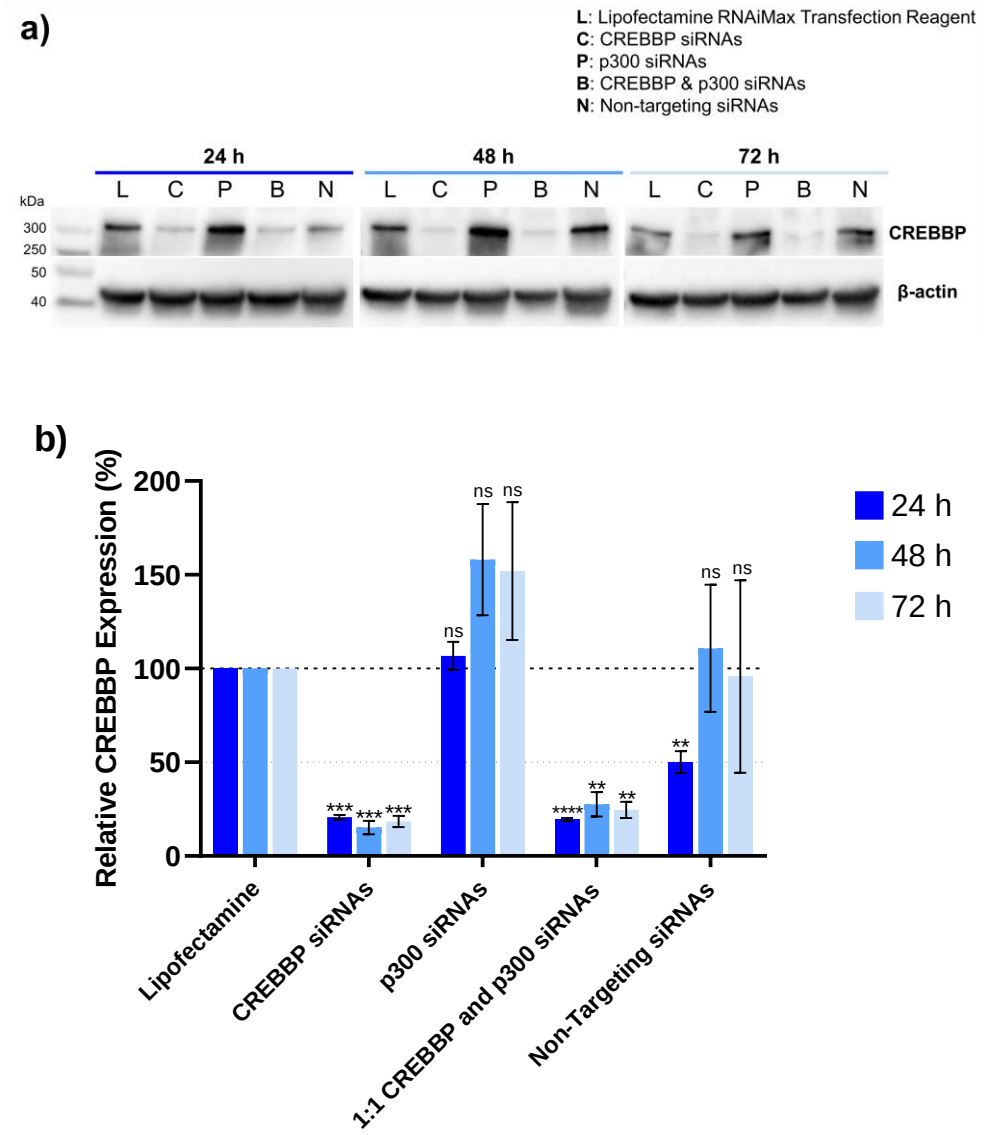

Figure 16. Quantification of relative cellular CREBBP levels following siRNA-mediated knockdown of CREBBP, p300, both CREBBP and p300, or non-targeting siRNA in HeLa cells for 24 h, 48 h, or 72 h, as indicated. Three biological repeats were performed. **a)** Representative western blot of cells treated with Lipofectamine RNAiMax Transfection Reagent and no siRNA (L), CREBBP-targeting siRNAs (C), p300-targeting siRNAs (P), 1:1 mixture of CREBBP and p300-targeting siRNAs (B), or non-targeting siRNAs (N) after 24 h (dark blue), 48 h (blue), or 72 h (light blue). CREBBP and p300 levels were assessed on separate blots from the same denatured protein sample instead of by stripping membranes and incubating with new antibodies. **b)** Relative protein expressions of CREBBP from Western Blot analysis. For each sample, the CREBBP band was normalised against the corresponding β-actin loading control and then relative to the β-actin-standardised lipofectamine control sample (Appendix Table 2). Average normalised CREBBP levels in the lipofectamine-treated cells were set to 100%. Western Blots were analysted using Image Lab (Bio-Rad) Software and the data was quantified using Excel. Data are reported as the mean relative expression over the three biological repeats and error bars are the standard error of the mean. A Student's t-test was performed for each sample relative to the lipofectamine control data for the corresponding timepoint. Significance is denoted as: **** - $p \leq 0.0001$, *** - $p \leq 0.001$, ** - $p \leq 0.01$, * - $p \leq 0.05$, ns - not statistically significant. 100% relative protein level indicated by dashed line, 50% relative protein level indicated by dotted line.

2.3.1.3 – siRNA-Mediated Knockdown Effect on p300 Cellular Levels

Each siRNA-mediated knockdown *in vitro* assay was measured for relative p300 levels as described above (Figure 17, quantification calculations available in Appendix Table 3, western blots of the three biological repeats shown in Appendix Figure 9). Treatment with the p300-targeting siRNAs caused a

reduction of p300 levels by >90% for all time points. Due to the low levels of p300 detected, it can be inferred that the p300-targeting primary antibody is selective for p300 over CREBBP. Incubation with the non-targeting siRNAs does not significantly affect relative p300 levels for any time point; indicating that siRNA-mediated p300 knockdown is an on-target effect.

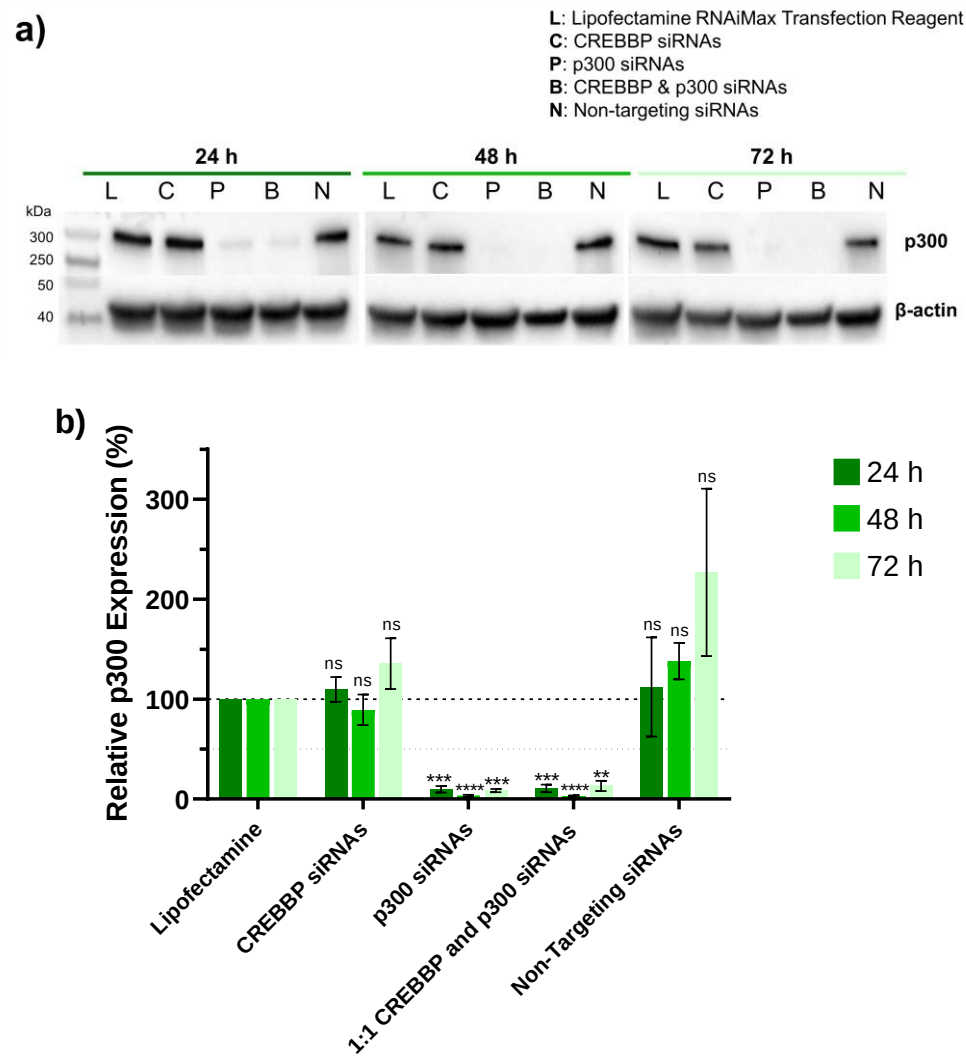

Figure 17. Quantification of relative cellular p300 levels following siRNA-mediated knockdown of CREBBP, p300, both CREBBP and p300, or non-targeting siRNA in HeLa cells for 24 h, 48 h, or 72 h, as indicated. Three biological repeats were performed. **a)** Representative western blot of cells treated with Lipofectamine RNAiMax Transfection Reagent and no siRNA (L), CREBBP-targeting siRNAs (C), p300-targeting siRNAs (P), 1:1 mixture of CREBBP and p300-targeting siRNAs (B), or non-targeting siRNAs (N) after 24 h (dark green), 48 h (green), or 72 h (light green). CREBBP and p300 levels were assessed on separate blots from the same denatured protein sample instead of by stripping membranes and incubating with new antibodies. **b)** Relative protein expressions of p300 from Western Blot analysis. Protein expression was quantified against the β-actin loading control and then relative to the β-actin-standardised lipofectamine control sample (Appendix Table 3). Average normalised p300 levels in the lipofectamine-treated cells were set to 100%. Western Blots were analysted using Image Lab (Bio-Rad) Software and the data was quantified using Excel. Data are reported as the mean relative expression over the three biological repeats and error bars are the standard error of the mean. A student's t-test was performed for each sample relative to the lipofectamine control data for the corresponding timepoint. Significance is denoted as: **** - $p \leq 0.0001$, *** - $p \leq 0.001$, ** - $p \leq 0.01$, * - $p \leq 0.05$, ns - not statistically significant. 100% relative protein level indicated by dashed line, 50% relative protein level indicated by dotted line.

2.3.1.4 – siRNA-Mediated CREBBP and p300 Knockdown Conclusions

The siRNA-mediated knockdown study confirmed the selectivity of the CREBBP and p300 primary antibodies to bind their target protein over the other paralogue. Comparable results were obtained for the siRNA-mediated knockdown of CREBBP and/or p300 in HEK293T cells (Appendix Figure 10, Appendix Table 5) which were performed in collaboration with Dr Pascal Heitel and investigated the 24 h timepoint without a non-targeting siRNA control. These assays have demonstrated that the western blotting conditions are suitable for measuring the relative protein levels of CREBBP and p300 and to determine whether there is preferential degradation of either paralogue over the other. Therefore, these conditions will be used to investigate the abilities of PROTACs **31** – **38** and HyTs **65** – **68** to degrade CREBBP and/or p300.

2.3.2 – Measuring the Abilities of PROTACs **31** – **38** and HyTs **65** – **68** to Induce the Degradation of CREBBP and/or p300

*2.3.2.1 – In Vitro Testing of VHL-Targeting PROTACs **31** – **34** and Cereblon-Targeting PROTACs **35** – **38***

In this section, HEK293T cells were selected for use in the *in vitro* experiments because of their rapid growth and high expression of proteins.[159] In later studies the cell line was changed to HeLa cells because they are expected to express CREBBP and p300 more equally than HEK293T cells (HeLa: CREBBP = 22.7, p300 = 22.8; HEK293T: CREBBP = 18.5, p300 = 32.2; values are the normalized transcript per million) which should eliminate the potential bias of degrading the more abundant paralogue over the other.[160,161]

In collaboration with Dr Pascal Heitel, the abilities of the VHL-targeting PROTACs **31** – **34** and the cereblon-targeting PROTACs **35** – **38** to degrade CREBBP and/or p300 in HEK293T cells at 10 μM concentration following 24 h incubation was assessed using western blotting and the relative protein levels were quantified (Figure 18, quantification calculations available in Appendix Table 6 and Appendix Table 7, western blots of the three biological repeats shown in Appendix Figure 11).

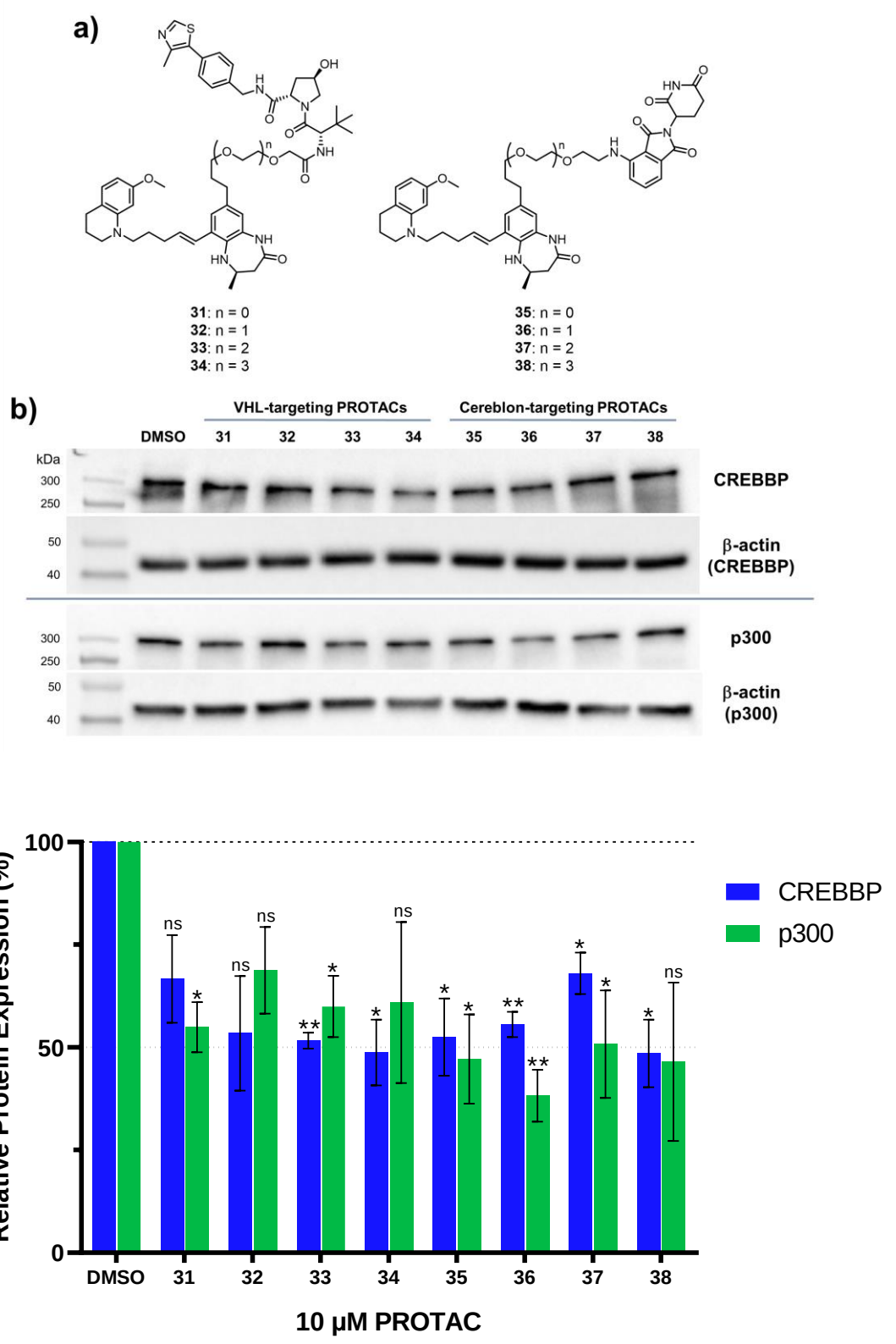

Figure 18. *In vitro* analysis of VHL-targeting PROTACs **31** – **34** (synthesised by Dr Pascal Heitel) and cereblon-targeting PROTACs **35** – **38**. *In vitro* assays and western blots were performed in collaboration with Dr Pascal Heitel as three biological repeats. **a)** Structures of VHL-targeting PROTACs **31** – **34** and cereblon-targeting PROTACs **35** – **38**. **b)** Representative western blots of CREBBP, p300 and their corresponding β-actin loading control levels in HEK293T cells treated with 10 μM PROTACs **31** – **38** or the vehicle (DMSO) control for 24 h. **c)** Relative protein levels of CREBBP and p300 from Western Blot analysis. Protein levels was quantified against the β-actin loading control and then relative to the β-actin-standardised DMSO control sample (Appendix Table 6, Appendix Table 7). Western blots were analysted using Image Lab and the data were quantified using Excel. Data are reported as the mean value of the three biological repeats and

error bars are the standard error of the mean. A Student's t-test was performed relative to the DMSO control data and significance is denoted as: ** – $p \leq 0.01$, * – $p \leq 0.05$, ns – not statistically significant.

Reductions in the relative cellular levels of CREBBP and p300 were observed for both VHL and cereblon-targeting PROTACs with many PROTACs reducing protein levels to around 50% relative to the DMSO control, which was set to 100% relative protein expression. For the statistically significant VHL-targeting PROTAC results, PROTACs **33** and **34** resulted in the reduction of CREBBP levels to 52% and 49%, respectively, while PROTACs **31** and **33** resulted in the reduction of p300 levels to 55% and 60%, respectively. All cereblon-targeting PROTACs led to the significant reduction in CREBBP levels in the range of 49 – 68%, while PROTACs **35** – **37** caused significant reduction in p300 levels in the range of 38 – 51%. There does not appear to be any preferential degradation of CREBBP over p300 or *vice versa* at this stage, and no optimal linker length could be identified to guide future PROTAC optimisation.

It should also be noted that the VHL-targeting PROTACs **31** – **34** caused phenotypic changes in the appearance of the HEK293T cells after the 24 h incubation, whereas cereblon-targeting PROTACs **35** – **38** did not (Figure 19). Such morphological changes were not observed in the siRNA-mediated CREBBP and/or p300 knockdown studies suggesting that PROTACs **31** – **34** are causing off-target cytotoxicity.

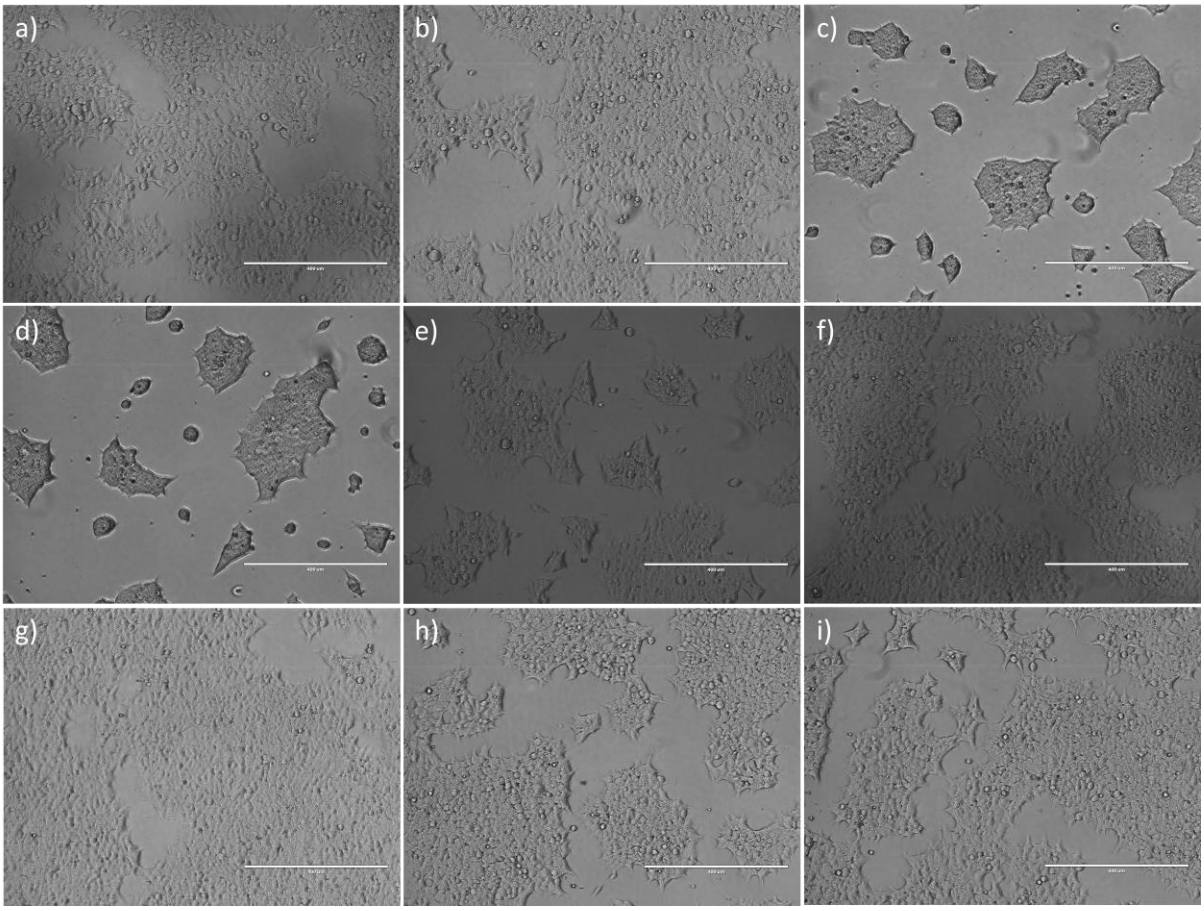

Figure 19. Images of HEK293T cells after 24 h treatment with the indicated PROTAC. Images depict changes in cell appearance following compound treatment and potential off-target cytotoxicity. **a)** 1% *v/v* DMSO. **b)** 10 μM **31** with 1% *v/v* DMSO. **c)** 10 μM **32** with 1% *v/v* DMSO. **d)** 10 μM **33** with 1% *v/v* DMSO. **e)** 10 μM **34** with 1% *v/v* DMSO. **f)** 10 μM **35** with 1% *v/v* DMSO. **g)** 10 μM **36** with 1% *v/v* DMSO. **h)** 10 μM **37** with 1% *v/v* DMSO. **i)** 10 μM **38** with 1% *v/v* DMSO. White bar represent 400 μm scale.

*2.3.2.2 – In Vitro Testing of **(R)-OXFBD05**-Based HyTs*

The ability of HyTs **65** – **68** to degrade CREBBP and p300 was investigated using the same conditions as for PROTACs **31** – **38**. HEK293T cells were incubated with HyTs **65** – **68** at 10 μM concentration for 24 h, and their ability to induce the degradation of CREBBP and/or p300 was assessed using western blotting (Figure 20). *In vitro* assays and western blots were performed by Dr Pascal Heitel as three biological repeats (Appendix Figure 11) and each sample was quantified relative to its β-actin loading control then relative to the β-actin-standardised DMSO control, and a mean value was calculated as the relative protein level (Figure 20c, Appendix Table 8, Appendix Table 9).

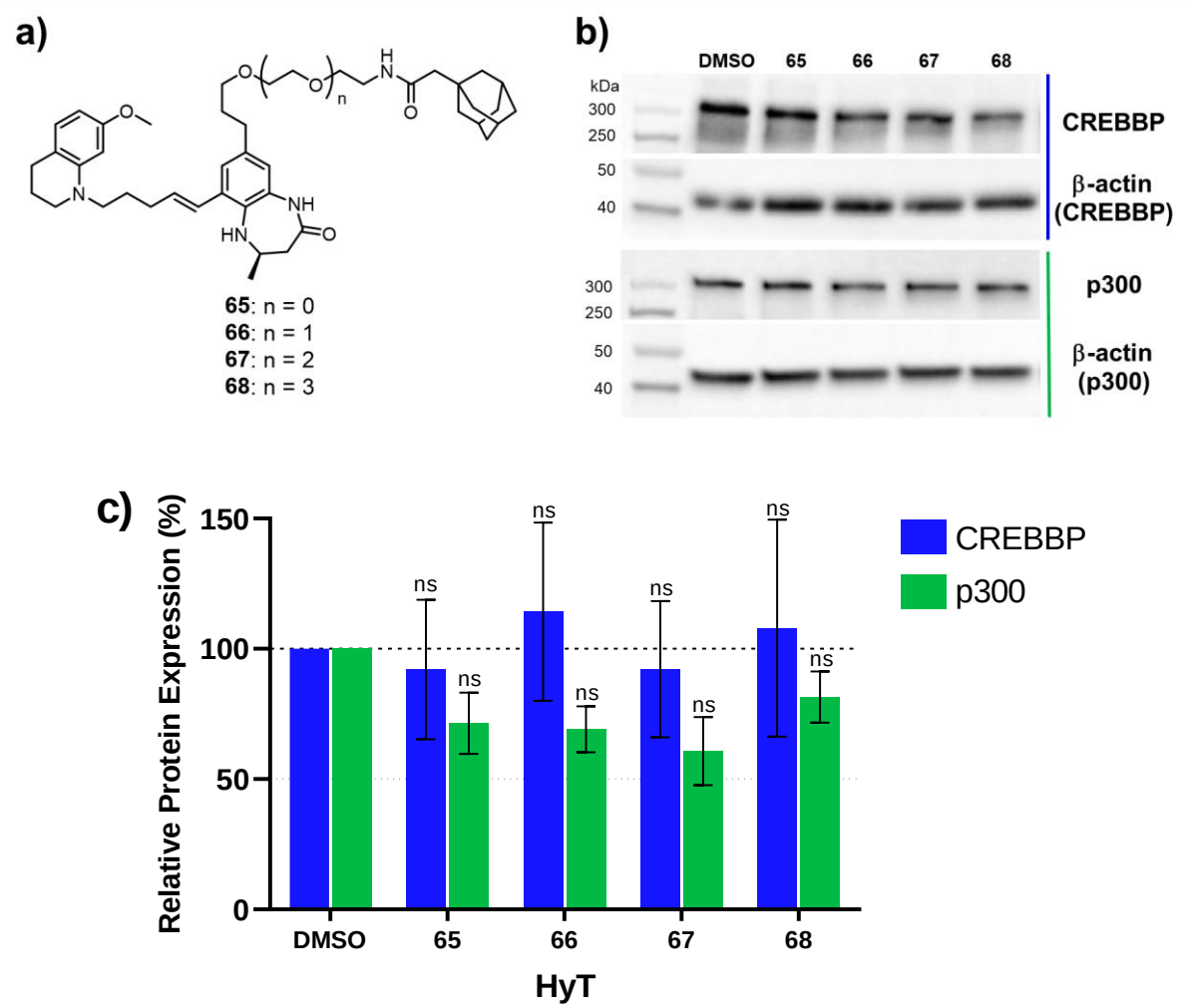

Figure 20. *In vitro* investigation into the ability of HyTs **65 – 68** to degrade CREBBP and p300. HEK293T cells were treated with 10 μM **65 – 68** over 24 h. *In vitro* assays and Western Blots were performed by Dr Pascal Heitel as three biological repeats. **a)** Structures of HyTs **65 – 68**. **b)** Representative western blots showing CREBBP, p300, and their corresponding β-actin protein bands for HEK293T cells treated with 10 μM **65 – 68** over 24 h. **c) d)** Relative protein levels of CREBBP and p300 from Western Blot analysis. Protein levels were quantified against the β-actin loading control and then relative to the β-actin-standardised DMSO control samples. Western blots were analysed using Image Lab and the data were quantified using Excel (Appendix Table 8, Appendix Table 9). Data are reported as the mean relative level over the three biological repeats and error bars are the standard error of the mean. A student's t-test was performed relative to the DMSO control data. No compound caused a significant change in CREBBP and p300 levels under the tested conditions. Significance is denoted as: ns – not statistically significant.

Under the tested conditions, no HyT (**65 – 68**) caused a significant reduction in the relative cellular levels of CREBBP or p300. Similar to the changes in cell morphologies observed following treatment with VHL-targeting PROTACs **31** – **34** in Section 2.3.2.1, incubation with HyTs **65 – 68** resulted in the formation of small clusters of cells with many detached into the media, indicating compound off-target cytotoxicity (Figure 21).

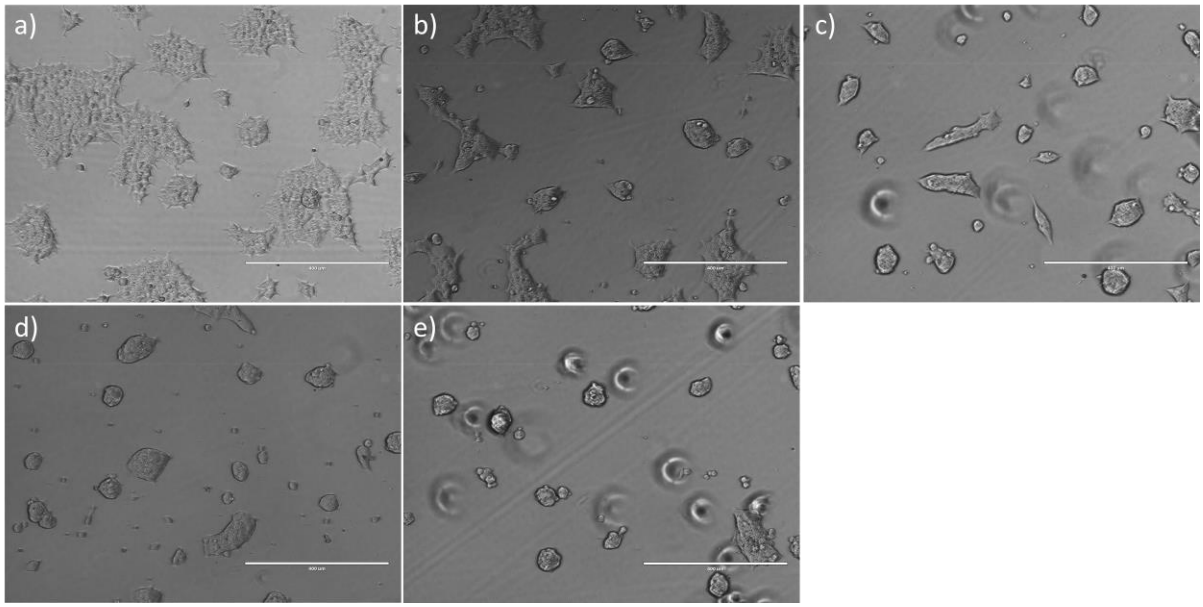

Figure 21. Images of HEK293T cells after 24 h treatment with the indicated HyT compound. Images depict changes in cell appearance following compound treatment and potential off-target cytotoxicity. **a)** 1% *v/v* DMSO. **b)** 10 μM **65** with 1% *v/v* DMSO. **c)** 10 μM **66** with 1% *v/v* DMSO. **d)** 10 μM **67** with 1% *v/v* DMSO. **e)** 10 μM **68** with 1% *v/v* DMSO. White bar represents 400 μm scale.

2.4 – The Rational Design of PROTACs and HyTs Using the CREBBP and p300 Bromodomain Ligand **(*R*)-OXFBD05** Conclusions

The work described in this chapter focused on the rational design of PROTACs and HyTs targeting the paralogues CREBBP and/or p300 for proteasomal degradation. Bifunctional molecules were designed using the CREBBP and p300 bromodomain ligand **(*R*)-OXFBD05**, which was developed in the Conway group.[43] An X-ray crystal structure was used to guide linker attachment to **(*R*)-OXFBD05** by identifying solvent exposed regions.[43] The position and functionality of linker attachment was then investigated through the synthesis of a small library of compounds, and ITC was used to assess the effect on bromodomain binding affinities. It was discovered that the attachment of a flexible propanol chain to the DHBD group of **(*R*)-OXFBD05** in compound **25** resulted in comparable CREBBP bromodomain binding affinity to the parent ligand, and therefore, the addition of flexible PEG linkers to this position appeared promising for PROTAC development.

As discussed in Chapter 1, PROTAC linkers play a key role in establishing a POI:PROTAC:E3 ligase ternary complex and the subsequent ability of the PROTAC to degrade the POI.[11,22,23,26,27] In this initial series of PROTACs and HyTs, PEG linkers of four lengths were investigated with the aim of finding an optimal linker length that could help guide future structure optimisation. Additionally, Chapter 1 discusses how the PROTAC E3 ligase ligand can affect ternary complex formation and PROTAC selectivity.[8,11,22,23] Therefore, the recruitment of two different E3 ligase enzymes, VHL and cereblon, was investigated using the ligands **VH032** and **pomalidomide** to afford PROTACs **31** – **38**.[8–10] A series of HyTs **65** – **68** was also synthesised by the addition of a lipophilic adamantane group as the E3 ligase ligand.[6,147,148]

All bifunctional compounds (**31** – **38** and **65** – **68**) were tested at 10 μM in HEK293T cells for 24 h and the resultant cellular levels of CREBBP and p300 were assessed by western blotting. None of the HyTs **65** – **68** induced the degradation of CREBBP or p300, while compounds from both the VHL- and cereblon-targeting series of PROTACs caused reductions in relative CREBBP and p300 levels. However, greater potency is desired and no optimal PEG linker length nor E3 ligase ligand for inducing CREBBP/p300 degradation was identified to help guide future compound optimisation. Additionally,

the VHL-targeting PROTACs **31** – **34** and the HyTs **65** – **68** appeared to cause off-target cytotoxic effects in the cells. A study by Nadanaciva, *et al.* showed that for a collection of lipophilic drug compounds, off-target cytotoxic effects could be attributed to compound recruitment to lysosomes causing lysosomal dysregulation and subsequent cell death.[162] This could provide one hypothesis for why incubation with PROTACs **31** – **35** and HyTs **65** – **68** appears to be causing cytotoxic effects. Evaluation of the $clogD_{pH7.4}$ values of the PROTACs **31** – **38** and HyTs **65** – **68** (Table 4) indicates that all compounds have a high lipophilicity and poor aqueous (pH 7.4) solubility and the compounds with the poorest predicted solubility tend to correlate with the greater observed changes in cell morphology. As, under the tested conditions, HyTs **65 – 68** did not cause any significant degradation of CREBBP or p300 and have a high inherent lipophilicity, it was decided to not develop these compounds further.

The synthetic strategy of adding PEG linkers to **(*R*)-OXFBD05** meant that compound derivatisation occurred early in the route and each final compound required multiple steps from a common intermediate. Therefore, the next series of PROTACs will aim to improve the throughput of obtaining final PROTAC molecules as well as enhancing compound hydrophilicity.

Table 4. Calculated $logD_{pH7.4}$, and Property Forecast Index (PFI) values of PROTACs **31** – **38** and HyTs **65** – **68**. Compound **25** has comparable binding affinity, $clogD_{pH7.4}$, and PFI values as the parent ligand **(*R*)-OXFBD05**, however, as the alkyl linker length increases in compounds **2** and **26**, the binding affinity for the CREBBP bromodomain decreases. This trend appears to correlate with the increasing lipophilicities of the compounds, where predicted aqueous solubility (pH 7.4) decreases with increasing alkyl linker length. Analogues **2** – **8** do not appear to follow a similar trend. Binding affinity K_d values were obtained using ITC. Darker green indicates higher binidng affinity of the compound to the CREBBP bromodomain, n.b. = no detectable binding. $clogD_{pH7.4}$ values were calculated using Chemicalize (http://www.chemicalize.com) and are coloured according to compound aqueous solubility observations by Hill and Young, where $x < 2$ predicts good solubility (green), $2 < \boldsymbol{x} \leq 4$ predicts moderate solubility (yellow), and $\boldsymbol{x} > 4$ predicts poor solubility (red).[20] The Property Forecast Index (PFI) is a measurement developed by GSK for predicting aqueous solubility (PFI = $clogD_{pH7.4}$ + #Ar rings).[21] PFI values are coloured according to compound aqueous solubility observations by Tinworth and Young, where $4 < \boldsymbol{x} \leq 8$ predicts moderate solubility (yellow), and $\boldsymbol{x} > 8$ predicts poor solubility (red), darker colour indicates higher value within category.[21]

Cpd.	Structure	$clogD_{pH7.4}$	PFI	Cpd.	Structure	$clogD_{pH7.4}$	PFI
31	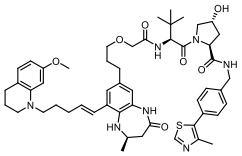	5.52	9.52	**37**	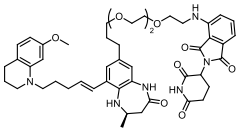	5.02	8.02
32	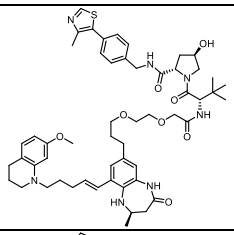	5.47	9.47	**38**	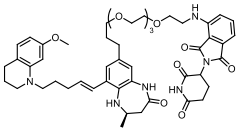	4.97	7.97
33	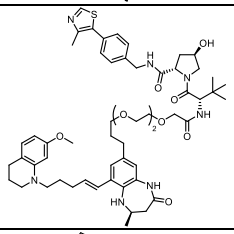	5.42	9.42	**65**	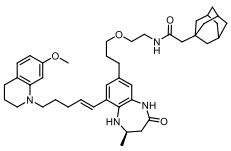	6.70	8.70
34	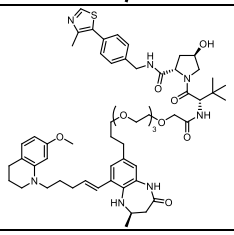	5.38	9.38	**66**	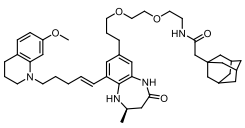	6.66	8.66
35	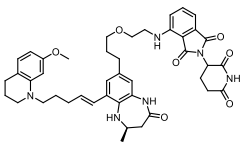	5.11	8.11	**67**	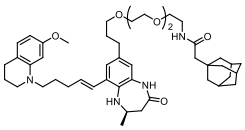	6.61	8.61
36	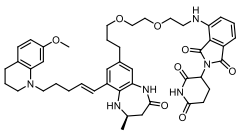	5.07	8.07	**68**	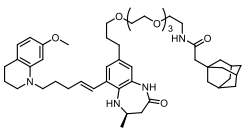	6.56	8.56

Chapter 3 – Higher Throughput Synthesis of PROTACs Using CREBBP and p300 Bromodomain Ligands

3.1 – Design of Novel Amine Terminal CREBBP and p300 Ligands to Facilitate Higher Throughput PROTAC Synthesis

3.1.1 – Modification of CREBBP and p300 Bromodomain Ligand **(*R*)-OXFBD05** with a Piperidine Ring for PROTAC Synthesis

In Chapter 2, development of **(*R*)-OXFBD05**-based PROTACs was impaired by a multistep, linear synthesis and, consequently, a higher throughput route to obtaining final PROTAC molecules was sought. One way to achieve this, is to functionalise the CREBBP and p300 ligand with an amine group to allow derivatisation into the final PROTACs in a final, amide coupling reaction step.

As introduced in Chapter 1, bromodomain inhibitor **GNE-781** was utilised as the POI ligand in the CREBBP and p300 degrading PROTAC, **dCBP-1** (Figure 22).[132,133] To enable linker attachment, the tetrahydropyran (THP) group of **GNE-781** was converted to a piperidine, which allowed the PEG linker to be attached by an amide bond.

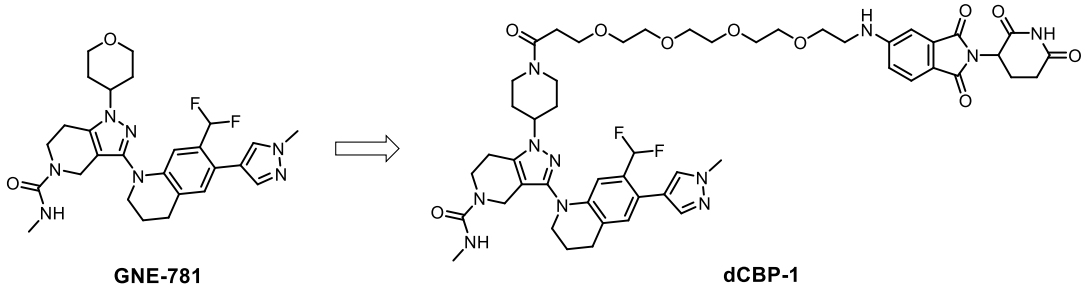

Figure 22. Structures of the CREBBP and p300 bromodomain inhibitor **GNE-781** and the CREBBP and p300 degrading PROTAC **dCBP-1**.[132,133]

An X-ray crystal structure of **GNE-781** bound to the bromodomain of CREBBP (PDB: 5W0E, Figure 23b)[132] shows the tetrahydropyrazolopyridine group occupying the deep KAc binding pocket. The urea moiety acts as a KAc mimic, forming H-bonds with residues N1168 and P1110, as well as a water-mediated H-bond with residue Y1125. The THQ-imidazole portion of the molecule binds an induced-fit pocket on the protein surface, where residue R1173 forms H-bonds with the difluoro methyl

group on the THQ. The THP group is directed out of the KAc binding site, becoming solvent exposed, and this is where the linker attaches to the ligand in **dCBP-1** (Figure 23b and d).[132]

Overlaying the X-ray structures of **GNE-781** (PDB: 5W0E)[132] and **(*R*)-OXFBD05** analogue **1** (PDB: 6YIM)[43] bound to the bromodomain of CREBBP shows high structural overlap of the ligand-bromodomain complexes where both ligands occupy similar space in the KAc binding site and an induced-fit pocket (Figure 23c–d).[43,132] Examination of the overlayed compounds indicates that compound **1**, and therefore its analogue **(*R*)-OXFBD05**, would accommodate addition of a 6-membered ring to the DHBD-group.

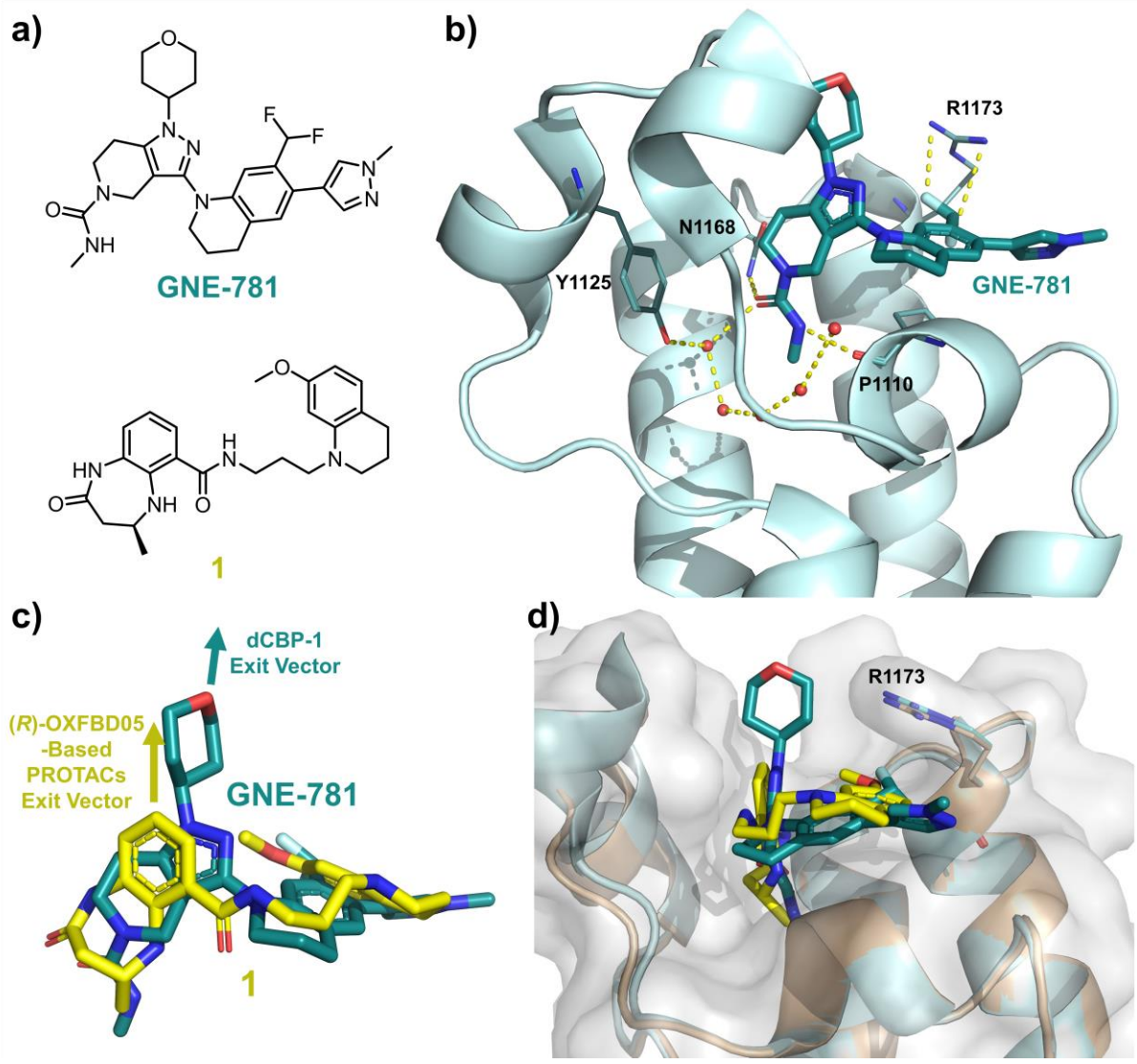

Figure 23. Examination of the X-ray crystal structures of bromodomain inhibitors **GNE-781** and **2** bound to the CREBBP bromodomain to inform modification of **(*R*)-OXFBD05** for PROTAC synthesis.[43,132] X-ray crystal structure images created using PyMOL. **a)** Chemical structures of CREBBP and p300 bromodomain inhibitors **GNE-781** and **(*R*)-OXFBD05** analogue **1**. **b)** X-Ray crystal structure of **GNE-781** (teal) bound to the CREBBP bromodomain (light cyan) (PBD: 5W0E).[132] Binding site protein residues are shown as wire lines, water

molecules are shown as red spheres, interactions are shown as yellow dotted lines. The urea moiety of the tetrahydro-pyrazolopyridine group acts as the KAc mimic and forms H-bonds with residues N1168 and P1110 and a water-mediate H-bond with residue Y1125. The THQ-imidazole portion of the molecule binds an induced fit pocket which is formed through H-bond interactions between residue R1173 and the difluoro methyl group on the THQ. The THP group points out that protein binding site becoming solvent exposed. **c)** Overlayed X-ray crystal structures of **GNE-781** (pink, PBD:5W0E)[132] and **(*R*)-OXFBD05** bioisostere **1** (yellow, PBD:6YIM)[43] bound to the CREBBP bromodomain (protein not shown for clarity) displaying high overlap of the protein-bound ligand structures. The exit vector of the linker from **GNE-781** in PROTAC **dCBP-1** is shown by a teal arrow, the exit vector used by the **(*R*)-OXFBD05**-based PROTACs **31 – 38** (described in Chapter 2) is shown by a yellow arrow. **d)** Overlayed X-ray crystal structures of the ligand-CREBBP bromodomain complexes of **GNE-781** (compound: teal, protein: light cyan, PBD: 5W0E)[132] and **1** (compound: yellow, protein: beige, PBD: 6YIM)[43]. Only the protein surface (transparent grey) of the **GNE-781**-bromodomain complex is displayed for clarity. Overlaying the complexes shows high structural overlap between both the compounds and the bromodomains. The structures indicate that a 6-membered ring could be added to the aromatic moiety of the DHBD group of ligand **1** and by extension **(*R*)-OXFBD05** to enable PROTAC synthesis.

Modification of **(*R*)-OXFBD05** with a piperidine ring to afford ligand **86** would enable PROTACs to be synthesised by amide couplings, similar to the synthesis of **dCBP-1** (Figure 24a). This would not only enhance synthetic throughput but would also help improve PROTAC properties. As discussed in Section 1.1.5, the potency of a PROTAC to degrade its POI can be enhanced through rigidification of the linker region due to the lower entropic loss of ternary complex formation.[26,27] Additionally, the optimisation of IRAK4-degrading PROTAC **dIRAK-1** to **dIRAK-2** demonstrated that modification of the linker region not only enhanced IRAK4 degradation by increased linker rigidity but also decreased the $clogD_{pH7.4}$ value from 6.44 to 4.97.[27] Using PROTAC **36** as a representative example, modification of the PEG linker to incorporate a piperidine group, while keeping a consistent distance between the two ligands, reduces the $clogD_{pH7.4}$ value from 5.07 to 3.44 which is a more preferable value for obtaining aqueous (pH 7.4) solubility (Figure 24b).

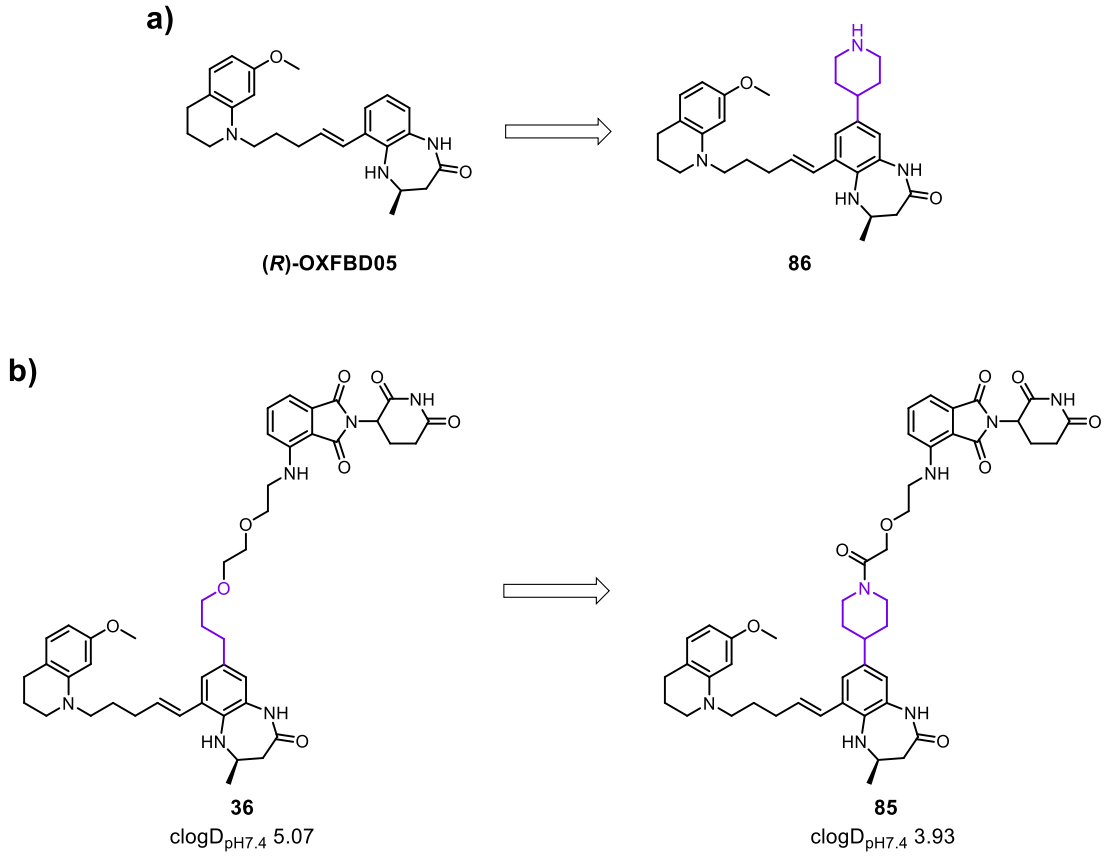

Figure 24. a) Modification of CREBBP and p300 bromodomain ligand **(*R*)-OXFBD05** with a piperidine ring to afford ligand **86**. This compound would allow PROTAC molecules to be synthesised in one, final amide coupling reaction. Piperazine ring modification highlighted in purple. **b)** Modification of PROTAC **36** with a piperidine ring (highlighted in purple) acts to enhancing linker rigidity and also decreases compound lipophilicity cauing a decrease in the $clogD_{pH7.4}$ value from 5.07 to 3.93. $clogD_{pH7.4}$ values calculated using Chemicalize (www.chemicalize.com).

3.1.2 – Modification of CREBBP and p300 Bromodomain Ligand **Inobrodib** with a Piperidine Ring for PROTAC Synthesis

Inobrodib is a high affinity inhibitor of the bromodomains of CREBBP and p300 with a high selectively against structurally similar BRD4 (SPR bromodomain binding affinities, CREBBP: K_d = 1.7 nM, p300: K_d = 1.3 nM, BRD4: K_d = 222 nM).[112] An X-ray crystal structure of **Inobrodib** bound to the CREBBP bromodomain was solved by Xu *et al*. (PDB: 7XH6) (Figure 25b).[163] The structure shows the dimethyl isoxazole moiety of **Inobrodib** bound to the KAc binding pocket of the bromodomain, forming an H-bond with residue N1168 and water-mediated H-bonds with residue Y1125. Additionally, the difluorophenyl group binds an induced-fit pocket by forming a cation-π interaction with residue R1173, which is further stabilised by an H-bond between residue R1173 and the piperidinone ring. **(*R*)-OXFBD05** analogue **1** forms a similar cation-π interaction with residue R1173, but overlaying the

ligand-bromodomain X-ray crystal structures shows that the induced-fit pockets to have different topologies (**1** PDB:6YIM) (Figure 25c).[43] The **Inobrodib**-bromodomain structure shows the cyclohexyl methoxy group to be solvent exposed and to project away from the bromodomain surface into a channel between the αA and αZ helices (the ZA channel) making this group promising for modification with a linker for PROTAC synthesis (Figure 25b, d–f). Overlaying the X-ray crystal structures of the **Inobrodib**-bromodomain and **1**-bromodomain complexes demonstrates that building off of the cyclohexyl methoxy group position of **Inobrodib** will access a different exit vector from the protein than the one addressed by the previous series of ***(R)*-OXFBD05**-based PROTACs (**31** – **38**) (Figure 25c–f).

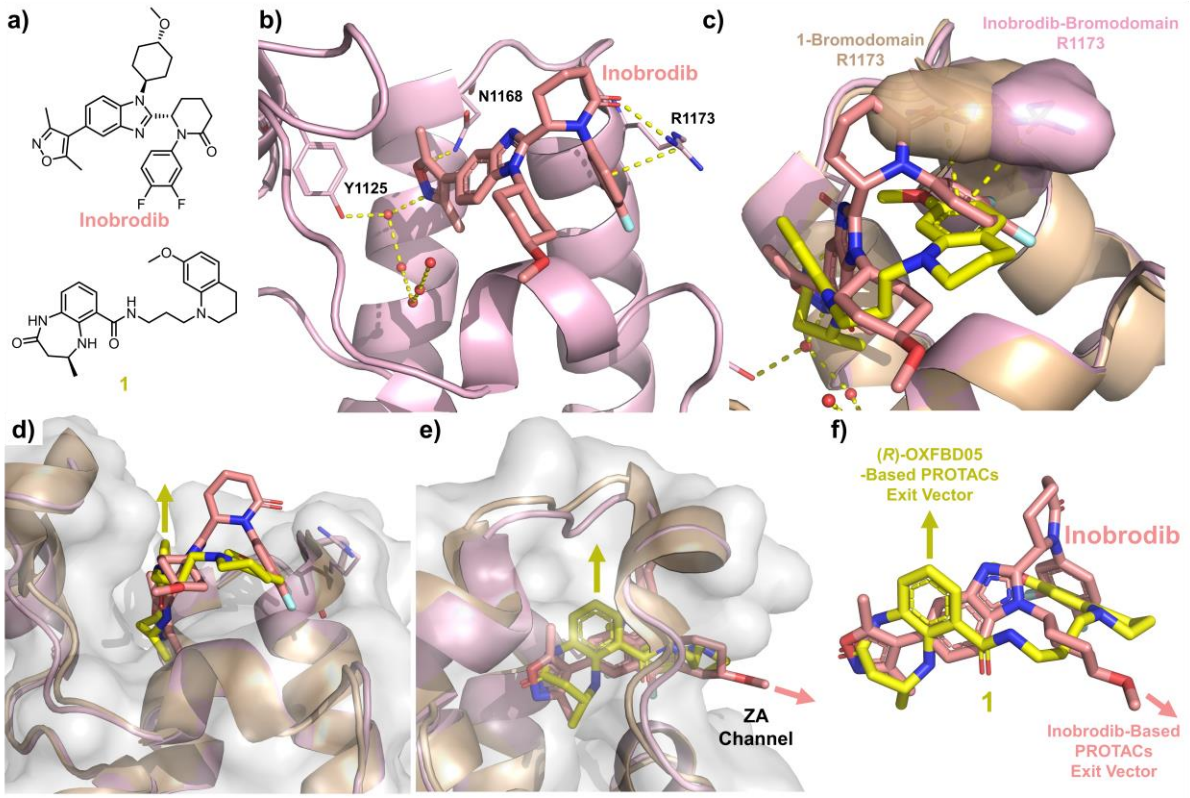

Figure 25. Ligand-bound X-ray crystal structures of **Inobrodib** and ***(R)*-OXFBD05** analogue **1** bound to the CREBBP bromodomain to guide modification of **Inobrodib** for PROTAC synthesis.[43,163] Key interacting protein residues depicted as wire lines, water molecules are depicted as spheres, and electrostatic interactions are depicted as yellow dashed lines. X-ray crystal structure images created using PyMOL. **a)** Compound structures of **Inobrodib** and ***(R)*-OXFBD05** analogue **1**.[43,112] **b)** X-Ray crystal structure of **Inobrodib** (pink) bound to the CREBBP bromodomain (light pink) (PDB: 7XH6).[163] Binding site protein residues are shown as lines, water molecules are shown as red dots, interactions are shown as yellow dotted lines. The isoxazole moiety binds the KAc pocket and forms an H-bond with residue N1168 and water mediated H-bonds with reside Y1125. An induced-fit pocket is created through residue R1173 forming a cation-π interaction with the difluoro phenyl group and an H-bond with the carbonyl of the piperidinone group. **c)** Overlay of the X-Ray crystal structures of the **Inobrodib**-bromodomain complex (compound: pink, protein: light pink, PDB: 7XH6)[163] and **1**-bromodomain complex (compound: yellow, protein: beige, PDB: 6YIM)[43] complexes showing different induced-fit pocket conformations. The surface of residue R1173 is shown in different positions depending upon which ligand had bound to the bromodomain (**Inobrodib**-bromodomain complex residue R1173 surface shown in transparent light pink, **1**-bromodomain complex residue R1173 surface shown in transparent beige). **d)** and **e)** Overlay of the X-Ray crystal structures of the **Inobrodib**-bromodomain complex (compound: pink, protein: light pink, PDB: 7XH6)[163] and **1**-bromodomain complex (compound: yellow, protein: beige, PDB: 6YIM)[43] showing the poor spatial overlap of the bound ligands and highlighting the different protein

exit vector that would be accessed by linker attachment from the cyclohexyl methoxy group position of **Inobrodib**. Exit vectors are shown as arrows from the linker attachment position of each ligand into the solvent (**(*R*)-OXFBD05**-based PROTACs exit vector: yellow, **Inobrodib**-based PROTACs exit vector: pink). For clarity, only the protein surface of the **Inobrodib**-bromodomain complex (transparent grey) is shown. **f)** Overlay of the X-Ray crystal structures of the bound **Inobrodib** and **(*R*)-OXFBD05** without the protein structure to show the different exit vectors of **(*R*)-OXFBD05**-based PROTACS and **Inobrodib**-based PROTACs. **Inobrodib**-bromodomain complex (compound: pink, PDB: 7XH6)[163] and **1**-bromodomain complex (compound: yellow, PDB: 6YIM)[43]. Exit vectors are shown as arrows from the linker attachment position of each ligand into the solvent (**(*R*)-OXFBD05**-based PROTACs exit vector: yellow, **Inobrodib**-based PROTACs exit vector: pink).

To modify **Inobrodib** to facilitate linker attachment by amide coupling reactions, it was proposed to convert the cyclohexyl methoxy group to a piperidine group to afford ligand **87** (Figure 26). The resultant PROTACs should access a different exit vector from the bromodomain than by **(*R*)-OXFBD05**-based PROTACs which could aid in the formation of stable POI:PROTAC:E3 ligase ternary complexes for inducing the degradation of CREBBP and/or p300.

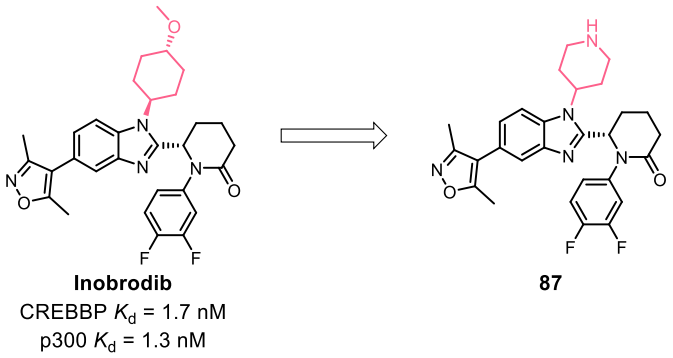

Figure 26. Proposed conversion of the cyclohexyl methoxy group in **Inobrodib** to a piperidine in ligand **87** to facilitate PROTAC synthesis by amide couplings with carboxylic acid terminal linkers.[112] Modification highlighted in pink.

3.1.3 – Modification of **Inobrodib** with an (*S*)-Methyl Ethyl Piperazine Group for PROTAC Synthesis

Inobrodib was developed from the CREBBP and p300 bromodomain inhibitor **SGC-CBP30** (Figure 27a).[164] The CREBBP and p300 bromodomain binding affinities of **Inobrodib** (CREBBP: K_d = 1.7 nM (SPR), p300: K_d = 1.3 nM (SPR)) were enhanced from those of **SGC-CBP30** (CREBBP: K_d = 21 nM (ITC)) by the rigidification of the compound and by the formation of additional stabilising interactions with the protein, for example an H-bond formed between the piperidinone ring of **Inobrodib** and CREBBP bromodomain residue R1173 (Figure 27b).[112,163,164]

Examining the overlayed X-ray crystal structures of **Inobrodib** (PDB: 7XH6)[163] and **SGC-CBP30** (PBD: 4NR7)[164] bound to the CREBBP bromodomain, reveals high spatial overlap between the two complexes, and shows the morpholine group of **SGC-CBP30** projecting further into the ZA channel than the cyclohexyl methoxy group of **Inobrodib** (Figure 27b–c).

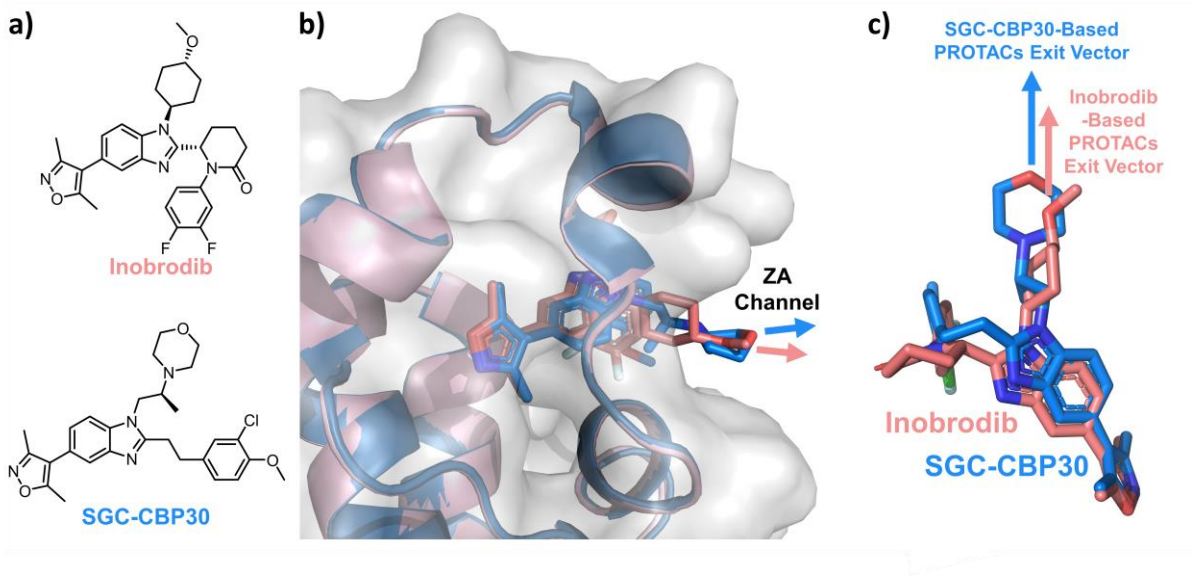

Figure 27. Overlayed X-ray crystal structures of **Inobrodib** and **SGC-CBP30** bound to the CREBBP or p300 bromodomain showing the morpholine ring of **SGC-CBP30** projecting further into the solvent region, away from the protein.[48,163] X-ray crystal structure images created using PyMOL. **a)** Compound structures of the CREBBP and p300 bromodomain inhibitors **Inobrodib** and **SGC-CBP30**.[112,164] **b)** Overlayed X-ray crystal structures of the ligand-bromodomain complexes of **Inobrodib** (compound: pink, protein: light pink, PDB: 7XH6)[163] and **SGC-CBP30** (compound: blue, protein: blue, PDB: 4NR7)[165] bound to the CREBBP bromodomain. For clarity, only the protein surface of the **Inobrodib**-bromodomain complex is displayed (transparent grey). The morpholine of **SCG-CBP30** is observed to project further into the ZA channel than the cyclohexyl methoxy group of **Inobrodib**. Modification to the morpholine position of **SGC-CBP30** with a linker would access a comparable exit vector from the bromodomain as with the cyclohexyl methoxy position of **Inobrodib**. Exit vectors are shown as arrows from the linker attachment position of each ligand into the solvent (**SGC-CBP30**-based PROTACs exit vector: blue, **Inobrodib**-based PROTACs exit vector: pink). **c)** Overlayed X-ray crystal structures of CREBBP bromodomain bound **SGC-CBP30** (compound: blue, PDB: 4NR7)[165] and **Inobrodib** (compound: pink, PDB: 7XH6)[163] without the protein structures. The compounds exhibit high spatial overlap and the morpholine of SGC-CBP30 extends further into the solvent than the cyclohexyl methoxy group of Inobrodib. Exit vectors are shown as arrows from the linker attachment position of each ligand into the solvent (**SGC-CBP30**-based PROTACs exit vector: blue, **Inobrodib**-based PROTACs exit vector: pink).

Modification of **Inobrodib** with a structurally similar group to the (*S*)-methyl ethyl morpholine in **SGC-CBP30**, but with amine functionality, could provide an alternative route for PROTAC synthesis. It was proposed to synthesise ligand **88** which comprises the difluorophenyl piperidinone moiety of **Inobrodib** and a (*S*)-methyl ethyl piperazine group to mimic the morpholine structure of **SGC-CBP30** but with amine functionality to enable PROTAC synthesis using amide coupling reactions (Figure 28). Such a ligand would assess a similar exit vector from the CREBBP and p300 bromodomain as ligand **87** the amide bond produced by attachment of a linker would be located further from the bromodomain

surface and there would be increased flexibility adjacent to the benzimidazole group. The variation in structures between ligand **87** and ligand **88** will help to explore PROTAC SAR for investigating optimal POI:PROTAC:E3 ligase ternary complex formation.

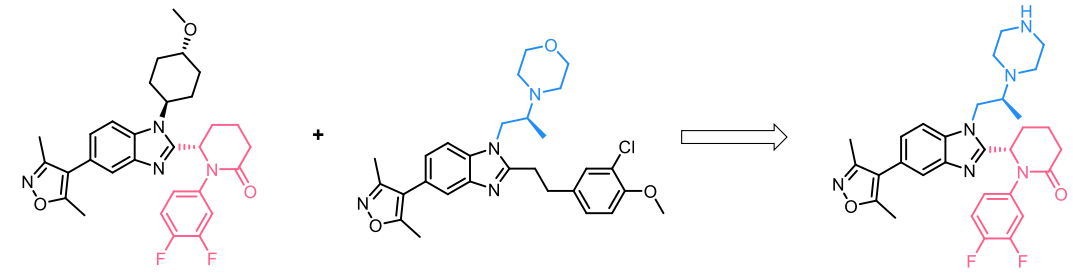

Figure 28. Proposed novel CREBBP and p300 ligand **88** that combines structural components of **Inobrodib** and **SGC-CBP30**.[112,164] Ligand **88** comprises the difluoro phenyl piperidinone group (pink) of **Inobrodib** and an (*S*)-methyl ethyl piperazine group (blue) to mimic the (*S*)-methyl ethyl morpholine group (blue) in **SGC-CBP30**.

3.2 – Synthesis of Novel Amine Terminal CREBBP and p300 Ligands

3.2.1 – Synthesis of Piperidine Modified **(*R*)-OXFBD05** Ligand **86**

*3.2.1.1 – Synthetic Route to Modify **(R)-OXFBD05** with a Piperidine group*

The strategy for obtaining ligand **86** was to use a similar route as for compounds **25** and **26** (described in Section 2.1.2.1) (Figure 29). First, DHBD-intermediate **24** could be functionalised with an unsaturated piperidine group, in a Suzuki-Miyaura coupling, to afford olefin **89**. The double bond could then be reduced to afford saturated piperidine intermediate **90** and, finally, ligand **86** could be obtained in a Suzuki-Miyaura coupling with THQ-containing intermediate **13**.

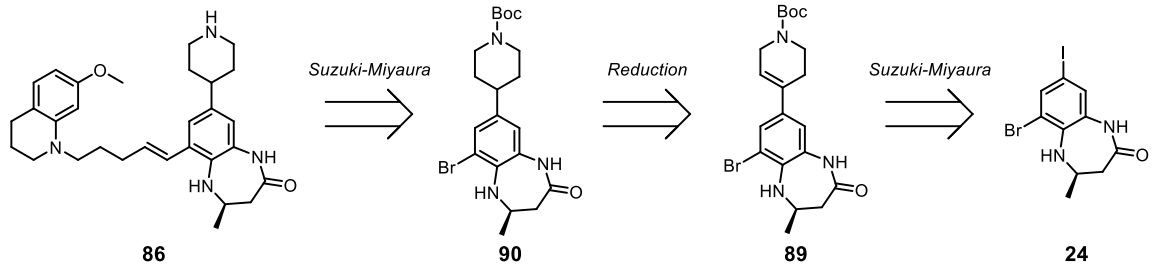

Figure 29. Proposed retrosynthesis of piperidine-modified **(*R*)-OXFBD05** ligand **86**. DHBH intermediate **24** is to be functionalised with an unsaturated piperidine group in a Suzuki-Miyaura coupling reaction to afford intermediate **89**. An unsaturated piperidine ring can then be formed by reducing the double bond to afford intermediate **90**. Ligand **86** could then be synthesised in a Suzuki-Miyaura coupling with intermediate **13**.

3.2.1.2 – Suzuki-Miyaura Coupling and Atmospheric Pressure Hydrogenation Reactions

Using the proposed synthetic route, intermediate **89** was obtained in a good yield of 72% from a Suzuki-Miyaura coupling between intermediate **24** and commercially available (1-*tert*-butoxycarbonyl-1,2,3,6-tetrahydropyridin-4-yl)boronic acid pinacol ester using Pd(dppf)Cl_2 as the catalyst (Scheme 12). Reduction of the double bond was initially performed with the same conditions as for the synthesis of intermediates **29** and **30** (described in Section 2.1.2.1), using H_2 (1 atm) and Wilkinson's catalyst in toluene at 60 °C for 15 h (Scheme 12). However, because the starting material and product share similar polarities, no change in R_f was observed when the reaction was monitored using TLC. Analysis using low resolution mass spectrometry (LRMS) detected *m/z* values corresponding to both the desired product (**90**) and the starting olefin (**89**), indicating partial reaction conversion. Attempts to separate the starting material and product using normal phase and reverse phase column chromatography were, however, unsuccessful with no clean fractions obtained.

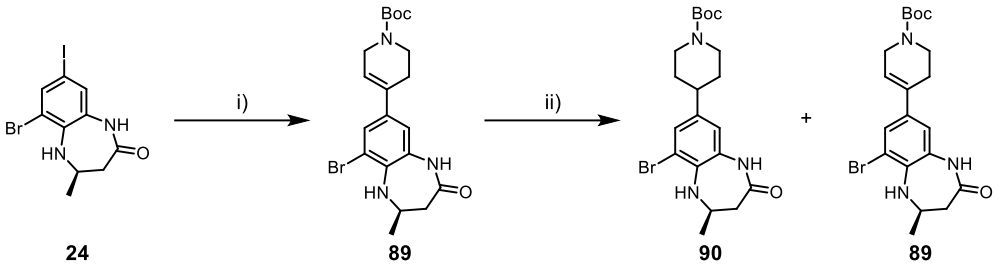

Scheme 12. Synthesis of intermediate **89** in a Suzuki-Miyaira coupling and subsequent hydrogenation which led to an inseparable mixture of intermediates **89** and **90**. *Reagents and conditions*: i) (1-*tert*-Butoxycarbonyl-1,2,3,6-tetrahydropyridin-4-yl)boronic acid pinacol ester, $Pd(dppf)Cl_2$, K_2CO_3, 1,4-dioxane, H_2O, Ar, 100 °C, 18 h; ii) H_2, $Rh(PPh_3)_3Cl$, solvent, 60 °C, 24 h, for solvent and reaction conversions see Table 5.

A study by Jourdant *et al.* discovered a large solvent effect on the reaction conversion of double bond reductions using hydrogenation reactions catalysed by Wilkinson's catalyst.[166] They showed that the use of a protic solvent greatly enhanced reaction conversion compared to aprotic solvents, and that this could be increased further by using a 1:1 mixture of aprotic and protic solvents (e.g. 1:1 THF: MeOH). The reduction of **89** was investigated using a range of solvent conditions, at a concentration of 0.1 M starting material, with 1 atm H_2. The reaction conversion was assessed after stirring at 60 °C for 24 h using ^{1}H NMR (Table 5, Appendix Figure 13).

Table 5. Reduction of olefin **89** using Wilkinson's catalyst and 1 atm H_2 in the given solvent at 0.1M starting material. Reaction mixtures were stirred at 60 °C for 24 h before the reaction conversion was measured using ^{1}H NMR. % conversion is reported as a mean value calculated using the integrals of the -C*H*$_3$ peak and the two Ar-*H* peaks of **89** and **90** (one Ar-*H* peak was obscured in the toluene sample so was not used in the calculation) (see Appendix Figure 13 for relevant ^{1}H NMR peaks).

Solvent	Reaction Conversion (^{1}H NMR)
Toluene	21%
MeOH	26%
THF	5%
1:1 THF:MeOH	15%
1:1 THF:*tert*-BuOH	9%

The original conditions using toluene as a solvent resulted in poor conversion with only 21% product (**90**) formation. A marginal improvement in was obtained using methanol with 26% product **90**, which correlates with the findings of Jourdant *et al.* that reaction conversion can be enhanced using a polar solvent. However, mixtures of either 1:1 THF: MeOH or 1:1 THF: ^{t}BuOH gave decreased reaction conversions of 15% and 9%, respectively, contrary to Jourdant *et al.* Reaction in THF alone gave the

lowest yield with only 5% product (**90**) formed. The poor reaction conversions when THF was used, either alone or in a mixture, could be due to poor compound solubility in this solvent.

As **89** and **90** share aromatic bromine functionality, if a mixture were used in the subsequent Suzuki-Miyaura coupling, both would react with intermediate **13** to produce a similar mixture of saturated and unsaturated piperidine products. Therefore, full reduction of the double bond was required. However, the use of more strongly reducing catalysts, such as Pd/C, instead of mild Wilkinson's catalyst would likely cause undesired dehalogenation of the aromatic bromine.[167]

3.2.1.3 – Higher Pressure Hydrogenation Reaction

As the previous hydrogenation reactions of **89** yielded little or no desired **90**, higher pressure conditions were investigated. A high pressure reactor was obtained from the Vincent Group, University of Oxford, enabling the reaction to be performed at a pressure of 4 bar H_2 (Scheme 13).

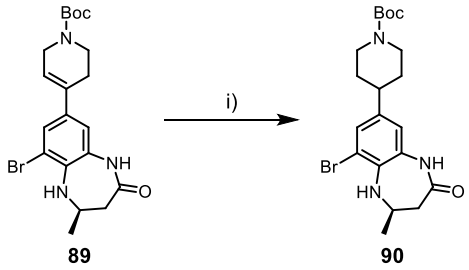

Scheme 13. Reduction of olefin **89** to unsaturated piperidine containing compound **90** by hydrogenation. *Reagents and conditions*: i) H_2 (4 bar), $Rh(PPh_3)_3Cl$, MeOH, 60 °C, 15 – 24 h, 64%.

In the reaction solvent screen above, the greatest reaction conversion was achieved using methanol (analysed using ^{1}H NMR) so this solvent was used for the higher pressure reaction, which was performed using Wilkinson's catalyst at 4 bar H_2 and 60 °C. ^{1}H NMR analysis of the crude reaction mixture after 22 h showed negligible remaining starting material (<3%). Restricted by the size of the reactor, the reaction was performed four times over 15 – 24 h and the crude material was pooled for purification to afford **90** in a yield of 64%. The loss in yield compared with conversion was due to coelution of $OPPh_3$ with the product causing difficulties in normal phase column chromatography purification.

3.2.1.4 – OXFBD05-Piperidine Ligand Synthesis

The Boc-protected ligand **91** was synthesised in a Suzuki-Miyaura coupling between intermediates **90** and **13** using Pd(dppf)Cl_2 as the catalyst (Scheme 14). After stirring at 100 °C for 18 h, TLC analysis showed full consumption of starting material **90** and remaining **13** which was in excess. However, the product (**91**) was only obtained in a 26% yield following purification. This reaction was repeated while on industrial placement at GSK, where it could be easily monitored using LCMS (data not shown), which displayed the fast consumption of intermediate **90** with a large peak of remaining intermediate **13**. This could suggest that intermediate **90** has a poor stability under the reaction conditions or that it was participating in undesired side-reactions, and the reaction could be progressed by the continual addition of intermediate **90**. The piperidine group of compound **91** was then Boc-deprotected by treatment with HCl for 4 h, and the crude hydrochloride salt of ligand **86** was used in subsequent amide coupling reactions.

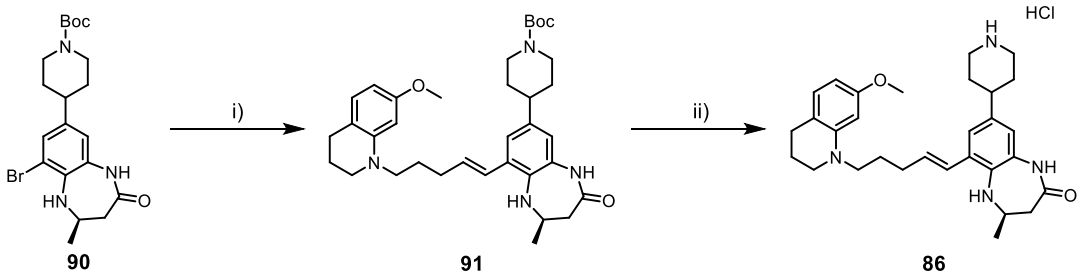

Scheme 14. Synthesis of **(*R*)-OXFBD05**-piperidine-based ligand **86** by Suzuki-Miyaura coupling and Boc-protection. *Reagents and conditions*: i) 7-Methoxy-1-[(4*E*)-5-(4,4,5,5-tetramethyl-1,3,2-dioxaborolan-2-yl)pent-4-en-1-yl]-1,2,3,4-tetrahydroquinoline **13**, Pd(dppf)Cl_2, K_2CO_3, 1,4-dioxane, H_2O, 100 °C, 18 h, 26%; ii) 4 M HCl in 1,4-dioxane, CH_2Cl_2, rt, 8 h, 100%.

3.2.2 – Synthesis of Piperidine-Modified **Inobrodib** Ligand **87**

Modification of the CREBBP and p300 bromodomain ligand **Inobrodib** with a piperidine group to afford novel ligand **87** was achieved using procedures reported by Liu *et al*. (Scheme 15).[168]

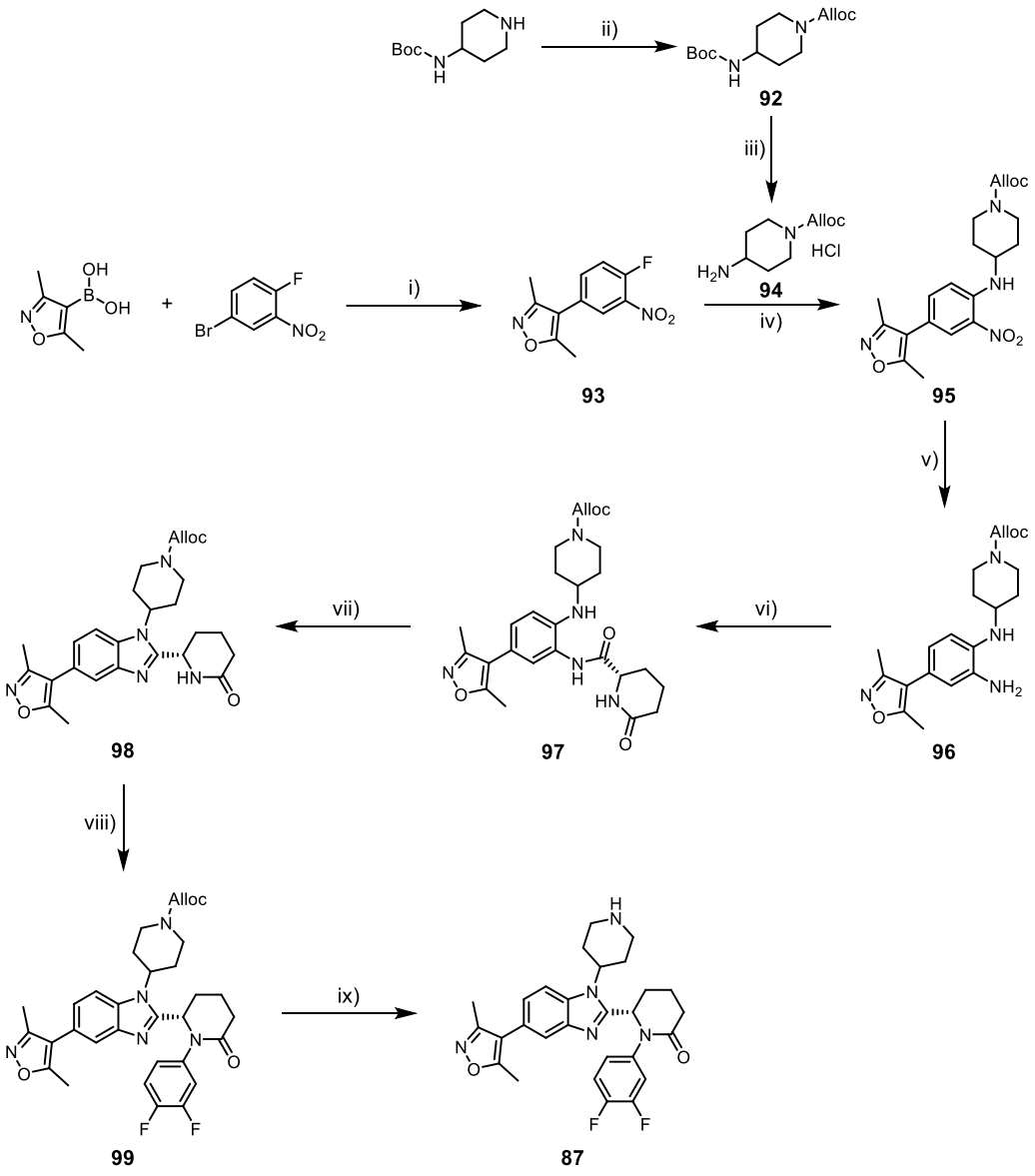

Scheme 15. Synthesis of piperidine-modified **Inobrodib** ligand **87** using procedures by Liu et al.[168] *Reagents and conditions*: i) $Pd(dppf)Cl_2$, K_2CO_3, 1,4-dioxane, H_2O, Ar, 100 °C, 17 h, 62%; ii) Allyl chloroformate, DBU, CH_2Cl_2, 0 °C, 3 h, 91%; iii) TFA, CH_2Cl_2, rt, 1.5 h; iv) DIPEA, MeCN, 80 °C, 15 h, 61% (two steps); v) $Na_2S_2O_4$, EtOAc, H_2O, 80 °C, 5 h; vi) (*S*)-6-Oxo-2-piperidine carboxylic acid, HATU, DIPEA, DMF, rt, 18 h; vii) Acetic acid, reflux, 72 h, 42% (two steps); viii) (3,4-Difluorophenyl)boronic acid, DBU, Cu-TMEDA, anhydrous CH_2Cl_2, 3 Å molecular sieves, air, rt, 18 h, 26%; ix) $Pd(PPh_3)_4$, K_2CO_3, MeOH, rt, N_2, 1.5 h, 66%.

It was decided to protect the piperidine amine with an Alloc group because the synthetic route includes acidic and basic steps, making the commonly used Boc and Fmoc protecting groups unsuitable. This

was achieved using commercially available 4-*N*-Boc-amino piperidine and allyl chloroformate to give intermediate **92** in a 91% yield.

The KAc memetic portion of the ligand was synthesised using a Suzuki-Miyaura coupling between commercially available 3,5-dimethylisoxazole boronic acid and 4-bromo-1-fluoro-2-nitronbenzene to afford intermediate **93** in a yield of 62%. The piperidine group was then introduced by first Boc-deprotecting intermediate **92** using TFA to afford intermediate **94**, followed by an S_NAr reaction with **93** at 80 °C for 15 h giving intermediate **95** in a 61% yield over the two steps. The nitro group was then reduced using sodium dithionite, at 80 °C for 5 h, to give aniline intermediate **96** in a 72% yield. The benzimidazole was formed using an amide coupling with commercially available (*S*)-6-oxo-2-piperidine carboxylic acid followed by heating under reflux in acetic acid for 72 h, producing intermediate **98** in a 42% yield over the two steps, which is consistent with yields obtained by Liu *et al*.[168]

The difluorophenyl group was introduced using a Chan-Evans-Lam amination reaction with commercially available (3,4-difluorophenyl)boronic acid using Cu-TMEDA (0.2 eq.) as the catalyst. Using the literature procedure, of stirring under an atmosphere of air with a drying tube and molecular sieves for 18 h at room temperature, resulted in poor reaction conversation (TLC) with the major spot corresponding to remaining starting intermediate **98**. Following reverse phase and normal phase column chromatography, the desired product (**99**) was obtained in a yield of 26%, which does not greatly exceed the proportion of catalyst used for the reaction. The reaction was repeated where Cu-TMEDA was continually added to the reaction mixture (4 × 0.2 eq.) over 48 h, and an improved yield of 61% was obtained. These findings would imply that, the Cu-TMEDA is not performing efficiently as a catalyst, however, Liu *et al*. obtained high yields using the given conditions.[168] The Chan-Evans-Lam catalytic cycle must be performed dry, but requires oxygen to recycle the catalyst back to the active Cu^{II} species from a reduced Cu^{I} species formed in the reaction.[169] The dry dichloromethane used for the reaction was stored under an inert atmosphere so it may the that, despite vigorous stirring, there was insufficient oxygen in the reaction mixture to recycle the catalyst.[170] However, it should be noted that it is not

uncommon for literature Chan-Evans-Lam couplings to use stoichiometric or excess equivalents of the copper catalyst.[170–174]

The Alloc group was then deprotected using mild palladium^0 conditions according to a procedure reported by Vutukuri *et al.*[175] A suspension of Alloc-protected ligand **99**, $Pd^0(PPh_3)_4$, and potassium carbonate in methanol was stirred at room temperature under an atmosphere of nitrogen. Initially when the reaction was performed, LCMS monitoring after 18 h showed no remaining starting **99** and 90% product (**87**) (Appendix Figure 14). However, upon opening the reaction mixture to air and concentrating under a flow of nitrogen, two new major peaks formed in the LCMS trace with *m/z* values that corresponded to the addition of water and methanol, respectively (Appendix Figure 15). As a result, **Inobrodib**-based ligand **87** was obtained in a yield of 15% following purification. This reaction was repeated, as above, and LCMS monitoring showed full conversion of the starting material after 1.5 h. In this instance, the reaction mixture was not concentrated, but directly purified using cation exchange chromatography, to afford ligand **87** in an improved yield of 66%.

3.2.3 – Attempted Synthesis of (*S*)-Methyl Ethyl Piperazine-Modified **Inobrodib** Ligand **88**

*3.2.3.1 – Proposed Synthetic Route to Modify **Inobrodib** with an (S)-Methyl Ethyl Piperazine Group*

For the synthesis of **Inobrodib**-based ligand **88**, the (*S*)-methyl ethyl piperazine group was not directly installed in an S_NAr reaction with intermediate **93**, like the piperazine group for intermediate **95** synthesis above, because a commercial source for an appropriate piperazine-containing starting material could not be identified (Figure 30a). As an alternative route, first the (*S*)-methyl ethyl group could be introduced to intermediate **93** and then the piperazine ring could be formed with in an intermolecular then intramolecular alkylation reaction using a diethyl amine compound with two terminal leaving groups (Figure 30b). The subsequent synthesis could then follow the same literature pathway used previously for the synthesis of piperidine-modified **Inobrodib** ligand **87**.[168]

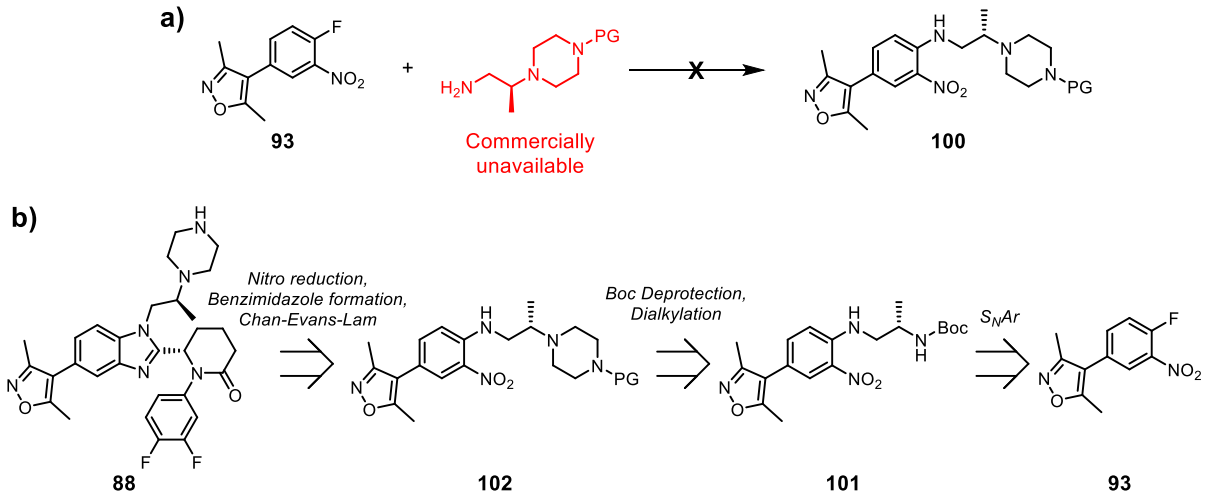

Figure 30. Proposed synthesis of (*S*)-methyl ethyl piperazine-modified **Inobrodib** ligand **88**. **a)** Proposed S_NAr reaction between **93** and an (*S*)-methyl ethyl piperidine compound which was not possible due to the commercial unavailability of the amine. PG – protecting group. **b)** Proposed retrosynthesis of ligand **88**. An (*S*)-propyl amine group could be couplied to intermediate **93** in an S_NAr reaction to afford intermediate **101**. The piperazine ring could then be formed in a double alkylation reaction with Boc-deprotected intermediate **101** to give intermediate **102**. The final **Inobrodib**-based ligand **88** could then be synthesised using the previously used methodology by Liu *et al.* of nitro reduction, formation of the benzimidazole group and Chan-Evans-Lam coupling.[168] PG – protecting group.

*3.2.3.2 – Synthesis Towards (S)-Methyl Ethyl-Modified **Inobrodib**-Based Ligand **88***

The S_NAr reaction between intermediate **93** and (*S*)-*tert*-butyl-1-aminopropan-2-carbamate afforded (*S*)-propyl amino intermediate **101** in a 93% yield (Scheme 16). The terminal amine could then be Boc-deprotected using HCl at room temperature for 2 h and the **103** HCl salt was directly used in subsequent alkylation reactions without purification.

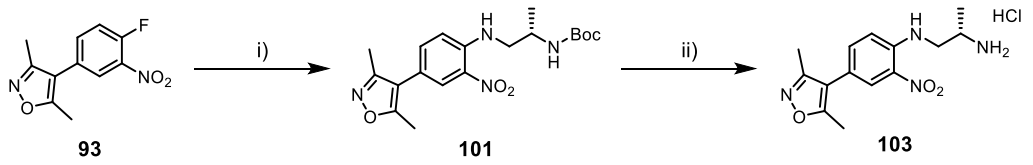

Scheme 16. Synthesis of intermediate **103** by S_NAr reaction followed by Boc-deprotection. *Reagents and conditions*: i) (*S*)-*tert*-Butyl-1-aminopropan-2-carbamate, DIPEA, MeCN, 80 °C, 18 h, 93%; ii) 4 M HCl in 1,4-dioxane, CH_2Cl_2, rt, 2 h, 100%.

To obtain the alkylating agent, first diol **104** was synthesised, then multiple conditions were investigated to activate the alcohols as good leaving groups for substitution reactions with intermediate **93** (Scheme 17, Scheme 18). Dibenzyl protected diol **105** was synthesised using a reductive amination reaction between commercially available benzyloxy acetaldehyde and 2-benzylaminoethanol in a yield of 84% (Scheme 17). The benzyl group was then selectively removed from the alcohol to afford diol **104** according to a procedure reported by Ramanathan and Hou using triphenylphosphine hydrogen bromide in anhydrous acetonitrile for 1 h at 100 °C under microwave irradiation.[176]

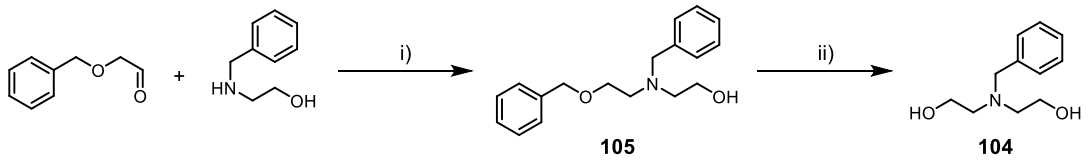

Scheme 17. Synthesis of diphenol intermediate **104** by reductive amination and selective benzyl ether deprotection. Selective benzyl-deprotection was achieved using a procedure reported by Ramanathan and Hou.[176] *Reagents and conditions*: i) $NaB(OAc)_3H$, anhydrous 1,2-dichloroethane, 0 °C – rt, 2 h, 84%. ii) $PPh_3 \cdot HBr$, anhydrous MeCN, 100 °C microwave, 1 h, 45%.

Ramanathan and Hou propose that the mechanism proceeds via protonation of the benzyl ether followed by nucleophilic attack by triphenylphosphine of the ether carbon with the most cationic character (Figure 31). An initial test reaction afforded desired diol **104** in an 88% yield, however, the ^{1}H NMR contained multiple peaks in the aromatic region from triphenylphosphine contamination. When the reaction was scaled up, an acidic extraction step was added to the work up to protonate the product and remove excess triphenylphosphine in the organic component. The aqueous component was then basified to recover the product and following purification, diol **104** was obtained in a lower yield of 45% but without triphenylphosphine contamination.

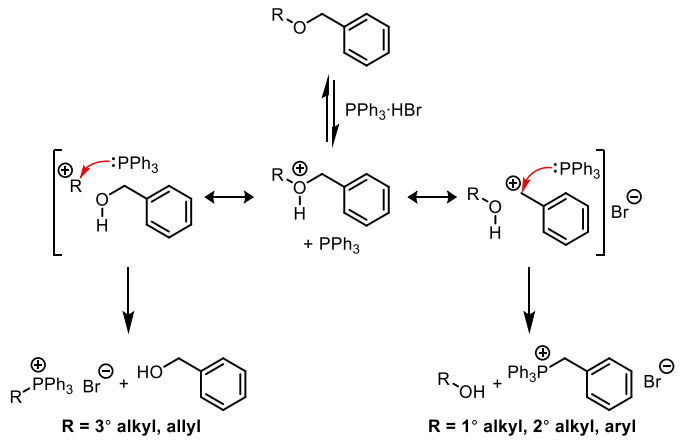

Figure 31. Proposed mechanism for the reaction of benzyl ethers with triphenylphosphine hydrogen bromide.[176] The ether is protonated by the hydrogen bromide and the triphenyl phosphine will react with the ether carbon that displays the greater cationic character. For reactions involving tertiary (3°) alkyl and allyl benzyl ethers, the tertiary and allyl carbocations have similar or greater stability than the benzyl carbocation so will react with the triphenylphosphine and the R-OH compound is not liberated in these instances. For reactions involving primary (1°) alkyl, secondary (2°) alkyl, and aryl benzyl ethers, the benzyl ether will form the more stable carbocation and react with triphenylphosphine to release the R-OH product. Figure modified from figure by Ramanathan and Hou.[176]

Multiple conditions were tested for the dialkylation reaction to form the piperazine ring in intermediate **102** and are summarised in Table 6 (Scheme 18). Monitoring the activated alkylating agents using LCMS proved difficult due to their apparent instability to mass spectrometry conditions and benzyl groups having relatively poor chromophores. However, ^{1}H NMR of the isolated dichloro and diiodo intermediates gave 2:4:4 peak integration patterns with different chemical shifts to those of diol **104** and each other, indicating the desired intermediates were formed. For reactions monitored using LCMS, the dialkylation step was monitored with respect to intermediate **103** consumption, and each trace showed the formation of multiple, low intensity peaks (unless no reaction took place), indicating undesired alkylation side-reactions were occurring.

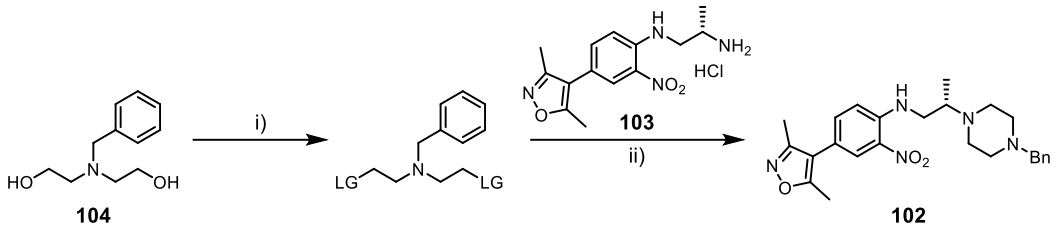

Scheme 18. Activation of diol **104** and subsequent dialkylation of intermediate **103** to afford piperazine intermediate **102**. For reaction reagents and conditions and results see Table **6**. LG – leaving group.

Table 6. Conditions for diol **104** activation and subsequent S_N2 reactions with (*S*)-amine intermediate **103** to form piperazine-intermediate **102**, see Scheme 18. Reactions were monitored with respect to intermediate **103** consumption. Int. – intermediate, Ref. – reference.

Reagents and Conditions	Activated Int. Structure	Results	Ref.
i) Ms_2O, MsOH, NEt_3, anhydrous MeCN, −10 °C, 30 min ii) NEt_3, 85 °C, 24 h	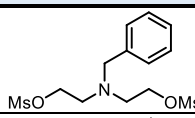	TLC: major **103**, minor **102** LCMS: 45% **103**, 19% **102**	177
i) $SOCl_2$, anhydrous CH_2Cl_2, rt, 5 h ii) DIPEA, anhydrous DMF, rt, 4 h	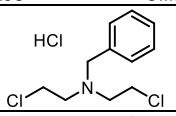	TLC: only **103** LCMS: 100% **103**	178
i) $SOCl_2$, anhydrous CH_2Cl_2, rt, 5 h ii) DIPEA, anhydrous DMF, rt, 28 h	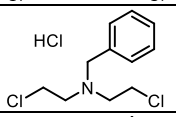	TLC: major **103**, minor **102**	178
i) $SOCl_2$, anhydrous CH_2Cl_2, rt, 5 h ii) DIPEA, anhydrous DMF, rt, 28 h then 100 °C microwave, 1 h	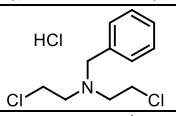	TLC: multiple spots	178
i) $SOCl_2$, anhydrous CH_2Cl_2, rt, 5 h ii) TBAI, DIPEA, anhydrous DMF, rt – 100 °C, 72 h	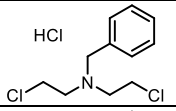	TLC: major **103**, minor **102** Purification: **102** isolated in 17% yield	178
i) $SOCl_2$, anhydrous CH_2Cl_2, rt, 5 h ii) TBAI, DIPEA, anhydrous EtOH, reflux, 40 h	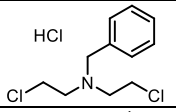	TLC: minor **103**, major **102** LCMS: 15% **103**, 62% **102** Purification: **102** isolated in 42% yield	178,179
i) $SOCl_2$, anhydrous CH_2Cl_2, rt, 5 h then NaI, anhydrous acetone, reflux, 16 h ii) DIPEA, DMF, 100 °C, 16 h	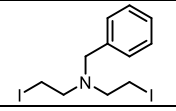	TLC: minor **103**, major **102**, many spots LCMS: 9% **103**, 40% **102**	178,180

The highest yielding dialkylation reaction occurred using the dichloro intermediate and ethanol as the reaction solvent. Despite the 62% conversion (LCMS) of this reaction, purification was challenged by the presence of side-products and **102** was isolated in a 42% yield. Typically, protic solvents are avoided for S_N2 reactions because nucleophilic attack is obstructed by H-bonds formed between the solvent and nucleophile. Therefore, if the reaction mechanism were purely S_N2 in nature, the corresponding reaction using polar aprotic DMF as the solvent would have been expected to afford intermediate **102** in a greater yield than the reaction in ethanol (intermediate **102** isolated in 17% yield for reaction in DMF). The compositions of the reaction mixtures were identical other than the solvent used, but were heated to

different temperatures for different times, and the reaction conversion in DMF was not quantitatively analysed by LCMS. Consequently, the two reactions are not directly comparable, and it is difficult to draw definitive conclusions as to why the reaction in ethanol afforded the greater isolated yield of **102**.

As the final **Inobrodib**-based ligand **88** was required for the synthesis of multiple PROTACs, and later steps in the synthetic pathway were moderate – low yielding when followed for the synthesis of **Inobrodib**-based ligand **87**, an alternative route for installation of the piperazine ring was sought.

3.2.4 – Synthesis of Ethyl Piperazine-Modified **Inobrodib** Ligand **106**

*3.2.4.1 –Modification of **Inobrodib** with an Ethyl Piperazine Group*

When **SGC-CBP30** was developed by Hay *et al*., an analogue without the (*S*)-methyl group, but otherwise structurally identical (**SGC-CBP30-A**), was also evaluated (Figure 32).[164] **SGC-CBP30-A** exhibits comparable binding affinity for the CREBBP bromodomain as **SGC-SCB30** (ITC binding affinities: **SGC-CBP30** K_d = 21 nM, **SGC-CBP30-A** K_d = 28 nM). Therefore, the modification of **Inobrodib** with an ethyl piperazine group to mimic the structure of **SGC-CBP30-A** in ligand **106** was viewed as a more synthetically tractable target than ligand **88** (Figure 32). If any PROTACs using ligand **106** were identified as degraders of CREBBP and/or p300, then the use of ligand **88** could be reevaluated to probe PROTAC SAR at this position.

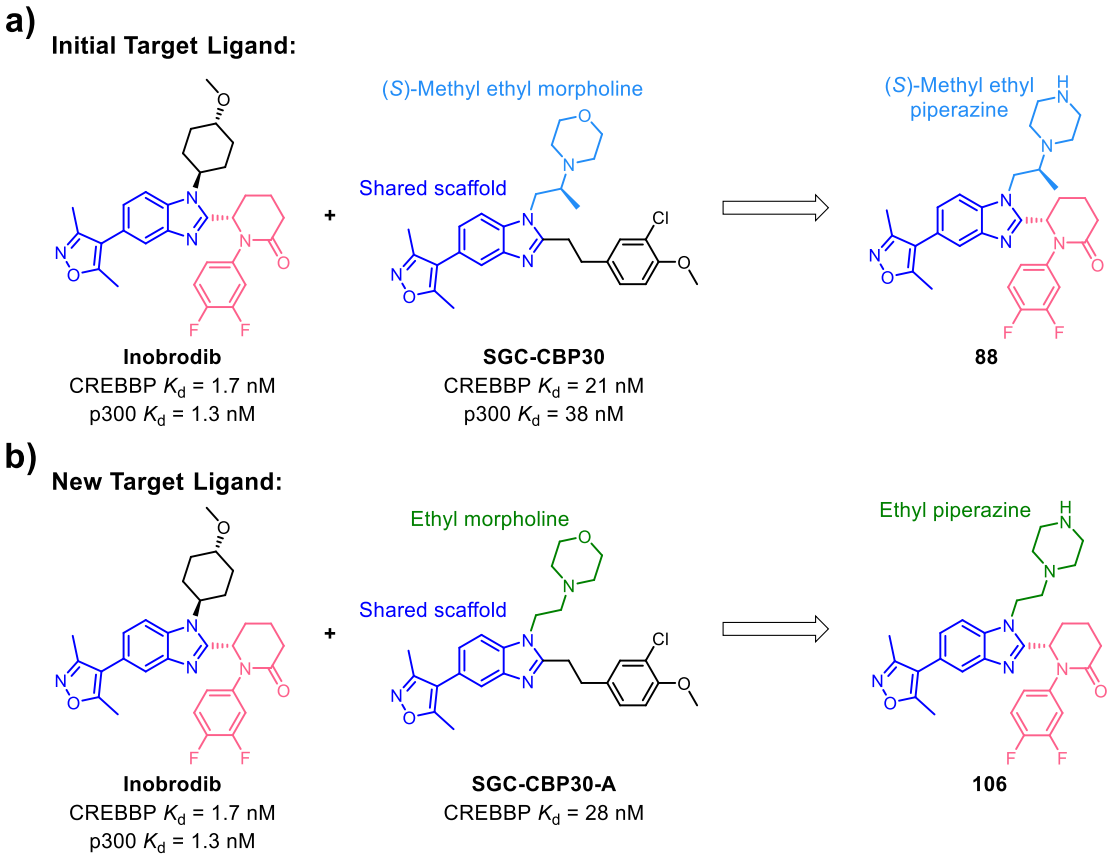

Figure 32. Design of CREBBP and p300 bromodomain ligands **88** and **106** that comprise structural features from the bromodomain inhibitors **Inobrodib**, **SGC-CBP30**, and **SGC-CBP30-A**.[112,164] All reported K_d values were measured using ITC. **a)** Design of the initial target CREBBP and p300 bromodomain ligand **88**, as described in Section 3.1.3. **Inobrodib**, **SGC-CBP30**, and ligand **88** share a dimethylisoxazole benzimidazole scaffold (dark blue) which is required for binding to the KAc binding site of the bromodomain. Ligand **88** comprises a difluorophenyl piperidinone moiety (pink) from **Inobrodib**, which is integral for the high **Inobrodib**-bromodomain binding affinity, and an (*S*)-methyl ethyl piperazine group (light blue) to mimic the (*S*)-methyl ethyl morpholine group (light blue) of **SGC-CBP30** but with amine functionality to enable subsequent PROTAC synthesis. Ligand **88** was not pursued due to synthetic intractability. **b)** Design of CREBBP and p300 bromodomain ligand **106**, which was viewed as a more synthetically tractable target than ligand **88**. **SGC-CBP30**, and **SGC-CBP30-A** share similar binding affinities for the CREBBP bromodomain and only differ by an (*S*)-methyl group. Ligand **106** comprises the dimethylisoxazole benzimidazole scaffold (dark blue) share with **Inobrodib**, **SGC-CBP30**, and **SGC-CBP30-A**; a difluorophenyl

piperidinone moiety (pink) from the **Inobrodib** structure; and an ethyl piperazine group (green) to mimic the ethyl morpholine group (green) of **SGC-CBP30-A** but with amine functionality to enable subsequent PROTAC synthesis.

*3.2.4.2 – Synthesis of Ethyl Piperazine-Modified **Inobrodib** Ligand **106***

Unlike for the proposed synthesis of ligand **88**, described in Section 3.2.3, the ethyl piperazine moiety of ligand **106** could be directly installed in an S_NAr reaction with intermediate **93** using a commercially available compound and did not need to be formed by cyclisation. Ligand **106** was obtained using the procedure reported by Liu *et al*. that was previously used in Section 3.2.2 for the synthesis of piperidine-modified **Inobrodib** ligand **87** (Scheme 19).[168]

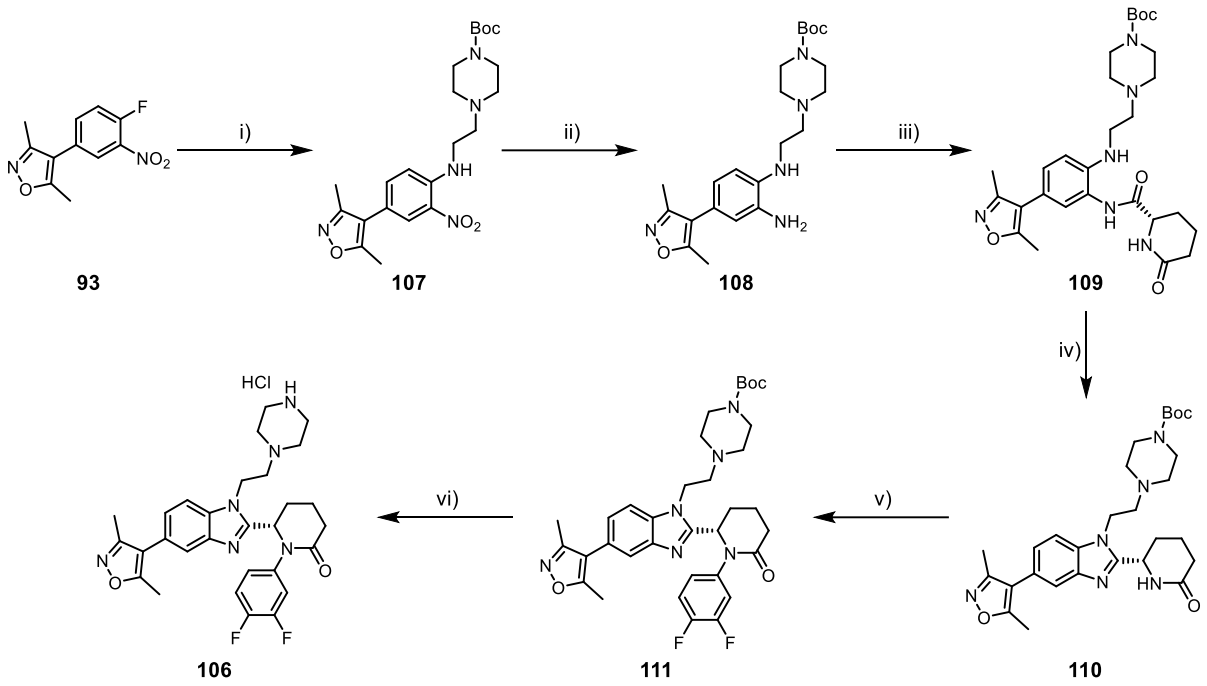

Scheme 19. Synthesis of piperazine-modified **Inobrodib** ligand **106** using a procedure reported by Liu *et al*.[168] *Reagents and conditions*: i) *tert*-Butyl 4-(2-aminoethyl)piperazine-1-carboxylate, DIPEA, MeCN, 80 °C, 18 h, 85%; ii) $Na_2S_2O_4$, EtOH, H_2O, 80 °C, 15 min, 84%; iii) (*S*)-6-Oxo-2-piperidinecarboxylic acid, HATU, DIPEA, DMF, rt, 16 h; iv) Toluene, Dean-Stark apparatus, reflux, 66 h, 27% (two steps); v) 3,4-Difluorophenylboronic acid, DBU, Cu-TMEDA, anhydrous CH_2Cl_2, 3 Å molecular sieves, air, rt, 18 h, 30%; vi) 4 M HCl in 1,4-dioxane, CH_2Cl_2, rt, 17 h, 94%.

The ethyl piperazine moiety was installed onto the isoxazole-containing intermediate **93** in an S_NAr reaction using commercially available *tert*-butyl 4-(2-aminoethyl)piperazine-1-carboxylate to afford intermediate **107** in an 85% yield. The nitro group was then reduced using sodium dithionite, at 80 °C for 15 min, giving aniline intermediate **108** in an 84% yield. The piperidinone group was then introduced in an amide coupling reaction with (*S*)-6-oxo-2-piperidinecarboxylic acid, using HATU as the coupling reagent, at room temperature for 16 h. TLC analysis showed no remaining intermediate

109 and, following work up, the crude product was used directly in the next step to form the benzimidazole group. The Liu *et al*. procedure forms the imidazole ring by heating the amide intermediate in acetic acid under reflux, however, in this case, the piperazine group is protected using an acid-labile Boc group. Instead, the reaction solvent was changed to toluene and intermediate **109** was heated under reflux using Dean-Stack apparatus to remove the water by-product and drive cyclisation. Intermediate **109** is poorly soluble in toluene causing the cyclisation reaction to proceed slowly but after 66 h, TLC analysis showed one major product spot with some remaining starting intermediate **109**. Following purification, benzimidazole **110** was obtained in a 27% yield over the two steps (amide coupling and cyclisation). This is lower than the yields obtained using acetic acid in the literature by Liu, *et al*., but not substantially.[168] The difluorophenyl group was then installed using a Chan-Evans-Lam coupling reaction with 3,4-difluorophenylboronic acid using Cu-TMEDA as the catalyst to afford the Boc-protected ligand (**111**) in a yield of 30% and unreacted starting material was also recovered. The Boc group was then removed by treating **111** with HCl, and the hydrochloride salt of ligand **106** was used directly, without purification, in the subsequent amide coupling reactions to afford final PROTACs.

3.3 – Higher Throughput PROTAC Synthesis Using Amide Coupling Reactions

3.3.1 – Amide Coupling Arrays

With amine functionalised ligands **86**, **87**, and **106** in hand, final PROTAC molecules could be synthesised using amide coupling reactions with compounds comprising an E3 ligase ligand attached to a carboxylic acid functionalised linker. This work was carried out on an industrial placement at GSK, Stevenage using their library of E3 ligase ligand-linker compounds. As for the series of PEG-PROTACs synthesised in Chapter 2, the E3 ubiquitin ligases cereblon and VHL were targeted using derivatives of the ligands **thalidomide** and **VH032**, respectively.[15,25] Amide couplings were performed using HATU as the coupling reagent in DMF at room temperature for 2 – 20 h. The crude reaction mixtures were directly purified using either preparative reverse phase column chromatography or mass directed auto purification (MDAP), to afford the final PROTACs. For the purposes of performing an initial higher throughput biological screen of the PROTACs to assess their abilities to cause the degradation of CREBBP and/or p300 (discussed in Chapter 4 and Chapter 5), the final compounds were not required to be >95% pure (for purities see Table 7**,** Table 8**,** and Table 9) and were not fully characterised. Any hits from the initial biological screen would then be validated using >95% pure, resynthesised compound that was fully characterised.

3.3.2 – Synthesis of PROTACs Using Piperidine-Modified **(*R*)-OXFBD05** Ligand **86**

Amide couplings between piperidine-modified **(*R*)-OXFBD05** ligand **86** and cereblon ligand-linker compounds afforded cereblon-targeting PROTACs **112 – 123** in yields of 3 – 26% (Scheme 20 and Table 7). <1 mg of PROTAC **123** was obtained so this compound was not biologically evaluated.

Surprisingly, amide couplings between ligand **86** and VHL ligand-linker compounds did not produce desired PROTACs **124 – 131**; instead forming products with *m/z* values of the desired mass −4, after stirring at room temperature for 18 h with no remaining ligand **86** (LCMS analysis) (Scheme 20 and Table 7). These products were isolated using mass directed auto purification (MDAP), but it was not possible to deduce their identity, so these compounds were not biologically tested. VHL-targeting PROTACs **132** and **133** were formed in their coupling reactions, however, the products were obtained in a low purity (LCMS purity: 34% and 50%, respectively) so were also not evaluated for their ability to degrade CREBBP and/or p300.

Of the 22 amide coupling reactions performed using ligand **86**, 11 afforded PROTACs in sufficient quantities and purities for the biological evaluation of their abilities to induce the degradation of CREBBP and/or p300 in Chapter 5. Each of these PROTACs (**112 – 122**) recruit the E3 ubiquitin ligase enzyme cereblon using ligands **thalidomide**, **pomalidomide**, or **lenalidomide** where the linker is either attached to the 4'-position or 5'-position of the ligand.[15] The final PROTACs investigate a range of linker lengths and flexibilities, including alkyl, PEG, and cyclic linker structures.

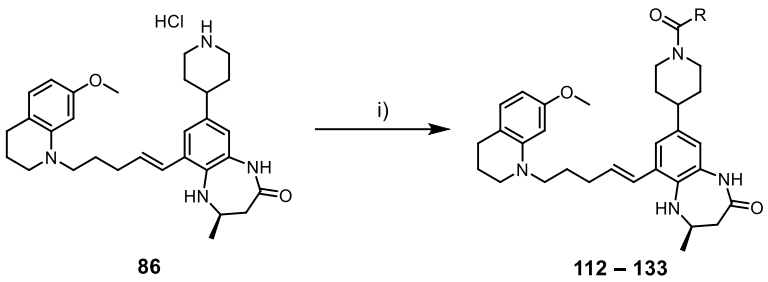

86 112 – 133

Scheme 20. General synthesis of PROTACs **112 – 123**, **132**, and **133**; and the attempted synthesis of PROTACs **124 – 131** using amide coupling reactions between ligand **86** with carboxylic acid functionalised linker-E3 ligase ligand compounds. *Reagents and conditions*: i) R-CO_2H, HATU, DIPEA, DMF, rt, 4 – 18 h, for R groups and results, see Table 7.

Table 7. Results of amide couplings between ligand **86** and E3 ligase ligand compounds R-CO_2H (Scheme 20). Purity values were measured using LCMS, formic acid method. Cpd – compound.

Cpd.	R Group Structure	Result
112	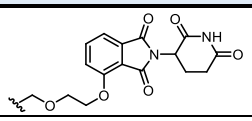	7.4 mg, 8.7 µmol, yield 22%, purity 94%
113	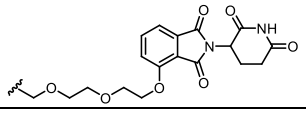	5.1 mg, 5.7 µmol, yield 26%, purity 92%
114	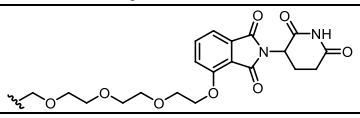	5.4 mg, 5.8 µmol, yield 15%, purity 96%
115	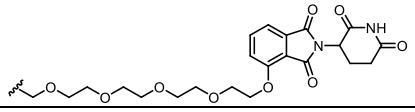	4.9 mg, 5.0 µmol, yield 24%, purity 91%
116	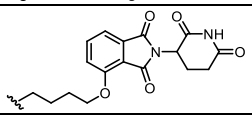	2.4 mg, 2.8 µmol, yield 13%, purity 89%
117	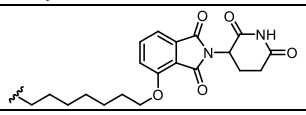	2.4 mg, 2.7 µmol, yield 13%, purity 88%
118	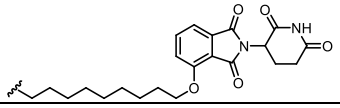	1.5 mg, 1.6 µmol, yield 7%, purity 86%
119	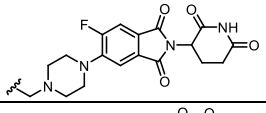	4.4 mg, 4.9 µmol, yield 21%, purity 80%
120	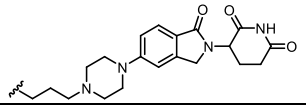	9.1 mg, 10 µmol, yield 24%, purity 89%
121	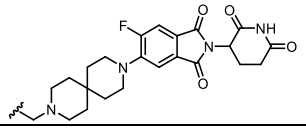	4.8 mg, 5.0 µmol, yield 23%, purity 88%
122	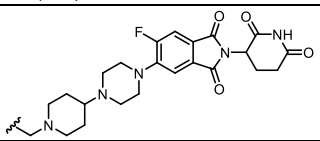	3.7 mg, 3.8 µmol, yield 16%, purity 79%

123	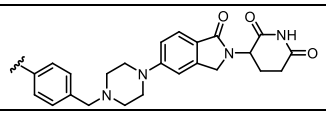	0.7 mg, 0.8 µmol, yield 3%, purity 80% Compound not biologically tested
124	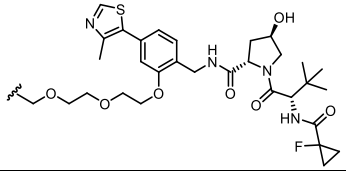	Failed reaction Expected *m/z* 1149.6 LCMS: *m/z* 1145.5, purity 36%
125	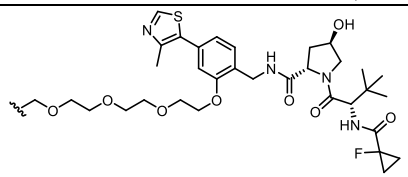	Failed reaction Expected *m/z* 1193.6 LCMS: *m/z* 1189.5, purity 29%
126	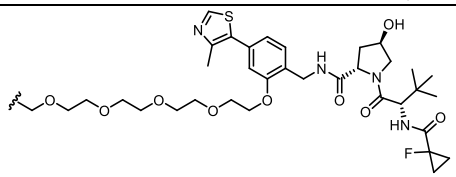	Failed reaction Expected *m/z* 1237.6 LCMS: *m/z* 1233.4, purity 55%
127	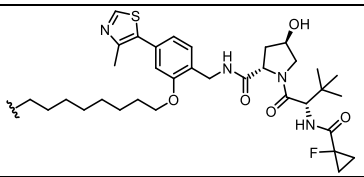	Failed reaction Expected *m/z* 1159.6 LCMS: *m/z* 1155.5, purity 54%
128	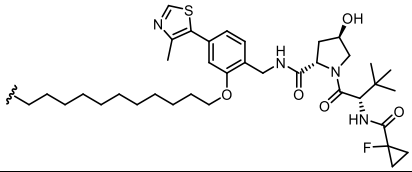	Failed reaction Expected *m/z* 1201.7 LCMS: *m/z* 1195.5, purity 55%
129	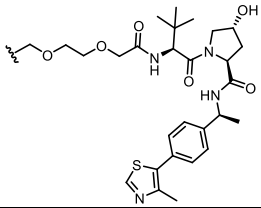	Failed reaction Expected *m/z* 1075.6 LCMS: *m/z* 1071.6, purity 37%
130	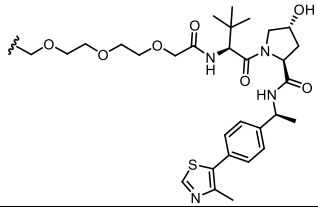	Failed reaction Expected *m/z* 1119.6 LCMS: *m/z* 1115.5, purity 46%
131	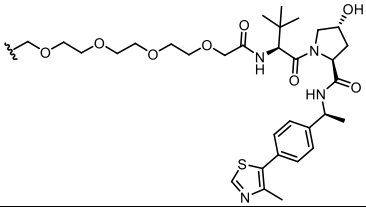	Failed reaction Expected *m/z* 1162.6 LCMS: *m/z* 1159.5, purity 36%
132	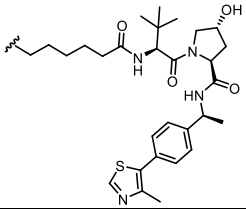	4.2 mg isolated, purity 39% Compound was not biologically tested

133	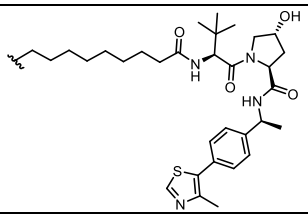	3.7 mg isolated, purity 50% Compound was not biologically tested

3.3.3 – Synthesis of PROTACs Using Piperidine-Modified **Inobrodib** Ligand **86**

Amide couplings between piperidine-modified **Inobrodib** ligand **86** and E3 ligase ligand-linker compounds afforded PROTACs **134 – 146** in moderate yields of 39 – 63% other than PROTAC **145** which was obtained in a 5% yield (Scheme 21 and Table 8). Overall, 13 novel CREBBP and p300-targeting PROTACs (**134 – 146**) were synthesised using ligand **87** and their ability to degrade CREBBP and/or p300 will be evaluated in Chapter 5. Each of these PROTACs target the E3 ubiquitin ligase enzyme cereblon for recruitment using a **thalidomide**-derivative, other than PROTAC **146** which targets VHL using ligand **VH101**.[14,15] The cereblon-targeting PROTACs **134 – 144** comprise flexible PEG and alkyl linkers of different lengths, which bind the 4'-position of **thalidomide**, as well as more rigid linkers which bind either **pomalidomide** or **lenalidomide** at the 5'-position.

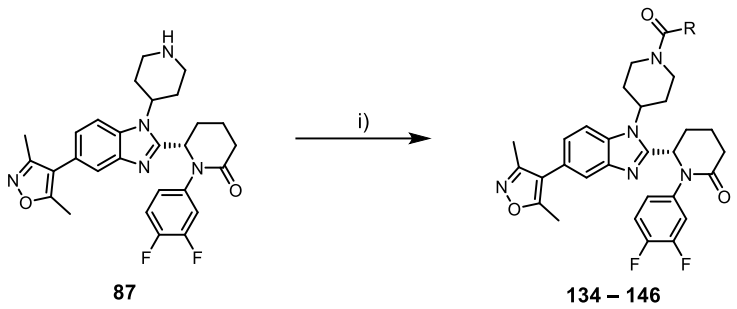

Scheme 21. General synthesis of PROTACs **134 – 146** using amide coupling reactions between ligand **87** and carboxylic acid functionalised linker-E3 ligase ligand compounds. *Reagents and conditions*: i) R-CO_2H, HATU, DIPEA, DMF, rt, 2 – 18 h, for R groups and results, see Table 8.

Table 8. Results of amide couplings between ligand **87** and E3 ligase ligand compounds R-CO_2H (Scheme 21). Purity values were measured using LCMS, formic acid method.

Cpd.	R Group Structure	Result
134	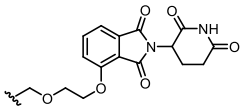	7.4 mg, 8.6 µmol, yield 43%, purity 99%
135	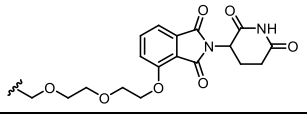	17.3 mg, 18.0 µmol, yield 59%, purity 92%
136	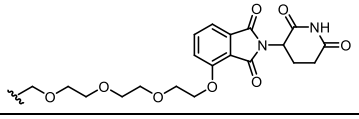	9.9 mg, 10 µmol, yield 53%, purity 100%
137	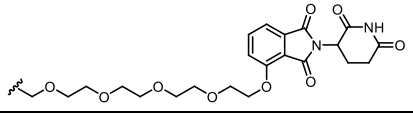	7.6 mg, 7.6 µmol, yield 39%, purity 100%
138	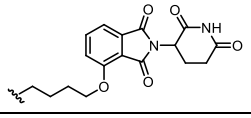	8.4 mg, 10 µmol, yield 49%, purity 100%

139	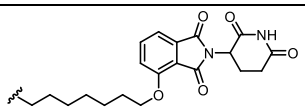	9.1 mg, 10 µmol, yield 51%, purity 100%
140	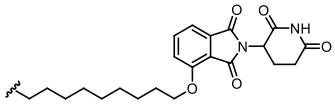	10.2 mg, 10.9 µmol, yield 55%, purity 100%
141	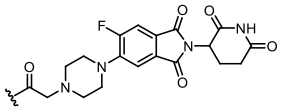	7.5 mg, 8.3 µmol, yield 41%, purity 98%
142	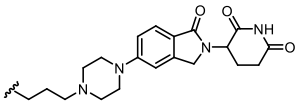	8.3 mg, 9.2 µmol, yield 46%, purity 98%
143	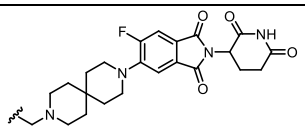	12.1 mg, 12.4 µmol, yield 63%, purity 100%
144	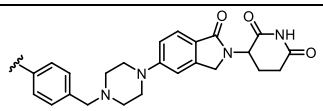	9.6 mg, 10 µmol, yield 44%, purity 87%
145	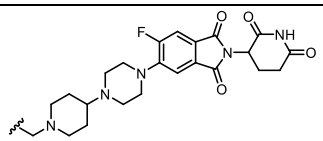	1.1 mg, 1.1 µmol, yield 5%, purity 97%
146	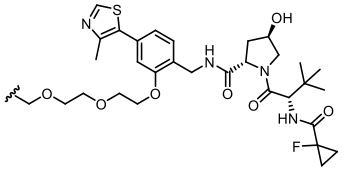	17.9 mg, 15.3 µmol, yield 52%, purity 100%

3.3.4 – Synthesis of PROTACs Using Ethyl Piperazine-Modified **Inobrodib** Ligand **106**

PROTACs recruiting both cereblon and VHL were synthesised from ethyl piperazine-modified **Inobrodib** ligand **106** (Scheme 22 and Table 9). Amide couplings using cereblon ligand-linker compounds afforded the desired PROTACs **147** – **157** in yields of 31 – 51% while PROTAC **158** degraded following purification using a high pH method, likely due to the instability of the glutarimide ring to basic aqueous conditions.[145]

Amide couplings between ligand **106** and VHL ligand-linker compounds for PROTACs **159** – **170** were more varied in their outcomes. For PROTACs **159** and **165** – **167**, after stirring at room temperature for 17 h, LCMS analysis showed negligible or no desired product formation with remaining ligand **106** and carboxylic acid starting materials. The temperatures of the reaction mixtures were increased to 50 °C for 6 h but no reaction evolution was detected using LCMS, and no desired products were obtained following MDAP purification. The other VHL-targeting PROTACs **160** – **164** and **168** – **170** were obtained in yields of 11 – 56%.

Overall, 19 novel CREBBP and p300-targeting PROTACs (**147 – 157, 160 – 164**, and **168 – 170**) were synthesised in sufficient quantities and purities using ligand **106** and their ability to degrade CREBBP and/or p300 will be investigated in Chapter 5. These PROTACs either recruit cereblon, using a **thalidomide**-derivative, or VHL using, **VH101** or **VH032**, and investigate different linker lengths, linker structures, and E3 ligase exit vectors.[14,15,25]

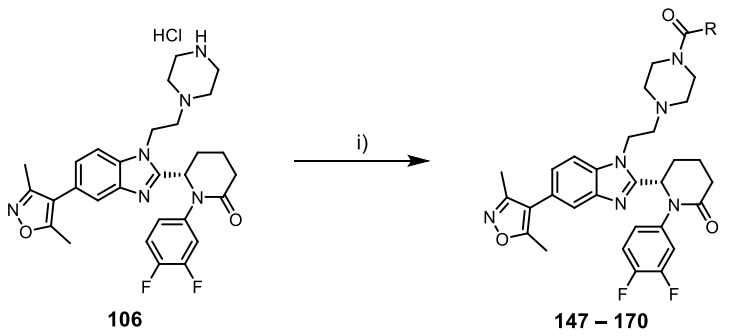

Scheme 22. General synthesis of PROTACs **147 – 157**, **160 – 164**, and **168 – 170** and the attempted synthesis of PROTACs **158**, **159**, **165 – 167** using amide coupling reactions between ligand **106** with carboxylic acid functionalised linker-E3 ligase ligand compounds. *Reagents and conditions*: i) R-CO_2H, HATU, DIPEA, DMF, rt, 2 – 20 h, for R groups and results, see Table 9.

Table 9. Results of amide couplings between ligand **106** and E3 ligase ligand compounds R-CO_2H (Scheme 22). Purity values were obtained using LCMS, formic acid method unless otherwise stated.

Cpd.	R Group Structure	Result
147	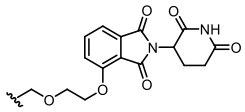	5.1 mg, 5.7 µmol, yield 31%, purity 100%
148	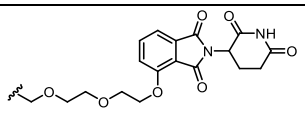	12.7 mg, 13.6 µmol, yield 50%, purity 84%
149	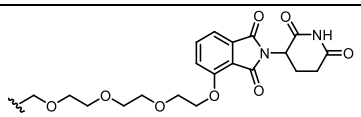	6.3 mg, 6.4 µmol, yield 34%, purity 100%
150	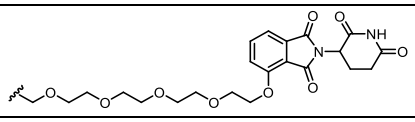	9.6 mg, 9.4 µmol, yield 48%, purity 96%
151	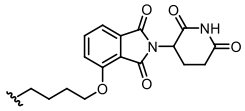	7.0 mg, 7.9 µmol, yield 42%, purity 100%
152	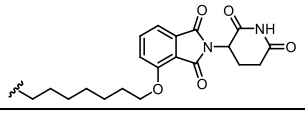	7.8 mg, 8.4 µmol, yield 44%, purity 99%
153	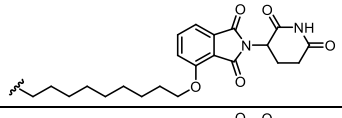	7.2 mg, 7.5 µmol, yield 37%, purity 96%
154	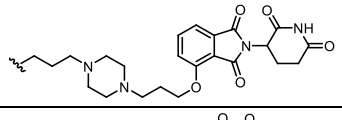	6.3 mg, 6.3 µmol, yield 34%, purity 100%
155	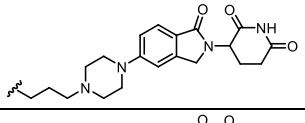	11.4 mg, 12.2 µmol, yield 65%, purity 100%
156	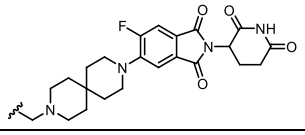	9.4 mg, 9.4 µmol, yield 50%, purity 100%
157	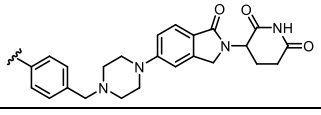	9.9 mg, 10 µmol, yield 51%, purity 95%

158	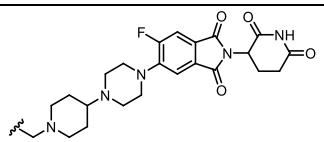	Degradation during purification 4.5 mg isolated, purity 9% (HpH)
159	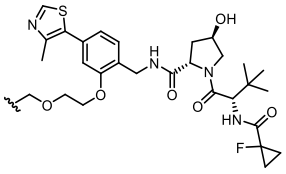	Failed reaction LCMS: *m/z* 576.7 $[M+2H]^{2+}$, purity 1% Purification: no product isolated
160	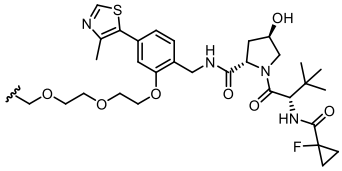	17.6 mg, 14.7 µmol, yield 56%, purity 99%
161	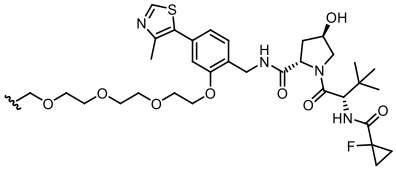	10.4 mg, 8.39 µmol, yield 42%, purity 94%
162	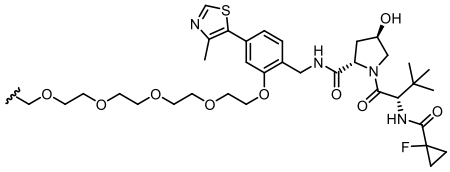	2.6 mg, 2.0 µmol, yield 11%, purity 99%
163	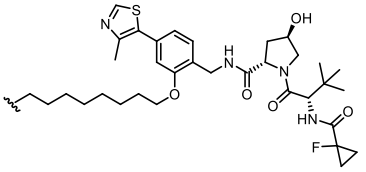	10.6 mg, 8.79 µmol, yield 47%, purity 100%
164	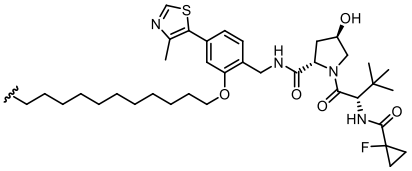	10.9 mg, 8.74 µmol, yield 47%, purity 100%
165	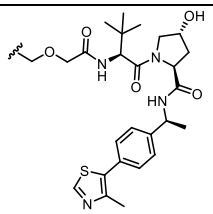	Failed reaction LCMS: no desired product formation Purification: no product isolated
166	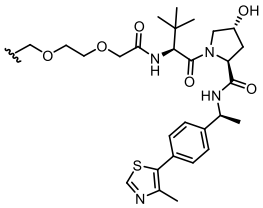	Failed reaction LCMS: *m/z* 561.7 $[M+2H]^{2+}$, 2% Purification: no product isolated
167	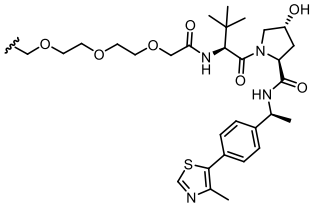	Failed reaction LCMS: *m/z* 583.7 $[M+2H]^{2+}$, 10% Purification: no product isolated

168	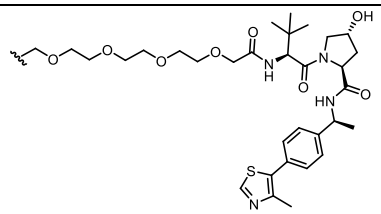	9.7 mg, 8.02 µmol, yield 42%, purity 99%
169	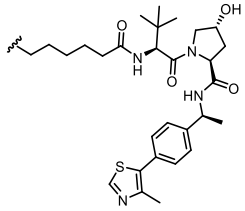	3.9 mg, 3.5 µmol, yield 18%, purity 94%
170	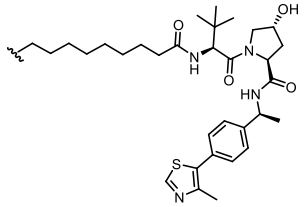	5.1 mg, 4.5 µmol, yield 23%, purity 96%

3.3 – Higher Throughput PROTAC Synthesis Conclusions

Chapter 2 described the synthesis of eight novel PROTACs (four of which were synthesised by Dr Pascal Heitel) and four novel HyTs. The synthesis of these compounds was hindered by a multistep, linear synthesis where the different PROTAC linkers needed to be incorporated onto the CREBBP and p300 ligand at an early stage in the synthetic route.

This chapter investigated streamlining the synthetic process for obtaining final PROTAC molecules, which enabled 42 novel PROTACs to be synthesised using three different CREBBP and p300-targeting ligands. This was achieved by functionalising the ligands **86**, **87**, and **106** with amine groups to enable PROTACs to be synthesised in a final amide coupling step. These amide coupling reactions were aided by access to GSK's equipment and their library of E3 ligase ligands functionalised with a variety of carboxylic acid-terminal linkers.

The CREBBP and p300 ligands (**86**, **87**, and **106**) developed for this series of amide linked PROTACs investigate two distinct exit vectors from the bromodomain binding site (discussed in Section 3.1) and the E3 ligase ligands similarly explore different linker attachment positions. Additionally, the final PROTACs (**112 – 122**, **134 – 157**, **160 – 164**, and **168 – 170**) comprise linkers of different structures and lengths with the aim of installing structural diversity into the final compounds. As discussed in Sections 1.1.4 and 1.1.5, PROTAC potencies and selectivities result from the formation of stabilising interactions within the POI:PROTAC:E3 ligase ternary complex. Therefore, evaluation of a diverse range of PROTACs will increase the chances of finding a potent or potentially selective degrader or CREBBP and/or p300. Additionally, the results from the biological evaluation of these compounds in Chapter 5 could give insights into the PROTAC structural features required for ternary complex formation and could help to guide future optimisation.

Chapter 4 – Optimisation of a Higher Throughput *in vitro* Assay for Assessing the Abilities of the Amide-Series of PROTACs to Induce the Degradation of CREBBP and/or p300

4.1 – Immunoassay Design

4.1.1 – Capillary Electrophoresis Immunoassay

Work in Chapter 4 was conducted during an industrial placement at GSK, Stevenage under the guidance Jenni Cryan and supervision of Dr John Harling.

Having synthesised a range of PROTACs in Chapter 3, it was necessary to evaluate their ability to degrade CREBBP and p300. Traditionally, the ability of PROTACs to degrade their target POI(s) is evaluated using western blotting, as for work in Chapter 2. However, this low-throughput technique can cause a bottleneck in the discovery of PROTACs due to the large samples of cell lysate required, multiple steps, and long workflows. Therefore, western blotting was deemed poorly suited to assessing the activities of the 42 novel CREBBP and p300-targeting PROTACs synthesised in Chapter 3 and, instead, a higher throughput automated capillary electrophoresis immunoassay was used.

Capillary electrophoresis immunoassays function in a similar manor to western blots, except the workflow occurs within a single capillary using reagents that have been pre-distributed into a 384-well plate (Figure 33a).[181,182] First, the capillaries are loaded with the stacking and separation matrices, the cell lysate sample is loaded, and the proteins are separated according to size by electrophoresis. The separated proteins are then immobilised to the capillary walls by UV irradiation, and the matrices are washed away. The system then sequentially flows reagents through the capillary to add the POI-targeting primary antibody, secondary horseradish peroxidase (HRP)-conjugated antibody, and then the luminol HRP chemiluminescence substrate. Each immunoassay provides a chemiluminescence trace and the subsequent peak areas can be used to quantitatively measure protein abundance using the manufacturer's software.[183] Other than reagent setup, the assay is fully automated and an overnight run can assess eight cycles comprising 11 immunoassays each (88 immunoassays total), greatly enhancing throughput compared to western blotting. Additionally, the capillary electrophoresis immunoassay only requires loading of 0.6 – 1.2 µg total protein amounts, which is far lower than the 30 µg total protein

used for the western blotting described in Chapter 2. This enables the cell work to be performed on a miniaturised scale, using 384-well plates and liquid handling machinery, which further acts to enhance assay throughput.

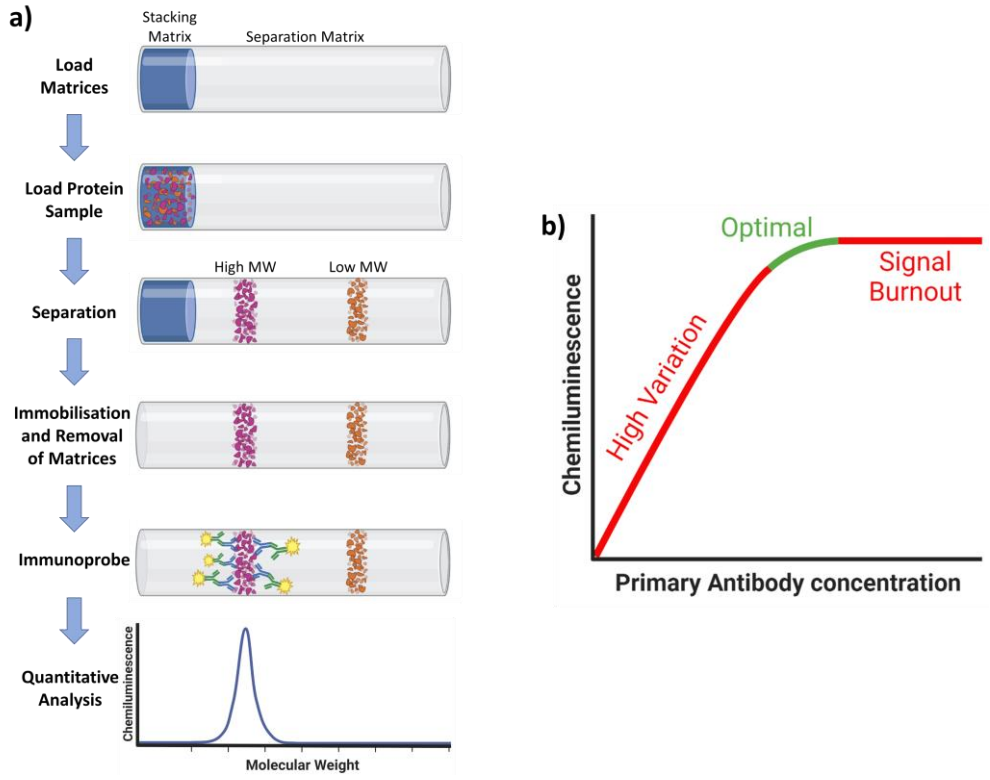

Figure 33. a) Capillary electrophoresis immunoassay workflow. The stacking matrix and separation matrix are loaded into the capillary and then the protein sample is loaded and separated by size using electrophoresis. The proteins are immobilised to walls of the capillary tube by irradiation with UV and the stacking and separation matrices are removed. The automated system then sequentially flows the POI-targeting primary antibody, the HRP-conjugated secondary antibody, and the luminol substrate for HRP through the capillary creating a chemiluminescent signal which can be quantified. Image created using BioRender (www.biorender.com) and was adapted from figure by Valerie M. Harris.[181] **b)** Relationship between chemiluminescence signal and the concentration of the POI-targeting primary antibody. As the primary antibody concentration increases, binding to the immobilised POI in the capillary will increase and there will be a downstream increase in chemiluminescence. At lower concentrations of primary antibody, any variation of primary antibody concentration or amount of POI will have a large effect on the chemiluminescence signal. At higher concentrations of primary antibody, the POI will become saturated, and the signal can exhibit burnout. Therefore, the optimal concentration of primary antibody is at the point near POI saturation. The same relationship is observed for POI concentration. Image created using BioRender (www.biorender.com).

To use such an immunoassay for measuring CREBBP and p300 levels in cell lysate, the assay parameters were first optimised. To achieve accurate measurements, the chemiluminescence signal should reach near saturation for untreated cells. This eliminates chemiluminescent signal burnout which results from high concentrations of HRP bound to the target protein, and minimises signal variation from lower protein-bound HRP concentrations that arise from small changes in protein or primary antibody concentrations (Figure 33b).[181,182,184] The HRP-conjugated secondary antibody concentration is fixed so the chemiluminescent signal intensity can be modified by changing the amount of primary

antibody bound to the POI in the capillary. This can be achieved by altering the primary antibody concentration or the amount of protein loaded into the assay.

During optimisation, combinations of different protein and primary antibody concentrations were investigated, and representative examples are described in the following sections of this chapter. Due to the large number of PROTACs to be analysed, it would not be efficient to individually evaluate the protein concentration of individual cell lysate samples, like for the western blots performed in Chapter 2. Instead, protein loading was optimised by altering the number of cells used in the cellular assays. A 384-well plate was seeded with a range of known cells densities and by extension, a range of total protein concentrations, then the optimal protein loading was assessed by using a set volume of the different cell lysate samples. Cells were not seeded at a density of $<0.01\times10^6$ cells/well because of the variability that could be introduced from using such a small number of cells, for example, by the displacement of cells during washing steps. Technical repeats refer to experiments which were performed in individual capillaries in the same immunoassay cycle using different cell lysate samples of equal cell densities.

4.1.2 – Immunoassay Parameter Optimisation

4.1.2.1 – Vinculin Loading Control Signal Optimisation

Vinculin was selected as the protein loading standard, as opposed to previously used β-actin, because its higher molecular weight (MW) was within the immunoassay detection range of 66 – 440 kDa (vinculin MW = 124, β-actin MW = 42 kDa).[185,186]. A vinculin-targeting rabbit (Rb) primary monoclonal antibody (mAb) that has been validated for similar assays in the group was used but, first, its dilution required optimisation.

High intensity chemiluminescence signals were obtained when using the vinculin-targeting mAb even at the highest tested dilution of 1:500 (Figure 34). At higher protein levels, the signals exhibit burnout as indicated by peak splitting (Figure 34a). Using a 1:2 dilution of 0.01×10^6 cells/ well lysate and 1:500 dilution of vinculin-targeting mAb produced a smooth, narrow peak, with no signal burnout (Figure 34e). Overlaying the chemiluminescence traces of three technical repeats shows a high signal overlap and indicates that these conditions will be effective for measuring vinculin levels in the PROTAC screening immunoassays (Figure 34f).

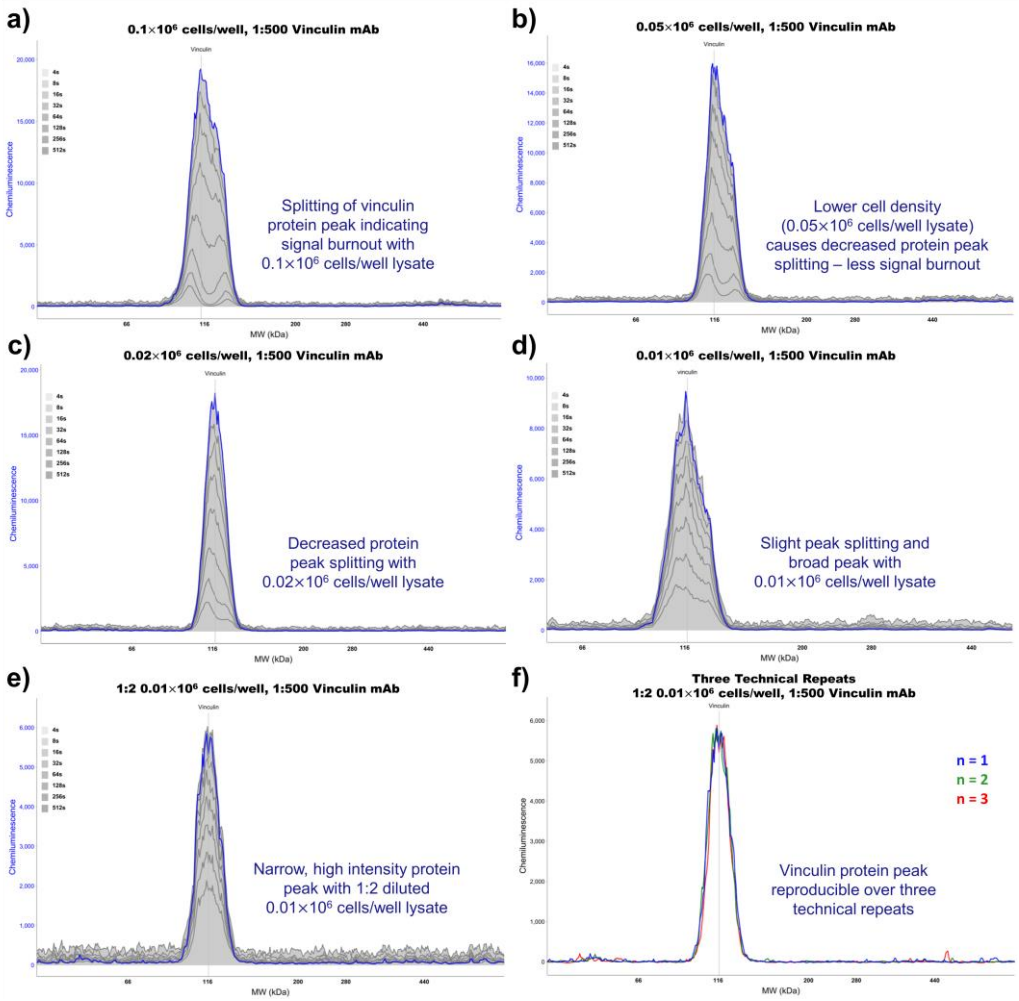

Figure 34. Optimisation of protein concentration and primary antibody dilution for detection of the vinculin loading control. **a)** Chemiluminescence signal using cell lysate from 0.1×10^6 cells/well sample and 1:500 vinculin-targeting primary mAb showing signal burnout. **b)** Chemiluminescence signal using cell lysate from 0.05×10^6 cells/well sample and 1:500 vinculin-targeting primary mAb showing signal burnout. **c)** Chemiluminescence signal using cell lysate from 0.02×10^6 cells/well sample and 1:500 vinculin-targeting primary mAb showing signal burnout. **d)** Chemiluminescence signal using cell lysate from 0.01×10^6 cells/well sample and 1:500 vinculin-targeting primary mAb showing signal burnout. **e)** Chemiluminescence signal using 1:2 diluted cell lysate from 0.01×10^6 cells/well sample and 1:500 vinculin-targeting primary mAb showing a smooth, narrow peak with no burnout. **f)** Overlay of the chemiluminescence signals from three technical repeats using 1:2 diluted cell lysate from 0.01×10^6 cells/well sample and 1:500 vinculin-targeting primary mAb showing high signal overlap between the repeats.

4.1.2.2 – CREBBP Signal Optimisation

The Simple Western™ Antibody Database was used to select primary antibodies to target CREBBP and p300 for the automated immunoassays.[187] The database recommended the same CREBBP-targeting primary mAb was used for western blotting in Chapter 2 so this was selected and the optimal mAb dilution was investigated.

A wide range of mAb dilutions were examined, and signals using the highest tested dilution of 1:250 are discussed (Figure 35). Assessment of 0.1×10^6 cells/well lysate, displayed a very broad peak that

exhibited signal burnout (Figure 35a). The signal profile improved as the cell lysate protein content decreased, where a high intensity peak with no signal burnout and a more symmetrical shape was obtained when using 1:2 diluted 0.01×10^6 cells/well lysate with 1:250 dilution of CREBBP-targeting mAb. This result was reproducible over three technical repeats (Figure 35e–f).

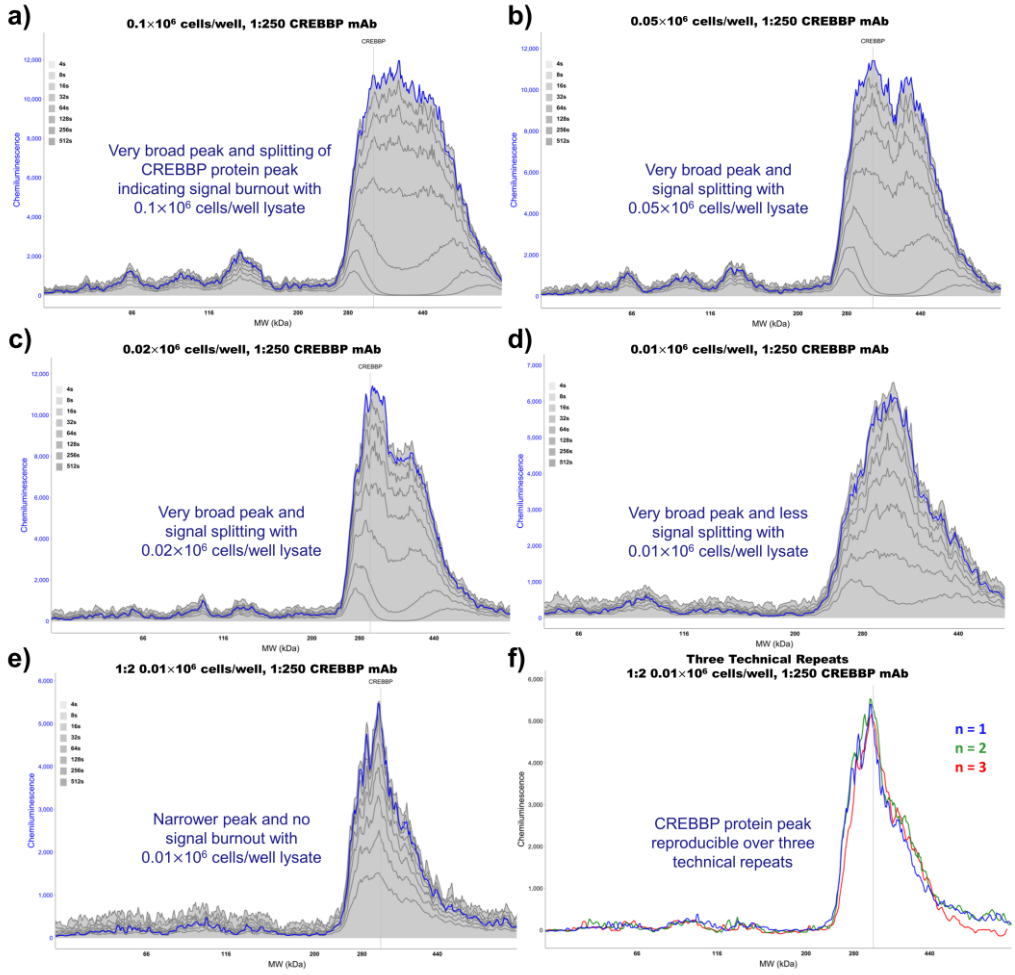

Figure 35. Optimisation of protein concentration and primary antibody dilution for detection of CREBBP. **a)** Chemiluminescence signal using cell lysate from 0.1×10^6 cells/ well sample and 1:250 CREBBP-targeting primary mAb showing signal burnout. **b)** Chemiluminescence signal using cell lysate from 0.05×10^6 cells/well sample and 1:250 CREBBP-targeting primary mAb showing signal burnout. **c)** Chemiluminescence signal using cell lysate from 0.02×10^6 cells/well sample and 1:250 CREBBP-targeting primary mAb showing signal burnout. **d)** Chemiluminescence signal using cell lysate from 0.01×10^6 cells/well sample and 1:250 CREBBP-targeting primary mAb showing signal burnout. **e)** Chemiluminescence signal using 1:2 diluted cell lysate from 0.01×10^6 cells/well sample and 1:250 CREBBP-targeting primary mAb showing a broad peak with a slight shoulder. **f)** Overlay of the chemiluminescence signals from three technical repeats using 1:2 diluted cell lysate from 0.01×10^6 cells/well sample and 1:250 CREBBP-targeting primary mAb showing high signal overlap between the repeats.

4.1.2.3 – Multiplexing Vinculin with CREBBP and Normalisation of the CREBBP Signal

To enable the cellular levels of CREBBP to be standardised against the vinculin loading control, the primary antibodies targeting CREBBP and vinculin were combined at their optimised dilutions of 1:250 and 1:500, respectively, and tested using 1:2 diluted 0.01×10^6 cells/well lysate (Figure 36). This

multiplexing of the primary antibodies means that the immunoassay trace will give two peaks (one for each protein) and allows the CREBBP peak area to be directly quantified relative to the vinculin peak area to calculate the relative CREBBP level in the cell lysate sample.

Over 11 technical repeats, no signal burnout was observed, but some variation was visible when overlaying the chemiluminescence traces (Figure 36b). Compass for Simple Western™ software was used to measure the area beneath each protein peak and to normalise the CREBBP signal relative to the corresponding vinculin signal. Calculating the % CREBBP area (normalised to vinculin) relative to the mean of the 11 repeats shows ten values to be within 10% of the mean (Figure 36c, ces

Appendix Table 10), therefore these assay conditions were deemed suitable for analysing the abilities of the PROTACs synthesised in Chapter 3 to induce the degradation of CREBBP.

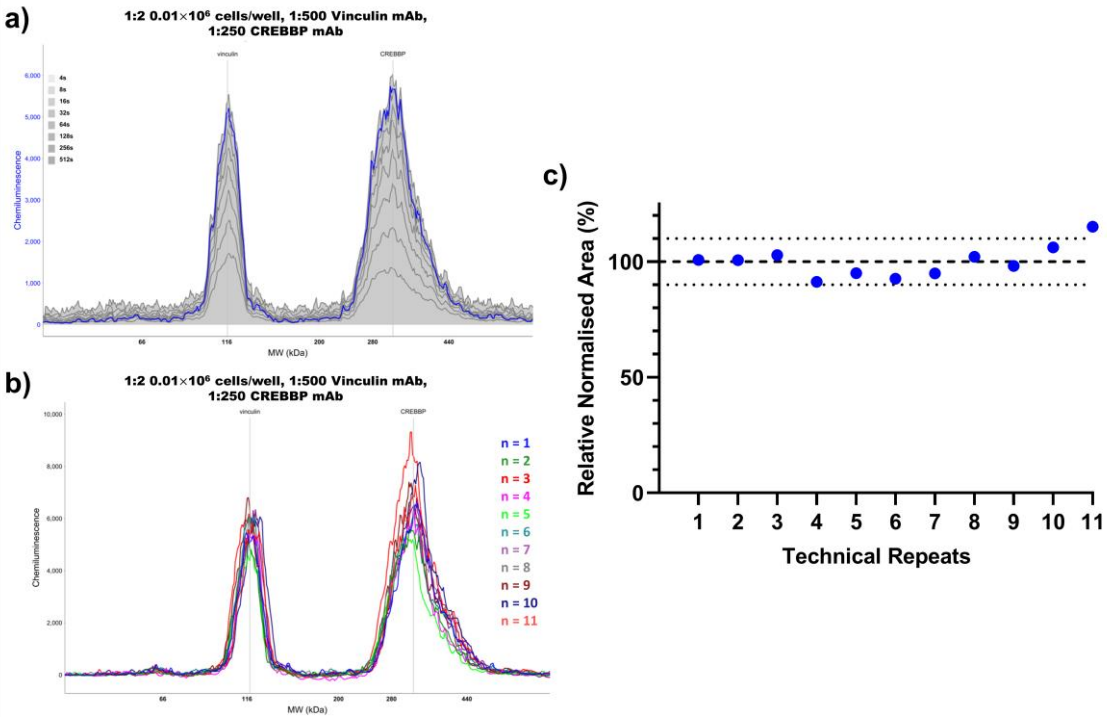

Figure 36. Multiplexing 1:500 vinculin-targeting primary mAb and 1:250 CREBBP-targeting primary mAb to enable cellular CREBBP levels to be standardised against the vinculin loading control levels. **a)** Representative chemiluminescence signals using 1:2 diluted 0.01×10^6 cells/well lysate and 1:500 vinculin-targeting primary mAb and 1:250 CREBBP-targeting primary mAb. **b)** Overlay of the chemiluminescence signals from 11 technical repeats using 1:2 diluted cell lysate from 0.01×10^6 cells/well sample and 1:500 vinculin-targeting primary mAb and 1:250 CREBBP-targeting primary mAb **c)** Plot of the vinculin- normalised CREBBP peak area for 11 technical repeats relative to the mean value (blue circles). Relative normalised area is given as a % value compared to the calculated mean of the 11 technical repeats (ces

Appendix **Table 10**). The CREBBP signal area was normalised against the corresponding vinculin signal using Compass for Simple Western™. The mean was calculated using Excel. The normalised area of each CREBBP signal relative to the mean was calculated in excel as follows: (100×normalised CREBBP area)/mean. 100% relative normalised area is depicted as a dashed line (and is equivalent to the mean). 90% and 110% relative normalised areas are depicted as dotted lines.

4.1.2.6 – p300 Signal Optimisation and Antibody Selection

The Simple Western™ Antibody Database recommended to use a goat (Gt) mAb to target p300 in the automated immunoassay.[187] A different, Rb mAb was used for the western blot assays discussed in Chapter 2 so it was decided to investigate the use of both of these antibodies for use in the capillary electrophoresis immunoassay and then select the best performing mAb for the degradation assays.

The p300-targeting Rb mAb used in previous work (Chapter 2) produced a very broad, poorly resolved peak of low intensity for all cell densities and antibody dilutions tested (Figure 37). Using 1:250 antibody dilution as a representative example, the signal shape could be improved by decreasing the total protein concentration. However, the chemiluminescence signal was low in intensity making it ill-suited as a red-out for p300 degradation, as decreases in the protein signal could be lost into the baseline noise (Figure 37a–d). Decreasing the primary antibody dilution to 1:10 marginally improved the signal intensity but resulted in peak broadening (Figure 37e).

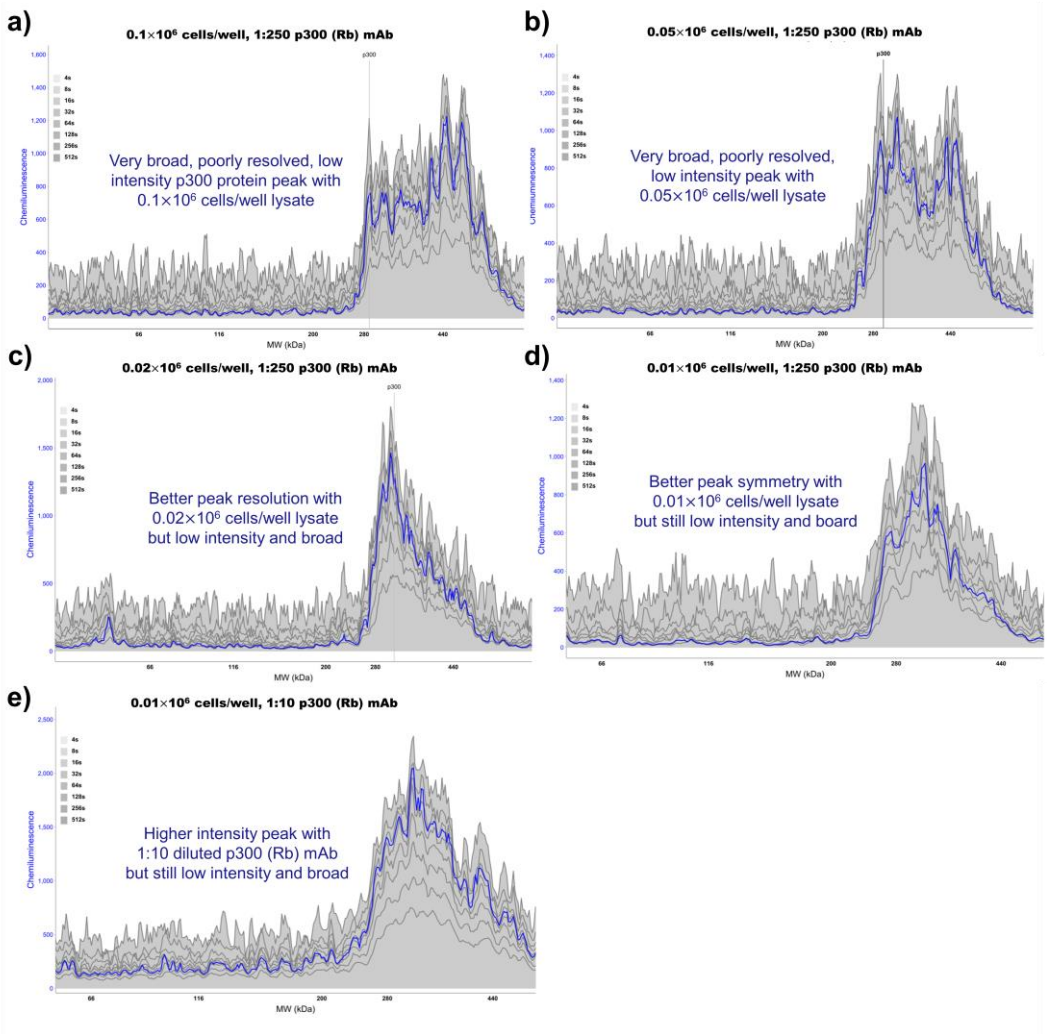

Figure 37. Investigation into the use of rabbit (Rb) p300-targeting primary antibody for immunoassays. **a)** Chemiluminescence signal using cell lysate from 0.1×10^6 cells/well sample and 1:250 p300-targeting primary antibody (Rb) showing weak, broad, unresolved peak. **b)** Chemiluminescence signal using cell lysate from 0.05×10^6 cells/well sample and 1:250 p300-targeting primary antibody (Rb) showing weak, broad, unresolved peak. **c)** Chemiluminescence signal using cell lysate from 0.02×10^6 cells/well sample and 1:250 p300-targeting primary antibody (Rb) showing sharper peak but still with low signal intensity. **d)** Chemiluminescence signal using cell lysate from 0.01×10^6 cells/well sample and 1:250 p300-targeting primary antibody (Rb) showing weak, broad peak. **e)** Chemiluminescence signal using cell lysate from 0.01×10^6 cells/well sample and 1:10 p300-targeting primary antibody (Rb) showing weak, broad peak.

Investigating the Simple Western™ Antibody Database recommended p300-targeting Gt mAb using 0.02×10^6 cells/well lysate, gave negligible signal at for 1:250 mAb dilution but caused signal burnout at 1:10 mAb dilution (Figure 38a–b). Decreasing the lysate cell density to the 0.01×10^6 cells/well sample and using 1:10 p300-targeting Gt mAb created a peak of higher intensity than the corresponding signal using 1:10 p300-targeting Rb mAb (Figure 38c–d). The signal peak could be sharpened by modifying the assay run times to have a shorter stacking and longer separation time, and these results were reproducible over 11 technical repeats (Figure 38e–f).

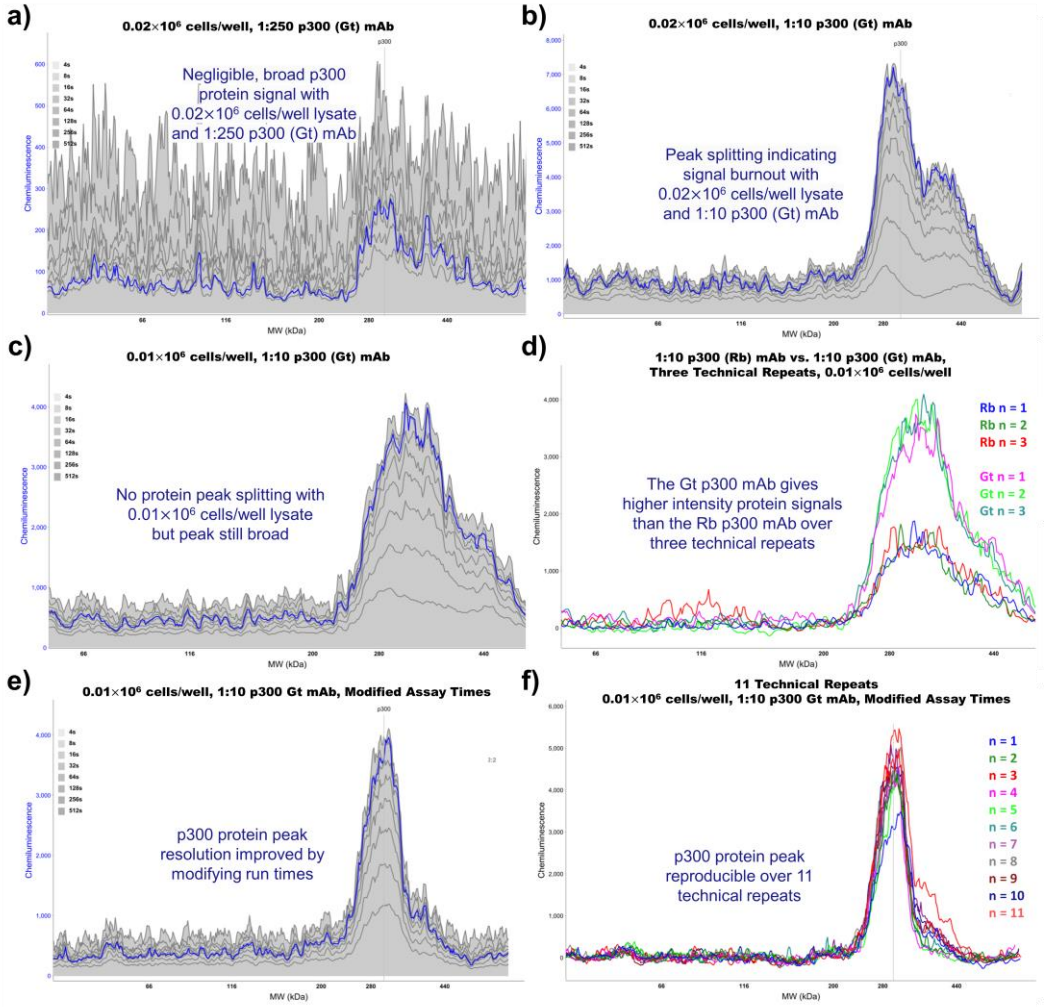

Figure 38. Investigation into the use of goat (Gt) p300-targeting primary mAb for immunoassays. **a)** Chemiluminescence signal using cell lysate from 0.02×10^6 cells/ well sample and 1:250 p300-targeting primary mAb (Gt) showing very weak signal. **b)** Chemiluminescence signal using cell lysate from 0.02×10^6 cells/ well sample and 1:10 p300-targeting primary mAb (Gt) showing signal burnout. **c)** Chemiluminescence signal using cell lysate from 0.01×10^6 cells/ well sample and 1:10 p300-targeting primary mAb (Gt) showing a strong, broad peak. **d)** Overlay of the chemiluminescence signals from three technical repeats using 1:2 diluted cell lysate from 0.01×10^6 cells/ well sample and either Rb or Gt 1:10 p300-targeting primary antibody showing high signal overlap between the repeats and a stronger signal when using the Gt mAb. **e)** Chemiluminescence signal using cell lysate from 0.01×10^6 cells/ well sample and 1:10 p300-targeting primary mAb (Gt) using modified assay timings showing strong, narrow peak. **f)** Overlay of the chemiluminescence signals from 11 technical repeats using 1:2 diluted cell lysate from 0.01×10^6 cells/ well sample and Gt 1:10 p300-targeting primary mAb (Gt) using modified assay timings showing high signal overlap between the repeats.

4.1.2.7 – Multiplexing Vinculin with p300 and Normalisation of the p300 Signal

The p300-targeting Gt mAb could achieve higher intensity peaks than the Rb mAb so was used for further assay development. Gt antibodies are not compatible with the standard diluent used for the automated immunoassays and instead must be diluted using a milk-free diluent and the assay should be run using milk-free conditions. To multiplex the p300-targeting Gt mAb with vinculin, first the compatibility of the vinculin-targeting Rb mAb with the milk-free diluent was investigated, and an

increase in the peak intensity was observed compared to using the standard diluent over three technical repeats (Figure 39a). The p300 (Gt) and vinculin primary mAbs were multiplexed at their optimised dilutions (1:500 vinculin-targeting mAb, 1:10 p300-targeting mAb) using the modified assay run times, however, negligible signal was detected for p300 (Figure 39b). Multiplexing the p300-targeting mAb with different dilutions of the vinculin-targeting mAb, similarly, resulted in negligible p300 detection (Figure 39c). It transpired that the anti-Rb secondary antibody is derived from a goat. Therefore, the anti-Gt secondary antibody will bind the anti-Rb secondary antibody in the multiplexed solution, making it unavailable to bind p300 via the primary antibody in the assay, resulting in no p300 signal being detected.

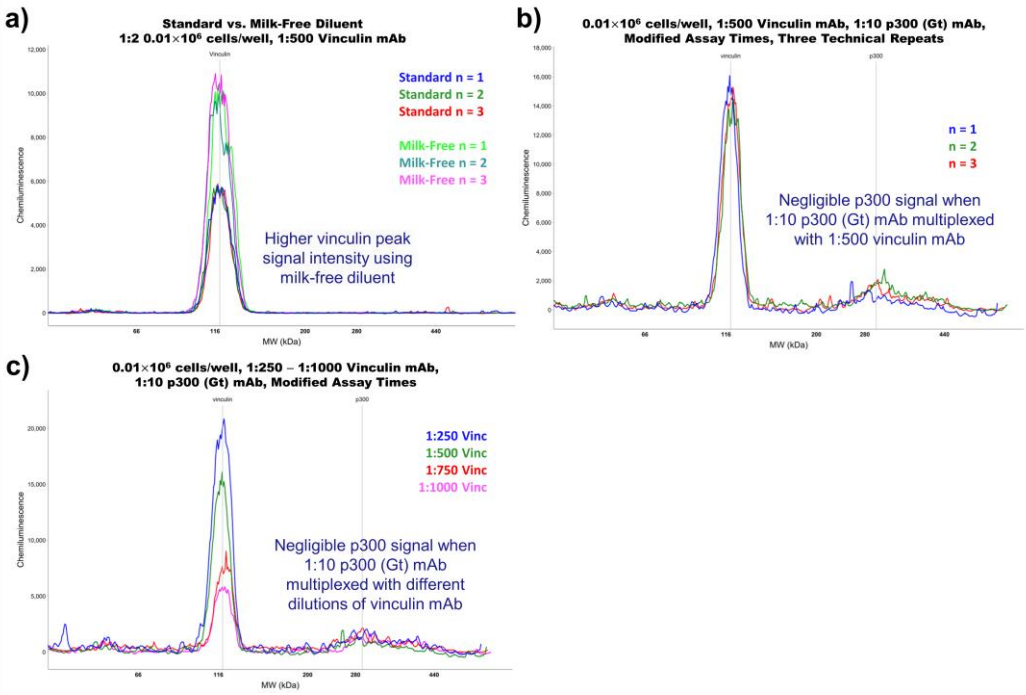

Figure 39. Investigation into multiplexing the p300-targeting Gt mAb and the vinculin-targeting Rb mAb. **a)** Overlay of vinculin chemiluminescence signals for three technical repeats using a 1:500 dilution of the vinculin-targeting mAb in either the standard diluent or a milk-free diluent using lysate from 0.01×10^6 cells/well samples. A higher chemiluminescence signal is observed when the milk-free diluent was used. **b)** Overlay of the chemiluminescence signals for three technical repeats using multiplexed 1:500 vinculin-targeting Rb mAb and 1:10 p300-targeting Gt mAb in milk-free diluent and using lysate from 0.01×10^6 cells/well samples. A strong, narrow peak is detected for vinculin but a very low intensity, broad peak is observed for p300. **c)** Overlay of the chemiluminescence signals when 1:10 p300-targeting Gt mAb was multiplexed with either 1:250, 1:500, 1:750, or 1:100 vinculin-targeting Rb mAb in milk-free diluent and using lysate from 0.01×10^6 cells/well samples. For all examples, a strong, narrow peak is detected for vinculin but a very low intensity, broad peak is observed for p300.

Due to the undesired interactions between the multiplexed secondary antibodies, it was decided to normalise p300 levels relative to the vinculin peak area in the corresponding CREBBP run. Both proteins would be assessed using the same cell lysate sample, but the sample would be diluted 1:2 for CREBBP and vinculin detection, by the addition of RIPA buffer to the assay reagent 384-well plate. Similar to the results for CREBBP, over 11 technical repeats there is some variation in chemiluminescence signal overlap (Figure 40a). To assess signal variation, each p300 signal area was normalised to the vinculin signal area in the corresponding CREBBP trace, and a mean value was calculated. Normalising each signal relative to the mean value showed 9 of the 11 normalised areas to be within 10% of the mean (Figure 40, ces

Appendix Table 10). Therefore, these conditions were deemed appropriate for analysing the abilities of the PROTACs synthesised in Chapter 3 to degrade p300 in the screening immunoassay.

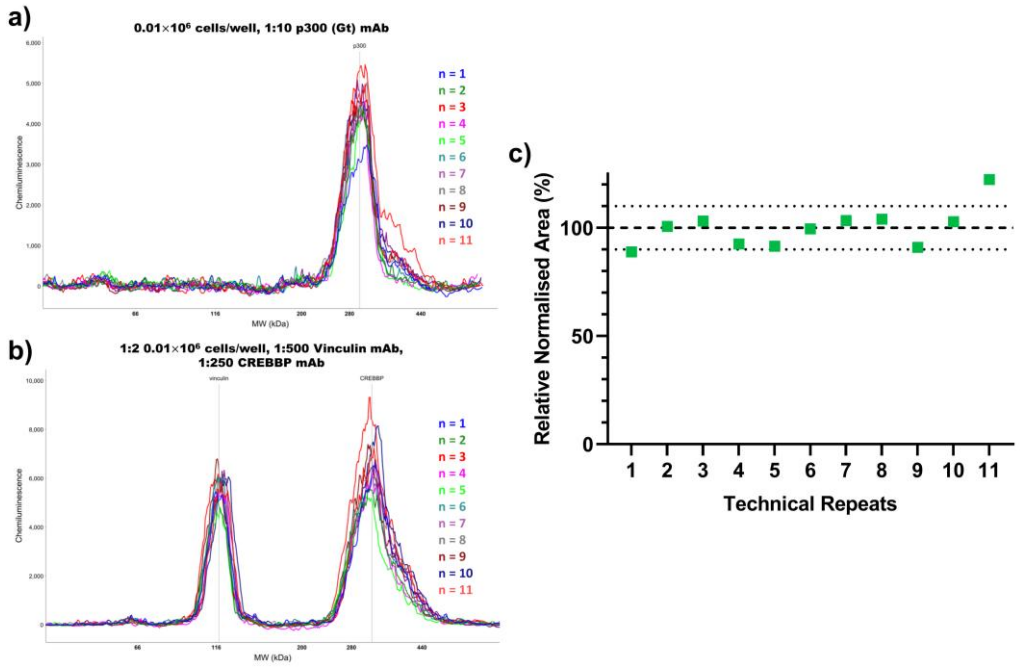

Figure 40. Standardisation of cellular p300 levels using the corresponding vinculin signal from the CREBBP run. Corresponding immunoassays used the same 0.01×10^6 cells/well lysate samples but vinculin is analysed by diluting the lysate 1:2 with RIPA buffer and p300 is analysed using neat lysate. **a)** Overlay of the chemiluminescent signals of 11 technical repeats using 1:10 p300-targeting primary mAb showing high signal overlap. The p300 signal areas were obtained using Compass for Simple Western™ software. **b)** Overlay of the chemiluminescent signals of 11 technical repeats using multiplexed 1:500 vinculin-targeting primary mAb and 1:250 CREBBP-targeting primary mAb showing high signal overlap. The vinculin signal areas were obtained using Compass for Simple Western™ software. **c)** Plot of the vinculin-normalised p300 peak area for 11 technical repeats relative to mean value (green squares). Relative normalised area is given as a % value compared to the calculated mean of the 11 technical repeats (ces

Appendix **Table 10**). The p300 signal area was normalised against the vinculin signal in the corresponding CREBBP trace in excel as follows: p300 area/ vinculin area. The mean was calculated and the normalised area of each p300 signal relative to the mean was calculated in excel as follows: (100×normalised p300 area)/mean. 100% relative normalised area is depicted as a dashed line (and is equivalent to the mean). 90% and 110% relative normalised areas are depicted as dotted lines.

4.2 – Capillary Electrophoresis Immunoassay Validation Using **dCBP-1**

To validate the immunoassay conditions for being able to detect CREBBP and/or p300 degradation, the previously reported CREBBP and p300-degrading PROTAC **dCBP-1** was tested as a positive control by treating HeLa cells with a concentration gradient of 0.51 nM – 10 µM **dCBP-1** for 24 h over three biological repeats.[133] **dCBP-1**-induced degradation of CREBBP and p300 has been reported in the literature over short timepoints (≤6 h), so these validation assays will also investigate the cellular activity of **dCBP-1** following a longer incubation time.[133,134] The 24 h timepoint was selected for initial PROTAC screening because it allows sufficient time for the cells to adhere in the miniaturised cellular assay, and for any active PROTACs to induce degradation. Optimal incubation times could then be investigated in subsequent timecourse assays for any compounds identified as active.

Inspection of the immunoassay chemiluminescent signals shows a large reduction in both the CREBBP and p300 signals relative to the DMSO control over the range of 1.1 – 10 µM **dCBP-1** and the signal then recovers to the control level as the PROTAC concentration decreases towards 0.51 nM (Appendix Figure 16, Appendix Figure 17). The CREBBP and p300 signals were quantified relative vehicle (DMSO) control treated cells and the relative protein levels are reported as mean values over the three biological repeats (Figure 41, Appendix Table 11, Appendix Table 12). Assessment of the relative CREBBP levels showed a significant reduction to <10% for cells treated with **dCBP-1** concentrations ranging 370 nM – 10 µM, with a maximum reduction to 4% for cells treated with 3.3 µM **dCBP-1**. The relative CREBBP levels then increase to the control level as the concentration of **dCBP-1** decreases to 0.51 nM. Measurement of p300 cellular levels gave more variable results compared to those for CREBBP but show a significant reduction in p300 levels for cells treated with **dCBP-1** concentrations ranging 120 nM – 10 µM, which increase to the control level as the PROTAC concentration is decreased. A maximum reduction in p300 levels to 30% is achieved for both 1.1 µM and 3.3 µM **dCBP-1** treated samples. DC_{50} values were calculated from the relative protein levels vs. **dCBP-1** concentration graphs, using GraphPad Prism Software, and gave values of 34 nM and 93 nM for

CREBBP and p300, respectively. These are both 49-fold lower than DC_{50} values reported by Thomas, *et al*. for 4 h incubation **dCBP-1** in RS4;11 cells (CREBBP DC_{50} = 0.8 nM, p300 DC_{50} = 1.9 nM) which could arise from numerous differences in the assays.[134] It has been reported in the literature that the **thalidomide**-based PROTACs **dBET1** and **BSJ-03-123** cause a large reduction in POI levels for short timepoints, but that protein levels begin to increase to the control levels as the timecourse increases to 24 h.[188,189] This phenomenon has been attributed to the poor stability of **thalidomide**-derivatives at physiological pH, therefore, the reduction in **dCBP-1** potency could result from compound instability over time.[145,190]

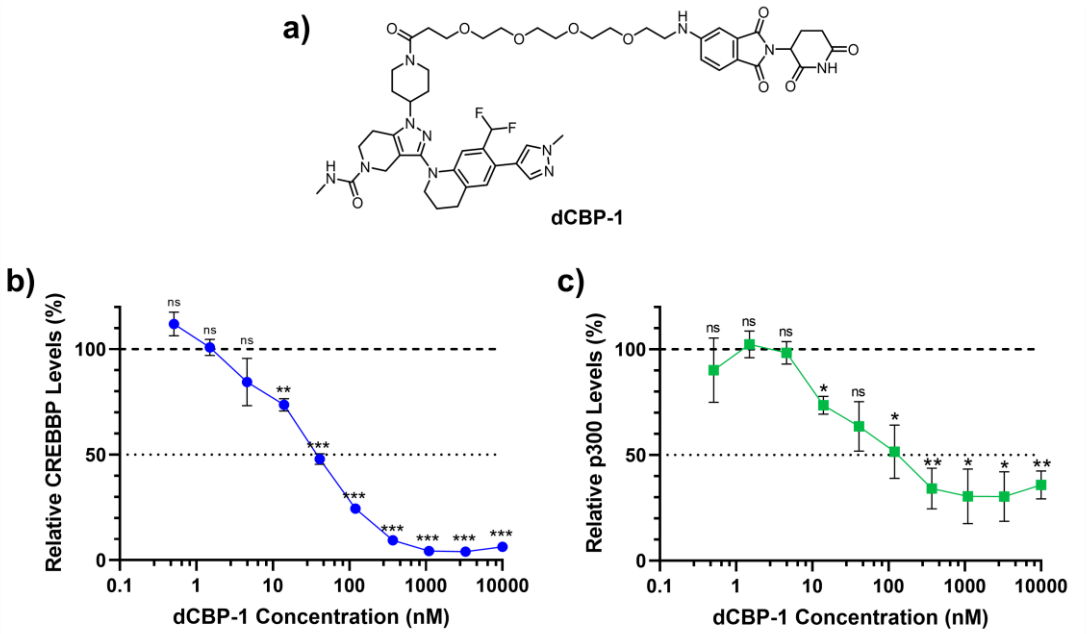

Figure 41. Assessment of the optimised capillary electrophoresis immunoassay using literature CREBBP and p300-degrading PROTAC **dCBP-1**.[133] **a)** Structure of **dCBP-1**. **b)** Quantification from the capillary electrophoresis immunoassay of the relative CREBBP protein levels (blue circles) in 1:2 diluted 0.01×10^6 HeLa cells/well treated for 24 h with a concentration gradient of dCBP-1, as indicated, with 0.625% *v/v* DMSO. Cellular assay performed as three biological repeats. Protein signal areas and vinculin-normalised CREBBP values were obtained using Compass for Protein Simple™ software. Each sample was normalised to the vinculin-normalised DMSO control, and a mean value was calculated for the relative protein level using Excel (Appendix Table 11). Data are reported as the mean relative expression over the three biological repeats and error bars are the standard error of the mean. A Student's t-test was performed relative to the DMSO control data and significance is denoted as: *** - $p \leq 0.001$, ** - $p \leq 0.01$, * - $p \leq 0.05$, n.s - not statistically significant. 100% relative protein level depicted as dashed line; 50% relative protein level depicted as dotted line. Graph created using GraphPad Prism Software. **c)** Quantification from the capillary electrophoresis immunoassay of the relative p300 protein levels (green squares) in 0.01×10^6 HeLa cells/well treated for 24 h with a concentration gradient of dCBP-1, as indicated, with 0.625% *v/v* DMSO. Cellular assay performed as three biological repeats. Protein signal areas were obtained using Compass for Protein Simple™ software. Each sample was normalised to the corresponding vinculin loading control in the CREBBP analysis, then to the vinculin-normalised DMSO control, and a mean value was calculated for the relative protein level using Excel (Appendix Table 12). Data are reported as the mean relative expression over the three biological repeats and error bars are the standard error of the mean. A Student's t-test was performed relative to the DMSO control data and significance is denoted as: *** - $p \leq 0.001$, ** - $p \leq 0.01$, * - $p \leq 0.05$, ns - not statistically significant. 100% relative protein level depicted as dashed line; 50% relative protein level depicted as dotted line. Graph created using GraphPad Prism Software.

While the variation in the p300 data could be an accurate representation of protein cellular levels following PROTAC treatment, it is also possible that variability has arisen due to standardisation against vinculin in the corresponding CREBBP trace. When reported by Vannam *et al*., the ability of **dCBP-1** to degrade CREBBP and p300 was measured using a similar capillary electrophoresis immunoassay, but it is difficult to directly compare the results as no signal quantification is given. Simulated western blots were, however, provided and the reduction in CREBBP and p300 bands reported is comparable, by eye, to those obtained using the above assay (Figure 42).[133] The blots show that the concentrations of **dCBP-1** for causing optimal CREBBP and p300 degradation differ between the two assay results, but this is likely due to different assay times and cell lines used (literature assays investigated degradation in HAP1 cells following 6 h incubation with 10 nM – 1 μM **dCBP-1**).

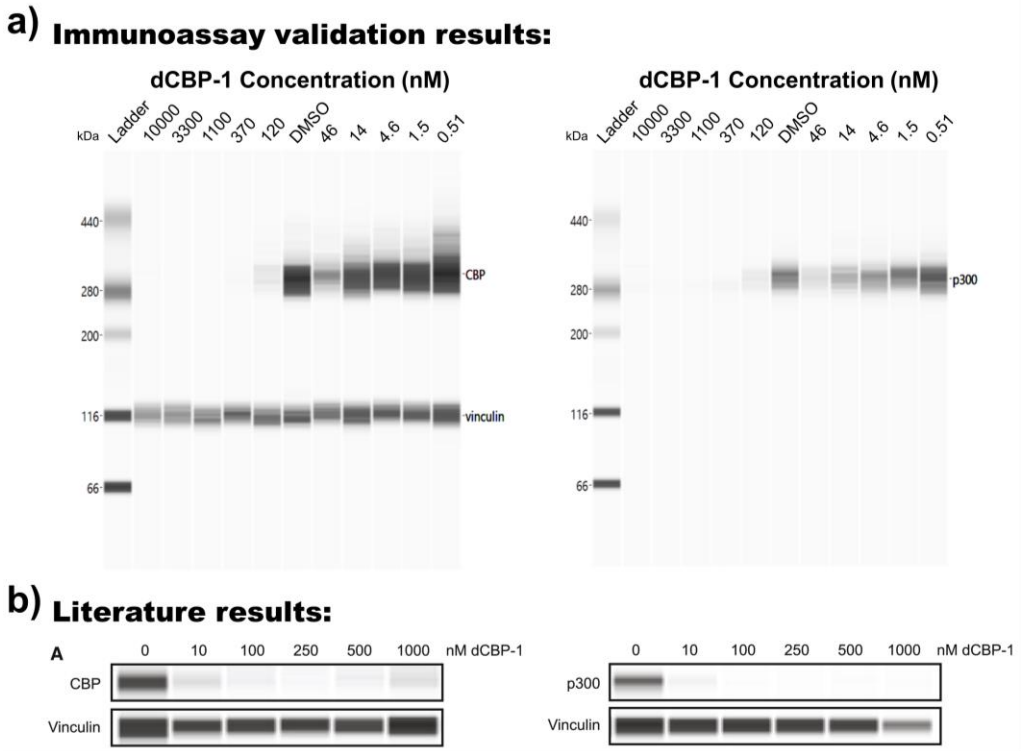

Figure 42. Comparison of the generated western blots measuring **dCBP-1**-induced degradation of CREBBP and p300 in the capillary electrophoresis immunoassays optimised in this chapter and those reported in the literature.[133] Both sets of results show large reductions in the band intensities for CREBBP and p300 following **dCBP-1** treatment. Optimal concentrtaions of **dCBP-1** for inducting protein degradation differ between the capillary electrophoresis immunoassay describes above and the one used in the literture. This is likely due to differences in the cellular assays. **a)** Representative generated western blots showing CREBBP, vinculin, and p300 protein bands bands following 24 h incubation of HeLa cells with the vehicle (DMSO) control treated cells and a concentration gradient of **dCBP-1**, as indicated. The simulated CREBBP western blot shows the complete loss of band for CREBBP over the range of 10 μM – 1.1 μM **dCBP-1**, faint CREBBP bands over the range of 120 nM – 46 nM **dCBP-1**, and strong CREBBP bands over the range of 14 nM – 0.51 nM and for the vehicle (DMSO) control sample. The simulated p300 western blot shows the complete loss of a band for p300 over the range of 10 μM – 1.1 μM **dCBP-1**, faint p300 bands over the range of 120 nM – 46 nM **dCBP-1**, and strong p300 bands (relative to the vehicle (DMSO) control) over the range of 14 nM – 0.51 nM **dCBP-1** and for the vehicle (DMSO) control sample. Western blots generated using Compass for Protein Simple™ software. **b)** Generated western blots reported in the literature by (DMSO) control sampleannam *et al.* Showing of CREBBP (CBP), p300, and vinculin protein bands following the treatment of HAP1 cells with concentration gradient of **dCBP-1**, as indicated, over 6 h.[133] The simulated CREBBP

western blot shows very faint bands for CREBBP over all tested concentrations of **dCBP-1** (10 nM – 1 μM). The p300 simulated western blot shows very faint p300 bands following treatment with 10 nM **dCBP-1** and complete loss of p300 bands over the range of 100 nM – 1 μM **dCBP-1**. Reprinted from 'Targeted degradation of the enhancer lysine acetyltransferases CBP and p300', Volume 28, Issue 4, 15 April 2021, Pages 503 – 514, Copyright (2021), with permission from Elsevier.[133]

Evaluation of the optimised capillary electrophoresis immunoassay conditions using **dCBP-1** confirmed that the protocol would be transferable for screening the abilities of the PROTACs synthesised in Chapter 3 to degrade CREBBP and/or p300. Any active compounds will be resynthesised and further assessed using western blotting to ensure the validity of the results.

Chapter 5 – Assessment of the Abilities of the Amide Series of PROTACs to Degrade CREBBP and p300 Using the Higher Throughput Screening Assay

5.1 – Assessment of Abilities of Piperidine-**(*R*)-OXFBD05**-Derived PROTACs to Degrade CREBBP and/or p300

5.1.1 – Capillary Electrophoresis Immunoassay Results for PROTACs **112** – **122**

The abilities of PROTACs synthesised using the piperidine-modified **(*R*)-OXFBD05** ligand **86** were assessed using the optimised capillary electrophoresis immunoassay described in Chapter 4. HeLa cells were treated with a concentration gradient (0.51 nM – 1.0 μM) of PROTACs **112** – **122** or the vehicle (DMSO) control for 24 h before being lysed. The cellular CREBBP and p300 levels were then measured using the immunoassay as two biological repeats. Quantification of the immunoassay results showed none of the PROTACs caused a reduction in CREBBP or p300 levels other than PROTAC **116** which reduced CREBBP levels to 86% at both 14 nM and 370 nM concentration (Figure 43). However, these data would need to be repeated to obtain three biological repeats and further validate the results, and higher PROTAC potency was desired.

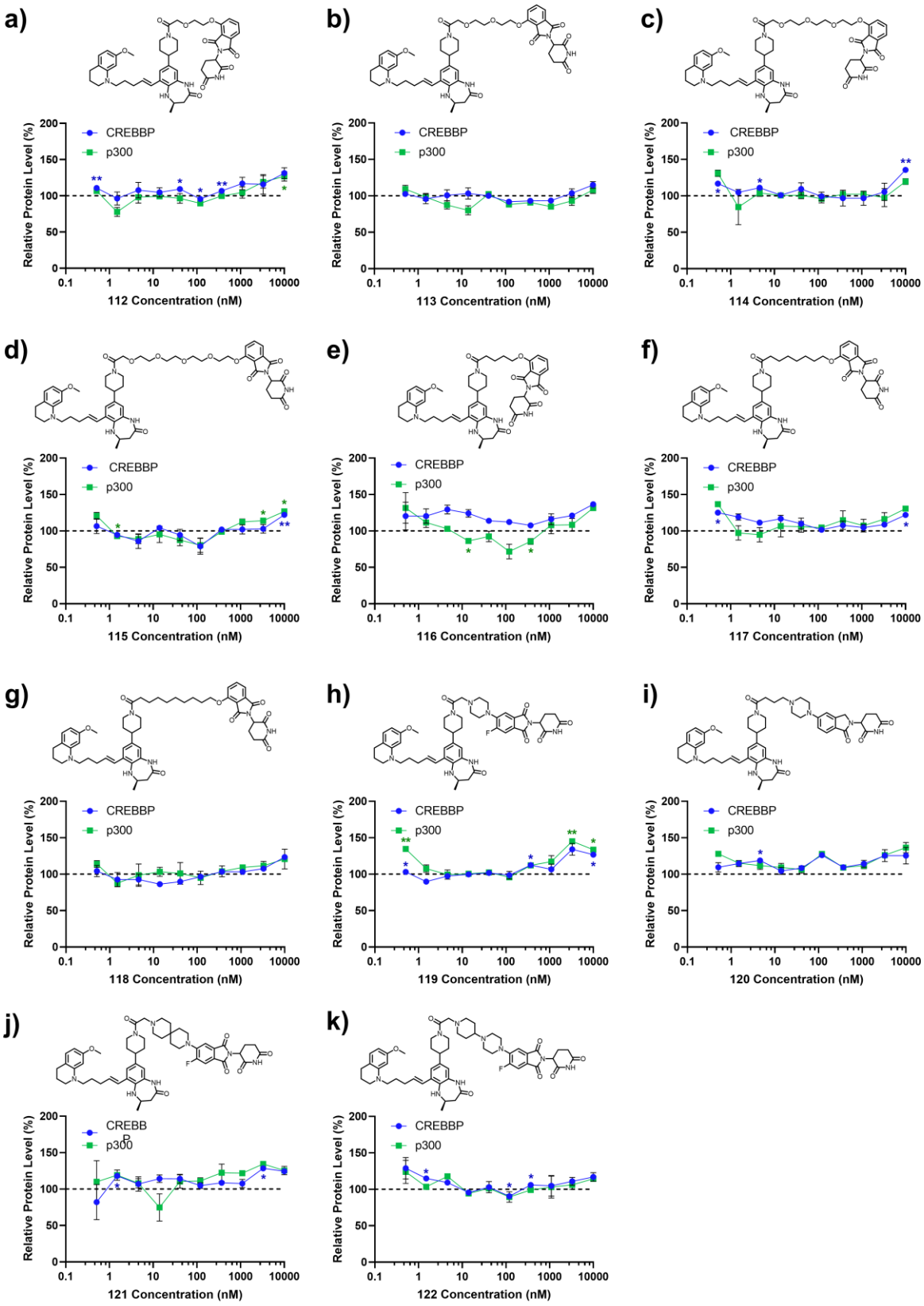

Figure 43. Quantification of CREBBP and p300 levels in for HeLa cells treated for 24 h with the indicated concentrations of **86**-based PROTACs **112** – **122** in 0.625% *v/v* DMSO. Assays were performed as two biological repeats using 0.01×10^6 HeLa cells/ well. CREBBP and the vinculin (loading control) levels were assessed by diluting the cell lysate samples 1:2 in the reagent plate of the immunoassay. CREBBP protein levels were normalised to the vinculin loading control using Compass for Simple Western™ software. The vinculin-normalised CREBBP values were then standardised against the DMSO control in excel and a mean value was calculated as the relative cellular CREBBP level. p300 levels were assessed using neat cell lysate and signal areas were obtained using Compass for Simple Western™ software and were

normalised against the corresponding vinculin signal areas using excel. The vinculin-normalised p300 values were then standardised against the DMSO control in excel and a mean value was calculated as the relative cellular p300 level. Examined PROTACs are as follows: **a) 112**, **b) 113**, **c) 114**, **d) 115**, **e) 116**, **f) 117**, **g) 118**, **h) 119**, **i) 120**, **j) 121**, **k) 122**. Error bars are reported as the standard error of the mean. CREBBP is shown as blue circles, p300 is shown as green squares and a black dotted line indicates 100% relative protein expression. A student's t test was performed relative to the vehicle (DMSO) control data, and significance is denoted as: ** - $p \leq 0.01$, * - $p \leq 0.05$, or is otherwise not statistically significant. CREBBP significe shown in blue, p300 significe shown in green. Graphs produced using GraphPad Prism Software.

5.1.2 – Discussion of Immunoassay Results for PROTACs **112** – **122**

As discussed in Chapter 3, the series of PROTACs synthesised using ligand **86** are predicted to access a comparable exit vector from the CREBBP and p300 bromodomain as the previously reported PROTAC **dCBP-1**.[133] **dCBP-1** caused the potent degradation of both CREBBP and p300 when tested using this assay in Section 4.1 (CREBBP DC_{50} = 34 nM, p300 DC_{50} = 93 nM), so the ligand **86** exit vector was viewed as promising for POI:PROTAC:E3 ligase ternary complex formation. Overlaying the X-ray crystal structures of **dCBP-1** ligand **GNE-781** (PBD: 5W0E)[132,133] and **(*R*)-OXFBD05** analogue **1** (PDB: 6YIM)[43] bound to the CREBBP bromodomain shows a high spatial overlap between the bound ligands, and indicates that modification of **(*R*)-OXFBD05** with a piperidine group would occupy the same space in the bromodomain binding site as the morpholine group in **GNE-781** (Figure 44). Despite the high overlap of the ligand binding poses, **GNE-781** has a higher bromodomain binding affinity than **(*R*)-OXFBD05** (**GNE-781**: CREBBP IC_{50} = 0.94 nM (TR-FRET),[132] **(*R*)-OXFBD05**: CREBBP K_d = 102 nM (ITC)[43]). While PROTAC potencies are dependent upon stabilising interactions formed within the full POI:PROTAC:E3 ligase ternary complex, and low affinity PROTACs have been reported in the literature to induce POI degradation (discussed in Section 1.1.4),[8] the CREBBP/p300 ligand-bromodomain binding interaction will play a role in stabilising ternary complex structures. Therefore, a higher affinity ligand may be required for potent protein degradation in this case.

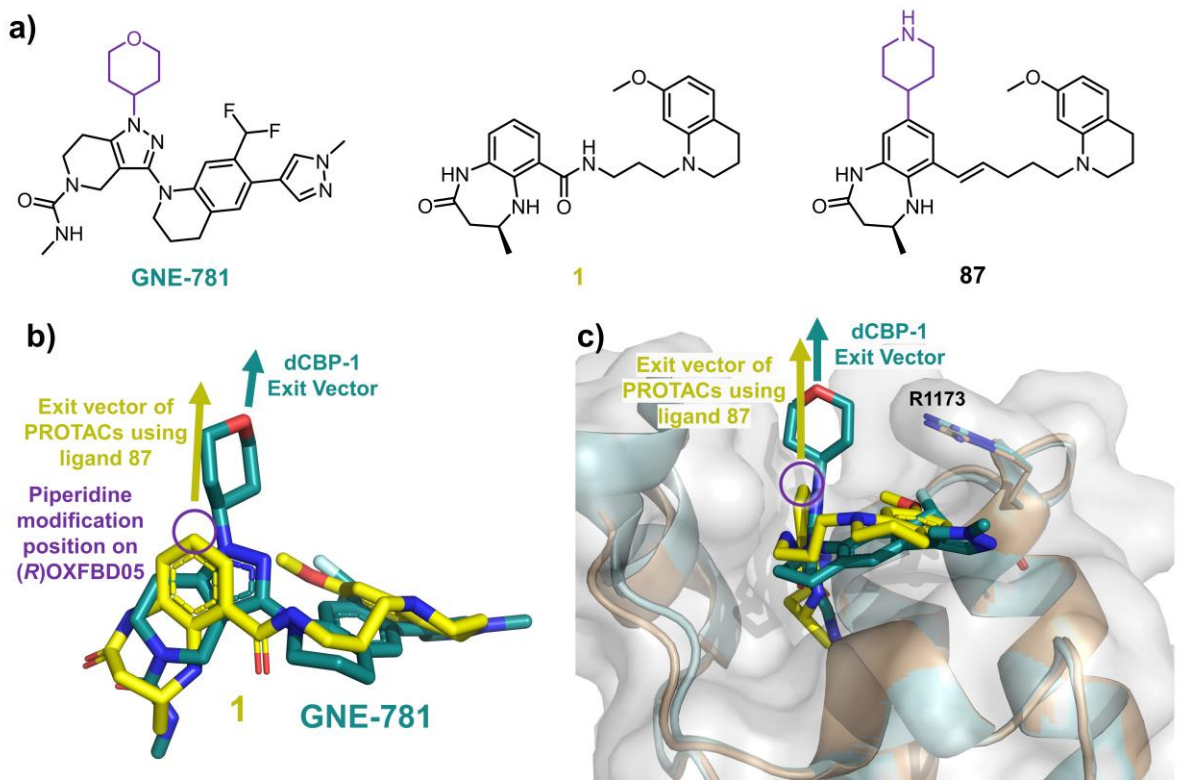

Figure 44. Comparison of the binding modes of CREBBP and p300 bromodomain ligands **GNE-781** and **1** (which is an analogue of **(*R*)-OXFBD05** and was used to model the binding of ligand **1**, as discussed in Section 2.1.1.1) with the CREBBP bromodomain. **GNE-781** was developed into the previously reported PROTAC **dCBP-1** by conversion of the morpholine group (purple) into a piperidine to enable PROTAC linker attachment using an amide coupling reaction. Examination of the overlayed crystal structures suggests that modification of **(*R*)-OXFBD05** with a piperidine group to afford ligand **86** would occupy the same bromodomain binding site space as the morpholine group in **GNE-781** and would allow PROTACs to be synthesised using amide coupling reactions. It is, therefore, predicted that PROTACs synthesised using ligand **86** would access an equivalent exit vector from the CREBBP and p300 bromodomain as **dCBP-1**. **a)** Structures of **GNE-781**, ligand **1**, and ligand **86**. The morpholine of **GNE-781** and the position where **(*R*)-OXFBD05** is modified with a piperidine group in ligand **86** are highlighted in purple. These groups are predicted to occupy equivalent space in the bromodomain binding site. **b)** Overlayed X-ray crystal structures of the CREBBP bromodomain bound ligands **GNE-781** (teal, PBD: 5W0E)[132] and **1** (yellow, PBD: 6YIM)[43] with the protein hidden to highlight the high spatial overlap of the ligands. The exit vector of dCBP-1 is shown with a teal arrow, the position where **(*R*)-OXFBD05** is modified with a piperidine group in ligand **86** is shown with a purple circle, and the predicted exit vector of PROTACs synthesised using ligand **86** is shown with a yellow arrow. **c)** Overlayed X-ray crystal structures of the CREBBP bromodomain bound ligands **GNE-781** (compound: teal, protein: light cyan, PBD: 5W0E)[132] and **1** (compound: yellow, protein: beige, PBD: 6YIM)[43] showing high spatial overlap of the ligands and the comparable PROTAC exit vectors. The exit vector of The exit vector of dCBP-1 is shown with a teal arrow, the position where **(*R*)-OXFBD05** is modified with a piperidine group in ligand **86** is shown with a purple circle, and the predicted exit vector of PROTACs synthesised using ligand **86** is shown with a yellow arrow. Only the protein surface (transparent grey) of the **GNE-781**-bromodomain complex is displayed for clarity.

dCBP-1 comprises a PEG4 linker bound to the 5'-position of the cereblon ligand **pomalidomide** (Figure 45a).[133] A corresponding PEG4-**pomalidomide** compound was not available in the GSK library for the synthesis of structurally comparable PROTAC **171** from ligand **86** (Figure 45c) so this compound was not evaluated. PROTAC **114** provides the greatest structural comparison with **dCBP-1** as it comprises a PEG4 linker, but this is attached to the 4'-position of **thalidomide** by an ether linkage (Figure 45b). The disparity in PROTAC activity between **114** and **dCBP-1** could be attributed to a variety of reasons including the exit vector from the cereblon ligand, difference in PROTAC binding

affinities for the CREBBP and p300 bromodomains, potential differences in cereblon ligand activities,[191] and poor PROTAC physicochemical properties (Table 10). Synthesis and evaluation of PROTAC **171** would be able to provide insights into the impact of using an **(*R*)-OXFBD05**-based ligand to bind the CREBBP and p300 bromodomain instead of a **GNE-781**-based ligand, because some of the unknown variables would be eliminated, such as cereblon exit vector.[43,132] However, PROTAC **171** is predicted to have a lower aqueous solubility than **dCBP-1** and to be partially charged at physiological pH which could interfere with assay results (Table 10).

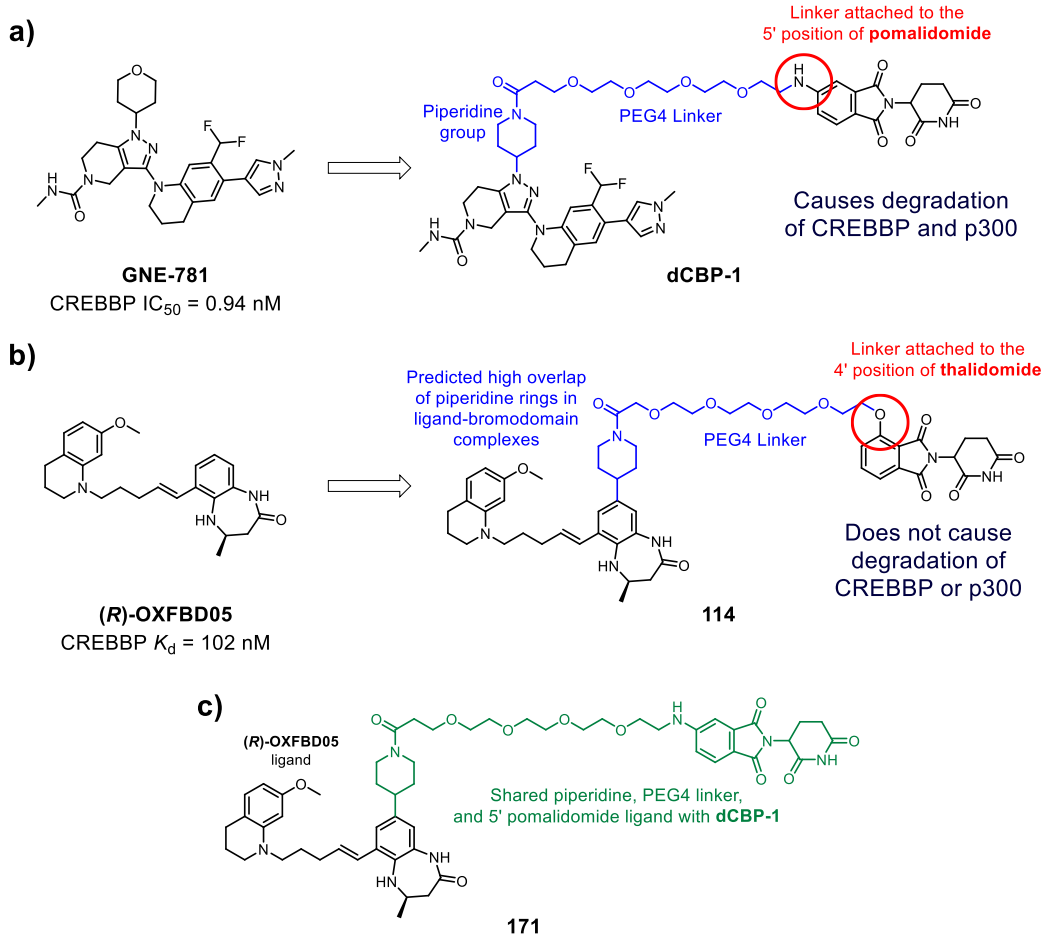

Figure 45. Comparison of the structures of literature PROTAC **dCBP-1** with **114** and design of proposed PROTAC **171** to examine the difference in the abilities of **GNE-784** and **(*R*)-OXFBD05**-based PROTACs to induce the degradation of CREBBP and p300.[43,132,133] **dCBP-1** induces the degradation of both CREBBP and p300 in the cell while **114** shows no activity. Both **dCBP-1** and PROTAC **114** comprise a PEG4 linker attached to a piperidine ring on the bromodomain ligand by an amide bond. The piperidine rings of these ligands are predicted to occupy a similar space in the bromodomain binding site so the PROTACs should access equivalent exit vectors from the CREBBP and p300 bromodomain. Both dCBP-1 and **114** target the E3 ubiquitin ligase cereblon, however, **dCBP-1** uses the ligand **pomalidomide** and the linker is attached at the 5'-position, while **114** uses **thalidomide** and the linker is attached at the 4'-position by an ether linkage. The proposed PROTAC **171** would offer a more direct comparison with **dCBP-1** to help understand the effect of ligand binding affinity and physicochemical properties on the ability to degrade CREBBP and p300. **a)** Development of CREBBP and p300 bromodomain ligand **GNE-781** into PROTAC **dCBP-1** reported in the literature by conversion of the morpholine into a piperidine group and attachment of a PEG4 linker bound to the 5'-position of **pomalidomide**.[132,133] **dCBP-1** induces the potent degradation of both CREBBP and p300. **b)** Development of CREBBP and p300 bromodomain ligand **(*R*)-OXFBD05** into PROTAC **114** by modification with a piperidine ring and attachment of a PEG4 linker bound to the 4'-position of thalidomide.[43] **171** did not cause the degradation of either CREBBP or p300 under the tested conditions. **c)** Structure of

proposed PROTAC **171** which comprises **(*R*)-OXFBD05** (black) and the piperidine, PEG4 linker, and 5'-**pomalidomide** of the **dCBP-1** structure (green).

The lack of CREBBP and/or p300 degradation achieved with PROTACs **112 – 122** could be attributed to their physicochemical properties. Evaluation of $logD_{pH7.4}$ (measured and calculated) and PFI values predict that **dCBP-1** has superior aqueous solubility at physiological pH than all PROTACs synthesised using ligand **86** (**112 - 122**), which are predicted to be poorly soluble (Table 10). Additionally, calculation of overall compound charge at pH 7.4 indicates that dCBP-1 will be neutral while PROTACs **112 – 122** each have a partial positive charge which is unfavourable for passive permeation into the cell.[192] These disfavourable properies of PROTACs **112 – 122** could be reducing the concentration of PROTAC available in the cell to induce protein degradation.

Table 10. Calculated $logD_{pH7.4}$, measured $logD_{pH7.4}$, Property Forecast Index (PFI), and charge at pH 7.4 values of literature PROTAC **dCBP-1** and **86**-based PROTACs **112** – **122**.[133] PROTAC **dCBP-1** has more favourable properties than PROTACs **112** – **122** indicating it will have a better solubility and permeability in the cellular assays. $clogD_{pH7.4}$ values were calculated using Chemicalize (http://www.chemicalize.com) and are coloured according to compound aqueous solubility observations by Hill and Young, where $x < 2$ predicts good solubility (green), $2 < \boldsymbol{x} \leq 4$ predicts moderate solubility (yellow), and $\boldsymbol{x} > 4$ predicts poor solubility (red), darker colour indicates higher value within category.[20] The Property Forecast Index (PFI) is a measurement developed by GSK for predicting aqueous solubility (PFI = $clogD_{pH7.4}$ + #Ar rings).[21] PFI was calculated using the measured $logD_{pH7.4}$ + the number of aromatic rings.[20,21,143] * - PFI calculated using calculated $clogD_{pH7.4}$. PFI values are coloured according to compound aqueous solubility observations by Tinworth and Young, where $4 < \boldsymbol{x} \leq 8$ predicts moderate solubility (yellow), and $\boldsymbol{x} > 8$ predicts poor solubility (red), darker colour indicates higher value within category.[21]

Cpd.	R Group Structure	Calculated $logD_{pH7.4}$	Measured $logD_{pH7.4}$	PFI	Charge @ pH7.4
Literature CREBBP and p300 PROTAC					
dCBP-1	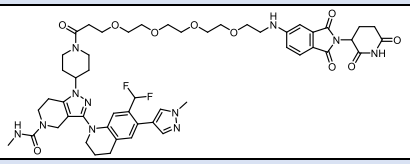	0.89	3.40	7.40	0.00
Ligand **86**-Derived PROTACs					
112	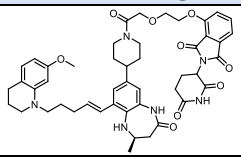	3.65	5.71	8.71	+0.24
113	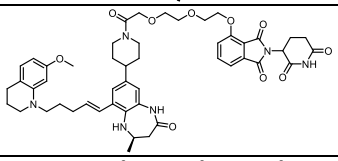	3.60	5.73	8.73	+0.24
114	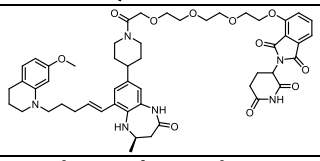	3.55	5.73	8.73	+0.24
115	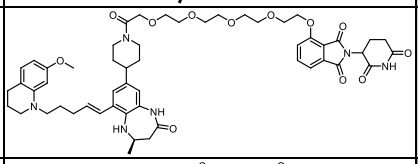	3.51	5.73	8.73	+0.24
116	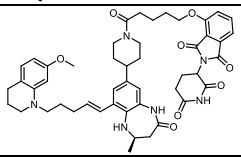	4.67	6.29	9.29	+0.24
117	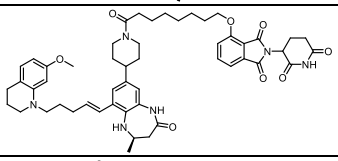	6.00	7.21	10.21	+0.24
118	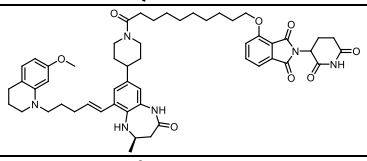	6.89	Insufficient compound	10.01*	+0.24
119	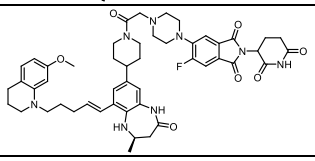	3.87	6.34	9.34	+0.45

120	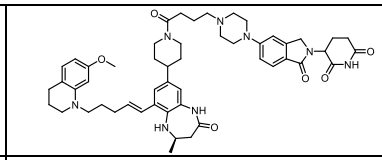	2.90	5.28	8.28	+1.21
121	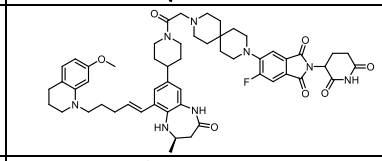	4.56	Not measured	7.56*	+0.60
122	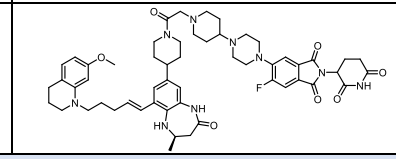	2.48	6.14	9.14	+1.22
Proposed Ligand **86**-Derived PROTAC					
171	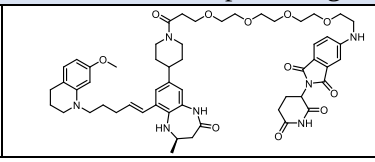	3.38	N/A	6.38*	+0.24

5.2 – Assessment of Abilities of Ethyl Piperazine-**Inobrodib**-Derived PROTACs to Degrade CREBBP and/or p300

5.2.1 – Capillary Electrophoresis Immunoassay Results for PROTACs **147** – **157**, **160** – **164**, and **168** – **170**

The abilities of PROTACs synthesised using the ethyl piperazine-modified **Inobrodib** ligand **106** were assessed using the optimised capillary electrophoresis immunoassay described in Chapter 4. HeLa cells were treated with a concentration gradient (0.51 nM – 1.0 μM) of PROTACs **147** – **157**, **160** – **164**, and **168** – **170** or the vehicle (DMSO) control for 24 h before being lysed. The cellular CREBBP and p300 levels were measured using the immunoassay as two biological repeats other than PROTACs **168** and **170** which were measured once. Quantification of the immunoassay results for PROTACs comprising the ethyl piperazine-modified **Inobrodib** ligand **106** identified only three PROTACs (**147**, **148**, and **163**) to cause small reductions in CREBBP or p300 levels, while the other PROTACs (**149** – **157**, **160** – **162**, **164**, and **168** – **170**) did not induce the degradation of either paralogue (Figure 46). PROTAC **147** caused reductions in CREBBP levels to 92% and 89% with 1.5 nM and 14 nM PROTAC concentrations, respectively; PROTAC **148** caused reductions in p300 levels to 78% and 91% with 4.6 nM and 14 nM PROTAC concentrations, respectively; and PROTAC **163** caused reductions in p300 levels to 86% with 41 nM PROTAC concentration. These results would need to be repeated to obtain three biological repeats for further validation, however, greater PROTAC potency was desired.

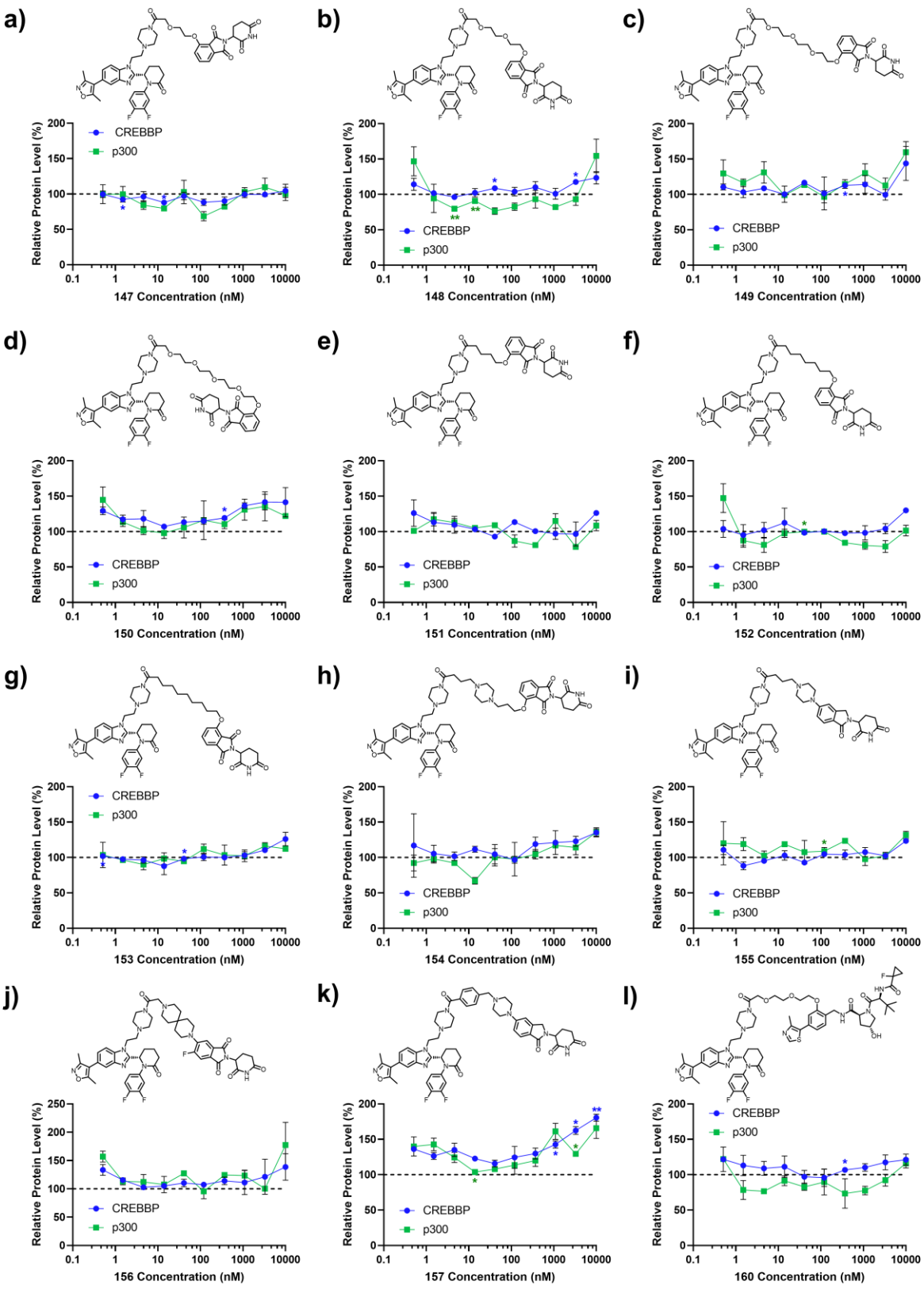
a)
b)
c)
d)
e)
f)
g)
h)
i)
j)
k)
l)
CREBBP
p300
Relative Protein Level (%)
147 Concentration (nM)
148 Concentration (nM)
149 Concentration (nM)
150 Concentration (nM)
151 Concentration (nM)
152 Concentration (nM)
153 Concentration (nM)
154 Concentration (nM)
155 Concentration (nM)
156 Concentration (nM)
157 Concentration (nM)
160 Concentration (nM)

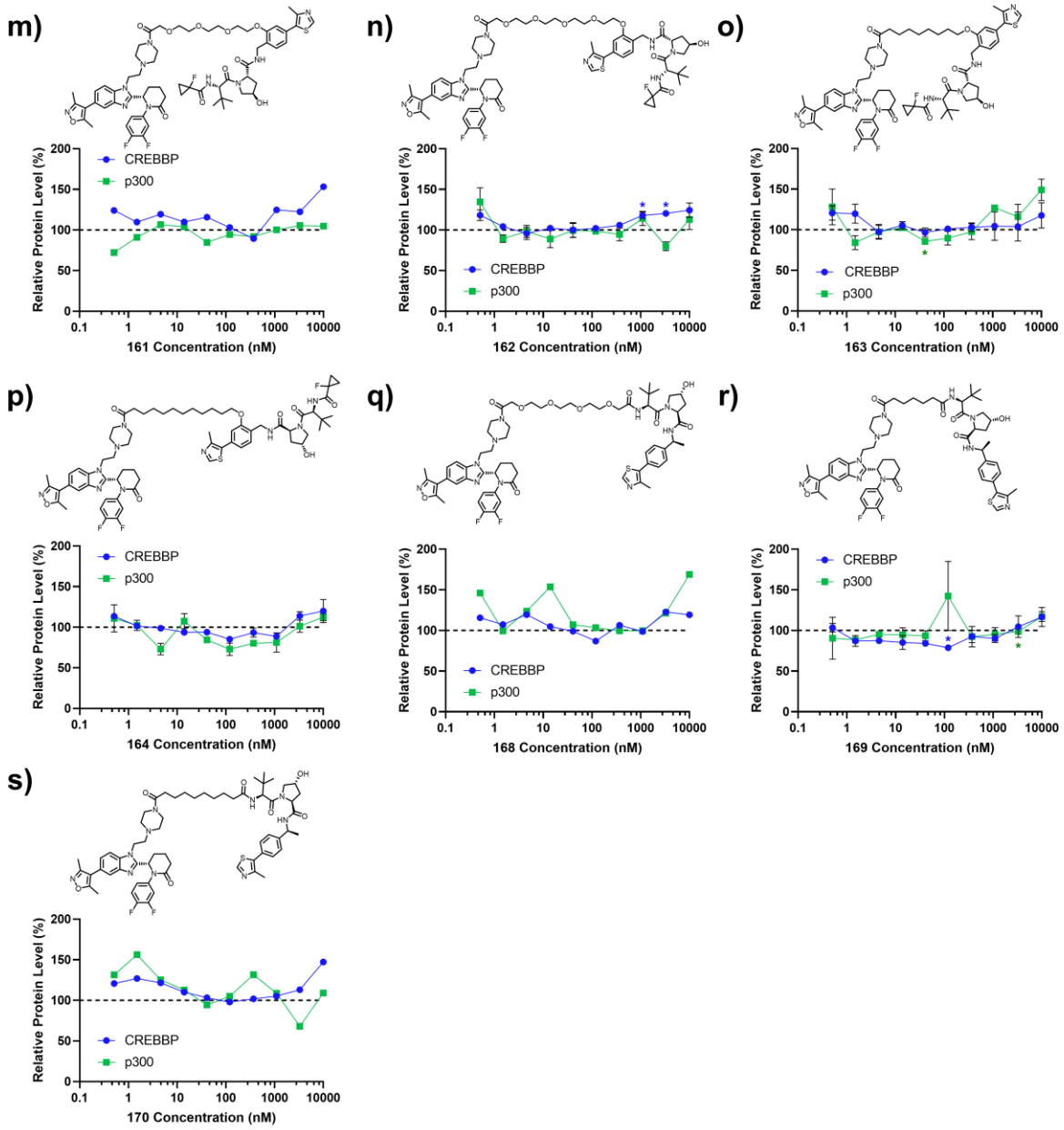

Figure 46. Quantification of CREBBP and p300 levels in for HeLa cells treated for 24 h with the indicated concentrations of **106**-based PROTACs **147 – 157, 160 – 164,** and **168 – 170** in 0.625% *v/v* DMSO. Assays were performed as two biological repeats, unless otherwise stated, using 0.01×10^6 HeLa cells/well. CREBBP and vinculin (loading control) levels were assessed by diluting the cell lysate samples 1:2 in the reagent plate of the immunoassay. CREBBP protein levels were normalised to the vinculin loading control using Compass for Simple Western™ software. The vinculin-normalised CREBBP values were then standardised against the DMSO control in excel and a mean value was calculated as the relative cellular CREBBP level. p300 levels were assessed using neat cell lysate and signal areas were obtained using Compass for Simple Western™ software and were normalised against the corresponding vinculin signal areas using excel. The vinculin-normalised p300 values were then standardised against the DMSO control in excel and a mean value was calculated as the relative cellular p300 level. Evaluated PROTACs are as follows: **a) 147**; **b) 148**; **c) 149**; **d) 150**; **e) 151**; **f) 152**; **g) 153**; **h) 154**; **i) 155**; **j) 156**; **k) 157**; **l) 160**; **m) 161**, tested n = 1; **n) 162**; **o) 163**; **p) 164**; **q) 168**, tested n = 1; **r) 169**; **p) 170**, tested n = 1. Error bars are reported as the standard error of the mean. CREBBP is shown as blue circles, p300 is shown as green squares and a black dotted line indicates 100% relative protein expression. A student's t test was performed relative to the vehicle (DMSO) control data, and significance is denoted as: ** - $p \leq 0.01$, * - $p \leq 0.05$, or is otherwise not statistically significant. CREBBP significe shown in blue, p300 significe shown in green. Graphs produced using GraphPad Prism Software.

5.2.2 – Discussion of Immunoassay Results for PROTACs **149** – **157**, **160** – **162**, **164**, and **168** – **170**

PROTACs synthesised using ligand **106** (**149** – **157**, **160** – **162**, **164**, and **168** – **170**) investigate a different exit vector from the CREBBP and p300 bromodomain than **dCBP-1** (Figure 47).[112,133,164] As discussed in Chapter 1, the potency and selectivity of PROTACs arises from stabilising interactions formed between the components of the POI:PROTAC:E3 ligase ternary complex. It may be that this exit vector is suboptimal for the formation and stabilisation of a ternary complex, which would lead to the inability of PROTACs to induce degradation.

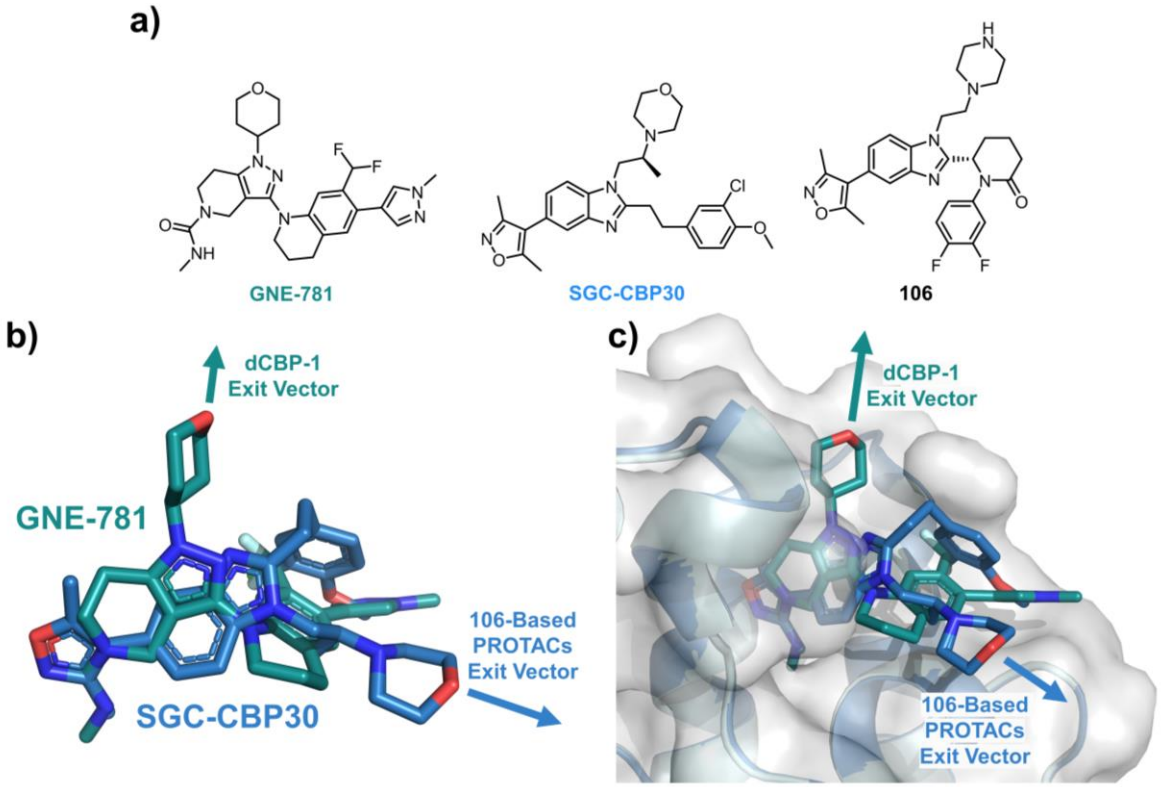

Figure 47. Comparison of the exit vector from the CREBBP and p300 bromodomain accessed by **dCBP-1** using ligand **GNE-781** and PROTACs synthesised using ligand **108**, which is structurally similar to bromdomain inhibitor **SGC-CBP30**.[132,133,164] Based on the overlayed X-ray crystal strauctures of **GNE-781** (PBD: 5W0E)[132] and **SGC-CBP30** (PBD: 4NR7)[164] bound to the bromdomain of CREBBP, PROTACs synthesised using ligand **108** would be predicted to access a different bromodomain exit vector than **dCBP-1**. **a)** Structures of CREBBP and p300 ligands **GNE-781**, **SGC-CBP30**, and **106**.[132,164]

PROTACs **149** – **157**, **160** – **162**, **164**, and **168** – **170** are predicted to have a moderate to low solubility and to be positively charged in aqueous buffer at physiological pH which may adversely affect their effective concentration in the cell, and subsequent abilities to degrade CREBBP and/ or p300 (Table 11). PROTACs **154** and **155** have lower measured $logD_{pH7.4}$ values (3.07 and 3.04, respectively) than

dCBP-1 (3.40) due to the presence of a second piperazine group which can be positively charged at physiological pH. However, this results in a calculated partial charge of +1.54 and +1.58 for **154** and **155**, respectively, which could reduce passive diffusion of the PROTAC into the cell through the lipophilic cell membrane.[192] PROTACs **147** – **150** have comparable measured $logD_{pH7.4}$ values (**147**: 3.49, **148**: 3.52, **149**: 3.56, **150**: 3.58) as **dCBP-1**, however, due to the four aromatic rings in the CREBBP and p300 ligand **106**, all PROTACs (**149** – **157**, **160** – **162**, **164**, and **168** – **170**) have greater PFI values than **dCBP-1**.

Table 11. Calculated $logD_{pH7.4}$, measured $logD_{pH7.4}$, Property Forecast Index (PFI), and charge at pH 7.4 values of literature PROTAC **dCBP-1** and **106**-based PROTACs **149 – 157**, **160 – 162**, **164**, and **168 – 170**.[133] PROTAC **dCBP-1** has more favourable properties than PROTACs **112** – **122** indicating it will have a better solubility and permeability in the cellular assays. $clogD_{pH7.4}$ values were calculated using Chemicalize (http://www.chemicalize.com) and are coloured according to compound aqueous solubility observations by Hill and Young, where $x < 2$ predicts good solubility (green), $2 < \boldsymbol{x} \leq 4$ predicts moderate solubility (yellow), and $\boldsymbol{x} > 4$ predicts poor solubility (red), darker colour indicates higher value within category.[20] The Property Forecast Index (PFI) is a measurement developed by GSK for predicting aqueous solubility (PFI = $clogD_{pH7.4}$ + #Ar rings).[21] PFI was calculated using the measured $logD_{pH7.4}$ + the number of aromatic rings.[20,21,143] * - PFI calculated using calculated $clogD_{pH7.4}$. PFI values are coloured according to compound aqueous solubility observations by Tinworth and Young, where $4 < \boldsymbol{x} \leq 8$ predicts moderate solubility (yellow), and $\boldsymbol{x} > 8$ predicts poor solubility (red), darker colour indicates higher value within category.[21]

Cpd.	R Group Structure	Calculated $logD_{pH7.4}$	Measured $logD_{pH7.4}$	PFI	Charge @ pH7.4
Literature CREBBP and p300 PROTAC					
dCBP-1	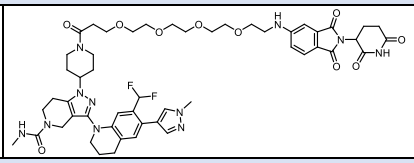	0.89	3.40	7.40	0.00
Ligand **106**-Derived PROTACs					
147	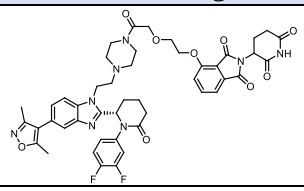	2.14	3.49	8.49	+0.56
148	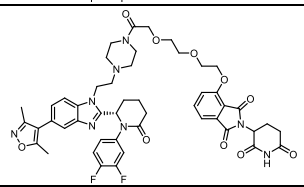	2.09	3.52	8.52	+0.56
149	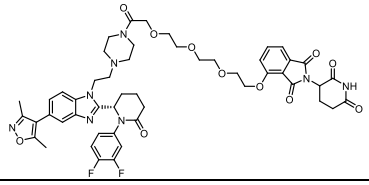	2.05	3.56	8.56	+0.56

150	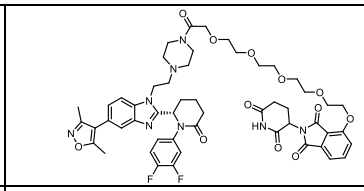	2.00	3.58	8.58	+0.56
151	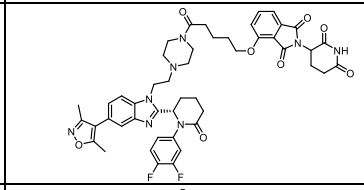	3.10	3.98	8.98	+0.62
152	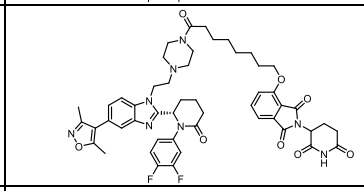	4.44	4.91	9.91	+0.62
153	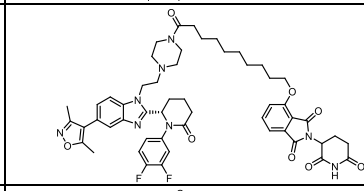	5.32	5.61	10.61	+0.62
154	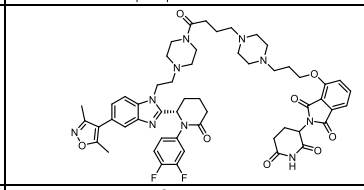	1.33	3.07	8.07	+1.54
155	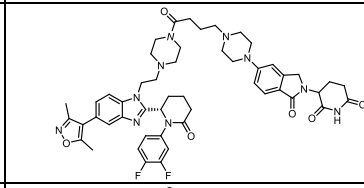	1.33	3.04	8.04	+1.58
156	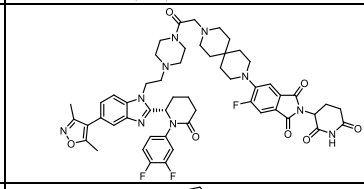	3.06	4.53	9.53	+0.81
157	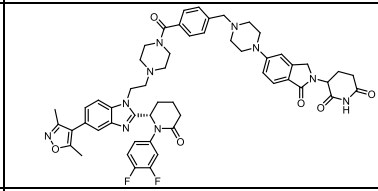	3.48	3.77	8.77	+1.36
160	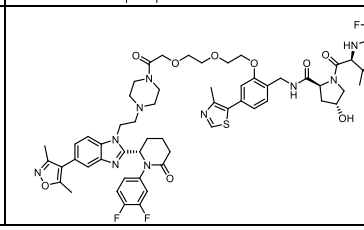	3.51	4.50	10.50	+0.56

161	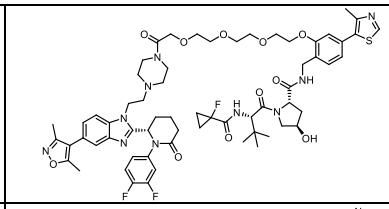	3.47	4.50	10.50	+0.56
162	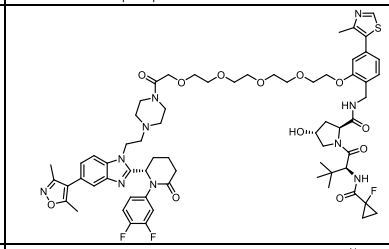	3.42	Insufficient compound	9.42*	+0.56
163	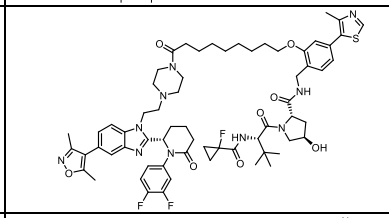	6.30	6.00	12.00	+0.62
164	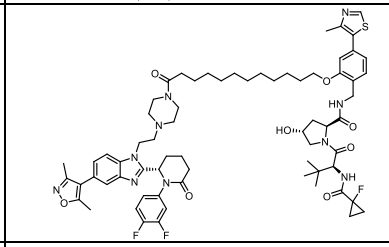	7.63	7.17	13.17	+0.62
168	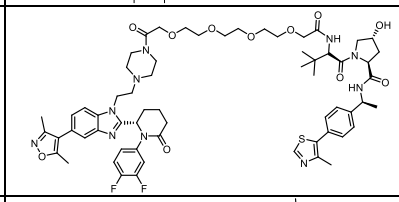	3.10	4.17	10.17	+0.56
169	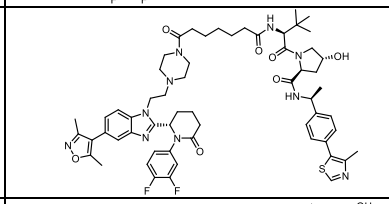	5.04	4.51	10.51	+0.62
170	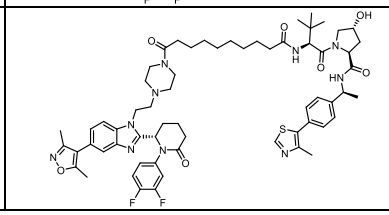	6.37	5.25	11.25	+0.62

5.3 – Assessment of Abilities of Piperidine-**Inobrodib**-Derived PROTACs to Degrade CREBBP and/or p300

5.3.1 – Capillary Electrophoresis Immunoassay Results for PROTACs **134** – **146**

The abilities of PROTACs synthesised using the piperidine-modified **Inobrodib** ligand **87** were assessed using the optimised capillary electrophoresis immunoassay described in Chapter 4. HeLa cells were treated with a concentration gradient (0.51 nM – 1.0 μM) of PROTACs **134** – **146** or the vehicle (DMSO) control for 24 h before being lysed. The cellular CREBBP and p300 levels were measured using the immunoassay as two biological repeats other than PROTAC **145** which was measured once.

Of the 13 PROTACs synthesised using ligand **87**, 12 PROTACs (**134** – **143**, **145**, and **146**) did cause a statistically significant reduction in the cellular levels of CREBBP or p300 under the tested conditions (Figure 48). Pleasingly, PROTAC **144** was able to induce significant reductions in CREBBP levels and gave more varied results for p300 (Figure 49, Appendix Table 13).

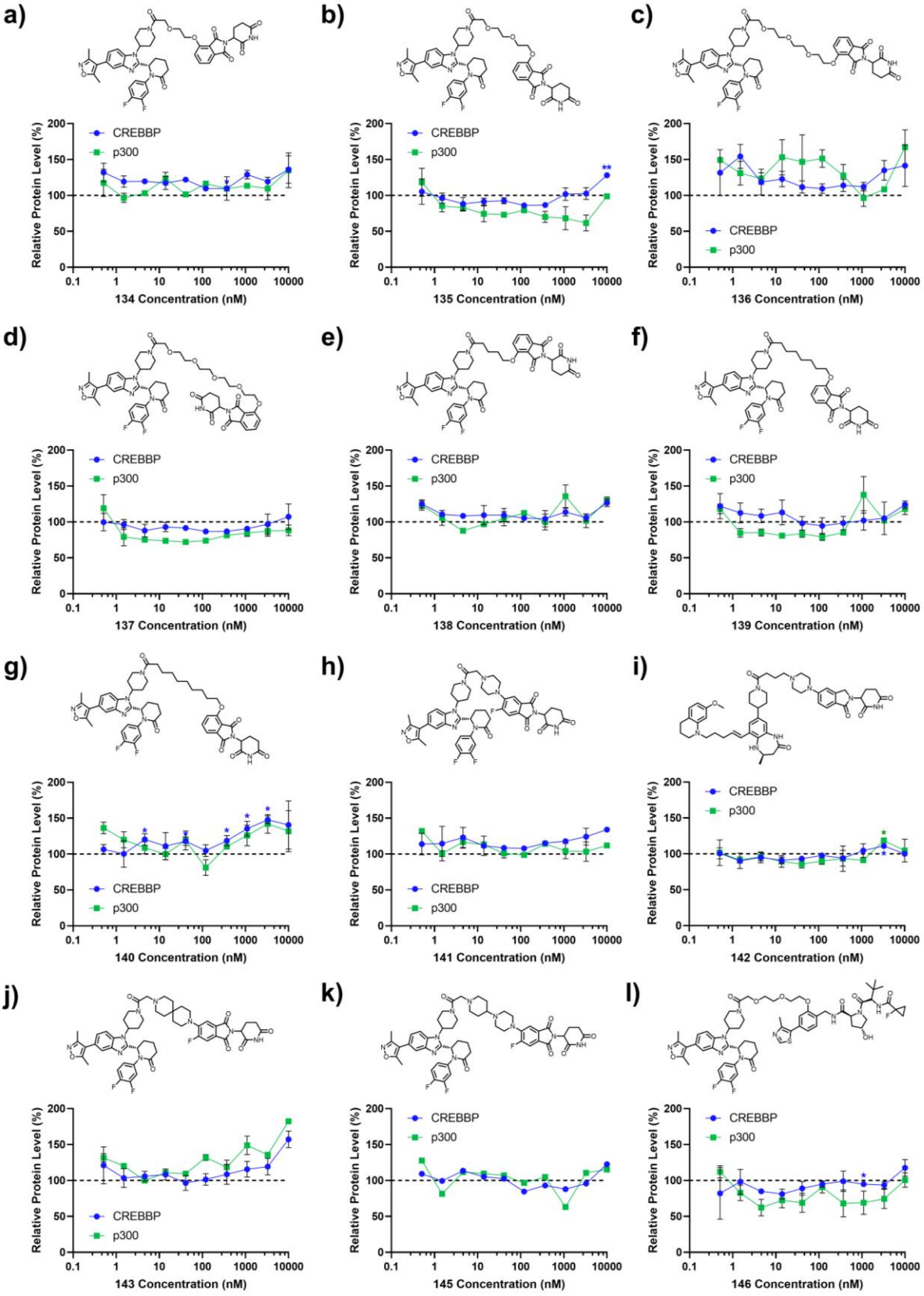

Figure 48. Quantification of CREBBP and p300 levels in for HeLa cells treated for 24 h with the indicated concentrations of Piperazine-Inobrodib-Derived PROTACs **134** – **143**, **145**, and **146** in 0.625% v/v DMSO. Assays were performed as two biological repeats, unless otherwise stated, using 0.01×10^6 HeLa cells/well. CREBBP and vinculin (loading control) levels were assessed by diluting the cell lysate samples 1:2 in the reagent plate of the immunoassay. CREBBP protein levels were normalised to the vinculin loading control using Compass for Simple Western™ software. The vinculin-normalised CREBBP values were then standardised against the DMSO control in

excel and a mean value was calculated as the relative cellular CREBBP level. p300 levels were assessed using neat cell lysate and signal areas were obtained using Compass for Simple Western™ software and were normalised against the corresponding vinculin signal areas using excel. The vinculin-normalised p300 values were then standardised against the DMSO control in excel and a mean value was calculated as the relative cellular p300 level. Evaluated PROTACs are as follows: **a) 134**; **b) 135**; **c) 136**; **d) 137**; **e) 138**; **f) 139**; **g) 140**; **h) 141**; **i) 142**; **j) 143**; **k) 145**, tested n = 1; **l) 146**. Error bars are reported as the standard error of the mean. CREBBP is shown as blue circles, p300 is shown as green squares and a black dotted line indicates 100% relative protein expression. A student's t test was performed relative to the vehicle (DMSO) control data, and significance is denoted as: ** - $p \leq 0.01$, * - $p \leq 0.05$, or is otherwise not statistically significant. CREBBP significe shown in blue, p300 significe shown in green. Graphs produced using GraphPad Prism Software.

Maximum CREBBP degradation was achieved using 370 nM **144**, where protein levels were reduced to 54% relative to the vehicle (DMSO) treated control cells, and a similar reduction in CREBBP to 56% was observed using 1.1 μM **144** (Figure 49, Appendix Table 13). The CREBBP level then recovers to that of the vehicle (DMSO) control treated cells as concentration of **144** decreases from 370 nM to 0.51 nM, showing a dose-response effect of the PROTAC (Figure 49, Appendix Table 13, Appendix Table 14). For higher concentrations of PROTAC **144**, a Hook effect is observed, which is evident by the bell shaped degradation profile (Figure 49b), where increasing PROTAC concentrations cause less protein to be degraded. This phenomenon occurs because at high PROTAC concentrations the POI binding sites become saturated, and non-functioning (with respect to POI degradation) binary complexes form (Figure 50).[2]

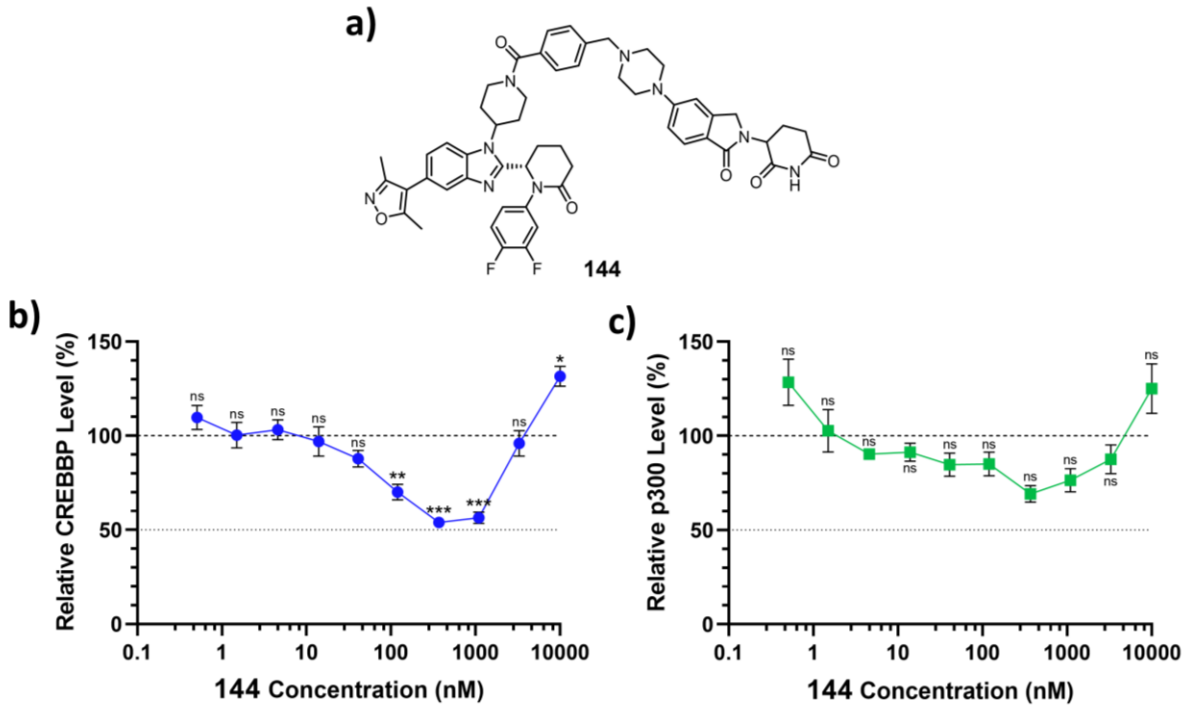

Figure 49. Evaluation of PROTAC **144**-induced CREBBP and/or p300 degradation in HeLa cells following 24 h PROTAC incubation. **a)** Structure of PROTAC **144**. **b)** Quantification from the capillary electrophoresis immunoassay of the relative CREBBP protein levels (blue circles) in 1:2 diluted 0.01×10^6 HeLa cells/well treated for 24 h with a concentration gradient of **144**, as indicated, with 0.625% *v/v* DMSO. Cellular assay performed as three biological repeats. Protein signal areas and vinculin-normalised CREBBP values were obtained using

Compass for Protein Simple™ software. Each sample was normalised to the vinculin-normalised DMSO control, and a mean value was calculated for the relative protein level using Excel (Appendix Table 13). Data are reported as the mean relative expression over the three biological repeats and error bars are the standard error of the mean. A Student's t-test was performed relative to the DMSO control data, and significance is denoted as: *** - $p \leq 0.001$, ** - $p \leq 0.01$, * - $p \leq 0.05$, n.s - not statistically significant. Graph created using GraphPad Prism. **c)** Quantification from the capillary electrophoresis immunoassay of the relative p300 protein levels in 0.01×10^6 HeLa cells/ well HeLa cells treated for 24 h with a concentration gradient of **144**, as indicated, with 0.625% v/v DMSO. Cellular assay performed as three biological repeats. Protein signal areas were obtained using Compass for Protein Simple™ software. Each sample was normalised to the corresponding vinculin loading control in the CREBBP analysis, then to the vinculin-normalised DMSO control, and a mean value was calculated for the relative protein level using Excel (Appendix Table 14). Data are reported as the mean relative expression over the three biological repeats and error bars are the standard error of the mean. A student's t-test was performed relative to the DMSO control data, and significance is denoted as: *** - $p \leq 0.001$, ** - $p \leq 0.01$, * - $p \leq 0.05$, n.s - not statistically significant.

Interestingly, treatment with 10 μM **144** causes a significant increase in the relative CREBBP level to 131%. Increases in CREBBP and/or p300 levels were also observed for **86**-based PROTACs **112**, **114**, **115**, **117**, **119**, and **121** (Figure 43); **106**-based PROTACs **148**, **157**, and **162** (Figure 46); and **87**-based PROTACs **140** and **142** (Figure 48). Where PROTACs are able to bind the CREBBP and p300 bromodomain, but not form a POI:PROTAC:E3 ligase ternary complex, they will not cause degradation but could instead act as inhibitors. Due to the Hook effect, at high concentrations, PROTAC **144** will form binary complexes with CREBBP and p300 and act to inhibit bromodomain function. It has been shown for the BET family of BCPs that bromodomain inhibition can lead to increased expression of the proteins, which is believed to occur through a feedback mechanism to compensate for the loss of bromodomain function.[193–195] This could explain the observed increases in CREBBP levels following 24 h PROTAC treatment.

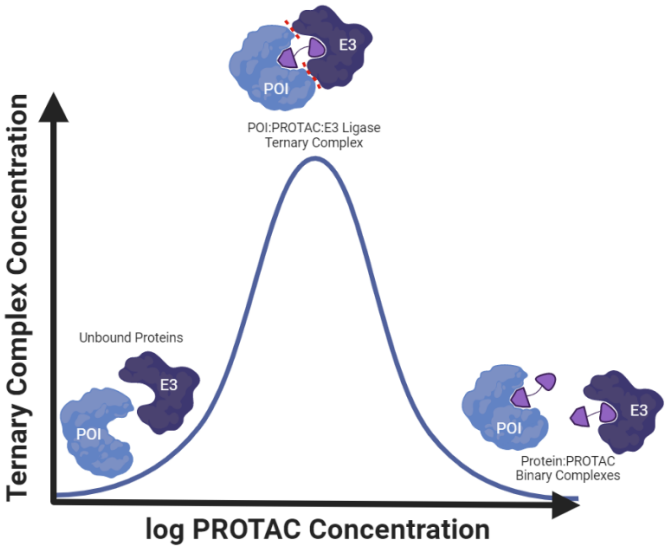

Figure 50. Illustration of the Hook effect. As the concentration of PROTAC increases, more is available to bind the POI and E3 ubiquitin ligase and form ternary complexes to induce the polyubiquitination and subsequent degradation of the POI. However, as the PROTAC concentration increases past an optimum, there is a decrease in ternary complex formation due to the formation of binary complexes, meaning that there will be a subsequent decrease in POI degradation. Red dotted lines indicate cooperative PPIs formed between the POI and E3 ubiquitin ligase in the ternary complex. Image was created using Biorender (www.biorender.com) and is based on a figure by Pettersson and Crews.[2]

5.2.2 – Discussion of Immunoassay Results for PROTACs **134** – **146**

Of the 13 PROTACs synthesised using ligand **87** (PROTACs **134** – **146**), only PROTAC **144** was able to induce protein degradation under the investigated conditions. Overlaying the X-ray crystal structures of the parent CREBBP and p300 ligands of PROTAC **144** and **dCBP-1** (**Inobrodib** (PDB: 7XH6)[163] and **GNE-781**(PDB: 5W0E)[132], respectively) bound to the CREBBP bromodomain, shows that the PROTACs should address different exit vectors from the bromodomain (Figure 51).[133] Therefore, these PROTACs could be forming different POI:PROTAC:E3 ligase ternary complex structures and parallel SAR investigations could give insights into the PROTAC structural features required for potent and potentially selective CREBBP and/or p300 degradation.

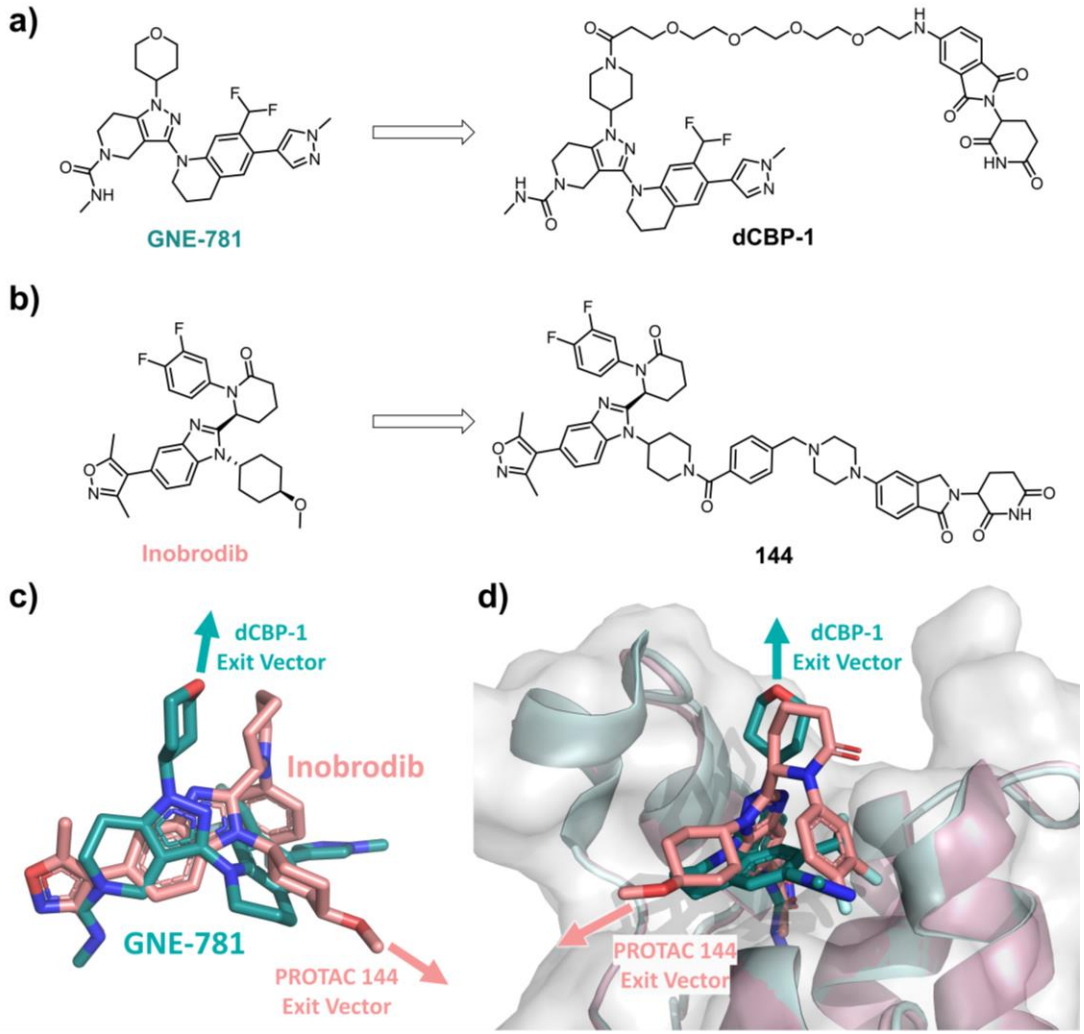

Figure 51. Comparison of the predicted CREBBP and p300 exit vectors accessed by previously reported **dCBP-1** and novel PROTAC **144**.[133] **a)** Structures of the CREBBP and p300 bromodomain inhibitor **GNE-781** and PROTAC **dCBP-1**.[132,133] **GNE-781** was developed into the bromodomain ligand of **dCBP-1** by conversion of the morpholine group to a piperidine group to allow linker attachment by an amide coupling reaction. **b)** Structures of the CREBBP and p300 bromodomain ligand **Inobrodib** and PROTAC **144**.[112] Inobrodib was developed into the bromodomain ligand of PROTAC **144** by conversion of the methoxycyclohexane group to a piperidine to allow a linker to be attached in an amide coupling reaction. **c)** Overlay of the X-ray crystal structures of the parent bromodomain ligands of **dCBP-1** and PROTAC **144** bound to the bromodomain of CREBBP (proteins not shown for clarity) indicating the different PROTAC exit vectors (**dCBP-1** exit vector indicated by teal arrow, PROTAC **144** exit vector indicated by pink arrow). **dCBP-1** was developed from the bromodomain ligand **GNE-781** (teal, PDB: 5W0E) where the THP group was modified to a piperidine to facilitate linker attachment.[132,133] PROTAC **144** comprises the bromodomain ligand **Inobrodib** (pink, PBD: 7XH6) where the cyclohexyl ring was modified to a piperidine group to facilitate linker attachment.[112,163] **d)** Overlay of the X-ray crystal structures of the parent bromodomain ligands of **dCBP-1** and PROTAC **144** bound to the bromodomain of CREBBP, with protein structures shown, indicating the different PROTAC exit vectors (dCBP-1 exit vector indicated by teal arrow, PROTAC **144** exit vector indicated by pink arrow). **dCBP-1** was developed from the bromodomain ligand **GNE-781** (compound: teal, protein: light blue, PDB: 5W0E) where the THP group was modified to a piperidine to facilitate linker attachment.[132,133] PROTAC **144** comprises the bromodomain ligand Inobrodib (compound: pink, protein: light pink, PBD: 7XH6) where the cyclohexyl ring was modified to a piperidine group to facilitate linker attachment.[112,163] For clarity only the surface of the Inobrodib-bromodomain complex is shown (transparent grey).

All PROTACs synthesised using ligand **87** (PROTACs **134** – **146**), are predicted to be moderately to poorly soluble in the cellular assays (Table 12). Poor aqueous solubility at physiological pH could be decreasing the effective concentration of the PROTACs in the cell. However, the majority of the

PROTACs synthesised using ligand **87** are predicted to be neutral at pH 7.4 (PROTACs **134** – **140** and **146**) which could promote the passive diffusion of the compounds into the cells (Table 12).[192] PROTACs **134** – **137** have similar measured $clogD_{pH7.4}$ values (**134**: 3.49, **135**: 3.54, **136**: 3.62, **137**: 3.65) to **dCBP-1** (3.40), however, they have greater PFI values, due to their higher number of aromatic rings, causing each compound to have a predicted low aqueous (pH 7.4) solubility according to observations by Tinworth and Young.[21] PROTAC **144** has a slightly higher measured $clogD_{pH7.4}$ value than **dCBP-1** (**144** $logD_{pH7.4}$ = 3.82, **dCBP-1** $logD_{pH7.4}$ = 3.40, Table 12) and both values would suggest moderate compound solubility in aqueous solutions at pH 7.4 according to observations by Hill and Young.[20] However, PROTAC **144** has a high PFI value (9.82) and is predicted to have a partial charge of +0.86 (aq., pH 7.4) (Table 12) which could reduce the concentration of PROTAC able to passively diffuse into the cells.[192] Therefore, optimisation of the physicochemical properties of **144** may be able to enhance its activity further.

Table 12. Calculated $logD_{pH7.4}$, measured $logD_{pH7.4}$, Property Forecast Index (PFI), and charge at pH 7.4 values of literature PROTAC **dCBP-1** and **87**-based PROTACs **134 – 146**.[133] $clogD_{pH7.4}$ values were calculated using Chemicalize (http://www.chemicalize.com) and are coloured according to compound aqueous solubility observations by Hill and Young, where $x < 2$ predicts good solubility (green), $2 < \boldsymbol{x} \leq 4$ predicts moderate solubility (yellow), and $\boldsymbol{x} > 4$ predicts poor solubility (red), darker colour indicates higher value within category.[20] The Property Forecast Index (PFI) is a measurement developed by GSK for predicting aqueous solubility (PFI = $clogD_{pH7.4}$ + #Ar rings).[21] PFI was calculated using the measured $logD_{pH7.4}$ + the number of aromatic rings.[20,21,143] * - PFI calculated using calculated $clogD_{pH7.4}$. PFI values are coloured according to compound aqueous solubility observations by Tinworth and Young, where $4 < \boldsymbol{x} \leq 8$ predicts moderate solubility (yellow), and $\boldsymbol{x} > 8$ predicts poor solubility (red), darker colour indicates higher value within category.[21]

Cpd.	R Group Structure	Calculated $logD_{pH7.4}$	Measured $logD_{pH7.4}$	PFI	Charge @ pH7.4
Literature CREBBP and p300 PROTAC					
dCBP-1	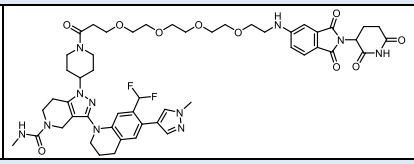	0.89	3.40	7.40	0.00
Active Ligand **87**-Derived PROTAC					
144	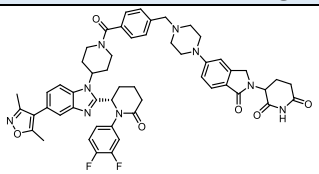	4.00	3.82	9.82	+0.86
Ligand **87**-Derived PROTACs					
134	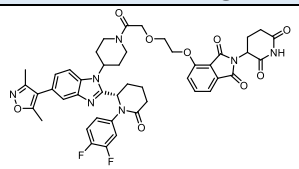	2.66	3.49	8.49	0.00
135	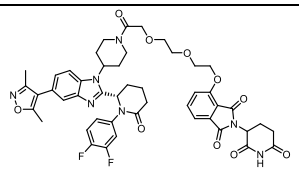	2.61	3.54	8.54	0.00
136	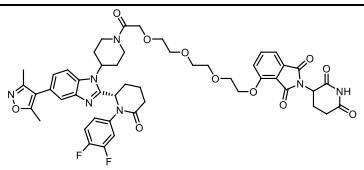	2.57	3.62	8.62	0.00
137	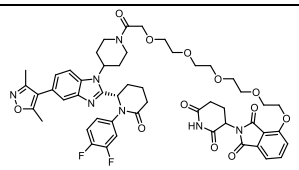	2.52	3.65	8.65	0.00
138	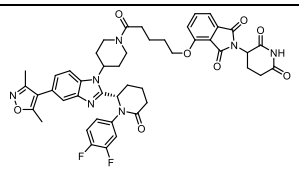	3.68	4.02	9.02	0.00
139	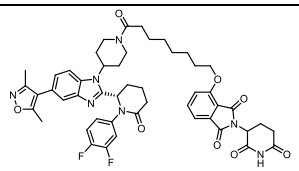	5.01	4.98	9.98	0.00

140	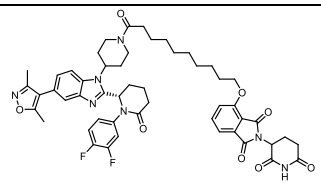	5.90	5.72	10.72	0.00
141	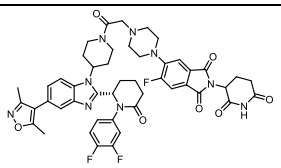	2.88	4.12	9.12	+0.18
142	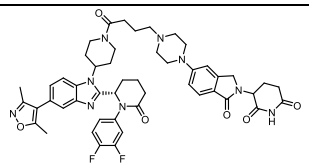	1.91	3.08	8.08	+0.97
143	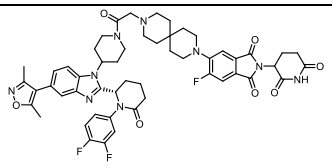	3.57	4.81	9.81	+0.41
145	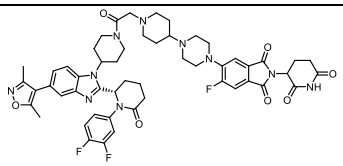	1.49	Insufficient compound	6.49*	+0.98
146	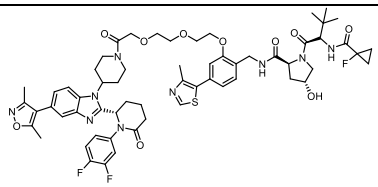	4.03	4.53	10.53	0.00

5.4 – Higher Throughput *in vitro* Testing of CREBBP and p300-Targeting PROTACs Conclusions

Using a capillary electrophoresis immunoassay (optimised in Chapter 4), the 42 novel PROTACs synthesised in Chapter 3 were assessed for their abilities to induce the degradation of CREBBP and/or p300. PROTAC **144** was shown to induce the statistically significant (Student's t-test) degradation of CREBBP, with more variable results for p300 degradation, and showed a dose-response relationship for lower PROTAC concentrations and a Hook effect for higher PROTAC concentrations, achieving a maximum degradation to 54% CREBBP with 370 nM PROTAC (Figure 49). Additionally, PROTACs **116**, **147**, **148**, and **163** caused small reductions in CREBBP/p300 levels over two biological repeats, but greater potency was desired, and these compounds were not investigated further.

Although the majority of the PROTACs did not induce CREBBP or p300 degradation, they offer structural insight for probing the SAR of CREBBP and p300-degrading PROTACs and could be used to guide the design of the next generation of compounds. **dCBP-1** is a potent degrader of both CREBBP and p300, and PROTACs developed using ligand **86** (PROTACs **112** – **122**) were designed to investigate the same bromodomain exit vector (Figure 44).[133] However, none of these PROTACs caused the degradation of either paralogue, but structural features of **dCBP-1** could be used to investigate the effect of binding the CREBBP and p300 bromodomain using the **(*R*)-OXFBD05** ligand (discussed in Section 5.1.2) (Figure 44, Figure 45). Additionally, the structures of PROTACs synthesised using the **Inobrodib**-based ligands **87** and **106** (PROTACs **134** – **157**, **160** – **164**, and **168** – **170**) could be used to investigate the SAR of active PROTAC **144.** The most structurally comparable PROTACs are **145** and **155** (Figure 52). Each of these PROTACs (**144**, **145**, and **155**) share an **Inobrodib**-based scaffold which is linked, by a chain of 14 atoms in length, from the benzimidazole group to the 5-position of a **thalidomide**-derivative cereblon ligand via a piperazine ring (Figure 52). However, neither **145** nor **155** showed any activity for degrading CREBBP or p300 under the examined conditions.

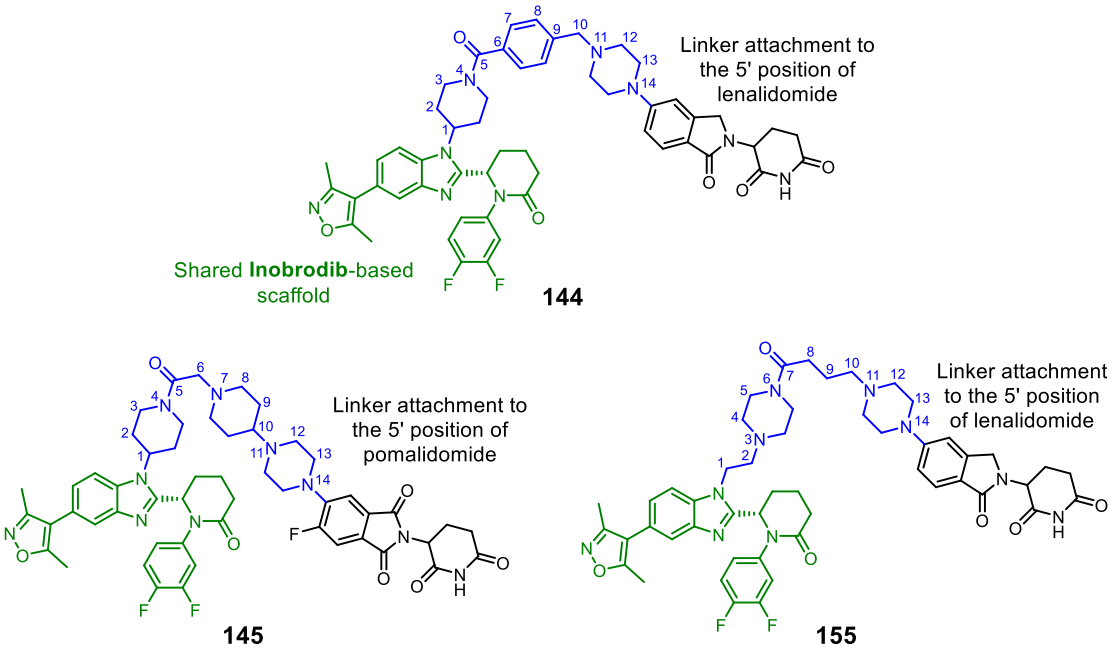

Figure 52. Comparison of the structures of **144** with **145** and **155**. Each compound shares the **Inobrodib**-based benzimidazole scaffold (green), comprises a chain of 14 atoms in length (blue), and is bound to the 5-position of the cereblon ligand (either lenalidomide or thalidomide) by a piperazine group. Neither PROTACs **145** nor **155** show any activity for degrading CREBBP or p300 in HeLa cells following 24 h incubation using a concentration gradient of 0.51 nM – 10 μM PROTAC.

Active PROTAC **144** have less favourable $clogD_{pH7.4}$ and PFI values than **145** and **155** (Table 13) so it is hypothesised that the difference in compound activities is due to the ability to form a stable POI:PROTAC:E3 ligase ternary complex and not as a result of compound solubility.[2] Section 1.1.5 discusses two examples of how modifications to the linker region of a PROTAC can enhance POI degradation,[26,27] therefore, the structures of **145** and **155** could be used to guide optimisation of PROTAC **144** further, for example to look at the importance of having a $-CH_2$ group adjacent to the piperazine ring.

PROTAC **144** showed a lower potency for degrading CREBBP and p300 than **dCBP-1** under the tested conditions. As discussed in Sections 3.1.2 and 5.2.2, these PROTACs are predicted to occupy different exit vectors from the CREBBP and p300 bromodomain which could cause the formation of different POI:PROTAC:E3 ligase ternary complex structures. It may be that **dCBP-1** is able to establish a more stable ternary complex structure than **144**, which is the driving force for PROTAC-induced protein degradation (discussed in Sections 1.1.4 and 1.1.5). Additionally, **dCBP-1** has more preferable physicochemical properties than PROTAC **144**, which may be hampering its ability to reduce cellular levels of CREBBP and/or p300 (Table 13).

Table 13. Calculated $logD_{pH7.4}$, measured $logD_{pH7.4}$, Property Forecast Index (PFI), and charge at pH 7.4 values of literature PROTAC **dCBP-1** and **Inobrodib**-based PROTACs **144**, **145**, and **155**.[133,196] $clogD_{pH7.4}$ values were calculated using Chemicalize (http://www.chemicalize.com) and are coloured according to compound aqueous solubility observations by Hill and Young, where $x < 2$ predicts good solubility (green), $2 < \boldsymbol{x} \leq 4$ predicts moderate solubility (yellow), and $\boldsymbol{x} > 4$ predicts poor solubility (red), darker colour indicates higher value within category.[20] The Property Forecast Index (PFI) is a measurement developed by GSK for predicting aqueous solubility (PFI = $clogD_{pH7.4}$ + #Ar rings).[21] PFI was calculated using the measured $logD_{pH7.4}$ + the number of aromatic rings.[20,21,143] * - PFI calculated using calculated $clogD_{pH7.4}$. PFI values are coloured according to compound aqueous solubility observations by Tinworth and Young, where $4 < \boldsymbol{x} \leq 8$ predicts moderate solubility (yellow), and $\boldsymbol{x} > 8$ predicts poor solubility (red), darker colour indicates higher value within category.[21]

Cpd.	R Group Structure	Calculated $logD_{pH7.4}$	Measured $logD_{pH7.4}$	PFI	Charge @ pH7.4
Literature CREBBP and p300 PROTAC					
dCBP-1	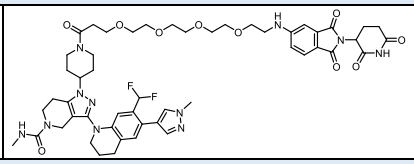	0.89	3.40	7.40	0.00
Active **Inobrodib**-based PROTAC					
144	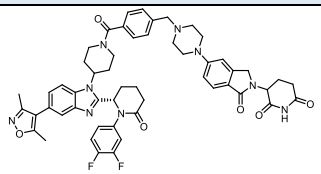	4.00	3.82	9.82	+0.86
Inactive **Inobrodib**-based PROTACs					
145	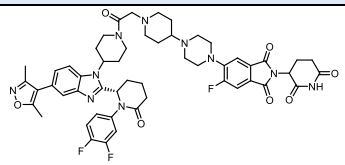	1.49	Insufficient compound	6.49*	+0.98
155	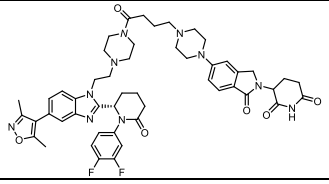	1.33	3.04	8.04	+1.58

Chapter 6 – Validation of the Ability of PROTAC **144** to Induce the Proteasomal Degradation of CREBBP and p300

6.1 – PROTAC **144** Activity Validation and Mechanism of Action Assay

6.1.1 –Larger Scale Cellular Assays and Western Blotting

To enhance the throughput of PROTAC synthesis and biological evaluation (described in Chapters 3 – 5), compounds were not required to have a purity of ≥95% and were not fully characterised. PROTAC **144**, which was found to induce reductions in cellular CREBBP levels for concentrations of 120 nM – 1.1 μM, was screened at a purity of 87% (LCMS). To validate the ability of PROTAC **144** to induce protein degradation, the compound was resynthesised, as previously described, to enable full compound characterisation and obtain a higher purity (HPLC: 98% pure). PROTAC **144** was reevaluated with larger scale cellular assays using a higher concentration of DMSO (1% *v/v* instead of 0.625% *v/v* used for the miniaturised cellular assays) to promote compound solubility, and the protein levels of CREBBP and p300 were then assessed using western blotting (Figure 53). 24 h PROTAC incubation at a concentration of 370 nM was investigated because this concentration caused the greatest CREBBP degradation in the capillary electrophoresis immunoassay, described in Section 5.3.

In parallel, the mechanism of action of PROTAC **144** was investigated to confirm the reduction in cellular protein levels was the result of on-target proteasomal degradation (Figure 53). To verify PROTAC **144** was binding the bromodomain of CREBBP and p300, a competition assay was performed, where cells were preincubated with **Inobrodib** for 4 h before the addition of **144** and further 24 h incubation.[112] Similarly, to confirm E3 ubiquitin ligase binding, cells were preincubated with the cereblon ligand **pomalidomide** for 4 h before 24 h incubation with PROTAC **144**.[15] To examine whether PROTAC **144-**induced protein degradation employs the proteasomal protein degradation pathway, two points of the pathway were inhibited to determine the impact on relative protein levels following **144** treatment. The proteasome was inhibited using **Carfilzomib**, and NEDD8-activating enzyme (NAE) was inhibited using **MLN4924**.[197–199] NAE was targeted because it is required for the neddylation and subsequent activation of cereblon as an E3 ubiquitin ligase enzyme.[199] To enable direct

comparison with the mechanism of action studies, cells treated with PROTAC **144** alone were first incubated with 1% *v/v* DMSO for 4 h before 24 h incubation with the PROTAC. Control experiments were performed for each of assays where PROTAC **144** was not added, and all assays were performed as three biological repeats.

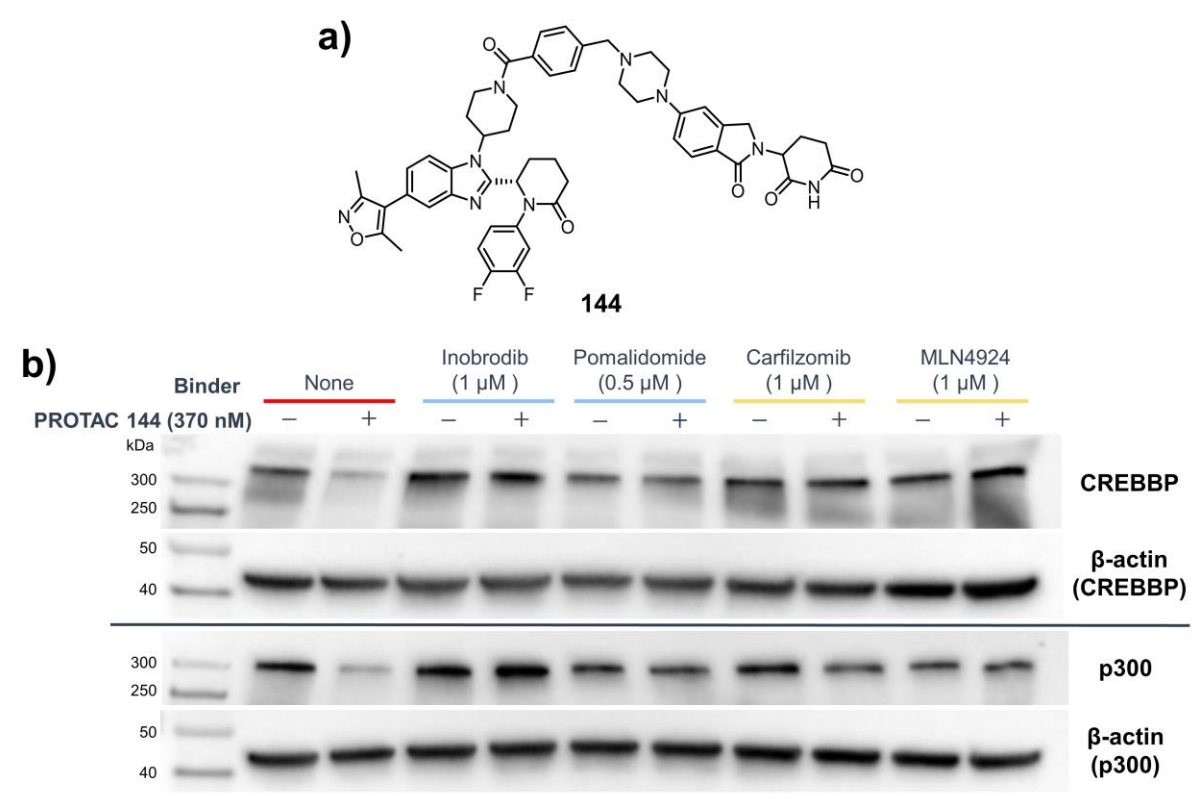

Figure 53. Assessment of the ability of PROTAC **144** to induce the degradation of CREBBP and p300 and investigation into the mechanism of action. Assays were performed using HeLa cells as three biological repeats and representative examples are shown, see Appendix Figure 18 for all western blots. Cells were preincubated with the relevant binder or the vehicle (DMSO) control at the given concentrations for 4 h before the addition of (±) PROTAC **144** (370 nM). Cells treated the PROTAC **144** alone were pre-treated with 1% *v/v* DMSO. The cells were incubated for a further 24 h before being harvested and lysed. Following cell lysis, protein levels were assessed using western blotting. **a)** Structure of PROTAC **144**. **b)** Representative western blots for CREBBP, p300 and the corresponding β-actin loading control. PROTAC **144** activity assays are highlighted in red, PROTAC **144** target engagement assays are highlighted in light blue, and PROTAC **144** degradation pathway investigation assays are highlighted in yellow. Blot images obtained using Image Lab (Bio-Rad) Software.

6.1.2 – The Ability of PROTAC **144** to Induce the Degradation of CREBBP and/or p300 in the Larger Scale Cellular Assays

Quantification of the western blots (Figure 53) for cells incubated with PROTAC **144** (370 nM) alone show a significant reduction in both CREBBP and p300 levels, to 37% and 27%, respectively, relative to the vehicle (DMSO) control treated cells (Figure 54, Appendix Table 15, Appendix Table 16).

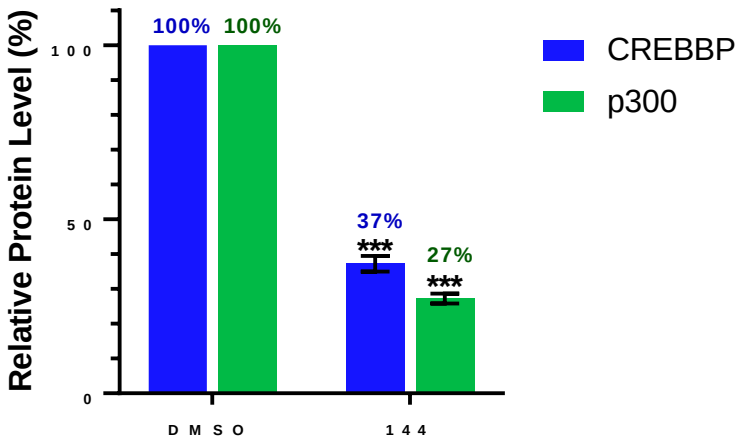

Figure 54. Quantification of CREBBP and p300 levels in HeLa cells following treatment with PROTAC **144** (370 nM) for 24 h relative to the vehicle (DMSO) control treated cells. Cells were preincubated with the compound vehicle (1% *v/v* DMSO) for 4 h. The vehicle (DMSO) control cells were then incubated for a further 24 h (28 h total). For the PROTAC **144** treated cells, following DMSO preincubation, PROTAC **144** (370 nM) was added and the cells were incubated for a further 24 h. Three biological repeats were performed, and protein levels were assessed using Western Blotting (Figure 53). Western Blot protein bands were analysed using Image Lab (Bio-Rad) software and the data were quantified using Excel (Appendix Table 15, Appendix Table 16). For each sample, the CREBBP/p300 band was normalised against the relevant β-actin loading control band then relative to the β-actin normalised DMSO control sample. A mean value was calculated as the % protein level relative to the vehicle (DMSO) control treated cells. CREBBP is reported in blue, p300 is reported in green. Error bars are the standard error of the mean. A Student's t-test was performed for each condition relative to the corresponding DMSO control data. Significance is denoted as: *** - $p \leq 0.001$, * - $p \leq 0.05$, ns - not statistically significant. Graph created using GraphPad Prism Software.

These data indicate superior degradation of CREBBP and p300 than observed in the screening immunoassay (described in Chapter 5), where 24 h treatment with PROTAC **144** (370 nM) resulted in the reduction of CREBBP levels to 54% but no significant reduction in p300 levels (both relative to the DMSO control). There are numerous variables associated with assessing relative protein levels in both the miniaturised, higher throughput immunoassay and the larger scale western blotting assay which could account for this.

One notable variation between the assays is the amount of DMSO used. The larger scale cellular assays used a higher percentage of DMSO in the cell media (1% *v/v* DMSO compared with 0.625% *v/v* for the miniaturised assays) and, additionally, cells were pre-incubated with the 1% *v/v* DMSO for 4 h before

addition of PROTAC **144**. These factors could both act to enhanced compound solubility and subsequently promote activity.[200] The cellular assays also differ in the method of adding compounds to the HeLa cells. To increase the throughput of the miniaturised assays, the compounds were pre-distributed into the 384-well plate before a suspension of the cells in media is added to the wells. Due to the high lipophilicity of PROTAC **144** (Table 13), the compound may have a high affinity for the plasticware of the assays and the miniaturised assay set-up may promote undesired interactions between the compound and well walls, thereby reducing the compound effective concentration.[201] However, these two hypotheses do not explain the Hook effect observed in the automated immunoassay (**Figure 49**) because you would expect protein levels to decrease further as the PROTAC concentration increased from 370 nM. Additional studies could be performed to better understand this disparity, such as investigating different concentrations of DMSO while keeping all other parameters identical.

6.1.3 – PROTAC **144** CREBBP/p300 and E3 Ubiquitin Ligase Target Engagement Assay Results

Quantification of the western blot bands for the PROTAC competition assays indicate that **144**-induced degradation of CREBBP and p300 is dependent on the on-target binding of both CREBBP/p300 and the E3 ubiquitin ligase cereblon (Figure 53, Figure 55). Competition of PROTAC **144** with the parent bromodomain ligand, **Inobrodib**, resulted in no significant change in CREBBP or p300 levels relative to the vehicle (DMSO) treated control cells. This demonstrates that degradation is reliant upon PROTAC interaction with the CREBBP and p300 bromodomain. Competition of PROTAC **144** with **pomalidomide** caused no significant reduction in CREBBP levels, but reduced the p300 level to 55% relative to the vehicle (DMSO) treated control cells (Figure 55, Appendix Table 16). However, a greater reduction in the relative p300 level to 27% was observed following incubation with PROTAC **144** alone (Figure 55, Appendix Table 16) suggesting that **pomalidomide** was interrupting PROTAC **144** binding cereblon but does not completely block the interaction. A study by Shahbazi *et al.* has shown **pomalidomide** to be unstable in human plasma, with 72% compound degradation observed after 24 h at room temperature.[202] Instability of **pomalidomide** in the competition assay would cause fewer

cereblon binding sites to be occupied, enabling binding of **144** to cereblon to induce CREBBP/p300 degradation. To investigate this further, higher concentrations of **pomalidomide** or shorter timepoints could be investigated but, overall, these data indicate that cereblon binding is required for PROTAC **144** activity.

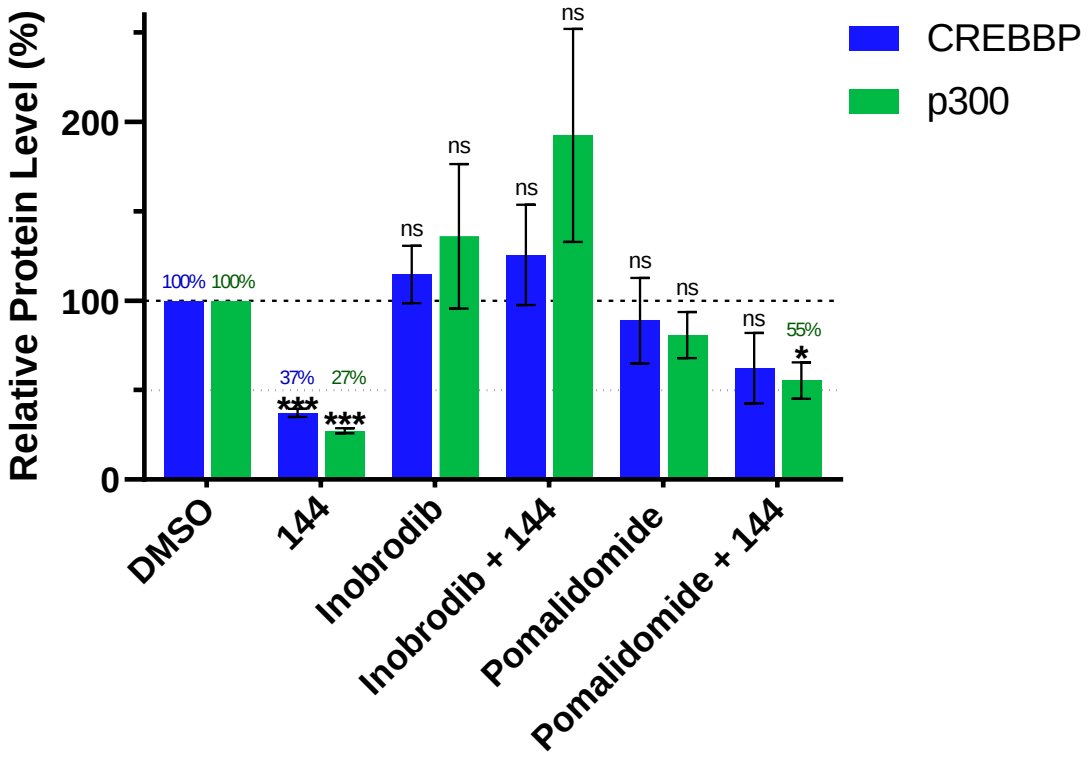

Figure 55. Quantification of CREBBP and p300 levels in HeLa cells ivestigating the target engagement of PROTAC **144** (370 nM) using competition assays with either CREBBP and p300 ligand **Inobrodib** (1 μM) or cereblon ligand **pomalidomide** (1 μM). HeLa cells were pre-treated with either the compound vehicle (DMSO), Inobrodib (1 μM), or pomalidomide (1 μM), as indicated, for 4 h before incubation with (±) PROTAC **144** (370 nM), as indicated, for 24 h. Three biological repeats were performed, and protein levels were assessed using Western Blotting (Figure 53). Western Blot protein bands were analysed using Image Lab (Bio-Rad) software and the data were quantified using Excel (Appendix Table 15, Appendix Table 16). For each sample, the CREBBP/p300 band was normalised against the relevant β-actin loading control band then relative to the β-actin normalised DMSO control sample. A mean value was calculated as the % protein level relative to the vehicle (DMSO) control treated cells. CREBBP is reported in blue, p300 is reported in green. Error bars are the standard error of the mean. A Student's t-test was performed for each condition relative to the corresponding DMSO control data. Significance is denoted as: *** - $p \leq 0.001$, * - $p \leq 0.05$, ns - not statistically significant. Graph created using GraphPad Prism Software.

6.1.4 – Investigation into the PROTAC **144**-Induced CREBBP and p300 Degradation Pathway Assay Results

Quantification of the western blot bands investigating the POI degradation pathway indicate that PROTAC **144** is utilising the expected proteasomal degradation pathway to remove CREBBP and p300 from the cell (Figure 53, Figure 56).[3] Inhibition of the proteasome using **Carfilzomib** followed by

PROTAC **144** incubation resulted in no significant changes to CREBBP or p300 levels relative to the vehicle (DMSO) treated control cells, signifying that the proteasome is required for the PROTAC mechanism of action (Figure 56).[197] Inhibition of the NAE using **MLN4924** and incubation with **144** caused no significant changes to CREBBP levels, but p300 levels were reduced to 67% relative to the DMSO control (Figure 56, Appendix Table 16). However, this reduction in p300 is less than for incubation with PROTAC **144** alone, where the relative protein level was reduced to 27%, and has a lower significance. Therefore, these data indicate that inhibition of the NAE is reducing the **144**-induced cereblon-mediated degradation of p300 and further studies could examine the effect of using different **MLN4924** concentrations or shorter timepoints.

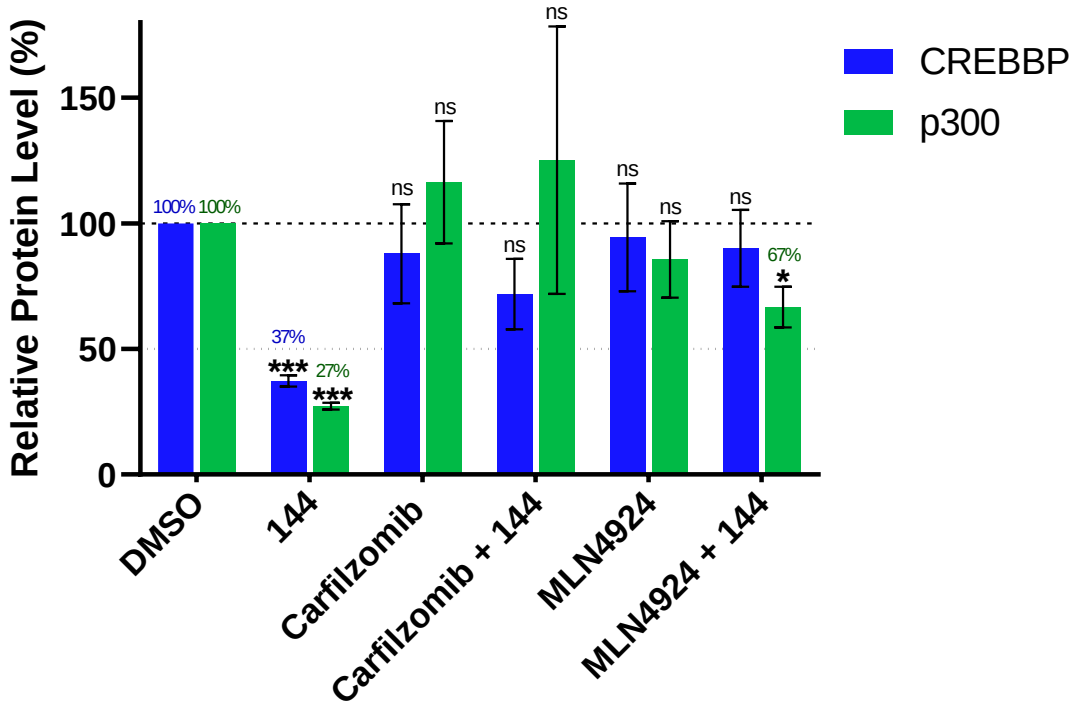

Figure 56. Quantification of CREBBP and p300 levels in HeLa cells ivestigating the pathway being utilised by PROTAC **144** to degrade CREBBP and p300. HeLa cells were pre-treated with either DMSO, **Carfilzomib** (0.5 μM), or **MLN4924** (1 μM), as indicated, for 4 h before incubation with (±) PROTAC **144** (370 nM), as indicated, for 24 h. Three biological repeats were performed, and protein levels were assessed using Western Blotting (Figure 53). Western Blot protein bands were analysed using Image Lab (Bio-Rad) software and the data were quantified using Excel (Appendix Table 15, Appendix Table 16). For each sample, the CREBBP/p300 band was normalised against the relevant β-actin loading control band then relative to the β-actin normalised DMSO control sample. A mean value was calculated as the % protein level relative to the vehicle (DMSO) control treated cells. CREBBP is reported in blue, p300 is reported in green. Error bars are the standard error of the mean. A Student's t-test was performed for each condition relative to the corresponding DMSO control data. Significance is denoted as: *** - $p \leq 0.001$, * - $p \leq 0.05$, ns - not statistically significant. Graph created using GraphPad Prism Software.

6.2 –PROTAC **144**-Induced Proteasomal Degradation of CREBBP and p300 Investigation Conclusions

These validation studies have shown that PROTAC **144** (370 nM) is able to cause reduction in cellular CREBBP and p300 levels by 63% and 73%, respectively, following 24 h incubation. These results show a greater PROTAC potency than was measured using the capillary electrophoresis immunoassay in Chapter 5 which could be due to numerous variables, including DMSO concentration and compound purity, which could be investigated further. Additionally, the larger scale cellular assay used in the chapter only investigated the 24 h timepoint and using 370 nM PROTAC concentration. Future assays could be used to find the optimal PROTAC incubation times and concentrations for inducing CREBBP and p300 degradation.

The work described in this chapter, also, validated the reduction in CREBBP and p300 cellular levels as an on-target effect by investigating the target engagement and mechanism of action of PROTAC **144**. Competition assays confirmed PROTAC **144** activity required binding of the CREBBP/p300 bromodomain and the E3 ubiquitin ligase cereblon, and the inhibition of two points of the proteasomal degradation pathway demonstrated that CREBBP/p300 degradation required the 26S proteasome and the activation of cereblon to have E3 ubiquitin ligase functionality.

Chapter 7 – Conclusions and Future Work

7.1 – Conclusions

The aim of the work described in this dissertation was to synthesise and biologically evaluate novel bifunctional molecules to induce the degradation of CREBBP and/or p300 in the cell. Such chemical probes would allow the overall cellular functions of CREBBP and/or p300 to be studied, and could also provide starting points for therapeutic development, because CREBBP and p300 are clinically relevant targets for cancer treatment.[109–114] This work describes the conversion of three CREBBP and p300 bromodomain ligands to bifunctional molecules and primarily focused on the synthesis of PROTAC chemical probes, but a small series of HyTs was also evaluated. Recently, three distinct CREBBP and p300-degrading PROTACs (**dCBP-1**, **JET-209**, and **JQAD1**) have been reported in the literature, displaying the high interest in this field. However, to effectively validate the biological results of these compounds, multiple, structurally orthogonal probes are required.[138,139] Additionally, selectively for degrading one paralogue over the other has only been displayed with **JQAD1**, but this PROTAC only causes moderate protein degradation (no quantification reported).[135] Furthermore, the abilities of **dCBP-1** and **JET-209** to induce CREBBP and p300 degradation were only reported for short timepoints, while it would be preferable for a chemical probe to cause a long lasting protein knockdown. Therefore, bifunctional optimisation is still required.

Initially, a rational design approach was used to develop bromodomain ligand **(*R*)-OXFBD05** into PROTACs recruiting the E3 ubiquitin ligases cereblon and VHL (described in Chapter 2, VHL-targeting PROTACs synthesised by Dr Pascal Heitel). Additionally, a small series of HyTs, that use a lipophilic adamantane group to non-specifically recruit an E3 ligase enzyme, was also investigated. An SAR investigation indicated that the addition of flexible PEG linkers to the DHBD group of **(*R*)-OXFBD05** was promising for PROTAC synthesis and four linker lengths were investigated for each bifunctional series in an attempt to discover the optimal structure for ternary complex formation and protein degradation. However, this initial approach was limited by a multistep, linear synthesis to obtain the final PROTAC molecules, as the linker needed to be coupled to an early stage **(*R*)-OXFBD05** intermediate, and this greatly reduced the throughput of obtaining final molecules for testing. Biological

evaluation found that the HyTs (**65** – **68**) did not reduce CREBBP or p300 levels when examined at 10 μM for 24 h using HET293T cells, and appeared to cause off-target cytotoxicity, so these were not investigated further. PROTACs from both the VHL and cereblon-targeting series caused moderate reductions in relative CREBBP and p300 cellular levels, but higher potency was desired. Additionally, the VHL series of PROTACs appeared to cause off-target cytotoxic effects on the cells. Analysis of the $clogD_{pH7.4}$ and PFI values for PROTACs (**31** – **38**) and HyTs (**65** – **68**) predicted each compound to be poorly soluble in the assay conditions, with the predicted least soluble bifunctional molecules appearing to correlate to the most cytotoxic. Therefore, the next series of compound looked to improve PROTACs physicochemical properties as well as improving the synthetic throughput.

To streamline PROTAC synthesis, CREBBP and p300 bromodomain ligands were functionalised with amine groups to enable the one-step derivatisation of the ligand into the final PROTACs using amide coupling reactions (discussed in Chapter 3). The DHBD group of **(*R*)-OXFBD05** was modified by addition of a piperidine ring to afford ligand **86** and two additional ligands were investigated that derive from the higher bromodomain binding affinity ligand **Inobrodib** (ITC binding affinities for CREBBP: **(*R*)-OXFBD05** K_d = 102 nM, **Inobrodib** K_d = 1.7 nM), which was modified with either a piperidine group (ligand **87**) or an ethyl piperazine moiety (ligand **106**). Together, these novel ligands enabled the facile synthesis of 42 novel PROTACs (discussed in Chapter 3) for biological evaluation which investigated a variety of linker lengths, linker compositions, and different cereblon or VHL-targeting ligands. Due to the number of PROTACs synthesised, it was necessary to develop a higher throughput assay for measuring their ability to degrade CREBBP and/or p300, which was achieved using an automated capillary electrophoresis immunoassay (optimised in Chapter 4). This immunoassay was used to measure the relative CREBBP and p300 levels of cells following 24 h incubation with a concentration gradient of each PROTAC (10 μM – 0.51 nM) (discussed in Chapter 5). The results showed that 37 PROTACs did not cause a reduction in CREBBP or p300, four PROTACs induced a small reduction in either CREBBP or p300, and PROTAC **144** resulted in the significant degradation of CREBBP. In this assay, **144** achieved a maximum reduction in CREBBP levels to 54% using 370 nM PROTAC and displayed a Hook effect with higher concentrations.[2]

Larger scale cellular assays using the optimal parameters from the capillary electrophoresis immunoassay (HeLa cells, 24 h, 370 nM) followed by western blot analysis (described in Chapter 6) found PROTAC **144** to induce the degradation of both CREBBP and p300, reducing the relative protein levels to 37% and 27%, respectively. The difference in assay results could arise from multiple variables and further experiments could investigate these (discussed in Chapter 6). Additionally, mechanism of action investigations confirmed that the reduction in CREBBP and p300 levels caused by **144** incubation was the result of on-target protein binding and that the 26S proteasome and neddylation pathway were required.

Overall, this work has identified a novel PROTAC for inducing the degradation of CREBBP and p300 in the cell. PROTAC **144** is structurally different to the other CREBBP and p300-targeting PROTACs, so could be used in combination to confirm subsequent effects as being on-target. Future studies could investigate optimal assay conditions to achieve maximal protein degradation using **144** and could also look at optimising the PROTAC structure further.

7.2 – Future Work

7.2.1 – Further Investigation into the Role of Cereblon on PROTAC **144** Activity

The PROTAC mechanism of action studies described in Chapter 6, showed some residual degradation of p300 in the **pomalidomide** competition assay and in the neddylation inhibition assay. Both of these assays investigate the role of cereblon in **144**-induced degradation of CREBBP and p300, where **pomalidomide** should inhibit PROTAC binding, and **MLN4924** should inhibit cereblon activation.[15,198] These experiments could be repeated using different compound concentrations or shorter timepoints to determine the subsequent effect on CREBBP and p300 degradation. Additionally, the role of cereblon function in **144**-induced degradation could be further validated using cereblon knockout cells, where you would expect no CREBBP or p300 degradation following PROTAC incubation.[203]

Compound **144** could be *N*-methylated on the lenalidomide glutarimide ring to produce a negative control compound that will not bind cereblon due to steric hinderance in the cereblon binding site (Figure 57).[204] This small modification should be able to identify PROTAC off-targets without interfering with the native cellular interactions of cereblon.

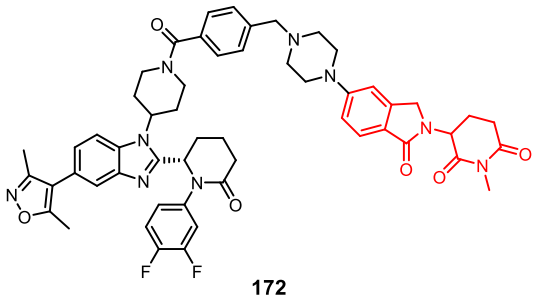

172

Figure 57. Structure of postulated negative control compound **172**. This compound comprises a *N*-methyl glutarimide ring which should not bind cereblon due to steric hindrance with the binding site.[204] N-methyl lenalidomide highlighted in red.

7.2.2 – Further Investigation into Optimal Conditions for CREBBP and p300 Degradation using PROTAC **144**

At present, the larger scale cellular assay has only investigated the ability of PROTAC **144** to cause the degradation of CREBBP and p300 in HeLa cells at 370 nM for 24 h. Further assays should be performed that investigate optimal **144** concentration for inducing protein degradation, and to calculate DC_{50} and D_{max} values. Additionally, a timecourse could be performed to determine the optimal incubation time for protein degradation. Longer timepoints would be able to show whether **144** can cause a sustained

knockdown of CREBBP and p300 in the cell, which would be desirable for chemical probes and therapeutics. Additionally, shorter timepoints could investigate the stability of **144** in cells. It has been reported in the literature that **thalidomide**-based PROTACs **dBET1** and **BSJ-03-123** cause a large initial degradation of their POIs, but that this decreases as the incubation time increases to 24 h due to poor PROTAC stability.[145,188–190] If the PROTAC were found to show a similar trend of large initial protein degradation that then decreases over time, this could suggest similar PROTAC stability issues which could be addressed in compound optimisation.

7.2.3 – Investigation into PROTAC **144** Stability

If a timecourse assay found that PROTAC **144** lost potency over time, the cereblon ligand, **lenalidomide**, could be changed for a ligand with greater aqueous stability to determine whether the poor stability of **thalidomide** analogues is contributing factor.[202] Min *et al.* have reported the optimisation of **dBET1** to **SJ995973** by modification of the **thalidomide** ligand to a ligand comprising a phenyl glutarimide (Figure 58).[205] This enhanced compound stability by removal of the hydrolysis-susceptible imide group and this, additionally, stabilised of the glutarimide ring against hydrolysis. Accordingly, **SJ995973** exhibited enhanced degradation of BRD4 than **dBET1** in HD-MB03 cells with a greater potency (**SJ995973** DC_{50} = 24 nM, **dBET1** DC_{50} = 230 nM, 12 h incubation, HD-MB03 cells) and showed sustained protein degradation over 96 h (Figure 58).

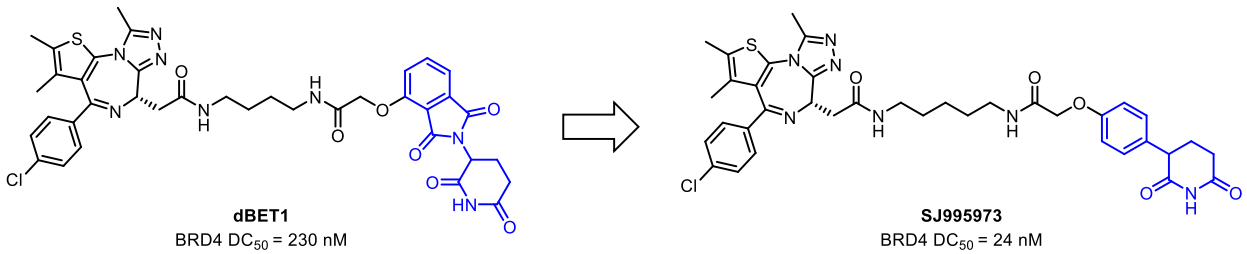

Figure 58. Optimisation of the BRD4-degrading PROTAC **dBET1** to **SJ995973**.[188,205] The cereblon ligand of **dBET1** (**thalidomide**) was modified to a phenyl glutarimide which shows a greater stability against hydrolysis and resulted in an increased potency for degrading BRD4. DC_{50} values were measured following 12 h incubation with HD-MB03 cells. Cereblon ligands highlighted in blue.

Jarusiewicz *et al.* later showed that replacement of the glutarimide stereogenic carbon with a nitrogen, to form a phenyl dihydrouracil, not only eliminated the known facile inversion of stereochemistry at

this position, but also enhanced the stability of the 6-membered ring against hydrolysis.[206] They found that optimisation of the phenyl glutarimide in LCK-degrading PROTAC **SJ11646** to a phenyl dihydrouracil in **SJ34739** retained a high potency for degrading LCK in cells (**SJ11646** DC_{50} = 8 nM, **SJ34739** DC_{50} = 15 nM, 4 h incubation, HiBit-tagged KOPT-K1 cells) and enhanced compound stability in cell media over a 50 h time course (Figure 59).[206,207]

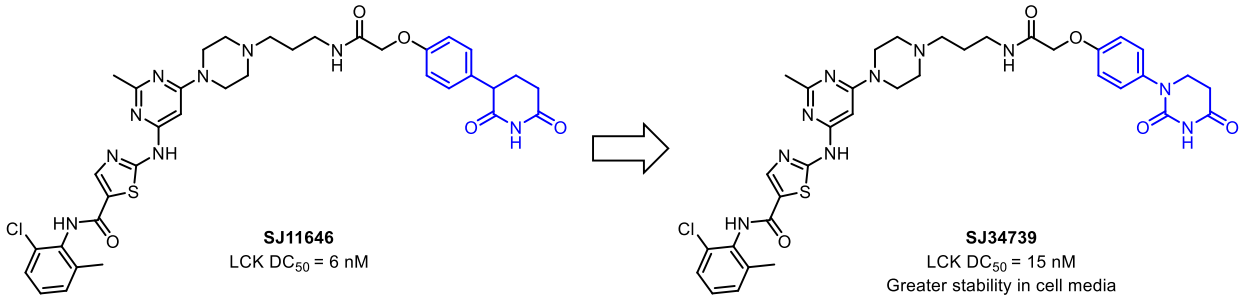

Figure 59. Optimisation of the LCK-degrading PROTAC **SJ11646** to **SJ34739**.[206,207] The phenyl glutarimide cereblon ligand of **SJ11646** was modified to a phenyl dihydrouracil which retained a high potency for degrading LCK in cells and exhibited greater stability in cell media. DC_{50} values were measured following 4 h incubation with HiBiT-tagged KOPT-K1 cells. Cereblon ligands highlighted in blue.

The **lenalidomide** ligand of PROTAC **144** could be similarly converted to a phenyl glutarimide or phenyl dihydrouracil (Figure 60), but due to the shorter distance between the linker attachment position and glutarimide/ dihydrouracil ring, the PROTAC linker length will likely need to be optimised. For the optimisation of **dBET1** to **SJ995973**, the linker was extended by one -CH_2 group.[205]

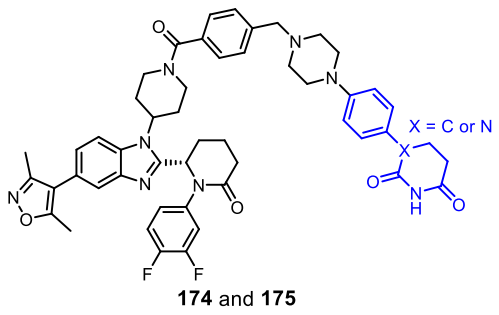

Figure 60. Proposed modification of the cereblon ligand (**lenalidomide**) of PROTAC **144** to a phenyl glutarimide (**174**) or phenyl dihydrouracil (**175**) which are reported to have enhanced stability in biological systems than **thalidomide**.[205,206]

7.2.4 –Investigation into the Consequences of PROTAC **144**-Induced CREBBP and p300 Degradation

There is currently clinical interest in inhibiting the bromodomain of CREBBP and p300 to treat a range of cancers with two compounds in clinical trials, including **Inobrodib**, which is used as the CREBBP and p300 ligand for PROTAC **144**.[112–114,196,208] Due to the potential of **Inobrodib** as a chemotherapeutic, it would be interesting to examine the phenotypic effects of **144**-induced CREBBP and p300 degradation in cancer cells and compare these to the effects of bromodomain inhibition alone. Such experiments could look at cell proliferation, cell mortality, and the effects on downstream protein expression levels. PROTAC-induced POI degradation can cause greater reductions in downstream cellular pathways and have a longer effect than the corresponding single domain inhibition with the PROTAC POI ligand.[115] *In vitro* experiments in castration-resistant prostate cancer showed **Inobrodib** inhibition of the CREBBP and p300 bromodomain to reduce the cellular levels of multiple proteins, including those involved in the androgen receptor (AR) signalling pathway, the upregulation of which is indicative of advanced disease.[129] Further studies displayed a greater antiproliferative activity of **Inobrodib** in AR-proficient cells ($IC_{50} < 100$ nmol/L) than AR-negative cells ($IC_{50} > 1000$ nmol/L), and mouse xenograft studies showed **Inobrodib** treatment to inhibit the AR signalling pathway, reduce tumour volumes, and increase mouse survival. Therefore, **Inobrodib**-based PROTACs, such as **144**, could cause greater anti-cancer effects than **Inobrodib** and could represent a starting point for chemotherapeutic development.

7.2.5 – PROTAC **144** SAR Investigation

As discussed in Section 1.1, PROTAC potencies and selectivities have been reportedly optimised by modifications to the linker region and E3 ubiquitin ligase ligand. For example, PROTAC **MZ1** was optimised to **AZ1** by conversion of a PEG linker to an alkyl linker and modification of the linker-E3 ligase ligand coupling position, which enhanced the PROTAC selectivity for BRD4 degradation over its paralogues.[11,23]

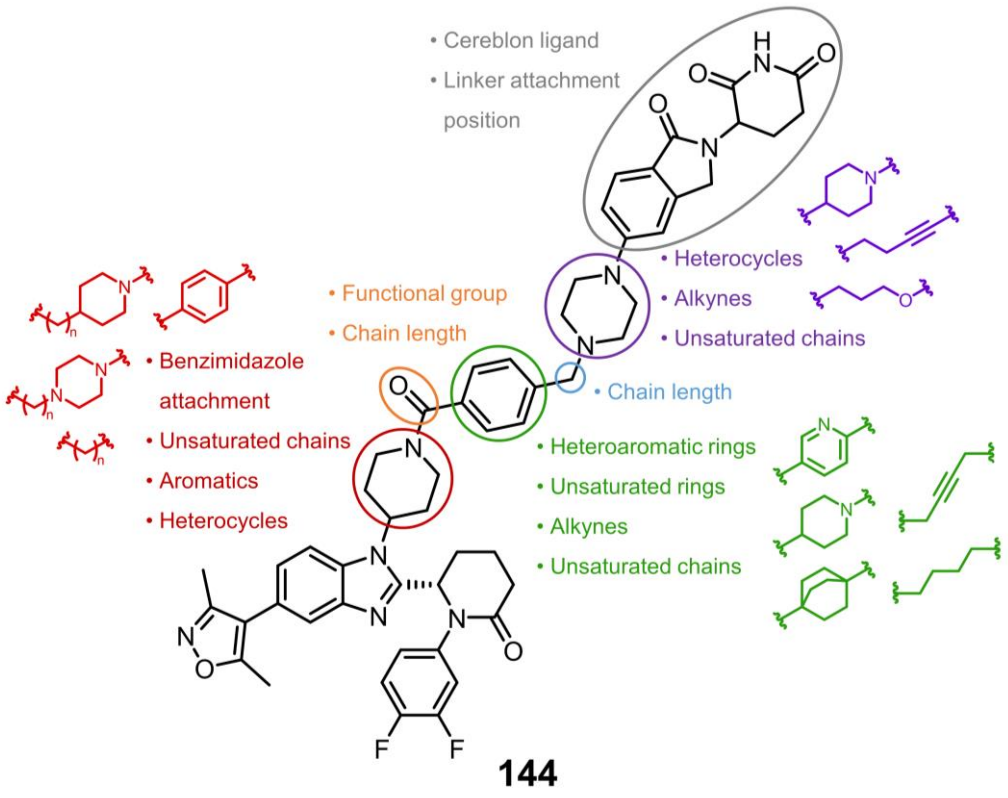

Figure 61. Positions of PROTAC **144** that could investigated to examine the compound's SAR with suggested modifications.

It may be possible to optimise the potency and selectivity of **144** by investigating the SAR of the compound. Additionally, compounds could be designed to improve the physicochemical properties of **144**, which was discussed as a potential obstacle for inducing protein degradation in cellular assays in Section 5.4. There are numerous possibilities of modifying PROTAC **144** including investigating the piperidine ring of the **Inobrodib**-based ligand **87**, altering the composition of the linker, and altering the linker attachment position to the cereblon ligand (Figure 61). The results of such an SAR study could provide information for gaining compound potency, increasing compound stability, and enhancing selectivity for CREBBP over p300 or *vice versa*.

Chapter 8 – Experimental

8.1 – Biochemical and Biophysical Methods

8.1.1 Biological reagents and pH measurements

Biologically tested compounds were synthesised according to the procedures described in Section 8.3 or were purchased from commercial sources, see Table 18. All biologically tested compounds were >95% pure unless otherwise stated.

Purified (Milli-Q) water was obtained from a Millipore Elix® Reverse Osmosis system which was further purified by a Millipore Milli-Q® Synthesis system with a 0.22 µm filter on the outlet.

Media, buffers, and gels were made with distilled H_2O, unless otherwise stated and adjusted to the required pH by the addition of aq. HCl or aq. NaOH solutions.

pH measurements were performed using an Oakton pH 550 Benchtop pH Meter Kit, with an Oakton pH electrode with temperature sensor. The electrode was stored in a 4 M aq. potassium chloride solution and calibration was carried out between pH 4.0 – 7.0 and 7.0 − 10.0 immediately before use, with pH 4.0, pH 7.0, pH 10.0 buffer solutions.

8.1.2 Protein Expression and Purification

Protein molecular weight and molar extinction coefficient were calculated using ProtParam on the ExPASy Bioinformatics Resource Portal.

Protein expression. Standard sterile practices were followed using an open flame, on sterilised surfaces using 70% *v/v* EtOH in H_2O. Media and equipment were sterilised by autoclaving at 121 °C for 15 min. Solutions of isopropyl ß-D-1-thiogalactopyranoside (IPTG), antibiotics and other labile compounds were sterilised by filtering through 0.22 µm filters. Competent *E. coli* BL21 (DE3) cells (20 µL) were thawed on ice and the CREBBP bromodomain plasmid (1.0 µL) was added. The cell solution was incubated on ice for 30 min, heated at 42 °C for 30 sec, incubated on ice for 5 min, then SOC outgrowth medium (500 µL) was added. The solution was incubated at 37 °C for 1 h before the transformation mixture (100 – 200 µL) was plated onto 2× TY Bacto agar plates containing kanamycin (50 µg/ mL) and incubated at 37 °C overnight. A single colony was harvested, transferred into 2× TY medium

(100 mL) containing kanamycin (50 μg/ mL), and incubated at 37 °C and 180 rpm overnight. The cell culture (10 mL) was added to 2× TY medium (1.0 L) containing kanamycin (50 μg/ mL). The culture was incubated at 37 °C and 180 rpm until an OD_{600} value of 0.6 was reached. OD_{600} values were measured in 1.6 mL cuvettes against a reference of 2× TY medium, using a Novaspec® II spectrophotometer measuring at 600 nm. The cultures were cooled to 16 °C and IPTG was added (0.1 mM final concentration). The cell cultures were fermented at 16 °C and 180 rpm overnight. Cells were harvested by centrifugation (4 °C, 11,325 ×*g*, 10 min) and the cell pellet was stored at −80 °C.

Table 14. Protein expression media/ agar recipes.

Media/ Agar	Reagent	Mass per litre (gL^{-1})
2× TY	Tryptone	16
	Yeast Extract	10
	NaCl	5
2× TY Bacto agar plates	Tryptone	16
	Yeast Extract	10
	NaCl	5
	Bacto agar	15

Protein purification. A cell pellet was suspended in extraction buffer (100 mL/ 20 g cell mass), Benzoase® Nuclease (25 Units (U)) was added, and the cells were lysed by sonication (30 × 5 sec bursts, 5 sec pause) on ice. 15% Polyethyleneimine was added, and the cells were incubated on ice for 15 min. The lysate was centrifuged, the supernatant decanted, and filtered through a 0.45 μm filter. The lysate was purified by Immobilised Metal Affinity Chromatography (IMAC) at 4 °C with a HisTrap™ column. The column was washed with Milli-Q water, then 100 mM $NiSO_4$, and equilibrated in binding buffer. The column was loaded with the cell lysate solution, washed (gradient of 9 – 12% elution buffer in binding buffer), then the protein was eluted (gradient of 60 – 100% elution buffer in binding buffer), and the column was washed with strip buffer. The eluted protein was collected, and fractions containing the highest levels of pure protein, as determined by purification UV trace and by SDS-PAGE of the fractions, were concentrated by centrifugation (4 °C, 4,000 ×g) using 10k MWCO spin protein concentrators. The protein was further purified by size-exclusion chromatography (SEC) using a 120/300 mL column with Superdex 75 resin that had been pre-equilibrated with gel filtration buffer. The protein was eluted in gel filtration buffer and fractions containing the highest levels of pure protein, as determined by SDS-PAGE, were concentrated by centrifugation (4 °C, 4,000 ×g) using 10k MWCO

spin protein concentrators. Protein concentration was measured using a NanoDrop Lite spectrophotometer using the predicted protein absorbance (CREBBP: ε_{280}: 26930 M^{-1} cm^{-1}). The concentrated protein solution was aliquoted, flash frozen in liquid N_2, and stored at −80 °C.

Table 15. Protein purification buffer recipes. Buffers were adjusted to the required pH, filtered through a 0.22 µm filter, and degassed. * - added immediately prior to use.

Buffer	Reagent	Concentration (mM)
Extraction buffer (pH 7.6)	HEPES	50
	NaCl	500
	Imidazole	5
	SigmaFAST Protease Inhibitor Cocktail Tablet, EDTA Free	1 tablet
IMAC binding buffer (pH 7.6)	HEPES	50
	NaCl	500
	Imidazole	5
	β-Mercaptoethanol*	10
IMAC elution buffer (pH 7.6)	HEPES	50
	NaCl	500
	Imidazole	500
IMAC strip buffer (pH 7.6)	HEPES	50
	NaCl	500
	EDTA	100
SEC gel filtration buffer (pH 7.6)	HEPES	50
	NaCl	500

Sodium dodecyl sulfate polyacrylamide gel electrophoresis (SDS-PAGE). Gels were prepared using 70 mm × 100 mm glass plates, with 0.75 mm spacers. The resolving gel was cast, then covered with a thin layer of methanol to ensure a level surface, which was removed before casting the stacking gel. Protein samples for SDS-PAGE were prepared with 10% *v/v* β-mercaptoethanol in 4× Laemmli sample buffer and denatured at 100 °C for 5 min. Protein samples were loaded onto the gel which was run in a Mini-PROTEAN® 3 Electrophoresis System at 100 V for 10 min then at 200 V until the loading dye reached the bottom of the gel. Following Electrophoresis, gels were stained with InstantBlue™ Coomasie® stain for 15 mins then destained with Milli-Q water.

Table 16. SDS-PAGE buffer recipe.

Buffer	Reagent	Concentration (mM)
SDS-PAGE running buffer	Tris-HCl	25
	Glycine	190
	SDS	3.5

Protein mass spectrometry utilised a Waters LCT Premier XE bench-top orthogonal acceleration time-of-flight LC/MS system equipped with desalting LC column for front end LC/MS and connected

to an Acquity Column Compartment, Acquity Sample Manager and Acquity Binary Solvent Manager. Inspection and deconvolution of the mass spectra were performed using MassLynx 4.1.

8.1.3 Isothermal Calorimetry

All calorimetric experiments were performed on a MicroCal PEAQ-ITC Automated and analysed with the MicroCal PEAQ-ITC Analysis software using a single binding site model. The first data point was excluded from the analysis. The CREBBP bromodomain was dialysed at 4 °C overnight in a Slide-A-Lyzer® MINI Dialysis Device in 0.2% DMSO *v/v* ITC buffer. Proteins were centrifuged to remove aggregates (3 min, 3,000 rpm, 25 °C). Protein concentrations were determined by measuring the absorbance at 280 nm using a NanoDrop Lite spectrophotometer using the predicted protein absorbance (CREBBP: ε_{280}: 26930 M^{-1} cm^{-1}). Tested compounds were dissolved as a DMSO stock solution (10 mM) and diluted to the required concentration in 0.2% (total) DMSO *v/v* ITC buffer. The cell was stirred at 750 rpm, reference power set to 5 µcal sec^{-1}, and temperature held at 25 ˚C. Small molecule solutions in the calorimetric cell (250 µL, (10 – 40 µM) were titrated with the protein solutions in the syringe (60 µL, 160 – 250 µM). After an initial delay of 60 sec, 20 × 2 µL injections (first injection 0.4 µL) were performed with a spacing of 150 sec.

Table 17. ITC buffer recipe.

Buffer	Reagent	Concentration (mM)
ITC buffer (pH 7.4)	HEPES	50
	NaCl	150

8.1.4 *In Vitro* Assays

Cell Culture. HEK293T and HeLa cells were cultured in Dulbecco's Modified Eagle Medium (DMEM) with high glucose, GlutaMAX™, and pyruvate supplemented with penicillin (100 U/mL), streptomycin (100 µg/mL), and 10% *v/v* fetal bovine serum (FBS), here-after referred to as “growth media”, at 37 °C and 5% CO_2. Standard sterile practices were followed. Cells were split 2 – 3 times/ week once 70 – 80% confluency was reached and were regularly tested for the presence of mycoplasma. Cells were either counted on a Countess™ II automated cell counter using a Countess™ Cell Counting Chamber Slide or on a NucleoCounter® NC-200™ using a Via1-Cassette™ according to the manufacturers’ guidelines.

si-RNA-mediated knockdown. HEK293T/ HeLa cells were seeded into 6-well plates at a concentration of 220,000 cells/ well in growth media (2 mL) and allowed to settle overnight at 37 °C and 5% CO_2. The media was discarded and replaced with Opti-MEM™ (750 µL). Transfection reagents were prepared in sterile Eppendorf tubes: Lipofectamine™ RNAiMAX Transfection Reagent (9 µL) was diluted in Opti-MEM™ (150 µL) and 10 µM siRNA (3 µL) was diluted in Opti-MEM™ (150 µL). The diluted siRNA solution (150 µL) was added to the diluted Lipofectamine™ RNAiMAX Transfection Reagent solution (150 µL) and incubated at rt for 5 min. The siRNA-lipid complex (250 µL, 25 pmol final siRNA, 7.5 µL final Lipofectamine™ RNAiMAX) was added to the relevant well and the plates were incubated at 37 °C and 5% CO_2 for 5 h before the media was replaced with growth media (2 mL). The plates were incubated at 37 °C and 5% CO_2 for the remainder of the assay time-course. Cells were harvested at 24 h, 48 h, and 72 h post-transfection by washing with PBS (1 mL), scraping into PBS (1 mL), and centrifuging (3,000 ×g, 5 min, 4 °C). The cell pellet was lysed in UTB buffer (50 µL) and sonicated (3 × 10 sec bursts, 10 sec pause) on a FB-505 sonic dismembrator with a 1/16" tapered microtip at 40% maximum power whilst being kept on ice between sonication bursts. The lysates were centrifuged (16,000 ×g, 10 min, 4 °C), the supernatants were transferred to a fresh tube, and stored at −20 °C.

Larger scale compound *in vitro* testing. 100 mm dishes were seeded with 2,200,000 cells/ dish in growth media and allowed to settle overnight at 37 °C and 5% CO_2. Cells were treated with 1% *v/v* DMSO in growth media ± test compound at the given concentrations and were incubated at 37 °C and 5% CO_2 for the given assay time. The cells were washed with PBS (2 × 3 mL), scraped into PBS (1 mL), and centrifuging (4 °C, 3,000 ×g, 5 min). The cell pellet was lysed in UTB buffer (100 µL) and sonicated (3 × 10 sec bursts, 20 sec pause) on a FB-505 sonic dismembrator with a 1/16" tapered microtip at 40% maximum power whilst being kept on ice between sonication bursts. The lysates were centrifuged (4 °C, 16,000 ×g, 10 min), the supernatants were transferred to a fresh tube, and then stored at −20 °C.

Bradford assay. Protein concentrations were measured using Pierce™ Coomassie (Bradford) Protein Assay Kit according to the manufacturer's guidelines. To a 96-well plate was added calibration curve

bovine serum albumin (BSA) and protein lysate of known dilutions (10 µL). To each protein sample (10 µL) was added Pierce Bradford reagent (300 µL) and the plate was incubated at rt for 10 min before absorption was measured at 595 nm on a FLUOstar Omega plate reader.

Western Blot Immunoassays. Protein samples for SDS-PAGE were prepared from cell lysate diluted in Milli-Q water and 10% *v/v* β-mercaptoethanol in 4× Laemmli sample buffer, and denatured at 100 °C for 5 min. The prepared samples (30 µg protein) were loaded into Mini-PROTEAN TGX gels, 4 – 20% along with the Spectra™ Multicolor High Range Protein Ladder and run in a Mini-PROTEAN Tetra Cell at 50 V for 5 min then at 200 V until the loading dye reached the bottom of the gel. Following electrophoresis, the proteins were transferred to a 0.2 µm PVDF membrane (7 x 8.5 cm) using a Trans-Blot Turbo Transfer System with the default high molecular weight mode. Membranes were washed with distilled water (3×) and shaken in blocking buffer (5% *w/v* Blotto non-fat dry milk, 0.1% *v/v* tween in TBS) (10 mL) at rt for 1 h. The membranes were cut at around 120 kDa and the gels were incubated with the relevant primary antibody diluted in blocking buffer (1:2000 CREBBP (D6C5) rabbit mAb, 1:2000 p300 (D8Z4E) rabbit mAb, 1:400 β-actin (AC-15) mouse mAb) and shaken at 4 °C overnight. The membranes were washed with 0.1% *v/v* tween in TBS (3×) before being incubated with the relevant HRP-conjugated secondary antibody diluted in blocking buffer (1:5000 anti-rabbit IgG (H+L), 1:5000 anti-mouse IgG (H+L)) at rt for 1 h. The membranes were washed with 0.1% *v/v* tween in TBS (3×) and imaged by incubating with Clarity Western ECL working substrate for 5 min and imaged with a Bio-Rad ChemiDoc XRS+ Imaging System. Signal intensities were quantified using ImageLab software and the data was exported to Excel for processing. Graphs were produced using GraphPad Prism.

Automated immunoassay optimisation sample preparation. HeLa (BIOCAT49509) cells were diluted to the desired concentration in growth media and distributed (80 µL/ well) to a V-bottomed 384-well plate using a Multidrop™ Combi Reagent Dispenser. The plate was incubated at 37 °C and 5% CO_2 for 24 h. The plate was centrifuged (400 ×g, 5 min, 4 °C) and the media was removed from each well using a Biomek FX^P Automated Workstation equipped with Biomek AP384 P30 tips. Cold PBS (80 µL) was added to each well using a Multidrop™ Combi Reagent Dispenser and the 'shake'

function was used for 5 – 10 sec. The plate was centrifuged (400 ×g, 5 min, 4 °C) and the PBS was removed from each well using a Biomek FX^P Automated Workstation. Cold PBS (80 µL) was added to each well using a Multidrop™ Combi Reagent Dispenser and the 'shake' function was used for 5 – 10 sec. The plate was centrifuged (400 ×g, 5 min, 4 °C) and the PBS was removed from each well using a Biomek FX^P Automated Workstation. Cold RIPA buffer (20 µL) containing Complete Mini-EDTA-free protease inhibitor tablets (1 tablet/ 10 mL) and Benzonase® Nuclease (1:500) was added to each well using a Multidrop™ Combi Reagent Dispenser, and the 'shake' function was used for 5 – 10 sec. The plate was incubated on ice for 30 min before being centrifuged (32000 ×g, 30 min, 4 °C), and stored at −20 °C.

Smaller scale compound *in vitro* testing. A concentration gradient of each compound in DMSO (0.5 µL) was distributed into a V-bottomed 384-well plate. HeLa (BIOCAT49509) cells were diluted to 125,000 cells/ mL in growth media and distributed (80 µL/ well, 10,000 cells/ well, 0.625% (final) *v/v* DMSO) to the 384-well plate using a Multidrop™ Combi Reagent Dispenser. The plate was incubated at 37 °C and 5% CO_2 for 24 h. The plate was centrifuged (400 ×g, 5 min, 4 °C) and the media was removed from each well using a Biomek FX^P Automated Workstation equipped with Biomek AP384 P30 tips. Cold PBS (80 µL) was added to each well using a Multidrop™ Combi Reagent Dispenser and the 'shake' function was used for 5 – 10 sec. The plate was centrifuged (400 ×g, 5 min, 4 °C) and the PBS was removed from each well using a Biomek FX^P Automated Workstation. Cold PBS (80 µL) was added to each well using a Multidrop™ Combi Reagent Dispenser and the 'shake' function was used for 5 – 10 sec. The plate was centrifuged (400 ×g, 5 min, 4 °C) and the PBS was removed from each well using a Biomek FX^P Automated Workstation. Cold RIPA buffer (20 µL) containing Complete Mini-EDTA-free protease inhibitor tablets (1 tablet/ 10 mL) and Benzonase® Nuclease (1:500) was added to each well using a Multidrop™ Combi Reagent Dispenser, and the 'shake' function was used for 5 – 10 sec. The plate was incubated on ice for 30 min before being centrifuged (32000 ×g, 30 min, 4 °C), and stored at −20 °C.

Automated Immunoassay. Assays were carried out on either a Sally Sue Simple Western or Peggy Sue Simple Western system – the Peggy Sue system features additional charge separation functionality

which was not used. EZ Standard Pack 3 High Molecular Weight reagents and ladders were reconstituted immediately prior to assay set-up according to the manufacturer's guidelines. Primary antibodies (CREBBP (D6C5) rabbit mAb, p300 (D8Z4E) rabbit mAb, Anti-h p300 goat mAb, and Vinculin (EPR8185) rabbit mAb) were diluted in either Antibody Diluent 2 (rabbit mAbs) or Milk Free Antibody Diluent (goat mAb) to the given dilutions. The secondary antibodies (1× Anti-Rabbit Secondary HRP Antibody, 1× Anti-Goat Secondary HRP Antibody) were used neat other than where anti-goat and anti-rabbit secondary antibodies were multiplexed (1:20 dilution of 20× Anti-Rabbit Secondary HRP Antibody in 1× Anti-Goat Secondary HRP Antibody). 5× Fluorescent Master Mix (1 µL) was added to the relevant wells of a 384-well PCR plate followed by cell lysate samples (4 µL). The plate was sealed with a microplate sealer, heated at 95 °C for 5 min, and allowed to cool. The 66-440 kDa protein ladder (5 µL), Stacking Matrix II (15 µL), 66-440 kDa Separation Matrix (15 µL), distilled H_2O (30 µL), Antibody Diluent 2 (15 µL), Milk Free Antibody Diluent (15 µL), the diluted primary antibodies (10 µL), the secondary antibodies (10 µL), Streptavidin-HRP (15 µL), and 1:1 luminol/ peroxide (15 µL) were added to the relevant wells of the 384-well PCR plate and the plate was centrifuged (1000 ×g, 5 min, 20 °C). Plate layouts and run times are available in the Supporting Information. Data was analysed using Compass for Simple Western software. The software was set to detect peaks corresponding to the analysed proteins (vinculin: MW = 117 ± 10%, CREBBP: MW = 330 ± 10%, and p300: MW = 300 ± 10%), and the 'peak find width' was adjusted from 9 to 14. Peak areas were exported to Excel for processing and graphs were produced using GraphPad Prism.

Table 18. Commercial suppliers of biological reagents and resources.

Reagent/ Resource	Supplier	Identifier
Cell lines, plasmids		
His_6Tev-CREBBP bromodomain plasmid	Addgene	Cat. # 38977
E. coli BL21(DE3) cells	Fisher Scientific	Cat. # EC0114
HEK293T cells	Obtained from the Hammond Group, University of Oxford	
HeLa cells	Obtained from the Hammond/ Russell Group, University of Oxford or from Biocat	BIOCAT49509
Antibodies		
CBP (D6C5) rabbit mAb	Cell Signaling Technology®	D6C5, cat. # 7389
p300 (D8Z4E) rabbit mAb	Cell Signaling Technology®	D8Z4E, cat. # 86377
β-Actin (AC-15) mouse mAb	Santa Cruz Biotechnologies	AC-15, cat. # sc-69879
Anti-h p300 goat mAb	R&D Systems	Cat. # AF3789, lot: XQM0522011
Vinculin (EPR8185) rabbit mAb	Abcam	Cat. # ab129002, lot: GR3270283-6
Anti-Rabbit IgG (H+L), HRP Conjugate	Promega UK Ltd.	Cat. # W4021
Anti-Mouse IgG (H+L), HRP Conjugate	Promega UK Ltd.	Cat. # W4011
1X Anti-Rabbit Secondary HRP Conjugate	ProteinSimple, Bio-techne®	Cat. # 042-206, lot: 94531
1X Anti-Goat Secondary HRP Conjugate	ProteinSimple, Bio-techne®	Cat. # 043-522, lot: 99983
20X Anti-Rabbit Secondary HRP Conjugate	ProteinSimple, Bio-techne®	Cat. # 043-426
siRNA		
siGENOME SMARTPool Human CREBBP siRNA	Horizon Discovery Biosciences Ltd.	Cat. # M-003477-02-0005
siGENOME SMARTPool Human p300 siRNA	Horizon Discovery Biosciences Ltd.	Cat. # M-003486-04-0005
siGENOME SMARTPool Non-Targeting siRNA Pool #2	Horizon Discovery Biosciences Ltd.	Cat. # D-001206-14-05
Biologically tested commercial compounds		
dCBP-1	MedChemExpress	Cat. # HY-134582, CAS: 2484739-25-3
Inobrodib	MedChemExpress	Cat. # HY-111784, CAS: 2222941-37-7
Pomalidomide	Sigma-Aldrich	SKU P0018, CAS: 19171-19-8
Carfilzomib	Cayman Chemicals	Cat. # 17554, CAS: 868540-17-4
MLN 4924	TOCRIS	Cat. # 6499, CAS: 905579-51-3
Biological reagents		
Oakton Buffer Pack	Oakton	Item # WZ-05942-10
SOC outgrowth medium	New England Biolabs Inc.	NEB # B9035
Isopropyl ß-D-1-thiogalactopyranoside (IPTG)	Apollo Scientific	Cat. # BIMB8001, CAS: 367-93-1
SigmaFAST™ Protease Inhibitor Cocktail Tablet, EDTA Free	Sigma-Aldrich	SKU: S8830-20TAB
SigmaFAST™ Protease Inhibitor Tablets	Sigma-Aldrich	SKU: S8820-20TAB
Complete Mini-EDTA-free protease inhibitor tablets	Roche	Cat. # 11836170001
Benzoase® Nuclease	Sigma Aldrich	E1014-25KU
Polyethyleneimine	Sigma Aldrich	SKU: 408727, CAS: 9002-98-6
4× Laemmli sample buffer	Bio-Rad	Cat. # 1610747
β-mercaptoethanol	Merck	SKU 8057400250, CAS: 60-24-2
InstantBlue™ Coomasie® stain	Abcam	Cat. # ab119211
Spectra™ Multicolor High Range Protein Ladder	Thermo Fisher Scientific Life Technologies	Cat. # 26625
DMEM, high glucose, GlutaMAX™ Supplement, pyruvate	Thermo Fisher Scientific Life Technologies	Cat. # 31966047
Fetal bovine serum	Merck Life Science	Cat # F7524-500ML
Penicillin-Streptomycin (10,000 U/mL)	Thermo Fisher Scientific Life Technologies	Cat # 15140122
Dulbecco′s Phosphate Buffered Saline (PBS) with $MgCl_2$ and $CaCl_2$	Merck Life Science	Cat. # 8662-500ML
Dulbecco′s Phosphate Buffered Saline (PBS) without $MgCl_2$ and $CaCl_2$	Thermo Fisher Scientific Life Technologies	Cat # 14190094
(10%) Australian non-heat inactivated FBS	Gibco	Cat. # 10099-141
Trypsin-EDTA solution (1×)	Merck Life Science	Cat. # 59430C-500ML
Trypsin-EDTA solution (1×)	Sigma Life Science	SKU T3924-100ML
TrypLE™ Express Enzyme (1X)	Gibco	Cat. # 12604013
RIPA buffer	Pierce, Thermo Scientific	Cat. # 89900
Lipofectamine™ RNAiMAX Transfection Reagent	Thermo Fisher Scientific Life Technologies	Cat. # 13778075
Opti-MEM™ I Reduced Serum Medium, GlutaMAX™ Supplement	Thermo Fisher Scientific Life Technologies	Cat. # 51985026
Biological grade DMSO	Sigma-Aldrich	SKU D8418-100ML, CAS: 67-68-5
TRIS-buffered saline (TBS, 10×) buffer pH 7.6	Thermo Scientific	Cat. # J62662.K7

Blotto, non-fat dry milk	Insight Biotechnology Ltd.	Cat. # sc-2324
Milk Free Antibody Diluent	ProteinSimple, Bio-techne®	Cat. # 043-524, lot # 99066

Instruments

Oakton PH 550 Benchtop pH Meter Kit	Oakton	Item # WZ-35419-30
Novaspec® II spectrometer	Pharmacia	Cat. # 5159
Novaspec® II spectrophotometer	No longer available to purchase	N/A
Sonic dismembrator ultrasonic processor	Thermo Fisher Scientific Life Technologies	FB-505
1/16" tapered microtip	Qsonica	Cat. # 4417
Heraeus Megafuge 8R centrifuge	Thermo Fisher Scientific Life Technologies	Biomax # 27695
Fresco™ 21 Microcentrifuge	Thermo Scientific™	Cat. # 75002555
VWR® Megastar 3.0R centrifuge	VWR, part of Avantor	Mega Star 3.0R
NanoDrop Lite spectrophotometer	Nanodrop® Technologies Inc.	Cat. # ND-LITE-PR
MicroCal PEAQ-ITC Automated	Malvern	
Mini-PROTEAN® 3 Electrophoresis System	Bio-Rad	Cat. # 165-3301
Mini-PROTEAN Tetra Vertical Electrophoresis Cell for Precast Gels, 4-gel	Bio-Rad	Cat. # 1658004EDU
Trans-Blot Turbo Transfer System	Bio-Rad	Cat. # 1704150
Countess™ II automated cell counter	Thermo Fisher Scientific Life Technologies	Cat. # I-CACC2
NucleoCounter® NC-200™	Chemometec	NucleoCounter® NC-200™
FLUOstar Omega plate reader	BMG Labtech	
Multidrop™ Combi Reagent Dispenser	Thermo Fisher Scientific Life Technologies	Cat. # 5840300, Asset # 064763 or 065379
Tubing set for standard dispensing cassette	Thermo Fisher Scientific Life Technologies	Cat. # 24070290
Bio-Rad ChemiDoc XRS+ Imaging System	Bio-Rad	Cat. # 1708265
Biomek FXP Automated Workstation	Beckman Coulter	No Longer Available for Purchase
Sally Sue Simple Western	ProteinSimple, Bio-techne®	OneTag # 2T31106
Peggy Sue Simple Western	ProteinSimple, Bio-techne®	Biomax # 24873

Consumables

0.22 µm filter, PES membrane	Merck Millipore Ltd.	Ref: SLGP033RS
0.45 µm filter, PVDF membrane	Merck Millipore Ltd.	Ref: SLHV033RS
Polyamide Membrane Filter, Nylon, 0.2 um, 47 mm	Sartorius	25007-47N
GSTrap™ High Performance Column, 5 mL	Cytiva	Cat. # 17528201
Superdex 75 resin	Cytiva	Cat. # 17104404
10k MWCO spin protein concentrators, 6 mL	Corning®	Cat. # 431483
10k MWCO spin protein concentrators, 20 mL	Corning®	Cat. # 431488
2000 MWCO Slide-A-Lyzer® MINI Dialysis Device	Thermo Fisher Scientific Life Technologies	Cat. # 88400
Mini-PROTEAN TGX Gels, 4–20%, 12-well,	Bio-Rad	Cat. # 4561095
Mini-PROTEAN TGX Gels, 4–20%, 15-well	Bio-Rad	Cat. # 4561096
Trans-Blot Turbo RTA Mini 0.2 µm PVDF Transfer Kit	Bio-Rad	Cat. # 1704272
Countess™ Cell Counting Chamber Slides-50 slides	Thermo Fisher Scientific Life Technologies	Cat. # C10228
Via1-Cassette™	Chemometec	Cat. # 941-0012
T175 cell culture flask	Sarstedt Ltd.	Cat # 83.3912.002
T75 cell culture flask	Sarstedt Ltd.	Cat # 83.3911.002
T25 cell culture flask	Sarstedt Ltd.	Cat # 83.3910.002
Corning™ Costar™ 6-well plates	Fisher Scientific	Cat. # 10578911
100mm CELLSTAR Culture dish	Greiner Bio-One Ltd.	Cat. # 664160
96-Well microplate	Greiner Bio-One Ltd.	Cat. # 655101
Sterile V-bottomed 384-well plate	Greiner	Cat. # 781281
Hard shell, 384-well PCR plates	Bio-Rad	Cat. # HSP3831
Universal lids for the sterile v-bottomed plates	Costar	Cat. # 3098
Microplate sealers	Greiner	Cat. # 676001
Pierce™ Coomassie (Bradford) Protein Assay Kit	Thermo Fisher Scientific Life Technologies	Cat. # 23236
MycoAlert Mycoplasma Detection Kit	Lonza Biologics PLC	Cat # F7524-500ML
Clarity Western ECL substrate	Bio-Rad	Cat. # 1705060
Peggy Sue and Sally Sue 66-440kDa Size Assay Separation Module Kit	ProteinSimple, Bio-techne®	Cat. # SM-S002-1, lot # 84317
No secondary Detection Module	ProteinSimple, Bio-techne®	Cat. # DM-003
EZ Standard Pack 3 High Molecular Weight	ProteinSimple, Bio-techne®	Cat. # PS-ST03EZ-8, lot # 24509
Biomek AP384 P30 Tips, Non-sterile, 30 µL	Beckman Coulter	Cat. # 719222
Capillary Boxes for Size based Separation in Peggy Sue/Sally Sue	ProteinSimple, Bio-techne®	Cat. # SS700

Software

ProtParam	ExPASy Bioinformatics Resource Portal	https://www.expasy.org/
MassLynx 4.1	Waters	Version 4.1
MicroCal PEAQ-ITC Analysis software	Malvern	Version 1.1.0.1262

Image Lab	Bio-rad	Version 6.1
Compass for SW (v4.1.0) - Used for Sally Sue data collection	ProteinSimple, Bio-techne®	Version 4.1.0, Build ID: 0923
Compass for SW (v3.1.8) - Used for Peggy Sue data collection	ProteinSimple, Bio-techne®	Version 3.1.8, Build ID: 0601
Compass for SW (v5.0.1) - Used for data analysis	ProteinSimple, Bio-techne®	Version 5.0.1, Build ID: 0911
GraphPad Prism (v9.5.1.733)	GraphPad Software, LLC	Version 9.5.1.733

8.2 – General Synthetic Methods

Chemicalize (www.chemicalize.com) developed by ChemAxon (www.chemaxon.com) was used to generate compound names and to calculate predicted physiochemical properties.

In vacuo refers to the removal of solvents under reduced pressure using a Büchi™ rotary evaporator in a water bath at 40 °C, unless otherwise stated.

Celite® refers to Celite® 545 filter aid, treated with sodium carbonate, flux-calcined which was purchased from Sigma Aldrich.

Chemicals were purchased from Acros UK, Apollo Scientific, Enamine, Sigma Aldrich UK, Alfa Aesar UK, Fisher Scientific UK, Fluka UK, Fluorochem, Merck, Argo International Limited, and TCI-Europe. All chemicals were used without further purification.

Brine refers to a saturated aqueous solution of sodium chloride.

Petroleum ether refers to the fraction of light petroleum ether boiling within the range of 40 – 60 °C.

High pressure hydrogenation reactions were performed using either a büchiglasuster® tinyclave steel small pressure reactor equipped with a 25 mL Borosilicate glass 3.3 chamber or using a büchiglasuster® miniclave steel small pressure reactor equipped with a 100 mL Borosilicate glass 3.3 chamber.

Normal phase column chromatography was performed either manually using Geduran silica gel 60 (40 – 63 μM) under a positive pressure of air/ nitrogen, or on a Biotage® Selekt Flash Purification System using Biotage® KP-Sil SNAP or Biotage® Sfär Silica cartridges.

Reverse phase column chromatography was performed on a Biotage® Selekt Flash Purification System using Biotage® C18 D Silica cartridges.

Semi-preparative reverse phase column chromatography was performed on an Agilent 1260 Infinity II® with a Agilent 5 Prep C18 [5 μM, 130 Å, 21.2 × 50 mm] column using a constant flow rate of 25.0 mL min^{-1} and gradient method of 95:5 A:B (1 min), 95:5 A:B → 5:95 A:B (14 min), 5:95 A:B (5 min) where eluent A = 0.1% *v/v* formic acid in H_2O and eluent B = 0.1% *v/v* formic acid in MeCN.

Preparative reverse phase column chromatography was performed on a Teledyne ISCO ACCQPrep® HP150 using a Waters XSelect CSH C18 OBD [5 μm, 130 Å, 30 mm × 100 mm] column with a constant flow rate of 40.0 mL min^{-1} at the given gradient.

Mass directed auto purification (MDAP) was performed using high-performance liquid chromatography (HPLC) separation with a Xselect CSH C18 [5 μm, 130 Å, 150 mm × 30 mm] column at rt with a constant flow rate of 40.0 mL min^{-1} and using standard elution gradients (methods A, B, C, D, extended A, and extended B). DAD detection was 210 – 350 nm and MS detection was 100 – 1250 AMU using alternate scan positive/ negative Electrospray. Method A = 100:0 A:B (4 min), 100:0 A:B → 70:0 A:B (8 min), 70:30 A:B → 1:99 A:B (0.5 min), 1:99 A:B (4.5 min); method B = 85:15 A:B (2.5 min), 85:15 A:B → 45:55 A:B (9.5 min), 45:55 A:B → 1:99 A:B (0.5 min), 1:99 A:B (4.5 min); method C = 70:30 A:B (2.5 min), 70:30 A:B → 15:85 A:B (9.5 min), 15:85 A:B → 1:99 A:B (0.5 min), 1:99 A:B (4.5 min); method D = 50:50 A:B (2.5 min), 50:50 A:B → 1:99 A:B (9.5 min), 1:99 A:B (5 min); extended method A = 100:0 A:B (1 min), 100:0 A:B → 75:25 A:B (19 min), 75:25 A:B → 1:99 A:B (0.5 min), 1:99 A:B (4.5 min); extended method B = 85:15 A:B (1 min), 85:15 A:B → 45:55 A:B (19 min), 45:55 A:B → 1:99 A:B (0.5 min), 1:99 A:B (4.5 min). Eluent A = 0.1% *v/v* formic acid in H_2O, eluent B = 0.1% *v/v* formic acid in MeCN.

Thin layer chromatography (TLC) was carried out on normal phase Merck silica gel 60 F_{254} aluminium-supported chromatography sheets. Visualisation was by absorption of UV light (λ_{max} 254 nm), exposure to iodine vapour or thermal development after dipping in either an ethanolic solution of ninhydrin or an aqueous solution of potassium permanganate.

Melting points were determined using a Leica Galen III hot stage microscope and are uncorrected. The solvents of crystallisation are shown in parentheses.

Infrared (IR) spectra were obtained from neat samples, either as liquids or solids using a diamond ATR module. The spectra were recorded on a Bruker Tensor 27 spectrometer. Absorption maxima are reported in wavenumbers (cm^{-1}) and reported as s (strong), m (medium), w (weak) or br (broad). Only the main, relevant peaks have been assigned.

Specific optical rotations were measured using a Schmidt + Haensch UniPol L2000 polarimeter, in cells with a path length of 1 dm, using a sodium lamp at 589 nm. The concentration (c) is expressed in g/100 mL (equivalent to g/0.1 dm^3). Specific rotations are denoted $[\alpha]_D^T$ and are given in implied units of $10^{-1}degcm^2g^{-1}$ at the temperature stated.

^{1}H NMR spectra were recorded on a Bruker AVIIIHD 400 (400 MHz), Bruker AVII 500 (500 MHz) with dual ^{13}C(^{1}H) cryoprobe, Bruker AVIIIHD 500 (500 MHz), Bruker AVIIIHD 600 (600 MHz), or Bruker NEO 600 (600 MHz) spectrometer in the stated solvent as a reference for the internal deuterium lock. The chemical shift data for each signal are given as δ_H in units of parts per million (ppm) relative to tetramethylsilane (TMS) where δ_H (TMS) = 0.00 ppm. The spectra are calibrated using the solvent peak with the data provided by Fulmer *et al*.[209] The multiplicity of each signal is indicated by s (singlet); br s (broad singlet); d (doublet); dd (doublet of doublets), ddd (doublet of doublet of doublets), t (triplet), td (triplet of doublets), q (quartet), p (quintet), dt (doublet of triplets), dq (doublet of quartets), or m (multiplet). The number of protons (n) for a given resonance signal is indicated by n H. Where appropriate, coupling constants (*J*) are quoted in Hz and are recorded to the nearest 0.1 Hz. Identical proton coupling constants (*J*) are averaged in each spectrum and reported to the nearest 0.1 Hz. Coupling constants were determined using MestReNova x64 software. ^{1}H spectra were assigned using 2D NMR experiments including COSY, HMBC, and HSQC.

^{13}C NMR spectra were recorded on a Bruker AVIIIHD 400 (101 MHz), Bruker AVII 500 (126 MHz), Bruker AVIIIHD 600 (151 MHz), or Bruker NEO 600 (151 MHz) spectrometer in the stated solvents, with broadband proton decoupling and an internal deuterium lock. The chemical shift data for each signal are given as δ_C in units of parts per million (ppm) relative to tetramethylsilane (TMS) where δ_C (TMS) = 0.00 ppm. The spectra are calibrated using the solvent peak with the data provided by *Fulmer et al*.[209] The shift values of resonances are quoted to 1 decimal place unless peaks have similar chemical shifts, in which case 2 decimal places are used. Coupling constants (*J*) are quoted in Hz and are recorded to the nearest 0.1 Hz. ^{13}C spectra were assigned using 2D NMR experiments including HMBC and HSQC. Diastereomers have been arbitrarily assigned as “diastereomer A” and “diastereomer B” where relevant.

^{19}F NMR spectra were recorded on a Bruker AVIIIHD 400 nanobay (376 MHz) or Bruker NEO 600 (471 MHz) spectrometer using a deuterium internal lock. The chemical shift data for each signal are given as δ_F in units of parts per million (ppm). The multiplicity of each signal is indicated by: s (singlet), d (doublet), or m (multiplet). Coupling constant (*J*) values are quoted in Hz and are recorded to the nearest 0.1 Hz. Coupling constants were determined by analysis using MestReNova x64 software. ^{19}F

spectra were assigned using coupling constant (*J*) values.

^{11}B NMR spectra were recorded on a Bruker AVIIIHD 500 (160 MHz) using a deuterium internal lock. The chemical shift data for each signal are given as δ_B in units of parts per million (ppm). The multiplicity of each signal is indicated by: s (singlet).

Low resolution mass spectrometry (LRMS) was performed on a Waters LCT Premier spectrometer or Agilent 6120 Quadrupole spectrometer. *m/z* values are reported in Daltons and followed by their percentage abundance in parentheses.

High resolution mass spectrometry (HRMS) was performed on either a Bruker MicroTOF spectrometer or on an ACQUITY I-Class PLUS UPLC System operating in positive or negative mode, as indicated. Samples were made as solutions in MeOH, MeCN or H_2O. *m/z* values are reported in Daltons and followed by their percentage abundance in parentheses. Electron ionisation/field ionisation (EI/FI) was carried out on a Waters GCT with a temperature programmed solids probe inlet.

Liquid chromatography mass spectrometry (LCMS) was performed on an Acquity UPLC using a CSH C18 column [1.7µm, 130 Å, 50mm x 2.1mm] at 40 °C with a constant flow rate of 1.0 mL min^{-1} and a gradient of 97:3 A:B → 3:97 A:B (1.5 min), 3:97 A:B (0.4 min). Formic acid method: eluent A = 0.1% *v/v* formic acid in H_2O, eluent B = 0.1% *v/v* formic acid in MeCN. High pH (HpH) method: eluent A = 10 mM NH_4HCO_3 in water adjusted to pH 10 with aq. NH_3, eluent B = MeCN. Purity is given as a summed signal from wavelengths of 210nm to 350nm.

Analytical high-performance liquid chromatography (HPLC) was performed on a PerkinElmer Flexar system with a Binary LC Pump and UV/VIS LC Detector (Methods 1 and 2) or on an Agilent 1260 Infinity II fitted with a Quaternary LC Pump and UV/VIS LC Detector (Method 3). Samples were prepared by dissolving in H_2O, MeOH, or MeCN and filtered through a Gilson Scientific Ltd® polytetrafluoroethylene (PTFE) syringe filter 13 mm, 0.22 µm. Purity is reported as an average value of UV absorption at two/ three different wavelengths. Methods 1 and 2: a Dionex Acclaim® 120 C18 [5 µm, 120 Å, 150 mm × 4.6 mm] reverse phase column was used with a constant flow rate of 1.5 mL min^{-1} and gradient method of 95:5 A:B (1 min), 95:5 A:B → 5:95 A:B (10 min), 5:95 A:B (5 min). Method 1: eluent A = H_2O, eluent B = MeCN. Method 2: eluent A = 0.1% *v/v* formic acid in H_2O, eluent B = 0.1% *v/v* formic acid in MeCN. Method 3: An Agilent Poroshell EC-C18 [4.0 µm, 120 Å,

4.6 mm × 100 mm] reverse phase column fitted with an Agilent Poroshell EC-C18 [4.0 μm, 120 Å, 4.6 mm × 5 mm] guard column was used at 40 °C with a constant flow rate of 1.0 mL min^{-1} and a gradient of 95:5 A:B (1 min), 95:5 A:B → 5:95 A:B (11 min), 5:95 A:B (5 min) where eluent A = 0.1% *v/v* formic acid in H_2O and eluent B = 0.1% *v/v* formic acid in MeCN.

8.3 – Synthesis

8.3.1 – Synthesis of Compounds in Chapter 2

7-Methoxy-3,4-dihydroquinolin-2(1*H*)-one (9)

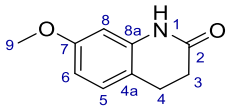

To a stirred suspension of 7-hydroxy-3,4-dihydroquinolin-2(1*H*)-one (3.40 g, 20.8 mmol, 1.0 eq.) and K_2CO_3 (5.76 mg, 41.7 mmol, 2.0 eq.) in DMF (35 mL) was added iodomethane (1.43 mL, 22.9 mmol, 1.1 eq.) at rt. The reaction mixture was stirred at 60 ºC for 18 h. The cooled suspension was diluted with EtOAc (250 mL) and washed with 1 M aq. K_2CO_3 (3 × 100 mL), 0.5 M aq. LiCl (3 × 100 mL), brine (200 mL), dried ($MgSO_4$), filtered, and concentrated *in vacuo*. The crude solid was recrystalised from EtOH (20 mL) to afford 7-methoxy-3,4-dihydroquinolin-2(1*H*)-one (**9**) (2.81 g, 15.9 mmol, 76%) as colourless crystals: R_f 0.13 (3:2 petroleum ether/ EtOAc); mp 128 – 134 ºC (EtOH), [lit.[210] 147 ºC]; ^{1}H NMR (400 MHz, $CDCl_3$) δ_H 7.74 (1 H, br s, NH-1), 7.06 (1 H, dt, *J* 8.3, 0.8, H-5), 6.53 (1 H, dd, *J* 8.3, 2.5, H-6), 6.30 (1 H, d, *J* 2.5, H-8), 3.78 (3 H, s, H-9), 2.95 – 2.85 (2 H, m, H-4), 2.66 – 2.56 (2 H, m, H-3); LRMS *m/z* (ESI$^+$) 178 ([M+H]$^+$, 100%). These data are in good accordance with the literature.[210]

7-Methoxy-1,2,3,4-tetrahydroquinoline (10)

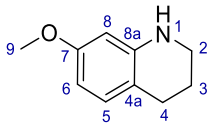

7-Methoxy-3,4-dihydroquinolin-2(1*H*)-one (**9**) (2.81 g, 15.9 mmol, 1.0 eq.) was suspended in anhydrous THF (90 mL) and added slowly to $LiAlH_4$ (905 mg, 23.9 mmol, 1.5 eq.) in anhydrous THF (75 mL) at 0 ºC. The suspension was warmed to rt and stirred for a further 3 h. The reaction mixture was cooled to 0 ºC and H_2O (0.90 mL), followed by 15% aq. NaOH (0.90 mL) then H_2O (2.7 mL) were added dropwise. $MgSO_4$ was added and the suspension was stirred at rt for 15 min (Fieser workup).

The salts were removed by filtration and washed with EtOAc (100 mL). The filtrate was concentrated *in vacuo* and the crude oil was purified using normal phase column chromatography (isocratic 10% EtOAc in petroleum ether) to afford 7-methoxy-1,2,3,4-tetrahedroquinoline (**10**) (2.13 g, 13.0 mmol, 82%) as a colourless oil: R_f 0.58 (3:2 petroleum ether/ EtOAc); ^{1}H NMR (400 MHz, $CDCl_3$) δ_H 6.85 (1 H, dt, *J* 8.2, 1.1, H-5), 6.21 (1 H, dd, *J* 8.2, 2.5, H-6), 6.04 (1 H, d, *J* 2.5, H-8), 3.83 (1 H, br s, NH-1), 3.74 (3 H, s, H-9), 3.33 – 3.22 (2 H, m, H-4), 2.70 (2 H, t, *J* 6.4, H-2), 1.99 – 1.91 (2 H, m, H-3); LRMS *m/z* (ESI$^+$) 164 ([M+H]$^+$, 100%). These data are in good accordance with the literature.[211]

Pent-4-yn-1-yl methanesulfonate (11)

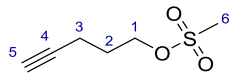

Methanesulfonyl chloride (2.8 mL, 35 mmol, 1.5 eq.) was added dropwise to a solution of 4-pentyn-1-ol (2.2 mL, 24 mmol, 1.0 eq.) and NEt_3 (6.6 mL, 47 mmol, 2.0 eq.) in CH_2Cl_2 (16 mL) at 0 ºC. The reaction was warmed to rt and stirred for 1.5 h before being diluted in CH_2Cl_2 (100 mL). The organic components were washed with water (3 × 70 mL), sat. aq. $NaHCO_3$ (70 mL), brine (70 mL), dried ($MgSO_4$), filtered, and concentrated *in vacuo* to afford pent-4-yn-1-yl methanesulfonate (**11**) (3.44 g, 21.2 mmol, 89%) as an orange oil which was used without purification: R_f 0.46 (3:2 petroleum ether/ EtOAc); ^{1}H NMR (400 MHz, $CDCl_3$) δ_H 4.36 (2 H, t, *J* 6.1, H-1), 3.03 (3 H, s, H-6), 2.37 (2 H, td, *J* 6.8, 2.7, H-3), 2.01 (1 H, t, *J* 2.7, H-5), 2.03 – 1.95 (2 H, m, H-2); LRMS *m/z* (ESI$^+$) 183 ([M+Na]$^+$, 100 %). These data are in good accordance with the literature.[212]

7-Methoxy-1-(pent-4-yn-1-yl)-1,2,3,4-tetrahydroquinoline (12)

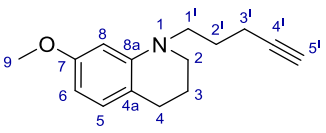

Pent-4-yn-1-yl methanesulfonate (**11**) (448 mg, 2.95 mmol, 1.5 eq.) was added to a solution of 7-methoxy-1,2,3,4-tetrahedroquinoline (**10**) (320 mg, 1.96 mmol, 1.0 eq.), potassium iodide (140 mg, 0.82 mmol, 0.5 eq.) and DIPEA (685 µL, 3.93 mmol, 2.0 eq.) in DMF (11 mL). The reaction mixture stirred at 100 ºC for 1 h under microwave irradiation. The cooled solution was diluted in Et_2O (75 mL), and the organic component was washed with water (3 × 75 mL), brine (50 mL), dried ($MgSO_4$), filtered, and concentrated *in vacuo*. The crude oil was purified using normal phase column chromatography (isocratic 10% EtOAc in petroleum ether) to afford 7-methoxy-1-(pent-4-yn-1-yl)-1,2,3,4-tetrahydroquinoline (**12**) (227 mg, 0.988 mmol, 51%) as a yellow oil: R_f 0.76 (3:2 petroleum ether/ EtOAc), ^{1}H NMR (400 MHz, $CDCl_3$) δ_H 6.84 (1 H, d, *J* 8.1, H-5), 6.19 (1 H, d, *J* 2.5, H-8), 6.14 (1 H, dd, *J* 8.1, 2.5, H-6), 3.76 (3 H, s, H-9), 3.40 – 3.33 (2 H, m, H-2), 3.31 – 3.25 (2 H, m, H-1^I), 2.69 (2 H, t, *J* 6.3, H-4), 2.26 (2 H, td, *J* 6.9, 2.7, H-3^I), 2.00 (1 H, t, *J* 2.6, H-5^I), 2.00 – 1.90 (2 H, m, H-2^I), 1.89 – 1.80 (2 H, m, H-3); LRMS *m/z* (ESI$^+$) 230 ([M+H]$^+$, 100%). These data are in good accordance with the literature.[43]

7-Methoxy-1-[(4*E*)-5-(4,4,5,5-tetramethyl-1,3,2-dioxaborolan-2-yl)pent-4-en-1-yl]-1,2,3,4-tetrahydroquinoline (13)

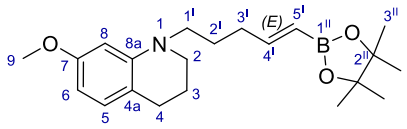

7-Methoxy-1-(pent-4-yn-1-yl)-1,2,3,4-tetrahydroquinoline (**12**) (300 mg, 1.31 mmol, 1.0 eq.) and bis(cyclopentadienyl)zirconium(IV) chloride hydride (34 mg, 0.13 mmol, 0.1 eq.) were added to a tapered microwave vial and sealed under an Ar atmosphere. NEt_3 (18 µL, 0.13 mmol, 0.1 eq.) and 4,4,5,5-tetramethyl-1,3,2-dioxaborolane (209 µL, 1.44 mmol, 1.1 eq.) were added and the reaction mixture was stirred at 60 ºC for 18 h under an atmosphere of Ar in the absence of light. The reaction mixture was directly purified using normal phase column chromatography (gradient of 5 – 30% EtOAc in petroleum ether) to afford 7-methoxy-1-[(4*E*)-5-(4,4,5,5-tetramethyl-1,3,2-dioxaborolan-2-yl)pent-4-en-1-yl]-1,2,3,4-tetrahydroquinoline (**13**) (265 mg, 0.742 mmol, 57%) as a yellow oil: R_f 0.17 (9:1

petroleum ether/ EtOAc); ^{1}H NMR (400 MHz, $CDCl_3$) δ_H 6.83 (1 H, d, *J* 8.3, H-5), 6.65 (1 H, dt, *J* 18.0, 6.4, H-4^{I}), 6.14 – 6.11 (1 H, m, H-6), 6.11 (1 H, s, H-8), 5.47 (1 H, dt, *J* 18.0, 1.5, H-5^{I}), 3.75 (3 H, s, H-9), 3.29 – 3.16 (4 H, m, H-1^{I}), 2.67 (2 H, t, *J* 6.3, H-4), 2.25 – 2.16 (2 H, m, H-3^{I}), 1.95 – 1.86 (2 H, m, H-2), 1.78 – 1.68 (2 H, m, H-2^{I}), 1.26 (12 H, s, H-3^{II}); ^{11}B-NMR (160 MHz, $CDCl_3$) δ_B 29.8 (s, B-1^{II}); LRMS *m/z* (ESI$^+$) 359 ([M+H]$^+$, 100%). These data are in good accordance with the literature.[43]

tert-Butyl (3*R*)-3-[benzyl(1*R*)-1-phenylethyl)amino]butanoate (14)

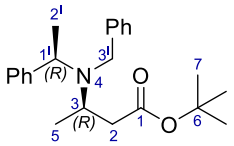

To a stirred solution of (*R*)-*N*-benzyl-1-phenylethan-1-amine (4.04 g, 19.1 mmol, 1.5 eq.) in anhydrous THF (22 mL) at −78 ºC was added 2.5 M *n*-BuLi in *n*-hexane (8.2 mL, 20 mmol, 1.6 eq.) dropwise over a period of 15 min. The resultant pink solution was stirred at −78 ºC for a further 30 min before the dropwise addition of *tert*-butyl crotonate (2.0 mL, 13 mmol, 1.0 eq.) in THF (16 mL) over a period of 1 h. The reaction mixture was stirred at −78 ºC for a further 3 h. The reaction mixture was quenched with dropwise addition of sat. aq. NH_4Cl (20 mL) and was warmed to rt. The aqueous component was extracted with CH_2Cl_2 (3 × 100 mL) and the combined organic components were washed with sat. aq. $NaHCO_3$ (150 mL), brine (150 mL), dried (Na_2SO_4), filtered and concentrated *in vacuo*. The crude colourless oil was purified using normal phase column chromatography (isocratic 3% Et_2O in petroleum ether) to afford *tert*-butyl (3*R*)-3-(benzyl(1*R*)-1-phenylethyl)amino)butanoate (**14**) (2.23 g, 6.31 mmol, 49%) as a colourless oil: R_f 0.51 (1:9 Et_2O/ hexane); $[\alpha]_D^{25} = -3.0$ (*c* 1.0, $CHCl_3$) [lit.[141] $[\alpha]_D^{25} = -5.2$ (*c* 1.1, $CHCl_3$)]; ^{1}H NMR (400 MHz, $CDCl_3$) δ_H 7.43 – 7.18 (10 H, m, Ar-H), 3.89 (1 H, q, *J* 6.9, H-1^{I}), 3.76 (1 H, d, *J* 15.0, H_AH_B-3^{I}), 3.61 (1 H, d, *J* 15.0, H_AH_B-3^{I}), 3.47 – 3.38 (1 H, m, H-3), 2.27 (1 H, dd, *J* 14.1, 4.7, H_AH_B-2), 2.01 (1 H, dd, *J* 14.1, 9.1, H_AH_B-2), 1.39 (9 H, s, H-7), 1.33 (3 H, d, *J* 6.9, H-2^{I}), 1.11 (3 H, d, *J* 6.6, H-5).; LRMS *m/z* (ESI$^+$) 354 ([M+H]$^+$, 100%). These data are in good accordance with the literature.[141]

***tert*-Butyl (3*R*)-3-aminobutanoate (15)**

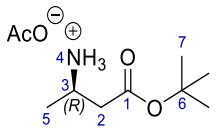

20% $Pd(OH)_2/C$ (832 mg, 1.19 mmol, 0.2 eq.) was added to a stirred solution of *tert*-butyl (3*R*)-3-(benzyl(1*R*)-1-phenylethyl)amino)butanoate (**14**) (2.10 g, 5.94 mmol, 1.0 eq.) in H_2O (3.4 mL), glacial acetic acid (2.2 mL) and MeOH (86 mL). The suspension was stirred at rt for 16 h before being filtered through Celite®, washed MeOH (20 mL), and concentrated *in vacuo* to afford *tert*-butyl (3*R*)-3-aminobutanoate (**15**) (1.16 g, 5.29 mmol, 89%) as a colourless solid which was used without purification: R_f 0.00 (EtOAc); $[\alpha]_D^{25} = -16.8$ (*c* 1.0, $CHCl_3$), [lit.[141] $[\alpha]_D^{25} = -22.2$ (*c* 0.5, $CHCl_3$)]; mp 72 – 77 ºC (toluene); ^{1}H NMR (400 MHz, $CDCl_3$) δ_H 3.68 (3 H, br s, NH-4), 3.47 – 3.31 (1 H, m, H-3), 2.39 (1 H, dd, *J* 16.0, 4.7, H_AH_B-2), 2.31 (1 H, dd, *J* 16.0, 8.1, H_AH_B-2), 2.03 (3 H, s, Ac-H), 1.45 (9 H, s, H-7), 1.17 (3 H, d, *J* 6.5, H-5); LRMS *m/z* (ESI$^+$) 160 ([M+H]$^+$, 100%). These data are in good accordance with the literature.[141]

***tert*-Butyl (3*R*)-3-(2-bromo-6-nitroanilino)butanoate (16)**

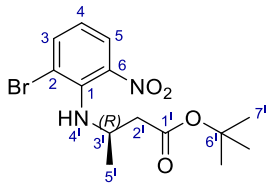

A suspension of 1-bromo-2-fluoro-3-nitrobenzene (220 mg, 1.00 mmol, 1.0 eq.), *tert*-butyl (3*R*)-3-aminobutanoate (**15**) (307 mg, 1.40 mmol, 1.4 eq.), and DIPEA (749 µL, 4.30 mmol, 4.3 eq.) in DMF (3.5 mL) was stirred at 80 ºC for 14 h. The reaction mixture was cooled to rt and concentrated under reduced pressure. H_2O (10 mL) was added and the aqueous component was extracted with Et_2O (3 × 10 mL). The combined organic components were dried (Na_2SO_4), filtered, and concentrated *in vacuo* to afford *tert*-butyl (3*R*)-3-(2-bromo-6-nitroanilino)butanoate (**16**) (354 mg, 0.985 mmol, 99%) as an orange oil which was used without purification: R_f 0.64 (1:4 petroleum ether/

EtOAc); $[\alpha]_D^{25} = -68.3$ (c 1.0, $CHCl_3$), [lit.[43] $[\alpha]_D^{25} = -74.3$ (c 1.0, $CHCl_3$)]; ^{1}H NMR (400 MHz, $CDCl_3$) δ_H 7.93 (1 H, dd, J 8.4, 1.6, H-5), 7.72 (1 H, dd, J 7.8, 1.6, H-3), 6.78 (1 H, dd, J 8.4, 7.8, H-4), 4.32 – 4.18 (1 H, m, H-3^I), 2.45 (2 H, d, J 6.1, H-2^I), 1.39 (9 H, s), 1.28 (3 H, d, J 6.5, H-5^I); LRMS *m/z* (ESI$^+$) 381 ([M(^{79}Br)+Na]$^+$, 100%), 383 ([M(^{81}Br)+Na]$^+$, 97%). These data are in good accordance with the literature.[43]

(4*R*)-6-Bromo-4-methyl-1,3,4,5-tetrahydro-2*H*-1,5-benzodiazepin-2-one (17)

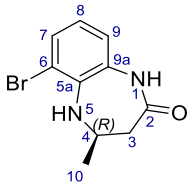

Step I:

To a solution of *tert*-butyl (3*R*)-3-(2-bromo-6-nitroanilino)butanoate (**16**) (354 mg, 0.985 mmol, 1.0 eq.) in CH_2Cl_2 (1.8 mL) at 0 ºC was added TFA (1.8 mL). The reaction mixture was stirred at 0 ºC for 10 mins then at rt for 2.5 h before being concentrated *in vacuo* to afford the carboxylic acid intermediate as a brown oil.

Step II:

The carboxylic acid intermediate was dissolved in glacial acetic acid (2.2 mL) and iron powder (276 mg, 4.95 mmol, 5.0 eq.) was added. The brown solution was stirred at reflux for 13 h. The reaction mixture was cooled to rt and concentrated *in vacuo*. H_2O (20 mL) was added, and the aqueous component was extracted with EtOAc (3 × 20 mL). The combined organic components were washed with brine (2 × 60 mL), dried (Na_2SO_4), filtered, and concentrated *in vacuo*. The crude brown oil was purified using normal phase column chromatography (gradient of 10 – 100% EtOAc in petroleum ether) to afford (4*R*)-6-bromo-4-methyl-1,3,4,5-tetrahydro-2*H*-1,5-benzodiazepin-2-one (**17**) (197 mg, 0.772 mmol, 78%) as a colourless solid: R_f 0.29 (2:1 petroleum ether/ EtOAc); mp 135 – 140 ºC (EtOAc); $[\alpha]_D^{25} = -4.4$ (c 1.0, $CHCl_3$), [lit.[43] $[\alpha]_D^{25} = -6.3$ (c 1.0, $CHCl_3$)]; ^{1}H NMR (400 MHz, $CDCl_3$) δ_H 7.70 (1 H, br s, NH-5), 7.33 (1 H, d, J 7.9, H-9), 6.85 (1 H, d, J 7.8, H-7), 6.73 (1 H, dd, J 7.9, 7.8,

H-8), 4.21 – 4.06 (1 H, m, H-4), 2.62 (1 H, dd, *J* 13.7, 3.7, H_AH_B-3), 2.45 (1 H, dd, *J* 13.6, 7.9, H_AH_B-3), 1.39 (3 H, d, *J* 6.1, H-10); LRMS *m/z* (ESI^+) 277 ([M(^{79}Br)+Na]$^+$, 96%), 279 ([M(^{81}Br)+Na]$^+$, 100%). These data are in good accordance with the literature.[43]

(4*R*)-6-[(1*E*)-5-(7-Methoxy-3,4-dihydroquinolin-1(2*H*)-yl)pent-1-en-1-yl]-4-methyl-1,3,4,5-tetrahydro-2*H*-1,5-benzodiazepin-2-one ((*R*)-OXFBD05)

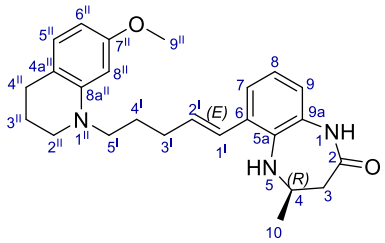

A suspension of (4*R*)-6-bromo-4-methyl-1,3,4,5-tetrahydro-2*H*-1,5-benzodiazepin-2-one (**17**) (108 mg, 0.423 mmol, 1.0 eq.), 7-methoxy-1-[(4*E*)-5-(4,4,5,5-tetramethyl-1,3,2-dioxaborolan-2-yl)pent-4-en-1-yl]-1,2,3,4-tetrahydroquinoline (**13**) (167 mg, 0.467 mmol, 1.1 eq.), and K_2CO_3 (145 mg, 1.05 mmol, 2.5 eq.) in 1,4-dioxane (3.6 mL) and H_2O (0.84 mL) was purged with Ar. $Pd(PPh_3)_2Cl_2$ (15 mg, 0.021 mmol, 0.05 eq.) was added and the reaction mixture was purged with Ar before being stirred at 100 ºC for 24 h. The reaction mixture was cooled to rt and was filtered through a Gilson Scientific Ltd® PTFE syringe filter 25 mm, 0.22 µm, washed with EtOAc (10 mL), and concentrated *in vacuo*. H_2O (10 mL) was added, and the aqueous component was extracted with EtOAc (2 × 10 mL). The combined organic components were washed with brine (30 mL), dried (Na_2SO_4), filtered, and concentrated *in vacuo*. The crude brown oil was purified using normal phase column chromatography (gradient of 12 – 100% EtOAc in petroleum ether) to afford (4*R*)-6-[(1*E*)-5-(7-methoxy-3,4-dihydroquinolin-1(2*H*)-yl)pent-1-en-1-yl]-4-methyl-1,3,4,5-tetrahydro-2*H*-1,5-benzodiazepin-2-one (**(*R*)-OXFBD05**) (98 mg, 0.24 mmol, 58%) as a pale brown oil: R_f 0.14 (1:1 petroleum ether/ EtOAc); $[\alpha]_D^{25} = -2.9$ (*c* 1.0, $CHCl_3$) [lit.[43] $[\alpha]_D^{22} = -3.7$ (*c* 1.0, $CHCl_3$)]; ^{1}H NMR (400 MHz, $CDCl_3$) δ_H 7.23 (1 H, br s, NH-5), 7.12 (1 H, dd, *J* 7.7, 1.5, H-9), 6.90 – 6.83 (2 H, m, H-7, H-5^{II}), 6.78 (1 H, dd, *J* 7.8, 1.5, H-8), 6.48 (1 H, d, *J* 15.5, H-1^I), 6.24 – 6.13 (2 H, m, H-6^{II}, H-8^{II}), 6.08 (1 H, dt, *J* 15.5, 6.9, H-2^I), 4.19 – 4.03

(1 H, m, H-4), 3.75 (3 H, s, H-9^{II}), 3.33 – 3.25 (4 H, m, H-5^{I}, H-2^{II}), 2.70 (2 H, t, *J* 6.4, H-4^{II}), 2.61 (1 H, dd, *J* 13.3, 4.7, H_AH_B-3), 2.39 (1 H, dd, *J* 13.3, 7.5, H_AH_B-3), 2.34 – 2.26 (2 H, m, H-3^{I}), 1.99 – 1.89 (2 H, m, H-3^{II}), 1.87 – 1.75 (2 H, m, H-4^{I}), 1.35 (3 H, d, *J* 6.3, H-10); LRMS *m/z* (ESI$^+$) 406 ([M+H]$^+$, 100%), HPLC (Method 2) t_R 8.8 min, purity 99.7%. These data are in good accordance with the literature.[43]

1-Bromo-2-fluoro-5-iodo-3-nitrobenzene (18)

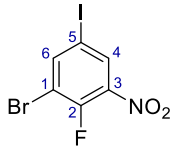

N-Iodosuccinimide (2.88 g, 12.8 mmol, 1.4 eq.) was added to a solution of 1-bromo-2-fluoro-3-nitrobenzene (2.00 g, 9.13 mmol, 1.0 eq.) in concentrated sulfuric acid (10 mL) and the reaction mixture was stirred at rt for 16 h. The reaction mixture was added slowly to ice (100 g) and the precipitate was extracted with CH_2Cl_2 (3 × 70 mL). The combined organic components were washed with 10% aq. $Na_2S_2O_3$ (100 mL), brine (100 mL), dried (Na_2SO_4), filtered, and concentrated *in vacuo*. The crude oil was purified using normal phase column chromatography (gradient of 0 – 10% EtOAc in petroleum ether) to afford 1-bromo-2-fluoro-5-iodo-3-nitrobenzene (**18**) (2.68 g, 7.75 mmol 85%) as a yellow solid: R_f 0.67 (1:9 EtOAc /petroleum ether); mp 36 – 39 ºC (CH_2Cl_2); ^{1}H NMR (400 MHz, $CDCl_3$) δ_H 8.28 (1 H, dd, *J* 6.2, 2.2, H-4), 8.16 (1 H, dd, *J* 5.5, 2.2, H-6); ^{19}F NMR (376 MHz, $CDCl_3$) δ_F −110.84 (dd, *J* 6.2, 5.5, F-2). These data are in good accordance with previous work in the group.

***tert*-Butyl (3*R*)-3-(2-bromo-4-iodo-6-nitroanilino)butanoate (19)**

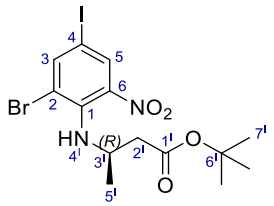

To a stirred suspension of 1-bromo-2-fluoro-5-iodo-3-nitrobenzene (**18**) (1.31 g, 3.78 mmol, 1.0 eq.) and Cs_2CO_3 (3.69 g, 5.29 mmol, 1.4 eq.) in toluene (60 mL) was added *tert*-butyl (3*R*)-3-aminobutanoate (**15**) (1.16 g, 5.29 mmol, 1.4 eq.) and the suspension was stirred at 85 ºC for 17 h. The suspension was cooled to rt, 1 M aq. K_2CO_3 (150 mL) was added, and the resulting mixture was extracted with EtOAc (3 × 150 mL). The combined organic components were washed with brine (80 mL), dried ($MgSO_4$), filtered, and concentrated *in vacuo*. The crude orange oil was purified using normal phase column chromatography (gradient of 0 – 10 % EtOAc in petroleum ether) to afford *tert*-butyl (3*R*)-3-(2-bromo-4-iodo-6-nitroanilino)butanoate (**19**) (1.71 g, 3.52 mmol, 93%) as an orange solid: R_f 0.48 (1:9 EtOAc/ petroleum ether); $[\alpha]_D^{25} = -55.5$ (*c* 1.0, $CHCl_3$); mp 52 – 57 ºC (EtOAc); ^{1}H NMR (400 MHz, $CDCl_3$) δ_H 8.20 (1 H, d, *J* 2.1, H-5), 7.98 (1 H, d, *J* 2.1, H-3), 6.40 (1 H, d, *J* 10.2, NH-4^I), 4.30 – 4.15 (1 H, m, H-3^I), 2.45 (1 H, d, *J* 2.4, H_AH_B-2^I), 2.43 (1H, d, *J* 2.4, H_AH_B-2^I) 1.39 (9 H, s, H-7^I), 1.27 (3 H, d, *J* 6.6, H-5^I); LRMS *m/z* (ESI$^-$) 483 ([M(^{79}Br)−H]$^-$, 100%), 485 ([M(^{79}Br)−H]$^-$, 100%). These data are in good accordance with previous work in the group.

***tert*-Butyl (3*R*)-3-(2-bromo-4-(5-hydroxypent-1-yn-1-yl)-6-nitroanilino)butanoate (20)**

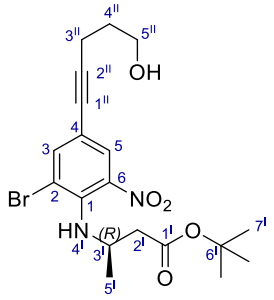

A solution of *tert*-butyl (3*R*)-3-(2-bromo-4-iodo-6-nitroanilino)butanoate (**19**) (775 mg, 1.60 mmol, 1.0 eq.), 4-pentyn-1-ol (0.179 mL, 1.92 mmol, 1.2 eq.), and NEt_3 (2.6 mL) in THF (4.5 mL) was purged with Ar before the addition of $Pd(PPh_3)_2Cl_2$ (23 mg, 0.032 mmol, 0.02 eq.) and CuI (9 mg, 0.05 mmol, 0.03 eq.). The reaction mixture was purged with Ar and stirred at rt under an atmosphere of Ar for 3.5 h. The reaction mixture was concentrated *in vacuo* and the residue was diluted in EtOAc (400 mL), washed with sat. aq. $NaHCO_3$ (3 × 200 mL), brine (90 mL), dried ($MgSO_4$), filtered, and concentrated *in vacuo*. The crude orange oil was purified using normal phase column chromatography (gradient of 20 – 30% EtOAc in petroleum ether) to afford *tert*-butyl (3*R*)-3-(2-bromo-4-(5-hydroxypent-1-yn-1-yl)-6-nitroanilino)butanoate (**20**) (544 mg, 1.23 mmol, 77%) as an orange solid: R_f 0.44 (1:1 petroleum ether/ EtOAc); $[\alpha]_D^{25} = -75.2$ (*c* 1.0, $CHCl_3$); mp 54 – 60 ºC; ^{1}H NMR (400 MHz, $CDCl_3$) δ_H 7.95 (1 H, d, *J* 2.0, H-5), 7.72 (1 H, d, *J* 2.0, H-3), 6.46 (1 H, d, *J* 10.2, NH-4^I), 4.34 – 4.19 (1 H, m, H-3^I), 3.80 (2 H, q, *J* 5.7, H-5^{II}), 2.52 (2 H, t, *J* 7.0, H-3^{II}), 2.44 (2 H, d, *J* 6.1, H-2^I), 1.93 – 1.80 (2 H, m, H-4^{II}), 1.39 (9 H, s, H-7^I), 1.27 (3 H, d, *J* 6.5, H-5^I); LRMS *m/z* (ESI$^+$) 463 ([M(^{79}Br)+Na]$^+$, 89%), 465 ([M(^{81}Br)+Na]$^+$, 100%). These data are in good accordance with previous work in the group.

***tert*-Butyl (3*R*)-3-(2-bromo-4-(5-hydroxypentyl)-6-nitroanilino)butanoate (21)**

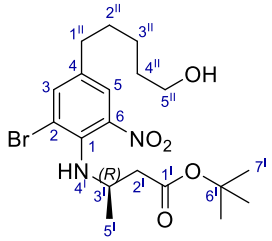

$Rh(PPh_3)_3Cl$ (29 mg, 0.031 mmol, 0.05 eq.) was added to a solution of *tert*-butyl (3*R*)-3-(2-bromo-4-(5-hydroxypent-1-yn-1-yl)-6-nitroanilino)butanoate (**20**) (270 mg, 0.616 mmol, 1.0 eq.) in toluene (8.1 mL). The resulting orange suspension was purged with H_2 and stirred at 60 ºC under an atmosphere of H_2 for 6 h. The reaction mixture was concentrated *in vacuo* and the crude orange oil was purified using normal phase column chromatography (isocratic 30% EtOAc in petroleum ether) to afford *tert*-butyl (3*R*)-3-(2-bromo-4-(5-hydroxypentyl)-6-nitroanilino)butanoate (**21**) (228 mg, 0.512 mmol,

83%) as an orange oil: R_f 0.26 (7:3 petroleum ether/ EtOAc): $[\alpha]_D^{25} = -62.9$ (*c* 1.0, $CHCl_3$); ^{1}H NMR (400 MHz, $CDCl_3$) δ_H 7.74 (1 H, d, *J* 2.0, H-3), 7.57 (1 H, d, *J* 2.0, H-5), 6.19 (1 H, d, *J* 10.5, NH-4^I), 4.27 – 4.11 (1 H, m, H-3^I), 3.65 (2 H, td, *J* 6.4, 4.8, H-5^{II}), 2.56 (2 H, t, *J* 7.7, H-1^{II}), 2.44 (1 H, d, *J* 2.6, H_AH_B-2^I), 2.42 (1 H, d, *J* 2.6, H_AH_B-2^I), 1.68 – 1.57 (4 H, m, H-2^{II}, H-4^{II}), 1.46 – 1.40 (2 H, m, H-3^{II}), 1.39 (9 H, s, H-7^I), 1.25 (3 H, d, *J* 6.5, H-5^I); LRMS *m/z* (ESI$^+$) 445 ([M(^{79}Br)+H$^+$], 98%), 447 ([M(^{81}Br)+H$^+$], 100%)These data are in good accordance with previous work in the group.

(4*R*)-6-Bromo-8-(5-hydroxypentyl)-4-methyl-1,3,4,5-tetrahydro-2*H*-1,5-benzodiazepin-2-one (22)

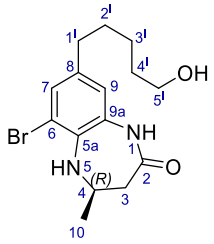

Step I:

To a solution of *tert*-butyl (3*R*)-3-(2-bromo-4-(5-hydroxypentyl)-6-nitroanilino)butanoate (**21**) (200 mg, 0.449 mmol, 1.0 eq.) in CH_2Cl_2 (1.7 mL) was added trifluoroacetic acid (1.7 mL). The orange solution was stirred at rt for 2 h before being concentrated *in vacuo* to afford the carboxylic acid intermediate as a brown oil.

Step II:

The crude carboxylic acid intermediate was dissolved in glacial acetic acid (4.0 mL) and iron powder (126 mg, 2.25 mmol, 5.0 eq.) was added. The brown suspension was heated at reflux for 5 h. The reaction mixture was cooled to rt before the addition of 1 M aq. K_2CO_3 (40 mL) and the aqueous component was extracted with EtOAc (3 × 40 mL). The combined organic components were washed with brine (40 mL), dried ($MgSO_4$), filtered, and concentrated *in vacuo* to afford the O-acetylated product.

Step III:

The brown O-acetylated product was dissolved in 3:2:1 THF/ MeOH/ H_2O (4.3 mL) and LiOH (108 mg, 4.49 mmol, 10 eq.) was added. The reaction mixture was stirred at rt for 2 h before being concentrated *in vacuo*. The residue was diluted in H_2O (20 mL) and the aqueous component was extracted with EtOAc (3 × 20 mL). The combined organic components were washed with brine (20 mL), dried ($MgSO_4$), filtered, and concentrated *in vacuo*. The crude brown oil was purified using normal phase column chromatography (gradient of 50 – 100% EtOAc in petroleum ether) to afford (4*R*)-6-bromo-8-(5-hydroxypentyl)-4-methyl-1,3,4,5-tetrahydro-2*H*-1,5-benzodiazepin-2-one (**22**) (97 mg, 0.28 mmol, 63%) as a colourless solid: R_f 0.18 (EtOAc): $[\alpha]_D^{25}$ = +15.2 (*c* 1.0, MeOH); mp 86 – 92 ºC (EtOAc); ^{1}H NMR (400 MHz, $CDCl_3$) δ_H 7.34 (1 H, br s, NH-1) 7.16 (1 H, d, *J* 1.9, H-7), 6.63 (1 H, d, *J* 1.9, H-9), 4.10 (1 H, m, H-4), 3.99 (1 H, br s, NH-5), 3.65 (2 H, td, *J* 6.6, 5.2, H-5^{I}), 2.59 (1 H, dd, *J* 13.5, 4.5 H_AH_B-3), 2.51 (2 H, t, *J* 7.8, H-1^{I}), 2.40 (1 H, dd, *J* 13.5, 8.0, H_AH_B-3), 1.66 – 1.57 (4 H, m, H-2^{I}, H-4^{I}), 1.44 – 1.38 (2 H, m, H-3^{I}), 1.36 (3 H, d, *J* 6.3, H-10). These data are in good accordance with previous work in the group.

(4*R*)-8-(5-Hydroxypentyl)-6-((1*E*)-5-(7-methoxy-3,4-dihydroquinolin-1(2*H*)-yl)pent-1-en-1-yl)-4-methyl-1,3,4,5-tetrahydro-2*H*-1,5-benzodiazepin-2-one (2)

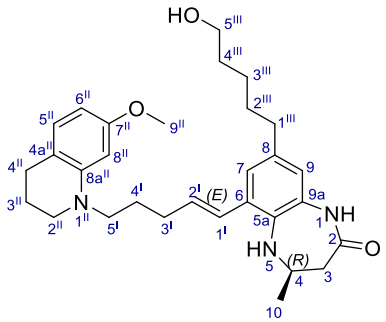

A suspension of (4*R*)-6-bromo-8-(5-hydroxypentyl)-4-methyl-1,3,4,5-tetrahydro-2*H*-1,5-benzodiazepin-2-one (**22**) (96 mg, 0.28 mmol, 1.0 eq.), 7-methoxy-1-[(4*E*)-5-(4,4,5,5-tetramethyl-1,3,2-dioxaborolan-2-yl)pent-4-en-1-yl]-1,2,3,4-tetrahydroquinoline (**13**) (151 mg, 0.422 mmol, 1.5 eq.) and K_2CO_3 (117 mg, 0.843 mmol, 3.0 eq.) in 1,4-dioxane (2.0 mL) and H_2O (0.5 mL) was

purged with Ar. $Pd(PPh_3)_2Cl_2$ (10 mg, 0.014 mmol, 0.05 eq.) was added and the reaction mixture was purged with Ar before being stirred at 100 ºC under an atmosphere of Ar for 16 h. The reaction mixture concentrated *in vacuo* and the residues was diluted with EtOAc (50 mL). The organic component was washed with brine (3 × 20 mL), dried ($MgSO_4$), filtered, and concentrated *in vacuo*. The crude brown oil was purified using normal phase column chromatography (isocratic EtOAc) to afford (4*R*)-8-(5-hydroxypentyl)-6-((1*E*)-5-(7-methoxy-3,4-dihydroquinolin-1(2*H*)-yl)pent-1-en-1-yl)-4-methyl-1,3,4,5-tetrahydro-2*H*-1,5-benzodiazepin-2-one (**2**) (45 mg, 92 μmol, 33 %) as a yellow oil: R_f 0.26 (EtOAc); $[\alpha]_D^{25} = +3.1$ (*c* 1.0, $CHCl_3$); $\bar{\upsilon}_{max}$ (thin film)/ cm^{-1} 3367 (O-H, w, br), 3215 (N-H, w, br), 2931 (C-H, m), 2931 (C-H, m), 2856 (C-H, m), 1665 (C=O, s), 1612 (C=C, m), 1577 (C=C, m); ^{1}H NMR (500 MHz, $CDCl_3$) δ_H 7.47 (1 H, br s, NH-1), 6.95 (1 H, d, *J* 2.0, H-7), 6.85 (1 H, d, *J* 8.0, H-5^{II}), 6.62 (1 H, d, *J* 2.0, H-9), 6.46 (1 H, d, *J* 15.5, H-1^{I}), 6.17 – 6.12 (2 H, m, H-6^{II}, H-8^{II}), 6.08 (1 H, dt, *J* 15.5, 6.9, H-2^{I}), 4.15 – 4.04 (1 H, m, H-4), 3.75 (3 H, s, H-9^{II}), 3.65 (2 H, t, *J* 6.6, H-5^{III}), 3.42 (1 H, br s, NH-5), 3.32 – 3.25 (4 H, m, H-5^{I}, H-2^{II}), 2.69 (2 H, t, *J* 6.3, H-4^{II}), 2.59 (1 H, dd, *J* 13.2, 4.9, H_AH_B-3), 2.53 (2 H, t, *J* 7.7, H-1^{III}), 2.35 (1 H, dd, *J* 13.2, 7.3, H_AH_B-3), 2.29 (2 H, q, *J* 6.9, H-3^{I}), 1.93 (2 H, p, *J* 6.3, H-3^{II}), 1.79 (2 H, p, *J* 7.5, H-4^{I}), 1.67 – 1.56 (4 H, m, H-2^{III}, H-4^{III}), 1.45 – 1.36 (2 H, m, H-3^{III}), 1.34 (3 H, d, *J* 6.3, H-10); ^{13}C NMR (126 MHz, $CDCl_3$) δ_C 173.1 (C-2), 159.4 (C-7^{II}), 146.2 (C-8a^{II}), 136.3 (C-8), 134.6 (C-2^{I}), 133.8 (C-5a), 131.1 (C-6), 130.5 (C-9a), 129.6 (C-5^{II}), 125.8 (C-1^{I}), 124.3 (C-7), 120.9 (C-9), 115.5 (C-4a^{II}), 99.4 (C-6^{II}), 97.7 (C-8^{II}), 63.0 (C-5^{III}), 55.8 (C-4), 55.3 (C-9^{II}), 51.2 (C-5^{I}), 49.6 (C-2^{II}), 40.7 (C-3), 35.2 (C-1^{III}), 32.7 (C-4^{II}), 31.3 (C-2^{II}), 31.2 (C-3^{I}), 27.5 (C-4^{II}), 26.1 (C-4^{I}), 25.5 (C-3^{III}), 24.1 (C-10), 22.6 (C-3^{II}); HRMS *m/z* (ESI$^+$) 492.3211 (492.3221 calculated for $[C_{30}H_{42}N_3O_3]^+$); LRMS *m/z* (ESI$^+$) 493 ($[M+H]^+$, 100%); HPLC (Method 1) t_R 10.4 min, purity 95.8%.

(4*R*)-6-Bromo-8-iodo-4-methyl-1,3,4,5-tetrahydro-2H-1,5-benzodiazepin-2-one (24)

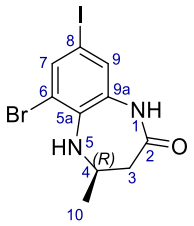

Step I:

To a solution of *tert*-butyl (3*R*)-3-(2-bromo-4-iodo-6-nitroanilino)butanoate (**19**) (500 mg, 1.03 mmol, 1.0 eq.) in CH_2Cl_2 (3.8 mL) was added TFA (3.8 mL) and the resulting orange solution was stirred at rt for 45 min. The reaction mixture was concentrated *in vacuo* to afford the carboxylic acid intermediate as a brown oil.

Step II:

The carboxylic acid intermediate was dissolved in glacial acetic acid (9.0 mL) and iron powder (288 mg, 5.15 mmol, 5.0 eq.) was added. The brown suspension was heated under reflux for 4 h. The reaction mixture was cooled to rt and 1 M aq. K_2CO_3 (60 mL) was added. The aqueous component was extracted with EtOAc (3 × 60 mL) and the combined organic components were washed with brine (60 mL), dried ($MgSO_4$), filtered, and concentrated *in vacuo*. The crude oil was purified using normal phase column gel chromatography (isocratic 50% EtOAc in petroleum ether) to afford (4*R*)-6-bromo-8-iodo-4-methyl-1,3,4,5-tetrahydro-2H-1,5-benzodiazepin-2-one (**24**) (370 mg, 0.971 mmol, 97%) as a colourless solid: R_f 0.45 (1:4 petroleum ether/ EtOAc)**;** mp 174 – 176 ºC (EtOAc); $[\alpha]_D^{25}$ = +25.2 (*c* 1.0, DMSO); ^{1}H NMR (400 MHz, DMSO-d_6) δ_H 9.66 (1 H, br s, NH-1), 7.57 (1 H, d, *J* 2.1, H-7), 7.20 (1 H, d, *J* 2.1, H-9), 4.80 (1 H, br s, NH-5), 3.99 (1 H, m, H-4), 2.45 (1H, dd, *J* 13.6, 4.1, H_AH_B-3), 2.26 (1 H, dd, *J* 13.6, 8.1, H_AH_B-3), 1.22 (3 H, d, *J* 6.3, H-10); LRMS *m/z* (ESI$^+$) 341 ([M(^{79}Br)+H]$^+$, 100%), 342 ([M(^{81}Br)+H$^+$], 99.9%). These data are in good accordance with previous work in the group.

(4*R*)-6-Bromo-8-(5-hydroxypent-1-yn-1-yl)-4-methyl-1,3,4,5-tetrahydro-2*H*-1,5-benzodiazepin-2-one (23)

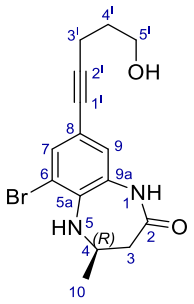

A solution of (4*R*)-6-bromo-8-iodo-4-methyl-1,3,4,5-tetrahydro-2H-1,5-benzodiazepin-2-one (**24**) (120 mg, 0.315 mmol, 1.0 eq.), 4-pentyn-1-ol (35 µL, 0.38 mmol, 1.2 eq.), and NEt_3 (0.48 mL) in DMF (0.84 mL) was purged with Ar before the addition of $Pd(PPh_3)_2Cl_2$ (4 mg, 6 µmol, 0.02 eq.) and CuI (2 mg, 0.01 mmol, 0.04 eq.). The suspension was purged with Ar before being stirred at 40 ºC under an atmosphere of Ar for 19 h. The reaction mixture was cooled to rt and diluted with EtOAc (80 mL). The organic component was washed with sat. aq. $NaHCO_3$ (3 × 50 mL), 0.5 M aq. LiCl (3 × 20 mL), brine (50 mL), dried ($MgSO_4$), filtered, and concentrated *in vacuo*. The crude orange oil was purified using normal phase column chromatography (gradient of 50 – 80% EtOAc in petroleum ether) to afford (4*R*)-6-bromo-8-(5 -hydroxypent-1-yn-1-yl)-4-methyl-1,3,4,5-tetrahydro-2*H*-1,5-benzodiazepin-2-one (**23**) (61 mg, 0.18 mmol, 57%) as a colourless solid: R_f 0.32 (1:4 petroleum ether/ EtOAc); mp 83 – 85 ºC (EtOAc); ^{1}H NMR (400 MHz, CD_3OD) δ_H 7.36 (1 H, d, *J* 1.8, H-7), 6.96 (1 H, d, *J* 1.9, H-9), 4.18 – 4.09 (1 H, m, H-4), 3.70 (2 H, t, *J* 6.3, H-5^I), 2.57 (1 H, dd, *J* 13.5, 4.3, H_AH_B-3), 2.50 (2 H, t, *J* 7.1, H-3^I), 2.38 (1 H, dd, *J* 13.5, 8.0, H_AH_B-3), 1.86 – 1.75 (2 H, m, H-4^I), 1.36 (3 H, d, *J* 6.3, H-10); LRMS *m/z* (ESI$^+$) 337 ([M(^{79}Br)+H]$^+$, 100%), 339 ([M(^{81}Br)+H]$^+$, 97%). These data are in good accordance with previous work in the group.

(4*R*)-8-(5-Hydroxypent-1-yn-1-yl)-6-((1*E*)-5-(7-methoxy-3,4-dihydroquinolin-1(2*H*)-yl)pent-1-en-1-yl)-4-methyl-1,3,4,5-tetrahydro-2*H*-1,5-benzodiazepin-2-one (3)

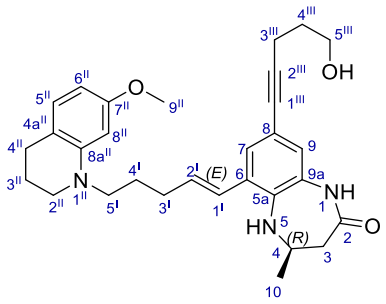

A suspension of (4*R*)-6-bromo-8-(5-hydroxypent-1-yn-1-yl)-4-methyl-1,3,4,5-tetrahydro-2*H*-1,5-benzodiazepin-2-one (**23**) (30 mg, 0.088 mmol, 1.0 eq.), 7-methoxy-1-[(4*E*)-5-(4,4,5,5-tetramethyl-1,3,2-dioxaborolan-2-yl)pent-4-en-1-yl]-1,2,3,4-tetrahydroquinoline (**13**) (47 mg, 0.13 mmol, 1.5 eq.), and K_2CO_3 (37 mg, 0.26 mmol, 3.0 eq.) in 1,4-dioxane (0.70 mL) and H_2O (0.18 mL) was purged with Ar. $Pd(PPh_3)_2Cl_2$ (3 mg, 4 µmol, 0.05 eq.) was added and the reaction mixture was purged with Ar before being stirred at 100 ºC under an atmosphere of Ar for 16 h. The reaction mixture was cooled to rt, concentrated *in vacuo*, and diluted with EtOAc (50 mL). The organic component was washed with brine (3 × 30 mL), dried ($MgSO_4$), filtered, and concentrated *in vacuo*. The crude brown oil was purified using normal phase column chromatography (gradient of 80 – 100% EtOAc in petroleum ether) to afford (4*R*)-8-(5-hydroxypent-1-yn-1-yl)-6-((1*E*)-5-(7-methoxy-3,4-dihydroquinolin-1(2*H*)-yl)pent-1-en-1-yl)-4-methyl-1,3,4,5-tetrahydro-2*H*-1,5-benzodiazepin-2-one (**3**) (6 mg, 0.01 mmol, 14%) as a yellow oil: R_f 0.36 (1:4 petroleum ether/ EtOAc); $[\alpha]_D^{25} = +16.5$ (*c* 0.2, $CHCl_3$); $\bar{\upsilon}_{max}$ (thin film)/ cm^{-1} 3362 (O-H, N-H, w, br), 2981 (C-H, s), 2929 (C-H, s), 1669 (C=O, m), 1613 (C=C, m), 1574 (C=C, w); ^{1}H NMR (400 MHz, $CDCl_3$) δ_H 7.48 (1 H, br s, NH-5), 7.14 (1 H, d, *J* 1.9, H-7), 6.86 (1 H, d, *J* 7.9, H-5^{II}), 6.83 (1 H, d, *J* 1.9, H-9), 6.38 (1 H, d, *J* 15.5, H-1^{I}), 6.18 – 6.13 (2 H, m, H-6^{II}, H-8^{II}), 6.08 (1 H, dt, *J* 15.5, 6.9, H-2^{I}), 4.14 – 4.03 (1 H, m, H-4), 3.81 (2 H, t, *J* 6.1, H-5^{III}), 3.75 (3 H, s, H-9^{II}), 3.61 (1 H, br s, NH-1), 3.33 – 3.23 (4 H, m, H-5^{I}, H-2^{II}), 2.69 (2 H, t, *J* 6.3, H-4^{II}), 2.60 (1 H, dd, *J* 13.4, 4.3, H_AH_B-3), 2.52 (2 H, t, *J* 6.9, H-3^{III}), 2.40 (1 H, dd, *J* 13.4, 7.7, H_AH_B-3), 2.32 – 2.24 (2 H, m, H-3^{I}), 1.97 – 1.89 (2 H, m, H-3^{II}), 1.89 – 1.81 (2 H, m, H-4^{III}), 1.83 – 1.74 (2 H, m, H-4^{I}), 1.34 (3 H, d, *J* 6.3, H-10); ^{13}C NMR (126 MHz, $CDCl_3$) δ_C 172.7 (C-2), 159.3 (C-7^{II}), 146.2 (C-8a^{II}), 135.79 (C-5a/ C-2^{I}),

135.76 (C-5a/ C-2^{I}), 130.6 (C-6), 129.7 (C-5^{II}), 129.0 (C-9a), 127.8 (H-7), 125.0 (C-1^{I}), 123.9 (C-9), 116.3 (C-8), 115.5 (C-4a^{II}), 99.6 (C-8^{II}), 97.64 (C-6^{II}), 88.6 (C-2^{III}), 80.5 (C-1^{III}), 62.0 (C-5^{III}), 55.3 (C-9^{II}), 54.9 (C-4), 51.1 (C-5^{I}), 49.6 (C-2^{II}), 40.9 (C-3), 31.5 (C-4^{III}), 31.1 (C-3^{I}), 27.5 (C-4^{II}), 26.0 (C-4^{I}), 24.3 (C-10), 22.6 (C-3^{II}), 16.1 (C-3^{III}); HRMS *m/z* (ESI^{+}) 488.2910 (488.2908 calculated for $[C_{30}H_{38}N_3O_3]^{+}$); LRMS *m/z* (ESI^{+}) 488 ([M+H]$^{+}$, 100%); HPLC (Method 1) t_R 10.1 min, purity 95.2%.

(4*R*)-6-Bromo-8-(3-hydroxyprop-1-yn-1-yl)-4-methyl-1,3,4,5-tetrahydro-2*H*-1,5-benzodiazepin-2-one (27)

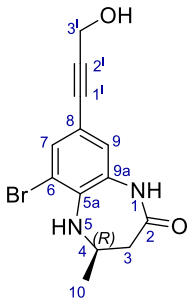

A solution of (4*R*)-6-bromo-8-iodo-4-methyl-1,3,4,5-tetrahydro-2*H*-1,5-benzodiazepin-2-one (**24**) (150 mg, 0.394 mmol, 1.0 eq.), propargyl alcohol (27 μL, 0.47 mmol, 1.2 eq.), and NEt_3 (0.6 mL) in DMF (1.0 mL) was purged with Ar before the addition of $Pd(PPh_3)_2Cl_2$ (6 mg, 8 μmol, 0.02 eq.) and CuI (3 mg, 0.02 mmol, 0.04 eq.). The reaction mixture was purged with Ar and stirred at rt under an atmosphere of Ar for 18 h. The reaction mixture was concentrated *in vacuo* and the orange residue was diluted in EtOAc (80 mL). The organic component was washed with sat. aq. $NaHCO_3$ (3 × 50 mL), 0.5 M aq. LiCl (3 × 20 mL), brine (50 mL), dried ($MgSO_4$), filtered, and concentrated *in vacuo*. The crude orange oil was purified using normal phase column chromatography (isocratic 75% EtOAc in petroleum ether) to afford (4*R*)-6-bromo-8-(3-hydroxyprop-1-yn-1-yl)-4-methyl-1,3,4,5-tetrahydro-2*H*-1,5-benzodiazepin-2-one (**27**) (75 mg, 0.24 mmol, 62%) as an orange solid: R_f 0.16 (1:1 petroleum ether/ EtOAc); $[\alpha]_D^{25} = -9.30$ (*c* 1.0, $CHCl_3$); **mp 116 – 121 ºC (EtOAc);** $\tilde{\upsilon}_{max}$ (thin film)/ cm^{-1} 3350 (OH, m, br), 3216 (N-H, m, br), 2967 (C-H, w), 1668 (C=O, s); ^{1}H NMR (500 MHz, $CDCl_3$) δ_H 7.77 (1 H, br s, NH-1), 7.40 (1 H, d, *J* 1.8, H-7), 6.89 (1 H, d, *J* 1.8, H-9), 4.46 (2 H, d, *J* 5.5, H-3^{I}), 4.37 (1 H, br s,

NH-5), 4.15 – 4.07 (1 H, m, H-4), 2.64 (1 H, dd, *J* 13.9, 3.5, H_AH_B-3), 2.49 (1 H, dd, *J* 13.9, 8.5, H_AH_B-3), 1.98 (1 H, br t, *J* 6.1, OH), 1.39 (3 H, d, *J* 6.3, H-10); ^{13}C NMR (126 MHz, $CDCl_3$) δ_C 172.4 (C-2), 137.0 (C-9a), 132.4 (C-7), 127.0 (C-5a), 124.8 (C-9), 114.77 (C-8), 114.68 (C-6), 87.6 (C-2^I), 83.8 (C-1^I), 53.6 (C-4), 51.7 (C-3^I), 41.7 (C-3), 24.2 (C-10); HRMS *m/z* (ESI^+) 309.0234 (309.0233 calculated for $[C_{13}H_{14}{}^{79}BrN_2O_2]^+$), 311.0213 (311.0213 calculated for $[C_{13}H_{14}{}^{81}BrN_2O_2]^+$); LRMS *m/z* ($ESI^+$) 309 ($[M(^{79}Br)+H]^+$, 100%), 311 ($[M(^{81}Br)+H]^+$, 83%); HPLC (Method 1) t_R 5.5 min, purity 97.0%.

(4*R*)-6-Bromo-8-(10-hydroxydec-1-yn-1-yl)-4-methyl-1,3,4,5-tetrahydro-2*H*-1,5-benzodiazepin-2-one (28)

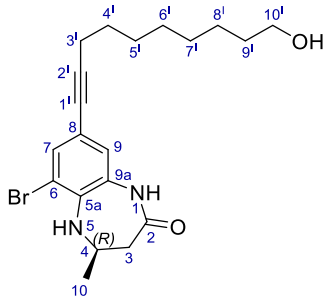

A solution of (4*R*)-6-bromo-8-iodo-4-methyl-1,3,4,5-tetrahydro-2H-1,5-benzodiazepin-2-one (**24**) (100 mg, 0.26 mmol, 1.0 eq.), 9-decyn-1-ol (60 µL, 0.31 mmol, 1.2 eq.), and NEt_3 (0.4 mL) in DMF (0.4 mL) was purged with Ar before the addition of $Pd(PPh_3)_2Cl_2$ (4 mg, 5 µmol, 0.02 eq.) and CuI (2 mg, 10 µmol, 0.04 eq.). The reaction mixture was purged with Ar and stirred at rt under an atmosphere of Ar for 20 h. The reaction mixture was concentrated *in vacuo* and the orange residue was diluted in EtOAc (80 mL). The organic component was washed with sat. aq. $NaHCO_3$ (3 × 50 mL), 0.5 M aq. LiCl (3 × 20 mL), brine (50 mL), dried ($MgSO_4$), filtered, and concentrated *in vacuo*. The crude orange oil was purified using normal phase column chromatography (isocratic 75% EtOAc in petroleum ether) to afford (4*R*)-6-bromo-8-(10-hydroxydec-1-yn-1-yl)-4-methyl-1,3,4,5-tetrahydro-2*H*-1,5-benzodiazepin-2-one (**28**) (103 mg, 0.253 mmol, 96%) as a colourless solid: R_f 0.28 (petroleum ether/ EtOAc 2:3); $[\alpha]_D^{25}$ = +1.6 (*c* 1.0, $CHCl_3$); mp 95 – 99 ºC (EtOAc); $\bar{\upsilon}_{max}$ (thin film)/ cm^{-1} 3360 (O-H, m,

br), 3210 (N-H, m, br), 2929 (C-H, m), 2855 (C-H, m), 1673 (C=O, s); ^{1}H NMR (500 MHz, $CDCl_3$) δ_H 7.77 (1 H, br s, NH-1), 7.36 (1 H, d, *J* 1.8, H-7), 6.87 (1 H, d, *J* 1.8, H-9), 4.25 (1 H, br s, NH-5), 4.10 (1 H, m, H-4), 3.65 (2 H, q, *J* 6.4, H-10^{I}), 2.61 (1 H, dd, *J* 13.8, 3.7, H_AH_B-3), 2.45 (1 H, dd, *J* 13.7, 8.3, H_AH_B-3), 2.37 (2 H, t, *J* 7.0, H-3^{I}), 1.61 – 1.53 (4 H, m, H-4^{I}, H-9^{I}), 1.51 – 1.39 (2 H, m, H-5^{I}), 1.37 (3 H, d, *J* 6.3, H-10), 1.36 – 1.32 (6 H, m, H-6^{I}, H-7^{I}, H-8^{I}); ^{13}C NMR (126 MHz, $CDCl_3$) δ_C 172.4 (C-2), 136.3 (C-5a), 132.1 (C-7), 127.7 (C-9a), 124.7 (C-9), 116.8 (C-8), 115.1 (C-6), 90.8 (C-2^{I}), 78.7 (C-1^{I}), 63.2 (C-10^{I}), 54.0 (C-4), 41.5 (C-3), 32.9 (C-9^{I}), 29.4 (C-7^{I}), 29.1 (C-6^{I}), 28.8 (H-5^{I}), 28.6 (C-4^{I}), 25.8 (C-8^{I}), 24.2 (C-10), 19.4 (C-3^{I}); HRMS *m/z* (ESI^{+}) 407.13270 (407.1329 calculated for $[C_{20}H_{28}BrN_2O_2]^{+}$); LRMS *m/z* (ESI^{+}) 407 ([M(^{79}Br)+H]$^{+}$, 100%), 409 ([M(^{81}Br)+H]$^{+}$, 94%); HPLC (Method 1) t_R 9.8 min, purity 98.2%.

(4*R*)-6-Bromo-8-(3-hydroxypropyl)-4-methyl-1,3,4,5-tetrahydro-2*H*-1,5-benzodiazepin-2-one (29)

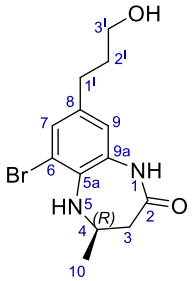

A suspension of (4*R*)-6-bromo-8-(3-hydroxyprop-1-yn-1-yl)-4-methyl-1,3,4,5-tetrahydro-2*H*-1,5-benzodiazepin-2-one (**27**) (74 mg, 0.24 mmol, 1.0 eq.) and $Rh(PPh_3)Cl$ (11 mg, 12 μmol, 0.05 eq.) in toluene (2.0 mL) was purged with H_2. The reaction mixture was stirred at 60 ºC under an atmosphere of H_2 for 6 h. The crude brown suspension was directly purified using normal phase column chromatography (isocratic EtOAc) to afford (4*R*)-6-bromo-8-(3-hydroxypropyl)-4-methyl-1,3,4,5-tetrahydro-2*H*-1,5-benzodiazepin-2-one (**29**) (49 mg, 0.16 mmol, 65%) as a yellow solid: R_f 0.28 (EtOAc); $[\alpha]_D^{25} = +3.3$ (*c* 1.0, $CHCl_3$); mp 92 – 94 ºC (EtOAc); $\bar{\upsilon}_{max}$ (thin film)/ cm^{-1} 3354 (O-H, w, br), 3219 (N-H, w, br), 2929 (C-H, w), 2864 (C-H, w), 1668 (C=O, s); ^{1}H NMR (500 MHz, $CDCl_3$) δ_H 8.36 (1 H, br s, NH-1), 7.17 (1 H, d, *J* 1.8, H-7), 6.73 (1 H, d, *J* 1.9, H-9), 4.16 – 4.04 (1 H, m, H-4), 4.00

(1 H, br s, NH-5), 3.65 (2 H, t, *J* 6.3, H-3^{I}), 2.64 – 2.55 (3 H, m, H_AH_B-3, H-1^{I}), 2.40 (1 H, dd, *J* 13.6, 8.1, H_AH_B-3), 1.89 (1 H, br s, OH), 1.86 – 1.79 (2 H, m, H-2^{I}), 1.35 (3 H, d, *J* 6.3, H-10); ^{13}C NMR (126 MHz, $CDCl_3$) δ_C 173.2 (C-2), 135.9 (C-9a), 134.8 (C-8), 129.5 (C-5a), 129.1 (C-7), 121.7 (C-9), 116.5 (C-6), 61.8 (C-3^{I}), 55.1 (C-4), 41.2 (C-3), 34.0 (C-2^{I}), 30.8 (C-1^{I}), 24.0 (C-10); HRMS *m/z* (ESI$^+$) 313.05466 (313.0546 calculated for $[C_{13}H_{18}{}^{79}BrN_2O_2]^+$), 315.05252 (315.0526 calculated for $[C_{13}H_{18}{}^{81}BrN_2O_2]^+$); LRMS *m/z* (ESI$^+$) 313 ([M(^{79}Br)+H]$^+$, 100%), 315 ([M(^{81}Br)+H]$^+$, 85%); HPLC (Method 1) t_R 5.4 min, purity 98.7%.

(4*R*)-6-Bromo-8-(10-hydroxydecyl)-4-methyl-1,3,4,5-tetrahydro-2*H*-1,5-benzodiazepin-2-one (30)

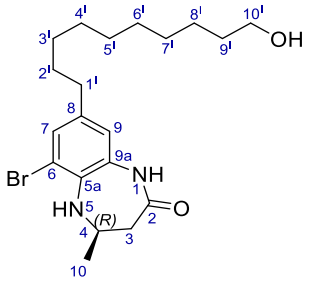

A suspension of (4*R*)-6-bromo-8-(10-hydroxydec-1-yn-1-yl)-4-methyl-1,3,4,5-tetrahydro-2*H*-1,5-benzodiazepin-2-one (**30**) (50 mg, 0.12 mmol, 1.0 eq.) **and** $Rh(PPh_3)_3Cl$ (6 mg, 6 μmol, 0.05 eq.) in toluene (1.6 mL) was purged with H_2. The reaction mixture was stirred at 60 ºC under an atmosphere of H_2 for 3.5 h. The crude brown suspension was directly purified using normal phase column chromatography (isocratic 40% EtOAc in petroleum ether). The yellow oil was further purified by normal phase column chromatography (isocratic Et_2O) to afford (4*R*)-6-bromo-8-(10-hydroxydecyl)-4-methyl-1,3,4,5-tetrahydro-2*H*-1,5-benzodiazepin-2-one (**30**) (32 mg, 77 μmol, 63%) as a colourless solid: R_f 0.24 (3:2 petroleum ether/ EtOAc); $[\alpha]_D^{25}$ = +4.6 (*c* 1.0, $CHCl_3$); mp 56 –59 ºC (Et_2O); $\bar{\upsilon}_{max}$ (thin film)/ cm^{-1} 3363 (O-H, m, br), 3213 (N-H, m, br), 2925 (C-H, m), 2853 (C-H, m), 1672 (C=O, s); ^{1}H NMR (500 MHz, $CDCl_3$) δ_H 7.99 (1 H, br s, NH-1), 7.15 (1 H, d, *J* 1.9, H-7), 6.67 (1 H, d, *J* 1.9, H-9), 4.15 – 4.06 (1 H, m, H-4), 3.97 (1 H, br s, NH-5), 3.63 (2 H, t, *J* 6.6, H-10^{I}), 2.58 (1 H, dd, *J* 13.5, 4.5, H_AH_B-3), 2.47 (2 H, t, *J* 8.0, H-1^{I}), 2.39 (1 H, dd, *J* 13.5, 8.0,

H_AH_B-3), 1.60 – 1.46 (4 H, m, H-2^I, H-9^I), 1.36 (3 H, d, *J* 6.3, H-10), 1.34 – 1.24 (12 H, m, *J* 6.1, H-3^I, H-4^I, H-5^I, H-6^I, H-7^I, H-8^I); ^{13}C NMR (126 MHz, $CDCl_3$) δ_C 173.0 (C-2), 137.1 (C-8), 134.6 (C-9a), 129.6 (C-5a), 129.1 (C-7), 121.5 (C-9), 116.5 (C-6), 63.1 (C-10^I), 55.2 (C-4), 41.1 (C-3), 34.8 (C-1^I), 32.9 (C-9^I), 31.3 (C-2^I), 29.6 (C-4^I/ C-5^I/ C-6^I/ C-7^I), 29.48‡ (C-4^I/ C-5^I/ C-6^I/ C-7^I), 29.48‡ (C-4^I/ C-5^I/ C-6^I/ C-7^I), 29.43 (C-4^I/ C-5^I/ C-6^I/ C-7^I), 29.2 (C-3^I), 25.8 (C-8^I), 24.0 (C-10); HRMS *m/z* (ESI^+) 411.1643 (411.1642 calculated for $[C_{20}H_{32}{}^{79}BrN_2O_2]^+$), 413.1622 (413.1621 calculated for $[C_{20}H_{32}{}^{81}BrN_2O_2]^+$); LRMS *m/z* ($ESI^+$) 411 ($[M(^{79}Br)+H]^+$, 100%), 413 ($[M(^{81}Br)+H]^+$, 91%); HPLC (Method 1) t_R 10.1 min, purity 98.6%. ‡ - Two carbon environments with equivalent ppm, evident by HSQC and HMBC.

(4*R*)-8-(3-Hydroxypropyl)-6-[(1*E*)-5-(7-methoxy-3,4-dihydroquinolin-1(2*H*)-yl)pent-1-en-1-yl]-4-methyl-1,3,4,5-tetrahydro-2*H*-1,5-benzodiazepin-2-one (25)

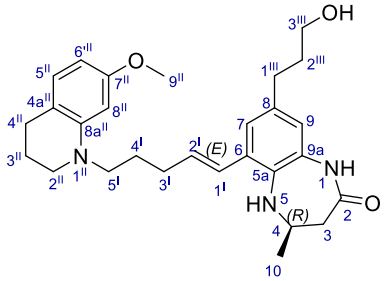

A suspension of (4*R*)-6-bromo-8-(3-hydroxypropyl)-4-methyl-1,3,4,5-tetrahydro-2*H*-1,5-benzodiazepin-2-one (**29**) (25 mg, 0.080 mmol, 1.0 eq.), 7-methoxy-1-[(4*E*)-5-(4,4,5,5-tetramethyl-1,3,2-dioxaborolan-2-yl)pent-4-en-1-yl]-1,2,3,4-tetrahydroquinoline (**13**) (31 g, 0.088 mmol, 1.1 eq.), and K_2CO_3 (28 mg, 0.20 mmol, 2.5 eq.) in 1,4-dioxane (0.55 mL) and H_2O (0.14 mL) was purged with Ar. $Pd(PPh_3)_2Cl_2$ (3 mg, 4 µmol, 0.05 eq.) was added and the reaction mixture was purged with Ar before being stirred at 100 ºC under an atmosphere of Ar for 17 h. The reaction mixture cooled to rt and diluted with EtOAc (20 mL). The organic components were washed with brine (3 × 20 mL), dried ($MgSO_4$), filtered, and concentrated *in vacuo*. The crude brown oil was purified using normal phase column chromatography (isocratic 90% EtOAc in petroleum ether) to afford (4*R*)-8-(3-hydroxypropyl)-6-[(1*E*)-5-(7-methoxy-3,4-dihydroquinolin-1(2*H*)-yl)pent-1-en-1-yl]-4-methyl-1,3,4,5-tetrahydro-2*H*-

1,5-benzodiazepin-2-one (**25**) (17 mg, 0.037 mmol, 46%) as a yellow oil: R_f 0.27 (petroleum ether/ EtOAc 1:9); $[\alpha]_D^{25}$ = +1.8 (*c* 1.0, $CHCl_3$); $\bar{\upsilon}_{max}$ (thin film)/ cm^{-1} 3368 (O-H, w, br), 3224 (N-H, w, br), 2981 (C-H, m), 2972 (C-H, m), 1666 (C=O, s); ^1H NMR (500 MHz, $CDCl_3$) δ_H 7.49 (1 H, br s, NH-5), 6.98 (1 H, d, *J* 2.0, H-7), 6.85 (1 H, dd, *J* 8.0, 1.1, H-5^{II}), 6.65 (1 H, d, *J* 2.0, H-9), 6.46 (1 H, dt, *J* 15.5, 1.6, H-1^{I}), 6.16 – 6.12 (2 H, m, H-6^{II}, H-8^{II}), 6.08 (1 H, dt, *J* 15.5, 6.9, H-2^{I}), 4.16 – 4.04 (1 H, m, H-4), 3.75 (3 H, s, H-9^{II}), 3.67 (2 H, t, *J* 6.4, H-3^{III}), 3.44 (1H, br s, NH-1), 3.31 – 3.24 (4 H, m, H-5^{I}, H-2^{II}), 2.69 (2 H, t, *J* 6.3, H-4^{II}), 2.65 – 2.56 (3 H, m, H_AH_B-3, H-1^{III}), 2.35 (1 H, dd, *J* 13.2, 7.3, H_AH_B-3), 2.32 – 2.26 (2 H, m, H-3^{I}), 1.96 – 1.89 (2 H, m, H-3^{II}), 1.89 – 1.83 (2 H, m, H-2^{III}), 1.79 (2 H, p, *J* 7.5, H-4^{I}), 1.33 (3 H, d, *J* 6.2, H-10); ^{13}C NMR (126 MHz, $CDCl_3$) δ_C 173.0 (C-2), 159.3 (C-7^{II}), 146.2 (C-$8a^{II}$), 135.5 (C-8), 134.8 (C-2^{I}), 133.9 (C-5a), 131.2 (C-9a), 130.5 (C-6), 129.6 (C-5^{II}), 125.7 (C-1^{I}), 124.3 (C-7), 120.9 (C-9), 115.5 (C-$4a^{II}$), 99.4 (C-8^{II}), 97.7 (C-6^{II}), 62.2 (C-3^{III}), 55.7 (C-4), 55.3 (C-9^{II}), 51.1 (C-5^{I}), 49.6 (C-2^{II}), 40.7 (C-3), 34.3 (C-2^{III}), 31.3 (C-1^{III}), 31.2 (C-3^{I}), 27.5 (C-4^{II}), 26.1 (C-4^{I}), 24.1 (C-10), 22.6 (C-3^{II}); HRMS *m/z* (ESI^+) 464.29062 (464.2908 calculated for $[C_{28}H_{38}N_3O_3]^+$); LRMS *m/z* (ESI^+) 464 ($[M+H]^+$, 100%); HPLC (Method 1) t_R 8.0 min, purity 96.8%.

(4*R*)-8-(10-Hydroxydecyl)-6-[(1*E*)-5-(7-methoxy-3,4-dihydroquinolin-1(2*H*)-yl)pent-1-en-1-yl]-4-methyl-1,3,4,5-tetrahydro-2*H*-1,5-benzodiazepin-2-one (26)

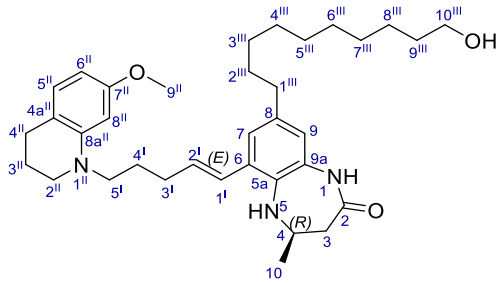

A suspension of (4*R*)-6-bromo-8-(10-hydroxydecyl)-4-methyl-1,3,4,5-tetrahydro-2*H*-1,5-benzodiazepin-2-one (**30**) (25 mg, 0.061 mmol, 1.0 eq.), 7-methoxy-1-[(4*E*)-5-(4,4,5,5-tetramethyl-1,3,2-dioxaborolan-2-yl)pent-4-en-1-yl]-1,2,3,4-tetrahydroquinoline (**13**) (24 mg, 0.067 mmol, 1.1 eq.), and K_2CO_3 (21 mg, 0.15 mmol, 2.5 eq.) in 1,4-dioxane (0.42 mL) and H_2O (0.11 mL) was purged with Ar. $Pd(PPh_3)_2Cl_2$ (2 mg, 3 μmol, 0.05 eq.) was added and the reaction mixture was purged

with Ar before being stirred at 100 ºC under an atmosphere of Ar for 17 h. The reaction mixture was diluted with EtOAc (20 mL), the organic component was washed with brine (3 × 20 mL), dried ($MgSO_4$), filtered, and concentrated *in vacuo*. The crude brown oil was purified using normal phase column chromatography (gradient of 80 – 100% EtOAc in petroleum ether) to afford (4*R*)-8-(10-hydroxydecyl)-6-[(1*E*)-5-(7-methoxy-3,4-dihydroquinolin-1(2*H*)-yl)pent-1-en-1-yl]-4-methyl-1,3,4,5-tetrahydro-2*H*-1,5-benzodiazepin-2-one (**26**) (16 mg, 0.029 mmol, 47%) as a yellow oil: R_f 0.21 (7:3 EtOAc/ petroleum ether)**;** $[\alpha]_D^{25}$ = +4.2 (*c* 0.7, $CHCl_3$); $\bar{\upsilon}_{max}$ (thin film)/ cm^{-1} 3363 (O-H, w, br), 3206 (N-H, w, br), 2926 (C-H, m), 2853 (C-H, m), 1668 (C=O); ^{1}H NMR (500 MHz, $CDCl_3$) δ_H 7.31 (1 H, br s, NH-5), 6.95 (1 H, d, *J* 2.0, H-7), 6.85 (1 H, d, *J* 8.0, H-5^{II}), 6.61 (1 H, d, *J* 2.0, H-9), 6.46 (1 H, d, *J* 15.6, H-1^{I}), 6.17 – 6.12 (2 H, m, H-6^{II}, H-8^{II}), 6.08 (1 H, dt, *J* 15.6, 6.9, H-2^{I}), 4.14 – 4.01 (1 H, m, H-4), 3.75 (3 H, s, H-9^{II}), 3.63 (2 H, t, *J* 6.6, H-10^{III}), 3.42 (1 H, br s, NH-1), 3.33 – 3.21 (4 H, m, H-5^{I}, H-2^{II}), 2.69 (2 H, t, *J* 6.4, H-4^{II}), 2.59 (1 H, dd, *J* 13.2, 5.0, H_AH_B-3), 2.53 – 2.47 (2 H, t, *J* 7.8, H-1^{III}), 2.35 (1 H, dd, *J* 13.2, 7.3, H_AH_B-3), 2.29 (2 H, q, *J* 7.1, H-3^{I}), 1.93 (2 H, p, *J* 6.2, H-3^{II}), 1.79 (2 H, p, *J* 7.5, H-4^{I}), 1.60 – 1.51 (4 H, m, H-2^{III}, H-9^{III}), 1.33 (3 H, d, *J* 6.3, H-10), 1.32 – 1.26 (12 H, m, H-3^{III}, H-4^{III}, H-5^{III}, H-6^{III}, H-7^{III}, H-8^{III}); ^{13}C NMR (126 MHz, $CDCl_3$) δ_C 173.0 (C-2), 159.4 (C-7^{II}), 146.2 (C-8a^{II}), 136.7 (C-8), 134.6 (C-2^{I}), 133.7 (C-5a), 131.1 (C-6), 130.4 (C-9a), 129.7 (C-5^{II}), 125.8 (C-1^{I}), 124.3 (C-7), 120.8 (C-9), 115.5 (C-4a^{II}), 99.5 (C-8^{II}), 97.7 (C-6^{II}), 63.2 (C-10^{III}), 55.8 (C-4), 55.3 (C-5^{I}), 51.2 (C-9^{II}), 49.6 (C-2^{II}), 40.7 (C-3), 35.3 (C-1^{III}), 32.9 (C-9^{III}), 31.6 (C-2^{III}), 31.2 (C-3^{I}), 29.6 (C-3^{III}/ C-4^{III}/ C-5^{III}/ C-6^{III}/ C-7^{III}), 29.54 (C-3^{III}/ C-4^{III}/ C-5^{III}/ C-6^{III}/ C-7^{III}), 29.51 (C-3^{III}/ C-4^{III}/ C-5^{III}/ C-6^{III}/ C-7^{III}), 29.50 (C-3^{III}/ C-4^{III}/ C-5^{III}/ C-6^{III}/ C-7^{III}), 29.3 (C-3^{III}/ C-4^{III}/ C-5^{III}/ C-6^{III}/ C-7^{III}), 27.5 (C-4^{II}), 26.1 (C-4^{I}), 25.9 (C-8^{III}), 24.0 (C-10), 22.6 (C-3^{II}); HRMS *m/z* (ESI$^+$) 562.39991 (562.4003 calculated for $[C_{35}H_{52}N_3O_3]^+$); LRMS *m/z* (ESI$^+$) 562 ($[M+H]^+$, 100%); HPLC (Method 1) t_R 12.4 min, purity 97.3%.

2-(2,6-Dioxopiperidin-3-yl)-4-fluoro-2,3-dihydro-1*H*-isoindole-1,3-dione (40)

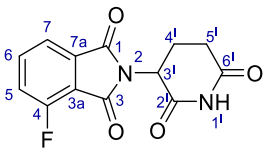

3-Fluorophthalic anhydride (2.00 g, 12.0 mmol, 1.0 eq.), 3-aminopiperidine-2,6-dione hydrochloride (1.98 g, 12.0 mmol, 1.0 eq.), and sodium acetate (1.27 g, 18.1 mmol, 1.5 eq.) in glacial acetic acid (50 mL) were stirred at reflux for 4 h. The reaction mixture was cooled to rt and concentrated *in vacuo*. H_2O (50 mL) was added to the resulting purple solid and the aqueous component was extracted with EtOAc (3 × 50 mL). The combined organic components were washed with sat. aq. $NaHCO_3$ (150 mL), dried ($MgSO_4$), filtered, and concentrated *in vacuo*. The lilac solid was purified using normal phase column chromatography (gradient of 50 – 100% EtOAc in petroleum ether) to afford 2-(2,6-dioxopiperidin-3-yl)-4-fluoro-2,3-dihydro-1*H*-isoindole-1,3-dione (**40**) (2.81 g, 10.2 mmol, 85%) as a colourless solid: R_f 0.39 (1:2 petroleum ether/ EtOAc); mp 235 – 239 ºC (EtOAc); ^{1}H NMR (400 MHz, DMSO) δ_H 11.15 (1 H, s, NH-1^I), 7.98 – 7.91 (1 H, m, H-6), 7.79 (1 H, d, *J* 7.3, H-7), 7.73 (1 H, t, *J* 8.9, H-5), 5.16 (1 H, dd, *J* 12.9, 5.4, H-3^I), 2.89 (1 H, ddd, *J* 17.2, 13.9, 5.4, H_AH_B-5^I), 2.61 (1 H, ddd, *J* 17.2, 4.5, 2.4, H_AH_B-5^I), 2.57 – 2.45 (1 H, m, H_AH_B-4^I), 2.10 – 2.02 (1 H, m, H_AH_B-4^I); ^{19}F NMR (376 MHz, DMSO) δ_F −114.65 (1 F, dd, *J* 9.7, 4.8, F-4); LRMS *m/z* (ESI$^+$) 299 ([M+Na]$^+$, 100%). These data are in good accordance with the literature.[213]

2-(2,6-Dioxopiperidin-3-yl)-4-((5-hydroxypentyl)amino)-1*H*-isoindole-1,3(2*H*)-dione (41)

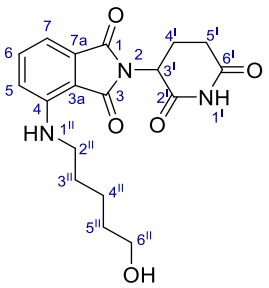

A suspension of 2-(2,6-dioxopiperidin-3-yl)-4-fluoro-2,3-dihydro-1*H*-isoindole-1,3-dione (**40**) (200 mg, 0.724 mmol, 1.0 eq.), 5-amino-1-pentanol (82 mg, 0.79 mmol, 1.1 eq.), and DIPEA (251 µL, 1.44 mmol, 2.0 eq.) in DMF (7.2 mL) was stirred at 90 ºC for 2 h. The reaction mixture was cooled to rt and brine (40 mL) was added. The aqueous component was extracted with EtOAc (3 × 40 mL), and the combined organic components were washed with brine (40 mL), dried (Na_2SO_4), filtered, and concentrated *in vacuo*. The crude yellow oil was purified using normal phase column chromatography (gradient of 5 – 100% EtOAc in petroleum ether) to afford 2-(2,6-dioxopiperidin-3-yl)-4-((5-hydroxypentyl)amino)-1*H*-isoindole-1,3(2*H*)-dione (**41**) (84 mg, 0.23 mmol, 32%) as a yellow amorphous solid: R_f 0.23 (1:4 petroleum ether/ EtOAc); $\bar{\upsilon}_{max}$ (thin film)/ cm^{-1} 3199 (C-H, w), 3092 (C-H, w), 1699 (C=O, s); ^{1}H NMR (500 MHz, $CDCl_3$) δ_H 8.34 (1 H, br s, NH-1^I), 7.48 (1 H, dd, *J* 8.6, 7.1, H-6), 7.08 (1 H, d, *J* 7.1, H-5), 6.87 (1 H, d, *J* 8.6, H-7), 6.24 (1 H, br t, *J* 5.7, NH-1^{II}), 4.91 (1 H, dd, *J* 12.3, 5.4, H-3^I), 3.66 (2 H, t, *J* 6.4, H-6^{II}), 3.31 – 3.25 (2 H, m, H-2^{II}), 2.93 – 2.67 (3 H, m, H-5^I, H_AH_B-4^I), 2.18 – 2.08 (1 H, m, H_AH_B-4^I), 1.74 – 1.66 (2 H, m, H-3^{II}), 1.67 – 1.53 (2 H, m, *J* 8.6, 6.0, H-5^{II}), 1.54 – 1.44 (2 H, m, H-4^{II}); ^{13}C NMR (126 MHz, $CDCl_3$) δ_C 171.3 (C-6^I), 169.7 (C-1), 168.6 (C-2^I), 167.8 (C-3), 147.1 (C-4), 136.3 (C-6), 132.6 (C-7a), 116.8 (C-7), 111.6 (C-5), 110.0 (C-3a), 62.7 (C-6^{II}), 49.0 (C-3^I), 42.7 (C-2^{II}), 32.4 (C-5^I), 31.5 (C-5^{II}), 29.1 (C-3^{II}), 23.3 (C-4^{II}), 22.9 (C-4^I); HRMS *m/z* (ESI$^+$) 360.1549 (360.1554 calculated for $[C_{18}H_{21}N_3O_{5F}]^+$); LRMS *m/z* (ESI$^+$) 360 ($[M+H]^+$, 100%); HPLC (Method 3) t_R 8.2 min, purity 99.9%.

4-((5-Hydroxypentyl)amino)-2-(1-(3-((2*R*)-9-((1*E*)-5-(7-methoxy-3,4-dihydroquinolin-1(2*H*)-yl)pent-1-en-1-yl)-2-methyl-4-oxo-2,3,4,5-tetrahydro-1*H*-1,5-benzodiazepin-7-yl)propyl)-2,6-dioxopiperidin-3-yl)-1*H*-isoindole-1,3(2*H*)-dione (42)

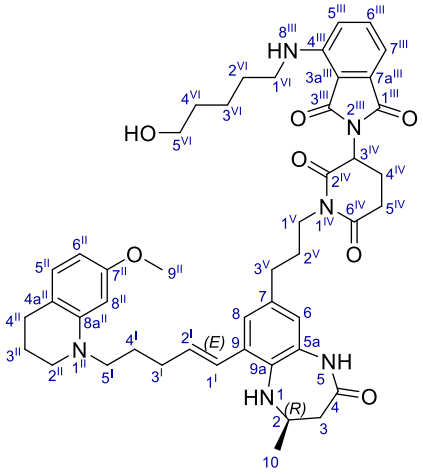

Step I:

Methanesulfonyl chloride (5 µL, 0.07 mmol, 1.5 eq.) was added to a solution of (4*R*)-8-(3-hydroxypropyl)-6-[(1*E*)-5-(7-methoxy-3,4-dihydroquinolin-1(2*H*)-yl)pent-1-en-1-yl]-4-methyl-1,3,4,5-tetrahydro-2*H*-1,5-benzodiazepin-2-one (**25**) (20 mg, 0.043 mmol, 1.0 eq.) and DIPEA (13 µL, 0.073 mmol, 1.7 eq.) in anhydrous CH_2Cl_2 (100 µL) at 0 ºC. The reaction mixture was stirred at 0 ºC for 3 h before being quenched by the addition of H_2O (250 µL) at 0 ºC, warmed to rt, and further H_2O (2 mL) was added. The aqueous component was extracted with CH_2Cl_2 (3 × 2 mL), the combined organic components were dried ($MgSO_4$), filtered, and concentrated *in vacuo* to afford the mesylate intermediate (**39**) as a brown oil.

Step II:

Sodium hydride 60% *w/w* in mineral oil (8 mg, 0.2 mmol, 4.7 eq.) was added portion-wise to a solution of 2-(2,6-dioxopiperidin-3-yl)-4-((5-hydroxypentyl)amino)-1*H*-isoindole-1,3(2*H*)-dione (**41**) (31 mg, 0.087 mmol, 2.0 eq.) in anhydrous DMF (200 µL) at 0 ºC. The reaction mixture was stirred at 0 ºC for 30 min before the addition of the mesylate intermediate (**39**) in anhydrous DMF (200 µL). The reaction mixture was stirred at 0 ºC for 4.5 h, then at rt for 16 h. The reaction mixture was cooled to 0 ºC, quenched with H_2O (1 mL), and allowed to warm to rt. Brine (1 mL) was added and the aqueous

component was extracted with EtOAc (3 × 2 mL). The combined organic components were dried ($MgSO_4$), filtered, and concentrated *in vacuo*. The crude yellow oil was purified using normal phase column chromatography (gradient of 0 – 10% acetone in EtOAc) to afford 4-((5-hydroxypentyl)amino)-2-(1-(3-((2*R*)-9-((1*E*)-5-(7-methoxy-3,4-dihydroquinolin-1(2*H*)-yl)pent-1-en-1-yl)-2-methyl-4-oxo-2,3,4,5-tetrahydro-1*H*-1,5-benzodiazepin-7-yl)propyl)-2,6-dioxopiperidin-3-yl)-1*H*-isoindole-1,3(2*H*)-dione (**42**) (3 mg, 4 μmol, 9%) as a yellow amorphous solid: R_f 0.16 (EtOAc); $[\alpha]_D^{25}$ = +0.9 (*c* 0.7, $CHCl_3$); $\bar{\upsilon}_{max}$ (thin film)/ cm^{-1} 3661 (O-H, w), 2981 (C-H, s), 2888 (C-H, m), 1677 (C=O, w); ^{1}H NMR (500 MHz, CDC_3) δ_H 7.51 (1 H, br d, *J* 9.8, NH-5), 7.48 (1 H, dd, *J* 8.6, 7.1, H-6^{III}), 7.08 (1 H, d, *J* 7.1, H-5^{III}), 6.97 (1 H, d, *J* 2.3, H-8), 6.87 (1 H, d, *J* 8.6, H-7^{III}), 6.85 (1 H, d, *J* 8.0, H-5^{II}), 6.66 (1 H, t, *J* 2.3, H-6), 6.45 (1 H, d, *J* 15.5, H-1^{I}), 6.28 (1 H, q, *J* 5.3, NH-8^{III}), 6.17 – 6.08 (3 H, m, H-2^{I}, H-6^{II}, H-8^{II}), 4.71 (1 H, td, *J* 12.6, 5.2, H-3^{IV}), 4.12 – 4.04 (1 H, m, H-2), 3.97 – 3.88 (1 H, m, H_AH_B-1^{V}), 3.87 – 3.79 (1 H, m, H_AH_B-1^{V}), 3.75 (3 H, s, H-9^{II}), 3.67 (2 H, t, *J* 6.3, H-5^{VI}), 3.40 (1 H, br s, NH-1), 3.33 – 3.25 (6 H, m, H-5^{I}, H-2^{II}, H-1^{VI}), 2.84 – 2.78 (1 H, m, H_AH_B-5^{IV}), 2.69 (2 H, t, *J* 6.3, H-4^{II}), 2.66 – 2.43 (5 H, m, H_AH_B-3, H_AH_B-4^{IV}, H_AH_B-5^{IV}, H-3^{V}), 2.34 (1 H, dd, *J* 13.1, 7.2, H_AH_B-3), 2.28 (2 H, q, *J* 6.7, H-3^{I}), 2.02 – 1.83 (5 H, m, H_AH_B-4^{IV}, H-3^{II}, H-2^{V}), 1.79 (2 H, p, *J* 7.5, H-4^{I}), 1.75 – 1.68 (2 H, m, H-2^{VI}), 1.67 – 1.57 (2 H, m, H-4^{VI}), 1.57 – 1.49 (2 H, m, H-3^{VI}), 1.32 (3 H, dd, *J* 6.1, 6.1, H-10); ^{13}C NMR (126 MHz, $CDCl_3$) δ_C 172.97 (C-4 diastereomer A), 172.95 (C-4 diastereomer B), 171.2 (C-6^{IV}), 169.95 (C-1^{III} diastereomer A), 169.94 (C-1^{III} diastereomer B), 169.04 (C-2^{IV} diastereomer A), 169.01 (C-2^{IV} diastereomer B), 168.01 (C-3^{III} diastereomer A), 168.00 (C-3^{III} diastereomer B), 159.4 (C-7^{II}), 147.1 (C-4^{III}), 146.3 (C-8a^{II}), 136.3 (C-6^{III}), 135.12 (C-2^{I} diastereomer A), 135.11 (C-2^{I} diastereomer B), 134.88 (C-7 diastereomer A), 134.85 (C-7 diastereomer B), 134.06 (C-9a diastereomer A), 133.97 (C-9a diastereomer B), 132.7 (C-5a), 131.11 (C-9 diastereomer A), 131.07 (C-9 diastereomer B), 130.64 (C-7^{III} diastereomer A), 130.58 (C-7^{III} diastereomer B), 129.6 (C-5^{II}), 125.60 (C-1^{I} diastereomer A), 125.58 (C-1^{I} diastereomer B), 124.32 (C-8 diastereomer A), 124.27 (C-8 diastereomer B), 120.8 (C-6), 116.8 (C-7a^{III}), 115.4 (C-4a^{II}), 111.5 (C-5^{III}), 110.0 (C-3a^{III}), 99.4 (C-6^{II}), 97.7 (C-8^{II}), 62.7 (C-5^{VI}), 55.97 (C-2 diastereomer A), 55.94 (C-2 diastereomer B), 55.3 (C-9^{II}), 51.1 (C-5^{I}), 49.9 (C-3^{IV}), 49.6 (C-2^{II}), 42.68 (C-1^{VI} diastereomer A), 42.67 (C-1^{VI} diastereomer B), 40.62 (C-3/ C-1^{V}), 40.60 (C-3/ C-1^{V}), 32.46 (C-3^{V}/ 4^{VI}), 32.43 (C-3^{V}/ 4^{VI}), 32.2 (C-5^{IV}), 31.2 (C-3^{I}), 29.07 (C-2^{VI}

diastereomer A), 29.06 (C-2^{VI} diastereomer B), 28.4 (C-2^{V} diastereomer A), 28.3 (C-2^{V} diastereomer B), 27.6 (C-4^{II}), 26.1 (C-4^{I}), 24.1 (C-10 diastereomer A), 24.0 (C-10 diastereomer B), 23.40 (C-3^{VI}), 22.6 (C-3^{II}), 22.02 (C-4^{IV} diastereomer A), 22.01 (C-4^{IV} diastereomer B); LRMS *m/z* (ESI^+) 805 ($[M+H]^+$, 100%); HPLC (Method 3) t_R 10.2 min, purity 96.8%.

tert-Butyl 3-(4-fluoro-1,3-dioxo-1,3-dihydro-2*H*-isoindol-2-yl)-2,6-dioxopiperidine-1-carboxylate (43)

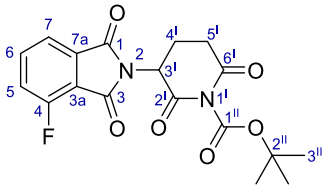

Di-*tert*-butyl dicarbonate (711 mg, 3.26 mmol, 1.5 eq.) was added portion-wise to a solution of 2-(2,6-dioxopiperidin-3-yl)-4-fluoro-2,3-dihydro-1*H*-isoindole-1,3-dione (**X**) (600 mg, 2.17 mmol, 1.0 eq.), and DMAP (27 mg, 0.22 mmol, 0.1 eq.) in 1,4-dioxane (22 mL) at 0 ºC and the reaction mixture was stirred at rt for 1.5 h. H_2O (2 mL) was added and the reaction mixture was concentrated *in vacuo*. H_2O (50 mL) was added to the residue and the aqueous component was extracted with EtOAc (3 × 50 mL). The combined organic components were dried ($MgSO_4$), filtered, and concentrated *in vacuo*. The crude orange oil was purified using normal phase column chromatography (gradient of 10 – 80% EtOAc in petroleum ether) to afford *tert*-butyl 3-(4-fluoro-1,3-dioxo-1,3-dihydro-2*H*-isoindol-2-yl)-2,6-dioxopiperidine-1-carboxylate (**X**) (735 mg, 1.95 mmol, 00%) as a colourless solid: R_f 0.29 (3:2 petroleum ether/ EtOAc); mp 232 – 238 ºC (EtOAc); ^{1}H NMR (500 MHz, DMSO) δ_H 8.00 – 7.94 (1 H, m, H-6), 7.81 (1 H, d, *J* 7.3, H-7), 7.76 (1 H, t, *J* 8.8, H-5), 5.45 (1 H, dd, *J* 13.2, 5.5, H-3^I), 3.10 (1 H, ddd, *J* 17.5, 13.8, 5.5, H_AH_B-5^I), 2.81 (1 H, ddd, *J* 17.5, 4.5, 2.4, H_AH_B-5^I), 2.59 (1 H, ddd, *J* 13.2, 4.5, H_AH_B-4^I), 2.12 (1 H, ddd, *J* 13.2, 5.5, 2.4, H_AH_B-4^I), 1.49 (9 H, s, H-3^{II}); ^{13}C-NMR (126 MHz, CDC_3) δ_C 170.0 (C-6^I), 167.4 (C-2^I), 165.9 (d, *J* 2.8, C-1), 163.8 (C-3), 156.8 (d, *J* 262.4, C-4), 148.3 (C-1^{II}), 138.2 (d, *J* 7.8, C-6), 133.4 (C-7a), 123.1 (d, *J* 19.5 C-5), 120.2 (d, *J* 3.3, C-7), 117.0 (d, *J* 12.5, C-3a), 86.1 (C-2^{II}), 48.8 (C-3^I), 30.7 (C-5^I), 27.0 (C-3^{II}), 21.0 (C-4^I); ^{19}F-NMR (376 MHz,

DMSO) δ_F -114.51 (dd, *J* 9.8, 5.0); LRMS *m/z* (ESI$^+$) 399 ([M+Na]$^+$, 100%); HRMS *m/z* (ESI$^+$) 399.0969 (399.0963 calculated for [$C_{18}H_{17}FN_2O_6Na$]$^+$).

tert-Butyl (2-hydroxyethyl)carbamate (45)

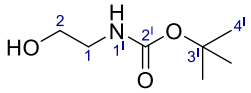

Ethanolamine (604 µL, 10.0 mmol, 1.0 eq.) was added dropwise to a solution of di-*tert*-butyl dicarbonate (2.18 g, 10.0 mmol, 1.0 eq.) in CH_2Cl_2 (30 mL) at 0 ºC. The colourless solution was stirred at rt for 3 h before being concentrated *in vacuo* and directly purified using normal phase column chromatography (isocratic 50% EtOAc in petroleum ether) to afford *tert*-butyl (2-hydroxyethyl)carbamate (**45**) (1.60 g, 9.93 mmol, 99%) as a colourless oil: R_f 0.35 (1:1 petroleum ether/ EtOAc); ^{1}H NMR (400 MHz, $CDCl_3$) 4.97 (1 H, br s, NH-1^I), 3.69 (2 H, q, *J* 5.4, H-2), 3.28 (2 H, q, *J* 5.4, H-1), 2.51 (1 H, br s, OH), 1.44 (9 H, s, H-4^I); LRMS *m/z* (ESI$^+$) 184 ([M+Na]$^+$, 100%). These data are in good accordance with the literature.[214]

tert-Butyl [2-(2-hydroxyethoxy)ethyl]carbamate (46)

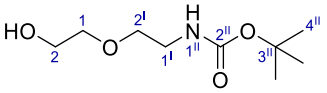

2-(2-Aminoethoxy)ethanol (1.00 mL, 10.0 mmol, 1.0 eq.) was added dropwise to a solution of di-*tert*-butyl dicarbonate (2.18 g, 10.0 mmol, 1.0 eq.) in CH_2Cl_2 (30 mL) at 0 ºC. The colourless solution was stirred at rt for 18 h before being concentrated *in vacuo* and directly purified using normal phase column chromatography (isocratic 50% EtOAc in petroleum ether) to afford *tert*-butyl [2-(2-hydroxyethoxy)ethyl]carbamate (**46**) (1.63 g, 7.94 mmol, 79%) as a colourless oil: R_f 0.50 (95:5 EtOAc/ MeOH); ^{1}H NMR (400 MHz, $CDCl_3$) δ_H 4.90 (1 H, br s, NH-1^{II}), 3.74 (2 H, t, *J* 4.5, H-2), 3.64 – 3.49

(4 H, m, H-1, H-2^{I}), 3.33 (2 H, q, *J* 5.4, H-1^{I}), 2.11 (1 H, br s, OH), 1.45 (9 H, s, H-4^{II}); LRMS *m/z* (ESI^{+}) 228 ([M+Na]$^{+}$, 100%). These data are in good accordance with the literature.[215]

***tert*-Butyl {2-[2-(2-hydroxyethoxy)ethoxy]ethyl}carbamate (47)**

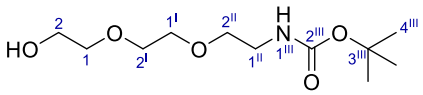

2-[2-(2-Aminoethoxy)ethanoxyl] ethanol (1.38 mL, 10.0 mmol, 1.0 eq.) was added dropwise to a solution of di-*tert*-butyl dicarbonate (2.18 g, 10.0 mmol, 1.0 eq.) in CH_2Cl_2 (30 mL) at 0 ºC. The colourless solution was stirred at rt for 18 h before being concentrated *in vacuo* and directly purified using column chromatography (isocratic 60% EtOAc in petroleum ether) to afford *tert*-butyl {2-[2-(2-hydroxyethoxy)ethoxy]ethyl}carbamate (**47**) (2.22 g, 8.92 mmol, 89%) as a yellow oil: R_f 0.18 (1:1 *n*-hexane/ EtOAc); ^{1}H NMR (400 MHz, $CDCl_3$) δ_H 5.08 (1 H, br s, NH-1^{III}), 3.79 – 3.71 (2 H, m, H-2), 3.69 – 3.59 (6 H, m, H-1, H-1^{I}, H-2^{I}), 3.56 (2 H, t, *J* 5.4, H-2^{II}), 3.31 (2 H, t, *J* 5.4, H-1^{II}), 2.39 (1 H, br s, OH), 1.44 (9 H, s, H-4^{III}); LRMS *m/z* (ESI^{+}) 272 ([M+Na]$^{+}$, 100%). These data are in good accordance with the literature.[16,216]

***tert*-Butyl (2-{2-[2-(2-hydroxyethoxy)ethoxy]ethoxy}ethyl)carbamate (48)**

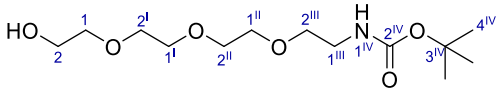

2-{2-[2-(2-Aminoethoxy)ethoxy]ethoxy}ethoxy)ethanol (1.93 g, 10.0 mmol, 1.0 eq.) was added dropwise to a solution of di-*tert*-butyl dicarbonate (2.18 g, 10.0 mmol, 1.0 eq.) in CH_2Cl_2 (30 mL) at 0 ºC. The colourless solution was stirred at rt for 27 h before being concentrated *in vacuo* and directly purified using column chromatography (isocratic 50% EtOAc in petroleum ether) to afford *tert*-butyl (2-{2-[2-(2-hydroxyethoxy)ethoxy]ethoxy}ethyl)carbamate (**48**) (2.91 g, 9.92 mmol, 99%) as a colourless oil which was used with used without purification: R_f 0.23 ($CHCl_3$/ MeOH 19:1);

^{1}H NMR (400 MHz, $CDCl_3$) δ_H 5.57 (1 H, br s, NH-1^{IV}), 3.76 – 3.68 (4 H, m, H-1, H-2), 3.68 – 3.59 (8 H, m, H-1^{I}, H-2^{I}, H-1^{II}, H-2^{II}), 3.55 – 3.51 (2 H, m, 4.5, H-2^{III}), 3.31 (2 H, t, *J* 5.0, H-1^{III}), 2.30 (1 H, br s, OH), 1.44 (9 H, s, H-9^{IV}); LRMS *m/z* (ESI$^+$) 194 ([M+2H−$C_5H_9O_2$]$^+$, 100%). These data are in good accordance with the literature.[217]

tert-Butyl {2-[(prop-2-yn-1-yl)oxy]ethyl}carbamate (49)

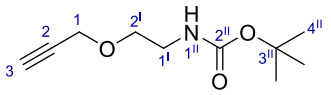

Sodium hydride 60% *w/w* in mineral oil (264 mg, 6.60 mmol, 1.1 eq.) was added portion-wise to a solution of *tert*-butyl (2-hydroxyethyl)carbamate (**45**) (967 mg, 6.00 mmol, 1.0 eq.) in anhydrous THF (60 mL) at 0 ºC and the resulting suspension was stirred at 0 ºC for 10 min. Propargyl bromide 80% *w/w* in toluene (735 µL, 6.60 mmol, 1.1 eq.) and TBAI (222 mg, 0.60 mmol, 0.1 eq.) were added at 0 ºC and the resulting yellow suspension was stirred at 50 ºC for 5 h. The reaction mixture was cooled to 0 ºC and quenched with sat. aq. NH_4Cl (6 mL) and concentrated *in vacuo*. The sat. aq. NH_4Cl (50 mL) was added to the residue and the aqueous component was extracted with EtOAc (3 × 50 mL). The combined organic components were washed with brine (150 mL), dried (Na_2SO_4), filtered, and concentrated *in vacuo*. The crude yellow oil was purified using normal phase column chromatography (gradient of 2 – 40% EtOAc in petroleum ether) to afford *tert*-butyl {2-[(prop-2-yn-1-yl)oxy]ethyl}carbamate (**49**) (648 mg, 3.25 mmol, 54%) as a pale yellow oil: R_f 0.51 (2:1 *n*-hexane/ EtOAc); ^{1}H NMR (400 MHz, $CDCl_3$) δ_H 4.88 (1 H, br s, NH-1^{II}), 4.15 (2 H, d, *J* 2.4, H-1), 3.58 (2 H, t, *J* 5.3, H-2^{I}), 3.34 (2 H, q, *J* 5.3, H-1^{I}), 2.44 (1 H, t, *J* 2.4, H-3), 1.44 (9 H, s, H-4^{II}); LRMS *m/z* (ESI$^+$) 222 ([M+Na]$^+$, 100%). These data are in good accordance with the literature.[218]

***tert*-Butyl (2-{2-[(prop-2-yn-1-yl)oxy]ethoxy}ethyl)carbamate (50)**

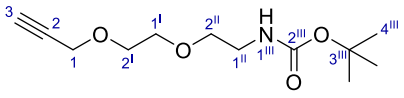

Sodium hydride 60% *w/w* in mineral oil (264 mg, 6.60 mmol, 1.1 eq.) was added portion-wise to a solution of *tert*-butyl {2-[2-(2-hydroxyethoxy)ethoxy]ethyl}carbamate (**46**) (1.20 g, 6.00 mmol, 1.0 eq.) in anhydrous THF (60 mL) at 0 ºC and the resulting suspension was stirred at 0 ºC for 10 min. Propargyl bromide 80% *w/w* in toluene (735 µL, 6.60 mmol, 1.1 eq.) and TBAI (222 mg, 0.600 mmol, 0.1 eq.) were added at 0 ºC, and the yellow suspension was stirred at rt for 24 h. The reaction mixture was cooled to 0 ºC, quenched with sat. aq. NH_4Cl (6 mL), then concentrated *in vacuo*. The sat. aq. NH_4Cl (50 mL) was added to the residue and the aqueous component was extracted with EtOAc (3 × 50 mL). The combined organic components were washed with brine (150 mL), dried (Na_2SO_4), filtered, and concentrated *in vacuo*. The crude yellow oil was purified using column chromatography (isocratic 30% EtOAc in petroleum ether) to afford *tert*-butyl (2-{2-[(prop-2-yn-1-yl)oxy]ethoxy}ethyl)carbamate (**50**) (804 mg, 3.30 mmol, 54%) as a yellow oil: R_f 0.55 (19:1 CH_3Cl/ MeOH); ^{1}H NMR (400 MHz, $CDCl_3$) δ_H 4.96 (1 H, br s, NH-1^{III}), 4.21 (2 H, d, *J* 2.4, H-1), 3.73 – 3.67 (2 H, m, H-2^{I}), 3.66 – 3.61 (2 H, m, H-1^{I}), 3.54 (2 H, t, *J* 5.3, H-2^{II}), 3.32 (2 H, q, *J* 5.3, H-1^{II}), 2.44 (1 H, t, *J* 2.4, H-3), 1.44 (9 H, s, H-4^{III}) 3.75 – 3.70 (2 H, m, H-2^{II}), 3.69 – 3.64 (2 H, m, H-1^{II}); LRMS *m/z* (ESI$^+$) 266 ([M+Na]$^+$, 100%). These data are in good accordance with the literature.[219]

***tert*-Butyl [2-(2-{2-[(prop-2-yn-1-yl)oxy]ethoxy}ethoxy)ethyl]carbamate (51)**

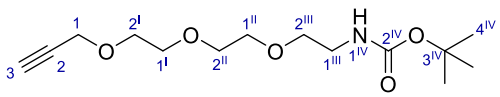

Sodium hydride 60% *w/w* in mineral oil (264 mg, 6.60 mmol, 1.1 eq.) was added portion-wise to a solution of *tert*-butyl {2-[2-(2-hydroxyethoxy)ethoxy]ethyl}carbamate (**47**) (1.50 g, 6.00 mmol, 1.0 eq.) in anhydrous THF (60 mL) at 0 ºC and the resulting suspension was stirred at 0 ºC for 10 min.

Propargyl bromide 80% *w/w* in toluene (735 µL, 6.60 mmol, 1.1 eq.) and TBAI (222 mg, 0.600 mmol, 0.1 eq.) were added at 0 ºC, and the yellow suspension was stirred at rt for 24 h. The reaction mixture was cooled to 0 ºC, quenched with sat. aq. NH_4Cl (6 mL), then concentrated *in vacuo*. sat. aq. NH_4Cl (50 mL) was added to the residue and the aqueous component was extracted with EtOAc (3 × 50 mL). The combined organic components were washed with brine (150 mL), dried (Na_2SO_4), filtered, and concentrated *in vacuo*. The crude yellow oil was purified using normal phase column chromatography (isocratic 30% EtOAc in petroleum ether) to afford *tert*-butyl [2-(2-{2-[(prop-2-yn-1-yl)oxy]ethoxy}ethoxy)ethyl]carbamate (**51**) (730 mg, 2.54 mmol, 42%) as a yellow oil: R_f 0.56 (CH_3Cl/ MeOH 19:1); ^{1}H NMR (400 MHz, $CDCl_3$) δ_H (500 MHz, $CDCl_3$) 5.03 (1 H, br s, NH-1^{IV}), 4.21 (2 H, d, *J* 2.4, H-1), 3.73 – 3.70 (2 H, m, H-2^{I}), 3.70 – 3.67 (2 H, m, H-1^{I}), 3.66 – 3.63 (2 H, m, H-1^{II}/ H-2^{II}), 3.63 – 3.60 (2 H, m, H-1^{II}/ H-2^{II}), 3.54 (2 H, t, *J* 5.2, H-2^{III}), 3.34 – 3.28 (2 H, m, H-1^{III}), 2.43 (1 H, t, *J* 2.4, H-3), 1.44 (9 H, s, H-4^{IV}); LRMS *m/z* 188 (ESI$^+$) ([M+H−$C_5H_9O_2$]$^+$, 100%). These data are in good accordance with the literature.[16]

***tert*-Butyl 3,6,9,12-tetraoxapentadec-14-yn-1-ylcarbamate (52)**

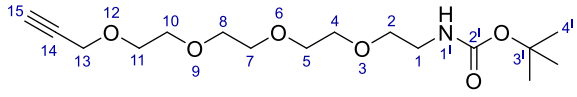

Sodium hydride 60% *w/w* in mineral oil (264 mg, 6.60 mmol, 1.1 eq.) was added portion-wise to a solution of *tert*-butyl (2-{2-[2-(2-hydroxyethoxy)ethoxy]ethoxy}ethyl)carbamate (**48**) (1.76 g, 6.00 mmol, 1.0 eq.) in anhydrous THF (60 mL) at 0 ºC and the resulting suspension was stirred at 0 ºC for 10 min. Propargyl bromide 80% *w/w* in toluene (735 µL, 6.6 mmol, 1.1 eq.) and TBAI (222 mg, 0.600 mmol, 0.1 eq.) were added at 0 ºC, and the yellow suspension was stirred at 50 ºC for 5 h. The reaction mixture was cooled to 0 ºC, quenched with sat. aq. NH_4Cl (6 mL), then concentrated *in vacuo*. sat. aq. NH_4Cl (50 mL) was added to the residue and the aqueous component was extracted with EtOAc (2 × 50 mL). The combined organic components were washed with brine (150 mL), dried (Na_2SO_4), filtered, and concentrated *in vacuo*. The crude yellow oil was purified using normal phase column

chromatography (gradient of 10 – 80% EtOAc in petroleum ether) to afford *tert*-butyl 3,6,9,12-tetraoxapentadec-14-yn-1-ylcarbamate (**52**) (1.26 g, 3.81 mmol, 63%) as a yellow oil: R_f 0.52 (19:1 CH_3Cl/ MeOH); ^{1}H NMR (400 MHz, $CDCl_3$) δ_H 4.21 (2 H, d, *J* 2.4, H-13), 3.72 – 3.70 (2 H, m, H-11), 3.69 – 3.68 (2 H, m, H-10), 3.67 – 3.66 (4 H, m, H-7, H-8), 3.66 – 3.63 (2 H, m, H-4/ H-5), 3.63 – 3.60 (2 H, m, H-4/ H-5), 3.54 (2 H, t, *J* 5.1, H-2), 3.35 – 3.28 (2 H, m, H-1), 2.43 (1 H, t, *J* 2.4, H-15), 1.44 (9 H, s, H-4^{I}); LRMS *m/z* (ESI$^+$) 354 ([M+Na]$^+$, 100%). These data are in good accordance with the literature.[220]

tert-Butyl [2-({3-[(2*R*)-9-bromo-2-methyl-4-oxo-2,3,4,5-tetrahydro-1*H*-1,5-benzodiazepin-7-yl]prop-2-yn-1-yl}oxy)ethyl]carbamate (53)

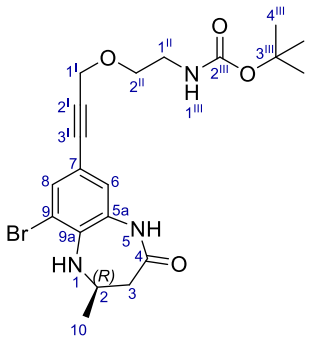

A yellow solution of (4*R*)-6-bromo-8-iodo-4-methyl-1,3,4,5-tetrahydro-2H-1,5-benzodiazepin-2-one (**24**) (267 mg, 0.700 mmol, 1.0 eq.), *tert*-butyl {2-[(prop-2-yn-1-yl)oxy]ethyl}carbamate (**49**) (167 mg, 0.838 mmol, 1.2 eq.), and NEt_3 (1.0 mL) in DMF (1.8 mL) was purged with Ar before the addition of $Pd(PPh_3)_2Cl_2$ (10 mg, 14 μmol, 0.02 eq.) and CuI (5 mg, 28 μmol, 0.04 eq.). The suspension was purged with Ar before being stirred at rt under an atmosphere of Ar for 16 h. The brown suspension was concentrated *in vacuo* and directly purified using normal phase column chromatography (isocratic 50% EtOAc in petroleum ether) to afford *tert*-butyl [2-({3-[(2*R*)-9-bromo-2-methyl-4-oxo-2,3,4,5-tetrahydro-1*H*-1,5-benzodiazepin-7-yl]prop-2-yn-1-yl}oxy)ethyl]carbamate (**53**) (248 mg, 0.548 mmol, 78%) as a brown oil: R_f 0.29 (1:1 petroleum ether/ EtOAc); $[\alpha]_D^{25} = -6.3$ (*c* 1.0, $CHCl_3$); $\bar{\upsilon}_{max}$ (thin film)/ cm^{-1} 3350 (N-H, w, br), 2975 (C-H, w), 2931 (C-H, w), 1676 (C=O, s); ^{1}H NMR (500 MHz, $CDCl_3$) δ_H 8.18 (1 H, br s, NH-5), 7.41 (1 H, d, *J* 1.8, H-6), 6.94 (1 H, d, *J* 1.8, H-8), 4.94

(1 H, br s, NH-1^{III}), 4.37 (1 H, br s, NH-1), 4.34 (2 H, s, H-1^{I}), 4.16 – 4.07 (1 H, m, H-2), 3.62 (2 H, t, *J* 5.3, H-2^{II}), 3.36 (2 H, q, *J* 5.3, H-1^{II}), 2.63 (1 H, dd, *J* 13.8, 3.5, H_AH_B-3), 2.49 (1 H, dd, *J* 13.8, 8.4, H_AH_B-3), 1.44 (9 H, s, H-4^{III}), 1.39 (3 H, d, *J* 6.4, H-10); ^{13}C NMR (126 MHz, $CDCl_3$) δ_C 172.6 (C-4), 156.1 (C-2^{III}), 137.1 (C-9a), 132.4 (C-6), 127.1 (C-5a), 125.0 (C-8), 114.7 (C-9), 114.6 (C-7), 85.0 (C-2^{II}), 84.7 (C-3^{I}), 79.5 (C-3^{III}), 69.3 (C-2^{II}), 59.1 (C-1^{I}), 53.6 (C-2), 41.7 (C-3), 40.5 (C-1^{II}), 28.5 (C-4^{III}), 24.2 (C-10); HRMS *m/z* (ESI^+) 452.1001 (452.1179 calculated for $[C_{20}H_{27}{}^{79}BrN_3O_4]^+$), 454.1157 (454.1159 calculated for $[C_{22}H_{27}{}^{80}BrN_3O_4]^+$); LRMS *m/z* ($ESI^+$) 474 ($[M(^{79}Br)+Na]^+$, 85%), 476 ($[M(^{81}Br)+Na]^+$, 100%); HPLC (Method 2) t_R 10.0 min, purity 98.4%.

tert-Butyl {2-[2-({3-[(2*R*)-9-bromo-2-methyl-4-oxo-2,3,4,5-tetrahydro-1*H*-1,5-benzodiazepin-7-yl]prop-2-yn-1-yl}oxy)ethoxy]ethyl}carbamate (54)

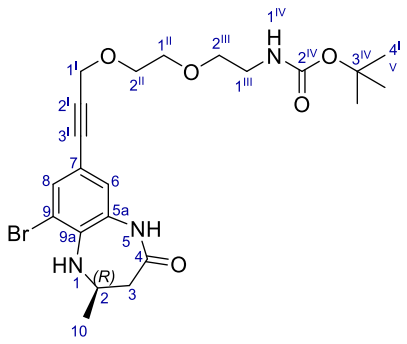

A yellow solution of (4*R*)-6-bromo-8-iodo-4-methyl-1,3,4,5-tetrahydro-2H-1,5-benzodiazepin-2-one (**24**) (381 mg, 1.00 mmol, 1.0 eq.), *tert*-butyl (2-{2-[(prop-2-yn-1-yl)oxy]ethoxy}ethyl)carbamate (**50**) (292 mg, 1.20 mmol, 1.2 eq.), and NEt_3 (1.4 mL) in DMF (2.6 mL) was purged with Ar before the addition of $Pd(PPh_3)_2Cl_2$ (14 mg, 0.020 mmol, 0.02 eq.) and CuI (8 mg, 0.040 mmol, 0.04 eq.). The suspension was purged with Ar before being stirred at rt under an atmosphere of Ar for 16 h. The brown suspension was concentrated *in vacuo* and directly purified using normal phase column chromatography (gradient of 15 – 100% EtOAc in petroleum ether) to afford *tert*-butyl {2-[2-({3-[(2*R*)-9-bromo-2-methyl-4-oxo-2,3,4,5-tetrahydro-1*H*-1,5-benzodiazepin-7-yl]prop-2-yn-1-yl}oxy)ethoxy]ethyl}carbamate (**54**) (412 mg, 0.831 mmol, 83%) as a brown oil: R_f 0.25 (2:3 petroleum ether/ EtOAc); $[\alpha]_D^{25} = -4.5$ (*c* 1.0, $CHCl_3$); $\tilde{\upsilon}_{max}$ (thin film)/ cm^{-1} 3343 (N-H, m, br), 3223 (N-H, w,

br), 2975 (C-H, m), 2931 (C-H, m), 2870 (C-H, m), 1676 (C=O, s); ^{1}H NMR (600 MHz, $CDCl_3$) δ_H 7.49 (1 H, br s, NH-5), 7.41 (1 H, d, *J* 1.9, H-6), 6.90 (1 H, s, H-8), 4.96 (1 H, br s, NH-1^{IV}), 4.39 (2 H, s, H-1^{I}), 4.38 (1 H, br s, NH-1), 4.15 – 4.05 (1 H, m, H-2), 3.75 – 3.70 (2 H, m, H-2^{II}), 3.69 – 3.64 (2 H, m, H-1^{II}), 3.56 (2 H, t, *J* 5.3, H-2^{III}), 3.36 – 3.31 (2 H, m, H-1^{III}), 2.64 (1 H, dd, *J* 13.9, 3.5, H_AH_B-3), 2.49 (1 H, dd, *J* 13.9, 8.4, H_AH_B-3), 1.44 (9 H, s, H-4^{IV}), 1.39 (3 H, d, *J* 6.4, H-10); ^{13}C NMR (151 MHz, $CDCl_3$) δ_C 172.0 (C-4), 156.2 (C-2^{IV}), 137.1 (C-9a), 132.4 (C-6), 127.0 (C-5a), 124.9 (C-8), 114.75 (C-7/ C-9), 114.74 (C-7/ C-9), 85.2 (C-2^{I}), 84.5 (C-3^{I}), 79.4 (C-3^{IV}), 70.5 (C-2^{III}), 70.3 (C-1^{II}), 69.3 (C-2^{II}), 59.3 (C-1^{I}), 53.5 (C-2), 41.7 (C-3), 40.5 (C-1^{III}), 28.6 (C-4^{IV}), 24.2 (C-10); HRMS *m/z* (ESI^+) 496.1443 (496.1442 calculated for $[C_{22}H_{31}{}^{79}BrN_3O_5]^+$), 498.1422 (498.1422 calculated for $[C_{22}H_{31}{}^{80}BrN_3O_5]^+$); LRMS *m/z* ($ESI^+$) 518 ($[M(^{79}Br)+Na]^+$, 91%), 520 ($[M(^{81}Br)+Na]^+$, 100%); HPLC (Method 2) t_R 10.0 min, purity 98.1%.

***tert*-Butyl (2-{2-[2-({3-[(2*R*)-9-bromo-2-methyl-4-oxo-2,3,4,5-tetrahydro-1*H*-1,5-benzodiazepin-7-yl]prop-2-yn-1-yl}oxy)ethoxy]ethoxy}ethyl)carbamate (55)**

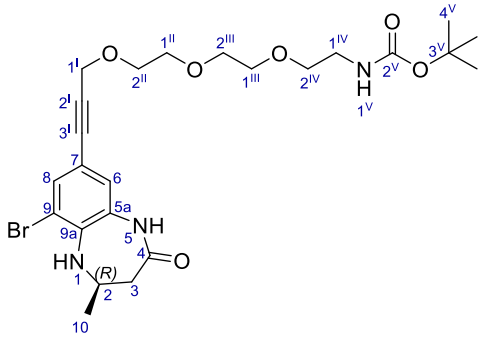

A yellow solution of (4*R*)-6-bromo-8-iodo-4-methyl-1,3,4,5-tetrahydro-2H-1,5-benzodiazepin-2-one (**24**) (381 mg, 1.00 mmol, 1.0 eq.), *tert*-butyl [2-(2-{2-[(prop-2-yn-1-yl)oxy]ethoxy}ethoxy)ethyl]carbamate (**51**) (345 mg, 1.20 mmol, 1.2 eq.), and NEt_3 (1.4 mL) in DMF (2.6 mL) was purged with Ar before the addition of $Pd(PPh_3)_2Cl_2$ (14 mg, 0.020 mmol, 0.02 eq.) and CuI (8 mg, 0.040 mmol, 0.04 eq.). The suspension was purged with Ar before being stirred at rt under an atmosphere of Ar for 16 h. The brown suspension was concentrated *in vacuo* and directly purified using normal phase column chromatography (gradient of

15 – 100% EtOAc in petroleum ether) to afford *tert*-butyl (2-{2-[2-({3-[(2*R*)-9-bromo-2-methyl-4-oxo-2,3,4,5-tetrahydro-1*H*-1,5-benzodiazepin-7-yl]prop-2-yn-1-yl}oxy)ethoxy]ethoxy}ethyl)carbamate (**55**) (528 mg, 0.977 mmol, 98%) as a brown oil: R_f 0.47 (EtOAc); $[\alpha]_D^{25} = -3.3$ (*c* 1.0, $CHCl_3$); $\bar{\upsilon}_{max}$ (thin film)/ cm^{-1} 3350 (N-H, w, br), 3225 (N-H, w, br), 2974 (C-H, m), 2930 (C-H, m), 2871 (C-H, m), 1677 (C=O, s); ^1H NMR (500 MHz, $CDCl_3$) δ_H 7.61 (1 H, br s, NH-5), 7.40 (1 H, d, *J* 1.9, H-6), 6.91 (1 H, d, *J* 1.9, H-8), 5.06 (1 H, br s, NH-1^V), 4.39 (2 H, s, H-1^I), 4.37 (1 H, br s, NH-1), 4.15 – 4.07 (1 H, m, H-2), 3.77 – 3.73 (2 H, m, H-2^{II}), 3.72 – 3.68 (2 H, m, H-1^{II}), 3.67 – 3.65 (2 H, m, H-1^{III}), 3.65 – 3.62 (2 H, m, H-2^{III}), 3.55 (2 H, t, *J* 5.3, H-2^{IV}), 3.31 (2 H, q, *J* 5.3, H-1^{IV}), 2.63 (1 H, dd, *J* 13.9, 3.5, H_AH_B-3), 2.49 (1 H, dd, *J* 13.9, 8.4, H_AH_B-3), 1.44 (9 H, s, H-4^V), 1.39 (3 H, d, *J* 6.4, H-10); ^{13}C NMR (126 MHz, $CDCl_3$) δ_C 172.1 (C-4), 156.2 (C-2^V), 137.0 (C-9a), 132.4 (C-6), 127.1 (C-5a), 124.9 (C-8), 114.8 (C-7/ C-9), 114.7 (C-7/ C-9), 85.3 (C-2^I), 84.5 (C-3^I), 79.4 (C-3^V), 70.8 (C-2^{III}), 70.6 (C-1^{II}), 70.4 (C-1^{III}), 70.3 (C-2^{IV}), 69.3 (C-2^{II}), 59.3 (C-1^I), 53.6 (C-2), 41.7 (C-3), 40.5 (C-1^{IV}), 28.6 (C-4^V), 24.2 (C-10); HRMS *m/z* (ESI^+) 562.1523 (562.1523 calculated for $[C_{24}H_{34}{}^{79}BrN_3O_6Na]^+$), 564.1503 (564.1503 calculated for $[C_{24}H_{34}{}^{80}BrN_3O_6Na]^+$); LRMS *m/z* ($ESI^+$) 562 ($[M(^{79}Br)+Na]^+$, 98%), 564 ($[M(^{81}Br)+Na]^+$, 100%); HPLC (Method 2) t_R 9.9 min, purity 99.0%.

tert-Butyl {15-[(2*R*)-9-bromo-2-methyl-4-oxo-2,3,4,5-tetrahydro-1*H*-1,5-benzodiazepin-7-yl]-3,6,9,12-tetraoxapentadec-14-yn-1-yl}carbamate (56)

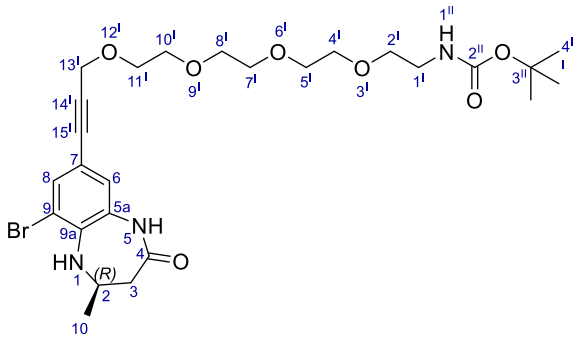

A yellow solution of (4*R*)-6-bromo-8-iodo-4-methyl-1,3,4,5-tetrahydro-2H-1,5-benzodiazepin-2-one (**24**) (381 mg, 1.00 mmol, 1.0 eq.), *tert*-butyl 3,6,9,12-tetraoxapentadec-14-yn-1-ylcarbamate (**52**) (398 mg, 1.20 mmol, 1.2 eq.), and NEt_3 (1.4 mL) in DMF (2.6 mL) was purged with Ar before the

addition of $Pd(PPh_3)_2Cl_2$ (14 mg, 0.020 mmol, 0.02 eq.) and CuI (8 mg, 0.04 mmol, 0.04 eq.). The suspension was purged with Ar before being stirred at rt under an atmosphere of Ar for 20 h. The brown suspension was concentrated *in vacuo* and purified using normal phase column chromatography (gradient of 0 – 100% EtOAc in petroleum ether) then using reverse phase column chromatography (gradient of 95 – 5% H_2O in MeCN) to afford *tert*-butyl {15-[(2*R*)-9-bromo-2-methyl-4-oxo-2,3,4,5-tetrahydro-1*H*-1,5-benzodiazepin-7-yl]-3,6,9,12-tetraoxapentadec-14-yn-1-yl}carbamate (**56**) (54 mg, 0.092 mmol, 9%) as a yellow oil: R_f 0.19 (EtOAc); $[\alpha]_D^{25} = -1.4$ (*c* 1.0, $CHCl_3$); $\bar{\upsilon}_{max}$ (thin film)/ cm^{-1} 3649 (N-H, w), 3357 (N-H, w, br), 2980 (C-H, s), 2867 (C-H, m), 1675 (C=O, s); ^1H NMR (500 MHz, $CDCl_3$) δ_H 7.98 (1 H, br s, NH-1), 7.40 (1 H, d, *J* 1.9 H-6), 6.93 (1 H, d, *J* 1.9, H-8), 5.08 (1 H, br s, NH-1^{III}), 4.38 (2 H, s, H-13^{II}), 4.15 – 4.07 (1 H, m, H-2), 3.75 – 3.72 (2 H, m, H-11^{I}), 3.72 – 3.69 (2 H, m, H-10^{I}), 3.69 – 3.65 (4 H, m, H-7^{I}, H-8^{I}), 3.65 – 3.63 (2 H, m, H-5^{I}), 3.63 – 3.60 (2 H, m, H-4^{I}), 3.53 (2 H, t, *J* 5.3, H-2^{I}), 3.30 (2 H, q, *J* 5.3, H-1^{I}), 2.63 (1 H, dd, *J* 13.9, 3.5, H_AH_B-3), 2.48 (1 H, dd, *J* 13.9, 8.4, H_AH_B-3), 1.43 (9 H, s, H-4^{II}), 1.39 (3 H, d, *J* 6.4, H-10); ^{13}C NMR (151 MHz, $CDCl_3$) δ_C 172.4 (C-4), 156.2 (C-2^{II}), 137.0 (C-9a), 132.3 (C-6), 127.2 (C-5a), 125.0 (C-8), 114.8 (C-9), 114.7 (C-7), 85.3 (C-14^{I}), 84.5 (C-15^{I}), 79.3 (C-3^{II}), 70.77 (C-7^{I}, C-8^{I})‡, 70.74 (C-10^{I}), 70.68 (C-5^{I}), 70.62 (C-6^{I}), 70.4 (C-2^{I}), 69.3 (C-11^{I}), 59.3 (C-13^{I}), 53.6 (C-2), 41.7 (C-3), 40.5 (C-1^{I}), 28.6 (C-4^{II}), 24.2 (C-10); LRMS *m/z* (ESI^+) 606 ($[M+Na]^+$, 100%), 608 ($[M+Na]^+$, 96%); HPLC (Method 2) t_R 9.9 min, purity 95.8%. ‡ - Two carbons with equivalent chemical shift, apparent by HSQC.

tert-Butyl (2-{3-[(2*R*)-9-bromo-2-methyl-4-oxo-2,3,4,5-tetrahydro-1*H*-1,5-benzodiazepin-7-yl]propoxy}ethyl)carbamate (57)

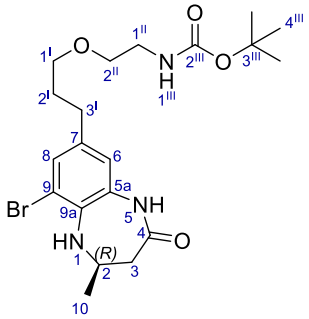

A suspension of *tert*-butyl [2-({3-[(2*R*)-9-bromo-2-methyl-4-oxo-2,3,4,5-tetrahydro-1*H*-1,5-benzodiazepin-7-yl]prop-2-yn-1-yl}oxy)ethyl]carbamate (**53**) (248 mg, 0.548 mmol, 1.0 eq.) and $Rh(PPh_3)_3Cl$ (25 mg, 27 μmol, 0.05 eq.) in toluene (5.5 mL) was purged with H_2 then stirred at 60 ºC under an atmosphere of H_2 for 4 h. The reaction mixture was cooled to rt before the further addition of $Rh(PPh_3)_3Cl$ (25 mg, 27 μmol, 0.05 eq.). The reaction mixture was purged with H_2 and stirred at 60 ºC under an atmosphere of H_2 for 16 h. The brown suspension was cooled to rt and directly purified using normal phase column chromatography (isocratic 60% EtOAc in petroleum ether). The product was further purified using normal phase column chromatography (isocratic Et_2O) to afford *tert*-butyl (2-{3-[(2*R*)-9-bromo-2-methyl-4-oxo-2,3,4,5-tetrahydro-1*H*-1,5-benzodiazepin-7-yl]propoxy}ethyl)carbamate (**57**) (146 mg, 0.320 mmol, 58%) as a pale brown oil: R_f 0.21 (1:1 petroleum ether/ EtOAc); $[\alpha]_D^{25} = +3.7$ (*c* 1.0, $CHCl_3$); $\bar{\upsilon}_{max}$ (thin film)/ cm^{-1} 3347 (N-H, w, br), 2929 (C-H, w), 2866 (C-H, w), 1673 (C=O, s); ^1H NMR (500 MHz, $CDCl_3$) δ_H 8.17 (1 H, br s, NH-5), 7.16 (1 H, d, *J* 1.9, H-6), 6.71 (1 H, d, *J* 1.9, H-8), 4.91 (1 H, br s, NH-1^{III}), 4.11 (1 H, m, H-2), 3.46 (2 H, t, *J* 5.2, H-2^{II}), 3.41 (2 H, t, *J* 6.3, H-1^{I}), 3.34 – 3.27 (2 H, m, H-1^{II}), 2.62 – 2.54 (3 H, m, H_AH_B-3, H-3^{I}), 2.40 (1 H, dd, *J* 13.5, 8.1, H_AH_B-3), 1.89 – 1.78 (2 H, m, H-2^{I}), 1.44 (9 H, s, H-4^{III}), 1.36 (3 H, d, *J* 6.3, H-10); ^{13}C NMR (126 MHz, $CDCl_3$) δ_C 172.9 (C-4), 156.1 (C-2^{III}), 136.0 (C-7), 134.7 (C-9a), 129.7 (C-5a), 129.1 (C-6), 121.7 (C-8), 116.5 (C-9), 79.5 (C-3^{III}), 69.90 (C-1^{I}/ C-2^{II}), 69.89 (C-1^{I}/ C-2^{II}), 55.2 (C-2), 41.2 (C-3), 40.6 (C-1^{II}), 31.13 (C-3^{I}), 31.08 (C-2^{I}), 28.6 (C-4^{III}), 24.0 (C-10); HRMS *m/z* (ESI^+) 456.1493 (456.1493 calculated for $[C_{20}H_{31}{}^{79}BrN_3O_4]^+$), 458.1471 (458.1472 calculated for $[C_{20}H_{31}{}^{81}BrN_3O_4]^+$); LRMS *m/z* ($ESI^+$) 478 ($[M(^{79}Br)+Na]^+$, 100%), 480 ($[M(^{81}Br)+Na]^+$, 95%); HPLC (Method 2) t_R 9.9 min, purity 97.0%.

tert-Butyl [2-(2-{3-[(2*R*)-9-bromo-2-methyl-4-oxo-2,3,4,5-tetrahydro-1*H*-1,5-benzodiazepin-7-yl]propoxy}ethoxy)ethyl]carbamate (58)

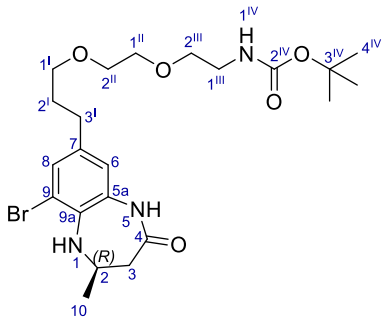

A suspension of *tert*-butyl {2-[2-({3-[(2*R*)-9-bromo-2-methyl-4-oxo-2,3,4,5-tetrahydro-1*H*-1,5-benzodiazepin-7-yl]prop-2-yn-1-yl}oxy)ethoxy]ethyl}carbamate (**54**) (302 mg, 0.610 mmol, 1.0 eq.) and $Rh(PPh_3)_3Cl$ (29 mg, 31 μmol, 0.05 eq.) in toluene (6.1 mL) was purged with H_2 and the reaction mixture was stirred at 60 ºC under an atmosphere of H_2 for 20 h. The brown suspension was cooled to rt and directly purified using normal phase column chromatography (gradient of 50 – 100% EtOAc in petroleum ether) then using reverse phase column chromatography (gradient of 80 – 30% H_2O in MeCN) to afford *tert*-butyl [2-(2-{3-[(2*R*)-9-bromo-2-methyl-4-oxo-2,3,4,5-tetrahydro-1*H*-1,5-benzodiazepin-7-yl]propoxy}ethoxy)ethyl]carbamate (**58**) (118 mg, 0.236 mmol, 39%) as a yellow oil: R_f 0.27 (EtOAc); $[\alpha]_D^{25}$ = +3.4 (*c* 1.0, $CHCl_3$); $\bar{\upsilon}_{max}$ (thin film)/ cm^{-1} 3659 (N-H, w, br), 2980 (C-H, s), 2886 (C-H, m), 1714 (C=O, w), 1673 (C=O, w); ^1H NMR (500 MHz, $CDCl_3$) δ_H 7.52 (1 H, br s, NH-5), 7.17 (1 H, d, *J* 2.0, H-6), 6.70 (1 H, d, *J* 2.0, H-8), 5.10 (1 H, br s, NH-1^{IV}), 4.16 – 4.04 (1 H, m, H-2), 3.64 – 3.60 (2 H, m, H-1^{II}), 3.60 – 3.53 (4 H, m, H-2^{II}, H-2^{III}), 3.43 (2 H, t, *J* 6.3, H-1^{I}), 3.36 – 3.30 (2 H, m, H-1^{III}), 2.62 – 2.56 (3 H, m, H_AH_B-3, H-3^{I}), 2.41 (1 H, dd, *J* 13.6, 8.1, H_AH_B-3), 1.89 – 1.79 (2 H, m, H-2^{I}), 1.43 (9 H, s, H-4^{IV}), 1.37 (3 H, d, *J* 6.3, H-10); ^{13}C NMR (126 MHz, $CDCl_3$) δ_C 172.5 ((C-4), 156.2 (C-3^{IV}), 135.8 (C-7), 134.7 (C-9a), 129.3 (C-5a), 129.2 (C-6), 121.8 (C-8), 116.4 (C-9), 79.4 (C-3^{IV}), 70.38 (C-1^{II}/ C-2^{III}), 70.35 (C-1^{II}/ C-2^{III}), 70.2 (C-2^{II}), 70.1 (C-1^{I}), 54.9 (C-2), 41.2 (C-3), 40.5 (C-1^{III}), 31.1 (C-3^{I}), 31.0 (C-2^{I}), 28.6 (C-4^{IV}), 24.0 (C-10); HRMS *m/z* (ESI^+) 500.1744 (500.1755 calculated for $[C_{22}H_{35}{}^{79}BrN_3O_5]^+$), 502.1722 (502.1735 calculated for $[C_{22}H_{35}{}^{81}BrN_3O_5]^+$); LRMS *m/z* ($ESI^+$) 500 ($[M(^{79}Br)+H]^+$, 100%), 502 ($[M(^{81}Br)+H]^+$, 90%); HPLC (Method 2) t_R 9.9 min, purity 99.9%.

***tert*-Butyl {2-[2-(2-{3-[(2*R*)-9-bromo-2-methyl-4-oxo-2,3,4,5-tetrahydro-1*H*-1,5-benzodiazepin-7-yl]propoxy}ethoxy)ethoxy]ethyl}carbamate (59)**

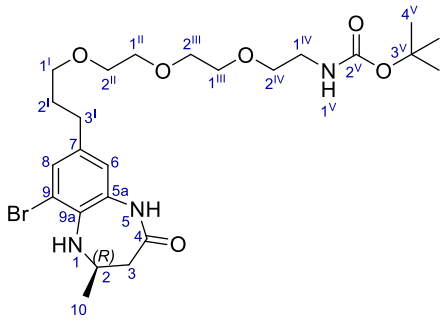

A suspension of *tert*-butyl (2-{2-[2-({3-[(2*R*)-9-bromo-2-methyl-4-oxo-2,3,4,5-tetrahydro-1*H*-1,5-benzodiazepin-7-yl]prop-2-yn-1-yl}oxy)ethoxy]ethoxy}ethyl)carbamate (**55**) (237 mg, 0.439 mmol, 1.0 eq.) and $Rh(PPh_3)_3Cl$ (20 mg, 22 μmol, 0.05 eq.) in toluene (4.5 mL) was purged with H_2 and stirred at 60 ºC under an atmosphere of H_2 for 7 h. The crude suspension was cooled to rt and directly purified by normal phase column chromatography (elution with a gradient of 40 – 100% EtOAc in petroleum ether) to afford *tert*-butyl {2-[2-(2-{3-[(2*R*)-9-bromo-2-methyl-4-oxo-2,3,4,5-tetrahydro-1*H*-1,5-benzodiazepin-7-yl]propoxy}ethoxy)ethoxy]ethyl}carbamate (**59**) (165 mg, 0.303 mmol, 67%) as a pale brown oil: R_f 0.19 (EtOAc); $[\alpha]_D^{25}$ = +2.6 (*c* 1.0, $CHCl_3$); $\bar{\upsilon}_{max}$ (thin film)/ cm^{-1} 3349 (N-H, m, br), 3251 (N-H, w, br), 2929 (C-H, m), 2866 (C-H, m), 1674 (C=O, s); ^{1}H NMR (500 MHz, $CDCl_3$) δ_H 7.65 (1 H, br s, NH-5), 7.16 (1 H, d, *J* 1.9, H-6), 6.74 (1 H, d, *J* 1.9, H-8), 5.14 (1 H, br s, NH-1^V), 4.14 – 4.05 (1 H, m, H-2), 4.00 (1 H, br d, *J* 2.1, NH-1), 3.67 – 3.62 (6 H, m, H-1^{II}, H-1^{III}, H-2^{III}), 3.60 – 3.52 (4 H, m, H-2^{II}, H-2^{IV}), 3.42 (2 H, t, *J* 6.2, H-1^I), 3.31 (2 H, q, *J* 5.4, H-1^{IV}), 2.64 – 2.55 (3 H, m, H_AH_B-3, H-3^I), 2.40 (1 H, dd, *J* 13.5, 8.0, H_AH_B-3), 1.88 – 1.78 (2 H, m, H-2^I), 1.43 (9 H, s, H-4^V), 1.36 (3 H, d, *J* 6.3, H-10); ^{13}C NMR (126 MHz, $CDCl_3$) δ_C 172.5 (C-4), 156.2 (C-2^V), 135.8 (C-7), 134.7 (C-9a), 129.4 (C-5a), 129.1 (C-6), 121.9 (C-8), 116.4 (C-9), 79.3 (C-3^V), 70.7 (C-1^{II}/ C-1^{III}/ C-2^{III}/ C-2^{II}/ C-2^{IV}), 70.6 (C-1^{II}/ C-1^{III}/ C-2^{III}/ C-2^{II}/ C-2^{IV}), 70.42‡ (C-1^{II}/ C-1^{III}/ C-2^{III}/ C-2^{II}/ C-2^{IV}), 70.42‡ (C-1^{II}/ C-1^{III}/ C-2^{III}/ C-2^{II}/ C-2^{IV}), 70.3 (C-2^{II}/ C-2^{IV}), 69.8 (C-1^I), 55.0 (C-2), 41.3 (C-3), 40.5 (C-1^{IV}), 31.01 (C-3^I), 30.96 (C-2^I), 28.6 (C-4^V), 24.1 (C-10); HRMS *m/z* (ESI$^+$) 544.2021 (544.2017 calculated for

$[C_{24}H_{39}{}^{79}BrN_3O_6]^+$), 546.2001 (546.1997 calculated for $[C_{24}H_{39}{}^{81}BrN_3O_6]^+$); LRMS *m/z* ($ESI^+$) 444.2 ($[M(^{79}Br)+H-C_5H_9O_2]^+$, 100%), 446.2 ($[M(^{81}Br)+H-C_5H_9O_2]^+$, 99%); HPLC (Method 2) t_R 9.8 min, purity 98.6%. ǂ - Two carbon environments located at the same ppm, evident by HSQC and HMBC.

tert-Butyl {15-[(2*R*)-9-bromo-2-methyl-4-oxo-2,3,4,5-tetrahydro-1*H*-1,5-benzodiazepin-7-yl]-3,6,9,12-tetraoxapentadecan-1-yl}carbamate (60)

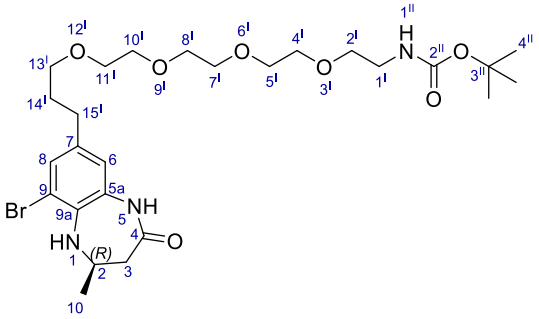

A suspension of *tert*-butyl {15-[(2*R*)-9-bromo-2-methyl-4-oxo-2,3,4,5-tetrahydro-1*H*-1,5-benzodiazepin-7-yl]-3,6,9,12-tetraoxapentadec-14-yn-1-yl}carbamate (**56**) (250 mg, 0.425 mmol, 1.0 eq.) and $Rh(PPh_3)_3Cl$ (20 mg, 21 μmol, 0.05 eq.) in toluene (4.2 mL) was purged with H_2. The reaction mixture was stirred at 60 ºC for under an atmosphere of H_2 for 20 h. The brown suspension was cooled to rt and directly purified using normal phase column chromatography (gradient of 60 – 100% EtOAc in petroleum ether) to afford *tert*-butyl {15-[(2*R*)-9-bromo-2-methyl-4-oxo-2,3,4,5-tetrahydro-1*H*-1,5-benzodiazepin-7-yl]-3,6,9,12-tetraoxapentadecan-1-yl}carbamate (**60**) (227 mg, 0.386 mmol, 92%) as a pale brown oil: R_f 0.16 (EtOAc); $[\alpha]_D^{25}$ = +4.7 (*c* 1.0, $CHCl_3$); $\tilde{\upsilon}_{max}$ (thin film)/ cm^{-1} 3658 (N-H, w, br), 2981 (C-H, s), 2889 (C-H, m), 1683 (C=O, m); ^1H NMR (500 MHz, $CDCl_3$) δ_H 7.84 (1 H, br s, NH-5), 7.16 (1 H, d, *J* 1.9, H-6), 6.75 (1 H, d, *J* 1.9, H-8), 5.12 (1 H, br s, NH-1^{II}), 4.13 – 4.06 (1 H, m, H-2), 3.70 – 3.66 (4 H, m, O-CH_2), 3.66 – 3.62 (4 H, m, O-CH_2), 3.62 – 3.58 (2 H, m, O-CH_2), 3.58 – 3.55 (2 H, m, O-CH_2), 3.51 (2 H, t, *J* 5.2, H-2^I), 3.41 (2 H, t, *J* 6.2, H-13^I), 3.31 – 3.25 (2 H, m, H-1^I), 2.62 – 2.55 (3 H, m, H_AH_B–3, H-15^I), 2.43 – 2.35 (1 H, m, H_AH_B–3), 1.87 – 1.79 (2 H, m, H-14^I), 1.43 (9 H, s, H-4^{II}), 1.36 (3 H, d, *J* 6.3, H-10); ^{13}C NMR (126 MHz, $CDCl_3$) δ_C 172.7 (C-4), 156.2 (C-2^{II}), 135.9 (C-7), 134.7 (C-9a), 129.5 (C-5a), 129.2 (C-6), 122.0 (C-8), 116.4 (C-9), 79.3 (C-3^{II}),

70.78 (O-*C*H$_2$), 70.71 (O-*C*H$_2$), 70.68 (O-*C*H$_2$), 70.63 (O-*C*H$_2$), 70.39 (C-2^{I}/ O-*C*H$_2$), 70.36 (C-2^{I}/ O-*C*H$_2$), 70.3 (C-2^{I}/ O-*C*H$_2$), 69.8 (C-13^{I}), 55.1 (C-2), 41.2 (C-3), 40.5 (C-1^{I}), 37.44, 31.00 (C-14^{I}/ C-15^{I}), 30.97 (C-14^{I}/ C-15^{I}), 28.6 (C-4^{II}), 24.0 (C-10); HRMS *m/z* (ESI$^+$) 588.2269 (588.2269 calculated for [$C_{26}H_{43}{}^{79}BrN_3O_7$]$^+$), 590.2250 (590.2259 calculated for [$C_{26}H_{43}{}^{81}BrN_3O_7$]$^+$); LRMS *m/z* (ESI$^+$) 588 ([M(^{79}Br)+H]$^+$, 100%), 590 ([M(^{81}Br)+H]$^+$, 98%); HPLC (Method 2) t_R 9.8 min, purity 97.8%.

tert-Butyl [2-(3-{(2*R*)-9-[(1*E*)-5-(7-methoxy-3,4-dihydroquinolin-1(2*H*)-yl)pent-1-en-1-yl]-2-methyl-4-oxo-2,3,4,5-tetrahydro-1*H*-1,5-benzodiazepin-7-yl}propoxy)ethyl]carbamate (61)

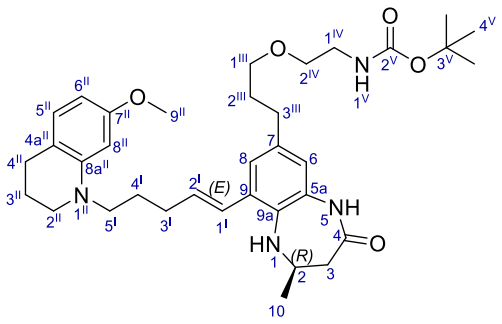

A mixture of *tert*-butyl (2-{3-[(2*R*)-9-bromo-2-methyl-4-oxo-2,3,4,5-tetrahydro-1*H*-1,5-benzodiazepin-7-yl]propoxy}ethyl)carbamate (**57**) (234 mg, 0.513 mmol, 1.0 eq.), 7-methoxy-1-[(4*E*)-5-(4,4,5,5-tetramethyl-1,3,2-dioxaborolan-2-yl)pent-4-en-1-yl]-1,2,3,4-tetrahydroquinoline (**13**) (202 mg, 0.564 mmol, 1.1 eq.), K_2CO_3 (176 mg, 1.28 mmol, 2.5 eq.) in 1,4-dioxane (3.6 mL) and H_2O (1.0 mL) was purged with Ar. Pd(dppf)Cl_2 (19 mg, 26 μmol, 0.05 eq.) was added and the reaction mixture was purged with Ar before being stirred at 100 ºC under an atmosphere of Ar for 16 h. The reaction mixture was cooled to rt and concentrated *in vacuo*. H_2O (20 mL) was added to the residue and the aqueous component was extracted with EtOAc (3 × 20 mL), dried (Na_2SO_4), filtered, and concentrated *in vacuo*. The crude brown oil was purified using normal phase column chromatography (gradient of 40 – 100% EtOAc in petroleum ether) to afford *tert*-butyl [2-(3-{(2*R*)-9-[(1*E*)-5-(7-methoxy-3,4-dihydroquinolin-1(2*H*)-yl)pent-1-en-1-yl]-2-methyl-4-oxo-2,3,4,5-tetrahydro-1*H*-1,5-benzodiazepin-7-yl}propoxy)ethyl]carbamate (**61**) (200 mg, 0.330 mmol, 65%) as a yellow oil: R_f 0.23 (2:3 petroleum ether/ EtOAc); $[\alpha]_D^{25} = +0.7$ (*c* 1.0, $CHCl_3$); $\tilde{\upsilon}_{max}$ (thin film)/ cm^{-1} 3351 (N-H, w, br),

3210 (N-H, w, br), 2932 (C-H, m), 2863 (C-H, m), 1697 (C=O, s), 1670 (C=O, s); ^{1}H NMR (500 MHz, $CDCl_3$) δ_H 7.80 (1 H, s, NH-5), 6.96 (1 H, d, *J* 2.0, H-8), 6.85 (1 H, d, *J* 8.0, H-5^{II}), 6.66 (1 H, d, *J* 2.0, H-6), 6.47 (1 H, d, *J* 15.1, H-1^{I}), 6.19 – 6.12 (2 H, m, H-6^{II}, H-8^{II}), 6.08 (1 H, dt, *J* 15.1, 6.9, H-2^{I}), 4.92 (1 H, s, NH-1^{V}), 4.08 (1 H, p, *J* 6.3, H-2), 3.75 (3 H, s, H-9^{II}), 3.50 – 3.41 (4 H, m, H-1^{III}, H-2^{IV}), 3.35 – 3.24 (6 H, m, H-5^{I}, H-2^{II}, H-1^{IV}), 2.69 (2 H, t, *J* 6.3, H-4^{II}), 2.62 – 2.55 (3 H, m, H_AH_B-3, H-3^{III}), 2.35 (1 H, dd, *J* 13.2, 7.3, H_AH_B-3), 2.32 – 2.26 (2 H, m, H-3^{I}), 1.97 – 1.89 (2 H, m, H-3^{II}), 1.89 – 1.82 (2 H, m, H-2^{III}), 1.82 – 1.75 (2 H, m, H-4^{I}), 1.44 (9 H, s, H-4^{V}), 1.33 (3 H, d, *J* 6.3, H-10); ^{13}C NMR (126 MHz, $CDCl_3$) δ_C 173.1 (C-4), 159.3 (C-7^{II}), 156.1 (C-2^{V}), 146.1 (C-8a^{II}), 135.5 (C-7), 134.6 (C-2^{I}), 133.9 (C-5a), 131.1 (C-9), 130.6 (C-9a), 129.6 (C-5^{II}), 125.8 (C-1^{I}), 124.2 (C-8), 121.0 (C-6), 115.5 (C-4a^{II}), 99.5 (C-6^{II}), 97.7 (C-8^{II}), 79.4 (C-3^{V}), 70.3 (C-1^{III}), 69.9 (C-2^{IV}), 55.8 (C-2), 55.3 (C-9^{II}), 51.2 (C-5^{I}), 49.6 (C-2^{II}), 40.7 (C-3), 40.6 (C-1^{IV}), 31.6 (C-3^{III}), 31.3 (C-2^{III}), 31.1 (C-3^{I}), 28.5 (C-4^{V}), 27.5 (C-4^{II}), 26.1 (C-4^{I}), 24.0 (C-10), 22.5 (C-3^{II}); HRMS *m/z* (ESI^{+}) 607.3851 (607.3854 calculated for $[C_{35}H_{51}N_4O_5]^{+}$); LRMS *m/z* (ESI^{+}) 607 ($[M+H]^{+}$, 100%); HPLC (Method 2) t_R 9.8 min, purity 95.9%.

tert-Butyl {2-[2-(3-{(2*R*)-9-[(1*E*)-5-(7-methoxy-3,4-dihydroquinolin-1(2*H*)-yl)pent-1-en-1-yl]-2-methyl-4-oxo-2,3,4,5-tetrahydro-1*H*-1,5-benzodiazepin-7-yl}propoxy)ethoxy]ethyl}carbamate (62)

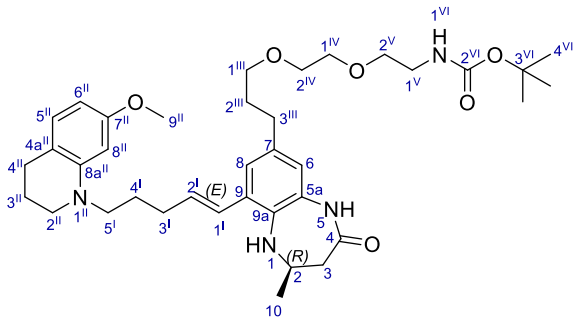

A mixture of *tert*-butyl [2-(2-{3-[(2*R*)-9-bromo-2-methyl-4-oxo-2,3,4,5-tetrahydro-1*H*-1,5-benzodiazepin-7-yl]propoxy}ethoxy)ethyl]carbamate (**58**) (118 mg, 0.236 mmol, 1.0 eq.), 7-methoxy-1-[(4*E*)-5-(4,4,5,5-tetramethyl-1,3,2-dioxaborolan-2-yl)pent-4-en-1-yl]-1,2,3,4-tetrahydroquinoline (**13**) (94 mg, 0.26 mmol, 1.1 eq.), K_2CO_3 (83 mg, 0.60 mmol, 2.5 eq.) in 1,4-dioxane (1.7 mL) and H_2O

(0.5 mL) was purged with Ar. $Pd(dppf)Cl_2$ (9 mg, 0.01 mmol, 0.05 eq.) was added and the reaction mixture was purged with Ar before being stirred at 100 ºC under an atmosphere of Ar for 26 h. The reaction mixture was cooled to rt and concentrated *in vacuo*. H_2O (20 mL) was added to the residue and the aqueous component was extracted with EtOAc (3 × 20 mL). The combined organic components were dried ($MgSO_4$), filtered, and concentrated *in vacuo*. The crude brown oil was purified using normal phase column chromatography (gradient of 50 – 100% EtOAc in petroleum ether) to afford *tert*-butyl {2-[2-(3-{(2*R*)-9-[(1*E*)-5-(7-methoxy-3,4-dihydroquinolin-1(2*H*)-yl)pent-1-en-1-yl]-2-methyl-4-oxo-2,3,4,5-tetrahydro-1*H*-1,5-benzodiazepin-7-yl}propoxy)ethoxy]ethyl}carbamate (**62**) (122 mg, 0.187 mmol, 78%) as a yellow oil: R_f 0.32 (EtOAc); $[\alpha]_D^{25} = -2.3$ (*c* 0.4, MeOH); $\bar{\upsilon}_{max}$ (thin film)/ cm^{-1} 3657 (N-H, w, br), 2980 (C-H, s), 2889 (C-H, m), 1698 (C=O, w), 1671 (C=O, w); ^1H NMR (500 MHz, $CDCl_3$) δ_H 7.31 (1 H, br s, NH-5), 6.96 (1 H, d, *J* 2.1, H-8), 6.85 (1 H, d, *J* 8.0, H-5^{II}), 6.65 (1 H, d, *J* 2.1, H-6), 6.46 (1 H, dt, *J* 15.5, 1.6, H-1^{I}), 6.17 – 6.12 (2 H, m, H-6^{II}, H-8^{II}), 6.08 (1 H, dt, *J* 15.5, 6.9, H-2^{I}), 5.08 (1 H, br s, NH-1^{VI}), 4.14 – 4.01 (1 H, m, H-2), 3.75 (3 H, s, H-9^{II}), 3.64 – 3.59 (2 H, m, H-1^{IV}), 3.59 – 3.54 (4 H, m, H-2^{IV}, H-2^{V}), 3.46 (2 H, t, *J* 6.4, H-1^{III}), 3.43 (1 H, br s, NH-1), 3.35 – 3.30 (1 H, m, H-1^{V}), 3.30 – 3.25 (4 H, m, H-5^{I}, H-2^{II}), 2.69 (2 H, t, *J* 6.3, H-4^{II}), 2.63 – 2.56 (3 H, m, H_AH_B-3, H-3^{III}), 2.35 (1 H, dd, *J* 13.2, 7.3, H_AH_B 3), 2.32 – 2.26 (2 H, m, H-3^{I}), 1.96 – 1.90 (2 H, m, H-3^{II}), 1.90 – 1.84 (2 H, m, H-2^{III}), 1.83 – 1.75 (2 H, m, H-4^{I}), 1.43 (9 H, s, H-4^{VI}), 1.34 (3 H, d, *J* 6.2, H-10); ^{13}C NMR (126 MHz, $CDCl_3$) δ_C 172.8 (C-4), 159.4 (C-7^{II}), 156.2 (C-2^{VI}), 146.2 (C-$8a^{II}$), 135.5 (C-7), 134.6 (C-2^{I}), 133.9 (C-5a), 131.1 (C-9), 130.4 (C-9a), 129.6 (C-5^{II}), 125.8 (C-1^{I}), 124.3 (C-8), 121.1 (C-6), 115.5 (C-$4a^{II}$), 99.4 (C-6^{II}), 97.7 (C-8^{II}), 79.3 (C-3^{IV}), 70.5 (C-1^{III}), 70.40 (C-1^{IV}/ C-2^{IV}/ C-2^{V}), 70.35 (C-1^{IV}/ C-2^{IV}/ C-2^{V}), 70.2 (C-1^{IV}/ C-2^{IV}/ C-2^{V}), 55.7 (C-2), 55.3 (C-9^{II}), 51.2 (C-5^{I}), 49.6 (C-2^{II}), 40.8 (C-3), 40.5 (C-1^{V}), 31.6 (C-3^{III}), 31.22 (C-3^{I}/ C-2^{III}), 31.18 (C-3^{I}/ C-2^{III}), 28.6 (C-4^{IV}), 27.6 (C-4^{II}), 26.1 (C-4^{I}), 24.1 (C-10), 22.6 (C-3^{II}); HRMS *m/z* (ESI^+) 651.4106 (651.4116 calculated for $[C_{37}H_{55}N_4O_6]^+$); LRMS *m/z* (ESI^+) 651 ($[M+H]^+$, 100%); HPLC (Method 2) t_R 9.8 min, purity 97.8%.

***tert*-Butyl (2-{2-[2-(3-{(2*R*)-9-[(1*E*)-5-(7-methoxy-3,4-dihydroquinolin-1(2*H*)-yl)pent-1-en-1-yl]-2-methyl-4-oxo-2,3,4,5-tetrahydro-1*H*-1,5-benzodiazepin-7-yl}propoxy)ethoxy]ethoxy}ethyl)carbamate (63)**

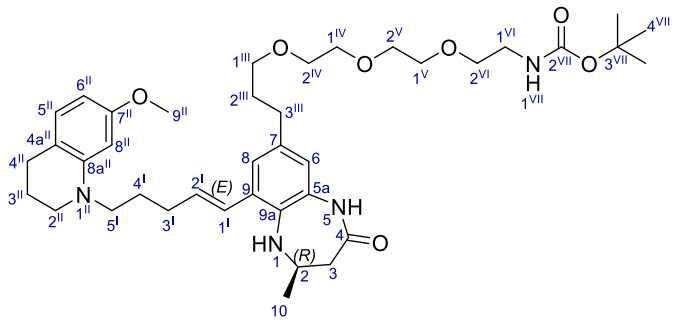

A mixture of *tert*-butyl {2-[2-(2-{3-[(2*R*)-9-bromo-2-methyl-4-oxo-2,3,4,5-tetrahydro-1*H*-1,5-benzodiazepin-7-yl]propoxy}ethoxy)ethoxy]ethyl}carbamate (**59**) (138 mg, 0.253 mmol, 1.0 eq.), 7-methoxy-1-[(4*E*)-5-(4,4,5,5-tetramethyl-1,3,2-dioxaborolan-2-yl)pent-4-en-1-yl]-1,2,3,4-tetrahydroquinoline (**13**) (99 mg, 0.28 mmol, 1.1 eq.), K_2CO_3 (86 mg, 0.63 mmol, 2.5 eq.) in 1,4-dioxane (1.8 mL) and H_2O (0.5 mL) was purged with Ar. $Pd(dppf)Cl_2$ (9 mg, 13 μmol, 0.05 eq.) was added and the reaction mixture was purged with Ar before being stirred at 100 ºC under an atmosphere of Ar for 16 h. The reaction mixture was cooled to rt and concentrated *in vacuo*. H_2O (20 mL) was added to the residue and the aqueous component was extracted with CH_2Cl_2 (3 × 20 mL). The combined organic components were dried ($MgSO_4$), filtered, and concentrated *in vacuo*. The crude brown oil was purified using normal phase column chromatography (gradient of 40 – 100% EtOAc in petroleum ether) to afford *tert*-butyl (2-{2-[2-(3-{(2*R*)-9-[(1*E*)-5-(7-methoxy-3,4-dihydroquinolin-1(2*H*)-yl)pent-1-en-1-yl]-2-methyl-4-oxo-2,3,4,5-tetrahydro-1*H*-1,5-benzodiazepin-7-yl}propoxy)ethoxy]ethoxy}ethyl)carbamate (**63**) (134 mg, 0.193 mmol, 77%) as a yellow oil: R_f 0.30 (EtOAc); $[\alpha]_D^{25} = +1.9$ (*c* 1.0, $CHCl_3$); $\bar{\upsilon}_{max}$ (thin film)/ cm^{-1} 3359 (N-H, w, br), 2931 (C-H, m), 2865 (C-H, m), 1671 (C=O, s), 1613 (C=C, m); ^1H NMR (500 MHz, $CDCl_3$) δ_H 7.63 (1 H, br s, NH-5), 6.95 (1 H, d, *J* 2.0, H-8), 6.85 (1 H, d, *J* 8.0, H-5^{II}), 6.68 (1 H, d, *J* 2.0, H-6), 6.46 (1 H, d, *J* 15.6, H-1^{I}), 6.16 – 6.11 (2 H, m, H-6^{II}, H-8^{II}), 6.07 (1 H, dt, *J* 15.6, 6.9, H-2^{I}), 5.14 (1 H, br s, NH-1^{VII}), 4.12 – 4.03 (1 H, m, H-2), 3.74 (3 H, s, H-9^{II}), 3.68 – 3.61 (6 H, m, H-1^{IV}, H-2^{IV}/ H-1^{v}, H-2^{V}), 3.61 – 3.57 (2 H, m, H-2^{IV}/ H-1^{v}), 3.54 (2 H, t, *J* 5.2, H-2^{VI}), 3.45 (2 H, t, *J* 6.3, H-1^{III}), 3.34 – 3.25 (6 H, m, H-5^{I},

H-2^{II}, H-1^{VI}), 2.69 (2 H, t, *J* 6.3, H-4^{II}), 2.65 – 2.53 (3 H, m, H_AH_B-3, H-3^{III}), 2.35 (1 H, dd, *J* 13.2, 7.3, H_AH_B-3), 2.32 – 2.25 (2 H, m, H-3^{I}), 1.97 – 1.88 (2 H, m, H-3^{II}), 1.91 – 1.82 (2 H, m, H-2^{III}), 1.83 – 1.75 (2 H, m, H-4^{I}), 1.43 (9 H, s, H-4^{VII}), 1.33 (3 H, d, *J* 6.2, H-10); ^{13}C NMR (126 MHz, $CDCl_3$) δ_C 173.0 (C-4), 159.3 (C-7^{II}), 156.2 (C-2^{VII}), 146.2 (C-8a^{II}), 135.5 (C-7), 134.5 (C-2^{I}), 133.8 (C-9a), 131.0 (C-9), 130.5 (C-5a), 129.6 (C-5^{II}), 125.8 (C-1^{I}), 124.2 (C-8), 121.2 (C-6), 115.4 (C-4a^{II}), 99.4 (C-6^{II}), 97.6 (C-8^{II}), 79.2 (C-3^{VII}), 70.7 (C-1^{IV}/ C-2^{V}), 70.6 (C-1^{IV}/ C-2^{V}), 70.39 (C-1^{III}/ C-2^{IV}/ C-2^{VI}/ C-1^{V}), 70.37 (C-1^{III}/ C-2^{IV}/ C-2^{VI}/ C-1^{V}), 70.31 (C-1^{III}/ C-2^{IV}/ C-2^{VI}/ C-1^{V}), 70.27 (C-1^{III}/ C-2^{IV}/ C-2^{VI}/ C-1^{V}), 55.7 (C-2), 55.3 (C-9^{II}), 51.1 (C-5^{I}), 49.6 (C-2^{II}), 40.8 (C-3), 40.5 (C-1^{VI}), 31.5 (C-3^{III}), 31.20 (C-3^{I}/ C-2^{III}), 31.15 (C-3^{I}/ C-2^{III}), 28.6 (C-4^{VII}), 27.5 (C-4^{II}), 26.1 (C-4^{I}), 24.1 (C-10), 22.6 (C-3^{II}); HRMS *m/z* (ESI$^+$) 695.4385 (695.4378 calculated for $[C_{39}H_{59}N_4O_7]^+$); LRMS *m/z* (ESI$^+$) 595 ($[M+H-C_5H_9O_2]^+$, 100%); HPLC (Method 2) t_R 9.7 min, purity 93%.

tert-Butyl (15-{(2*R*)-9-[(1*E*)-5-(7-methoxy-3,4-dihydroquinolin-1(2*H*)-yl)pent-1-en-1-yl]-2-methyl-4-oxo-2,3,4,5-tetrahydro-1*H*-1,5-benzodiazepin-7-yl}-3,6,9,12-tetraoxapentadecan-1-yl)carbamate (64)

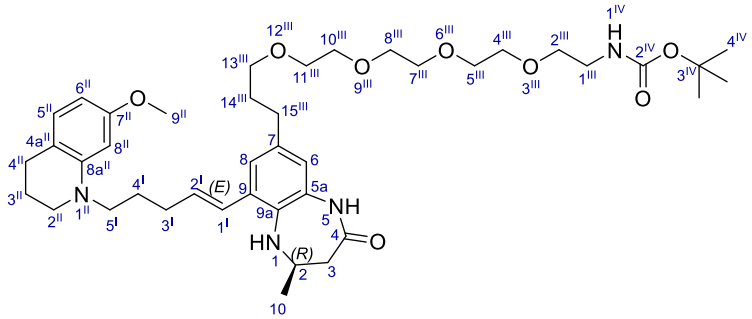

A mixture of *tert*-butyl {15-[(2*R*)-9-bromo-2-methyl-4-oxo-2,3,4,5-tetrahydro-1*H*-1,5-benzodiazepin-7-yl]-3,6,9,12-tetraoxapentadecan-1-yl}carbamate (**60**) (178 mg, 0.302 mmol, 1.0 eq.), 7-methoxy-1-[(4*E*)-5-(4,4,5,5-tetramethyl-1,3,2-dioxaborolan-2-yl)pent-4-en-1-yl]-1,2,3,4-tetrahydroquinoline (**13**) (119 mg, 0.333 mmol, 1.1 eq.), K_2CO_3 (104 mg, 0.752 mmol, 2.5 eq.) in 1,4-dioxane (2.1 mL) and H_2O (0.63 mL) was purged with Ar. $Pd(dppf)Cl_2$ (11 mg, 15 μmol, 0.050 eq.) was added and the reaction mixture was purged with Ar before being stirred at 100 ºC under an atmosphere of Ar for 26 h. The

reaction mixture was cooled to rt and concentrated *in vacuo*. H_2O (20 mL) was added to the residue and the aqueous phase component was extracted with EtOAc (3 × 20 mL). The combined organic components were dried ($MgSO_4$), filtered, and concentrated *in vacuo*. The crude brown oil was purified using normal phase column chromatography (gradient of 0 – 15% acetone in EtOAc) to afford *tert*-butyl (15-{(2*R*)-9-[(1*E*)-5-(7-methoxy-3,4-dihydroquinolin-1(2*H*)-yl)pent-1-en-1-yl]-2-methyl-4-oxo-2,3,4,5-tetrahydro-1*H*-1,5-benzodiazepin-7-yl}-3,6,9,12-tetraoxapentadecan-1-yl)carbamate (**64**) (129 mg, 0.175 mmol, 58%) as a yellow oil: R_f 0.21 (9:1 EtOAc/ acetone); $[\alpha]_D^{25} = +1.6$ (*c* 1.0, $CHCl_3$); $\bar{\upsilon}_{max}$ (thin film)/ cm^{-1} 3337 (N-H, w, br), 2933 (C-H, m), 2865 (C-H, m), 1699 (C=O, s), 1671 (C=O, s), 1614 (C=C, m); ^{1}H NMR (500 MHz, $CDCl_3$) δ_H 7.42 (1 H, br s, NH-5), 6.96 (1 H, d, *J* 2.0, H-8), 6.86 (1 H, d, *J* 8.1, H-5^{II}), 6.68 (1 H, d, *J* 2.0, H-6), 6.46 (1 H, d, *J* 15.6, H-1^{I}), 6.18 (1 H, d, *J* 2.4, H-8^{II}), 6.15 (1 H, dd, *J* 8.1, 2.4, H-6^{II}), 6.08 (1 H, dt, *J* 15.6, 6.9, H-2^{I}), 5.09 (1 H, br s, NH-1^{IV}), 4.12 – 4.05 (1 H, m, H-2), 3.75 (3 H, s, H-9^{II}), 3.68 – 3.67 (4 H, m, O-CH_2), 3.67 – 3.63 (4 H, m, O-CH_2), 3.62 – 3.59 (2 H, m, O-CH_2), 3.59 – 3.57 (2 H, m, O-CH_2), 3.52 (2 H, t, *J* 5.2, H-2^{III}), 3.45 (2 H, t, *J* 6.3, H-13^{III}), 3.32 – 3.26 (6 H, m, H-5^{I}, H-2^{II}, H-1^{III}), 2.70 (2 H, t, *J* 6.4, H-4^{II}), 2.62 – 2.56 (3 H, m, H_AH_B-3, H-15^{III}), 2.35 (1 H, dd, *J* 13.3, 7.3, H_AH_B-3), 2.33 – 2.26 (2 H, m, H-3^{I}), 1.96 – 1.90 (2 H, m, H-3^{II}), 1.89 – 1.83 (2 H, m, H-14^{III}), 1.83 – 1.76 (2 H, m, H-4^{I}), 1.44 (9 H, s, H-4^{IV}), 1.34 (3 H, d, *J* 6.3, H-10); ^{13}C NMR (126 MHz, $CDCl_3$) δ_C 172.8 (C-4), 159.4 (C-7^{II}), 156.2 (C-2^{IV}), 146.1 (C-8a^{II}), 135.6 (C-7), 134.6 (C-2^{I}), 133.9 (C-9a), 131.1 (C-9), 130.5 (C-5a), 129.7 (C-5^{II}), 125.8 (C-1^{I}), 124.3 (C-8), 121.2 (C-6), 115.6 (C-4a^{II}), 99.7 (C-6^{II}), 97.9 (C-8^{II}), 79.3 (C-3^{IV}), 70.8 (O-*C*H_2), 70.74 (O-*C*H_2), 70.73 (O-*C*H_2), 70.66 (O-*C*H_2), 70.4 (C-2^{III}, O-*C*H_2), 70.30 (C-2^{III}, O-*C*H_2), 70.25 (C-2^{III}, O-*C*H_2), 55.7 (C-2), 55.3 (C-9^{II}), 51.3 (C-5^{I}), 49.6 (C-2^{II}), 40.8 (C-3), 40.5 (C-1^{III}), 31.5 (C-15^{III}), 31.24 (C-14^{III}), 31.17 (C-3^{I}), 28.6 (C-4^{IV}), 27.5 (C-4^{II}), 26.1 (C-4^{I}), 24.1 (C-10), 22.5 (C-3^{II}); HRMS *m/z* (ESI$^+$) 739.4630 (739.4640 calculated for $[C_{41}H_{63}N_4O_8]^+$); LRMS *m/z* (ESI$^+$) 739 ($[M+H]^+$, 100%); HPLC (Method 2) t_R 9.7 min, 97.1% purity.

2-(2,6-Dioxopiperidin-3-yl)-4-{[2-(3-{(2*R*)-9-[(1*E*)-5-(7-methoxy-3,4-dihydroquinolin-1(2*H*)-yl)pent-1-en-1-yl]-2-methyl-4-oxo-2,3,4,5-tetrahydro-1*H*-1,5-benzodiazepin-7-yl}propoxy)ethyl]amino}-1*H*-isoindole-1,3(2*H*)-dione (35)

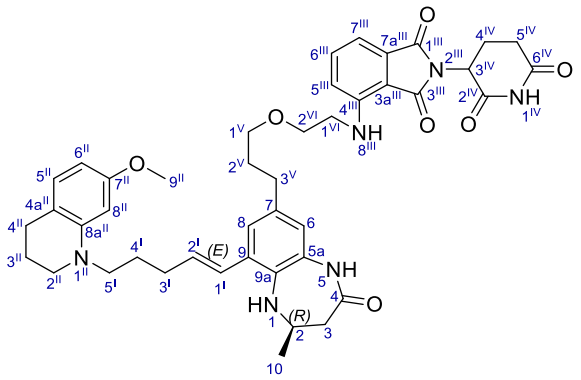

Step I:

To a solution of *tert*-butyl [2-(3-{(2*R*)-9-[(1*E*)-5-(7-methoxy-3,4-dihydroquinolin-1(2*H*)-yl)pent-1-en-1-yl]-2-methyl-4-oxo-2,3,4,5-tetrahydro-1*H*-1,5-benzodiazepin-7-yl}propoxy)ethyl]carbamate (**61**) (30 mg, 0.050 mmol, 1.0 eq.) in CH_2Cl_2 (0.50 mL) at 0 ºC was added 4 M HCl in 1,4-dioxane (63 µL, 0.25 mmol, 5.0 eq.). The resulting suspension was stirred at rt for 1 h. The suspension was concentrated under a flow of N_2, 1 M aq. NaOH (3 mL) was added to the residue, and the aqueous component was extracted with CH_2Cl_2 (3 × 3 mL). The combined organic components were dried (Na_2SO_4), filtered, and concentrated *in vacuo* to afford the amine intermediate as a yellow oil.

Step II:

A yellow solution of the amine intermediate, 2-(2,6-dioxopiperidin-3-yl)-4-fluoro-2,3-dihydro-1*H*-isoindole-1,3-dione (**40**) (17 mg, 0.060 mmol, 1.2 eq.), and DIPEA (44 µL, 0.25 mmol, 5.0 eq.) in DMF (0.50 mL) was stirred was stirred at 90 ºC for 4 h. The reaction mixture was cooled to rt before being diluted with EtOAc (30 mL). The organic component was washed with brine (2 × 30 mL), dried (Na_2SO_4), filtered, and concentrated *in vacuo*. The crude brown oil was purified using normal phase column chromatography (gradient of 60 – 80% EtOAc in petroleum ether) to afford 2-(2,6-dioxopiperidin-3-yl)-4-{[2-(3-{(2*R*)-9-[(1*E*)-5-(7-methoxy-3,4-dihydroquinolin-1(2*H*)-yl)pent-1-en-1-yl]-2-methyl-4-oxo-2,3,4,5-tetrahydro-1*H*-1,5-benzodiazepin-7-yl}propoxy)ethyl]amino}-1*H*-isoindole-1,3(2*H*)-dione (**35**) (10 mg, 0.013 mmol, 26%) as a yellow oil: R_f 0.17 (petroleum ether/

EtOAc 1:4); $[\alpha]_D^{25}$ = +4.4 (*c* 0.4, MeCN); $\bar{\upsilon}_{max}$ (thin film)/ cm^{-1} 3377 (N-H, w, br), 2310 (N-H, w, br), 2930 (C-H, m), 2860 (C-H, m), 1698 (C=O, s), 1667 (C=O, m), 1624 (C=C, m); ^{1}H NMR (500 MHz, CD_3CN) δ_H 9.14 (1 H, br s, NH-1^{IV}), 7.89 (1 H, br d, *J* 5.2, NH-5), 7.54 (1 H, t, *J* 7.8, H-6^{III}), 7.09 – 6.94 (3 H, m, H-8, H-5^{III}, H-7^{III}), 6.77 (1 H, d, *J* 8.1, H-5^{II}), 6.63 (1 H, s, H-6), 6.60 – 6.51 (2 H, m, H-1^{I}, NH-8^{III}), 6.17 – 6.09 (2 H, m, H-2^{I}, H-8^{II}), 6.05 (1 H, dd, *J* 8.1, 2.5, H-6^{II}), 4.96 (1 H, dd, *J* 12.3, 5.4, H-3^{IV}), 4.03 – 3.93 (1 H, m, H-2), 3.75 (1 H, br s, NH-1), 3.65 (3 H, s, H-9^{II}), 3.62 (2 H, t, *J* 5.4, H-2^{VI}), 3.50 – 3.40 (4 H, m, H-1^{V}, H-1^{VI}), 3.33 – 3.19 (4 H, m, H-5^{I}, H-2^{II}), 2.79 – 2.59 (5 H, m, H-4^{II}, H_AH_B-4^{IV}, H-5^{IV}), 2.56 (2 H, t, *J* 7.5, H-3^{V}), 2.49 – 2.39 (1 H, m, H_AH_B-3), 2.30 – 2.21 (2 H, m, H-3^{I}), 2.19 – 2.10‡ (1 H, m, H_AH_B-3), 2.10 – 2.02 (1 H, m, H_AH_B-4^{IV}), 1.89 – 1.82 (2 H, m, H-3^{II}), 1.83 – 1.75 (2 H, m, H-2^{V}), 1.76 – 1.68 (2 H, m, H-4^{I}), 1.33 – 1.05 (3 H, m, H-10); ^{13}C NMR (126 MHz, CD_3CN) δ_C 173.4 (C-4), 172.9 (C-6^{IV}), 170.90 (C-2^{IV}), 170.88 (C-6^{IV}), 170.6 (C-1^{III}), 168.6 (C-3^{III}), 160.2 (C-7^{II}), 148.0 (C-4^{III}), 147.1 (C-$8a^{II}$), 137.1 (C-6^{III}), 136.12 (C-7), 135.14 (C-9a diastereomer A), 135.05 (C-9a diastereomer B), 134.4 (C-2^{I}), 133.5 (C-$7a^{III}$), 132.48 (C-5a diastereomer A), 132.45 (C-5a diastereomer B), 131.87 (C-9 diastereomer A), 131.85 (C-9 diastereomer B), 130.4 (C-5^{II}), 126.8 (C-1^{I}), 124.0 (C-8), 121.6 (C-6), 118.1 (C-8^{III}), 116.0 (C-$4a^{II}$), 111.8 (C-7^{III}), 110.9 (C-$3a^{III}$), 100.8 (C-6^{II}), 97.8 (C-8^{II}), 70.3 (C-1^{V}), 69.6 (C-2^{VI}), 56.73 (C-2 diastereomer A), 56.71 (C-2 diastereomer B), 55.4 (C-9^{II}), 51.3 (C-5^{I}), 49.89 (C-2^{II}/ C-3^{IV}), 49.84 (C-2^{II}/ C-3^{IV}), 43.0 (C-1^{VI}), 41.18 (C-3 diastereomer A), 41.13 (C-3 diastereomer B), 32.00 (C-2^{V}/ C-5^{IV}), 31.95 (C-2^{V}/ C-5^{IV}), 31.85 (C-3^{V}), 31.4 (C-3^{I}), 28.0 (C-4^{II}), 26.4 (C-4^{I}), 23.72 (C-10 diastereomer A), 23.66 (C-10 diastereomer B), 23.25 (C-3^{II}/ C-4^{IV}), 23.20 (C-3^{II}/ C-4^{IV}); HRMS *m/z* (ESI^+) 763.3810 (763.3814 calculated for $[C_{43}H_{51}N_6O_7]^+$); LRMS *m/z* (ESI^+) 763 ($[M+H]^+$, 100%); HPLC (Method 2) t_R 9.7 min, purity 95.8%. ‡ - Located beneath H_2O peak, ppm obtained through HSQC and HMBC.

2-(2,6-Dioxopiperidin-3-yl)-4-({2-[2-(3-{(2*R*)-9-[(1*E*)-5-(7-methoxy-3,4-dihydroquinolin-1(2*H*)-yl)pent-1-en-1-yl]-2-methyl-4-oxo-2,3,4,5-tetrahydro-1*H*-1,5-benzodiazepin-7-yl}propoxy)ethoxy]ethyl}amino)-1*H*-isoindole-1,3(2*H*)-dione (36)

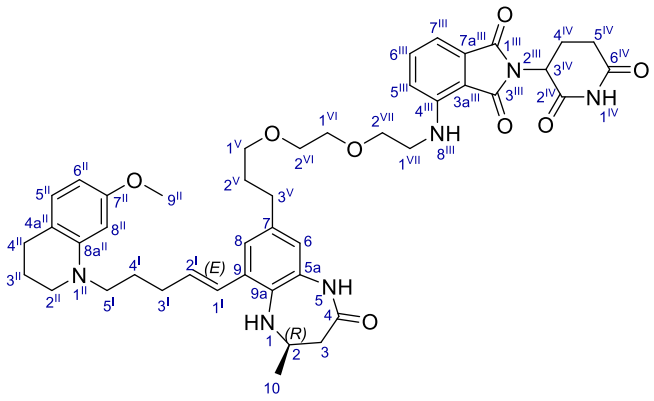

Step I:

To a solution of *tert*-butyl {2-[2-(3-{(2*R*)-9-[(1*E*)-5-(7-methoxy-3,4-dihydroquinolin-1(2*H*)-yl)pent-1-en-1-yl]-2-methyl-4-oxo-2,3,4,5-tetrahydro-1*H*-1,5-benzodiazepin-7-yl}propoxy)ethoxy]ethyl}carbamate (**36**) (33 mg, 0.050 mmol, 1.0 eq.) in CH_2Cl_2 (0.50 mL) at 0 ºC was added 4 M HCl in 1,4-dioxane (63 µL, 0.25 mmol, 5.0 eq.). The resulting suspension was stirred at rt for 2 h. The suspension was concentrated under a flow of N_2, sat. aq. K_2CO_3 (5 mL) was added to the residue, and the aqueous component was extracted with CH_2Cl_2 (3 × 5 mL). The combined organic components were dried (Na_2SO_4), filtered, and concentrated *in vacuo* to afford the amine intermediate as a yellow oil.

Step II:

A yellow solution of the amine intermediate, 2-(2,6-dioxopiperidin-3-yl)-4-fluoro-2,3-dihydro-1*H*-isoindole-1,3-dione (**13**) (17 mg, 0.060 mmol, 1.2 eq.), and DIPEA (44 µL, 0.25 mmol, 5.0 eq.) in DMF (0.50 mL) was stirred at 90 ºC for 2 h. The reaction mixture was concentrated *in vacuo* and the crude brown oil was purified using normal phase column chromatography (isocratic EtOAc) to afford 2-(2,6-dioxopiperidin-3-yl)-4-({2-[2-(3-{(2*R*)-9-[(1*E*)-5-(7-methoxy-3,4-dihydroquinolin-1(2*H*)-yl)pent-1-en-1-yl]-2-methyl-4-oxo-2,3,4,5-tetrahydro-1*H*-1,5-benzodiazepin-7-yl}propoxy)ethoxy]ethyl}amino)-1*H*-isoindole-1,3(2*H*)-dione (**36**) (4 mg, 5 µmol, 10%) as a yellow

oil: R_f 0.20 (EtOAc); $[\alpha]_D^{25} = +16.3$ (c 0.4, $CHCl_3$); $\bar{\upsilon}_{max}$ (thin film)/ cm^{-1} 3650 (N-H, w, br), 2972 (C-H, s), 2888 (C-H, m), 1698 (C=O, s), 1670 (C=O, w); ^1H NMR (500 MHz, $(CD_3)_2CO$) δ_H 9.91 (1 H, br s, NH-1^{IV}), 8.42 (1 H, br s, NH-5), 7.56 (1 H, dd, J 8.5, 7.1, H-6^{III}), 7.12 (1 H, d, J 8.5, H-7^{III}), 7.06 (1 H, d, J 2.0, H-8), 7.02 (1 H, d, J 7.1, H-5^{III}), 6.78 – 6.71 (3 H, m, H-6, H-1^{I}, H-5^{II}), 6.63 (1 H, br t, J 5.8, NH-8^{III}), 6.19 (1 H, dt, J 15.5, 6.9, H-2^{I}), 6.13 (1 H, d, J 2.4, H-8^{II}), 6.07 (1 H, dd, J 8.1, 2.4, H-6^{II}), 5.04 (1 H, dd, J 12.7, 5.4, H-3^{IV}), 4.08 (1 H, br s, NH-1), 4.07 – 4.00 (1 H, m, H-2), 3.75 (2 H, t, J 5.3, H-2^{VII}), 3.66 (3 H, s, H-9^{II}), 3.66 – 3.63 (2 H, m, H-1^{VI}), 3.59 – 3.56 (2 H, m, H-2^{VI}), 3.56 – 3.52 (2 H, m, H-1^{VII}), 3.45 (2 H, t, J 6.3, H-1^{V}), 3.34 – 3.29 (2 H, m, H-5^{I}), 3.29 – 3.26 (2 H, m, H-2^{II}), 2.97 – 2.86 (1 H, m, H_AH_B-5^{IV}), 2.76 – 2.68 (2 H, m, H_AH_B-4^{IV}, H_AH_B-5^{IV}), 2.62 (2 H, t, J 6.4, H-4^{II}), 2.58 (2 H, t, J 7.7, H-3^{V}), 2.47 (1 H, ddd, J 12.9, 5.3, 2.8, H_AH_B-3), 2.35 – 2.27 (2 H, m, H-3^{I}), 2.23 – 2.11 (2 H, m, H_AH_B-3, H_AH_B-4^{IV}), 1.91 – 1.84 (2 H, m, H-3^{II}), 1.83 – 1.73 (4 H, m, H-4^{I}, H-2^{V}), 1.28 (3 H, d, J 6.1, H-10); ^{13}C NMR (126 MHz, $(CD_3)_2CO$) δ_C 172.8 (C-2^{IV}), 172.6 (C-4), 170.5 (C-1^{III}), 170.4 (C-6^{IV}), 168.4 (C-3^{III}), 160.4 (C-7^{II}), 148.0 (C-4^{III}), 147.1 (C-$8a^{II}$), 137.0 (C-6^{III}), 136.1 (C-7), 135.3 (C-9a), 133.8 (C-2^{I}), 133.7 (C-$7a^{III}$), 133.3 (C-5a), 131.8 (C-9), 130.3 (C-5^{II}), 127.3 (C-1^{I}), 123.8 (C-8), 121.6 (C-6), 118.0 (C-5^{III}), 115.7 (C-$4a^{II}$), 111.6 (C-7^{III}), 111.2 (C-$3a^{III}$), 100.9 (C-6^{II}), 98.1 (C-8^{II}), 71.5 (C-1^{IV}), 71.1 (C-2^{VI}), 70.9 (C-1^{V}), 70.4 (C-2^{VII}), 56.9 (C-2), 55.3 (C-9^{II}), 51.5 (C-5^{I}), 50.1 (C-2^{II}), 50.0 (C-3^{IV}), 43.2 (C-1^{VII}), 41.4 (C-3), 32.5 (C-2^{V}), 32.4 (C-3^{V}), 32.1 (C-5^{IV}), 31.7 (C-3^{I}), 28.3 (C-4^{II}), 26.7 (C-4^{I}), 24.0 (C-10), 23.5 (C-4^{IV}), 23.4 (C-3^{II}); HRMS m/z (ESI^+) 807.4066 (807.4076 calculated for $[C_{45}H_{55}N_6O_8]^+$); LRMS m/z (ESI^+) 807 ($[M+H]^+$, 100%); HPLC (Method 2) t_R 9.4 min, 96.2% purity.

2-(2,6-Dioxopiperidin-3-yl)-4-[(2-{2-[2-(3-{(2*R*)-9-[(1*E*)-5-(7-methoxy-3,4-dihydroquinolin-1(2*H*)-yl)pent-1-en-1-yl]-2-methyl-4-oxo-2,3,4,5-tetrahydro-1*H*-1,5-benzodiazepin-7-yl}propoxy)ethoxy]ethoxy}ethyl)amino]-1*H*-isoindole-1,3(2*H*)-dione (37)

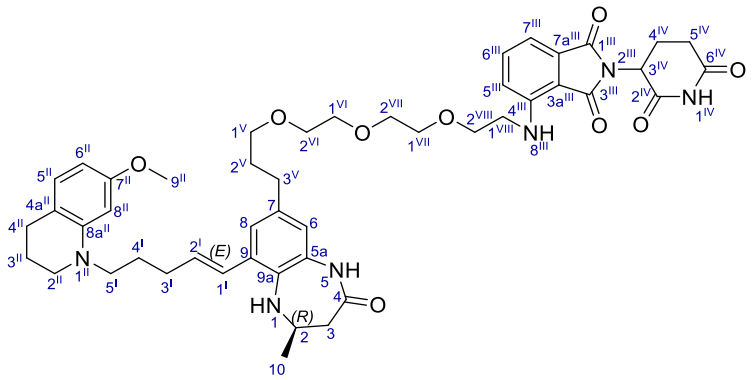

Method 1:

Step I:

To a solution of *tert*-butyl (2-{2-[2-(3-{(2*R*)-9-[(1*E*)-5-(7-methoxy-3,4-dihydroquinolin-1(2*H*)-yl)pent-1-en-1-yl]-2-methyl-4-oxo-2,3,4,5-tetrahydro-1*H*-1,5-benzodiazepin-7-yl}propoxy)ethoxy]ethoxy}ethyl)carbamate (**63**) (35 mg, 0.050 mmol, 1.0 eq.) in CH_2Cl_2 (0.50 mL) at 0 ºC was added 4 M HCl in 1,4-dioxane (63 µL, 0.25 mmol, 5.0 eq.). The resulting suspension was stirred at rt for 1.5 h. The suspension was concentrated under a flow of N_2, 1 M aq. NaOH (5.0 mL) was added to the residue, and the aqueous component was extracted with CH_2Cl_2 (2 × 5.0 mL). The combined organic components were dried (Na_2SO_4), filtered, and concentrated *in vacuo* to afford the amine intermediate as a yellow oil.

Step II:

A yellow solution of the amine intermediate, 2-(2,6-dioxopiperidin-3-yl)-4-fluoro-2,3-dihydro-1*H*-isoindole-1,3-dione (**X**) (17 mg, 0.060 mmol, 1.2 eq.), and DIPEA (44 µL, 0.25 mmol, 5.0 eq.) in DMF (0.50 mL) was stirred was stirred at 90 ºC for 3.5 h. The reaction mixture was cooled to rt before being diluted with EtOAc (30 mL). The organic component was washed with brine (2 × 30 mL), dried (Na_2SO_4), filtered, and concentrated *in vacuo*. The crude brown oil was purified using normal phase column chromatography (gradient of 60 – 80% EtOAc in petroleum ether) to afford 2-(2,6-dioxopiperidin-3-yl)-4-[(2-{2-[2-(3-{(2*R*)-9-[(1*E*)-5-(7-methoxy-3,4-dihydroquinolin-1(2*H*)-

yl)pent-1-en-1-yl]-2-methyl-4-oxo-2,3,4,5-tetrahydro-1*H*-1,5-benzodiazepin-7-yl}propoxy)ethoxy]ethoxy}ethyl)amino]-1*H*-isoindole-1,3(2*H*)-dione (**37**) (9 mg, 11 μmol, 21%) as a yellow oil: R_f 0.21 (EtOAc); $[\alpha]_D^{25}$ = +2.0 (*c* 0.3, MeCN); $\tilde{\upsilon}_{max}$ (thin film)/ cm^{-1} 3226 (N-H, w, br), 2926 (C-H, m), 2861 (C-H, m), 1698 (C=O, s); ^{1}H NMR (500 MHz, CD_3CN) δ_H 9.04 (1 H, br s, NH-1^{IV}), 7.77 (1 H, br s, NH-5), 7.51 (1 H, dd, *J* 8.4, 7.3, H-6^{III}), 7.05 – 6.99 (3 H, m, H-8, H-5^{III}, H-7^{III}), 6.77 (1 H, dt, *J* 8.2, 1.1, H-5^{II}), 6.66 (1 H, d, *J* 2.0, H-6), 6.58 (1 H, dt, *J* 15.6, 1.6, H-1^{I}), 6.47 (1 H, br t, *J* 5.6, NH-8^{III}), 6.15 (1 H, dt, *J* 15.6, 7.1, H-2^{I}), 6.11 (1 H, d, *J* 2.5, H-8^{II}), 6.06 (1 H, dd, *J* 8.2, 2.5, H-6^{II}), 4.91 (1 H, dd, *J* 12.5, 5.2, H-3^{IV}), 4.03 – 3.93 (1 H, m, H-2), 3.73 (1 H, br s, NH-1), 3.67 (2 H, t, *J* 5.4, H-2^{VIII}), 3.65 (3 H, s, H-9^{II}), 3.62 – 3.58 (2 H, m, H-1^{VII}/ H-2^{VII}), 3.58 – 3.55 (2 H, m, H-1^{VII}/ H-2^{VII}), 3.55 – 3.53 (2 H, m, H-1^{VI}), 3.49 – 3.46 (2 H, m, H-2^{VI}), 3.47 – 3.40 (2 H, m, H-1^{VIII}), 3.38 (2 H, t, *J* 6.4, H-1^{V}), 3.31 – 3.23 (4 H, m, H-5^{I}, H-2^{II}), 2.78 – 2.65 (3 H, m, H_AH_B-4^{IV}, H-5^{IV}), 2.62 (2 H, t, *J* 6.3, H-4^{II}), 2.53 (2 H, t, *J* 7.6, H-3^{V}), 2.44 (1 H, dd, *J* 13.0, 5.3, H_AH_B-3), 2.31 – 2.23 (2 H, m, H-3^{I}), 2.17 – 2.12 (1 H, m, H_AH_B-3), 2.10 – 2.03 (1 H, m, H_AH_B-4^{IV}), 1.90 – 1.81 (2 H, m, H-3^{II}), 1.79 – 1.71 (4 H, m, H-4^{I}, H-2^{V}), 1.23 (3 H, d, *J* 6.2, H-10); ^{13}C NMR (126 MHz, CD_3CN) δ_C 173.2 (C-4), 172.9 (C-6^{IV}), 170.6 (C-2^{IV}), 170.4 (C-1^{III}), 168.6 (C-3^{III}), 160.2 (C-7^{II}), 147.8 (C-4^{III}), 147.1 (C-$8a^{II}$), 137.0 (C-6^{III}), 136.3 (C-7), 135.1 (C-9a), 134.4 (C-2^{I}), 133.5 (C-$7a^{III}$), 132.7 (C-5a), 131.9 (C-9), 130.4 (C-5^{II}), 126.8 (C-1^{I}), 124.0 (C-8), 121.5 (C-6), 117.2 (C-5^{III})*, 116.0 (C-$4a^{II}$), 111.7 (C-7^{III}), 110.8 (C-$3a^{III}$), 100.8 (C-6^{II}), 97.8 (C-8^{II}), 71.24 (C-1^{VI}/ C-1^{VII}/ C-2^{VII}), 71.22 (C-1^{VI}/ C-1^{VII}/ C-2^{VII}), 71.15 (C-1^{VI}/ C-1^{VII}/ C-2^{VII}), 70.8 (C-2^{VI}), 70.6 (C-1^{V}), 70.1 (C-2^{VIII}), 56.9 (C-2), 55.4 (C-9^{II}), 51.3 (C-5^{I}), 49.9 (C-2^{II}/ C-3^{IV}), 49.8 (C-2^{II}/ C-3^{IV}), 43.0 (C-1^{VIII}), 41.1 (C-3), 32.11 (C-4^{II}/ C-3^{V}/ C-2^{V}), 32.06 (C-4^{II}/ C-3^{V}/ C-2^{V}), 31.99 (C-4^{II}/ C-3^{V}/ C-2^{V}), 31.4 (C-3^{I}), 28.0 (C-5^{IV}), 26.4 (C-4^{I}), 23.7 (C-10), 23.3 (C-4^{IV}), 23.2 (C-3^{II}); HRMS *m/z* (ESI^+) 851.4326 (851.4338 calculated for $[C_{47}H_{59}N_6O_9]^+$); LRMS *m/z* (ESI^+) 851 ($[M+H]^+$, 100%); HPLC (Method 2) t_R 9.1 min, purity 97.1%. ǂ - Located beneath H_2O peak, ppm obtained from HSQC and HMBC. * - Located beneath solvent peak, ppm obtained from HSQC.

Method 2:

Step I:

To a solution of *tert*-butyl (2-{2-[2-(3-{(2*R*)-9-[(1*E*)-5-(7-methoxy-3,4-dihydroquinolin-1(2*H*)-yl)pent-1-en-1-yl]-2-methyl-4-oxo-2,3,4,5-tetrahydro-1*H*-1,5-benzodiazepin-7-yl}propoxy)ethoxy]ethoxy}ethyl)carbamate (**63**) (35 mg, 0.050 mmol, 1.0 eq.) in CH_2Cl_2 (0.50 mL) at 0 ºC was added 4 M HCl in 1,4-dioxane (63 µL, 0.25 mmol, 5.0 eq.). The resulting suspension was stirred at rt for 45 min. The suspension was concentrated under a flow of N_2, 1 M aq. NaOH (5 mL) was added to the residue, and the aqueous component was extracted with CH_2Cl_2 (3 × 5 mL). The combined organic components were dried (Na_2SO_4), filtered, and concentrated *in vacuo* to afford the amine intermediate as a yellow oil.

Step II:

A yellow solution of the amine intermediate, 2-(2,6-dioxopiperidin-3-yl)-4-fluoro-2,3-dihydro-1*H*-isoindole-1,3-dione (**13**) (17 mg, 0.060 mmol, 1.2 eq.), and DIPEA (44 µL, 0.25 mmol, 5.0 eq.) in DMSO (0.50 mL) was stirred was stirred at 90 ºC for 3 h. The reaction mixture was cooled to rt and concentrated under a flow of N_2. The crude brown oil was purified using reverse phase column chromatography (gradient of 95 – 5% H_2O in MeCN) to afford 2-(2,6-dioxopiperidin-3-yl)-4-[(2-{2-[2-(3-{(2*R*)-9-[(1*E*)-5-(7-methoxy-3,4-dihydroquinolin-1(2*H*)-yl)pent-1-en-1-yl]-2-methyl-4-oxo-2,3,4,5-tetrahydro-1*H*-1,5-benzodiazepin-7-yl}propoxy)ethoxy]ethoxy}ethyl)amino]-1*H*-isoindole-1,3(2*H*)-dione (**37**) (14 mg, 16 µmol, 33%) as a yellow oil: physical data as for Method 1; HPLC (Method 3) t_R 10.9 min, purity 95.5%.

2-(2,6-Dioxopiperidin-3-yl)-4-[(15-{(2*R*)-9-[(1*E*)-5-(7-methoxy-3,4-dihydroquinolin-1(2*H*)-yl)pent-1-en-1-yl]-2-methyl-4-oxo-2,3,4,5-tetrahydro-1*H*-1,5-benzodiazepin-7-yl}-3,6,9,12-tetraoxapentadecan-1-yl)amino]-1*H*-isoindole-1,3(2*H*)-dione (38)

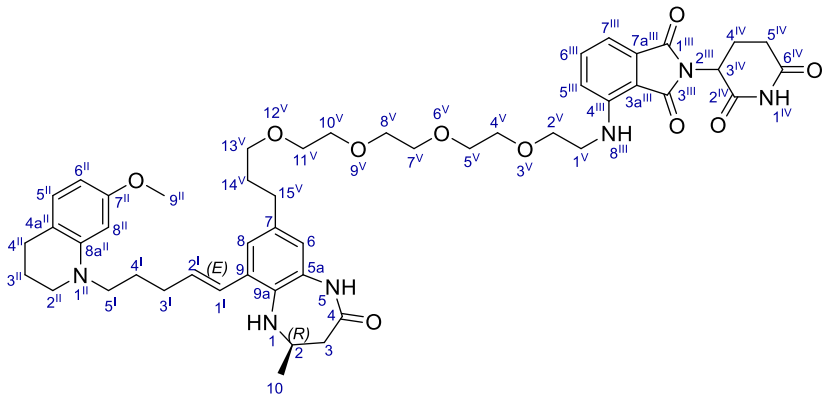

Step I:

To a solution of *tert*-butyl (15-{(2*R*)-9-[(1*E*)-5-(7-methoxy-3,4-dihydroquinolin-1(2*H*)-yl)pent-1-en-1-yl]-2-methyl-4-oxo-2,3,4,5-tetrahydro-1*H*-1,5-benzodiazepin-7-yl}-3,6,9,12-tetraoxapentadecan-1-yl)carbamate (**64**) (37 mg, 0.050 mmol, 1.0 eq.) in CH_2Cl_2 (0.50 mL) at 0 ºC was added 4 M HCl in 1,4-dioxane (63 µL, 0.25 mmol, 5.0 eq.). The resulting suspension was stirred at rt for 2 h. The suspension was concentrated under a flow of N_2, sat. aq. K_2CO_3 (5 mL) was added to the residue, and the aqueous phase was extracted with CH_2Cl_2 (3 × 5 mL). The combined organic phases were dried (Na_2SO_4), filtered, and concentrated *in vacuo* to afford the amine intermediate as a yellow oil.

Step II:

A yellow solution of the amine intermediate, 2-(2,6-dioxopiperidin-3-yl)-4-fluoro-2,3-dihydro-1*H*-isoindole-1,3-dione (**13**) (17 mg, 0.060 mmol, 1.2 eq.), and DIPEA (44 µL, 0.25 mmol, 5.0 eq.) in DMF (0.50 mL) was stirred was stirred at 90 ºC for 3 h. The reaction mixture was concentrated *in vacuo* and the crude brown oil was purified using column chromatography (isocratic 2% MeOH in EtOAc) to afford 2-(2,6-dioxopiperidin-3-yl)-4-[(15-{(2*R*)-9-[(1*E*)-5-(7-methoxy-3,4-dihydroquinolin-1(2*H*)-yl)pent-1-en-1-yl]-2-methyl-4-oxo-2,3,4,5-tetrahydro-1*H*-1,5-benzodiazepin-7-yl}-3,6,9,12-tetraoxapentadecan-1-yl)amino]-1*H*-isoindole-1,3(2*H*)-dione (**38**) (6 mg, 7 µmol, 13%) as a yellow oil: R_f 0.18 (98:2 EtOAc/ MeOH); $[\alpha]_D^{25}$ = +4.1 (*c* 0.4, MeCN); $\bar{\upsilon}_{max}$ (thin film)/ cm^{-1} 3385 (N-H, w, br),

3229 (N-H, w, br), 2926 (C-H, m), 2864 (C-H, m), 1698 (C=O, s); ^{1}H NMR (500 MHz, CD_3CN) δ_H 9.04 (1 H, br s, NH-1^{IV}), 7.78 (1 H, br s, NH-5), 7.52 (1 H, dd, *J* 8.5, 7.2, H-6^{III}), 7.03 – 7.02 (2 H, m, H-8, H-7^{III}), 7.01 (1 H, d, *J* 2.7, H-5^{III}), 6.77 (1 H, d, *J* 8.1, H-5^{II}), 6.68 (1 H, d, *J* 2.0, H-6), 6.58 (1 H, dt, *J* 15.7, 1.7, H-1^{I}), 6.46 (1 H, br t, *J* 5.8, NH-8^{III}), 6.15 (1 H, dt, *J* 15.7, 7.0, H-2^{I}), 6.11 (1 H, d, *J* 2.5, H-8^{II}), 6.06 (1 H, dd, *J* 8.1, 2.5, H-6^{II}), 4.92 (1 H, dd, *J* 12.4, 5.4, H-3^{IV}), 4.02 – 3.94 (1 H, m, H-2), 3.74 (1 H, br s, NH-1), 3.66 – 3.63 (5 H, m, H-9^{II}, H-2^{V}), 3.60 – 3.57 (2 H, m, H-4^{V}), 3.57 – 3.55 (2 H, m, H-5^{V}), 3.55 – 3.47 (8 H, m, H-7^{V}, H-8^{V}, H-10^{V}, H-11^{V}), 3.44 – 3.40 (2 H, m, H-1^{V}), 3.38 (2 H, t, *J* 6.4, H-13^{V}), 3.31 – 3.23 (4 H, m, H-5^{I}, H-2^{II}), 2.76 – 2.64 (3 H, m, H_AH_B-4^{IV}, H-5^{IV}), 2.62 (2 H, t, *J* 6.3, H-4^{II}), 2.54 (2 H, t, *J* 7.6, H-15^{V}), 2.44 (1 H, dd, *J* 13.0, 5.3, H_AH_B-3), 2.30 – 2.24 (2 H, m, H-3^{I}), 2.17 – 2.12 (1 H, m, H_AH_B-3)‡, 2.11 – 2.05 (1 H, m, H_AH_B-4^{IV}), 1.89 – 1.82 (2 H, m, H-3^{II}), 1.82 – 1.70 (4 H, m, H-4^{I}, H-14^{V}), 1.23 (3 H, d, *J* 6.2, H-10); ^{13}C NMR (126 MHz, CD_3CN) δ_C 173.1 (C-4), 173.0 (C-6^{IV}), 170.6 (C-2^{IV}), 170.4 (C-3^{III}), 168.6 (C-1^{III}), 160.2 (C-7^{II}), 147.8 (C-4^{III}), 147.1 (C-8a^{II}), 137.1 (C-6^{III}), 136.3 (C-7), 135.1 (C-9a), 134.4 (C-2^{I}), 133.5 (C-3a^{III}), 132.7 (C-7a^{III}), 131.9 (C-9), 130.4 (C-5^{II}), 126.8 (C-1^{I}), 124.0 (C-8), 121.6 (C-6), 118.2* (C-5^{III}), 115.9 (C-4a^{II}), 111.7 (C-5a), 110.8 (C-7^{III}), 100.8 (C-6^{II}), 97.8 (C-8^{II}), 71.23 (C-4^{V}/ C-5^{V}/ C-7^{V}/ C-8^{V}/ C-10^{V}/ C-11^{V}), 71.17 (C-4^{V}/ C-5^{V}/ C-7^{V}/ C-8^{V}/ C-10^{V}/ C-11^{V}), 71.14 (C-4^{V}/ C-5^{V}/ C-7^{V}/ C-8^{V}/ C-10^{V}/ C-11^{V}), 71.12 (C-4^{V}/ C-5^{V}/ C-7^{V}/ C-8^{V}/ C-10^{V}/ C-11^{V}), 71.11 (C-4^{V}/ C-5^{V}/ C-7^{V}/ C-8^{V}/ C-10^{V}/ C-11^{V}), 71.10 (C-4^{V}/ C-5^{V}/ C-7^{V}/ C-8^{V}/ C-10^{V}/ C-11^{V}), 70.8 (C-12^{V}), 70.6 (C-13^{V}), 70.0 (C-2^{V}), 56.9 (C-2), 55.4 (C-9^{II}), 51.3 (C-5^{I}), 49.85 (C-2^{II}/ C-3^{IV}), 49.84 (C-2^{II}/ C-3^{IV}), 43.0 (C-1^{V}), 41.1 (C-3), 36.48, 32.09 (C-5^{IV}/ C-14^{V}/ C-15^{V}), 32.05 (C-5^{IV}/ C-14^{V}/ C-15^{V}), 31.99 (C-5^{IV}/ C-14^{V}/ C-15^{V}), 31.4 (C-3^{I}), 28.0 (C-4^{II}), 26.4 (C-4^{I}), 23.7 (C-10), 23.3 (C-3^{II}), 23.2 (C-4^{IV}); HRMS *m/z* (ESI^{+}) 895.4590 (895.4600 calculated for $[C_{49}H_{63}N_6O_8]^{+}$); LRMS *m/z* (ESI^{+}) 895 ($[M+H]^{+}$, 100%); HPLC (Method 2) t_R 9.4 min, purity 96.9%. ‡ - Located beneath H_2O peak, ppm obtained from HSQC and HMBC. * - Located beneath solvent peak, ppm value obtained from HMBC.

2-(Adamantan-1-yl)-*N*-[2-(3-{(2*R*)-9-[(1*E*)-5-(7-methoxy-3,4-dihydroquinolin-1(2*H*)-yl)pent-1-en-1-yl]-2-methyl-4-oxo-2,3,4,5-tetrahydro-1*H*-1,5-benzodiazepin-7-yl}propoxy)ethyl]acetamide (65)

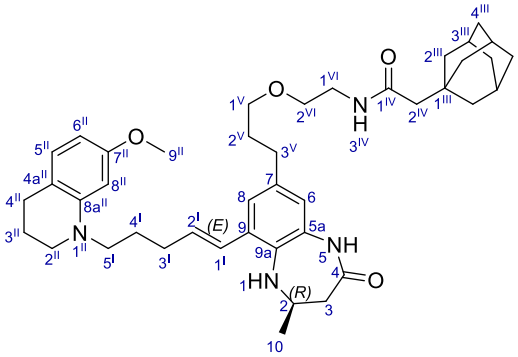

Step I:

To a solution of *tert*-butyl [2-(3-{(2*R*)-9-[(1*E*)-5-(7-methoxy-3,4-dihydroquinolin-1(2*H*)-yl)pent-1-en-1-yl]-2-methyl-4-oxo-2,3,4,5-tetrahydro-1*H*-1,5-benzodiazepin-7-yl}propoxy)ethyl]carbamate (**61**) (30 mg, 0.050 mmol, 1.0 eq.) in CH_2Cl_2 (0.50 mL) at 0 ºC was added 4 M HCl in 1,4-dioxane (63 µL, 0.25 mmol, 5.0 eq.). The resulting suspension was stirred at rt for 1 h. The suspension was concentrated under a flow of N_2, 1 M aq. NaOH (3 mL) was added to the residue, and the aqueous component was extracted with CH_2Cl_2 (3 × 3 mL). The combined organic components were dried (Na_2SO_4), filtered, and concentrated *in vacuo* to afford the amine intermediate as a yellow oil.

Step II:

A solution of 1-adamantaneacetic acid (12 mg, 0.060 mmol, 1.2 eq.), HATU (23 mg, 0.060 mmol, 1.2 eq.), and DIPEA (44 µL, 0.25 mmol, 5.0 eq.) in DMF (0.50 mL) was stirred at rt for 15 min before being added to the amine intermediate. The resulting yellow solution was stirred at rt for a further 3 h. The reaction mixture was concentrated *in vacuo*, sat. aq. $NaHCO_3$ (30 mL) was added to the residue, and the aqueous component was extracted with EtOAc (3 × 30 mL). The combined organic components were washed with brine (90 mL), dried (Na_2SO_4), filtered, and concentrated *in vacuo*. The crude brown oil was purified using normal phase column chromatography (gradient of 80 – 100% EtOAc in petroleum ether) to afford 2-(adamantan-1-yl)-*N*-[2-(3-{(2*R*)-9-[(1*E*)-5-(7-methoxy-3,4-dihydroquinolin-1(2*H*)-yl)pent-1-en-1-yl]-2-methyl-4-oxo-2,3,4,5-tetrahydro-1*H*-1,5-benzodiazepin-

7-yl}propoxy)ethyl]acetamide (**65**) (20 mg, 0.029 mmol, 59%) as a yellow oil: R_f 0.07 (EtOAc); $[\alpha]_D^{25}$ = +5.8 (*c* 0.2, MeCN); $\bar{\upsilon}_{max}$ (thin film)/ cm^{-1} 3316 (N-H, w, br), 2903 (C-H, m), 2846 (C-H, m), 1668 (C=O, s); ^{1}H NMR (500 MHz, CD_3CN) δ_H 7.73 (1 H, br s, NH-5), 7.03 (1 H, d, *J* 2.1, H-8), 6.78 (1 H, d, *J* 8.1, H-5^{II}), 6.67 (1 H, d, *J* 2.1, H-6), 6.60 (1 H, dd, *J* 15.7, 1.6, H-1^{I}), 6.27 (1 H, br s, NH-3^{IV}), 6.16 (1 H, dt, *J* 15.7, 7.1, H-2^{I}), 6.12 (1 H, d, *J* 2.5, H-8^{II}), 6.07 (1 H, dd, *J* 8.1, 2.5, H-6^{II}), 4.03 – 3.95 (1 H, m, H-2), 3.74 (1 H, br s, NH-1), 3.66 (3 H, s, H-9^{II}), 3.44 – 3.38 (4 H, m, H-1^{V}, H-2^{VI}), 3.33 – 3.23 (6 H, m, H-5^{I}, H-2^{II}, H-1^{VI}), 2.63 (2 H, t, *J* 6.4, H-4^{II}), 2.56 (2 H, dd, *J* 8.7, 6.7, H-3^{V}), 2.44 (1 H, dd, *J* 13.0, 5.4, H_AH_B-3), 2.33 – 2.23 (2 H, m, H-3^{I}), 2.18 – 2.09‡ (1 H, m, H_AH_B-3), 1.92 – 1.88 (3 H, m, H-3^{III}), 1.88 – 1.85 (2 H, m, H-3^{II}), 1.85 (2 H, s, H-2^{IV}), 1.82 – 1.72 (4 H, m, H-4^{I}, H-2^{V}), 1.71 – 1.59 (6 H, m, H-4^{III}), 1.59 (6 H, d, *J* 3.0, H-2^{III}), 1.23 (3 H, d, *J* 6.2, H-10); ^{13}C NMR (126 MHz, CD_3CN) δ_C 173.0 (C-4), 171.4 (C-1^{IV}), 160.3 (C-7^{II}), 147.1 (C-8a^{II}), 136.4 (C-7), 135.2 (C-9a), 134.4 (C-2^{I}), 132.8 (C-5a), 132.0 (C-9), 130.4 (C-5^{II}), 126.9 (C-1^{I}), 124.0 (C-8), 121.5 (C-6), 116.0 (C-4a^{II}), 100.8 (C-6^{II}), 97.8 (C-8^{II}), 70.5 (C-1^{V}), 70.0 (C-2^{VI}), 56.9 (C-2), 55.5 (C-9^{II}), 51.8 (C-2^{IV}), 51.3 (C-5^{I}), 49.9 (C-2^{II}), 43.2 (C-2^{III}), 41.1 (C-3), 39.7 (C-1^{VI}), 37.5 (C-4^{III}), 33.3 (C-1^{III}), 32.14 (C-2^{V}/ C-3^{V}), 32.09 (C-2^{V}/ C-3^{V}), 31.4 (C-3^{I}), 29.6 (C-3^{III}), 28.0 (C-4^{II}), 26.4 (C-4^{I}), 23.7 (C-10), 23.2 (C-3^{II}); HRMS *m/z* (ESI$^+$) 683.4528 (683.4531 calculated for $[C_{42}H_{59}N_4O_4]^+$); LRMS *m/z* (ESI$^+$) 683.4 ([M+H]$^+$, 100%); HPLC (Method 2) t_R 10.5 min, purity 93.4%. ǂ - Located beneath H_2O peak, ppm obtained from HSQC and HMBC.

2-(Adamantan-1-yl)-*N*-{2-[2-(3-{(2*R*)-9-[(1*E*)-5-(7-methoxy-3,4-dihydroquinolin-1(2*H*)-yl)pent-1-en-1-yl]-2-methyl-4-oxo-2,3,4,5-tetrahydro-1*H*-1,5-benzodiazepin-7-yl}propoxy)ethoxy]ethyl}acetamide (66)

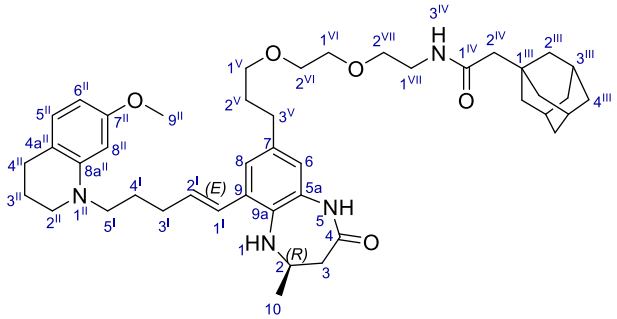

Step I:

To a solution of *tert*-butyl {2-[2-(3-{(2*R*)-9-[(1*E*)-5-(7-methoxy-3,4-dihydroquinolin-1(2*H*)-yl)pent-1-en-1-yl]-2-methyl-4-oxo-2,3,4,5-tetrahydro-1*H*-1,5-benzodiazepin-7-yl}propoxy)ethoxy]ethyl}carbamate (**62**) (33 mg, 0.050 mmol, 1.0 eq.) in CH_2Cl_2 (0.50 mL) at 0 ºC was added 4 M HCl in 1,4-dioxane (63 µL, 0.25 mmol, 5.0 eq.). The resulting suspension was stirred at rt for 2 h. The suspension was concentrated under a flow of N_2, 1 M aq. NaOH (3 mL) was added to the residue, and the aqueous component was extracted with CH_2Cl_2 (3 × 3.0 mL). The combined organic components were dried (Na_2SO_4), filtered, and concentrated *in vacuo* to afford the amine intermediate as a yellow oil.

Step II:

A solution of 1-adamantaneacetic acid (12 mg, 0.060 mmol, 1.2 eq.), HATU (23 mg, 0.060 mmol, 1.2 eq.), and DIPEA (44 µL, 0.25 mmol, 5.0 eq.) in DMF (0.50 mL) was stirred at rt for 15 min before being added to the amine intermediate. The resulting yellow solution was stirred at rt for 13 h. The reaction mixture was concentrated *in vacuo*, sat. aq. $NaHCO_3$ (5 mL) was added to the residue, and the aqueous component was extracted with EtOAc (2 × 5 mL). The combined organic components were washed with brine (15 mL), dried (Na_2SO_4), filtered, and concentrated *in vacuo*. The crude brown oil was purified using normal phase column chromatography (isocratic 5% MeOH in EtOAc) to afford 2-(adamantan-1-yl)-*N*-{2-[2-(3-{(2*R*)-9-[(1*E*)-5-(7-methoxy-3,4-dihydroquinolin-1(2*H*)-yl)pent-1-en-1-yl]-2-methyl-4-oxo-2,3,4,5-tetrahydro-1*H*-1,5-benzodiazepin-7-yl}propoxy)ethoxy]ethyl}acetamide (**66**) (27 mg, 37 µmol, 74%) as a yellow amorphous solid: R_f 0.22 (19:1 EtOAc/ MeOH); $[\alpha]_D^{25} = +12.0$ (*c* 0.2, MeCN); $\bar{\upsilon}_{max}$ (thin film)/ cm^{-1} 3317 (N-H, w, br), 2901 (C-H, m), 2846 (C-H, m), 1670 (C=O, s); ^{1}H NMR (600 MHz, CD_3CN) δ_H 7.79 (1 H, br s, NH-5), 7.03 (1 H, d, *J* 2.0, H-8), 6.78 (1 H, dd, *J* 8.1, 1.2, H-5^{II}), 6.69 (1 H, d, *J* 2.0, H-6), 6.60 (1 H, dt, *J* 15.5, 1.6, H-1^{I}), 6.30 (1 H, br s, NH-3^{IV}), 6.16 (1 H, dt, *J* 15.5, 7.0, H-2^{I}), 6.12 (1 H, d, *J* 2.5, H-8^{II}), 6.07 (1 H, dd, *J* 8.1, 2.5, H-6^{II}), 4.03 – 3.95 (1 H, m, H-2), 3.74 (1 H, br s, NH-1), 3.66 (3 H, s, H-9^{II}), 3.56 – 3.53 (2 H, m, H-2^{VI}), 3.53 – 3.50 (2 H, m, H-1^{VI}), 3.47 (2 H, t, *J* 5.6, H-2^{VII}), 3.42 (2 H, t, *J* 6.4, H-1^{V}), 3.32 – 3.24 (6 H, m, H-5^{I}, H-2^{II}, H-1^{VII}), 2.63 (2 H, t, *J* 6.3, H-4^{II}), 2.57 (2 H, t, *J* 7.7, H-3^{V}), 2.45 (1 H, dd, *J* 13.0, 5.3, H_AH_B-3), 2.32 – 2.25 (2 H, m, H-3^{I}), 2.17 – 2.14‡ (1 H, m, H_AH_B-3), 1.92 – 1.84 (5 H, m, H-3^{II}, H-3^{III}), 1.83 (2 H, s, H-2^{IV}),

1.82 – 1.78 (2 H, m, H-2^{V}), 1.78 – 1.73 (2 H, m, H-4^{I}), 1.68 (3 H, d, *J* 11.9, H_AH_B-4^{III}), 1.60 (3 H, d, *J* 11.9, H_AH_B-4^{III}), 1.57 (6 H, d, *J* 2.9, H-2^{III}), 1.23 (3 H, d, *J* 6.2, H-10); ^{13}C NMR (151 MHz, CD_3CN) δ_C 173.0 (C-4), 171.4 (C-1^{IV}), 160.3 (C-7^{II}), 147.2 (C-8a^{II}), 136.3 (C-7), 135.2 (C-9a), 134.4 (C-2^{I}), 132.8 (C-5a), 132.0 (C-9), 130.4 (C-5^{II}), 126.9 (C-1^{I}), 124.0 (C-8), 121.7 (C-6), 116.0 (C-4a^{II}), 100.9 (C-6^{II}), 97.9 (C-8^{II}), 70.9 (C-1^{VI}/ C-2^{VI}), 70.8 (C-1^{VI}/ C-2^{VI}), 70.7 (C-1^{V}), 70.4 (C-2^{VII}), 56.9 (C-2), 55.5 (C-9^{II}), 51.8 (C-2^{IV}), 51.4 (C-5^{I}), 49.9 (C-2^{II}), 43.3 (C-2^{III}), 41.2 (C-3), 39.7 (C-1^{VII}), 37.5 (C-4^{III}), 33.3 (C-1^{III}), 32.2 (C-2^{V}), 32.1 (C-3^{V}), 31.5 (C-3^{I}), 29.7 (C-3^{III}), 28.1 (C-4^{II}), 26.5 (C-4^{I}), 23.7 (C-10), 23.3 (C-3^{II}); HRMS *m/z* (ESI$^+$) 727.4772 (727.4793 calculated for $[C_{44}H_{63}N_4O_5]^+$); LRMS *m/z* (ESI$^+$) 727 ($[M+H]^+$, 100%); HPLC (Method 2) t_R 10.7 min, 97.3% purity. ǂ - Located beneath H_2O peak, ppm obtained from HSQC and HMBC.

2-(Adamantan-1-yl)-*N*-(2-{2-[2-(3-{(2*R*)-9-[(1*E*)-5-(7-methoxy-3,4-dihydroquinolin-1(2*H*)-yl)pent-1-en-1-yl]-2-methyl-4-oxo-2,3,4,5-tetrahydro-1*H*-1,5-benzodiazepin-7-yl}propoxy)ethoxy]ethoxy}ethyl)acetamide (67)

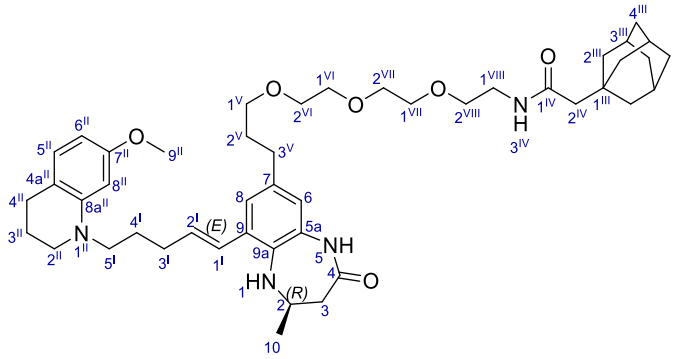

Step I:

To a solution of *tert*-butyl (2-{2-[2-(3-{(2*R*)-9-[(1*E*)-5-(7-methoxy-3,4-dihydroquinolin-1(2*H*)-yl)pent-1-en-1-yl]-2-methyl-4-oxo-2,3,4,5-tetrahydro-1*H*-1,5-benzodiazepin-7-yl}propoxy)ethoxy]ethoxy}ethyl)carbamate (**63**) (35 mg, 0.050 mmol, 1.0 eq.) in CH_2Cl_2 (0.50 mL) at 0 ºC was added 4 M HCl in 1,4-dioxane (63 µL, 0.25 mmol, 5.0 eq.). The resulting suspension was stirred at rt for 1.5 h. The suspension was concentrated under a flow of N_2, 1 M aq. NaOH (3.0 mL) was

added, and the aqueous phase was extracted with CH_2Cl_2 (3 × 3.0 mL). The combined organic phases were dried (Na_2SO_4), filtered, and concentrated *in vacuo* to afford the amine intermediate as a yellow oil.

Step II:

A solution of 1-adamantaneacetic acid (12 mg, 0.060 mmol, 1.2 eq.), HATU (23 mg, 0.060 mmol, 1.2 eq.), and DIPEA (44 μL, 0.25 mmol, 5.0 eq.) in DMF (0.50 mL) was stirred at rt for 15 min before being added to the amine intermediate. The resulting yellow solution was stirred at rt for 3 h. The reaction mixture was concentrated *in vacuo*, $NaHCO_3$ (30 mL) was added to the residue, and the aqueous component was extracted with EtOAc (3 × 30 mL). The combined organic components were washed with brine (90 mL), dried (Na_2SO_4), filtered, and concentrated *in vacuo*. The crude brown oil was purified using normal phase column chromatography (gradient of 80 – 100% EtOAc in petroleum ether) to afford 2-(adamantan-1-yl)-*N*-(2-{2-[2-(3-{(2*R*)-9-[(1*E*)-5-(7-methoxy-3,4-dihydroquinolin-1(2*H*)-yl)pent-1-en-1-yl]-2-methyl-4-oxo-2,3,4,5-tetrahydro-1*H*-1,5-benzodiazepin-7-yl}propoxy)ethoxy]ethoxy}ethyl)acetamide (**67**) (22 mg, 0.029 mmol, 57%) as a yellow oil: R_f 0.46 (9:1 CH_2Cl_2/ MeOH); $[\alpha]_D^{25} = +2.3$ (*c* 0.7, MeCN); $\bar{\upsilon}_{max}$ (thin film)/ cm^{-1} 3297 (N-H, w, br), 2902 (C-H, m), 2947 (C-H, m); ^{1}H NMR (500 MHz, CD_3CN) δ_H 7.82 (1 H, br s, NH-5), 7.04 (1 H, d, *J* 2.0, H-8), 6.77 (1 H, dd, *J* 8.2, 1.0, H-5^{II}), 6.70 (1 H, d, *J* 2.0, H-6), 6.60 (1 H, dd, *J* 15.6, 1.6, H-1^{I}), 6.41 (1 H, br s, NH-3^{IV}), 6.16 (1 H, dt, *J* 15.6, 6.9, H-2^{I}), 6.12 (1 H, d, *J* 2.5, H-8^{II}), 6.07 (1 H, dd, *J* 8.2, 2.5, H-6^{II}), 4.04 – 3.94 (1 H, m, H-2), 3.75 (1 H, br s, NH-1), 3.66 (3 H, s, H-9^{II}), 3.58 – 3.53 (6 H, m, H-1^{VI}, H-2^{VII}, H-2^{VI}/ H-1^{VIII}), 3.53 – 3.50 (2 H, m, H-2^{VI}/ H-1^{VIII}), 3.46 (2 H, t, *J* 5.4, H-2^{VIII}), 3.42 (2 H, t, *J* 6.4, H-1^{V}), 3.32 – 3.24 (6 H, m, H-5^{I}, H-2^{II}, H-1^{VIII}), 2.65 – 2.61 (2 H, m, H-4^{II}), 2.56 (2 H, t, *J* 7.6, H-3^{V}), 2.45 (1 H, dd, *J* 13.0, 5.3, H$_A$H$_B$-3), 2.32 – 2.25 (2 H, m, H-3^{I}), 2.18 – 2.11‡ (1 H, m, H$_A$H$_B$-3), 1.92 – 1.89 (3 H, m, H-3^{III}), 1.89 – 1.84 (2 H, m, H-3^{II}), 1.84 – 1.79 (4 H, m, H-2^{IV}, H-2^{V}), 1.79 – 1.72 (2 H, m, H-4^{I}), 1.68 (3 H, d, *J* 12.5, H$_A$H$_B$-4^{III}), 1.61 (3 H, d, *J* 12.5, H$_A$H$_B$-4^{III}), 1.57 (6 H, d, *J* 2.8, H-2^{III}), 1.23 (3 H, d, *J* 6.2, H-10); ^{13}C NMR (126 MHz, CD_3CN) δ_C 173.1 (C-4), 171.8 (C-1^{IV}), 160.2 (C-7^{II}), 147.1 (C-8a), 136.2 (C-7), 135.2 (C-9a), 134.4 (C-2^{I}), 132.8 (C-5a), 131.9 (C-9), 130.4 (C-5^{II}), 126.9 (C-1^{I}), 124.0 (C-8), 121.7 (C-6), 116.0 (C-4a), 100.8 (C-6^{II}), 97.8 (C-8^{II}), 71.07 (C-1^{VI}/ C-2^{VII}), 70.95 (C-1^{VI}/ C-2^{VII}), 70.80 (C-1^{V}/ C-2^{VI}/ C-1^{VII}/ C-2^{VIII}), 70.74 (C-1^{V}/ C-2^{VI}/ C-1^{VII}/ C-2^{VIII}), 70.70* (C-1^{V}/ C-2^{VI}/

C-1^{VII}/ C-2^{VIII}), 70.70* (C-1^{V}/ C-2^{VI}/ C-1^{VII}/ C-2^{VIII}), 56.9 (C-2), 55.5 (C-9^{II}), 51.7 (C-2^{IV}), 51.3 (C-5^{I}), 49.9 (C-2^{II}), 43.2 (C-2^{III}), 41.1 (C-3), 39.6 (C-1^{VIII}), 37.5 (C-4^{III}), 33.3 (C-1^{III}), 32.03* (C-2^{V}), 32.03* (C-3^{V}), 31.4 (C-3^{I}), 29.6 (C-3^{III}), 28.0 (C-4^{II}), 26.4 (C-4^{I}), 23.7 (C-10), 23.2 (C-3^{II}); HRMS *m/z* (ESI^{+}) 771.5040 (771.5055 calculated for $[C_{46}H_{67}N_4O_6]^{+}$); LRMS *m/z* (ESI^{+}) 771 ([M+H]$^{+}$, 100%); HPLC (Method 2) t_R 10.3 min, purity 95.0%. ǂ - Located beneath H_2O peak, ppm obtained from HSQC and HMBC. * - Two carbon environments located at the same ppm, evident by HSQC and HMBC.

2-(Adamantan-1-yl)-*N*-(15-{(2*R*)-9-[(1*E*)-5-(7-methoxy-3,4-dihydroquinolin-1(2*H*)-yl)pent-1-en-1-yl]-2-methyl-4-oxo-2,3,4,5-tetrahydro-1*H*-1,5-benzodiazepin-7-yl}-3,6,9,12-tetraoxapentadecan-1-yl)acetamide (68)

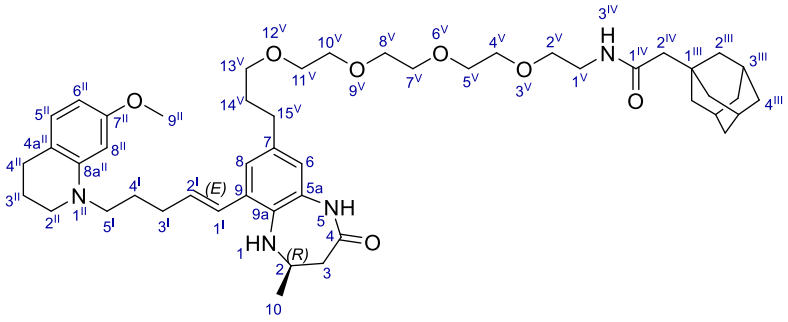

Step I:

To a solution of *tert*-butyl (15-{(2*R*)-9-[(1*E*)-5-(7-methoxy-3,4-dihydroquinolin-1(2*H*)-yl)pent-1-en-1-yl]-2-methyl-4-oxo-2,3,4,5-tetrahydro-1*H*-1,5-benzodiazepin-7-yl}-3,6,9,12-tetraoxapentadecan-1-yl)carbamate (**64**) (37 mg, 0.050 mmol, 1.0 eq.) in CH_2Cl_2 (0.50 mL) at 0 ºC was added 4 M HCl in 1,4-dioxane (63 µL, 0.25 mmol, 5.0 eq.). The resulting suspension was stirred at rt for 2 h. The suspension was concentrated under a flow of N_2, 1 M aq. NaOH (3 mL) was added to the residue, and the aqueous component was extracted with CH_2Cl_2 (2 × 3 mL). The combined organic components were dried (Na_2SO_4), filtered, and concentrated *in vacuo* to afford the amine intermediate as a yellow oil.

Step II:

A solution of 1-adamantaneacetic acid (12 mg, 0.060 mmol, 1.2 eq.), HATU (23 mg, 0.060 mmol, 1.2 eq.), and DIPEA (44 μL, 0.25 mmol, 5.0 eq.) in DMF (0.50 mL) was stirred at rt for 15 min before being added to the amine intermediate. The resulting yellow solution was stirred at rt for 20 h. The reaction mixture was concentrated *in vacuo*, sat. aq. $NaHCO_3$ (5 mL) was added, and the aqueous component was extracted with EtOAc (3 × 5 mL). The combined organic components were washed with brine (15 mL), dried (Na_2SO_4), filtered, and concentrated *in vacuo*. The crude brown oil was purified using normal phase column chromatography (isocratic 5% MeOH in EtOAc) to afford 2-(adamantan-1-yl)-*N*-(15-{(2*R*)-9-[(1*E*)-5-(7-methoxy-3,4-dihydroquinolin-1(2*H*)-yl)pent-1-en-1-yl]-2-methyl-4-oxo-2,3,4,5-tetrahydro-1*H*-1,5-benzodiazepin-7-yl}-3,6,9,12-tetraoxapentadecan-1-yl)acetamide (**68**) (9 mg, 0.01 mmol, 22%) as a yellow oil: R_f 0.20 (19:1 EtOAc/ MeOH); $[\alpha]_D^{25} = +7.3$ (*c* 0.3, MeCN); $\bar{\upsilon}_{max}$ (thin film)/ cm^{-1} 3330 (N-H, w, br), 2901 (C-H, m), 2847 (C-H, m), 1670 (C=O, s); ^{1}H NMR (500 MHz, CD_3CN) δ_H 7.83 (1 H, br s, NH-5), 7.04 (1 H, d, *J* 2.0, H-8), 6.77 (1 H, dt, *J* 8.1, 1.1, H-5^{II}), 6.70 (1 H, d, *J* 2.0, H-6), 6.60 (1 H, dt, *J* 15.6, 1.6, H-1^{I}), 6.34 (1 H, br s, H-3^{IV}), 6.17 (1 H, dt, *J* 15.6, 7.0, H-2^{I}), 6.12 (1 H, d, *J* 2.5, H-8^{II}), 6.07 (1 H, dd, *J* 8.1, 2.5, H-6^{II}), 4.03 – 3.95 (1 H, m, H-2), 3.75 (1 H, br s, NH-1), 3.66 (3 H, s, H-9^{II}), 3.57 – 3.49 (12 H, m, H-4^{V}, H-5^{V}, H-7^{V}, H-8^{V}, H-10^{V}, H-11^{V}), 3.44 (2 H, t, *J* 5.5, H-2^{V}), 3.41 (2 H, t, *J* 6.4, H-13^{V}), 3.31 – 3.23 (6 H, m, H-5^{I}, H-2^{II}, H-1^{V}), 2.63 (2 H, t, *J* 6.3, H-4^{II}), 2.56 (2 H, t, *J* 7.6, H-15^{V}), 2.45 (1 H, dd, *J* 13.0, 5.3, H_AH_B-3), 2.32 – 2.25 (2 H, m, H-3^{I}), 2.18 – 2.12‡ (1 H, m, H_AH_B-3), 1.92 – 1.89 (3 H, m, H-3^{III}), 1.89 – 1.84 (2 H, m, H-3^{II}), 1.83 (2 H, s, H-2^{IV}), 1.82 – 1.72 (4 H, m, H-4^{I}, H-14^{V}), 1.69 (3 H, d, *J* 12.0, H_AH_B-4^{III}), 1.61 (3 H, d, *J* 12.0, H_AH_B-4^{III}), 1.58 (6 H, d, *J* 2.9, H-2^{III}), 1.23 (3 H, d, *J* 6.2, H-10); ^{13}C NMR (126 MHz, CD_3CN) δ_C 173.0 (C-4), 171.4 (C-1^{IV}), 160.3 (C-7^{II}), 147.1 (C-8a^{II}), 136.3 (C-7), 135.1 (C-9a), 134.4 (C-2^{I}), 132.8 (C-5a), 131.9 (C-9), 130.4 (C-5^{II}), 126.9 (C-1^{I}), 124.0 (C-8), 121.7 (C-6), 116.0 (C-4a^{II}), 100.8 (C-6^{II}), 97.8 (C-8^{II}), 71.18 (C-4^{V}/ C-5^{V}/ C-7^{V}/ C-8^{V}/ C-10^{V}/ C-11^{V}), 71.15* (C-4^{V}/ C-5^{V}/ C-7^{V}/ C-8^{V}/ C-10^{V}/ C-11^{V}), 71.15* (C-4^{V}/ C-5^{V}/ C-7^{V}/ C-8^{V}/ C-10^{V}/ C-11^{V}), 71.06 (C-4^{V}/ C-5^{V}/ C-7^{V}/ C-8^{V}/ C-10^{V}/ C-11^{V}), 70.85 (C-4^{V}/ C-5^{V}/ C-7^{V}/ C-8^{V}/ C-10^{V}/ C-11^{V}), 70.82 (C-4^{V}/ C-5^{V}/ C-7^{V}/ C-8^{V}/ C-10^{V}/ C-11^{V}), 70.6 (C-13^{V}), 70.4 (C-2^{V}), 56.9 (C-2), 55.5 (C-9^{II}), 51.7 (C-2^{IV}), 51.3 (C-5^{I}), 49.9 (C-2^{II}), 43.2 (C-2^{III}), 41.1 (C-3), 39.6 (C-1^{V}), 33.3 (C-1^{III}), 32.12 (C-14^{V}/ C-15^{V}), 32.07 (C-14^{V}/ C-15^{V}), 31.4 (C-3^{I}), 29.64,

28.0 (C-4^{II}), 26.4 (C-4^{I}), 23.7 (C-10), 23.2 (C-3^{II}); HRMS *m/z* (ESI^+) 815.5308 (815.5317 calculated for $[C_{48}H_{71}N_4O_7]^+$); LRMS *m/z* (ESI^+) 815 ($[M+H]^+$, 100%); HPLC (Method 2) t_R 10.7 min, purity 97.2%. ǂ - Located beneath H_2O peak, ppm obtained from HSQC and HMBC. * - Two carbon environments located at the same ppm, evident by HSQC and HMBC.

8.3.2 – Synthesis of Compounds in Chapter 3

tert-Butyl 4-[(2_R_)-9-bromo-2-methyl-4-oxo-2,3,4,5-tetrahydro-1H-1,5-benzodiazepin-7-yl]-1,2,3,6-tetrahydropyridine-1-carboxylate (89)

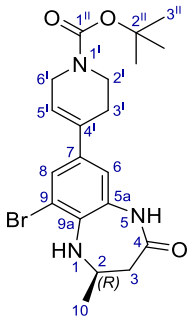

A yellow solution of (4*R*)-6-bromo-8-iodo-4-methyl-1,3,4,5-tetrahydro-2H-1,5-benzodiazepin-2-one (**24**) (4.00 g, 10.5 mmol, 1.0 eq.), (1-*tert*-butoxycarbonyl-1,2,3,6-tetrahydropyridin-4-yl)boronic acid pinacol ester (5.57 g, 11.5 mmol, 1.1 eq.), and K_2CO_3 (3.63 g, 26.3 mmol, 2.5 eq.) in 1,4-dioxane (73 mL) and H_2O (20 mL) was purged with Ar before the addition of Pd(dppf)Cl_2 (253 mg, 0.327 mmol, 0.033 eq.). The suspension was purged with Ar before being stirred at 100 °C under an atmosphere of Ar for 18 h. The brown suspension was filtered through celite®, washed with EtOAc (50 mL), and the filtrate was concentrated *in vacuo*. H_2O (250 mL) was added to the residue and the aqueous component was extracted with EtOAc (3 × 250 mL). The combined organic components were dried (Na_2SO_4), filtered, and concentrated *in vacuo*. The crude brown residue was purified using normal phase column chromatography (gradient of 0 – 60% EtOAc in petroleum ether) to afford *tert*-butyl 4-[(2*R*)-9-bromo-2-methyl-4-oxo-2,3,4,5-tetrahydro-1H-1,5-benzodiazepin-7-yl]-1,2,3,6-tetrahydropyridine-1-carboxylate (**89**) (3.32 g, 7.61 mmol, 72%) as a yellow solid: R_f 0.21 (1:1 petroleum ether/ EtOAc); mp 57 – 60 °C (EtOAc); $[\alpha]_D^{25}$ = +0.9 (*c* 1.0, $CHCl_3$); $\bar{\upsilon}_{max}$ (thin film)/ cm^{-1} 3643 (N-H, w, br), 3624 (N-H, w, br), 2981 (C-H, s), 2889 (C-H, s), 1689 (C=O, m), 1678 (C=O, m); ^{1}H NMR (600 MHz, $CDCl_3$) δ_H 7.69 (1 H, br s, NH-1), 7.35 (1 H, d, *J* 2.1, H-8), 6.84 (1 H, d, *J* 2.1, H-6), 5.99 – 5.90 (1 H, m, H-5^I), 4.15 – 4.08 (1 H, m, H-4), 4.07 – 4.04 (2 H, m, H-6^I), 3.61 (2 H, t, *J* 5.7, H-2^I), 2.62 (1 H, dd, *J* 13.7, 4.0, H_AH_B-3), 2.48 – 2.40 (3 H, m, H_AH_B-3, H-3^I), 1.49 (9 H, s, H-3^{II}), 1.38 (3 H, d, *J* 6.3, H-10); ^{13}C NMR (151 MHz, $CDCl_3$) δ_C 172.5 (C-2), 154.9 (C-1^{II}), 135.8 (C-5a), 134.3 (C-9a), 133.3 (C-4^I), 128.5 (C-8), 125.9 (C-7), 121.0 (C-5^I), 118.2 (C-9), 116.3 (C-6), 80.0 (C-2^{II}), 54.5 (C-4), 43.7 (C-6^I),

41.4 (C-3), 39.9 (C-2^{I}), 28.6 (C-3^{II}), 27.4 (C-3^{I}), 24.2 (C-10); HRMS *m/z* (ESI^+) 436.1259 (436.1230 calculated for $[C_{20}H_{27}{}^{79}BrN_3O_3]^+$); LRMS *m/z* ($ESI^+$) 436 ($[M(^{79}Br)+H]^+$, 100%), 438 ($[M(^{81}Br)+H]^+$, 88%); HPLC (Method 3) t_R 10.1 min, purity 98.4%.

tert-Butyl 4-[(2*R*)-9-bromo-2-methyl-4-oxo-1,2,3,5-tetrahydro-1,5-benzodiazepin-7-yl]piperidine-1-carboxylate (90)

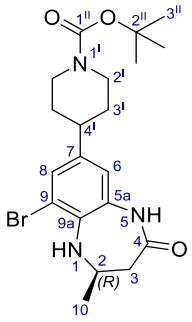

Four reactions were performed at the given quantities and the crude materials were combined for purification. *tert*-Butyl 4-[(2*R*)-9-bromo-2-methyl-4-oxo-2,3,4,5-tetrahydro-1H-1,5-benzodiazepin-7-yl]-1,2,3,6-tetrahydropyridine-1-carboxylate (**89**) (660 mg, 1.51 mmol, 1.0 eq.) and $Rh(PPh_3)_3Cl$ (70 mg, 76 μmol, 0.05 eq.) in MeOH (15 mL) was purged with H_2 (4 bar, 3×) before being stirred under an atmosphere of H_2 (4 bar) at 60 °C for 15 – 24 h. The reaction mixtures were combined, concentrated *in vacuo*, and purified using normal phase column chromatography (gradient of 0 – 100% EtOAc in petroleum ether) to afford *tert*-butyl 4-[(2*R*)-9-bromo-2-methyl-4-oxo-1,2,3,5-tetrahydro-1,5-benzodiazepin-7-yl]piperidine-1-carboxylate (**90**) (1.70 g, 3.88 mmol, 64%) as a light brown solid: R_f 0.21 (1:1 petroleum ether/ EtOAc); mp 57 – 60 ºC (EtOAc); $[\alpha]_D^{25}$ = +3.2 (*c* 1.0, $CHCl_3$); $\bar{\upsilon}_{max}$ (thin film)/ cm^{-1} 3662 (N-H, w, br), 3643 (N-H, w, br), 2981 (C-H, s), 2889 (C-H, m), 1678 (C=O, s); ^1H NMR (600 MHz, $CDCl_3$) δ_H 7.37 (1 H, br s, NH-5), 7.18 (1 H, d, *J* 1.9, H-8), 6.64 (1 H, d, *J* 1.9, H-6), 4.31 – 4.16 (2 H, m, H_AH_B-2^{I}), 4.14 – 4.07 (1 H, m, H-2), 4.03 (1 H, br s, NH-1), 2.82 – 2.70 (2 H, m, H_AH_B-2^{I}), 2.60 (1 H, dd, *J* 13.6, 4.3, H_AH_B-3), 2.53 (1 H, tt, *J* 12.2, 3.6, H-4^{I}), 2.42 (1 H, dd, *J* 13.6, 8.1, H_AH_B-3), 1.81 – 1.74 (2 H, m, H_AH_B-3^{I}), 1.56 – 1.49 (2 H, m, H_AH_B-3^{I}), 1.48 (9 H, s, H-3^{II}), 1.37 (3 H, d, *J* 6.3, H-10); ^{13}C NMR (151 MHz, $CDCl_3$) δ_C 172.4

(C-4), 154.9 (C-1^{II}), 139.7 (C-7), 135.2 (C-9a), 129.20, 127.6 (C-8), 120.0 (C-5a), 116.6 (C-9), 79.7 (C-2^{II}), 54.8 (C-2), 44.3 (C-2^{I}), 41.7 (C-4^{I}), 41.2 (C-3), 33.3 (C-3^{I}), 28.6 (C-3^{II}), 24.1 (C-10); HRMS *m/z* (ESI$^+$) 460.1215 (460.1206 calculated for $[C_{20}H_{28}{}^{79}BrN_3O_3Na]^+$), 462.1198 (462.1186 calculated for $[C_{20}H_{28}{}^{81}BrN_3O_3Na]^+$); LRMS *m/z* (ESI$^+$) 460 ($[M(^{79}Br)+Na]^+$, 100%), 462 ($[M(^{81}Br)+Na]^+$, 91%); HPLC (Method 3) t_R 10.0 min, purity 97.4%.

tert-Butyl 4-[(2*R*)-9-[(1*E*)-5-(7-methoxy-1,2,3,4-tetrahydroquinolin-1-yl)pent-1-en-1-yl]-2-methyl-4-oxo-2,3,4,5-tetrahydro-1*H*-1,5-benzodiazepin-7-yl]piperidine-1-carboxylate (91)

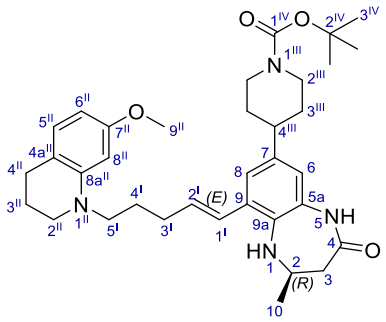

A suspension of *tert*-butyl 4-[(2*R*)-9-bromo-2-methyl-4-oxo-2,3,4,5-tetrahydro-1H-1,5-benzodiazepin-7-yl]-1,2,3,6-tetrahydropyridine-1-carboxylate (**90**) (248 mg, 0.566 mmol, 1.0 eq.), 7-methoxy-1-[(4*E*)-5-(4,4,5,5-tetramethyl-1,3,2-dioxaborolan-2-yl)pent-4-en-1-yl]-1,2,3,4-tetrahydroquinoline (**13**) (208 mg, 0.906 mmol, 1.6 eq.), K_2CO_3 (164 mg, 1.19 mmol, 2.5 eq.) in 1,4-dioxane (4.0 mL) and H_2O (1.2 mL) was purged with Ar. $Pd(dppf)Cl_2$ (21 mg, 28 μmol, 0.05 eq.) was added and the reaction mixture was purged with Ar before being stirred at 100 ºC under an atmosphere of Ar for 18 h. The reaction mixture was concentrated under a flow of N_2, brine (100 mL) was added to the residue, and the aqueous component was extracted with EtOAc (3 × 100 mL). The combined organic components were dried ($MgSO_4$), filtered, and concentrated *in vacuo*. The crude product was purified using normal phase column chromatography (gradient of 70 – 100% EtOAc in petroleum ether) to afford *tert*-butyl 4-[(2*R*)-9-[(1*E*)-5-(7-methoxy-1,2,3,4-tetrahydroquinolin-1-yl)pent-1-en-1-yl]-2-methyl-4-oxo-2,3,4,5-tetrahydro-1*H*-1,5-benzodiazepin-7-yl]piperidine-1-carboxylate (**91**) (86 mg, 0.15 mmol, 26%) as a brown oil: R_f 0.26 (1:4 petroleum ether/ EtOAc)

$[\alpha]_D^{25}$ = +6.3 (*c* 1.0, $CHCl_3$); $\bar{\upsilon}_{max}$ (thin film)/ cm^{-1} 3209 (N-H, w, br), 2980 (C-H, m), 2934 (C-H, m), 1675 (C=O, s), 1578 (C=C, m); ^{1}H NMR (600 MHz, $CDCl_3$) δ_H 7.22 (1 H, br s, NH-5), 6.96 (1 H, d, *J* 2.0, H-8), 6.88 (1 H, d, *J* 8.1, H-5^{II}), 6.61 (1 H, d, *J* 2.0, H-6), 6.48 (1 H, d, *J* 15.5, H-1^{I}), 6.26 – 6.13 (2 H, m, H-6^{II}, H-8^{II}), 6.08 (1 H, dt, *J* 15.5, 6.9, H-2^{I}), 4.29 – 4.17 (2 H, m H_AH_B-2^{III}), 4.13 – 4.04 (1 H, m, H-2), 3.75 (3 H, s, H-9^{II}), 3.32 – 3.28 (4 H, m, H-5^{I}, H-2^{II}), 2.84 – 2.75 (2 H, m, H_AH_B-2^{III}), 2.71 (2 H, t, *J* 6.4, H-4^{II}), 2.60 (1 H, dd, *J* 13.3, 4.8, H_AH_B-3), 2.54 (1 H, tt, *J* 12.2, 3.6, H-4^{III}), 2.36 (1 H, dd, *J* 13.3, 7.4, H_AH_B-3), 2.30 (2 H, dt, *J* 7.4, 6.9, H-3^{I}), 1.99 – 1.92 (2 H, m, H-3^{II}), 1.87 – 1.76 (3 H, m, H-4^{I}, H_AH_B-3^{III}), 1.60 – 1.53 (2 H, m, H_AH_B-3^{III}), 1.48 (9 H, s, H-3^{IV}), 1.34 (3 H, d, *J* 6.2, H-10); ^{13}C NMR (151 MHz, $CDCl_3$) δ_C 172.7 (C-4), 159.3 (C-7^{II}), 155.0 (C-1^{IV}), 146.2 (C-8a^{II}), 139.5 (C-7), 134.7 (C-2^{I}), 134.3 (C-9a), 131.1 (C-9), 130.3 (C-5a), 129.8 (C-5^{II}), 125.9 (C-1^{I}), 122.7 (C-8), 119.3 (C-6), 115.7 (C-4a^{I}), 79.6 (C-2^{IV}), 55.6 (C-2), 55.4 (C-9^{II}), 49.5 (C-5^{II}), 44.5 (C-2^{III}), 42.1 (C-4^{III}), 40.8 (C-3), 33.4 (C-3^{III}), 31.1 (C-3^{I}), 28.6 (C-3^{IV}), 27.4 (C-4^{II}), 26.0 (C-4^{I}), 24.1 (C-10), 22.3 (C-3^{II}); HRMS *m/z* (ESI$^+$) 589.3750 (589.3748 calculated for $[C_{35}H_{49}N_4O_4]^+$); LRMS *m/z* (ESI$^+$) 589 ($[M+H]^+$, 100%); HPLC (Method 3) t_R 12.4 min, purity 93.3%.

(4*R*)-6-[(1*E*)-5-(7-Methoxy-1,2,3,4-tetrahydroquinolin-1-yl)pent-1-en-1-yl]-4-methyl-8-(piperidin-4-yl)-2,3,4,5-tetrahydro-1*H*-1,5-benzodiazepin-2-one Hydrochloride (86)

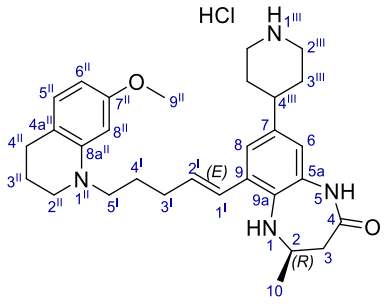

To a solution of *tert*-butyl 4-[(2*R*)-9-[(1*E*)-5-(7-methoxy-1,2,3,4-tetrahydroquinolin-1-yl)pent-1-en-1-yl]-2-methyl-4-oxo-2,3,4,5-tetrahydro-1*H*-1,5-benzodiazepin-7-yl]piperidine-1-carboxylate (**91**) (231 mg, 392 µmol 1.0 eq.) in DCM (3 mL) was added 4 M HCl in dioxane (981 µL, 3.92 mmol, 10.0 eq.). The reaction mixture was stirred at rt for 8 h before being concentrated under a flow of N_2.

(4*R*)-6-[(1*E*)-5-(7-Methoxy-1,2,3,4-tetrahydroquinolin-1-yl)pent-1-en-1-yl]-4-methyl-8-(piperidin-4-yl)-2,3,4,5-tetrahydro-1*H*-1,5-benzodiazepin-2-one hydrochloride (231 mg, 0.413 mmol, 100%) was obtained as a brown solid which was used without purification: R_f 0.00 (acetone); $[\alpha]_D^{25}$ – solubility too low for measurement; $\bar{\upsilon}_{max}$ (thin film)/ cm^{-1} 3001 (N-H, w, br), 2931 (C-H, m), 2844 (C-H, m), 1669 (C=O, s), 1613 (C=O, m), 1509 (C=C, s); ^{1}H NMR (400 MHz, $CDCl_3$) δ_H 7.69 (1 H, br s, NH-5), 6.99 (1 H, d, *J* 2.0, H-8), 6.85 (1 H, d, *J* 8.1, H-5^{II}), 6.66 (1 H, d, *J* 2.0, H-6), 6.46 (1 H, d, *J* 15.4, H-1^{I}), 6.16 – 6.11 (2 H, m, H-6^{II}, H-8^{II}), 6.11 – 6.05 (1 H, m, H-2^{I}), 4.11 – 4.04 (1 H, m, H-2), 3.74 (3 H, s, H-9^{II}), 3.42 (1 H, br s, NH-1^{III}), 3.31 – 3.24 (4 H, m, H-5^{I}, H-2^{II}), 3.21 – 3.16 (2 H, m, H_AH_B-2^{III}), 2.75 – 2.70 (2 H, m, H_AH_B-2^{III}), 2.70 – 2.67 (2 H, m, H-4^{II}), 2.60 – 2.56 (1 H, m, H_AH_B-3), 2.52 (1 H, tt, *J* 12.5, 3.9, H-4^{III}), 2.36 (1 H, dd, *J* 13.2, 7.4, H_AH_B-3), 2.32 – 2.26 (2 H, m, H-3^{I}), 1.95 – 1.90 (2 H, m, H-3^{II}), 1.82 – 1.77 (4 H, m, H-4^{I}, H_AH_B-3^{III}), 1.65 – 1.54 (2 H, m, H_AH_B-3^{III}), 1.33 (3 H, d, *J* 6.2, H-10); ^{13}C NMR (151 MHz, $CDCl_3$) δ_C 173.0 (C-4), 159.3 (C-7^{II}), 146.2 (C-8a^{II}), 140.4 (C-7), 134.6 (C-2^{I}), 134.1 (C-9a), 131.0 (C-9), 130.5 (C-5a), 129.6 (C-5^{II}), 125.9 (C-1^{I}), 122.6 (C-8), 119.3 (C-6), 115.6 (C-4a^{I}), 99.5 (C-8^{II}), 97.7 (C-6^{II}), 55.7 (C-2), 55.3 (C-9^{II}), 51.2 (C-5^{I}), 49.6 (C-2^{II}), 47.1 (C-2^{III}), 42.3 (C-4^{II}), 40.8 (C-3), 34.6 (C-3^{III}), 31.2 (C-3^{I}), 27.5 (C-4^{II}), 26.1 (C-4^{I}), 24.1 (C-10), 22.6 (C-3^{II}); LCMS (formic acid): t_R 0.80 min, *m/z* (ESI$^+$) 489.3 $[M+H]^+$, purity 94%. ^{1}H and ^{13}C NMRs were performed after a basic extraction to remove the HCl salt.

4-(4-Fluoro-3-nitrophenyl)-3,5-dimethyl-1,2-oxazole (93)

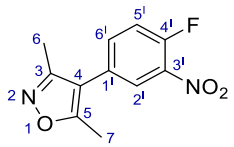

A solution of 4-bromo-1-fluoro-2-nitronbenzene (2.50 mL, 20.4 mmol, 1.0 eq.), 3,5-dimethylisoxazole boronic acid (3.16 g, 22.4 mmol, 1.1 eq.), K_2CO_3 (7.05 g, 51.0 mmol, 2.5 eq.) in 1,4-dioxane (140 mL) and H_2O (40 mL) was purged with Ar. Pd(dppf)Cl_2 (500 mg, 0.683 mmol, 0.034 eq.) was added and the brown solution was stirred at 100 ºC for 17 h. The reaction mixture was cooled to rt, filtered through

silica, washed with EtOAc (50 mL), and concentrated *in vacuo*. Brine (300 mL) was added to the residue and the aqueous component was extracted with EtOAc (3 × 300 mL). The combined organic components were dried (Na_2SO_4), filtered, and concentrated *in vacuo*. The crude brown oil was purified using normal phase silica gel column chromatography (gradient of 0 – 30% EtOAc in petroleum ether) to afford 4-(4-fluoro-3-nitrophenyl)-3,5-dimethyl-1,2-oxazole (**93**) (3.42 g, 12.7 mmol, 62%) as a yellow solid: R_f 0.31 (EtOAc/ *n*-hexane 3:7); mp 116 – 120 °C; ^{1}H NMR (400 MHz, $CDCl_3$) δ_H 7.95 (1 H, dd, *J* 6.9, 2.3, H-2^I), 7.53 (1 H, ddd, *J* 8.6, 4.2, 2.3, H-6^I), 7.40 (1 H, dd, *J* 10.7, 8.6, H-5^I), 2.43 (3 H, s, H-7), 2.28 (3 H, s, H-6); ^{19}F NMR (377 MHz, $CDCl_3$) δ_F −118.5 (1 F, ddd, *J* 10.7, 6.9, 4.2, F-4^I); LRMS *m/z* (ESI$^+$) 237 ([M+H]$^+$, 100%). These data are in good accordance with the literature.[164]

Prop-2-en-1-yl 4-{[(*tert*-butoxy)carbonyl]amino}piperidine-1-carboxylate (92)

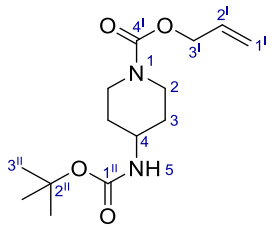

A solution of allyl chloroformate (4.68 µL, 44.0 mmol, 1.1 eq.) in CH_2Cl_2 (8.0 mL) was added dropwise at 0 °C to a solution of 4-*N*-Boc-amino piperidine (8.01 g, 40.0 mmol, 1.0 eq.) and DBU (7.18 mL, 48.0 mmol, 1.2 eq.) in CH_2Cl_2 (80 mL). The reaction mixture was stirred at 0 °C for 3 h before acetic acid (80 mL) was added at 0 °C. The mixture was allowed to warm to rt, the phases were separated, and the organic component was washed with sat. aq. $NaHCO_3$ (2 × 80 mL), dried (Na_2SO_4), filtered, and concentrated *in vacuo* to afford prop-2-en-1-yl 4-{[(*tert*-butoxy)carbonyl]amino}piperidine-1-carboxylate (**92**) (10.3 g, 36.2 mmol, 91%) as a colourless solid which was used without purification: R_f 0.19 (4:1 petroleum ether/ EtOAc); 65 – 68 °C; $\tilde{\upsilon}_{max}$ (thin film)/ cm^{-1} 3341 (N-H, w, br), 2979 (C-H, w), 2942 (C-H, w), 1773 (C=O, m), 1749 (C=O, m), 1696 (C=C, s); ^{1}H NMR (400 MHz, $CDCl_3$) δ_H 5.90 (1 H, ddt, *J* 17.2, 10.5, 5.4, H-2^I), 5.26 (1 H, dq, *J* 17.2, 1.7, H_AH_B-1^I), 5.17 (1 H, dq, *J* 10.5, 1.5, H_AH_B-1^I), 4.55 (2 H, dt, *J* 5.4, 1.5, H-3^I), 4.13 – 3.97 (2 H, m, H_AH_B-2), 3.65 – 3.51 (1 H, m, C-4),

2.96 – 2.82 (2 H, m, H_AH_B-2), 1.96 – 1.84 (2 H, m, H_AH_B-3), 1.41 (9 H, s, H-3^{II}), 1.35 – 1.22 (2 H, m, H_AH_B-3); ^{13}C NMR (101 MHz, $CDCl_3$) δ_C 155.0 (C-4^I/ C-1^{II}), 154.9 (C-4^I/ C-1^{II}), 133.0 (C-2^I), 117.2 (C-1^I), 79.3 (C-2^{II}), 65.9 (C-3^I), 47.7 (C-4), 42.7 (C-2), 32.3 (C-3), 28.3 (C-3^{II}); HRMS *m/z* (ESI^+) 285.1819 (285.1809 calculated for $[C_{14}H_{25}N_2O_4]^+$); LRMS (ESI^+) *m/z* 307 ($[M+Na]^+$, 100%); HPLC - poor chromophore.

Prop-2-en-1-yl 4-{[4-(3,5-dimethyl-1,2-oxazol-4-yl)-2-nitrophenyl]amino}piperidine-1-carboxylate (95)

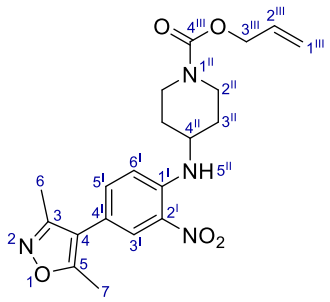

Step I:

Trifluoroacetic acid (4.04 mL, 52.8 mmol, 6.0 eq.) was added dropwise to a solution of prop-2-en-1-yl 4-{[(*tert*-butoxy)carbonyl]amino}piperidine-1-carboxylate (**92**) (3.00 g, 10.6 mmol, 1.2 eq.) in CH_2Cl_2 (106 mL). The reaction mixture was stirred at rt for 1.5 h before being concentrated *in vacuo* to afford the amine salt intermediate (**94**) as a colourless solid.

Step II:

A suspension of the amine salt intermediate, 4-(4-fluoro-3-nitrophenyl)-3,5-dimethyl-1,2-oxazole (**X**) (2.39 g, 8.83 mmol, 1.0 eq.), and DIPEA (7.45 mL, 44.2 mmol, 5.0 eq.) in MeCN (160 mL) was stirred at 80 °C for 15 h. The reaction mixture was cooled to rt, concentrated *in vacuo*, and directly purified using normal phase column chromatography (isocratic 40% EtOAc in petroleum ether) to afford prop-2-en-1-yl 4-{[4-(3,5-dimethyl-1,2-oxazol-4-yl)-2-nitrophenyl]amino}piperidine-1-carboxylate (**95**) (2.59 g, 6.47 mmol, 61%) as an orange oil: R_f 0.33 (petroleum ether/ EtOAc 1:1); ῡmax (thin film)/ cm^{-1} 3663 (N-H, w, br), 2981 (C-H, s), 2888 (C-H, m), 1383 (N=O, m); ^{1}H NMR (600 MHz, $CDCl_3$)

δ_H 8.15 (1 H, br d, *J* 7.4, NH-5^{II}), 8.09 (1 H, dd, *J* 1.9, H-2^{I}), 7.34 (1 H, dd, *J* 8.7, 1.9, H-6^{I}), 6.96 (1 H, d, *J* 8.7, H-5^{I}), 6.01 – 5.91 (1 H, m, H-2^{III}), 5.32 (1 H, dt, *J* 17.3, 1.5, H_AH_B-1^{III}), 5.24 (1 H, dt, *J* 10.4, 1.5, H_AH_B-1^{III}), 4.62 (2 H, dq, *J* 5.6, 1.5, H-3^{III}), 4.18 – 4.05 (2 H, m, H_AH_B-2^{II}), 3.79 – 3.70 (1 H, m, H-4^{II}), 3.23 – 3.10 (2 H, m, H_AH_B-2^{II}), 2.40 (3 H, s, H-7), 2.26 (3 H, s, H-6), 2.16 – 2.08 (2 H, m, H_AH_B-3^{II}), 1.68 – 1.58 (2 H, m, H_AH_B-3^{II}); ^{13}C NMR (151 MHz, $CDCl_3$) δ_C 165.6 (C-5), 158.7 (C-3), 155.2 (C-4^{III}), 143.5 (C-1^{I}), 137.0 (C-5^{I}), 133.1 (C-2^{III}), 132.2 (C-2^{I}), 127.5 (C-3^{I}), 117.9 (C-4^{I}), 117.8 (C-1^{III}), 114.9 (C-4), 114.7 (C-6^{I}), 66.4 (C-3^{III}), 49.4 (C-4^{II}), 42.4 (C-2^{II}), 31.9 (C-3^{II}), 11.7 (C-7), 10.9 (C-6); HRMS *m/z* (ESI$^-$) 399.1695 (399.1674 calculated for $[C_{20}H_{23}N_4O_5]^-$); LRMS (ESI$^+$) *m/z* 399 ([M−H]$^-$, 100%); HPLC (Method 3) t_R 10.2 min, purity 94.5%.

Prop-2-en-1-yl 4-{[2-amino-4-(3,5-dimethyl-1,2-oxazol-4-yl)phenyl]amino}piperidine-1-carboxylate (96)

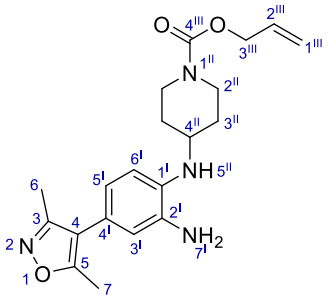

To an orange solution of prop-2-en-1-yl 4-{[4-(3,5-dimethyl-1,2-oxazol-4-yl)-2-nitrophenyl]amino}piperidine-1-carboxylate (**95**) (1.35 g, 3.37 mmol, 1.0 eq.) in 1:1 EtOAc/ H_2O (62 mL) was added $Na_2S_2O_4$ (4.62 g, 27.0 mmol, 8.0 eq.) and the resulting suspension was stirred at 80 °C for 5 h. The reaction mixture was concentrated *in vacuo*, 10% aq. NH_3 (200 mL) was added to the residue, and the aqueous component was extracted with EtOAc (3 × 200 mL). The combined organic components were dried (Na_2SO_4), filtered, and concentrated *in vacuo*. The crude solid was purified using normal phase column chromatography (gradient of 0 – 100% EtOAc in petroleum ether) to afford prop-2-en-1-yl 4-{[2-amino-4-(3,5-dimethyl-1,2-oxazol-4-yl)phenyl]amino}piperidine-1-carboxylate (**96**) (898 mg, 2.42 mmol, 72%) as a colourless oil: R_f 0.40

(petroleum ether/ EtOAc 1:4); ῡmax (thin film)/ cm^{-1} 3388 (w, br, N-H), 3269 (N-H, w, br), 2946 (C-H, w), 2861 (C-H, w), 1686 (C=O, s), 1525 (N-O, m); ^{1}H NMR (600 MHz, $CDCl_3$) δ_H 6.71 (1 H, d, *J* 8.0, H-6^{I}), 6.68 (1 H, dd, *J* 8.0, 1.9, H-5^{I}), 6.61 (1 H, d, *J* 1.9, H-3^{I}), 6.01 – 5.91 (1 H, m, H-2^{III}), 5.31 (1 H, d, *J* 17.2, H_AH_B-1^{III}), 5.22 (1 H, d, *J* 10.4, H_AH_B-1^{III}), 4.61 (2 H, d, *J* 5.4, H-3^{III}), 4.19 – 4.06 (2 H, m, H_AH_B-2^{II}), 3.46 (1 H, p, *J* 6.1, H-4^{II}), 3.40 (2 H, br s, NH-7^{I}), 3.30 (1 H, br s, NH-5^{II}), 3.11 – 3.02 (2 H, m, H_AH_B-2^{II}), 2.38 (3 H, s, H-7), 2.25 (3 H, s, H-6), 2.09 (2 H, d, *J* 11.8, H_AH_B-3^{II}), 1.51 – 1.41 (2 H, m, H_AH_B-3^{II}); ^{13}C NMR (151 MHz, $CDCl_3$) δ_C 164.7 (C-5), 159.1 (C-3), 155.3 (C-4^{III}), 135.6 (C-2^{I}), 135.0 (C-1^{I}), 133.3 (C-2^{III}), 121.7 (C-5^{I}), 121.0 (C-4^{I}), 117.7 (C-3^{I}), 117.5 (C-1^{III}), 116.8 (C-4), 113.2 (C-6^{I}), 66.2 (C-3^{III}), 50.1 (C-4^{II}), 42.8 (C-2^{II}), 32.6 (C-3^{II}), 11.7 (C-7), 11.0 (C-6); HRMS *m/z* (ESI^+) 371.2094 (371.2078 calculated for $[C_{20}H_{27}N_4O_3]^+$); LRMS (ESI^+) *m/z* 371 ($[M+H]^+$, 100%); HPLC (Method 3) t_R 7.88 min, purity 96.9%.

Prop-2-en-1-yl 4-[5-(3,5-dimethyl-1,2-oxazol-4-yl)-2-[(2*S*)-6-oxopiperidin-2-yl]-1*H*-1,3-benzodiazol-1-yl]piperidine-1-carboxylate (98)

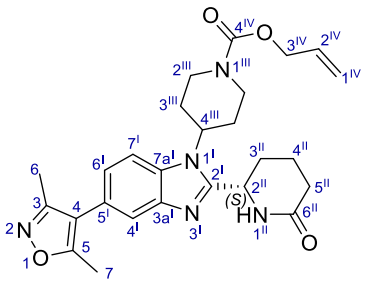

Step I:

A solution of (*S*)-6-oxo-2-piperidine carboxylic acid (415 mg, 2.90 mmol, 1.2 eq.), HATU (1.47 g, 3.87 mmol, 1.6 eq.), and DIPEA (817 µL, 4.84 mmol, 2.0 eq.) in DMF (20 mL) was stirred at rt for 30 min before the addition of a solution of prop-2-en-1-yl 4-{[2-amino-4-(3,5-dimethyl-1,2-oxazol-4-yl)phenyl]amino}piperidine-1-carboxylate (**96**) (895 mg, 2.42 mmol, 1.0 eq.) in DMF (4.0 mL). The reaction mixture was stirred at rt for 18 h before being concentrated *in vacuo*. Brine (100 mL) was added, and the aqueous component was extracted with EtOAc (3 × 100 mL). The combined organic components were washed with brine (200 mL), dried (Na_2SO_4), filtered, and concentrated *in vacuo* to

afford the amide intermediate (**97**) as a brown solid.

Step II:

The amide intermediate was dissolved in acetic acid (24 mL) and heated at reflux for 72 h. The reaction mixture was cooled to rt and concentrated *in vacuo*. Sat. aq. $NaHCO_3$ (200 mL) was added, and the aqueous component was extracted with EtOAc (3 × 100 mL). The combined organic components were washed with brine (400 mL), dried (Na_2SO_4), filtered, and concentrated *in vacuo.* The crude brown oil was purified using reverse phase column chromatography (gradient of 95 – 5% H_2O in MeCN) to afford prop-2-en-1-yl 4-[5-(3,5-dimethyl-1,2-oxazol-4-yl)-2-[(2*S*)-6-oxopiperidin-2-yl]-1*H*-1,3-benzodiazol-1-yl]piperidine-1-carboxylate (**98**) (486 mg, 1.02 mmol, 42%) as a cream solid: R_f 0.17 (acetone); mp 128 – 131 °C (H_2O); $[\alpha]_D^{25} = -0.6$ (*c* 1.0, $CHCl_3$); ῡmax (thin film)/ cm^{-1} 3505 (N-H, w, br), 3254 (N-H, w, br), 2951 (C-H, m), 2872 (C-H, w), 1694 (C=O, s), 1653 (C=N, s), 1508 (N-O, s); ^{1}H NMR (600 MHz, $CDCl_3$) δ_H 7.68 (1 H, d, *J* 1.8, H-4^{I}), 7.57 (1 H, d, *J* 8.5, H-7^{I}), 7.16 (1 H, dd, *J* 8.5, 1.8, H-6^{I}), 6.69 (1 H, br s, H-1^{II}), 6.04 – 5.94 (1 H, m, H-2^{IV}), 5.36 (1 H, dq, *J* 17.2, 1.5, H_AH_B-1^{IV}), 5.27 (1 H, dq, *J* 10.5, 1.5, H_AH_B-1^{IV}), 5.18 – 5.07 (1 H, m, H-2^{II}), 4.67 (2 H, d, *J* 5.6, H-3^{IV}), 4.58 – 4.38 (3 H, m, H_AH_B-2^{III}, H-4^{III}), 3.07 – 2.92 (2 H, m, H_AH_B-2^{III}), 2.57 – 2.47 (4 H, m, H-5^{II}, H_AH_B-3^{III}), 2.41 (3 H, s, H-7), 2.30 – 2.23 (4 H, m, H-6, H_AH_B-3^{II}), 2.15 – 1.91 (5 H, m, H_AH_B-3^{II}, H-4^{II}, H_AH_B-3^{III}); ^{13}C NMR (151 MHz, $CDCl_3$) δ_C 171.9 (C-6^{II}), 165.5 (C-5), 158.9 (C-3), 155.1 (C-4^{IV}), 153.4 (C-2^{I}), 132.9 (C-1^{IV}), 124.8 (C-6^{I}), 120.6 (C-4^{I}), 118.1 (C-2^{IV}), 116.6 (C-4), 112.9 (C-7^{I}), 66.7 (C-3^{IV}), 55.1 (C-4^{III}), 51.0 (C-2^{II}), 43.7 (C-2^{III}), 31.4 (C-5^{II}), 30.6 (C-3^{III}), 30.5 (C-5^{II}), 28.8 (C-3^{II}), 19.8 (C-4^{II}), 11.7 (C-7), 11.0 (C-6); HRMS *m/z* (ESI$^+$) 478.2462 (478.2449 calculated for $[C_{26}H_{31}N_5O_4]^+$); LRMS (ESI$^+$) *m/z* 478 ($[M+H]^+$, 100%); HPLC (Method 3) t_R 7.3 min, purity 94.7%.

Prop-2-en-1-yl 4-{2-[(2*S*)-1-(3,4-difluorophenyl)-6-oxopiperidin-2-yl]-5-(3,5-dimethyl-1,2-oxazol-4-yl)-1*H*-1,3-benzodiazol-1-yl}piperidine-1-carboxylate (99)

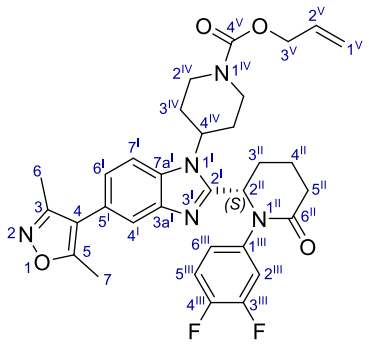

Method I:

A solution of prop-2-en-1-yl 4-[5-(3,5-dimethyl-1,2-oxazol-4-yl)-2-[(2*S*)-6-oxopiperidin-2-yl]-1*H*-1,3-benzodiazol-1-yl]piperidine-1-carboxylate (**98**) (384 mg, 0.804 mmol, 1.0 eq.) and DBU (265 µL, 1.77 mmol, 2.2 eq.) in anhydrous CH_2Cl_2 (26 mL) was stirred at rt for 10 min with 3 Å molecular sieves and a drying tube containing P_2O_5. Cu-TMEDA (75 mg, 0.161 mmol, 0.20 eq.) was added and the reaction mixture was stirred at rt for 10 min before the addition of (3,4-difluorophenyl)boronic acid (254 mg, 1.61 mmol, 2.0 eq.) and the reaction mixture was stirred at rt for a further 18 h. Sat. aq. $NaHCO_3$ (100 mL) was added and the aqueous component was extracted with CH_2Cl_2 (3 × 100 mL). The combined organic components were dried (Na_2SO_4), filtered, and concentrated *in vacuo*. The crude residue was purified using reverse phase column chromatography (gradient of 95 – 5% H_2O in MeCN) then using normal phase column chromatography (gradient of 0 – 30% acetone in EtOAc) to afford prop-2-en-1-yl 4-{2-[(2*S*)-1-(3,4-difluorophenyl)-6-oxopiperidin-2-yl]-5-(3,5-dimethyl-1,2-oxazol-4-yl)-1*H*-1,3-benzodiazol-1-yl}piperidine-1-carboxylate (**99**) (121 mg, 0.205 mmol, 26%) as a yellow oil: R_f 0.17 (EtOAc/ acetone 4:1); $[\alpha]_D^{25} = -0.9$ (*c* 1.0, $CHCl_3$); ῡmax (thin film)/ cm^{-1} 3658 (N-H, w, br), 2981 (C-H, s), 2888 (C-H, m), 1699 (C=O, s), 1651 (C=N, s); ^{1}H NMR (600 MHz, $CDCl_3$) δ_H 7.68 (1 H, d, *J* 1.9, H-4^{I}), 7.45 (1 H, d, *J* 8.4, H-7^{I}), 7.16 – 7.08 (2 H, m, H-6^{I}, H-5^{III}), 7.04 (1 H, q, *J* 9.2, H-2^{III}), 6.99 – 6.94 (1 H, m, H-6^{III}), 6.02 – 5.92 (1 H, m, H-2^{V}), 5.34 (1 H, dq, *J* 17.2, 1.6, H_AH_B-1^{V}), 5.28 – 5.24 (2 H, m, H-2^{II}, H_AH_B-1^{V}), 4.65 (2 H, dt, *J* 5.8, 1.6, H-3^{V}), 4.50 – 4.31 (2 H, m, H_AH_B-2^{IV}), 4.21 – 4.13 (1 H, m, H-4^{IV}), 2.98 – 2.78 (3 H, m, H_AH_B-4^{II}, H_AH_B-2^{IV}), 2.70 – 2.61 (1 H, m, H_AH_B-4^{II}), 2.47 – 2.37

(5 H, m, H-7, H_AH_B-3^{II}), 2.36 – 2.29 (5 H, m, H-6, H_AH_B-3^{IV}), 2.29 – 2.23 (1 H, m, H_AH_B-5^{II}), 2.23 – 2.14 (1 H, m, H_AH-$_B$-3^{II}), 1.95 – 1.86 (1 H, m, H_AH_B-5^{II}), 1.84 – 1.77 (2 H, m, H_AH_B-3^{IV}); ^{13}C NMR (151 MHz, $CDCl_3$) δ_C 170.9 (C-6^{II}), 165.3 (C-5), 159.0 (C-3), 155.0 (C-4^{V}), 152.4 (C-2^{I}), 150.7 (dd, *J* 93.8, 13.0, C-3^{III}), 149.03 (dd, *J* 93.2, 13.0, C-4^{III}), 143.4 (C-$3a^{I}$), 138.6 (dd, *J* 7.6, 3.6, C-1^{III}), 132.84 (C-2^{V}), 132.8 (C-$7a^{I}$), 124.9 (C-5^{I}), 124.3 (C-6^{III}), 124.1 (C-6^{I}), 121.2 (C-4^{I}), 118.1 (C-1^{V}), 117.95 (d, *J* 18.1, C-5^{III}), 117.55 (d, *J* 18.0, C-2^{III}), 116.8 (C-4), 112.4 (C-7^{I}), 66.7 (C-3^{V}), 57.9 (C-2^{II}), 54.6 (C-4^{IV}), 43.68 (C-2^{IV}), 43.64 (C-2^{IV}), 32.5 (C-4^{II}), 30.56 (C-3^{IV}), 29.8 (C-3^{II}), 11.8 (C-7), 11.0 (C-6); ^{19}F NMR (565 MHz, $CDCl_3$) δ_F −135.18 (dt, *J* 21.3, 9.2, F-3^{III}), −138.01 (d, *J* 21.3, F-4^{III}); HRMS *m/z* (ESI^+) 590.2601 (590.2673 calculated for $[C_{32}H_{33}F_2N_5O_4]^+$); LRMS ($ESI^+$) *m/z* 590 ($[M+H]^+$, 100%); HPLC (Method 3) t_R 9.0 min, purity 99.5%.

Method II:

A suspension of prop-2-en-1-yl 4-[5-(3,5-dimethyl-1,2-oxazol-4-yl)-2-[(2*S*)-6-oxopiperidin-2-yl]-1*H*-1,3-benzodiazol-1-yl]piperidine-1-carboxylate (**98**) (1.66 g, 3.48 mmol, 1.0 eq.), (3,4-difluorophenyl)boronic acid (1.10 g, 6.95 mmol, 2.0 eq.), Cu-TMEDA (323 mg, 0.695 mmol, 0.20 eq.), and DBU (1.15 mL, 7.65 mmol, 2.2 eq.) in anhydrous CH_2Cl_2 (112 mL) with 3 Å molecular sieves was stirred at rt for 4.5 h. Further Cu-TMEDA (323 mg, 0.695 mmol, 0.20 eq.) was added and the reaction mixture was stirred at rt for 18 h. Further (3,4-difluorophenyl)boronic acid (549 mg, 3.48 mmol, 1.0 eq.) and Cu-TMEDA (323 mg, 0.695 mmol, 0.20 eq.) were added and the reaction mixture was stirred at rt for a further 23 h before the further addition of DBU (1.05 mL, 6.95 mmol, 2.0 eq.) and Cu-TMEDA (323 mg, 0.695 mmol, 0.20 eq.) were added and the reaction mixture was stirred at rt for 4.5 h. The reaction mixture was added to brine (100 mL), the phases were separated, and the aqueous component was extracted with CH_2Cl_2 (2 × 100 mL). The combined organic components were filtered through an Isolute® Phase Separator and the filtrate was concentrated *in vacuo*. The crude product was purified using normal phase column chromatography (gradient of 0 – 100% (1:3 EtOH/ EtOAc) in EtOAc) to afford prop-2-en-1-yl 4-{2-[(2*S*)-1-(3,4-difluorophenyl)-6-oxopiperidin-2-yl]-5-(3,5-dimethyl-1,2-oxazol-4-yl)-1*H*-1,3-benzodiazol-1-yl}piperidine-1-carboxylate (**99**) (1.44 g, 2.13 mmol, 61%) as a yellow oil: **LCMS** (formic acid): t_R 1.08 min, *m/z* 590.1 $[M+H]^+$, purity 87%.

(6*S*)-1-(3,4-Difluorophenyl)-6-[5-(3,5-dimethyl-1,2-oxazol-4-yl)-1-(piperidin-4-yl)-1*H*-1,3-benzodiazol-2-yl]piperidin-2-one (87)

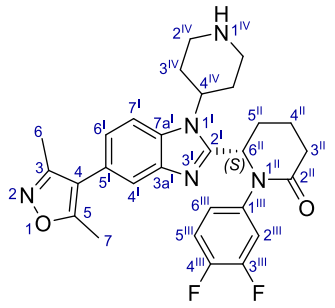

Method 1:

A suspension of allyl (*S*)-4-(2-(1-(3,4-difluorophenyl)-6-oxopiperidin-2-yl)-5-(3,5-dimethylisoxazol-4-yl)-1*H*-benzo[d]imidazol-1-yl)piperidine-1-carboxylate (**99**) (399 mg, 0.677 mmol, 1.0 eq.) and K_2CO_3 (560 mg, 4.05 mmol 6.0 eq.) in MeOH (6.8 mL) was purged with N_2 before the addition of $(PPh_3)_4Pd^0$ (16.0 mg, 13.8 μmol, 0.02 eq.). The reaction mixture purged with N_2 and stirred at rt under an atmosphere of N_2 for 2.5 h. The reaction mixture was concentrated under a flow of N_2. To the solid residue was added sat. aq. $NaHCO_3$ (100 mL) and the aqueous component was extracted with CH_2Cl_2 (3 × 100 mL). The combined organic components were filtered through an Isolute® Phase Separator and the filtrate was concentrated *in vacuo*. The crude product was purified using cation exchange chromatography with a Biotage® Isolute® SCX SPE column (washed: MeOH (5 CV), elution: 4 M NH_3 in MeOH (5 CV)). The filtrate was concentrated *in vacuo* and the crude product was repurified using preparative reverse phase column chromatography (gradient of 20 – 55% MeCN in 10 mM aq. $(NH_4)HCO_3$ (pH 10)) to afford (*S*)-1-(3,4-difluorophenyl)-6-(5-(3,5-dimethylisoxazol-4-yl)-1-(piperidin-4-yl)-1*H*-benzo[d]imidazol-2-yl)piperidin-2-one (**87**) (54.5 mg, 0.108 mmol, 15%) as a yellow solid: ^{1}H NMR (600 MHz, $CDCl_3$) δ_H 7.68 (1 H, d, *J* 1.7, H-4^{I}), 7.67 – 7.64 (1 H, m, H-7^{I}), 7.15 (1 H, ddd, *J* 10.7, 7.1, 2.4, H-2^{III}), 7.10 (1 H, dd, *J* 8.4, 1.7, H-6^{I}), 7.03 (1 H, dd, *J* 18.2, 8.8, H-5^{III}), 6.97 (1 H, d, *J* 8.8, H-6^{III}), 5.31 (1 H, t, *J* 5.2, H-6^{II}), 4.21 – 4.13 (1 H, m, H-4^{IV}), 3.36 (1 H, d, *J* 12.4, $H_AH_BH_CH_D$-3^{IV}), 3.30 (1 H, d, *J* 12.4, $H_AH_BH_CH_D$-3^{IV}), 2.91 – 2.81 (2 H, m, H_AH_B-4^{II}, $H_AH_BH_CH_D$-3^{IV}), 2.76 (1 H, t, *J* 12.4, $H_AH_BH_CH_D$-3^{IV}), 2.71 – 2.61 (1 H, m, H_AH_B-4^{II}), 2.56 – 2.46 (2 H, m, $H_AH_BH_CH_D$-3^{IV}), 2.46 – 2.37 (4 H, m, H-7, H_AH_B-5^{II}), 2.36 – 2.23 (4 H, m, H-6, H_AH_B-3^{II}), 2.23 – 2.16

(2 H, m, H_AH_B-5^{II}), 1.97 – 1.88 (1 H, m, H_AH_B-3^{II}), 1.78 (1 H, d, *J* 13.2, $H_AH_BH_CH_D$-3^{IV}), 1.36 (1 H, d, *J* 12.8, $H_AH_BH_CH_D$-3^{IV}); ^{13}C NMR (151 MHz, $CDCl_3$) δ_C 171.0 (C-3^{II}), 165.3 (C-5), 159.0 (C-3), 150.67 (dd, *J* 95.5, 13.0, C-3^{III}), 149.02 (dd, *J* 94.9, 13.0, C-4^{III}), 138.59 (dd, *J* 7.6, 3.7, C-1^{III}), 133.0 (C-$7a^{I}$), 132.18 (C-$3a^{I}$), 124.8 (C-5^{I}), 124.45 (C-6^{III}), 124.1 (C-6^{I}), 121.1 (C-4^{I}), 118.00 (d, *J* 18.0, C-2^{III}), 117.50 (d, *J* 18.0, C-5^{III}), 116.8 (C-4), 112.5 (C-7^{I}), 57.9 (C-6^{II}), 54.3 (C-4^{IV}), 46.0 (C-2^{IV}), 32.6 (C-4^{II}), 31.0 (C-3^{IV}), 29.8 (C-5^{II}), 18.3 (C-3^{II}), 11.8 (C-7), 11.05 (C-6); ^{19}F NMR (565 MHz, $CDCl_3$) δ_F 135.39 (1 F, dd, *J* 21.5, 10.7, F-3^{III}), 138.22 (1 F, d, *J* 21.5, F-4^{III}); **LCMS** (HpH): t_R 0.85 min, *m/z* 506.1 $[M+H]^+$, purity 96%.

Method 2:

A suspension of (*S*)-4-(2-(1-(3,4-difluorophenyl)-6-oxopiperidin-2-yl)-5-(3,5-dimethylisoxazol-4-yl)-1*H*-benzo[d]imidazol-1-yl)piperidine-1-carboxylate (**99**) (200 mg, 0.339 mmol, 1.0 eq.) and K_2CO_3 (281 mg, 2.03 mmol 6.0 eq.) in MeOH (3.4 mL) was purged with N_2 before the addition of $(PPh_3)_4Pd^0$ (7.8 mg, 6.8 μmol, 0.02 eq.).The reaction mixture was purged with N_2 before being stirred at rt under an atmosphere of N_2 for 1.5 h. The reaction mixture was filtered, the solid was washed with MeOH (2 mL), and the filtrate was directly purified using cation exchange chromatography with a Biotage® Isolute SCX-2 column (washed with MeOH (5 CV), elution with 4 M NH_3 in MeOH (5 CV)). The filtrate was concentrated *in vacuo* to afford (*S*)-1-(3,4-difluorophenyl)-6-(5-(3,5-dimethylisoxazol-4-yl)-1-(piperidin-4-yl)-1*H*-benzo[d]imidazol-2-yl)piperidin-2-one (**87**) (139 mg, 0.223 mmol, 66%) as a yellow solid: physical data as for Method 1; LCMS (formic acid): t_R 0.57 min, *m/z* 506.2 $[M+H]^+$, purity 81%.

***tert*-Butyl *N*-[(2*S*)-1-{[4-(3,5-dimethyl-1,2-oxazol-4-yl)-2-nitrophenyl]amino}propan-2-yl]carbamate (101)**

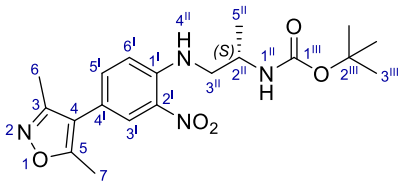

A yellow solution of 4-(4-fluoro-3-nitrophenyl)-3,5-dimethyl-1,2-oxazole (**93**) (129 mg, 0.478 mmol, 1.0 eq.), (*S*)-*tert*-butyl-1-aminopropan-2-carbamate (100 mg, 0.574 mmol, 1.2 eq.), and DIPEA (242 µL, 1.43 mmol, 3.0 eq.) in MeCN (8.7 mL) was stirred at 80 °C for 18 h. The orange solution was concentrated *in vacuo* and directly purified using normal phase column chromatography (gradient of 0 – 40% EtOAc in petroleum ether) to afford *tert*-butyl *N*-[(2*S*)-1-{[4-(3,5-dimethyl-1,2-oxazol-4-yl)-2-nitrophenyl]amino}propan-2-yl]carbamate (**101**) (173 mg, 0.443 mmol, 93%) as an orange oil: R_f 0.30 (7:3 petroleum ether/ EtOAc); $[\alpha]_D^{25} = +12.9$ (*c* 1.0, $CHCl_3$); ῡmax (thin film)/ cm^{-1} 3651 (N-H, w, br), 3369 (N-H, w, br), 2981 (C-H, s), 2889 (C-H, m), 1704 (C=O, s), 1622 (C=N, s), 1564 (N-O, s), 1530 (N-O, s); ^{1}H NMR (600 MHz, $CDCl_3$) δ_H 8.32 (1 H, br s, NH-1^{II}), 8.07 (1 H, d, *J* 2.2, H-3^{I}), 7.35 (1 H, dd, *J* 8.9, 2.2, H-5^{I}), 7.14 (1 H, d, *J* 8.9, H-6^{I}), 4.51 (1 H, br s, NH-4^{II}), 4.01 (1 H, p, *J* 6.8, H-2^{II}), 3.53 – 3.45 (1 H, m, H_AH_B-3^{II}), 3.39 – 3.32 (1 H, m, H_AH_B-3^{II}), 2.40 (3 H, s, H-7), 2.26 (3 H, s, H-6), 1.46 (9 H, s, H-3^{III}), 1.28 (3 H, d, *J* 6.8, H-5^{II}); ^{13}C NMR (151 MHz, $CDCl_3$) δ_C 165.5 (C-5), 158.7 (C-3), 155.6 (C-1^{III}), 144.9 (C-1^{I}), 137.1 (C-5^{I}), 132.2 (C-2^{I}), 127.1 (C-3^{I}), 117.9 (C-4^{I}), 115.0 (C-6^{I}), 114.9 (C-4), 80.1 (C-2^{III}), 48.6 (C-3^{II}), 45.6 (C-2^{II}), 28.5 (C-3^{III}), 18.7 (C-5^{II}), 11.7 (C-7), 10.9 (C-6); HRMS *m/z* (ESI$^+$) 391.1984 (391.1976 calculated for $[C_{19}H_{27}N_4O_5]^+$); LRMS (ESI$^+$) *m/z* 391 ($[M+H]^+$, 100%); HPLC (Method 3) t_R 10.1 min, purity 96.2%.

2-{Benzyl[2-(benzyloxy)ethyl]amino}ethan-1-ol (105)

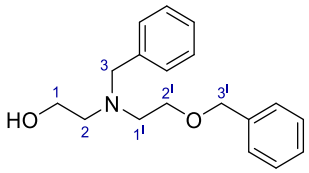

A solution of benzyloxy acetaldehyde (1.26 mL, 9.00 mmol, 1.0 eq.) and 2-benzylaminoethanol (1.28 mL, 9.00 mmol, 1.0 eq.) in anhydrous 1,2-dichloroethane (60 mL) was stirred at rt for 30 min before being cooled to 0 °C and sodium tris(acetoxy)borohydride (2.67 g, 12.6 mmol, 1.4 eq.) was added portion-wise. The reaction mixture was stirred at rt for 2 h before being cooled to 0 °C and sat. aq. $NaHCO_3$ (60 mL) was added. The components were separated, and the aqueous component was

extracted with CH_2Cl_2 (2 × 60 mL). The combined organic components were dried (Na_2SO_4), filtered, and concentrated *in vacuo*. The crude yellow oil was purified using normal phase column chromatography (gradient of 0 – 100% EtOAc in petroleum ether) to afford 2-{benzyl[2-(benzyloxy)ethyl]amino}ethan-1-ol (**105**) (2.17 g, 7.60 mmol, 84%) as a colourless oil: R_f 0.22 (7:3 PE/EtOAc); ῡmax (thin film)/ cm^{-1} 3434 (O-H, w, br), 2980 (C-H, m), 2883 (C-H, m); ^{1}H NMR (600 MHz, $CDCl_3$) δ_H 7.37 – 7.23 (10 H, m, Ar-H), 4.49 (2 H, s, H-3^I), 3.71 (2 H, s, H-3), 3.57 – 3.53 (4 H, m, H-1, H-2^I), 3.11 (1 H, br s, OH), 2.78 (2 H, t, *J* 5.6, H-1^I), 2.73 (2 H, t, *J* 5.3, H-2); ^{13}C NMR (151 MHz, $CDCl_3$) δ_C 139.2 (Ar-C), 138.3 (Ar-C), 129.0 (Ar-C), 128.6 (Ar-C), 128.5 (Ar-C), 127.8 (Ar-C), 127.8 (Ar-C), 127.3 (Ar-C), 73.2 (C-3^I), 68.8 (C-2^I), 59.5 (C-3), 59.2 (C-1), 56.0 (C-2), 53.2 (C-1^I); HRMS *m/z* (ESI$^+$) 308.1621 (308.1621 calculated for $[C_{18}H_{23}NO_2Na]^+$); LRMS (ESI$^+$) *m/z* 286 ($[M+H]^+$, 100%); HPLC - poor chromophore.

2-[Benzyl(2-hydroxyethyl)amino]ethan-1-ol (104)

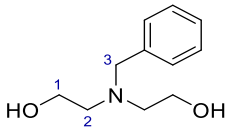

Four reactions of equal same scale performed separately then combined for work up and purification. A solution of 2-{benzyl[2-(benzyloxy)ethyl]amino}ethan-1-ol (**105**) (150 mg, 0.525 mmol, 1.0 eq.) and triphenylphosphine hydrobromide (378 mg, 1.10 mmol, 2.1 eq.) in anhydrous acetonitrile (600 µL) was stirred at 100 °C for 1 h. The combined reaction mixtures were concentred *in vacuo* and the residue was dissolved in 1 M aq. HCl (15 mL). To remove excess triphenylphosphine, the aqueous component was washed with EtOAc (2 × 15 mL) before being adjusted to pH 14 using 2 M aq. NaOH. The aqueous component was extracted with EtOAc (3 × 20 mL) and the combined organic components were dried (Na_2SO_4), filtered, and concentrated *in vacuo*. The crude oil was purified using normal phase column chromatography (gradient of 0 – 100% EtOAc in petroleum ether) to afford 2-[benzyl(2-hydroxyethyl)amino]ethan-1-ol (**104**) (185 mg, 0.948 mmol, 45%) as a yellow oil: R_f 0.19 (EtOAc); ῡmax (thin film)/ cm^{-1} 3451 (O-H, m, br), 2949 (C-H, m), 2870 (C-H, m), 1583 (C=C,

m), 737 (C-H, s), 700 (C-H, s); ^{1}H NMR (400 MHz, $CDCl_3$) δ_H 7.36 – 7.23 (5 H, m, Ar-H), 3.71 (2 H, s, H-3), 3.65 – 3.59 (4 H, t, *J* 5.4, H-1), 2.72 (4 H, t, *J* 5.4, H-2), 2.55 (2 H, br s, OH); LRMS (ESI^+) *m/z* 413 ($[2M+Na]^+$, 100%). These data are in good accordance with the literature.[221]

_N_-[(2_S_)-2-(4-Benzylpiperazin-1-yl)propyl]-4-(3,5-dimethyl-1,2-oxazol-4-yl)-2-nitroaniline (102)

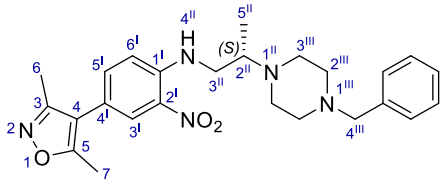

Step I:

To a solution of *tert*-butyl *N*-[(2*S*)-1-{[4-(3,5-dimethyl-1,2-oxazol-4-yl)-2-nitrophenyl]amino}propan-2-yl]carbamate (**101**) (179 mg, 0.453 mmol, 1.0 eq.) in CH_2Cl_2 (2.0 mL) was added 4 M HCl in 1,4-dioxane (1.13 mL, 4.53 mmol, 10 eq.). The reaction mixture was stirred at rt for 3 h before being concentrated *in vacuo* to afford (2*S*)-*N*1-[4-(3,5-dimethyl-1,2-oxazol-4-yl)-2-nitrophenyl]propane-1,2-diamine hydrochloride (**103**) as a colourless solid which was used without purification.

Step II.I:

Thionyl chloride (34 µL, 0.461 mmol, 3.0 eq.) was added dropwise to a solution of 2-[benzyl(2-hydroxyethyl)amino]ethan-1-ol (**104**) (30 mg, 0.154 mmol, 1.0 eq.) in anhydrous CH_2Cl_2 (500 µL) at 0 °C. The reaction mixture was stirred at rt for 3 h before being concentrated *in vacuo* to afford the benzylbis(2-chloroethyl)amine hydrochloride intermediate as a colourless solid.

Step II.II:

To the benzylbis(2-chloroethyl)amine hydrochloride intermediate was added (2*S*)-*N*1-[4-(3,5-dimethyl-1,2-oxazol-4-yl)-2-nitrophenyl]propane-1,2-diamine hydrochloride (**103**) (55 mg, 0.169 mmol, 1.1 eq), TBAI (11 mg, 0.031 mmol, 0.2 eq.), DIPEA (134 µL, 0.770 mmol, 5.0 eq.), and anhydrous EtOH (2.0 mL) and the reaction mixture was stirred at 80 °C for 40 h. The reaction mixture was directly purified by reverse phase column chromatography (gradient of 95 – 5% H_2O in MeCN) to afford *N*-[(2*S*)-2-(4-Benzylpiperazin-1-yl)propyl]-4-(3,5-dimethyl-1,2-oxazol-4-yl)-2-nitroaniline

(**102**) (32 mg, 0.072 mmol, 42%) as an orange amorphous solid: ^{1}H NMR (600 MHz, $CDCl_3$) δ_H 8.83 (1 H, br d, *J* 6.1, NH-4^{II}), 8.09 (1 H, d, *J* 2.2, H-3^{I}), 7.34 – 7.29 (5 H, m, H-5^{I}, Ar-*H*), 7.26 – 7.22 (1 H, m, Ar-*H*), 6.88 (1 H, d, *J* 8.8, H-6^{I}), 3.53 (2 H, s, H-4^{III}), 3.31 – 3.26 (1 H, m, H_AH_B-3^{II}), 3.13 – 3.08 (1 H, m, H_AH_B-3^{II}), 3.08 – 3.01 (1 H, m, H-2^{II}), 2.71 – 2.48 (8 H, m, H-2^{III}, H-3^{III}), 2.40 (3 H, s, H-7), 2.26 (3 H, s, H-6), 1.10 (3 H, d, *J* 6.4, H-5^{II}); ^{13}C NMR (151 MHz, $CDCl_3$) δ_C 165.4 (C-5), 158.8 (C-3), 144.4 (C-1^{I}), 138.5 (Ar), 136.7 (C-5^{I}), 131.9 (C-2^{I}), 129.4 (Ar), 128.3 (Ar), 127.16 (C-3^{I}), 127.12 (Ar) 117.0 (C-4^{I}), 115.14 (C-6^{I}), 115.10 (C-4), 63.2 (C-4^{III}), 57.2 (C-2^{II}), 54.0 (C-2^{III}/ C-3^{III}), 53.7 (C-2^{III}/ C-3^{III}), 45.7 (C-3^{II}), 11.7 (C-5^{II}), 11.5 (C-7), 10.9 (C-6); LRMS (ESI^{+}) *m/z* 450 ([M+H]$^{+}$, 100%).

tert-Butyl 4-(2-{[4-(3,5-dimethyl-1,2-oxazol-4-yl)-2-nitrophenyl]amino}ethyl)piperazine-1-carboxylate (107)

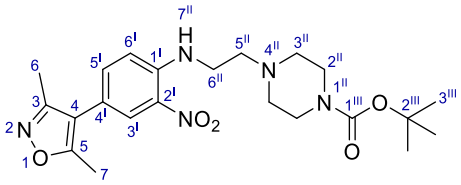

A yellow solution of 4-(4-fluoro-3-nitrophenyl)-3,5-dimethyl-1,2-oxazole (1.27 g, 4.70 mmol, 1.0 eq.), *tert*-butyl 4-(2-aminoethyl)piperazine-1-carboxylate (1.19 g, 5.17 mmol, 1.1 eq.), and DIPEA (2.38 mL, 14.1 mmol, 3.0 eq.) in MeCN (78 mL) was stirred at 80 °C for 18 h. The orange solution was concentrated *in vacuo* and directly purified by normal phase column chromatography (elution with a gradient of 0 – 50% EtOAc in PE) to afford *tert*-butyl 4-(2-{[4-(3,5-dimethyl-1,2-oxazol-4-yl)-2-nitrophenyl]amino}ethyl)piperazine-1-carboxylate (**107**) (1.79 g, 4.02 mmol, 85%) as an orange foam: R_f 0.13 (3:2 petroleum ether/ EtOAc); ῡmax (thin film)/ cm^{-1} 3348 (N-H, w, br), 2929 (C-H, w), 2862 (C-H, w), 2819 (C-H, w), 1694 (C=O, s), 1622 (C=C, m), 1558 (N=O, m); ^{1}H NMR (500 MHz, $CDCl_3$) δ_H 8.58 (1 H, br t, *J* 4.7, NH-7^{II}), 8.08 (1 H, d, *J* 2.2, H-3^{I}), 7.34 (1 H, dd, *J* 8.8, 2.2, H-5^{I}), 6.91 (1 H, d, *J* 8.8, H-6^{I}), 3.49 (4 H, t, *J* 5.1, H-2^{II}), 3.41 (2 H, dt, *J* 6.1, 4,7, H-6^{II}), 2.76 (2 H, t, *J* 6.1, H-5^{II}), 2.48 (4 H, t, *J* 5.1, H-3^{II}), 2.40 (3 H, s, H-7), 2.26 (3 H, s, H-6), 1.46 (9 H, s, H-3^{III}); ^{13}C NMR (151 MHz, $CDCl_3$) δ_C 165.5 (C-3), 158.7 (C-5), 154.9 (C-1^{III}), 144.5 (C-1^{I}), 136.9 (C-5^{I}),

132.1 (C-2^{I}), 127.2 (C-3^{I}), 117.4 (C-4^{I}), 115.1 (C-4), 114.8 (C-6^{I}), 79.9 (C-2^{III}), 55.7 (C-5^{II}), 52.6 (C-3^{II}), 43.3 (C-2^{II}), 39.8 (C-6^{II}), 28.6 (C-3^{III}), 11.7 (C-7), 10.9 (C-6); HRMS *m/z* (ESI^+) 446.2405 (446.2398 calculated for $[C_{22}H_{32}N_5O_5]^+$); LRMS (ESI^+) *m/z* 446 ($[M+H]^+$, 100%); HPLC (Method 3) t_R 7.3 min, purity 98.5%.

***tert*-Butyl 4-(2-{[2-amino-4-(3,5-dimethyl-1,2-oxazol-4-yl)phenyl]amino}ethyl)piperazine-1-carboxylate (108)**

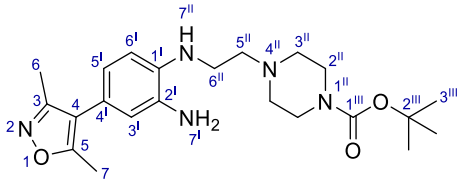

An orange solution of *tert*-butyl 4-(2-{[4-(3,5-dimethyl-1,2-oxazol-4-yl)-2-nitrophenyl]amino}ethyl)piperazine-1-carboxylate (**107**) (1.50 g, 3.37 mmol, 1.0 eq.) and $Na_2S_2O_4$ (5.76 g, 33.7 mmol, 10 eq.) in 1:1 EtOH/ H_2O (120 mL) was stirred at 80 °C for 15 min. The colourless solution was concentrated *in vacuo*, diluted with 35% aq. NH_3 (100 mL), and the aqueous component was extracted with EtOAc (3 × 100 mL). The combined organic components were washed with brine (300 mL), dried (Na_2SO_4), filtered, and concentrated *in vacuo*. *tert*-Butyl 4-(2-{[2-amino-4-(3,5-dimethyl-1,2-oxazol-4-yl)phenyl]amino}ethyl)piperazine-1-carboxylate (**108**) (1.17 g, 2.82 mmol, 84%) was obtained as an amorphous colourless solid and was used without purification: R_f 0.33 (9:1 CH_2Cl_2/ MeOH); ῡmax (thin film)/ cm^{-1} 3400 (N-H, w, br), 2978 (C-H, w), 2931 (C-H, w), 2863 (C-H, w), 1683 (C=O, s); ^1H NMR (500 MHz, $CDCl_3$) δ_H 6.69 – 6.67 (2 H, m, H-5^{I}, H-6^{I}), 6.58 (1 H, s, H-3^{I}), 3.44 (4 H, t, *J* 5.1, H-2^{II}), 3.20 (2 H, t, *J* 5.8, H-6^{II}), 2.71 (2 H, t, *J* 5.8, H-5^{II}), 2.44 (4 H, t, *J* 5.1, H-3^{II}), 2.37 (3 H, s, C-7), 2.25 (3 H, s, C-6), 1.46 (9 H, s, H-3^{III}); ^{13}C NMR (151 MHz, $CDCl_3$) δ_C 164.6 (C-3), 159.1 (C-5), 154.9 (C-1^{III}), 137.2 (C-1^{I}), 134.7 (C-2^{I}), 121.5 (C-5^{I}), 120.5 (C-4^{I}), 116.9 (C-4), 116.8 (C-3^{I}), 112.0 (C-6^{I}), 79.8 (C-2^{III}), 57.0 (C-5^{II}), 52.9 (C-3^{II}), 43.5 (C-2^{II}), 40.7 (C-6^{II}), 28.6 (C-3^{III}), 11.7 (C-7), 11.0 (C-6); HRMS *m/z* (ESI^+) 438.2492 (438.2476 calculated for $[C_{22}H_{33}N_5O_3Na]^+$); LRMS (ESI^+) *m/z* 416 ($[M+H]^+$, 100%); HPLC (Method 3) t_R 6.4 min, purity 99.0%.

***tert*-Butyl 4-{2-[5-(3,5-dimethyl-1,2-oxazol-4-yl)-2-[(2*S*)-6-oxopiperidin-2-yl]-1*H*-1,3-benzodiazol-1-yl]ethyl}piperazine-1-carboxylate (110)**

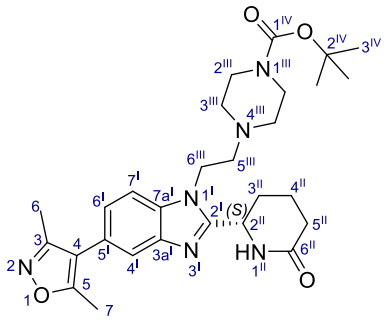

Step I:

A solution of *tert*-butyl 4-(2-{[2-amino-4-(3,5-dimethyl-1,2-oxazol-4-yl)phenyl]amino}ethyl)piperazine-1-carboxylate (**108**) (1.09 g, 2.63 mmol, 1.0 eq.), (*S*)-6-oxo-2-piperidinecarboxylic acid (452 mg, 3.16 mmol, 1.2 eq.), HATU (1.20 g, 3.16 mmol, 1.2 eq.), and DIPEA (888 µL, 5.26 mmol, 2.0 eq.) in DMF (26.0 mL) was stirred at rt for 16 h. The reaction mixture was concentrated *in vacuo*, sat. aq. $NaHCO_3$ (200 mL) was added to the residue and the aqueous component was extracted with EtOAc (3 × 200 mL). The combined organic components were dried (Na_2SO_4), filtered, and concentrated *in vacuo* to afford the amide intermediate.

Step II:

The amide intermediate was suspended in toluene (40 mL) and heated at reflux using a Dean Stark apparatus for 66 h. The reaction mixture was concentrated *in vacuo* and the crude residue was purified using normal phase column chromatography (gradient of 0 – 10% MeOH in CH_2Cl_2) to afford *tert*-butyl 4-{2-[5-(3,5-dimethyl-1,2-oxazol-4-yl)-2-[(2*S*)-6-oxopiperidin-2-yl]-1*H*-1,3-benzodiazol-1-yl]ethyl}piperazine-1-carboxylate (**110**) (377 mg, 0.721 mmol, 27%) as an amorphous yellow solid: R_f 0.27 (9:1 CH_2Cl_2/ MeOH); $[\alpha]_D^{25}$ = +19.1 (*c* 1.0, $CHCl_3$); ῡmax (thin film)/ cm^{-1} 3650 (N-H, w, br), 2981 (C-H, s), 2824 (C-H, m), 1684 (C=O, s), 1665 (C=O, s); ^{1}H NMR (600 MHz, $CDCl_3$) δ_H 8.05 (1 H, br s, NH-1^{II}), 7.67 (1 H, d, *J* 1.6, H-4^{I}), 7.41 (1 H, d, *J* 8.3, H-7^{I}), 7.20 (1 H, dd, *J* 8.3, 1.6, H-6^{I}), 4.88 – 4.81 (1 H, m, H-2^{II}), 4.42 – 4.28 (2 H, m, H-6^{III}), 3.61 – 3.47 (4 H, m, H-2^{III}), 3.00 – 2.91 (1 H, m, H_AH_B-5^{III}), 2.86 – 2.75 (1 H, m, H_AH_B-5^{III}), 2.62 – 2.44 (5 H, m, H_AH_B-3^{II}, H-5^{II}, H_AH_B-3^{III}), 2.42 (3 H, s, H-7), 2.34 – 2.24 (3 H, m, H_AH_B-3^{II}, H_AH_B-3^{III}), 2.28 (3 H, s, H-6), 2.24 – 2.17 (1 H, m,

H_AH_B-4^{II}), 1.95 – 1.85 (1 H, m, H_AH_B-4^{II}), 1.42 (9 H, s, H-3^{IV}); ^{13}C NMR (151 MHz, $CDCl_3$) δ_C 171.7 (C-6^{II}), 165.3 (C-3), 159.0 (C-5), 154.6 (C-1^{IV}), 154.1 (C-2^{I}), 142.6 (C-3a^{I}), 134.2 (C-7a^{I}), 125.5 (C-5^{I}), 124.8 (C-6^{I}), 121.0 (C-4^{I}), 116.9 (C-4), 110.1 (C-7^{I}), 79.9 (C-2^{IV}), 57.5 (C-5^{III}), 54.5 (), 49.4 (C-2^{II}), 42.8 (C-6^{III}), 42.6 (C-2^{III}), 31.7 (C-5^{II}), 28.5 (C-3^{IV}), 27.1 (C-3^{III}), 20.3 (C-4^{II}), 18.79, 17.52, 11.7 (C-7), 11.0 (C-6); HRMS *m/z* (ESI$^+$) 523.3041 (523.3027 calculated for $[C_{28}H_{39}N_6O_4]^+$); LRMS (ESI$^+$) *m/z* 523 ($[M+H]^+$, 100%); HPLC (Method 3) t_R 6.7 min, purity 96.7%.

tert-Butyl 4-(2-{2-[(2*S*)-1-(3,4-difluorophenyl)-6-oxopiperidin-2-yl]-5-(3,5-dimethyl-1,2-oxazol-4-yl)-1*H*-1,3-benzodiazol-1-yl}ethyl)piperazine-1-carboxylate (111)

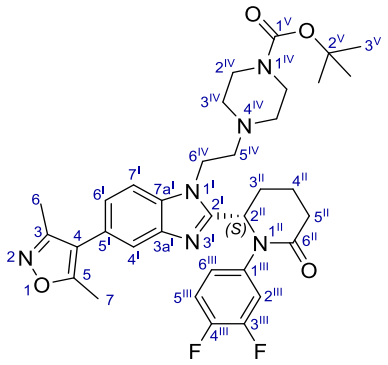

A solution of *tert*-butyl 4-{2-[5-(3,5-dimethyl-1,2-oxazol-4-yl)-2-[(2*S*)-6-oxopiperidin-2-yl]-1*H*-1,3-benzodiazol-1-yl]ethyl}piperazine-1-carboxylate (**110**) (477 mg, 0.913 mmol, 1.0 eq.) and DBU (300 µL, 2.01 mmol, 2.2 eq.) in anhydrous CH_2Cl_2 (30 mL) was stirred over 3 Å molecular sieves for 10 min before the addition of Cu-TMEDA (85 mg, 0.18 mmol, 0.2 eq.). The suspension was stirred at rt for 5 min before the addition of 3,4-difluorophenylboronic acid (288 mg, 1.83 mmol, 2.0 eq.) and was stirred at rt for a further 18 h. The reaction mixture was diluted with CH_2Cl_2 (100 mL) and washed with sat. aq. $NaHCO_3$ (100 mL). The aqueous component was extracted with EtOAc (2 × 100 mL) and the combined organic components were dried (Na_2SO_4), filtered, and concentrated *in vacuo*. The crude product was purified using reverse phase column chromatography (gradient of 95 – 5% H_2O in MeCN) then using normal phase column chromatography (gradient of 0 – 30% acetone in EtOAc) to afford *tert*-butyl 4-(2-{2-[(2*S*)-1-(3,4-difluorophenyl)-6-oxopiperidin-2-yl]-5-

(3,5-dimethyl-1,2-oxazol-4-yl)-1*H*-1,3-benzodiazol-1-yl}ethyl)piperazine-1-carboxylate (**111**) (174 mg, 0.274 mmol, 30%) as a yellow amorphous solid: R_f 0.27 (9:1 CH_2Cl_2/ MeOH); $[\alpha]_D^{25} = -72.7$ (*c* 1.0, $CHCl_3$); ῡmax (thin film)/ cm^{-1} 3504 (N-H, w, br), 2981 (C-H, m), 2818 (C-H, m), 1687 (C=O, s), 1661 (C=O, s), 1542 (C=C, s); ^{1}H NMR (600 MHz, $CDCl_3$) δ_H 7.68 (1 H, s, H-4^{I}), 7.30 (1 H, d, *J* 8.3, H-7^{I}), 7.15 (1 H, d, *J* 8.3, H-6^{I}), 7.10 – 7.00 (2 H, m, H-2^{III}, H-5^{III}), 6.94 – 6.88 (1 H, m, H-6^{III}), 5.24 – 5.15 (1 H, m, H-2^{II}), 4.04 – 3.96 (2 H, m, H-6^{IV}), 3.45 – 3.23 (4 H, m, H-2^{IV}), 2.86 (1 H, dt, *J* 17.8, 5.4, H$_A$H$_B$-4^{II}), 2.65 (1 H, dt, *J* 17.8, 7.0, H$_A$H$_B$-4^{II}), 2.58 – 2.50 (1 H, m, H$_A$H$_B$-5^{IV}), 2.44 (3 H, s, H-7), 2.43 – 2.24 (6 H, m, H-3^{II}, H$_A$H$_B$-5^{II}, H$_A$H$_B$-5^{IV}, H$_A$H$_B$-3^{IV}), 2.31 (3 H, s, H-6), 1.94 – 1.86 (1 H, m, H$_A$H$_B$-5^{II}), 1.66 – 1.59 (2 H, m, H$_A$H$_B$-3^{IV}), 1.46 (9 H, s, H-3^{V}); ^{13}C NMR (151 MHz, $CDCl_3$) δ_C 170.9 (C-6^{II}), 165.3 (C-3), 159.0 (C-5), 154.7 (C-1^{V}), 153.2 (C-2^{I}), 150.8 (dd, *J* 79.3, 11.4, C-3^{III}), 149.16 (dd, *J* 79.2, 12.3, C-4^{III}), 142.9 (C-3a^{I}), 138.6 (C-1^{III}), 134.2 (C-7a^{I}), 125.2 (C-5^{I}), 124.6 (C-6^{III}), 124.5 (C-6^{I}), 121.0 (C-4^{I}), 118.2 (d, *J* 17.6, C-2^{III}), 117.61 (d, *J* 17.9, C-5^{III}), 117.0 (C-4), 109.9 (C-7^{I}), 80.2 (C-2^{V}), 57.6‡ (C-2^{II}), 57.6‡ (C-5^{IV}), 53.6 (C-3^{IV}), 43.1 (C-2^{IV}), 41.9 (C-5^{IV}), 32.5 (C-4^{II}), 29.5 (C-3^{II}), 28.5 (C-3^{V}), 18.3 (C-5^{II}), 11.8 (C-7), 11.1 (C-6); ^{19}F NMR (565 MHz, $CDCl_3$) δ_F −(135.2 – 135.0) (1 F, m, F-3^{III}), −(138.0 – 137.8) (1 F, m, F-4^{III}); HRMS *m/z* (ESI$^+$) 657.2971 (657.2994 calculated for $[C_{34}H_{40}F_2N_6O_4Na]^+$); LRMS (ESI$^+$) *m/z* 635 ([M+H]$^+$, 100%); HPLC (Method 3) t_R 8.2 min, purity 92.8%. ‡ - Two carbon environments with equivalent ppm, evident by HSQC.

(6*S*)-1-(3,4-Difluorophenyl)-6-[5-(3,5-dimethyl-1,2-oxazol-4-yl)-1-[2-(piperazin-1-yl)ethyl]-1*H*-1,3-benzodiazol-2-yl]piperidin-2-one hydrochloride (106)

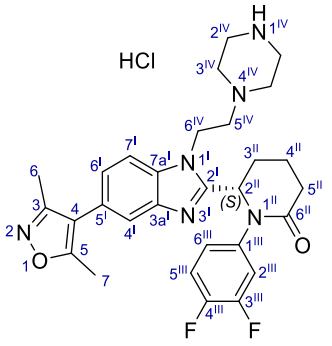

To a solution of *tert*-butyl 4-(2-{2-[(2S)-1-(3,4-difluorophenyl)-6-oxopiperidin-2-yl]-5-(3,5-dimethyl-1,2-oxazol-4-yl)-1*H*-1,3-benzodiazol-1-yl}ethyl)piperazine-1-carboxylate (**111**) (291 mg, 458 μmol, 1.0 eq.) in CH_2Cl_2 (2.3 mL) was added 4 M HCl in dioxane (573 μL, 2.29 mmol, 5.0 eq.). The reaction mixture was stirred at rt for 6 h before the further addition of CH_2Cl_2 (2.3 mL) and 4 M HCl in dioxane (573 μL, 2.29 mmol, 5.0 eq.) to the resultant suspension. The reaction mixture was stirred at rt for 17 h before being concentrated *in vacuo* to afford (6*S*)-1-(3,4-difluorophenyl)-6-[5-(3,5-dimethyl-1,2-oxazol-4-yl)-1-[2-(piperazin-1-yl)ethyl]-1*H*-1,3-benzodiazol-2-yl]piperidin-2-one hydrochloride (**106**) (251 mg, 0.431 mmol, 94%) as a pale yellow solid which was used without purification: R_f 0.00 (acetone); ^{1}H NMR (400 MHz, CD_3OD) δ_H 8.04 (1 H, d, *J* 8.6, H-7^{I}), 7.80 (1 H, d, *J* 1.5, H-4^{I}), 7.62 (1 H, dd, *J* 8.6, 1.5, H-6^{I}), 7.45 (1 H, ddd, *J* 11.3, 7.1, 2.5, H-5^{III}), 7.28 (1 H, dt, *J* 10.1, 8.5, H-2^{III}), 7.24 – 7.19 (1 H, m, H-6^{III}), 6.14 (1 H, br t, *J* 6.0, NH-1^{IV}), 4.73 – 4.67 (1 H, m, H-2^{II}), 3.76 – 3.64 (2 H, m, H-6^{IV}), 3.29 – 3.26 (2 H, m, H-2^{IV}), 3.13 – 3.05 (4 H, m, CH_2), 3.01 – 2.95 (2 H, m, CH_2), 2.91 – 2.81 (2 H, m, CH_2), 2.77 – 2.68 (2 H, m, CH_2), 2.45 (3 H, s, H-7), 2.43 – 2.43 (2 H, m, CH_2), 2.28 (3 H, s, H-6), 2.19 – 2.12 (2 H, m, H_AH_B-3^{IV}); F NMR (400 MHz, $CDCl_3$) δ_F −135.11 (1 F, d, *J* 21.6, F-3^{III}), −137.89 (1 F, d, *J* 21.6, F-4^{III}); LCMS (HpH) t_R 0.85 min, *m/z* (ESI$^+$) 535.2 $[M+H]^+$, purity 98%.

General Amide Coupling Method I.I:

To each carboxylic acid building block (20.9 μmol, 1.1 eq.) was added a solution of HATU (8.7 mg, 23 μmol 1.2 eq.) and DIPEA (14 μL, 80 μmol, 4.2 eq.) in DMF (100 μL) followed by a solution of (*R*,*E*)-6-(5-(7-methoxy-3,4-dihydroquinolin-1(2*H*)-yl)pent-1-en-1-yl)-4-methyl-8-(piperidin-4-yl)-1,3,4,5-tetrahydro-2*H*-benzo[b][1,4]diazepin-2-one hydrochloride (**86**) (10.0 mg, 19.0 μmol, 1.0 eq.) in DMF (100 μL). The reaction mixtures were stirred at rt for 18 h before being directly purified using mass directed auto purification (MDAP). The relevant fractions were concentrated under a flow of N_2 at 40 °C.

General Amide Coupling Method I.II:

Solutions of (*R*,*E*)-6-(5-(7-methoxy-3,4-dihydroquinolin-1(2*H*)-yl)pent-1-en-1-yl)-4-methyl-8-(piperidin-4-yl)-1,3,4,5-tetrahydro-2*H*-benzo[b][1,4]diazepin-2-one hydrochloride (**86**) (20.0 mg, 38.0 μmol, 1.0 eq.), each carboxylic acid building block (41.9 μmol, 1.1 eq.), HATU (17.4 mg, 45.7 μmol 1.2 eq.), and DIPEA (27 μL, 160 μmol, 4.1 eq.) in DMF (380 μL). The reaction mixtures were stirred at rt for 4 h before being directly purified using preparative reverse phase column chromatography. The relevant fractions were concentrated under a flow of N_2 at 40 °C.

General Amide Coupling Method II:

To each carboxylic acid building block (21.8 μmol, 1.1 eq.) was added a solution of HATU (9.0 mg, 24 μmol, 1.2 eq.) and DIPEA (11 μL, 63 μmol, 3.2 eq.) in DMF (100 μL) followed by a solution of (*S*)-1-(3,4-difluorophenyl)-6-(5-(3,5-dimethylisoxazol-4-yl)-1-(piperidin-4-yl)-1*H*-benzo[d]imidazol-2-yl)piperidin-2-one (**87**) (10.0 mg, 19.8 μmol, 1.0 eq.) in DMF (100 μL). The reaction mixtures were stirred at rt for 18 h before being directly purified using MDAP. The relevant fractions were concentrated under a flow of N_2 at 40 °C.

General Amide Coupling Method III:

To each carboxylic acid building block (20.6 μmol, 1.1 eq.) was added a solution of HATU (8.5 mg, 22 μmol, 1.2 eq.) and DIPEA (13 μL, 75 μmol, 4.0 eq.) in DMF (100 μL) followed by a solution of (6*S*)-1-(3,4-difluorophenyl)-6-[5-(3,5-dimethyl-1,2-oxazol-4-yl)-1-[2-(piperazin-1-yl)ethyl]-1*H*-1,3-benzodiazol-2-yl]piperidin-2-one hydrochloride (**106**) (10.0 mg, 18.7 μmol, 1.0 eq.) in DMF (100 μL). The reaction mixtures were stirred at rt for 4 – 20 h before being directly purified by MDAP. The relevant fractions were concentrated under a flow of N_2 at 40 °C.

2-(2,6-Dioxopiperidin-3-yl)-4-[2-(2-{4-[(2*R*)-9-[(1*E*)-5-(7-methoxy-1,2,3,4-tetrahydroquinolin-1-yl)pent-1-en-1-yl]-2-methyl-4-oxo-2,3,4,5-tetrahydro-1*H*-1,5-benzodiazepin-7-yl]piperidin-1-yl}-2-oxoethoxy)ethoxy]-2,3-dihydro-1*H*-isoindole-1,3-dione (112)

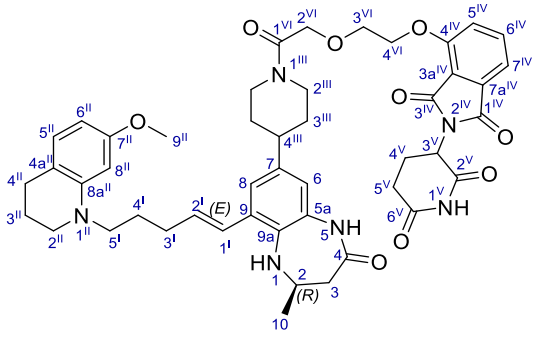

Synthesised according to 'General Amide Coupling Method I.II'. The crude reaction mixture was directly purified using preparative reverse phase column chromatography (gradient of 30 – 99% MeCN in H_2O each with 0.1% *v/v* formic acid) to afford 2-(2,6-dioxopiperidin-3-yl)-4-[2-(2-{4-[(2*R*)-9-[(1*E*)-5-(7-methoxy-1,2,3,4-tetrahydroquinolin-1-yl)pent-1-en-1-yl]-2-methyl-4-oxo-2,3,4,5-tetrahydro-1*H*-1,5-benzodiazepin-7-yl]piperidin-1-yl}-2-oxoethoxy)ethoxy]-2,3-dihydro-1*H*-isoindole-1,3-dione (**112**) (7.4 mg, 8.7 µmol, 22%): R_f 0.10 (acetone); ^{1}H NMR (400 MHz, $CO(CD_3)_2$) δ_H 9.95 – 9.84 (1 H, m, NH-1^V), 8.49 (1 H, br s, NH-5), 7.80 (1 H, dd, *J* 8.6, 7.3, H-6^{IV}), 7.53 – 7.40 (3 H, m, H-8, H-5^{IV}, H-7^{IV}), 6.83 – 6.73 (3 H, m, H-6, H-1^I, H-5^{II}), 6.29 – 6.12 (3 H, m, H-2^I, H-6^{II}, H-8^{II}), 5.09 (1 H, dd, *J* 12.6, 5.5, H-3^V), 4.61 – 4.53 (1 H, m, CH_2), 4.45 (2 H, s, H-2^{VI}), 4.11 – 3.96 (4 H, m, CH_2), 3.67 (3 H, s, H-9^{II}), 3.39 – 3.31 (4 H, m, CH_2), 3.09 – 3.18 (1 H, m, CH_2), 2.96 – 2.84 (2 H, m, CH_2), 2.74 – 2.64 (6 H, m, CH_2), 2.51 (2 H, dd, *J* 13.1, 5.0, H-4^{III}), 2.35 – 2.28 (2 H, m, CH_2), 2.27 – 2.20 (1 H, m, CH_2), 2.17 – 2.11 (1 H, m, CH_2), 1.94 – 1.87 (2 H, m, CH_2), 1.86 – 1.76 (5 H, m, CH_2), 1.66 – 1.56 (1 H, m, CH_2), 1.53 – 1.43 (1 H, m, CH_2), 1.31 (3 H, d, *J* 6.1, H-10); HRMS *m/z* (ESI$^+$) 847.4044 (847.4025 calculated for $[C_{47}H_{55}N_6O_9]^+$); LCMS (formic acid) t_R 1.18 min, *m/z* (ESI$^+$) 847.3 $[M+H]^+$, purity 94%.

2-(2,6-Dioxopiperidin-3-yl)-4-{2-[2-(2-{4-[(2*R*)-9-[(1*E*)-5-(7-methoxy-1,2,3,4-tetrahydroquinolin-1-yl)pent-1-en-1-yl]-2-methyl-4-oxo-2,3,4,5-tetrahydro-1*H*-1,5-benzodiazepin-7-yl]piperidin-1-yl}-2-oxoethoxy)ethoxy]ethoxy}-2,3-dihydro-1*H*-isoindole-1,3-dione (113)

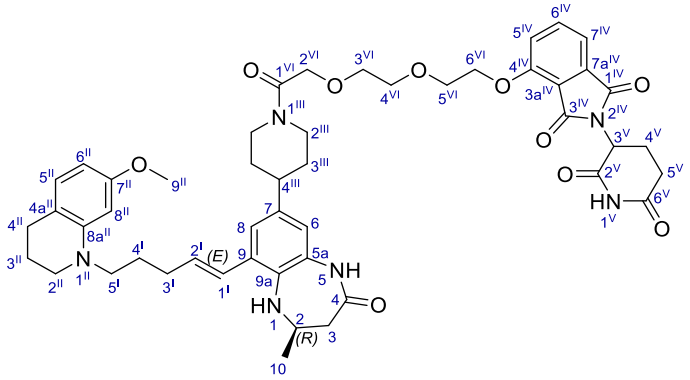

Synthesised according to 'General Amide Coupling Method I.I'. The crude reaction mixture was directly purified using MDAP (method C) to afford 2-(2,6-dioxopiperidin-3-yl)-4-{2-[2-(2-{4-[(2*R*)-9-[(1*E*)-5-(7-methoxy-1,2,3,4-tetrahydroquinolin-1-yl)pent-1-en-1-yl]-2-methyl-4-oxo-2,3,4,5-tetrahydro-1*H*-1,5-benzodiazepin-7-yl]piperidin-1-yl}-2-oxoethoxy)ethoxy]ethoxy}-2,3-dihydro-1*H*-isoindole-1,3-dione (**113**) (5.1 mg, 5.7 µmol, 26%): R_f 0.32 (acetone); ^{1}H NMR (400 MHz, CD_3CN) δ_H 8.99 (1 H, br s, NH-1^V), 8.03 (1 H, br s, NH-5), 7.87 – 7.62 (2 H, m, H-6^{IV}), 7.43 (1 H, d, *J* 7.3, H-7^{IV}), 7.40 – 7.35 (1 H, m, H-5^{IV}), 7.03 (1 H, d, *J* 2.0, H-8), 6.85 (1 H, d, *J* 7.6, H-5^{II}), 6.68 (1 H, d, *J* 2.0, H-6), 6.59 (1 H, d, *J* 15.5, H-1^I), 6.28 – 6.20 (2 H, m, H-6^{II}, H-8^{II}), 6.15 (1 H, dt, *J* 15.5, 6.9, H-2^I), 5.03 – 4.91 (1 H, m, H-3^V), 4.73 – 4.60 (1 H, m, CH_2), 4.57 – 4.48 (1 H, m, CH_2), 4.33 (2 H, t, *J* 4.5), 4.26 – 4.13 (2 H, m, CH_2), 4.00 (1 H, dd, *J* 12.0, 6.4, H-2), 3.92 – 3.76 (3 H, m, H-9^{II}), 3.75 – 3.69 (2 H, m, CH_2), 3.69 – 3.62 (4 H, m, CH_2), 3.39 – 3.26 (3 H, m, CH_2), 3.10 – 2.98 (1 H, m, CH_2), 2.79 – 2.56 (6 H, m, CH_2), 2.45 (2 H, dd, *J* 13.2, 5.1, H-4^{III}), 2.34 – 2.25 (2 H, m, CH_2), 2.24 – 2.01 (7 H, m, CH_2), 1.92 – 1.87 (2 H, m, CH_2), 1.85 – 1.70 (3 H, m, CH_2), 1.62 – 1.37 (2 H, m, CH_2), 1.24 (3 H, d, *J* 6.4, H-10); HRMS *m/z* (ESI$^+$) 891.4289 (891.4287 calculated for $[C_{49}H_{59}N_6O_{10}]^+$); LCMS (formic acid) t_R 1.18 min, *m/z* (ESI$^+$) 891.5 $[M+H]^+$, purity 92%.

2-(2,6-Dioxopiperidin-3-yl)-4-(2-{2-[2-(2-{4-[(2*R*)-9-[(1*E*)-5-(7-methoxy-1,2,3,4-tetrahydroquinolin-1-yl)pent-1-en-1-yl]-2-methyl-4-oxo-2,3,4,5-tetrahydro-1*H*-1,5-benzodiazepin-7-yl]piperidin-1-yl}-2-oxoethoxy)ethoxy]ethoxy}ethoxy)-2,3-dihydro-1*H*-isoindole-1,3-dione (114)

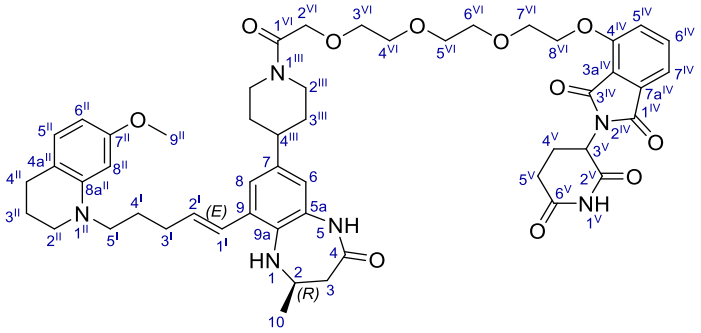

Synthesised according to 'General Amide Coupling Method I.II'. The crude reaction mixture was directly purified using preparative reverse phase column chromatography (gradient of 30 – 99% MeCN in H_2O each with 0.1% *v/v* formic acid) to afford 2-(2,6-dioxopiperidin-3-yl)-4-(2-{2-[2-(2-{4-[(2*R*)-9-[(1*E*)-5-(7-methoxy-1,2,3,4-tetrahydroquinolin-1-yl)pent-1-en-1-yl]-2-methyl-4-oxo-2,3,4,5-tetrahydro-1*H*-1,5-benzodiazepin-7-yl]piperidin-1-yl}-2-oxoethoxy)ethoxy]ethoxy}ethoxy)-2,3-dihydro-1*H*-isoindole-1,3-dione (**114**) (5.4 mg, 5.8 µmol, 15%): R_f 0.12 (acetone); ^{1}H NMR (400 MHz, $CO(CD_3)_2$) δ_H 9.95 (1 H, br s, NH-1^V), 8.69 (1 H, br s, NH-5), 7.81 (1 H, dd, *J* 8.6, 7.3, H-6^{IV}), 7.51 (1 H, d, *J* 8.6, H-5^{IV}), 7.45 (1 H, d, *J* 7.1, H-7^{IV}), 7.23 (1 H, s, H-8), 7.03 (1 H, d, *J* 7.1, H-5^{II}), 6.90 (1 H, s, H-6), 6.87 (d, *J* 15.7, H-1^I), 6.63 – 6.53 (2 H, m, H-6^{II}, H-8^{II}), 6.42 – 6.32 (1 H, m, H-2^I), 5.11 (1 H, dd, *J* 12.5, 5.4, H-3^V), 4.50 – 4.44 (1 H, m, CH_2), 4.42 (2 H, t, *J* 4.5, CH_2), 4.32 – 4.26 (2 H, m, CH_2), 4.22 – 4.17 (1 H, m, CH_2), 4.03 – 3.95 (1 H, m, H-2), 3.94 – 3.90 (2 H, m, CH_2), 3.77 – 3.74 (2 H, m, CH_2), 3.73 (3 H, s, H-9^{II}), 3.66 – 3.63 (6 H, m, CH_2), 3.59 – 3.91 (4 H, m, CH_2), 3.16 – 3.06 (2 H, m, CH_2), 3.01 – 2.89 (2 H, m, CH_2), 2.82 – 2.72 (6 H, m, CH_2), 2.58 (2 H, dd, *J* 13.2, 5.4, H-4^{III}), 2.44 – 2.36 (2 H, m, CH_2), 2.30 (1 H, dd, *J* 13.2, 7.6, H$_A$H$_B$-3), 2.25 – 2.17 (1 H, m, CH_2), 2.04 – 1.96 (3 H, m, CH_2), 1.87 – 1.80 (1 H, m, CH_2), 1.78 – 1.66 (2 H, m, CH_2), 1.40 (3 H, d, *J* 6.1, H-10); HRMS *m/z* (ESI$^+$) 935.4583 (935.4549 calculated for $[C_{51}H_{63}N_6O_{11}]^+$); LCMS (formic acid) t_R 1.18 min, *m/z* (ESI$^+$) 935.4 $[M+H]^+$, purity 96%.

2-(2,6-Dioxopiperidin-3-yl)-4-[(14-{4-[(2*R*)-9-[(1*E*)-5-(7-methoxy-1,2,3,4-tetrahydroquinolin-1-yl)pent-1-en-1-yl]-2-methyl-4-oxo-2,3,4,5-tetrahydro-1*H*-1,5-benzodiazepin-7-yl]piperidin-1-yl}-14-oxo-3,6,9,12-tetraoxatetradecan-1-yl)oxy]-2,3-dihydro-1*H*-isoindole-1,3-dione (115)

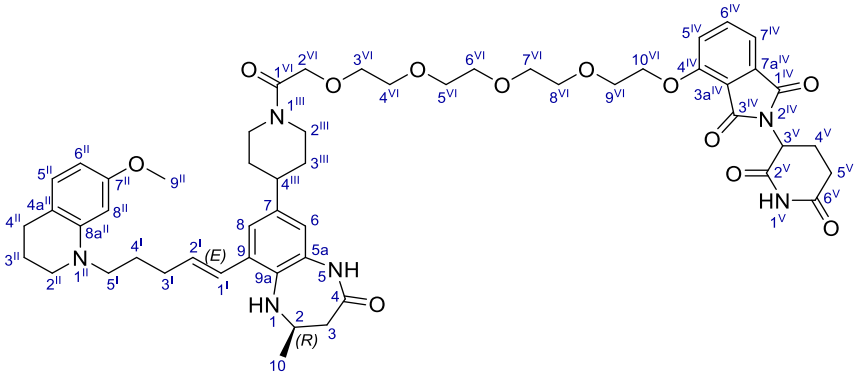

Synthesised according to 'General Amide Coupling Method I.I'. The crude reaction mixture was directly purified using MDAP (method C) to afford 2-(2,6-dioxopiperidin-3-yl)-4-[(14-{4-[(2*R*)-9-[(1*E*)-5-(7-methoxy-1,2,3,4-tetrahydroquinolin-1-yl)pent-1-en-1-yl]-2-methyl-4-oxo-2,3,4,5-tetrahydro-1*H*-1,5-benzodiazepin-7-yl]piperidin-1-yl}-14-oxo-3,6,9,12-tetraoxatetradecan-1-yl)oxy]-2,3-dihydro-1*H*-isoindole-1,3-dione (**115**) (4.9 mg, 5.0 µmol, 24%): R_f 0.10 (acetone); ^{1}H NMR (400 MHz, $CO(CD_3)_2$) δ_H 9.99 – 9.82 (1 H, m, NH-1^V), 8.19 (1 H, br s, NH-5), 7.79 (1 H, dd, *J* 8.5, 7.3, H-6^{IV}), 7.49 (1 H, d, *J* 8.5, H-5^{IV}), 7.44 (1 H, d, *J* 7.3, H-7^{IV}), 7.10 (1 H, d, *J* 2.0, H-8), 6.80 (1 H, d, *J* 2.0, H-6), 6.78 – 6.71 (2 H, m, H-1^I, H-5^{II}), 6.22 (1 H, dt, *J* 15.6, 7.0, H-2^I), 6.13 (1 H, d, *J* 2.5, H-8^{II}), 6.07 (1 H, dd, *J* 7.9, 2.5, H-6^{II}), 5.10 (1 H, dd, *J* 12.8, 5.4, H-3^V), 4.63 – 4.54 (1 H, m, CH_2), 4.40 – 4.35 (2 H, m, CH_2), 4.24 – 4.12 (2 H, m, CH_2), 4.09 – 4.01 (2 H, m, H-2), 3.88 (2 H, dd, *J* 5.4, 3.9, CH_2), 3.70 (1 H, d, *J* 3.9, CH_2), 3.68 (1 H, t, *J* 3.5, CH_2), 3.66 (3 H, s, H-9^{II}), 3.63 – 3.56 (11 H, m, CH_2), 3.34 – 3.25 (5 H, m, CH_2), 3.02 – 2.89 (2 H, m, CH_2), 2.84 – 2.66 (4 H, m, CH_2), 2.63 (2 H, t, *J* 6.2, H-10^{VI}), 2.48 (1 H, dd, *J* 13.0, 5.2, H-4^{III}), 2.35 – 2.27 (2 H, m, CH_2), 2.23 – 2.17 (2 H, m, CH_2), 1.90 – 1.76 (6 H, m, CH_2), 1.28 (3 H, d, *J* 5.9, H-10); HRMS *m/z* (ESI$^+$) 979.4810 (979.4812 calculated for $[C_{53}H_{67}N_6O_{12}]^+$); LCMS (formic acid) t_R 1.19 min, *m/z* (ESI$^+$) 979.6 $[M+H]^+$, purity 91%.

2-(2,6-Dioxopiperidin-3-yl)-4-[(5-{4-[(2*R*)-9-[(1*E*)-5-(7-methoxy-1,2,3,4-tetrahydroquinolin-1-yl)pent-1-en-1-yl]-2-methyl-4-oxo-2,3,4,5-tetrahydro-1*H*-1,5-benzodiazepin-7-yl]piperidin-1-yl}-5-oxopentyl)oxy]-2,3-dihydro-1*H*-isoindole-1,3-dione (116)

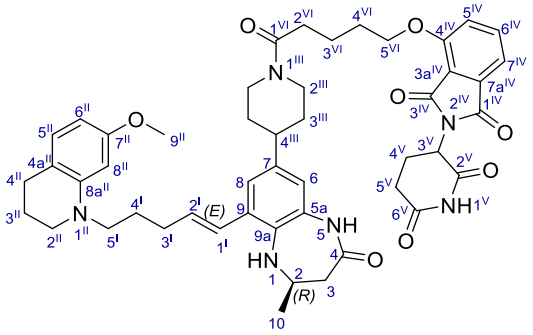

Synthesised according to 'General Amide Coupling Method I.I'. The crude reaction mixture was purified using MDAP (method C) to afford 2-(2,6-dioxopiperidin-3-yl)-4-[(5-{4-[(2*R*)-9-[(1*E*)-5-(7-methoxy-1,2,3,4-tetrahydroquinolin-1-yl)pent-1-en-1-yl]-2-methyl-4-oxo-2,3,4,5-tetrahydro-1*H*-1,5-benzodiazepin-7-yl]piperidin-1-yl}-5-oxopentyl)oxy]-2,3-dihydro-1*H*-isoindole-1,3-dione (**116**) (2.4 mg, 2.8 μmol, 13%): R_f 0.18 (acetone); ^{1}H NMR (400 MHz, $CO(CD_3)_2$) δ_H 9.87 – 9.80 (1 H, m, NH-1^V), 8.42 (1 H, br s, NH-5), 7.79 (1 H, dd, *J* 8.6, 7.3, H-6^{IV}), 7.48 – 7.46 (1 H, m, H-5^{IV}), 7.41 (1 H, d, *J* 7.3, H-7^{IV}), 7.11 (1 H, d, *J* 2.0, H-8), 6.80 (1 H, d, *J* 2.0, H-6), 6.75 (2 H, d, *J* 15.8, H-1^I), 6.27 – 6.07 (3 H, m, H-2^I, H-6^{II}, H-8^{II}), 5.08 (1 H, dd, *J* 12.6, 5.2, H-3^V), 4.72 – 4.63 (1 H, m, CH_2), 4.29 (2 H, t, *J* 5.9, H-2^{VI}), 4.16 – 4.02 (2 H, m, H-2), 3.66 (3 H, s, H-9^{II}), 3.38 – 3.27 (4 H, m, CH_2), 3.12 (1 H, br t, *J* 13.0, H-4^{III}), 2.97 – 2.86 (2 H, m, CH_2), 2.69 – 2.45 (9 H, m, CH_2), 2.36 – 2.27 (2 H, m, CH_2), 2.25 – 2.12 (3 H, m, CH_2), 1.92 – 1.77 (10 H, m, CH_2), 1.29 (3 H, d, *J* 5.9, H-10); HRMS *m/z* (ESI$^+$) 845.4212 (845.4232 calculated for $[C_{48}H_{57}N_6O_8]^+$); LCMS (formic acid) t_R 1.25 min, *m/z* (ESI$^+$) 845.4 $[M+H]^+$, purity 89%.

2-(2,6-Dioxopiperidin-3-yl)-4-[(8-{4-[(2*R*)-9-[(1*E*)-5-(7-methoxy-1,2,3,4-tetrahydroquinolin-1-yl)pent-1-en-1-yl]-2-methyl-4-oxo-2,3,4,5-tetrahydro-1*H*-1,5-benzodiazepin-7-yl]piperidin-1-yl}-8-oxooctyl)oxy]-2,3-dihydro-1*H*-isoindole-1,3-dione (117)

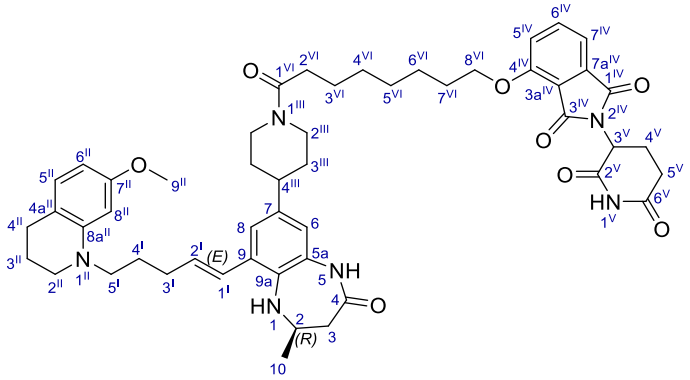

Synthesised according to 'General Amide Coupling Method I.I'. The crude reaction mixture was directly purified using MDAP (method D) to afford 2-(2,6-dioxopiperidin-3-yl)-4-[(8-{4-[(2*R*)-9-[(1*E*)-5-(7-methoxy-1,2,3,4-tetrahydroquinolin-1-yl)pent-1-en-1-yl]-2-methyl-4-oxo-2,3,4,5-tetrahydro-1*H*-1,5-benzodiazepin-7-yl]piperidin-1-yl}-8-oxooctyl)oxy]-2,3-dihydro-1*H*-isoindole-1,3-dione (**117**) (2.4 mg, 2.7 μmol, 13%): R_f 0.23 (acetone); ^{1}H NMR (400 MHz, $CO(CD_3)_2$) δ_H 9.87 (1 H, br s, NH-1^V), 8.37 (1 H, br s, NH-5), 7.79 (1 H, dd, *J* 8.5, 7.1, H-6^{IV}), 7.47 (1 H, d, *J* 8.5, H-5^{IV}), 7.42 (1 H, d, *J* 7.1, H-7^{IV}), 7.10 (1 H, d, *J* 2.0, H-8), 6.80 (1 H, d, *J* 2.0, H-6), 6.78 – 6.75 (1 H, m, H-5^{II}), 6.75 – 6.72 (1 H, m, H-1^I), 6.22 (1 H, dt, *J* 15.6, 7.0, H-2^I), 6.13 (1 H, d, *J* 2.5, H-8^{II}), 6.07 (1 H, dd, *J* 7.9, 2.5, H-6^{II}), 5.09 (1 H, dd, *J* 12.8, 5.4, H-3^V), 4.69 (1 H, d, *J* 10.3, CH_2), 4.26 (2 H, t, *J* 6.4, H-2^{VI}), 4.12 – 4.01 (2 H, m, H-2), 3.66 (3 H, s, H-9^{II}), 3.35 – 3.25 (4 H, m, CH_2), 2.63 (2 H, t, *J* 6.4, H-8^{VI}), 2.58 – 2.52 (1 H, m, CH_2), 2.48 (1 H, dd, *J* 12.8, 4.9, H-4^{III}), 2.40 – 2.34 (3 H, m, CH_2), 2.34 – 2.28 (2 H, m, CH_2), 2.24 – 2.16 (3 H, m, CH_2), 1.91 – 1.83 (5 H, m, CH_2), 1.83 – 1.74 (4 H, m, CH_2), 1.68 – 1.51 (6 H, m, CH_2), 1.51 – 1.35 (6 H, m, CH_2), 1.28 (3 H, d, *J* 6.4, H-10); HRMS *m/z* (ESI$^+$) 887.4719 (887.4702 calculated for $[C_{51}H_{63}N_6O_8]^+$); LCMS (formic acid) t_R 1.36 min, *m/z* (ESI$^+$) 887.6 $[M+H]^+$, purity 88%.

2-(2,6-Dioxopiperidin-3-yl)-4-[(10-{4-[(2*R*)-9-[(1*E*)-5-(7-methoxy-1,2,3,4-tetrahydroquinolin-1-yl)pent-1-en-1-yl]-2-methyl-4-oxo-2,3,4,5-tetrahydro-1*H*-1,5-benzodiazepin-7-yl]piperidin-1-yl}-10-oxodecyl)oxy]-2,3-dihydro-1*H*-isoindole-1,3-dione (118)

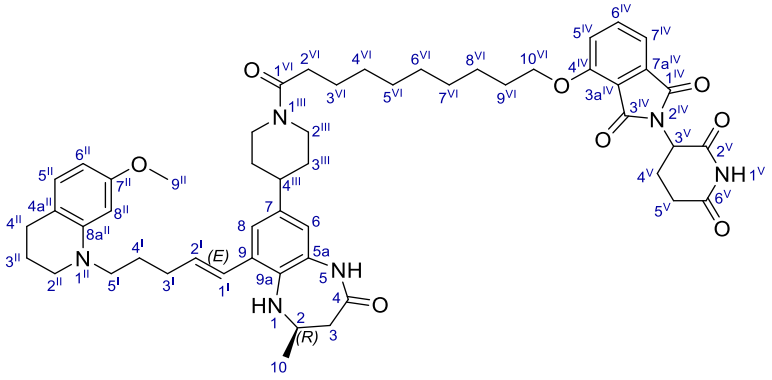

Synthesised according to 'General Amide Coupling Method I.I'. The crude reaction mixture was directly purified using MDAP (method D) to afford 2-(2,6-dioxopiperidin-3-yl)-4-[(10-{4-[(2*R*)-9-[(1*E*)-5-(7-methoxy-1,2,3,4-tetrahydroquinolin-1-yl)pent-1-en-1-yl]-2-methyl-4-oxo-2,3,4,5-tetrahydro-1*H*-1,5-benzodiazepin-7-yl]piperidin-1-yl}-10-oxodecyl)oxy]-2,3-dihydro-1*H*-isoindole-1,3-dione (**118**) (1.5 mg, 1.6 µmol, 7%): R_f 0.63 (acetone); ^{1}H NMR (400 MHz, $CO(CD_3)_2$) δ_H 9.93 (1 H, br s, NH-1^V), 8.39 (1 H, br s, NH-5), 7.81 (1 H, dd, *J* 8.4, 7.1, H-6^{IV}), 7.48 (1 H, d, *J* 8.4, H-5^{IV}), 7.46 – 7.42 (1 H, m, H-7^{IV}), 7.12 (1 H, d, *J* 2.0, H-8), 6.82 (1 H, d, *J* 2.0, H-6), 6.80 – 6.77 (1 H, m, H-5^{II}), 6.77 – 6.74 (1 H, m, H-1^I), 6.24 (1 H, dt, *J* 15.4, 6.9, H-2^I), 6.15 (1 H, d, *J* 2.5, H-8^{II}), 6.09 (1 H, dd, *J* 8.1, 2.5, H-6^{II}), 5.11 (1 H, dd, *J* 12.6, 5.5, H-3^V), 4.75 – 4.66 (2 H, m, H-2), 4.27 (2 H, t, *J* 6.4, H-2^{VI}), 3.68 (3 H, s, H-9^{II}), 3.36 – 3.27 (4 H, m, CH_2), 2.65 (2 H, t, *J* 6.2, H-10^{VI}), 2.50 (2 H, dd, *J* 13.0, 4.9, H-4^{III}), 2.41 – 2.30 (6 H, m, CH_2), 2.26 – 2.18 (3 H, m, CH_2), 1.93 – 1.76 (10 H, m, CH_2), 1.67 – 1.52 (8 H, m, CH_2), 1.46 – 1.39 (5 H, m, CH_2), 1.30 (3 H, d, *J* 6.1, H-10); HRMS *m/z* (ESI$^+$) 915.5023 (915.5015 calculated for $[C_{53}H_{66}N_6O_8]^+$); LCMS (formic acid) t_R 1.45 min, *m/z* (ESI$^+$) 915.6 $[M+H]^+$, purity 86%.

2-(2,6-Dioxopiperidin-3-yl)-5-fluoro-6-[4-(2-{4-[(2*R*)-9-[(1*E*)-5-(7-methoxy-1,2,3,4-tetrahydroquinolin-1-yl)pent-1-en-1-yl]-2-methyl-4-oxo-2,3,4,5-tetrahydro-1*H*-1,5-benzodiazepin-7-yl]piperidin-1-yl}-2-oxoethyl)piperazin-1-yl]-2,3-dihydro-1*H*-isoindole-1,3-dione (119)

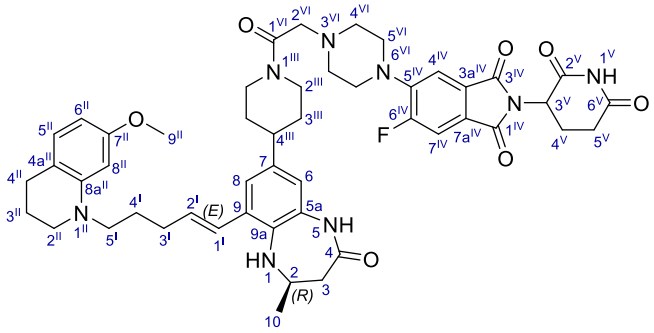

Synthesised according to 'General Amide Coupling Method I.I'. The crude reaction mixture was directly purified using MDAP (method B) to afford 2-(2,6-dioxopiperidin-3-yl)-5-fluoro-6-[4-(2-{4-[(2*R*)-9-[(1*E*)-5-(7-methoxy-1,2,3,4-tetrahydroquinolin-1-yl)pent-1-en-1-yl]-2-methyl-4-oxo-2,3,4,5-tetrahydro-1*H*-1,5-benzodiazepin-7-yl]piperidin-1-yl}-2-oxoethyl)piperazin-1-yl]-2,3-dihydro-1*H*-isoindole-1,3-dione (**119**) (4.4 mg, 4.9 μmol, 21%): R_f 0.10 (acetone); ^{1}H NMR (400 MHz, $CO(CD_3)_2$) δ_H 9.86 (1 H, br s, NH-1^V), 8.37 (1 H, br s, NH-5), 7.53 (1 H, d, *J* 11.3, H-7^{IV}), 7.42 (1 H, d, *J* 7.3, H-4^{IV}), 7.11 (1 H, d, *J* 2.0, H-8), 6.82 (1 H, d, *J* 2.0, H-6), 6.79 – 6.72 (2 H, m, H-1^I, H-5^{II}), 6.21 (1 H, dt, *J* 15.4, 7.0, H-2^I), 6.11 (1 H, d, *J* 2.3, H-8^{II}), 6.06 (1 H, dd, *J* 8.0, 2.3, H-6^{II}), 5.09 (1 H, dd, *J* 12.7, 5.4, H-3^V), 4.70 – 4.62 (1 H, m, CH_2), 4.40 – 4.30 (2 H, m, CH_2), 4.10 – 3.99 (2 H, m, CH_2), 3.65 (3 H, s, H-9^{II}), 3.37 (4 H, t, *J* 4.9, CH_2), 3.32 – 3.28 (2 H, m, CH_2), 3.28 – 3.24 (2 H, m, CH_2), 2.79 – 2.69 (9 H, m, CH_2), 2.63 – 2.60 (2 H, m, CH_2), 2.47 (2 H, dd, *J* 13.0, 5.1, H-4^{III}), 2.34 – 2.27 (2 H, m, CH_2), 2.24 – 2.16 (3 H, m, CH_2), 1.90 – 1.81 (5 H, m, CH_2), 1.80 – 1.72 (3 H, m, CH_2), 1.28 (3 H, d, *J* 6.4, H-10); ^{19}F NMR (376 MHz, $CO(CD_3)_2$) δ_F −113.08 (1 F, s, F-6^{IV}); HRMS *m/z* (ESI$^+$) 889.4389 (889.4407 calculated for $[C_{49}H_{58}FN_8O_7]^+$); LCMS (formic acid) t_R 0.90 min, *m/z* (ESI$^+$) 889.5 $[M+H]^+$, purity 80%.

3-{5-[4-(4-{4-[(2*R*)-9-[(1*E*)-5-(7-Methoxy-1,2,3,4-tetrahydroquinolin-1-yl)pent-1-en-1-yl]-2-methyl-4-oxo-2,3,4,5-tetrahydro-1*H*-1,5-benzodiazepin-7-yl]piperidin-1-yl}-4-oxobutyl)piperazin-1-yl]-1-oxo-2,3-dihydro-1*H*-isoindol-2-yl}piperidine-2,6-dione (120)

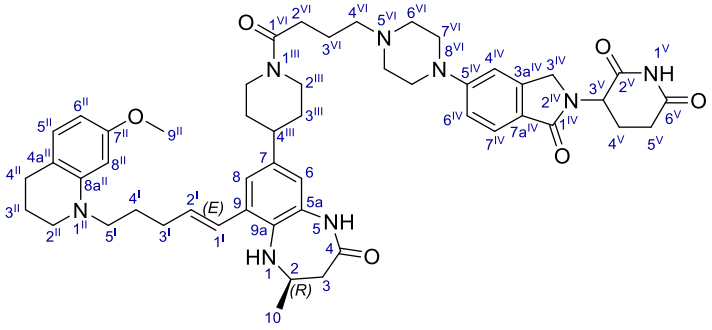

Synthesised according to 'General Amide Coupling Method I.II'. The crude reaction mixture was purified using preparative reverse phase column chromatography, (elution with a gradient of 20 – 85% MeCN in H_2O each with 0.1% *v/v* formic acid) to afford 3-{5-[4-(4-{4-[(2*R*)-9-[(1*E*)-5-(7-methoxy-1,2,3,4-tetrahydroquinolin-1-yl)pent-1-en-1-yl]-2-methyl-4-oxo-2,3,4,5-tetrahydro-1*H*-1,5-benzodiazepin-7-yl]piperidin-1-yl}-4-oxobutyl)piperazin-1-yl]-1-oxo-2,3-dihydro-1*H*-isoindol-2-yl}piperidine-2,6-dione (**120**) (9.1 mg, 10 µmol, 24%): R_f 0.12 (acetone); ^{1}H NMR (400 MHz, $(CD_3)_2SO$) δ_H 10.93 (1 H, br s, NH-1^V), 9.34 (1 H, br s, NH-5), 8.19 – 8.14 (1 H, m), 8.16 (1 H, s), 7.52 (1 H, d, *J* 9.1), 7.06 (1 H, s, H-8), 7.04 (1 H, d, *J* 1.5, H-6), 6.77 – 6.65 (3 H, m, H-5^{II}), 6.21 – 6.13 (1 H, m, H-1^I), 6.09 – 6.02 (3 H, m, H-2^I, H-6^{II}, H-8^{II}), 5.05 (1 H, dd, *J* 13.3, 5.0, H_AH_B-3^{IV}), 4.55 (1 H, d, *J* 11.7, H-3^V), 4.36 – 4.29 (1 H, m, CH_2), 4.25 – 4.18 (1 H, m, CH_2), 3.99 (1 H, d, *J* 13.3, H_AH_B-3^{IV}), 3.95 – 3.88 (1 H, m, H-2), 3.61 (3 H, s, H-9^{II}), 3.34 – 3.21 (9 H, m, CH_2), 3.12 – 3.04 (1 H, m, CH_2), 2.96 – 2.85 (1 H, m, CH_2), 2.69 – 2.55 (6 H, m, CH_2), 2.41 – 2.31 (7 H, m, CH_2), 2.29 – 2.22 (2 H, m, CH_2), 2.10 – 2.03 (1 H, m, CH_2), 2.00 – 1.93 (1 H, m, CH_2), 1.86 – 1.66 (9 H, m, CH_2), 1.55 – 1.45 (1 H, m, CH_2), 1.44 – 1.33 (1 H, m, CH_2), 1.18 (3 H, d, *J* 6.1, H-10); HRMS *m/z* (ESI$^+$) 885.5022 (885.5022 calculated for $[C_{51}H_{65}N_8O_6]^+$); LCMS (formic acid) t_R 0.86 min, *m/z* (ESI$^+$) 885.6 $[M+H]^+$, purity 89%.

2-(2,6-Dioxopiperidin-3-yl)-5-fluoro-6-[9-(2-{4-[(2*R*)-9-[(1*E*)-5-(7-methoxy-1,2,3,4-tetrahydroquinolin-1-yl)pent-1-en-1-yl]-2-methyl-4-oxo-2,3,4,5-tetrahydro-1*H*-1,5-benzodiazepin-7-yl]piperidin-1-yl}-2-oxoethyl)-3,9-diazaspiro[5.5]undecan-3-yl]-2,3-dihydro-1*H*-isoindole-1,3-dione (121)

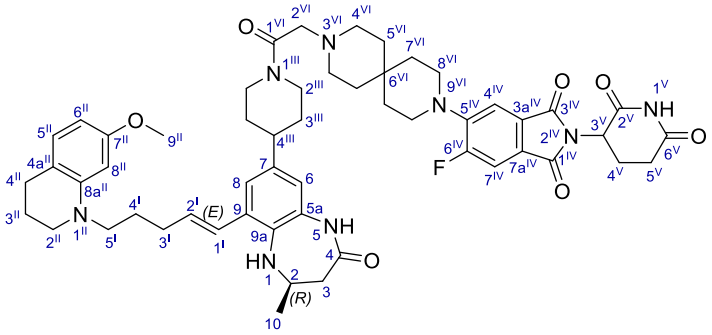

Synthesised according to 'General Amide Coupling Method I.I'. The crude reaction mixture was directly purified using MDAP (method B) to afford 2-(2,6-dioxopiperidin-3-yl)-5-fluoro-6-[9-(2-{4-[(2*R*)-9-[(1*E*)-5-(7-methoxy-1,2,3,4-tetrahydroquinolin-1-yl)pent-1-en-1-yl]-2-methyl-4-oxo-2,3,4,5-tetrahydro-1*H*-1,5-benzodiazepin-7-yl]piperidin-1-yl}-2-oxoethyl)-3,9-diazaspiro[5.5]undecan-3-yl]-2,3-dihydro-1*H*-isoindole-1,3-dione (**121**) (4.8 mg, 5.0 μmol, 23%): R_f 0.00 (acetone); ^{1}H NMR (400 MHz, $CO(CD_3)_2$) δ_H 9.85 (1 H, br s, NH-1^V), 8.38 (1 H, s, NH-5), 7.51 (1 H, d, *J* 11.5, H-7^{IV}), 7.42 (1 H, d, *J* 7.6, H-4^{IV}), 7.11 (1 H, d, *J* 2.1, H-8), 6.82 (1 H, d, *J* 2.1, H-6), 6.78 (1 H, d, *J* 15.5, H-1^I), 6.22 (1 H, dt, *J* 15.5, 7.0, H-2^I), 6.12 (1 H, d, *J* 2.4, H-8^{II}), 6.06 (1 H, dd, *J* 8.2, 2.4, H-6^{II}), 5.09 (1 H, dd, *J* 12.6, 5.3, H-3^V), 4.64 (1 H, dd, *J* 13.7, 2.9, CH_2), 4.41 – 4.29 (2 H, m, CH_2), 4.10 – 4.00 (1 H, m, H-2), 3.65 (3 H, s, H-9^{II}), 3.34 – 3.25 (11 H, m, CH_2), 2.80 – 2.78 (2 H, m, CH_2), 2.74 (2 H, d, *J* 6.4, CH_2), 2.60 (2 H, t, *J* 6.4, CH_2), 2.54 – 2.46 (7 H, m, CH_2), 2.35 – 2.30 (2 H, m, CH_2), 2.23 – 2.18 (2 H, m, CH_2), 1.88 – 1.77 (7 H, m, CH_2), 1.69 – 1.66 (4 H, m, CH_2), 1.63 (4 H, t, *J* 5.5, CH_2), 1.29 (3 H, d, *J* 6.4, H-10); ^{19}F NMR (376 MHz, $CO(CD_3)_2$) δ_F −113.32 (1 F, s); HRMS *m/z* (ESI$^+$) 957.5054 (957.5033 calculated for $[C_{54}H_{66}N_8O_7]^+$); LCMS (formic acid) t_R 0.96 min, *m/z* (ESI$^+$) 957.6 $[M+H]^+$, purity 88%.

2-(2,6-Dioxopiperidin-3-yl)-5-fluoro-6-{4-[1-(2-{4-[(2*R*)-9-[(1*E*)-5-(7-methoxy-1,2,3,4-tetrahydroquinolin-1-yl)pent-1-en-1-yl]-2-methyl-4-oxo-2,3,4,5-tetrahydro-1*H*-1,5-benzodiazepin-7-yl]piperidin-1-yl}-2-oxoethyl)piperidin-4-yl]piperazin-1-yl}-2,3-dihydro-1*H*-isoindole-1,3-dione (122)

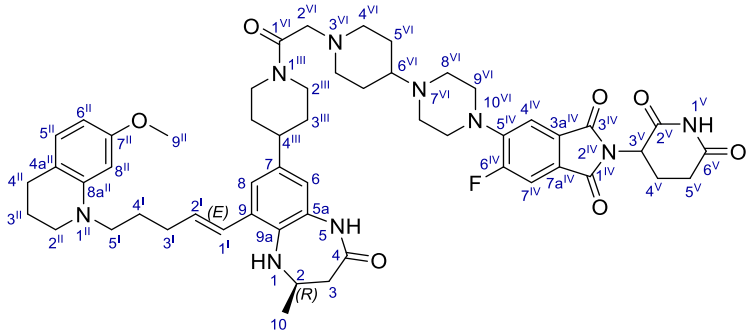

Synthesised according to 'General Amide Coupling Method I.I'. The crude reaction mixture was directly purified using MDAP (method B) to afford 2-(2,6-dioxopiperidin-3-yl)-5-fluoro-6-{4-[1-(2-{4-[(2*R*)-9-[(1*E*)-5-(7-methoxy-1,2,3,4-tetrahydroquinolin-1-yl)pent-1-en-1-yl]-2-methyl-4-oxo-2,3,4,5-tetrahydro-1*H*-1,5-benzodiazepin-7-yl]piperidin-1-yl}-2-oxoethyl)piperidin-4-yl]piperazin-1-yl}-2,3-dihydro-1*H*-isoindole-1,3-dione (**123**) (3.7 mg, 3.8 μmol, 16%): R_f 0.00 (acetone); ^{1}H NMR (400 MHz, $CO(CD_3)_2$) δ_H 9.86 (1 H, br s, NH-1^V), 8.40 (1 H, br s, NH-5), 7.52 (1 H, d, *J* 11.5, H-7^{IV}), 7.39 (1 H, d, *J* 7.6, H-4^{IV}), 7.11 (1 H, d, *J* 2.1, H-8), 6.82 (1 H, d, *J* 2.1, H-6), 6.79 – 6.72 (2 H, m, H-1^I, H-5^{II}), 6.22 (1 H, dt, *J* 15.5, 6.9, H-2^I), 6.11 (1 H, d, *J* 2.4, H-8^{II}), 6.06 (1 H, dd, *J* 8.2, 2.4, H-6^{II}), 5.09 (1 H, dd, *J* 12.6, 5.5, H-3^V), 4.67 – 4.61 (1 H, m, H-2), 4.37 – 4.30 (1 H, m, H-6^{VI}), 4.09 – 4.02 (1 H, m, H-2), 3.65 (3 H, s, H-9^{II}), 3.31 – 3.25 (10 H, m, CH_2), 3.12 – 3.07 (5 H, m, CH_2), 3.01 – 2.93 (8 H, m, CH_2), 2.80 – 2.72 (9 H, m, CH_2), 2.61 (2 H, t, *J* 6.1, CH_2), 2.33 – 2.30 (2 H, m, CH_2), 1.89 – 1.83 (5 H, m, CH_2), 1.82 – 1.77 (2 H, m, CH_2), 1.63 – 1.54 (2 H, m, CH_2), 1.28 (3 H, d, *J* 6.1, H-10); ^{19}F NMR (376 MHz, $CO(CD_3)_2$) δ_F −113.09 (1 F, s, F-6^{IV}); HRMS *m/z* (ESI$^+$) 972.5090 (972.5142 calculated for $[C_{54}H_{67}FN_9O_7]^+$); LCMS (formic acid) t_R 0.76 min, *m/z* (ESI$^+$) 972.6 $[M+H]^+$, purity 79%.

3-(5-{4-[(4-{4-[(2*R*)-9-[(1*E*)-5-(7-Methoxy-1,2,3,4-tetrahydroquinolin-1-yl)pent-1-en-1-yl]-2-methyl-4-oxo-2,3,4,5-tetrahydro-1*H*-1,5-benzodiazepin-7-yl]piperidine-1-carbonyl}phenyl)methyl]piperazin-1-yl}-1-oxo-2,3-dihydro-1*H*-isoindol-2-yl)piperidine-2,6-dione (123)

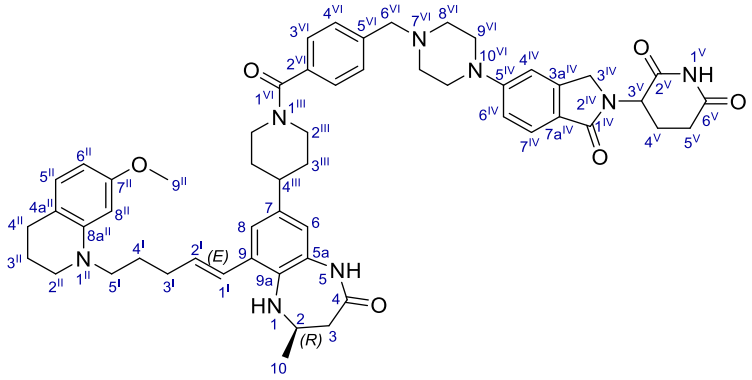

Synthesised according to 'General Amide Coupling Method I.I'. The crude reaction mixture was directly purified using MDAP (method B) to afford 3-(5-{4-[(4-{4-[(2*R*)-9-[(1*E*)-5-(7-methoxy-1,2,3,4-tetrahydroquinolin-1-yl)pent-1-en-1-yl]-2-methyl-4-oxo-2,3,4,5-tetrahydro-1*H*-1,5-benzodiazepin-7-yl]piperidine-1-carbonyl}phenyl)methyl]piperazin-1-yl}-1-oxo-2,3-dihydro-1*H*-isoindol-2-yl)piperidine-2,6-dione (**122**) (0.7 mg, 0.8 μmol, 3%): R_f 0.029 (acetone); LCMS (formic acid) t_R 0.89 min, *m/z* (ESI$^+$) 933.5 $[M+H]^+$, purity 80%. Compound was not tested, no further data collected.

4-{2-[2-(4-{2-[(2*S*)-1-(3,4-Difluorophenyl)-6-oxopiperidin-2-yl]-5-(3,5-dimethyl-1,2-oxazol-4-yl)-1*H*-1,3-benzodiazol-1-yl}piperidin-1-yl)-2-oxoethoxy]ethoxy}-2-(2,6-dioxopiperidin-3-yl)-2,3-dihydro-1*H*-isoindole-1,3-dione (134)

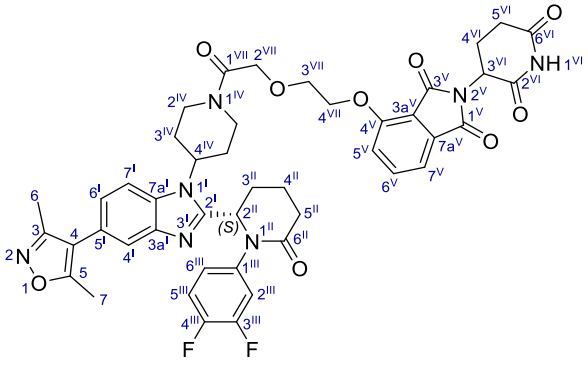

Synthesised according to 'General Amide Coupling Method II'. The crude reaction mixture was directly purified by MDAP (method B) to afford 4-{2-[2-(4-{2-[(2S)-1-(3,4-difluorophenyl)-6-oxopiperidin-2-yl]-5-(3,5-dimethyl-1,2-oxazol-4-yl)-1H-1,3-benzodiazol-1-yl}piperidin-1-yl)-2-oxoethoxy]ethoxy}-2-(2,6-dioxopiperidin-3-yl)-2,3-dihydro-1H-isoindole-1,3-dione (**134**) (7.4 mg, 8.6 µmol, 43%): R_f 0.06 (1:1 EtOAc/ acetone); ^{1}H NMR (400 MHz, CD_3CN) δ_H 8.86 (1 H, br s, NH-1^{VI}), 7.72 (1 H, dd, *J* 8.3, 7.3, H-6^{V}), 7.60 (1 H, d, *J* 1.0, H-4^{I}), 7.55 (1 H, d, *J* 7.8, H-7^{I}), 7.43 – 7.35 (2 H, m, H-5^{V}, H-6^{V}), 7.23 – 7.06 (2 H, m, H-2^{III}, H-6^{I}), 7.06 – 6.99 (1 H, m, H-6^{III}), 5.46 (1 H, t, *J* 4.4, H-2^{II}), 4.89 (1 H, dd, *J* 12.5, 5.4, H-3^{VI}), 4.56 – 4.34 (3 H, m, CH_2), 4.06 – 3.88 (3 H, m, H-4^{IV}), 3.22 – 3.01 (1 H, m, CH_2), 2.75 – 2.48 (7 H, m, CH_2), 2.47 – 2.31 (9 H, m, H-7, CH_2), 2.22 (3 H, s, H-6), 2.16 – 2.07 (2 H, m, CH_2), 1.87 – 1.80 (1 H, m, CH_2), 1.44 – 1.28 (1 H, m, CH_2); ^{19}F NMR (376 MHz, CD_3CN) δ_F −138.71 (1 F, dd, *J* 21.2, 5.7, F-4^{III}), −141.35 (1 F, dd, *J* 21.2, 5.2, F-3^{III}); HRMS *m/z* (ESI$^+$) 864.3189 (864.3163 calculated for $[C_{45}H_{44}F_2N_7O_9]^+$); LCMS (formic acid) t_R 0.88 min, *m/z* (ESI$^+$) 864.4 $[M+H]^+$, purity 99%.

4-(2-(2-(2-(4-(2-((*S*)-1-(3,4-Difluorophenyl)-6-oxopiperidin-2-yl)-5-(3,5-dimethylisoxazol-4-yl)-1*H*-benzo[d]imidazol-1-yl)piperidin-1-yl)-2-oxoethoxy)ethoxy)ethoxy)-2-(2,6-dioxopiperidin-3-yl)isoindoline-1,3-dione (135)

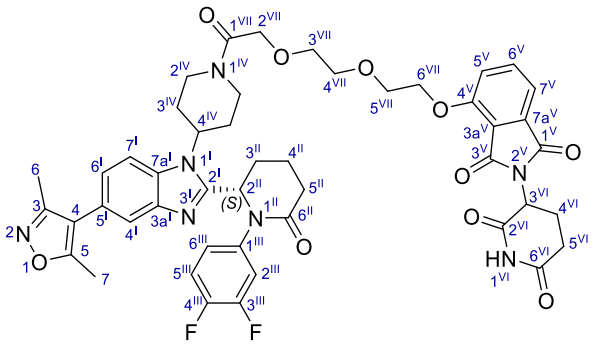

A solution of (*S*)-1-(3,4-difluorophenyl)-6-(5-(3,5-dimethylisoxazol-4-yl)-1-(piperidin-4-yl)-1*H*-benzo[d]imidazol-2-yl)piperidin-2-one (**87**) (15.0 mg, 29.7 µmol, 1.0 eq.), 2-(2-(2-((2-(2,6-dioxopiperidin-3-yl)-1,3-dioxoisoindolin-4-yl)oxy)ethoxy)ethoxy)acetic acid (14.0 mg, 33.3 µmol, 1.1 eq.), HATU (14.0 mg, 36.8 µmol, 1.2 eq.), and DIPEA (16 µL, 92 µmol, 3.1 eq.) in DMF (300 µL) was stirred at rt for 2 h. The crude reaction mixture was directly purified using preparative reverse phase column chromatography (gradient of 30 – 99% MeCN in 10 mM aq. $(NH_4)HCO_3$ (pH 10)) to afford 4-(2-(2-(2-(4-(2-((*S*)-1-(3,4-Difluorophenyl)-6-oxopiperidin-2-yl)-5-(3,5-dimethylisoxazol-4-yl)-1*H*-benzo[d]imidazol-1-yl)piperidin-1-yl)-2-oxoethoxy)ethoxy)ethoxy)-2-(2,6-dioxopiperidin-3-yl)isoindoline-1,3-dione (**135**) (17.3 mg, 18.0 µmol, 59%): R_f 0.04 (1:1 EtOAC/ acetone); ^{1}H NMR (400 MHz, CD_3CN) δ_H 8.97 (1 H, br s, NH-1^{VI}), 7.70 – 7.62 (1 H, m, H-6^{V}), 7.61 (1 H, d, *J* 1.7, H-4^{I}), 7.58 (1 H, d, *J* 8.6, H-7^{I}), 7.40 – 7.35 (1 H, m, H-6^{I}), 7.28 (1 H, d, *J* 8.1, H-5^{V}), 7.22 – 7.09 (3 H, m, H-2^{III}, H-5^{III}, H-7^{V}), 7.05 – 6.99 (1 H, m, H-6^{III}), 5.46 (1 H, m, H-2^{II}), 5.00 – 4.90 (1 H, m, H-3^{VI}), 4.69 – 4.52 (1 H, m, CH_2), 4.48 – 4.34 (1 H, m, CH_2), 4.30 – 4.15 (3 H, m, CH_2), 4.06 – 3.88 (1 H, m, H-4^{IV}), 3.87 – 3.80 (2 H, m, CH_2), 3.75 – 3.64 (3 H, m, CH_2), 3.19 – 3.01 (1 H, m, CH_2), 2.76 – 2.53 (5 H, m, CH_2), 2.47 – 2.39 (1 H, m, CH_2), 2.37 (3 H, s, H-7), 2.31 – 2.12 (9 H, m, H-6), 2.11 – 1.99 (3 H, m, CH_2), 1.87 – 1.78 (1 H, m, CH_2), 1.44 – 1.26 (1 H, m, CH_2); ^{19}F NMR (376 MHz, CD_3CN) δ_F −138.69 (1 F, dd, *J* 21.2, 10.3, F-4^{III}), −141.33 (1 F, d, *J* 21.2, F-3^{III}); HRMS *m/z* (ESI$^+$) 908.3475

(908.3425 calculated for $[C_{47}H_{48}F_2N_7O_{10}]^+$); LCMS (HpH): t_R 0.94 min, *m/z* (ESI$^+$) 908.3 $[M+H]^+$, purity 92%.

4-[2-(2-{2-[2-(4-{2-[(2*S*)-1-(3,4-Difluorophenyl)-6-oxopiperidin-2-yl]-5-(3,5-dimethyl-1,2-oxazol-4-yl)-1*H*-1,3-benzodiazol-1-yl}piperidin-1-yl)-2-oxoethoxy]ethoxy}ethoxy)ethoxy]-2-(2,6-dioxopiperidin-3-yl)-2,3-dihydro-1*H*-isoindole-1,3-dione (136)

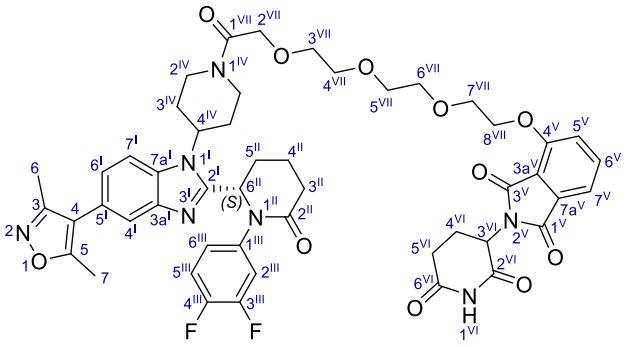

Synthesised according to 'General Amide Coupling Method II'. The crude reaction mixture was directly purified using MDAP (method B) to afford 4-[2-(2-{2-[2-(4-{2-[(2*S*)-1-(3,4-difluorophenyl)-6-oxopiperidin-2-yl]-5-(3,5-dimethyl-1,2-oxazol-4-yl)-1*H*-1,3-benzodiazol-1-yl}piperidin-1-yl)-2-oxoethoxy]ethoxy}ethoxy)ethoxy]-2-(2,6-dioxopiperidin-3-yl)-2,3-dihydro-1*H*-isoindole-1,3-dione (**136**) (9.9 mg, 10 µmol, 53%): R_f 0.07 (acetone); ^{1}H NMR (400 MHz, CD_3CN) δ_H 9.17 – 8.99 (1 H, m, NH-1^{VI}), 7.71 (1 H, dd, *J* 7.5, H-6^{V}), 7.62 – 7.58 (2 H, m, H-4^{I}, H-7^{V}), 7.42 – 7.36 (1 H, m, H-7^{I}), 7.34 (1 H, d, *J* 8.6, H-5^{V}), 7.23 – 7.00 (4 H, m, H-6^{I}, H-2^{III}, H-5^{III}, H-6^{III}), 5.50 – 5.44 (1 H, m, H-6^{II}), 4.95 (1 H, dd, *J* 12.4, 5.3, H-3^{VI}), 4.69 – 4.51 (1 H, m, C*H*$_2$), 4.49 – 4.38 (1 H, m, C*H*$_2$), 4.30 – 4.20 (3 H, m, C*H*$_2$), 4.19 – 4.09 (1 H, m, H-4^{IV}), 4.05 – 3.91 (1 H, m, C*H*$_2$), 3.79 – 3.69 (2 H, m, C*H*$_2$), 3.65 – 3.53 (8 H, m, C*H*$_2$), 3.22 – 3.04 (1 H, m, C*H*$_2$), 2.77 – 2.50 (8 H, m, C*H*$_2$), 2.48 – 2.40 (2 H, m, C*H*$_2$), 2.37 (3 H, s, H-7), 2.21 (3 H, s, H-6), 2.16 – 2.04 (3 H, m, C*H*$_2$), 1.90 – 1.80 (2 H, m, C*H*$_2$); ^{19}F NMR (376 MHz, CD_3CN) δ_F −138.71 (1 F, d, *J* 21.2, F-4^{III}), −(141.20 – 141.45) (1 F, m, F-3^{III}); HRMS *m/z* (ESI$^+$) 952.3666 (952.3687 calculated for $[C_{49}H_{52}F_2N_7O_{11}]^+$); LCMS (formic acid) t_R 0.90 min, *m/z* (ESI$^+$) 952.4 $[M+H]^+$, purity 100%.

4-{[14-(4-{2-[(2*S*)-1-(3,4-Difluorophenyl)-6-oxopiperidin-2-yl]-5-(3,5-dimethyl-1,2-oxazol-4-yl)-1*H*-1,3-benzodiazol-1-yl}piperidin-1-yl)-14-oxo-3,6,9,12-tetraoxatetradecan-1-yl]oxy}-2-(2,6-dioxopiperidin-3-yl)-2,3-dihydro-1*H*-isoindole-1,3-dione (137)

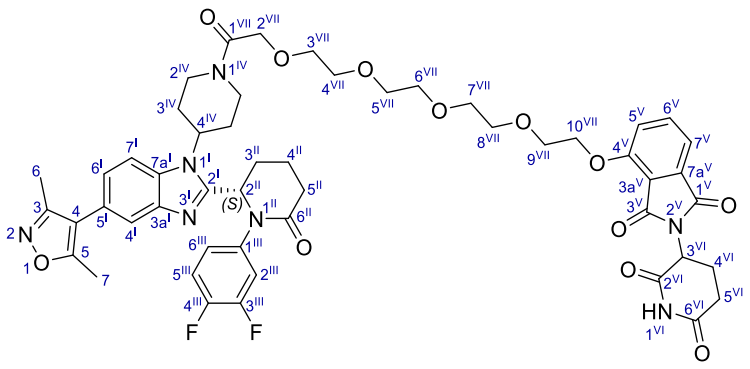

Synthesised according to 'General Amide Coupling Method II'. The crude reaction mixture was directly purified using MDAP (extended method B) to afford 4-{[14-(4-{2-[(2*S*)-1-(3,4-difluorophenyl)-6-oxopiperidin-2-yl]-5-(3,5-dimethyl-1,2-oxazol-4-yl)-1*H*-1,3-benzodiazol-1-yl}piperidin-1-yl)-14-oxo-3,6,9,12-tetraoxatetradecan-1-yl]oxy}-2-(2,6-dioxopiperidin-3-yl)-2,3-dihydro-1*H*-isoindole-1,3-dione (**137**) (7.6 mg, 7.6 µmol, 39%): R_f 0.04 (acetone); ^{1}H NMR (400 MHz, CD_3CN) δ_H 9.05 (1 H, br s, NH-1^{VI}), 7.72 (1 H, dd, *J* 8.4, 7.6, H-6^{V}), 7.61 (1 H, d, *J* 1.2, H-4^{I}), 7.59 (1 H, d, *J* 8.6, H-7^{I}), 7.40 (1 H, d, *J* 7.6, H-7^{V}), 7.37 (1 H, d, *J* 8.6, H-6^{I}), 7.23 – 7.16 (1 H, m, H-5^{V}), 7.16 – 7.09 (2 H, m, H-2^{III}, H-5^{III}), 7.06 – 7.00 (1 H, m, H-6^{III}), 5.47 (1 H, dd, *J* 5.1, 3.9, H-2^{II}), 5.00 - 4.92 (1 H, m, H-3^{VI}), 4.68 – 4.50 (1 H, m, CH_2), 4.48 – 4.38 (1 H, m, CH_2), 4.32 – 4.28 (2 H, m, CH_2), 4.26 – 4.12 (2 H, m, CH_2), 4.04 – 3.89 (1 H, m, H-4^{IV}), 3.82 – 3.79 (2 H, m, CH_2), 3.64 – 3.59 (5 H, m, CH_2), 3.53 – 3.48 (5 H, m, CH_2), 2.72 – 2.45 (12 H, m, CH_2), 2.38 (s, 3 H, H-7), 2.22 (3 H, s, H-6), 2.17 – 2.01 (4 H, m, CH_2), 1.89 – 1.81 (2 H, m, CH_2); ^{19}F NMR (376 MHz, CD_3CN) δ_F −138.71 (1 F, d, *J* 21.2, F-4^{III}), −141.35 (1 F, d, *J* 21.2, F-3^{III}); HRMS *m/z* (ESI$^+$) 996.3983 (996.3950 calculated for $[C_{51}H_{56}F_2N_7O_{12}]^+$); LCMS (formic acid) t_R 0.90 min, *m/z* (ESI$^+$) 996.5 $[M+H]^+$, purity 100%.

4-{[5-(4-{2-[(2*S*)-1-(3,4-Difluorophenyl)-6-oxopiperidin-2-yl]-5-(3,5-dimethyl-1,2-oxazol-4-yl)-1*H*-1,3-benzodiazol-1-yl}piperidin-1-yl)-5-oxopentyl]oxy}-2-(2,6-dioxopiperidin-3-yl)-2,3-dihydro-1*H*-isoindole-1,3-dione (138)

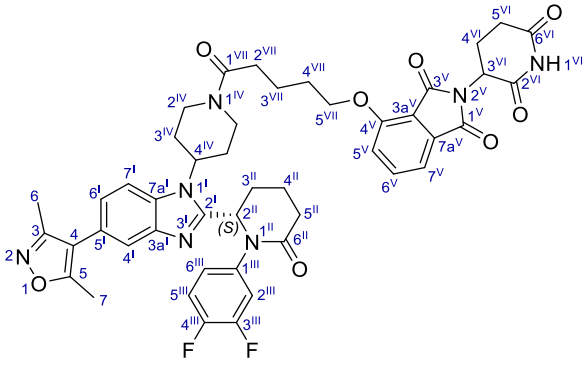

Synthesised according to 'General Amide Coupling Method II'. The crude reaction mixture was directly purified using MDAP (method B) to afford 4-{[5-(4-{2-[(2*S*)-1-(3,4-difluorophenyl)-6-oxopiperidin-2-yl]-5-(3,5-dimethyl-1,2-oxazol-4-yl)-1*H*-1,3-benzodiazol-1-yl}piperidin-1-yl)-5-oxopentyl]oxy}-2-(2,6-dioxopiperidin-3-yl)-2,3-dihydro-1*H*-isoindole-1,3-dione (**138**) (8.4 mg, 10 µmol, 49%): R_f 0.15 (1:1 EtOAc/ acetone); ^{1}H NMR (400 MHz, CD_3CN) δ_H 8.88 (1 H, br s, NH-1^{VI}), 7.74 (1 H, dd, *J* 8.4, 7.5, H-6^{V}), 7.61 (1 H, d, *J* 1.2, H-4^{I}), 7.60 – 7.55 (1 H, m, H-7^{I}), 7.41 – 7.35 (2 H, m, H-5^{V}, H-7^{V}), 7.23 – 7.06 (3 H, m, H-6^{I}, H-2^{III}, H-5^{III}), 7.06 – 7.00 (1 H, m, H-6^{III}), 5.48 (1 H, t, *J* 4.5, H-2^{II}), 4.95 – 4.86 (1 H, m, H-3^{VI}), 4.76 – 4.58 (1 H, m), 4.48 – 4.37 (1 H, m), 4.29 – 4.22 (2 H, m), 4.15 – 3.97 (1 H, m, H-4^{IV}), 3.22 – 3.07 (1 H, m, CH_2), 2.67 – 2.49 (10 H, m, CH_2), 2.38 (3 H, s, H-7), 2.22 (3 H, s, H-6), 2.16 – 1.98 (4 H, m, CH_2), 1.92 – 1.81 (6 H, m, CH_2), 1.42 – 1.31 (1 H, m, CH_2); ^{19}F NMR (376 MHz, CD_3CN) δ_F −138.70 (1 F, d, *J* 21.2, F-4^{III}), −(141.41 – 141.26) (1 F, m, F-3^{III}); HRMS *m/z* (ESI$^+$) 862.3355 (862.3370 calculated for $[C_{46}H_{46}F_2N_7O_8]^+$); LCMS (formic acid) t_R 0.95 min, *m/z* (ESI$^+$) 862.4 $[M+H]^+$, purity 100%.

4-{[8-(4-{2-[(2*S*)-1-(3,4-Difluorophenyl)-6-oxopiperidin-2-yl]-5-(3,5-dimethyl-1,2-oxazol-4-yl)-1*H*-1,3-benzodiazol-1-yl}piperidin-1-yl)-8-oxooctyl]oxy}-2-(2,6-dioxopiperidin-3-yl)-2,3-dihydro-1*H*-isoindole-1,3-dione (139)

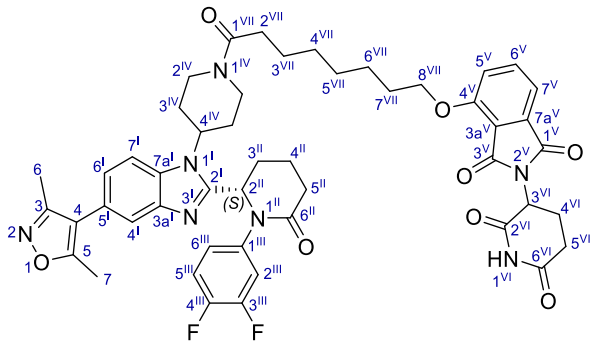

Synthesised according to 'General Amide Coupling Method II'. The crude reaction mixture was directly purified using MDAP (method C) to afford 4-{[8-(4-{2-[(2*S*)-1-(3,4-difluorophenyl)-6-oxopiperidin-2-yl]-5-(3,5-dimethyl-1,2-oxazol-4-yl)-1*H*-1,3-benzodiazol-1-yl}piperidin-1-yl)-8-oxooctyl]oxy}-2-(2,6-dioxopiperidin-3-yl)-2,3-dihydro-1*H*-isoindole-1,3-dione (**139**) (9.1 mg, 10 µmol, 51%): R_f 0.22 (1:1 EtOAc/ acetone); ^{1}H NMR (400 MHz, CD_3CN) δ_H 9.03 – 8.92 (1 H, m, NH-1^{VI}), 7.71 (1 H, dd, *J* 8.6, 7.2, H-6^{V}), 7.61 (1 H, d, *J* 1.2, H-4^{I}), 7.58 (1 H, d, *J* 8.6, H-7^{I}), 7.38 (1 H, d, *J* 7.2, H-7^{V}), 7.35 (1 H, d, *J* 8.6, H-5^{V}), 7.22 – 7.15 (1 H, m, H-6^{I}), 7.15 – 7.09 (1 H, m, H-5^{III}), 7.05 – 7.00 (1 H, m, H-2^{III}), 5.47 (1 H, dd, *J* 5.0, 3.8, H-2^{II}), 4.98 – 4.91 (1 H, m, H-3^{VI}), 4.78 – 4.60 (1 H, m, CH_2), 4.48 – 4.37 (1 H, m, CH_2), 4.20 (2 H, t, *J* 6.4, H-2^{VI}), 4.10 – 3.95 (1 H, m, H-4^{IV}), 3.23 – 3.06 (1 H, m, CH_2), 2.77 – 2.52 (6 H, m, CH_2), 2.37 (3 H, s, H-7), 2.27 – 2.06 (12 H, m, H-6, CH_2), 1.89 – 1.78 (4 H, m, CH_2), 1.66 – 1.57 (2 H, m, CH_2), 1.56 – 1.48 (2 H, m, CH_2), 1.45 – 1.35 (4 H, m, CH_2); ^{19}F NMR (376 MHz, CD_3CN) δ_F −138.72 (1 F, d, *J* 21.2, F-4^{III}), −141.35 (1 F, d, *J* 21.2, F-3^{III}); HRMS *m/z* (ESI$^+$) 904.3847 (904.3840 calculated for $[C_{49}H_{52}F_2N_7O_8]^+$); LCMS (formic acid) t_R 1.06 min, *m/z* (ESI$^+$) 904.5 $[M+H]^+$, purity 100%.

4-{[10-(4-{2-[(2*S*)-1-(3,4-Difluorophenyl)-6-oxopiperidin-2-yl]-5-(3,5-dimethyl-1,2-oxazol-4-yl)-1*H*-1,3-benzodiazol-1-yl}piperidin-1-yl)-10-oxodecyl]oxy}-2-(2,6-dioxopiperidin-3-yl)-2,3-dihydro-1*H*-isoindole-1,3-dione (140)

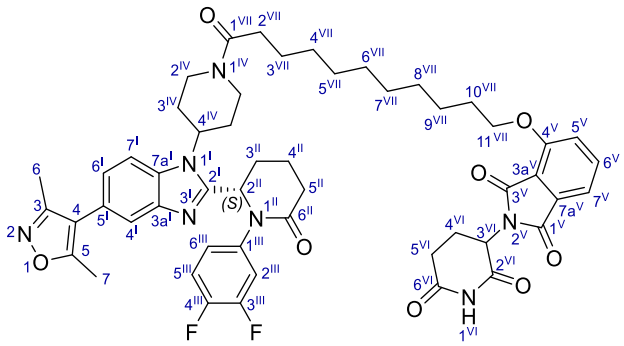

Synthesised according to 'General Amide Coupling Method II'. The crude reaction mixture was directly purified using MDAP (method C) to afford 4-{[10-(4-{2-[(2*S*)-1-(3,4-difluorophenyl)-6-oxopiperidin-2-yl]-5-(3,5-dimethyl-1,2-oxazol-4-yl)-1*H*-1,3-benzodiazol-1-yl}piperidin-1-yl)-10-oxodecyl]oxy}-2-(2,6-dioxopiperidin-3-yl)-2,3-dihydro-1*H*-isoindole-1,3-dione (**140**) (10.2 mg, 10.9 µmol, 55%): R_f 0.08 (EtOAc); ^{1}H NMR (400 MHz, CD_3CN) δ_H 9.19 – 9.05 (1 H, m, NH-1^{VI}), 7.74 (1 H, dd, *J* 7.8, H-6^{V}), 7.64 (1 H, s, H-4^{I}), 7.61 (1 H, d, *J* 8.6, H-7^{I}), 7.41 (1 H, dd, *J* 6.4, H-7^{V}), 7.37 (1 H, d, *J* 8.6, H-6^{I}), 7.25 – 7.19 (1 H, m, H-5^{V}), 7.18 – 7.12 (2 H, m, H-2^{III}, H-5^{III}), 7.08 – 7.03 (1 H, m, H-6^{III}), 5.51 (1 H, dd, *J* 5.3, 3.8, H-2^{II}), 5.02 – 4.94 (1 H, m, H-3^{VI}), 4.81 – 4.64 (1 H, m, CH_2), 4.52 – 4.40 (1 H, m, CH_2), 4.26 – 4.15 (2 H, m, CH_2), 4.13 – 3.97 (1 H, m, H-4^{IV}), 3.27 – 3.09 (1 H, m, CH_2), 2.81 – 2.56 (6 H, m, CH_2), 2.52 – 2.42 (2 H, m, CH_2), 2.25 (3 H, s, H-7) 2.41 (3 H, s, H-6), 2.23 —2.16 (4 H, m, CH_2), 2.15 – 2.09 (2 H, m, CH_2), 1.93 – 1.79 (4 H, m, CH_2), 1.67 – 1.58 (2 H, m, CH_2), 1.57 – 1.48 (2 H, m, CH_2), 1.46 – 1.34 (9 H, m, CH_2); ^{19}F NMR (376 MHz, CD_3CN) δ_F −138.69 (1 F, d, *J* 21.2, F-4^{III}), −141.32 (1 F, d, *J* 21.2, F-3^{III}); HRMS *m/z* (ESI$^+$) 932.4155 (932.4153 calculated for $[C_{51}H_{56}F_2N_7O_8]^+$); LCMS (formic acid) t_R 1.16 min, *m/z* (ESI$^+$) 932.5 $[M+H]^+$, purity 100%.

5-{4-[2-(4-{2-[(2S)-1-(3,4-Difluorophenyl)-6-oxopiperidin-2-yl]-5-(3,5-dimethyl-1,2-oxazol-4-yl)-1H-1,3-benzodiazol-1-yl}piperidin-1-yl)-2-oxoethyl]piperazin-1-yl}-2-(2,6-dioxopiperidin-3-yl)-6-fluoro-2,3-dihydro-1H-isoindole-1,3-dione (141)

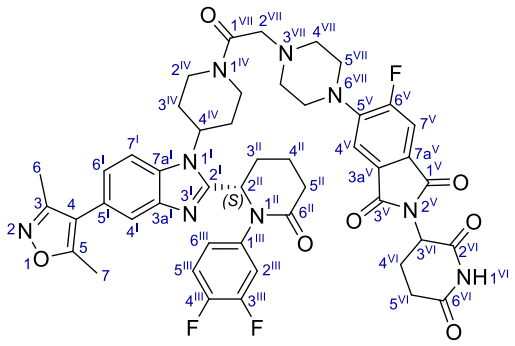

Synthesised according to 'General Amide Coupling Method II'. The crude reaction mixture was directly purified using MDAP (method B) to afford 5-{4-[2-(4-{2-[(2*S*)-1-(3,4-difluorophenyl)-6-oxopiperidin-2-yl]-5-(3,5-dimethyl-1,2-oxazol-4-yl)-1*H*-1,3-benzodiazol-1-yl}piperidin-1-yl)-2-oxoethyl]piperazin-1-yl}-2-(2,6-dioxopiperidin-3-yl)-6-fluoro-2,3-dihydro-1*H*-isoindole-1,3-dione (**141**) (7.5 mg, 8.3 µmol, 41%): R_f 0.11 (1:1 EtOAc/ acetone); ^{1}H NMR (400 MHz, CD_3CN) δ_H 8.93 (1 H, br s, NH-1^{VI}), 7.61 (1 H, d, *J* 1.0, H-4^{I}), 7.56 (1 H, d, *J* 8.6, H-7^{I}), 7.51 (1 H, d, *J* 11.5, H-7^{V}), 7.41 – 7.34 (1 H, m, H-4^{V}), 7.25 – 7.18 (1 H, m, H-6^{I}), 7.18 – 7.10 (2 H, m, H-2^{III}, H-5^{III}), 7.07 – 7.00 (1 H, m, H-6^{III}), 5.49 (1 H, dd, *J* 5.4, 3.8, H-2^{II}), 4.94 (1 H, dd, *J* 12.5, 5.4, H-3^{VI}), 4.75 – 4.58 (1 H, m, C*H*$_2$), 4.53 – 4.43 (1 H, m, C*H*$_2$), 4.35 – 4.17 (1 H, m, H-4^{IV}), 3.46 (2 H, d, *J* 13.2, C*H*$_2$), 3.35 – 3.26 (4 H, m, C*H*$_2$), 3.21 – 3.09 (3 H, m, C*H*$_2$), 2.78 – 2.64 (8 H, m, C*H*$_2$), 2.63 – 2.55 (2 H, m, C*H*$_2$), 2.55 – 2.41 (2 H, m, C*H*$_2$), 2.34 (3 H, s, H-7), 2.19 (3 H, s, H-6), 2.17 - 2.05 (3 H, m, C*H*$_2$), 1.89 – 1.82 (1 H, m, C*H*$_2$), 1.48 – 1.34 (2 H, m, C*H*$_2$); ^{19}F NMR (376 MHz, CD_3CN) δ_F −113.09 (1 F, s, F-4^{III}), −138.71 (1 F, d, *J* 20.9, F-3^{III}), −141.35 (1 F, d, *J* 20.9); HRMS *m/z* (ESI$^+$) 906.3548 (906.3545 calculated for $[C_{47}H_{47}F_3N_9O_7]^+$); LCMS (formic acid) t_R 0.70 min, *m/z* (ESI$^+$) 906.4 $[M+H]^+$, purity 98%.

3-(5-{4-[4-(4-{2-[(2*S*)-1-(3,4-Difluorophenyl)-6-oxopiperidin-2-yl]-5-(3,5-dimethyl-1,2-oxazol-4-yl)-1*H*-1,3-benzodiazol-1-yl}piperidin-1-yl)-4-oxobutyl]piperazin-1-yl}-1-oxo-2,3-dihydro-1*H*-isoindol-2-yl)piperidine-2,6-dione (142)

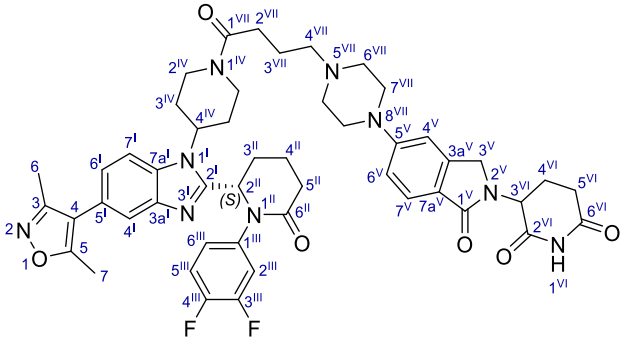

Synthesised according to 'General Amide Coupling Method II'. The crude reaction mixture was directly purified using MDAP (method A) to afford 3-(5-{4-[4-(4-{2-[(2*S*)-1-(3,4-difluorophenyl)-6-oxopiperidin-2-yl]-5-(3,5-dimethyl-1,2-oxazol-4-yl)-1*H*-1,3-benzodiazol-1-yl}piperidin-1-yl)-4-oxobutyl]piperazin-1-yl}-1-oxo-2,3-dihydro-1*H*-isoindol-2-yl)piperidine-2,6-dione (**142**) (8.3 mg, 9.2 µmol, 46%): R_f 0.04 (acetone); ^{1}H NMR (400 MHz, CD_3CN) δ_H 8.85 – 8.74 (1 H, m, NH-1^{VI}), 8.13 – 8.09 (1 H, m, H-6^{V}), 7.62 (1 H, d, *J* 1.7, H-4^{I}), 7.62 – 7.59 (1 H, m, H-6^{V}), 7.56 (1 H, d, *J* 8.3, H-7^{I}), 7.22 – 7.16 (1 H, m, H-6^{I}), 7.15 – 7.10 (2 H, m, H-2^{III}, H-5^{III},), 7.06 – 7.00 (3 H, m, H-6^{III}, H-4^{V}, H-6^{V}), 5.48 (1 H, dd, *J* 5.3, 4.0, H-2^{II}), 5.02 (1 H, dd, *J* 13.5, 5.1, H-3^{VI}), 4.81 – 4.62 (1 H, m, CH_2), 4.49 – 4.38 (2 H, m, CH_2), 4.35 – 4.19 (3 H, m, CH_2), 4.14 – 3.97 (3 H, m, H-4^{IV}), 3.39 – 3.31 (4 H, m, CH_2), 3.25 – 3.08 (3 H, m, CH_2), 2.75 – 2.67 (5 H, m, CH_2), 2.63 – 2.43 (7 H, m, CH_2), 2.38 (3 H, s, H-7), 2.22 (3 H, s, H-6), 2.16 – 2.06 (3 H, m, CH_2), 1.91 – 1.81 (4 H, m, CH_2), 1.43 – 1.32 (1 H, m, CH_2); ^{19}F NMR (376 MHz, CD_3CN) δ_F −138.71 (1 F, d, *J* 21.2, F-4^{III}), −141.34 (1 F, d, *J* 21.2, F-3^{III}); HRMS *m/z* (ESI$^+$) 902.4178 (902.4160 calculated for $[C_{49}H_{53}F_2N_9O_6]^+$); LCMS (formic acid) t_R 0.63 min, *m/z* (ESI$^+$) 902.5 $[M+H]^+$, purity 98%.

5-{9-[2-(4-{2-[(2*S*)-1-(3,4-Difluorophenyl)-6-oxopiperidin-2-yl]-5-(3,5-dimethyl-1,2-oxazol-4-yl)-1*H*-1,3-benzodiazol-1-yl}piperidin-1-yl)-2-oxoethyl]-3,9-diazaspiro[5.5]undecan-3-yl}-2-(2,6-dioxopiperidin-3-yl)-6-fluoro-2,3-dihydro-1*H*-isoindole-1,3-dione (143)

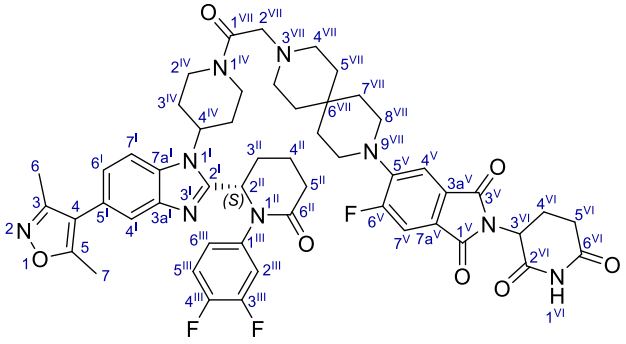

Synthesised according to 'General Amide Coupling Method II'. The crude reaction mixture was directly purified using MDAP (method B) to afford 5-{9-[2-(4-{2-[(2*S*)-1-(3,4-difluorophenyl)-6-oxopiperidin-2-yl]-5-(3,5-dimethyl-1,2-oxazol-4-yl)-1*H*-1,3-benzodiazol-1-yl}piperidin-1-yl)-2-oxoethyl]-3,9-diazaspiro[5.5]undecan-3-yl}-2-(2,6-dioxopiperidin-3-yl)-6-fluoro-2,3-dihydro-1*H*-isoindole-1,3-dione (**143**) (12.1 mg, 12.4 μmol, 63%): R_f 0.08 (EtOAc); ^{1}H NMR (400 MHz, CD_3CN) δ_H 9.05 – 8.88 (1 H, m, H-6^V), 7.63 (1 H, d, *J* 1.3, H-4^I), 7.61 (1 H, dd, *J* 8.7, 1.3, H-6^I), 7.48 (1 H, d, *J* 11.5, H-7^V), 7.42 (1 H, d, *J* 7.6, H-7^I), 7.26 – 7.11 (3 H, m, H-4^V, H-2^{III}, H-5^{III}), 7.08 – 7.01 (1 H, m, H-6^{III}), 5.50 (1 H, t, *J* 4.5, H-2^{II}), 5.00 – 4.91 (1 H, m, H-3^{VI}), 4.73 – 4.55 (1 H, m, CH_2), 4.53 – 4.42 (1 H, m, CH_2), 4.13 – 3.97 (1 H, m, H-4^{IV}), 3.65 – 3.46 (9 H, m, CH_2), 3.27 – 3.22 (4 H, m, CH_2), 3.21 – 3.08 (1 H, m, CH_2), 2.92 – 2.79 (4 H, m, CH_2), 2.77 – 2.54 (6 H, m, CH_2), 2.39 (3 H, s, H-7), 2.23 (3 H, s, H-6), 2.14 – 2.07 (2 H, m, CH_2), 1.90 – 1.82 (1 H, m, CH_2), 1.74 – 1.70 (3 H, m, CH_2), 1.67 – 1.64 (3 H, m, CH_2), 1.45 – 1.34 (1 H, m, CH_2); ^{19}F NMR (376 MHz, CD_3CN) δ_F −113.37 (1 F, s, F-6^V), −138.68 (1 F, dd, *J* 21.2, 2.9, F-4^{III}), −141.32 (1 F, dd, *J* 21.2, 8.9, F-3^{III}); HRMS *m/z* (ESI$^+$) 974.4163 (974.4171 calculated for $[C_{52}H_{55}F_3N_9O_7]^+$); LCMS (formic acid) t_R 0.76 min, *m/z* (ESI$^+$) 974.5 $[M+H]^+$, purity 100%.

3-[5-(4-{[4-(4-{2-[(2*S*)-1-(3,4-Difluorophenyl)-6-oxopiperidin-2-yl]-5-(3,5-dimethyl-1,2-oxazol-4-yl)-1*H*-1,3-benzodiazol-1-yl}piperidine-1-carbonyl)phenyl]methyl}piperazin-1-yl)-1-oxo-2,3-dihydro-1*H*-isoindol-2-yl]piperidine-2,6-dione (144)

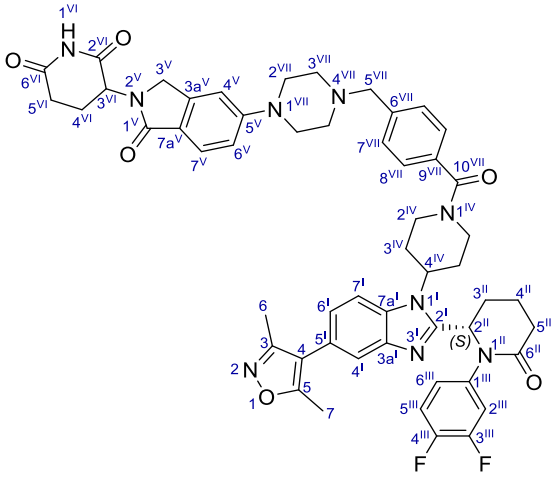

Method I:

Synthesised according to 'General Amide Coupling Method II'. The crude reaction mixture was directly purified by MDAP (method A) to afford 3-[5-(4-{[4-(4-{2-[(2*S*)-1-(3,4-difluorophenyl)-6-oxopiperidin-2-yl]-5-(3,5-dimethyl-1,2-oxazol-4-yl)-1*H*-1,3-benzodiazol-1-yl}piperidine-1-carbonyl)phenyl]methyl}piperazin-1-yl)-1-oxo-2,3-dihydro-1*H*-isoindol-2-yl]piperidine-2,6-dione (**144**) (9.6 mg, 10 µmol, 44%): R_f 0.08 (acetone); ^{1}H NMR (400 MHz, CD_3CN) δ_H 8.79 (1 H, br s, NH-1^{VI}), 7.71 (1 H, d, *J* 8.3, H-6^{V}), 7.63 (1 H, d, *J* 1.0, H-4^{I}), 7.58 – 7.54 (1 H, m, H-7^{V}), 7.49 – 7.41 (4 H, m, H-7^{VII}, H-8^{VII}), 7.23 – 7.08 (3 H, m, H-2^{III}, H-5^{III}, H-5^{V}), 7.06 – 7.01 (2 H, m, H-6^{III}, H-6^{V}), 7.00 (1 H, s, H-4^{V}), 5.50 (1 H, dd, *J* 5.2, 4.0, H-2^{II}), 5.02 (1 H, dd, *J* 13.5, 5.2, H-3^{VI}), 4.55 – 4.43 (1 H, m, CH_2), 4.34 – 4.19 (2 H, m, H-4^{VI}, CH_2), 3.62 (2 H, s, H-5^{VII}), 3.35 – 3.29 (5 H, m, CH_2), 2.86 – 2.63 (4 H, m, CH_2), 2.62 – 2.59 (4 H, m, CH_2), 2.58 – 2.41 (4 H, m, CH_2), 2.40 (3 H, s, H-7), 2.39 – 2.27 (3 H, m, CH_2), 2.24 (3 H, s, H-6), 2.23 – 2.20 (1 H, m, CH_2), 2.18 – 2.02 (4 H, m, CH_2), 1.89 – 1.81 (2 H, m, CH_2); ^{19}F NMR (376 MHz, CD_3CN) δ_F −138.67 (1 F, d, *J* 21.2, F-4^{III}), −141.28 (1 F, d, *J* 21.2, F-3^{III}); HRMS *m/z* (ESI$^+$) 950.4146 (950.4160 calculated for $[C_{53}H_{54}F_2N_9O_6]^+$); LCMS (formic acid) t_R 0.68 min, *m/z* (ESI$^+$) 950.5 $[M+H]^+$, purity 87%.

Method II:

A solution of (*S*)-1-(3,4-difluorophenyl)-6-(5-(3,5-dimethylisoxazol-4-yl)-1-(piperidin-4-yl)-1H-benzo[d]imidazol-2-yl)piperidin-2-one (**87**) (40.0 mg, 79.1 μmol, 1.0 eq.), 4-((4-(2-(2,6-dioxopiperidin-3-yl)-1-oxoisoindolin-5-yl)piperazin-1-yl)methyl)benzoic acid (40.3 mg, 87.0 μmol, 1.1 eq.), HATU (36.1 mg, 94.9 μmol, 1.2 eq.), and DIPEA (41 μL, 240 μmol, 3.0 eq.) in DMF (800 μL) was stirred at rt for 1 h. The reaction mixture was directly purified using preparative reverse phase column chromatography (gradient of 20 – 85% MeCN in H_2O each with 0.1% *v/v* formic acid) to afford 3-[5-(4-{[4-(4-{2-[(2*S*)-1-(3,4-difluorophenyl)-6-oxopiperidin-2-yl]-5-(3,5-dimethyl-1,2-oxazol-4-yl)-1*H*-1,3-benzodiazol-1-yl}piperidine-1-carbonyl)phenyl]methyl}piperazin-1-yl)-1-oxo-2,3-dihydro-1*H*-isoindol-2-yl]piperidine-2,6-dione (**144**) (21.7 mg, 0.023 mmol, 29%) as a colourless solid: R_f 0.08 (acetone); mp 80 – 82 °C (H_2O); $[\alpha]_D^{25} = -19.3$ (*c* 0.71, DMSO); $\tilde{\upsilon}_{max}$ (thin film)/ cm^{-1} 3450 (N-H, w, br), 2974 (C-H, w), 2926 (C-H, w), 2851 (C-H, w), 2831 (C-H, w), 1701 (C=O, m), 1663 (C=O, m), 1615 (C=C, s); ^{1}H NMR (600 MHz, DMSO) δ_H 10.93 (1 H, s, NH-1^{VI}), 8.36 (1 H, 0.43 eq., s, *H*COOH), 7.83 (1 H, d, *J* 8.5, H-7^{I}), 7.72 (1 H, d, *J* 1.7, H-4^{I}), 7.53 – 7.48 (3 H, m, H-7^{V}, H-8^{VII}), 7.43 (2 H, d, *J* 7.9, H-7^{VII}), 7.40 – 7.30 (2 H, m, H-2^{III}, H-5^{III}), 7.19 (1 H, dd, *J* 8.5, 1.7, H-6^{I}), 7.07 – 7.03 (3 H, m, H-6^{III}, H-4^{V}, H-6^{V}), 5.79 (1 H, dd, *J* 4.4, 4.4, H-2^{II}), 5.04 (1 H, dd, *J* 13.3, 5.1, H-3^{VI}), 4.74 – 4.64 (1 H, m, H-4^{IV}), 4.32 (1 H, d, *J* 16.8, H_AH_B-3^{V}), 4.20 (1 H, d, *J* 16.8, H_AH_B-3^{V}), 3.59 (2 H, s, H-5^{VII}), 3.30 (4 H, t, *J* 5.2, H-2^{VII}), 2.93 – 2.85 (1 H, m, H_AH_B-5^{VI}), 2.63 – 2.51 (7 H, m, H-5^{II}, H-2^{VI}, H_AH_B-5^{VI}, H-3^{VII}), 2.41 (3 H, s H-7), 2.41 – 2.30 (2 H, m, H_AH_B-4^{VI}, H_AH_B-3^{II}), 2.30 – 2.23 (2 H, m, H-3^{IV}), 2.24 (3 H, s, H-6), 2.11 – 2.03 (1 H, m, H_AH_B-3^{II}), 2.03 – 1.93 (2 H, m, H_AH_B-4^{II}, H_AH_B-4^{VI}), 1.82 – 1.74 (1 H, m, H_AH_B-4^{II}); ^{13}C NMR (151 MHz, DMSO) δ_c 172.9 (C-2^{VI}), 171.3 (C-6^{VI}), 169.8 (C-6^{II}), 169.1 (C-10^{VII}), 168.3 (C-1^{V}), 164.8 (C-3), 158.3 (C-5), 153.7 (C-5^{V}), 153.6 (C-2^{I}), 148.95 (dd, *J* 131.9, 12.1, C-3^{III}), 147.32 (dd, *J* 131.2, 12.7, C-4^{III}), 144.0 (C-7a^{V}), 142.9 (C-3a^{I}), 139.6 (C-6^{VII}), 139.2 (dd, *J* 7.9, 7.6, C-1^{III}), 134.7 (C-9^{VII}), 132.7 (C-7a^{I}) 128.7 (C-7^{VII}), 127.0 (C-8^{VII}), 124.4 (C-6^{III}), 123.7 (C-7^{V}), 123.4 (C-5^{I}), 123.3 (C-6^{I}), 121.5 (C-3a^{V}), 119.8 (C-4^{I}), 117.2 (d, *J* 21.1, H-2^{III}/ H-5^{III}), 117.0 (d, *J* 18.1, H-2^{III}/ H-5^{III}), 116.2 (C-4), 114.7 (C-6^{V}), 113.1 (C-7^{I}), 108.4 (C-4^{V}), 61.6 (C-5^{VII}), 56.3 (C-2^{II}), 52.9 (C-4^{IV}), 52.3 (C-3^{VII}), 51.4 (C-3^{VI}), 47.6 (C-2^{VII}), 47.0 (C-3^{V}), 40.1 (C-2^{IV}), 32.1 (C-5^{II}), 31.2 (C-5^{VI}), 30.5 (C-3^{IV}), 28.6 (C-3^{II}), 22.6 (C-4^{VI}), 17.3 (C-4^{II}), 11.3 (C-7), 10.5 (C-6); ^{19}F NMR

(471 MHz, DMSO) δ_F −137.80 (1 F, d, *J* 22.7, F-4^{III}), −140.55 (1 F, d, *J* 22.7, F-3^{III}); LCMS (formic acid): t_R 0.68 min, *m/z* (ESI$^+$) 950.5 $[M+H]^+$, purity 99%; HPLC (Method 3) t_R 7.13 min, purity 98.1%.

5-(4-{1-[2-(4-{2-[(2*S*)-1-(3,4-Difluorophenyl)-6-oxopiperidin-2-yl]-5-(3,5-dimethyl-1,2-oxazol-4-yl)-1*H*-1,3-benzodiazol-1-yl}piperidin-1-yl)-2-oxoethyl]piperidin-4-yl}piperazin-1-yl)-2-(2,6-dioxopiperidin-3-yl)-6-fluoro-2,3-dihydro-1*H*-isoindole-1,3-dione (145)

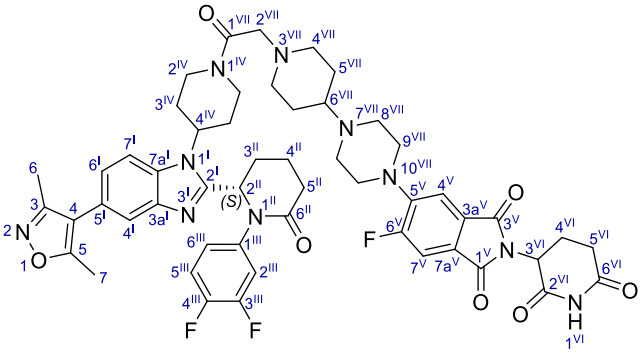

Synthesised according to 'General Amide Coupling Method II'. The crude reaction mixture was directly purified using MDAP (extended method A) to afford 5-(4-{1-[2-(4-{2-[(2*S*)-1-(3,4-difluorophenyl)-6-oxopiperidin-2-yl]-5-(3,5-dimethyl-1,2-oxazol-4-yl)-1*H*-1,3-benzodiazol-1-yl}piperidin-1-yl)-2-oxoethyl]piperidin-4-yl}piperazin-1-yl)-2-(2,6-dioxopiperidin-3-yl)-6-fluoro-2,3-dihydro-1*H*-isoindole-1,3-dione (**145**) (1.1 mg, 1.1 µmol, 5%): R_f 0.04 (acetone); ^{1}H NMR (400 MHz, CD_3OD) δ_H 8.43 (1 H, br s, NH-1^{VI}), 7.65 (1 H, d, *J* 1.2, H-4^I), 7.62 (1 H, d, *J* 8.6, H-7^I), 7.55 (1 H, d, *J* 11.3, H-7^V), 7.46 (1 H, d, *J* 7.3, H-4^V), 7.30 – 7.22 (1 H, m, H-6^I), 7.22 – 7.15 (2 H, m, H-2^{III}, H-5^{III}), 7.11 – 7.04 (1 H, m, H-6^{III}), 5.73 (1 H, dd, *J* 4.8, H-2^{II}), 5.09 (1 H, dd, *J* 12.4, 5.3, H-3^{VI}), 4.72 – 4.64 (1 H, m, C*H*$_2$), 4.33 – 4.14 (1 H, m, H-4^{IV}), 3.73 – 3.63 (2 H, m, C*H*$_2$), 3.43 – 3.35 (7 H, m, C*H*$_2$), 3.29 – 3.18 (4 H, m, C*H*$_2$), 2.93 – 2.60 (12 H, m, C*H*$_2$), 2.56 – 2.45 (3 H, m, C*H*$_2$), 2.40 (3 H, s, H-7), 2.21 (3 H, s, H-6), 2.16 – 2.07 (2 H, m, C*H*$_2$), 2.04 – 1.94 (3 H, m, C*H*$_2$), 1.78 – 1.65 (2 H, m, C*H*$_2$), 1.36 – 1.26 (1 H, m, C*H*$_2$); ^{19}F NMR (376 MHz, CD_3OD) δ_F −113.42 (1 F, s, F-6^V), −138.50 (1 F, dd, *J* 21.2, 10.3, F-4^{III}), −140.82 (1 F, d, *J* 21.2, F-3^{III}); HRMS (ESI$^+$) 989.4290 (989.4280 calculated for $[C_{52}H_{56}F_3N_{10}O_7]^+$); LCMS (formic acid) t_R 0.59 min, *m/z* (ESI$^+$) 989.5 $[M+H]^+$, purity 97%.

(2*S*,4*R*)-*N*-(2-(2-(2-(2-(4-(2-((*S*)-1-(3,4-Difluorophenyl)-6-oxopiperidin-2-yl)-5-(3,5-dimethylisoxazol-4-yl)-1*H*-benzo[d]imidazol-1-yl)piperidin-1-yl)-2-oxoethoxy)ethoxy)ethoxy)-4-(4-methylthiazol-5-yl)benzyl)-1-((*S*)-2-(1-fluorocyclopropane-1-carboxamido)-3,3-dimethylbutanoyl)-4-hydroxypyrrolidine-2-carboxamide (146)

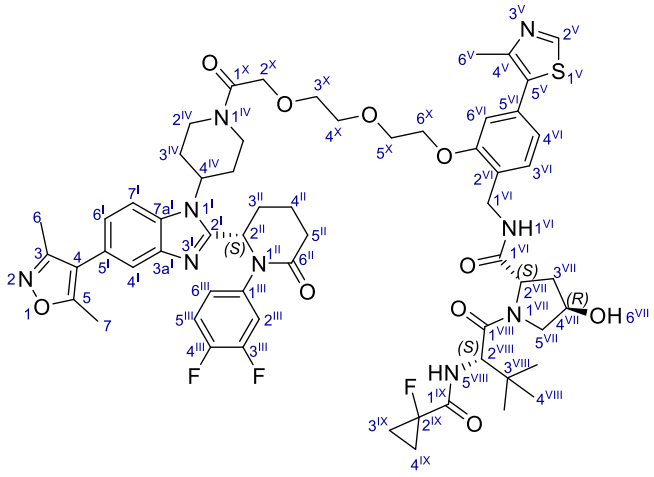

A solution of (*S*)-1-(3,4-difluorophenyl)-6-(5-(3,5-dimethylisoxazol-4-yl)-1-(piperidin-4-yl)-1*H*-benzo[d]imidazol-2-yl)piperidin-2-one (**87**) (15.0 mg, 29.7 µmol, 1.0 eq.), 2-(2-(2-(2-(((2*S*,4*R*)-1-((*S*)-2-(1-fluorocyclopropane-1-carboxamido)-3,3-dimethylbutanoyl)-4-hydroxypyrrolidine-2-carboxamido)methyl)-5-(4-methylthiazol-5-yl)phenoxy)ethoxy)ethoxy)acetic acid (22.0 mg, 32.4 µmol, 1.1 eq.), HATU (14.0 mg, 36.8 µmol, 1.2 eq.), and DIPEA (16 µL, 92 µmol, 3.1 eq.) in DMF (300 µL) was stirred at rt for 2 h. The crude reaction mixture was directly purified using preparative reverse phase column chromatography (gradient of 30 – 99% MeCN in 10 mM aq. $(NH_4)HCO_3$ (pH 10)) to afford (2*S*,4*R*)-*N*-(2-(2-(2-(2-(4-(2-((*S*)-1-(3,4-difluorophenyl)-6-oxopiperidin-2-yl)-5-(3,5-dimethylisoxazol-4-yl)-1*H*-benzo[*d*]imidazol-1-yl)piperidin-1-yl)-2-oxoethoxy)ethoxy)ethoxy)-4-(4-methylthiazol-5-yl)benzyl)-1-((*S*)-2-(1-fluorocyclopropane-1-carboxamido)-3,3-dimethylbutanoyl)-4-hydroxypyrrolidine-2-carboxamide (**146**) (17.9 mg, 15.3 µmol, 52%): R_f 0.12 (acetone); ^{1}H NMR (400 MHz, CD_3CN) δ_H 8.71 (1 H, s, H-2^{V}), 7.62 – 7.57 (2 H, m, H-4^{I}, H-7^{I}), 7.36 (1 H, d, *J* 7.8, H-4^{VI}), 7.28 – 6.92 (8 H, m, H-6^{I}, H-2^{III}, H-5^{III}, H-6^{III}, H-3^{VI}, NH-1^{VI}, H-6^{VI}, NH-5^{VIII}), 5.50 – 5.42 (1 H, m, H-2^{II}), 4.65 – 4.59 (1 H, m, CH_2), 4.50 (1 H, t, *J* 8.2, CH_2), 4.42 – 4.27 (4 H, m, CH_2), 4.21 – 4.14 (2 H, m, CH_2), 4.06 – 3.89 (1 H, m, H-4^{IV}), 3.87 – 3.82 (2 H, m, CH_2), 3.74 – 3.71 (2 H, m, CH_2), 3.69 – 3.64

(2 H, m, CH_2), 3.38 (1 H, br s, OH), 3.21 – 3.01 (1 H, m, CH_2), 2.62 – 2.51 (2 H, m, CH_2), 2.77 – 2.50 (2 H, m, CH_2), 2.44 (3 H, s, H-6^{V}), 2.37 (3 H, s, H-7), 2.22 (3 H, s, H-6), 2.19 – 2.15 (8 H, m, CH_2), 2.13 – 2.01 (4 H, m, CH_2), 1.90 – 1.74 (2 H, m, CH_2), 1.41 – 1.31 (1 H, m, CH_2), 1.28 – 1.18 (3 H, m, CH_2), 0.94 (9 H, s, H-4^{VIII}); ^{19}F NMR (376 MHz, CD_3CN) δ_F −(138.73 – 138.57) (1 F, m, F-4^{III}), −(141.39 – 141.19) (1 F, m, F-3^{III}), −198.24 (1 F, s, F-2^{IX}); HRMS *m/z* (ESI$^+$) 1166.4998 (1166.4991 calculated for $[C_{60}H_{71}F_3N_9O_{10}S]^+$); LCMS (HpH) t_R 1.06 min, *m/z* (ESI$^+$) 583.9 $[M+2H]^{2+}$, purity 100%.

4-(2-{2-[4-(2-{2-[(2*S*)-1-(3,4-Difluorophenyl)-6-oxopiperidin-2-yl]-5-(3,5-dimethyl-1,2-oxazol-4-yl)-1*H*-1,3-benzodiazol-1-yl}ethyl)piperazin-1-yl]-2-oxoethoxy}ethoxy)-2-(2,6-dioxopiperidin-3-yl)-2,3-dihydro-1*H*-isoindole-1,3-dione (147)

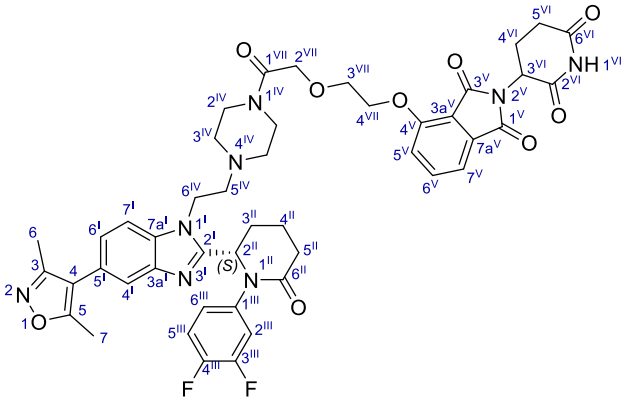

Synthesised according to 'General Amide Coupling Method III'. The crude reaction mixture was directly purified using MDAP (extended method B) to afford 4-(2-{2-[4-(2-{2-[(2*S*)-1-(3,4-difluorophenyl)-6-oxopiperidin-2-yl]-5-(3,5-dimethyl-1,2-oxazol-4-yl)-1*H*-1,3-benzodiazol-1-yl}ethyl)piperazin-1-yl]-2-oxoethoxy}ethoxy)-2-(2,6-dioxopiperidin-3-yl)-2,3-dihydro-1*H*-isoindole-1,3-dione (**147**) (5.1 mg, 5.7 µmol, 31%): R_f 0.13 (acetone); ^{1}H NMR (400 MHz, CD_3CN) δ_H 8.92 (1 H, br s, NH-1^{VI}), 7.75 (1 H, dd, *J* 8.6, 7.3, H-6^{V}), 7.64 – 7.60 (1 H, m, H-4^{I}), 7.50 – 7.36 (3 H, m, H-7^{I}, H-5^{V}, H-7^{V}), 7.23 – 7.07 (3 H, m, H-6^{I}, H-2^{III}, H-5^{III}), 7.04 – 6.98 (1 H, m, H-6^{III}), 5.37 – 5.31 (1 H, m, H-2^{II}), 4.99 – 4.91 (1 H, m, H-3^{VI}), 4.38 – 4.33 (2 H, m), 4.26 (2 H, s, H-2^{VII}), 4.12

– 4.05 (2 H, m, CH_2), 3.91 – 3.86 (2 H, m, CH_2), 3.32 – 3.26 (2 H, m, CH_2), 3.26 – 3.20 (2 H, m, CH_2), 2.76 – 2.41 (11 H, m, CH_2), 2.40 (3 H, s, H-7), 2.31 – 2.25 (4 H, m, H-6), 2.15 – 2.05 (3 H, m, CH_2), 1.88 – 1.79 (1 H, m, CH_2); ^{19}F NMR (376 MHz, CD_3CN) δ_F −138.50 (1 F, d, *J* 21.2), −141.10 (1 F, d, *J* 21.2); HRMS *m/z* (ESI^+) 893.3416 (893.3429 calculated for $[C_{46}H_{47}F_2N_8O_9]^+$); LCMS (formic acid) t_R 0.80 min, *m/z* (ESI^+) 893.5 $[M+H]^+$, purity 100%.

4-[2-(2-{2-[4-(2-{2-[(2*S*)-1-(3,4-Difluorophenyl)-6-oxopiperidin-2-yl]-5-(3,5-dimethyl-1,2-oxazol-4-yl)-1*H*-1,3-benzodiazol-1-yl}ethyl)piperazin-1-yl]-2-oxoethoxy}ethoxy)ethoxy]-2-(2,6-dioxopiperidin-3-yl)-2,3-dihydro-1*H*-isoindole-1,3-dione (148)

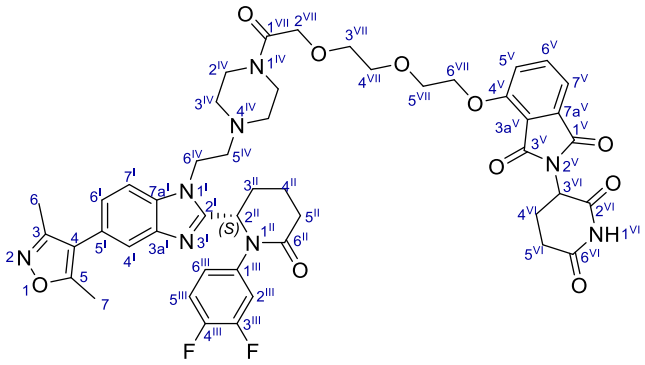

A solution of (6*S*)-1-(3,4-difluorophenyl)-6-[5-(3,5-dimethyl-1,2-oxazol-4-yl)-1-[2-(piperazin-1-yl)ethyl]-1*H*-1,3-benzodiazol-2-yl]piperidin-2-one hydrochloride (**106**) (15.0 mg, 26.3 µmol, 1.0 eq.), 2-(2-(2-((2-(2,6-dioxopiperidin-3-yl)-1,3-dioxoisoindolin-4-yl)oxy)ethoxy)ethoxy)acetic acid (12.0 mg, 28.6 µmol 1.1 eq.), HATU (12.0 mg, 31.6 µmol, 1.2 eq.), and DIPEA (18 µL, 100 µmol, 3.9 eq.) in DMF (260 µL) was stirred at rt for 2 h. The reaction mixture was directly purified using preparative reverse phase column chromatography (gradient of 30 – 99% MeCN in 10 mM aq. $(NH_4)HCO_3$ (pH 10)) to afford 4-[2-(2-{2-[4-(2-{2-[(2*S*)-1-(3,4-difluorophenyl)-6-oxopiperidin-2-yl]-5-(3,5-dimethyl-1,2-oxazol-4-yl)-1*H*-1,3-benzodiazol-1-yl}ethyl)piperazin-1-yl]-2-oxoethoxy}ethoxy)ethoxy]-2-(2,6-dioxopiperidin-3-yl)-2,3-dihydro-1*H*-isoindole-1,3-dione (**148**) (12.7 mg, 13.6 µmol, 50%): R_f 0.11 (acetone); ^{1}H NMR (400 MHz, CD_3CN) δ_H 9.01 (1 H, br s, NH-1^{VI}), 7.71 (1 H, dd, *J* 8.6, 7.3, H-6^V), 7.63 – 7.61 (1 H, m, H-4^I), 7.46 (1 H, d, *J* 8.3, H-7^I),

7.42 – 7.36 (2 H, m, H-5^{V}, H-7^{V}), 7.21 – 7.09 (3 H, m, H-6^{I}, H-2^{III}, H-5^{III}), 7.04 – 6.99 (1 H, m, H-6^{III}), 5.33 (1 H, dd, *J* 5.4, 3.9, H-2^{II}), 5.00 – 4.92 (1 H, m, H-3^{VI}), 4.34 – 4.30 (2 H, m), 4.09 (2 H, s, H-2^{VII}), 4.08 – 4.04 (2 H, m, C*H*$_2$), 3.87 – 3.83 (2 H, m, C*H*$_2$), 3.72 – 3.68 (2 H, m, C*H*$_2$), 3.62 – 3.58 (2 H, m, C*H*$_2$), 3.32 – 3.24 (2 H, m, C*H*$_2$), 3.24 – 3.16 (2 H, m, C*H*$_2$), 2.75 – 2.47 (7 H, m, C*H*$_2$), 2.46 – 2.42 (2 H, m, C*H*$_2$), 2.40 (3 H, s, H-7), 2.29 – 2.25 (3 H, m, C*H*$_2$), 2.24 (3 H, s, H-6), 2.13 – 2.07 (3 H, m, C*H*$_2$), 1.84 (2 H, dt, *J* 6.5, 3.5, C*H*$_2$); ^{19}F NMR (376 MHz, CD_3CN) δ_F −138.51 (1 F, d, *J* 21.2, F-4^{III}), −141.10 (1 F, d, *J* 21.2, F-3^{III}); HRMS *m/z* (ESI$^+$) 937.3713 (937.3691 calculated for $[C_{48}H_{50}F_2N_8O_{10}]^+$); LCMS (HpH) t_R 0.94 min, *m/z* (ESI$^+$) 937.4 $[M+H]^+$, purity 96%.

4-{2-[2-(2-{2-[4-(2-{2-[(2*S*)-1-(3,4-Difluorophenyl)-6-oxopiperidin-2-yl]-5-(3,5-dimethyl-1,2-oxazol-4-yl)-1*H*-1,3-benzodiazol-1-yl}ethyl)piperazin-1-yl]-2-oxoethoxy}ethoxy)ethoxy]ethoxy}-2-(2,6-dioxopiperidin-3-yl)-2,3-dihydro-1*H*-isoindole-1,3-dione (149)

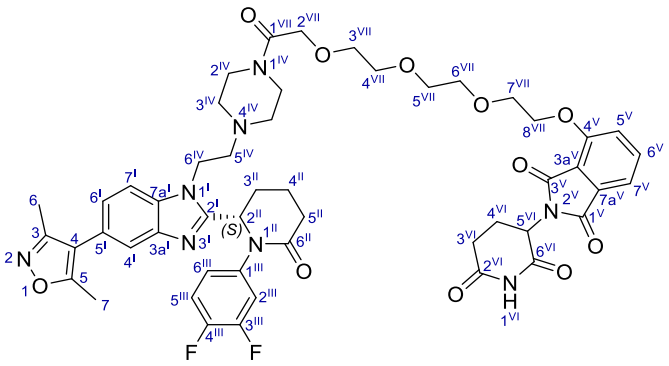

Synthesised according to 'General Amide Coupling Method III'. The crude reaction mixture was directly purified using MDAP (extended method B) to afford 4-{2-[2-(2-{2-[4-(2-{2-[(2*S*)-1-(3,4-difluorophenyl)-6-oxopiperidin-2-yl]-5-(3,5-dimethyl-1,2-oxazol-4-yl)-1*H*-1,3-benzodiazol-1-yl}ethyl)piperazin-1-yl]-2-oxoethoxy}ethoxy)ethoxy]ethoxy}-2-(2,6-dioxopiperidin-3-yl)-2,3-dihydro-1*H*-isoindole-1,3-dione (**149**) (6.3 mg, 6.4 μmol, 34%): R_f 0.03 (acetone); ^{1}H NMR (400 MHz, CD_3CN) δ_H 9.17 – 8.96 (1 H, m, NH-1^{VI}), 7.74 – 7.66 (1 H, m, H-6^{VI}), 7.63 – 7.56 (2 H, m, H-4^{I}, H-7^{I}), 7.43 – 7.36 (1 H, m, H-7^{V}), 7.34 (1 H, d, *J* 8.6, H-5^{V}), 7.23 – 6.98 (4 H, m, H-6^{I}, H-2^{III}, H-5^{III}, H-6^{III}), 5.50 – 5.44 (1 H, m, H-2^{II}), 4.95 (1 H, dd, *J* 12.4, 5.3, H-3^{VI}), 4.69 – 4.50 (1 H, m, C*H*$_2$), 4.49 – 4.38

(1 H, m, CH_2), 4.29 – 4.20 (3 H, m, CH_2), 4.19 – 4.06 (1 H, m, CH_2), 4.06 – 3.90 (1 H, m, CH_2), 3.79 – 3.69 (2 H, m, CH_2), 3.66 – 3.53 (8 H, m, CH_2), 3.22 – 3.03 (1 H, m, CH_2), 2.77 – 2.42 (10 H, m, CH_2), 2.37 (3 H, s, H-7), 2.33 – 2.27 (1 H, m, CH_2), 2.21 (3 H, s, H-6), 2.16 – 1.98 (4 H, m, CH_2), 1.91 – 1.78 (2 H, m, CH_2), 1.44 – 1.34 (1 H, m, CH_2); ^{19}F NMR (376 MHz, CD_3CN) δ_F −138.48 (1 F, d, *J* 21.2, F-4^{III}), −141.06 (1 F, d, *J* 21.2, F-3^{III}); HRMS *m/z* (ESI$^+$) 981.3956 (981.3953 calculated for $[C_{50}H_{55}F_2N_8O_{11}]^+$); LCMS (formic acid) t_R 0.80 min, *m/z* (ESI$^+$) 891.6 $[M+H]^+$, purity 100%.

4-({14-[4-(2-{2-[(2*S*)-1-(3,4-Difluorophenyl)-6-oxopiperidin-2-yl]-5-(3,5-dimethyl-1,2-oxazol-4-yl)-1*H*-1,3-benzodiazol-1-yl}ethyl)piperazin-1-yl]-14-oxo-3,6,9,12-tetraoxatetradecan-1-yl}oxy)-2-(2,6-dioxopiperidin-3-yl)-2,3-dihydro-1*H*-isoindole-1,3-dione (150)

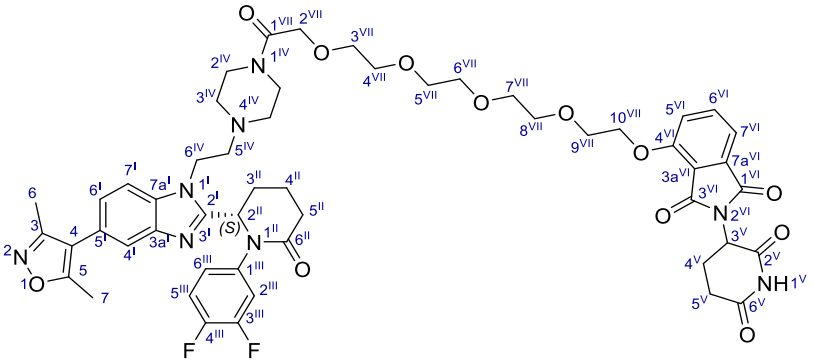

Synthesised according to 'General Amide Coupling Method III'. The crude reaction mixture was directly purified using MDAP (method B) to afford 4-({14-[4-(2-{2-[(2*S*)-1-(3,4-difluorophenyl)-6-oxopiperidin-2-yl]-5-(3,5-dimethyl-1,2-oxazol-4-yl)-1*H*-1,3-benzodiazol-1-yl}ethyl)piperazin-1-yl]-14-oxo-3,6,9,12-tetraoxatetradecan-1-yl}oxy)-2-(2,6-dioxopiperidin-3-yl)-2,3-dihydro-1*H*-isoindole-1,3-dione (**150**) (9.6 mg, 9.4 µmol, 48%): R_f 0.03 (acetone); ^{1}H NMR (400 MHz, CD_3CN) δ_H 9.06 (1 H, br s, NH-1^{VI}), 7.73 (1 H, dd, *J* 8.6, 7.3, H-6^V), 7.62 (1 H, d, *J* 1.0, H-4^I), 7.48 (1 H, d, *J* 8.3, H-7^I), 7.42 (1 H, d, *J* 7.3, H-7^V), 7.38 (1 H, d, *J* 8.6, H-5^V), 7.23 – 7.09 (3 H, m, H-6^I, H-2^{III}, H-5^{III}), 7.05 – 6.98 (1 H, m, H-6^{III}), 5.34 (1 H, dd, *J* 5.3, 4.0, H-2^{II}), 5.00 – 4.93 (1 H, m, H-3^{VI}), 4.32 (1 H, dd, *J* 5.3, 3.8, CH_2), 4.10 – 4.06 (2 H, m, CH_2), 4.06 (2 H, s, H-2^{VII}), 3.87 – 3.82 (2 H, m, CH_2), 3.68 – 3.65 (2 H, m, CH_2), 3.57 – 3.54 (9 H, m, CH_2), 3.30 – 3.24 (2 H, m, CH_2), 3.21 – 3.15 (2 H, m, CH_2), 2.75 – 2.41 (10 H, m, CH_2), 2.40 (3 H, s, H-7), 2.31 – 2.26 (3 H, m, CH_2), 2.24 (3 H, s, H-6), 2.16 – 2.06 (2 H, m, CH_2),

1.89 – 1.80 (1 H, m, CH_2); ^{19}F NMR (376 MHz, CD_3CN) δ_F −138.47 (1 F, d, *J* 21.2), −141.06 (1 F, d, *J* 21.2); HRMS *m/z* (ESI$^+$) 1025.4227 (1025.4215 calculated for $[C_{52}H_{59}F_2N_8O_{12}]^+$); LCMS (formic acid) t_R 0.83 min, *m/z* (ESI$^+$) 513.3 $[M+2H]^{2+}$, purity 96%.

4-({5-[4-(2-{2-[(2*S*)-1-(3,4-Difluorophenyl)-6-oxopiperidin-2-yl]-5-(3,5-dimethyl-1,2-oxazol-4-yl)-1*H*-1,3-benzodiazol-1-yl}ethyl)piperazin-1-yl]-5-oxopentyl}oxy)-2-(2,6-dioxopiperidin-3-yl)-2,3-dihydro-1*H*-isoindole-1,3-dione (151)

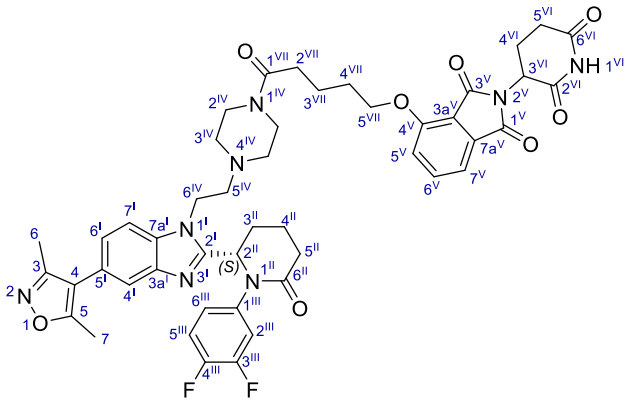

Synthesised according to 'General Amide Coupling Method III'. The crude reaction mixture was directly purified using MDAP (extended method B) to afford 4-({5-[4-(2-{2-[(2*S*)-1-(3,4-difluorophenyl)-6-oxopiperidin-2-yl]-5-(3,5-dimethyl-1,2-oxazol-4-yl)-1*H*-1,3-benzodiazol-1-yl}ethyl)piperazin-1-yl]-5-oxopentyl}oxy)-2-(2,6-dioxopiperidin-3-yl)-2,3-dihydro-1*H*-isoindole-1,3-dione (**151**) (7.0 mg, 7.9 μmol, 42%): R_f 0.14 (acetone); ^{1}H NMR (400 MHz, CD_3CN) δ_H 8.91 (1 H, br s, NH-1^{VI}), 7.74 (1 H, dd, *J* 8.4, 7.3, H-6^{V}), 7.64 – 7.61 (1 H, m, H-4^{I}), 7.49 (1 H, d, *J* 8.3, H-7^{I}), 7.41 (1 H, d, *J* 7.3, H-7^{V}), 7.37 (1 H, d, *J* 8.4, H-5^{V}), 7.20 (1 H, dd, *J* 8.3, 1.7, H-6^{I}), 7.18 – 7.09 (2 H, m, H-2^{III}, H-5^{III}), 7.05 – 7.00 (1 H, m, H-6^{III}), 5.35 (1 H, t, *J* 4.7, H-2^{II}), 5.00 – 4.92 (1 H, m, H-3^{VI}), 4.22 (2 H, t, *J* 6.1, H-2^{VII}), 4.10 (2 H, td, *J* 5.9, 2.6, CH_2), 3.32 – 3.20 (3 H, m, CH_2), 2.75 – 2.44 (8 H, m, CH_2), 2.41 – 2.35 (5 H, m, CH_2), 2.30 – 2.25 (4 H, m, H-7, CH_2), 2.24 (3 H, s, H-6), 2.17 – 2.05 (4 H, m, CH_2), 1.87 – 1.81 (3 H, m, CH_2), 1.79 – 1.71 (2 H, m, CH_2); ^{19}F NMR (376 MHz, CD_3CN) δ_F −138.52 (1 F, dd, *J* 21.2, 2.3, F-4^{III}), −141.13 (1 F, d, *J* 21.2, F-3^{III}); HRMS *m/z* (ESI$^+$) 891.3646

(891.3636 calculated for $[C_{47}H_{49}F_2N_8O_8]^+$); LCMS (formic acid) t_R 0.84 min, *m/z* (ESI^+) 891.5 $[M+H]^+$, purity 100%.

4-({8-[4-(2-{2-[(2*S*)-1-(3,4-Difluorophenyl)-6-oxopiperidin-2-yl]-5-(3,5-dimethyl-1,2-oxazol-4-yl)-1*H*-1,3-benzodiazol-1-yl}ethyl)piperazin-1-yl]-8-oxooctyl}oxy)-2-(2,6-dioxopiperidin-3-yl)-2,3-dihydro-1*H*-isoindole-1,3-dione (152)

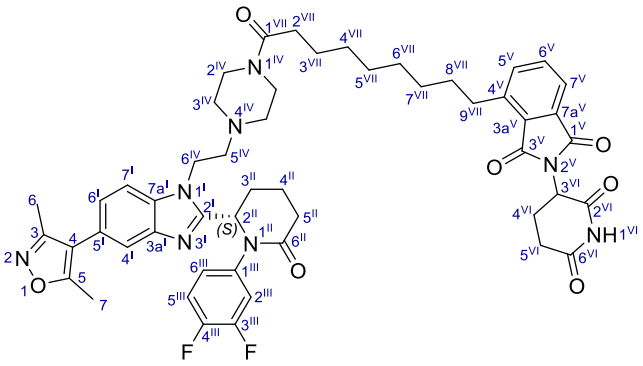

Synthesised according to 'General Amide Coupling Method III'. The crude reaction mixture was directly purified using MDAP (method C) to afford 4-({8-[4-(2-{2-[(2*S*)-1-(3,4-difluorophenyl)-6-oxopiperidin-2-yl]-5-(3,5-dimethyl-1,2-oxazol-4-yl)-1*H*-1,3-benzodiazol-1-yl}ethyl)piperazin-1-yl]-8-oxooctyl}oxy)-2-(2,6-dioxopiperidin-3-yl)-2,3-dihydro-1*H*-isoindole-1,3-dione (**152**) (7.8 mg, 8.4 μmol, 44%): R_f 0.21 (acetone); ^{1}H NMR (400 MHz, CD_3CN) δ_H 9.00 (1 H, br s, NH-1^{VI}), 7.73 (1 H, dd, *J* 8.3, 7.1, H-6^{V}), 7.62 (1 H, d, *J* 1.0, H-4^{I}), 7.48 (1 H, d, *J* 8.3, H-7^{I}), 7.40 (1 H, d, *J* 7.1, H-7^{V}), 7.36 (1 H, d, *J* 8.3, H-5^{V}), 7.24 – 7.08 (3 H, m, H-6^{I}, H-2^{III}, H-5^{III}), 7.06 – 7.00 (1 H, m, H-6^{III}), 5.35 (1 H, dd, *J* 5.1, 3.9, H-2^{II}), 4.96 (1 H, dd, *J* 12.2, 5.4, H-3^{VI}), 4.19 (2 H, t, *J* 6.4, H-2^{VII}), 4.10 (2 H, td, *J* 6.0, 3.7, CH_2), 3.34 – 3.25 (2 H, m, CH_2), 3.25 – 3.13 (2 H, m, CH_2), 2.74 – 2.46 (8 H, m, CH_2), 2.40 (3 H, s, H-7), 2.28 – 2.23 (9 H, m, H-6, CH_2), 2.14 – 2.07 (3 H, m, CH_2), 1.83 – 1.78 (2 H, m, CH_2), 1.56 – 1.47 (4 H, m, CH_2), 1.42 – 1.32 (4 H, m, CH_2); ^{19}F NMR (376 MHz, CD_3CN) δ_F −138.51 (1 F, d, *J* 20.2, F-4^{III}), −141.09 (1 F, d, *J* 21.2, F-3^{III}); HRMS *m/z* (ESI^+) 933.4123 (933.4105 calculated for $[C_{50}H_{55}F_2N_8O_8]^+$); LCMS (formic acid) t_R 0.97 min, *m/z* (ESI^+) 933.3 $[M+H]^+$, purity 99%.

4-({10-[4-(2-{2-[(2*S*)-1-(3,4-Difluorophenyl)-6-oxopiperidin-2-yl]-5-(3,5-dimethyl-1,2-oxazol-4-yl)-1*H*-1,3-benzodiazol-1-yl}ethyl)piperazin-1-yl]-10-oxodecyl}oxy)-2-(2,6-dioxopiperidin-3-yl)-2,3-dihydro-1*H*-isoindole-1,3-dione (153)

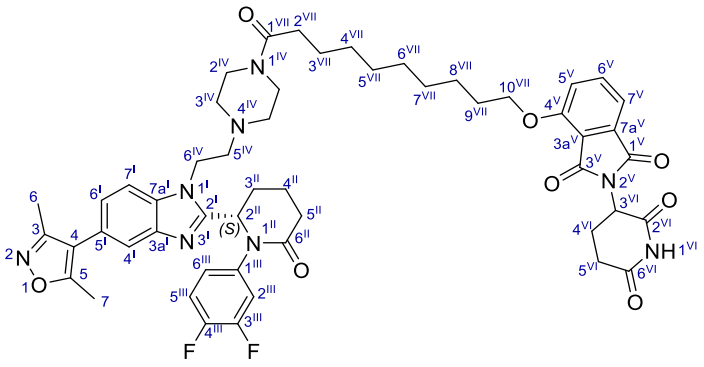

Synthesised according to 'General Amide Coupling Method III'. The crude reaction mixture was directly purified using MDAP (method C) to afford 4-({10-[4-(2-{2-[(2*S*)-1-(3,4-difluorophenyl)-6-oxopiperidin-2-yl]-5-(3,5-dimethyl-1,2-oxazol-4-yl)-1*H*-1,3-benzodiazol-1-yl}ethyl)piperazin-1-yl]-10-oxodecyl}oxy)-2-(2,6-dioxopiperidin-3-yl)-2,3-dihydro-1*H*-isoindole-1,3-dione (**153**) (7.2 mg, 7.5 µmol, 37%): R_f 0.29 (acetone); ^{1}H NMR (400 MHz, CD_3CN) δ_H 9.08 (1 H, br s, NH-1^{VI}), 7.76 (1 H, dd, *J* 8.6, 7.3, H-6^{V}), 7.68 – 7.63 (1 H, m, H-4^{I}), 7.55 – 7.48 (1 H, m, H-7^{I}), 7.44 – 7.41 (1 H, m, H-7^{V}), 7.39 (1 H, d, *J* 8.6, H-5^{V}), 7.25 – 7.10 (3 H, m, H-6^{I}, H-2^{III}, H-6^{III}), 7.09 – 7.02 (1 H, m, H-6^{III}), 5.37 (1 H, dd, *J* 5.3, 3.8, H-2^{II}), 5.04 – 4.95 (1 H, m, H-3^{VI}), 4.22 (2 H, t, *J* 6.4, H-2^{VII}), 4.17 – 4.07 (2 H, m, CH_2), 3.36 – 3.30 (2 H, m, CH_2), 3.28 – 3.16 (2 H, m, CH_2), 2.77 – 2.44 (9 H, m, CH_2), 2.43 (3 H, s, H-7), 2.31 – 2.24 (10 H, m, H-6, CH_2), 2.16 – 2.09 (2 H, m, CH_2), 1.90 – 1.79 (3 H, m, CH_2), 1.58 – 1.47 (4 H, m, CH_2), 1.42 – 1.32 (7 H, m, CH_2); ^{19}F NMR (376 MHz, CD_3CN) δ_F −138.52 (1 F, d, *J* 21.2, F-4^{III}), −141.11 (1 F, d, *J* 21.2, F-3^{III}); HRMS *m/z* (ESI$^+$) 961.4395 (961.4418 calculated for $[C_{52}H_{59}F_2N_8O_8]^+$); LCMS (formic acid) t_R 1.07 min, *m/z* (ESI$^+$) 961.3 $[M+H]^+$, purity 96%.

4-[3-(4-{4-[4-(2-{2-[(2*S*)-1-(3,4-Difluorophenyl)-6-oxopiperidin-2-yl]-5-(3,5-dimethyl-1,2-oxazol-4-yl)-1*H*-1,3-benzodiazol-1-yl}ethyl)piperazin-1-yl]-4-oxobutyl}piperazin-1-yl)propoxy]-2-(2,6-dioxopiperidin-3-yl)-2,3-dihydro-1*H*-isoindole-1,3-dione (154)

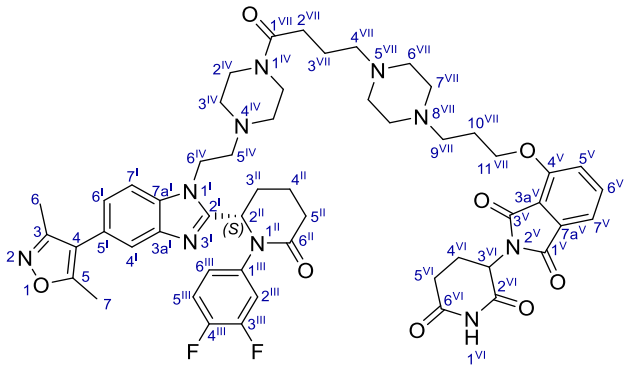

Synthesised according to 'General Amide Coupling Method III'. The crude reaction mixture was directly purified using MDAP (method A) to afford 4-[3-(4-{4-[4-(2-{2-[(2*S*)-1-(3,4-difluorophenyl)-6-oxopiperidin-2-yl]-5-(3,5-dimethyl-1,2-oxazol-4-yl)-1*H*-1,3-benzodiazol-1-yl}ethyl)piperazin-1-yl]-4-oxobutyl}piperazin-1-yl)propoxy]-2-(2,6-dioxopiperidin-3-yl)-2,3-dihydro-1*H*-isoindole-1,3-dione (**154**) (6.3 mg, 6.3 μmol, 34%): R_f 0.00 (acetone); ^{1}H NMR (400 MHz, CD_3OD) δ_H 8.48 (1 H, m, NH-1^{VI}), 7.80 (1 H, dd, *J* 8.6, 7.3, H-6^{V}), 7.65 (1 H, d, *J* 1.0, H-4^{I}), 7.59 (1 H, d, *J* 8.3, H-7^{I}), 7.49 (1 H, d, *J* 7.1, H-5^{V}), 7.46 (1 H, d, *J* 8.6, H-7^{V}), 7.32 – 7.23 (2 H, m, H-6^{I}, H-2^{III}), 7.19 (1 H, dt, *J* 10.3, 8.8, H-5^{III}), 7.12 – 7.05 (1 H, m, H-6^{III}), 5.53 (1 H, t, *J* 5.0), 5.11 (2 H, dd, *J* 12.7, 5.6, H-2^{II}), 4.34 (2 H, dd, *J* 5.6, H-3^{VI}), 4.30 – 4.21 (2 H, m, CH_2), 3.40 (2 H, t, *J* 4.8, H-2^{VII}), 3.37 – 3.32 (1 H, m, CH_2), 3.05 – 2.44 (20 H, m, CH_2), 2.42 (3 H, s, H-7), 2.40 – 2.28 (m, 5 H, CH_2), 2.27 (3 H, s, H-6), 2.23 – 2.11 (4 H, m, CH_2), 2.00 – 1.91 (2 H, m, CH_2), 1.90 – 1.81 (2 H, m, CH_2); ^{19}F NMR (376 MHz, CD_3OD) δ_F −138.24 (1 F, d, *J* 21.2, F-4^{III}), −140.59 (1 F, d, *J* 21.2, F-3^{III}); HRMS *m/z* (ESI$^+$) 1003.4622 (1003.4636 calculated for $[C_{53}H_{61}F_2N_{10}O_8]^+$); LCMS (formic acid) t_R 0.59 min, *m/z* (ESI$^+$) 502.5 $[M+2H]^{2+}$, purity 100%.

3-[5-(4-{4-[4-(2-{2-[(2*S*)-1-(3,4-Difluorophenyl)-6-oxopiperidin-2-yl]-5-(3,5-dimethyl-1,2-oxazol-4-yl)-1*H*-1,3-benzodiazol-1-yl}ethyl)piperazin-1-yl]-4-oxobutyl}piperazin-1-yl)-1-oxo-2,3-dihydro-1*H*-isoindol-2-yl]piperidine-2,6-dione (155)

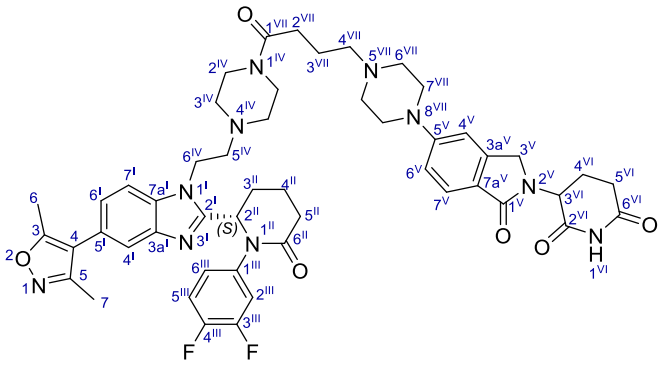

Synthesised according to 'General Amide Coupling Method III'. The crude reaction mixture was directly purified using MDAP (method A) to afford 3-[5-(4-{4-[4-(2-{2-[(2*S*)-1-(3,4-difluorophenyl)-6-oxopiperidin-2-yl]-5-(3,5-dimethyl-1,2-oxazol-4-yl)-1*H*-1,3-benzodiazol-1-yl}ethyl)piperazin-1-yl]-4-oxobutyl}piperazin-1-yl)-1-oxo-2,3-dihydro-1*H*-isoindol-2-yl]piperidine-2,6-dione (**155**) (11.4 mg, 12.2 μmol, 65%): R_f 0.00 (acetone); ^{1}H NMR (400 MHz, CD_3CN) δ_H 8.78 (1 H, br s, NH-1^{VI}), 7.63 – 7.60 (1 H, m, H-4^{I}), 7.60 – 7.54 (1 H, m, H-7^{I}), 7.52 – 7.46 (1 H, m, H-7^{V}), 7.22 – 7.10 (3 H, m, H-2^{III}, H-5^{III}, H-5^{V}), 7.05 – 7.01 (3 H, m, H-6^{III}, H-4^{V}, H-6^{V}), 5.35 (1 H, dd, *J* 5.3, 3.9, H-2^{II}), 5.02 (1 H, dd, *J* 13.5, 5.3, H-3^{VI}), 4.36 – 4.20 (2 H, m, CH_2), 4.15 – 4.05 (2 H, m, CH_2), 3.34 – 3.31 (4 H, m, CH_2), 3.27 – 3.20 (2 H, m, CH_2), 2.76 – 2.66 (20 H, m, CH_2), 2.51 – 2.46 (4 H, m, CH_2), 2.40 (3 H, s, H-7), 2.37 – 2.33 (2 H, m, CH_2), 2.31 – 2.25 (4 H, m, CH_2), 2.24 (3 H, s, H-6); ^{19}F NMR (376 MHz, CD_3CN) δ_F −138.51 (1 F, d, *J* 21.2, F-4^{III}), −141.11 (1 F, d, *J* 21.2, F-3^{III}); HRMS *m/z* (ESI$^+$) 931.4444 (931.4425 calculated for $[C_{50}H_{57}F_2N_{10}O_6]^+$); LCMS (formic acid) t_R 0.60 min, *m/z* (ESI$^+$) 931.6 $[M+H]^+$, purity 100%.

5-(9-{2-[4-(2-{2-[(2*S*)-1-(3,4-Difluorophenyl)-6-oxopiperidin-2-yl]-5-(3,5-dimethyl-1,2-oxazol-4-yl)-1*H*-1,3-benzodiazol-1-yl}ethyl)piperazin-1-yl]-2-oxoethyl}-3,9-diazaspiro[5.5]undecan-3-yl)-2-(2,6-dioxopiperidin-3-yl)-6-fluoro-2,3-dihydro-1*H*-isoindole-1,3-dione (156)

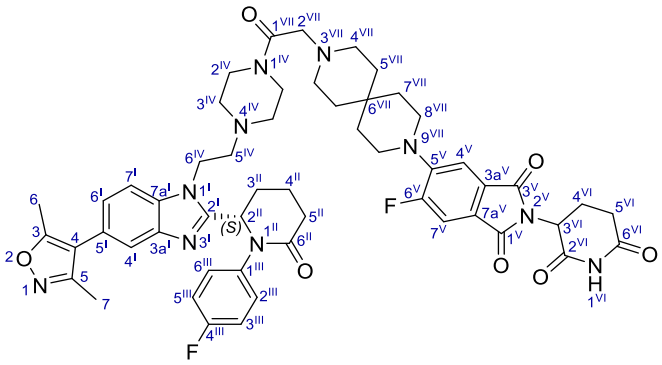

Synthesised according to 'General Amide Coupling Method III'. The crude reaction mixture was directly purified using MDAP (method B) to afford 5-(9-{2-[4-(2-{2-[(2*S*)-1-(3,4-difluorophenyl)-6-oxopiperidin-2-yl]-5-(3,5-dimethyl-1,2-oxazol-4-yl)-1*H*-1,3-benzodiazol-1-yl}ethyl)piperazin-1-yl]-2-oxoethyl}-3,9-diazaspiro[5.5]undecan-3-yl)-2-(2,6-dioxopiperidin-3-yl)-6-fluoro-2,3-dihydro-1*H*-isoindole-1,3-dione (**156**) (9.4 mg, 9.4 μmol, 50%): R_f 0.00 (acetone); ^{1}H NMR (400 MHz, CD_3CN) δ_H 8.93 (1 H, br s, NH-1^{VI}), 7.65 – 7.61 (1 H, m, H-4^{I}), 7.53 – 7.46 (2 H, m, H-7^{I}, H-4^{V}), 7.42 (1 H, d, *J* 7.3, H-7^{V}), 7.24 – 7.10 (3 H, m, H-6^{I}, H-2^{III}, H-5^{III}), 7.08 – 7.00 (1 H, m, H-6^{III}), 5.36 (1 H, dd, *J* 5. 3, 4.0, H-2^{II}), 5.00 – 4.91 (1 H, m, H-3^{VI}), 4.14 – 4.07 (2 H, m), 3.44 (2 H, s, H-2^{VII}), 3.35 – 3.29 (2 H, m, CH_2), 3.27 – 3.22 (5 H, m, CH_2), 2.79 – 2.45 (12 H, m, CH_2), 2.40 (3 H, s, H-7), 2.38 – 2.21 (9 H, m, H-6, CH_2), 2.18 – 2.05 (3 H, m, CH_2), 1.90 – 1.80 (1 H, m, CH_2), 1.69 – 1.64 (7 H, m, CH_2); ^{19}F NMR (376 MHz, CD_3CN) δ_F −113.39 (1 F, s, F-6^{V}), −138.46 (1 F, d, *J* 21.2, F-4^{III}), −141.05 (1 F, d, *J* 21.2, F-3^{III}); HRMS *m/z* (ESI$^+$) 1003.4427 (1003.4437 calculated for $[C_{53}H_{58}F_3N_{10}O_7]^+$); LCMS (formic acid) t_R 0.72 min, *m/z* (ESI$^+$) 502.5 $[(M+2H)/2]^{2+}$, purity 100%.

3-{5-[4-({4-[4-(2-{2-[(2*S*)-1-(3,4-Difluorophenyl)-6-oxopiperidin-2-yl]-5-(3,5-dimethyl-1,2-oxazol-4-yl)-1*H*-1,3-benzodiazol-1-yl}ethyl)piperazine-1-carbonyl]phenyl}methyl)piperazin-1-yl]-1-oxo-2,3-dihydro-1*H*-isoindol-2-yl}piperidine-2,6-dione (157)

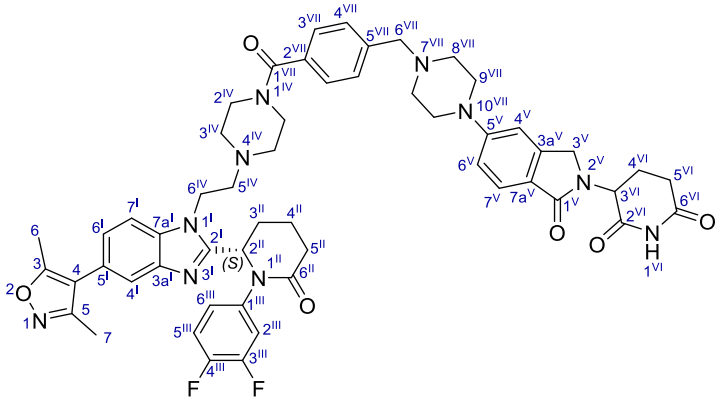

Synthesised according to 'General Amide Coupling Method III'. The crude reaction mixture was directly purified using MDAP (method A) to afford 3-{5-[4-({4-[4-(2-{2-[(2*S*)-1-(3,4-difluorophenyl)-6-oxopiperidin-2-yl]-5-(3,5-dimethyl-1,2-oxazol-4-yl)-1*H*-1,3-benzodiazol-1-yl}ethyl)piperazine-1-carbonyl]phenyl}methyl)piperazin-1-yl]-1-oxo-2,3-dihydro-1*H*-isoindol-2-yl}piperidine-2,6-dione (**157**) (9.9 mg, 10 μmol, 51%): R_f 0.015 (acetone); ^{1}H NMR (400 MHz, CD_3CN) δ_H 8.79 (1 H, br s, NH-1^{VI}), 7.62 (1 H, d, *J* 1.0, H-4^{I}), 7.60 – 7.55 (1 H, m, H-7^{I}), 7.52 – 7.47 (1 H, m, H-7^{V}), 7.43 (2 H, d, *J* 8.1, H-3^{VI}), 7.36 – 7.30 (2 H, m, H-4^{VI}), 7.24 – 7.00 (6 H, m, H-6^{I}, H-2^{III}, H-5^{III}, H-6^{III}, H-4^{V}, H-6^{V}), 5.35 (1 H, dd, *J* 5.4, 3.9), 5.02 (1 H, dd, *J* 13.3, 5.0, H-3^{VI}), 4.37 – 4.20 (2 H, m, CH_2), 4.14 – 4.07 (1 H, m, CH_2), 3.74 (2 H, s, H-6^{VII}), 3.37 – 3.33 (2 H, m, CH_2), 2.80 – 2.41 (21 H, m, CH_2), 2.40 (3 H, s, H-7), 2.37 – 2.25 (4 H, m, CH_2), 2.24 (3 H, s, H-6), 2.14 – 2.04 (2 H, m, CH_2), 1.90 – 1.79 (1 H, m, CH_2); ^{19}F NMR (376 MHz, CD_3CN) δ_F −138.49 (1 F, d, *J* 21.2, F-4^{III}), −141.05 (1 F, d, *J* 21.2, F-3^{III}); HRMS *m/z* (ESI$^+$) 979.4411 (979.4425 calculated for $[C_{54}H_{57}F_2N_{10}O_6]^+$); LCMS (formic acid) t_R 0.63 min, *m/z* (ESI$^+$) 979.7 $[M+H]^+$, purity 95%.

(2*S*,4*R*)-*N*-({2-[2-(2-{2-[4-(2-{2-[(2*S*)-1-(3,4-Difluorophenyl)-6-oxopiperidin-2-yl]-5-(3,5-dimethyl-1,2-oxazol-4-yl)-1*H*-1,3-benzodiazol-1-yl}ethyl)piperazin-1-yl]-2-oxoethoxy}ethoxy)ethoxy]-4-(4-methyl-1,3-thiazol-5-yl)phenyl}methyl)-1-[(2*S*)-2-[(1-fluorocyclopropyl)formamido]-3,3-dimethylbutanoyl]-4-hydroxypyrrolidine-2-carboxamide (160)

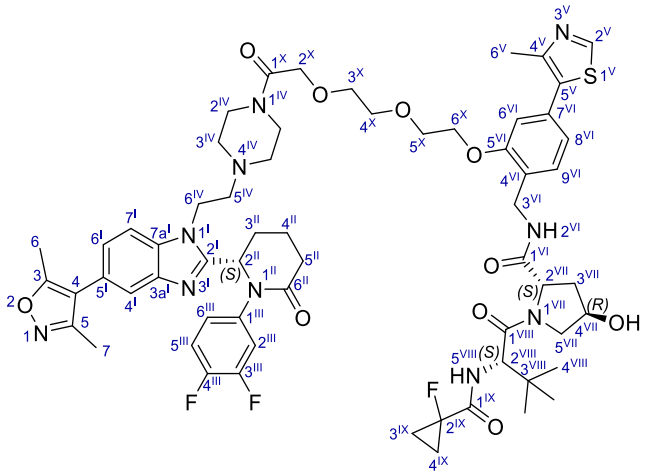

A solution of (6*S*)-1-(3,4-difluorophenyl)-6-[5-(3,5-dimethyl-1,2-oxazol-4-yl)-1-[2-(piperazin-1-yl)ethyl]-1*H*-1,3-benzodiazol-2-yl]piperidin-2-one hydrochloride (**106**) (15.0 mg, 26.3 µmol, 1.0 eq.), 2-(2-(2-(2-(((2*S*,4*R*)-1-((*S*)-2-(1-fluorocyclopropane-1-carboxamido)-3,3-dimethylbutanoyl)-4-hydroxypyrrolidine-2-carboxamido)methyl)-5-(4-methylthiazol-5-yl)phenoxy)ethoxy)ethoxy)acetic acid (20.0 mg, 29.5 µmol, 1.1 eq.), HATU (12.0 mg, 31.6 µmol, 1.2 eq.) and DIPEA (18 µL, 100 µmol, 3.9 eq.) in DMF (260 µL) was stirred at rt for 2 h. The reaction mixture was directly purified using preparative reverse phase column chromatography (gradient of 30 – 99% MeCN in 10 mM aq. $(NH_4)HCO_3$ (pH 10)) to afford (2*S*,4*R*)-*N*-({2-[2-(2-{2-[4-(2-{2-[(2*S*)-1-(3,4-difluorophenyl)-6-oxopiperidin-2-yl]-5-(3,5-dimethyl-1,2-oxazol-4-yl)-1*H*-1,3-benzodiazol-1-yl}ethyl)piperazin-1-yl]-2-oxoethoxy}ethoxy)ethoxy]-4-(4-methyl-1,3-thiazol-5-yl)phenyl}methyl)-1-[(2*S*)-2-[(1-fluorocyclopropyl)formamido]-3,3-dimethylbutanoyl]-4-hydroxypyrrolidine-2-carboxamide (**160**) (17.6 mg, 14.7 µmol, 56%): R_f 0.09 (acetone); ^{1}H NMR (400 MHz, CD_3CN) δ_H 8.71 (1 H, s, H-2^{V}), 7.64 – 7.60 (1 H, m, H-4^{I}), 7.44 (1 H, d, *J* 7.8, H-7^{I}), 7.38 (1 H, d, *J* 7.6, H-8^{VI}), 7.26 – 6.97 (8 H, m, H-6^{I}, H-2^{III}, H-5^{III}, H-6^{III}, NH-2^{VI}, H-6^{VI}, H-9^{VI}, NH-5^{VIII}), 5.37 – 5.27 (1 H, m, H-2^{II}), 4.63 (2 H, d,

J 9.3, H-3^{VI}), 4.50 (1 H, t, *J* 8.2, H-2^{VII}), 4.42 – 4.29 (4 H, m, C*H*$_2$), 4.23 – 4.18 (2 H, m, C*H*$_2$), 4.14 – 4.01 (5 H, m, C*H*$_2$), 4.10 (2 H, s, H-2^{X}), 4.07 – 4.02 (2 H, m, C*H*$_2$), 3.86 – 3.82 (2 H, m, C*H*$_2$), 3.71 – 3.67 (4 H, m, C*H*$_2$), 3.66 – 3.59 (3 H, m, C*H*$_2$), 3.35 – 3.23 (3 H, m, C*H*$_2$), 3.22 – 3.17 (2 H, m, C*H*$_2$), 2.61 – 2.47 (3 H, m, C*H*$_2$), 2.46 (3 H, s, H-6^{V}), 2.46 – 2.40 (3 H, m, C*H*$_2$), 2.39 (3 H, s, H-7), 2.27 – 2.25 (2 H, m, C*H*$_2$), 2.24 (3 H, s, H-6), 2.10 – 2.05 (2 H, m, C*H*$_2$), 1.31 – 1.20 (5 H, m, C*H*$_2$), 0.96 (9 H, s, H-4^{VIII}); ^{19}F NMR (376 MHz, CD_3CN) δ_F −138.47 (1 F, d, *J* 21.2, F-4^{III}), −141.07 (1 F, d, *J* 21.2, F-3^{III}), −198.25 (1 F, s, F-2^{IX}); HRMS *m/z* (ESI$^+$) 1195.5266 (1195.5257 calculated for $[C_{61}H_{74}F_3N_{10}O_{10}S]^+$); LCMS (HpH): t_R 1.06 min, *m/z* (ESI$^+$) 598.4 $[M+2H]^{2+}$, purity 100%.

(2*S*,4*R*)-*N*-[(2-{2-[2-(2-{2-[4-(2-{2-[(2*S*)-1-(3,4-Difluorophenyl)-6-oxopiperidin-2-yl]-5-(3,5-dimethyl-1,2-oxazol-4-yl)-1*H*-1,3-benzodiazol-1-yl}ethyl)piperazin-1-yl]-2-oxoethoxy}ethoxy)ethoxy]ethoxy}-4-(4-methyl-1,3-thiazol-5-yl)phenyl)methyl]-1-[(2*S*)-2-[(1-fluorocyclopropyl)formamido]-3,3-dimethylbutanoyl]-4-hydroxypyrrolidine-2-carboxamide (161)

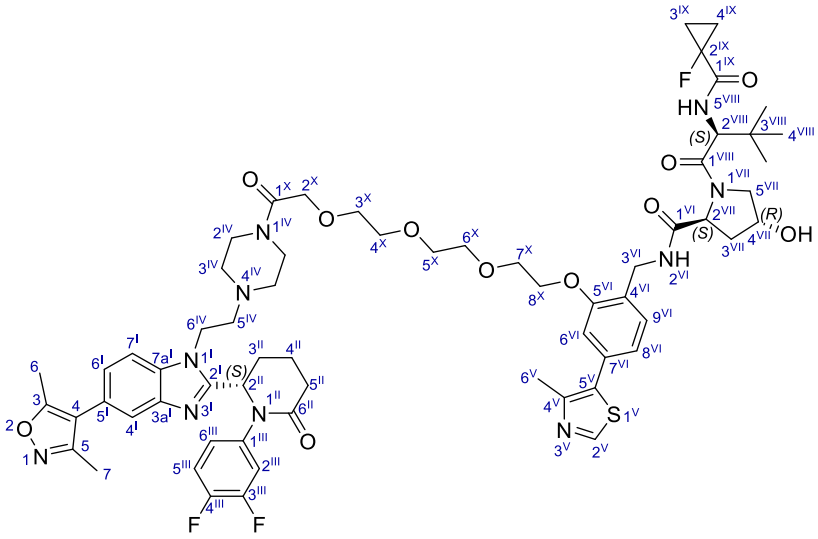

Synthesised according to 'General Amide Coupling Method III'. The crude reaction mixture was directly purified using MDAP (method B) to afford (2*S*,4*R*)-*N*-[(2-{2-[2-(2-{2-[4-(2-{2-[(2*S*)-1-(3,4-difluorophenyl)-6-oxopiperidin-2-yl]-5-(3,5-dimethyl-1,2-oxazol-4-yl)-1*H*-1,3-benzodiazol-1-yl}ethyl)piperazin-1-yl]-2-oxoethoxy}ethoxy)ethoxy]ethoxy}-4-(4-methyl-1,3-thiazol-5-

yl)phenyl)methyl]-1-[(2*S*)-2-[(1-fluorocyclopropyl)formamido]-3,3-dimethylbutanoyl]-4-hydroxypyrrolidine-2-carboxamide (**161**) (10.4 mg, 8.39 μmol, 42%): R_f 0.03 (acetone); ^{1}H NMR (400 MHz, CD_3CN) δ_H 8.72 (1 H, br s, H-2^{V}), 7.62 (1 H, d, *J* 1.0, H-4^{I}), 7.47 (1 H, d, *J* 8.3, H-7^{I}), 7.38 (1 H, d, *J* 7.6, H-4^{VI}), 7.26 (1 H, dd, *J* 6.0, H-8^{VI}), 7.22 – 6.97 (8 H, m, H-6^{I}, H-2^{III}, H-5^{III}, H-6^{III}, NH-2^{VI}, H-6^{VI}, H-9^{VI}, NH-5^{VIII}), 5.34 (1 H, dd, *J* 5.0, 4.3, H-2^{II}), 4.66 – 4.60 (1 H, m, H-3^{VI}), 4.50 (1 H, t, *J* 8.1, H-2^{VII}), 4.44 – 4.40 (1 H, m, H-1^{VIII}), 4.36 (2 H, dd, *J* 16.4, 6.1, CH_2), 4.21 – 4.17 (2 H, m, CH_2), 4.11 – 4.05 (4 H, m, CH_2), 3.85 – 3.81 (2 H, m, CH_2), 3.71 – 3.65 (5 H, m, CH_2), 3.62 – 3.54 (8 H, m, CH_2), 3.31 – 3.25 (1 H, m, CH_2), 3.21 – 3.15 (2 H, m, CH_2), 2.62 – 2.50 (2 H, m, CH_2), 2.47 (3H, s, H-6^{V}), 2.46 – 2.44 (1 H, m, CH_2), 2.39 (3 H, s, H-7), 2.31 – 2.25 (4 H, m, CH_2), 2.23 (3 H, s, H-6), 2.14 – 2.04 (3 H, m, CH_2), 1.88 – 1.79 (1 H, m, CH_2), 1.34 – 1.20 (5 H, m, CH_2), 0.96 (9 H, s, H-4^{VIII}); ^{19}F NMR (376 MHz, CD_3CN) δ_F −138.41 (1 F, d, *J* 21.2, F-4^{III}), −140.99 (1 F, d, *J* 21.2, F-3^{III}), −198.25 (1 F, s, F-2^{IX}); HRMS *m/z* (ESI$^+$) 1239.5516 (1239.5519 calculated for $[C_{63}H_{78}F_3N_{10}O_{11}S]^+$); LCMS (formic acid) t_R 0.93 min, *m/z* (ESI$^+$) 620.7 $[M+2H]^{2+}$, purity 94%.

(2*S*,4*R*)-*N*-{[2-({14-[4-(2-{2-[(2*S*)-1-(3,4-Difluorophenyl)-6-oxopiperidin-2-yl]-5-(3,5-dimethyl-1,2-oxazol-4-yl)-1*H*-1,3-benzodiazol-1-yl}ethyl)piperazin-1-yl]-14-oxo-3,6,9,12-tetraoxatetradecan-1-yl}oxy)-4-(4-methyl-1,3-thiazol-5-yl)phenyl]methyl}-1-[(2*S*)-2-[(1-fluorocyclopropyl)formamido]-3,3-dimethylbutanoyl]-4-hydroxypyrrolidine-2-carboxamide (162)

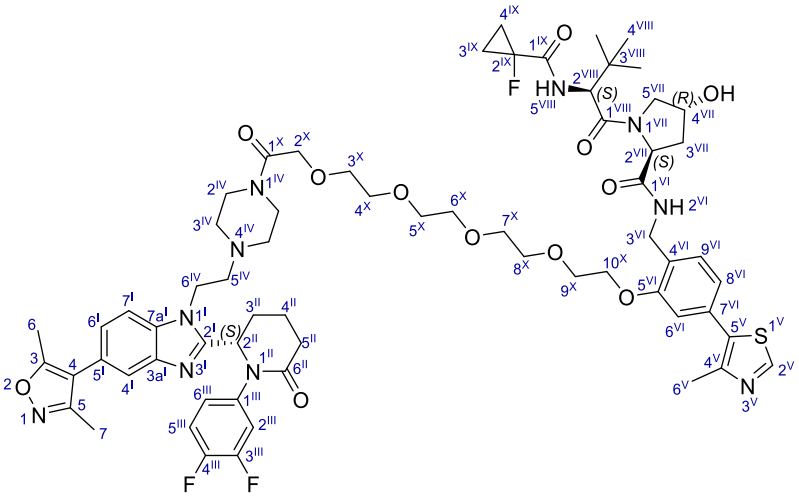

Synthesised according to 'General Amide Coupling Method III'. The crude reaction mixture was directly purified using MDAP (method B) to afford (2*S*,4*R*)-*N*-{[2-({14-[4-(2-{2-[(2*S*)-1-(3,4-difluorophenyl)-6-oxopiperidin-2-yl]-5-(3,5-dimethyl-1,2-oxazol-4-yl)-1*H*-1,3-benzodiazol-1-yl}ethyl)piperazin-1-yl]-14-oxo-3,6,9,12-tetraoxatetradecan-1-yl}oxy)-4-(4-methyl-1,3-thiazol-5-yl)phenyl]methyl}-1-[(2*S*)-2-[(1-fluorocyclopropyl)formamido]-3,3-dimethylbutanoyl]-4-hydroxypyrrolidine-2-carboxamide (**162**) (2.6 mg, 2.0 μmol, 11%): R_f 0.03 (acetone); ^{1}H NMR (400 MHz, CD_3CN) δ_H 8.71 (1 H, s, H-2^V), 7.62 (1 H, d, *J* 1.7, H-4^I), 7.47 (1 H, d, *J* 8.3, H-7^I), 7.39 (1 H, d, *J* 7.8, H-8^{VI}), 7.26 – 6.97 (8 H, m, H-6^I, H-2^{III}, H-5^{III}, H-6^{III}, NH-2^{VI}, H-6^{VI}, H-9^{VI}, NH-5^{VIII}), 5.33 (1 H, dd, *J* 5.3, 4.0, H-2^{II}), 4.63 (1 H, dd, *J* 9.3, 1.2, H-3^{VI}), 4.50 (1 H, t, *J* 8.2, H-2^{VII}), 4.44 – 4.28 (3 H, m, H-1^{VIII}, CH_2), 4.22 – 4.15 (2 H, m, CH_2), 4.11 – 4.03 (4 H, m, CH_2), 3.84 (2 H, t, *J* 4.7, CH_2), 3.73 – 3.64 (4 H, m, CH_2), 3.60 – 3.57 (2 H, m, CH_2), 3.56 – 3.54 (6 H, m, CH_2), 3.32 – 3.23 (2 H, m, CH_2), 3.20 – 3.13 (2 H, m, CH_2), 2.62 – 2.50 (6 H, m, CH_2), 2.47 (3 H, s, H-6^V), 2.39 (3 H, s, H-7), 2.29 – 2.24 (4 H, m, CH_2), 2.24 (3 H, s, H-6), 2.14 – 2.04 (5 H, m, CH_2), 1.87 – 1.82 (1 H, m, CH_2), 1.32 – 1.21 (4 H, m, CH_2), 0.96 (9 H, s, H-4^{VIII}); ^{19}F NMR (376 MHz, CD_3CN) δ_F −138.47 (1 F, d,

J 21.2, F-4^{III}), −141.06 (1 F, d, *J* 21.2, F-3^{III}), −198.28 (1 F, s, F-2^{IX}); HRMS *m/z* (ESI$^+$) 1283.5809 (1283.5781 calculated for $[C_{65}H_{82}F_3N_{10}O_{12}S]^+$); LCMS (formic acid) t_R 0.94 min, *m/z* (ESI$^+$) 642.8 $[M+2H]^{2+}$, purity 99%.

(2*S*,4*R*)-*N*-{[2-({9-[4-(2-{2-[(2*S*)-1-(3,4-Difluorophenyl)-6-oxopiperidin-2-yl]-5-(3,5-dimethyl-1,2-oxazol-4-yl)-1*H*-1,3-benzodiazol-1-yl}ethyl)piperazin-1-yl]-9-oxononyl}oxy)-4-(4-methyl-1,3-thiazol-5-yl)phenyl]methyl}-1-[(2*S*)-2-[(1-fluorocyclopropyl)formamido]-3,3-dimethylbutanoyl]-4-hydroxypyrrolidine-2-carboxamide (163)

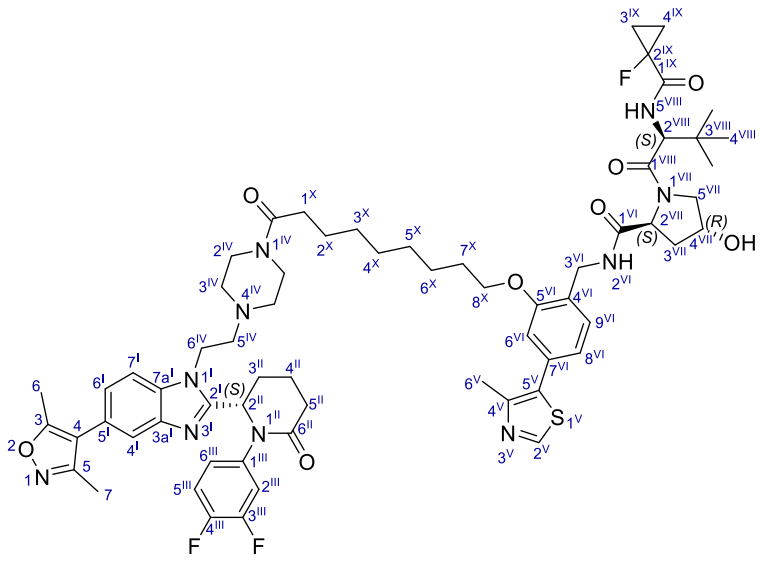

Synthesised according to 'General Amide Coupling Method III'. The crude reaction mixture was directly purified using MDAP (method C) to afford (2*S*,4*R*)-*N*-{[2-({9-[4-(2-{2-[(2*S*)-1-(3,4-difluorophenyl)-6-oxopiperidin-2-yl]-5-(3,5-dimethyl-1,2-oxazol-4-yl)-1*H*-1,3-benzodiazol-1-yl}ethyl)piperazin-1-yl]-9-oxononyl}oxy)-4-(4-methyl-1,3-thiazol-5-yl)phenyl]methyl}-1-[(2*S*)-2-[(1-fluorocyclopropyl)formamido]-3,3-dimethylbutanoyl]-4-hydroxypyrrolidine-2-carboxamide (**163**) (10.6 mg, 8.79 μmol, 47%): R_f 0.13 (acetone); ^{1}H NMR (400 MHz, CD_3CN) δ_H 8.72 (1 H, s, H-2^V), 7.62 (1 H, d, *J* 2.2, H-4^I), 7.51 – 7.45 (1 H, m, H-7^I), 7.38 (1 H, d, *J* 7.8, H-8^{VI}), 7.21 – 6.95 (8 H, m, H-6^I, H-2^{III}, H-5^{III}, H-6^{III}, NH-2^{VI}, H-6^{VI}, H-9^{VI}, NH-5^{VIII}), 5.34 (1 H, dd, *J* 5.3, 3.8, H-2^{II}), 4.63 (1 H, dd, *J* 9.3, 1.2, H-3^{VI}), 4.52 (1 H, t, *J* 8.1, H-2^{VII}), 4.45 – 4.36 (2 H, m, CH_2), 4.29 (1 H, dd, *J* 15.7, 5.6, CH_2), 4.12 – 4.07 (2 H, m, CH_2), 4.05 (2 H, t, *J* 6.4, CH_2), 3.75 – 3.63 (2 H, m, CH_2), 3.29 (2 H, d, *J* 4.7,

CH_2), 3.24 – 3.13 (2 H, m, CH_2), 2.66 – 2.48 (5 H, m, CH_2), 2.47 (3 H, s, H-6^{V}), 2.40 (3 H, s, H-7), 2.28 – 2.25 (5 H, m, CH_2), 2.24 (3 H, s, H-6), 2.23 – 2.21 (2 H, m, CH_2), 2.16 – 2.06 (4 H, m, CH_2), 1.85 – 1.76 (3 H, m, CH_2), 1.54 – 1.45 (4 H, m, CH_2), 1.37 – 1.30 (6 H, m, CH_2), 1.28 – 1.21 (4 H, m, CH_2), 0.95 (9 H, s, H-4^{VIII}); ^{19}F NMR (376 MHz, CD_3CN) δ_F −138.45 (1 F, d, *J* 21.2, F-4^{III}), −141.04 (1 F, d, *J* 21.2, F-3^{III}), −198.27 (1 F, s, F-2^{IX}); HRMS *m/z* (ESI$^+$) 1205.5836 (1205.5828 calculated for $[C_{64}H_{80}F_3N_{10}O_8S]^+$); LCMS (formic acid) t_R 1.11 min, *m/z* (ESI$^+$) 603.7 $[M+2H]^{2+}$, purity 100%.

(2*S*,4*R*)-*N*-{[2-({12-[4-(2-{2-[(2*S*)-1-(3,4-Difluorophenyl)-6-oxopiperidin-2-yl]-5-(3,5-dimethyl-1,2-oxazol-4-yl)-1*H*-1,3-benzodiazol-1-yl}ethyl)piperazin-1-yl]-12-oxododecyl}oxy)-4-(4-methyl-1,3-thiazol-5-yl)phenyl]methyl}-1-[(2*S*)-2-[(1-fluorocyclopropyl)formamido]-3,3-dimethylbutanoyl]-4-hydroxypyrrolidine-2-carboxamide (164)

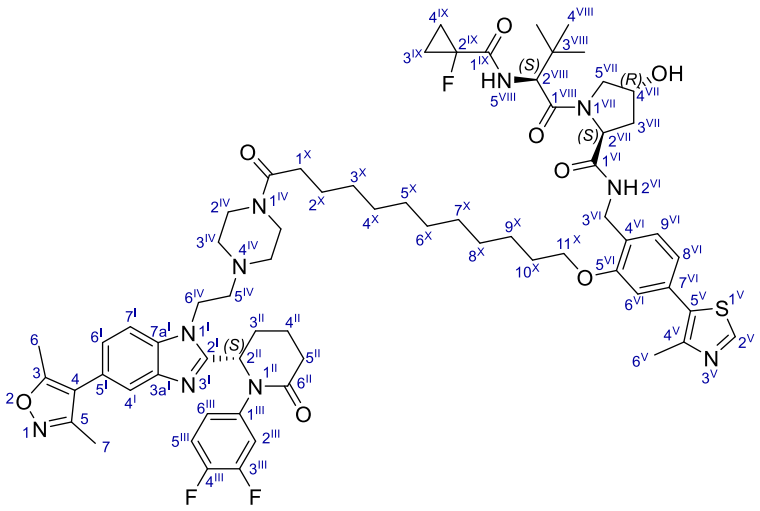

Synthesised according to 'General Amide Coupling Method III'. The crude reaction mixture was directly purified using MDAP (method C) to afford (2*S*,4*R*)-*N*-{[2-({12-[4-(2-{2-[(2*S*)-1-(3,4-difluorophenyl)-6-oxopiperidin-2-yl]-5-(3,5-dimethyl-1,2-oxazol-4-yl)-1*H*-1,3-benzodiazol-1-yl}ethyl)piperazin-1-yl]-12-oxododecyl}oxy)-4-(4-methyl-1,3-thiazol-5-yl)phenyl]methyl}-1-[(2*S*)-2-[(1-fluorocyclopropyl)formamido]-3,3-dimethylbutanoyl]-4-hydroxypyrrolidine-2-carboxamide (**164**) (10.9 mg, 8.74 μmol, 47%): R_f 0.15 (acetone); ^{1}H NMR (400 MHz, CD_3CN) δ_H 8.76 (1 H, s, H-2^{V}), 7.68 – 7.66 (1 H, m, H-4^{I}), 7.54 (1 H, d, *J* 7.8, H-7^{I}), 7.41 (1 H, d, *J* 8.4, H-8^{VI}), 7.27 (1 H, d, *J* 8.4,

H-9^{VI}), 7.24 – 6.98 (7 H, m, H-6^{I}, H-2^{III}, H-5^{III}, H-6^{III}, NH-2^{VI}, H-6^{VI}, NH-5^{VIII}), 5.38 (1 H, dd, *J* 5.4, 4.2, H-2^{II}), 4.66 (1 H, dd, *J* 9.3, 1.2, H-3^{VI}), 4.55 (1 H, t, *J* 8.1, H-2^{VII}), 4.48 – 4.39 (2 H, m), 4.36 – 4.29 (1 H, m), 4.22 (2 H, t, *J* 6.2, H-2^{X}), 4.10 – 4.05 (2 H, m, CH_2), 3.78 – 3.72 (1 H, m, CH_2), 3.72 – 3.66 (1 H, m, CH_2), 3.50 – 3.33 (4 H, m, CH_2), 2.67 – 2.52 (8 H, m, CH_2), 2.50 (3 H, s, H-6^{V}), 2.49 – 2.46 (1 H, m, CH_2), 2.42 (3 H, s, H-7), 2.31 – 2.28 (1 H, m, CH_2), 2.27 (3 H, s, H-6), 2.17 – 2.11 (3 H, m, CH_2), 1.89 – 1.79 (3 H, m, CH_2), 1.57 – 1.48 (4 H, m, CH_2), 1.43 – 1.24 (18 H, m, CH_2), 0.98 (9 H, s, H-4^{VIII}); ^{19}F NMR (376 MHz, CD_3CN) δ_F −138.22 (1 F, d, *J* 21.2, F-4^{III}), −140.81 (1 F, d, *J* 21.2, F-3^{III}), −198.27 (1 F, s, F-2^{IX}); HRMS *m/z* (ESI$^+$) 1247.6275 (1247.6297 calculated for $[C_{67}H_{86}F_3N_{10}O_8S]^+$); LCMS (formic acid) t_R 1.26 min, *m/z* (ESI$^+$) 624.8 $[M+2H]^{2+}$, purity 100%.

(2*S*,4*R*)-1-[(2*S*)-2-{14-[4-(2-{2-[(2*S*)-1-(3,4-Difluorophenyl)-6-oxopiperidin-2-yl]-5-(3,5-dimethyl-1,2-oxazol-4-yl)-1*H*-1,3-benzodiazol-1-yl}ethyl)piperazin-1-yl]-14-oxo-3,6,9,12-tetraoxatetradecanamido}-3,3-dimethylbutanoyl]-4-hydroxy-*N*-[(1*S*)-1-[4-(4-methyl-1,3-thiazol-5-yl)phenyl]ethyl]pyrrolidine-2-carboxamide (168)

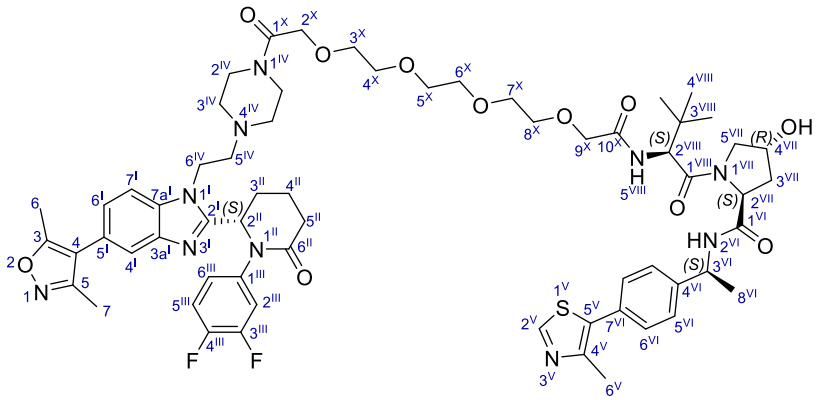

Synthesised according to 'General Amide Coupling Method III'. The crude reaction mixture was directly purified using MDAP (method B) to afford (2*S*,4*R*)-1-[(2*S*)-2-{14-[4-(2-{2-[(2*S*)-1-(3,4-difluorophenyl)-6-oxopiperidin-2-yl]-5-(3,5-dimethyl-1,2-oxazol-4-yl)-1*H*-1,3-benzodiazol-1-yl}ethyl)piperazin-1-yl]-14-oxo-3,6,9,12-tetraoxatetradecanamido}-3,3-dimethylbutanoyl]-4-hydroxy-*N*-[(1*S*)-1-[4-(4-methyl-1,3-thiazol-5-yl)phenyl]ethyl]pyrrolidine-2-carboxamide (**168**) (9.7 mg, 8.02 μmol, 42%): R_f 0.02 (acetone); ^{1}H NMR (400 MHz, CD_3CN) δ_H 8.72 (1 H, s, H-2^{V}), 7.62

(1 H, d, *J* 1.0, H-4^{I}), 7.49 – 7.10 (11 H, m, H-6^{I}, H-7^{I}, H-2^{III}, H-5^{III}, NH-2^{VI}, H-5^{VI}, H-6^{VI}, H-9^{VI}, NH-5^{VIII}), 7.04 – 6.99 (1 H, m, H-6^{III}), 5.34 (1 H, dd, *J* 5.4, 3.9, H-2^{II}), 4.99 – 4.90 (1 H, m, H-3^{VI}), 4.61 (1 H, d, *J* 9.5, H-2^{VIII}), 4.48 (1 H, t, *J* 8.2, H-2^{VII}), 4.39 – 4.34 (1 H, m, H-4^{VII}), 4.10 (2 H, s, H-9^{X}), 4.09 – 4.07 (1 H, m, CH_2), 3.95 (2 H, d, *J* 1.7, CH_2), 3.76 – 3.71 (1 H, m, CH_2), 3.68 – 3.58 (15 H, m, CH_2), 3.33 – 3.27 (2 H, m, CH_2), 3.24 – 3.18 (2 H, m, CH_2), 2.62 – 2.47 (5 H, m, CH_2), 2.46 (3 H, s, H-6^{V}), 2.39 (3 H, s, H-7), 2.35 – 2.25 (5 H, m, CH_2), 2.24 (3 H, s, H-6), 2.13 – 2.05 (2 H, m, CH_2), 2.03 – 1.98 (1 H, m, CH_2), 1.89 – 1.80 (1 H, m, CH_2), 1.42 (3 H, d, *J* 7.1, H-8^{VI}), 0.99 (9 H, s, H-4^{VIII}); ^{19}F NMR (376 MHz, CD_3CN) δ_F −138.44 (1 F, d, *J* 21.2, F-4^{III}), −141.04 (1 F, d, *J* 21.2, F-3^{III}); HRMS *m/z* (ESI$^+$) 1209.5635 (1209.5613 calculated for $[C_{62}H_{79}F_2N_{10}O_{11}S]^+$); LCMS (formic acid) t_R 0.90 min, *m/z* (ESI$^+$) 605.7 $[M+2H]^{2+}$, purity 99%.

(2*S*,4*R*)-1-[(2*S*)-2-{7-[4-(2-{2-[(2*S*)-1-(3,4-Difluorophenyl)-6-oxopiperidin-2-yl]-5-(3,5-dimethyl-1,2-oxazol-4-yl)-1*H*-1,3-benzodiazol-1-yl}ethyl)piperazin-1-yl]-7-oxoheptanamido}-3,3-dimethylbutanoyl]-4-hydroxy-*N*-[(1*S*)-1-[4-(4-methyl-1,3-thiazol-5-yl)phenyl]ethyl]pyrrolidine-2-carboxamide (169)

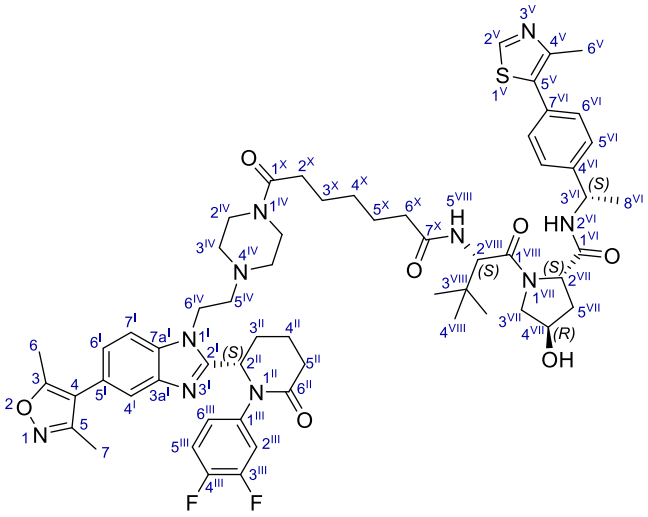

Synthesised according to 'General Amide Coupling Method III'. The crude reaction mixture was directly purified using MDAP (method B) to afford (2*S*,4*R*)-1-[(2*S*)-2-{7-[4-(2-{2-[(2*S*)-1-(3,4-difluorophenyl)-6-oxopiperidin-2-yl]-5-(3,5-dimethyl-1,2-oxazol-4-yl)-1*H*-1,3-benzodiazol-1-

yl}ethyl)piperazin-1-yl]-7-oxoheptanamido}-3,3-dimethylbutanoyl]-4-hydroxy-*N*-[(1*S*)-1-[4-(4-methyl-1,3-thiazol-5-yl)phenyl]ethyl]pyrrolidine-2-carboxamide (**169**) (3.9 mg, 3.5 μmol, 18%): R_f 0.04 (acetone); ^{1}H NMR (400 MHz, CD_3CN) δ_H 8.74 (1 H, s, H-2^{V}), 7.64 (1 H, d, *J* 1.0, H-4^{I}), 7.51 (1 H, d, *J* 8.5, H-7^{I}), 7.46 – 7.41 (2 H, m, H-6^{VI}), 7.40 – 7.35 (2 H, m, H-5^{VI}), 7.24 (1 H, d, *J* 8.5, H-6^{I}), 7.22 – 7.09 (3 H, m, H-2^{III}, H-5^{III}, NH-5^{VIII}), 7.06 – 7.00 (1 H, m, H-6^{III}), 6.58 (1 H, br d, *J* 8.8, NH-2^{VI}), 5.36 (1 H, dd, *J* 4.7, H-2^{II}), 4.99 – 4.89 (1 H, m, H-3^{VI}), 4.54 (1 H, d, *J* 9.1, H-2^{VIII}), 4.44 (1 H, t, *J* 8.1, H-2^{VII}), 4.39 – 4.34 (1 H, m, H-4^{VII}), 4.18 (1 H, br s, OH), 3.81 (1 H, d, *J* 11.0, CH_2), 3.64 (1 H, dd, *J* 11.0, 3.9, CH_2), 2.64 – 2.50 (4 H, m, CH_2), 2.47 (3 H, s, H-6^{V}), 2.40 (3 H, s, H-7), 2.24 (3 H, s, H-6), 2.23 – 2.06 (18 H, m, CH_2), 1.90 – 1.83 (1 H, m, CH_2), 1.60 – 1.49 (4 H, m, CH_2), 1.42 (3 H, d, *J* 6.9, H-8^{VI}), 1.36 – 1.25 (3 H, m, CH_2), 0.98 (9 H, s, H-4^{VIII}); ^{19}F NMR (376 MHz, CD_3CN) δ_F −138.29 (1 F, d, *J* 21.2, F-4^{III}), −140.88 (1 F, d, *J* 21.2, F-3^{III}); HRMS *m/z* (ESI$^+$) 1103.5360 (1103.5347 calculated for $[C_{59}H_{73}F_2N_{10}O_7S]^+$); LCMS (formic acid) t_R 0.94 min, *m/z* (ESI$^+$) 552.4 $[M+2H]^{2+}$, purity 94%.

(2*S*,4*R*)-1-[(2*S*)-2-{10-[4-(2-{2-[(2*S*)-1-(3,4-Difluorophenyl)-6-oxopiperidin-2-yl]-5-(3,5-dimethyl-1,2-oxazol-4-yl)-1*H*-1,3-benzodiazol-1-yl}ethyl)piperazin-1-yl]-10-oxodecanamido}-3,3-dimethylbutanoyl]-4-hydroxy-*N*-[(1*S*)-1-[4-(4-methyl-1,3-thiazol-5-yl)phenyl]ethyl]pyrrolidine-2-carboxamide (170)

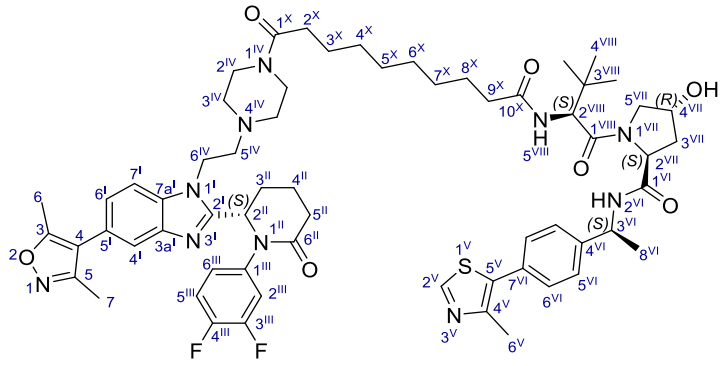

Synthesised according to 'General Amide Coupling Method III'. The crude reaction mixture was directly purified using MDAP (extended method C) to afford (2*S*,4*R*)-1-[(2*S*)-2-{10-[4-(2-{2-[(2*S*)-1-(3,4-difluorophenyl)-6-oxopiperidin-2-yl]-5-(3,5-dimethyl-1,2-oxazol-4-yl)-1*H*-1,3-benzodiazol-1-

yl}ethyl)piperazin-1-yl]-10-oxodecanamido}-3,3-dimethylbutanoyl]-4-hydroxy-*N*-[(1*S*)-1-[4-(4-methyl-1,3-thiazol-5-yl)phenyl]ethyl]pyrrolidine-2-carboxamide (**170**) (5.1 mg, 4.5 μmol, 23%): R_f 0.07 (acetone); ^{1}H NMR (400 MHz, CD_3CN) δ_H 8.73 (1 H, s, H-2^V), 7.64 – 7.61 (1 H, m, H-4^I), 7.50 – 7.36 (5 H, m, H-7^I, H-5^{VI}, H-6^{VI}), 7.23 – 7.09 (4 H, m, H-6^I, H-2^{III}, H-5^{III}, NH-5^{VIII}), 7.05 – 7.00 (1 H, m, H-6^{III}), 6.57 (1 H, br d, *J* 8.8, NH-2^{VI}), 5.35 (1 H, dd, *J* 5.4, 3.9, H-2^{II}), 5.00 – 4.90 (1 H, m, H-3^{VI}), 4.55 (1 H, d, *J* 9.1, H-2^{VIII}), 4.46 (1 H, t, *J* 8.2, H-2^{VII}), 4.38 – 4.33 (1 H, m, H-4^{VII}), 4.13 – 4.06 (2 H, m, CH_2), 3.81 (1 H, d, *J* 11.1, CH_2), 3.62 (1 H, dd, *J* 11.1, 4.0, CH_2), 3.33 – 3.25 (2 H, m, CH_2), 3.24 – 3.15 (2 H, m, CH_2), 2.60 – 2.48 (9 H, m, CH_2), 2.47 (3 H, s, H-6^{VI}), 2.40 (3 H, s, H-7), 2.28 – 2.25 (4 H, m, CH_2), 2.24 (3 H, s, H-6), 2.23 - 2.14 (4 H, m, CH_2), 1.88 – 1.81 (1 H, m, CH_2), 1.57 – 1.48 (4 H, m, CH_2), 1.42 (3 H, d, *J* 7.1, H-8^{VI}), 1.31 – 1.26 (8 H, m, CH_2), 0.98 (9 H, s, H-4^{VIII}); ^{19}F NMR (376 MHz, CD_3CN) δ_F −138.48 (1 F, d, *J* 21.2, F-4^{III}), −141.07 (1 F, d, *J* 21.2, F-3^{III}); HRMS *m/z* (ESI$^+$) 1145.5809 (1145.5817 calculated for $[C_{62}H_{79}F_2N_{10}O_7S]^+$); LCMS (formic acid) t_R 1.02 min, *m/z* (ESI$^+$) 573.7 $[M+2H]^{2+}$, purity 96%.

Bibliography

(1) Paiva, S.-L.; Crews, C. M. Targeted Protein Degradation: Elements of PROTAC Design. *Next Gener. Ther.* **2019**, *50*, 111–119. https://doi.org/10.1016/j.cbpa.2019.02.022.

(2) Pettersson, M.; Crews, C. M. PROteolysis TArgeting Chimeras (PROTACs) — Past, Present and Future. *Drug Discovery Today: Technologies*. Elsevier Ltd April 1, 2019, pp 15–27. https://doi.org/10.1016/j.ddtec.2019.01.002.

(3) Békés, M.; Langley, D. R.; Crews, C. M. PROTAC Targeted Protein Degraders: The Past Is Prologue. *Nat. Rev. Drug Discov.* **2022**, *21* (3), 181–200. https://doi.org/10.1038/s41573-021-00371-6.

(4) Navon, A.; Ciechanover, A. The 26 S Proteasome: From Basic Mechanisms to Drug Targeting. *Journal of Biological Chemistry*. Papers in Press December 4, 2009, pp 33713–33718. https://doi.org/10.1074/jbc.R109.018481.

(5) Finley, D. Recognition and Processing of Ubiquitin-Protein Conjugates by the Proteasome. *Annu. Rev. Biochem.* **2009**, *78* (1), 477–513. https://doi.org/10.1146/annurev.biochem.78.081507.101607.

(6) Lai, A. C.; Crews, C. M. Induced Protein Degradation: An Emerging Drug Discovery Paradigm. *Nat. Rev. Drug Discov.* **2017**, *16* (2), 101–114. https://doi.org/10.1038/nrd.2016.211.

(7) George, A. J.; Hoffiz, Y. C.; Charles, A. J.; Zhu, Y.; Mabb, A. M. A Comprehensive Atlas of E3 Ubiquitin Ligase Mutations in Neurological Disorders. *Front. Genet.* **2018**, *9*, 1–17. https://doi.org/https://doi.org/10.3389/fgene.2018.00029.

(8) Bondeson, D. P.; Smith, B. E.; Burslem, G. M.; Buhimschi, A. D.; Hines, J.; Jaime-Figueroa, S.; Wang, J.; Hamman, B. D.; Ishchenko, A.; Crews, C. M. Lessons in PROTAC Design from Selective Degradation with a Promiscuous Warhead. *Cell Chem. Biol.* **2018**, *25* (1), 78-87.e5. https://doi.org/10.1016/j.chembiol.2017.09.010.

(9) Buckley, D. L.; Van Molle, I.; Gareiss, P. C.; Tae, H. S.; Michel, J.; Noblin, D. J.; Jorgensen, W. L.; Ciulli, A.; Crews, C. M. Targeting the von Hippel–Lindau E3 Ubiquitin Ligase Using Small Molecules To Disrupt the VHL/HIF-1α Interaction. *J. Am. Chem. Soc.* **2012**, *134* (10), 4465–4468. https://doi.org/10.1021/ja209924v.

(10) Zhu, Y. X.; Braggio, E.; Shi, C.-X.; Bruins, L. A.; Schmidt, J. E.; Van Wier, S.; Chang, X.-B.; Bjorklund, C. C.; Fonseca, R.; Bergsagel, P. L.; Orlowski, R. Z.; Stewart, A. K. Cereblon Expression Is Required for the Antimyeloma Activity of Lenalidomide and Pomalidomide. *Blood* **2011**, *118* (18), 4771–4779. https://doi.org/10.1182/blood-2011-05-356063.

(11) Zengerle, M.; Chan, K. H.; Ciulli, A. Selective Small Molecule Induced Degradation of the BET Bromodomain Protein BRD4. *ACS Chem. Biol.* **2015**, *10* (8), 1770–1777. https://doi.org/10.1021/acschembio.5b00216.

(12) Soares, P.; Gadd, M. S.; Frost, J.; Galdeano, C.; Ellis, L.; Epemolu, O.; Rocha, S.; Read, K. D.; Ciulli, A. Group-Based Optimization of Potent and Cell-Active Inhibitors of the von Hippel–Lindau (VHL) E3 Ubiquitin Ligase: Structure–Activity Relationships Leading to the Chemical Probe (2S,4R)-1-((S)-2-(1-Cyanocyclopropanecarboxamido)-3,3-Dimethylbutanoyl)-4-Hydr. *J. Med. Chem.* **2018**, *61* (2), 599–618. https://doi.org/10.1021/acs.jmedchem.7b00675.

(13) Diehl, C. J.; Ciulli, A. Discovery of Small Molecule Ligands for the von Hippel-Lindau (VHL) E3 Ligase and Their Use as Inhibitors and PROTAC Degraders. *Chem. Soc. Rev.* **2022**, *51* (19), 8216–8257. https://doi.org/10.1039/D2CS00387B.

(14) Girardini, M.; Maniaci, C.; Hughes, S. J.; Testa, A.; Ciulli, A. Cereblon versus VHL: Hijacking E3 Ligases against Each Other Using PROTACs. *Bioorg. Med. Chem.* **2019**, *27* (12), 2466–2479. https://doi.org/https://doi.org/10.1016/j.bmc.2019.02.048.

(15) Lopez-Girona, A.; Mendy, D.; Ito, T.; Miller, K.; Gandhi, A. K.; Kang, J.; Karasawa, S.; Carmel, G.; Jackson, P.; Abbasian, M.; Mahmoudi, A.; Cathers, B.; Rychak, E.; Gaidarova, S.; Chen, R.; Schafer, P. H.; Handa, H.; Daniel, T. O.; Evans, J. F.; Chopra, R. Cereblon Is a Direct Protein Target for Immunomodulatory and Antiproliferative Activities of Lenalidomide and Pomalidomide. *Leukemia* **2012**, *26* (11), 2326–2335. https://doi.org/10.1038/leu.2012.119.

(16) Steinebach, C.; Sosič, I.; Lindner, S.; Bricelj, A.; Kohl, F.; Ng, Y. L. D.; Monschke, M.; Wagner, K. G.; Krönke, J.; Gütschow, M. A MedChem Toolbox for Cereblon-Directed PROTACs. *Medchemcomm* **2019**, *10* (6), 1037–1041. https://doi.org/10.1039/c9md00185a.

(17) Ermondi, G.; Garcia Jimenez, D.; Rossi Sebastiano, M.; Caron, G. Rational Control of Molecular Properties Is Mandatory to Exploit the Potential of PROTACs as Oral Drugs. *ACS Med. Chem. Lett.* **2021**, *12* (7), 1056–1060. https://doi.org/10.1021/acsmedchemlett.1c00298.

(18) Pike, A.; Williamson, B.; Harlfinger, S.; Martin, S.; McGinnity, D. F. Optimising Proteolysis-Targeting Chimeras (PROTACs) for Oral Drug Delivery: A Drug Metabolism and Pharmacokinetics Perspective. *Drug Discov. Today* **2020**, *25* (10), 1793–1800. https://doi.org/https://doi.org/10.1016/j.drudis.2020.07.013.

(19) Atilaw, Y.; Poongavanam, V.; Svensson Nilsson, C.; Nguyen, D.; Giese, A.; Meibom, D.; Erdelyi, M.; Kihlberg, J. Solution Conformations Shed Light on PROTAC Cell Permeability. *ACS Med. Chem. Lett.* **2021**, *12* (1), 107–114. https://doi.org/10.1021/acsmedchemlett.0c00556.

(20) Hill, A. P.; Young, R. J. Getting Physical in Drug Discovery: A Contemporary Perspective on Solubility and Hydrophobicity. *Drug Discov. Today* **2010**, *15* (15), 648–655. https://doi.org/https://doi.org/10.1016/j.drudis.2010.05.016.

(21) Tinworth, C. P.; Young, R. J. Facts, Patterns, and Principles in Drug Discovery: Appraising the Rule of 5 with Measured Physicochemical Data. *J. Med. Chem.* **2020**, *63* (18), 10091–10108. https://doi.org/10.1021/acs.jmedchem.9b01596.

(22) Winter, G. E.; Buckley, D. L.; Paulk, J.; Roberts, J. M.; Souza, A.; Dhe-Paganon, S.; Bradner, J. E. Phthalimide Conjugation as a Strategy for in Vivo Target Protein Degradation. *Science (80-.).* **2015**, *348* (6241), 1376 LP – 1381. https://doi.org/10.1126/science.aab1433.

(23) Gadd, M. S.; Testa, A.; Lucas, X.; Chan, K.-H.; Chen, W.; Lamont, D. J.; Zengerle, M.; Ciulli, A. Structural Basis of PROTAC Cooperative Recognition for Selective Protein Degradation. *Nat. Chem. Biol.* **2017**, *13* (5), 514–521. https://doi.org/10.1038/nchembio.2329.

(24) Kataoka, Y.; Mukohara, T.; Tomioka, H.; Funakoshi, Y.; Kiyota, N.; Fujiwara, Y.; Yashiro, M.; Hirakawa, K.; Hirai, M.; Minami, H. Foretinib (GSK1363089), a Multi-Kinase Inhibitor of MET and VEGFRs, Inhibits Growth of Gastric Cancer Cell Lines by Blocking Inter-Receptor Tyrosine Kinase Networks. *Invest. New Drugs* **2012**, *30* (4), 1352–1360. https://doi.org/10.1007/s10637-011-9699-0.

(25) Galdeano, C.; Gadd, M. S.; Soares, P.; Scaffidi, S.; Van Molle, I.; Birced, I.; Hewitt, S.; Dias, D. M.; Ciulli, A. Structure-Guided Design and Optimization of Small Molecules Targeting the Protein–Protein Interaction between the von Hippel–Lindau (VHL) E3 Ubiquitin Ligase and the Hypoxia Inducible Factor (HIF) Alpha Subunit with in Vitro Nanomolar Affinities. *J. Med. Chem.* **2014**, *57* (20), 8657–8663. https://doi.org/10.1021/jm5011258.

(26) Farnaby, W.; Koegl, M.; Roy, M. J.; Whitworth, C.; Diers, E.; Trainor, N.; Zollman, D.; Steurer, S.; Karolyi-Oezguer, J.; Riedmueller, C.; Gmaschitz, T.; Wachter, J.; Dank, C.; Galant, M.; Sharps, B.; Rumpel, K.; Traxler, E.; Gerstberger, T.; Schnitzer, R.; Petermann, O.;

Greb, P.; Weinstabl, H.; Bader, G.; Zoephel, A.; Weiss-Puxbaum, A.; Ehrenhöfer-Wölfer, K.; Wöhrle, S.; Boehmelt, G.; Rinnenthal, J.; Arnhof, H.; Wiechens, N.; Wu, M.-Y.; Owen-Hughes, T.; Ettmayer, P.; Pearson, M.; McConnell, D. B.; Ciulli, A. BAF Complex Vulnerabilities in Cancer Demonstrated via Structure-Based PROTAC Design. *Nat. Chem. Biol.* **2019**, *15* (7), 672–680. https://doi.org/10.1038/s41589-019-0294-6.

(27) Nunes, J.; McGonagle, G. A.; Eden, J.; Kiritharan, G.; Touzet, M.; Lewell, X.; Emery, J.; Eidam, H.; Harling, J. D.; Anderson, N. A. Targeting IRAK4 for Degradation with PROTACs. *ACS Med. Chem. Lett.* **2019**, *10* (7), 1081–1085. https://doi.org/10.1021/acsmedchemlett.9b00219.

(28) Troup, R. I.; Fallan, C.; Baud, M. G. J. Current Strategies for the Design of PROTAC Linkers: A Critical Review. *Explor. Target. Anti-tumor Ther.* **2020**, *1* (5), 273–312. https://doi.org/10.37349/etat.2020.00018.

(29) Chrivia, J. C.; Kwok, R. P. S.; Lamb, N.; Hagiwara, M.; Montminy, M. R.; Goodman, R. H. Phosphorylated CREB Binds Specifically to the Nuclear Protein CBP. *Nature* **1993**, *365* (6449), 855–859. https://doi.org/10.1038/365855a0.

(30) Eckner, R.; Ewen, M. E.; Newsome, D.; Gerdes, M.; DeCaprio, J. A.; Lawrence, J. B.; Livingston, D. M. Molecular Cloning and Functional Analysis of the Adenovirus E1A-Associated 300-KD Protein (P300) Reveals a Protein with Properties of a Transcriptional Adaptor. *Genes Dev.* **1994**, *8* (8), 869–884. https://doi.org/10.1101/gad.8.8.869.

(31) Filippakopoulos, P.; Picaud, S.; Mangos, M.; Keates, T.; Lambert, J.-P.; Barsyte-Lovejoy, D.; Felletar, I.; Volkmer, R.; Müller, S.; Pawson, T.; Gingras, A.-C.; Arrowsmith, C. H.; Knapp, S. Histone Recognition and Large-Scale Structural Analysis of the Human Bromodomain Family. *Cell* **2012**, *149* (1), 214–231. https://doi.org/10.1016/j.cell.2012.02.013.

(32) Ogryzko, V. V; Schiltz, R. L.; Russanova, V.; Howard, B. H.; Nakatani, Y. The Transcriptional Coactivators P300 and CBP Are Histone Acetyltransferases. *Cell* **1996**, *87* (5), 953–959. https://doi.org/10.1016/S0092-8674(00)82001-2.

(33) De Guzman, R. N.; Wojciak, J. M.; Martinez-Yamout, M. A.; Dyson, H. J.; Wright, P. E. CBP/P300 TAZ1 Domain Forms a Structured Scaffold for Ligand Binding. *Biochemistry* **2005**, *44* (2), 490–497. https://doi.org/10.1021/bi048161t.

(34) Ponting, C. P.; Blake, D. J.; Davies, K. E.; Kendrick-Jones, J.; Winder, S. J. ZZ and TAZ: New Putative Zinc Fingers in Dystrophin and Other Proteins. *Trends Biochem. Sci.* **1996**, *21* (1), 11–13.

(35) Park, S.; Stanfield, R. L.; Martinez-Yamout, M. A.; Dyson, H. J.; Wilson, I. A.; Wright, P. E. Role of the CBP Catalytic Core in Intramolecular SUMOylation and Control of Histone H3 Acetylation. *Proc. Natl. Acad. Sci. U. S. A.* **2017**, *114* (27), E5335–E5342. https://doi.org/10.1073/pnas.1703105114.

(36) Delvecchio, M.; Gaucher, J.; Aguilar-Gurrieri, C.; Ortega, E.; Panne, D. Structure of the P300 Catalytic Core and Implications for Chromatin Targeting and HAT Regulation. *Nat. Struct. Mol. Biol.* **2013**, *20* (9), 1040–1046. https://doi.org/10.1038/nsmb.2642.

(37) Legge, G. B.; Martinez-Yamout, M. A.; Hambly, D. M.; Trinh, T.; Lee, B. M.; Dyson, H. J.; Wright, P. E. ZZ Domain of CBP: An Unusual Zinc Finger Fold in a Protein Interaction Module. *J. Mol. Biol.* **2004**, *343* (4), 1081–1093. https://doi.org/10.1016/j.jmb.2004.08.087.

(38) Parker, D.; Ferreri, K.; Nakajima, T.; LaMorte, V. J.; Evans, R.; Koerber, S. C.; Hoeger, C.; Montminy, M. R. Phosphorylation of CREB at Ser-133 Induces Complex Formation with CREB-Binding Protein via a Direct Mechanism. *Mol. Cell. Biol.* **1996**, *16* (2), 694–703. https://doi.org/10.1128/mcb.16.2.694.

(39) Chakravarti, D.; LaMorte, V. J.; Nelson, M. C.; Nakajima, T.; Schulman, I. G.; Juguilon, H.; Montminy, M.; Evans, R. M. Role of CBP/P300 in Nuclear Receptor Signalling. *Nature* **1996**, *383* (6595), 99–103. https://doi.org/10.1038/383099a0.

(40) Lee, C. W.; Martinez-Yamout, M. A.; Dyson, H. J.; Wright, P. E. Structure of the P53 Transactivation Domain in Complex with the Nuclear Receptor Coactivator Binding Domain of CREB Binding Protein. *Biochemistry* **2010**, *49* (46), 9964–9971. https://doi.org/10.1021/bi1012996.

(41) Kamei, Y.; Xu, L.; Heinzel, T.; Torchia, J.; Kurokawa, R.; Gloss, B.; Lin, S. C.; Heyman, R. A.; Rose, D. W.; Glass, C. K.; Rosenfeld, M. G. A CBP Integrator Complex Mediates Transcriptional Activation and AP-1 Inhibition by Nuclear Receptors. *Cell* **1996**, *85* (3), 403–414. https://doi.org/10.1016/S0092-8674(00)81118-6.

(42) Thakur, J. K.; Yadav, A.; Yadav, G. Molecular Recognition by the KIX Domain and Its Role in Gene Regulation. *Nucleic Acids Res.* **2014**, *42* (4), 2112–2125. https://doi.org/10.1093/nar/gkt1147.

(43) Brand, M.; Clayton, J.; Moroglu, M.; Schiedel, M.; Picaud, S.; Bluck, J. P.; Skwarska, A.; Bolland, H.; Chan, A. K. N.; Laurin, C. M. C.; Scorah, A. R.; See, L.; Rooney, T. P. C.; Andrews, K. H.; Fedorov, O.; Perell, G.; Kalra, P.; Vinh, K. B.; Cortopassi, W. A.; Heitel, P.; Christensen, K. E.; Cooper, R. I.; Paton, R. S.; Pomerantz, W. C. K.; Biggin, P. C.; Hammond, E. M.; Filippakopoulos, P.; Conway, S. J. Controlling Intramolecular Interactions in the Design of Selective, High-Affinity Ligands for the CREBBP Bromodomain. *J. Med. Chem.* **2021**, *64* (14), 10102–10123. https://doi.org/10.1021/acs.jmedchem.1c00348.

(44) Ferreon, J. C.; Martinez-Yamout, M. A.; Dyson, H. J.; Wright, P. E. Structural Basis for Subversion of Cellular Control Mechanisms by the Adenoviral E1A Oncoprotein. *Proc. Natl. Acad. Sci. U. S. A.* **2009**, *106* (32), 13260–13265. https://doi.org/10.1073/pnas.0906770106.

(45) Demarest, S. J.; Martinez-Yamout, M.; Chung, J.; Chen, H.; Xu, W.; Jane Dyson, H.; Evans, R. M.; Wright, P. E. Mutual Synergistic Folding in Recruitment of Cbp/P300 by P160 Nuclear Receptor Coactivators. *Nature* **2002**, *415* (6871), 549–553. https://doi.org/10.1038/415549a.

(46) UniProt, Q92793, CBP_HUMAN https://www.uniprot.org/uniprotkb/Q92793/entry (accessed May 22, 2023).

(47) Consortium, T. U. UniProt: A Worldwide Hub of Protein Knowledge. *Nucleic Acids Res.* **2019**, *47* (D1), D506–D515. https://doi.org/10.1093/nar/gky1049.

(48) Tallant, C.; Hay, D. A.; Krojer, T.; Nunez-Alonso, G. A.; Picaud, S.; Newman, J. A.; Fedorov, O.; Arrowsmith, C. H.; Edwards, A. M.; Bountra, C.; Brennan, P. E.; Knapp, S. Crystal Structure of EP300 Bromodomain in Complex with SGC-CBP30 Chemical Probe. *Worldw. Protein Data Bank* **2015**. https://doi.org/https://doi.org/10.2210/pdb5bt3/pdb.

(49) Zhang, Y.; Xue, Y.; Shi, J.; Ahn, J.; Mi, W.; Ali, M.; Wang, X.; Klein, B. J.; Wen, H.; Li, W.; Shi, X.; Kutateladze, T. G. The ZZ Domain of P300 Mediates Specificity of the Adjacent HAT Domain for Histone H3. *Nat. Struct. Mol. Biol.* **2018**, *25* (9), 841–849. https://doi.org/10.1038/s41594-018-0114-9.

(50) Lochhead, M. R.; Brown, A. D.; Kirlin, A. C.; Chitayat, S.; Munro, K.; Findlay, J. E.; Baillie, G. S.; LeBrun, D. P.; Langelaan, D. N.; Smith, S. P. Structural Insights into TAZ2 Domain-Mediated CBP/P300 Recruitment by Transactivation Domain 1 of the Lymphopoietic Transcription Factor E2A. *J. Biol. Chem.* **2020**, *295* (13), 4303–4315. https://doi.org/10.1074/jbc.RA119.011078.

(51) UniProt, Q09472, EP300_HUMAN https://www.uniprot.org/uniprotkb/Q09472/ (accessed May 22, 2023).

(52) Altschul, S. F.; Madden, T. L.; Schäffer, A. A.; Zhang, J.; Zhang, Z.; Miller, W.; Lipman, D. J. Gapped BLAST and PSI-BLAST: A New Generation of Protein Database Search Programs. *Nucleic Acids Res.* **1997**, *25* (17), 3389–3402. https://doi.org/10.1093/nar/25.17.3389.

(53) Altschul, S. F.; Wootton, J. C.; Gertz, E. M.; Agarwala, R.; Morgulis, A.; Schäffer, A. A.; Yu, Y.-K. Protein Database Searches Using Compositionally Adjusted Substitution Matrices. *FEBS J.* **2005**, *272* (20), 5101–5109. https://doi.org/https://doi.org/10.1111/j.1742-4658.2005.04945.x.

(54) AlphaFold structure prediction of CREB-Binding Protein from UniProt Q92793 https://alphafold.ebi.ac.uk/entry/Q92793 (accessed May 23, 2023).

(55) Jumper, J.; Evans, R.; Pritzel, A.; Green, T.; Figurnov, M.; Ronneberger, O.; Tunyasuvunakool, K.; Bates, R.; Žídek, A.; Potapenko, A.; Bridgland, A.; Meyer, C.; Kohl, S. A. A.; Ballard, A. J.; Cowie, A.; Romera-Paredes, B.; Nikolov, S.; Jain, R.; Adler, J.; Back, T.; Petersen, S.; Reiman, D.; Clancy, E.; Zielinski, M.; Steinegger, M.; Pacholska, M.; Berghammer, T.; Bodenstein, S.; Silver, D.; Vinyals, O.; Senior, A. W.; Kavukcuoglu, K.; Kohli, P.; Hassabis, D. Highly Accurate Protein Structure Prediction with AlphaFold. *Nature* **2021**, *596* (7873), 583–589. https://doi.org/10.1038/s41586-021-03819-2.

(56) Varadi, M.; Anyango, S.; Deshpande, M.; Nair, S.; Natassia, C.; Yordanova, G.; Yuan, D.; Stroe, O.; Wood, G.; Laydon, A.; Žídek, A.; Green, T.; Tunyasuvunakool, K.; Petersen, S.; Jumper, J.; Clancy, E.; Green, R.; Vora, A.; Lutfi, M.; Figurnov, M.; Cowie, A.; Hobbs, N.; Kohli, P.; Kleywegt, G.; Birney, E.; Hassabis, D.; Velankar, S. AlphaFold Protein Structure Database: Massively Expanding the Structural Coverage of Protein-Sequence Space with High-Accuracy Models. *Nucleic Acids Res.* **2022**, *50* (D1), D439–D444. https://doi.org/10.1093/nar/gkab1061.

(57) Delvecchio, M.; Gaucher, J.; Aguilar-Gurrieri, C.; Ortega, E.; Panne, D. Structure of the P300 Catalytic Core and Implications for Chromatin Targeting and HAT Regulation. *Nat. Struct. Mol. Biol.* **2013**, *20* (9), 1040–1046. https://doi.org/10.1038/nsmb.2642.

(58) Dyson, H. J.; Wright, P. E. Role of Intrinsic Protein Disorder in the Function and Interactions of the Transcriptional Coactivators CREB-Binding Protein (CBP) and P300. *J. Biol. Chem.* **2016**, *291* (13), 6714–6722. https://doi.org/10.1074/jbc.R115.692020.

(59) Sterner, D. E.; Berger, S. L. Acetylation of Histones and Transcription-Related Factors. *Microbiol. Mol. Biol. Rev.* **2000**, *64* (2), 435 LP – 459. https://doi.org/10.1128/MMBR.64.2.435-459.2000.

(60) Josling, G. A.; Selvarajah, S. A.; Petter, M.; Duffy, M. F. The Role of Bromodomain Proteins in Regulating Gene Expression. *Genes*. MDPI AG 2012, pp 320–343. https://doi.org/10.3390/genes3020320.

(61) Dancy, B. M.; Cole, P. A. Protein Lysine Acetylation by P300/CBP. *Chem. Rev.* **2015**, *115* (6), 2419–2452. https://doi.org/10.1021/cr500452k.

(62) Weinert, B. T.; Narita, T.; Satpathy, S.; Srinivasan, B.; Hansen, B. K.; Schölz, C.; Hamilton, W. B.; Zucconi, B. E.; Wang, W. W.; Liu, W. R.; Brickman, J. M.; Kesicki, E. A.; Lai, A.; Bromberg, K. D.; Cole, P. A.; Choudhary, C. Time-Resolved Analysis Reveals Rapid Dynamics and Broad Scope of the CBP/P300 Acetylome. *Cell* **2018**, *174* (1), 231-244.e12. https://doi.org/https://doi.org/10.1016/j.cell.2018.04.033.

(63) Chan, H. M.; La Thangue, N. B. P300/CBP Proteins: HATs for Transcriptional Bridges and Scaffolds. *J. Cell Sci.* **2001**, *114* (13), 2363 LP – 2373.

(64) Bedford, D. C.; Kasper, L. H.; Fukuyama, T.; Brindle, P. K. Target Gene Context Influences the Transcriptional Requirement for the KAT3 Family of CBP and P300 Histone Acetyltransferases. *Epigenetics* **2010**, *5* (1), 9–15. https://doi.org/10.4161/epi.5.1.10449.

(65) Freedman, S. J.; Sun, Z.-Y. J.; Poy, F.; Kung, A. L.; Livingston, D. M.; Wagner, G.; Eck, M. J. *Structural Basis for Recruitment of CBPp300 by Hypoxia-Inducible Factor-1*; 2002.

(66) Lindström, I.; Andersson, E.; Dogan, J. The Transition State Structure for Binding between TAZ1 of CBP and the Disordered Hif-1α CAD. *Sci. Rep.* **2018**, *8* (1), 1–8. https://doi.org/10.1038/s41598-018-26213-x.

(67) Mukherjee, S. P.; Behar, M.; Birnbaum, H. A.; Hoffmann, A.; Wright, P. E.; Ghosh, G. Analysis of the RelA:CBP/P300 Interaction Reveals Its Involvement in NF-KB-Driven Transcription. *PLoS Biol.* **2013**, *11* (9), e1001647. https://doi.org/10.1371/journal.pbio.1001647.

(68) Bhattacharya, S.; Eckner, R.; Grossman, S.; Oldread, E.; Arany, Z.; D'Andrea, A.; Livingston, D. M. Cooperation of Stat2 and P300/CBP in Signalling Induced by Interferon-α. *Nature* **1996**, *383* (6598), 344–347. https://doi.org/10.1038/383344a0.

(69) Wojciak, J. M.; Martinez-Yamout, M. A.; Dyson, H. J.; Wright, P. E. Structural Basis for Recruitment of CBP/P300 Coactivators by STAT1 and STAT2 Transactivation Domains. *EMBO J.* **2009**, *28* (7), 948–958. https://doi.org/10.1038/emboj.2009.30.

(70) Zeng, X.; Li, X.; Miller, A.; Yuan, Z.; Yuan, W.; Kwok, R. P. S.; Goodman, R.; Lu, H. The N-Terminal Domain of P73 Interacts with the CH1 Domain of P300/CREB Binding Protein and Mediates Transcriptional Activation and Apoptosis. *Mol. Cell. Biol.* **2000**, *20* (4), 1299–1310. https://doi.org/10.1128/mcb.20.4.1299-1310.2000.

(71) Nelson, M. L.; Kang, H. S.; Lee, G. M.; Blaszczak, A. G.; Lau, D. K. W.; McIntosh, L. P.; Graves, B. J. Ras Signaling Requires Dynamic Properties of Ets1 for Phosphorylation-Enhanced Binding to Coactivator CBP. *Proc. Natl. Acad. Sci. U. S. A.* **2010**, *107* (22), 10026–10031. https://doi.org/10.1073/pnas.0915137107.

(72) Bui, J. M.; Gsponer, J. Phosphorylation of an Intrinsically Disordered Segment in Ets1 Shifts Conformational Sampling toward Binding-Competent Substates. *Structure* **2014**, *22* (8), 1196–1203. https://doi.org/10.1016/j.str.2014.06.002.

(73) De Guzman, R. N.; Martinez-Yamout, M. A.; Dyson, H. J.; Wright, P. E. Interaction of the TAZ1 Domain of the CREB-Binding Protein with the Activation Domain of CITED2: Regulation by Competition between Intrinsically Unstructured Ligands for Non-Identical Binding Sites. *J. Biol. Chem.* **2004**, *279* (4), 3042–3049. https://doi.org/10.1074/jbc.M310348200.

(74) Teufel, D. P.; Freund, S. M.; Bycroft, M.; Fersht, A. R. Four Domains of P300 Each Bind Tightly to a Sequence Spanning Both Transactivation Subdomains of P53. *Proc. Natl. Acad. Sci. U. S. A.* **2007**, *104* (17), 7009–7014. https://doi.org/10.1073/pnas.0702010104.

(75) Van Orden, K.; Giebler, H. A.; Lemasson, I.; Gonzales, M.; Nyborg, J. K. Binding of P53 to the KIX Domain of CREB Binding Protein. A Potential Link to Human T-Cell Leukemia Virus, Type I-Associated Leukemogenesis. *J. Biol. Chem.* **1999**, *274* (37), 26321–26328. https://doi.org/10.1074/jbc.274.37.26321.

(76) Zor, T.; De Guzman, R. N.; Dyson, H. J.; Wright, P. E. Solution Structure of the KIX Domain of CBP Bound to the Transactivation Domain of C-Myb. *J. Mol. Biol.* **2004**, *337* (3), 521–534. https://doi.org/10.1016/j.jmb.2004.01.038.

(77) Lee, Y. H.; Bedford, M. T.; Stallcup, M. R. Regulated Recruitment of Tumor Suppressor BRCA1 to the P21 Gene by Coactivator Methylation. *Genes Dev.* **2011**, *25* (2), 176–188. https://doi.org/10.1101/gad.1975811.

(78) Goto, N. K.; Zor, T.; Martinez-Yamout, M.; Dyson, H. J.; Wright, P. E. Cooperativity in Transcription Factor Binding to the Coactivator CREB-Binding Protein (CBP): The Mixed

Lineage Leukemia Protein (MLL) Activation Domain Binds to an Allosteric Site on the KIX Domain. *J. Biol. Chem.* **2002**, *277* (45), 43168–43174. https://doi.org/10.1074/jbc.M207660200.

(79) Campbell, K. M.; Lumb, K. J. Structurally Distinct Modes of Recognition of the KIX Domain of CBP by Jun and CREB. *Biochemistry* **2002**, *41* (47), 13956–13964. https://doi.org/10.1021/bi026222m.

(80) F, W.; CB, M.; K, Y.; GY, L.; GM, G.-S.; H, O.; TW, M.; M, I. Structures of KIX Domain of CBP in Complex With Two FOXO3a Transactivation Domains Reveal Promiscuity and Plasticity in Coactivator Recruitment. *Proc. Natl. Acad. Sci. U. S. A.* **2012**, *109* (16). https://doi.org/10.1073/PNAS.1119073109.

(81) Yang, F.; Vought, B. W.; Satterlee, J. S.; Walker, A. K.; Jim Sun, Z. Y.; Watts, J. L.; DeBeaumont, R.; Mako Saito, R.; Hyberts, S. G.; Yang, S.; Macol, C.; Iyer, L.; Tjian, R.; Van Den Heuvel, S.; Hart, A. C.; Wagner, G.; Näär, A. M. An ARC/Mediator Subunit Required for SREBP Control of Cholesterol and Lipid Homeostasis. *Nature* **2006**, *442* (7103), 700–704. https://doi.org/10.1038/nature04942.

(82) Dhalluin, C.; Carlson, J. E.; Zeng, L.; He, C.; Aggarwal, A. K.; Zhou, M. M. Structure and Ligand of a Histone Acetyltransferase Bromodomain. *Nature* **1999**, *399* (6735), 491–496. https://doi.org/10.1038/20974.

(83) Xu, L.; Cheng, A.; Huang, M.; Zhang, J.; Jiang, Y.; Wang, C.; Li, F.; Bao, H.; Gao, J.; Wang, N.; Liu, J.; Wu, J.; Wong, C. C. L.; Ruan, K. Structural Insight into the Recognition of Acetylated Histone H3K56ac Mediated by the Bromodomain of CREB-Binding Protein. *FEBS J.* **2017**, *284* (20), 3422–3436. https://doi.org/https://doi.org/10.1111/febs.14198.

(84) Zeng, L.; Zhang, Q.; Gerona-Navarro, G.; Moshkina, N.; Zhou, M. M. Structural Basis of Site-Specific Histone Recognition by the Bromodomains of Human Coactivators PCAF and CBP/P300. *Structure* **2008**, *16* (4), 643–652. https://doi.org/10.1016/j.str.2008.01.010.

(85) Mujtaba, S.; He, Y.; Zeng, L.; Yan, S.; Plotnikova, O.; Sachchidanand; Sanchez, R.; Zeleznik-Le, N. J.; Ronai, Z.; Zhou, M. M. Structural Mechanism of the Bromodomain of the Coactivator CBP in P53 Transcriptional Activation. *Mol. Cell* **2004**, *13* (2), 251–263. https://doi.org/10.1016/S1097-2765(03)00528-8.

(86) Plotnikov, A. N.; Yang, S.; Zhou, T. J.; Rusinova, E.; Frasca, A.; Zhou, M.-M. Structural Insights into Acetylated-Histone H4 Recognition by the Bromodomain-PHD Finger Module of Human Transcriptional Coactivator CBP. *Structure* **2014**, *22* (2), 353–360. https://doi.org/10.1016/j.str.2013.10.021.

(87) Polesskaya, A.; Naguibneva, I.; Duquet, A.; Bengal, E.; Robin, P.; Harel-Bellan, A. Interaction between Acetylated MyoD and the Bromodomain of CBP and/or P300. *Mol. Cell. Biol.* **2001**, *21* (16), 5312–5320. https://doi.org/10.1128/MCB.21.16.5312-5320.2001.

(88) Rack, J. G. M.; Lutter, T.; Kjæreng Bjerga, G. E.; Guder, C.; Ehrhardt, C.; Värv, S.; Ziegler, M.; Aasland, R. The PHD Finger of P300 Influences Its Ability to Acetylate Histone and Non-Histone Targets. *J. Mol. Biol.* **2015**, *426* (24), 3960–3972. https://doi.org/10.1016/j.jmb.2014.08.011.

(89) Ringel, A. E.; Wolberger, C. A New RING Tossed into an Old HAT. *Structure* **2013**, *21* (9), 1479–1481. https://doi.org/https://doi.org/10.1016/j.str.2013.08.011.

(90) Colino-Sanguino, Y.; Cornett, E. M.; Moulder, D.; Smith, G. C.; Hrit, J.; Cordeiro-Spinetti, E.; Vaughan, R. M.; Krajewski, K.; Rothbart, S. B.; Clark, S. J.; Valdés-Mora, F. A Read/Write Mechanism Connects P300 Bromodomain Function to H2A.Z Acetylation. *iScience* **2019**, *21*, 773–788. https://doi.org/10.1016/j.isci.2019.10.053.

(91) Hogg, S. J.; Motorna, O.; Cluse, L. A.; Johanson, T. M.; Coughlan, H. D.; Raviram, R.; Myers, R. M.; Costacurta, M.; Todorovski, I.; Pijpers, L.; Bjelosevic, S.; Williams, T.; Huskins, S. N.; Kearney, C. J.; Devlin, J. R.; Fan, Z.; Jabbari, J. S.; Martin, B. P.; Fareh, M.; Kelly, M. J.; Dupéré-Richer, D.; Sandow, J. J.; Feran, B.; Knight, D.; Khong, T.; Spencer, A.; Harrison, S. J.; Gregory, G.; Wickramasinghe, V. O.; Webb, A. I.; Taberlay, P. C.; Bromberg, K. D.; Lai, A.; Papenfuss, A. T.; Smyth, G. K.; Allan, R. S.; Licht, J. D.; Landau, D. A.; Abdel-Wahab, O.; Shortt, J.; Vervoort, S. J.; Johnstone, R. W. Targeting Histone Acetylation Dynamics and Oncogenic Transcription by Catalytic P300/CBP Inhibition. *Mol. Cell* **2021**, *81* (10), 2183-2200.e13. https://doi.org/https://doi.org/10.1016/j.molcel.2021.04.015.

(92) Henry, R. A.; Kuo, Y.-M.; Andrews, A. J. Differences in Specificity and Selectivity Between CBP and P300 Acetylation of Histone H3 and H3/H4. *Biochemistry* **2013**, *52* (34), 5746–5759. https://doi.org/10.1021/bi400684q.

(93) Jenkins, L. M. M.; Yamaguchi, H.; Hayashi, R.; Cherry, S.; Tropea, J. E.; Miller, M.; Wlodawer, A.; Appella, E.; Mazur, S. J. Two Distinct Motifs within the P53 Transactivation Domain Bind to the Taz2 Domain of P300 and Are Differentially Affected by Phosphorylation. *Biochemistry* **2009**, *48* (6), 1244–1255. https://doi.org/10.1021/bi801716h.

(94) Ferreon, J. C.; Lee, C. W.; Arai, M.; Martinez-Yamout, M. A.; Dyson, H. J.; Wright, P. E. Cooperative Regulation of P53 by Modulation of Ternary Complex Formation with CBP/P300 and HDM2. *Proc. Natl. Acad. Sci. U. S. A.* **2009**, *106* (16), 6591–6596. https://doi.org/10.1073/pnas.0811023106.

(95) Bhaumik, P.; Davis, J.; Tropea, J. E.; Cherry, S.; Johnson, P. F.; Miller, M. Structural Insights into Interactions of C/EBP Transcriptional Activators with the Taz2 Domain of P300. *Acta Crystallogr. Sect. D Biol. Crystallogr.* **2014**, *70* (7), 1914–1921. https://doi.org/10.1107/S1399004714009262.

(96) He, J.; Ye, J.; Cai, Y.; Riquelme, C.; Liu, J. O.; Liu, X.; Han, A.; Chen, L. Structure of P300 Bound to MEF2 on DNA Reveals a Mechanism of Enhanceosome Assembly. *Nucleic Acids Res.* **2011**, *39* (10), 4464–4474. https://doi.org/10.1093/nar/gkr030.

(97) Oka, O.; Waters, L. C.; Strong, S. L.; Dosanjh, N. S.; Veverka, V.; Muskett, F. W.; Renshaw, P. S.; Klempnauer, K.-H.; Carr, M. D. Interaction of the Transactivation Domain of B-Myb with the TAZ2 Domain of the Coactivator P300: Molecular Features and Properties of the Complex. *PLoS One* **2012**, *7* (12), e52906. https://doi.org/10.1371/journal.pone.0052906.

(98) Lin, C. H.; Hare, B. J.; Wagner, G.; Harrison, S. C.; Maniatis, T.; Fraenkel, E. A Small Domain of CBP/P300 Binds Diverse Proteins: Solution Structure and Functional Studies. *Mol. Cell* **2001**, *8* (3), 581–590. https://doi.org/https://doi.org/10.1016/S1097-2765(01)00333-1.

(99) Sheppard, H. M.; Harries, J. C.; Hussain, S.; Bevan, C.; Heery, D. M. Analysis of the Steroid Receptor Coactivator 1 (SRC1)-CREB Binding Protein Interaction Interface and Its Importance for the Function of SRC1. *Mol. Cell. Biol.* **2001**, *21* (1), 39–50. https://doi.org/10.1128/MCB.21.1.39-50.2001.

(100) Fauquier, L.; Azzag, K.; Parra, M. A. M.; Quillien, A.; Boulet, M.; Diouf, S.; Carnac, G.; Waltzer, L.; Gronemeyer, H.; Vandel, L. CBP and P300 Regulate Distinct Gene Networks Required for Human Primary Myoblast Differentiation and Muscle Integrity. *Sci. Rep.* **2018**, *8* (1), 12629. https://doi.org/10.1038/s41598-018-31102-4.

(101) Kung, A. L.; Rebel, V. I.; Bronson, R. T.; Ch'ng, L. E.; Sieff, C. A.; Livingston, D. M.; Yao, T. P. Gene Dose-Dependent Control of Hematopoiesis and Hematologic Tumor Suppression by CBP. *Genes Dev.* **2000**, *14* (3), 272–277.

(102) Yao, T.-P.; Oh, S. P.; Fuchs, M.; Zhou, N.-D.; Ch'ng, L.-E.; Newsome, D.; Bronson, R. T.; Li, E.; Livingston, D. M.; Eckner, R. Gene Dosage–Dependent Embryonic Development and Proliferation Defects in Mice Lacking the Transcriptional Integrator P300. *Cell* **1998**, *93* (3),

361–372. https://doi.org/10.1016/S0092-8674(00)81165-4.

(103) Shikama, N.; Lutz, W.; Kretzschmar, R.; Sauter, N.; Roth, J.-F.; Marino, S.; Wittwer, J.; Scheidweiler, A.; Eckner, R. Essential Function of P300 Acetyltransferase Activity in Heart, Lung and Small Intestine Formation. *EMBO J.* **2003**, *22* (19), 5175–5185. https://doi.org/10.1093/emboj/cdg502.

(104) Breen, M. E.; Mapp, A. K. Modulating the Masters: Chemical Tools to Dissect CBP and P300 Function. *Mol. Imaging / Chem. Genet. Epigenetics* **2018**, *45*, 195–203. https://doi.org/10.1016/j.cbpa.2018.06.005.

(105) Ono, M.; Lai, K. K. Y.; Wu, K.; Nguyen, C.; Lin, D. P.; Murali, R.; Kahn, M. Nuclear Receptor/Wnt Beta-Catenin Interactions Are Regulated via Differential CBP/P300 Coactivator Usage. *PLoS One* **2018**, *13* (7), e0200714. https://doi.org/10.1371/journal.pone.0200714.

(106) Radhakrishnan, I.; Pérez-Alvarado, G. C.; Parker, D.; Dyson, H. J.; Montminy, M. R.; Wright, P. E. Solution Structure of the KIX Domain of CBP Bound to the Transactivation Domain of CREB: A Model for Activator:Coactivator Interactions. *Cell* **1997**, *91* (6), 741–752. https://doi.org/10.1016/S0092-8674(00)80463-8.

(107) De Guzman, R. N.; Liu, H. Y.; Martinez-Yamout, M.; Dyson, H. J.; Wright, P. E. Solution Structure of the TAZ2 (CH3) Domain of the Transcriptional Adaptor Protein CBP. *J. Mol. Biol.* **2000**, *303* (2), 243–253. https://doi.org/10.1006/JMBI.2000.4141.

(108) Kjaergaard, M.; Teilum, K.; Poulsen, F. M. Conformational Selection in the Molten Globule State of the Nuclear Coactivator Binding Domain of CBP. *Proc. Natl. Acad. Sci.* **2010**, *107* (28), 12535 LP – 12540. https://doi.org/10.1073/pnas.1001693107.

(109) Goodman, R. H.; Smolik, S. CBP/P300 in Cell Growth, Transformation, and Development. *Genes and Development*. Cold Spring Harbor Laboratory Press July 1, 2000, pp 1553–1577. https://doi.org/10.1101/gad.14.13.1553.

(110) Iyer, N. G.; Özdag, H.; Caldas, C. P300/CBP and Cancer. *Oncogene* **2004**, *23* (24), 4225–4231. https://doi.org/10.1038/sj.onc.1207118.

(111) Chen, Q.; Yang, B.; Liu, X.; Zhang, X. D.; Zhang, L.; Liu, T. Histone Acetyltransferases CBP/P300 in Tumorigenesis and CBP/P300 Inhibitors as Promising Novel Anticancer Agents. *Theranostics* **2022**, *12* (11), 4935–4948. https://doi.org/10.7150/thno.73223.

(112) Brooks, N.; Raja, M.; Young, B. W.; Spencer, G. J.; Somervaille, T. C. P.; Pegg, N. A. CCS1477: A Novel Small Molecule Inhibitor of P300/CBP Bromodomain for the Treatment of Acute Myeloid Leukaemia and Multiple Myeloma. *Blood* **2019**, *134* (Supplement_1), 2560. https://doi.org/10.1182/blood-2019-124707.

(113) De Bono, J. S.; Cojocaru, E.; Plummer, E. R.; Knurowski, T.; Clegg, K.; Ashby, F.; Pegg, N.; West, W.; Brooks, A. N. An Open Label Phase I/IIa Study to Evaluate the Safety and Efficacy of CCS1477 as Monotherapy and in Combination in Patients with Advanced Solid/Metastatic Tumors. *J. Clin. Oncol.* **2019**, *37* (15_suppl), TPS5089–TPS5089. https://doi.org/10.1200/JCO.2019.37.15_suppl.TPS5089.

(114) van Gils, N.; Martiañez Canales, T.; Vermue, E.; Rutten, A.; Denkers, F.; van der Deure, T.; Ossenkoppele, G. J.; Giles, F.; Smit, L. The Novel Oral BET-CBP/P300 Dual Inhibitor NEO2734 Is Highly Effective in Eradicating Acute Myeloid Leukemia Blasts and Stem/Progenitor Cells. *HemaSphere* **2021**, *5* (8).

(115) Burslem, G. M.; Smith, B. E.; Lai, A. C.; Jaime-Figueroa, S.; McQuaid, D. C.; Bondeson, D. P.; Toure, M.; Dong, H.; Qian, Y.; Wang, J.; Crew, A. P.; Hines, J.; Crews, C. M. The Advantages of Targeted Protein Degradation Over Inhibition: An RTK Case Study. *Cell Chem. Biol.* **2018**, *25* (1), 67-77.e3.

https://doi.org/https://doi.org/10.1016/j.chembiol.2017.09.009.

(116) Huang, A.; Garraway, L. A.; Ashworth, A.; Weber, B. Synthetic Lethality as an Engine for Cancer Drug Target Discovery. *Nat. Rev. Drug Discov.* **2020**, *19* (1), 23–38. https://doi.org/10.1038/s41573-019-0046-z.

(117) Ryan, C. J.; Mehta, I.; Kebabci, N.; Adams, D. J. Targeting Synthetic Lethal Paralogs in Cancer. *Trends in Cancer* **2023**, *9* (5), 397–409. https://doi.org/10.1016/j.trecan.2023.02.002.

(118) Diss, G.; Ascencio, D.; DeLuna, A.; Landry, C. R. Molecular Mechanisms of Paralogous Compensation and the Robustness of Cellular Networks. *J. Exp. Zool. Part B Mol. Dev. Evol.* **2014**, *322* (7), 488–499. https://doi.org/https://doi.org/10.1002/jez.b.22555.

(119) Raina, K.; Lu, J.; Qian, Y.; Altieri, M.; Gordon, D.; Rossi, A. M. K.; Wang, J.; Chen, X.; Dong, H.; Siu, K.; Winkler, J. D.; Crew, A. P.; Crews, C. M.; Coleman, K. G. PROTAC-Induced BET Protein Degradation as a Therapy for Castration-Resistant Prostate Cancer. *Proc. Natl. Acad. Sci.* **2016**, *113* (26), 7124. https://doi.org/10.1073/pnas.1521738113.

(120) Chan, K. H.; Zengerle, M.; Testa, A.; Ciulli, A. Impact of Target Warhead and Linkage Vector on Inducing Protein Degradation: Comparison of Bromodomain and Extra-Terminal (BET) Degraders Derived from Triazolodiazepine (JQ1) and Tetrahydroquinoline (I-BET726) BET Inhibitor Scaffolds. *J. Med. Chem.* **2018**, *61* (2), 504–513. https://doi.org/10.1021/acs.jmedchem.6b01912.

(121) Vidler, L. R.; Brown, N.; Knapp, S.; Hoelder, S. Druggability Analysis and Structural Classification of Bromodomain Acetyl-Lysine Binding Sites. *J. Med. Chem.* **2012**, *55* (17), 7346–7359. https://doi.org/10.1021/jm300346w.

(122) Filippakopoulos, P.; Picaud, S.; Mangos, M.; Keates, T.; Lambert, J. P.; Barsyte-Lovejoy, D.; Felletar, I.; Volkmer, R.; Müller, S.; Pawson, T.; Gingras, A. C.; Arrowsmith, C. H.; Knapp, S. Histone Recognition and Large-Scale Structural Analysis of the Human Bromodomain Family. *Cell* **2012**, *149* (1), 214–231. https://doi.org/10.1016/j.cell.2012.02.013.

(123) Mujtaba, S.; Zeng, L.; Zhou, M. M. Structure and Acetyl-Lysine Recognition of the Bromodomain. *Oncogene*. Nature Publishing Group August 13, 2007, pp 5521–5527. https://doi.org/10.1038/sj.onc.1210618.

(124) Zhang, X.; Chen, K.; Wu, Y.-D.; Wiest, O. Protein Dynamics and Structural Waters in Bromodomains. *PLoS One* **2017**, *12* (10), e0186570. https://doi.org/10.1371/journal.pone.0186570.

(125) Rooney, T. P. C.; Filippakopoulos, P.; Fedorov, O.; Picaud, S.; Cortopassi, W. A.; Hay, D. A.; Martin, S.; Tumber, A.; Rogers, C. M.; Philpott, M.; Wang, M.; Thompson, A. L.; Heightman, T. D.; Pryde, D. C.; Cook, A.; Paton, R. S.; Müller, S.; Knapp, S.; Brennan, P. E.; Conway, S. J. A Series of Potent CREBBP Bromodomain Ligands Reveals an Induced-Fit Pocket Stabilized by a Cation-π Interaction. *Angew. Chem. Int. Ed. Engl.* **2014**, *53* (24), 6126–6130. https://doi.org/10.1002/anie.201402750.

(126) Picaud, S.; Fedorov, O.; Thanasopoulou, A.; Leonards, K.; Jones, K.; Meier, J.; Olzscha, H.; Monteiro, O.; Martin, S.; Philpott, M.; Tumber, A.; Filippakopoulos, P.; Yapp, C.; Wells, C.; Che, K. H.; Bannister, A.; Robson, S.; Kumar, U.; Parr, N.; Lee, K.; Lugo, D.; Jeffrey, P.; Taylor, S.; Vecellio, M. L.; Bountra, C.; Brennan, P. E.; O'Mahony, A.; Velichko, S.; Muller, S.; Hay, D.; Daniels, D. L.; Urh, M.; La Thangue, N. B.; Kouzarides, T.; Prinjha, R.; Schwaller, J.; Knapp, S. Generation of a Selective Small Molecule Inhibitor of the CBP/P300 Bromodomain for Leukemia Therapy. *Cancer Res.* **2015**, *75* (23), 5106–5119. https://doi.org/10.1158/0008-5472.CAN-15-0236.

(127) Taylor, A. M.; Côté, A.; Hewitt, M. C.; Pastor, R.; Leblanc, Y.; Nasveschuk, C. G.; Romero, F. A.; Crawford, T. D.; Cantone, N.; Jayaram, H.; Setser, J.; Murray, J.; Beresini, M. H.; De

Leon Boenig, G.; Chen, Z.; Conery, A. R.; Cummings, R. T.; Dakin, L. A.; Flynn, E. M.; Huang, O. W.; Kaufman, S.; Keller, P. J.; Kiefer, J. R.; Lai, T.; Li, Y.; Liao, J.; Liu, W.; Lu, H.; Pardo, E.; Tsui, V.; Wang, J.; Wang, Y.; Xu, Z.; Yan, F.; Yu, D.; Zawadzke, L.; Zhu, X.; Zhu, X.; Sims, R. J.; Cochran, A. G.; Bellon, S.; Audia, J. E.; Magnuson, S.; Albrecht, B. K. Fragment-Based Discovery of a Selective and Cell-Active Benzodiazepinone CBP/EP300 Bromodomain Inhibitor (CPI-637). *ACS Med. Chem. Lett.* **2016**, *7* (5), 531–536. https://doi.org/10.1021/acsmedchemlett.6b00075.

(128) Hammitzsch, A.; Tallant, C.; Fedorov, O.; O'Mahony, A.; Brennan, P. E.; Hay, D. A.; Martinez, F. O.; Al-Mossawi, M. H.; De Wit, J.; Vecellio, M.; Wells, C.; Wordsworth, P.; Müller, S.; Knapp, S.; Bowness, P. CBP30, a Selective CBP/P300 Bromodomain Inhibitor, Suppresses Human Th17 Responses. *Proc. Natl. Acad. Sci. U. S. A.* **2015**, *112* (34), 10768–10773. https://doi.org/10.1073/pnas.1501956112.

(129) Rasool, R. ur; Natesan, R.; Asangani, I. A. Toppling the HAT to Treat Lethal Prostate Cancer. *Cancer Discov.* **2021**, *11* (5), 1011–1013. https://doi.org/10.1158/2159-8290.CD-21-0184.

(130) Hügle, M.; Lucas, X.; Ostrovskyi, D.; Regenass, P.; Gerhardt, S.; Einsle, O.; Hau, M.; Jung, M.; Breit, B.; Günther, S.; Wohlwend, D. Beyond the BET Family: Targeting CBP/P300 with 4-Acyl Pyrroles. *Angew. Chemie - Int. Ed.* **2017**, *56* (41), 12476–12480. https://doi.org/10.1002/anie.201705516.

(131) Lai, K. W.; Romero, F. A.; Tsui, V.; Beresini, M. H.; de Leon Boenig, G.; Bronner, S. M.; Chen, K.; Chen, Z.; Choo, E. F.; Crawford, T. D.; Cyr, P.; Kaufman, S.; Li, Y.; Liao, J.; Liu, W.; Ly, J.; Murray, J.; Shen, W.; Wai, J.; Wang, F.; Zhu, C.; Zhu, X.; Magnuson, S. Design and Synthesis of a Biaryl Series as Inhibitors for the Bromodomains of CBP/P300. *Bioorg. Med. Chem. Lett.* **2018**, *28* (1), 15–23. https://doi.org/https://doi.org/10.1016/j.bmcl.2017.11.025.

(132) Romero, F. A.; Murray, J.; Lai, K. W.; Tsui, V.; Albrecht, B. K.; An, L.; Beresini, M. H.; De Leon Boenig, G.; Bronner, S. M.; Chan, E. W.; Chen, K. X.; Chen, Z.; Choo, E. F.; Clagg, K.; Clark, K.; Crawford, T. D.; Cyr, P.; De Almeida Nagata, D.; Gascoigne, K. E.; Grogan, J. L.; Hatzivassiliou, G.; Huang, W.; Hunsaker, T. L.; Kaufman, S.; Koenig, S. G.; Li, R.; Li, Y.; Liang, X.; Liao, J.; Liu, W.; Ly, J.; Maher, J.; Masui, C.; Merchant, M.; Ran, Y.; Taylor, A. M.; Wai, J.; Wang, F.; Wei, X.; Yu, D.; Zhu, B. Y.; Zhu, X.; Magnuson, S. GNE-781, A Highly Advanced Potent and Selective Bromodomain Inhibitor of Cyclic Adenosine Monophosphate Response Element Binding Protein, Binding Protein (CBP). *J. Med. Chem.* **2017**, *60* (22), 9162–9183. https://doi.org/10.1021/acs.jmedchem.7b00796.

(133) Vannam, R.; Sayilgan, J.; Ojeda, S.; Karakyriakou, B.; Hu, E.; Kreuzer, J.; Morris, R.; Herrera Lopez, X. I.; Rai, S.; Haas, W.; Lawrence, M.; Ott, C. J. Targeted Degradation of the Enhancer Lysine Acetyltransferases CBP and P300. *Cell Chem. Biol.* **2021**. https://doi.org/https://doi.org/10.1016/j.chembiol.2020.12.004.

(134) Thomas, J. E. I. I.; Wang, M.; Jiang, W.; Wang, M.; Wang, L.; Wen, B.; Sun, D.; Wang, S. Discovery of Exceptionally Potent, Selective, and Efficacious PROTAC Degraders of CBP and P300 Proteins. *J. Med. Chem.* **2023**. https://doi.org/10.1021/acs.jmedchem.3c00492.

(135) Durbin, A. D.; Wang, T.; Wimalasena, V. K.; Zimmerman, M. W.; Li, D.; Dharia, N. V; Mariani, L.; Shendy, N. A. M.; Nance, S.; Patel, A. G.; Shao, Y.; Mundada, M.; Maxham, L.; Park, P. M. C.; Sigua, L. H.; Morita, K.; Conway, A. S.; Robichaud, A. L.; Perez-Atayde, A. R.; Bikowitz, M. J.; Quinn, T. R.; Wiest, O.; Easton, J.; Schönbrunn, E.; Bulyk, M. L.; Abraham, B. J.; Stegmaier, K.; Look, A. T.; Qi, J. EP300 Selectively Controls the Enhancer Landscape of MYCN-Amplified Neuroblastoma. *Cancer Discov.* **2022**, *12* (3), 730–751. https://doi.org/10.1158/2159-8290.CD-21-0385.

(136) Wang, R.; He, Y.; Robinson, V.; Yang, Z.; Hessler, P.; Lasko, L. M.; Lu, X.; Bhathena, A.; Lai, A.; Uziel, T.; Lam, L. T. Targeting Lineage-Specific MITF Pathway in Human Melanoma

Cell Lines by A-485, the Selective Small-Molecule Inhibitor of P300/CBP. *Mol. Cancer Ther.* **2018**, *17* (12), 2543 LP – 2550. https://doi.org/10.1158/1535-7163.MCT-18-0511.

(137) Lasko, L. M.; Jakob, C. G.; Edalji, R. P.; Qiu, W.; Montgomery, D.; Digiammarino, E. L.; Hansen, T. M.; Risi, R. M.; Frey, R.; Manaves, V.; Shaw, B.; Algire, M.; Hessler, P.; Lam, L. T.; Uziel, T.; Faivre, E.; Ferguson, D.; Buchanan, F. G.; Martin, R. L.; Torrent, M.; Chiang, G. G.; Karukurichi, K.; Langston, J. W.; Weinert, B. T.; Choudhary, C.; de Vries, P.; Kluge, A. F.; Patane, M. A.; Van Drie, J. H.; Wang, C.; McElligott, D.; Kesicki, E.; Marmorstein, R.; Sun, C.; Cole, P. A.; Rosenberg, S. H.; Michaelides, M. R.; Lai, A.; Bromberg, K. D. Discovery of a Selective Catalytic P300/CBP Inhibitor That Targets Lineage-Specific Tumours. *Nature* **2017**, *550* (7674), 128–132. https://doi.org/10.1038/nature24028.

(138) Bunnage, M. E.; Chekler, E. L. P.; Jones, L. H. Target Validation Using Chemical Probes. *Nat. Chem. Biol.* **2013**, *9* (4), 195–199. https://doi.org/10.1038/nchembio.1197.

(139) Arrowsmith, C. H.; Audia, J. E.; Austin, C.; Baell, J.; Bennett, J.; Blagg, J.; Bountra, C.; Brennan, P. E.; Brown, P. J.; Bunnage, M. E.; Buser-Doepner, C.; Campbell, R. M.; Carter, A. J.; Cohen, P.; Copeland, R. A.; Cravatt, B.; Dahlin, J. L.; Dhanak, D.; Edwards, A. M.; Frye, S. V.; Gray, N.; Grimshaw, C. E.; Hepworth, D.; Howe, T.; Huber, K. V. M.; Jin, J.; Knapp, S.; Kotz, J. D.; Kruger, R. G.; Lowe, D.; Mader, M. M.; Marsden, B.; Mueller-Fahrnow, A.; Müller, S.; O'Hagan, R. C.; Overington, J. P.; Owen, D. R.; Rosenberg, S. H.; Roth, B.; Ross, R.; Schapira, M.; Schreiber, S. L.; Shoichet, B.; Sundström, M.; Superti-Furga, G.; Taunton, J.; Toledo-Sherman, L.; Walpole, C.; Walters, M. A.; Willson, T. M.; Workman, P.; Young, R. N.; Zuercher, W. J. The Promise and Peril of Chemical Probes. *Nature Chemical Biology*. Nature Publishing Group July 21, 2015, pp 536–541. https://doi.org/10.1038/nchembio.1867.

(140) Li, F.; Hu, Q.; Zhang, X.; Sun, R.; Liu, Z.; Wu, S.; Tian, S.; Ma, X.; Dai, Z.; Yang, X.; Gao, S.; Bai, F. DeepPROTACs Is a Deep Learning-Based Targeted Degradation Predictor for PROTACs. *Nat. Commun.* **2022**, *13* (1), 7133. https://doi.org/10.1038/s41467-022-34807-3.

(141) Davies, S. G.; Mulvaney, A. W.; Russell, A. J.; Smith, A. D. Parallel Synthesis of Homochiral β-Amino Acids. *Tetrahedron Asymmetry* **2007**, *18* (13), 1554–1566. https://doi.org/10.1016/j.tetasy.2007.06.008.

(142) Ritchie, T. J.; Macdonald, S. J. F. The Impact of Aromatic Ring Count on Compound Developability – Are Too Many Aromatic Rings a Liability in Drug Design? *Drug Discov. Today* **2009**, *14* (21), 1011–1020. https://doi.org/https://doi.org/10.1016/j.drudis.2009.07.014.

(143) Young, R. J.; Green, D. V. S.; Luscombe, C. N.; Hill, A. P. Getting Physical in Drug Discovery II: The Impact of Chromatographic Hydrophobicity Measurements and Aromaticity. *Drug Discov. Today* **2011**, *16* (17), 822–830. https://doi.org/https://doi.org/10.1016/j.drudis.2011.06.001.

(144) Maple, H. J.; Clayden, N.; Baron, A.; Stacey, C.; Felix, R. Developing Degraders: Principles and Perspectives on Design and Chemical Space. *Medchemcomm* **2019**, *10* (10), 1755–1764. https://doi.org/10.1039/C9MD00272C.

(145) Schumacher, H.; Smith, R. L.; Williams, R. T. The Metabolism of Thalidomide: The Spontaneous Hydrolysis of Thalidomide in Solution. *Br. J. Pharmacol. Chemother.* **1965**, *25* (2), 324–337. https://doi.org/10.1111/j.1476-5381.1965.tb02053.x.

(146) Brownsey, D. K.; Rowley, B. C.; Gorobets, E.; Gelfand, B. S.; Derksen, D. J. Rapid Synthesis of Pomalidomide-Conjugates for the Development of Protein Degrader Libraries. *Chem. Sci.* **2021**, *12* (12), 4519–4525. https://doi.org/10.1039/D0SC05442A.

(147) Neklesa, T. K.; Tae, H. S.; Schneekloth, A. R.; Stulberg, M. J.; Corson, T. W.; Sundberg, T. B.; Raina, K.; Holley, S. A.; Crews, C. M. Small-Molecule Hydrophobic Tagging-Induced Degradation of HaloTag Fusion Proteins. *Nat. Chem. Biol.* **2011**, *7* (8), 538–543. https://doi.org/10.1038/nchembio.597.

(148) Tae, H. S.; Sundberg, T. B.; Neklesa, T. K.; Noblin, D. J.; Gustafson, J. L.; Roth, A. G.; Raina, K.; Crews, C. M. Identification of Hydrophobic Tags for the Degradation of Stabilized Proteins. *ChemBioChem* **2012**, *13* (4), 538–541. https://doi.org/10.1002/cbic.201100793.

(149) Omni Calculator. Protein Molecular Weight Calculator https://www.bioinformatics.org/sms/prot_mw.html (accessed Jun 29, 2023).

(150) Hannus, M.; Beitzinger, M.; Engelmann, J. C.; Weickert, M.-T.; Spang, R.; Hannus, S.; Meister, G. SiPools: Highly Complex but Accurately Defined SiRNA Pools Eliminate off-Target Effects. *Nucleic Acids Res.* **2014**, *42* (12), 8049–8061. https://doi.org/10.1093/nar/gku480.

(151) Anderson, E. M.; Birmingham, A.; Baskerville, S.; Reynolds, A.; Maksimova, E.; Leake, D.; Fedorov, Y.; Karpilow, J.; Khvorova, A. Experimental Validation of the Importance of Seed Complement Frequency to SiRNA Specificity. *RNA* **2008**, *14*, 8538–8561. https://doi.org/10.1261/rna.704708.

(152) Jackson, A. L.; Burchard, J.; Leake, D.; Reynolds, A.; Schelter, J.; Guo, J.; Johnson, J. M.; Lim, L.; Karpilow, J.; Nichols, K.; Marshall, W.; Khvorova, A.; Linsley, P. S. Position-Specific Chemical Modification of SiRNAs Reduces "off-Target" Transcript Silencing. *RNA* **2006**, *12*, 1197–1205. https://doi.org/10.1261/rna.30706.

(153) Birmingham, A.; Anderson, E. M.; Reynolds, A.; Ilsley-Tyree, D.; Leake, D.; Fedorov, Y.; Baskerville, S.; Maksimova, E.; Robinson, K.; Karpilow, J.; Marshall, W. S.; Khvorova, A. 3′ UTR Seed Matches, but Not Overall Identity, Are Associated with RNAi off-Targets. *Nat. Methods* **2006**, *3* (3), 199–204. https://doi.org/10.1038/nmeth854.

(154) Kittler, R.; Putz, G.; Pelletier, L.; Poser, I.; Heninger, A.-K.; Drechsel, D.; Fischer, S.; Konstantinova, I.; Habermann, B.; Grabner, H.; Yaspo, M.-L.; Himmelbauer, H.; Korn, B.; Neugebauer, K.; Pisabarro, M. T.; Buchholz, F. An Endoribonuclease-Prepared SiRNA Screen in Human Cells Identifies Genes Essential for Cell Division. *Nature* **2004**, *432* (7020), 1036–1040. https://doi.org/10.1038/nature03159.

(155) Zhou, H.; Xu, M.; Huang, Q.; Gates, A. T.; Zhang, X. D.; Castle, J. C.; Stec, E.; Ferrer, M.; Strulovici, B.; Hazuda, D. J.; Espeseth, A. S. Genome-Scale RNAi Screen for Host Factors Required for HIV Replication. *Cell Host Microbe* **2008**, *4* (5), 495–504. https://doi.org/https://doi.org/10.1016/j.chom.2008.10.004.

(156) Ambike, S.; Cheng, C.-C.; Feuerherd, M.; Velkov, S.; Baldassi, D.; Afridi, S. Q.; Porras-Gonzalez, D.; Wei, X.; Hagen, P.; Kneidinger, N.; Stoleriu, M. G.; Grass, V.; Burgstaller, G.; Pichlmair, A.; Merkel, O. M.; Ko, C.; Michler, T. Targeting Genomic SARS-CoV-2 RNA with SiRNAs Allows Efficient Inhibition of Viral Replication and Spread. *Nucleic Acids Res.* **2022**, *50* (1), 333–349. https://doi.org/10.1093/nar/gkab1248.

(157) Bass, J. J.; Wilkinson, D. J.; Rankin, D.; Phillips, B. E.; Szewczyk, N. J.; Smith, K.; Atherton, P. J. An Overview of Technical Considerations for Western Blotting Applications to Physiological Research. *Scand. J. Med. Sci. Sports* **2017**, *27* (1), 4–25. https://doi.org/https://doi.org/10.1111/sms.12702.

(158) Jackson, A. L.; Linsley, P. S. Noise amidst the Silence: Off-Target Effects of SiRNAs? *Trends Genet.* **2004**, *20* (11), 521–524. https://doi.org/https://doi.org/10.1016/j.tig.2004.08.006.

(159) Lin, Y.-C.; Boone, M.; Meuris, L.; Lemmens, I.; Van Roy, N.; Soete, A.; Reumers, J.; Moisse, M.; Plaisance, S.; Drmanac, R.; Chen, J.; Speleman, F.; Lambrechts, D.; Van de Peer, Y.; Tavernier, J.; Callewaert, N. Genome Dynamics of the Human Embryonic Kidney 293 Lineage in Response to Cell Biology Manipulations. *Nat. Commun.* **2014**, *5*, 4767. https://doi.org/10.1038/ncomms5767.

(160) Thul, P. J.; Åkesson, L.; Wiking, M.; Mahdessian, D.; Geladaki, A.; Ait Blal, H.; Alm, T.;

Asplund, A.; Björk, L.; Breckels, L. M.; Bäckström, A.; Danielsson, F.; Fagerberg, L.; Fall, J.; Gatto, L.; Gnann, C.; Hober, S.; Hjelmare, M.; Johansson, F.; Lee, S.; Lindskog, C.; Mulder, J.; Mulvey, C. M.; Nilsson, P.; Oksvold, P.; Rockberg, J.; Schutten, R.; Schwenk, J. M.; Sivertsson, Å.; Sjöstedt, E.; Skogs, M.; Stadler, C.; Sullivan, D. P.; Tegel, H.; Winsnes, C.; Zhang, C.; Zwahlen, M.; Mardinoglu, A.; Pontén, F.; von Feilitzen, K.; Lilley, K. S.; Uhlén, M.; Lundberg, E. A Subcellular Map of the Human Proteome. *Science (80-.).* **2017**, *356* (6340), eaal3321. https://doi.org/10.1126/science.aal3321.

(161) The Human Protein Atlas - CREBBP and p300 Expression in Different Cell Lines https://www.proteinatlas.org/ENSG00000005339-CREBBP/cell+line (accessed May 21, 2023).

(162) Nadanaciva, S.; Lu, S.; Gebhard, D. F.; Jessen, B. A.; Pennie, W. D.; Will, Y. A High Content Screening Assay for Identifying Lysosomotropic Compounds. *Toxicol. Vitr.* **2011**, *25* (3), 715–723. https://doi.org/https://doi.org/10.1016/j.tiv.2010.12.010.

(163) Xu, H.; Luo, G.; Wu, T.; Hu, J.; Wang, C.; Wu, X.; Zhang, Y.; Xu, Y.; Xiang, Q. Structural Insights Revealed by the Cocrystal Structure of CCS1477 in Complex with CBP Bromodomain. *Biochem. Biophys. Res. Commun.* **2022**, *623*, 17–22. https://doi.org/https://doi.org/10.1016/j.bbrc.2022.07.021.

(164) Hay, D. A.; Fedorov, O.; Martin, S.; Singleton, D. C.; Tallant, C.; Wells, C.; Picaud, S.; Philpott, M.; Monteiro, O. P.; Rogers, C. M.; Conway, S. J.; Rooney, T. P. C.; Tumber, A.; Yapp, C.; Filippakopoulos, P.; Bunnage, M. E.; Müller, S.; Knapp, S.; Schofield, C. J.; Brennan, P. E. Discovery and Optimization of Small-Molecule Ligands for the CBP/P300 Bromodomains. *J. Am. Chem. Soc.* **2014**, *136* (26), 9308–9319. https://doi.org/10.1021/ja412434f.

(165) Filippakopoulos, P.; Picaud, S.; Felletar, I.; Hay, D. A.; Fedorov, O.; Schwalm, M. P.; Krojer, T.; Nowak, R. P.; von Delft, F.; Brennan, P. E.; Arrowsmith, C. H.; Edwards, A. M.; Bountra, C.; Knapp, S. Crystal Structure of the Bromodomain of Human CREBBP in Complex with an Isoxazolyl-Benzimidazole Ligand. PDB Entry - 4NR7. *Worldw. Protein Data Bank* **2013**. https://doi.org/https://doi.org/10.2210/pdb4nr7/pdb.

(166) Jourdant, A.; González-Zamora, E.; Zhu, J. Wilkinson's Catalyst Catalyzed Selective Hydrogenation of Olefin in the Presence of an Aromatic Nitro Function: A Remarkable Solvent Effect. *J. Org. Chem.* **2002**, *67* (9), 3163–3164. https://doi.org/10.1021/jo025595q.

(167) Ma, X.; Liu, S.; Liu, Y.; Gu, G.; Xia, C. Comparative Study on Catalytic Hydrodehalogenation of Halogenated Aromatic Compounds over Pd/C and Raney Ni Catalysts. *Sci. Reports 2016 61* **2016**, *6* (1), 1–11. https://doi.org/10.1038/srep25068.

(168) Liu, R.; Yang, H.; Chen, Z.; Zhou, K.; Shi, Q.; Li, J.; Huang, Y.; Huang, X.; Li, Y. Design, Synthesis and Biological Evaluation of (R)-5-Methylpyrrolidin-2-Ones as P300 Bromodomain Inhibitors with Anti-Tumor Activities in Multiple Tumor Lines. *Bioorg. Chem.* **2022**, *124*, 105803. https://doi.org/https://doi.org/10.1016/j.bioorg.2022.105803.

(169) King, A. E.; Brunold, T. C.; Stahl, S. S. Mechanistic Study of Copper-Catalyzed Aerobic Oxidative Coupling of Arylboronic Esters and Methanol: Insights into an Organometallic Oxidase Reaction. *J. Am. Chem. Soc.* **2009**, *131* (14), 5044–5045. https://doi.org/10.1021/ja9006657.

(170) Evans, D. A.; Katz, J. L.; West, T. R. Synthesis of Diaryl Ethers through the Copper-Promoted Arylation of Phenols with Arylboronic Acids. An Expedient Synthesis of Thyroxine. *Tetrahedron Lett.* **1998**, *39* (19), 2937–2940. https://doi.org/https://doi.org/10.1016/S0040-4039(98)00502-4.

(171) Lam, P. Y. S.; Clark, C. G.; Saubern, S.; Adams, J.; Winters, M. P.; Chan, D. M. T.; Combs, A. New Aryl/Heteroaryl C□N Bond Cross-Coupling Reactions via Arylboronic Acid/Cupric

Acetate Arylation. *Tetrahedron Lett.* **1998**, *39* (19), 2941–2944. https://doi.org/https://doi.org/10.1016/S0040-4039(98)00504-8.

(172) Grayson, J. D.; Dennis, F. M.; Robertson, C. C.; Partridge, B. M. Chan–Lam Amination of Secondary and Tertiary Benzylic Boronic Esters. *J. Org. Chem.* **2021**, *86* (14), 9883–9897. https://doi.org/10.1021/acs.joc.1c00976.

(173) Shade, R. E.; Hyde, A. M.; Olsen, J.-C.; Merlic, C. A. Copper-Promoted Coupling of Vinyl Boronates and Alcohols: A Mild Synthesis of Allyl Vinyl Ethers. *J. Am. Chem. Soc.* **2010**, *132* (4), 1202–1203. https://doi.org/10.1021/ja907982w.

(174) González, I.; Mosquera, J.; Guerrero, C.; Rodríguez, R.; Cruces, J. Selective Monomethylation of Anilines by Cu(OAc)2-Promoted Cross-Coupling with MeB(OH)2. *Org. Lett.* **2009**, *11* (8), 1677–1680. https://doi.org/10.1021/ol802882k.

(175) Vutukuri, D. R.; Bharathi, P.; Yu, Z.; Rajasekaran, K.; Tran, M.-H.; Thayumanavan, S. A Mild Deprotection Strategy for Allyl-Protecting Groups and Its Implications in Sequence Specific Dendrimer Synthesis. *J. Org. Chem.* **2003**, *68* (3), 1146–1149. https://doi.org/10.1021/jo026469p.

(176) Ramanathan, M.; Hou, D.-R. Cleavage of Benzyl Ethers by Triphenylphosphine Hydrobromide. *Tetrahedron Lett.* **2010**, *51* (47), 6143–6145. https://doi.org/https://doi.org/10.1016/j.tetlet.2010.09.065.

(177) Heeres, A.; Willigers-Hogg, S.; Borst, M. L.; Dröge, M. J. WO2015069110A1 MULTIPLE D2 A(NTA)GONISTS/H3 ANTAGONISTS FOR TREATMENT OF CNS-RELATED DISORDERS, 2015.

(178) Garcia-Lopez, M.; Almansa-Rosales, C.; LLorente-Fernandez, V. A.; Garriga-Sanahuja, L.; Christmann, U. WO2017016669A1 SUBSTITUTED AMIDE DERIVATIVES HAVING MULTIMODAL ACTIVITY AGAINST PAIN, 2017.

(179) Thede, K.; Johnston, S. W.; Bender, E.; Golz, S.; Hägebarth, A.; Lienau, P.; Puehler, F.; Basting, D.; Schneider, D.; Möwes, M. WO2014147182A2 NOVEL COMPOUNDS, 2014.

(180) Chambon, S.; Clary, L.; Schuppli, M. WO2011033009A1 N- [2-HYDROXYCARBAMOYL-2- (PIPERAZINYL) ETHYL] BENZAMIDE COMPOUNDS, THEIR PREPARATION AND THEIR USE AS TACE INHIBITORS, 2011.

(181) Harris, V. M. Protein Detection by Simple Western™ Analysis BT - Western Blotting: Methods and Protocols; Kurien, B. T., Scofield, R. H., Eds.; Springer New York: New York, NY, 2015; pp 465–468. https://doi.org/10.1007/978-1-4939-2694-7_47.

(182) Gentalen, E.; White, T.; Proctor, J. Peggy™: Size- or Charge-Based Western Blotting at the Push of a Button. *Nat. Methods* **2013**, *10* (6), i–ii. https://doi.org/10.1038/nmeth.f.365.

(183) ProteinSimple. Compass for Simple Western User Guide Technical Notes https://resources.bio-techne.com/bio-techne-assets/docs/software/Simple Western/CompassforSW_6.1.0/User Guides/Compass SW Software User Guide.pdf (accessed May 2, 2023).

(184) Nelson, G. M.; Guynn, J. M.; Chorley, B. N. Procedure and Key Optimization Strategies for an Automated Capillary Electrophoretic-Based Immunoassay Method. *J. Vis. Exp.* **2017**, *10* (127), 55911. https://doi.org/10.3791/55911.

(185) Vinculin molecular weight obtained from proteintech® https://www.ptglab.com/products/Vinculin-Antibody-66305-1-Ig.htm (accessed May 9, 2023).

(186) Beta actin molecular weight obtained from proteintech® https://www.ptglab.com/products/featured-products/beta-actin-antibody/#:~:text=beta-actin – a

housekeeping protein,-Actin is a&text=Though beta-actin has a,fragments on a Western blot. (accessed May 9, 2023).

(187) SimpleWestern™. Simple Western Antibody Database https://www.bio-techne.com/resources/simple-western-antibody-database (accessed May 2, 2023).

(188) Winter, G. E.; Buckley, D. L.; Paulk, J.; Roberts, J. M.; Souza, A.; Dhe-Paganon, S.; Bradner, J. E. Selective Target Protein Degradation via Phthalimide Conjugation. *Science* **2015**, *348* (6241), 1376. https://doi.org/10.1126/SCIENCE.AAB1433.

(189) Steinebach, C.; Ng, Y. L. D.; Sosič, I.; Lee, C.-S.; Chen, S.; Lindner, S.; Vu, L. P.; Bricelj, A.; Haschemi, R.; Monschke, M.; Steinwarz, E.; Wagner, K. G.; Bendas, G.; Luo, J.; Gütschow, M.; Krönke, J. Systematic Exploration of Different E3 Ubiquitin Ligases: An Approach towards Potent and Selective CDK6 Degraders. *Chem. Sci.* **2020**, *11* (13), 3474–3486. https://doi.org/10.1039/D0SC00167H.

(190) Bricelj, A.; Dora Ng, Y. L.; Ferber, D.; Kuchta, R.; Müller, S.; Monschke, M.; Wagner, K. G.; Krönke, J.; Sosič, I.; Gütschow, M.; Steinebach, C. Influence of Linker Attachment Points on the Stability and Neosubstrate Degradation of Cereblon Ligands. *ACS Med. Chem. Lett.* **2021**, *12* (11), 1733–1738. https://doi.org/10.1021/acsmedchemlett.1c00368.

(191) Sievers, Q. L.; Petzold, G.; Bunker, Richard, D.; Renneville, A.; Slabicki, M.; Liddicoat, B. J.; Abdulrahman, W.; Słabick, M.; Ebert, B. L.; Thomä, N. H. Defining the Human C2H2 Zinc-Finger Degrome Targeted by Thalidomide Analogs through CRBN. *Science (80-.).* **2019**, *362* (6414). https://doi.org/10.1126/science.aat0572.

(192) Adson, A.; Raub, T. J.; Burton, P. S.; Barsuhn, C. L.; Hilgers, A. R.; Audus, K. L.; Ho, N. F. H. Quantitative Approaches To Delineate Paracellular Diffusion in Cultured Epithelial Cell Monolayers. *J. Pharm. Sci.* **1994**, *83* (11), 1529–1536. https://doi.org/https://doi.org/10.1002/jps.2600831103.

(193) Quintela, M.; James, D. W.; Pociute, A.; Powell, L.; Edwards, K.; Coombes, Z.; Garcia, J.; Garton, N.; Das, N.; Lutchman-Singh, K.; Margarit, L.; Beynon, A. L.; Rioja, I.; Prinjha, R. K.; Harker, N. R.; Gonzalez, D.; Conlan, R. S.; Francis, L. W. Bromodomain Inhibitor I-BET858 Triggers a Unique Transcriptional Response Coupled to Enhanced DNA Damage, Cell Cycle Arrest and Apoptosis in High-Grade Ovarian Carcinoma Cells. *Clin. Epigenetics* **2023**, *15* (1), 63. https://doi.org/10.1186/s13148-023-01477-x.

(194) Zhou, X.; Sun, T.; Meng, Y.; Luo, J.; Chen, J.; Xia, B.; Zhang, Z.; Cheng, Z.; Wang, X. BET Inhibitors Combined with Chemotherapy Synergistically Inhibit the Growth of NSCLC Cells. *Oncol. Rep.* **2021**, *45* (5), 1–12. https://doi.org/10.3892/or.2021.8021.

(195) Bhattacharya, S.; Piya, S.; Borthakur, G. Bromodomain Inhibitors: What Does the Future Hold? *Clin. Adv. Hematol. Oncol.* **2018**, *16* (7), 504–515.

(196) Brooks, N.; Knurowski, T.; Hughes, A.; Clegg, K.; West, W.; Pegg, N. A.; Spencer, G. J.; Chadwick, J.; Somervaille, T. C. P. CCS1477, a Novel P300/CBP Bromodomain Inhibitor, Enhances Efficacy of Azacitidine and Venetoclax in Pre-Clinical Models of Acute Myeloid Leukaemia and Lymphoma. *Blood* **2021**, *138*, 3291. https://doi.org/https://doi.org/10.1182/blood-2021-148295.

(197) Demo, S. D.; Kirk, C. J.; Aujay, M. A.; Buchholz, T. J.; Dajee, M.; Ho, M. N.; Jiang, J.; Laidig, G. J.; Lewis, E. R.; Parlati, F.; Shenk, K. D.; Smyth, M. S.; Sun, C. M.; Vallone, M. K.; Woo, T. M.; Molineaux, C. J.; Bennett, M. K. Antitumor Activity of PR-171, a Novel Irreversible Inhibitor of the Proteasome. *Cancer Res.* **2007**, *67* (13), 6383–6391. https://doi.org/10.1158/0008-5472.CAN-06-4086.

(198) Swords, R. T.; Erba, H. P.; DeAngelo, D. J.; Bixby, D. L.; Altman, J. K.; Maris, M.; Hua, Z.; Blakemore, S. J.; Faessel, H.; Sedarati, F.; Dezube, B. J.; Giles, F. J.; Medeiros, B. C.

Pevonedistat (MLN4924), a First-in-Class NEDD8-Activating Enzyme Inhibitor, in Patients with Acute Myeloid Leukaemia and Myelodysplastic Syndromes: A Phase 1 Study. *Br. J. Haematol.* **2015**, *169* (4), 534–543. https://doi.org/https://doi.org/10.1111/bjh.13323.

(199) Petillo, S.; Capuano, C.; Molfetta, R.; Fionda, C.; Mekhloufi, A.; Pighi, C.; Antonangeli, F.; Zingoni, A.; Soriani, A.; Petrucci, M. T.; Galandrini, R.; Paolini, R.; Santoni, A.; Cippitelli, M. Immunomodulatory Effect of NEDD8-Activating Enzyme Inhibition in Multiple Myeloma: Upregulation of NKG2D Ligands and Sensitization to Natural Killer Cell Recognition. *Cell Death Dis.* **2021**, *12* (9), 836. https://doi.org/10.1038/s41419-021-04104-w.

(200) Timm, M.; Saaby, L.; Moesby, L.; Hansen, E. W. Considerations Regarding Use of Solvents in in Vitro Cell Based Assays. *Cytotechnology* **2013**, *65* (5), 887–894. https://doi.org/10.1007/s10616-012-9530-6.

(201) Fukazawa, T.; Yamazaki, Y.; Miyamoto, Y. Reduction of Non-Specific Adsorption of Drugs to Plastic Containers Used in Bioassays or Analyses. *J. Pharmacol. Toxicol. Methods* **2010**, *61* (3), 329–333. https://doi.org/https://doi.org/10.1016/j.vascn.2009.12.005.

(202) Shahbazi, S.; Peer, C. J.; Polizzotto, M. N.; Uldrick, T. S.; Roth, J.; Wyvill, K. M.; Aleman, K.; Zeldis, J. B.; Yarchoan, R.; Figg, W. D. A Sensitive and Robust HPLC Assay with Fluorescence Detection for the Quantification of Pomalidomide in Human Plasma for Pharmacokinetic Analyses. *J. Pharm. Biomed. Anal.* **2014**, *92*, 63–68. https://doi.org/https://doi.org/10.1016/j.jpba.2014.01.001.

(203) Lu, G.; Middleton, R. E.; Sun, H.; Naniong, M.; Ott, C. J.; Mitsiades, C. S.; Wong, K.-K.; Bradner, J. E.; Kaelin, W. G. The Myeloma Drug Lenalidomide Promotes the Cereblon-Dependent Destruction of Ikaros Proteins. *Science (80-.).* **2014**, *343* (6168), 305–309. https://doi.org/10.1126/science.1244917.

(204) Akuffo, A. A.; Alontaga, A. Y.; Metcalf, R.; Beatty, M. S.; Becker, A.; McDaniel, J. M.; Hesterberg, R. S.; Goodheart, W. E.; Gunawan, S.; Ayaz, M.; Yang, Y.; Rezaul Karim, M.; Orobello, M. E.; Daniel, K.; Guida, W.; Yonder, J. A.; Rajadhyaksha, A. M.; Schönbrunn, E.; Lawrence, H. R.; Lawrence, N. J.; Epling-Burnette, P. K. Ligand-Mediated Protein Degradation Reveals Functional Conservation among Sequence Variants of the CUL4-Type E3 Ligase Substrate Receptor Cereblon. *J. Biol. Chem.* **2018**, *298* (16), 6187–6200. https://doi.org/10.1074/jbc.M117.816868.

(205) Min, J.; Mayasundari, A.; Keramatnia, F.; Jonchere, B.; Yang, S. W.; Jarusiewicz, J.; Actis, M.; Das, S.; Young, B.; Slavish, J.; Yang, L.; Li, Y.; Fu, X.; Garrett, S. H.; Yun, M.-K.; Li, Z.; Nithianantham, S.; Chai, S.; Chen, T.; Shelat, A.; Lee, R. E.; Nishiguchi, G.; White, S. W.; Roussel, M. F.; Potts, P. R.; Fischer, M.; Rankovic, Z. Phenyl-Glutarimides: Alternative Cereblon Binders for the Design of PROTACs. *Angew. Chemie Int. Ed.* **2021**, *60* (51), 26663–26670. https://doi.org/https://doi.org/10.1002/anie.202108848.

(206) Jarusiewicz, J. A.; Yoshimura, S.; Mayasundari, A.; Actis, M.; Aggarwal, A.; McGowan, K.; Yang, L.; Li, Y.; Fu, X.; Mishra, V.; Heath, R.; Narina, S.; Pruett-Miller, S. M.; Nishiguchi, G.; Yang, J. J.; Rankovic, Z. Phenyl Dihydrouracil: An Alternative Cereblon Binder for PROTAC Design. *ACS Med. Chem. Lett.* **2023**, *14* (2), 141–145. https://doi.org/10.1021/acsmedchemlett.2c00436.

(207) Hu, J.; Jarusiewicz, J.; Du, G.; Nishiguchi, G.; Yoshimura, S.; Panetta, J. C.; Li, Z.; Min, J.; Yang, L.; Chepyala, D.; Actis, M.; Reyes, N.; Smart, B.; Pui, C.-H.; Teachey, D. T.; Rankovic, Z.; Yang, J. J. Preclinical Evaluation of Proteolytic Targeting of LCK as a Therapeutic Approach in T Cell Acute Lymphoblastic Leukemia. *Sci. Transl. Med.* **2023**, *14* (659), eabo5228. https://doi.org/10.1126/scitranslmed.abo5228.

(208) Knurowski, T.; Clegg, K.; Brooks, N.; Ashby, F.; Pegg, N. A.; West, W.; Walter, H. S.; Somervaille, T. C. P.; Knapper, S.; Davies, A. An Open-Label Phase I/IIa Study to Evaluate

the Safety and Efficacy of CCS1477, a First in Clinic Inhibitor of the P300/CPB Bromodomains, As Monotherapy in Patients with Advanced Haematological Malignancies. *Blood* **2019**, *134*, 1266. https://doi.org/https://doi.org/10.1182/blood-2019-124797.

(209) Fulmer, G. R.; Miller, A. J. M.; Sherden, N. H.; Gottlieb, H. E.; Nudelman, A.; Stoltz, B. M.; Bercaw, J. E.; Goldberg, K. I. NMR Chemical Shifts of Trace Impurities: Common Laboratory Solvents, Organics, and Gases in Deuterated Solvents Relevant to the Organometallic Chemist. *Organometallics* **2010**, *29* (9), 2176–2179. https://doi.org/10.1021/om100106e.

(210) Tsuritani, T.; Yamamoto, Y.; Kawasaki, M.; Mase, T. Novel Approach to 3,4-Dihydro-2(1H)-Quinolinone Derivatives via Cyclopropane Ring Expansion. *Org. Lett.* **2009**, *11* (5), 1043–1045. https://doi.org/10.1021/ol802669r.

(211) Pauff, S. M.; Miller, S. C. Synthesis of Near-IR Fluorescent Oxazine Dyes with Esterase-Labile Sulfonate Esters. *Org. Lett.* **2011**, *13* (23), 6196–6199. https://doi.org/10.1021/ol202619f.

(212) Delso, I.; Valero-Gonzalez, J.; Gomollón-Bel, F.; Castro-López, J.; Fang, W.; Navratilova, I.; van Aalten, D. M. F.; Tejero, T.; Merino, P.; Hurtado-Guerrero, R. Inhibitors against Fungal Cell Wall Remodeling Enzymes. *ChemMedChem* **2018**, *13* (2), 128–132. https://doi.org/10.1002/cmdc.201700720.

(213) Bradner, J.; Buckley, D.; Ishoey, M.; Winter, G. WO2018098280A1, 2018.

(214) Zhang, R.; McIntyre, P. J.; Collins, P. M.; Foley, D. J.; Arter, C.; von Delft, F.; Bayliss, R.; Warriner, S.; Nelson, A. Construction of a Shape-Diverse Fragment Set: Design, Synthesis and Screen against Aurora-A Kinase. *Chem. – A Eur. J.* **2019**, *25* (27), 6831–6839. https://doi.org/10.1002/chem.201900815.

(215) Heller, K.; Ochtrop, P.; Albers, M. F.; Zauner, F. B.; Itzen, A.; Hedberg, C. Covalent Protein Labeling by Enzymatic Phosphocholination. *Angew. Chemie Int. Ed.* **2015**, *54* (35), 10327–10330. https://doi.org/10.1002/anie.201502618.

(216) McGregor, Y. Bin; Kettle, J. G.; Hayhow, T. G. C.; Rasmusson, T. G.; Nissink Wilhelmus Maria, J.; Fallan, C.; Lamont, G. US2019194190 (A1) - Compounds and Their Use in Treating Cancer.

(217) Friese, A.; Kapoor, S.; Schneidewind, T.; Vidadala, S. R.; Sardana, J.; Brause, A.; Förster, T.; Bischoff, M.; Wagner, J.; Janning, P.; Ziegler, S.; Waldmann, H. Chemical Genetics Reveals a Role of DCTP Pyrophosphatase 1 in Wnt Signaling. *Angew. Chemie Int. Ed.* **2019**, *58* (37), 13009–13013. https://doi.org/https://doi.org/10.1002/anie.201905977.

(218) Chang, T. C.; Lai, C. H.; Chien, C. W.; Liang, C. F.; Adak, A. K.; Chuang, Y. J.; Chen, Y. J.; Lin, C. C. Synthesis and Evaluation of a Photoactive Probe with a Multivalent Carbohydrate for Capturing Carbohydrate-Lectin Interactions. *Bioconjug. Chem.* **2013**, *24* (11), 1895–1906. https://doi.org/10.1021/bc400306g.

(219) Oliveira, B. L.; Oliveira, B. L.; Stenton, B. J.; Unnikrishnan, V. B.; De Almeida, C. R.; Conde, J.; Negrão, M.; Schneider, F. S. S.; Cordeiro, C.; Ferreira, M. G.; Ferreira, M. G.; Caramori, G. F.; Domingos, J. B.; Fior, R.; Bernardes, G. J. L.; Bernardes, G. J. L. Platinum-Triggered Bond-Cleavage of Pentynoyl Amide and N-Propargyl Handles for Drug-Activation. *J. Am. Chem. Soc.* **2020**, *142* (24), 10869–10880. https://doi.org/10.1021/jacs.0c01622.

(220) Heinrich, T.; Wallrodt, S. WO2020152067 (A1) - Heterocyclic Derivatives, 2020.

(221) Le Coz, E.; Roueindeji, H.; Roisnel, T.; Dorcet, V.; Carpentier, J.-F.; Sarazin, Y. Barium Complexes with Crown-Ether-Functionalised Amidinate and Iminoanilide Ligands for the Hydrophosphination of Vinylarenes. *Dalt. Trans.* **2019**, *48* (25), 9173–9180. https://doi.org/10.1039/C9DT01512D.

Appendices

Chapter 1 Appendices

Human CREBBP Protein Sequence:

MAENLLDGPPNPKRAKLSSPGFSANDSTDFGSLFDLENDLPDELIPNGGELGLLNSGNLVPDA
ASKHKQLSELLRGGSGSSINPGIGNVSASSPVQQGLGGQAQGQPNSANMASLSAMGKSPLSQ
GDSSAPSLPKQAASTSGPTPAASQALNPQAQKQVGLATSSPATSQTGPGICMNANFNQTHPGL
LNSNSGHSLINQASQGQAQVMNGSLGAAGRGRGAGMPYPTPAMQGASSSVLAETLTQVSPQ
MTGHAGLNTAQAGGMAKMGITGNTSPFGQPFSQAGGQPMGATGVNPQLASKQSMVNSLPT
FPTDIKNTSVTNVPNMSQMQTSVGIVPTQAIATGPTADPEKRKLIQQQLVLLLHAHKCQRREQ
ANGEVRACSLPHCRTMKNVLNHMTHCQAGKACQVAHCASSRQIISHWKNCTRHDCPVCLPL
KNASDKRNQQTILGSPASGIQNTIGSVGTGQQNATSLSNPNPIDPSSMQRAYAALGLPYMNQP
QTQLQPQVPGQQPAQPQTHQQMRTLNPLGNNPMNIPAGGITTDQQPPNLISESALPTSLGATN
PLMNDGSNSGNIGTLSTIPTAAPPSSTGVRKGWHEHVTQDLRSHLVHKLVQAIFPTPDPAALK
DRRMENLVAYAKKVEGDMYESANSRDEYYHLLAEKIYKIQKELEEKRRSRLHKQGILGNQPA
LPAPGAQPPVIPQAQPVRPPNGPLSLPVNRMQVSQGMNSFNPMSLGNVQLPQAPMGPRAASP
MNHSVQMNSMGSVPGMAISPSRMPQPPNMMGAHTNNMMAQAPAQSQFLPQNQFPSSSGA
MSVGMGQPPAQTGVSQGQVPGAALPNPLNMLGPQASQLPCPPVTQSPLHPTPPPASTAAGMP
SLQHTTPPGMTPPQPAAPTQPSTPVSSSGQTPTPTPGSVPSATQTQSTPTVQAAAQAQVTPQPQ
TPVQPPSVATPQSSQQQPTPVHAQPPGTPLSQAAASIDNRVPTPSSVASAETNSQQPGPDVPVL
EMKTETQAEDTEPDPGESKGEPRSEMMEEDLQGASQVKEETDIAEQKSEPMEVDEKKPEVK
VEVKEEEESSSNGTASQSTSPSQPRKKIFKPEELRQALMPTLEALYRQDPESLPFRQPVDPQLL
GIPDYFDIVKNPMDLSTIKRKLDTGQYQEPWQYVDDVWLMFNNAWLYNRKTSRVYKFCSKL
AEVFEQEIDPVMQSLGYCCGRKYEFSPQTLCCYGKQLCTIPRDAAYYSYQNRYHFCEKCFTEI
QGENVTLGDDPSQPQTTISKDQFEKKKNDTLDPEPFVDCKECGRKMHQICVLHYDIIWPSGF
VCDNCLKKTGRPRKENKFSAKRLQTTRLGNHLEDRVNKFLRRQNHPEAGEVFVRVVASSDK
TVEVKPGMKSRFVDSGEMSESFPYRTKALFAFEEIDGVDVCFFGMHVQEYGSDCPPPNTRRV
YISYLDSIHFFRPRCLRTAVYHEILIGYLEYVKKLGYVTGHIWACPPSEGDDYIFHCHPPDQKIP
KPKRLQEWYKKMLDKAFAERIIHDYKDIFKQATEDRLTSAKELPYFEGDFWPNVLEESIKELE
QEEEERKKEESTAASETTEGSQGDSKNAKKKNNKKTNKNKSSISRANKKKPSMPNVSNDLSQ
KLYATMEKHKEVFFVIHLHAGPVINTLPPIVDPDPLLSCDLMDGRDAFLTLARDKHWEFSSLR
RSKWSTLCMLVELHTQGQDRFVYTCNECKHHVETRWHCTVCEDYDLCINCYNTKSHAHKM
VKWGLGLDDEGSSQGEPQSKSPQESRRLSIQRCIQSLVHACQCRNANCSLPSCQKMKRVVQH
TKGCKRKTNGGCPVCKQLIALCCYHAKHCQENKCPVPFCLNIKHKLRQQQIQHRLQQAQLM
RRRMATMNTRNVPQQSLPSPTSAPPGTPTQQPSTPQTPQPPAQPQPSPVSMSPAGFPSVARTQP
PTTVSTGKPTSQVPAPPPPAQPPPAAVEAARQIEREAQQQQHLYRVNINNSMPPGRTGMGTPGS
QMAPVSLNVPRPNQVSGPVMPSMPPGQWQQAPLPQQQPMPGLPRPVISMQAQAAVAGPRMP
SVQPPRSISPSALQDLLRTLKSPSSPQQQQQVLNILKSNPQLMAAFIKQRTAKYVANQPGMQP
QPGLQSQPGMQPQPGMHQQPSLQNLNAMQAGVPRPGVPPQQQAMGGLNPQGQALNIMNPG
HNPNMASMNPQYREMLRRQLLQQQQQQQQQQQQQQQQQQGSAGMAGGMAGHGQFQQP
QGPGGYPPAMQQQQRMQQHLPLQGSSMGQMAAQMGQLGQMGQPGLGADSTPNIQQALQQ
RILQQQQMKQQIGSPGQPNPMSPQQHMLSGQPQASHLPGQQIATSLSNQVRSPAPVQSPRPQS
QPPHSSPSPRIQPQPSPHHVSPQTGSPHPGLAVTMASSIDQGHLGNPEQSAMLPQLNTPSRSAL
SSELSLVGDTTGDTLEKFVEGL. Protein sequence obtained from UniProt.[46,47]

Human p300 Protein Sequence:

MAENVVEPGPPSAKRPKLSSPALSASASDGTDFGSLFDLEHDLPDELINSTELGLTNGGDINQL
QTSLGMVQDAASKHKQLSELLRSGSSPNLNMGVGGPGQVMASQAQQSSPGLGLINSMVKSP
MTQAGLTSPNMGMGTSGPNQGPTQSTGMMNSPVNQPAMGMNTGMNAGMNPGMLAAGNG
QGIMPNQVMNGSIGAGRGRQNMQYPNPGMGSAGNLLTEPLQQGSPQMGGQTGLRGPQPLK
MGMMNNPNPYGSPYTQNPGQQIGASGLGLQIQTKTVLSNNLSPFAMDKKAVPGGGMPNMG
QQPAPQVQQPGLVTPVAQGMGSGAHTADPEKRKLIQQQLVLLLHAHKCQRREQANGEVRQC
NLPHCRTMKNVLNHMTHCQSGKSCQVAHCASSRQIISHWKNCTRHDCPVCLPLKNAGDKRN
QQPILTGAPVGLGNPSSLGVGQQSAPNLSTVSQIDPSSIERAYAALGLPYQVNQMPTQPQVQA
KNQQNQQPGQSPQGMRPMSNMSASPMGVNGGVGVQTPSLLSDSMLHSAINSQNPMMSENA
SVPSLGPMPTAAQPSTTGIRKQWHEDITQDLRNHLVHKLVQAIFPTPDPAALKDRRMENLVAY
ARKVEGDMYESANNRAEYYHLLAEKIYKIQKELEEKRRTRLQKQNMLPNAAGMVPVSMNP
GPNMGQPQPGMTSNGPLPDPSMIRGSVPNQMMPRITPQSGLNQFGQMSMAQPPIVPRQTPPL
QHHGQLAQPGALNPPMGYGPRMQQPSNQGQFLPQTQFPSQGMNVTNIPLAPSSGQAPVSQA
QMSSSSCPVNSPIMPPGSQGSHIHCPQLPQPALHQNSPSPVPSRTPTPHHTPPSIGAQQPPATTIP
APVPTPPAMPPGPQSQALHPPPRQTPTPPTTQLPQQVQPSLPAAPSADQPQQQPRSQQSTAASV
PTPTAPLLPPQPATPLSQPAVSIEGQVSNPPSTSSTEVNSQAIAEKQPSQEVKMEAKMEVDQPEP
ADTQPEDISESKVEDCKMESTETEERSTELKTEIKEEEDQPSTSATQSSPAPGQSKKKIFKPEEL
RQALMPTLEALYRQDPESLPFRQPVDPQLLGIPDYFDIVKSPMDLSTIKRKLDTGQYQEPWQY
VDDIWLMFNNAWLYNRKTSRVYKYCSKLSEVFEQEIDPVMQSLGYCCGRKLEFSPQTLCCY
GKQLCTIPRDATYYSYQNRYHFCEKCFNEIQGESVSLGDDPSQPQTTINKEQFSKRKNDTLDP
ELFVECTECGRKMHQICVLHHEIIWPAGFVCDGCLKKSARTRKENKFSAKRLPSTRLGTFLEN
RVNDFLRRQNHPESGEVTVRVVHASDKTVEVKPGMKARFVDSGEMAESFPYRTKALFAFEEI
DGVDLCFFGMHVQEYGSDCPPPNQRRVYISYLDSVHFFRPKCLRTAVYHEILIGYLEYVKKLG
YTTGHIWACPPSEGDDYIFHCHPPDQKIPKPKRLQEWYKKMLDKAVSERIVHDYKDIFKQATE
DRLTSAKELPYFEGDFWPNVLEESIKELEQEEEERKREENTSNESTDVTKGDSKNAKKKNNK
KTSKNKSSLSRGNKKKPGMPNVSNDLSQKLYATMEKHKEVFFVIRLIAGPAANSLPPIVDPDP
LIPCDLMDGRDAFLTLARDKHLEFSSLRRAQWSTMCMLVELHTQSQDRFVYTCNECKHHVE
TRWHCTVCEDYDLCITCYNTKNHDHKMEKLGLGLDDESNNQQAAATQSPGDSRRLSIQRCI
QSLVHACQCRNANCSLPSCQKMKRVVQHTKGCKRKTNGGCPICKQLIALCCYHAKHCQENK
CPVPFCLNIKQKLRQQQLQHRLQQAQMLRRRMASMQRTGVVGQQQGLPSPTPATPTTPTGQ
QPTTPQTPQPTSQPQPTPPNSMPPYLPRTQAAGPVSQGKAAGQVTPPTPPQTAQPPLPGPPPAA
VEMAMQIQRAAETQRQMAHVQIFQRPIQHQMPPMTPMAPMGMNPPPMTRGPSGHLEPGMG
PTGMQQQPPWSQGGLPQPQQLQSGMPRPAMMSVAQHGQPLNMAPQPGLGQVGISPLKPGTV
SQQALQNLLRTLRSPSSPLQQQQVLSILHANPQLLAAFIKQRAAKYANSNPQPIPGQPGMPQG
QPGLQPPTMPGQQGVHSNPAMQNMNPMQAGVQRAGLPQQQPQQQLQPPMGGMSPQAQQM
NMNHNTMPSQFRDILRRQQMMQQQQQQGAGPGIGPGMANHNQFQQPQGVGYPPQQQQRM
QHHMQQMQQGNMGQIGQLPQALGAEAGASLQAYQQRLLQQQMGSPVQPNPMSPQQHMLP
NQAQSPHLQGQQIPNSLSNQVRSPQPVPSPRPQSQPPHSSPSPRMQPQPSPHHVSPQTSSPHPG
LVAAQANPMEQGHFASPDQNSMLSQLASNPGMANLHGASATDLGLSTDNSDLNSNLSQSTL
DIH. Protein sequence obtained from UniProt.[47,51]

Chapter 2 Appendices

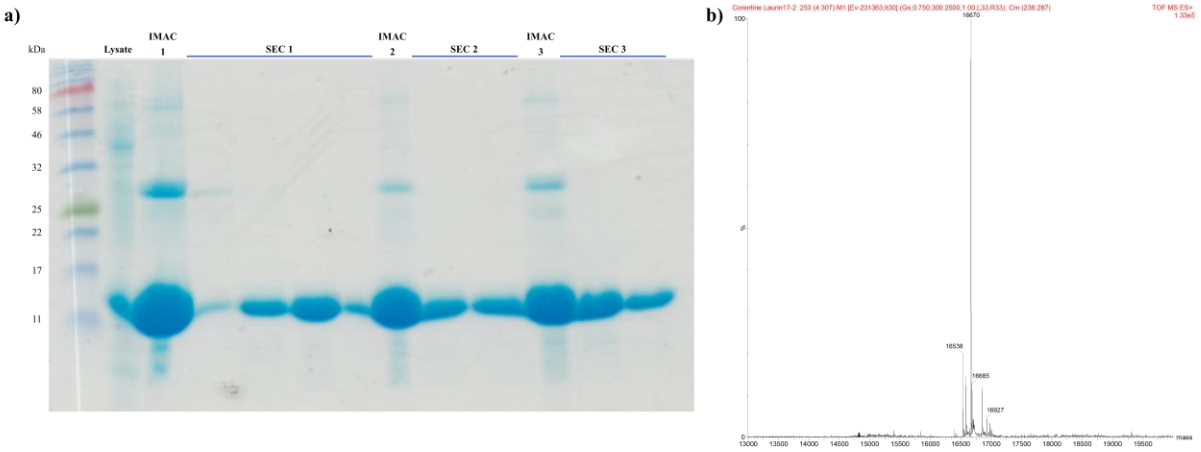

Appendix Figure 1. a) SDS-Page analysis of CREBBP fractions from IMAC and SEC purifications. Ladder: Colour Prestained Protein Standard, Broad Range (11 – 245 kDa) (New England Biolabs). Lystae: Unpurified cell lysate. IMAC 1: IMAC-purified fraction 6. SEC 2: SEC-purified fractions 14 – 17. IMAC 2: IMAC-purified fractions 4 – 5. SEC 2: SEC-purified fractions 15 – 16. IMAC-purified fractions 7 – 8. SEC 2: SEC-purified fractions 15 – 16. b) Protein mass spectra of purified CREBBP bromodomain from combined fractions 15 – 16 from each SEC purification *m/z* (ESI^+) 16670.00 (16673.04 expected). Protein molecular weight was calculated using ProtParam on the ExPASy Bioinformatics Resource Portal.

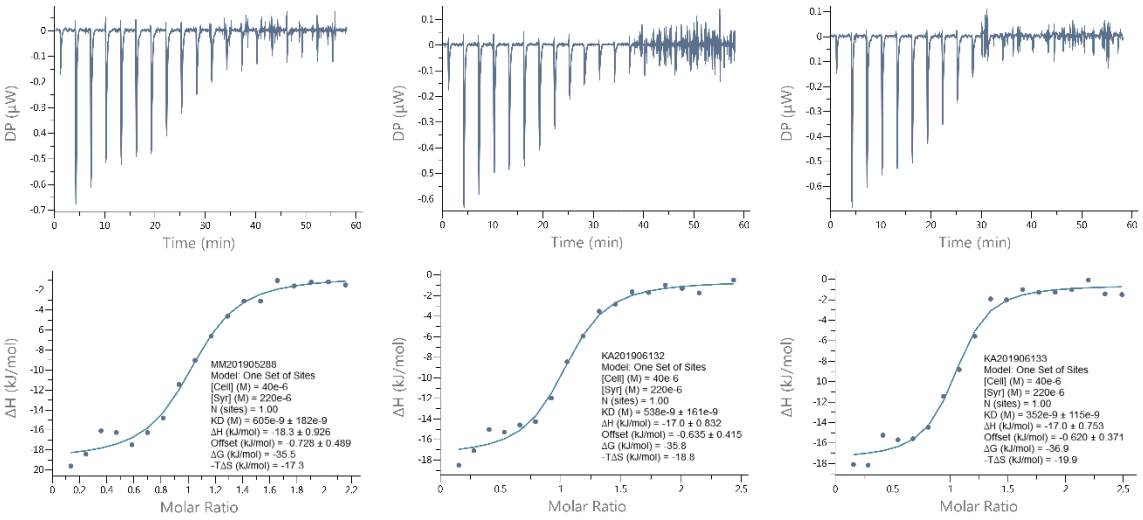

Appendix Figure 2. ITC traces to assess the binding affinity of analogue **2** to the CREBBP bromodomain. Assay performed as three technical repeats. The ITC cell contained 40 µM analogue **2** and titrated with 220 µM protein. Data was analysed using MicroCal PEAQ-ITC software.

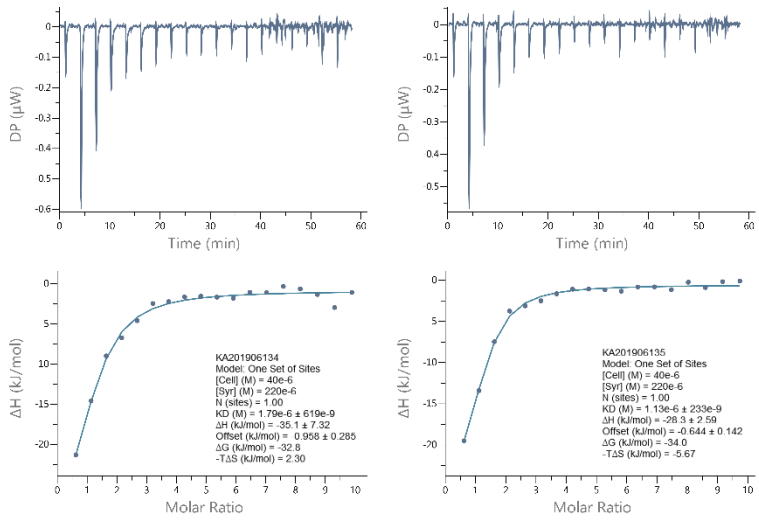

Appendix Figure 3. ITC traces to assess the binding affinity of analogue **3** and the CREBBP bromodomain. Assay performed as two technical repeats. The ITC cell contained 40 µM analogue **3** and titrated with 220 µM protein. Data was analysed using MicroCal PEAQ-ITC software.

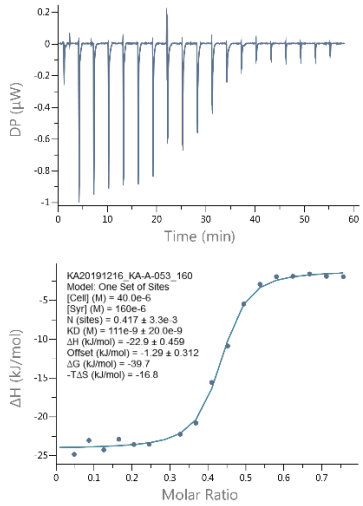

Appendix Figure 4. ITC trace to assess the binding affinity of analogue **25** and the CREBBP bromodomain. The ITC cell contained 40 µM analogue **25** and titrated with 220 µM protein. Data was analysed using MicroCal PEAQ-ITC software.

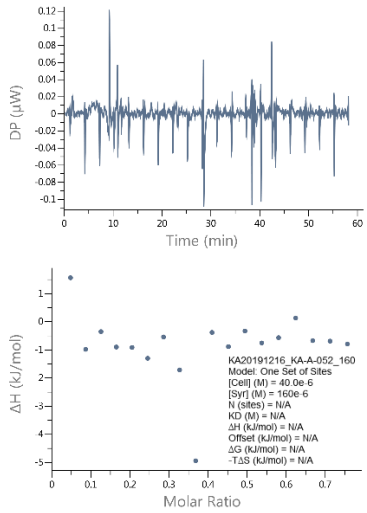

Appendix Figure 5. ITC trace to assess the binding affinity of analogue **26** and the CREBBP bromodomain. The ITC cell contained 40 µM analogue **26** and titrated with 220 µM protein. Data was analysed using MicroCal PEAQ-ITC software.

Appendix Table 1. Ligand binding affinities for the CREBBP bromodomain, $clogD_{pH7.4}$, and Property Forecast Index (PFI) values of **(*R*)-OXFBD05** and analogues **2** – **8**, **25**, and **26**. Compound **25** has comparable binding affinity, $clogD_{pH7.4}$, and PFI values as the parent ligand **(*R*)-OXFBD05**, however, as the alkyl linker length increases in compounds **2** and **26**, the binding affinity for the CREBBP bromodomain decreases. This trend appears to correlate with the increasing lipophilicities of the compounds, where predicted aqueous solubility (pH 7.4) decreases with increasing alkyl linker length. Analogues **2** – **8** do not appear to follow a similar trend. Binding affinity K_d values were obtained using ITC. Darker green indicates higher binidng affinity of the compound to the CREBBP bromodomain, n.b. = no detectable binding. $clogD_{pH7.4}$ values were calculated using Chemicalize (http://www.chemicalize.com) and are coloured according to compound aqueous solubility observations by Hill and Young, where $x < 2$ predicts good solubility (green), $2 < \boldsymbol{x} \leq 4$ predicts moderate solubility (yellow), and $\boldsymbol{x} > 4$ predicts poor solubility (red), darker colour indicates higher value within category.[20] The Property Forecast Index (PFI) is a measurement developed by GSK for predicting aqueous solubility (PFI = $clogD_{pH7.4}$ + #Ar rings).[21] PFI values are coloured according to compound aqueous solubility observations by Tinworth and Young, where $x < 4$ predicts good solubility (green), $4 < \boldsymbol{x} \leq 8$ predicts moderate solubility (yellow), and $\boldsymbol{x} > 8$ predicts poor solubility (red), darker colour indicates higher value within category.[21]

Cpd.	Structure	K_d (nM)	$clogD_{pH7.4}$	PFI
(*R*)-OXFBD05	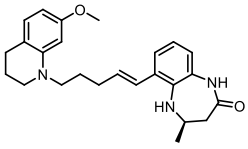	102	4.54	6.54
25	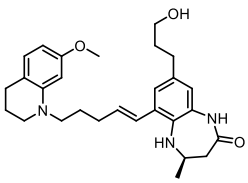	111	4.50	6.50
2	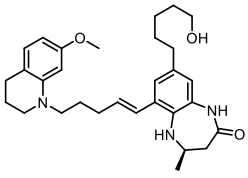	538	5.39	7.39

26	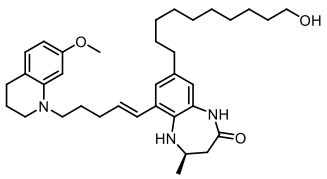	n.b.	7.61	9.61
3	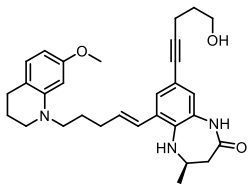	1460	5.38	7.38
4	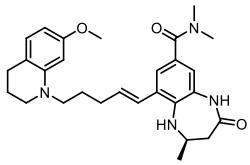	1300	4.06	6.08
5	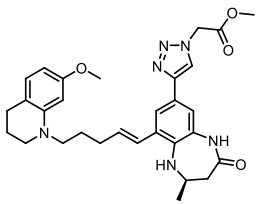	1310	4.65	7.65
6	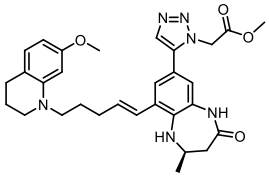	1260	4.18	7.18
7	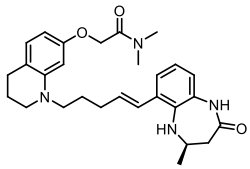	n.b.	4.06	6.06
8	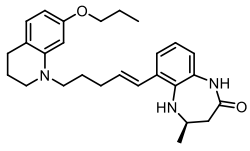	1450	5.82	7.82

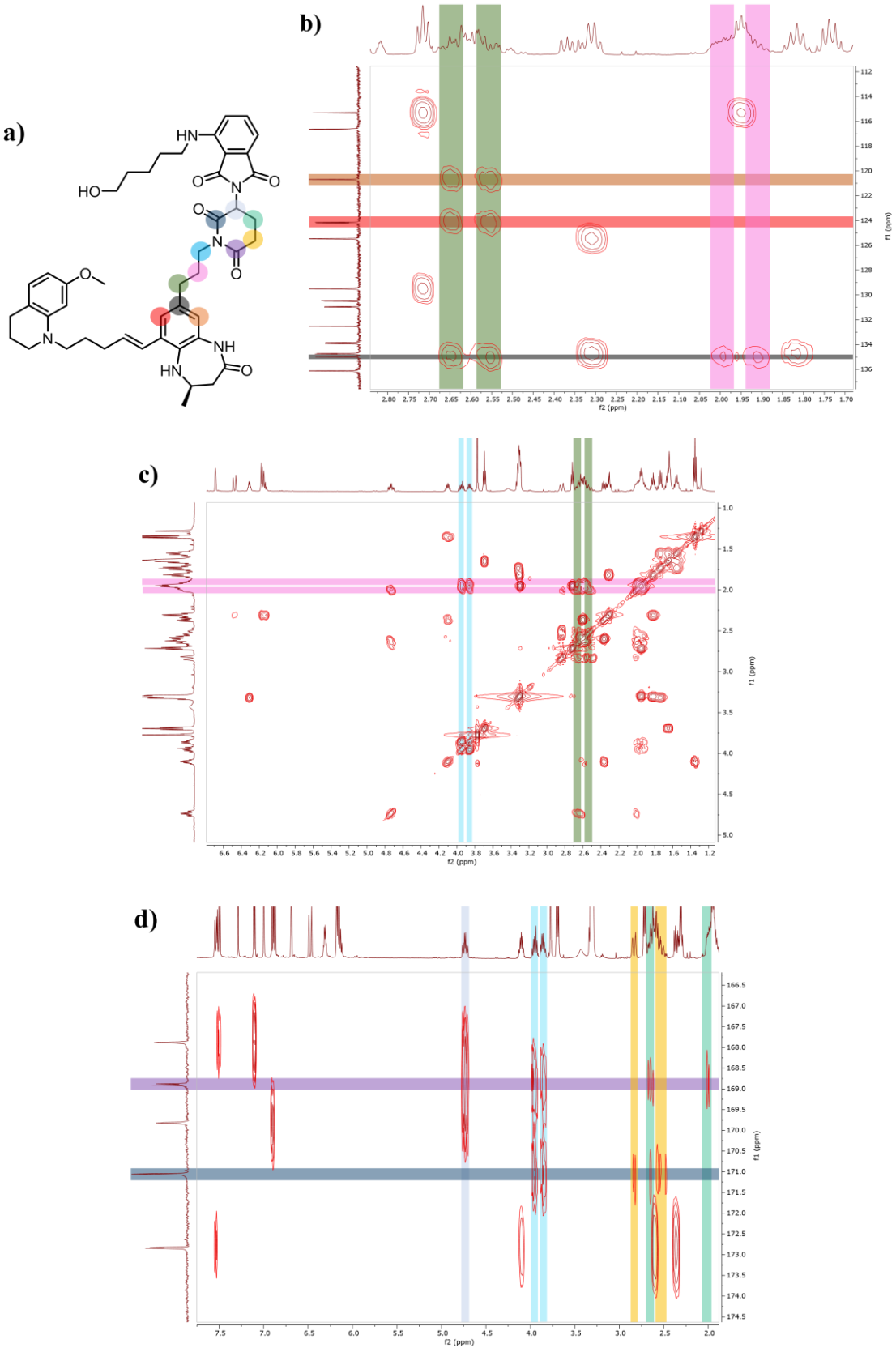

Appendix Figure 6. Assignment of undesired alkylation product **42**. **a)** Structure of compound **42**. Relevant atoms for compound assignment are highlighted in coloured circles that correspond to highlighted peaks in the 2D NMR spectra. **b)** HMBC spectra of compound **42** expanded into area to show the coupling interactions between the -CH_2 protons (green and pink) of the propanyl chain and carbons on the DHBD group (brown, red, and grey). **c)** COSY spectra of compound **42** expanded into area to show the coupling interactions between the -CH_2 protons

(green, pink, and cyan) of the propanyl chain. **c)** HMBC spectra of compound **42** expanded into area to show the coupling interactions between the -CH_2 protons (green and pink) of the propanyl chain and carbons on the DHBD group (brown, red, and grey).

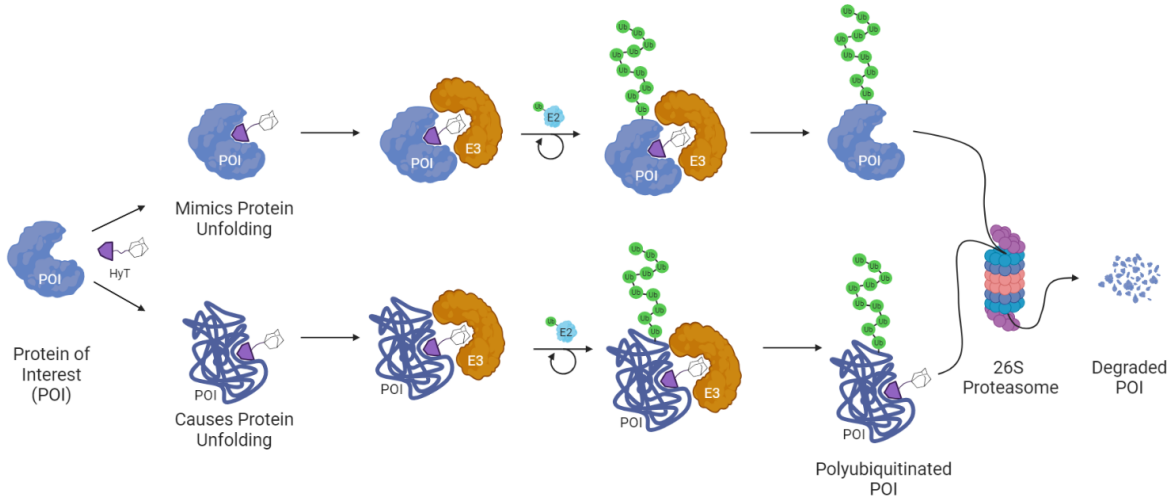

Appendix Figure 7. Two proposed mechanism of actions of HyTs.[6,147,148] HyTs function using a similar mechanism as PROTACs. Binding of the HyT to the POI either mimics protein unfolding or causes partial unfolding of the POI. This induces the recruitment of a non-specific E3 ubiqutin ligase enzyme which forms a complex with the POI and mediates the transfer of a polyubiqutin chain onto the POI using the UPS. The polyubiquitinated POI can then be recognised and degraded by the 26S proteasome. This process removes the full POI from the cell. Image created using Biorender (www.biorender.com).

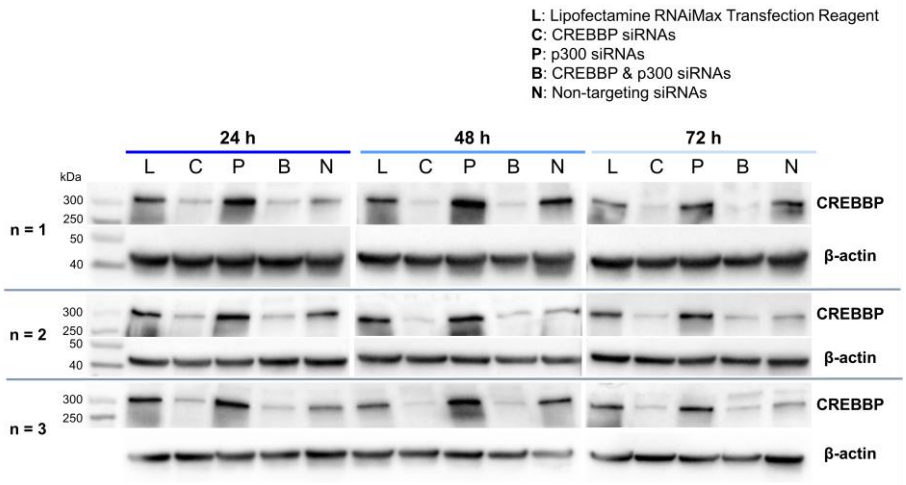

Appendix Figure 8. Western blots showing CREBBP and β-actin protein bands for the three biological repeats of the CREBBP and/or p300 siRNA-mediated knockdown assay. HeLa cells were treated with the vehicle (Lipofectamine RNAiMax Transfection Reagent) control (L), CREBBP-targeting siRNAs (C), p300-targeting siRNAs (P), 1:1 mixture of CREBBP and p300-targeting siRNAs (B), or non-targeting siRNAs (N) for 24 h (dark blue), 48 h (blue), or 72 h (light blue).

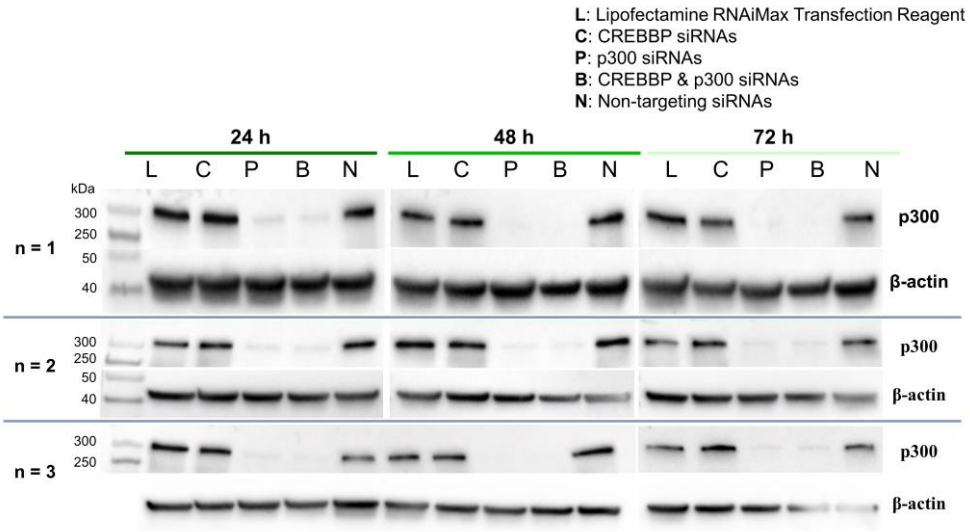

Appendix Figure 9. Western blots showing p300 and β-actin protein bands for the three biological repeats of the CREBBP and/or p300 siRNA-mediated knockdown assay. HeLa cells were treated with the vehicle (Lipofectamine RNAiMax Transfection Reagent) control (L), CREBBP-targeting siRNAs (C), p300-targeting siRNAs (P), 1:1 mixture of CREBBP and p300-targeting siRNAs (B), or non-targeting siRNAs (N) for 24 h (dark green), 48 h (green), or 72 h (light green).

Appendix Table 2. Quantification of CREBBP levels in HeLa cells following treatment with siRNAs targeting CREBBP, p300, both CREBBP and p300, or non-human firefly luciferase for 24 h, 48 h, or 72 h, as indicated. Cellular assays were performed as three biological repeats and protein levels were assessed using western blotting (Appendix Figure 8). Western Blot signals were analysed using Image Lab (Bio-Rad) software then quantified using Excel. For each sample, the CREBBP signal was normalised against the β-actin loading control using equation CREBBP signal/β-actin signal, then against the untreated (lipofectamine) sample for the same timepoint using equation 100 × β-actin normalised CREBBP signal/lipofectamine normalised CREBBP signal. This provides the relative protein level of each sample as a percentage relative to the untreated (lipofectamine) cells. An average (mean) was calculated for the relative protein expression value (%), and the standard deviation (SD) and standard error of the mean (SEM) were calculated. A Student's t-test was performed relative to the lipofectamine control data, and significance (sig.) is denoted as **** - $p \leq 0.0001$, *** - $p \leq 0.001$, ** - $p \leq 0.01$, * $p - \leq 0.05$, ns - not statistically significant.

		n = 1				n = 2				n = 3				Mean (%)	SD	SEM	t-test	Sig.
		CREBBP	β-actin	β-Actin normalised	Lipofectamine normalised (%)	CREBBP	β-actin	β-Actin normalised	Lipofectamine normalised (%)	CREBBP	β-actin	β-Actin normalised	Lipofectamine normalised (%)					
24 h	Lipofectamine	4676152	8021864	0.582925864	100.00	5081344	6424356	0.790949941	100.00	4434870	11158600	0.397439643	100.00	100.00	0.00	0.00	-	-
	CREBBP siRNAs	901810	8483700	0.106299138	18.24	960510	5674095	0.169279859	21.40	1169280	13095425	0.089289198	22.47	20.70	2.20	1.27	0.00013	***
	p300 siRNAs	5400330	8278543	0.652328556	111.91	4583616	6279770	0.729901891	92.28	5655309	12237015	0.462147754	116.28	106.82	12.78	7.38	0.22640	ns
	1:1 CREBBP and p300 siRNAs	899288	8468580	0.106191121	18.22	1247040	8241713	0.151308351	19.13	1046498	12556296	0.083344483	20.97	19.44	1.40	0.81	0.00005	****
	Non-Targeting siRNAs	1845725	7383600	0.249976299	42.88	4295874	8806040	0.487832669	61.68	2944672	16206999	0.181691379	45.72	50.09	10.13	5.85	0.00673	**
48 h	Lipofectamine	4122117	8635712	0.477333774	100.00	4296096	7430368	0.578180785	100.00	3672928	14173468	0.259141094	100.00	100.00	0.00	0.00	-	-
	CREBBP siRNAs	350714	7458360	0.047022938	9.85	862389	6824020	0.126375509	21.86	461216	12846432	0.035902265	13.85	15.19	6.11	3.53	0.00086	***
	p300 siRNAs	4396056	8922330	0.492702691	103.22	7489482	6321824	1.184702706	204.90	5672568	13170780	0.430693399	166.20	158.11	51.32	29.63	0.09445	ns
	1:1 CREBBP and p300 siRNAs	466125	6716332	0.069401721	14.54	1021760	5091120	0.200694543	34.71	895872	10390485	0.086220422	33.27	27.51	11.25	6.50	0.00397	**
	Non-Targeting siRNAs	4700403	9115947	0.515624213	108.02	1519650	4913850	0.309258524	53.49	3502851	7907192	0.442995567	170.95	110.82	58.78	33.94	0.39004	ns
72 h	Lipofectamine	1247352	8469088	0.147282919	100.00	2250600	8377236	0.268656631	100.00	2889120	8387160	0.344469403	100.00	100.00	0.00	0.00	-	-
	CREBBP siRNAs	237682	7330504	0.032423691	22.01	437370	7831425	0.055848074	20.79	469020	10866493	0.043162039	12.53	18.44	5.16	2.98	0.00067	***
	p300 siRNAs	2219328	8029230	0.276406081	187.67	3558560	6979038	0.509892624	189.79	2449280	9059276	0.270361561	78.49	151.98	63.66	36.75	0.14643	ns
	1:1 CREBBP and p300 siRNAs	218064	7336942	0.029721374	20.18	669321	7481376	0.089464959	33.30	526163	7528140	0.069892829	20.29	24.59	7.54	4.36	0.00166	**
	Non-Targeting siRNAs	2428900	8343900	0.291098887	197.65	1220850	8285225	0.147352667	54.85	1267435	10578152	0.119816297	34.78	95.76	88.81	51.27	0.13518	ns

Appendix Table 3. Quantification of p300 levels in HeLa cells following treatment with siRNAs targeting CREBBP, p300, both CREBBP and p300, or non-human firefly luciferase for 24 h, 48 h, or 72 h, as indicated. Cellular assays were performed as three biological repeats and protein levels were assessed using western blotting (Appendix Figure 9). Western blot signals were analysed using Image Lab (Bio-Rad) software then quantified using Excel. For each sample, the p300 signal was normalised against the β-actin loading control using equation $p300\ signal/\beta\text{-actin signal}$, then against the untreated (lipofectamine) sample for the same timepoint using equation $100 \times \beta\text{-actin normalised p300 signal/lipofectamine normalised p300 signal}$. This provides the relative protein level of each sample as a percentage relative to the untreated (lipofectamine) cells. An average (mean) was calculated for the relative protein expression value (%), and the standard deviation (SD) and standard error of the mean (SEM) were calculated. A Student's t-test was performed relative to the lipofectamine control data, and significance (sig.) is denoted as **** - $p \leq 0.0001$, *** - $p \leq 0.001$, ** - $p \leq 0.01$, * p - ≤ 0.05, ns - not statistically significant.

		n = 1				n = 2				n = 3								
		p300	β-actin	β-Actin normalised	Lipofectamine normalised (%)	p300	β-actin	β-Actin normalised	Lipofectamine normalised (%)	p300	β-actin	β-Actin normalised	Lipofectamine normalised (%)	Mean (%)	SD	SEM	t-test	Sig.
24 h	Lipofectamine	4385706	8158332	0.537573857	100.00	2485756	8725000	0.284900401	100.00	4935140	11494924	0.429332112	100.00	100.00	0.00	0.00	-	-
	CREBBP siRNAs	4945434	8304990	0.595477418	110.77	2959138	7955830	0.371945856	130.55	3830856	10182546	0.376217893	87.63	109.65	21.48	12.40	0.25898	ns
	p300 siRNAs	373037	8144040	0.045804908	8.52	350436	7711200	0.045445067	15.95	241824	11689484	0.020687312	4.82	9.76	5.67	3.27	0.00066	***
	1:1 CREBBP and p300 siRNAs	319150	7244440	0.044054475	8.20	361788	6934320	0.052173537	18.31	266040	11058456	0.024057608	5.60	10.70	6.72	3.88	0.00094	***
	Non-Targeting siRNAs	3655206	7474315	0.489035584	90.97	4068288	6904942	0.589184963	206.80	2624123	15704988	0.167088507	38.92	112.23	85.94	49.62	0.41414	ns
48 h	Lipofectamine	3230325	8052448	0.401160616	100.00	5193780	7217886	0.7195708	100.00	3262268	11910444	0.273899781	100.00	100.00	0.00	0.00	-	-
	CREBBP siRNAs	3128100	7717625	0.405318994	101.04	3525066	8313516	0.424016265	58.93	3423769	11617047	0.29471939	107.60	89.19	26.41	15.25	0.27591	ns
	p300 siRNAs	167923	8218110	0.020433287	5.09	158301	7291060	0.021711658	3.02	46152	9976865	0.004625902	1.69	3.27	1.72	0.99	0.00005	****
	1:1 CREBBP and p300 siRNAs	76176	6628791	0.011491688	2.86	148764	4773475	0.031164718	4.33	57424	10676091	0.005378748	1.96	3.05	1.19	0.69	0.00003	****
	Non-Targeting siRNAs	3578822	7947740	0.450294297	112.25	3686280	3978182	0.926624272	128.77	4988969	10527768	0.473886678	173.01	138.01	31.42	18.14	0.08555	ns
72 h	Lipofectamine	3052280	7786735	0.391984574	100.00	1622927	8486064	0.191246142	100.00	2872864	12443400	0.23087452	100.00	100.00	0.00	0.00	-	-
	CREBBP siRNAs	2084950	6155970	0.338687485	86.40	2437073	7433370	0.327855737	171.43	4029360	11747916	0.342985088	148.56	135.46	44.00	25.40	0.14874	ns
	p300 siRNAs	153360	6154740	0.024917381	6.36	164430	7346484	0.022382135	11.70	170176	10065528	0.016906813	7.32	8.46	2.85	1.64	0.00016	***
	1:1 CREBBP and p300 siRNAs	70148	6192180	0.011328482	2.89	217260	6486516	0.033494098	17.51	210428	4787532	0.043953335	19.04	13.15	8.92	5.15	0.00175	**
	Non-Targeting siRNAs	2164184	7139524	0.303127211	77.33	2612260	5777850	0.452116272	236.41	2365142	2793564	0.846639633	366.71	226.82	144.93	83.67	0.19551	ns

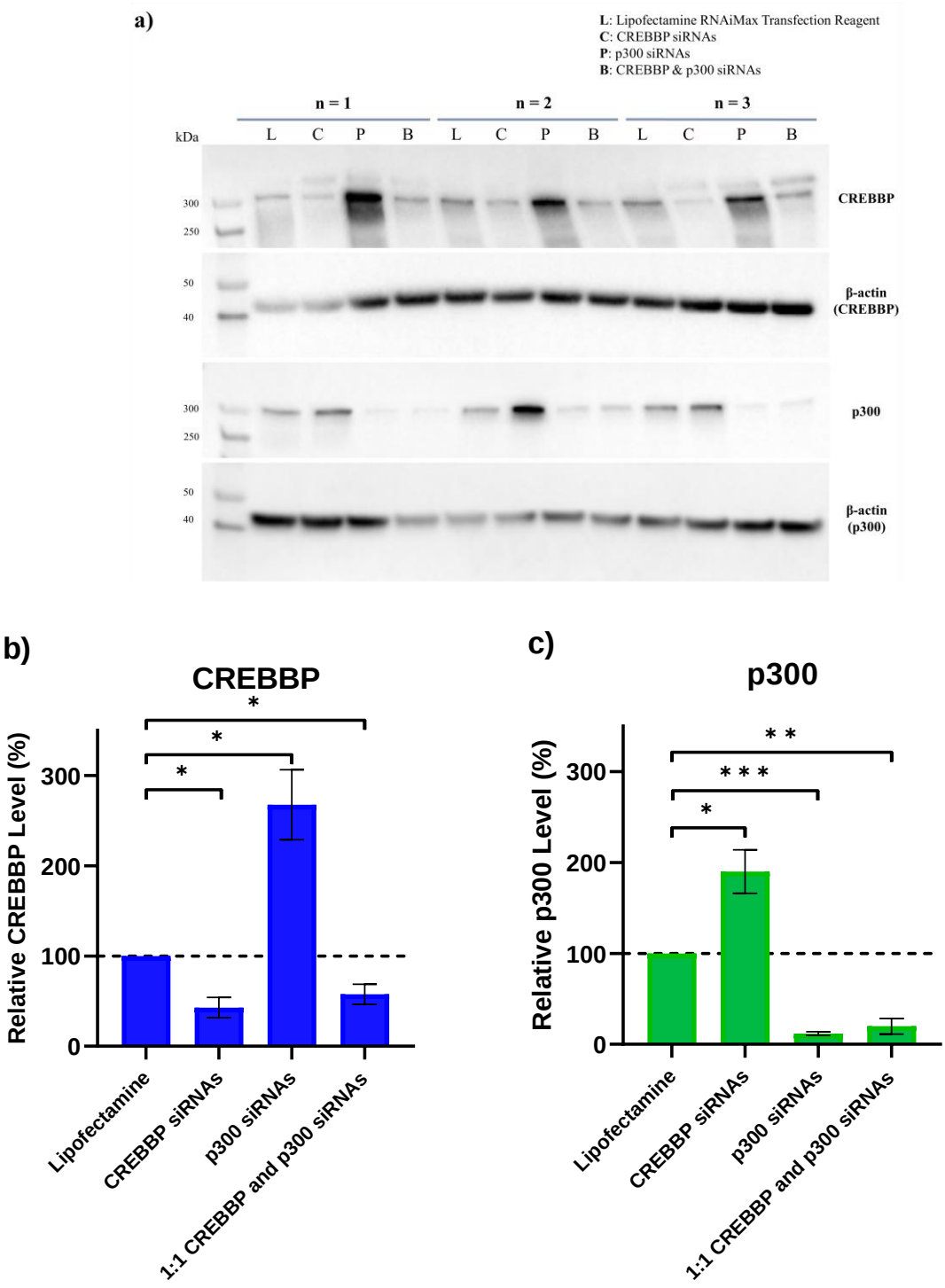

Appendix Figure 10. Quantification of relative cellular CREBBP and p300 levels following siRNA-mediated knockdown of CREBBP, p300, or both CREBBP and p300 in HEK293T cells after 24 h. **a)** Western blots of cells treated with Lipofectamine RNAiMax Transfection Reagent and no siRNA (L), CREBBP-targeting siRNAs (C), p300-targeting siRNAs (P), or a 1:1 mixture of CREBBP and p300-targeting siRNAs (B) after 24 h (dark green), 48 h (green), or 72 h (light green). Three biological repeats (n) were performed. CREBBP and p300 levels were assessed on separate blots from the same denatured protein sample instead of by stripping membranes and incubating with new antibodies. **b)** Relative protein expressions of CREBBP from Western Blot analysis. Protein expression was quantified against the β-actin loading control and then relative to the β-actin-standardised lipofectamine control sample (Appendix Table 4). Average normalised CREBBP levels in the lipofectamine-treated cells were set to 100%. **c)** Relative protein expressions of p300 from Western Blot analysis. Protein levels were quantified against the β-actin loading control and then relative to the β-actin-standardised lipofectamine control sample (Appendix Table 5). Average normalised p300 levels in the lipofectamine-treated cells were set to 100%. Western Blots were analysted using Image Lab (Bio-Rad) Software and the data was quantified using Excel. Data are reported as the mean relative expression over the three biological repeats and error

bars are the standard error of the mean. A student's t-test was performed for each sample relative to the corresponding lipofectamine control data. Significance is denoted as: **** - $p \leq 0.0001$, *** - $p \leq 0.001$, ** - $p \leq 0.01$, * - $p \leq 0.05$. 100% relative protein expression indicated by dahsed line.

Appendix Table 4. Quantification of CREBBP levels in HEK293T cells following treatment with siRNAs targeting CREBBP, p300, both CREBBP and p300, or non-human firefly luciferase for 24 h. Cellular assays were performed as three biological repeats and protein levels were assessed using western blotting (Appendix Figure 10). Western blot signals were analysed using Image Lab (Bio-Rad) software then quantified using Excel. For each sample, the CREBBP signal was normalised against the β-actin loading control using equation CREBBP signal/β-actin signal, then against the untreated (lipofectamine) sample for the same timepoint using equation 100 × β-actin normalised CREBBP signal/β-actin normalised lipofectamine CREBBP signal. This provides the relative protein level of each sample as a percentage relative to the untreated (lipofectamine) cells. An average (mean) was calculated for the relative protein expression value (%), and the standard deviation (SD) and standard error of the mean (SEM) were calculated. A Student's t-test was performed relative to the lipofectamine control data, and significance (sig.) is denoted as **** - $p \leq 0.0001$, *** - $p \leq 0.001$, ** - $p \leq 0.01$, * p - ≤ 0.05, ns - not statistically significant.

	n = 1				n = 2				n = 3				Mean (%)	SD	SEM	t-test	Sig.
	CREBBP	β-actin	β-Actin normalised	Lipofectamine normalised (%)	CREBBP	β-actin	β-Actin normalised	Lipofectamine normalised (%)	CREBBP	β-actin	β-Actin normalised	Lipofectamine normalised (%)					
Lipofectamine	564165	566660	0.995597007	100.00	1005925	2115000	0.475614657	100.00	1155357	2001042	0.577377686	100.00	100.00	0.00	0.00	-	-
CREBBP siRNA	302975	635911	0.476442458	47.85	550025	1948621	0.282263714	59.35	311310	2524640	0.12330867	21.36	42.85	19.48	11.25	0.0183	*
p300 siRNA	4245410	1780148	2.384863506	239.54	3363975	2053653	1.638044499	344.41	3129390	2476782	1.263490287	218.83	267.59	67.32	38.87	0.0249	*
CREBBP and p300 siRNA	770607	2160740	0.356640318	35.82	659325	1930122	0.341597578	71.82	1059330	2803355	0.377879362	65.45	57.70	19.21	11.09	0.0312	*

Appendix Table 5. Quantification of p300 levels in HEK293T cells following treatment with siRNAs targeting CREBBP, p300, both CREBBP and p300, or non-human firefly luciferase for 24 h. Cellular assays were performed as three biological repeats and protein levels were assessed using western blotting (Appendix Figure 10). Western blot signals were analysed using Image Lab (Bio-Rad) software then quantified using Excel. For each sample, the p300 signal was normalised against the β-actin loading control using equation p300 signal/β-actin signal, then against the untreated (lipofectamine) sample for the same timepoint using equation 100 × β-actin normalised p300 signal/β-actin normalised lipofectamine p300 signal. This provides the relative protein level of each sample as a percentage relative to the untreated (lipofectamine) cells. An average (mean) was calculated for the relative protein expression value (%), and the standard deviation (SD) and standard error of the mean (SEM) were calculated. A Student's t-test was performed relative to the lipofectamine control data, and significance (sig.) is denoted as **** - $p \leq 0.0001$, *** - $p \leq 0.001$, ** - $p \leq 0.01$, * p - ≤ 0.05, ns - not statistically significant.

	n = 1				n = 2				n = 3				Mean (%)	SD	SEM	t-test	Sig.
	p300	β-actin	β-Actin normalised	Lipofectamine normalised (%)	p300	β-actin	β-Actin normalised	Lipofectamine normalised (%)	p300	β-actin	β-Actin normalised	Lipofectamine normalised (%)					
Lipofectamine	798275	2579420	0.309478487	100.00	888914	592840	1.499416369	100.00	978857	1552740	0.63040625	100.00	100.00	0.00	0.00	-	-
CREBBP siRNA	1447794	2484820	0.582655484	188.27	3122802	896420	3.483637134	232.33	1550545	1644735	0.942732416	149.54	190.05	41.42	23.92	0.0319	*
p300 siRNA	97630	2018560	0.048366162	15.63	193660	1246875	0.155316291	10.36	118375	2012418	0.058822273	9.33	11.77	3.38	1.95	0.0002	***
CREBBP and p300 siRNA	83550	747973	0.111701893	36.09	289224	1172214	0.246733105	16.46	94328	2143466	0.044007229	6.98	19.84	14.85	8.57	0.0056	**

Appendix Table 6. Quantification of CREBBP levels in HEK293T cells treated with 10 μM PROTACs **31** – **38** or the vehicle (DMSO) control for 24 h. Western blot signals were analysed using Image Lab (Bio-Rad) software then quantified using Excel. For each sample, the CREBBP signal was normalised against the β-actin loading control using equation CREBBP signal/β-actin signal, then against the corresponding vehcile (DMSO) treated sample using the equation 100 × β-actin normalised CREBBP signal/β-actin normalised DMSO CREBBP signal. This provides the relative protein level of each sample as a percentage relative to the vehicle (DMSO) control treated cells. An average (mean) was calculated for the relative protein expression value (%), and the standard deviation (SD) and standard error of the mean (SEM) were calculated. A Student's t-test was performed relative to the lipofectamine control data, and significance (sig.) is denoted as **** - $p \leq 0.0001$, *** - $p \leq 0.001$, ** - $p \leq 0.01$, * p - ≤ 0.05, ns - not statistically significant.

	n = 1				n = 2				n = 3				Mean (%)	SD	SEM	ttest	Sig.
	CREBBP	β-Actin	β-Actin normalised	DMSO normalised (%)	CREBBP	β-Actin	β-Actin normalised	DMSO normalised (%)	CREBBP	β-Actin	β-Actin normalised	DMSO normalised (%)					
DMSO	3398174	2117324	1.60493812	100.00	3375584	1530672	2.20529545	100.00	3703552	1808016	2.0484067	100.00	100.00	0.00	0.00		
31	3264907	2299374	1.41991125	88.47	2061117	2163912	0.95249576	43.19	2422022	1730169	1.399876	68.34	66.67	18.52	10.69	0.0630	ns
32	3416310	2465012	1.38592023	86.35	1740798	2701728	0.64432763	29.22	2369619	2586144	0.916275	44.73	53.43	24.12	13.93	0.0560	ns
33	2364726	2638445	0.89625745	55.84	2630300	2502744	1.05096646	47.66	2398184	2277713	1.0528912	51.40	51.63	3.35	1.93	0.0012	**
34	1728168	2884821	0.59905554	37.33	1979019	2208336	0.89615847	40.64	3081337	2202848	1.3987969	68.29	48.75	13.88	8.01	0.0174	*
35	2454114	3190248	0.76925493	47.93	2345058	3018425	0.77691445	35.23	3658292	2400878	1.5237309	74.39	52.52	16.31	9.42	0.0271	*
36	2378324	2999832	0.79281906	49.40	3083570	2544973	1.21163171	54.94	2726145	2133538	1.2777579	62.38	55.57	5.32	3.07	0.0035	**
37	3301159	2658639	1.24167252	77.37	4757334	3066646	1.55131502	70.34	3054222	2645713	1.1544041	56.36	68.02	8.73	5.04	0.0177	*
38	2965140	2832335	1.04688887	65.23	2164374	3231891	0.66969276	30.37	2838288	2767072	1.025737	50.07	48.56	14.27	8.24	0.0182	*

Appendix Table 7. Quantification of p300 levels in HEK293T cells treated with 10 μM PROTACs **31** – **38** or the vehicle (DMSO) control for 24 h. Western blot signals were analysed using Image Lab (Bio-Rad) software then quantified using Excel. For each sample, the p300 signal was normalised against the β-actin loading control using equation p300 signal/β-actin signal, then against the corresponding vehcile (DMSO) treated sample using the equation $100 \times$ β-actin normalised p300 signal/β-actin normalised DMSO p300 signal. This provides the relative protein level of each sample as a percentage relative to the vehicle (DMSO) control treated cells. An average (mean) was calculated for the relative protein expression value (%), and the standard deviation (SD) and standard error of the mean (SEM) were calculated. A Student's t-test was performed relative to the lipofectamine control data, and significance (sig.) is denoted as **** - $p \leq 0.0001$, *** - $p \leq 0.001$, ** - $p \leq 0.01$, * p - ≤ 0.05, ns - not statistically significant.

	n = 1				n = 2				n = 3				Mean (%)	SD	SEM	ttest	Sig.
	p300	β-Actin	β-Actin normalised	DMSO normalised (%)	p300	β-Actin	β-Actin normalised	DMSO normalised (%)	p300	β-Actin	β-Actin normalised	DMSO normalised (%)					
DMSO	2783781	1906148	1.46042228	100.00	2843506	1714800	1.65821437	100.00	2477720	1423818	1.7401943	100.00	100.00	0.00	0.00		
31	2185677	2220658	0.98424746	67.39	1438784	2084697	0.69016457	41.62	1463476	1507066	0.9710763	55.80	54.94	10.54	6.09	0.0131	*
32	3197178	2409549	1.32687818	90.86	1386336	1813734	0.76435464	46.10	2681700	2222968	1.2063601	69.32	68.76	18.28	10.55	0.0684	n.s.
33	2110887	2039088	1.03521133	70.88	1702068	2455680	0.69311474	41.80	3102976	2652636	1.1697707	67.22	59.97	12.93	7.47	0.0242	*
34	2490669	1678862	1.483546	101.58	871695	2851100	0.30573989	18.44	2550604	2336984	1.0914084	62.72	60.91	33.97	19.61	0.1226	n.s.
35	2475765	2404604	1.02959365	70.50	1115208	2752548	0.40515479	24.43	2002812	2473614	0.8096704	46.53	47.15	18.81	10.86	0.0290	*
36	1541754	2789578	0.5526836	37.84	1156275	2781413	0.41571496	25.07	2070824	2293720	0.9028234	51.88	38.26	10.95	6.32	0.0077	**
37	2210841	1829234	1.20861574	82.76	1709559	2857092	0.5983563	36.08	1814792	3109876	0.5835577	33.53	50.79	22.63	13.06	0.0457	*
38	3108220	2273376	1.36722654	93.62	1046520	3070800	0.34079719	20.55	1397256	3165024	0.4414677	25.37	46.51	33.37	19.26	0.0758	n.s.

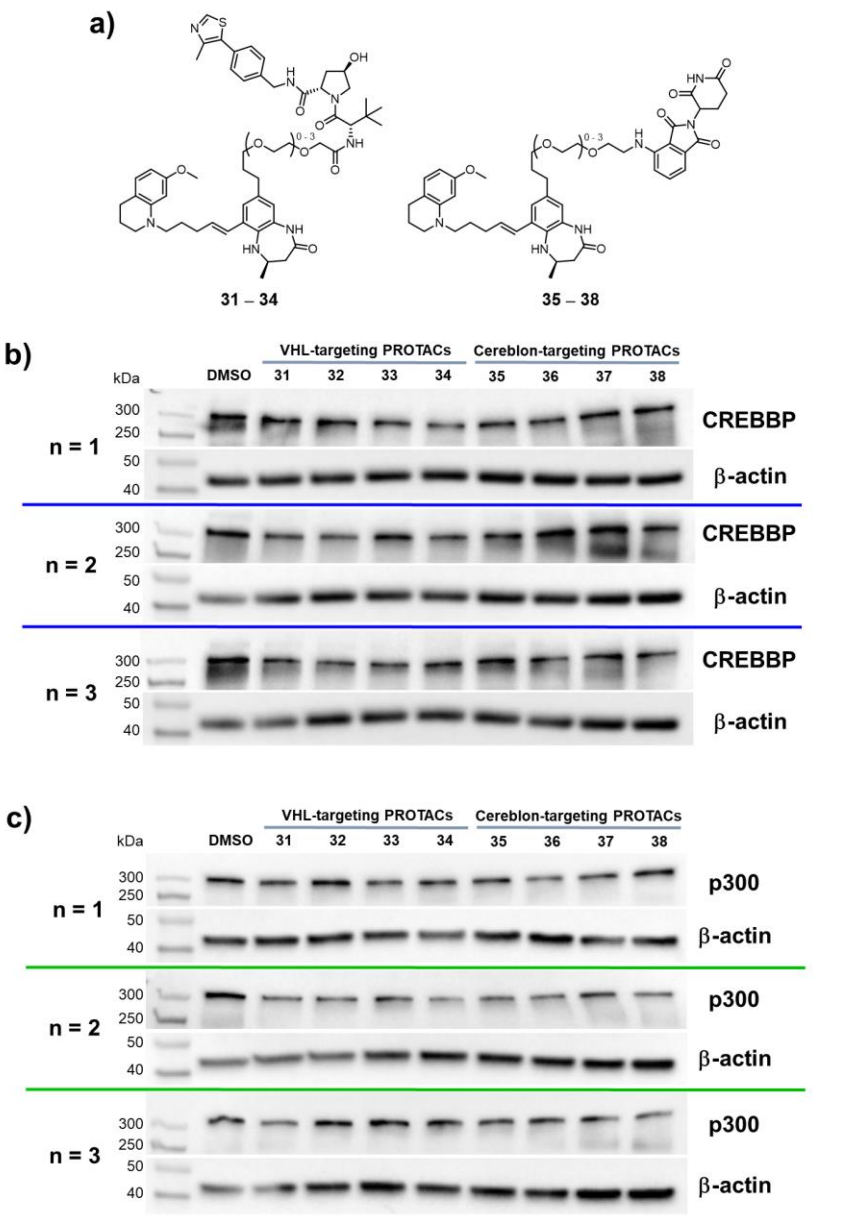

Appendix Figure 11. Wesetern blots for CREBBP, p300, and their corresponding β-actin loading control for the three biological repeats (n) of 24 h treatment of HEK293T cells with 10 μM PROTACs **31** – **38** or the vehicle (DMSO) control, as indicated. **a)** Structures of PROTACS **31** – **38**. **b)** Western blots of CREBBP and β-actin for the three biological repeats (n) of HEK293T cells treated with PROTACs **31** – **38** or the vehicle (DMSO) control, as indicated, for 24 h. Western Blots were analysted using Image Lab (Bio-Rad) Software and the relative protein levels were quantified using Excel (Appendix Table 6). **c)** Western blots of p300 and β-actin for the three biological repeats (n) of HEK293T cells treated with PROTACs **31** – **38** or the vehicle (DMSO) control, as indicated, for 24 h. Western Blots were analysted using Image Lab (Bio-Rad) Software and the relative protein levels were quantified using Excel (Appendix Table 7).

Appendix Table 8. Quantification of CREBBP levels in HEK293T cells treated with 10 μM HyTs **65** – **68** or the vehicle (DMSO) control for 24 h. Western blot signals were analysed using Image Lab (Bio-Rad) software then quantified using Excel. For each sample, the CREBBP signal was normalised against the β-actin loading control using equation CREBBP signal/β-actin signal, then against the corresponding vehcile (DMSO) treated sample using the equation 100 × β-actin normalised CREBBP signal/β-actin normalised DMSO CREBBP signal. This provides the relative protein level of each sample as a percentage relative to the vehicle (DMSO) control treated cells. An average (mean) was calculated for the relative protein expression value (%), and the standard deviation (SD) and standard error of the mean (SEM) were calculated. A Student's t-test was performed relative to the lipofectamine control data, and significance (sig.) is denoted as **** - $p \leq 0.0001$, *** - $p \leq 0.001$, ** - $p \leq 0.01$, * p - ≤ 0.05, ns - not statistically significant.

	n = 1				n = 2				n = 3				Mean (%)	SD	SEM	ttest	Sig.
	CREBBP	β-Actin	β-Actin normalised	DMSO normalised (%)	CREBBP	β-Actin	β-Actin normalised	DMSO normalised (%)	CREBBP	β-Actin	β-Actin normalised	DMSO normalised (%)					
DMSO	4035660	1628208	2.478589959	100.00	3509784	2027736	0.57773812	100.00	3263517	2486461	1.3125149	100.00	100.00	0.00	0.00		
65	3817590	2906376	1.313522407	52.99	3303535	2998211	0.90757658	157.09	2446200	2824752	0.8659875	65.98	92.02	46.32	26.74	0.4151	ns
66	4923265	3429576	1.435531681	57.92	2546640	2885557	1.13308399	196.12	3036744	2603810	1.1662694	88.86	114.30	59.22	34.19	0.3489	ns
67	2724680	3725011	0.731455558	29.51	2656935	2068462	0.77851434	134.75	4584384	3112774	1.4727648	112.21	92.16	45.24	26.12	0.3487	ns
68	2442880	3723375	0.656092926	26.47	1949805	2272272	1.16538423	201.71	2443440	1944504	1.2565878	95.74	107.97	72.06	41.61	0.4040	ns

Appendix Table 9. Quantification of p300 levels in HEK293T cells treated with 10 μM HyTs **65** – **68** or the vehicle (DMSO) control for 24 h. Western blot signals were analysed using Image Lab (Bio-Rad) software then quantified using Excel. For each sample, the p300 signal was normalised against the β-actin loading control using equation p300 signal/β-actin signal, then against the corresponding vehcile (DMSO) treated sample using the equation 100 × β-actin normalised p300 signal/β-actin normalised DMSO p300 signal. This provides the relative protein level of each sample as a percentage relative to the vehicle (DMSO) control treated cells. An average (mean) was calculated for the relative protein expression value (%), and the standard deviation (SD) and standard error of the mean (SEM) were calculated. A Student's t-test was performed relative to the lipofectamine control data, and significance (sig.) is denoted as **** - $p \leq 0.0001$, *** - $p \leq 0.001$, ** - $p \leq 0.01$, * p - ≤ 0.05, ns - not statistically significant.

	n = 1				n = 2				n = 3				Mean (%)	SD	SEM	ttest	Sig.
	p300	β-Actin	β-Actin normalised	DMSO normalised (%)	p300	β-Actin	β-Actin normalised	DMSO normalised (%)	p300	β-Actin	β-Actin normalised	DMSO normalised (%)					
DMSO	1759926	2400046	0.733288445	100.00	1746981	2582950	0.67635107	100.00	2244645	2249400	0.9978861	100.00	100.00	0.00	0.00		
65	1310696	3449770	0.379937213	51.81	1674702	2488301	0.67303031	99.51	1816344	2890536	0.6283762	62.97	71.43	20.37	11.76	0.0929	ns
66	1218420	3093926	0.393810324	53.70	1382238	2275656	0.607402	89.81	1793826	2814602	0.6373285	63.87	69.13	15.20	8.78	0.4523	ns
67	779289	3299340	0.236195421	32.21	1454814	2449475	0.5939289	87.81	1814778	2922380	0.6209932	62.23	60.75	22.72	13.12	0.3451	ns
68	1593548	2335100	0.682432444	93.06	1413612	2226055	0.63503013	93.89	1773846	3093040	0.573496	57.47	81.48	16.98	9.80	0.1821	ns

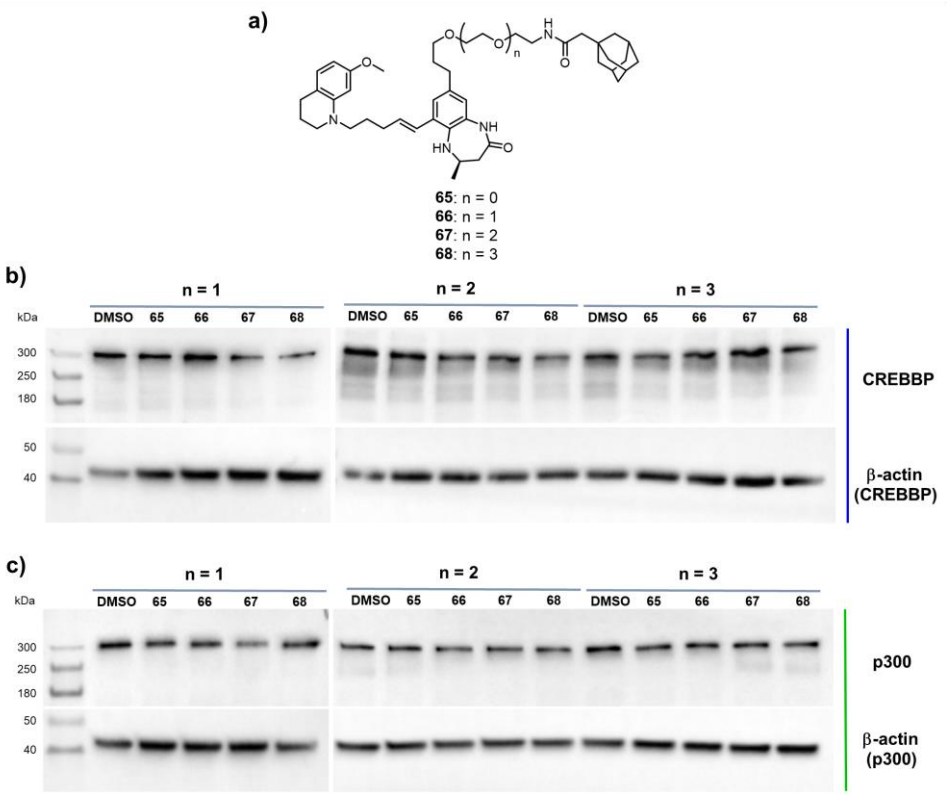

Appendix Figure 12. Wesetern blots for CREBBP, p300, and their corresponding β-actin loading control for the three biological repeats (n) of 24 h treatment of HEK293T cells with 10 μM HyTs **65** – **68** or the vehicle (DMSO) control, as indicated. **a)** Structures of HyTs **65** – **68**. **b)** Western blots of CREBBP and β-actin for the three biological repeats (n) of HEK293T cells treated with HyTs **65** – **68** or the vehicle (DMSO) control, as indicated, for 24 h. Western Blots were analysted using Image Lab (Bio-Rad) Software and the relative protein levels were quantified using Excel (Appendix Table 8). **c)** Western blots of p300 and β-actin for the three biological repeats (n) of HEK293T cells treated with HyTs **65** – **68** or the vehicle (DMSO) control, as indicated, for 24 h. Western Blots were analysted using Image Lab (Bio-Rad) Software and the relative protein levels were quantified using Excel (Appendix Table 9).

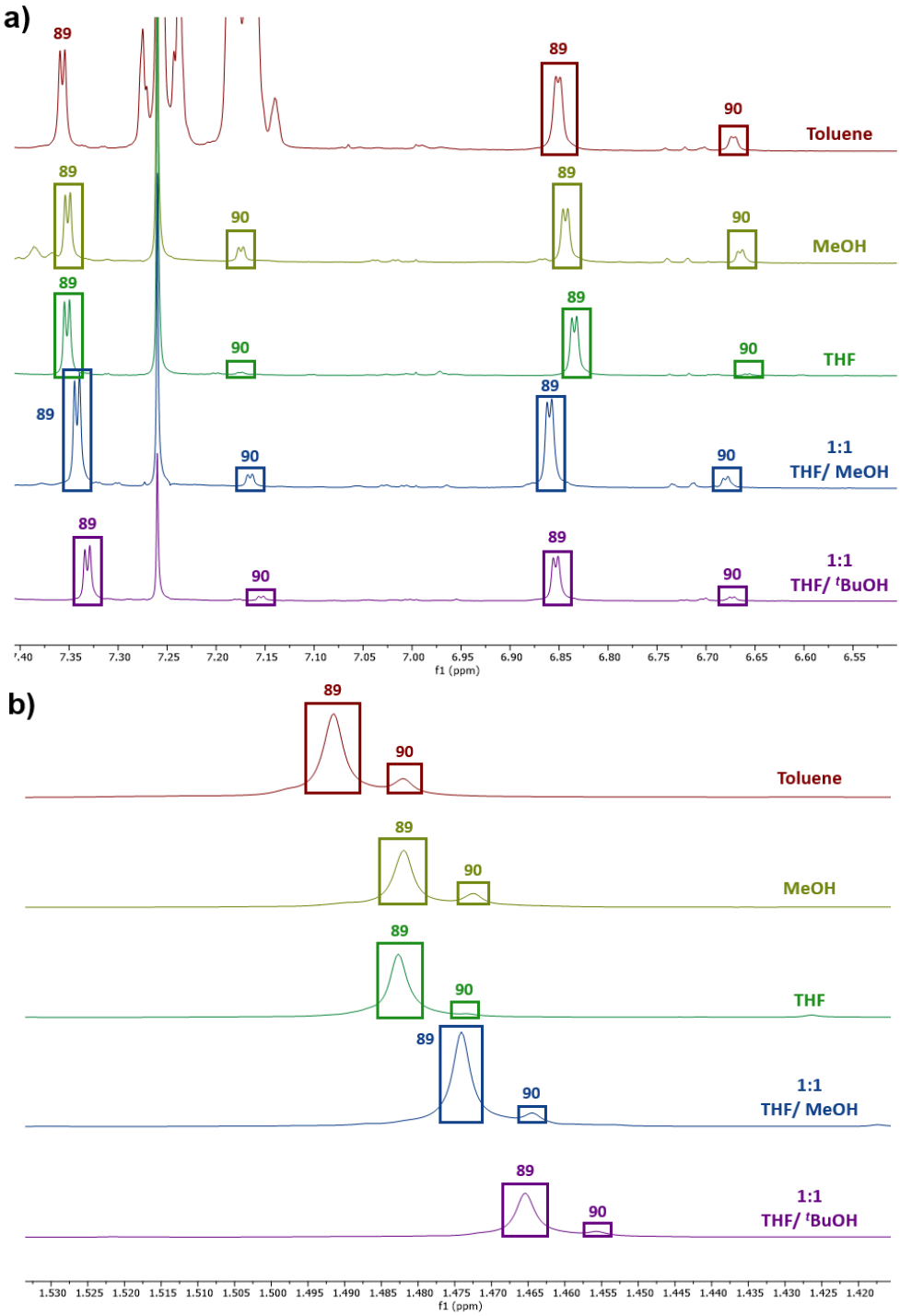

Appendix Figure 13. Stacked ^{1}H NMR traces for Wilkinson's catalysed hydrogenation of **89** to **90** using 1 atm H_2 with different solvent conditions, as indicated, at 60 °C. ^{1}H NMR traces were used to measure the % conversion of the reactions (see Table 5). Average values were calculated using the ratios of the two Ar-*H* peaks (other than for the toluene reaction where the toluene peaks obstruct one Ar-*H*) and the -C*H*$_3$ peak to calculate reaction conversion. Peaks used for the calculations are highlighted with boxes and the corresponding compound number.

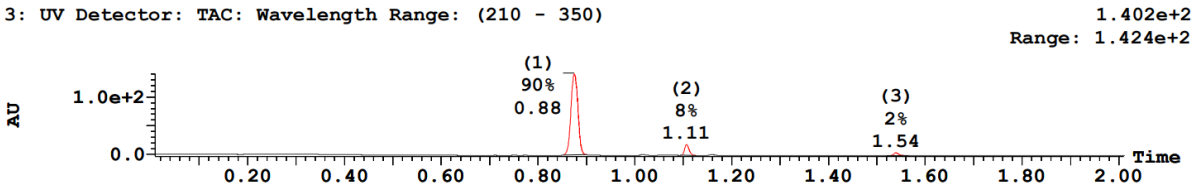

Appendix Figure 14. LCMS trace of the Alloc-deprotection of intermediate **99** to ligand **87** using $Pd(PPh_3)_4$ and K_2CO_3 in MeOH after stirring at rt for 18 h under an atmosphere of N_2. The trace shows no remaining **99** and a peak (t_R 0.88 min, *m/z* 506.2) with a 90% area corresponding to ligand **87**.

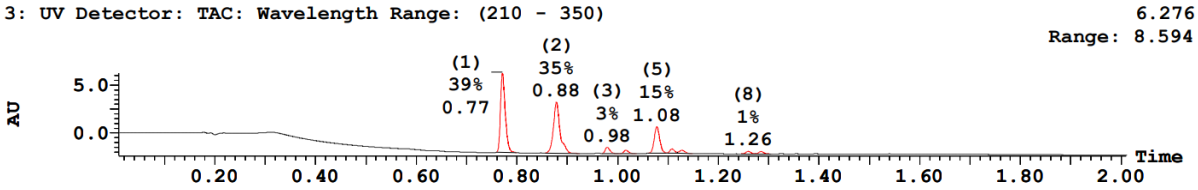

Appendix Figure 15. LCMS trace after concentrating the Alloc-deprotection of intermediate **99** to ligand **87** under a flow of nitrogen showing the formation of two major peaks corresponding to the addition of water (t_R 0.77 min, *m/z* 524.2) and the addition of methanol (t_R 1.08 min, *m/z* 538.2).

Chapter 4 Appendices

Appendix Table 10. Vinculin-normalised chemiluminescence signal areas for CREBBP and p300 over 11 technical repeats. Peak signal areas were measured using Compass for Protein Simple™ software. CREBBP was normalised to the vinculin loading control using Protein Simple™ software and p300 was normalised to the vinculin loading control using excel. A mean value of the normalised CREBBP and p300 values was determined and used to calculate the relative % of each value to the mean.

Repeats	Normalised CREBBP	% of Mean
1	196.6	100.79
2	196.3	100.65
3	200.6	102.82
4	178.2	91.33
5	185.4	95.06
6	180.7	92.64
7	185.3	94.98
8	199.3	102.15
9	191.6	98.21
10	207.2	106.22
11	224.6	115.15
Mean	195.1	

Repeats	Vinculin	p300	normalised p300	% of Mean
1	137803.3	138662.4	100.62	88.94
2	125243.8	142616.5	113.87	100.65
3	149087.7	174093.1	116.77	103.21
4	133417.5	139704.2	104.71	92.55
5	146140.2	151356.4	103.57	91.54
6	118898.5	133906.5	112.62	99.55
7	151445.2	177122.9	116.96	103.38
8	151477.5	178220.7	117.65	103.99
9	154416.9	158968.9	102.95	90.99
10	158147.6	184017.2	116.36	102.85
11	165819.7	229522.5	138.42	122.34
Mean			113.14	

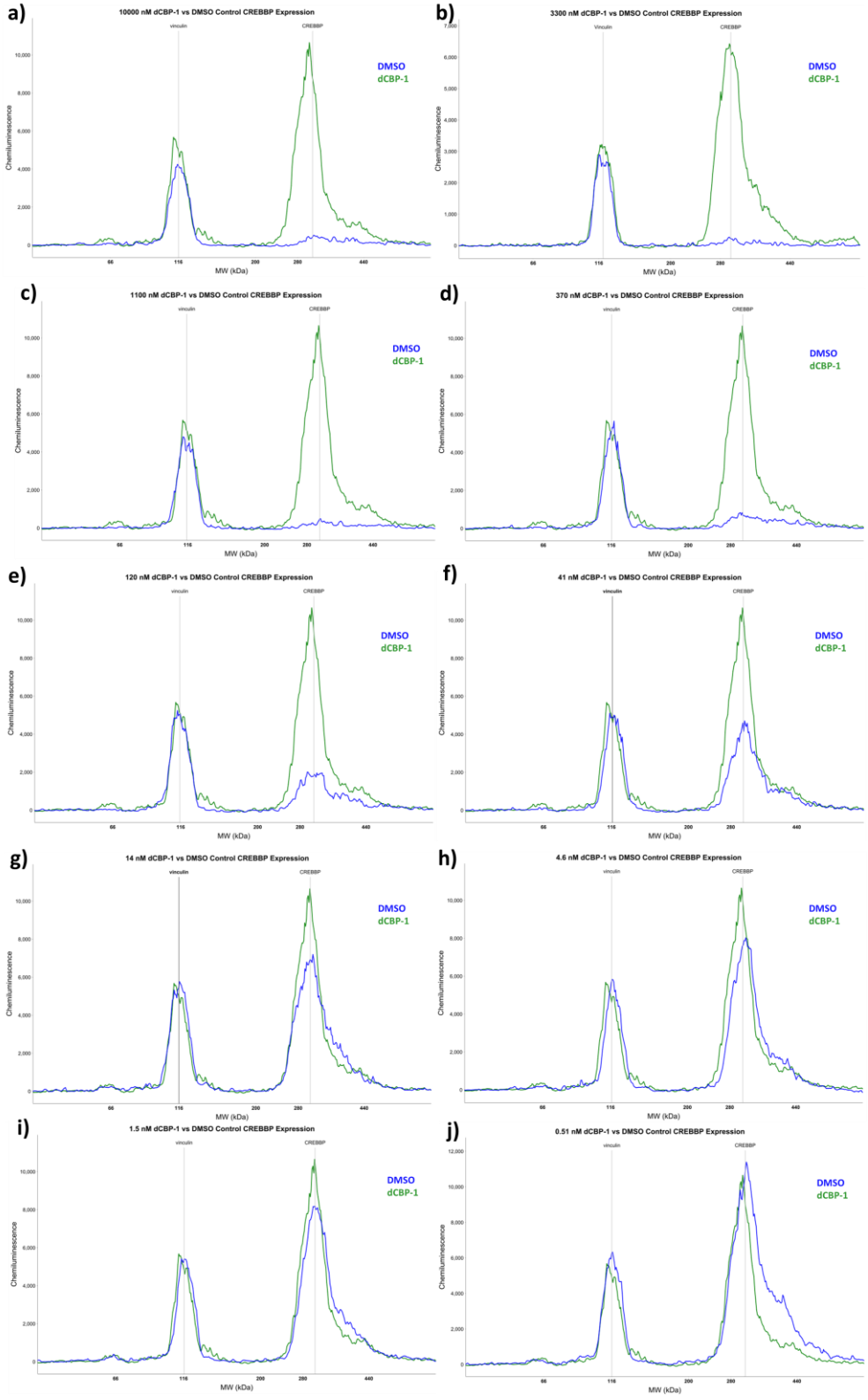

Appendix Figure 16. Representative chemiluminescence traces of CREBBP and the vinculin loading control for each of the tested concentrations of **dCBP-1** in 0.625% *v/v* DMSO overlayed with the 0.625% *v/v* DMSO control sample. In a 384-well plate, 0.01×10^6 HeLa cells/well were incubated with the compound concentration gradient for 24 h before being lysed. 1:2 diluted cell lysate in RIPA buffer was assessed for CREBBP and vinculin loading control cellular protein levels. Concentrations of **dCBP-1** are as follows: **a)** 10 μM; **b)** 3.3 μM; **c)** 1.1 μM; **d)** 370 nM; **e)** 120 nM; **f)** 41 nM; **g)** 14 nM; **h)** 4.6 nM; **i)** 1.5 nM; **j)** 0.51 nM.

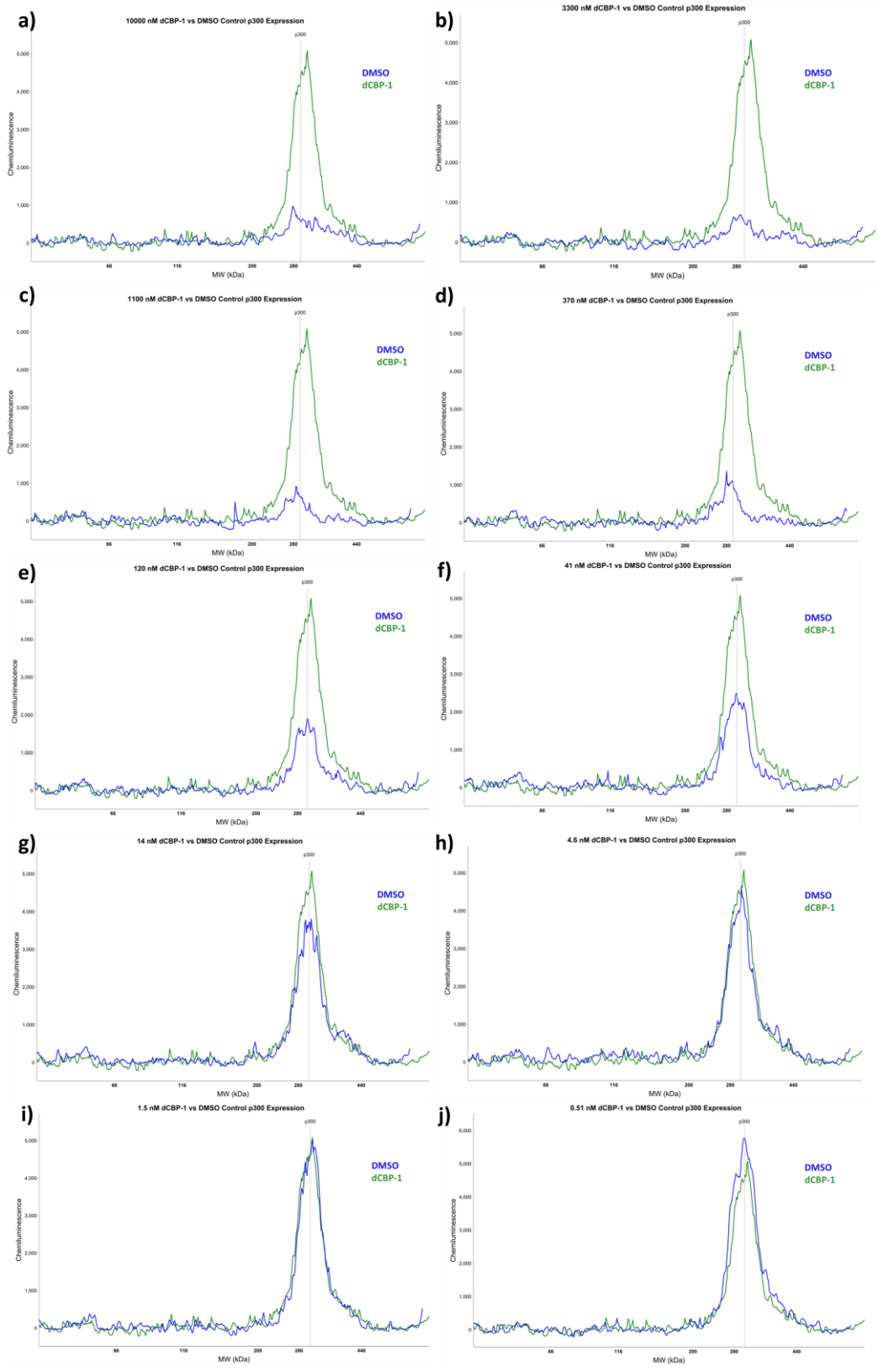

Appendix Figure 17. Representative chemiluminescence traces of p300 for each of the tested concentrations of **dCBP-1** in 0.625% *v/v* DMSO overlayed with the 0.625% DMSO control sample. In a 384-well plate, 0.01×10^6 HeLa cells/well were incubated with the compound concentration gradient for 24 h before being lysed. Neat cell lysate was assessed for p300 cellular protein levels using modified assay run times to decrease stacking time and increase separation time. Concentrations of **dCBP-1** are as follows: **a)** 10 μM; **b)** 3.3 μM; **c)** 1.1 μM; **d)** 370 nM; **e)** 120 nM; **f)** 41 nM; **g)** 14 nM; **h)** 4.6 nM; **i)** 1.5 nM; **j)** 0.51 nM.

Appendix Table 11. Quantification of relative CREBBP levels in HeLa cells treated for 24 h with a gradient of 0.51 nM – 10 μM of literature PROTAC **dCBP-1** in 0.625% v/v DMSO.[133] Data shown is each sample quantified relative to the vinculin loading control and then relative to the vinculin-standardised 0.625% v/v DMSO treated cells. An average (mean) was taken as the relative protein level, and the standard deviation (SD) and standard error of the mean (SEM) were calculated. A Student's t-test was performed relative to the vinculin-standardised DMSO control data, and significance is denoted as *** - $p \leq 0.001$, ** - $p \leq 0.01$, * - $p \leq 0.05$, n.s – not statistically significant. Data analysed using Excel.

Concentration	n = 1	n = 2	n = 3	Average	SD	SEM	Ttest	Significance
1.00E-05	4.0799	8.9438	6.1171	6.3803	1.9944	1.1515	0.0003	***
3.33E-06	2.9203	4.6183	4.5082	4.0156	0.7758	0.4479	0.0007	***
1.11E-06	4.6567	4.3867	3.9825	4.3420	0.2771	0.1600	0.0008	***
3.70E-07	8.0299	9.9602	10.4812	9.4905	1.0544	0.6088	0.0007	***
1.23E-07	21.0252	27.3191	25.1012	24.4819	2.6065	1.5049	0.0003	***
4.12E-08	41.9243	51.5528	50.3536	47.9436	4.2843	2.4736	0.0004	***
1.37E-08	78.9286	66.9546	75.1548	73.6793	4.9985	2.8859	0.0054	**
4.57E-09	108.8804	61.4422	83.1268	84.4831	19.3903	11.1950	0.2251	n.s.
1.52E-09	108.1191	102.3558	91.9767	100.8172	6.6793	3.8563	0.3004	n.s.
5.08E-10	124.2254	100.3637	111.1337	111.9076	9.7569	5.6331	0.0793	n.s.
DMSO	98.1238	103.5893	90.3414	97.3515	5.4360	3.1385		

Appendix Table 12. Quantification of relative p300 levels in HeLa cells treated for 24 h with a gradient of 0.51 nM – 10 μM of literature PROTAC **dCBP-1** in 0.625% v/v DMSO.[133] Data shown is each sample quantified relative to the vinculin loading control and then relative to the vinculin-standardised 0.625% v/v DMSO treated cells. An average (mean) was taken as the relative protein level, and the standard deviation (SD) and standard error of the mean (SEM) were calculated. A Student's t-test was performed relative to the vinculin-standardised DMSO control data, and significance is denoted as *** - $p \leq 0.001$, ** - $p \leq 0.01$, * - $p \leq 0.05$, n.s – not statistically significant. Data analysed using Excel.

Concentration	n = 1	n = 2	n = 3	Average	SD	SEM	Ttest	Significance
1.00E-05	51.35837607	23.53703371	32.75926335	35.88489104	11.57105394	6.6806	0.003113049	**
3.33E-06	59.14692737	16.08828774	15.92906195	30.38809235	20.33567115	11.7408	0.012830806	*
1.11E-06	62.01988565	14.18430467	15.05851699	30.42090244	22.34670545	12.9019	0.017204271	*
3.70E-07	57.82629856	22.50279381	21.98377476	34.10428904	16.77533203	9.6852	0.008073929	**
1.23E-07	82.06260662	31.84217761	40.83771001	51.58083141	21.86448971	12.6235	0.041183255	*
4.12E-08	90.54048673	41.47918051	58.53328029	63.51764917	20.33692687	11.7415	0.06815866	n.s.
1.37E-08	79.68043502	63.40254683	77.60439321	73.56245835	7.233963367	4.1765	0.043460299	*
4.57E-09	85.45908858	103.7342085	105.8479355	98.34707754	9.153948328	5.2850	0.427933961	n.s.
1.52E-09	87.03456456	110.6655732	109.3809056	102.3603478	10.84964873	6.2640	0.308527468	n.s.
5.08E-10	54.94270762	96.96091509	118.6762988	90.19330718	26.45553565	15.2741	0.392179421	n.s.
DMSO	84.44513056	92.89948372	111.6784721	96.34102878	11.38118028	6.5709		

Chapter 5 Appendices

Appendix Table 13. Quantification of relative CREBBP levels in HeLa cells treated for 24 h with a gradient of 0.51 nM – 10 μM of PROTAC **144** in 0.625% *v/v* DMSO. Data shown is each sample quantified relative to the vinculin loading control and then relative to the vinculin-standardised 0.625% *v/v* vehicle (DMSO) treated cells. An average (mean) was taken as the relative protein level, and the standard deviation (SD) and standard error of the mean (SEM) were calculated. A Student's t-test was performed relative to the vinculin-standardised DMSO control data, and significance is denoted as *** - $p \leq 0.001$, ** - $p \leq 0.01$, * - $p \leq 0.05$, n.s – not statistically significant. Data analysed using Excel.

Concentration	n = 1	n = 2	n = 3	Average	SD	SEM	Ttest	Signifigance
1.00E-05	138.8349	137.3756	118.6035	131.6047	9.2125	5.3188	0.0118	*
3.33E-06	110.5676	95.2283	81.8812	95.8924	11.7206	6.7669	0.4297	n.s.
1.11E-06	55.2976	63.4207	50.6741	56.4641	5.2688	3.0419	0.0007	***
3.70E-07	57.6321	52.5593	51.6346	53.9420	2.6364	1.5221	0.0001	***
1.23E-07	73.9729	76.2449	59.9291	70.0489	7.2157	4.1660	0.0091	**
4.12E-08	97.7619	85.9543	79.6803	87.7988	7.4961	4.3279	0.0989	n.s.
1.37E-08	96.2042	113.7126	80.8490	96.9219	13.4261	7.7515	0.4753	n.s.
4.57E-09	94.2828	115.7208	99.4581	103.1539	9.1339	5.2734	0.2446	n.s.
1.52E-09	105.3405	111.4827	84.2076	100.3436	11.6822	6.7447	0.3881	n.s.
5.08E-10	97.2283	124.0095	107.9375	109.7251	11.0062	6.3544	0.1278	n.s.
DMSO	101.4638	98.3135	93.0186	97.5986	3.4846	2.0118		

Appendix Table 14. Quantification of relative p300 levels in HeLa cells treated for 24 h with a gradient of 0.51 nM – 10 μM of PROTAC **144** in 0.625% *v/v* DMSO. Data shown is each sample quantified relative to the vinculin loading control and then relative to the vinculin-standardised 0.625% *v/v* vehicle (DMSO) treated cells. An average (mean) was taken as the relative protein level, and the standard deviation (SD) and standard error of the mean (SEM) were calculated. A Student's t-test was performed relative to the vinculin-standardised DMSO control data, and significance is denoted as *** - $p \leq 0.001$, ** - $p \leq 0.01$, * - $p \leq 0.05$, n.s – not statistically significant. Data analysed using Excel.

Concentration	n = 1	n = 2	n = 3	Average	SD	SEM	Ttest	Signifigance
1.00E-05	155.3682069	119.227586	100.5068085	125.0342005	22.77031454	13.1464	0.079556319	n.s.
3.33E-06	104.494169	85.88958254	72.26706647	87.55027267	13.20896042	7.6262	0.394372669	n.s.
1.11E-06	86.0492822	81.64872771	61.52700196	76.40833729	10.67494968	6.1632	0.133626583	n.s.
3.70E-07	79.66357798	62.67891553	65.20176095	69.18141815	7.483223159	4.3204	0.054371164	n.s.
1.23E-07	100.1443889	74.6912772	80.30225926	85.04597513	10.9191683	6.3042	0.311787888	n.s.
4.12E-08	93.15507354	69.56939016	91.28658894	84.67035088	10.7052034	6.1807	0.300168958	n.s.
1.37E-08	99.89621493	79.99009611	93.95489446	91.28040183	8.343783103	4.8173	0.496777965	n.s.
4.57E-09	86.81491294	90.76017871	93.53410964	90.36973376	2.756959256	1.5917	0.466848622	n.s.
1.52E-09	130.1781198	86.68348414	91.36953518	102.7437131	19.49315735	11.2544	0.261681265	n.s.
5.08E-10	147.4247161	98.80419216	139.1140757	128.4476613	21.2339058	12.2594	0.057554387	n.s.
DMSO	95.37931515	74.6385749	103.5522433	91.19004445	12.169978	7.0263		

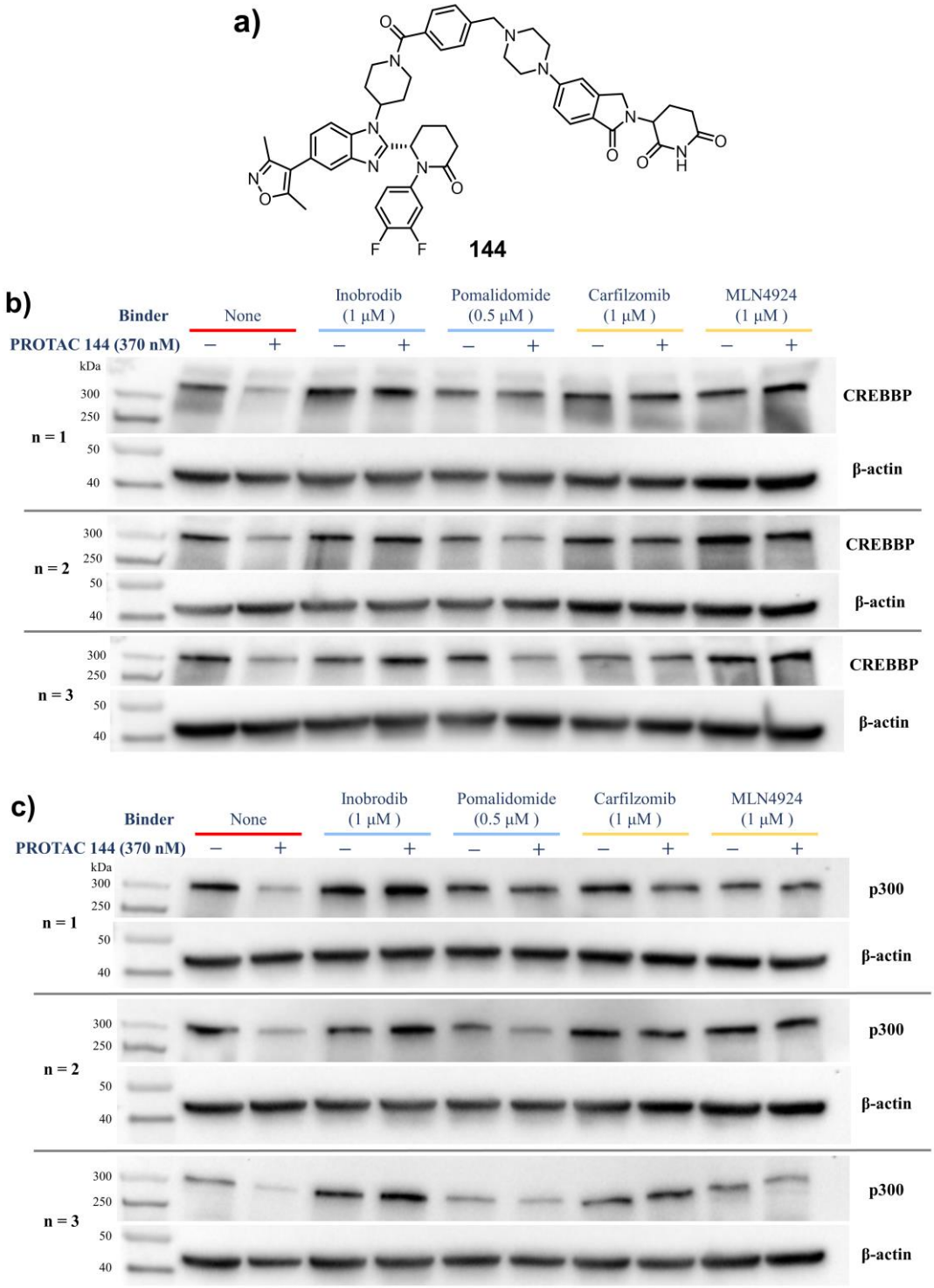

Appendix Figure 18. Assessment of the ability of PROTAC **144** to degrade CREBBP and p300 and investigation into the PROTAC's mechanism of action. Assays were performed using HeLa cells as three biological repeats. Cells were preincubated with the relevant binder or the vehicle (DMSO) control at the given concentrations for 4 h before the addition of (±) PROTAC **144** (370 nM). The cells were incubated for a further 24 h before being harvested and lysed. Cells treated the PROTAC alone were pre-treated with 1% *v/v* DMSO for 4 h before the addition of PROTAC **144** (370 nM). Following cell lysis, protein levels were assessed using western blotting. **a)** Structure of PROTAC **144**. **b)** Western blots for the three biological repeats (n) showing CREBBP and the corresponding β-actin loading control bands. PROTAC **144** activity assays highlighted in red, PROTAC **144** target engagement assays highlighted in light blue, PROTAC **144** degradation pathway

investigation assays highlighted in yellow. Blot images obtained using Image Lab Software. **c)** Western blots for the three biological repeats (n) showing p300 and the corresponding β-actin loading control bands. PROTAC **144** activity assays highlighted in red, PROTAC **144** target engagement assays highlighted in light blue, PROTAC **144** degradation pathway investigation assays highlighted in yellow. Blot images obtained using Image Lab Software.

Appendix Table 15. Quantification of relative CREBBP levels in HeLa cells treated with the vehicle (DMSO) control, PROTAC **144** (370 nM), **Inobrodib** (1 μM), **Inobrodib** (1 μM) + PROTAC **144** (370 nM), **pomalidomide** (1 μM), **pomalidomide** (1 μM) + PROTAC **144** (370 nM), **Carfilzomib** (500 nM), **Carfilzomib** (500 nM) + PROTAC **144** (370 nM), **MLN4924** (1 μM), or **MLN4924** (1 μM) + PROTAC **144** (370 nM). Cells were preincubated with the relevant binder before the addition of (±) PROTAC **144**. Western blot signals were analysed using Image Lab (Bio-Rad) software then quantified using Excel. For each sample, the CREBBP signal was normalised against the β-actin loading control using equation **CREBBP signal/β-actin signal**, then against the corresponding vehcile (DMSO) treated sample using the equation **100 × β-actin normalised CREBBP signal/β-actin normalised DMSO CREBBP signal**. This provides the relative protein level of each sample as a percentage relative to the vehicle (DMSO) control treated cells. An average (mean) was calculated for the relative protein expression value (%), and the standard deviation (SD) and standard error of the mean (SEM) were calculated. A Student's t-test was performed relative to the lipofectamine control data, and significance (sig.) is denoted as **** - $p \leq 0.0001$, *** - $p \leq 0.001$, ** - $p \leq 0.01$, * p - ≤ 0.05, ns - not statistically significant.

	n = 1				n = 2				n = 3								
	CREBBP	β-actin	β-Actin normalised	DMSO normalised (%)	CREBBP	β-actin	β-Actin normalised	DMSO normalised (%)	CREBBP	β-actin	β-Actin normalised	DMSO normalised (%)	Mean (%)	SD	SEM	t-test	Sig.
DMSO	3074346	9043281	0.339959137	100.00	3200556	4509612	0.709718708	100.00	1678123	5654880	0.296756607	100.00	100.00	0.00	0.00	-	-
370 nM Compound	1194399	8469370	0.14102572	41.48	1415640	5900538	0.239917106	33.80	514192	4763649	0.107940782	36.37	37.22	3.91	2.26	0.00064	***
1 μM Inobrodib	2509698	7811810	0.321269719	94.50	3545400	4841028	0.732365109	103.19	2269510	5224882	0.43436579	146.37	114.69	27.78	16.04	0.22823	ns
1 μM Inobrodib + 370 nM Compound	3130064	6109018	0.512367782	150.71	2945440	5941515	0.495738881	69.85	2107812	4540462	0.46422853	156.43	125.67	48.42	27.96	0.22775	ns
1 μM Pomalidomide	2499250	5730270	0.436148733	128.29	1716960	5278827	0.325254076	45.83	1158220	4224058	0.274196046	92.40	88.84	41.35	23.87	0.34307	ns
1 μM Pomalidomide + 370 nM Compound	1413510	7017158	0.201436251	59.25	1208400	5688898	0.212413722	29.93	1285500	4425102	0.290501778	97.89	62.36	34.09	19.68	0.09796	ns
500 nM Carfilzomib	2221593	6378120	0.348314707	102.46	2635476	7587300	0.347353604	48.94	1756048	5267892	0.333349279	112.33	87.91	34.11	19.69	0.30089	ns
500 nM Carfilzomib + 370 nM Compound	1998864	7073913	0.282568361	83.12	2201160	7048611	0.312282803	44.00	1525230	5804370	0.262772704	88.55	71.89	24.30	14.03	0.09152	ns
1 μM MLN4924	3858368	8403156	0.459157012	135.06	3685815	8320923	0.44295747	62.41	1616526	6355936	0.254333272	85.70	94.39	37.10	21.42	0.40899	ns
1 μM MLN4924 + 370 nM Compound	2893128	7998126	0.361725734	106.40	3517890	8323187	0.422661416	59.55	2575636	8330350	0.309187009	104.19	90.05	26.43	15.26	0.29063	ns

Appendix Table 16. Quantification of relative CREBBP levels in HeLa cells treated with the vehicle (DMSO) control, PROTAC **144** (370 nM), **Inobrodib** (1 μM), **Inobrodib** (1 μM) + PROTAC **144** (370 nM), **pomalidomide** (1 μM), **pomalidomide** (1 μM) + PROTAC **144** (370 nM), **Carfilzomib** (500 nM), **Carfilzomib** (500 nM) + PROTAC **144** (370 nM), **MLN4924** (1 μM), or **MLN4924** (1 μM) + PROTAC **144** (370 nM). Cells were preincubated with the relevant binder before the addition of (±) PROTAC **144**. Western blot signals were analysed using Image Lab (Bio-Rad) software then quantified using Excel. For each sample, the p300 signal was normalised against the β-actin loading control using equation **p300 signal/β-actin signal**, then against the corresponding vehcile (DMSO) treated sample using the equation **100 × β-actin normalised p300 signal/β-actin normalised DMSO p300 signal**. This provides the relative protein level of each sample as a percentage relative to the vehicle (DMSO) control treated cells. An average (mean) was calculated for the relative protein expression value (%), and the standard deviation (SD) and standard error of the mean (SEM) were calculated. A Student's t-test was performed relative to the lipofectamine control data, and significance (sig.) is denoted as **** - $p \leq 0.0001$, *** - $p \leq 0.001$, ** - $p \leq 0.01$, * p - ≤ 0.05, ns - not statistically significant.

	n = 1				n = 2				n = 3								
	p300	β-actin	β-Actin normalised	DMSO normalised (%)	p300	β-actin	β-Actin normalised	DMSO normalised (%)	p300	β-actin	β-Actin normalised	DMSO normalised (%)	Mean (%)	SD	SEM	t-test	Sig.
DMSO	1674942	6079088	0.27552521	100.00	3617090	7176975	0.503985314	100.00	3699840	5739300	0.644650044	100.00	100.00	0.00	0.00	-	-
370 nM Compound	277740	3934735	0.07058671	25.62	976701	6452820	0.151360335	30.03	1005300	5985088	0.167967455	26.06	27.24	2.43	1.40	0.00019	***
1 μM Inobrodib	3180848	5357052	0.593768364	215.50	2413830	5787900	0.417047634	82.75	4544490	6404160	0.709615313	110.08	136.11	70.10	40.47	0.23321	ns
1 μM Inobrodib + 370 nM Compound	4166016	4853280	0.85839185	311.55	3738900	5397116	0.692758873	137.46	5108970	6166206	0.828543516	128.53	192.51	103.19	59.57	0.13033	ns
1 μM Pomalidomide	1403724	4932026	0.284614071	103.30	1611090	5436576	0.296342772	58.80	2983008	5755588	0.518280322	80.40	80.83	22.25	12.85	0.13712	ns
1 μM Pomalidomide + 370 nM Compound	722610	4424867	0.163306603	59.27	1021020	5602873	0.182231509	36.16	2844237	6237665	0.455977838	70.73	55.39	17.61	10.17	0.02411	*
500 nM Carfilzomib	2393362	5261400	0.454890713	165.10	3112768	6611197	0.47083274	93.42	4212224	7217656	0.583599994	90.53	116.35	42.24	24.39	0.28582	ns
500 nM Carfilzomib + 370 nM Compound	2912130	4574988	0.636532817	231.03	3084120	7479612	0.412336897	81.82	2793952	6915720	0.404000162	62.67	125.17	92.17	53.22	0.34141	ns
1 μM MLN4924	1904970	6472558	0.29431486	106.82	3732260	7863721	0.474617551	94.17	2474577	6859790	0.360736553	55.96	85.65	26.48	15.29	0.22351	ns
1 μM MLN4924 + 370 nM Compound	1198320	6618096	0.181067183	65.72	3390210	8295437	0.408683714	81.09	2177631	6348300	0.343025849	53.21	66.67	13.96	8.06	0.02692	*

NMR Spectra of Novel Compounds

(4*R*)-8-(5-Hydroxypentyl)-6-((1*E*)-5-(7-methoxy-3,4-dihydroquinolin-1(2*H*)-yl)pent-1-en-1-yl)-4-methyl-1,3,4,5-tetrahydro-2*H*-1,5-benzodiazepin-2-one (2)

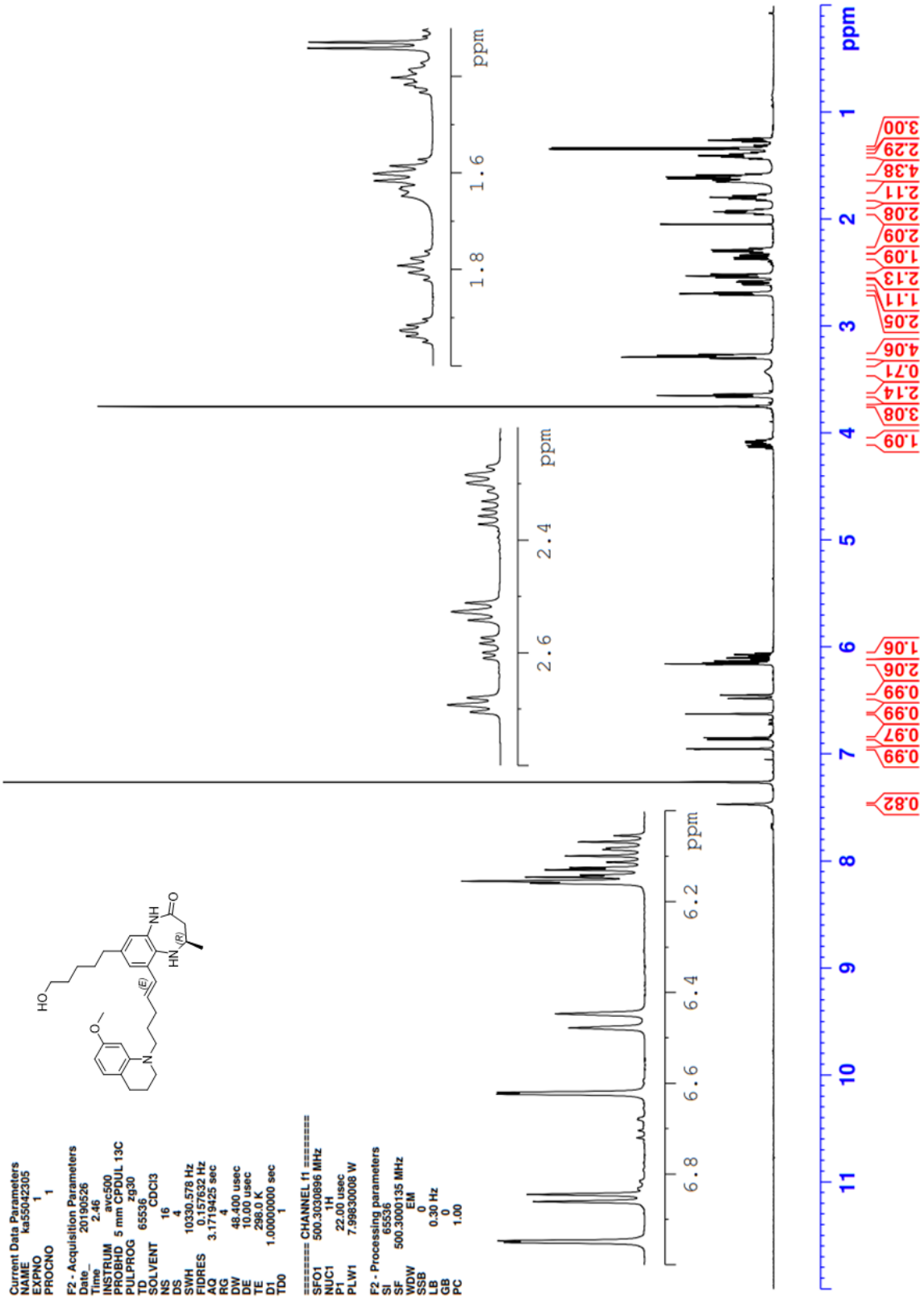

(4*R*)-8-(5-Hydroxypentyl)-6-((1*E*)-5-(7-methoxy-3,4-dihydroquinolin-1(2*H*)-yl)pent-1-en-1-yl)-4-methyl-1,3,4,5-tetrahydro-2*H*-1,5-benzodiazepin-2-one (2)

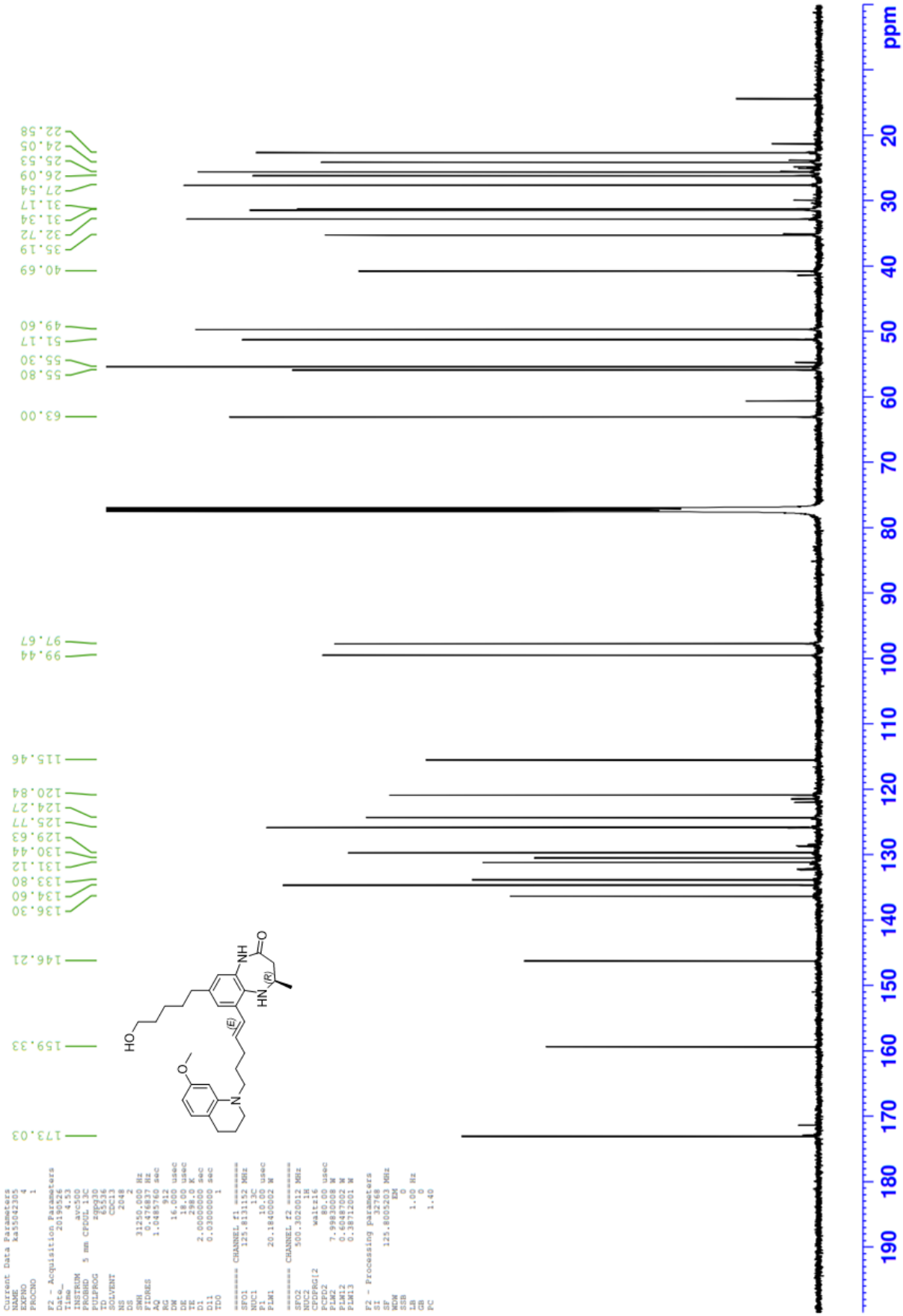

(4*R*)-8-(5-Hydroxypent-1-yn-1-yl)-6-((1*E*)-5-(7-methoxy-3,4-dihydroquinolin-1(2*H*)-yl)pent-1-en-1-yl)-4-methyl-1,3,4,5-tetrahydro-2*H*-1,5-benzodiazepin-2-one (3)

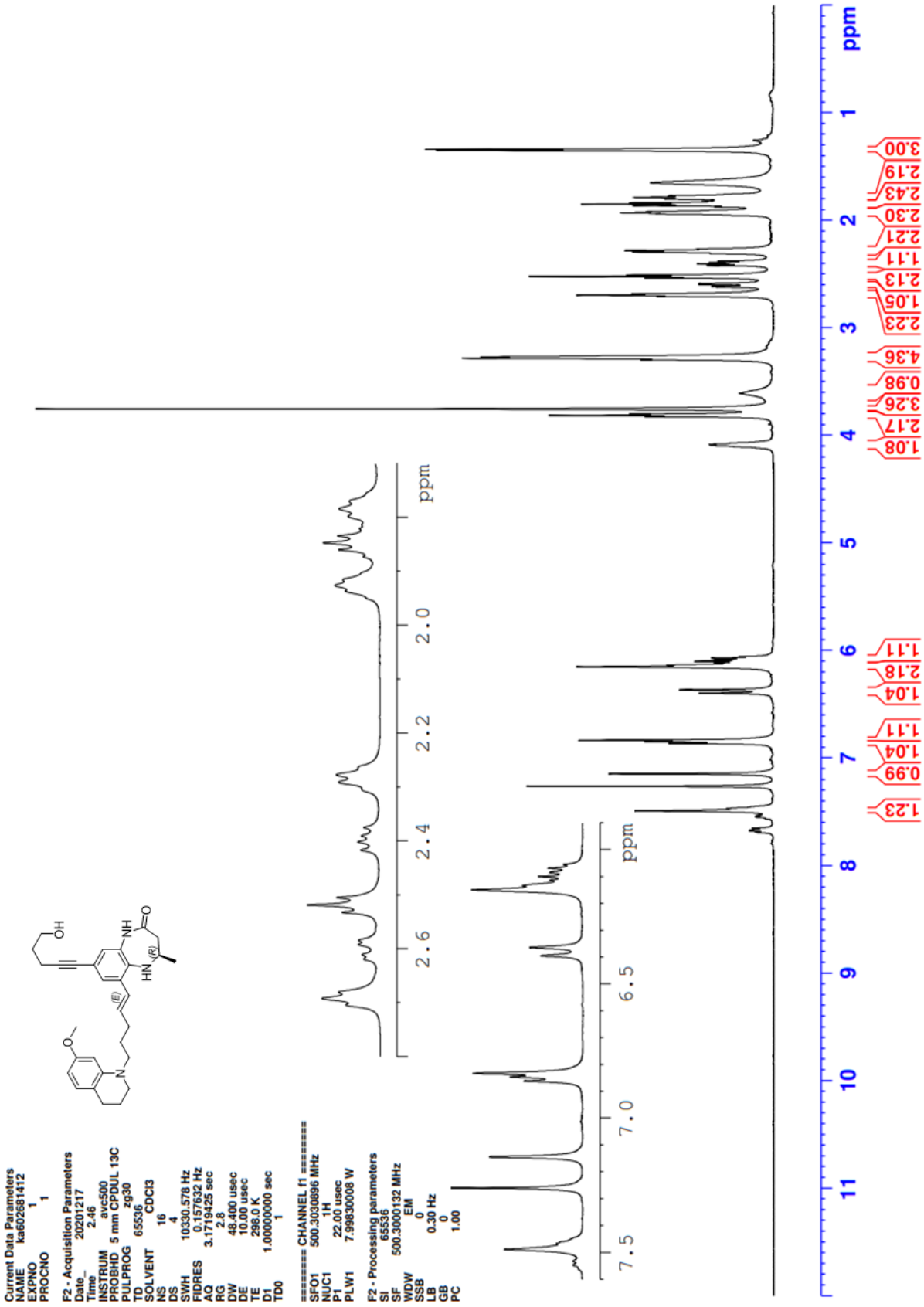

(4*R*)-8-(5-Hydroxypent-1-yn-1-yl)-6-((1*E*)-5-(7-methoxy-3,4-dihydroquinolin-1(2*H*)-yl)pent-1-en-1-yl)-4-methyl-1,3,4,5-tetrahydro-2*H*-1,5-benzodiazepin-2-one (3)

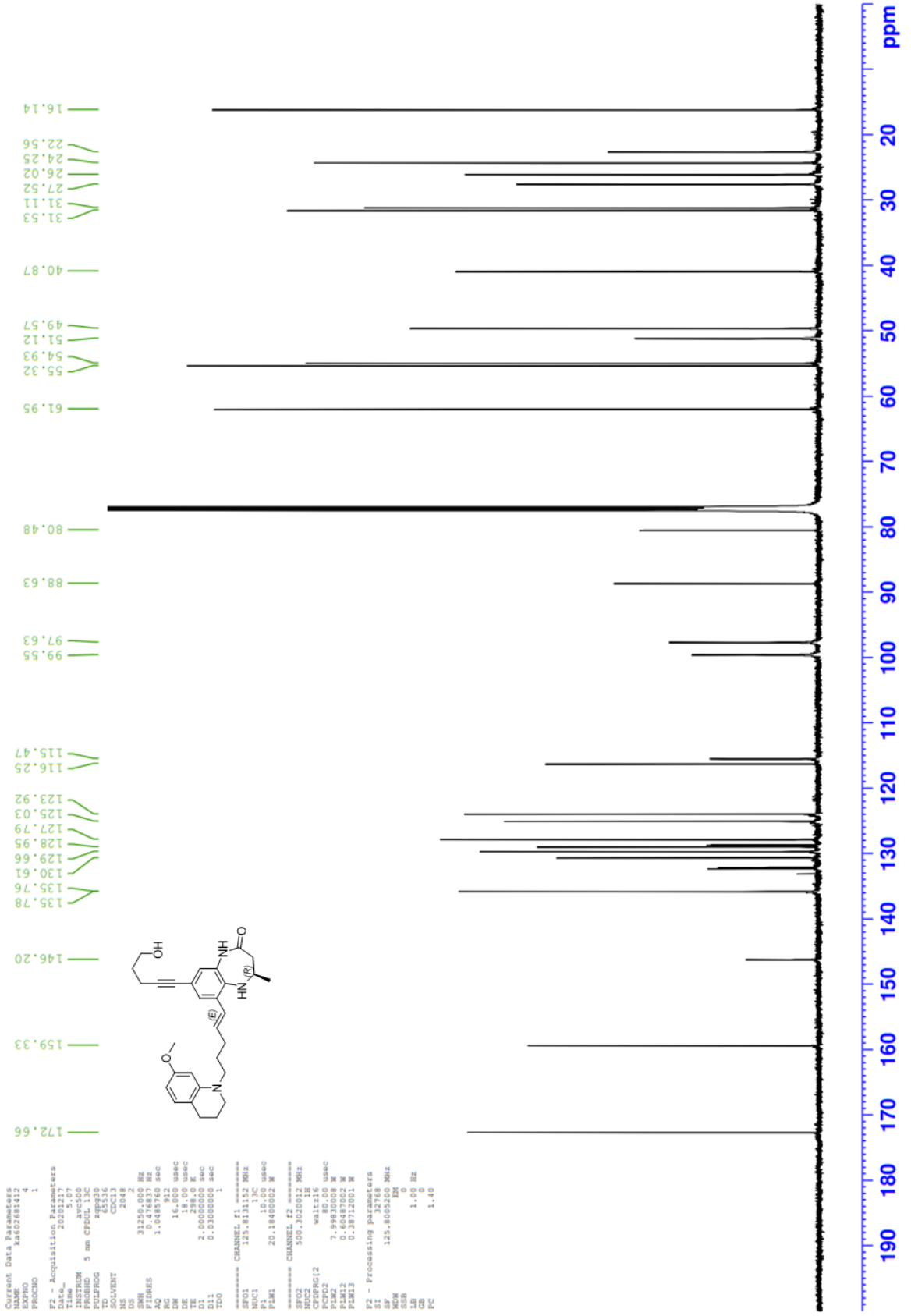

(4*R*)-6-Bromo-8-(3-hydroxyprop-1-yn-1-yl)-4-methyl-1,3,4,5-tetrahydro-2*H*-1,5-benzodiazepin-2-one (27)

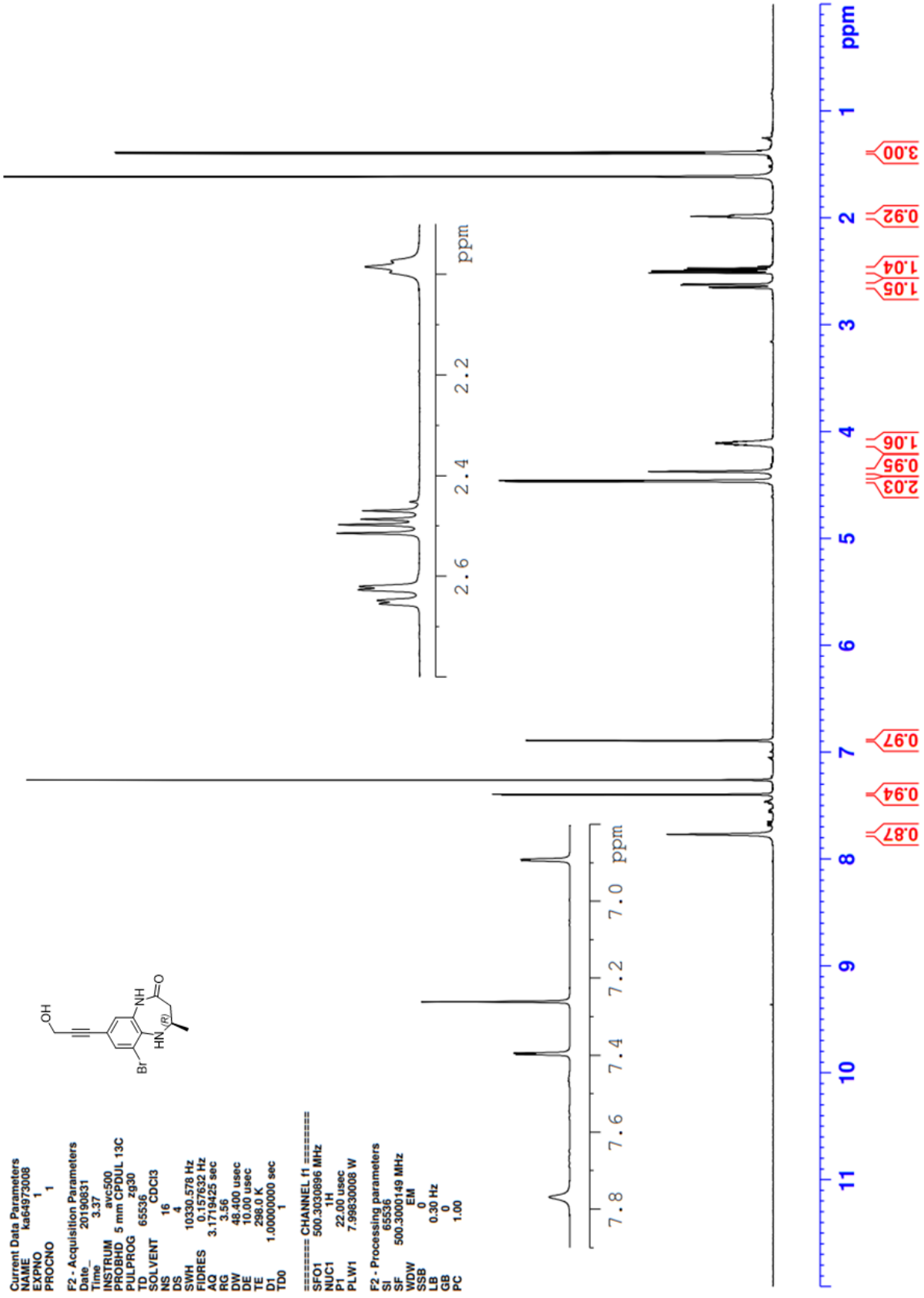

(4*R*)-6-Bromo-8-(3-hydroxyprop-1-yn-1-yl)-4-methyl-1,3,4,5-tetrahydro-2*H*-1,5-benzodiazepin-2-one (27)

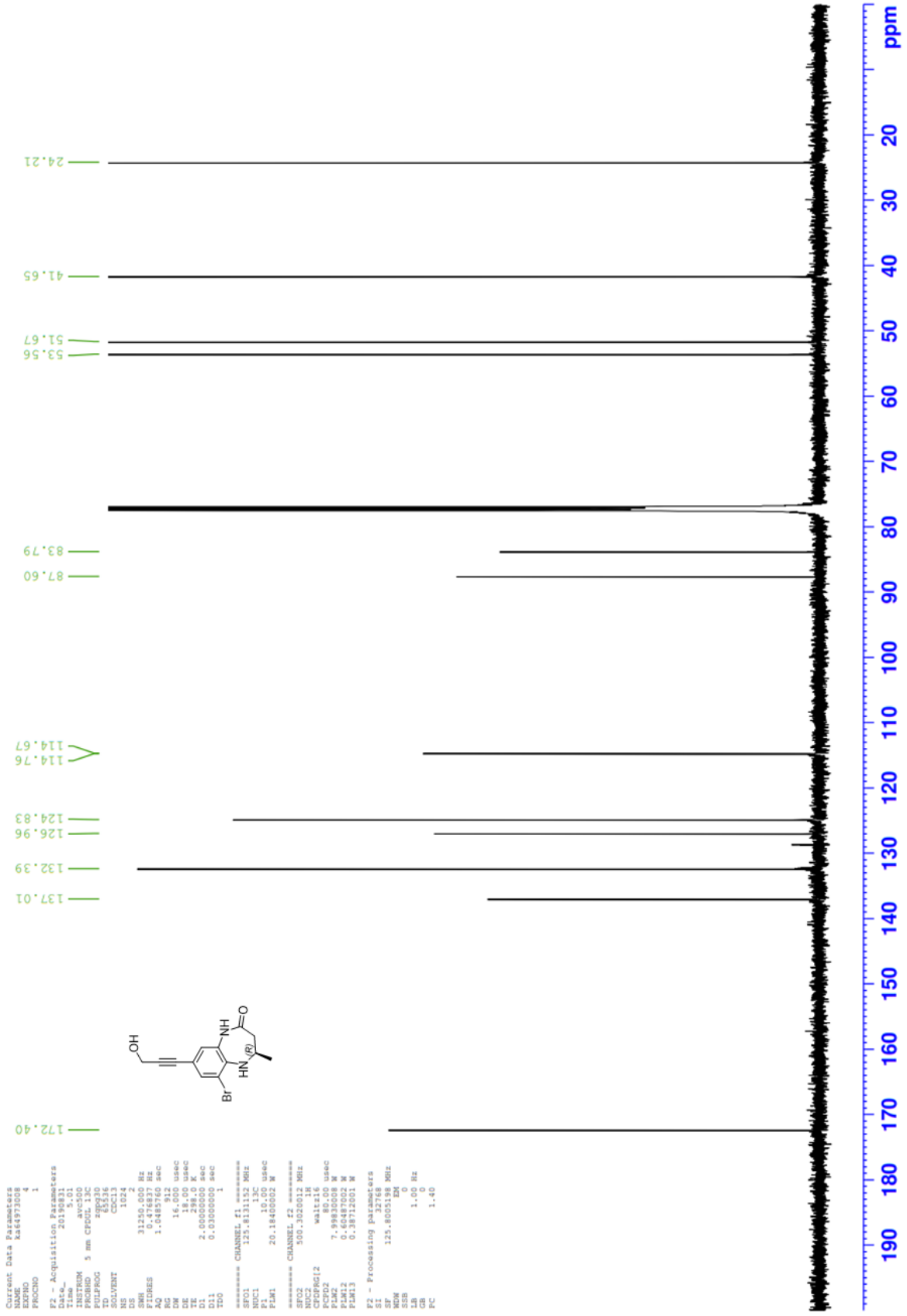

(4*R*)-6-Bromo-8-(10-hydroxydec-1-yn-1-yl)-4-methyl-1,3,4,5-tetrahydro-2*H*-1,5-benzodiazepin-2-one (28)

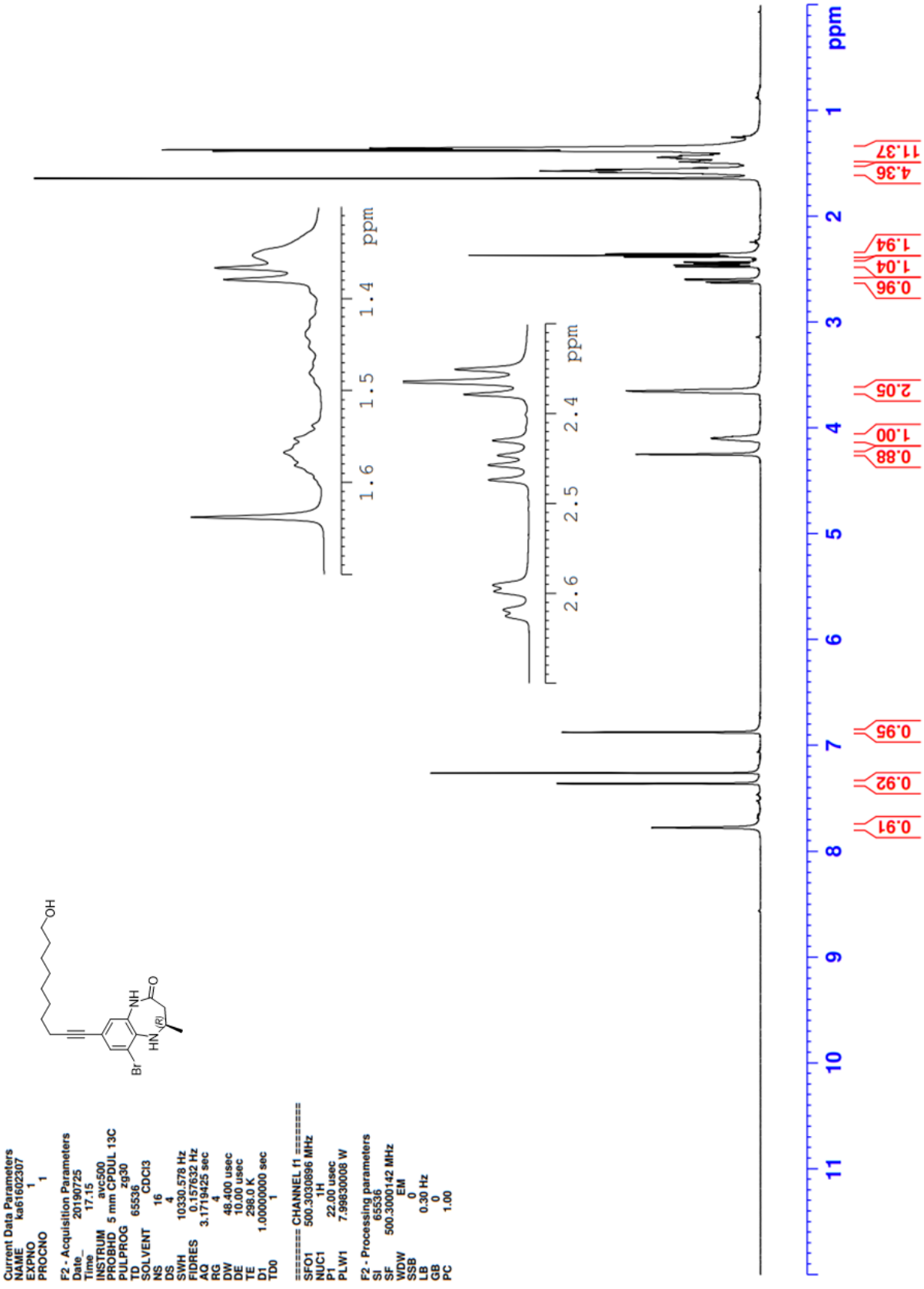

(4*R*)-6-Bromo-8-(10-hydroxydec-1-yn-1-yl)-4-methyl-1,3,4,5-tetrahydro-2*H*-1,5-benzodiazepin-2-one (28)

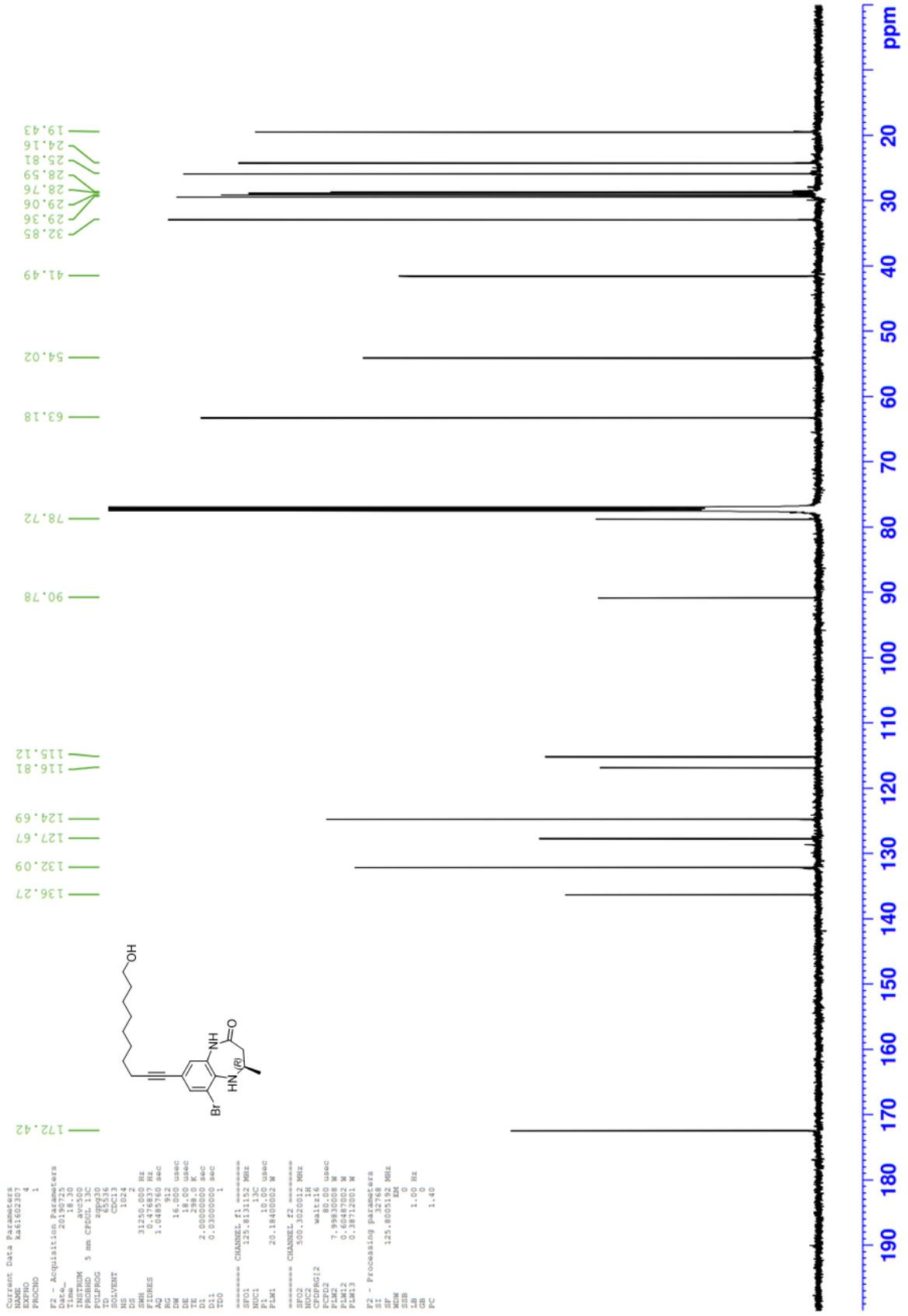

(4*R*)-6-Bromo-8-(3-hydroxypropyl)-4-methyl-1,3,4,5-tetrahydro-2*H*-1,5-benzodiazepin-2-one

(29)

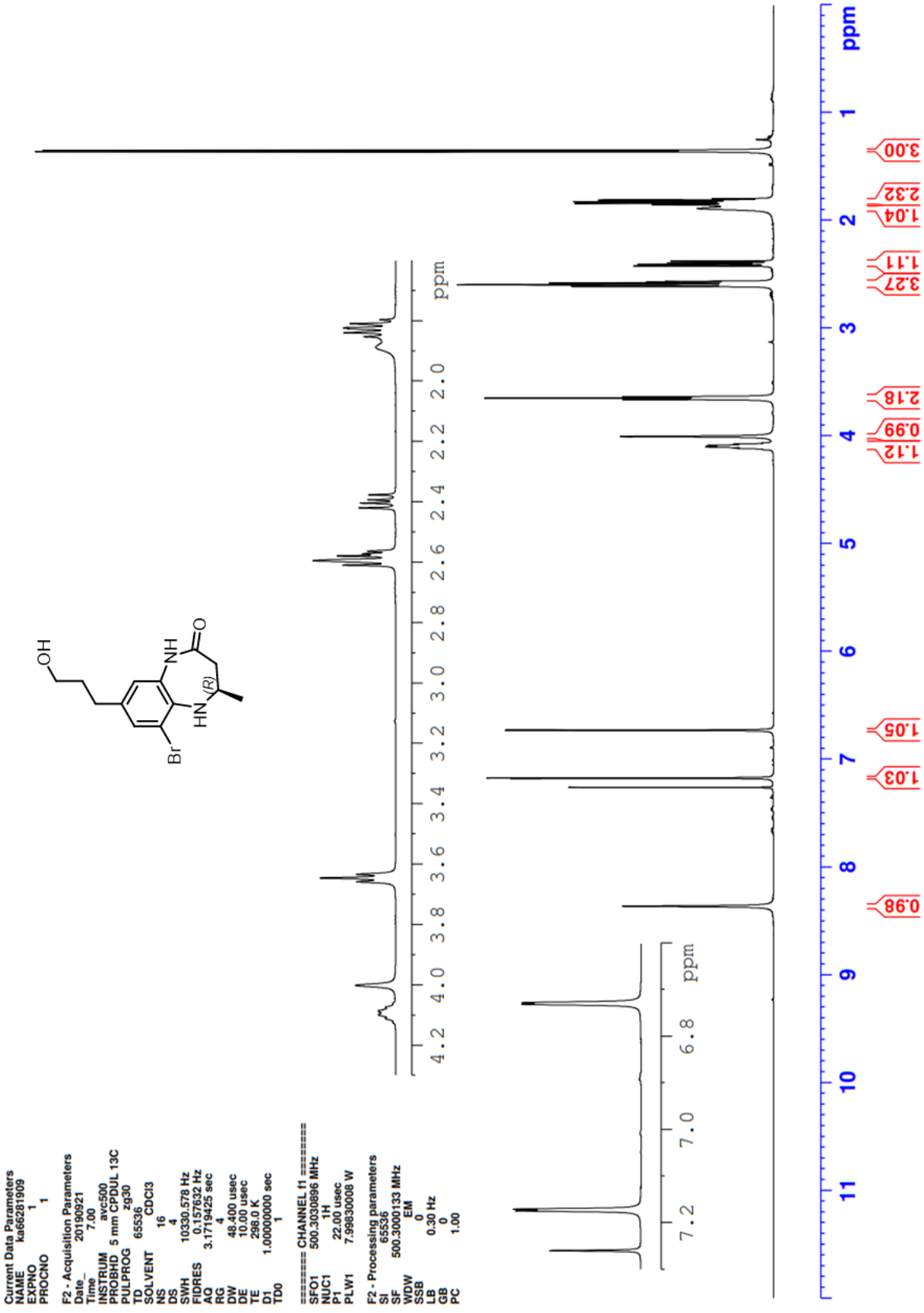

(4*R*)-6-Bromo-8-(3-hydroxypropyl)-4-methyl-1,3,4,5-tetrahydro-2*H*-1,5-benzodiazepin-2-one

(29)

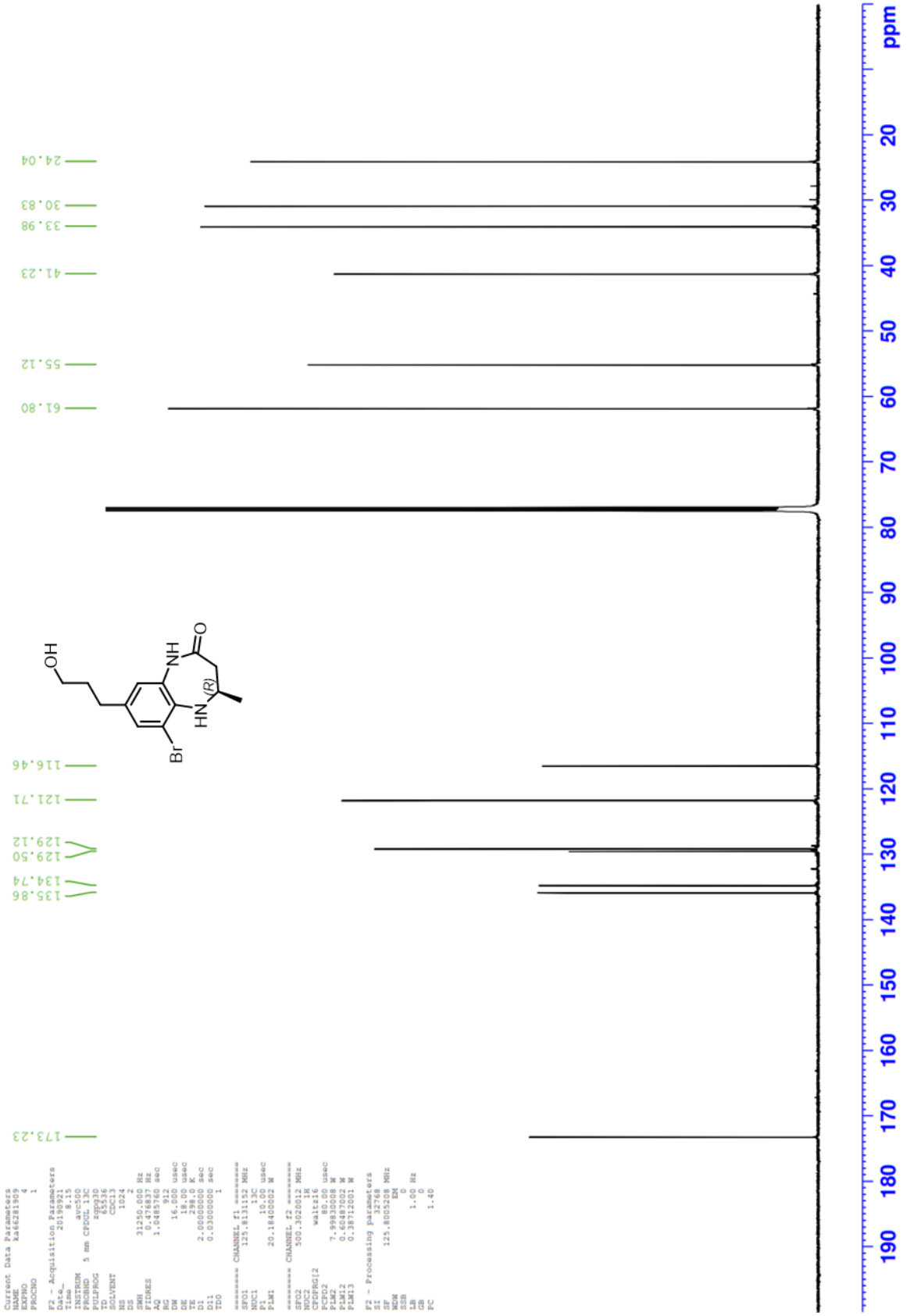

(4*R*)-6-Bromo-8-(10-hydroxydecyl)-4-methyl-1,3,4,5-tetrahydro-2*H*-1,5-benzodiazepin-2-one

(30)

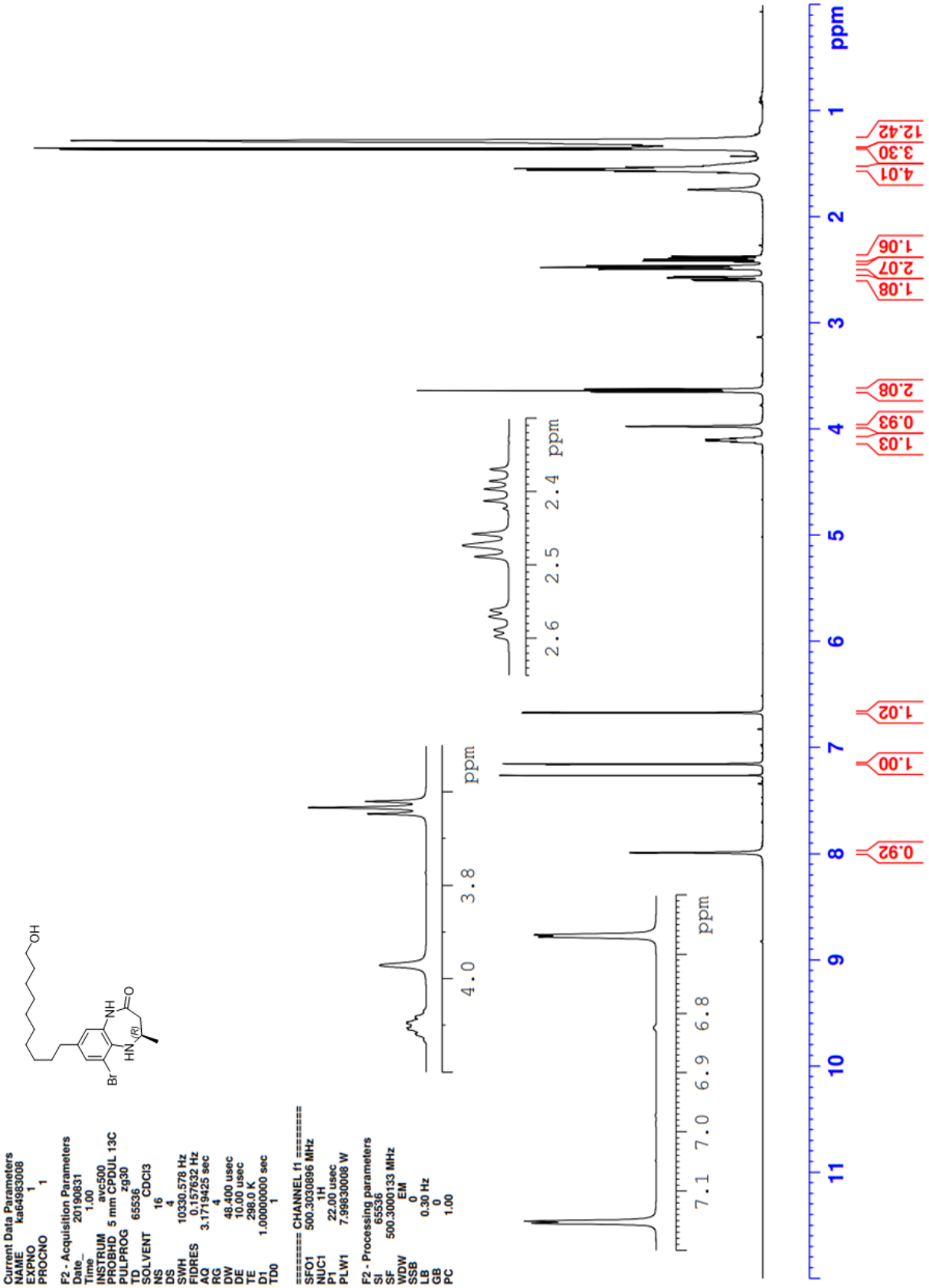

(4*R*)-6-Bromo-8-(10-hydroxydecyl)-4-methyl-1,3,4,5-tetrahydro-2*H*-1,5-benzodiazepin-2-one

(30)

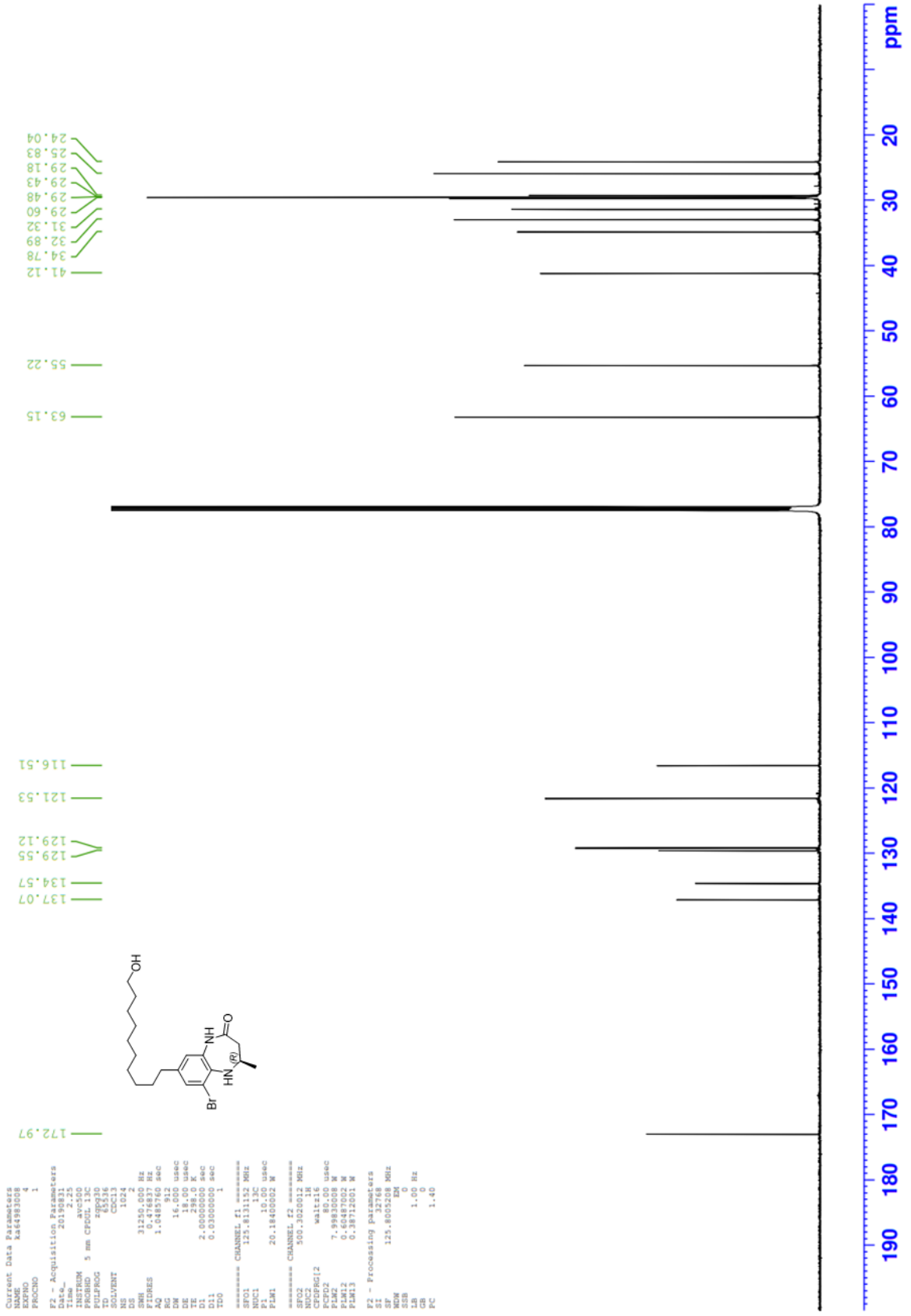

(4*R*)-8-(3-Hydroxypropyl)-6-[(1*E*)-5-(7-methoxy-3,4-dihydroquinolin-1(2*H*)-yl)pent-1-en-1-yl]-4-methyl-1,3,4,5-tetrahydro-2*H*-1,5-benzodiazepin-2-one (25)

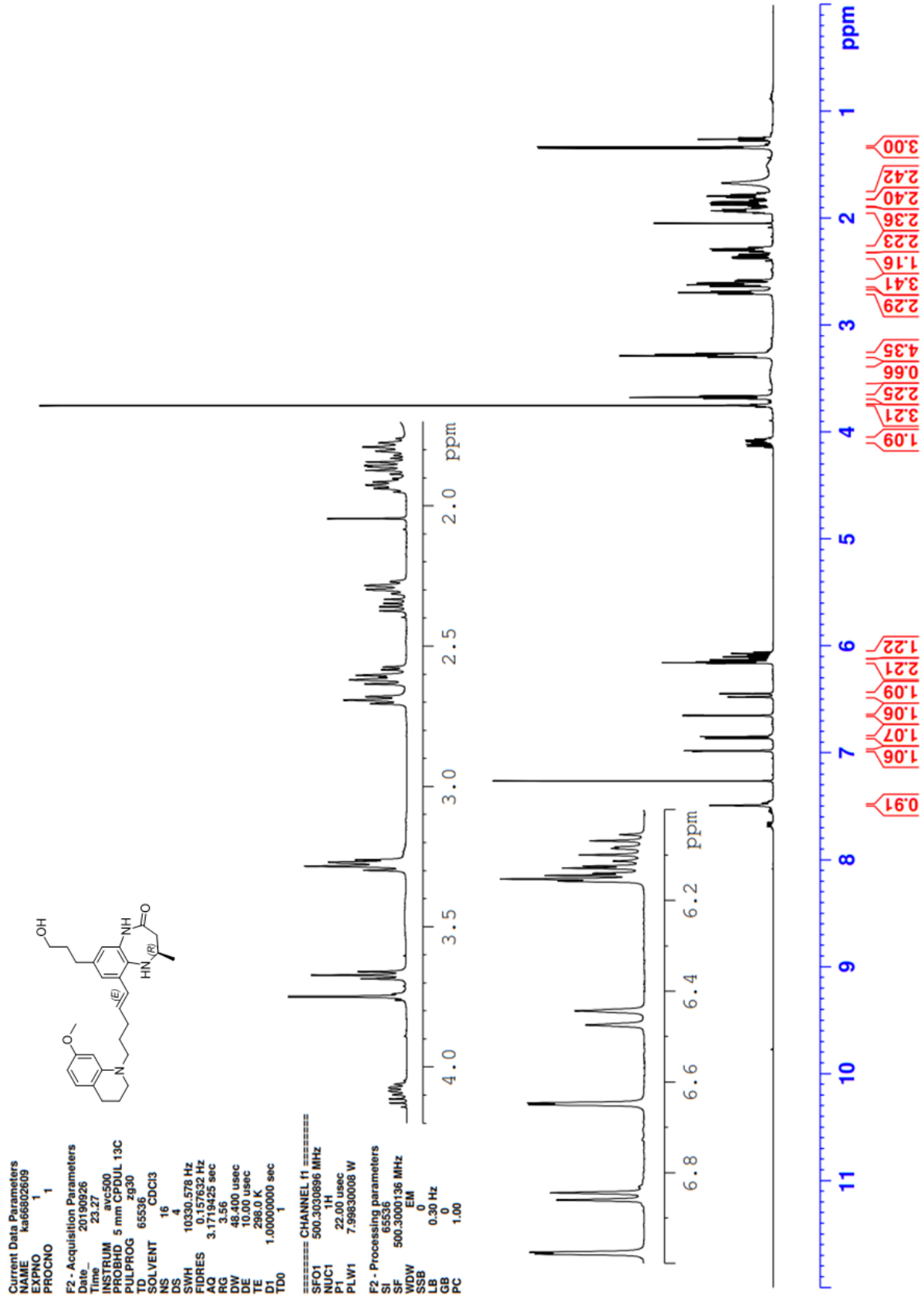

(4*R*)-8-(3-Hydroxypropyl)-6-[(1*E*)-5-(7-methoxy-3,4-dihydroquinolin-1(2*H*)-yl)pent-1-en-1-yl]-4-methyl-1,3,4,5-tetrahydro-2*H*-1,5-benzodiazepin-2-one (25)

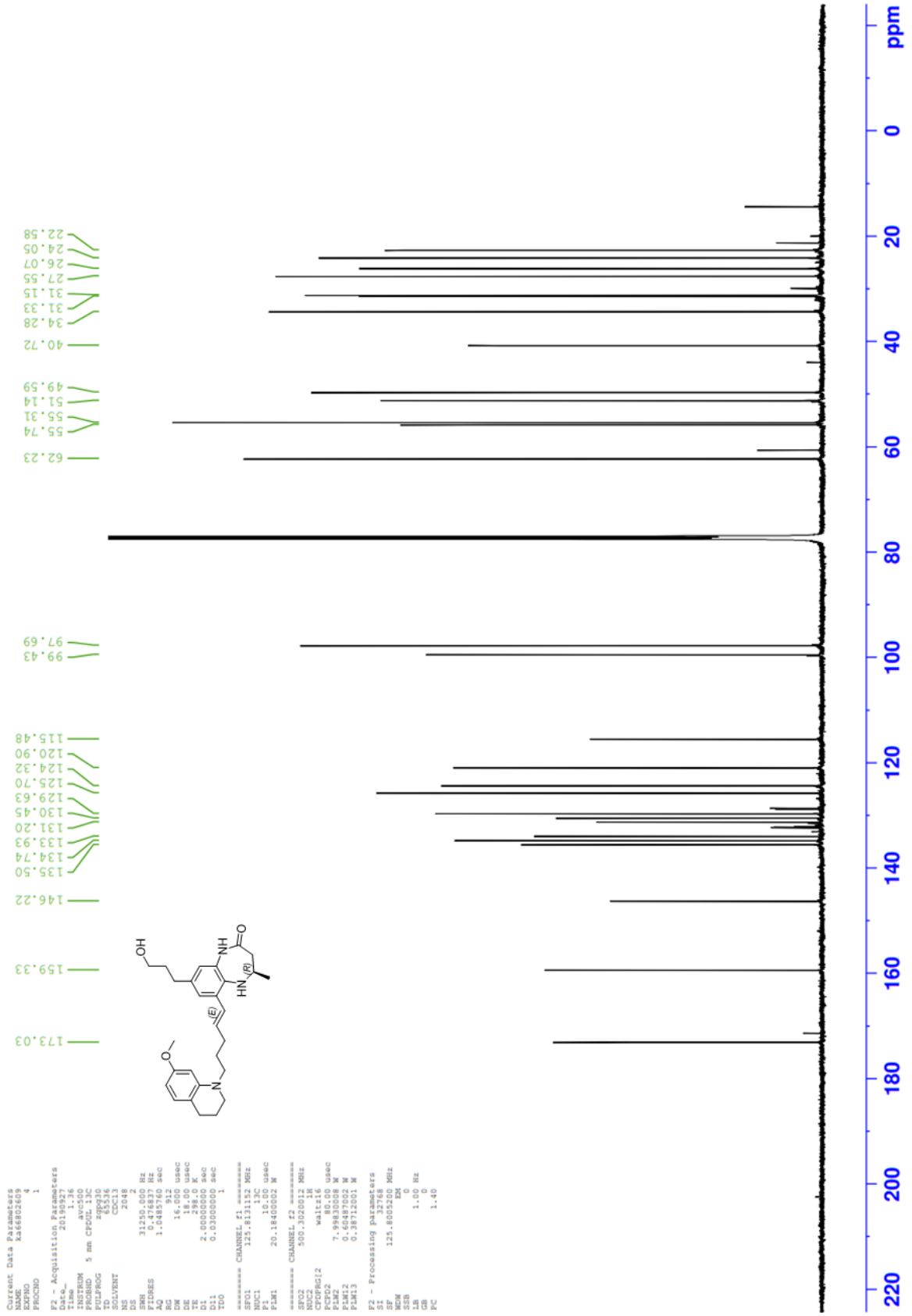

(4*R*)-8-(10-Hydroxydecyl)-6-[(1*E*)-5-(7-methoxy-3,4-dihydroquinolin-1(2*H*)-yl)pent-1-en-1-yl]-4-methyl-1,3,4,5-tetrahydro-2*H*-1,5-benzodiazepin-2-one (26)

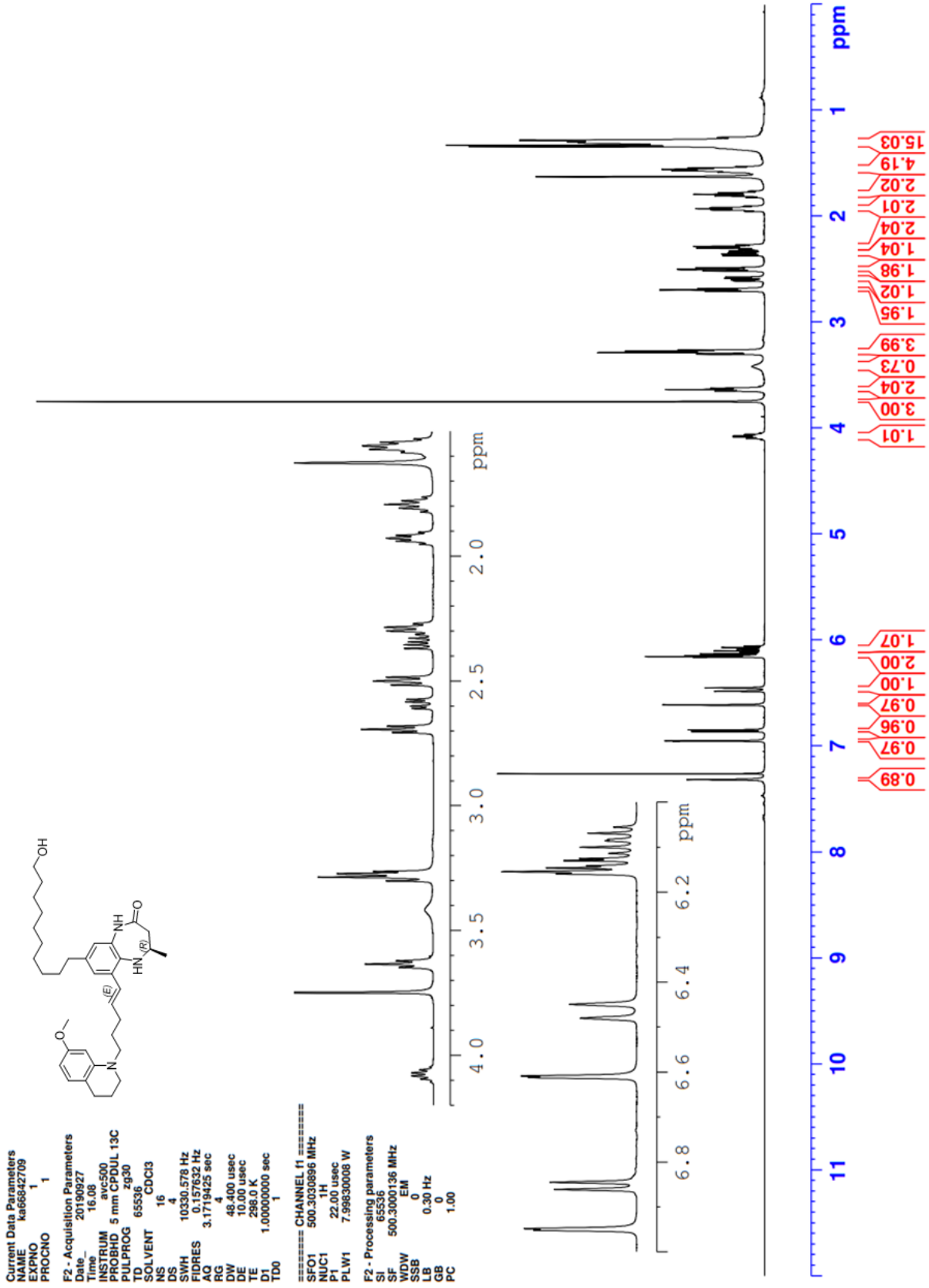

(4*R*)-8-(10-Hydroxydecyl)-6-[(1*E*)-5-(7-methoxy-3,4-dihydroquinolin-1(2*H*)-yl)pent-1-en-1-yl]-4-methyl-1,3,4,5-tetrahydro-2*H*-1,5-benzodiazepin-2-one (26)

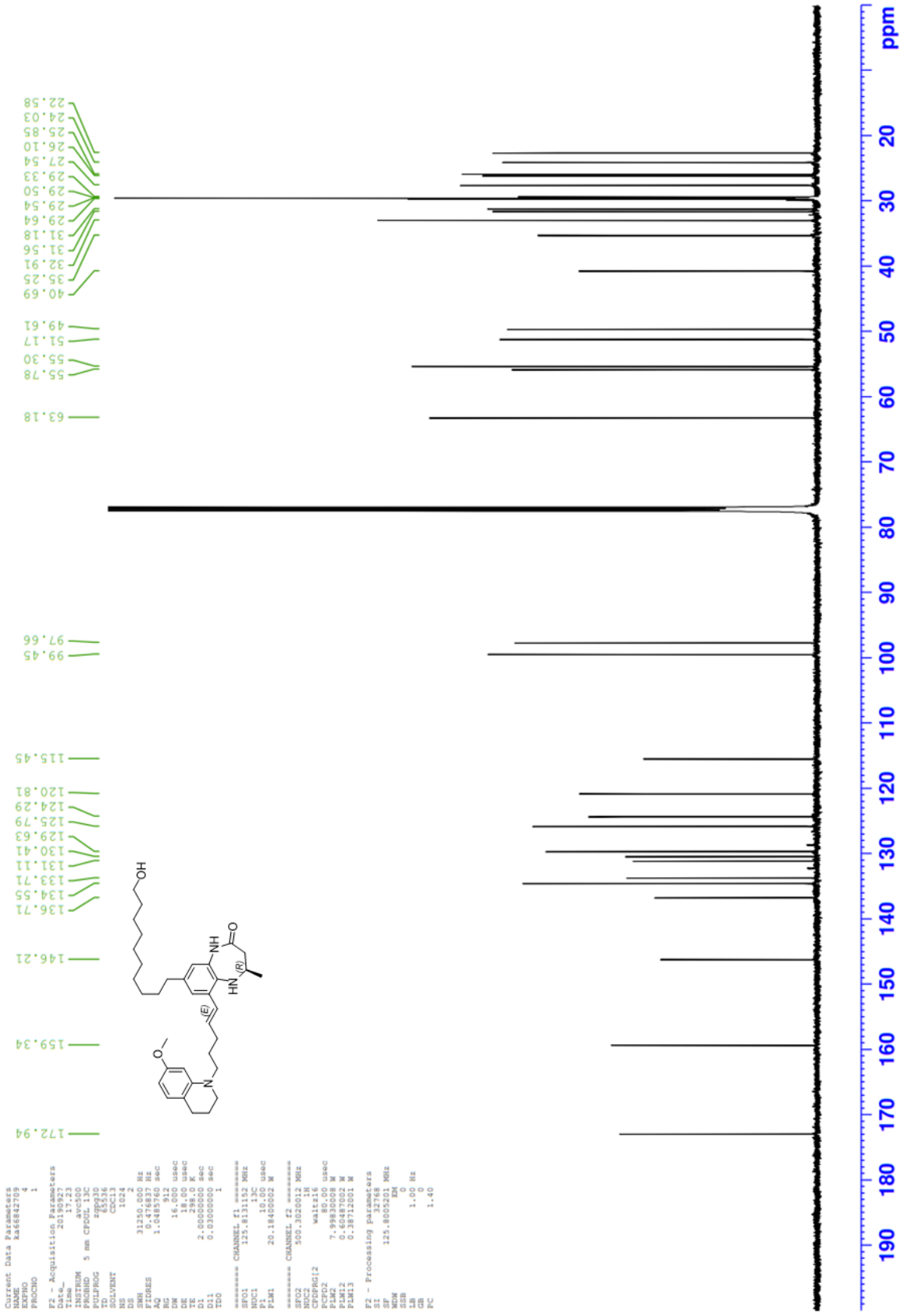

4-((5-Hydroxypentyl)amino)-2-(1-(3-((2*R*)-9-((1*E*)-5-(7-methoxy-3,4-dihydroquinolin-1(2*H*)-yl)pent-1-en-1-yl)-2-methyl-4-oxo-2,3,4,5-tetrahydro-1*H*-1,5-benzodiazepin-7-yl)propyl)-2,6-dioxopiperidin-3-yl)-1*H*-isoindole-1,3(2*H*)-dione (42)

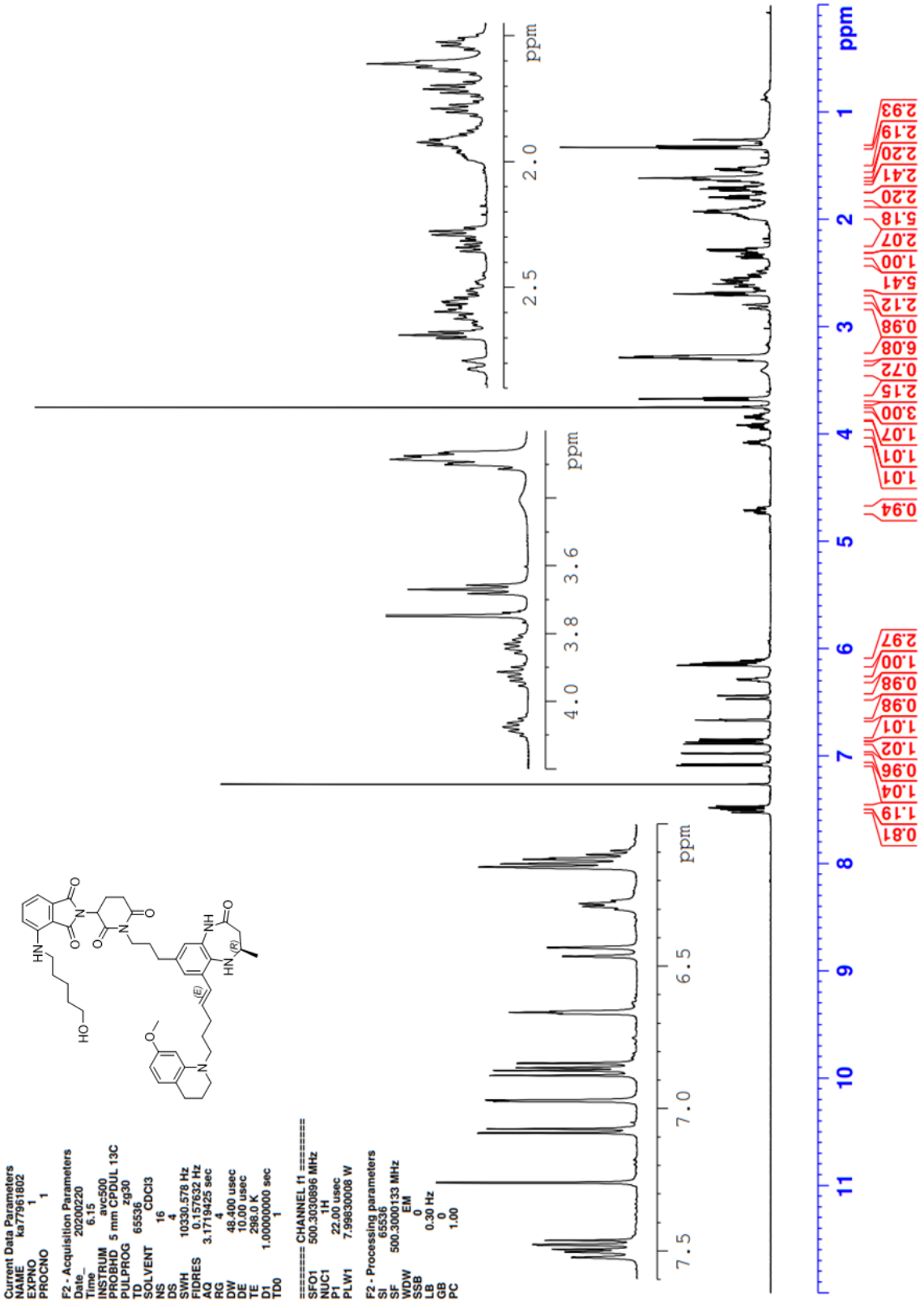

4-((5-Hydroxypentyl)amino)-2-(1-(3-((2*R*)-9-((1*E*)-5-(7-methoxy-3,4-dihydroquinolin-1(2*H*)-yl)pent-1-en-1-yl)-2-methyl-4-oxo-2,3,4,5-tetrahydro-1*H*-1,5-benzodiazepin-7-yl)propyl)-2,6-dioxopiperidin-3-yl)-1*H*-isoindole-1,3(2*H*)-dione (42)

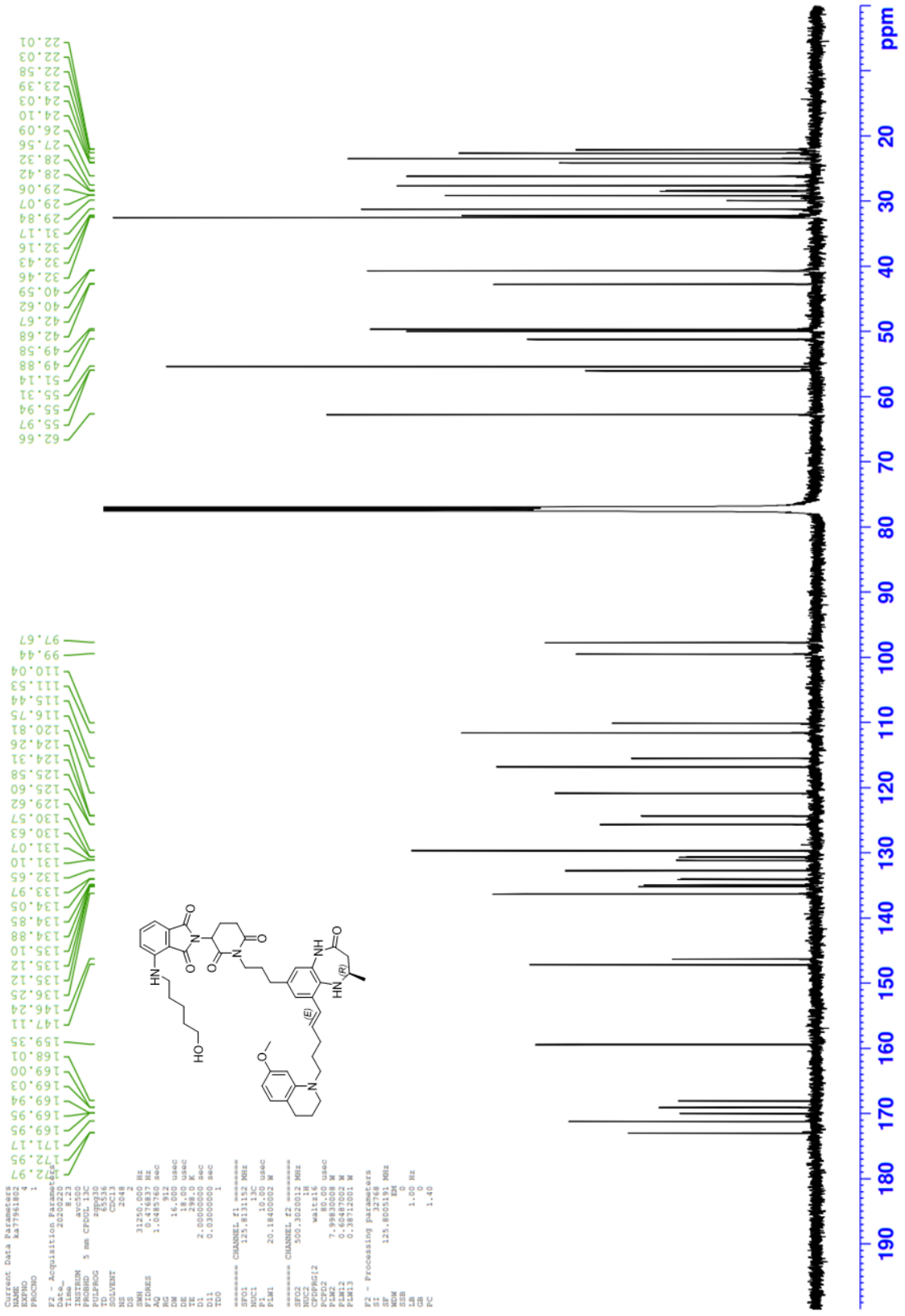

***tert*-Butyl [2-({3-[(2*R*)-9-bromo-2-methyl-4-oxo-2,3,4,5-tetrahydro-1*H*-1,5-benzodiazepin-7-yl]prop-2-yn-1-yl}oxy)ethyl]carbamate (53)**

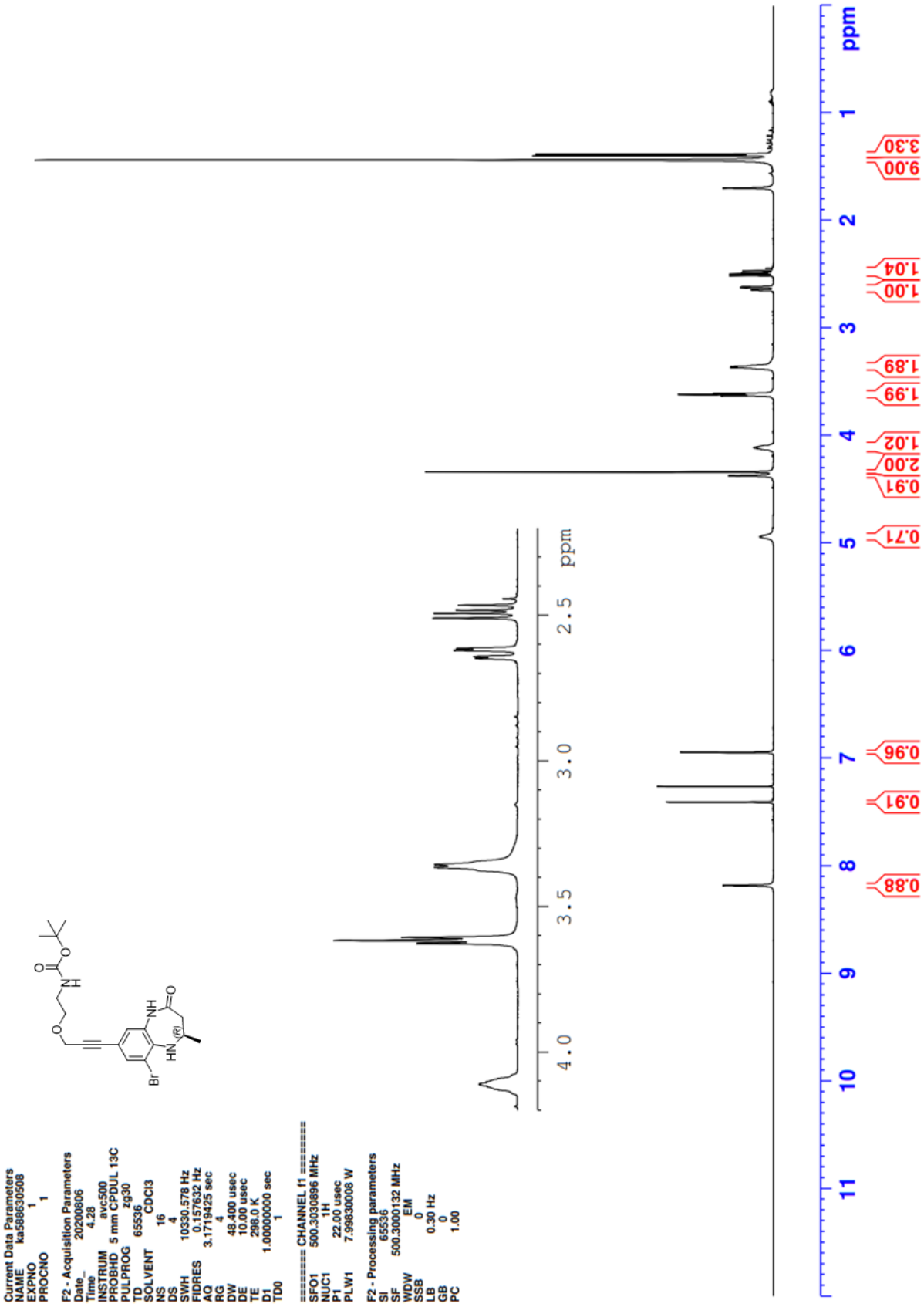

tert-Butyl [2-({3-[(2*R*)-9-bromo-2-methyl-4-oxo-2,3,4,5-tetrahydro-1*H*-1,5-benzodiazepin-7-yl]prop-2-yn-1-yl}oxy)ethyl]carbamate (53)

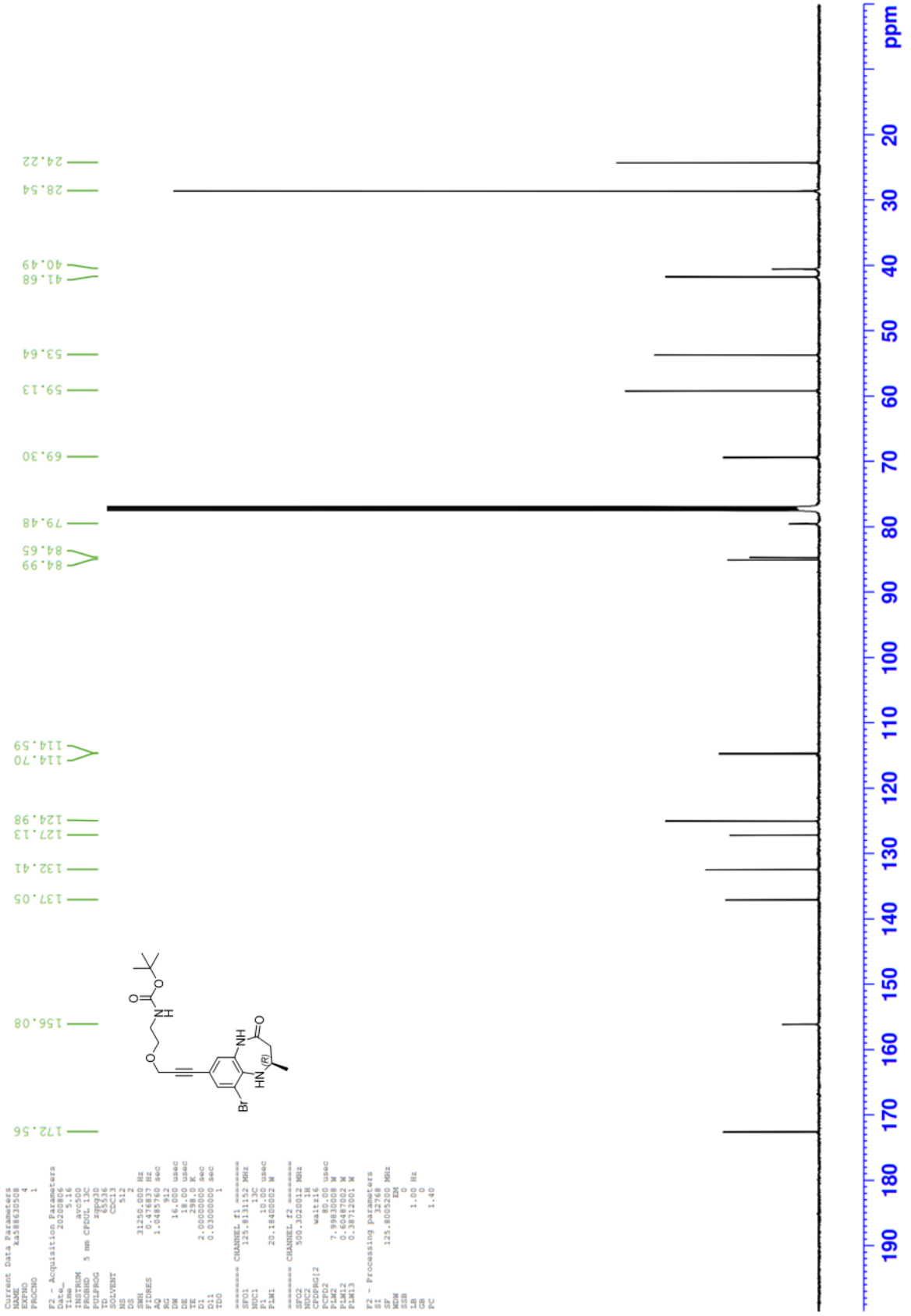

***tert*-Butyl {2-[2-({3-[(2*R*)-9-bromo-2-methyl-4-oxo-2,3,4,5-tetrahydro-1*H*-1,5-benzodiazepin-7-yl]prop-2-yn-1-yl}oxy)ethoxy]ethyl}carbamate (54)**

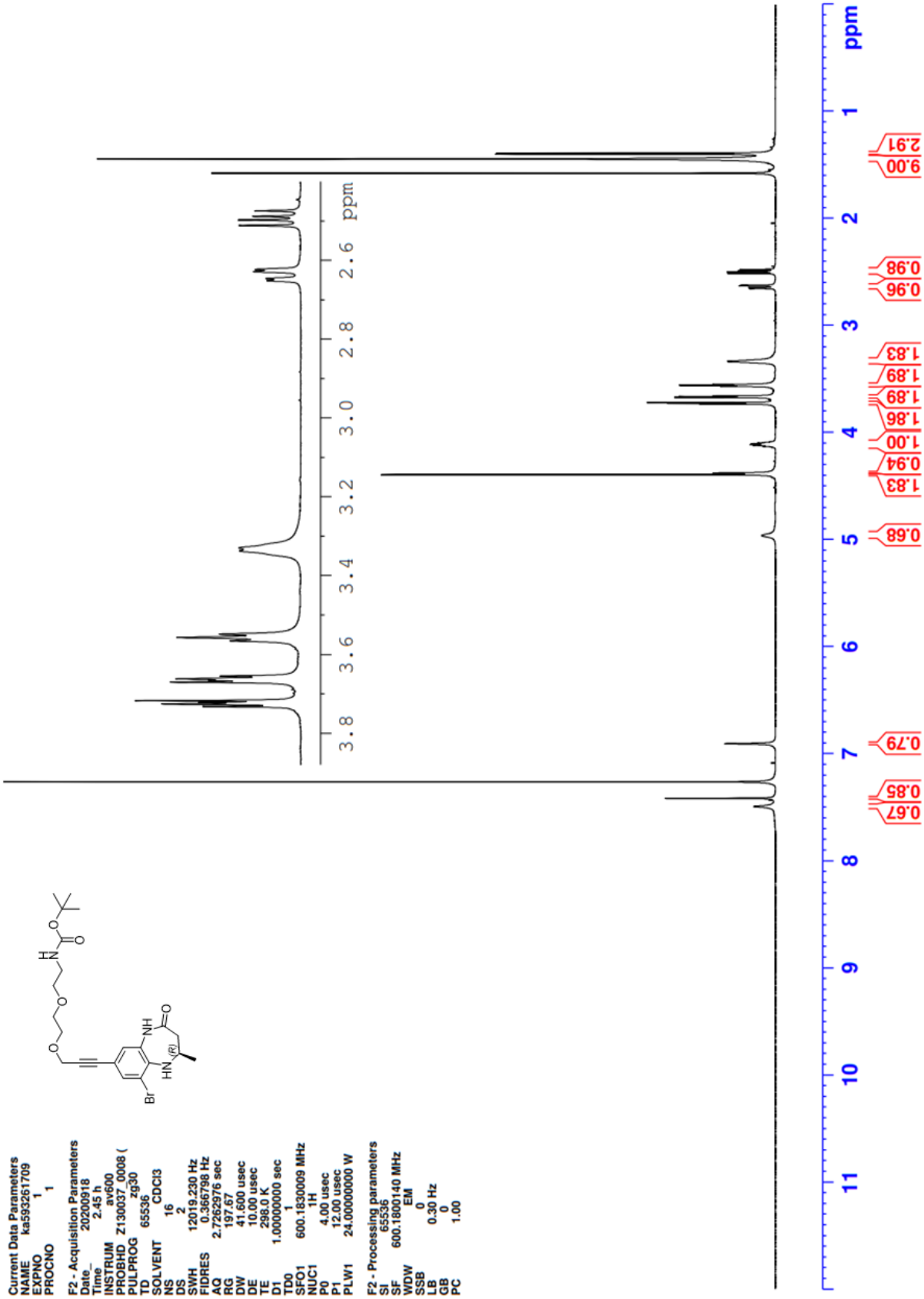

tert-Butyl {2-[2-({3-[(2*R*)-9-bromo-2-methyl-4-oxo-2,3,4,5-tetrahydro-1*H*-1,5-benzodiazepin-7-yl]prop-2-yn-1-yl}oxy)ethoxy]ethyl}carbamate (54)

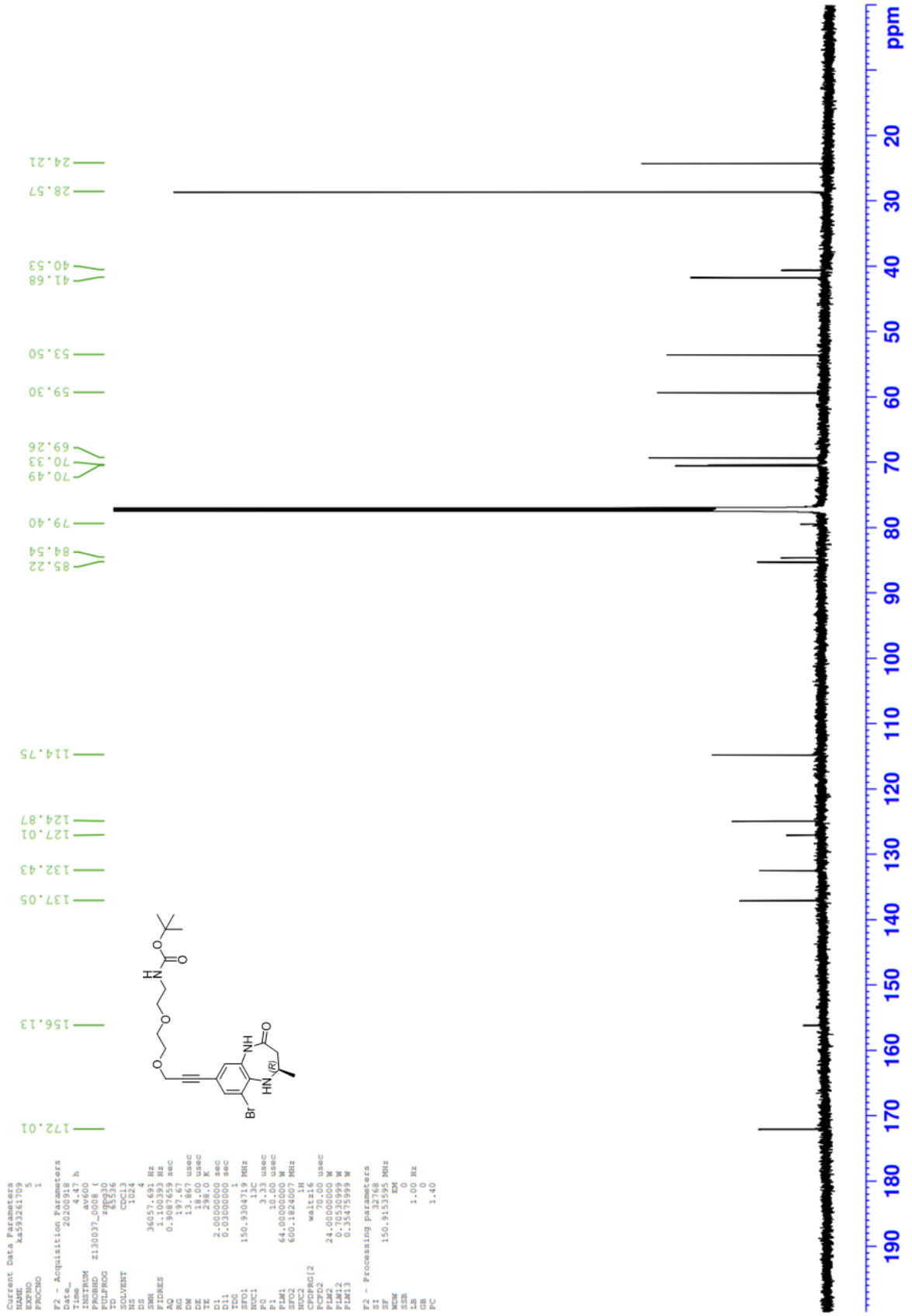

***tert*-Butyl (2-{2-[2-({3-[(2*R*)-9-bromo-2-methyl-4-oxo-2,3,4,5-tetrahydro-1*H*-1,5-benzodiazepin-7-yl]prop-2-yn-1-yl}oxy)ethoxy]ethoxy}ethyl)carbamate (55)**

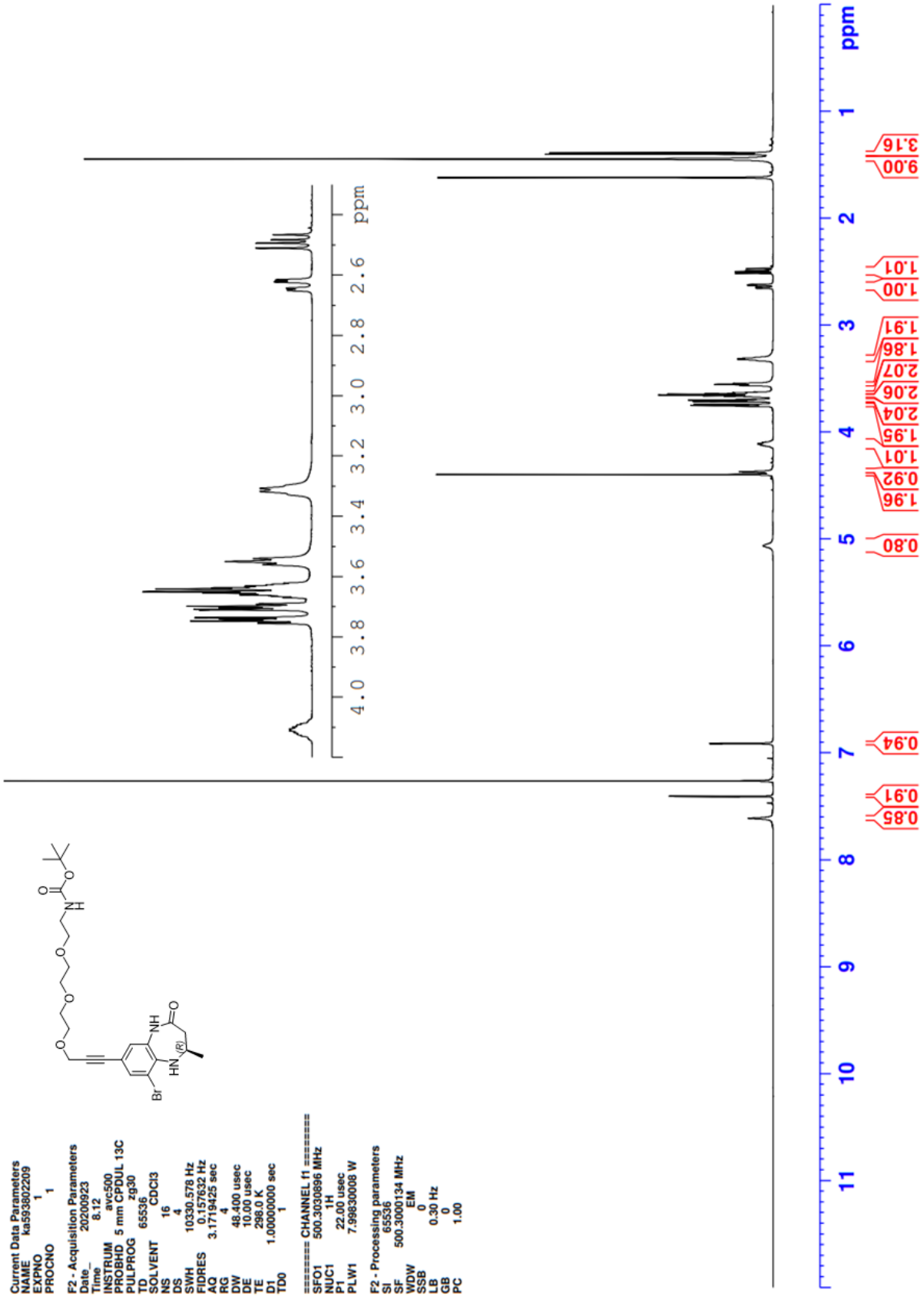

***tert*-Butyl (2-{2-[2-({3-[(2*R*)-9-bromo-2-methyl-4-oxo-2,3,4,5-tetrahydro-1*H*-1,5-benzodiazepin-7-yl]prop-2-yn-1-yl}oxy)ethoxy]ethoxy}ethyl)carbamate (55)**

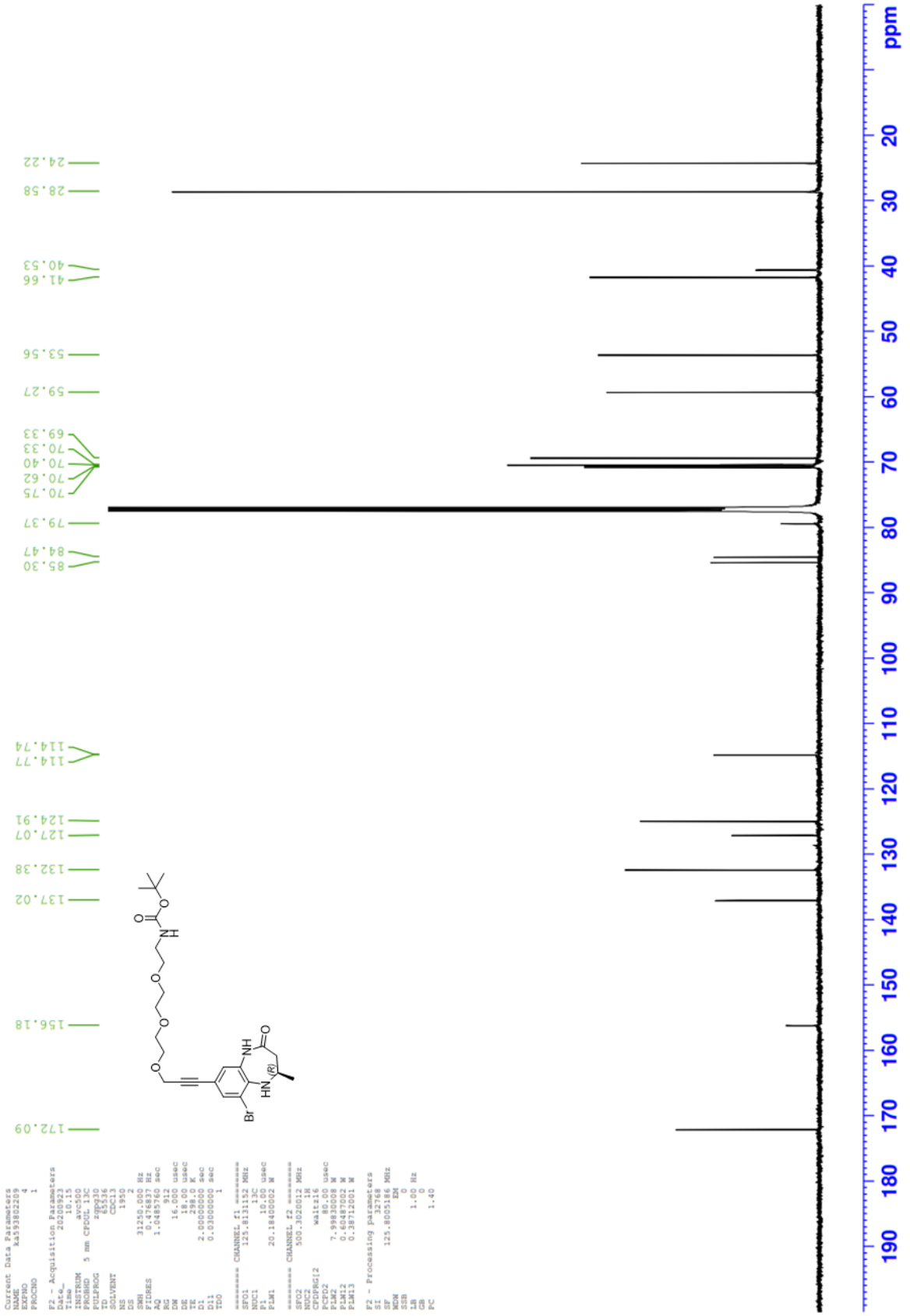

tert-Butyl {15-[(2*R*)-9-bromo-2-methyl-4-oxo-2,3,4,5-tetrahydro-1*H*-1,5-benzodiazepin-7-yl]-3,6,9,12-tetraoxapentadec-14-yn-1-yl}carbamate (56)

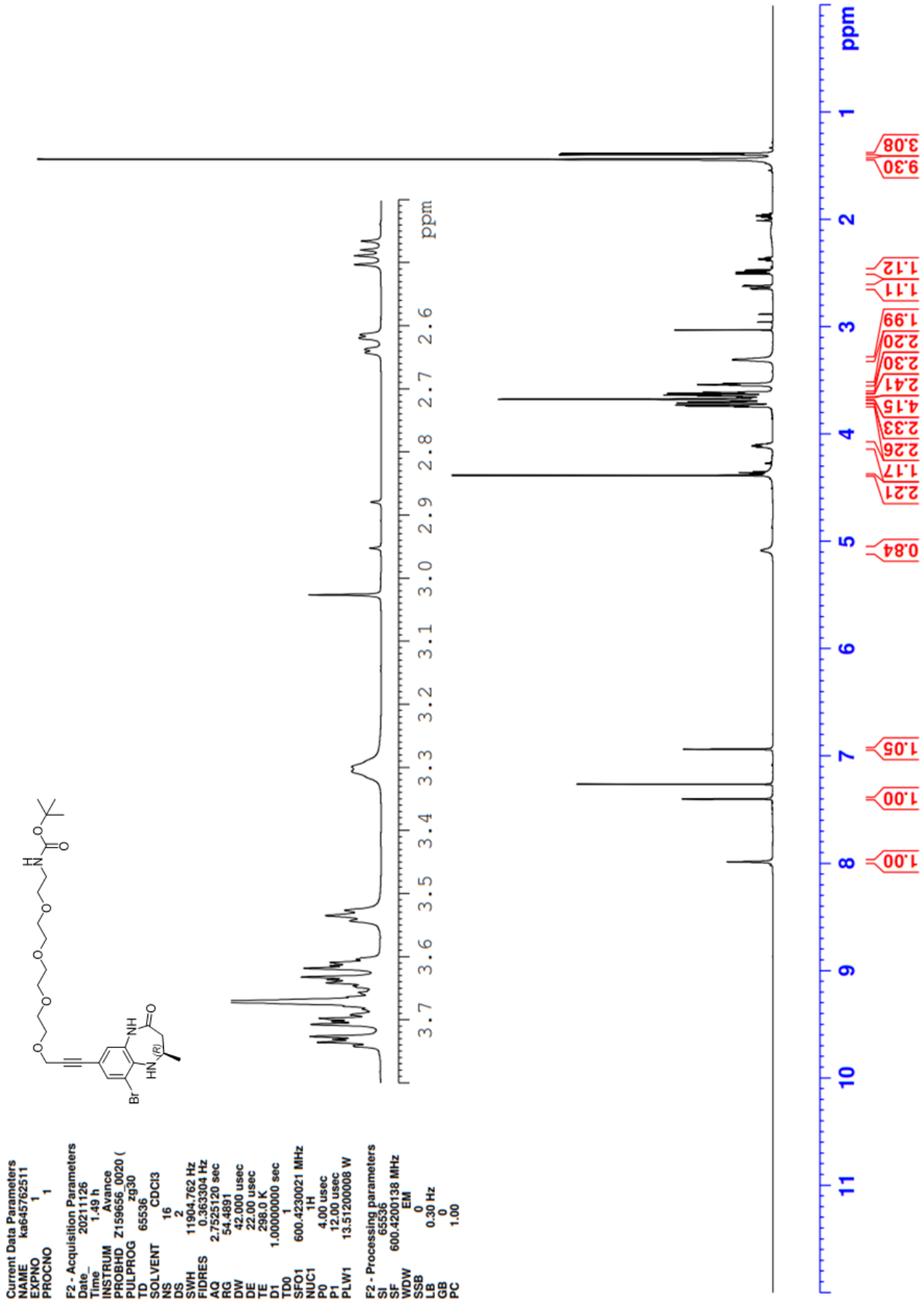

tert-Butyl {15-[(2*R*)-9-bromo-2-methyl-4-oxo-2,3,4,5-tetrahydro-1*H*-1,5-benzodiazepin-7-yl]-3,6,9,12-tetraoxapentadec-14-yn-1-yl}carbamate (56)

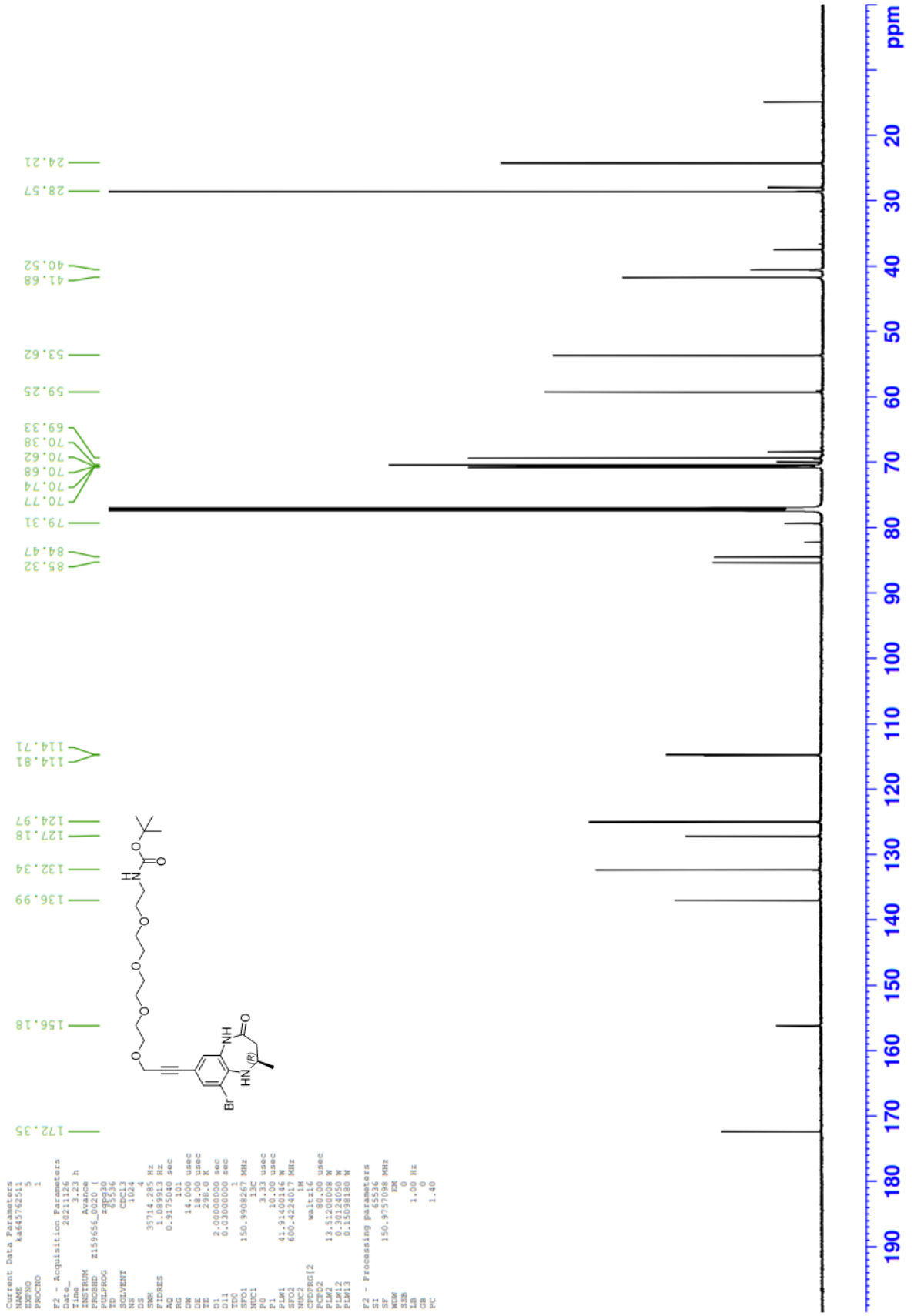

***tert*-Butyl (2-{3-[(2*R*)-9-bromo-2-methyl-4-oxo-2,3,4,5-tetrahydro-1*H*-1,5-benzodiazepin-7-yl]propoxy}ethyl)carbamate (57)**

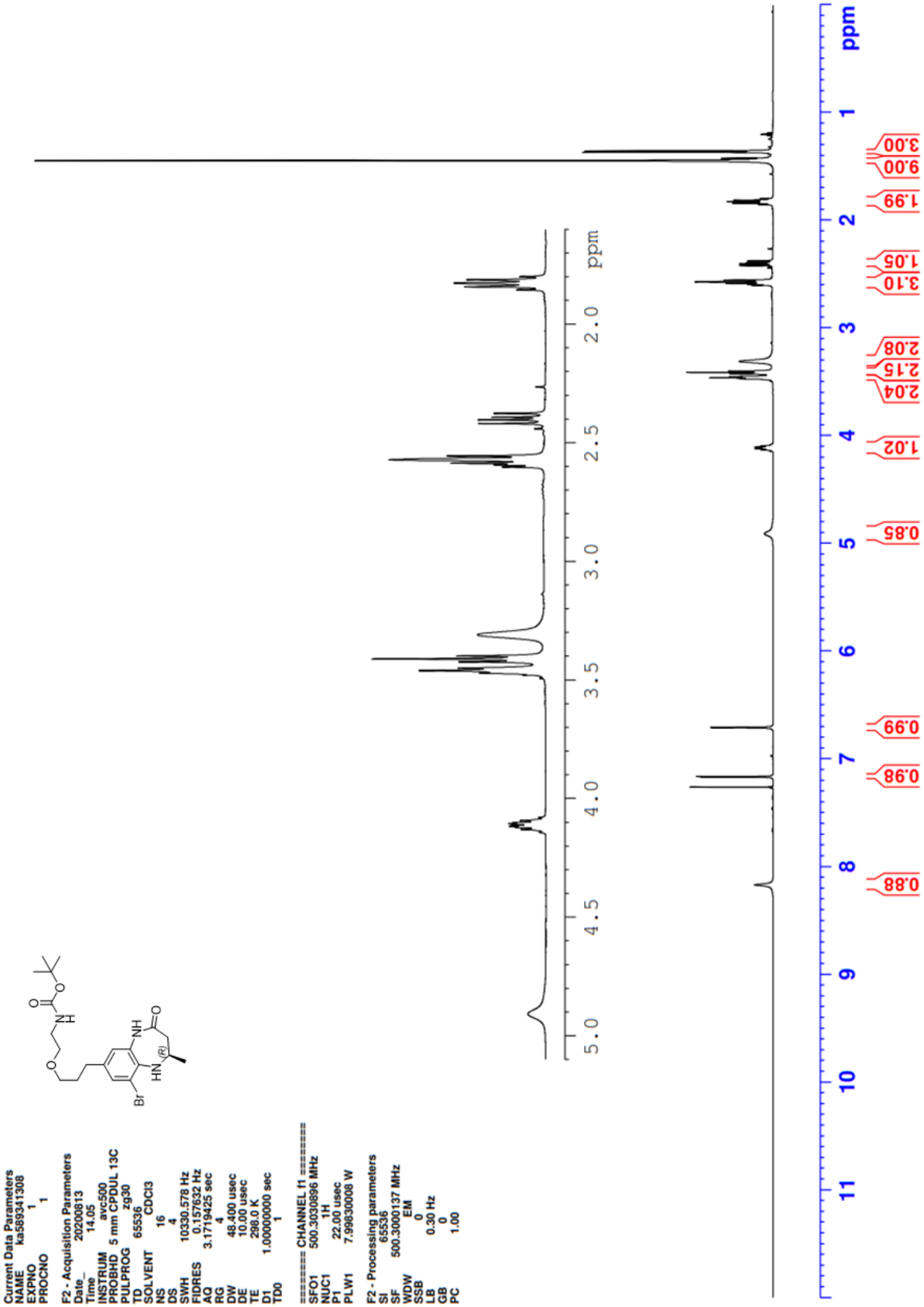

tert-Butyl (2-{3-[(2*R*)-9-bromo-2-methyl-4-oxo-2,3,4,5-tetrahydro-1*H*-1,5-benzodiazepin-7-yl]propoxy}ethyl)carbamate (57)

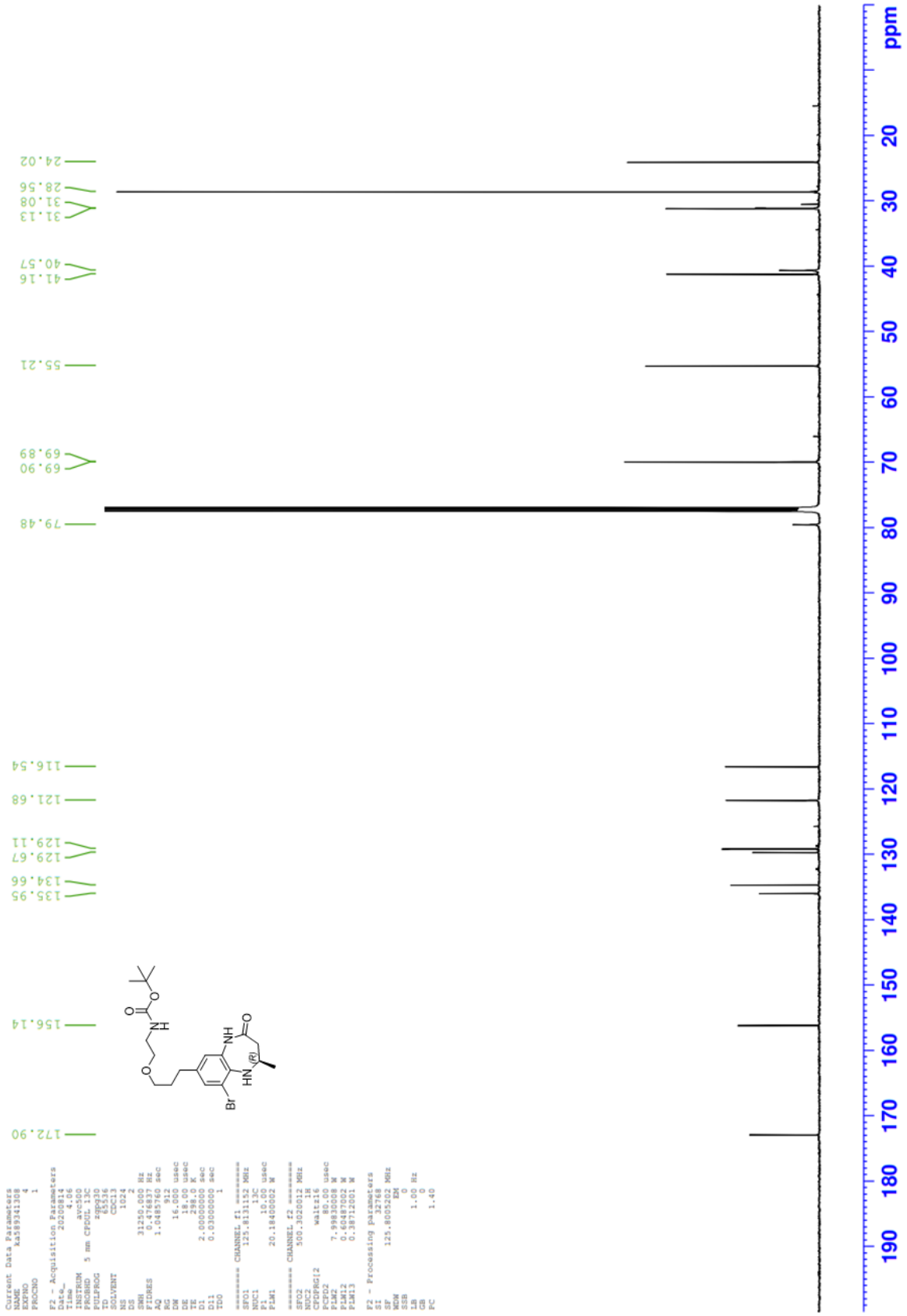

tert-Butyl [2-(2-{3-[(2*R*)-9-bromo-2-methyl-4-oxo-2,3,4,5-tetrahydro-1*H*-1,5-benzodiazepin-7-yl]propoxy}ethoxy)ethyl]carbamate (58)

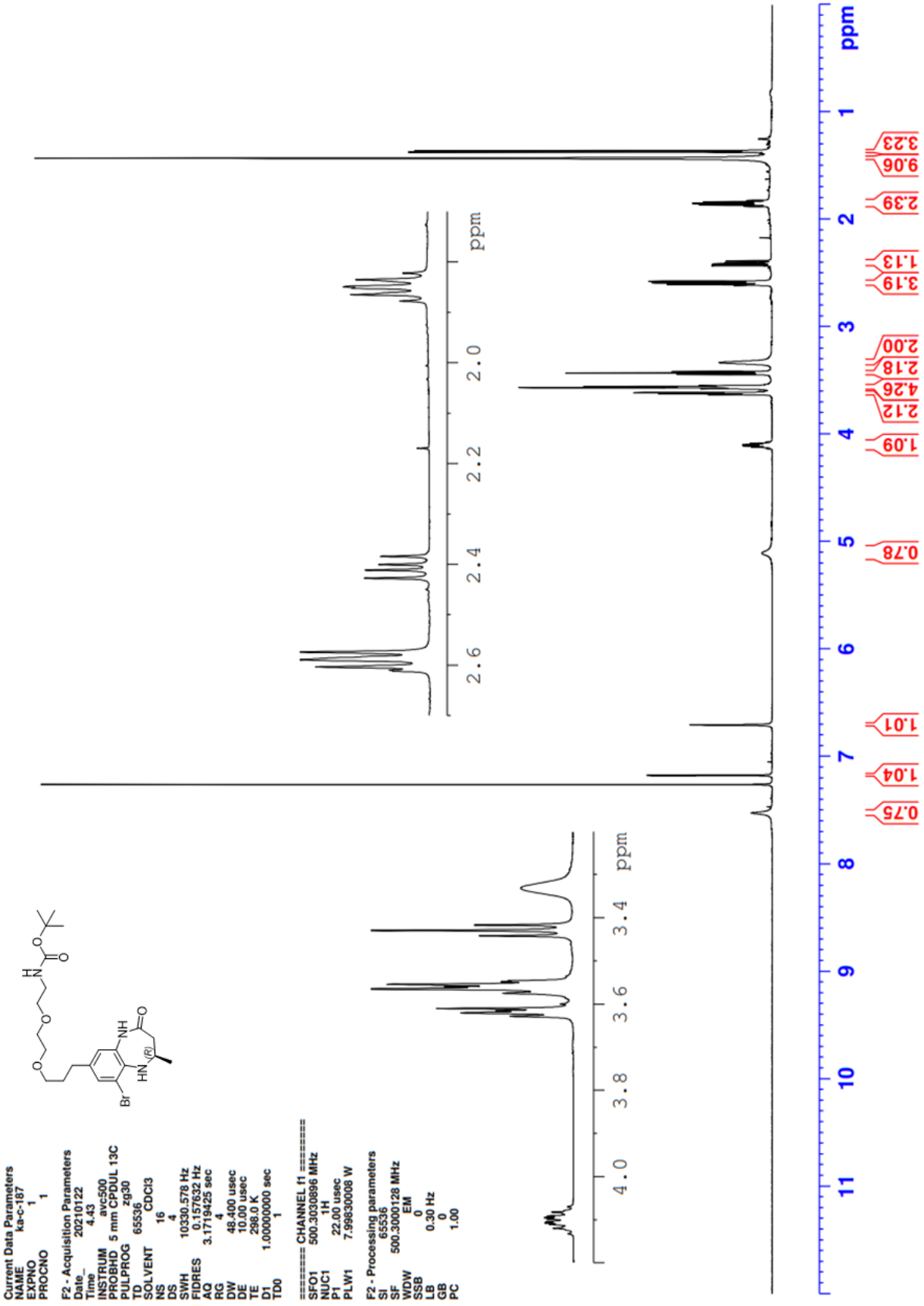

tert-Butyl [2-(2-{3-[(2*R*)-9-bromo-2-methyl-4-oxo-2,3,4,5-tetrahydro-1*H*-1,5-benzodiazepin-7-yl]propoxy}ethoxy)ethyl]carbamate (58)

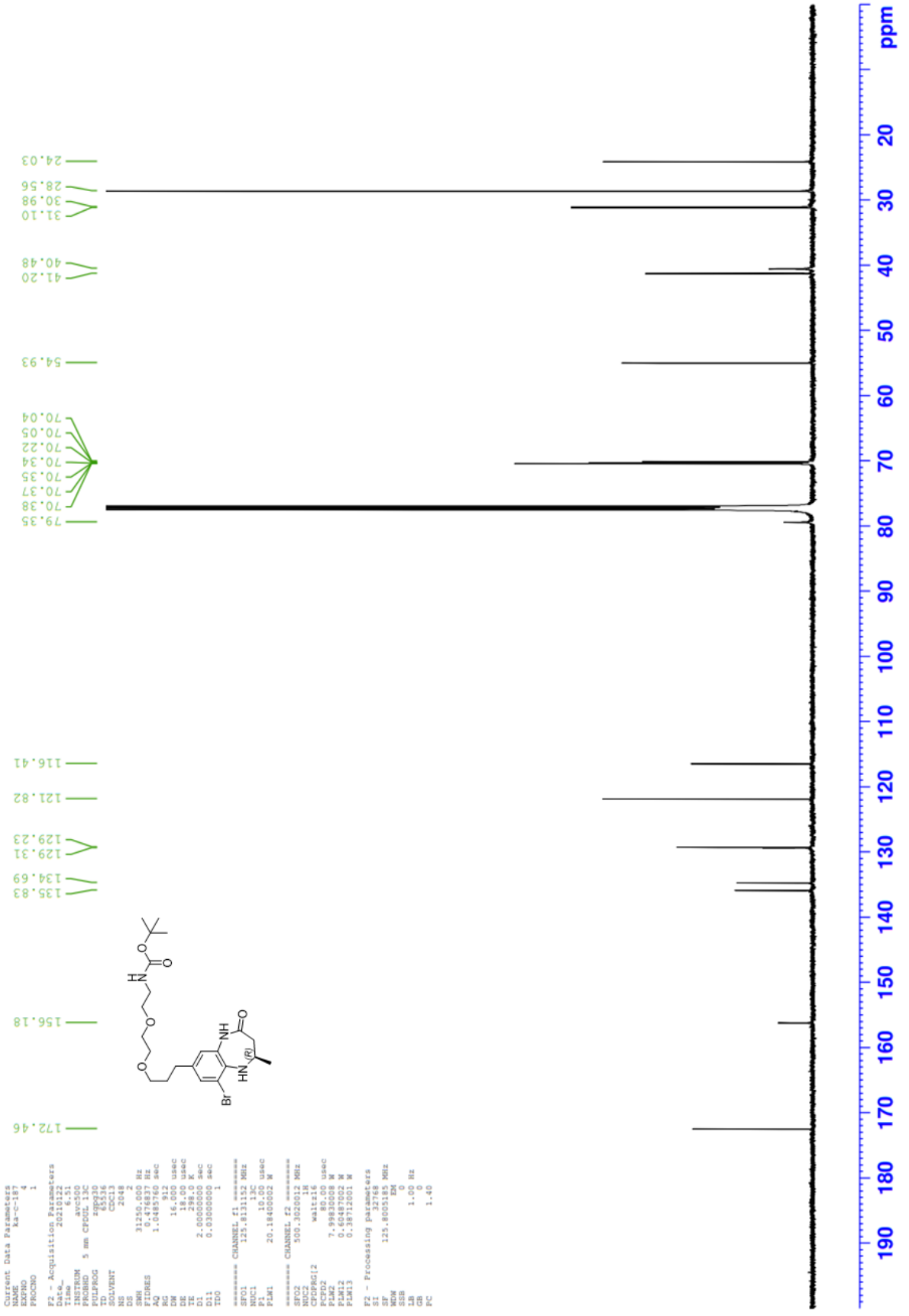

***tert*-Butyl {2-[2-(2-{3-[(2*R*)-9-bromo-2-methyl-4-oxo-2,3,4,5-tetrahydro-1*H*-1,5-benzodiazepin-7-yl]propoxy}ethoxy)ethoxy]ethyl}carbamate (59)**

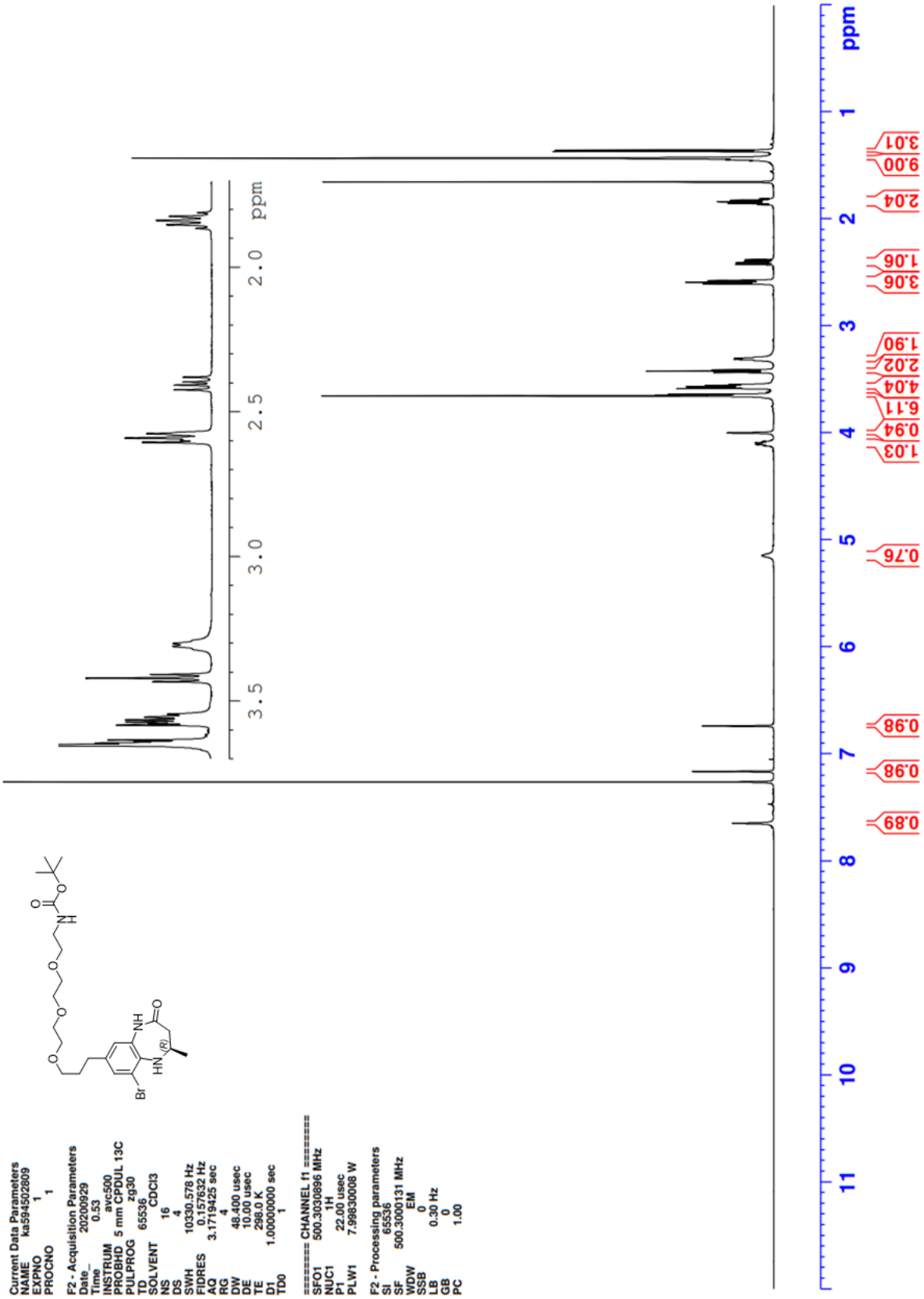

tert-Butyl {2-[2-(2-{3-[(2*R*)-9-bromo-2-methyl-4-oxo-2,3,4,5-tetrahydro-1*H*-1,5-benzodiazepin-7-yl]propoxy}ethoxy)ethoxy]ethyl}carbamate (59)

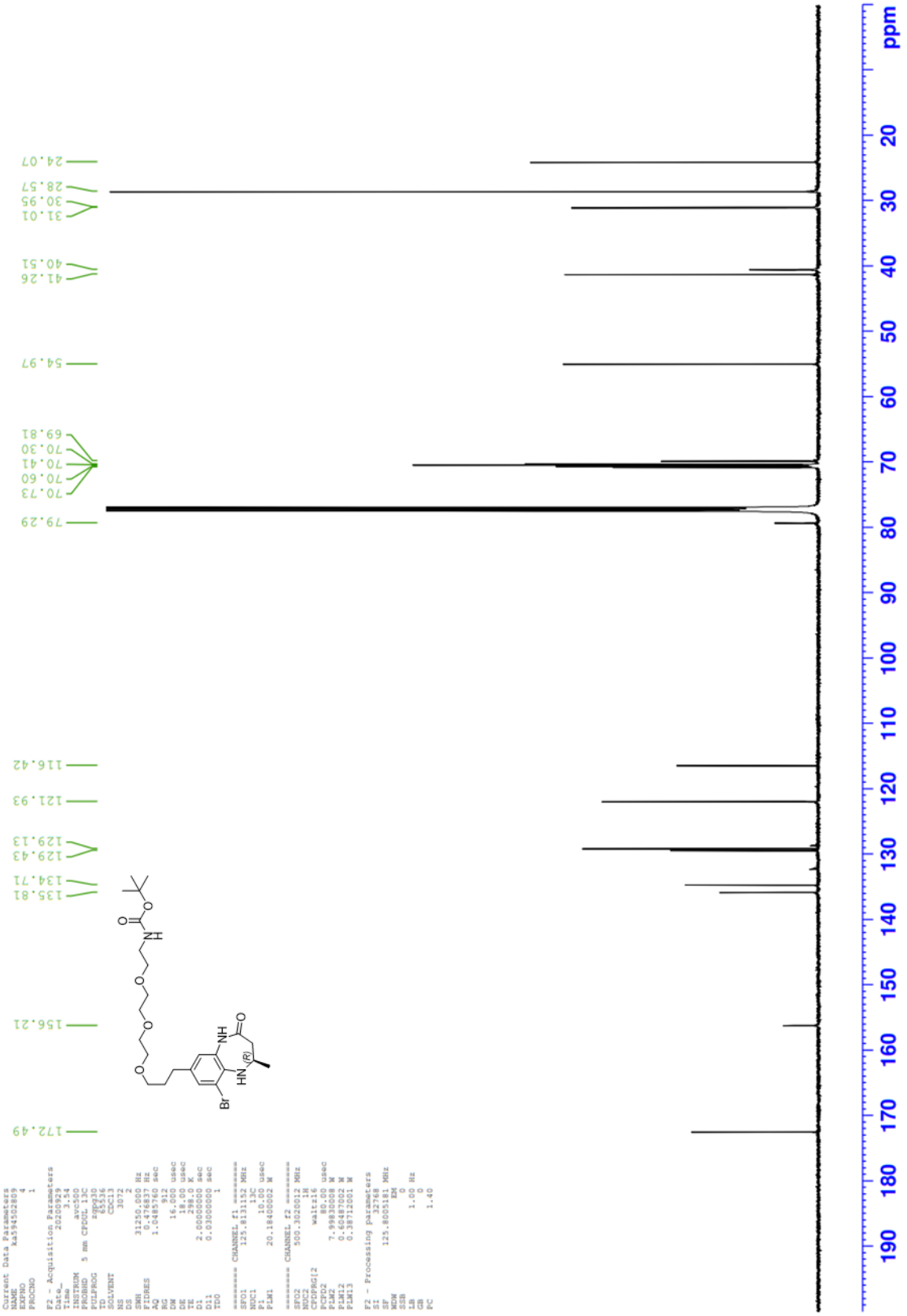

***tert*-Butyl {15-[(2*R*)-9-bromo-2-methyl-4-oxo-2,3,4,5-tetrahydro-1*H*-1,5-benzodiazepin-7-yl]-3,6,9,12-tetraoxapentadecan-1-yl}carbamate (60)**

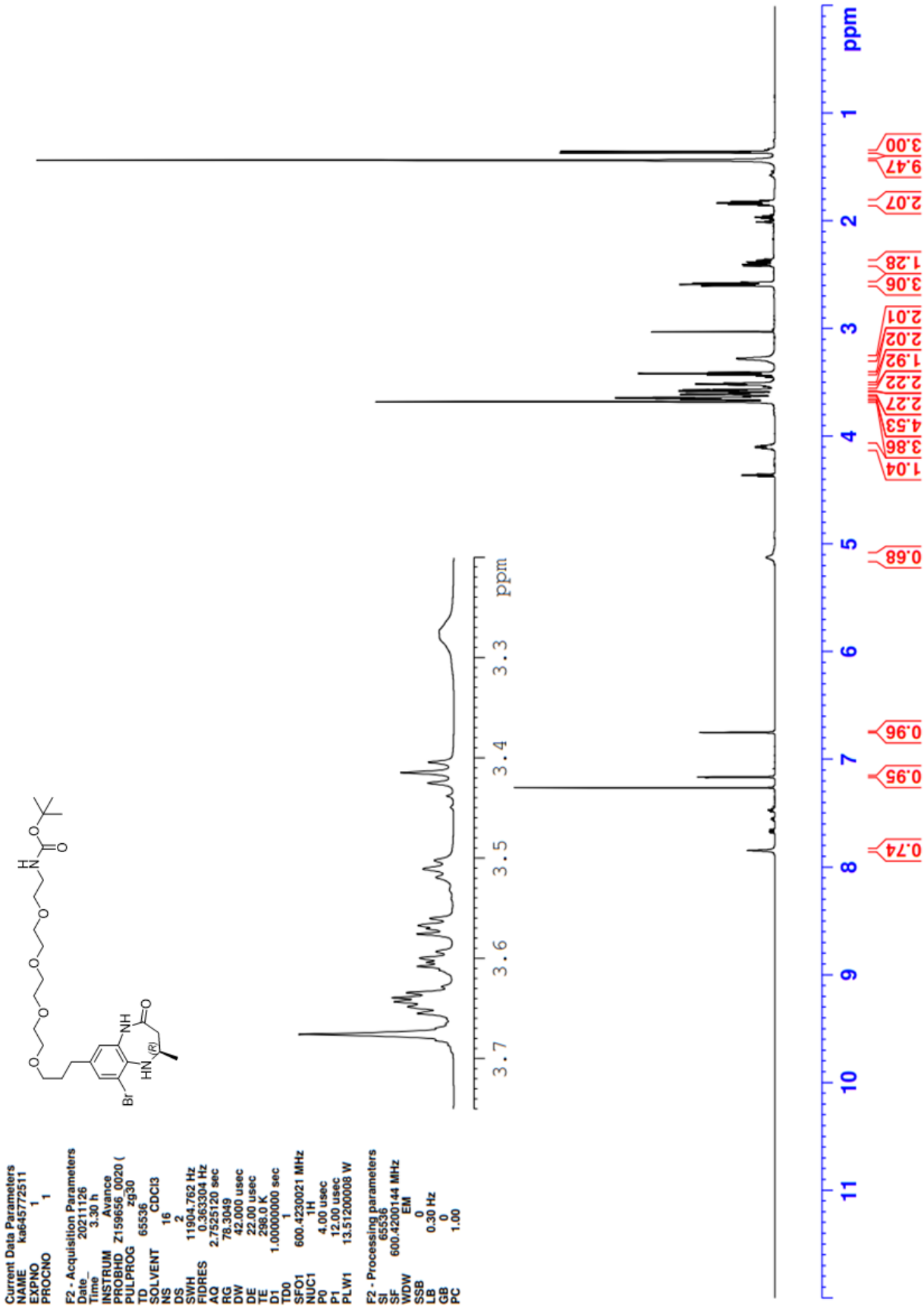

***tert*-Butyl {15-[(2*R*)-9-bromo-2-methyl-4-oxo-2,3,4,5-tetrahydro-1*H*-1,5-benzodiazepin-7-yl]-3,6,9,12-tetraoxapentadecan-1-yl}carbamate (60)**

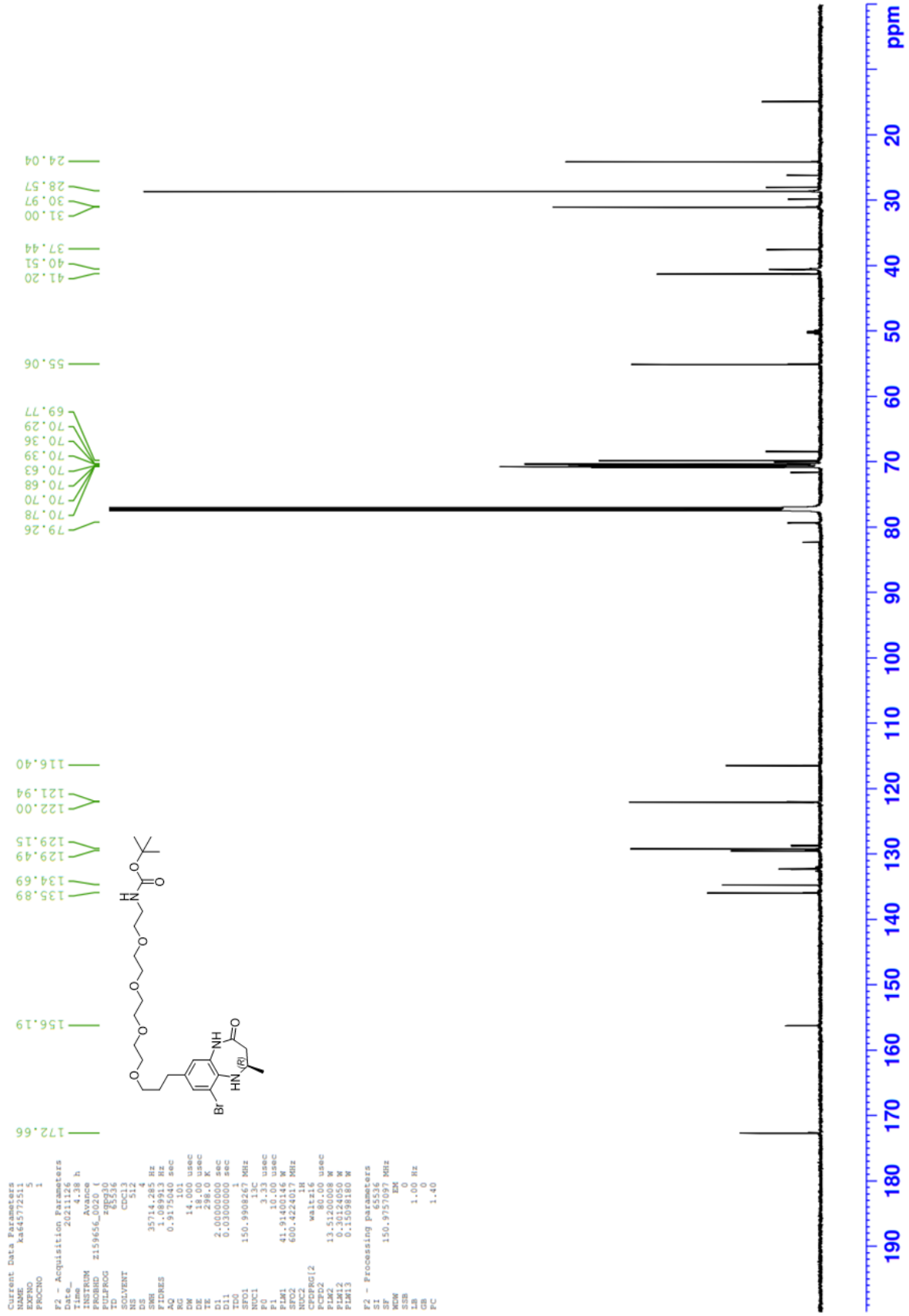

***tert*-Butyl [2-(3-{(2*R*)-9-[(1*E*)-5-(7-methoxy-3,4-dihydroquinolin-1(2*H*)-yl)pent-1-en-1-yl]-2-methyl-4-oxo-2,3,4,5-tetrahydro-1*H*-1,5-benzodiazepin-7-yl}propoxy)ethyl]carbamate (61)**

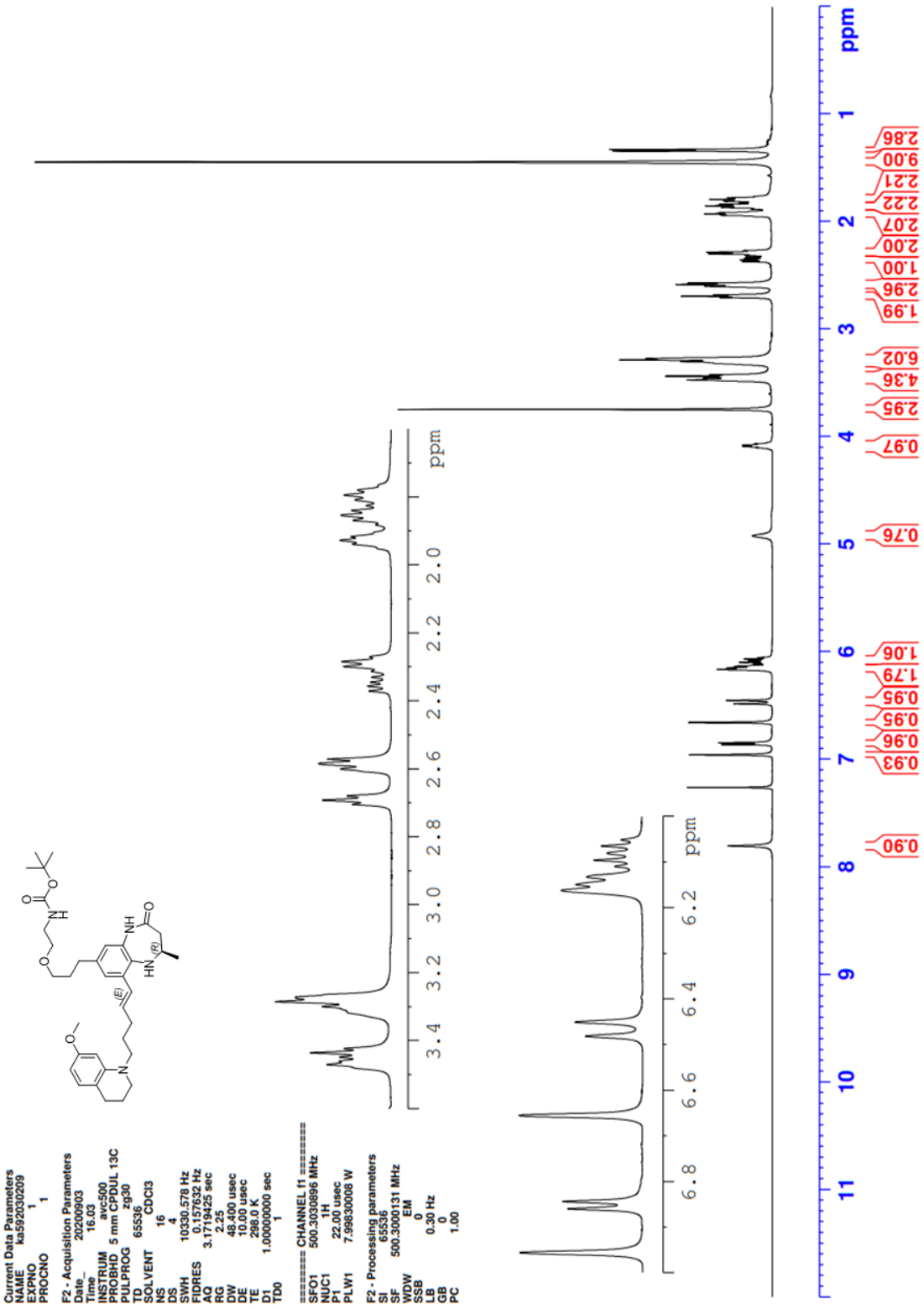

***tert*-Butyl [2-(3-{(2*R*)-9-[(1*E*)-5-(7-methoxy-3,4-dihydroquinolin-1(2*H*)-yl)pent-1-en-1-yl]-2-methyl-4-oxo-2,3,4,5-tetrahydro-1*H*-1,5-benzodiazepin-7-yl}propoxy)ethyl]carbamate (61)**

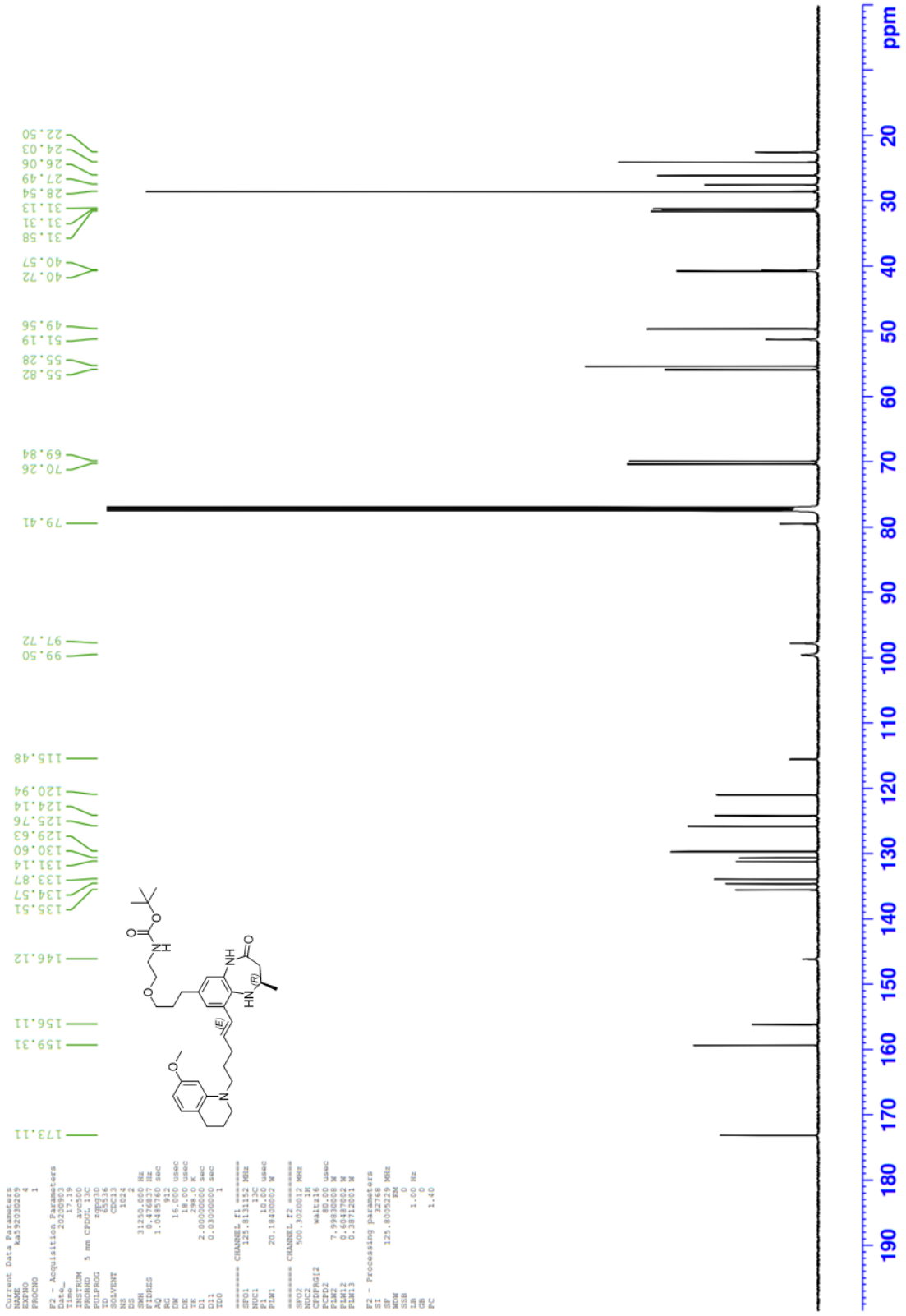

***tert*-Butyl {2-[2-(3-{(2*R*)-9-[(1*E*)-5-(7-methoxy-3,4-dihydroquinolin-1(2*H*)-yl)pent-1-en-1-yl]-2-methyl-4-oxo-2,3,4,5-tetrahydro-1*H*-1,5-benzodiazepin-7-yl}propoxy)ethoxy]ethyl}carbamate (62)**

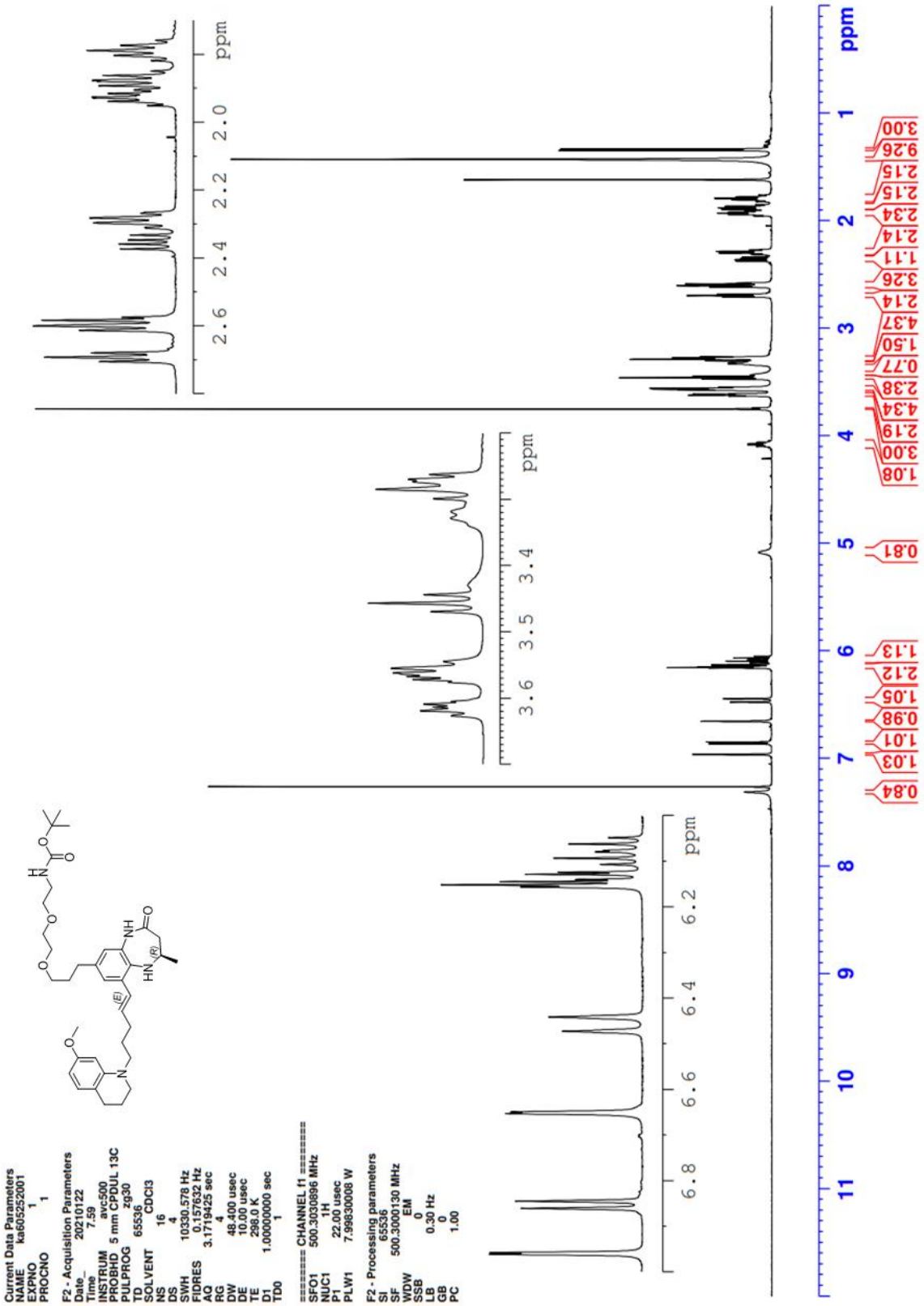

***tert*-Butyl {2-[2-(3-{(2*R*)-9-[(1*E*)-5-(7-methoxy-3,4-dihydroquinolin-1(2*H*)-yl)pent-1-en-1-yl]-2-methyl-4-oxo-2,3,4,5-tetrahydro-1*H*-1,5-benzodiazepin-7-yl}propoxy)ethoxy]ethyl}carbamate (62)**

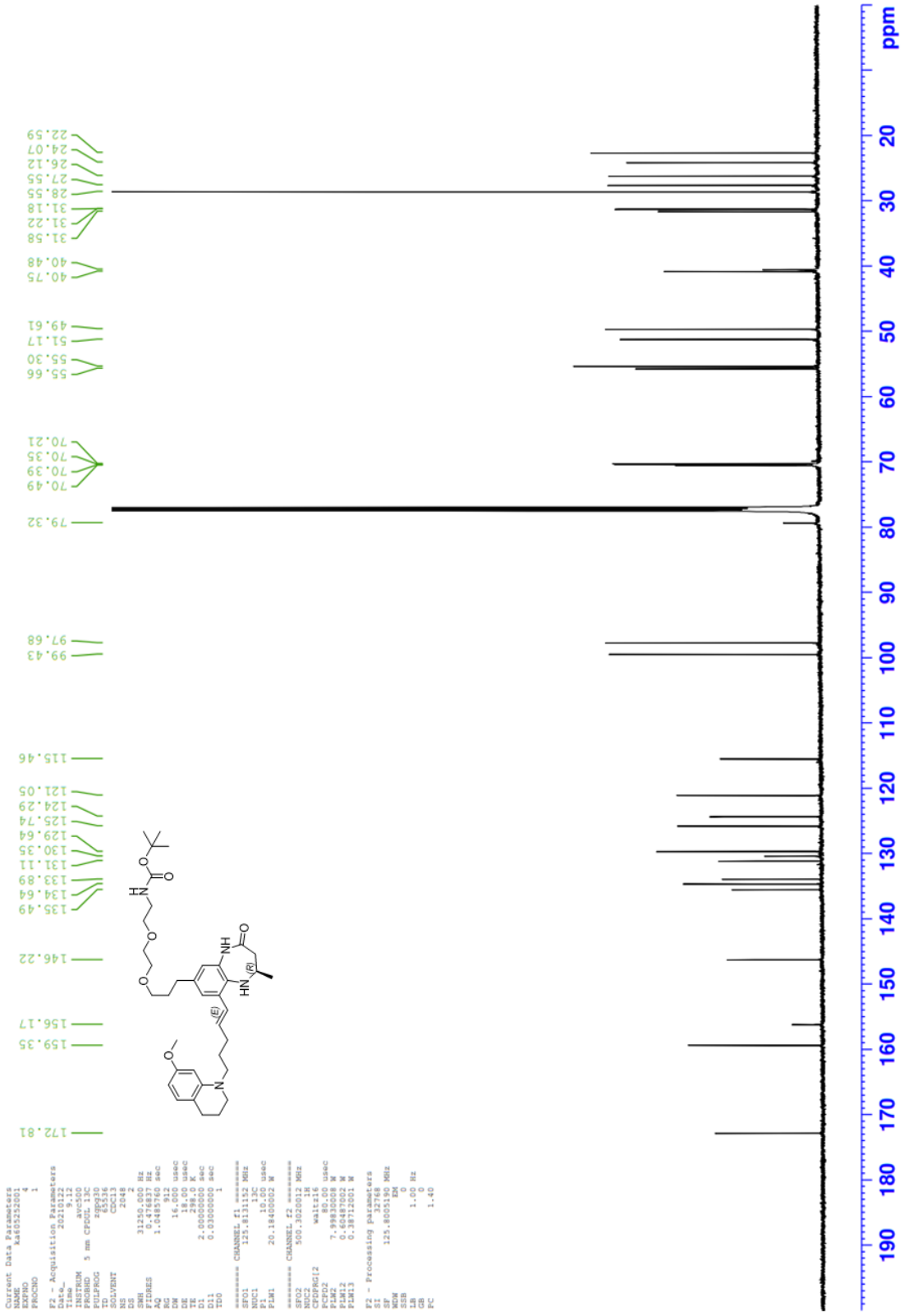

***tert*-Butyl (2-{2-[2-(3-{(2*R*)-9-[(1*E*)-5-(7-methoxy-3,4-dihydroquinolin-1(2*H*)-yl)pent-1-en-1-yl]-2-methyl-4-oxo-2,3,4,5-tetrahydro-1*H*-1,5-benzodiazepin-7-yl}propoxy)ethoxy]ethoxy}ethyl)carbamate (63)**

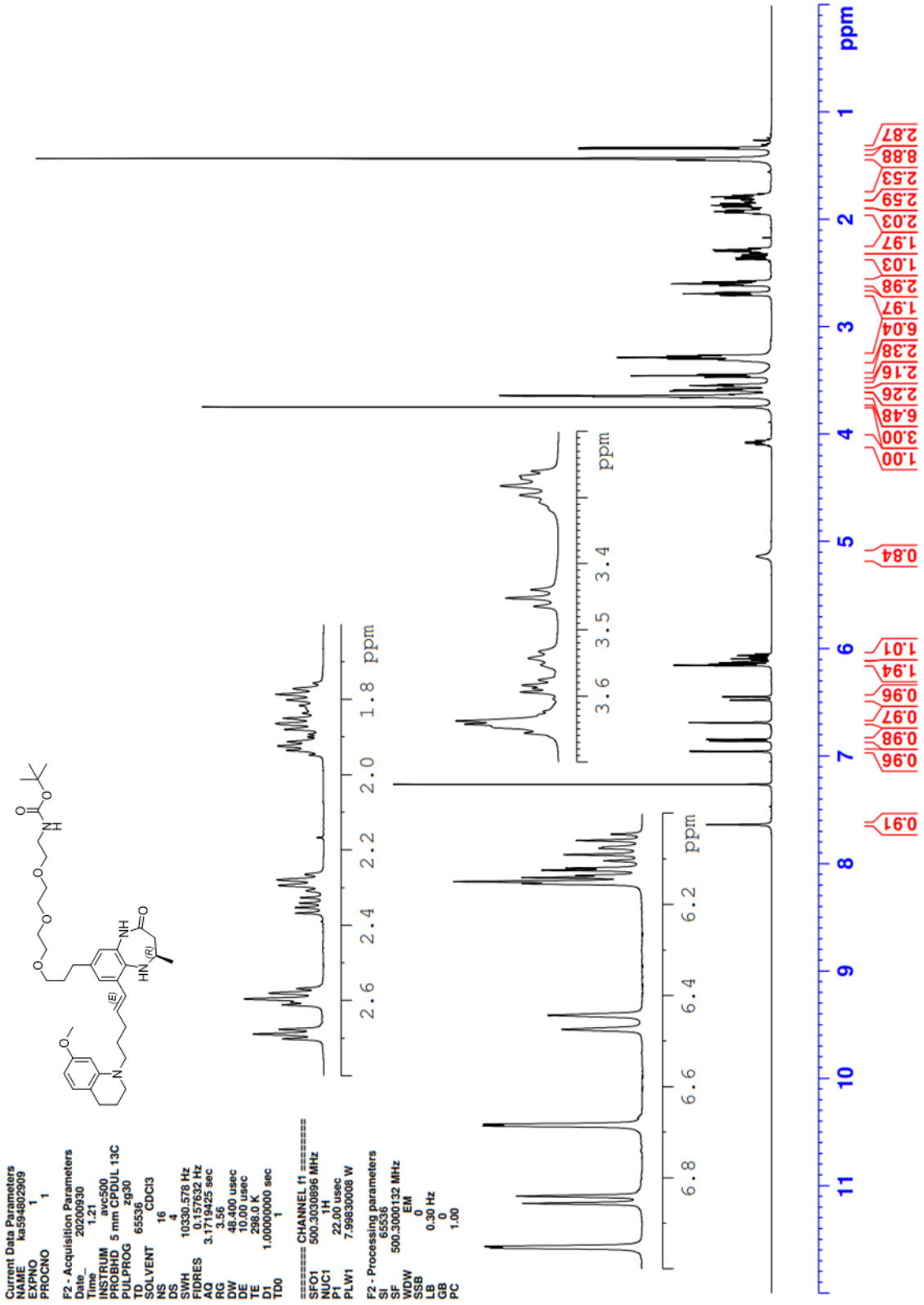

***tert*-Butyl (2-{2-[2-(3-{(2*R*)-9-[(1*E*)-5-(7-methoxy-3,4-dihydroquinolin-1(2*H*)-yl)pent-1-en-1-yl]-2-methyl-4-oxo-2,3,4,5-tetrahydro-1*H*-1,5-benzodiazepin-7-yl}propoxy)ethoxy]ethoxy}ethyl)carbamate (63)**

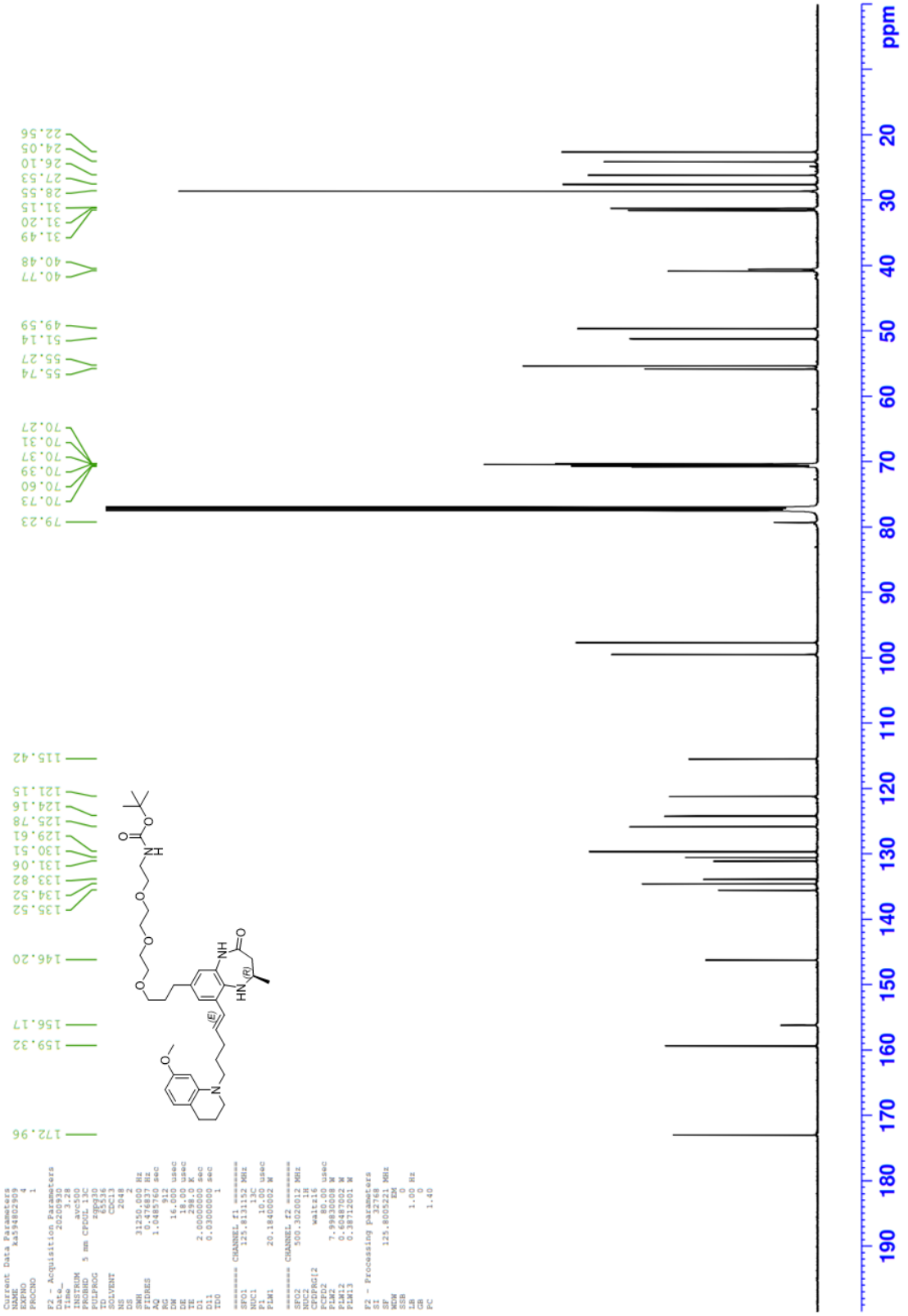

***tert*-Butyl (15-{(2*R*)-9-[(1*E*)-5-(7-methoxy-3,4-dihydroquinolin-1(2*H*)-yl)pent-1-en-1-yl]-2-methyl-4-oxo-2,3,4,5-tetrahydro-1*H*-1,5-benzodiazepin-7-yl}-3,6,9,12-tetraoxapentadecan-1-yl)carbamate (64)**

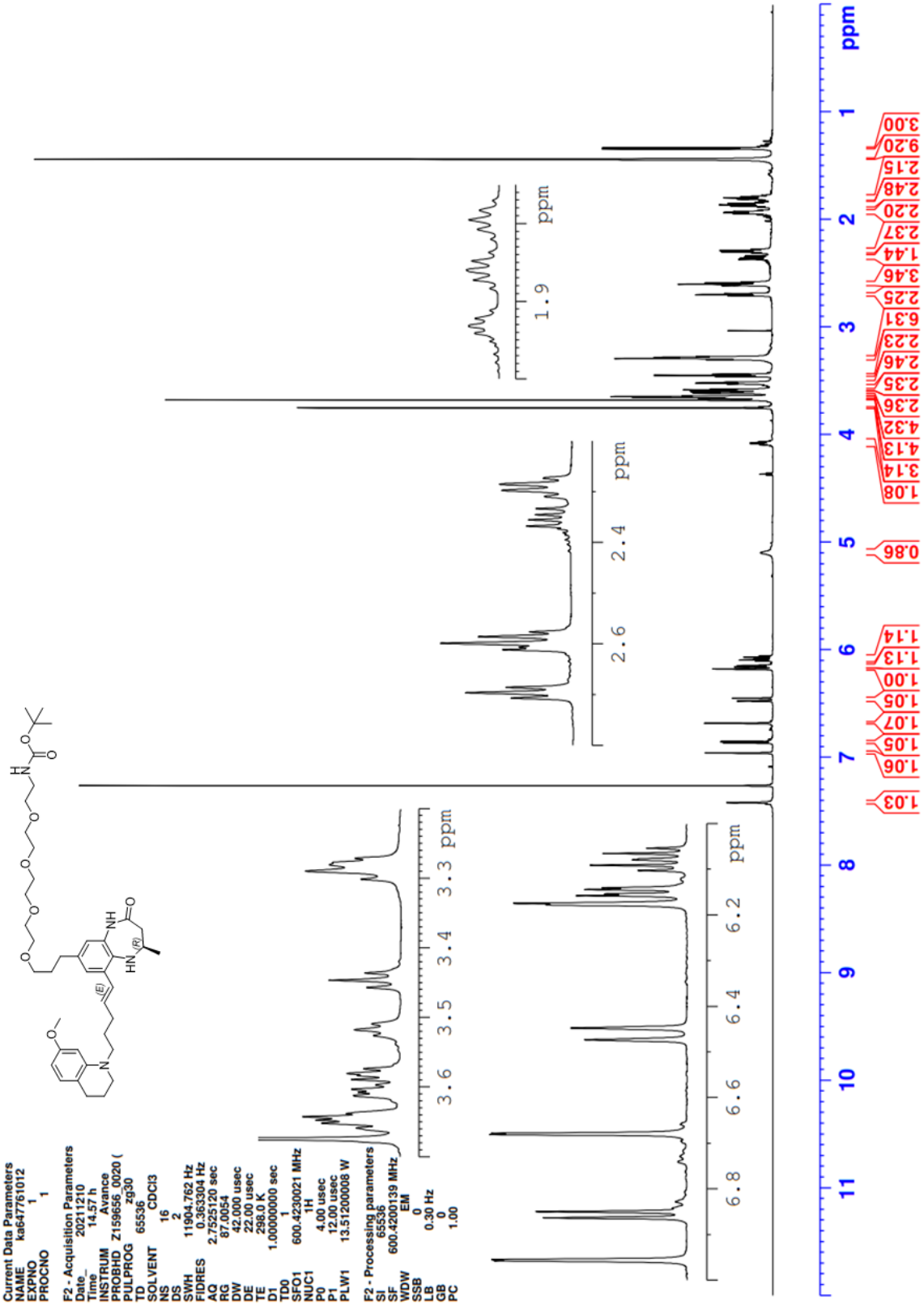

***tert*-Butyl (15-{(2*R*)-9-[(1*E*)-5-(7-methoxy-3,4-dihydroquinolin-1(2*H*)-yl)pent-1-en-1-yl]-2-methyl-4-oxo-2,3,4,5-tetrahydro-1*H*-1,5-benzodiazepin-7-yl}-3,6,9,12-tetraoxapentadecan-1-yl)carbamate (64)**

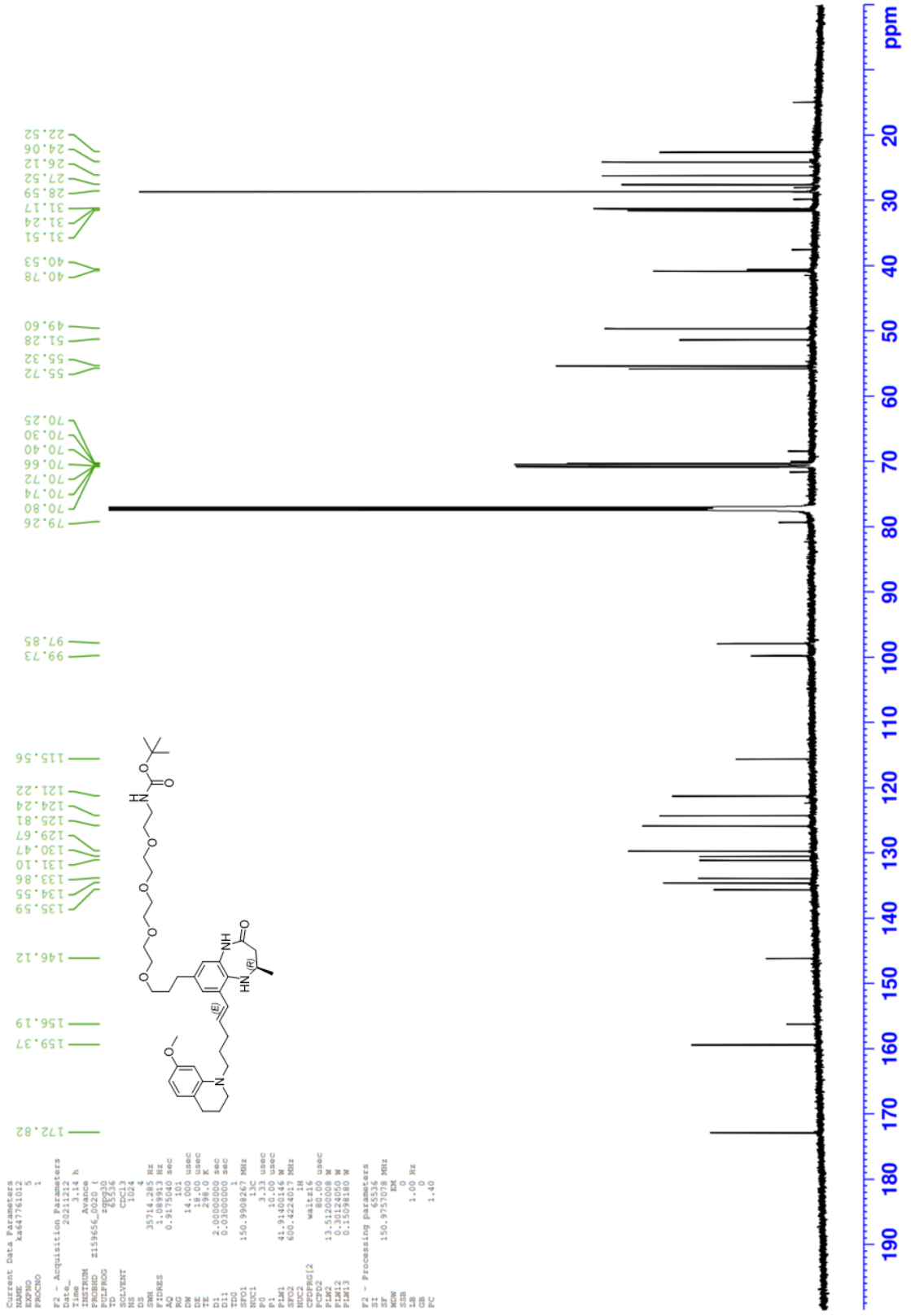

2-(2,6-Dioxopiperidin-3-yl)-4-{[2-(3-{(2*R*)-9-[(1*E*)-5-(7-methoxy-3,4-dihydroquinolin-1(2*H*)-yl)pent-1-en-1-yl]-2-methyl-4-oxo-2,3,4,5-tetrahydro-1*H*-1,5-benzodiazepin-7-yl}propoxy)ethyl]amino}-1*H*-isoindole-1,3(2*H*)-dione (35)

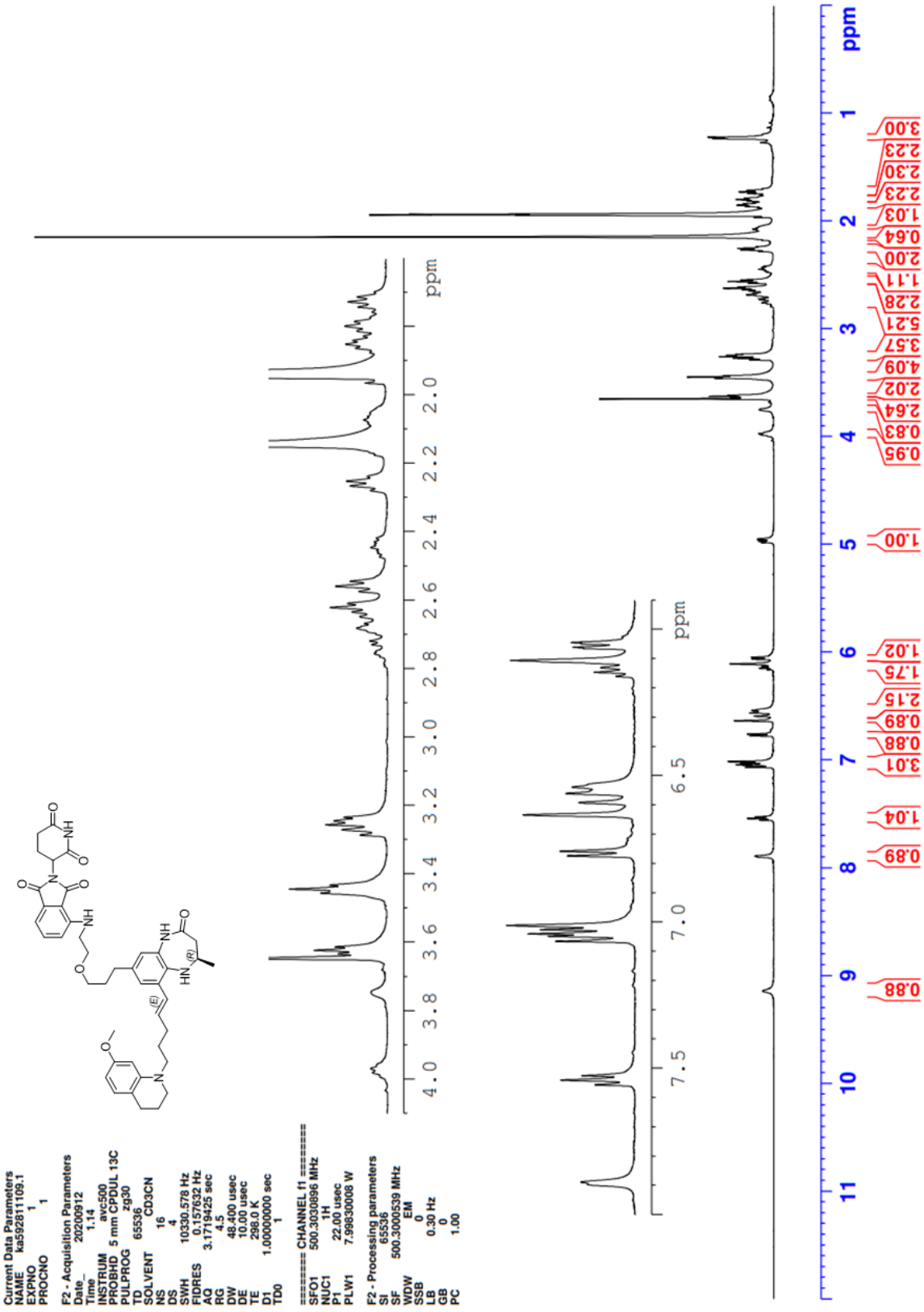

2-(2,6-Dioxopiperidin-3-yl)-4-{[2-(3-{(2*R*)-9-[(1*E*)-5-(7-methoxy-3,4-dihydroquinolin-1(2*H*)-yl)pent-1-en-1-yl]-2-methyl-4-oxo-2,3,4,5-tetrahydro-1*H*-1,5-benzodiazepin-7-yl}propoxy)ethyl]amino}-1*H*-isoindole-1,3(2*H*)-dione (35)

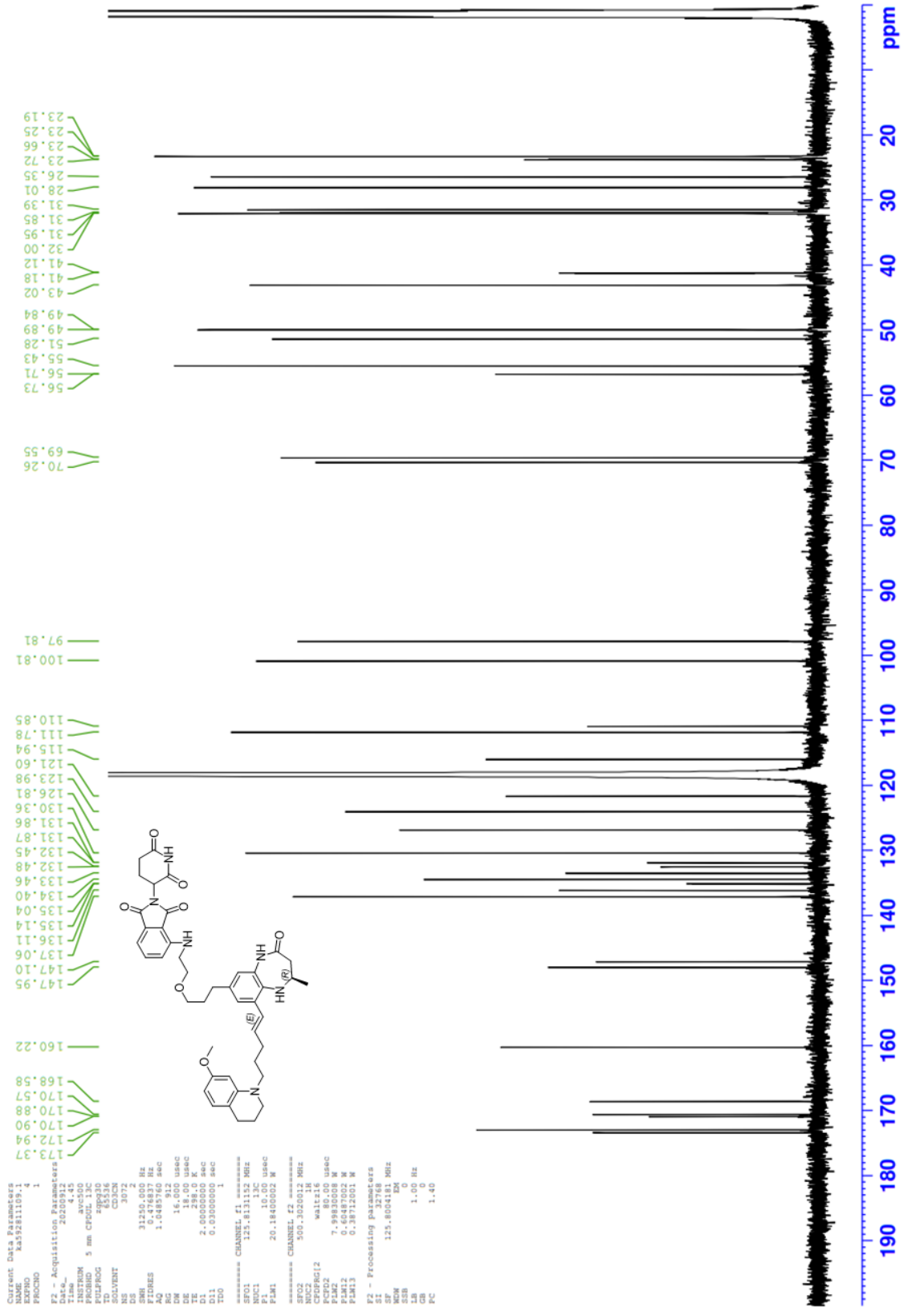

2-(2,6-Dioxopiperidin-3-yl)-4-({2-[2-(3-{(2*R*)-9-[(1*E*)-5-(7-methoxy-3,4-dihydroquinolin-1(2*H*)-yl)pent-1-en-1-yl]-2-methyl-4-oxo-2,3,4,5-tetrahydro-1*H*-1,5-benzodiazepin-7-yl}propoxy)ethoxy]ethyl}amino)-1*H*-isoindole-1,3(2*H*)-dione (36)

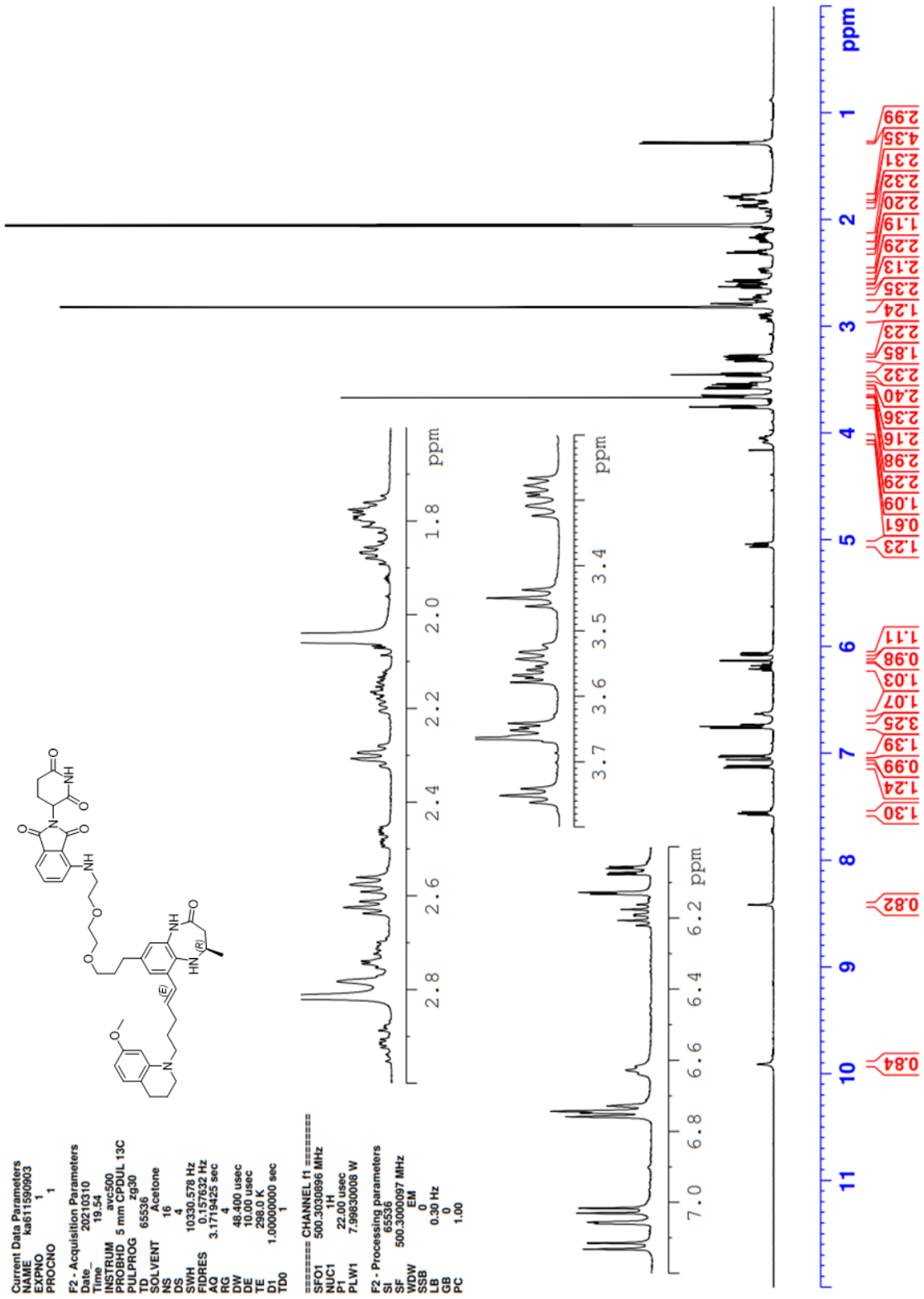

2-(2,6-Dioxopiperidin-3-yl)-4-({2-[2-(3-{(2*R*)-9-[(1*E*)-5-(7-methoxy-3,4-dihydroquinolin-1(2*H*)-yl)pent-1-en-1-yl]-2-methyl-4-oxo-2,3,4,5-tetrahydro-1*H*-1,5-benzodiazepin-7-yl}propoxy)ethoxy]ethyl}amino)-1*H*-isoindole-1,3(2*H*)-dione (36)

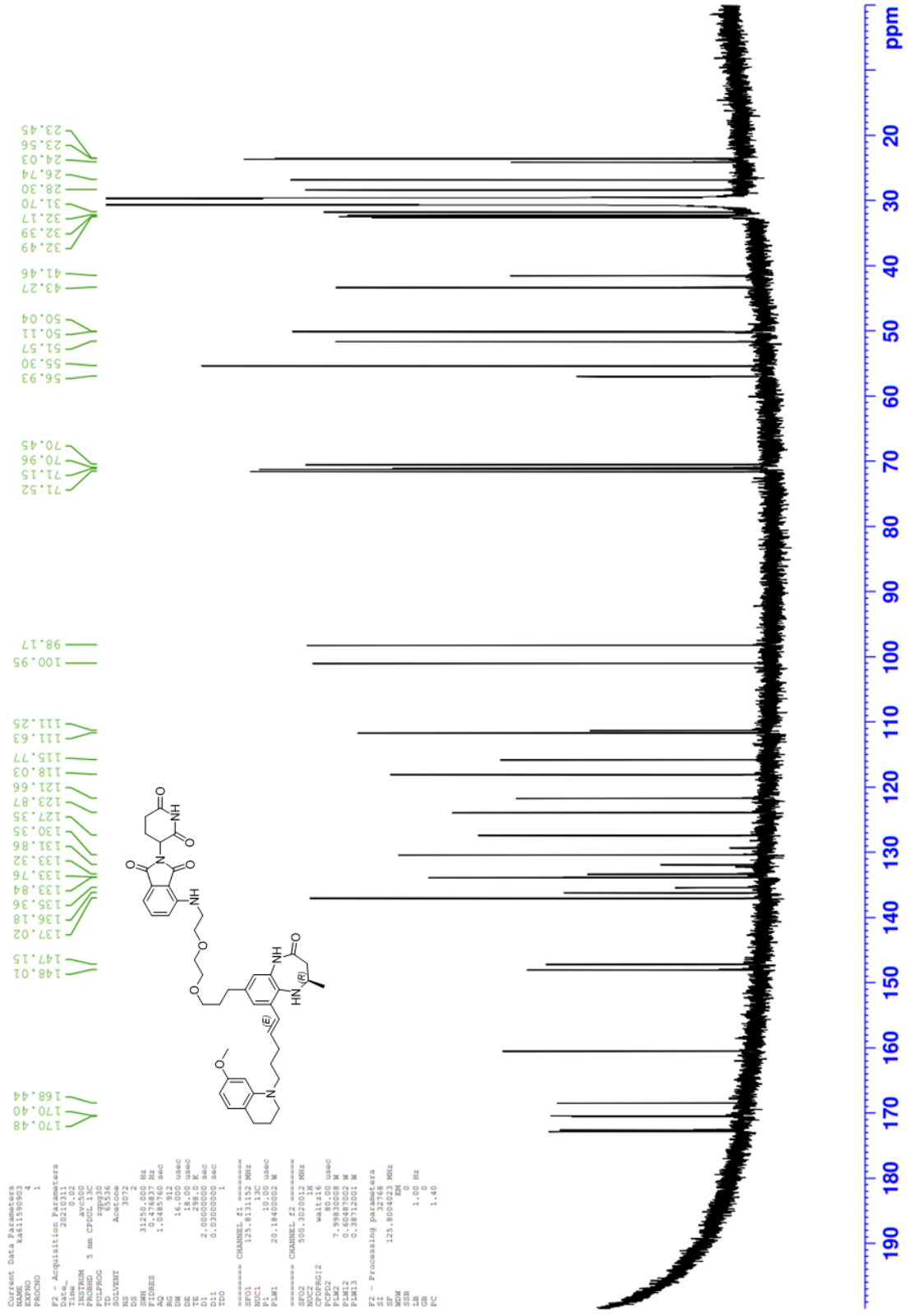

2-(2,6-Dioxopiperidin-3-yl)-4-[(2-{2-[2-(3-{(2*R*)-9-[(1*E*)-5-(7-methoxy-3,4-dihydroquinolin-1(2*H*)-yl)pent-1-en-1-yl]-2-methyl-4-oxo-2,3,4,5-tetrahydro-1*H*-1,5-benzodiazepin-7-yl}propoxy)ethoxy]ethoxy}ethyl)amino]-1*H*-isoindole-1,3(2*H*)-dione (37)

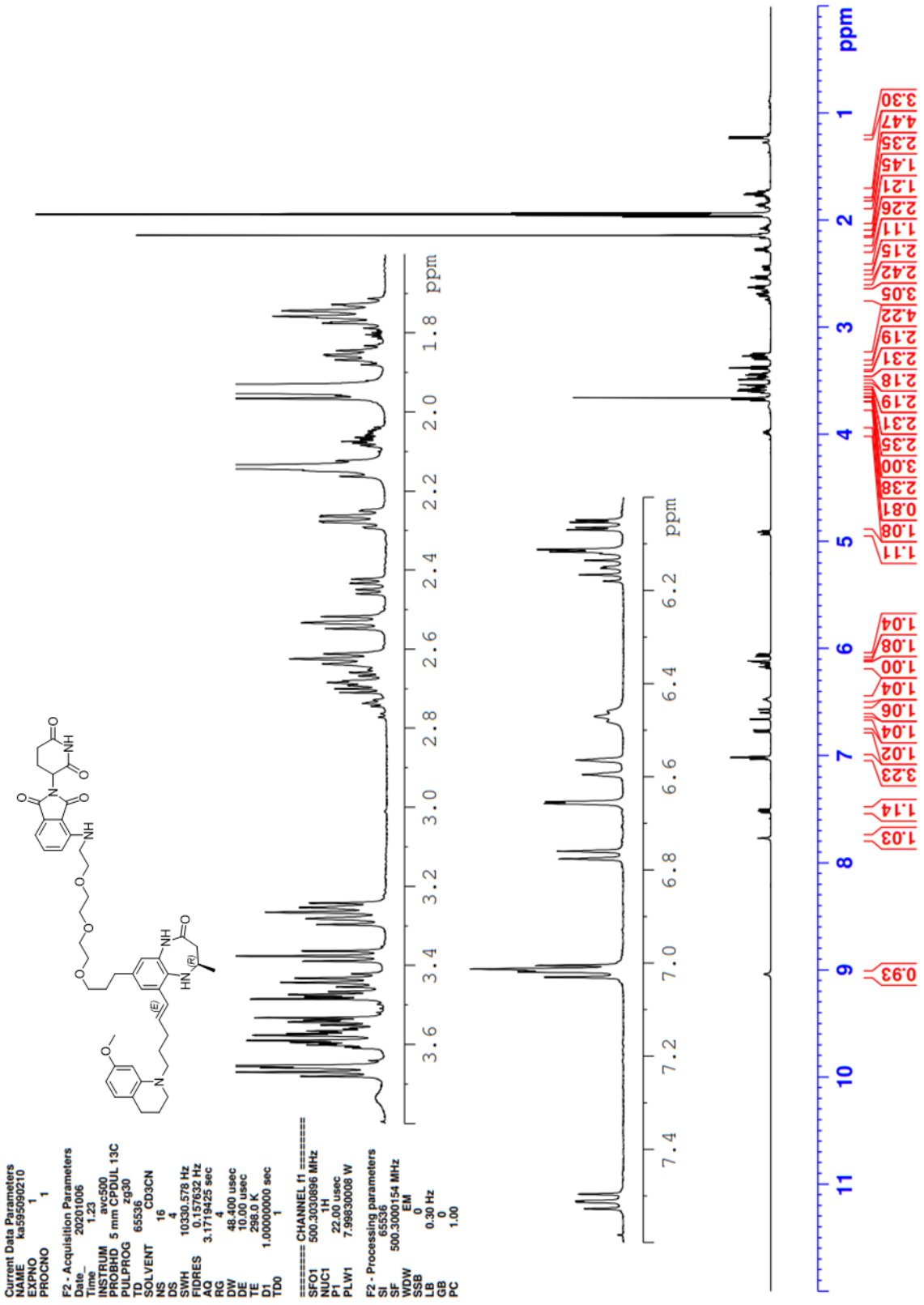

2-(2,6-Dioxopiperidin-3-yl)-4-[(2-{2-[2-(3-{(2*R*)-9-[(1*E*)-5-(7-methoxy-3,4-dihydroquinolin-1(2*H*)-yl)pent-1-en-1-yl]-2-methyl-4-oxo-2,3,4,5-tetrahydro-1*H*-1,5-benzodiazepin-7-yl}propoxy)ethoxy]ethoxy}ethyl)amino]-1*H*-isoindole-1,3(2*H*)-dione (37)

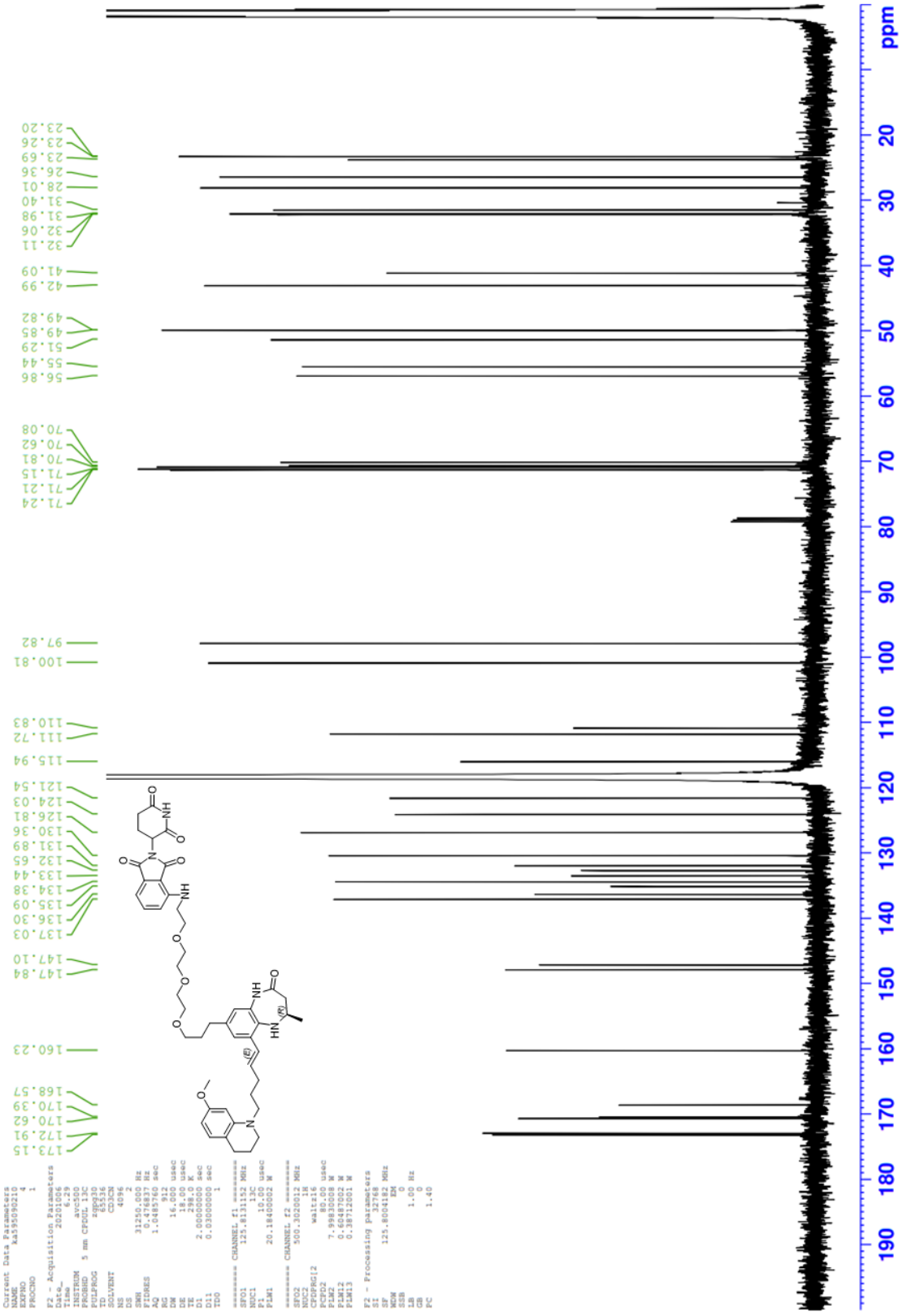

2-(2,6-Dioxopiperidin-3-yl)-4-[(15-{(2*R*)-9-[(1*E*)-5-(7-methoxy-3,4-dihydroquinolin-1(2*H*)-yl)pent-1-en-1-yl]-2-methyl-4-oxo-2,3,4,5-tetrahydro-1*H*-1,5-benzodiazepin-7-yl}-3,6,9,12-tetraoxapentadecan-1-yl)amino]-1*H*-isoindole-1,3(2*H*)-dione (38)

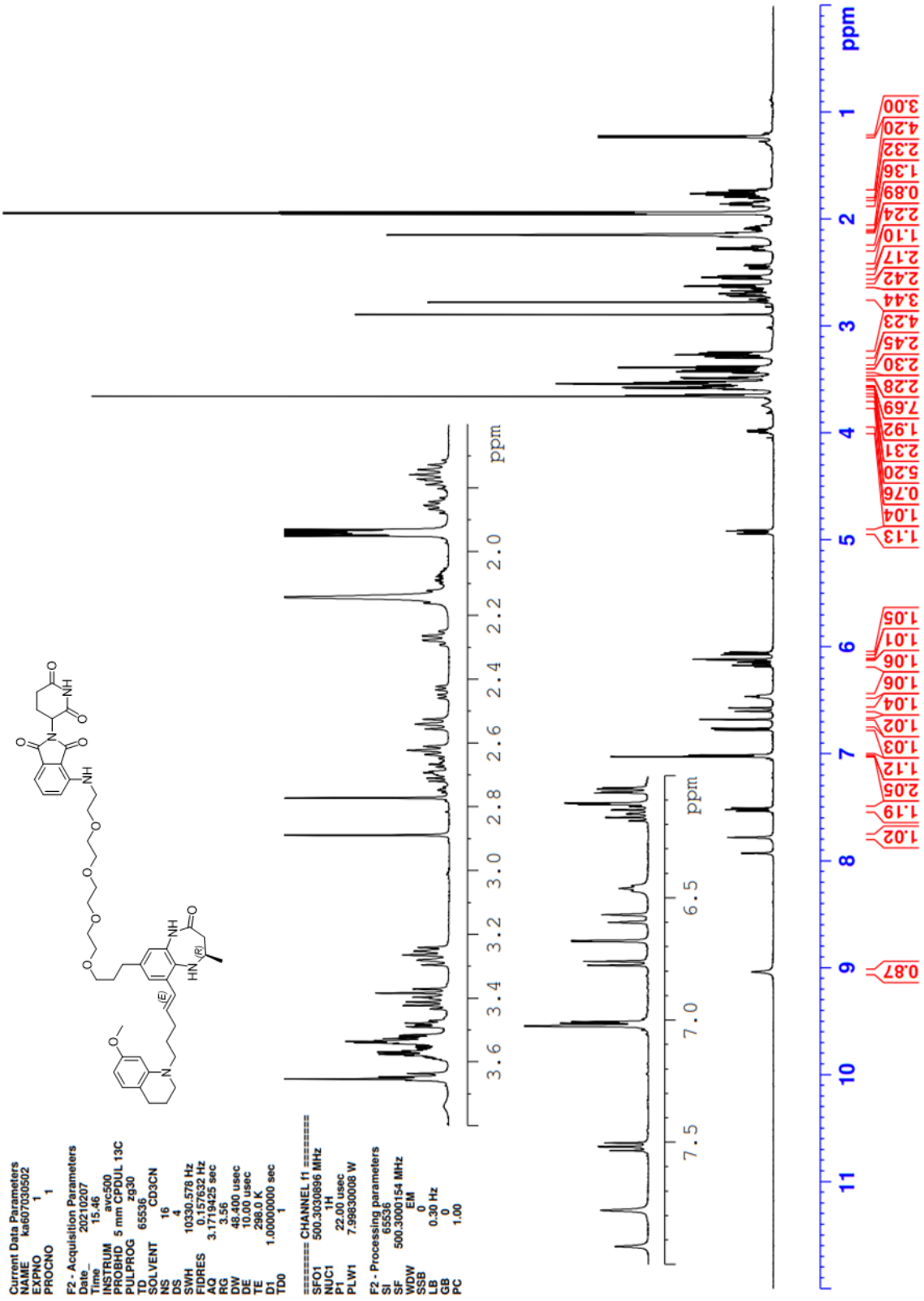

2-(2,6-Dioxopiperidin-3-yl)-4-[(15-{(2*R*)-9-[(1*E*)-5-(7-methoxy-3,4-dihydroquinolin-1(2*H*)-yl)pent-1-en-1-yl]-2-methyl-4-oxo-2,3,4,5-tetrahydro-1*H*-1,5-benzodiazepin-7-yl}-3,6,9,12-tetraoxapentadecan-1-yl)amino]-1*H*-isoindole-1,3(2*H*)-dione (38)

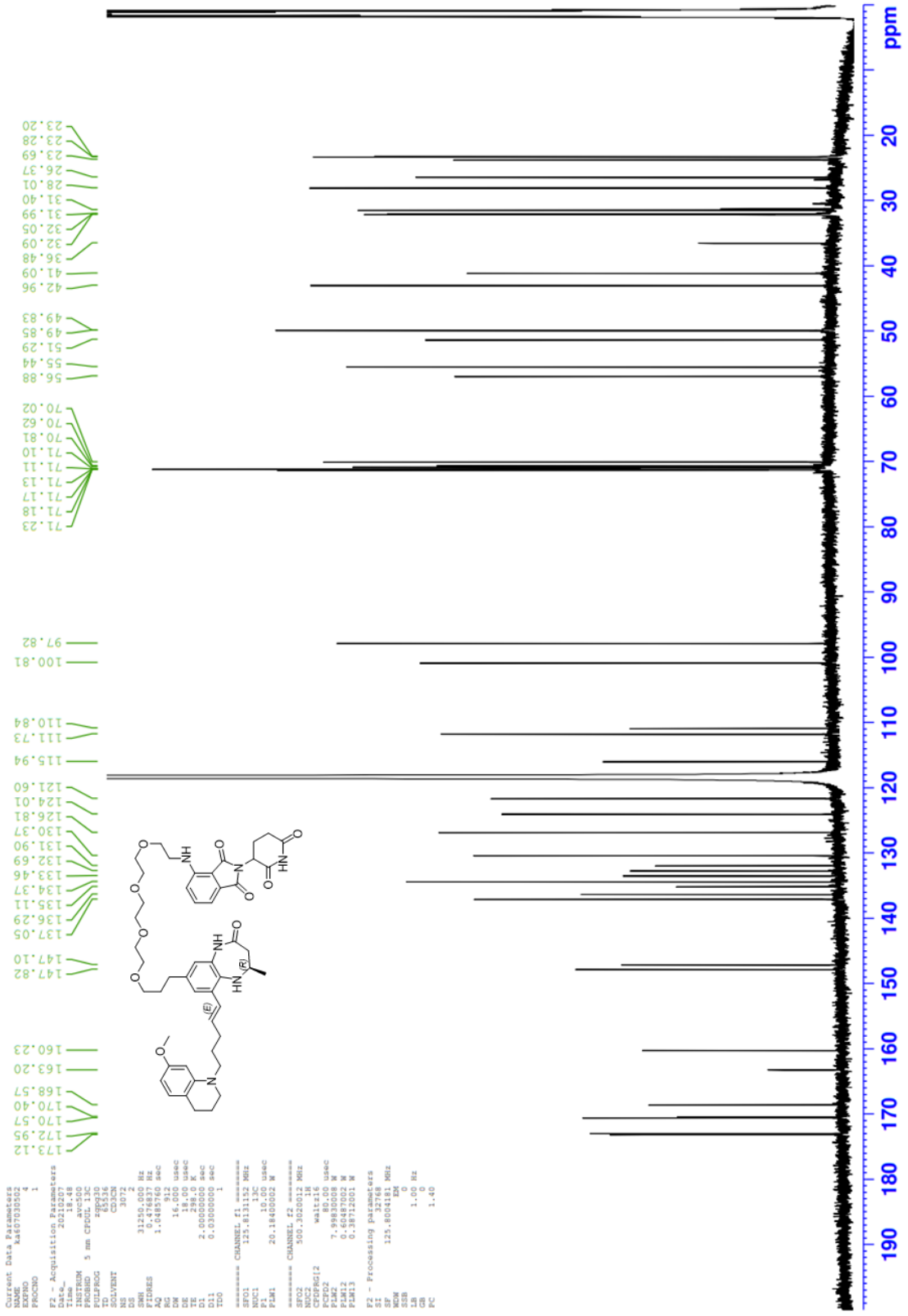

2-(Adamantan-1-yl)-*N*-[2-(3-{(2*R*)-9-[(1*E*)-5-(7-methoxy-3,4-dihydroquinolin-1(2*H*)-yl)pent-1-en-1-yl]-2-methyl-4-oxo-2,3,4,5-tetrahydro-1*H*-1,5-benzodiazepin-7-yl}propoxy)ethyl]acetamide (65)

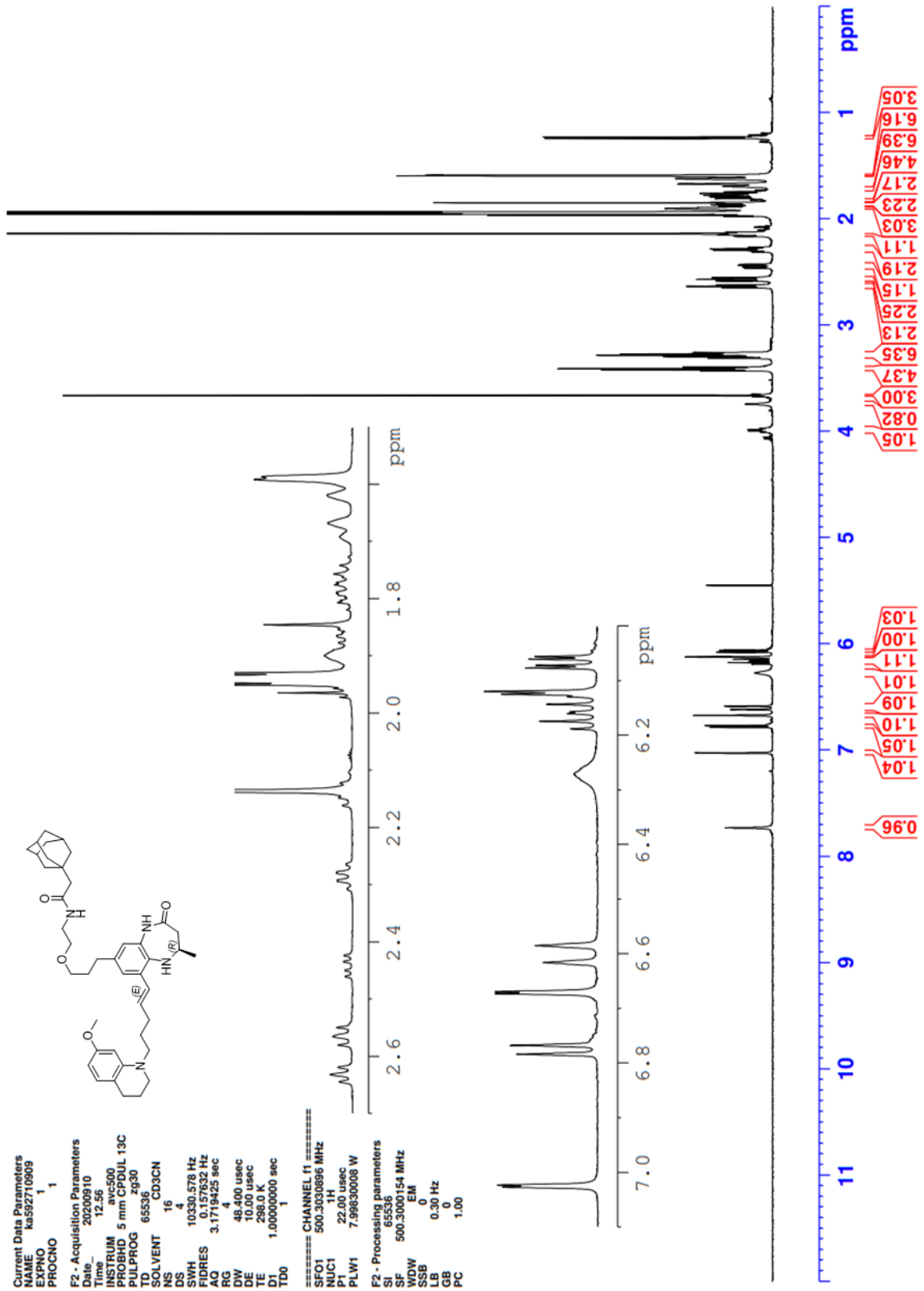

2-(Adamantan-1-yl)-*N*-[2-(3-{(2*R*)-9-[(1*E*)-5-(7-methoxy-3,4-dihydroquinolin-1(2*H*)-yl)pent-1-en-1-yl]-2-methyl-4-oxo-2,3,4,5-tetrahydro-1*H*-1,5-benzodiazepin-7-yl}propoxy)ethyl]acetamide (65)

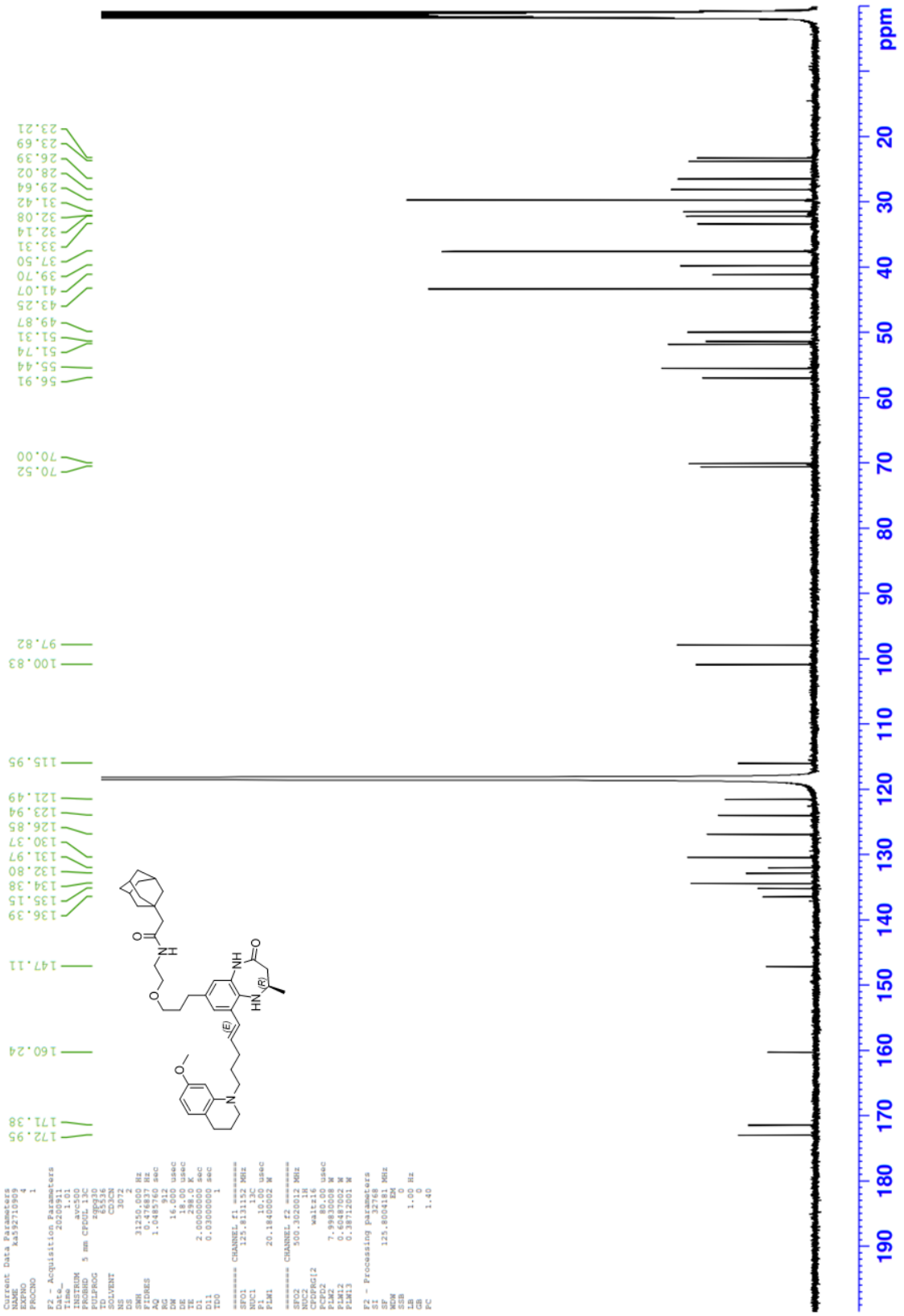

2-(Adamantan-1-yl)-*N*-{2-[2-(3-{(2*R*)-9-[(1*E*)-5-(7-methoxy-3,4-dihydroquinolin-1(2*H*)-yl)pent-1-en-1-yl]-2-methyl-4-oxo-2,3,4,5-tetrahydro-1*H*-1,5-benzodiazepin-7-yl}propoxy)ethoxy]ethyl}acetamide (66)

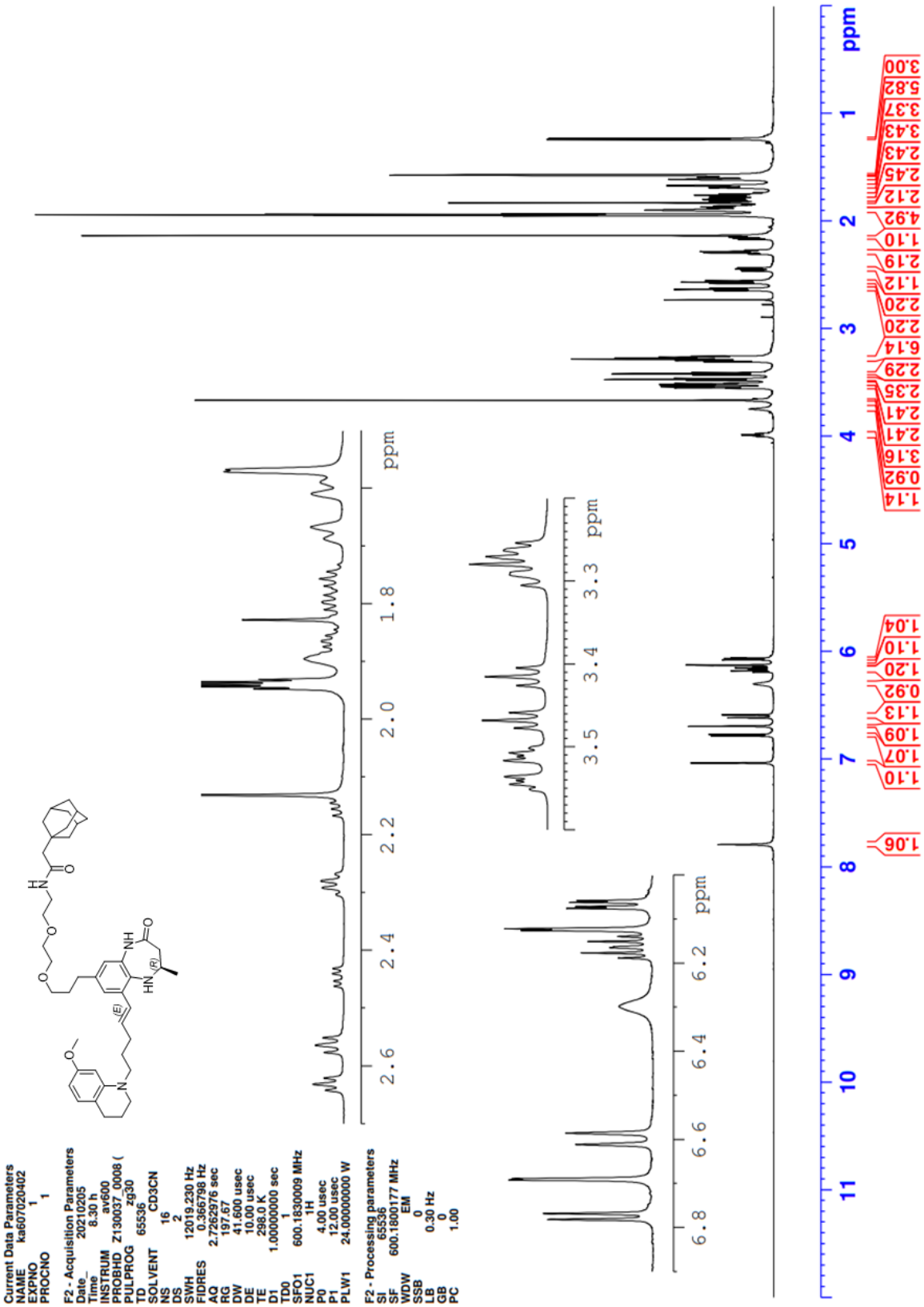

2-(Adamantan-1-yl)-*N*-{2-[2-(3-{(2*R*)-9-[(1*E*)-5-(7-methoxy-3,4-dihydroquinolin-1(2*H*)-yl)pent-1-en-1-yl]-2-methyl-4-oxo-2,3,4,5-tetrahydro-1*H*-1,5-benzodiazepin-7-yl}propoxy)ethoxy]ethyl}acetamide (66)

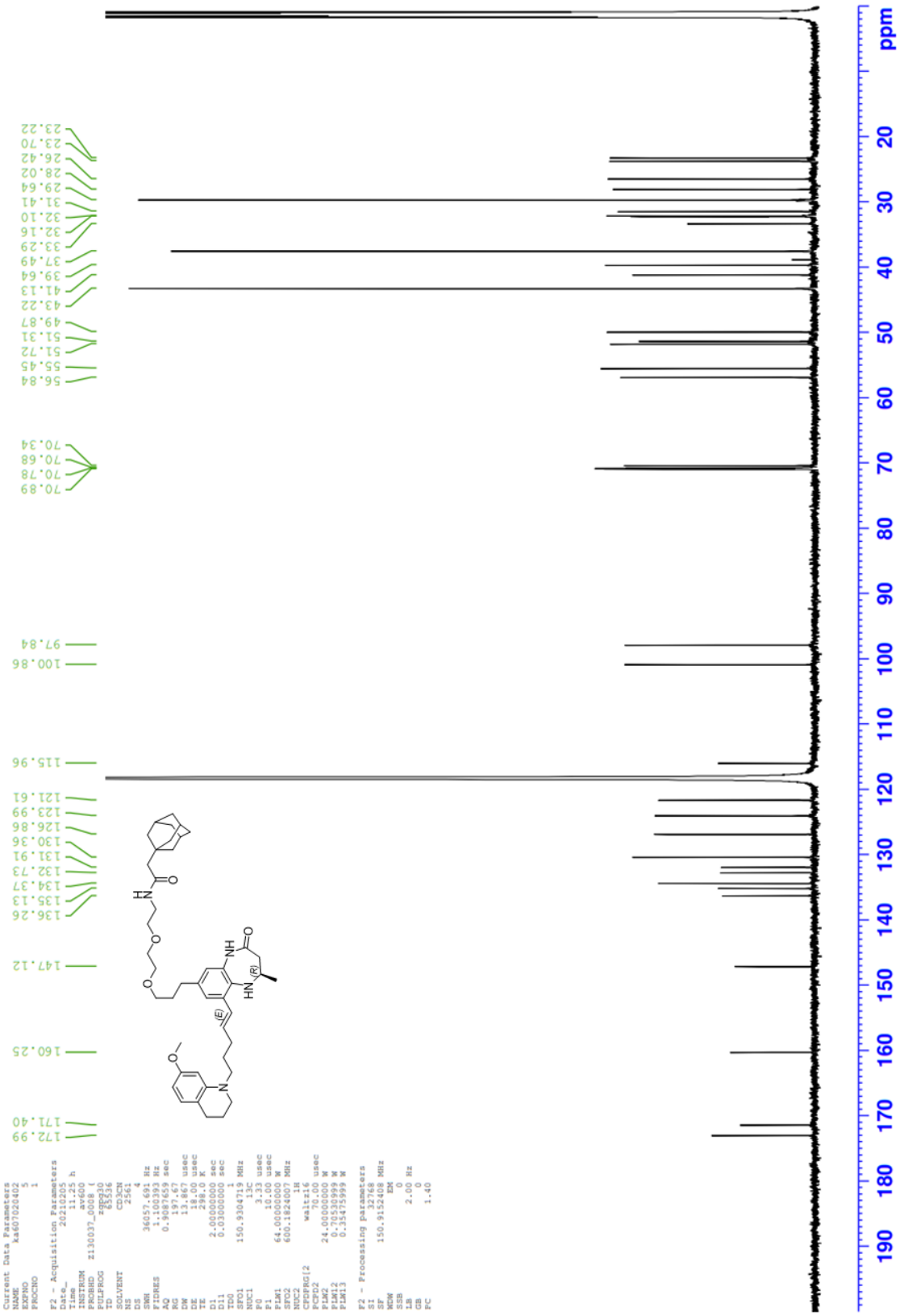

2-(Adamantan-1-yl)-*N*-(2-{2-[2-(3-{(2*R*)-9-[(1*E*)-5-(7-methoxy-3,4-dihydroquinolin-1(2*H*)-yl)pent-1-en-1-yl]-2-methyl-4-oxo-2,3,4,5-tetrahydro-1*H*-1,5-benzodiazepin-7-yl}propoxy)ethoxy]ethoxy}ethyl)acetamide (67)

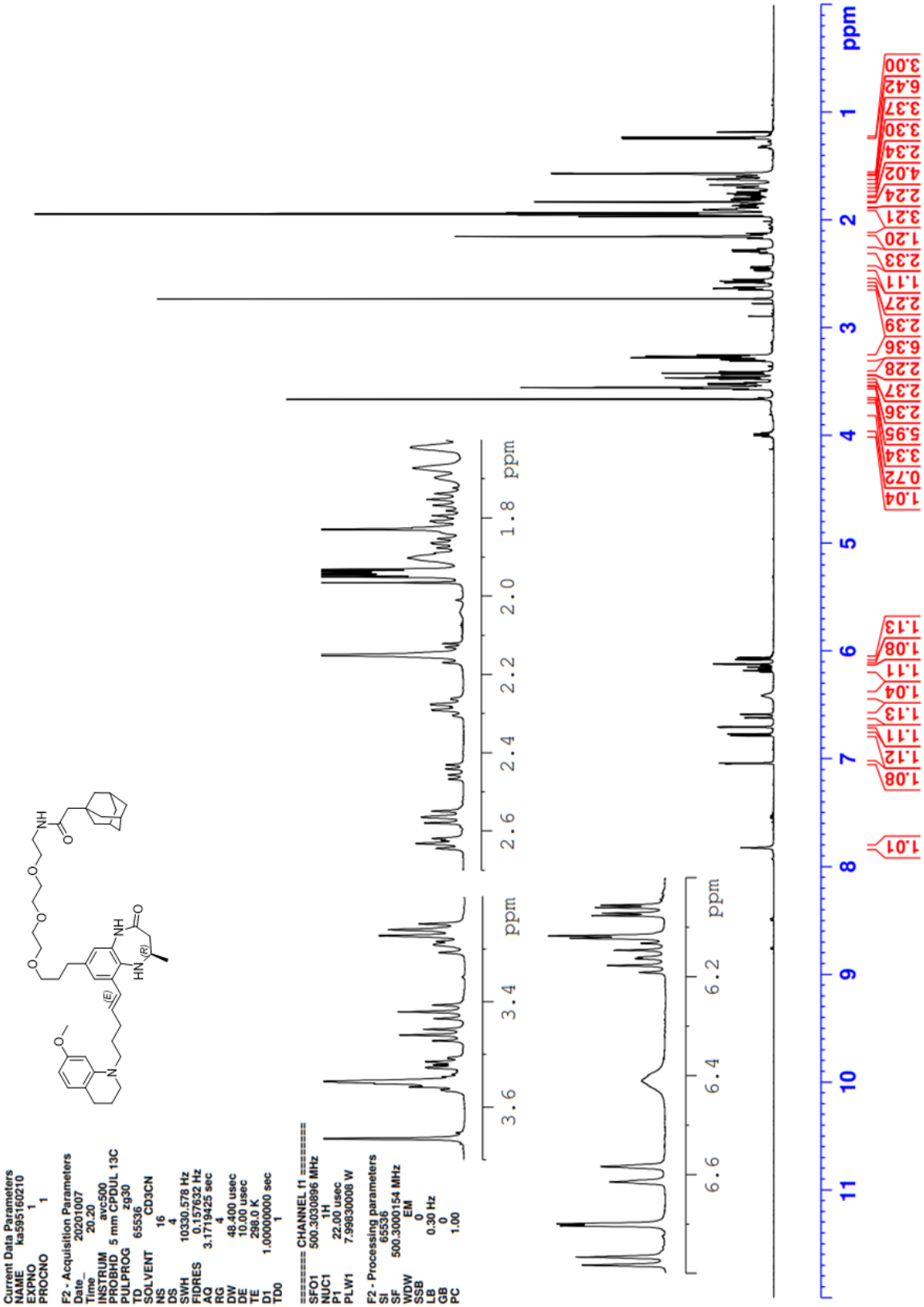

2-(Adamantan-1-yl)-*N*-(2-{2-[2-(3-{(2*R*)-9-[(1*E*)-5-(7-methoxy-3,4-dihydroquinolin-1(2*H*)-yl)pent-1-en-1-yl]-2-methyl-4-oxo-2,3,4,5-tetrahydro-1*H*-1,5-benzodiazepin-7-yl}propoxy)ethoxy]ethoxy}ethyl)acetamide (67)

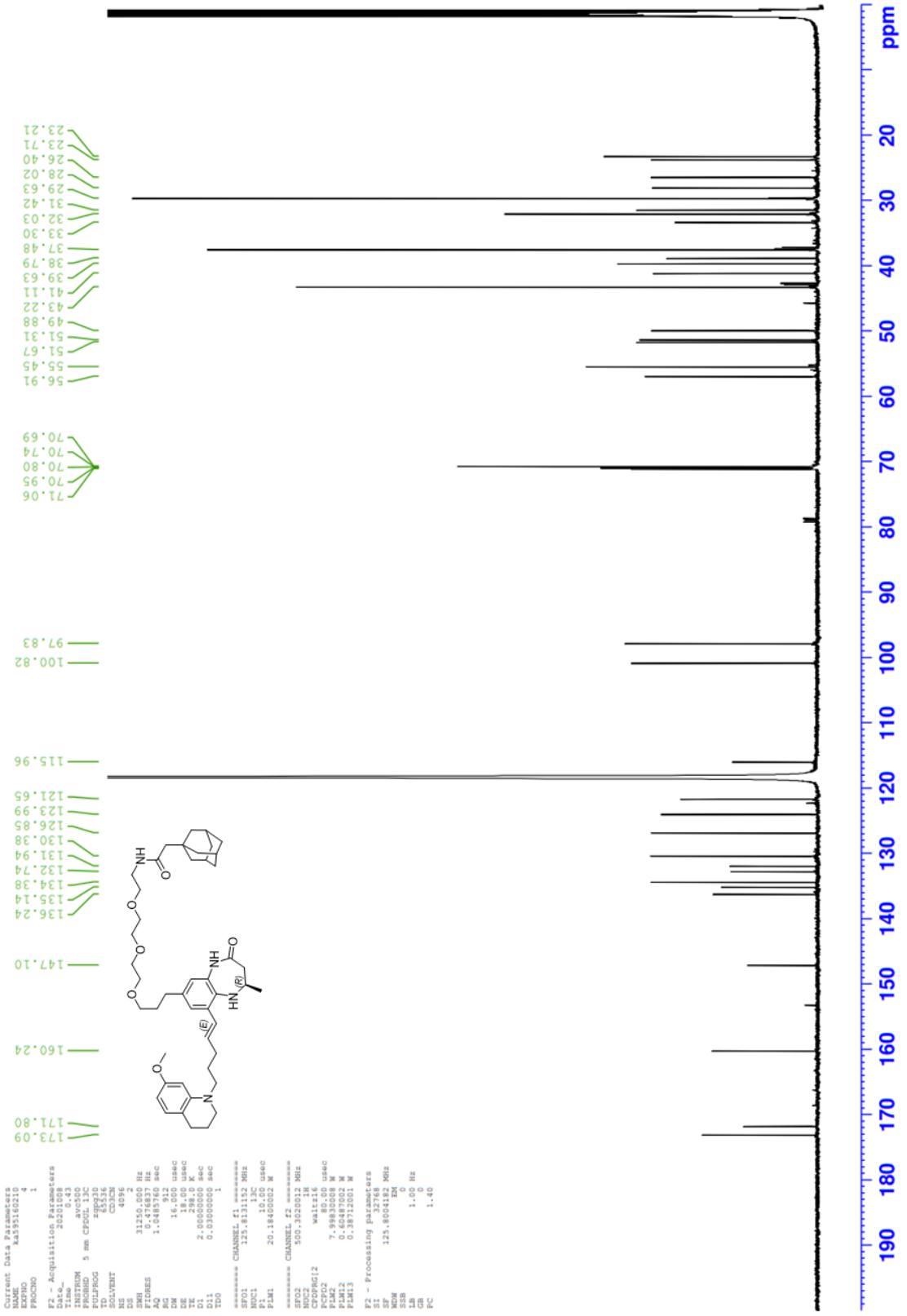

2-(Adamantan-1-yl)-*N*-(15-{(2*R*)-9-[(1*E*)-5-(7-methoxy-3,4-dihydroquinolin-1(2*H*)-yl)pent-1-en-1-yl]-2-methyl-4-oxo-2,3,4,5-tetrahydro-1*H*-1,5-benzodiazepin-7-yl}-3,6,9,12-tetraoxapentadecan-1-yl)acetamide (68)

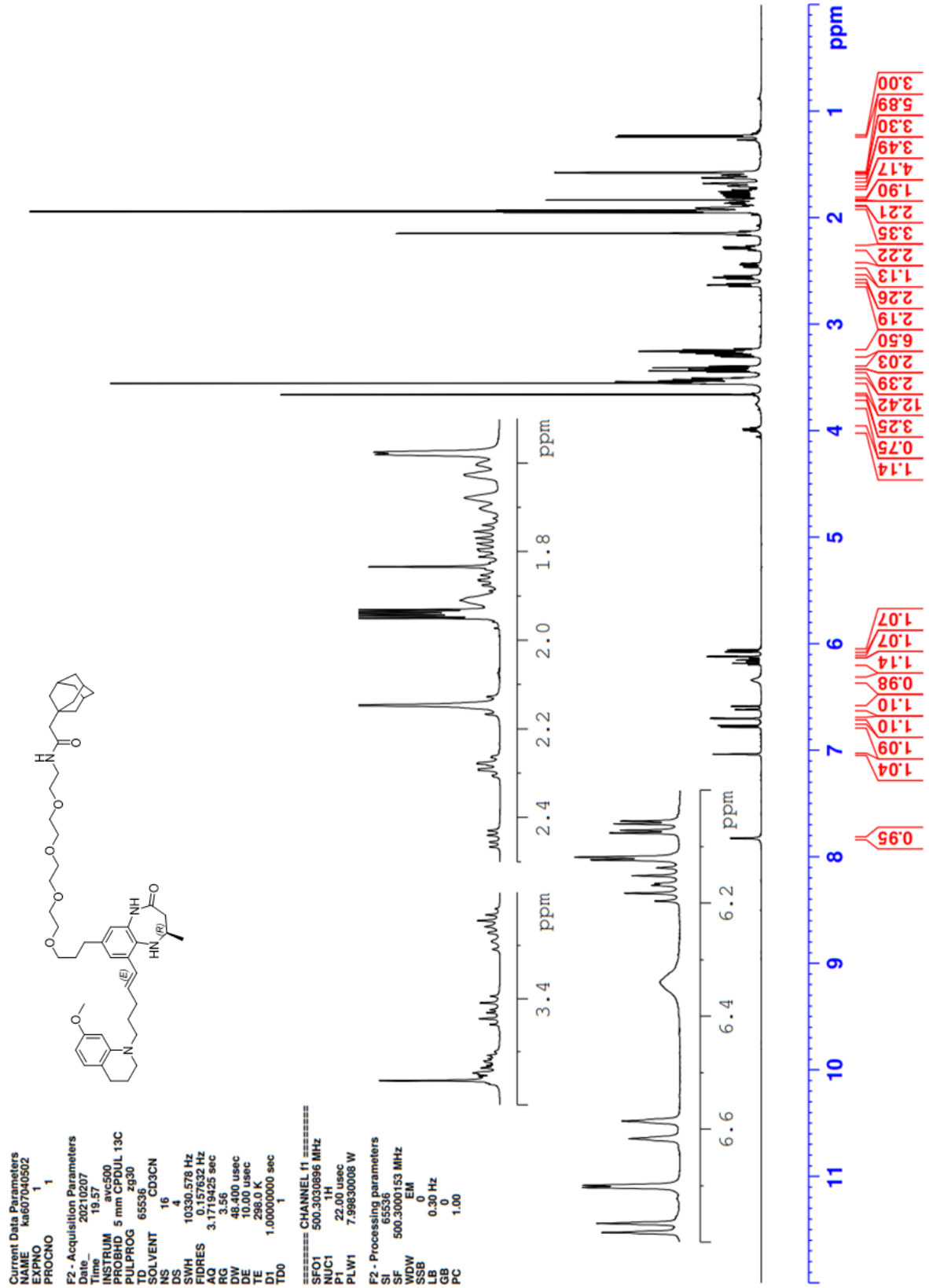

2-(Adamantan-1-yl)-*N*-(15-{(2*R*)-9-[(1*E*)-5-(7-methoxy-3,4-dihydroquinolin-1(2*H*)-yl)pent-1-en-1-yl]-2-methyl-4-oxo-2,3,4,5-tetrahydro-1*H*-1,5-benzodiazepin-7-yl}-3,6,9,12-tetraoxapentadecan-1-yl)acetamide (68)

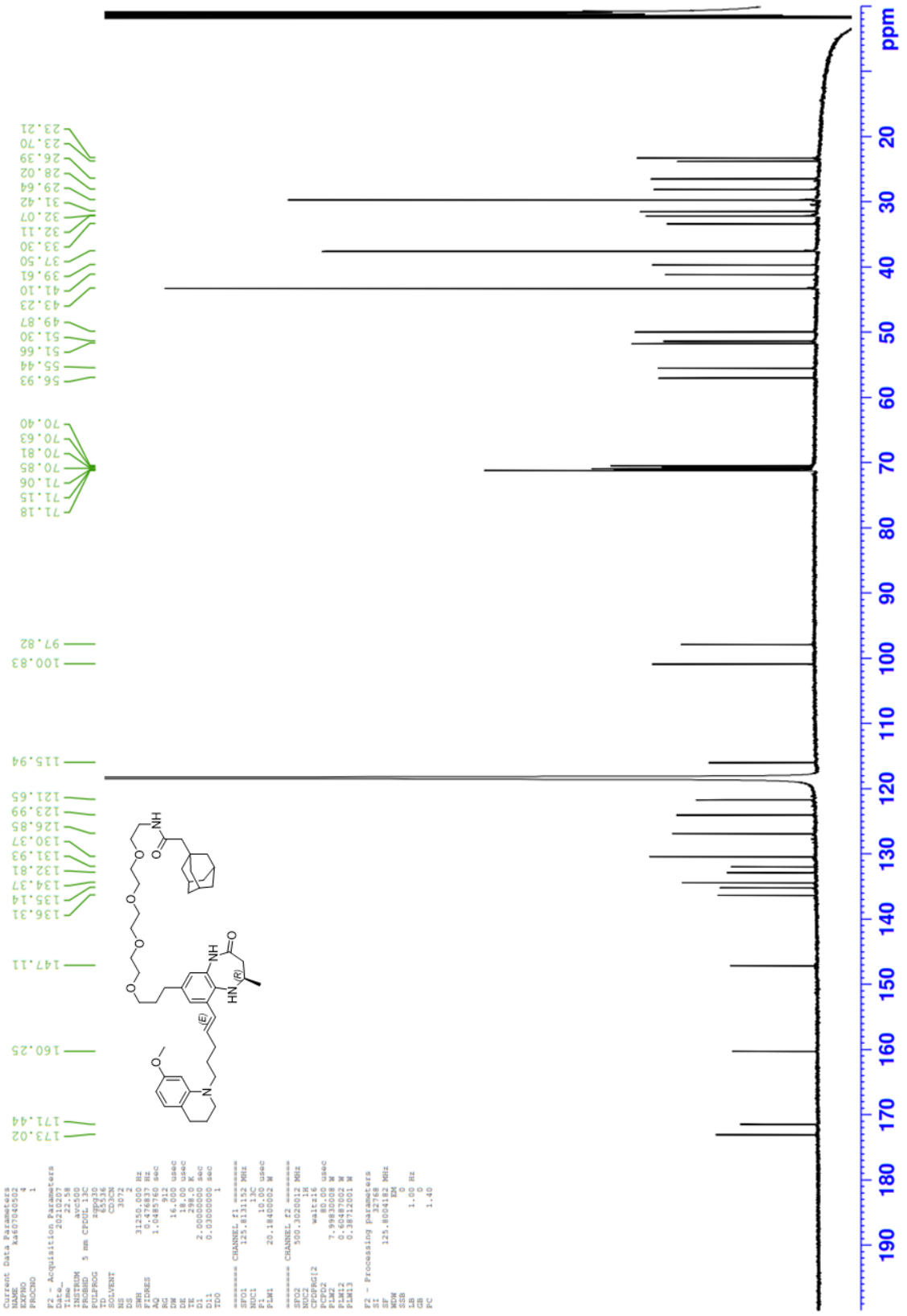

***tert*-Butyl 4-[(2*R*)-9-bromo-2-methyl-4-oxo-2,3,4,5-tetrahydro-1H-1,5-benzodiazepin-7-yl]-1,2,3,6-tetrahydropyridine-1-carboxylate (89)**

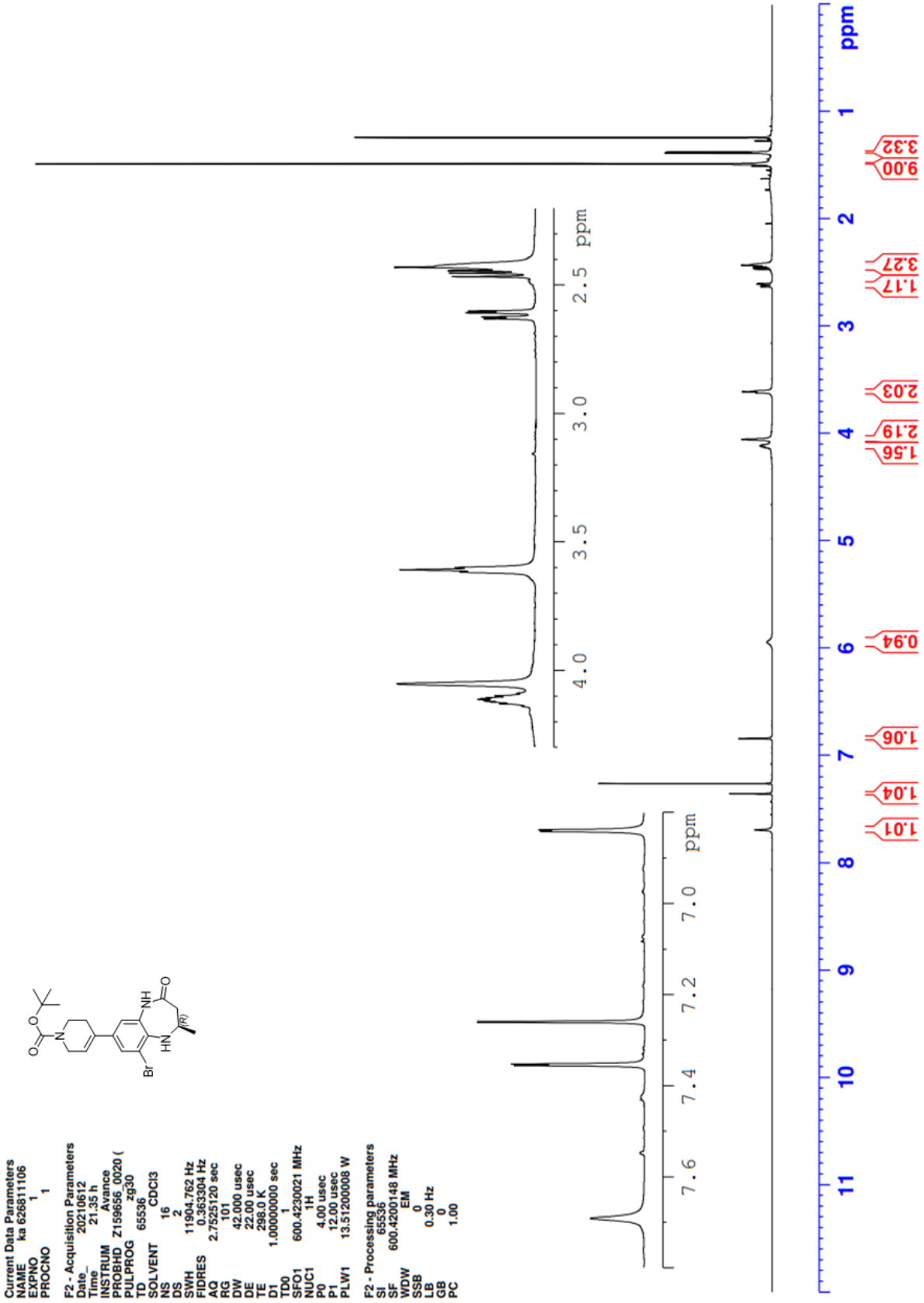

tert-Butyl 4-[(2*R*)-9-bromo-2-methyl-4-oxo-2,3,4,5-tetrahydro-1H-1,5-benzodiazepin-7-yl]-1,2,3,6-tetrahydropyridine-1-carboxylate (89)

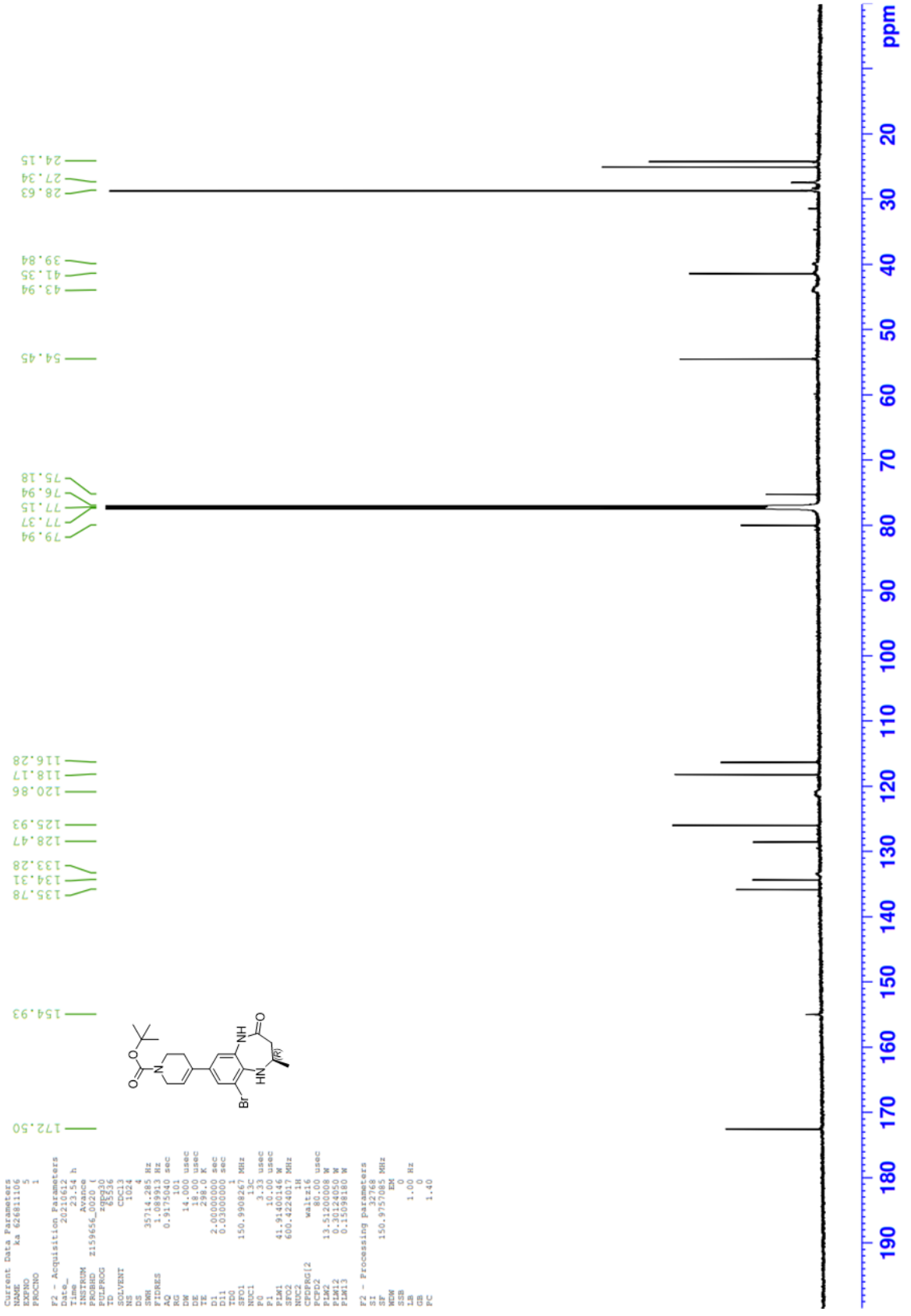

tert-Butyl 4-[(2*R*)-9-bromo-2-methyl-4-oxo-1,2,3,5-tetrahydro-1,5-benzodiazepin-7-yl]piperidine-1-carboxylate (90)

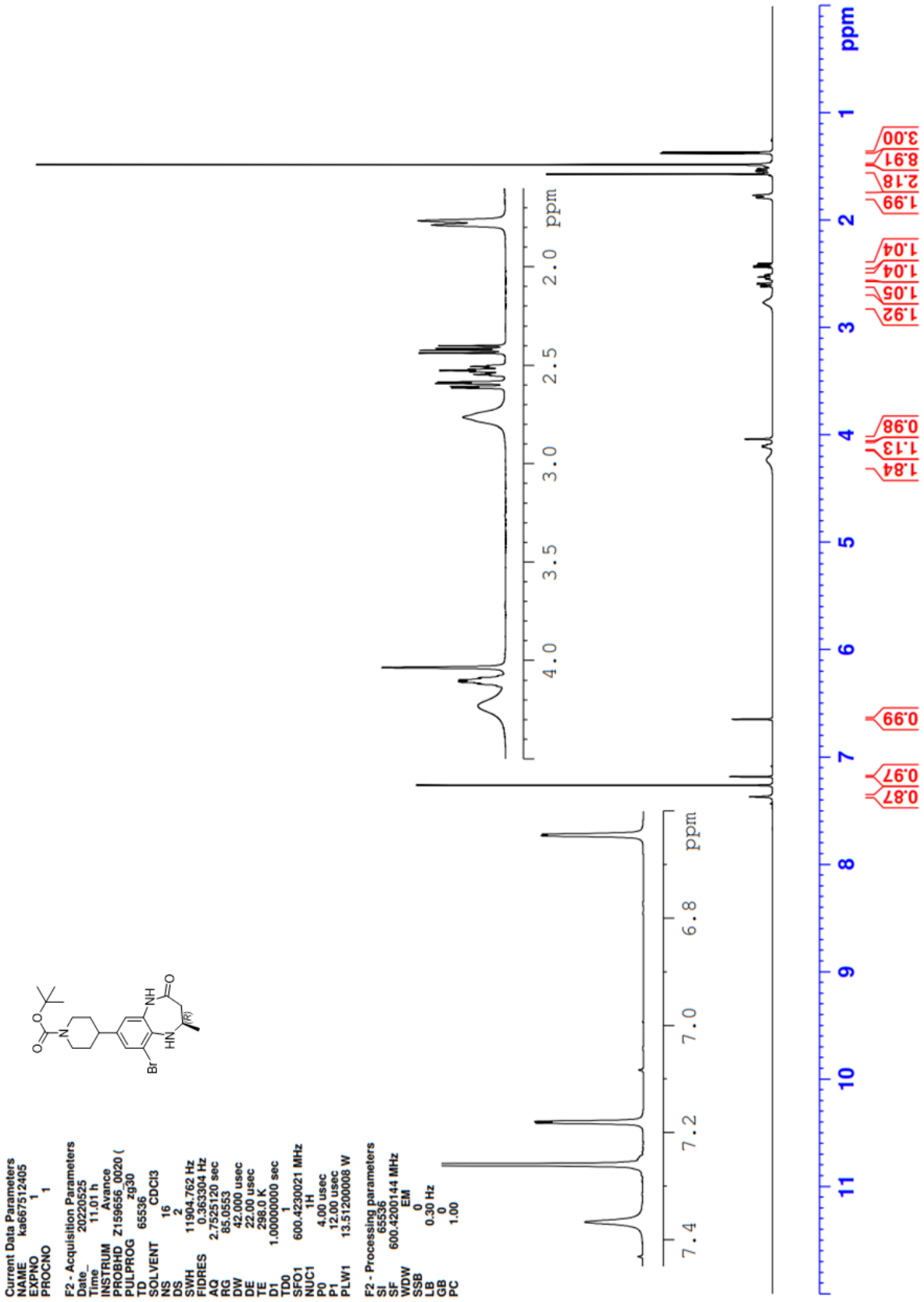

***tert*-Butyl 4-[(2*R*)-9-bromo-2-methyl-4-oxo-1,2,3,5-tetrahydro-1,5-benzodiazepin-7-yl]piperidine-1-carboxylate (90)**

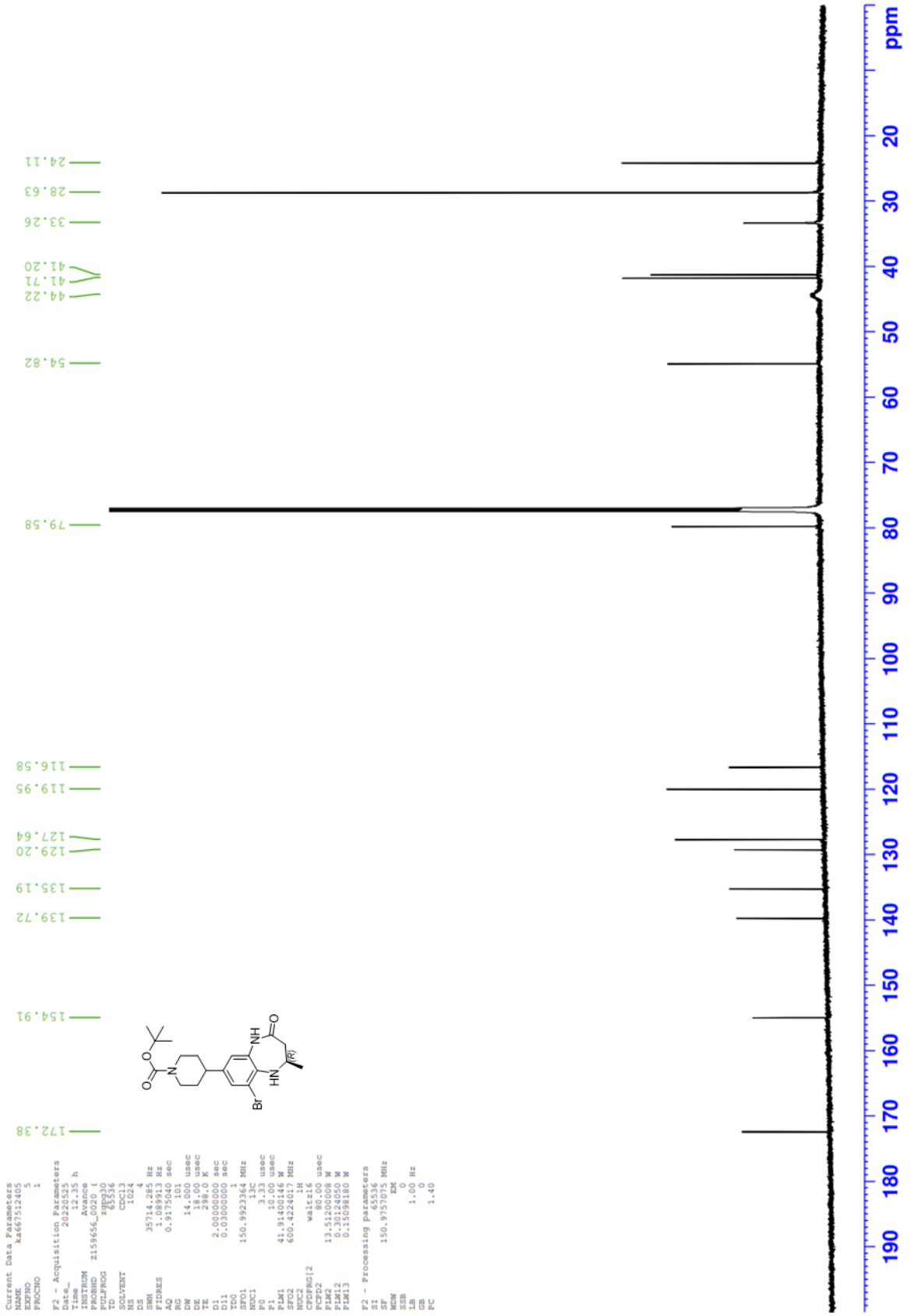

***tert*-Butyl 4-[(2*R*)-9-[(1*E*)-5-(7-methoxy-1,2,3,4-tetrahydroquinolin-1-yl)pent-1-en-1-yl]-2-methyl-4-oxo-2,3,4,5-tetrahydro-1*H*-1,5-benzodiazepin-7-yl]piperidine-1-carboxylate (91)**

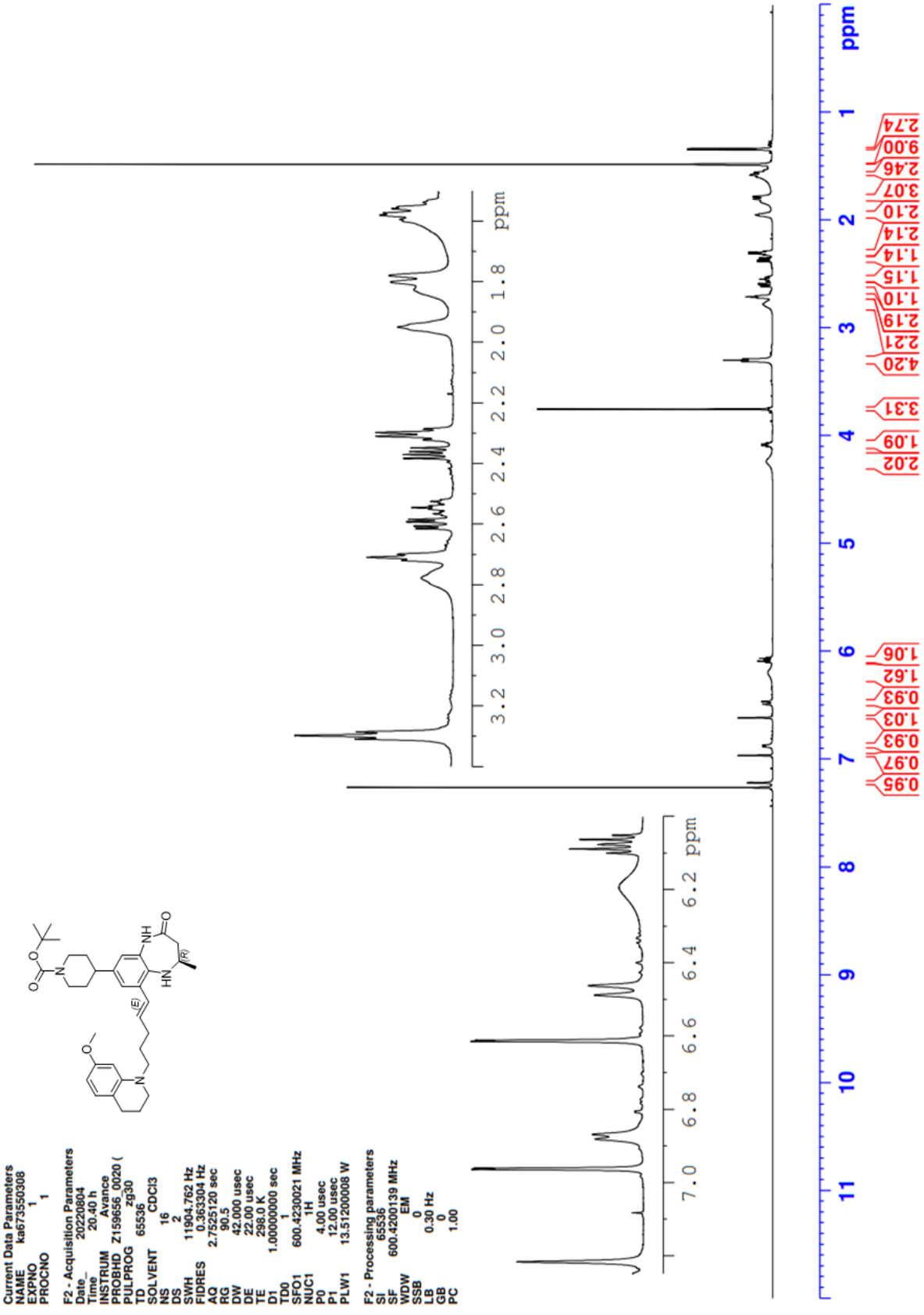

***tert*-Butyl 4-[(2*R*)-9-[(1*E*)-5-(7-methoxy-1,2,3,4-tetrahydroquinolin-1-yl)pent-1-en-1-yl]-2-methyl-4-oxo-2,3,4,5-tetrahydro-1*H*-1,5-benzodiazepin-7-yl]piperidine-1-carboxylate (91)**

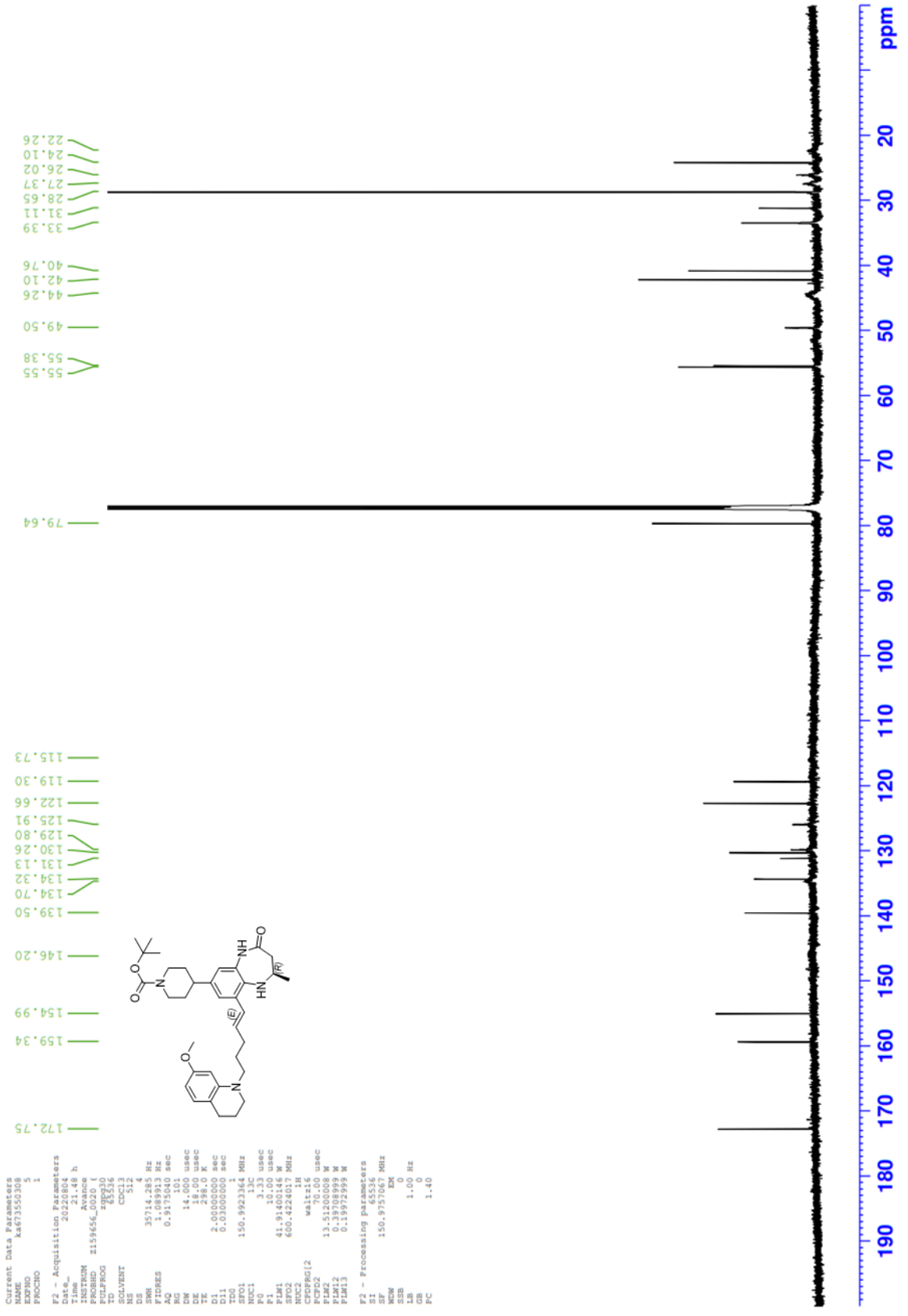

(4*R*)-6-[(1*E*)-5-(7-Methoxy-1,2,3,4-tetrahydroquinolin-1-yl)pent-1-en-1-yl]-4-methyl-8-(piperidin-4-yl)-2,3,4,5-tetrahydro-1*H*-1,5-benzodiazepin-2-one (86)

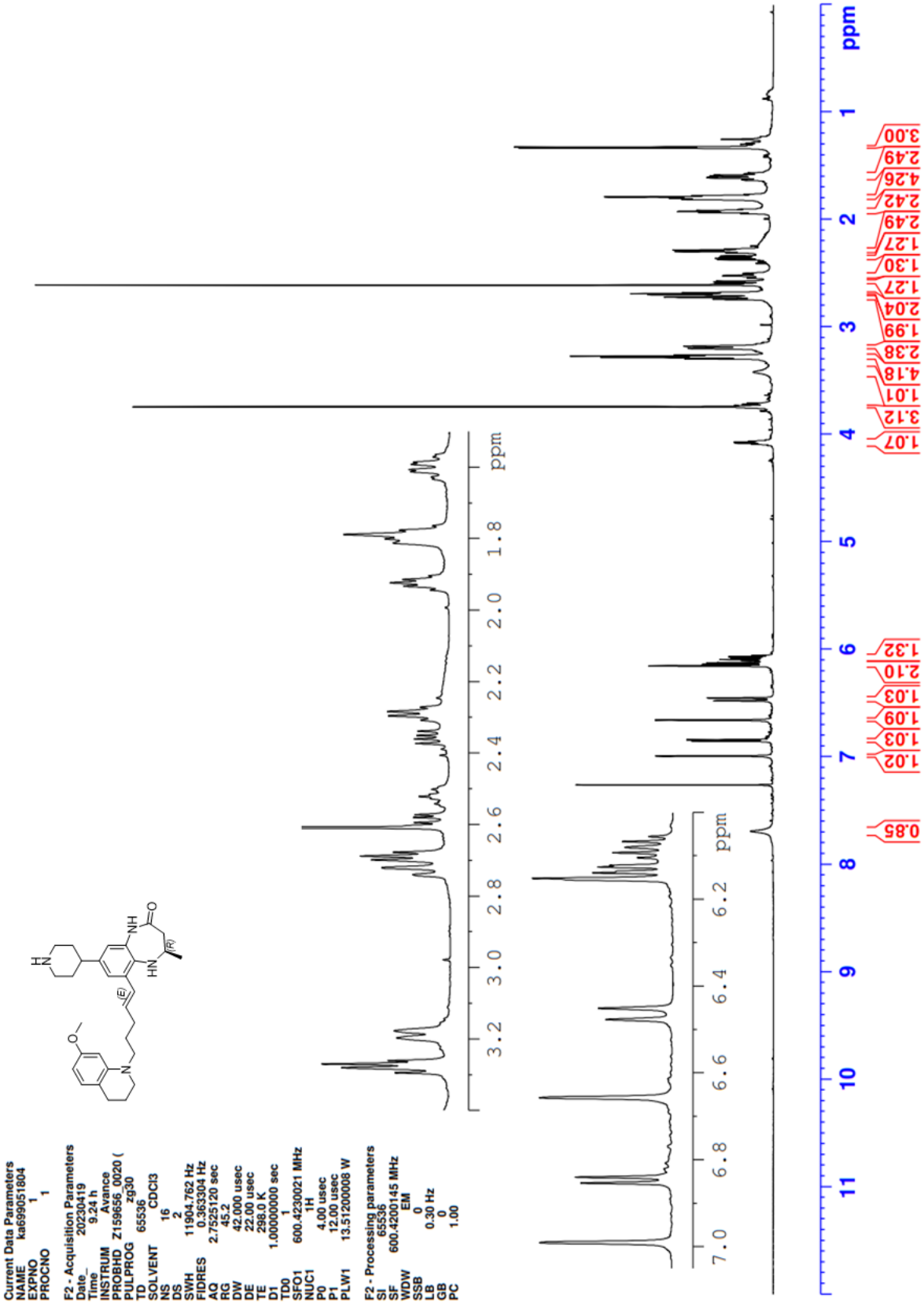

(4*R*)-6-[(1*E*)-5-(7-Methoxy-1,2,3,4-tetrahydroquinolin-1-yl)pent-1-en-1-yl]-4-methyl-8-(piperidin-4-yl)-2,3,4,5-tetrahydro-1*H*-1,5-benzodiazepin-2-one (86)

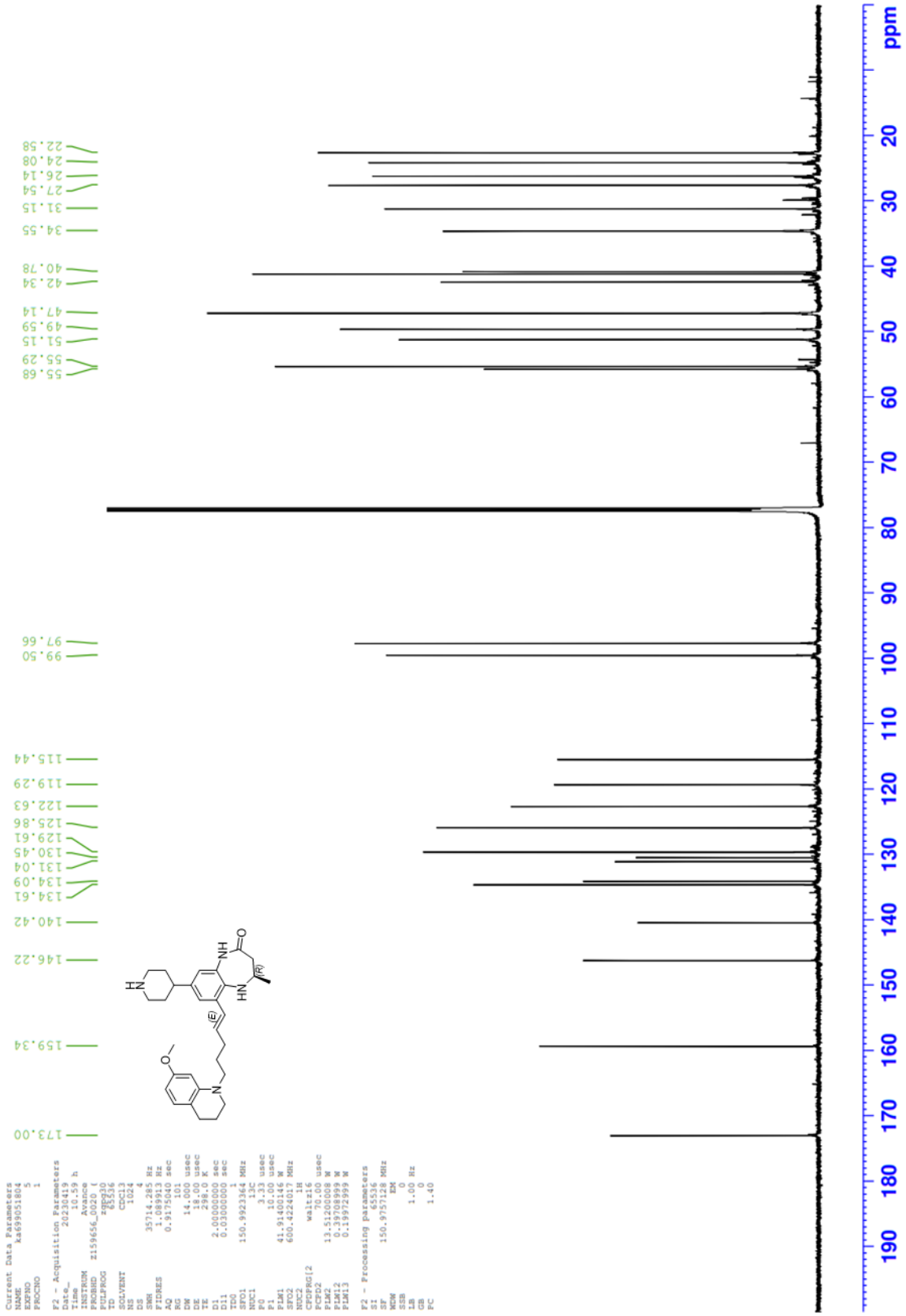

Prop-2-en-1-yl 4-{[(*tert*-butoxy)carbonyl]amino}piperidine-1-carboxylate (92)

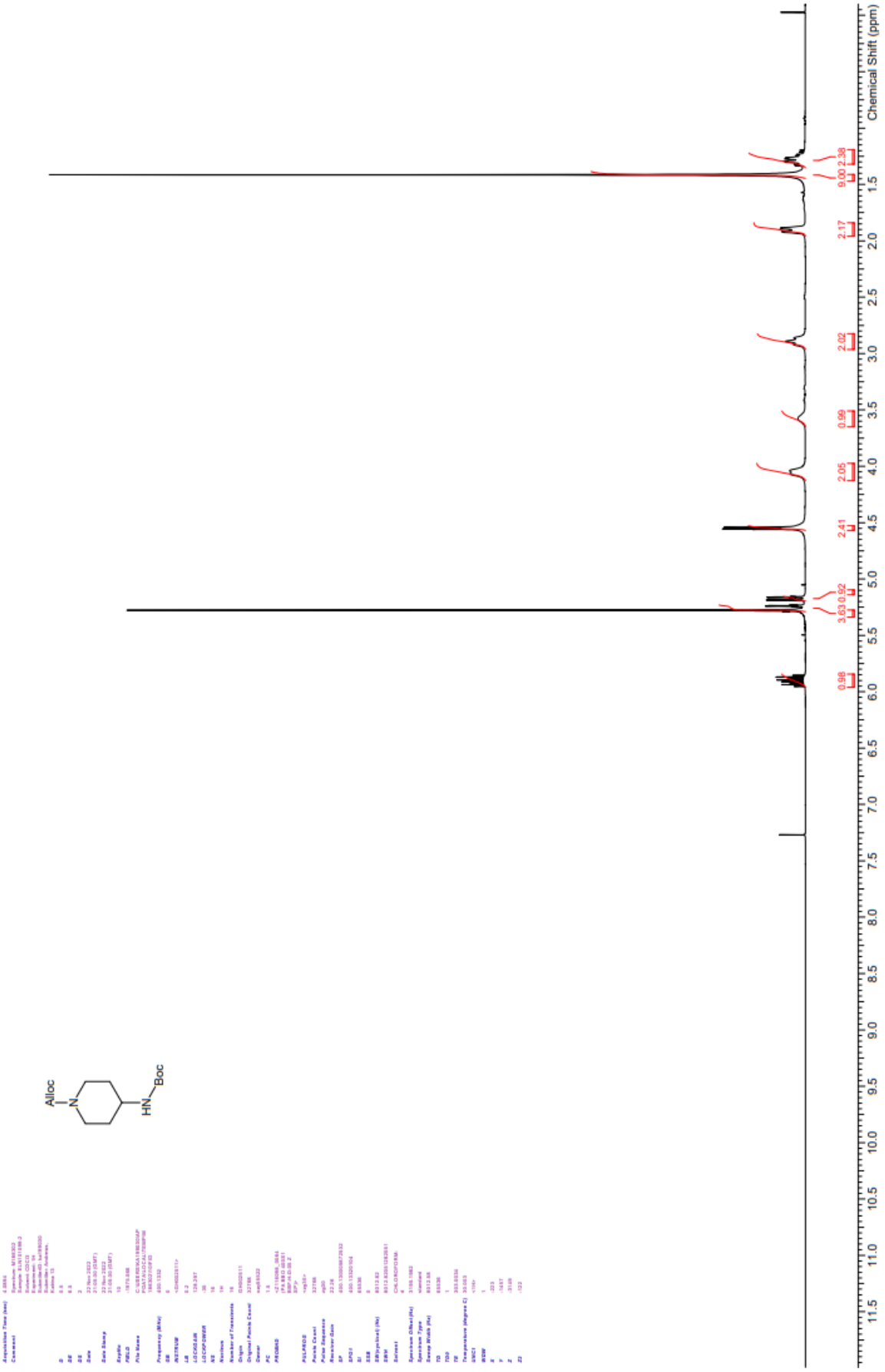

Prop-2-en-1-yl 4-{[(*tert*-butoxy)carbonyl]amino}piperidine-1-carboxylate (92)

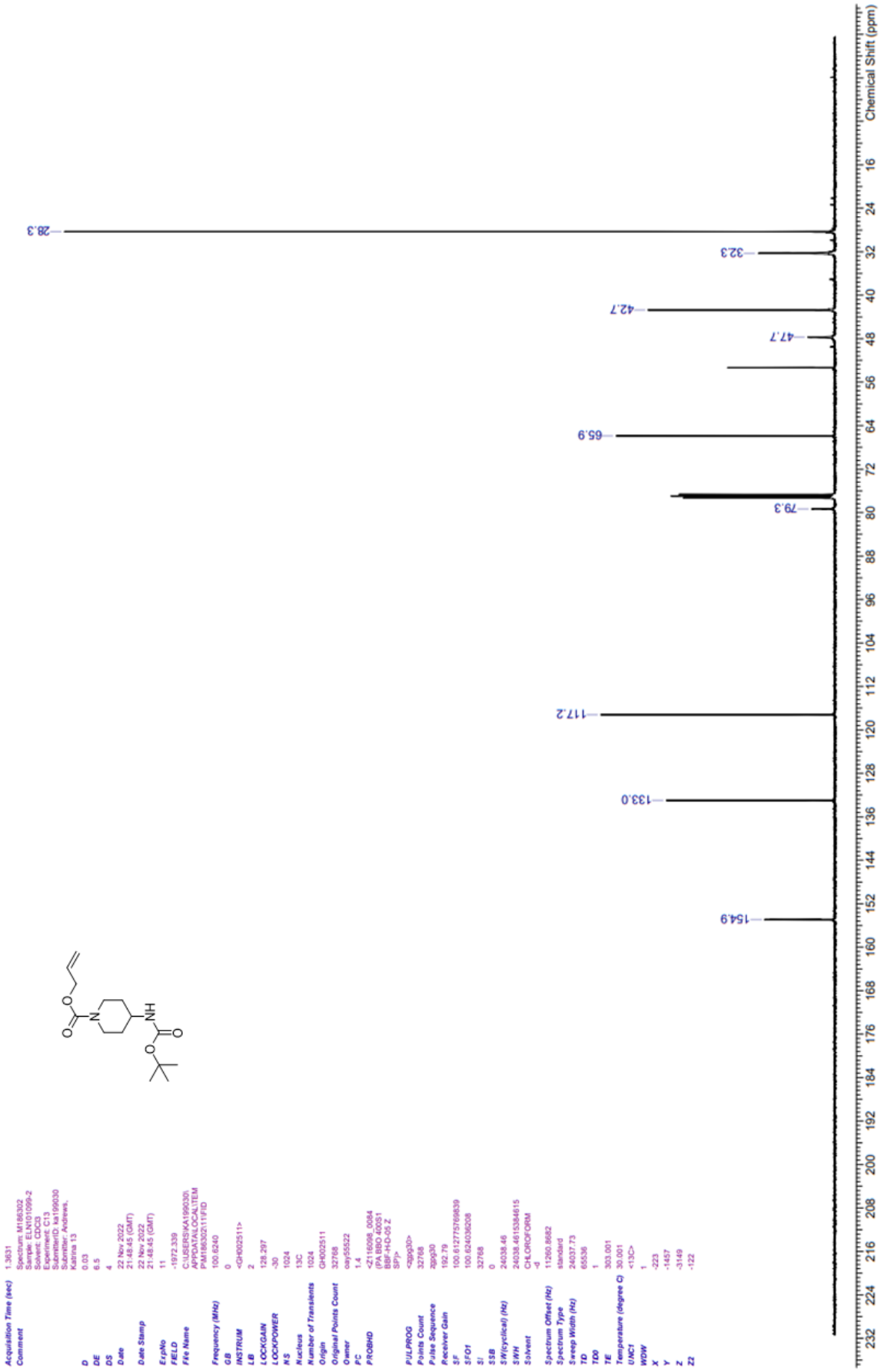

Prop-2-en-1-yl 4-{[4-(3,5-dimethyl-1,2-oxazol-4-yl)-2-nitrophenyl]amino}piperidine-1-carboxylate (95)

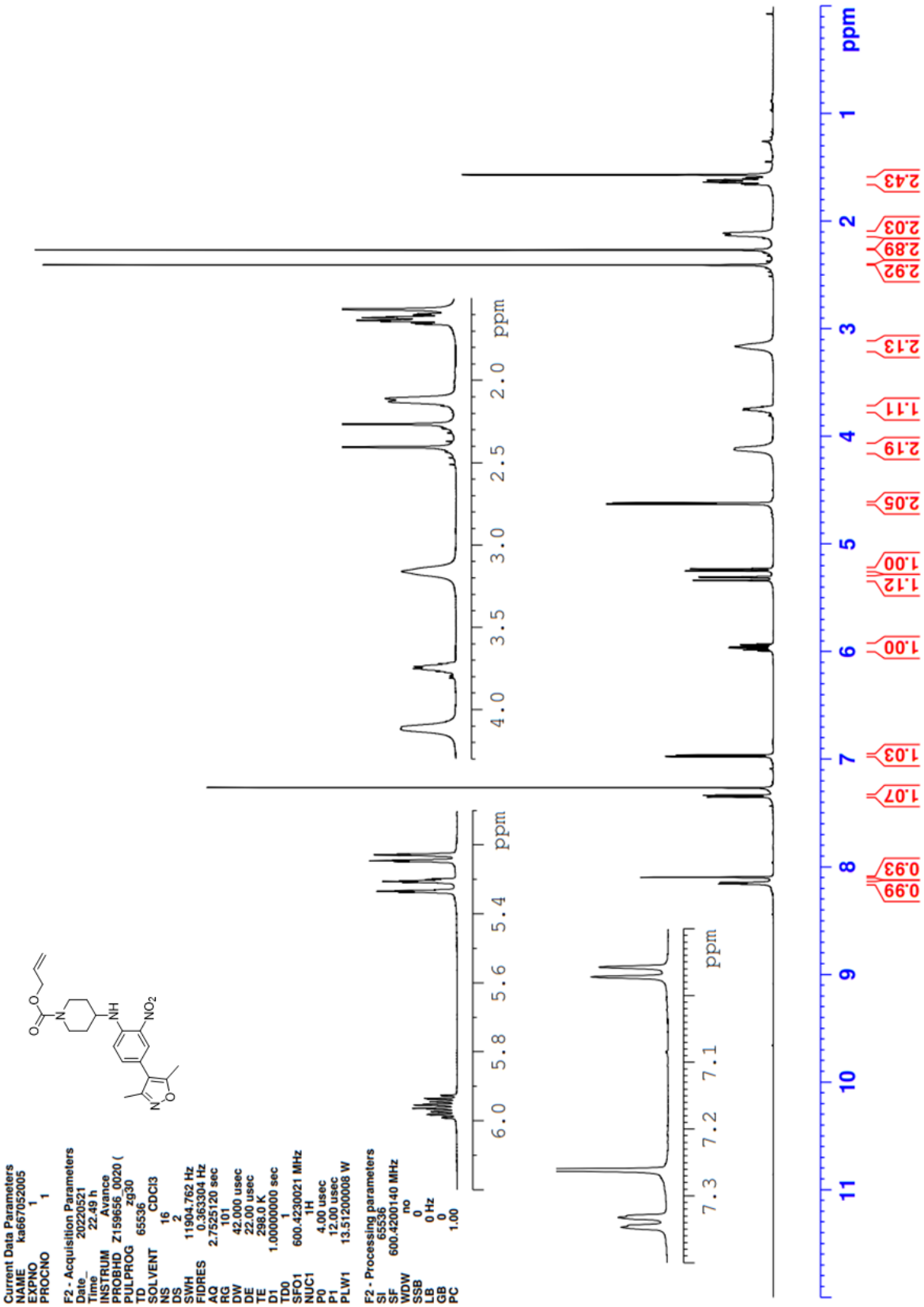

Prop-2-en-1-yl 4-{[4-(3,5-dimethyl-1,2-oxazol-4-yl)-2-nitrophenyl]amino}piperidine-1-carboxylate (95)

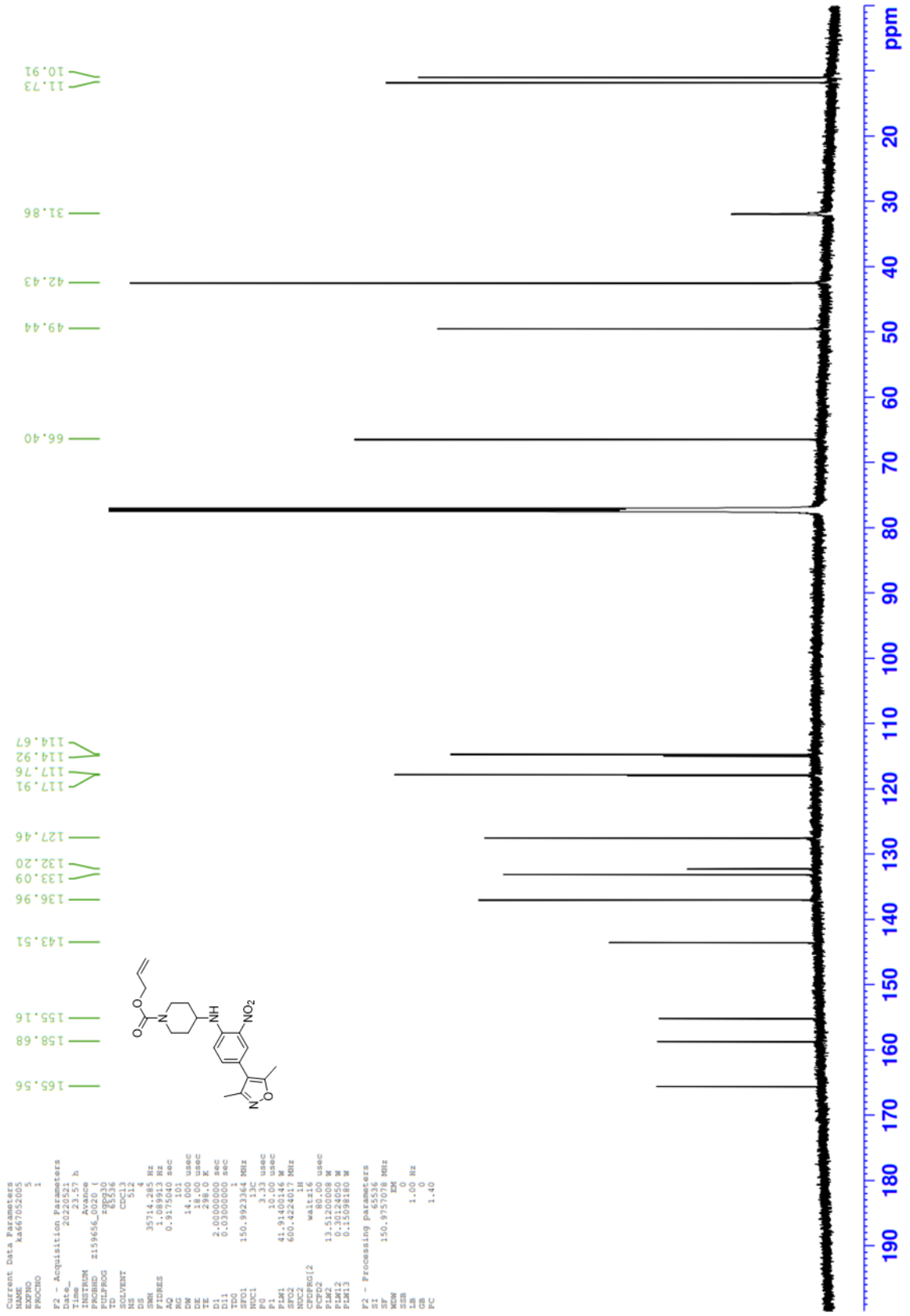

Prop-2-en-1-yl 4-{[2-amino-4-(3,5-dimethyl-1,2-oxazol-4-yl)phenyl]amino}piperidine-1-carboxylate (96)

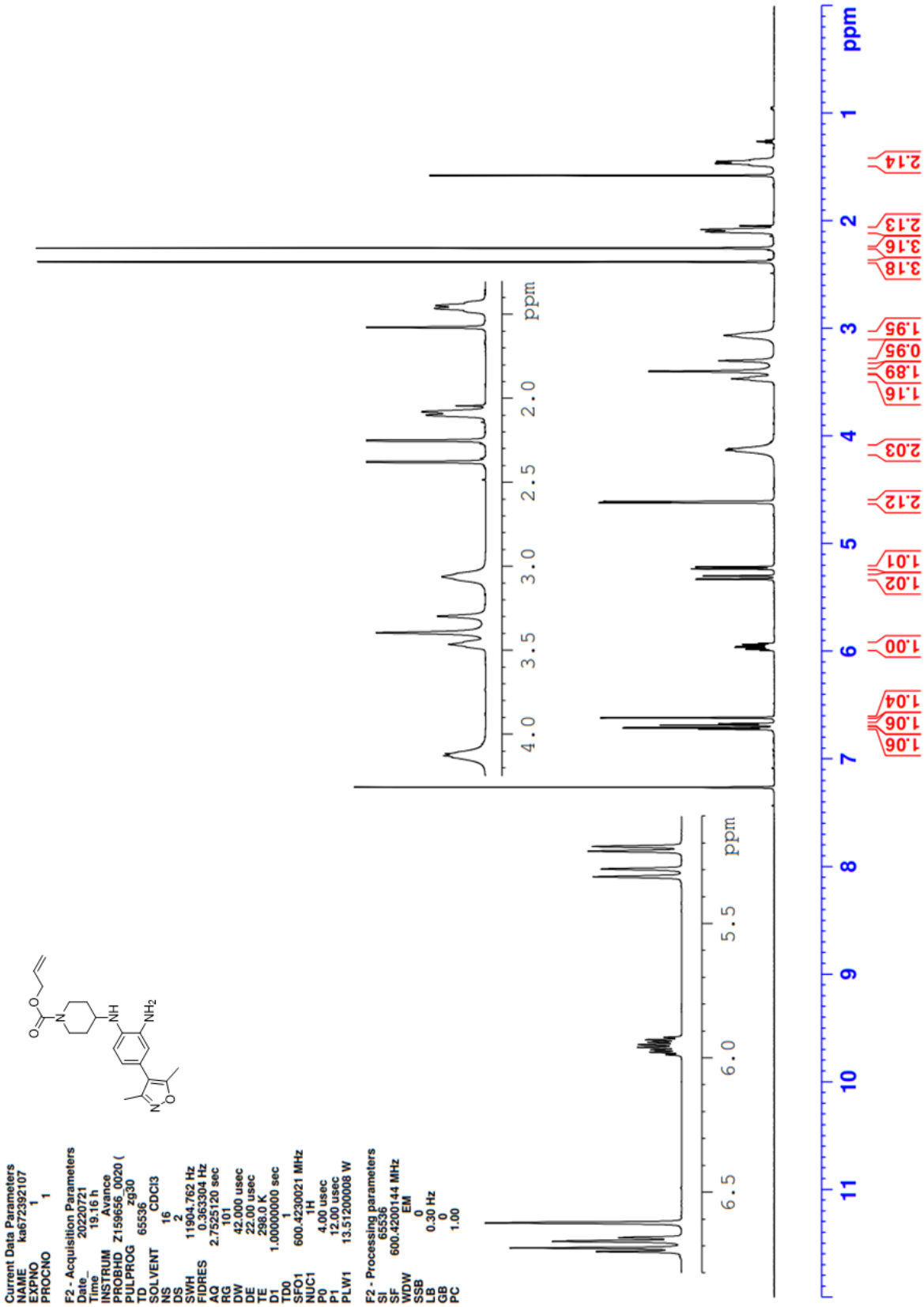

Prop-2-en-1-yl 4-{[2-amino-4-(3,5-dimethyl-1,2-oxazol-4-yl)phenyl]amino}piperidine-1-carboxylate (96)

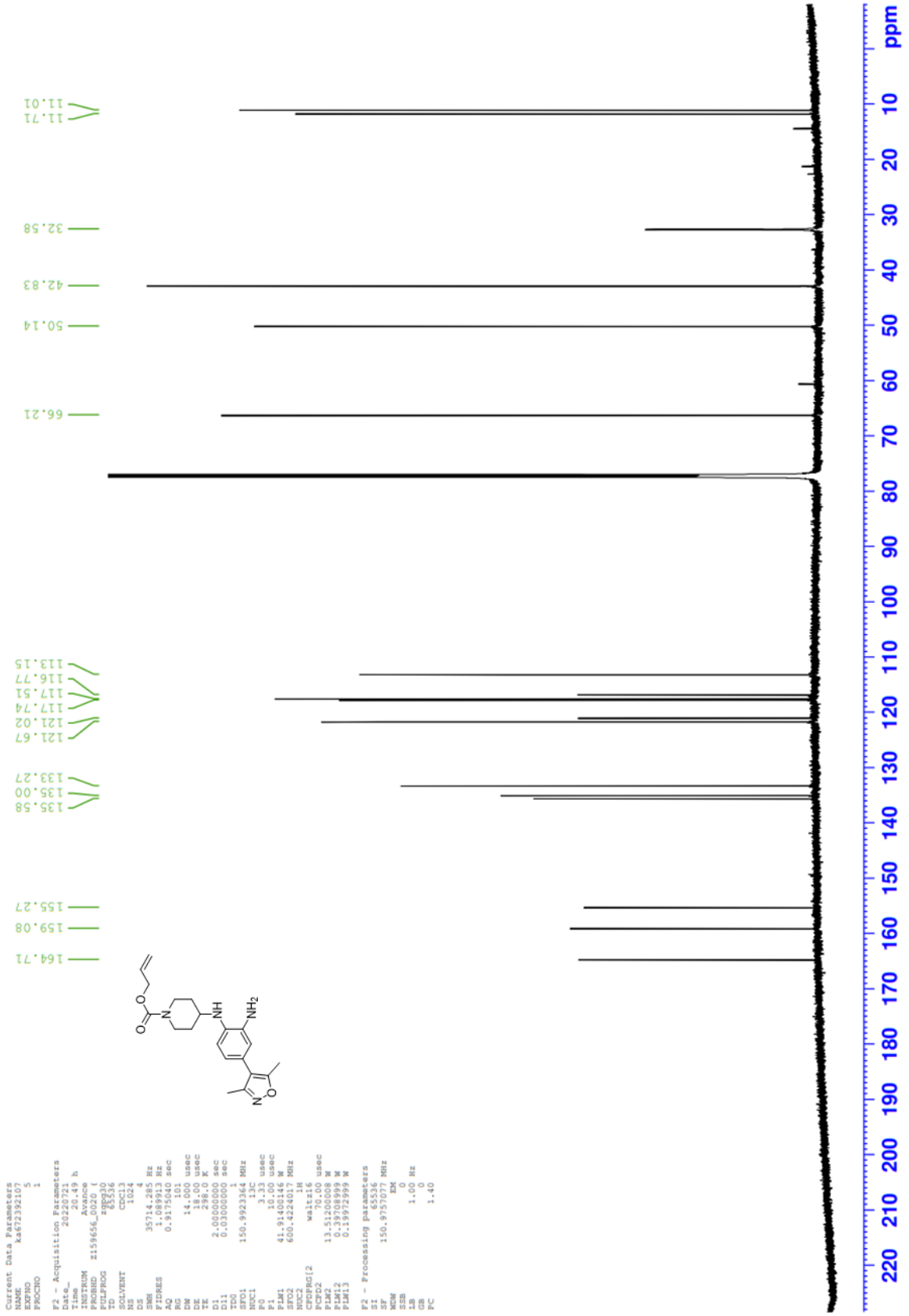

Prop-2-en-1-yl 4-[5-(3,5-dimethyl-1,2-oxazol-4-yl)-2-[(2*S*)-6-oxopiperidin-2-yl]-1*H*-1,3-benzodiazol-1-yl]piperidine-1-carboxylate (98)

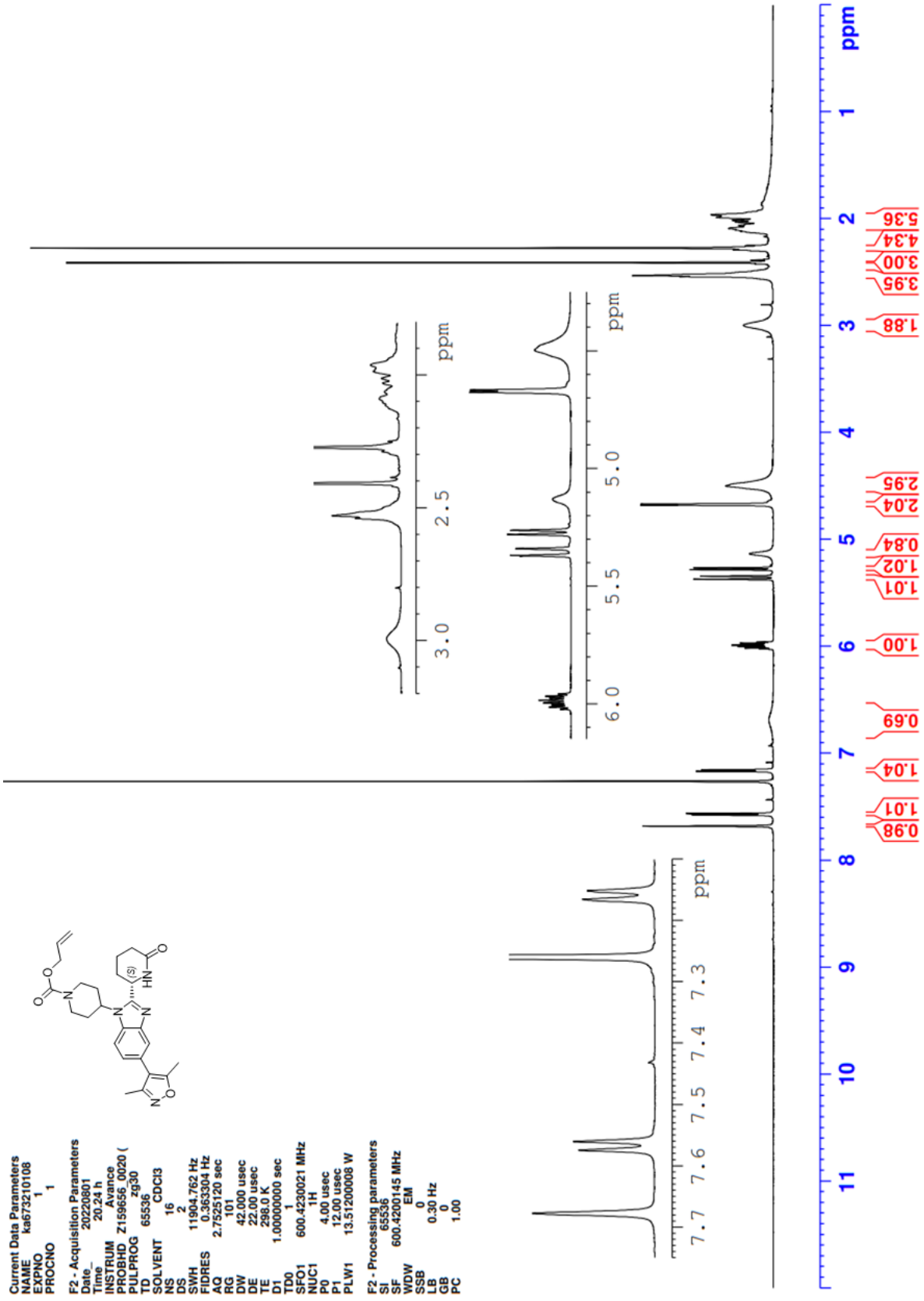

Prop-2-en-1-yl 4-[5-(3,5-dimethyl-1,2-oxazol-4-yl)-2-[(2*S*)-6-oxopiperidin-2-yl]-1*H*-1,3-benzodiazol-1-yl]piperidine-1-carboxylate (98)

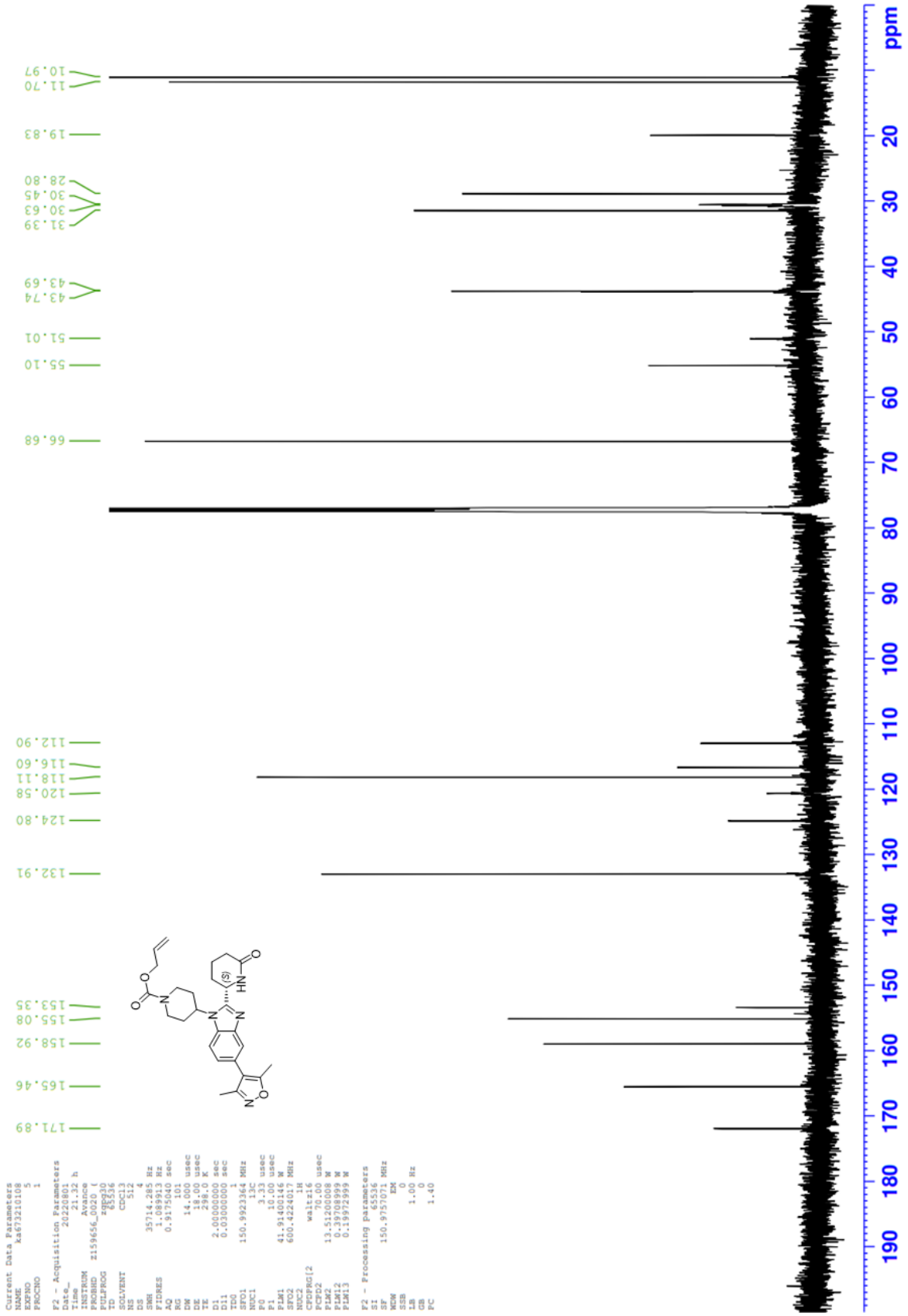

Prop-2-en-1-yl 4-{2-[(2*S*)-1-(3,4-difluorophenyl)-6-oxopiperidin-2-yl]-5-(3,5-dimethyl-1,2-oxazol-4-yl)-1*H*-1,3-benzodiazol-1-yl}piperidine-1-carboxylate (99)

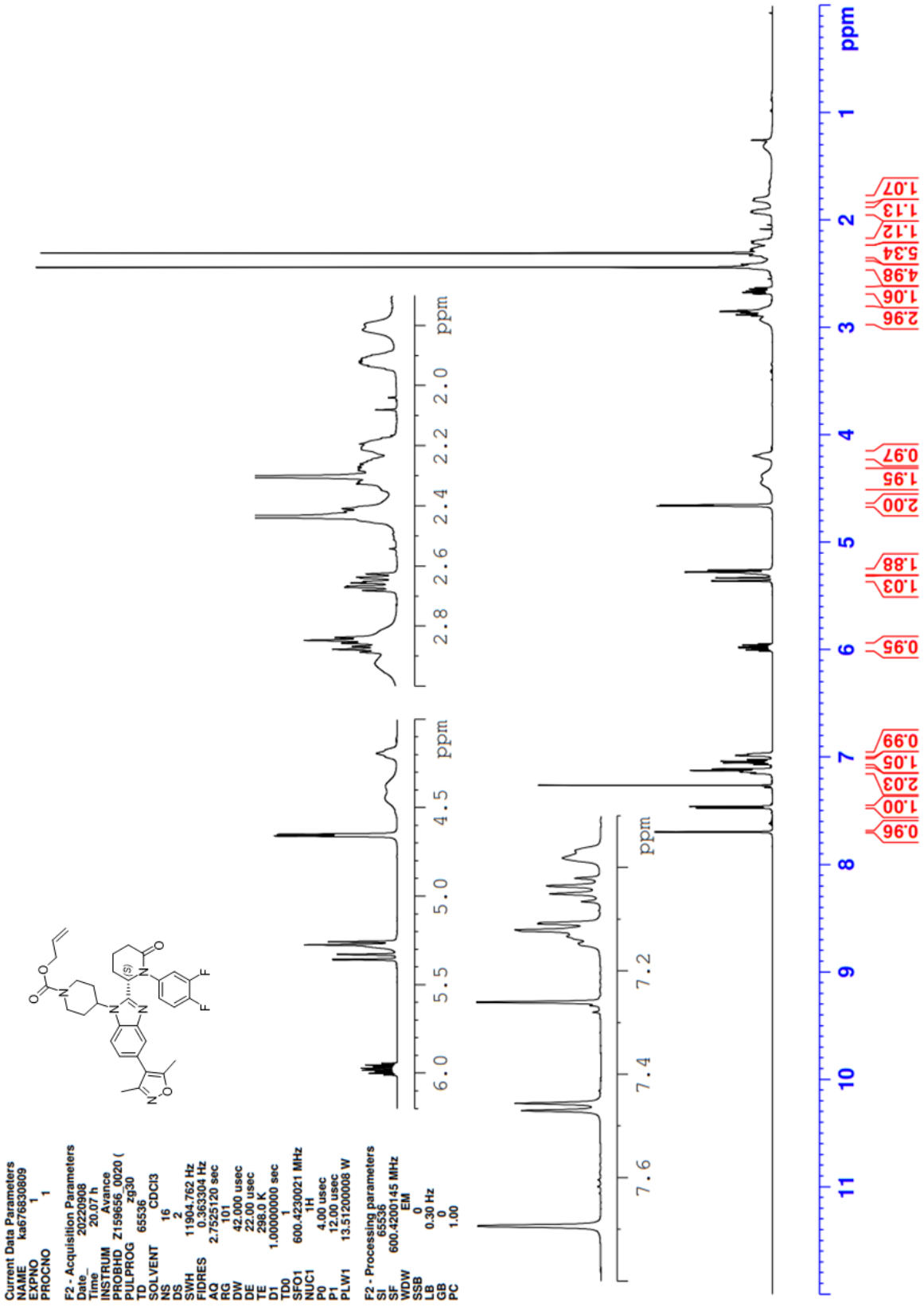

Prop-2-en-1-yl 4-{2-[(2*S*)-1-(3,4-difluorophenyl)-6-oxopiperidin-2-yl]-5-(3,5-dimethyl-1,2-oxazol-4-yl)-1*H*-1,3-benzodiazol-1-yl}piperidine-1-carboxylate (99)

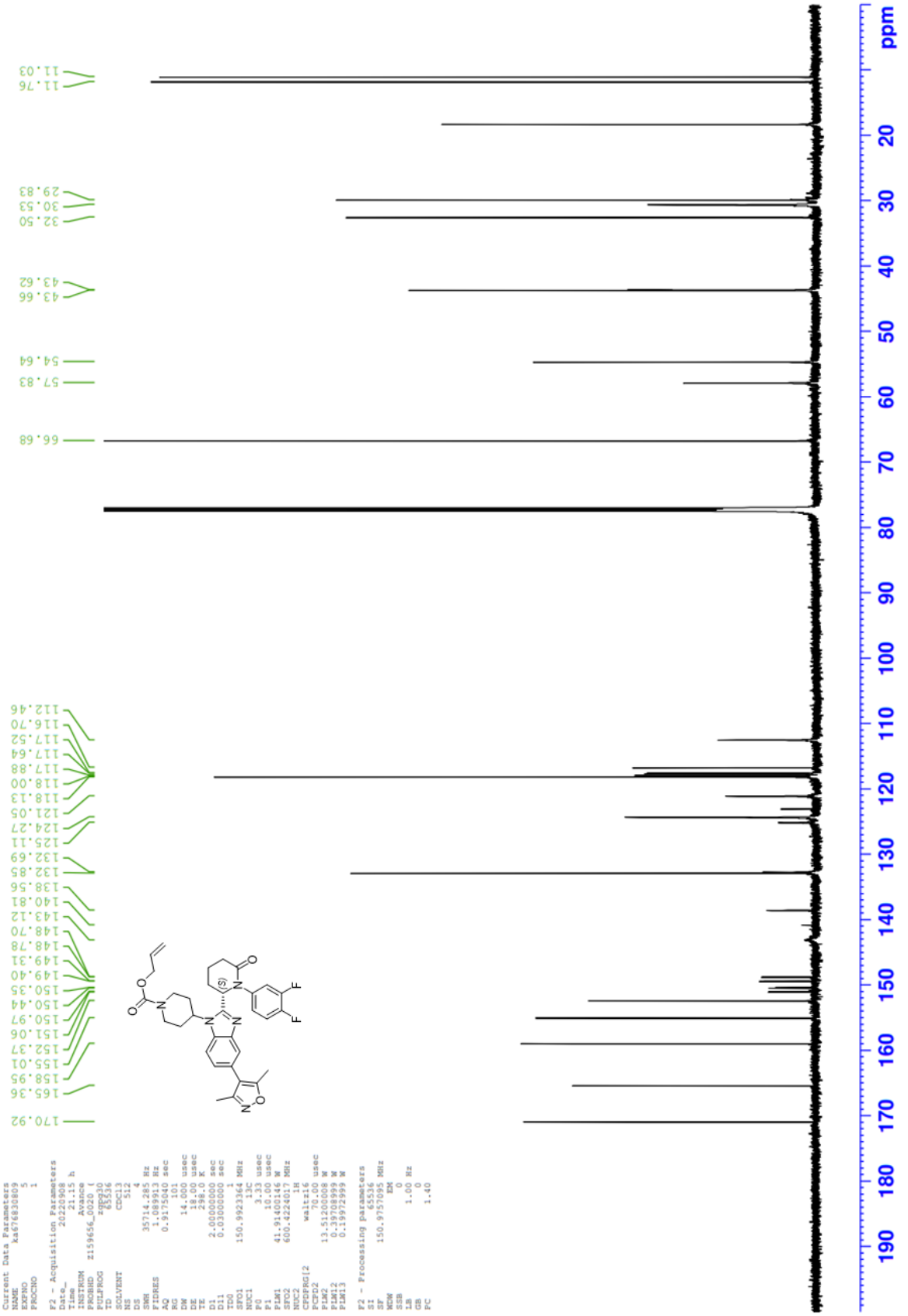

Prop-2-en-1-yl 4-{2-[(2*S*)-1-(3,4-difluorophenyl)-6-oxopiperidin-2-yl]-5-(3,5-dimethyl-1,2-oxazol-4-yl)-1*H*-1,3-benzodiazol-1-yl}piperidine-1-carboxylate (99)

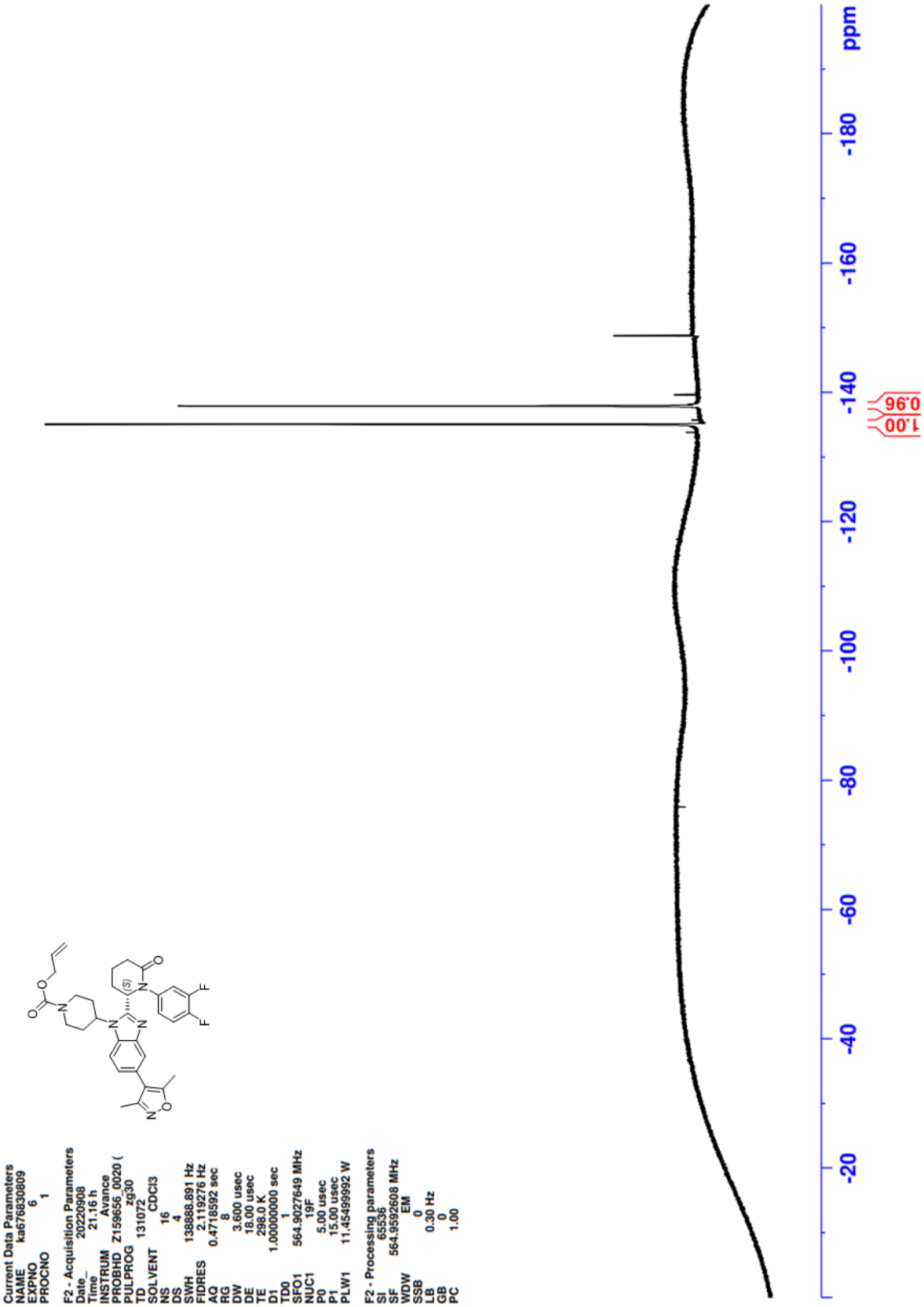

***tert*-Butyl *N*-[(2*S*)-1-{[4-(3,5-dimethyl-1,2-oxazol-4-yl)-2-nitrophenyl]amino}propan-2-yl]carbamate (101)**

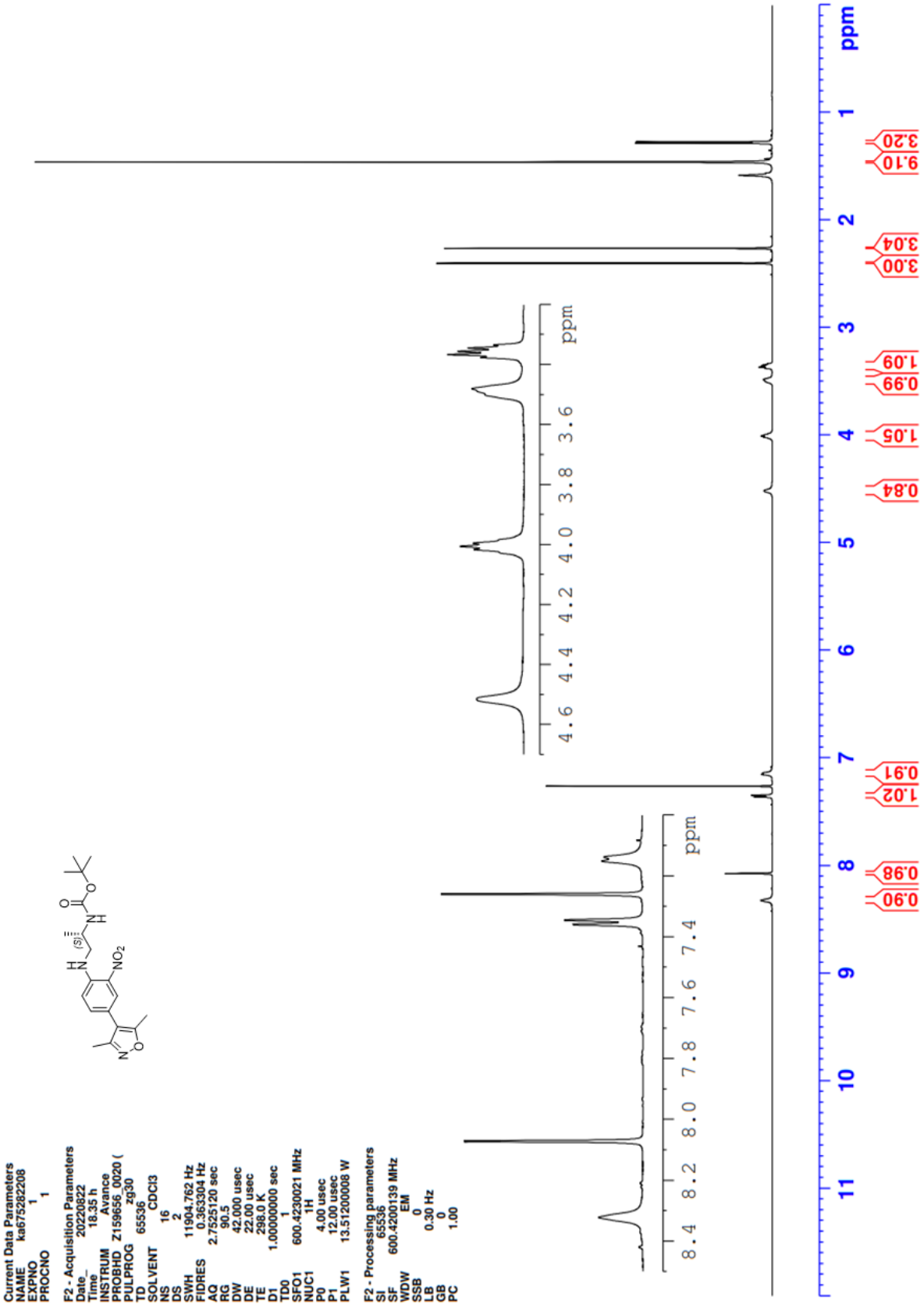

***tert*-Butyl *N*-[(2*S*)-1-{[4-(3,5-dimethyl-1,2-oxazol-4-yl)-2-nitrophenyl]amino}propan-2-yl]carbamate (101)**

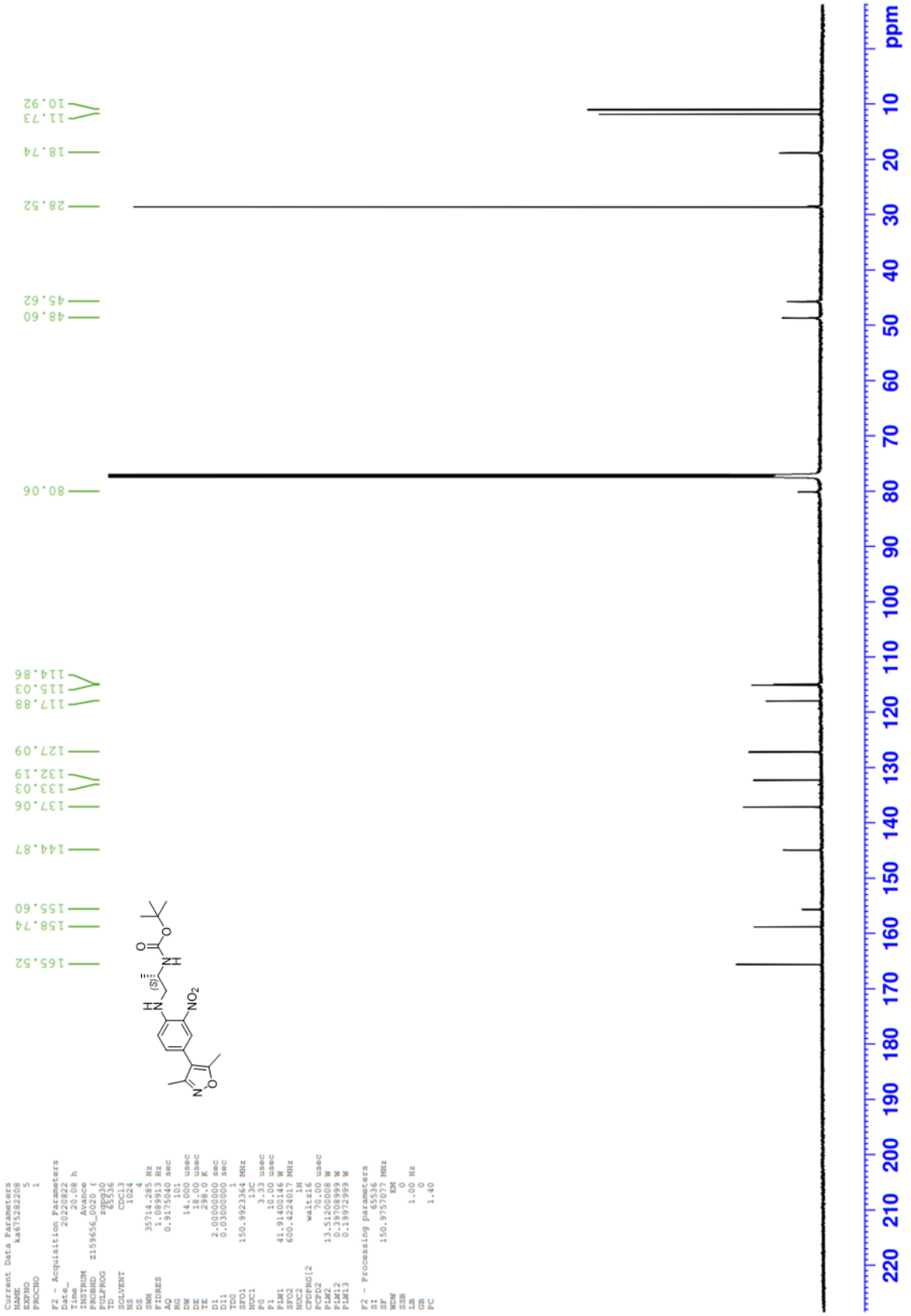

2-{Benzyl[2-(benzyloxy)ethyl]amino}ethan-1-ol (105)

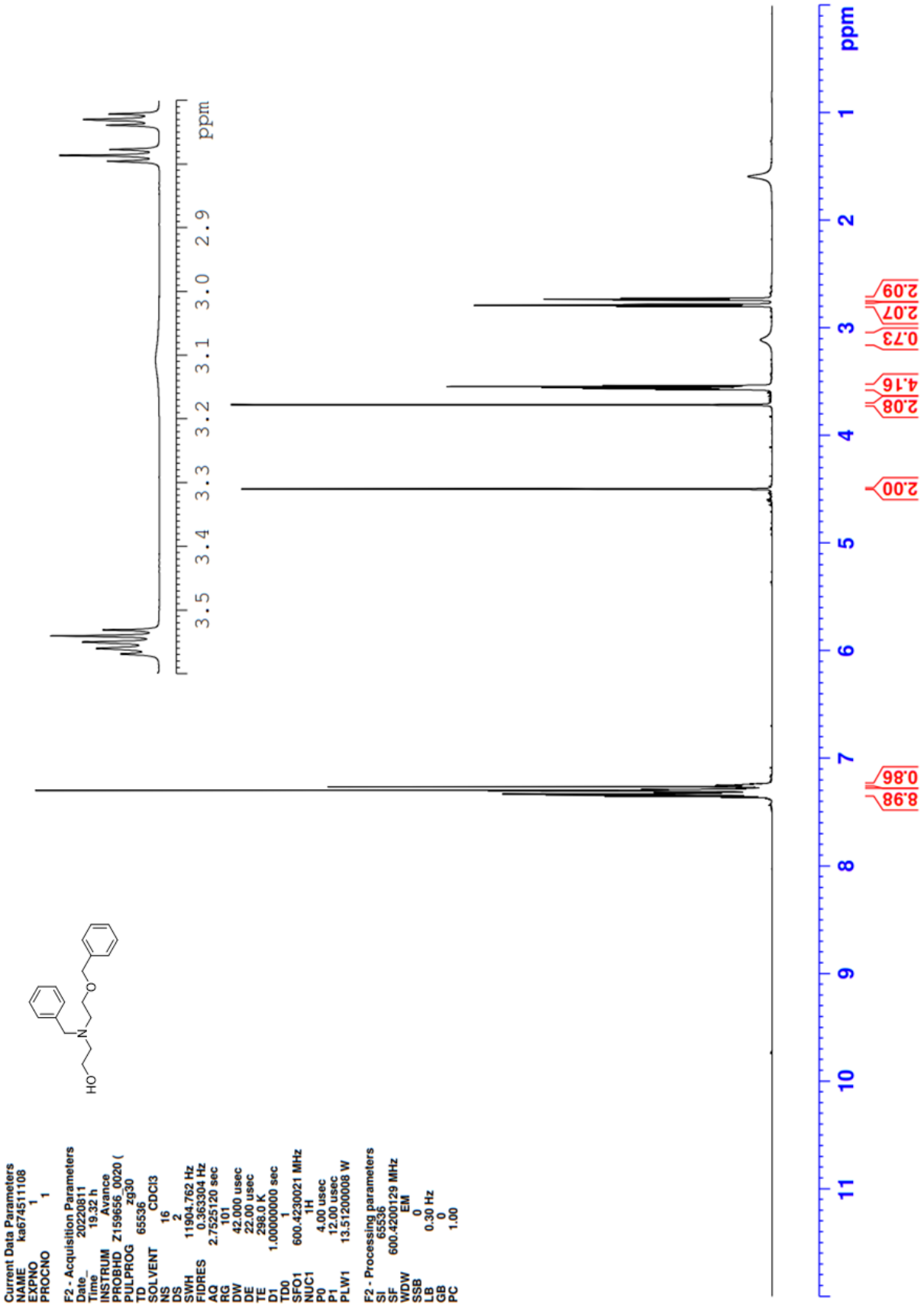

2-{Benzyl[2-(benzyloxy)ethyl]amino}ethan-1-ol (105)

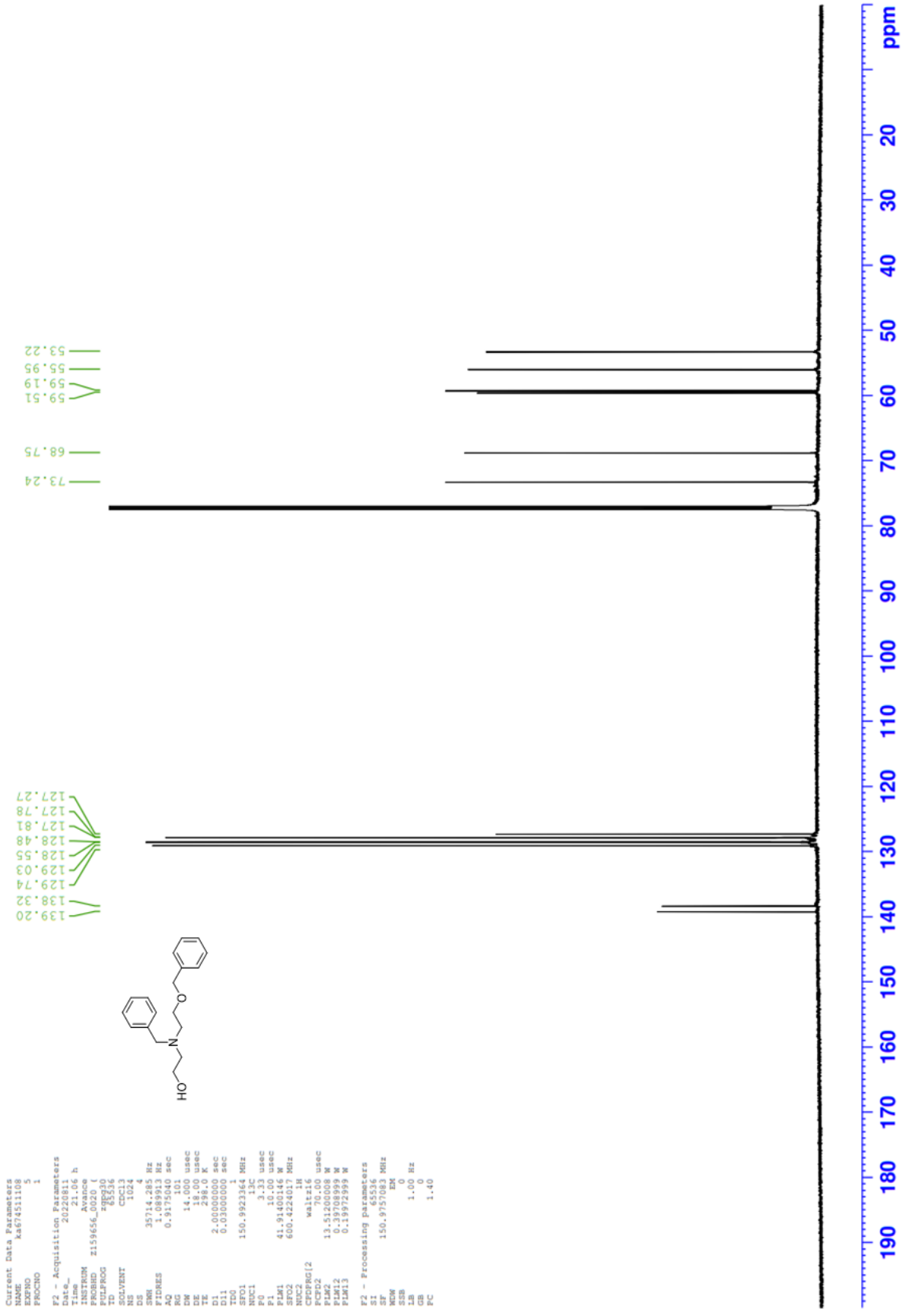

_N_-[(2_S_)-2-(4-Benzylpiperazin-1-yl)propyl]-4-(3,5-dimethyl-1,2-oxazol-4-yl)-2-nitroaniline (102)

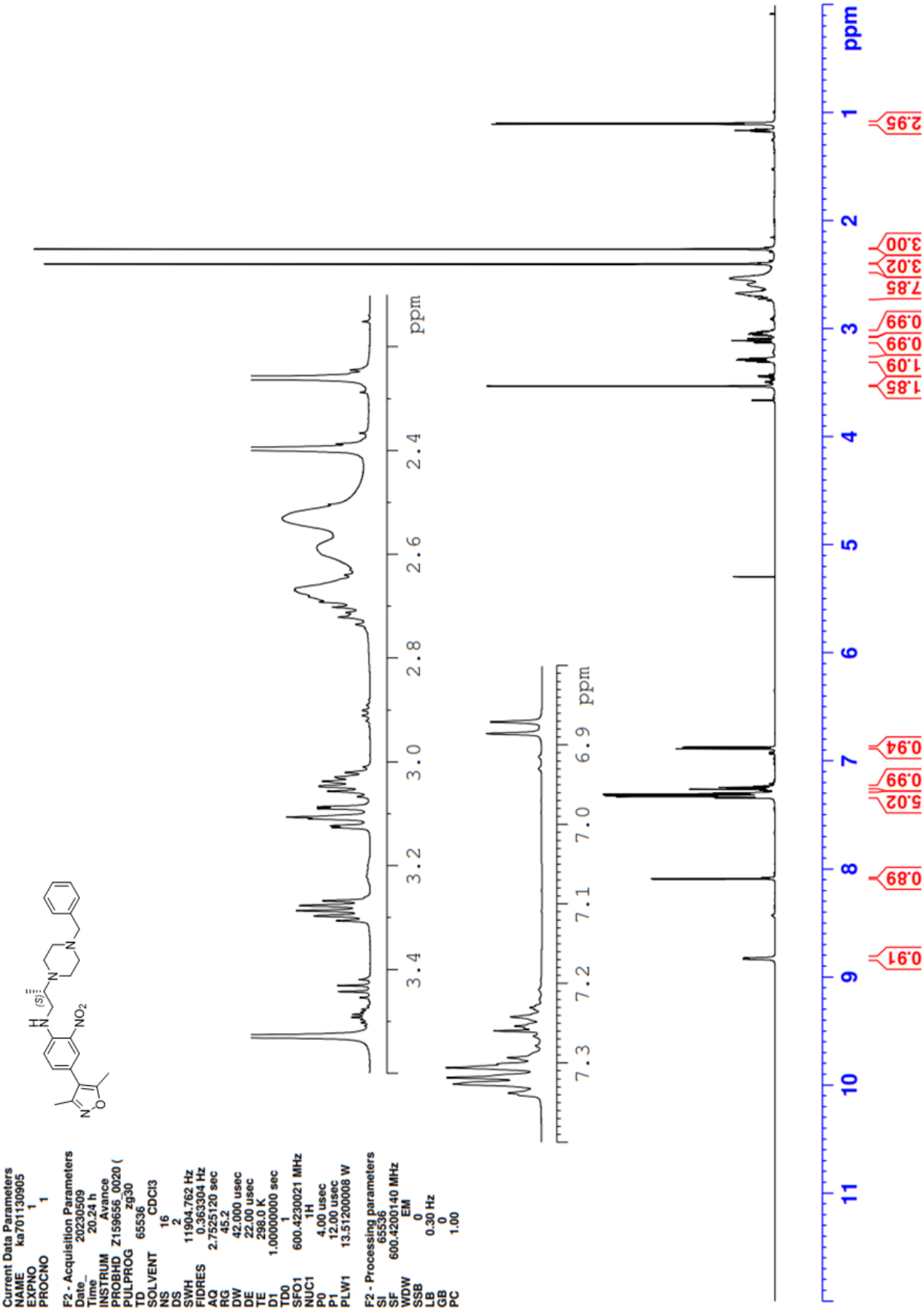

***N*-[(2*S*)-2-(4-Benzylpiperazin-1-yl)propyl]-4-(3,5-dimethyl-1,2-oxazol-4-yl)-2-nitroaniline (102)**

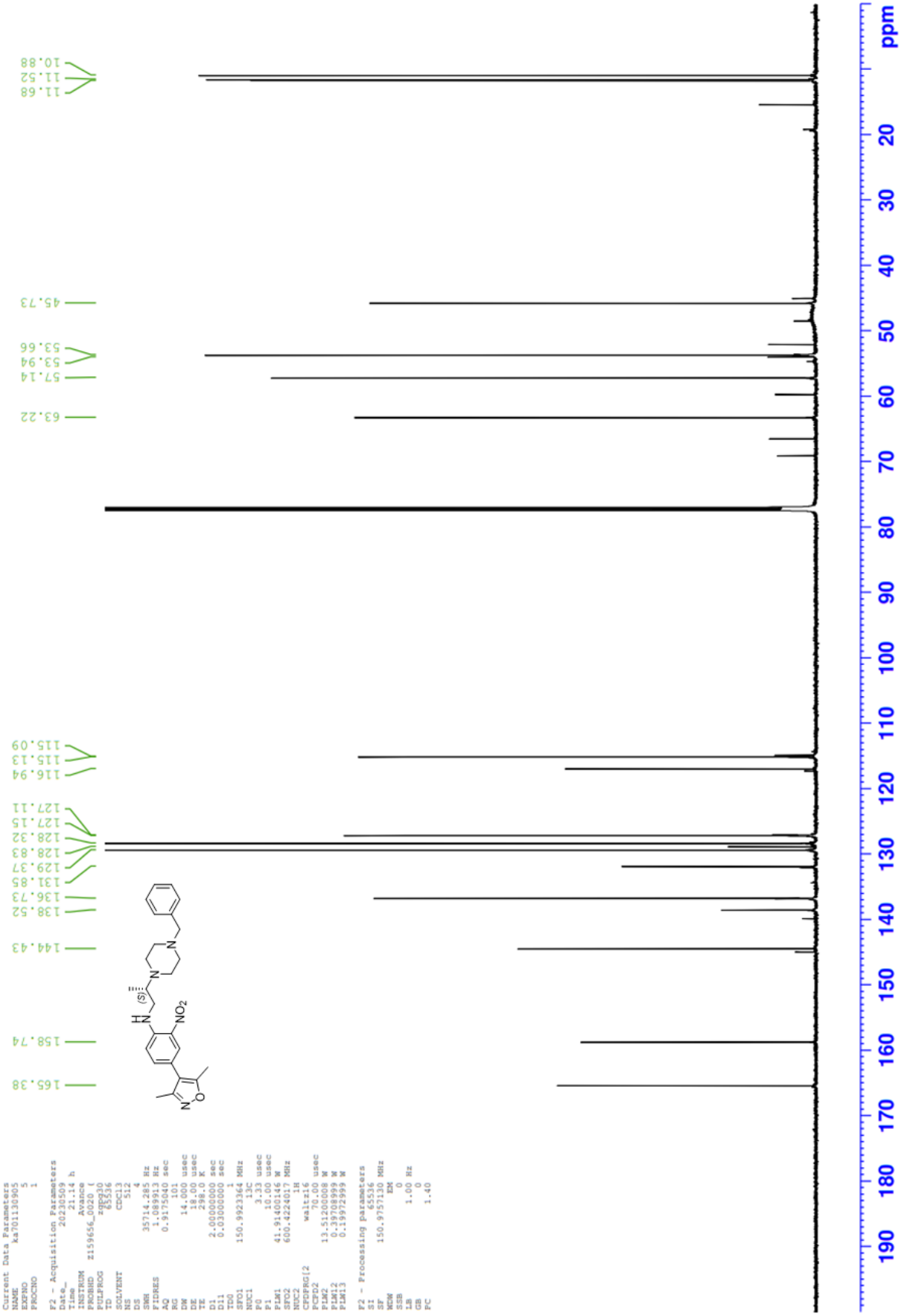

tert-Butyl 4-(2-{[4-(3,5-dimethyl-1,2-oxazol-4-yl)-2-nitrophenyl]amino}ethyl)piperazine-1-carboxylate (107)

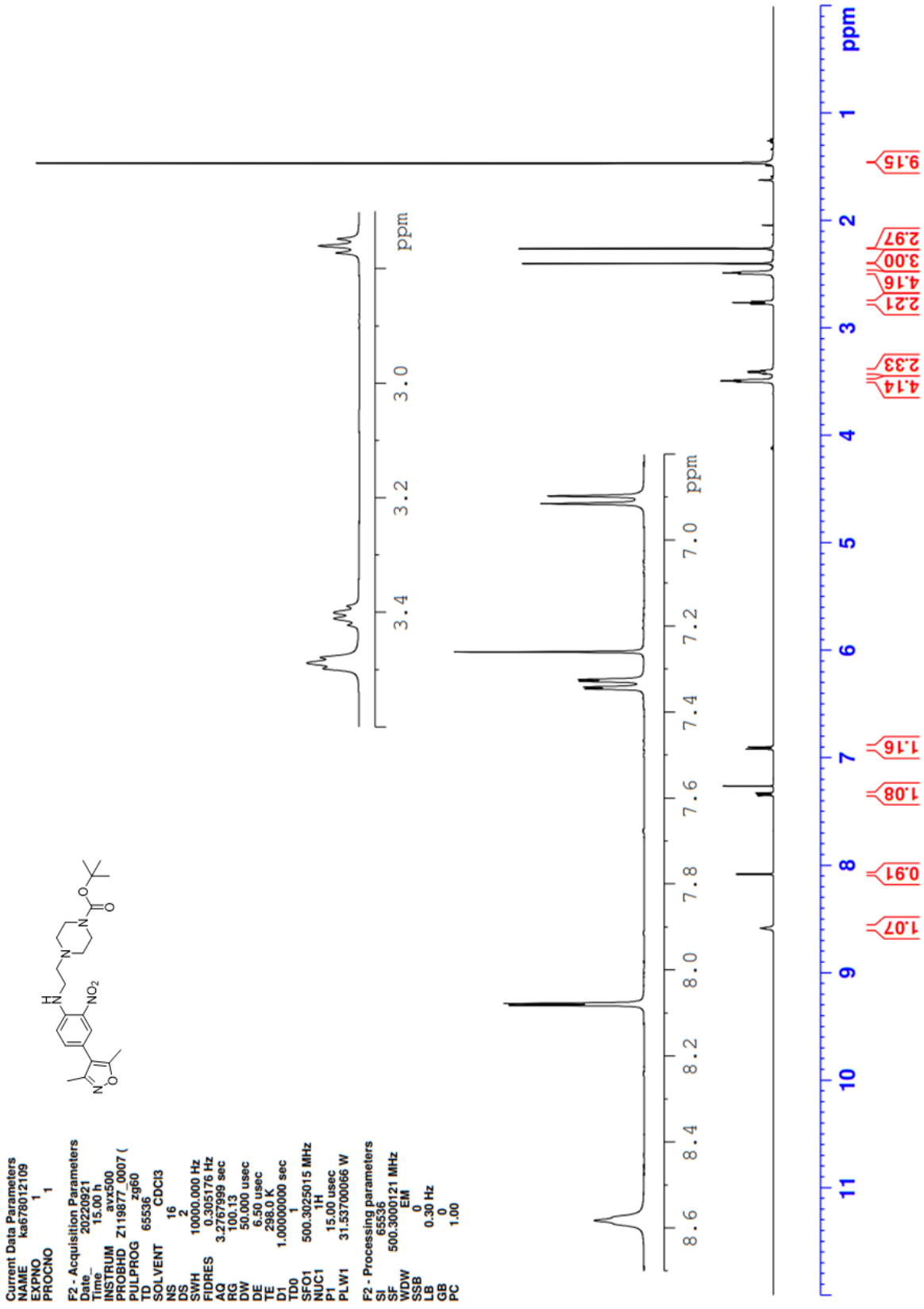

***tert*-Butyl 4-(2-{[4-(3,5-dimethyl-1,2-oxazol-4-yl)-2-nitrophenyl]amino}ethyl)piperazine-1-carboxylate (107)**

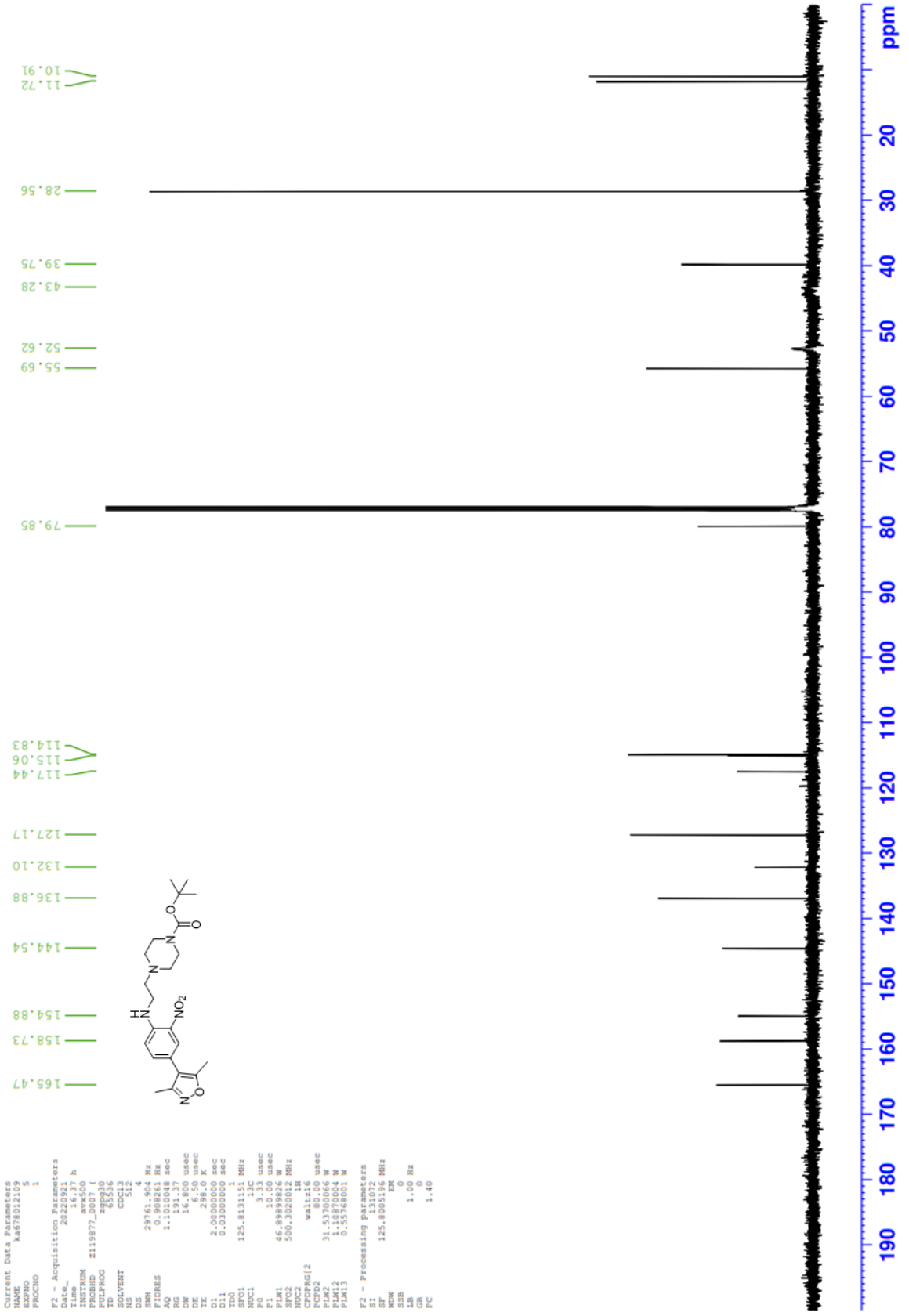

tert-Butyl 4-(2-{[2-amino-4-(3,5-dimethyl-1,2-oxazol-4-yl)phenyl]amino}ethyl)piperazine-1-carboxylate (108)

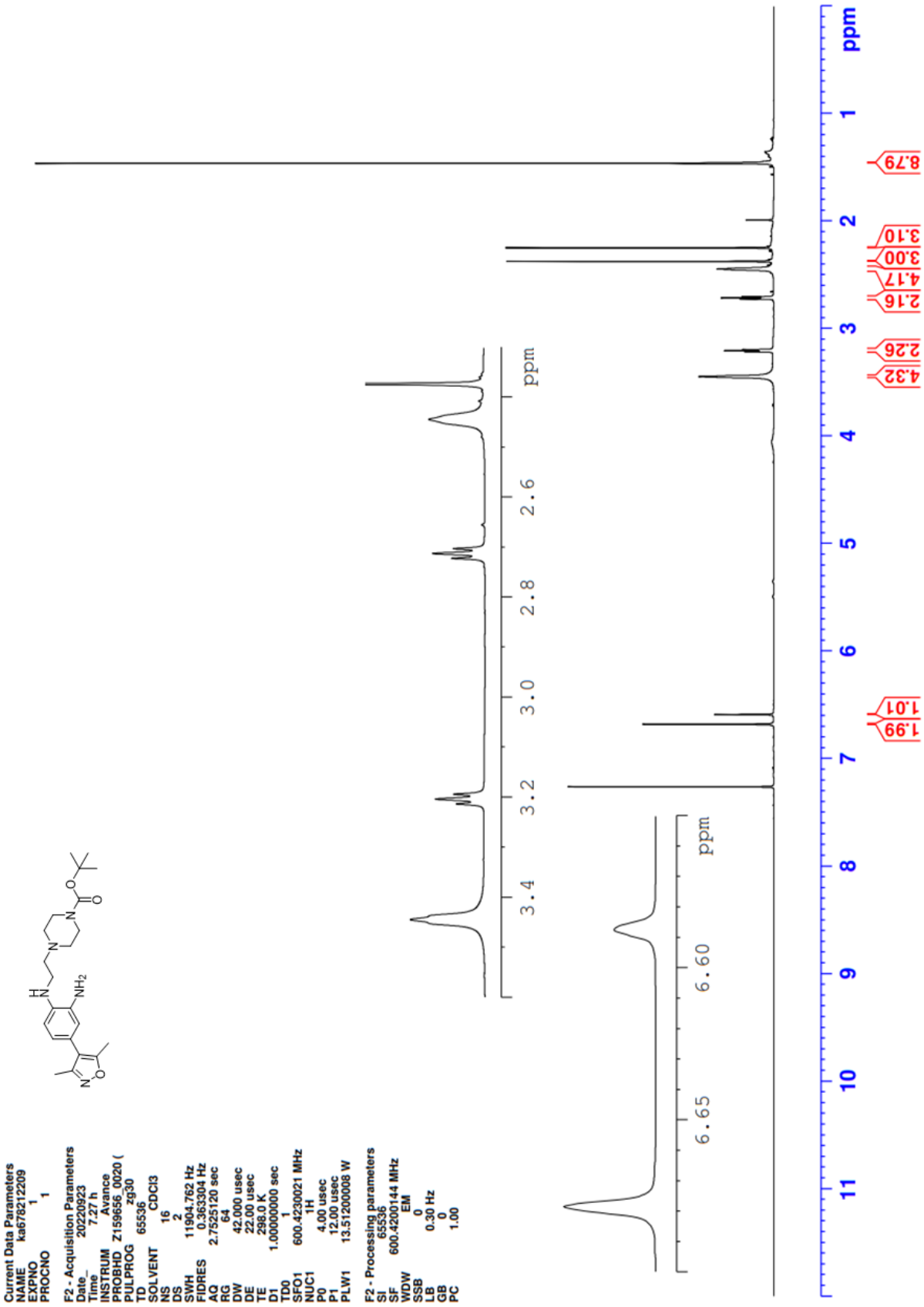

***tert*-Butyl 4-(2-{[2-amino-4-(3,5-dimethyl-1,2-oxazol-4-yl)phenyl]amino}ethyl)piperazine-1-carboxylate (108)**

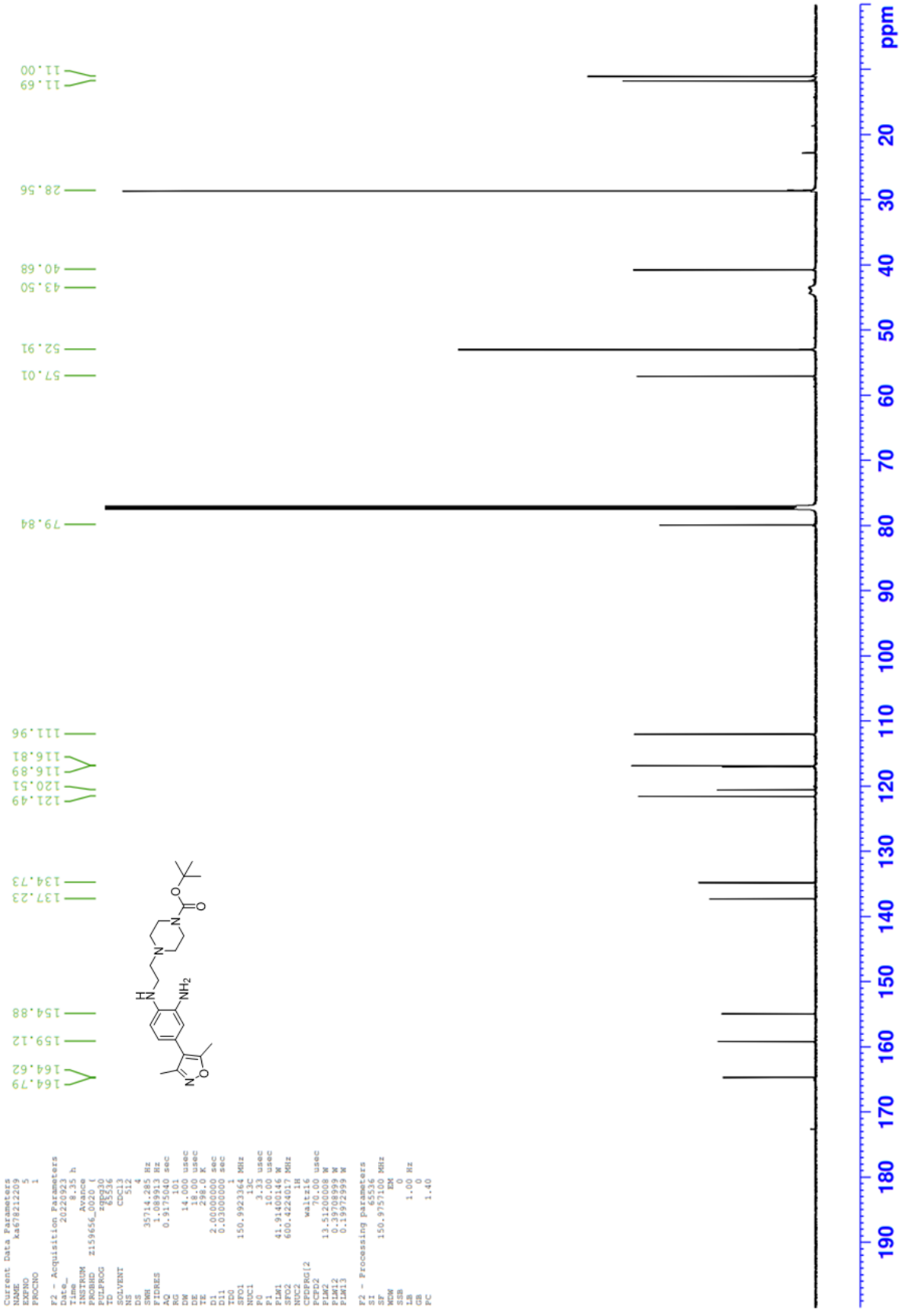

***tert*-Butyl 4-{2-[5-(3,5-dimethyl-1,2-oxazol-4-yl)-2-[(2*S*)-6-oxopiperidin-2-yl]-1*H*-1,3-benzodiazol-1-yl]ethyl}piperazine-1-carboxylate (110)**

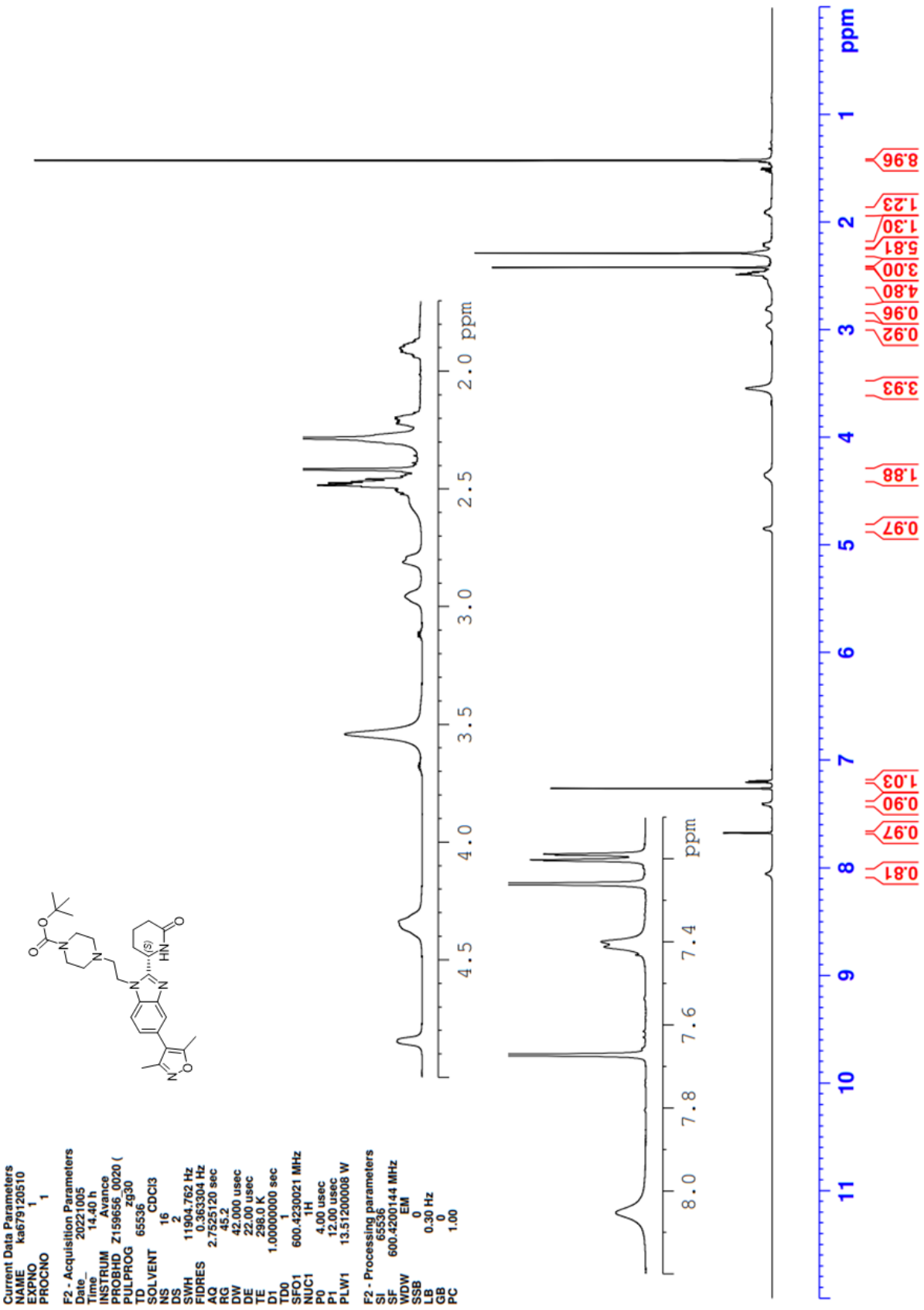

tert-Butyl 4-{2-[5-(3,5-dimethyl-1,2-oxazol-4-yl)-2-[(2*S*)-6-oxopiperidin-2-yl]-1*H*-1,3-benzodiazol-1-yl]ethyl}piperazine-1-carboxylate (110)

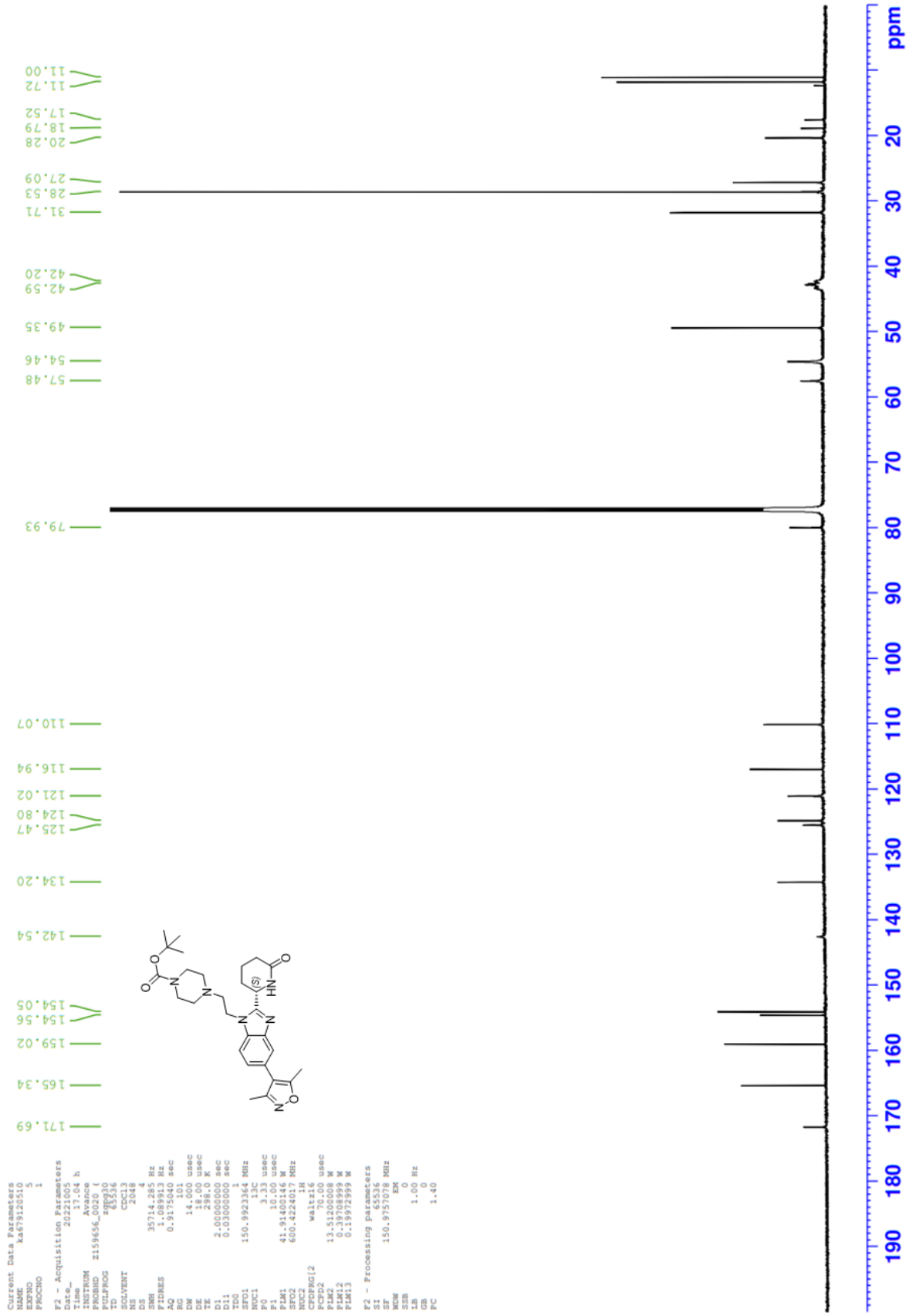

***tert*-Butyl 4-(2-{2-[(2*S*)-1-(3,4-difluorophenyl)-6-oxopiperidin-2-yl]-5-(3,5-dimethyl-1,2-oxazol-4-yl)-1*H*-1,3-benzodiazol-1-yl}ethyl)piperazine-1-carboxylate (111)**

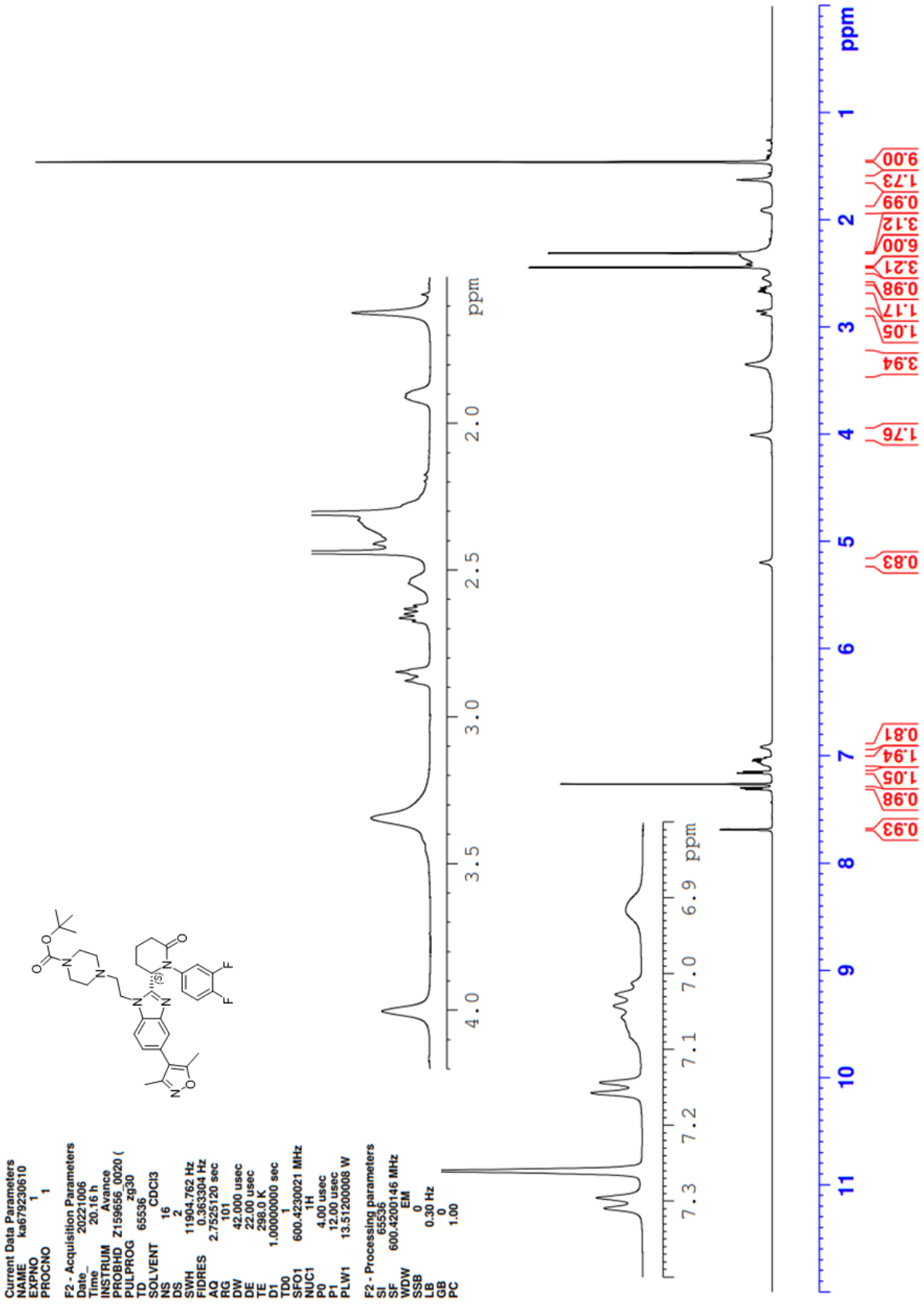

***tert*-Butyl 4-(2-{2-[(2*S*)-1-(3,4-difluorophenyl)-6-oxopiperidin-2-yl]-5-(3,5-dimethyl-1,2-oxazol-4-yl)-1*H*-1,3-benzodiazol-1-yl}ethyl)piperazine-1-carboxylate (111)**

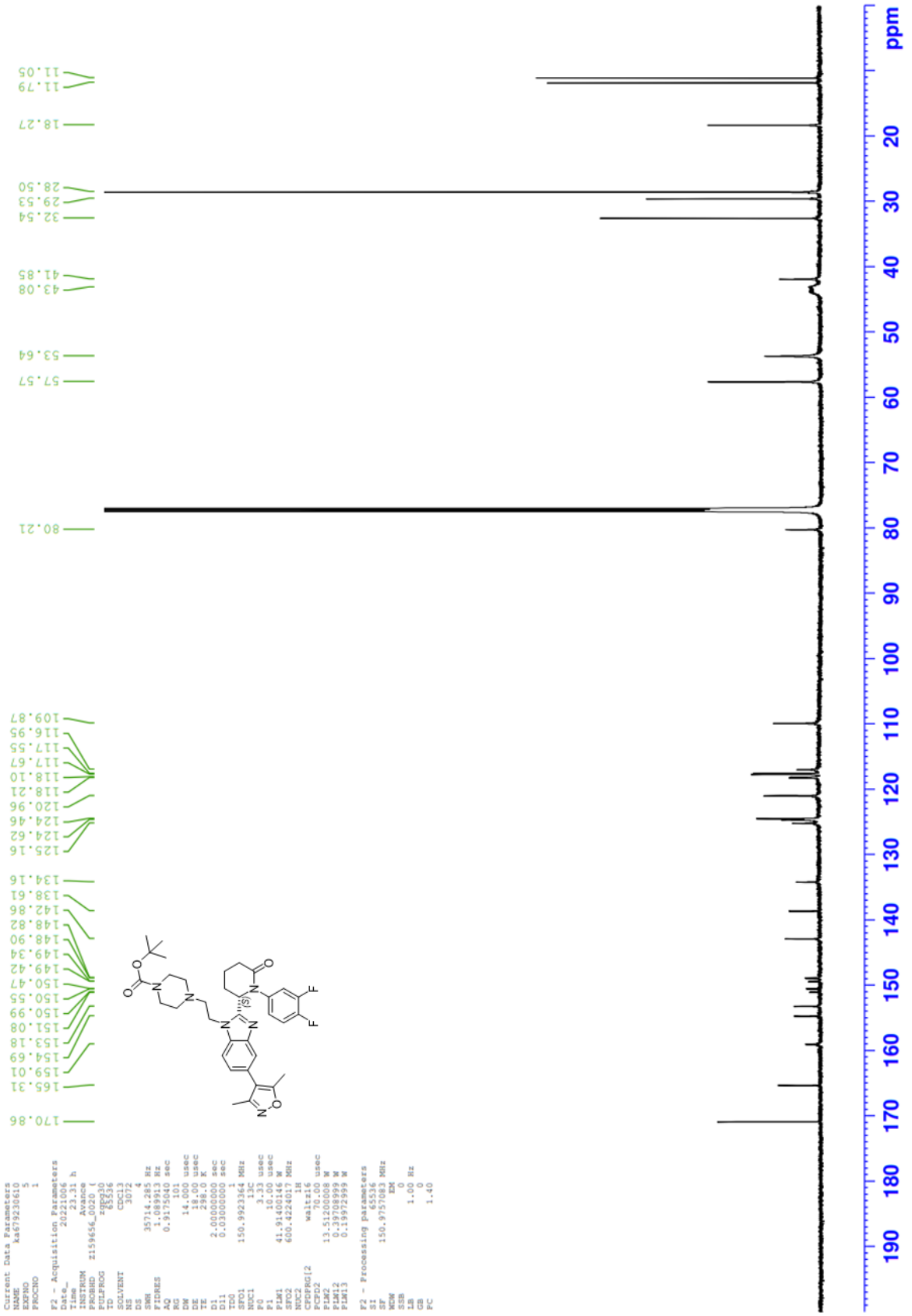

***tert*-Butyl 4-(2-{2-[(2*S*)-1-(3,4-difluorophenyl)-6-oxopiperidin-2-yl]-5-(3,5-dimethyl-1,2-oxazol-4-yl)-1*H*-1,3-benzodiazol-1-yl}ethyl)piperazine-1-carboxylate (111)**

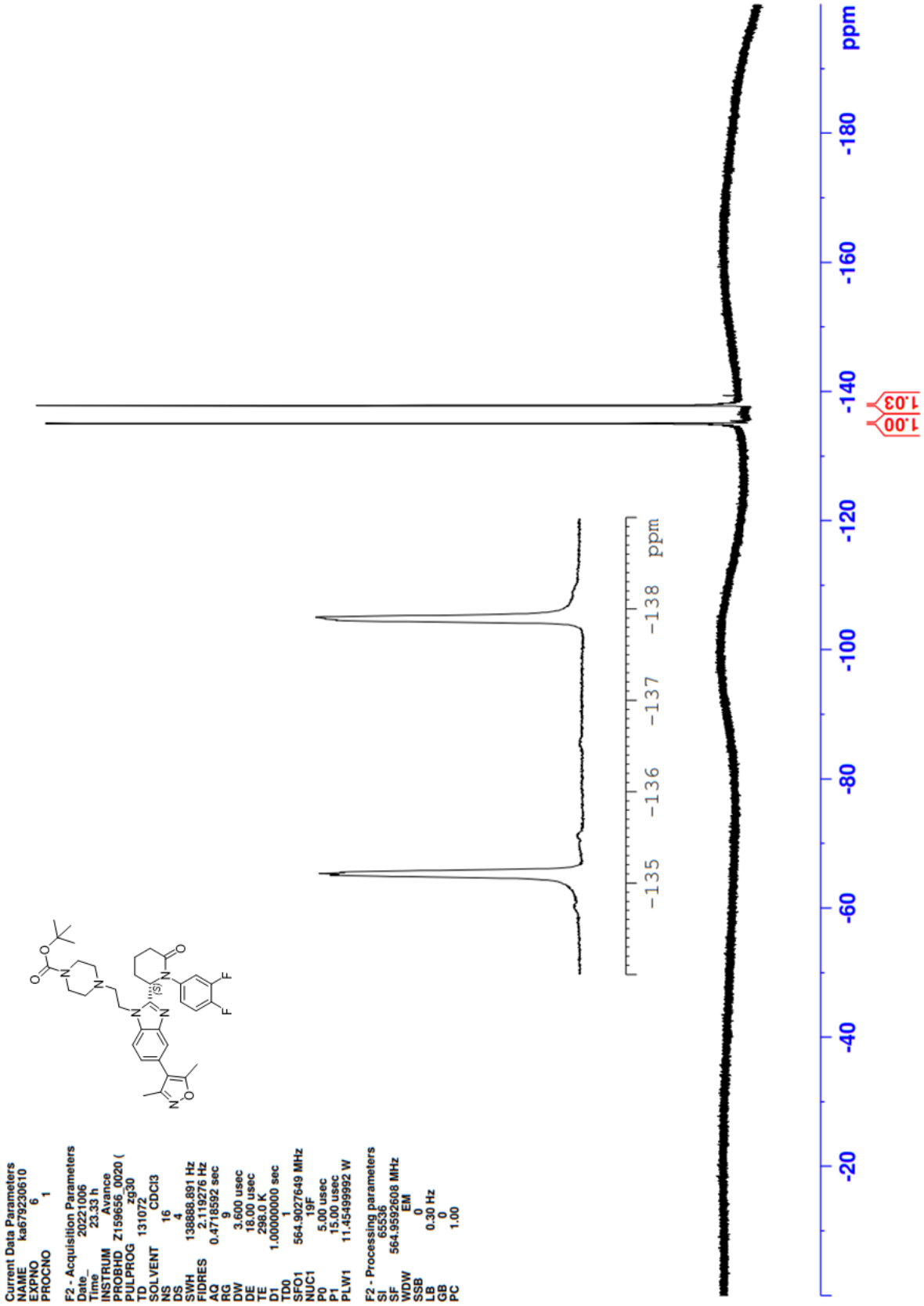

2-(2,6-Dioxopiperidin-3-yl)-4-[2-(2-{4-[(2*R*)-9-[(1*E*)-5-(7-methoxy-1,2,3,4-tetrahydroquinolin-1-yl)pent-1-en-1-yl]-2-methyl-4-oxo-2,3,4,5-tetrahydro-1*H*-1,5-benzodiazepin-7-yl]piperidin-1-yl}-2-oxoethoxy)ethoxy]-2,3-dihydro-1*H*-isoindole-1,3-dione (112)

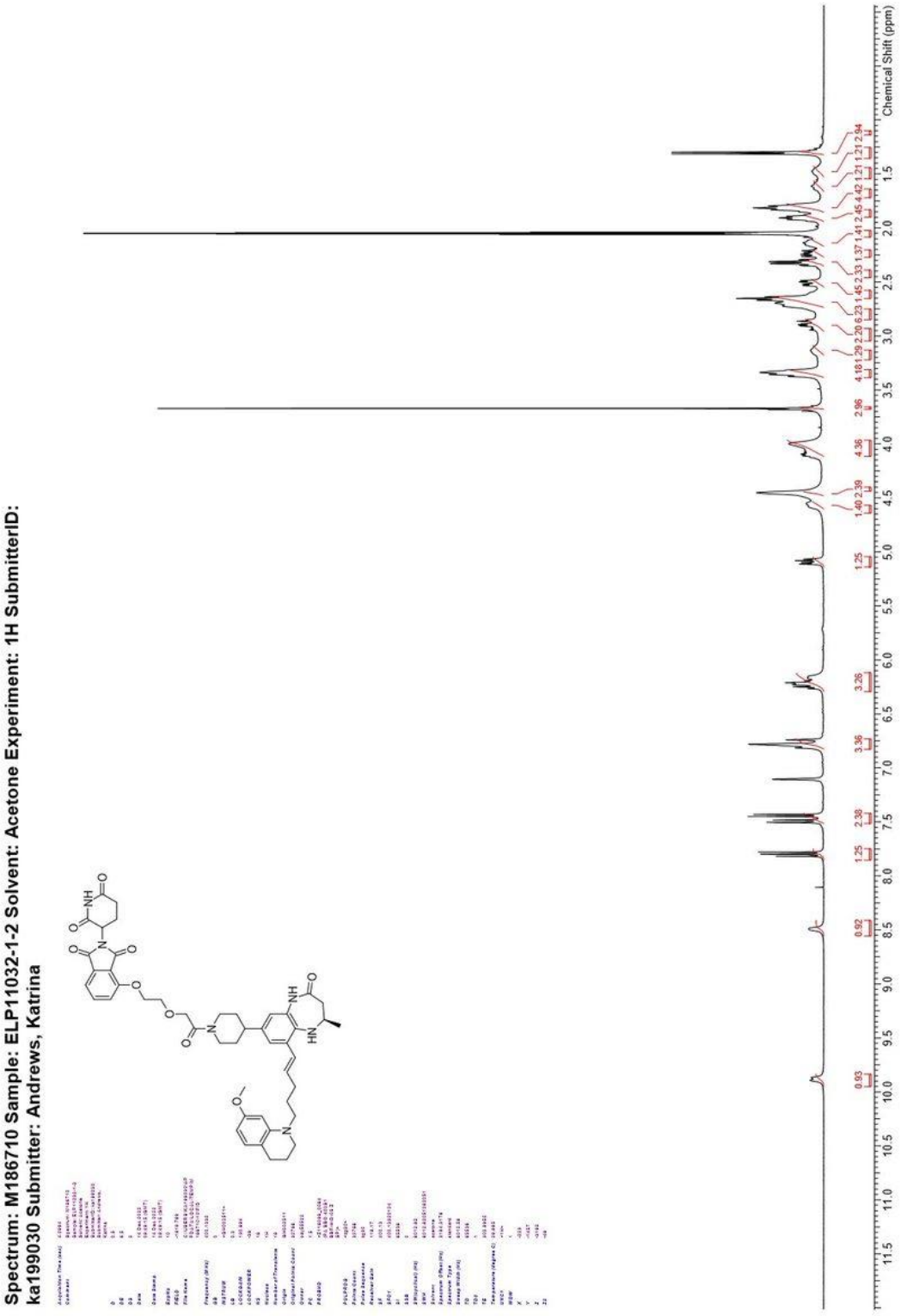

2-(2,6-Dioxopiperidin-3-yl)-4-{2-[2-(2-{4-[(2*R*)-9-[(1*E*)-5-(7-methoxy-1,2,3,4-tetrahydroquinolin-1-yl)pent-1-en-1-yl]-2-methyl-4-oxo-2,3,4,5-tetrahydro-1*H*-1,5-benzodiazepin-7-yl]piperidin-1-yl}-2-oxoethoxy)ethoxy]ethoxy}-2,3-dihydro-1*H*-isoindole-1,3-dione (113)

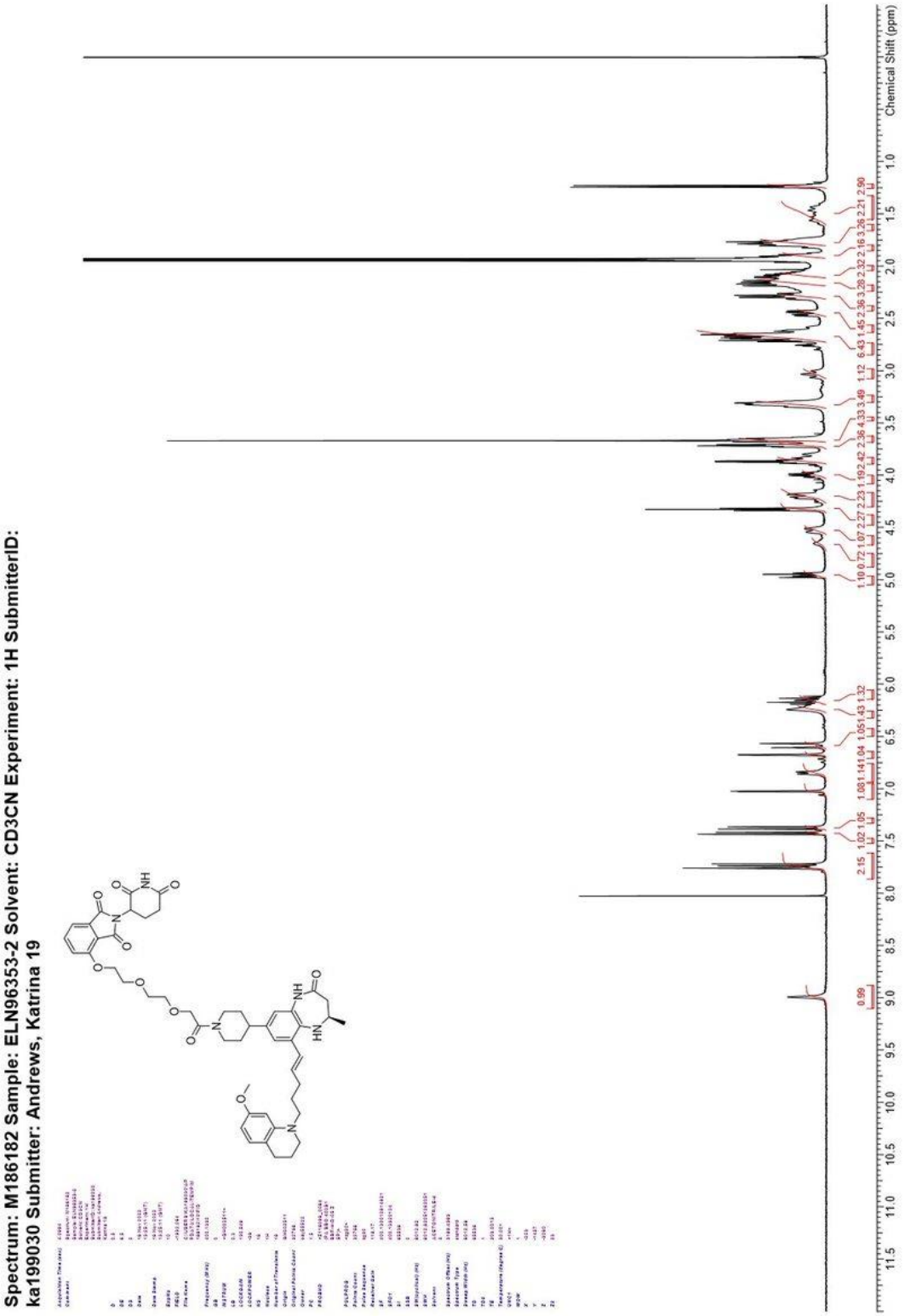

2-(2,6-Dioxopiperidin-3-yl)-4-(2-{2-[2-(2-{4-[(2*R*)-9-[(1*E*)-5-(7-methoxy-1,2,3,4-tetrahydroquinolin-1-yl)pent-1-en-1-yl]-2-methyl-4-oxo-2,3,4,5-tetrahydro-1*H*-1,5-benzodiazepin-7-yl]piperidin-1-yl}-2-oxoethoxy)ethoxy]ethoxy}ethoxy)-2,3-dihydro-1*H*-isoindole-1,3-dione (114)

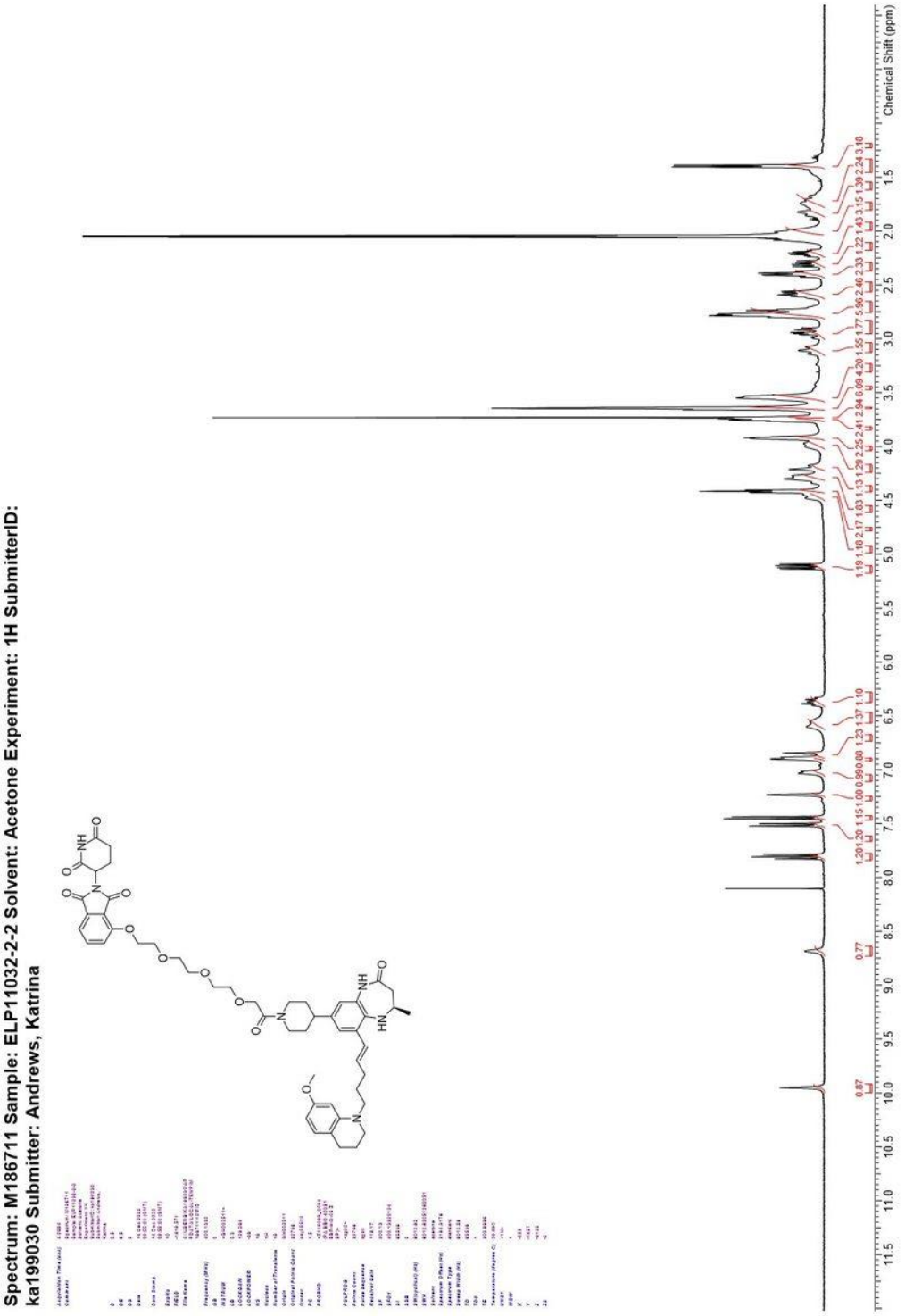

2-(2,6-Dioxopiperidin-3-yl)-4-[(14-{4-[(2*R*)-9-[(1*E*)-5-(7-methoxy-1,2,3,4-tetrahydroquinolin-1-yl)pent-1-en-1-yl]-2-methyl-4-oxo-2,3,4,5-tetrahydro-1*H*-1,5-benzodiazepin-7-yl]piperidin-1-yl}-14-oxo-3,6,9,12-tetraoxatetradecan-1-yl)oxy]-2,3-dihydro-1*H*-isoindole-1,3-dione (115)

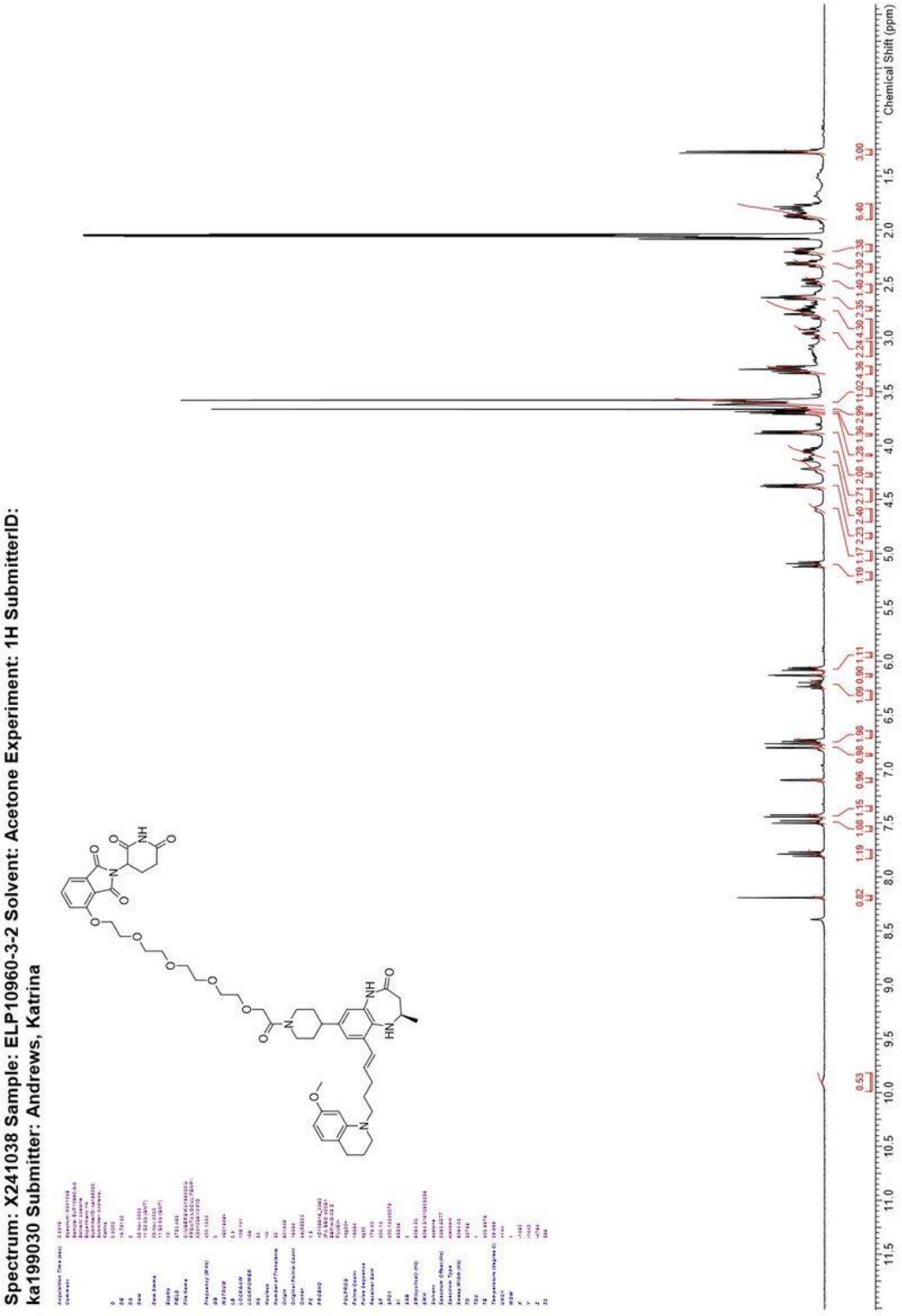

2-(2,6-Dioxopiperidin-3-yl)-4-[(5-{4-[(2*R*)-9-[(1*E*)-5-(7-methoxy-1,2,3,4-tetrahydroquinolin-1-yl)pent-1-en-1-yl]-2-methyl-4-oxo-2,3,4,5-tetrahydro-1*H*-1,5-benzodiazepin-7-yl]piperidin-1-yl}-5-oxopentyl)oxy]-2,3-dihydro-1*H*-isoindole-1,3-dione (116)

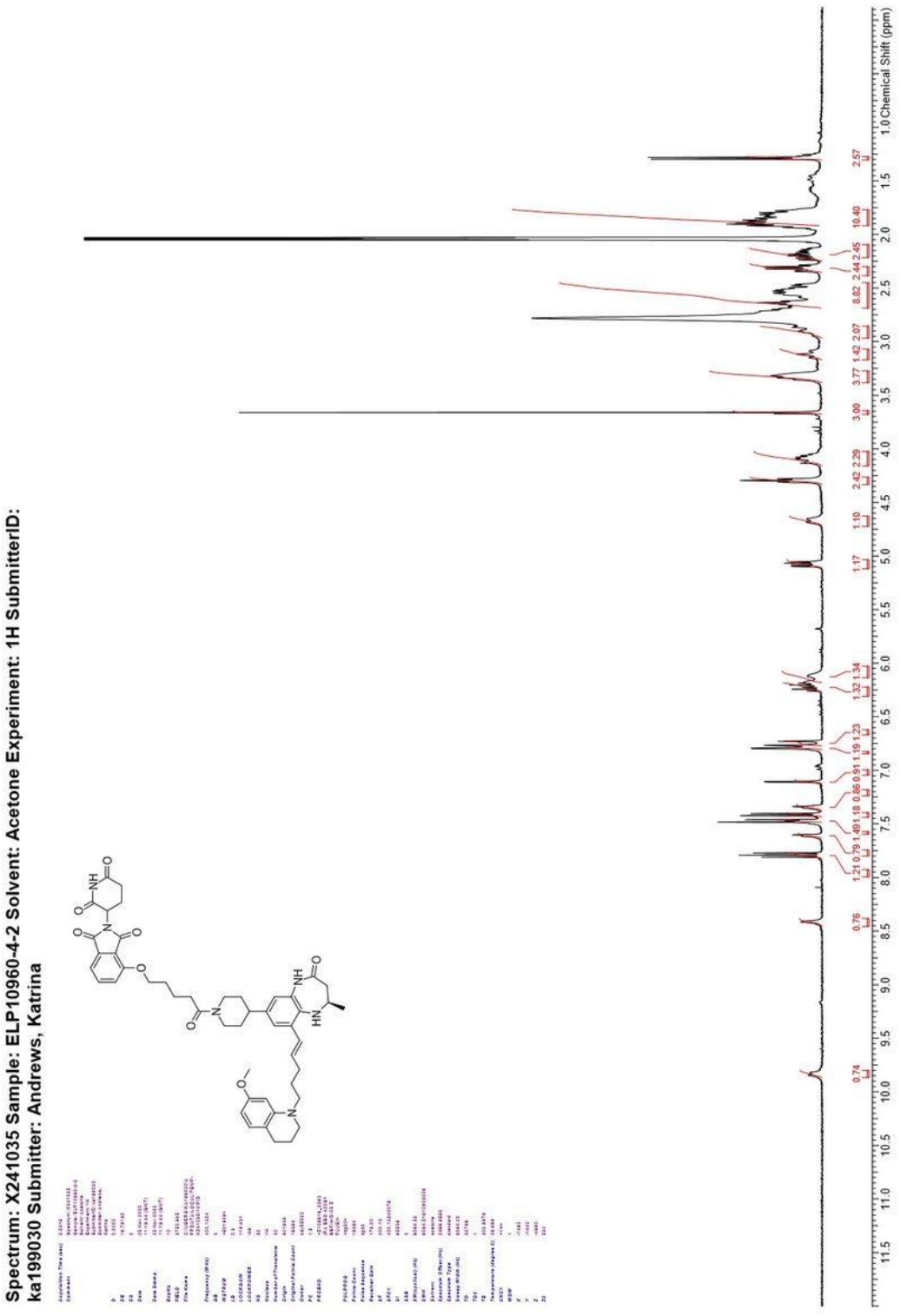

2-(2,6-Dioxopiperidin-3-yl)-4-[(8-{4-[(2*R*)-9-[(1*E*)-5-(7-methoxy-1,2,3,4-tetrahydroquinolin-1-yl)pent-1-en-1-yl]-2-methyl-4-oxo-2,3,4,5-tetrahydro-1*H*-1,5-benzodiazepin-7-yl]piperidin-1-yl}-8-oxooctyl)oxy]-2,3-dihydro-1*H*-isoindole-1,3-dione (117)

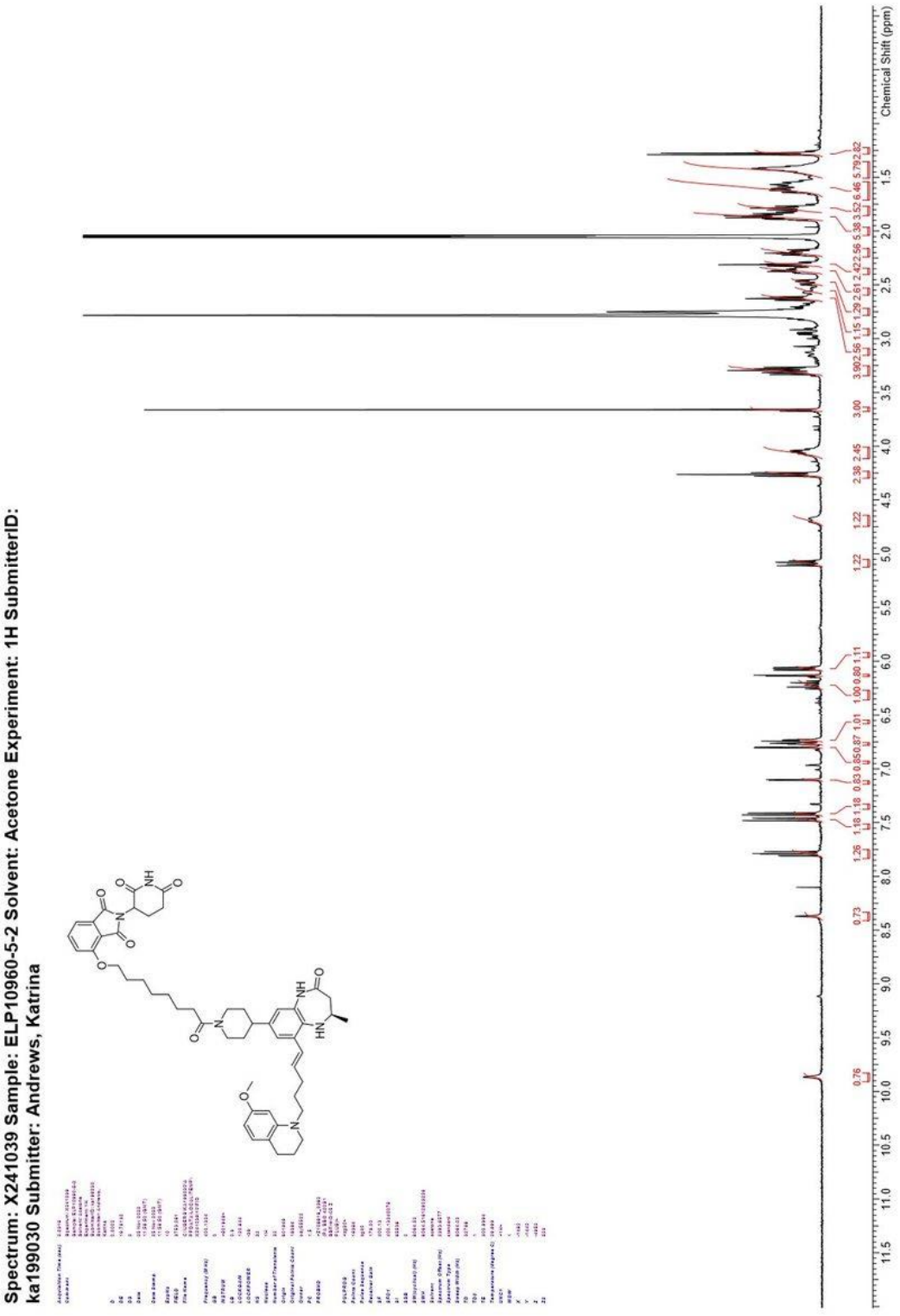

2-(2,6-Dioxopiperidin-3-yl)-4-[(10-{4-[(2*R*)-9-[(1*E*)-5-(7-methoxy-1,2,3,4-tetrahydroquinolin-1-yl)pent-1-en-1-yl]-2-methyl-4-oxo-2,3,4,5-tetrahydro-1*H*-1,5-benzodiazepin-7-yl]piperidin-1-yl}-10-oxodecyl)oxy]-2,3-dihydro-1*H*-isoindole-1,3-dione (118)

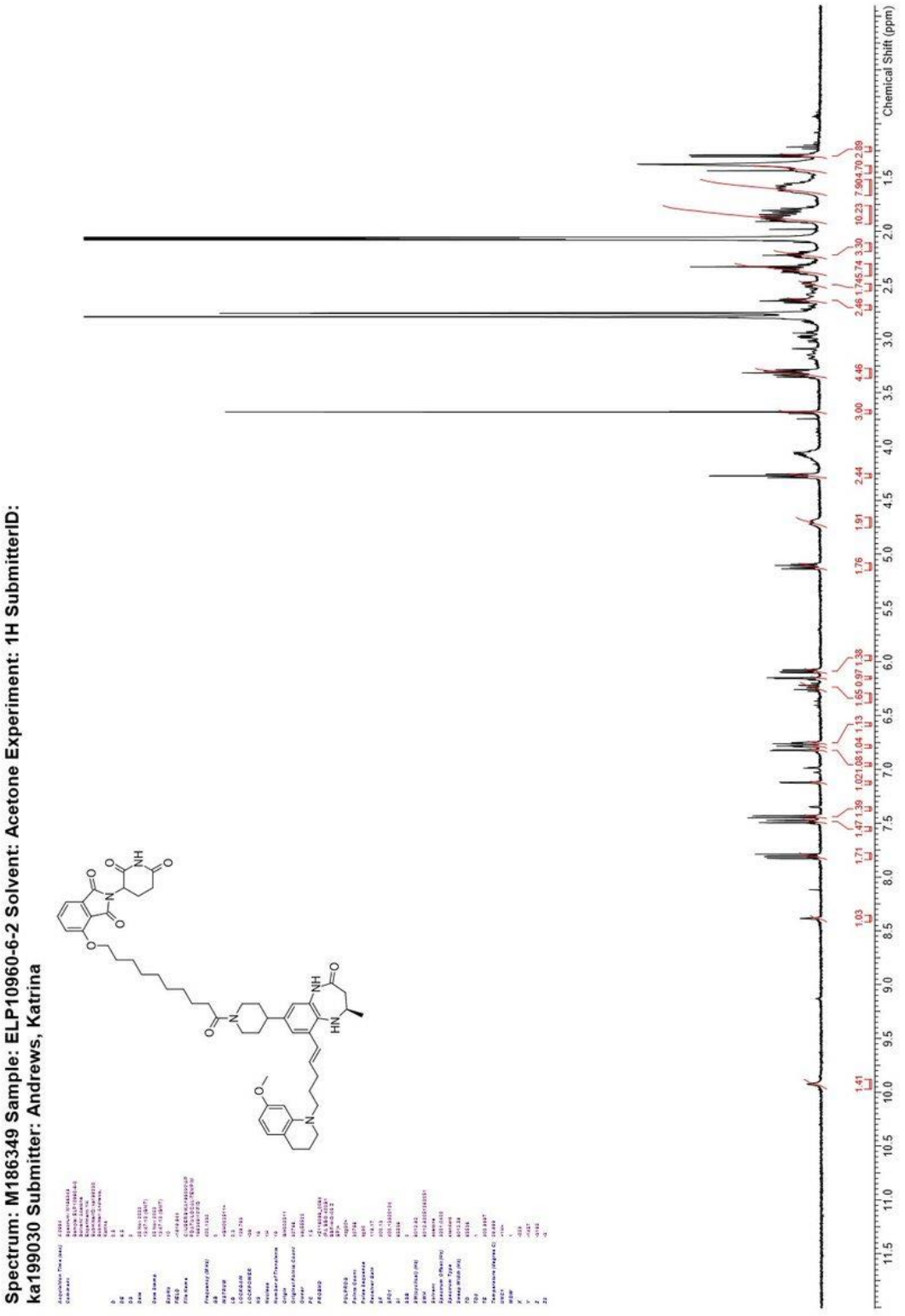

2-(2,6-Dioxopiperidin-3-yl)-5-fluoro-6-[4-(2-{4-[(2*R*)-9-[(1*E*)-5-(7-methoxy-1,2,3,4-tetrahydroquinolin-1-yl)pent-1-en-1-yl]-2-methyl-4-oxo-2,3,4,5-tetrahydro-1*H*-1,5-benzodiazepin-7-yl]piperidin-1-yl}-2-oxoethyl)piperazin-1-yl]-2,3-dihydro-1*H*-isoindole-1,3-dione (119)

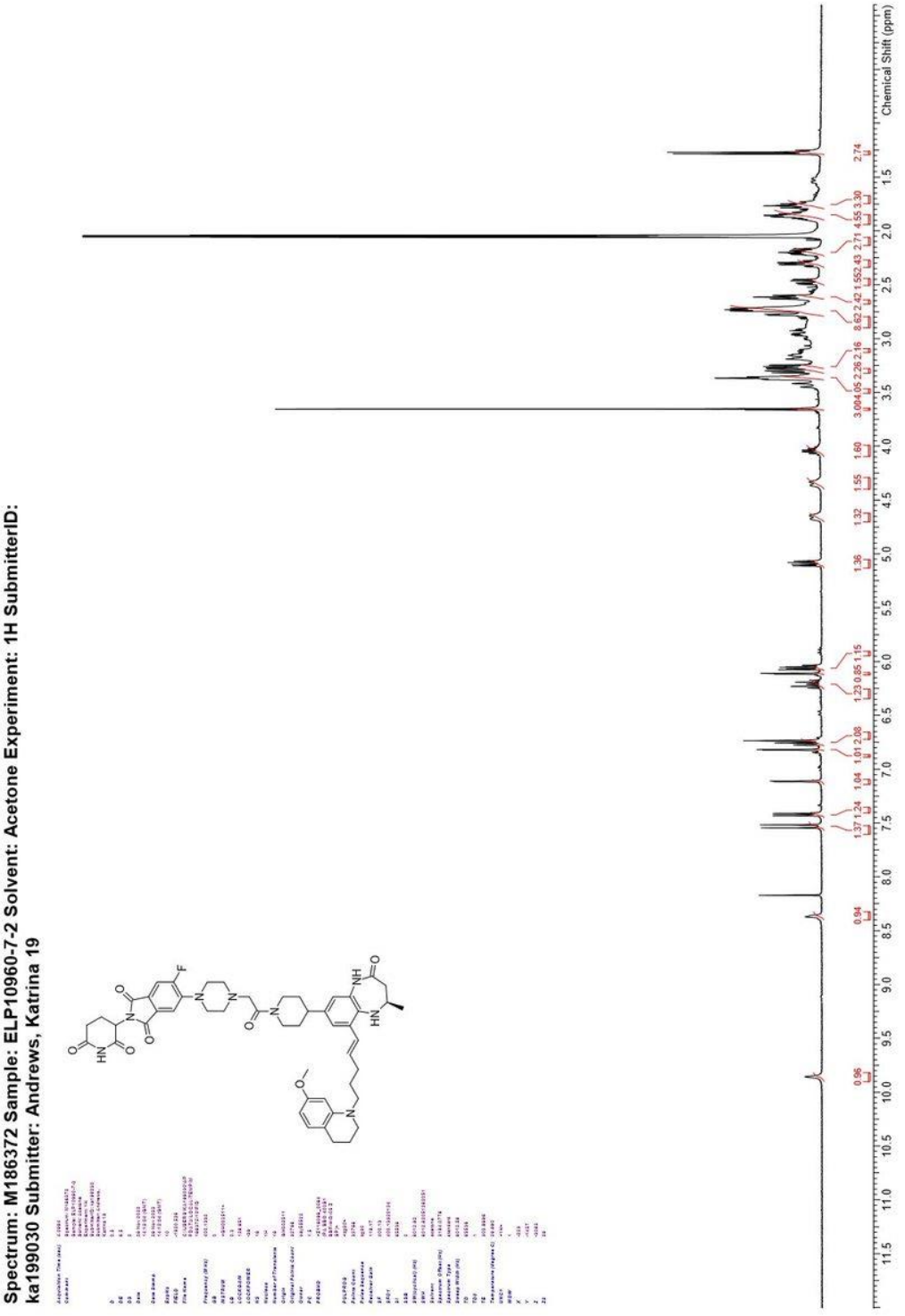

2-(2,6-Dioxopiperidin-3-yl)-5-fluoro-6-[4-(2-{4-[(2*R*)-9-[(1*E*)-5-(7-methoxy-1,2,3,4-tetrahydroquinolin-1-yl)pent-1-en-1-yl]-2-methyl-4-oxo-2,3,4,5-tetrahydro-1*H*-1,5-benzodiazepin-7-yl]piperidin-1-yl}-2-oxoethyl)piperazin-1-yl]-2,3-dihydro-1*H*-isoindole-1,3-dione (119)

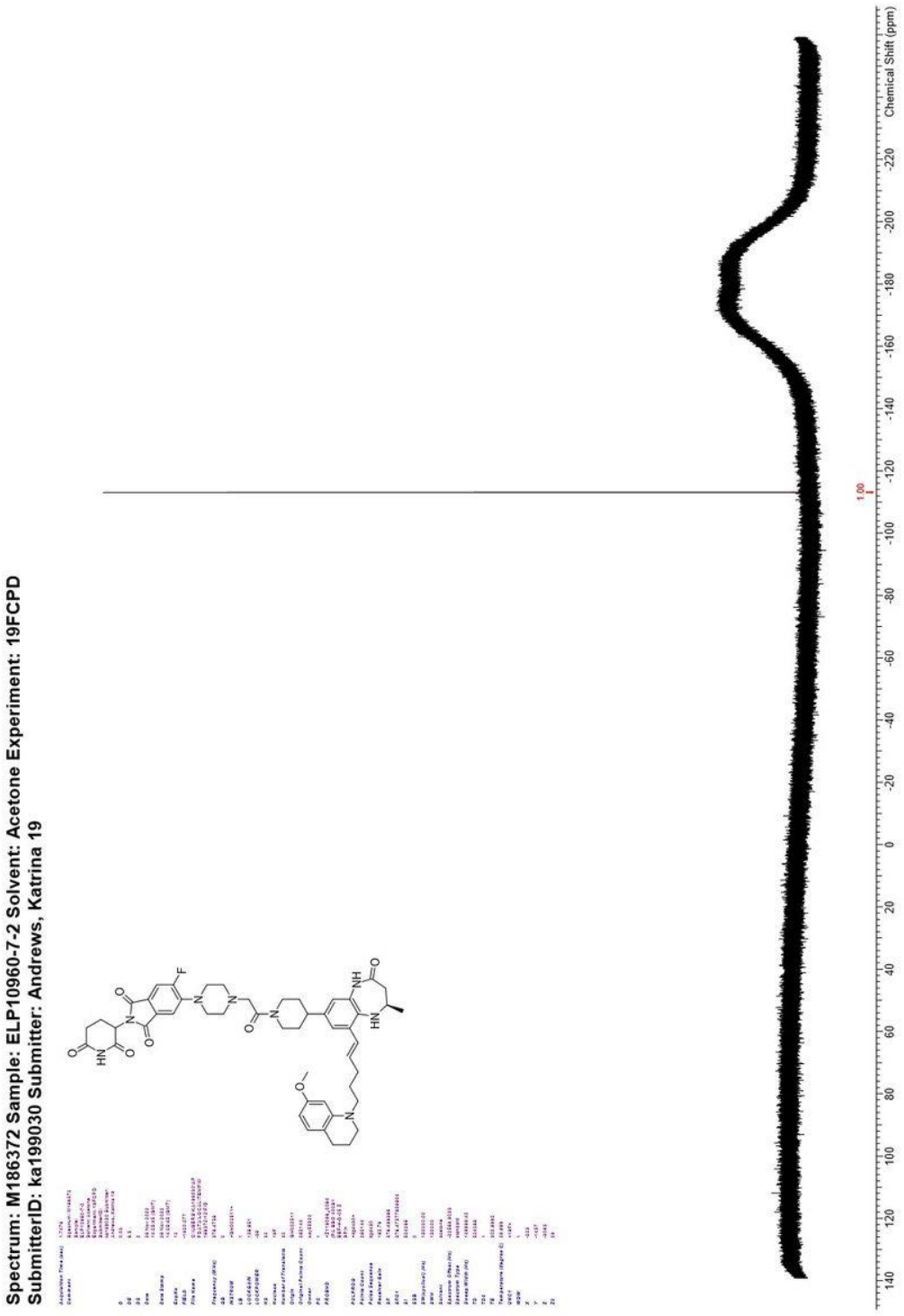

3-{5-[4-(4-{4-[(2*R*)-9-[(1*E*)-5-(7-Methoxy-1,2,3,4-tetrahydroquinolin-1-yl)pent-1-en-1-yl]-2-methyl-4-oxo-2,3,4,5-tetrahydro-1*H*-1,5-benzodiazepin-7-yl]piperidin-1-yl}-4-oxobutyl)piperazin-1-yl]-1-oxo-2,3-dihydro-1*H*-isoindol-2-yl}piperidine-2,6-dione (120)

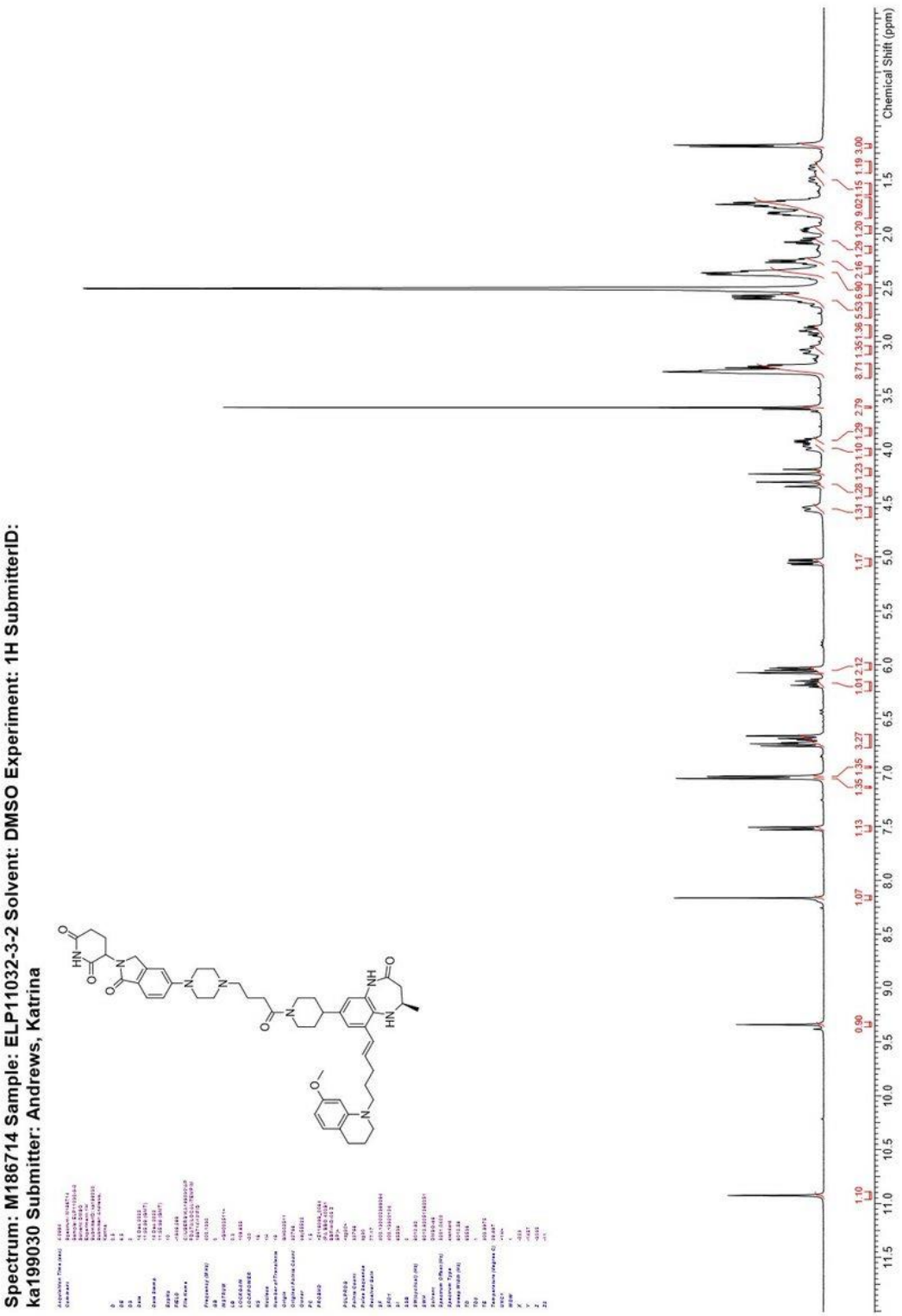

2-(2,6-Dioxopiperidin-3-yl)-5-fluoro-6-[9-(2-{4-[(2*R*)-9-[(1*E*)-5-(7-methoxy-1,2,3,4-tetrahydroquinolin-1-yl)pent-1-en-1-yl]-2-methyl-4-oxo-2,3,4,5-tetrahydro-1*H*-1,5-benzodiazepin-7-yl]piperidin-1-yl}-2-oxoethyl)-3,9-diazaspiro[5.5]undecan-3-yl]-2,3-dihydro-1*H*-isoindole-1,3-dione (121)

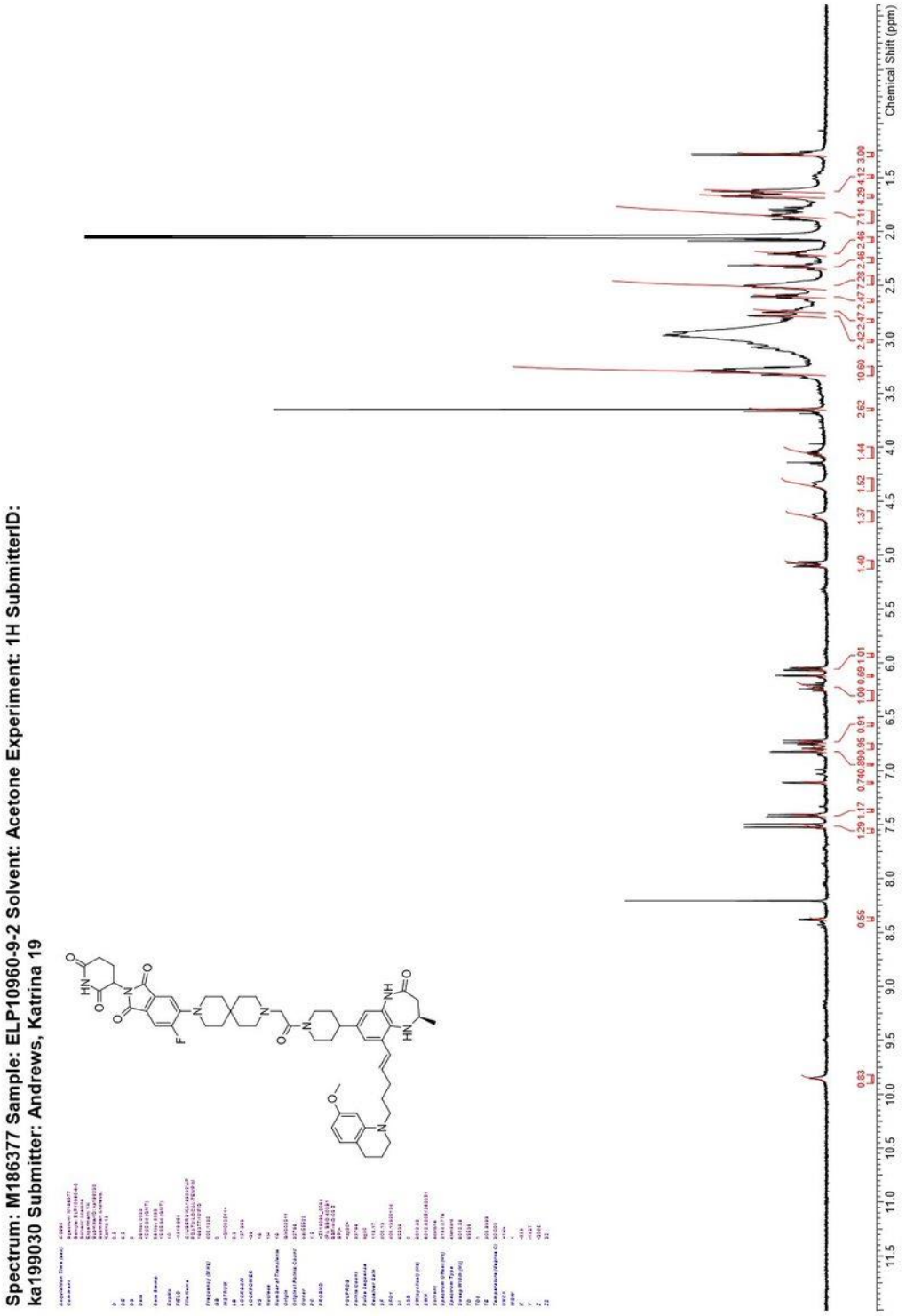

2-(2,6-Dioxopiperidin-3-yl)-5-fluoro-6-[9-(2-{4-[(2*R*)-9-[(1*E*)-5-(7-methoxy-1,2,3,4-tetrahydroquinolin-1-yl)pent-1-en-1-yl]-2-methyl-4-oxo-2,3,4,5-tetrahydro-1*H*-1,5-benzodiazepin-7-yl]piperidin-1-yl}-2-oxoethyl)-3,9-diazaspiro[5.5]undecan-3-yl]-2,3-dihydro-1*H*-isoindole-1,3-dione (121)

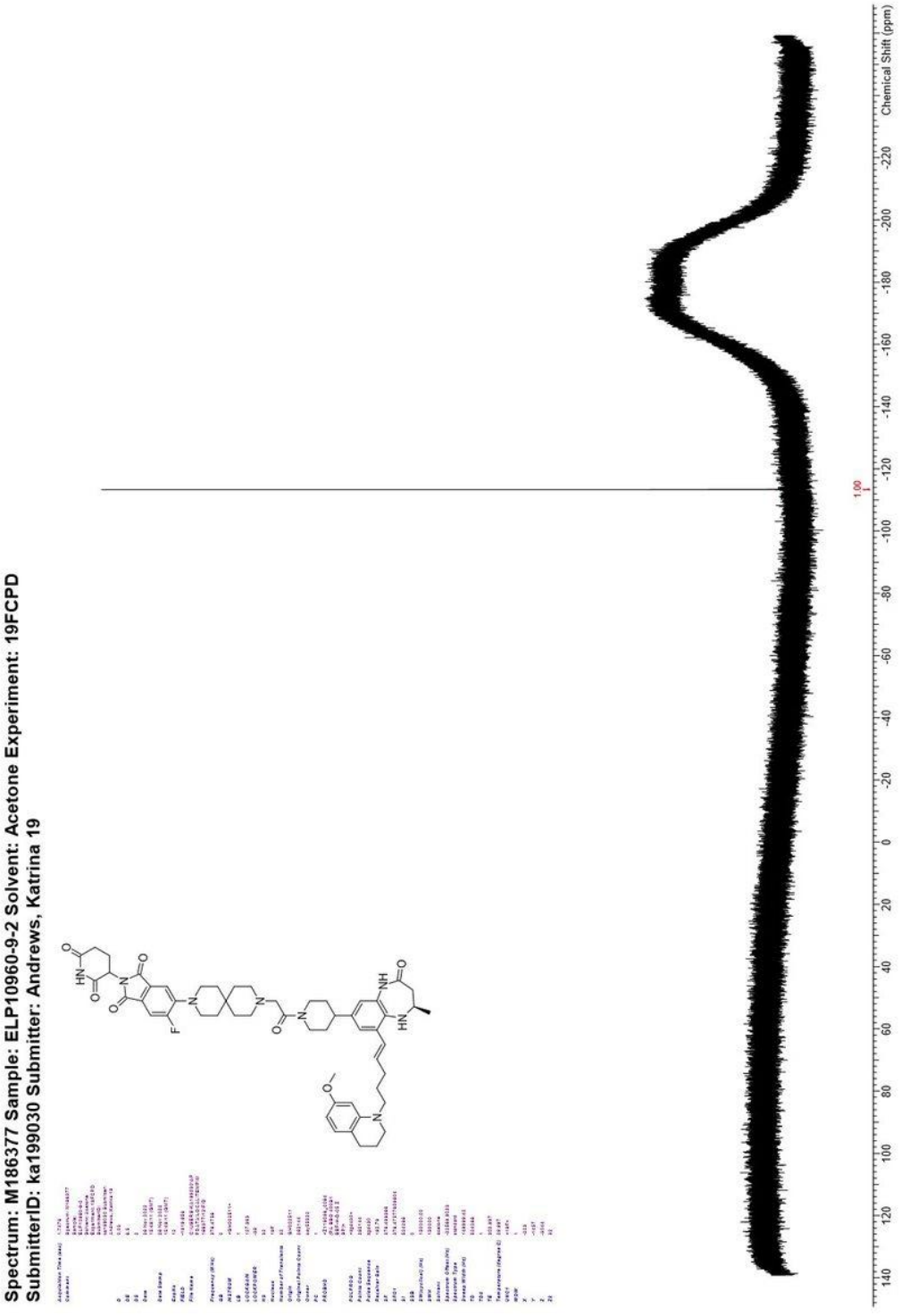

2-(2,6-Dioxopiperidin-3-yl)-5-fluoro-6-{4-[1-(2-{4-[(2*R*)-9-[(1*E*)-5-(7-methoxy-1,2,3,4-tetrahydroquinolin-1-yl)pent-1-en-1-yl]-2-methyl-4-oxo-2,3,4,5-tetrahydro-1*H*-1,5-benzodiazepin-7-yl]piperidin-1-yl}-2-oxoethyl)piperidin-4-yl]piperazin-1-yl}-2,3-dihydro-1*H*-isoindole-1,3-dione (122)

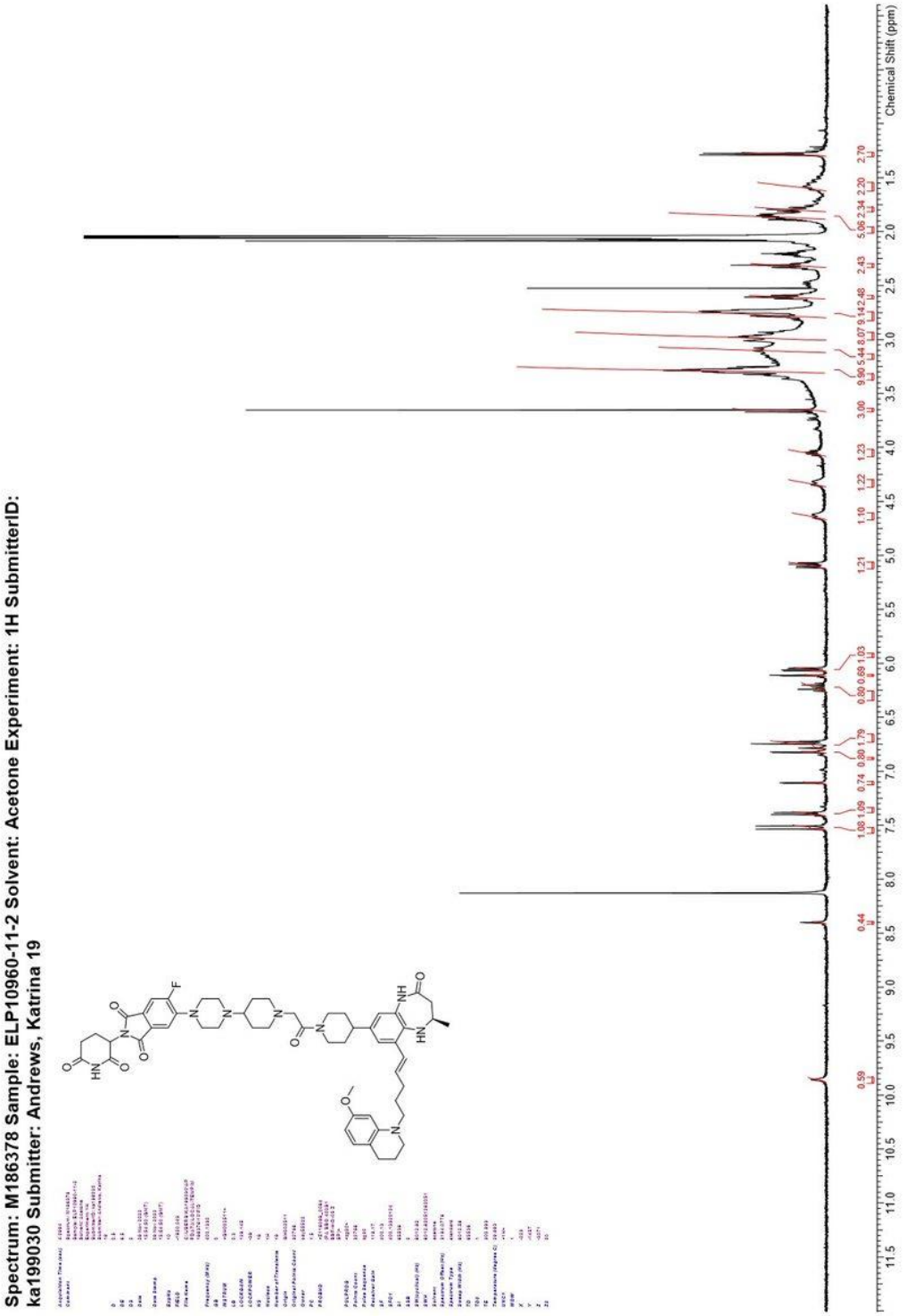

2-(2,6-Dioxopiperidin-3-yl)-5-fluoro-6-{4-[1-(2-{4-[(2*R*)-9-[(1*E*)-5-(7-methoxy-1,2,3,4-tetrahydroquinolin-1-yl)pent-1-en-1-yl]-2-methyl-4-oxo-2,3,4,5-tetrahydro-1*H*-1,5-benzodiazepin-7-yl]piperidin-1-yl}-2-oxoethyl)piperidin-4-yl]piperazin-1-yl}-2,3-dihydro-1*H*-isoindole-1,3-dione (122)

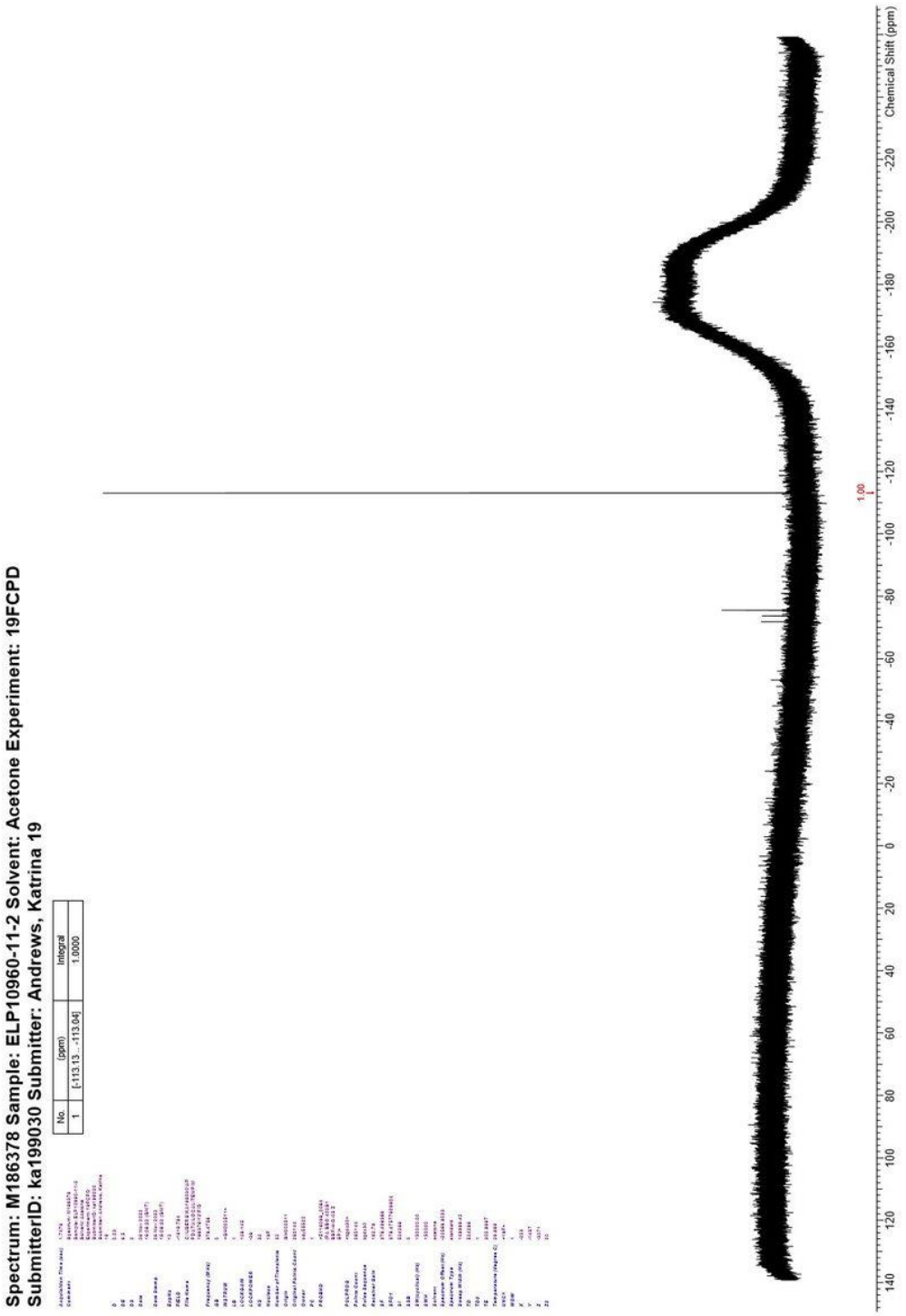

4-{2-[2-(4-{2-[(2*S*)-1-(3,4-Difluorophenyl)-6-oxopiperidin-2-yl]-5-(3,5-dimethyl-1,2-oxazol-4-yl)-1*H*-1,3-benzodiazol-1-yl}piperidin-1-yl)-2-oxoethoxy]ethoxy}-2-(2,6-dioxopiperidin-3-yl)-2,3-dihydro-1*H*-isoindole-1,3-dione (134)

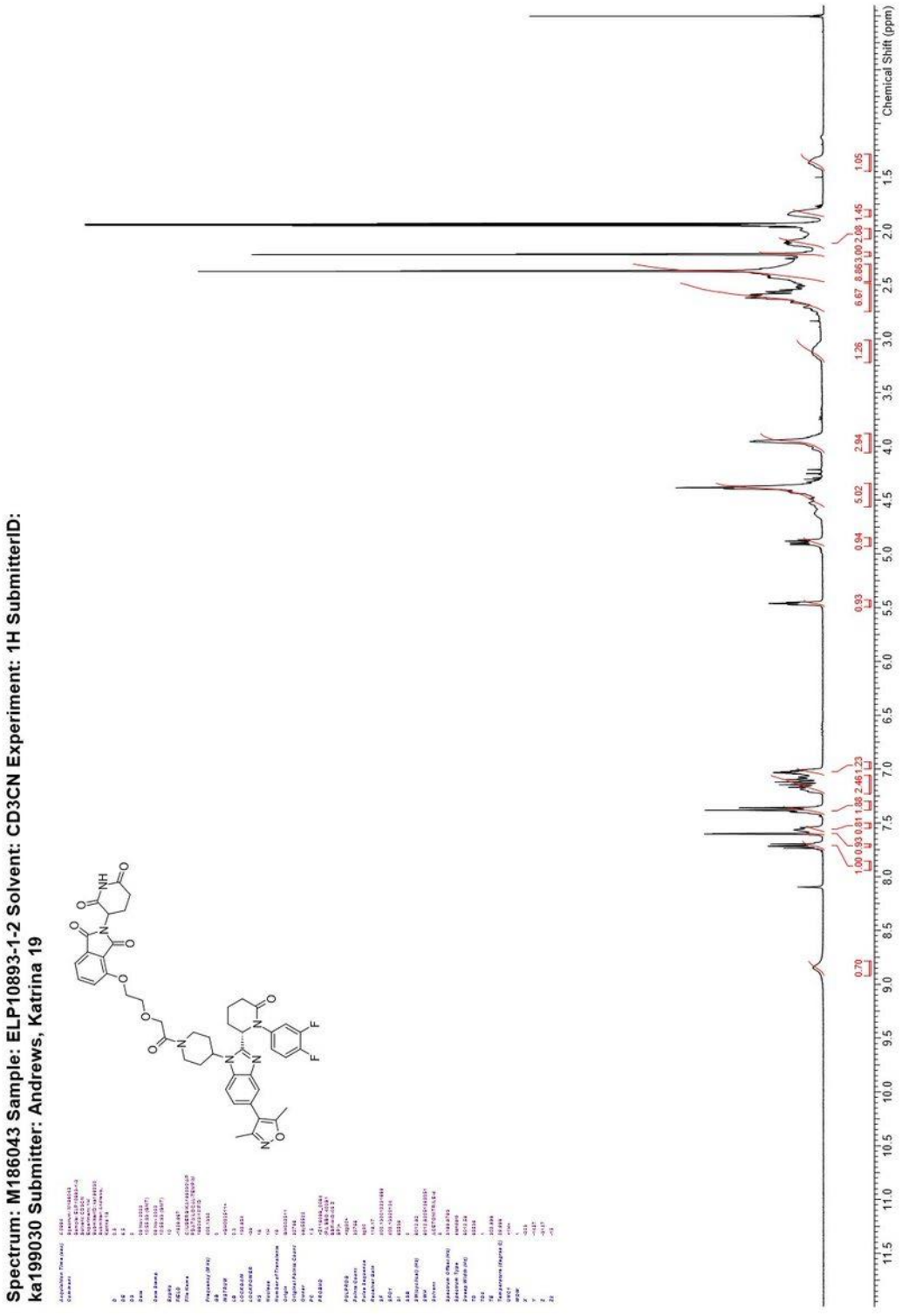

4-{2-[2-(4-{2-[(2*S*)-1-(3,4-Difluorophenyl)-6-oxopiperidin-2-yl]-5-(3,5-dimethyl-1,2-oxazol-4-yl)-1*H*-1,3-benzodiazol-1-yl}piperidin-1-yl)-2-oxoethoxy]ethoxy}-2-(2,6-dioxopiperidin-3-yl)-2,3-dihydro-1*H*-isoindole-1,3-dione (134)

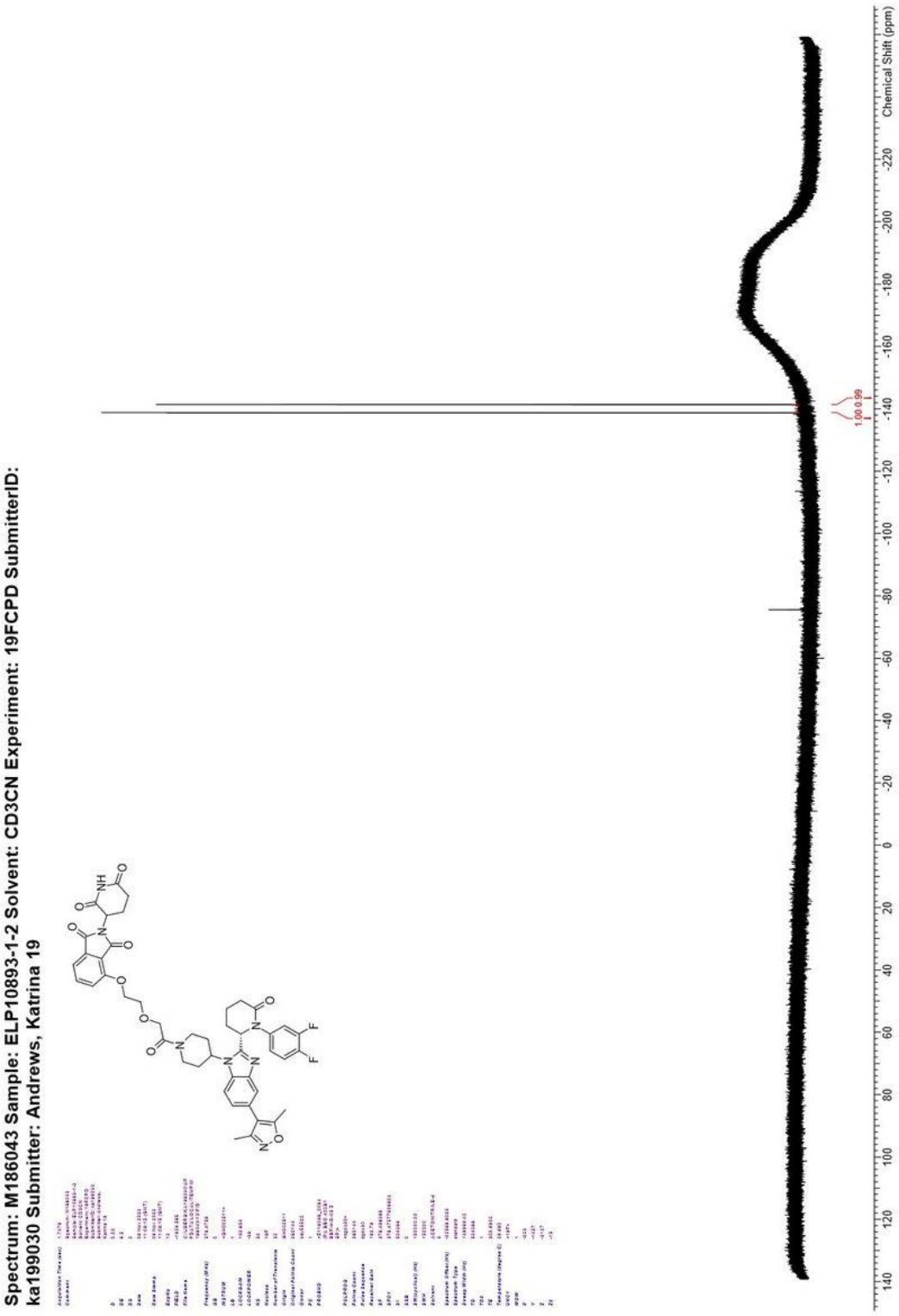

4-(2-(2-(2-(4-(2-((*S*)-1-(3,4-Difluorophenyl)-6-oxopiperidin-2-yl)-5-(3,5-dimethylisoxazol-4-yl)-1*H*-benzo[d]imidazol-1-yl)piperidin-1-yl)-2-oxoethoxy)ethoxy)ethoxy)-2-(2,6-dioxopiperidin-3-yl)isoindoline-1,3-dione (135)

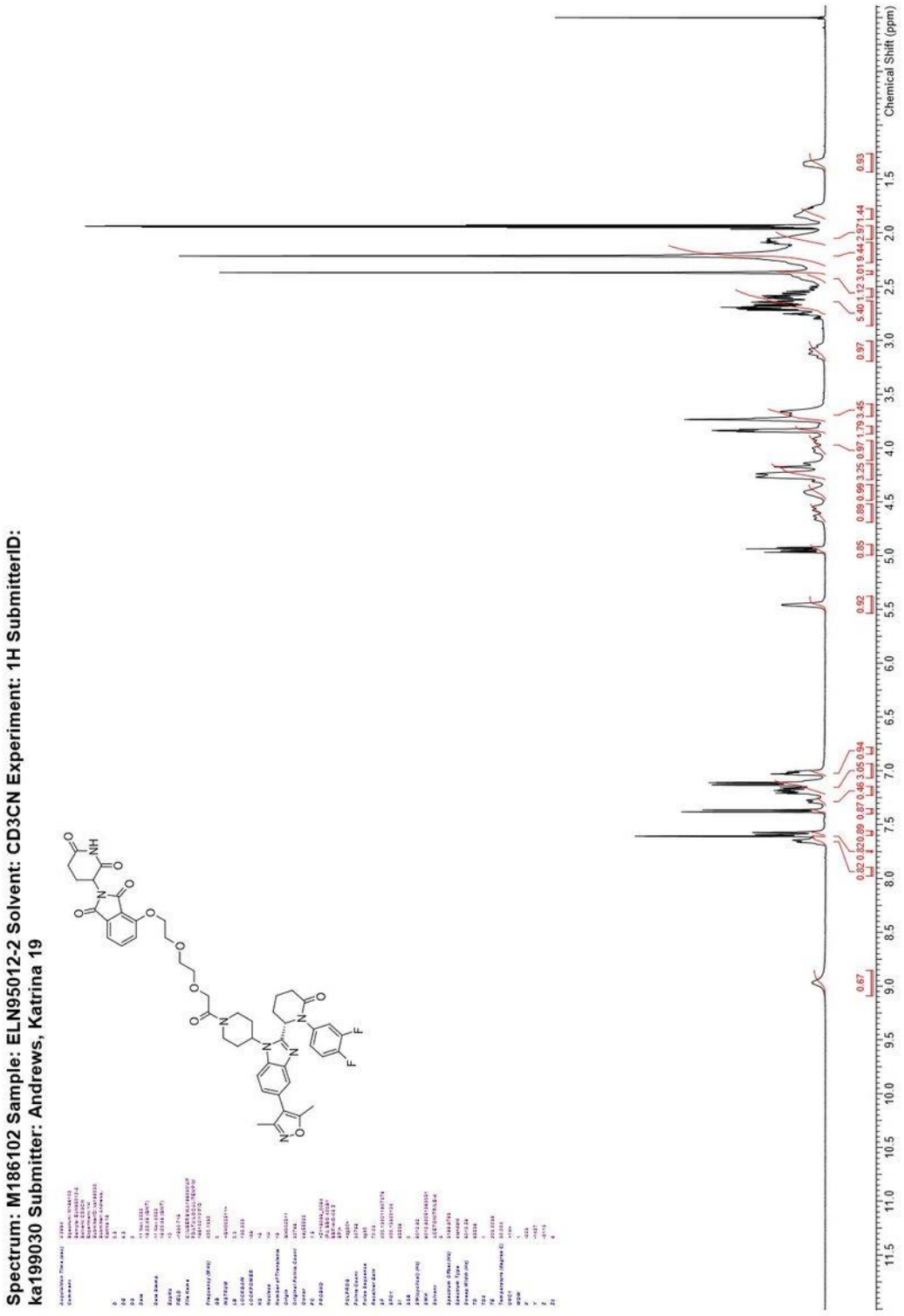

4-(2-(2-(2-(4-(2-((*S*)-1-(3,4-Difluorophenyl)-6-oxopiperidin-2-yl)-5-(3,5-dimethylisoxazol-4-yl)-1*H*-benzo[d]imidazol-1-yl)piperidin-1-yl)-2-oxoethoxy)ethoxy)ethoxy)-2-(2,6-dioxopiperidin-3-yl)isoindoline-1,3-dione (135)

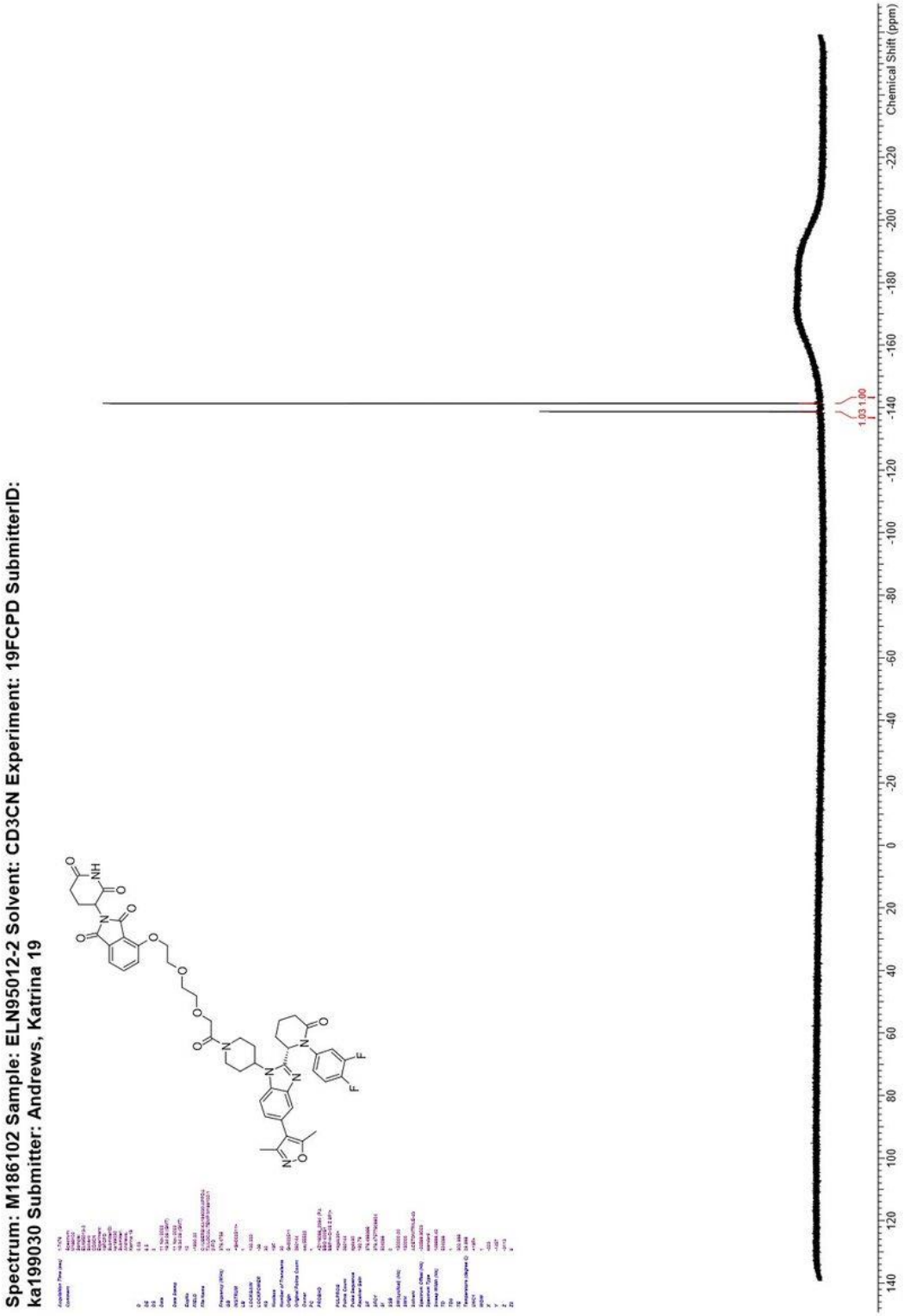

4-[2-(2-{2-[2-(4-{2-[(2*S*)-1-(3,4-Difluorophenyl)-6-oxopiperidin-2-yl]-5-(3,5-dimethyl-1,2-oxazol-4-yl)-1*H*-1,3-benzodiazol-1-yl}piperidin-1-yl)-2-oxoethoxy]ethoxy}ethoxy)ethoxy]-2-(2,6-dioxopiperidin-3-yl)-2,3-dihydro-1*H*-isoindole-1,3-dione (136)

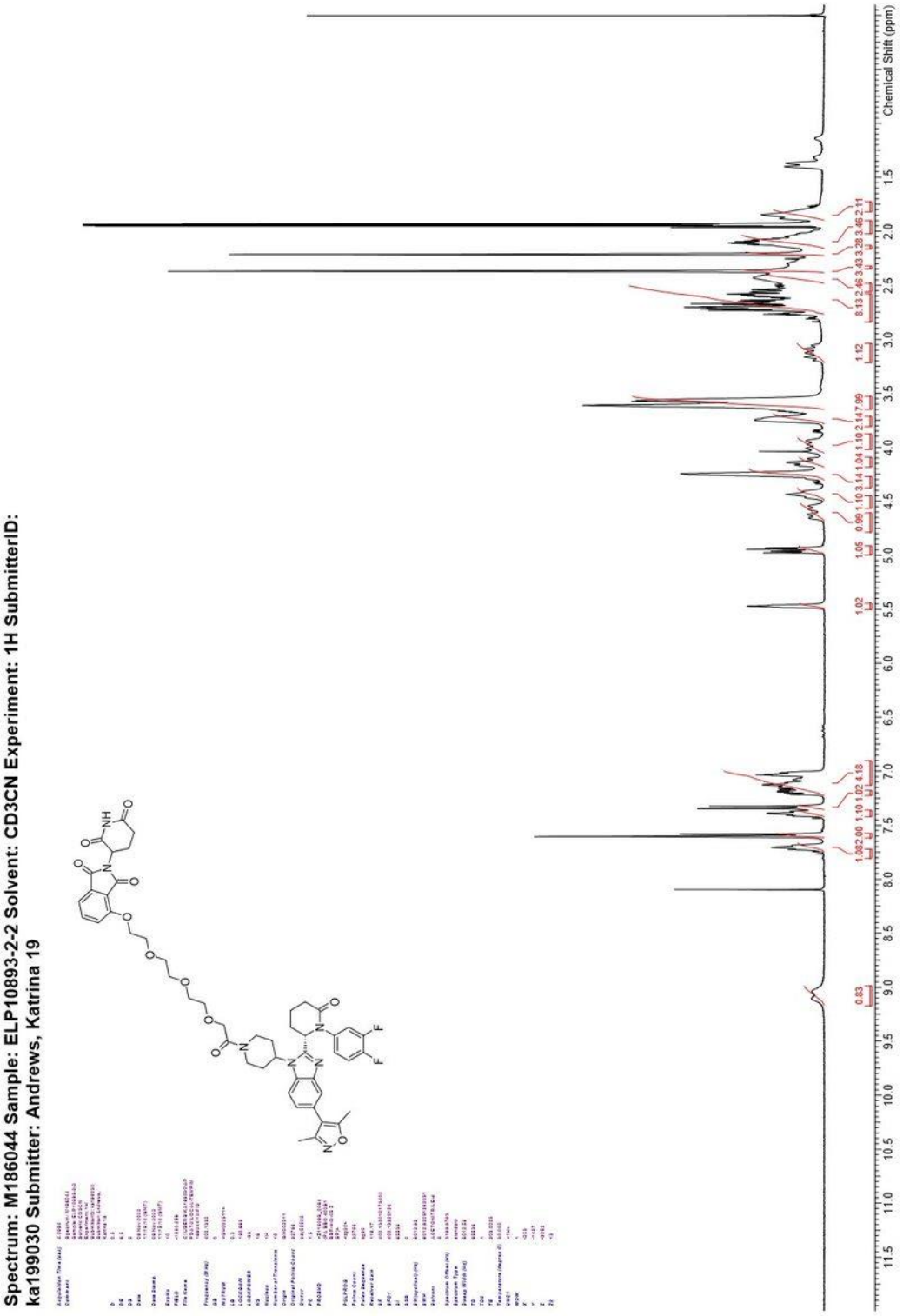

4-[2-(2-{2-[2-(4-{2-[(2*S*)-1-(3,4-Difluorophenyl)-6-oxopiperidin-2-yl]-5-(3,5-dimethyl-1,2-oxazol-4-yl)-1*H*-1,3-benzodiazol-1-yl}piperidin-1-yl)-2-oxoethoxy]ethoxy}ethoxy)ethoxy]-2-(2,6-dioxopiperidin-3-yl)-2,3-dihydro-1*H*-isoindole-1,3-dione (136)

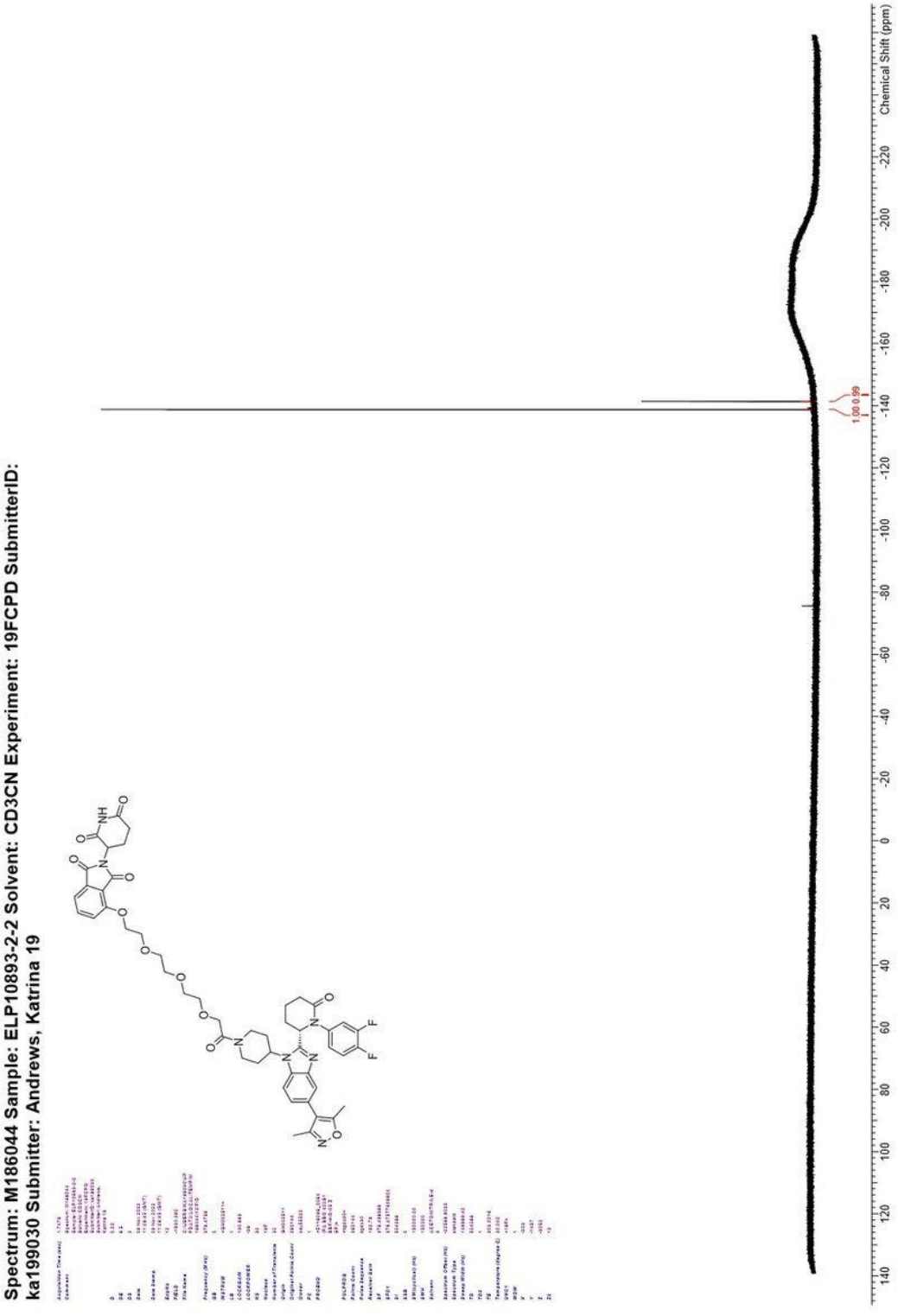

4-{[14-(4-{2-[(2*S*)-1-(3,4-Difluorophenyl)-6-oxopiperidin-2-yl]-5-(3,5-dimethyl-1,2-oxazol-4-yl)-1*H*-1,3-benzodiazol-1-yl}piperidin-1-yl)-14-oxo-3,6,9,12-tetraoxatetradecan-1-yl]oxy}-2-(2,6-dioxopiperidin-3-yl)-2,3-dihydro-1*H*-isoindole-1,3-dione (137)

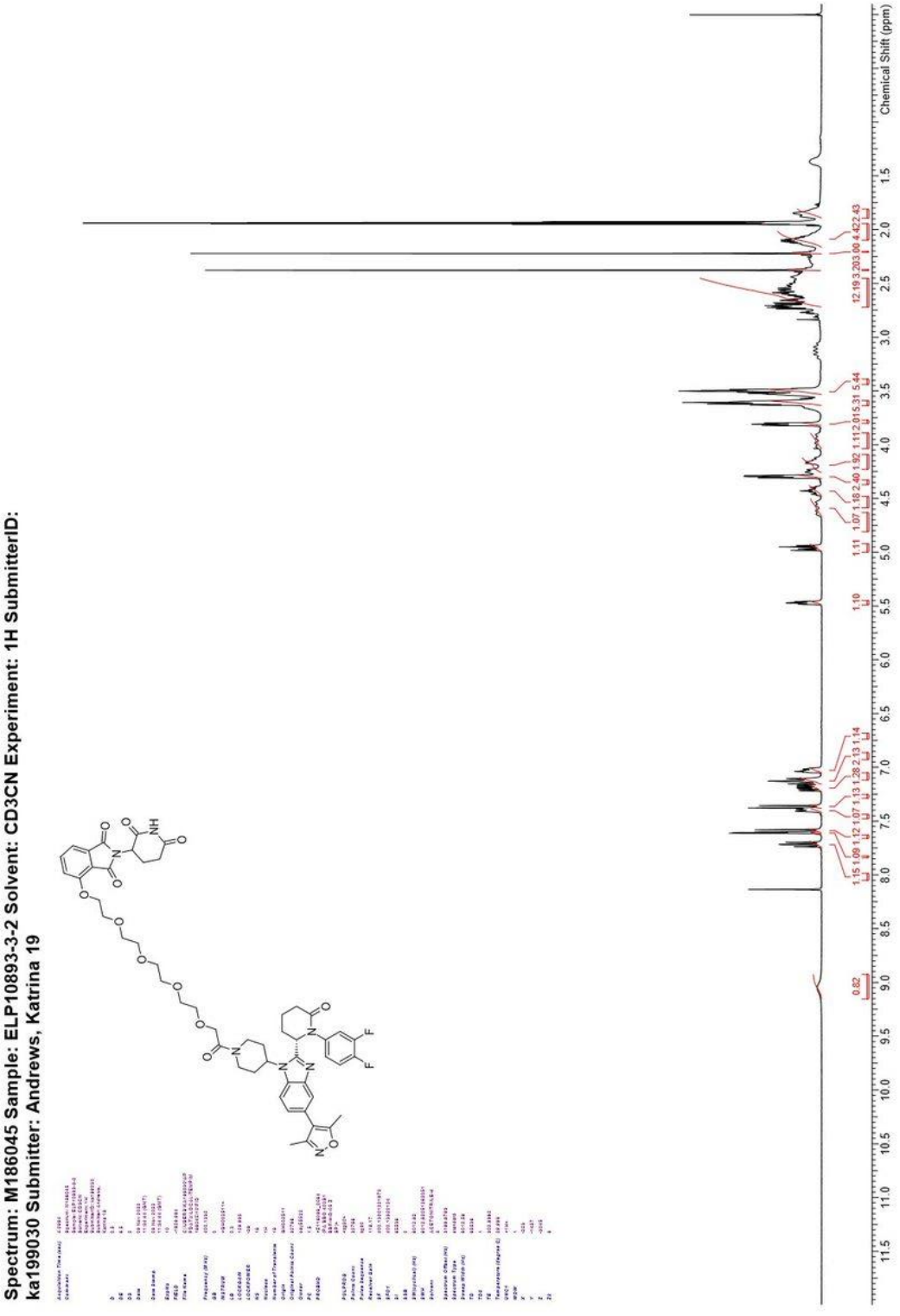

4-{[14-(4-{2-[(2*S*)-1-(3,4-Difluorophenyl)-6-oxopiperidin-2-yl]-5-(3,5-dimethyl-1,2-oxazol-4-yl)-1*H*-1,3-benzodiazol-1-yl}piperidin-1-yl)-14-oxo-3,6,9,12-tetraoxatetradecan-1-yl]oxy}-2-(2,6-dioxopiperidin-3-yl)-2,3-dihydro-1*H*-isoindole-1,3-dione (137)

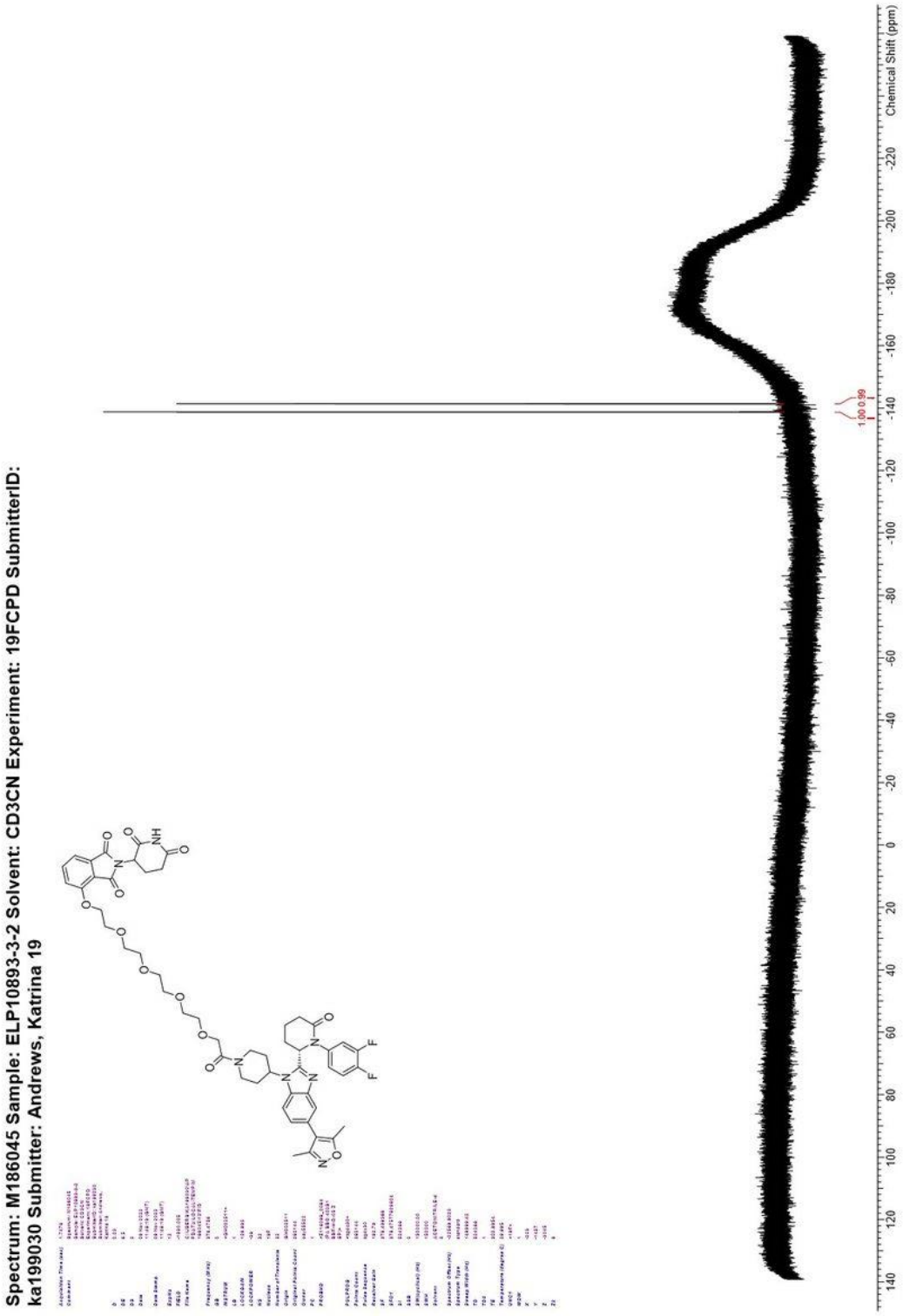

4-{[5-(4-{2-[(2*S*)-1-(3,4-Difluorophenyl)-6-oxopiperidin-2-yl]-5-(3,5-dimethyl-1,2-oxazol-4-yl)-1*H*-1,3-benzodiazol-1-yl}piperidin-1-yl)-5-oxopentyl]oxy}-2-(2,6-dioxopiperidin-3-yl)-2,3-dihydro-1*H*-isoindole-1,3-dione (138)

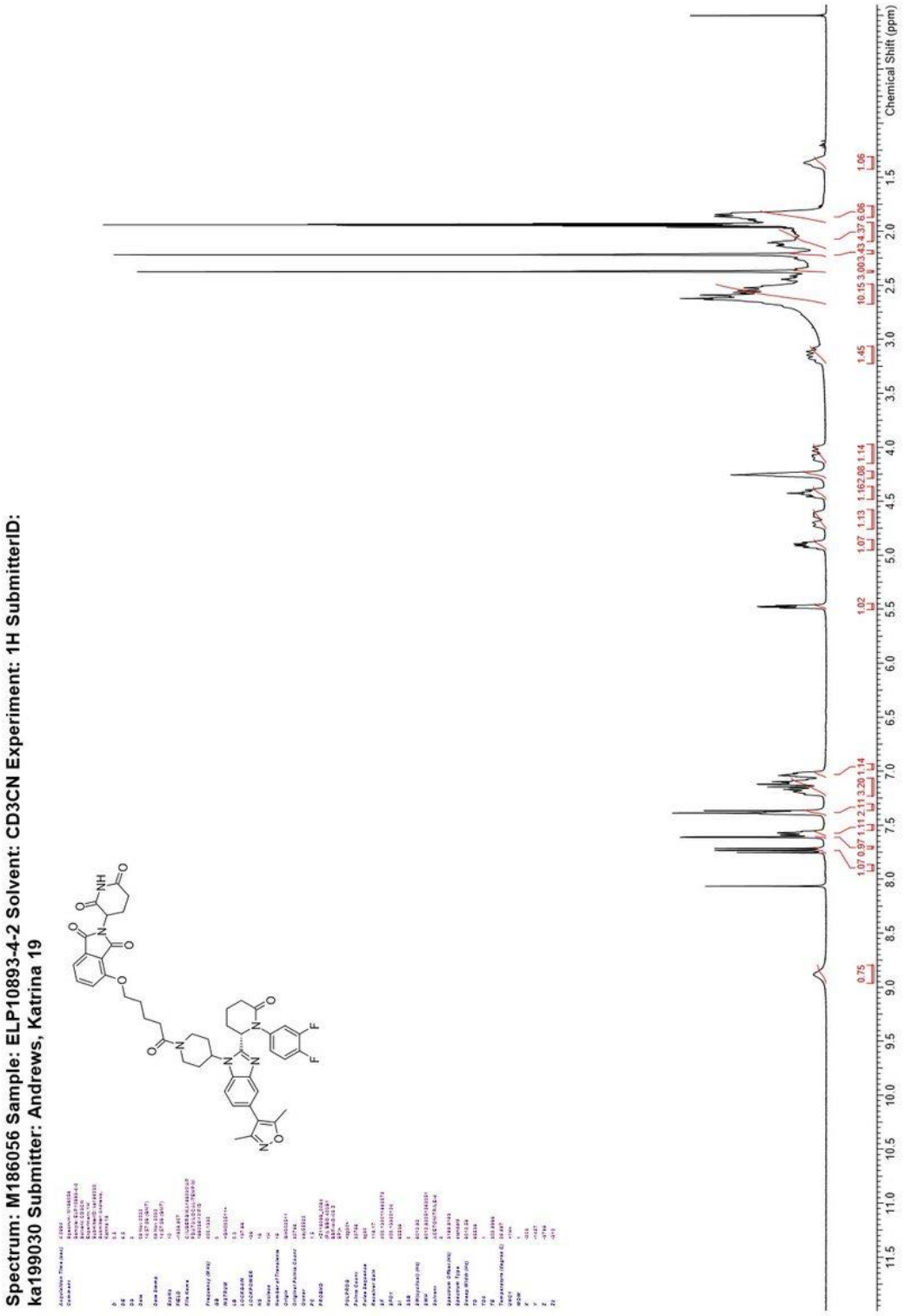

4-{[5-(4-{2-[(2*S*)-1-(3,4-Difluorophenyl)-6-oxopiperidin-2-yl]-5-(3,5-dimethyl-1,2-oxazol-4-yl)-1*H*-1,3-benzodiazol-1-yl}piperidin-1-yl)-5-oxopentyl]oxy}-2-(2,6-dioxopiperidin-3-yl)-2,3-dihydro-1*H*-isoindole-1,3-dione (138)

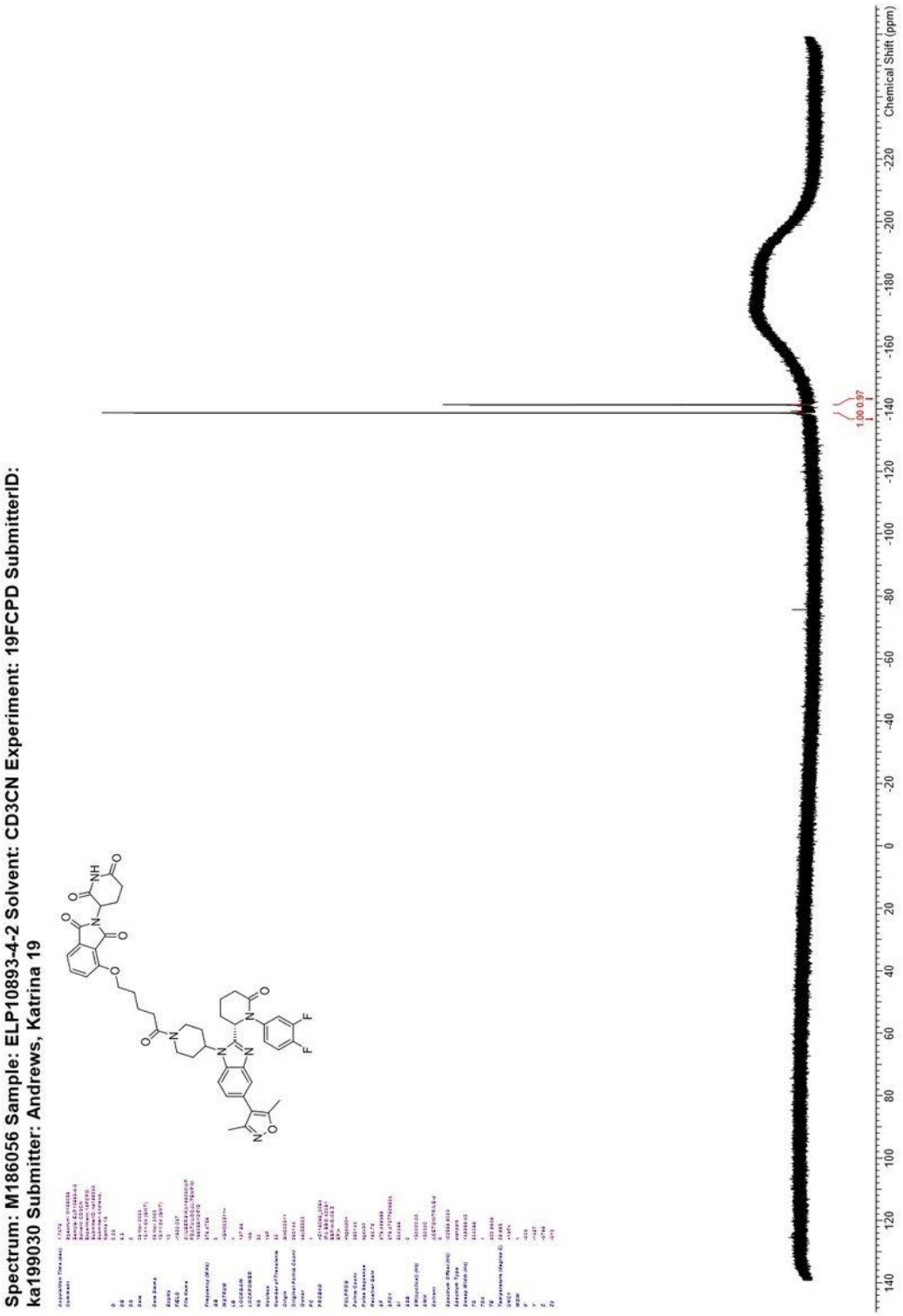

4-{[8-(4-{2-[(2*S*)-1-(3,4-Difluorophenyl)-6-oxopiperidin-2-yl]-5-(3,5-dimethyl-1,2-oxazol-4-yl)-1*H*-1,3-benzodiazol-1-yl}piperidin-1-yl)-8-oxooctyl]oxy}-2-(2,6-dioxopiperidin-3-yl)-2,3-dihydro-1*H*-isoindole-1,3-dione (139)

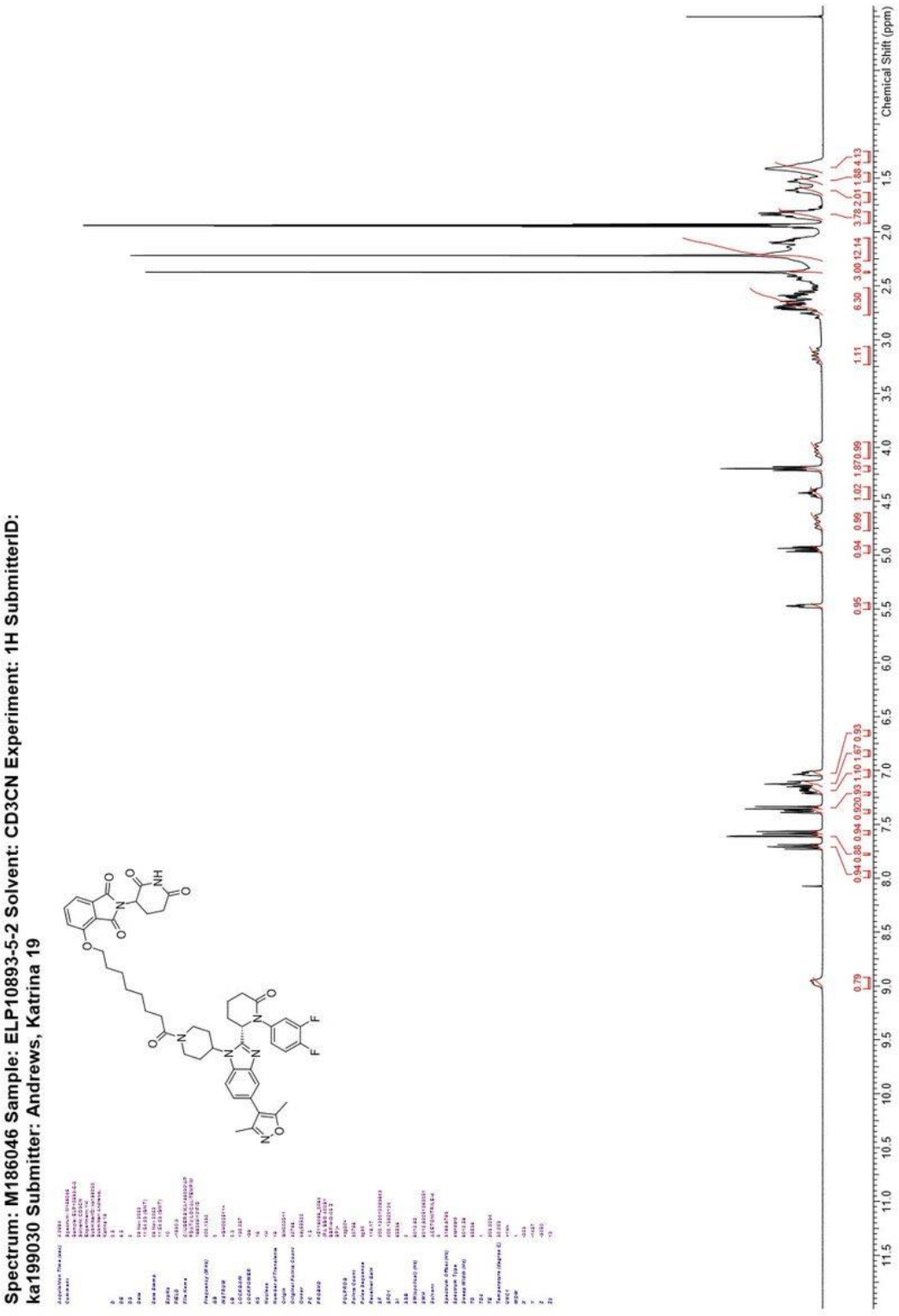

4-{[8-(4-{2-[(2*S*)-1-(3,4-Difluorophenyl)-6-oxopiperidin-2-yl]-5-(3,5-dimethyl-1,2-oxazol-4-yl)-1*H*-1,3-benzodiazol-1-yl}piperidin-1-yl)-8-oxooctyl]oxy}-2-(2,6-dioxopiperidin-3-yl)-2,3-dihydro-1*H*-isoindole-1,3-dione (139)

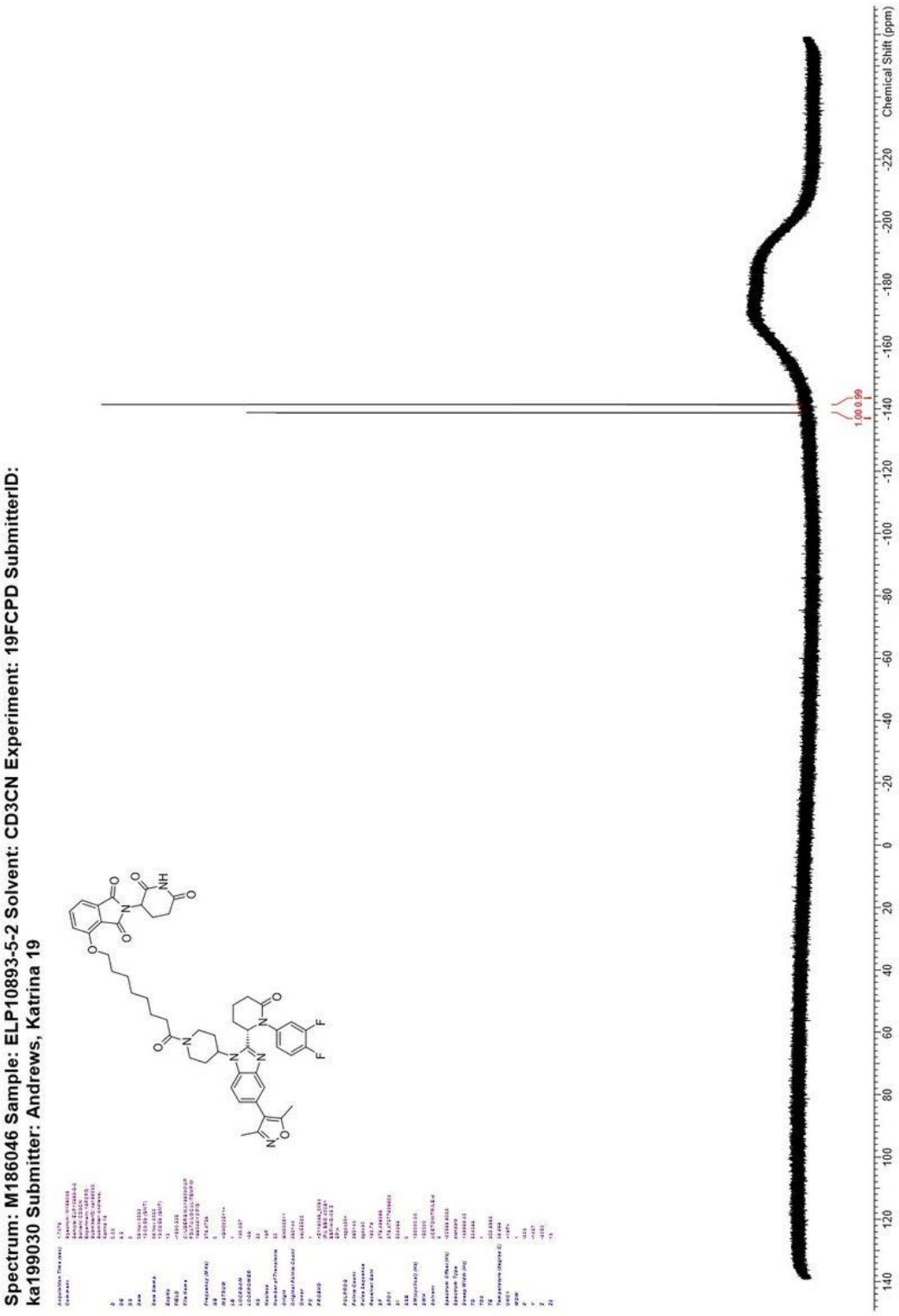

4-{[10-(4-{2-[(2*S*)-1-(3,4-Difluorophenyl)-6-oxopiperidin-2-yl]-5-(3,5-dimethyl-1,2-oxazol-4-yl)-1*H*-1,3-benzodiazol-1-yl}piperidin-1-yl)-10-oxodecyl]oxy}-2-(2,6-dioxopiperidin-3-yl)-2,3-dihydro-1*H*-isoindole-1,3-dione (140)

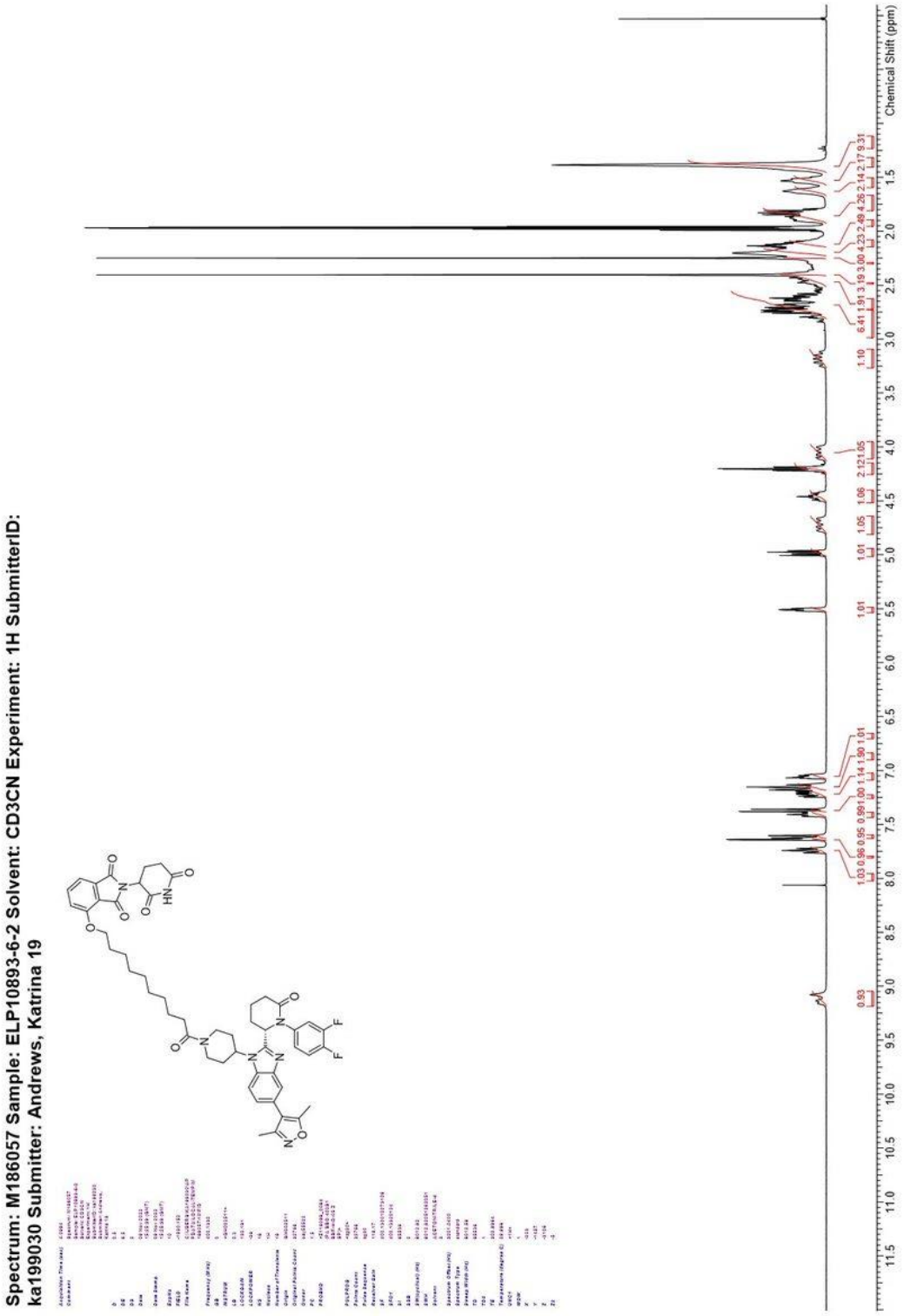

4-{[10-(4-{2-[(2*S*)-1-(3,4-Difluorophenyl)-6-oxopiperidin-2-yl]-5-(3,5-dimethyl-1,2-oxazol-4-yl)-1*H*-1,3-benzodiazol-1-yl}piperidin-1-yl)-10-oxodecyl]oxy}-2-(2,6-dioxopiperidin-3-yl)-2,3-dihydro-1*H*-isoindole-1,3-dione (140)

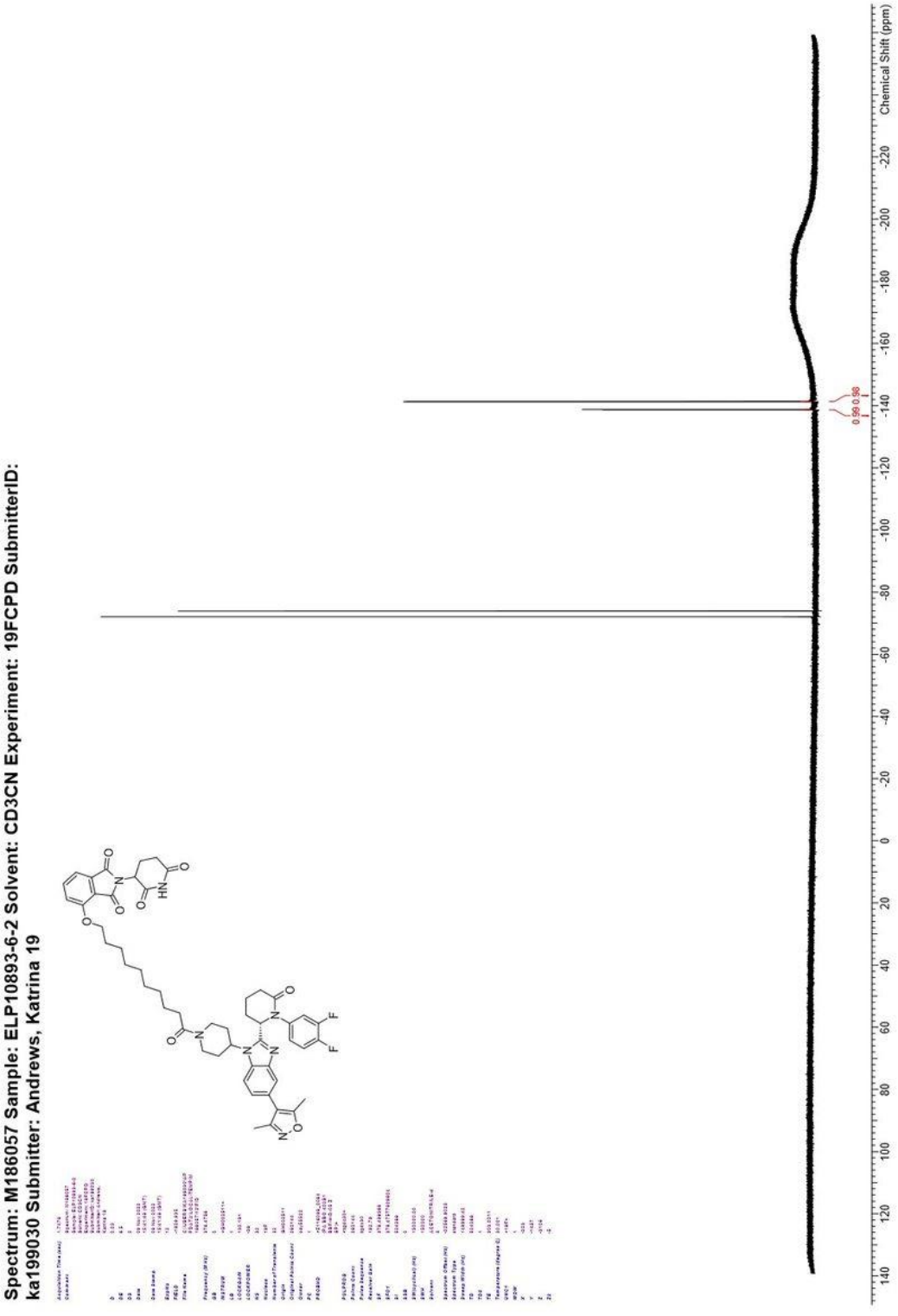

5-{4-[2-(4-{2-[(2S)-1-(3,4-Difluorophenyl)-6-oxopiperidin-2-yl]-5-(3,5-dimethyl-1,2-oxazol-4-yl)-1H-1,3-benzodiazol-1-yl}piperidin-1-yl)-2-oxoethyl]piperazin-1-yl}-2-(2,6-dioxopiperidin-3-yl)-6-fluoro-2,3-dihydro-1H-isoindole-1,3-dione (141)

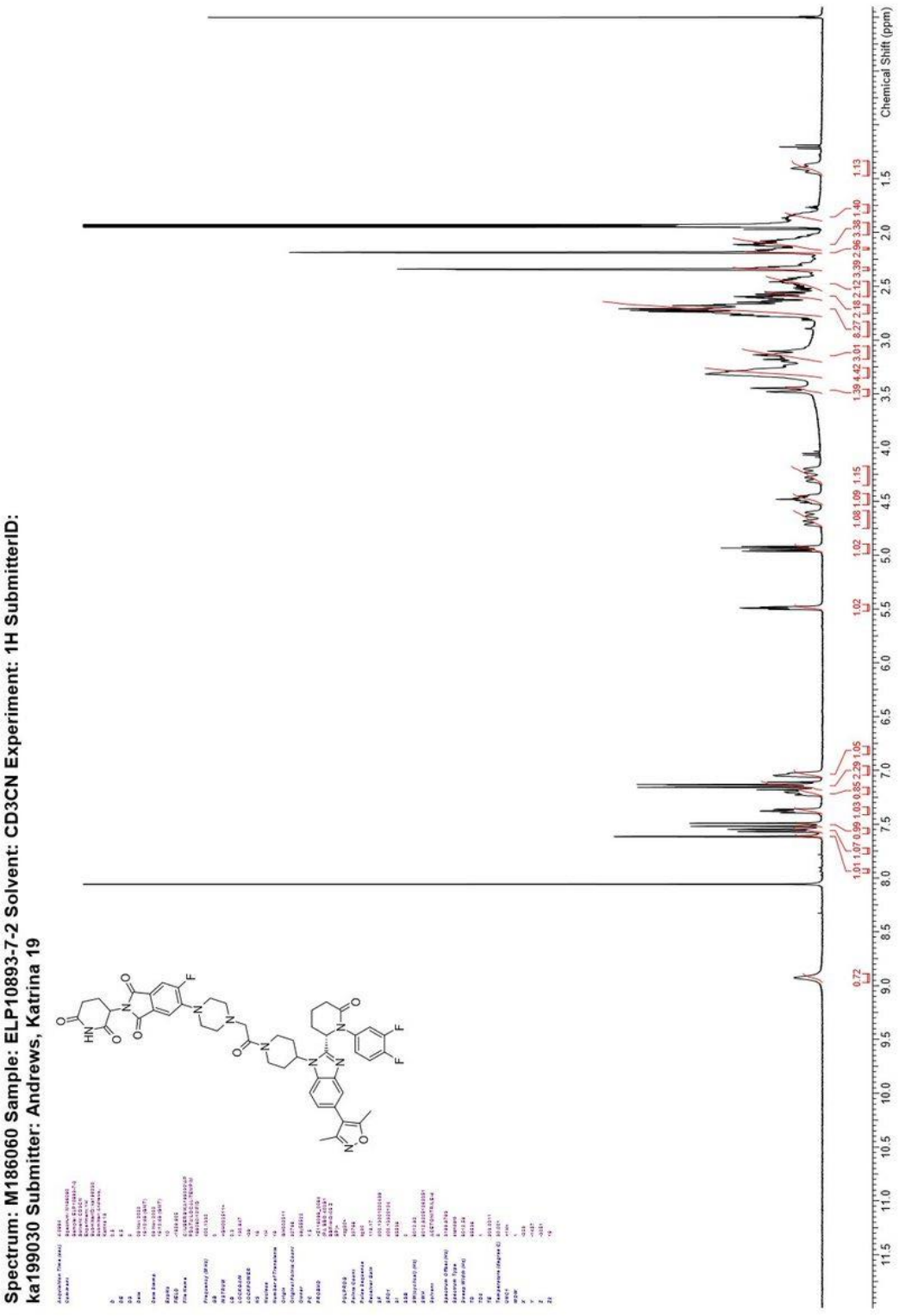

5-{4-[2-(4-{2-[(2S)-1-(3,4-Difluorophenyl)-6-oxopiperidin-2-yl]-5-(3,5-dimethyl-1,2-oxazol-4-yl)-1H-1,3-benzodiazol-1-yl}piperidin-1-yl)-2-oxoethyl]piperazin-1-yl}-2-(2,6-dioxopiperidin-3-yl)-6-fluoro-2,3-dihydro-1H-isoindole-1,3-dione (141)

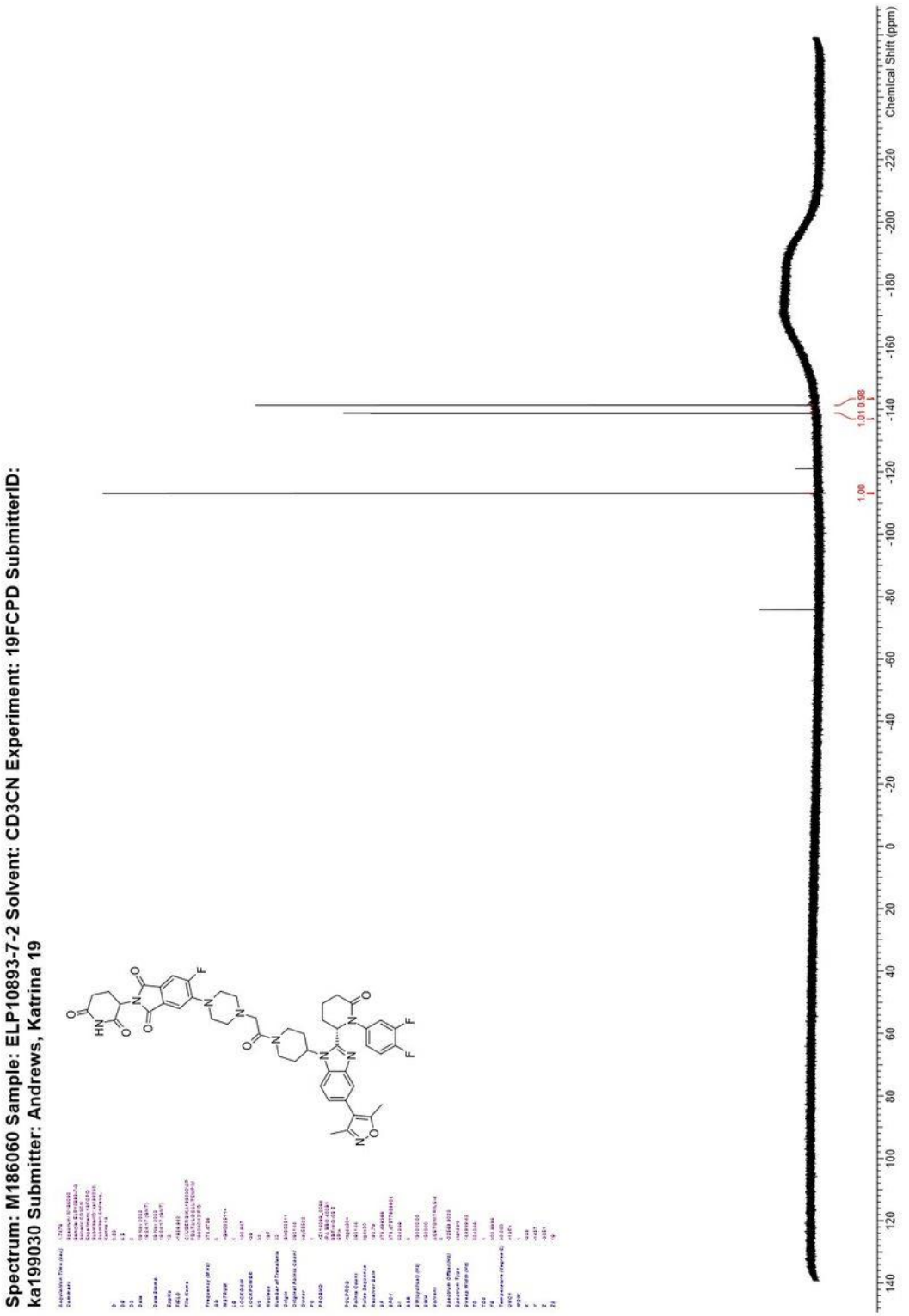

3-(5-{4-[4-(4-{2-[(2*S*)-1-(3,4-Difluorophenyl)-6-oxopiperidin-2-yl]-5-(3,5-dimethyl-1,2-oxazol-4-yl)-1*H*-1,3-benzodiazol-1-yl}piperidin-1-yl)-4-oxobutyl]piperazin-1-yl}-1-oxo-2,3-dihydro-1*H*-isoindol-2-yl)piperidine-2,6-dione (142)

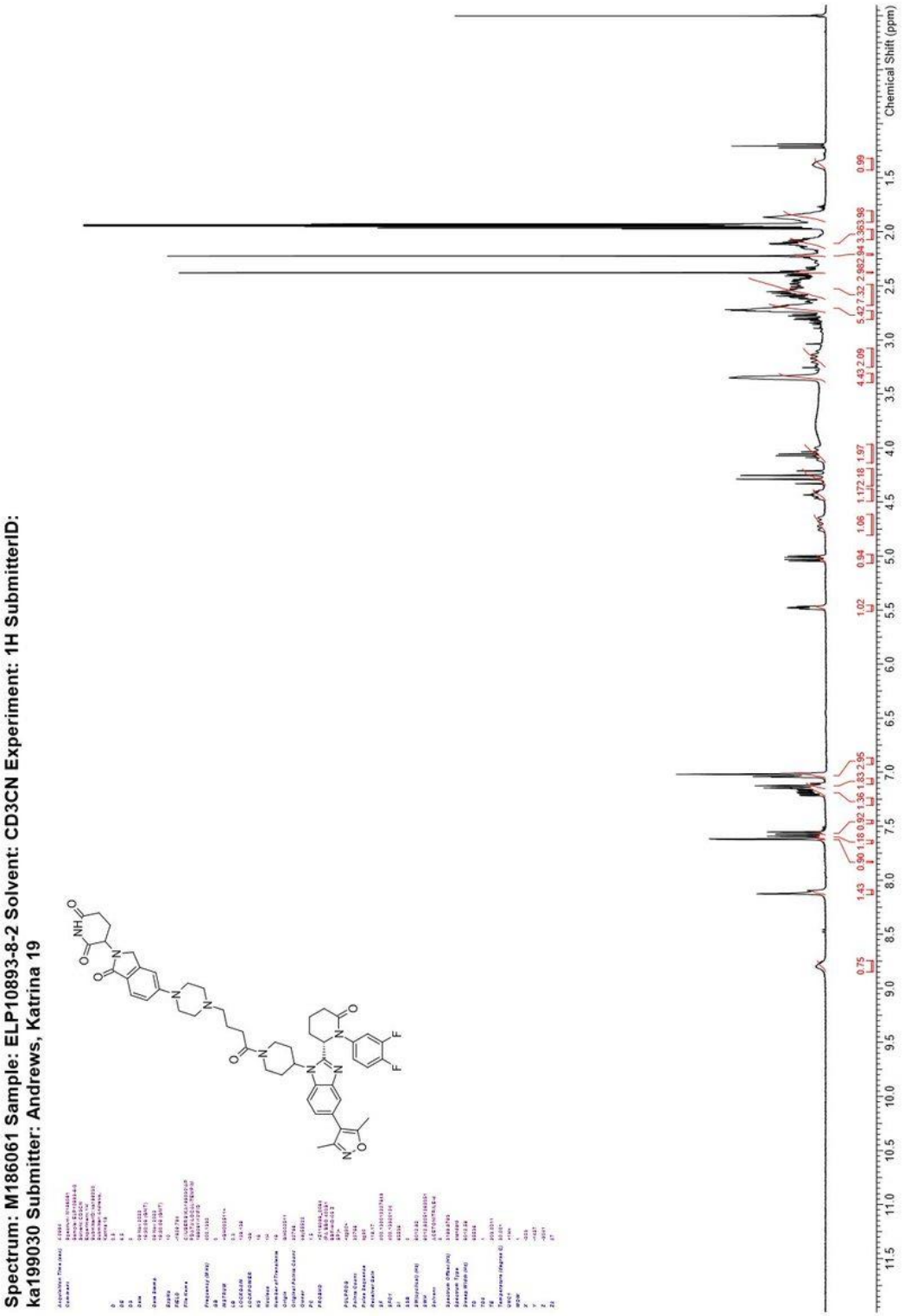

3-(5-{4-[4-(4-{2-[(2*S*)-1-(3,4-Difluorophenyl)-6-oxopiperidin-2-yl]-5-(3,5-dimethyl-1,2-oxazol-4-yl)-1*H*-1,3-benzodiazol-1-yl}piperidin-1-yl)-4-oxobutyl]piperazin-1-yl}-1-oxo-2,3-dihydro-1*H*-isoindol-2-yl)piperidine-2,6-dione (142)

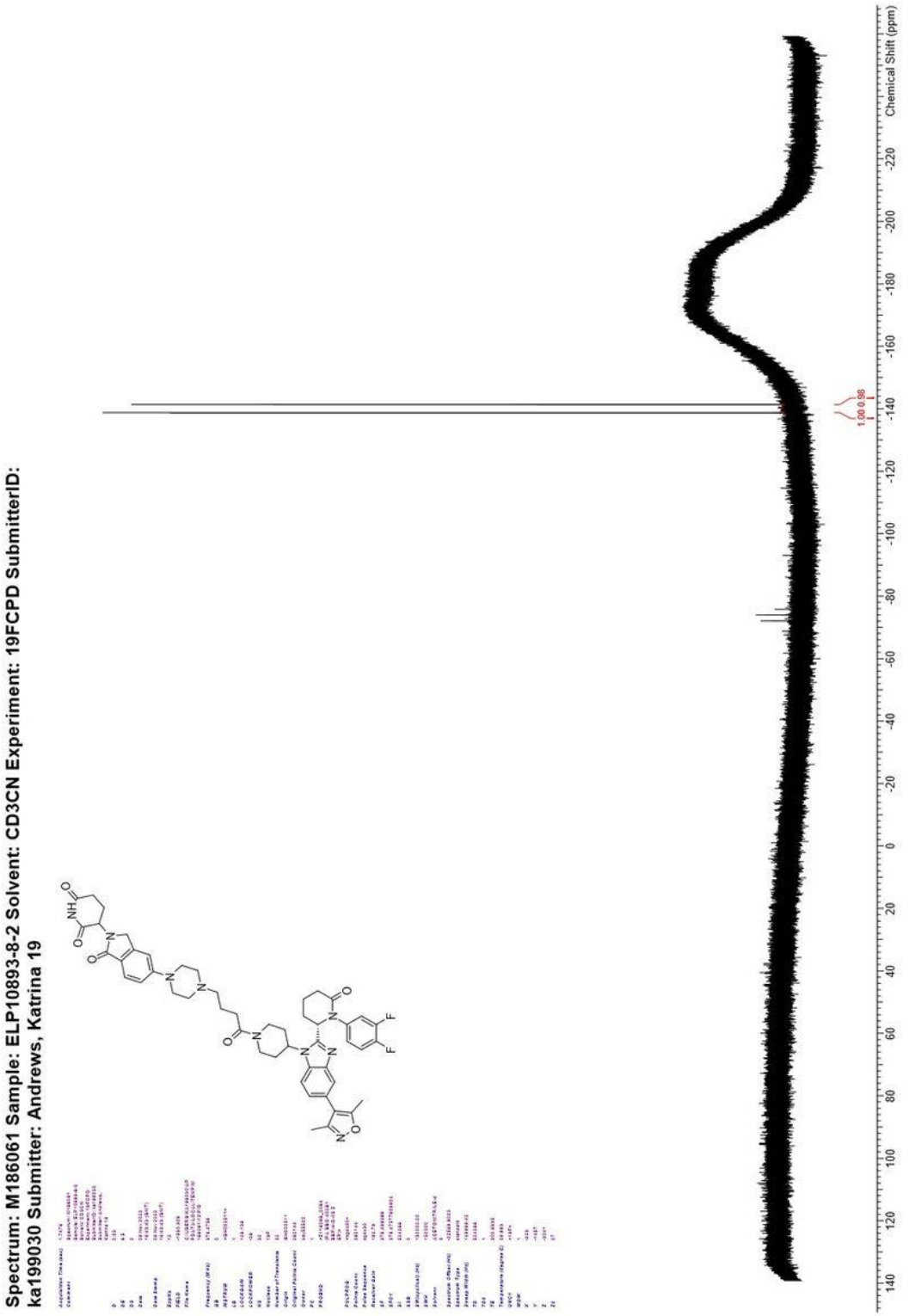

5-{9-[2-(4-{2-[(2*S*)-1-(3,4-Difluorophenyl)-6-oxopiperidin-2-yl]-5-(3,5-dimethyl-1,2-oxazol-4-yl)-1*H*-1,3-benzodiazol-1-yl}piperidin-1-yl)-2-oxoethyl]-3,9-diazaspiro[5.5]undecan-3-yl}-2-(2,6-dioxopiperidin-3-yl)-6-fluoro-2,3-dihydro-1*H*-isoindole-1,3-dione (143)

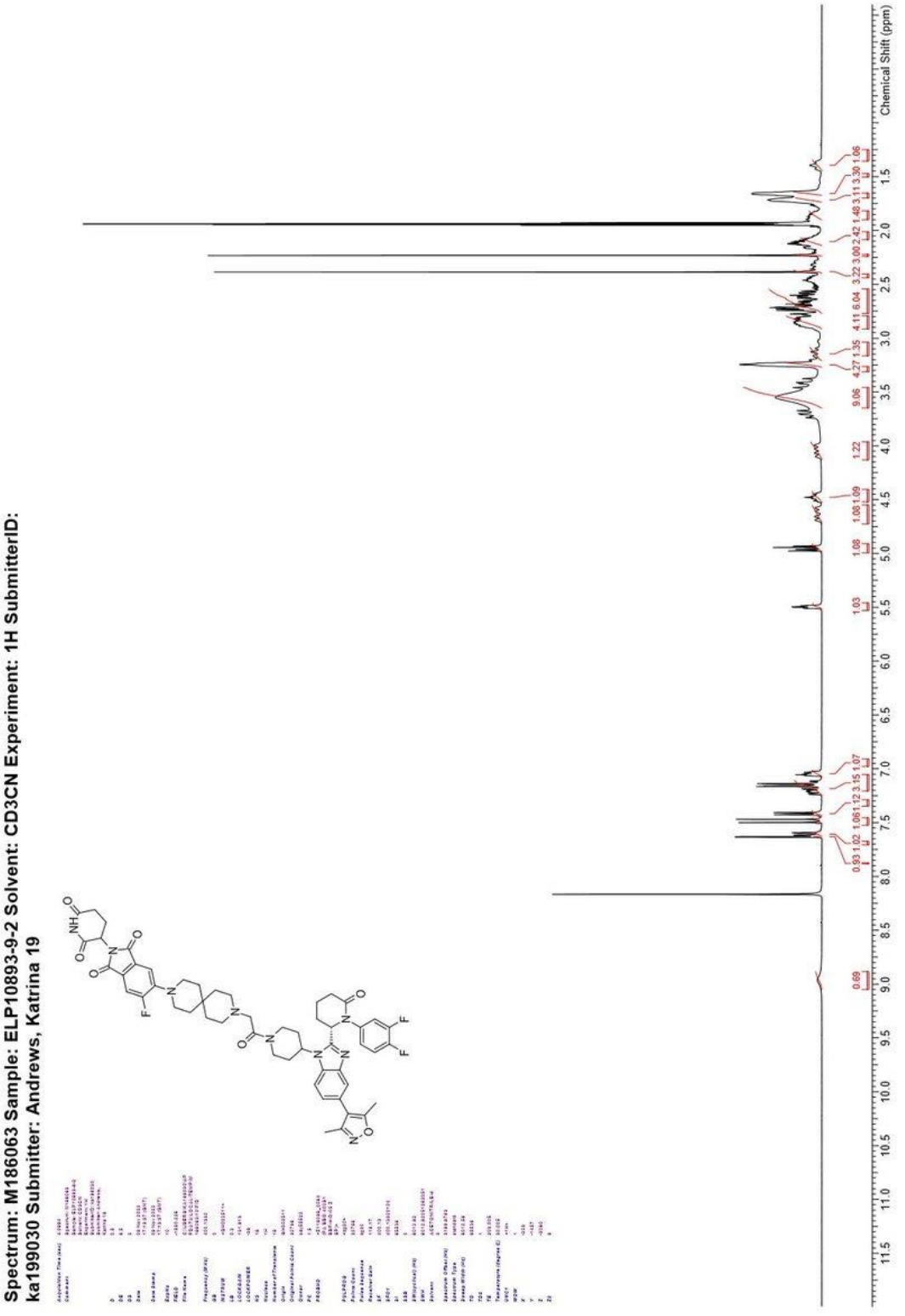

5-{9-[2-(4-{2-[(2*S*)-1-(3,4-Difluorophenyl)-6-oxopiperidin-2-yl]-5-(3,5-dimethyl-1,2-oxazol-4-yl)-1*H*-1,3-benzodiazol-1-yl}piperidin-1-yl)-2-oxoethyl]-3,9-diazaspiro[5.5]undecan-3-yl}-2-(2,6-dioxopiperidin-3-yl)-6-fluoro-2,3-dihydro-1*H*-isoindole-1,3-dione (143)

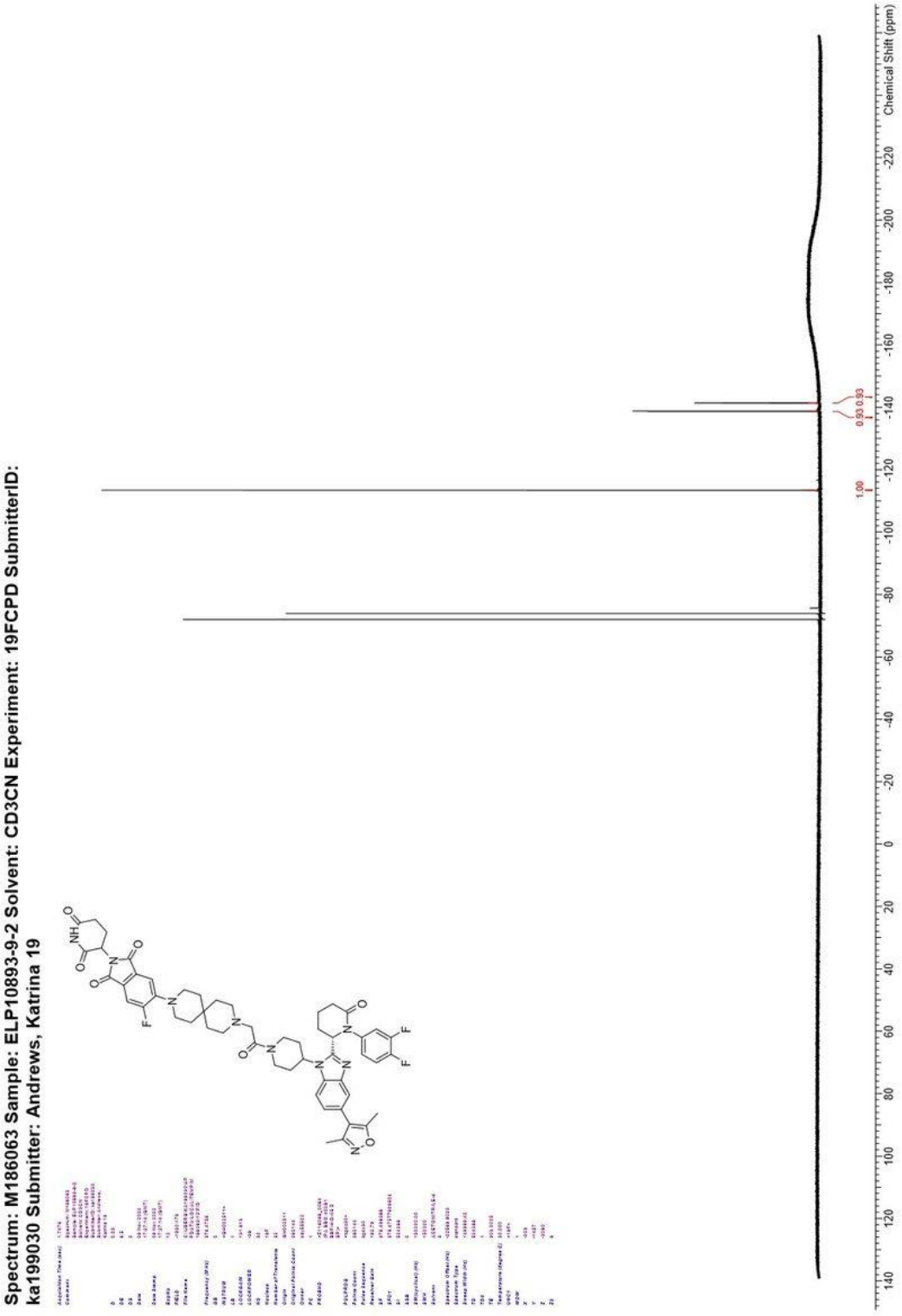

3-[5-(4-{[4-(4-{2-[(2*S*)-1-(3,4-Difluorophenyl)-6-oxopiperidin-2-yl]-5-(3,5-dimethyl-1,2-oxazol-4-yl)-1*H*-1,3-benzodiazol-1-yl}piperidine-1-carbonyl)phenyl]methyl}piperazin-1-yl)-1-oxo-2,3-dihydro-1*H*-isoindol-2-yl]piperidine-2,6-dione (144)

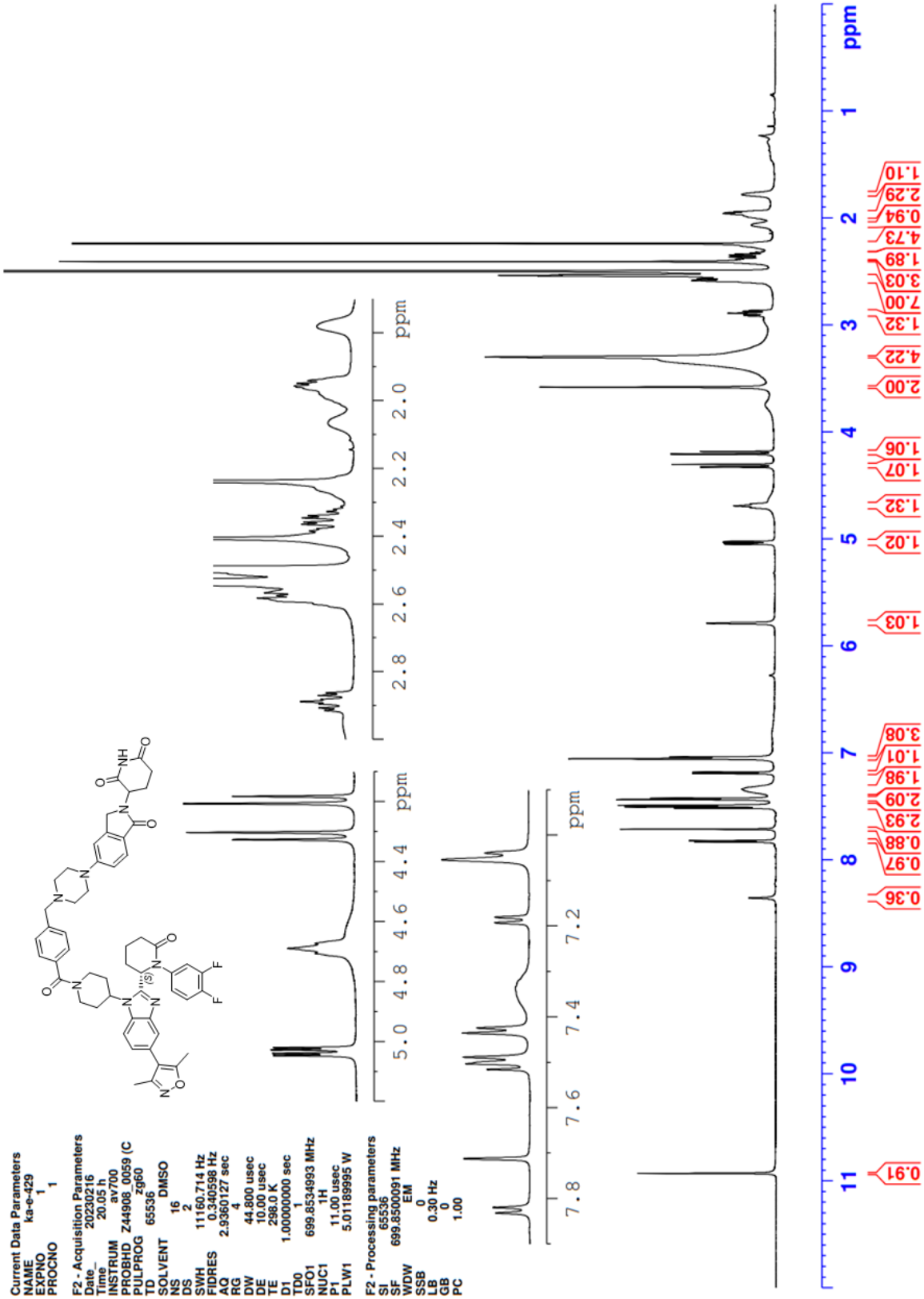

3-[5-(4-{[4-(4-{2-[(2*S*)-1-(3,4-Difluorophenyl)-6-oxopiperidin-2-yl]-5-(3,5-dimethyl-1,2-oxazol-4-yl)-1*H*-1,3-benzodiazol-1-yl}piperidine-1-carbonyl)phenyl]methyl}piperazin-1-yl)-1-oxo-2,3-dihydro-1*H*-isoindol-2-yl]piperidine-2,6-dione (144)

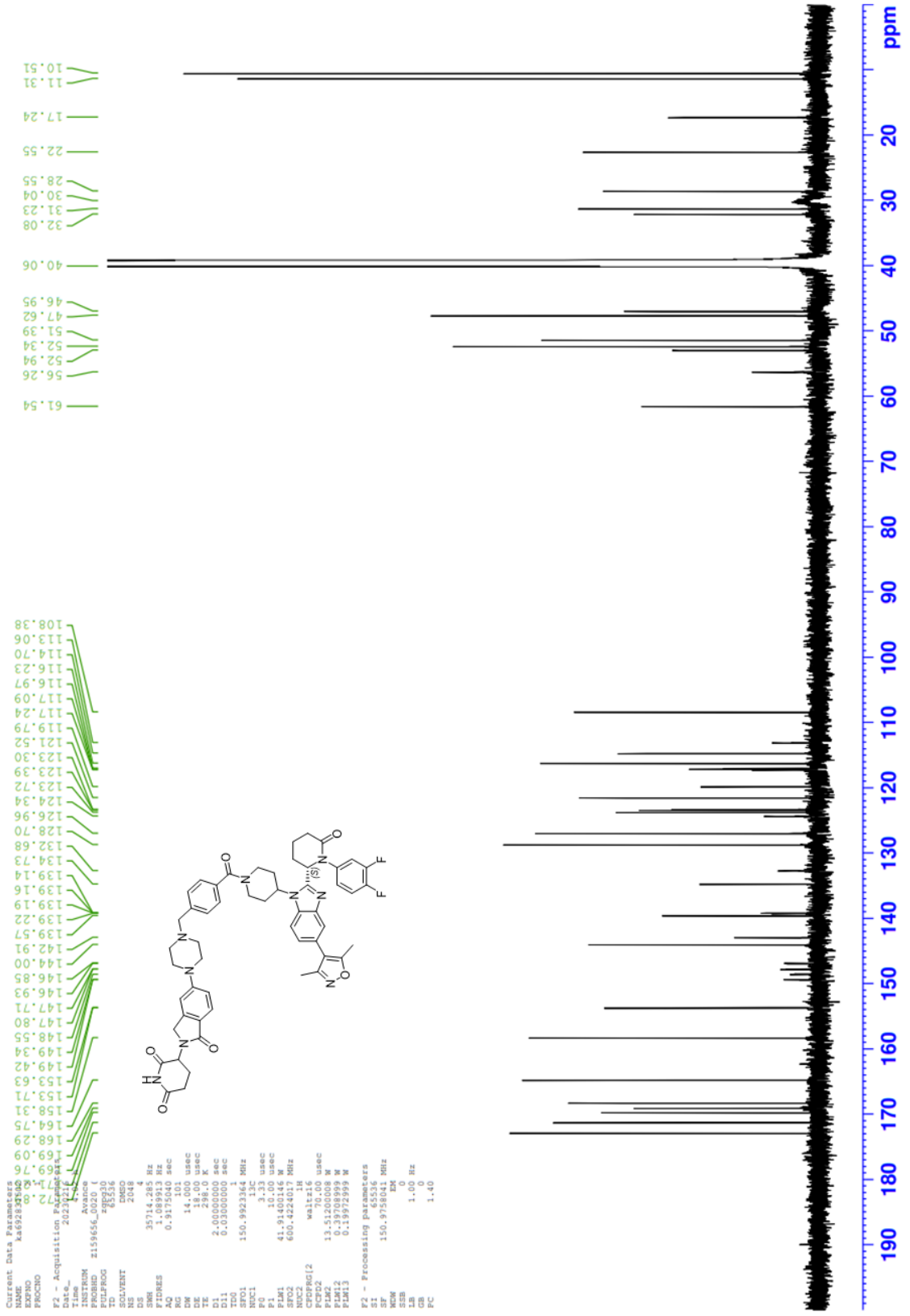

3-[5-(4-{[4-(4-{2-[(2*S*)-1-(3,4-Difluorophenyl)-6-oxopiperidin-2-yl]-5-(3,5-dimethyl-1,2-oxazol-4-yl)-1*H*-1,3-benzodiazol-1-yl}piperidine-1-carbonyl)phenyl]methyl}piperazin-1-yl)-1-oxo-2,3-dihydro-1*H*-isoindol-2-yl]piperidine-2,6-dione (144)

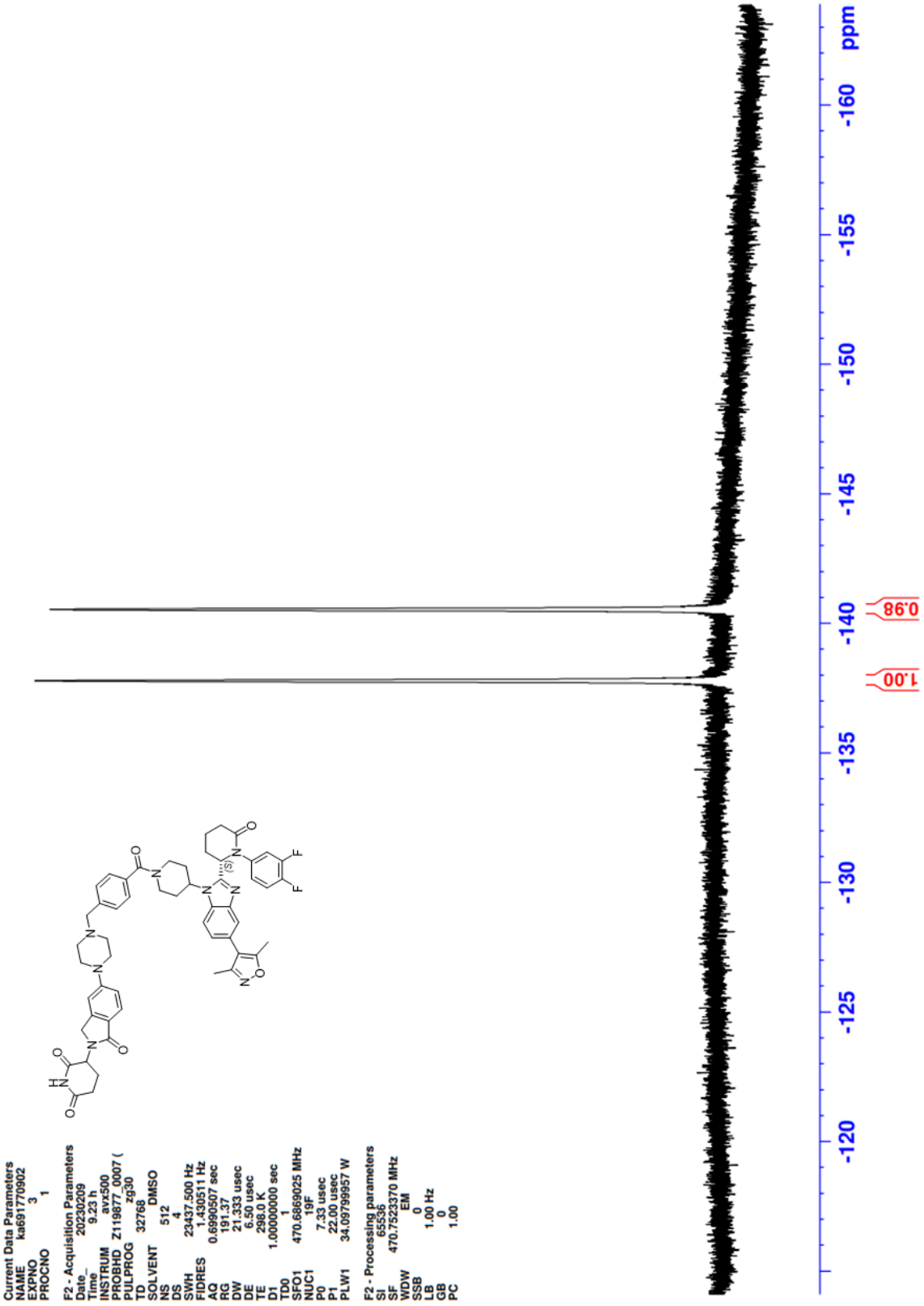

5-(4-{1-[2-(4-{2-[(2*S*)-1-(3,4-Difluorophenyl)-6-oxopiperidin-2-yl]-5-(3,5-dimethyl-1,2-oxazol-4-yl)-1*H*-1,3-benzodiazol-1-yl}piperidin-1-yl)-2-oxoethyl]piperidin-4-yl}piperazin-1-yl)-2-(2,6-dioxopiperidin-3-yl)-6-fluoro-2,3-dihydro-1*H*-isoindole-1,3-dione (145)

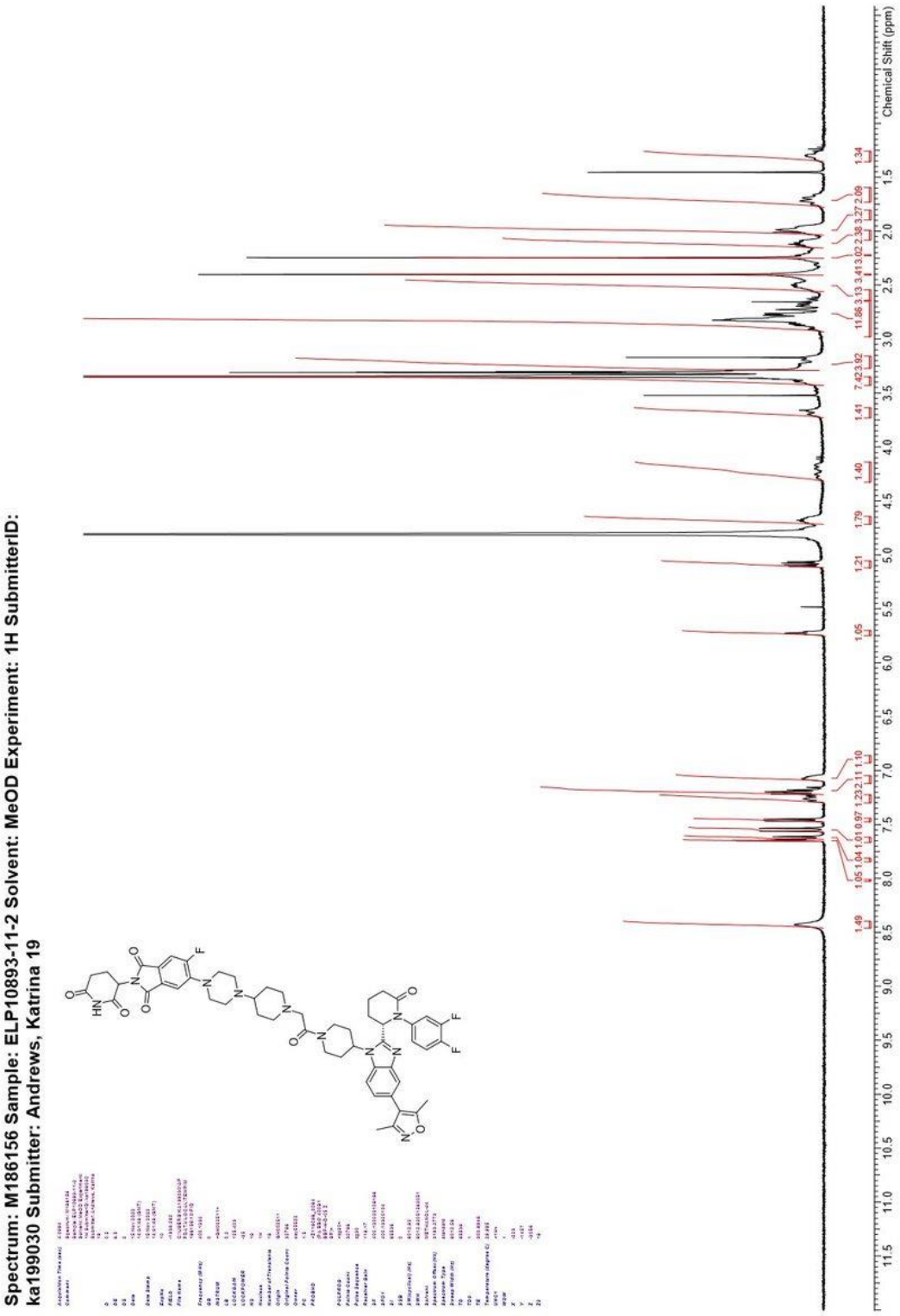

5-(4-{1-[2-(4-{2-[(2*S*)-1-(3,4-Difluorophenyl)-6-oxopiperidin-2-yl]-5-(3,5-dimethyl-1,2-oxazol-4-yl)-1*H*-1,3-benzodiazol-1-yl}piperidin-1-yl)-2-oxoethyl]piperidin-4-yl}piperazin-1-yl)-2-(2,6-dioxopiperidin-3-yl)-6-fluoro-2,3-dihydro-1*H*-isoindole-1,3-dione (145)

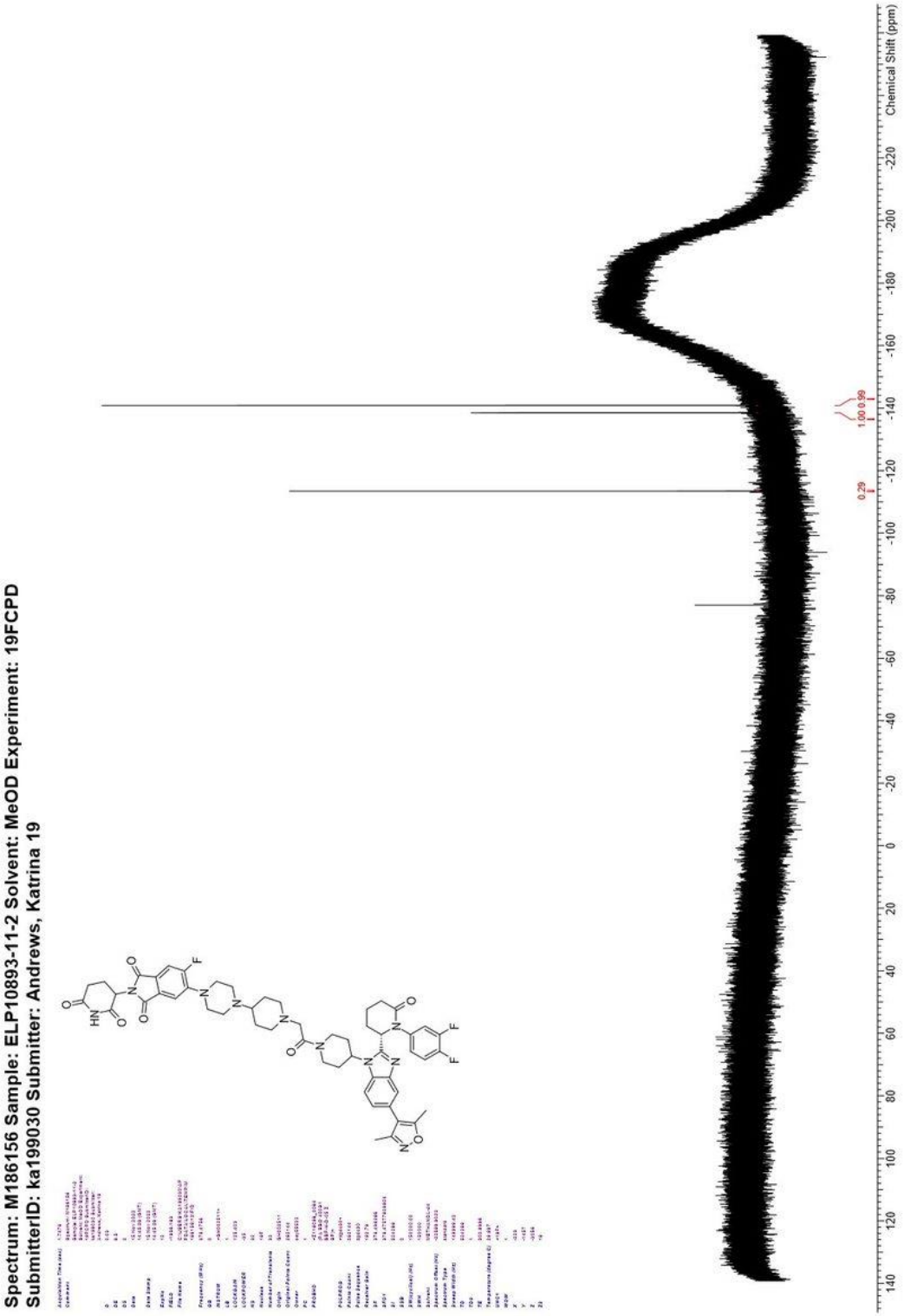

(2*S*,4*R*)-*N*-(2-(2-(2-(2-(4-(2-((*S*)-1-(3,4-Difluorophenyl)-6-oxopiperidin-2-yl)-5-(3,5-dimethylisoxazol-4-yl)-1*H*-benzo[d]imidazol-1-yl)piperidin-1-yl)-2-oxoethoxy)ethoxy)ethoxy)-4-(4-methylthiazol-5-yl)benzyl)-1-((*S*)-2-(1-fluorocyclopropane-1-carboxamido)-3,3-dimethylbutanoyl)-4-hydroxypyrrolidine-2-carboxamide (146)

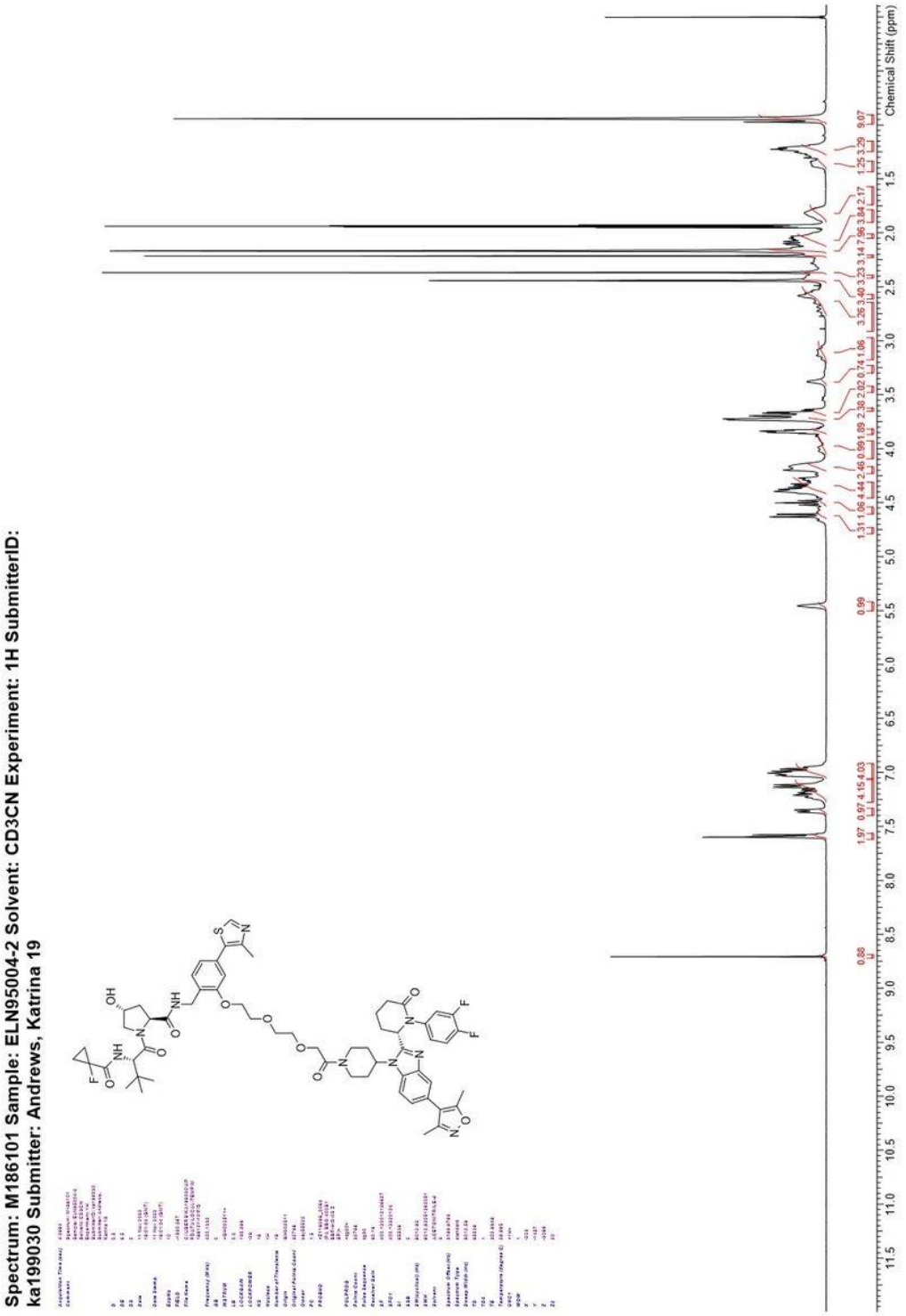

(2*S*,4*R*)-*N*-(2-(2-(2-(2-(4-(2-((*S*)-1-(3,4-Difluorophenyl)-6-oxopiperidin-2-yl)-5-(3,5-dimethylisoxazol-4-yl)-1*H*-benzo[d]imidazol-1-yl)piperidin-1-yl)-2-oxoethoxy)ethoxy)ethoxy)-4-(4-methylthiazol-5-yl)benzyl)-1-((*S*)-2-(1-fluorocyclopropane-1-carboxamido)-3,3-dimethylbutanoyl)-4-hydroxypyrrolidine-2-carboxamide (146)

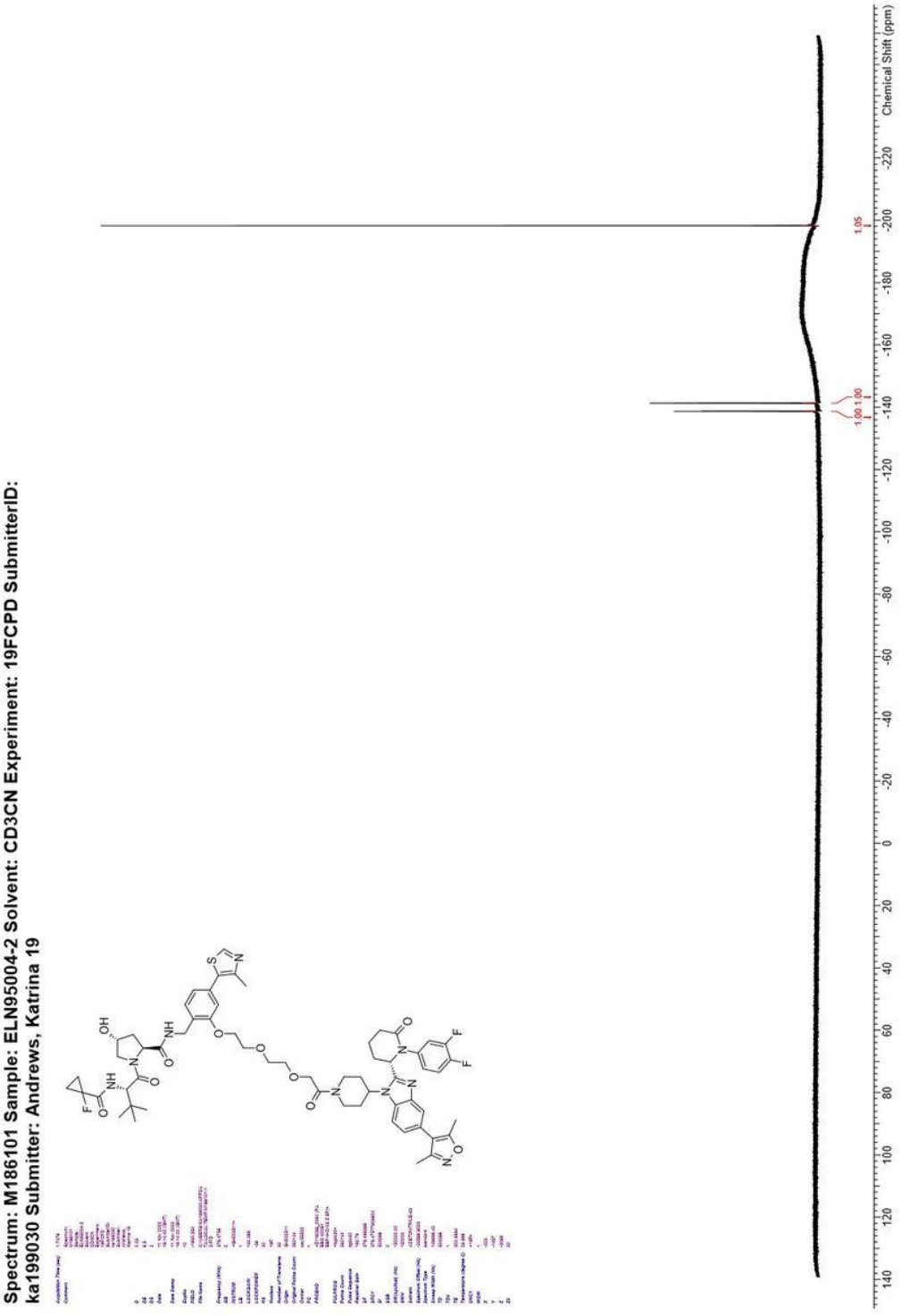

4-(2-{2-[4-(2-{2-[(2*S*)-1-(3,4-Difluorophenyl)-6-oxopiperidin-2-yl]-5-(3,5-dimethyl-1,2-oxazol-4-yl)-1*H*-1,3-benzodiazol-1-yl}ethyl)piperazin-1-yl]-2-oxoethoxy}ethoxy)-2-(2,6-dioxopiperidin-3-yl)-2,3-dihydro-1*H*-isoindole-1,3-dione (147)

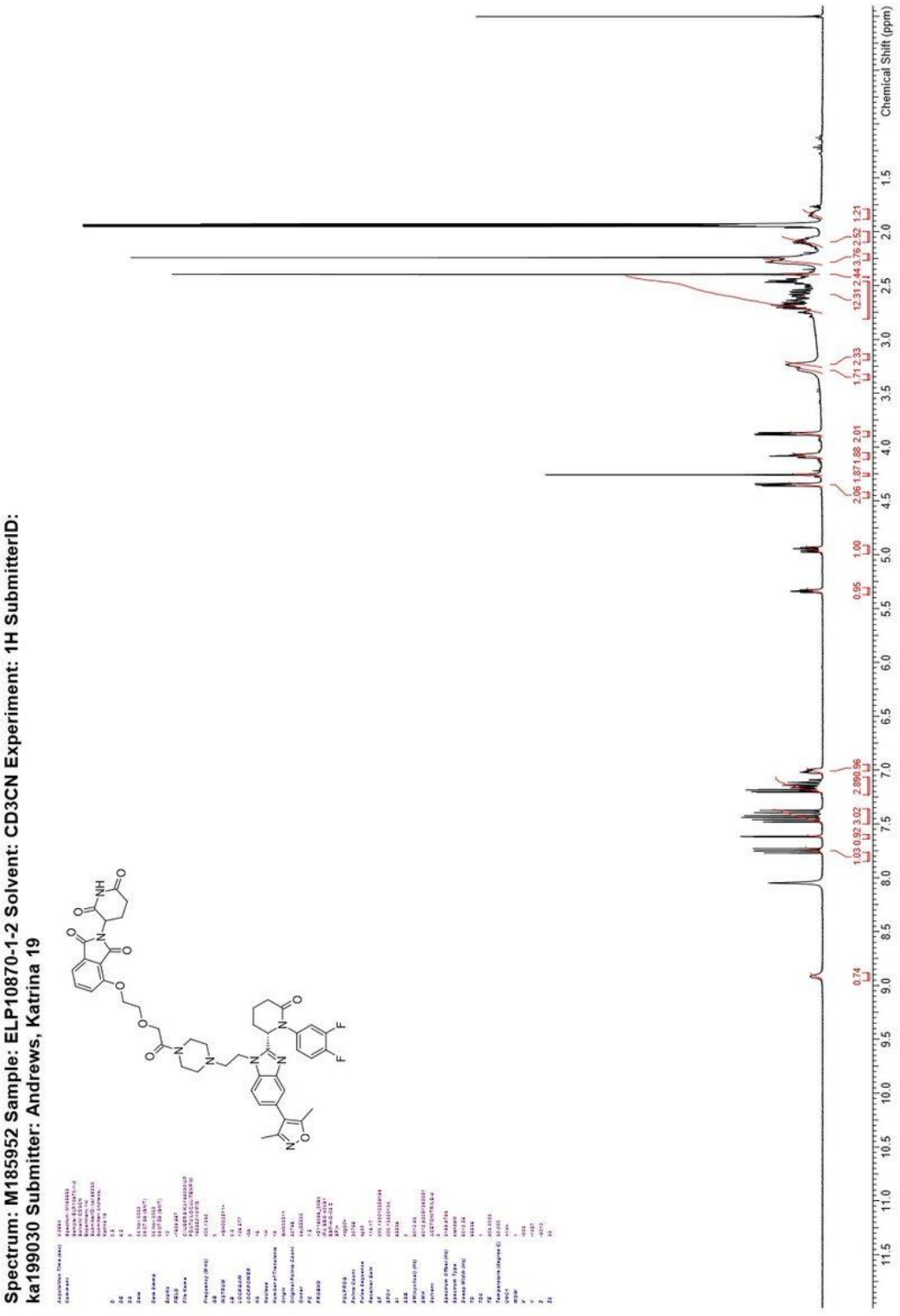

4-(2-{2-[4-(2-{2-[(2*S*)-1-(3,4-Difluorophenyl)-6-oxopiperidin-2-yl]-5-(3,5-dimethyl-1,2-oxazol-4-yl)-1*H*-1,3-benzodiazol-1-yl}ethyl)piperazin-1-yl]-2-oxoethoxy}ethoxy)-2-(2,6-dioxopiperidin-3-yl)-2,3-dihydro-1*H*-isoindole-1,3-dione (147)

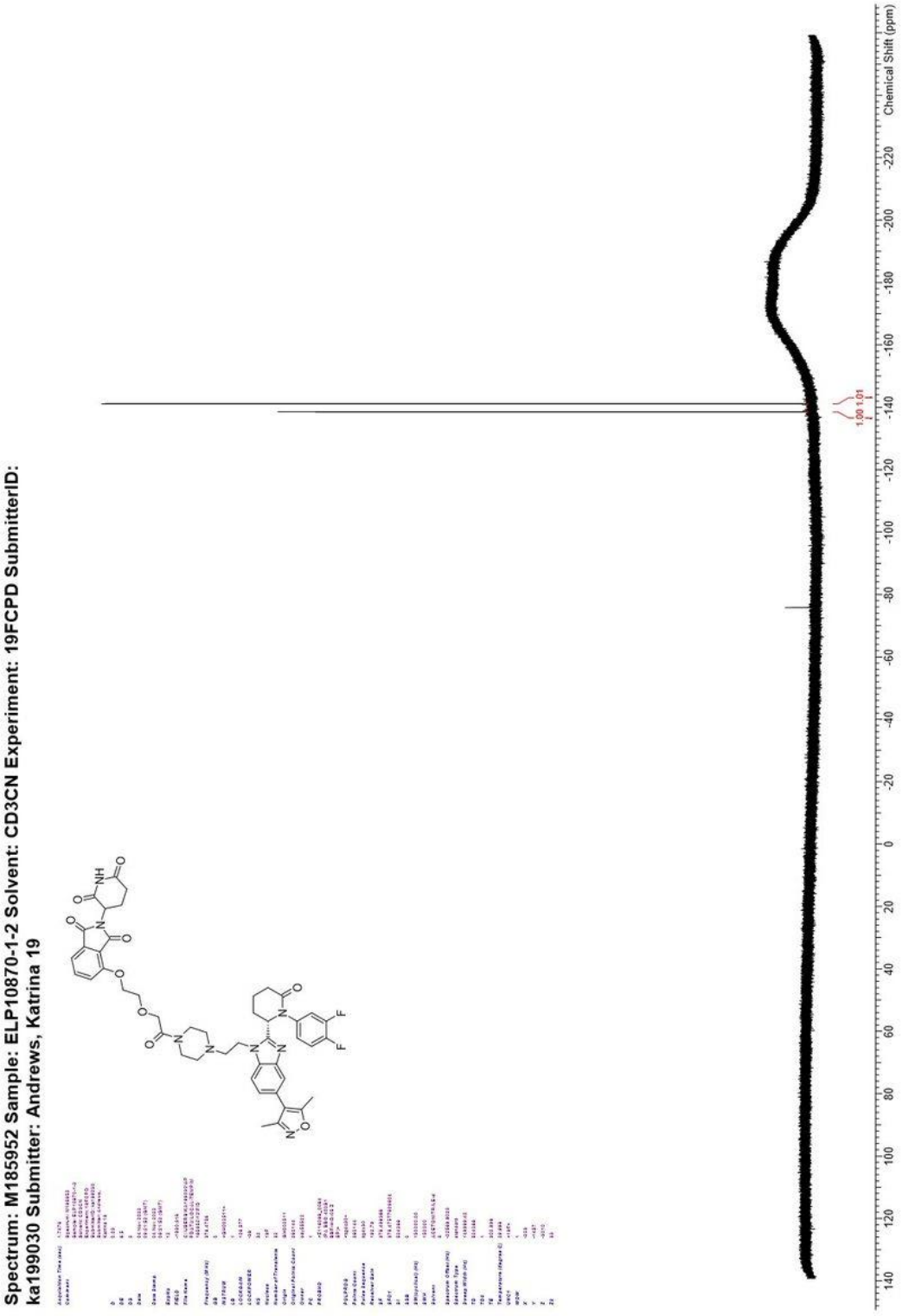

4-[2-(2-{2-[4-(2-{2-[(2*S*)-1-(3,4-Difluorophenyl)-6-oxopiperidin-2-yl]-5-(3,5-dimethyl-1,2-oxazol-4-yl)-1*H*-1,3-benzodiazol-1-yl}ethyl)piperazin-1-yl]-2-oxoethoxy}ethoxy)ethoxy]-2-(2,6-dioxopiperidin-3-yl)-2,3-dihydro-1*H*-isoindole-1,3-dione (148)

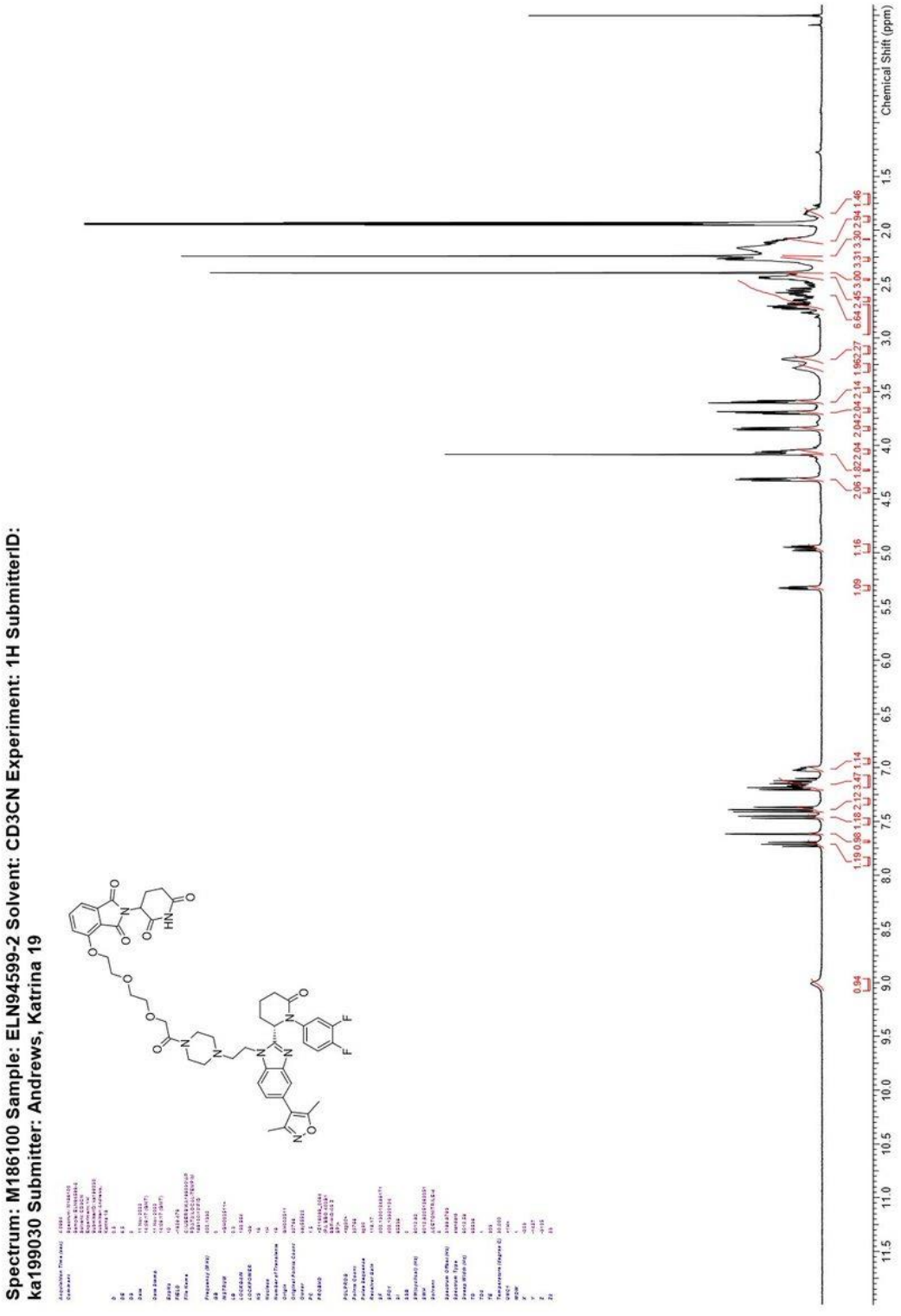

4-[2-(2-{2-[4-(2-{2-[(2*S*)-1-(3,4-Difluorophenyl)-6-oxopiperidin-2-yl]-5-(3,5-dimethyl-1,2-oxazol-4-yl)-1*H*-1,3-benzodiazol-1-yl}ethyl)piperazin-1-yl]-2-oxoethoxy}ethoxy)ethoxy]-2-(2,6-dioxopiperidin-3-yl)-2,3-dihydro-1*H*-isoindole-1,3-dione (148)

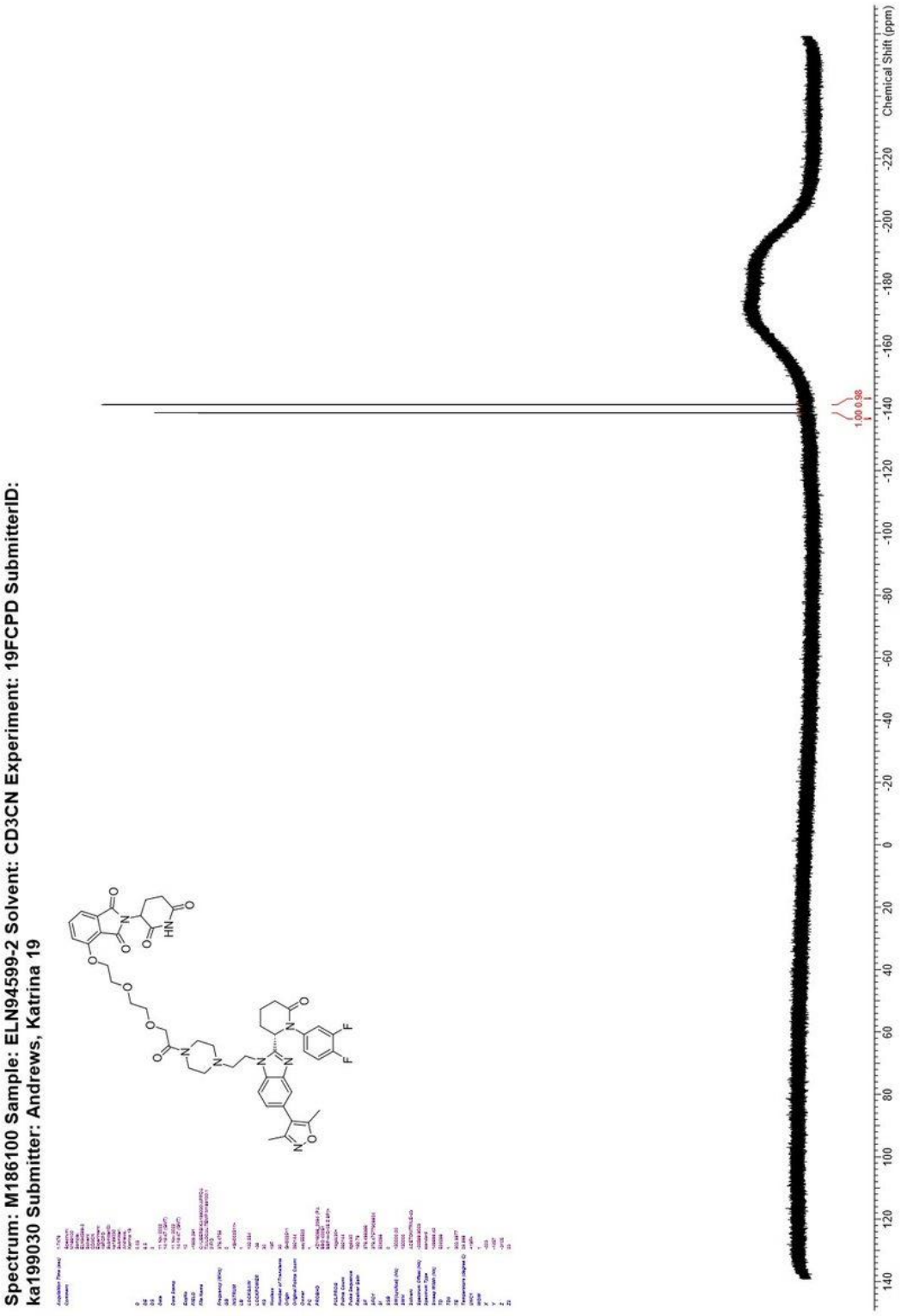

4-{2-[2-(2-{2-[4-(2-{2-[(2*S*)-1-(3,4-Difluorophenyl)-6-oxopiperidin-2-yl]-5-(3,5-dimethyl-1,2-oxazol-4-yl)-1*H*-1,3-benzodiazol-1-yl}ethyl)piperazin-1-yl]-2-oxoethoxy}ethoxy)ethoxy]ethoxy}-2-(2,6-dioxopiperidin-3-yl)-2,3-dihydro-1*H*-isoindole-1,3-dione (149)

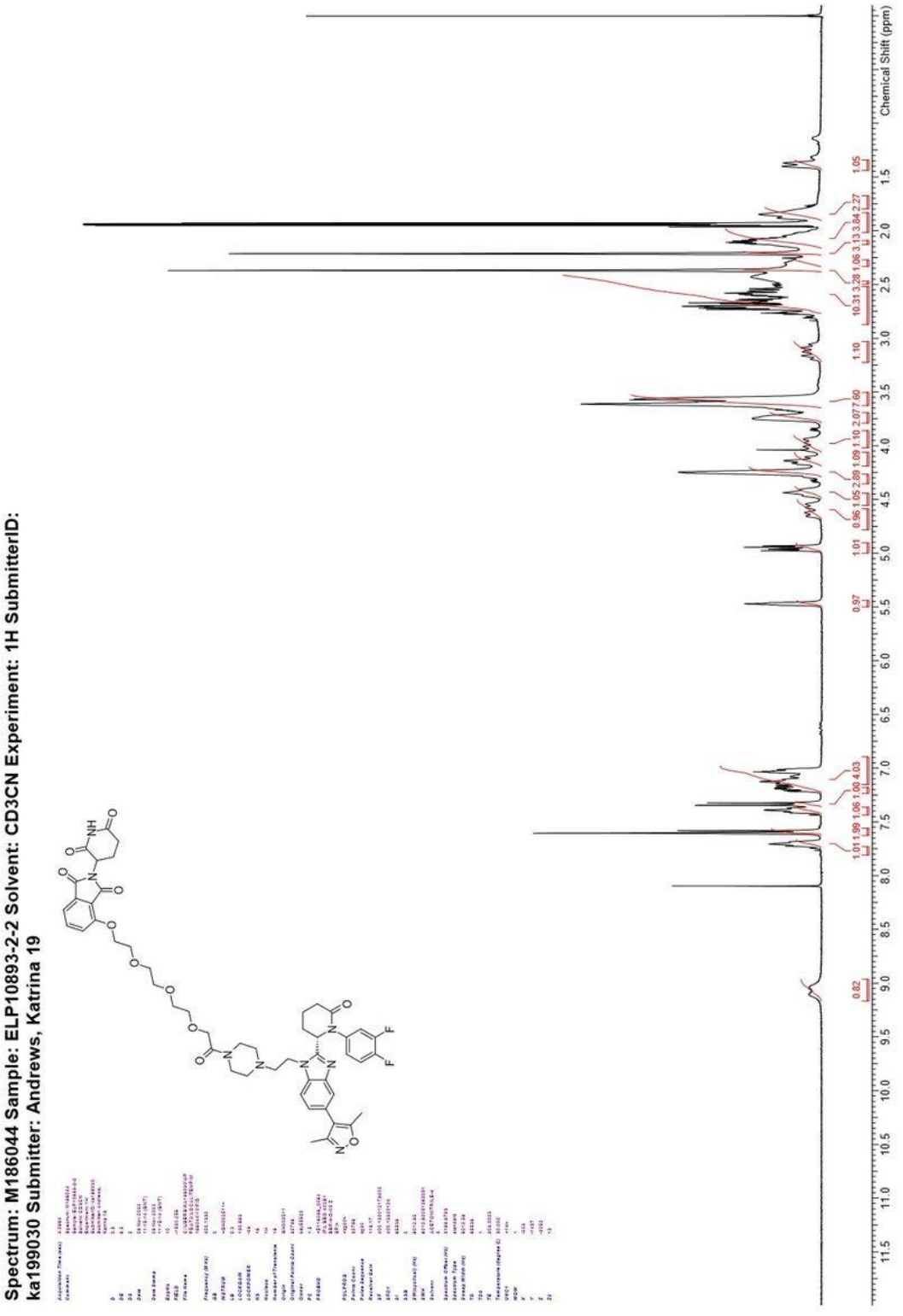

4-{2-[2-(2-{2-[4-(2-{2-[(2*S*)-1-(3,4-Difluorophenyl)-6-oxopiperidin-2-yl]-5-(3,5-dimethyl-1,2-oxazol-4-yl)-1*H*-1,3-benzodiazol-1-yl}ethyl)piperazin-1-yl]-2-oxoethoxy}ethoxy)ethoxy]ethoxy}-2-(2,6-dioxopiperidin-3-yl)-2,3-dihydro-1*H*-isoindole-1,3-dione (149)

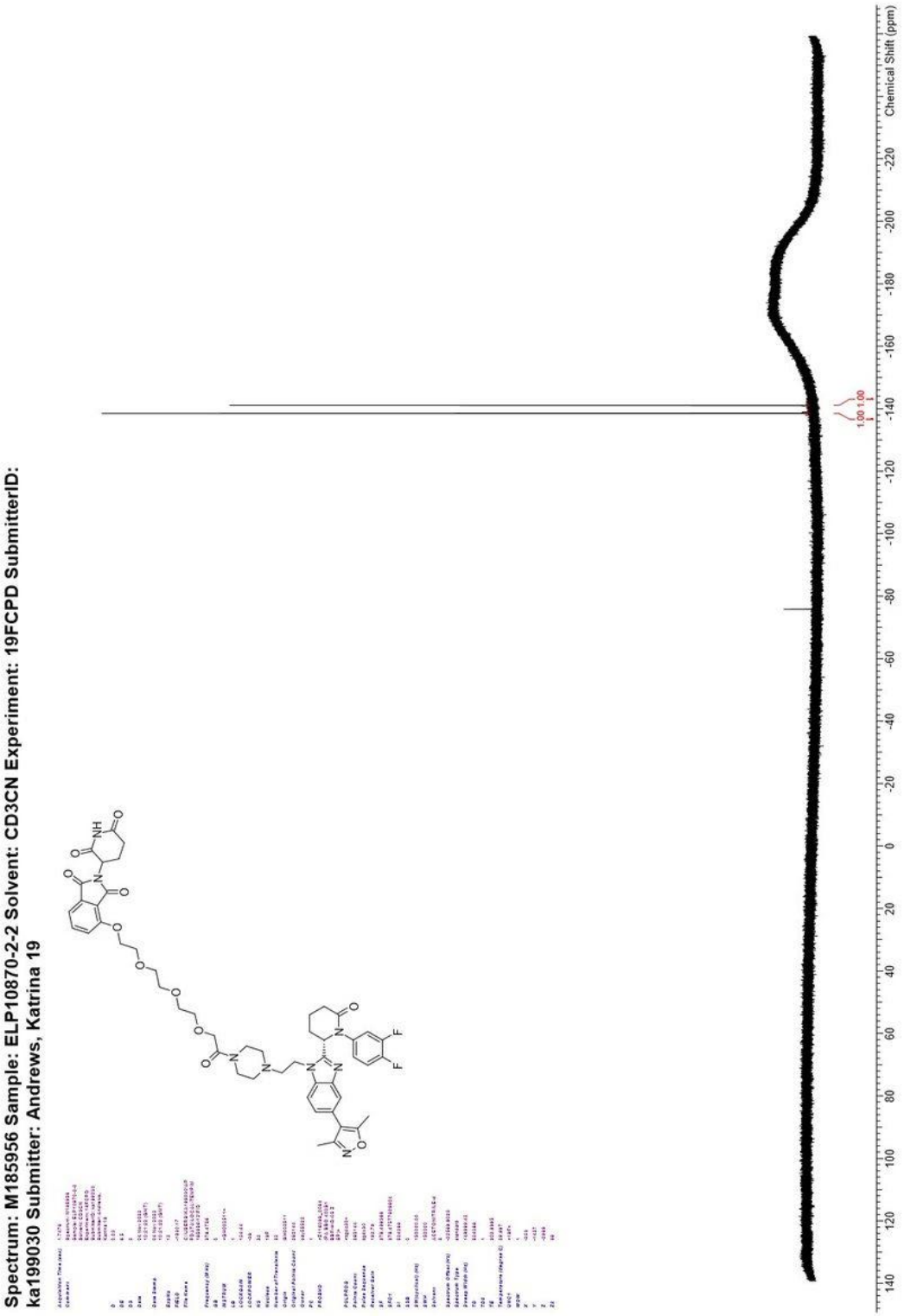

4-({14-[4-(2-{2-[(2*S*)-1-(3,4-Difluorophenyl)-6-oxopiperidin-2-yl]-5-(3,5-dimethyl-1,2-oxazol-4-yl)-1*H*-1,3-benzodiazol-1-yl}ethyl)piperazin-1-yl]-14-oxo-3,6,9,12-tetraoxatetradecan-1-yl}oxy)-2-(2,6-dioxopiperidin-3-yl)-2,3-dihydro-1*H*-isoindole-1,3-dione (150)

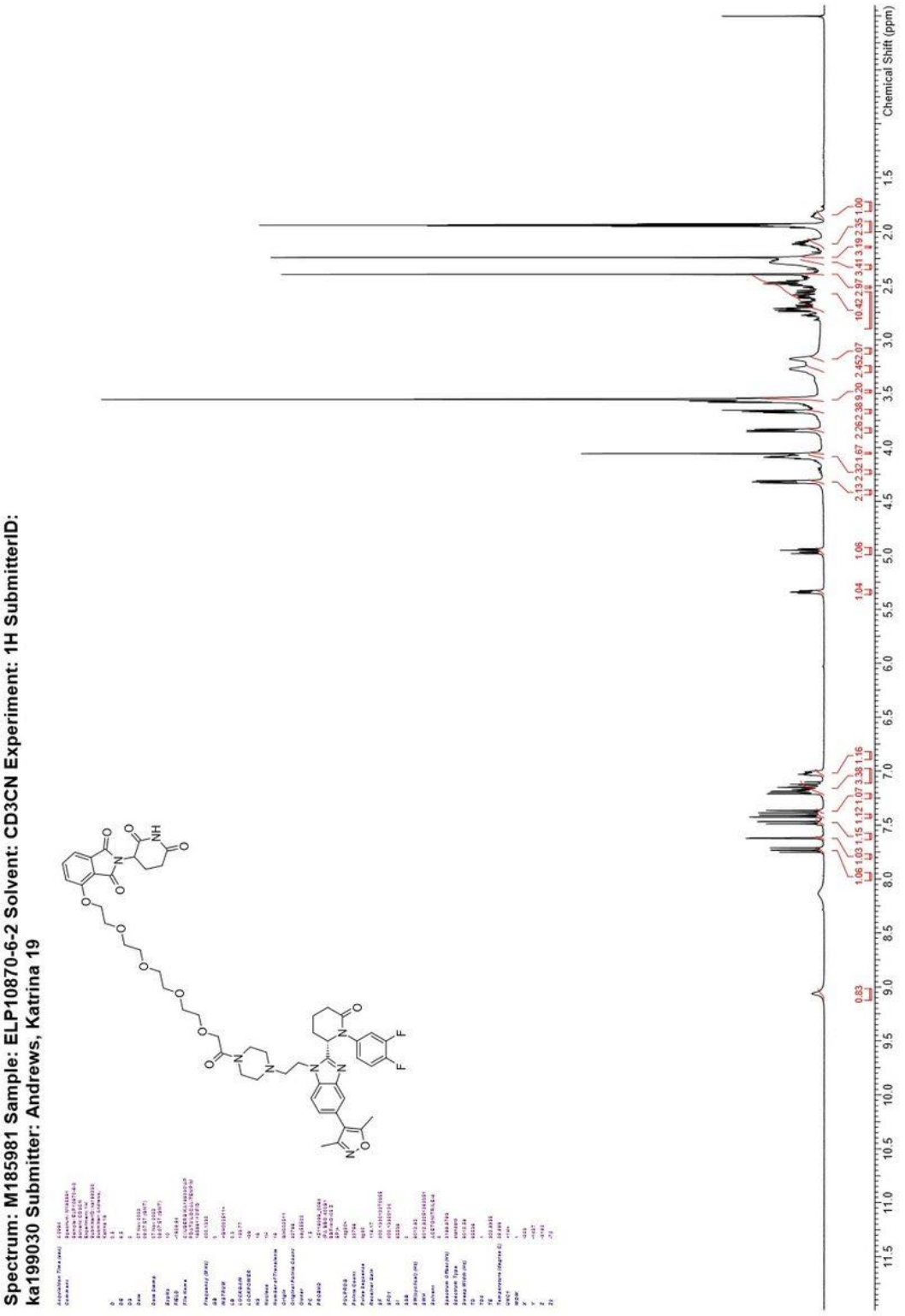

4-({14-[4-(2-{2-[(2*S*)-1-(3,4-Difluorophenyl)-6-oxopiperidin-2-yl]-5-(3,5-dimethyl-1,2-oxazol-4-yl)-1*H*-1,3-benzodiazol-1-yl}ethyl)piperazin-1-yl]-14-oxo-3,6,9,12-tetraoxatetradecan-1-yl}oxy)-2-(2,6-dioxopiperidin-3-yl)-2,3-dihydro-1*H*-isoindole-1,3-dione (150)

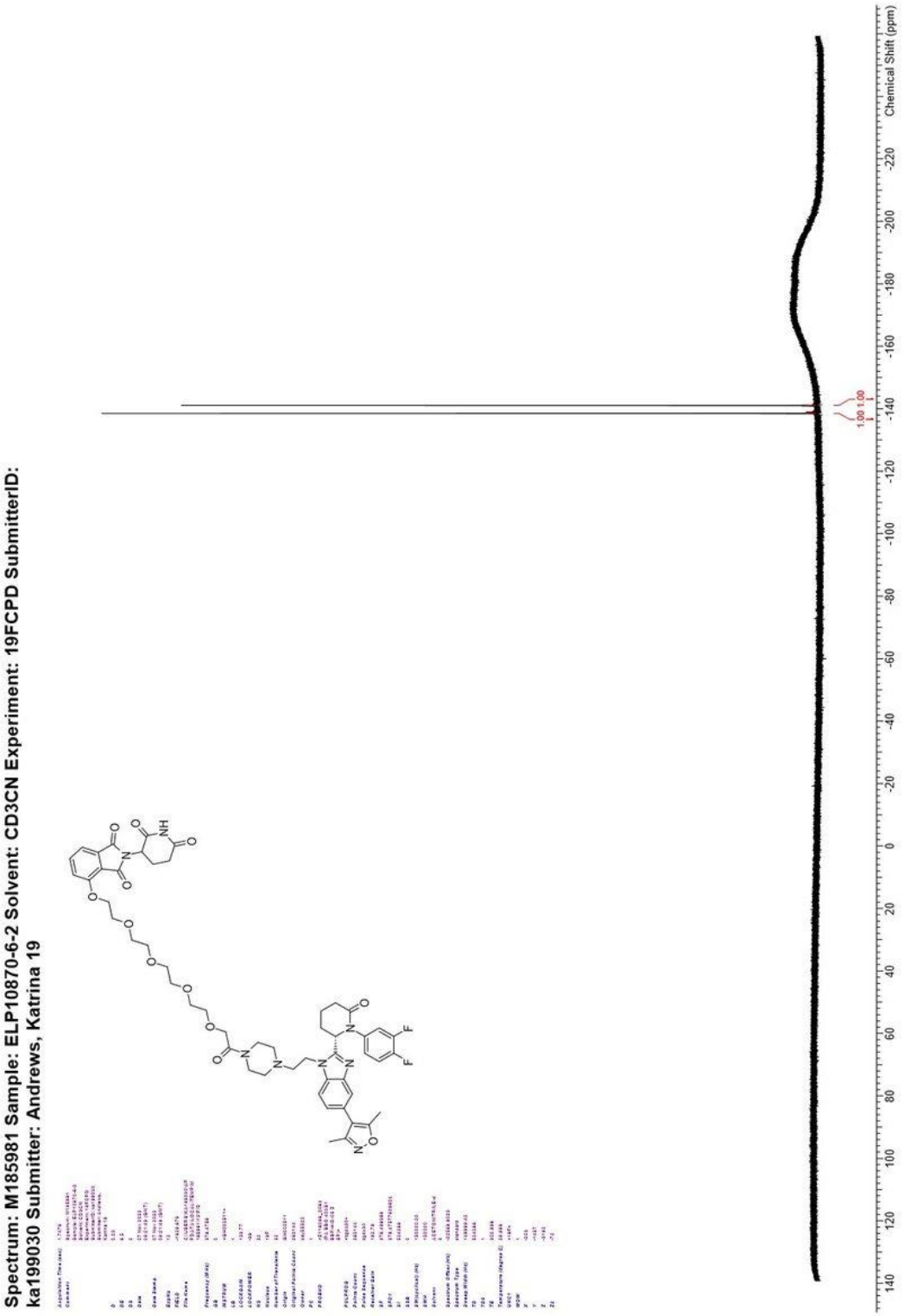

4-({5-[4-(2-{2-[(2*S*)-1-(3,4-Difluorophenyl)-6-oxopiperidin-2-yl]-5-(3,5-dimethyl-1,2-oxazol-4-yl)-1*H*-1,3-benzodiazol-1-yl}ethyl)piperazin-1-yl]-5-oxopentyl}oxy)-2-(2,6-dioxopiperidin-3-yl)-2,3-dihydro-1*H*-isoindole-1,3-dione (151)

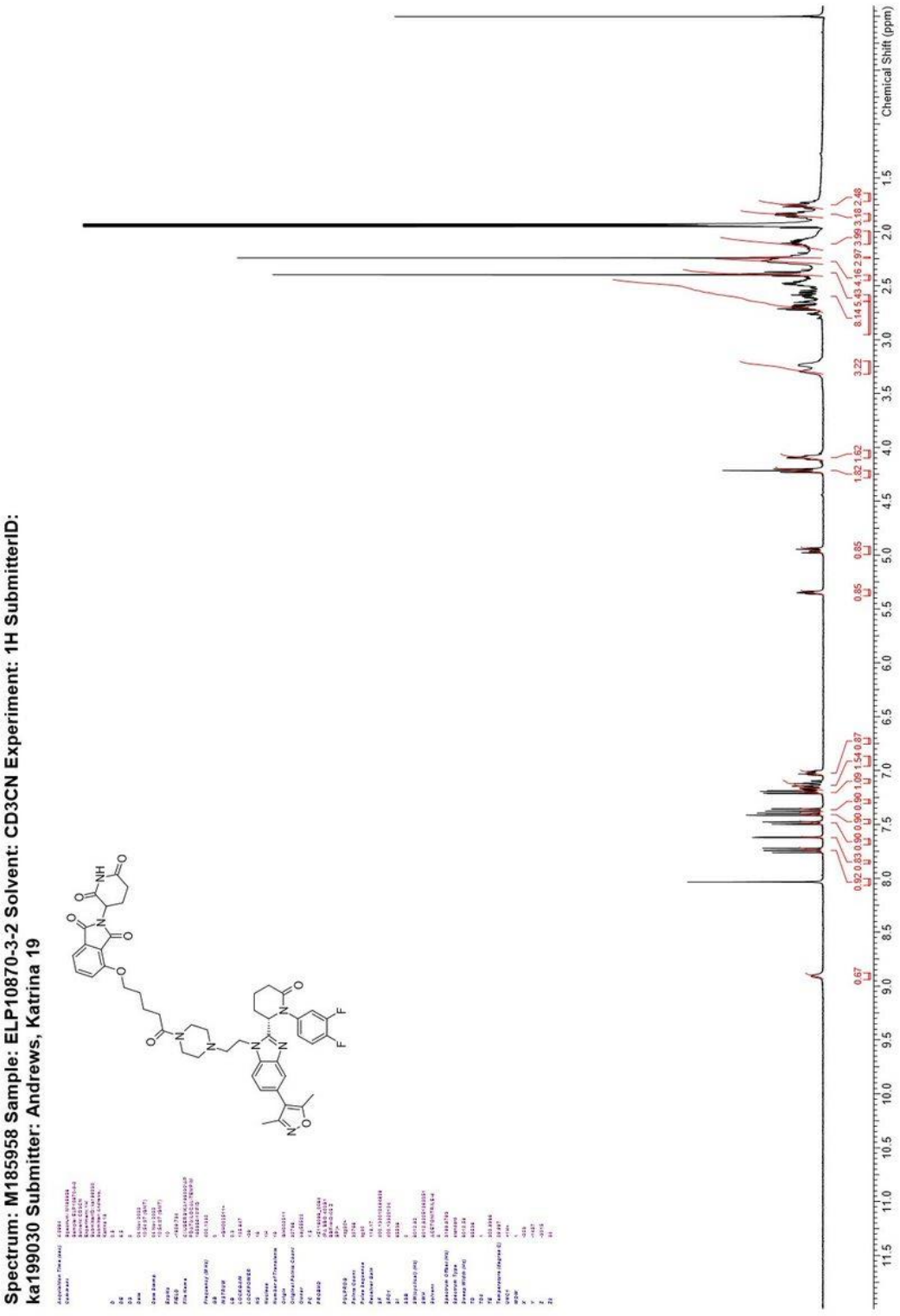

4-({5-[4-(2-{2-[(2*S*)-1-(3,4-Difluorophenyl)-6-oxopiperidin-2-yl]-5-(3,5-dimethyl-1,2-oxazol-4-yl)-1*H*-1,3-benzodiazol-1-yl}ethyl)piperazin-1-yl]-5-oxopentyl}oxy)-2-(2,6-dioxopiperidin-3-yl)-2,3-dihydro-1*H*-isoindole-1,3-dione (151)

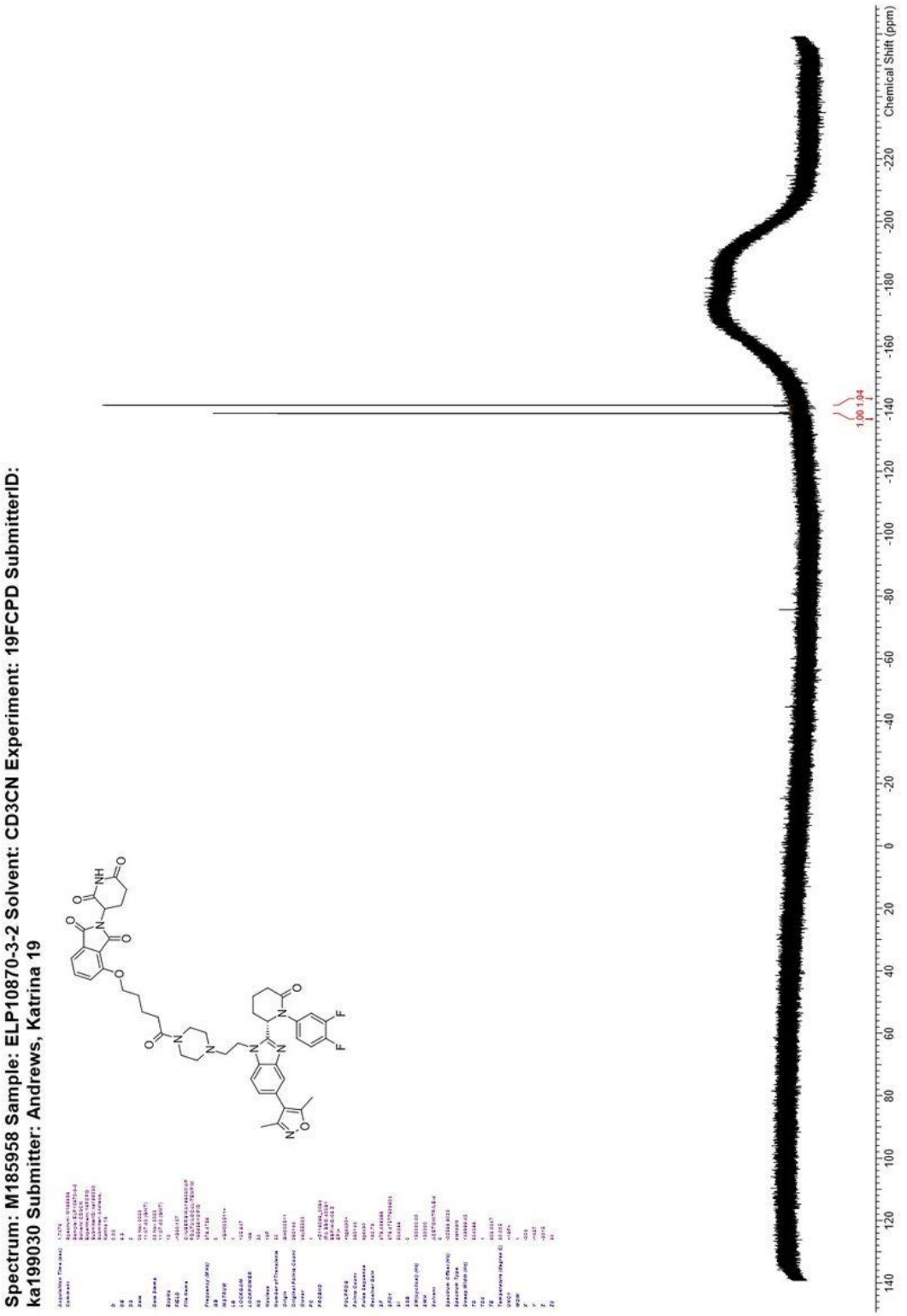

4-({8-[4-(2-{2-[(2*S*)-1-(3,4-Difluorophenyl)-6-oxopiperidin-2-yl]-5-(3,5-dimethyl-1,2-oxazol-4-yl)-1*H*-1,3-benzodiazol-1-yl}ethyl)piperazin-1-yl]-8-oxooctyl}oxy)-2-(2,6-dioxopiperidin-3-yl)-2,3-dihydro-1*H*-isoindole-1,3-dione (152)

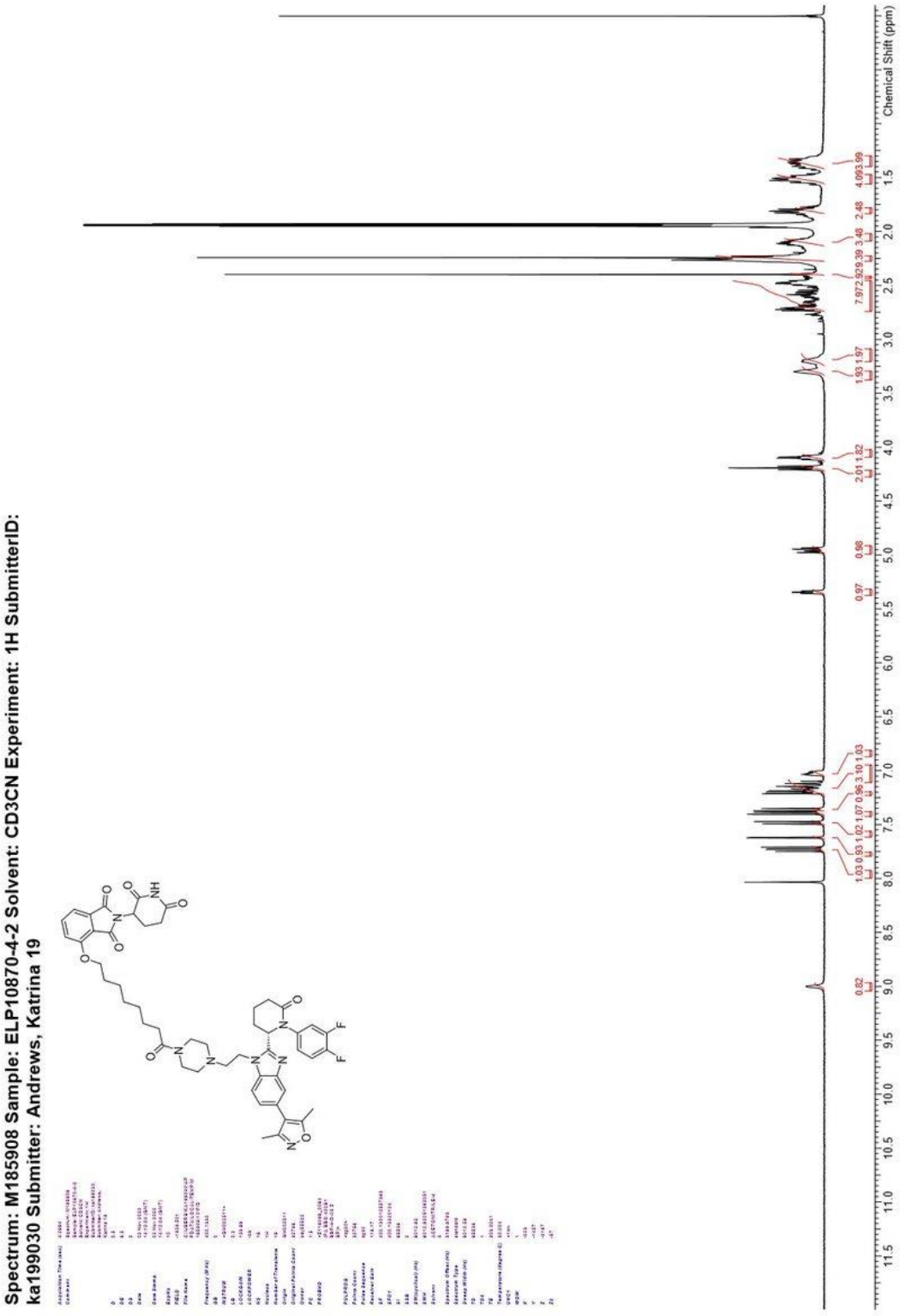

4-({8-[4-(2-{2-[(2*S*)-1-(3,4-Difluorophenyl)-6-oxopiperidin-2-yl]-5-(3,5-dimethyl-1,2-oxazol-4-yl)-1*H*-1,3-benzodiazol-1-yl}ethyl)piperazin-1-yl]-8-oxooctyl}oxy)-2-(2,6-dioxopiperidin-3-yl)-2,3-dihydro-1*H*-isoindole-1,3-dione (152)

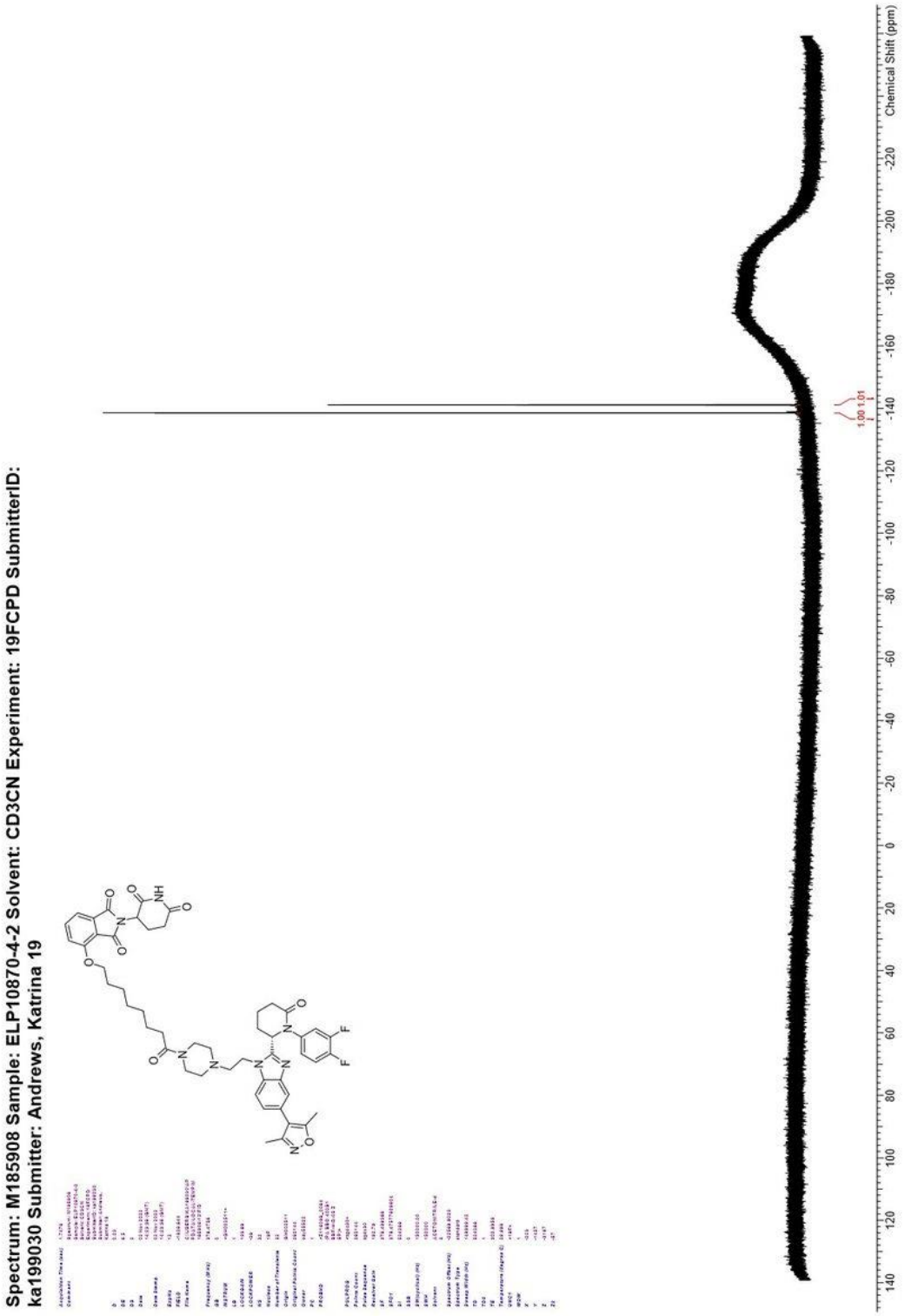

4-({10-[4-(2-{2-[(2*S*)-1-(3,4-Difluorophenyl)-6-oxopiperidin-2-yl]-5-(3,5-dimethyl-1,2-oxazol-4-yl)-1*H*-1,3-benzodiazol-1-yl}ethyl)piperazin-1-yl]-10-oxodecyl}oxy)-2-(2,6-dioxopiperidin-3-yl)-2,3-dihydro-1*H*-isoindole-1,3-dione (153)

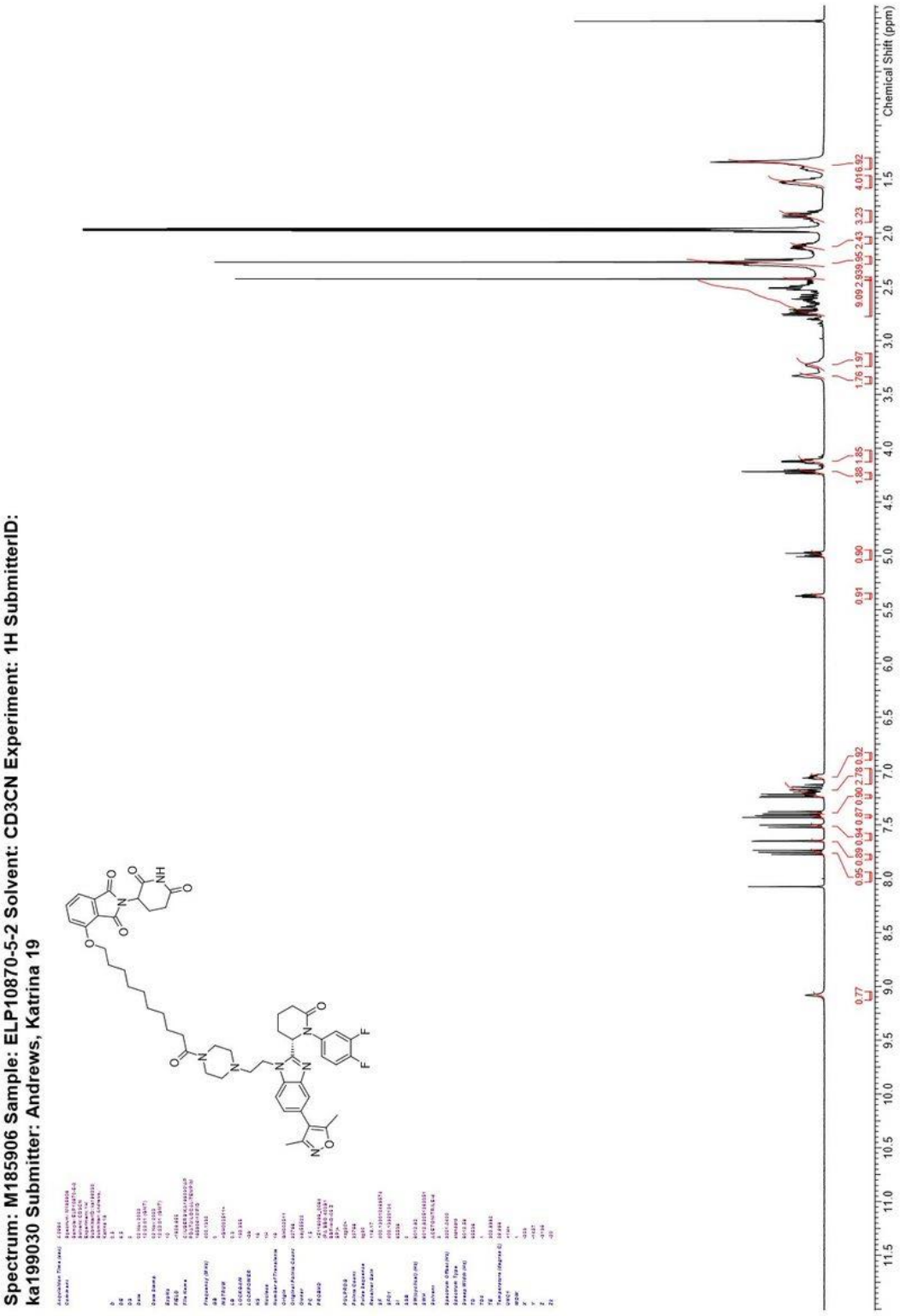

4-({10-[4-(2-{2-[(2*S*)-1-(3,4-Difluorophenyl)-6-oxopiperidin-2-yl]-5-(3,5-dimethyl-1,2-oxazol-4-yl)-1*H*-1,3-benzodiazol-1-yl}ethyl)piperazin-1-yl]-10-oxodecyl}oxy)-2-(2,6-dioxopiperidin-3-yl)-2,3-dihydro-1*H*-isoindole-1,3-dione (153)

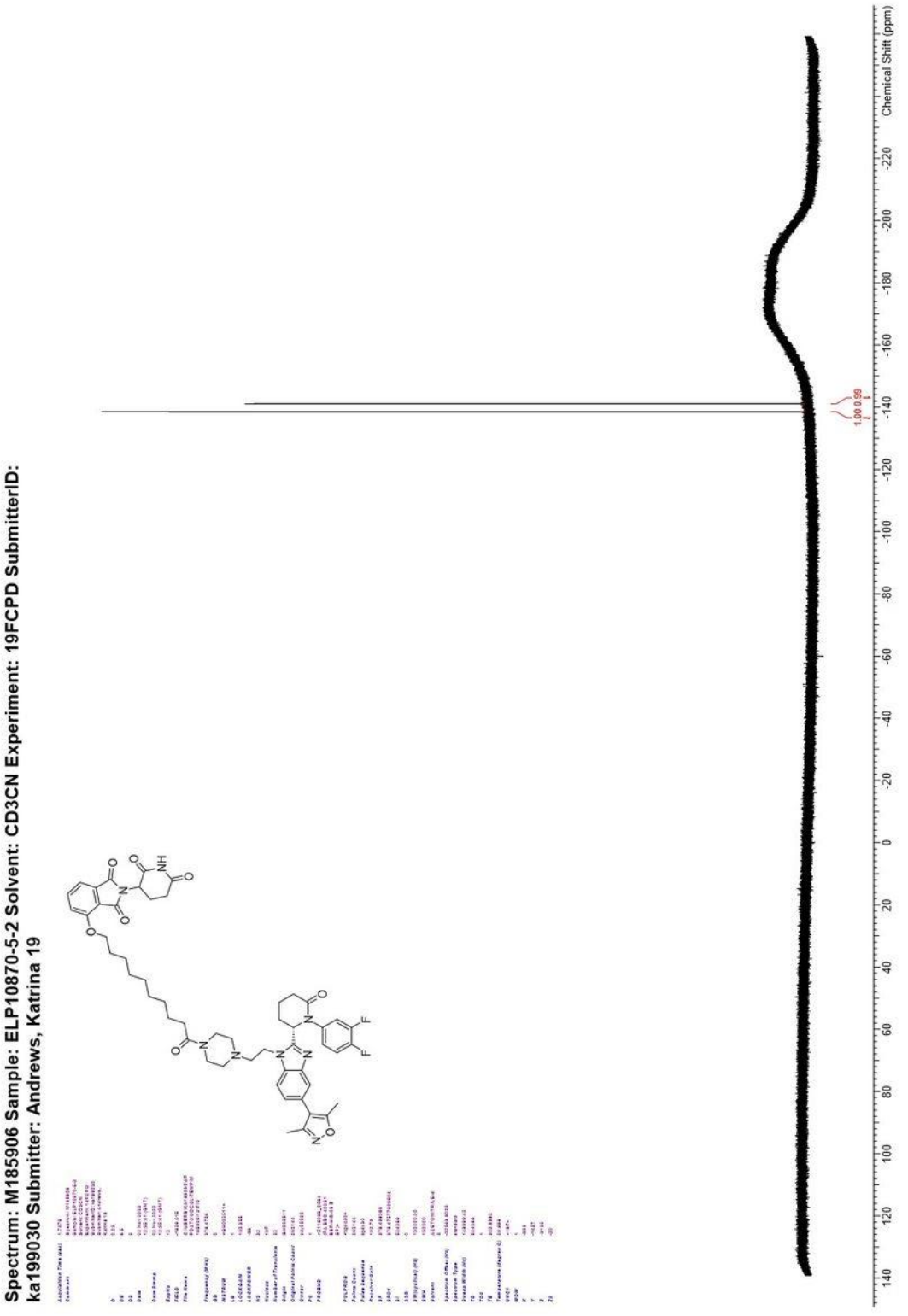

4-[3-(4-{4-[4-(2-{2-[(2*S*)-1-(3,4-Difluorophenyl)-6-oxopiperidin-2-yl]-5-(3,5-dimethyl-1,2-oxazol-4-yl)-1*H*-1,3-benzodiazol-1-yl}ethyl)piperazin-1-yl]-4-oxobutyl}piperazin-1-yl)propoxy]-2-(2,6-dioxopiperidin-3-yl)-2,3-dihydro-1*H*-isoindole-1,3-dione (154)

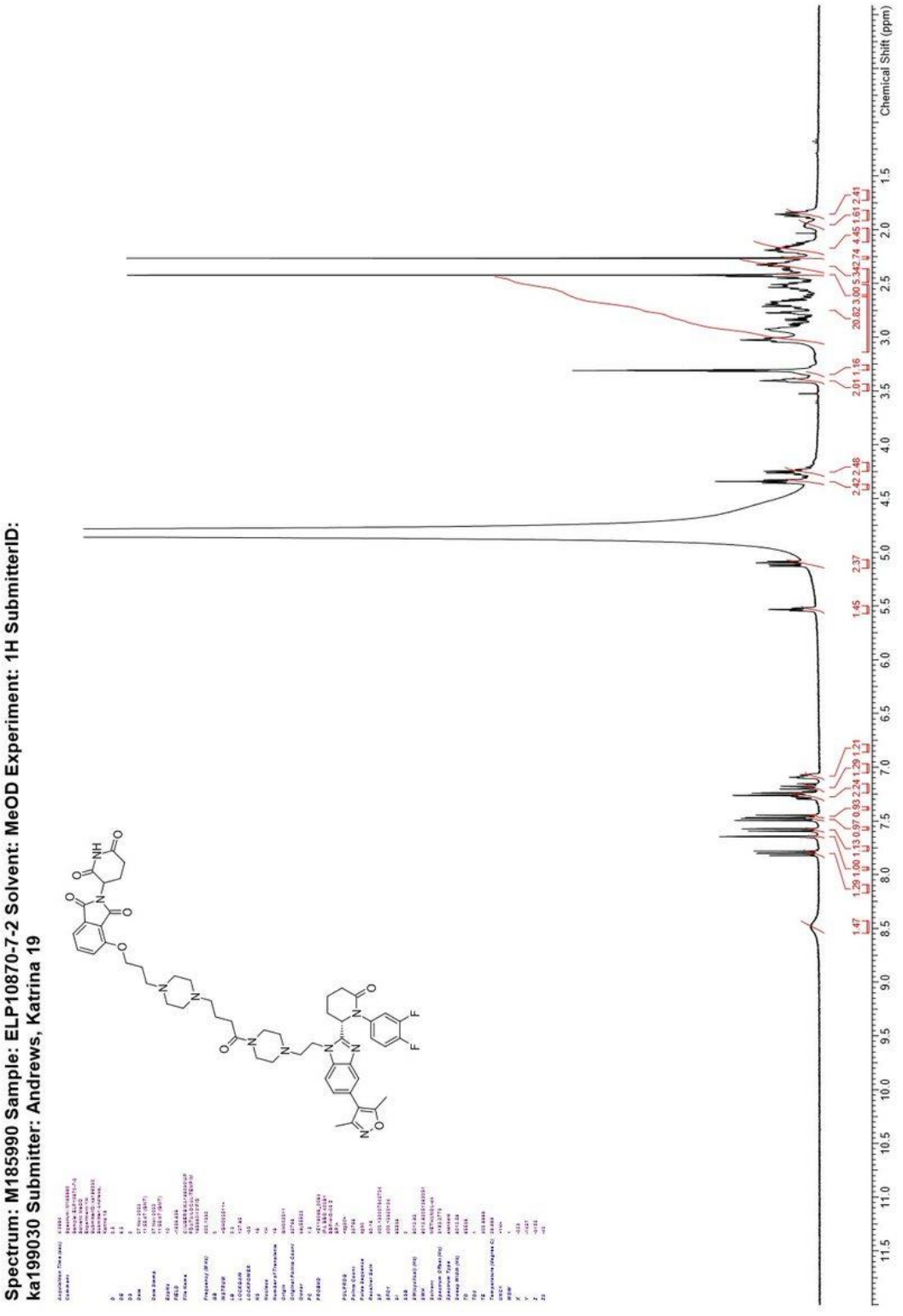

4-[3-(4-{4-[4-(2-{2-[(2*S*)-1-(3,4-Difluorophenyl)-6-oxopiperidin-2-yl]-5-(3,5-dimethyl-1,2-oxazol-4-yl)-1*H*-1,3-benzodiazol-1-yl}ethyl)piperazin-1-yl]-4-oxobutyl}piperazin-1-yl)propoxy]-2-(2,6-dioxopiperidin-3-yl)-2,3-dihydro-1*H*-isoindole-1,3-dione (154)

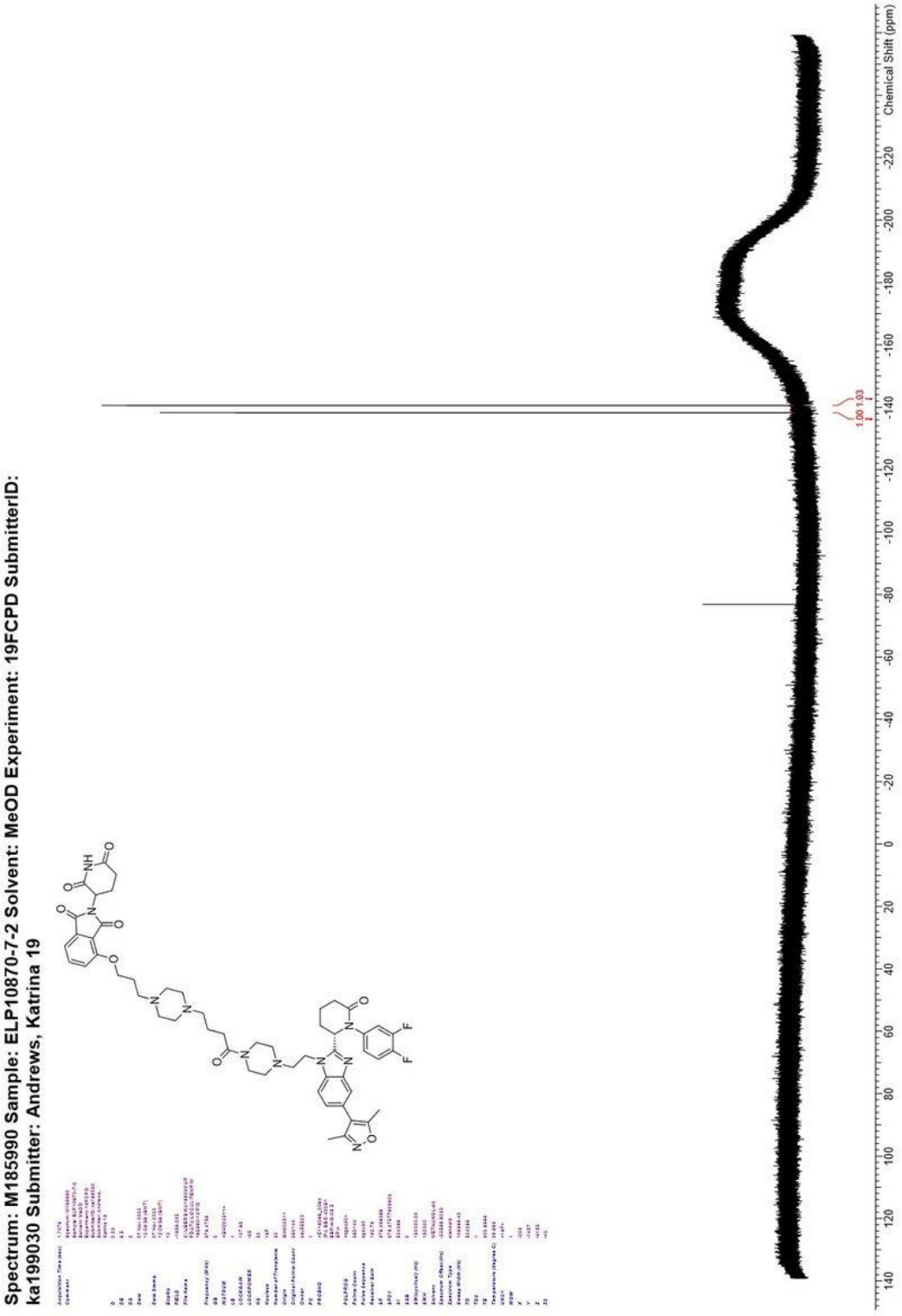

3-[5-(4-{4-[4-(2-{2-[(2*S*)-1-(3,4-Difluorophenyl)-6-oxopiperidin-2-yl]-5-(3,5-dimethyl-1,2-oxazol-4-yl)-1*H*-1,3-benzodiazol-1-yl}ethyl)piperazin-1-yl]-4-oxobutyl}piperazin-1-yl)-1-oxo-2,3-dihydro-1*H*-isoindol-2-yl]piperidine-2,6-dione (155)

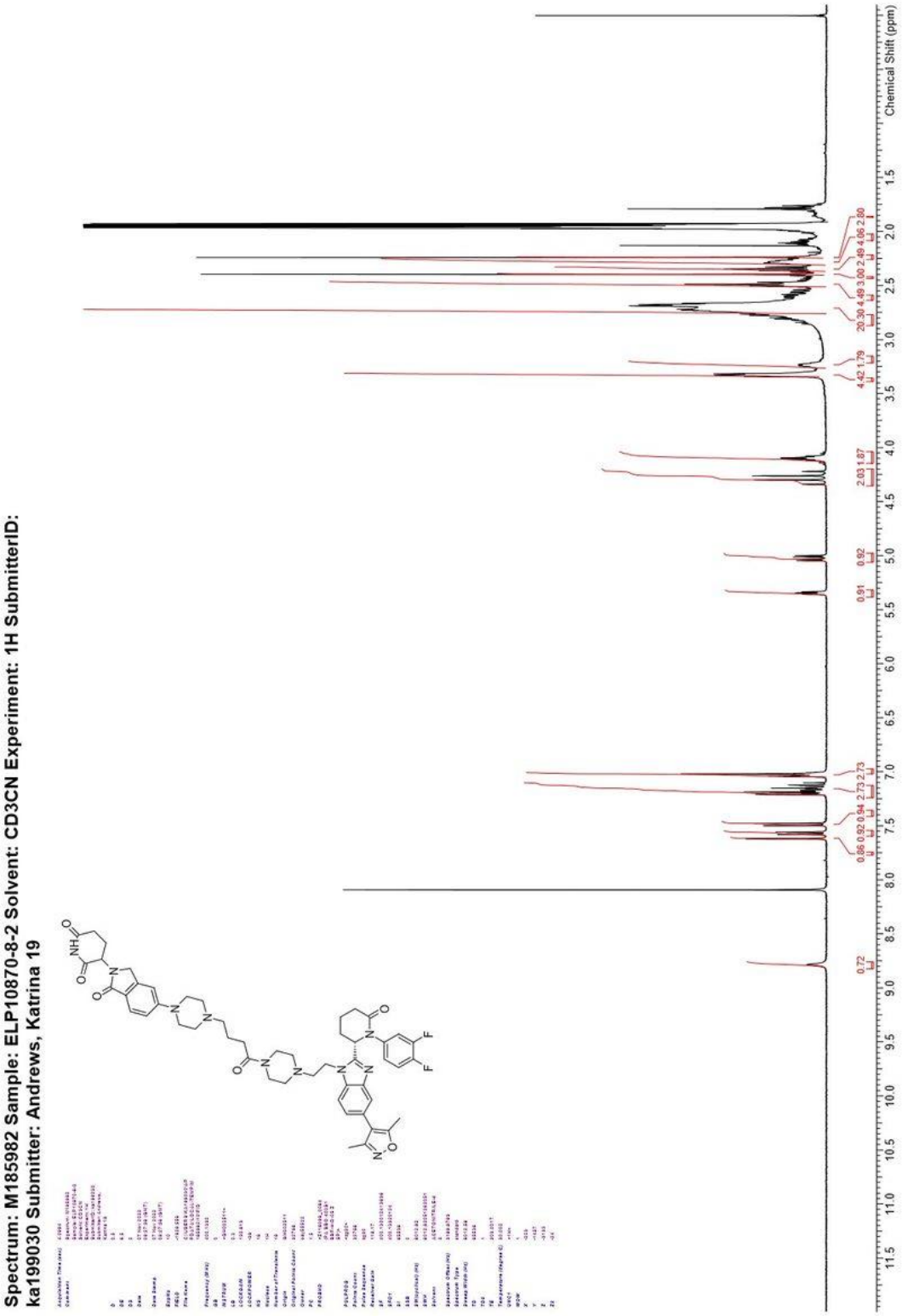

3-[5-(4-{4-[4-(2-{2-[(2*S*)-1-(3,4-Difluorophenyl)-6-oxopiperidin-2-yl]-5-(3,5-dimethyl-1,2-oxazol-4-yl)-1*H*-1,3-benzodiazol-1-yl}ethyl)piperazin-1-yl]-4-oxobutyl}piperazin-1-yl)-1-oxo-2,3-dihydro-1*H*-isoindol-2-yl]piperidine-2,6-dione (155)

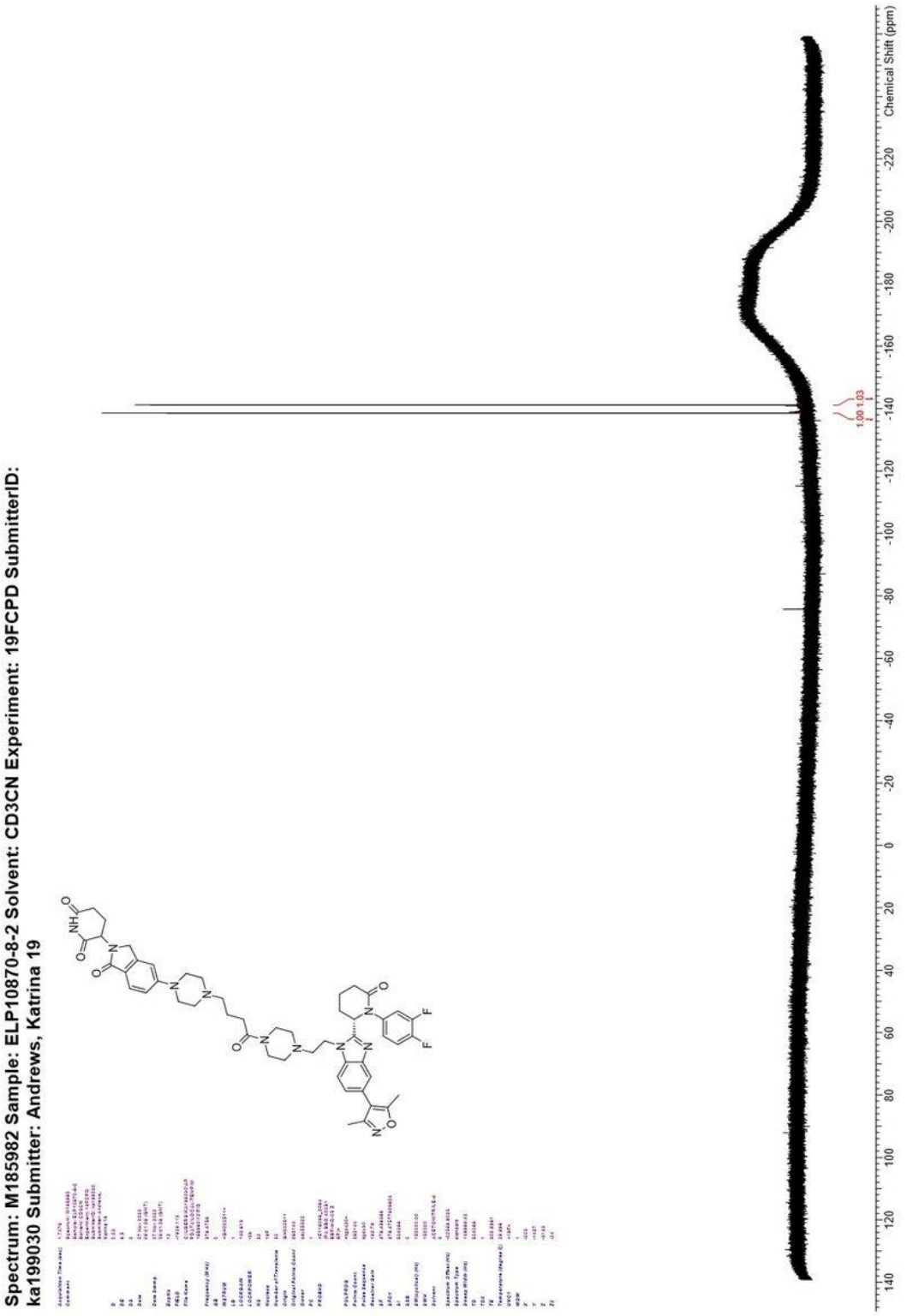

5-(9-{2-[4-(2-{2-[(2*S*)-1-(3,4-Difluorophenyl)-6-oxopiperidin-2-yl]-5-(3,5-dimethyl-1,2-oxazol-4-yl)-1*H*-1,3-benzodiazol-1-yl}ethyl)piperazin-1-yl]-2-oxoethyl}-3,9-diazaspiro[5.5]undecan-3-yl)-2-(2,6-dioxopiperidin-3-yl)-6-fluoro-2,3-dihydro-1*H*-isoindole-1,3-dione (156)

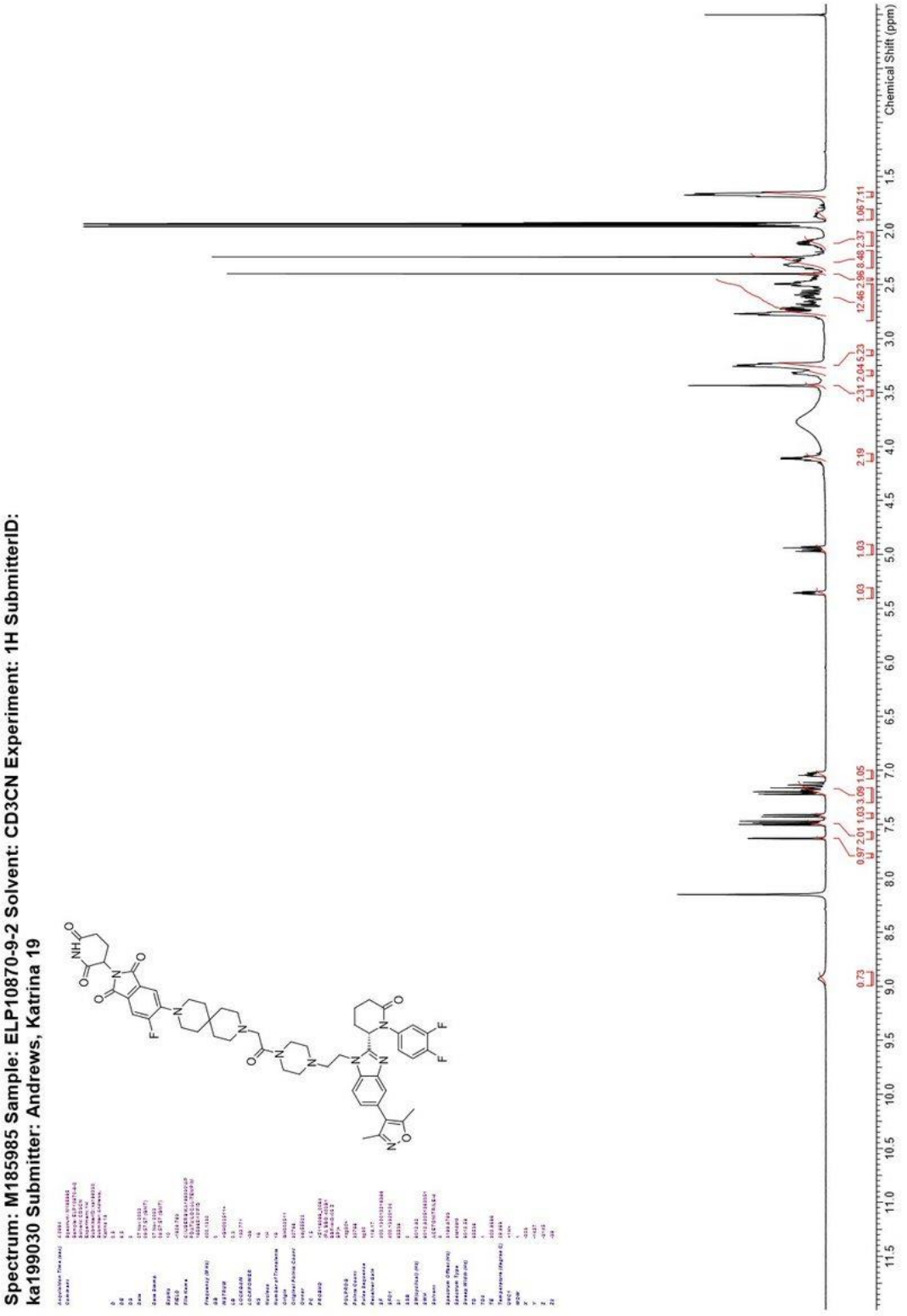

5-(9-{2-[4-(2-{2-[(2*S*)-1-(3,4-Difluorophenyl)-6-oxopiperidin-2-yl]-5-(3,5-dimethyl-1,2-oxazol-4-yl)-1*H*-1,3-benzodiazol-1-yl}ethyl)piperazin-1-yl]-2-oxoethyl}-3,9-diazaspiro[5.5]undecan-3-yl)-2-(2,6-dioxopiperidin-3-yl)-6-fluoro-2,3-dihydro-1*H*-isoindole-1,3-dione (156)

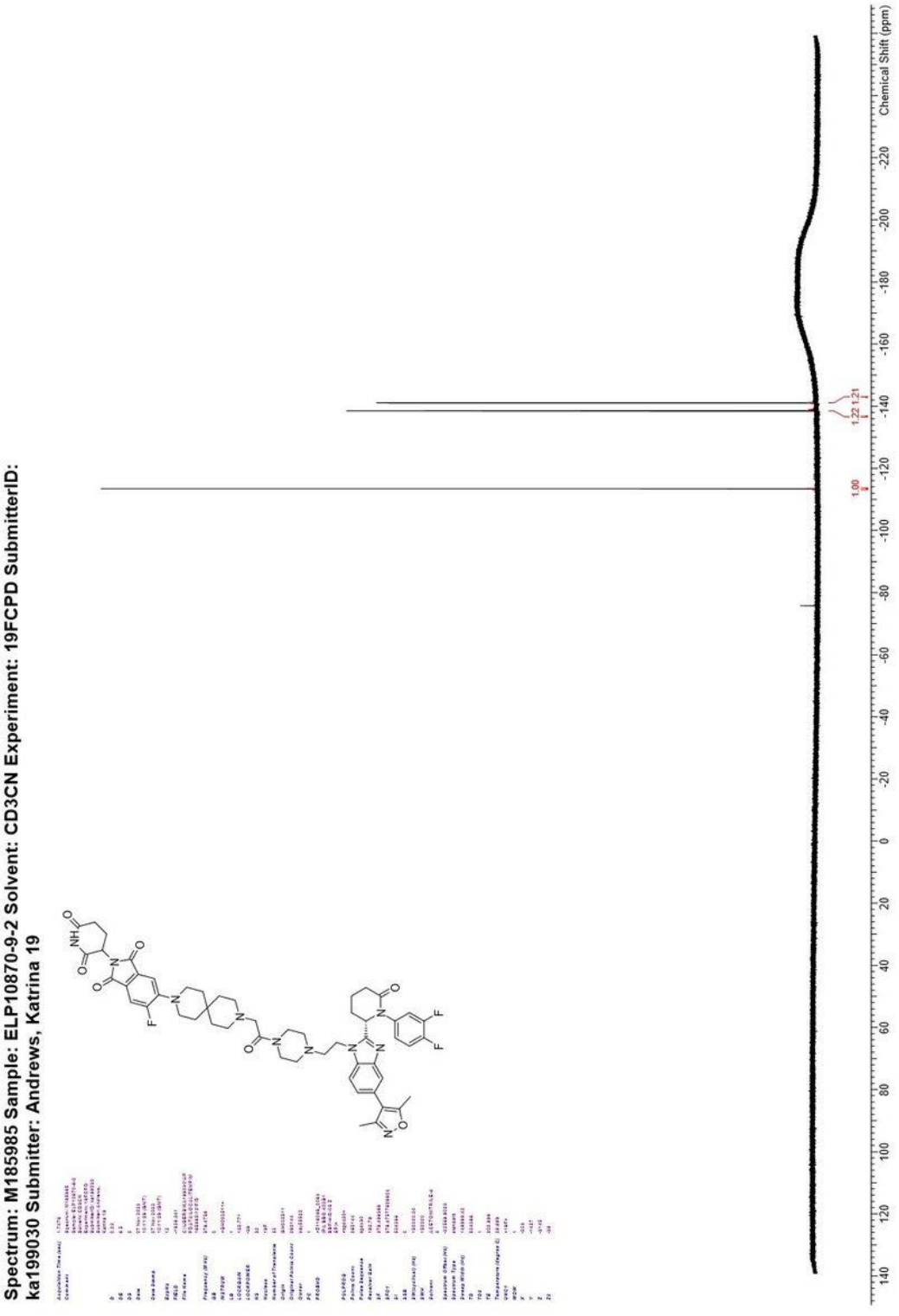

3-{5-[4-({4-[4-(2-{2-[(2*S*)-1-(3,4-Difluorophenyl)-6-oxopiperidin-2-yl]-5-(3,5-dimethyl-1,2-oxazol-4-yl)-1*H*-1,3-benzodiazol-1-yl}ethyl)piperazine-1-carbonyl]phenyl}methyl)piperazin-1-yl]-1-oxo-2,3-dihydro-1*H*-isoindol-2-yl}piperidine-2,6-dione (157)

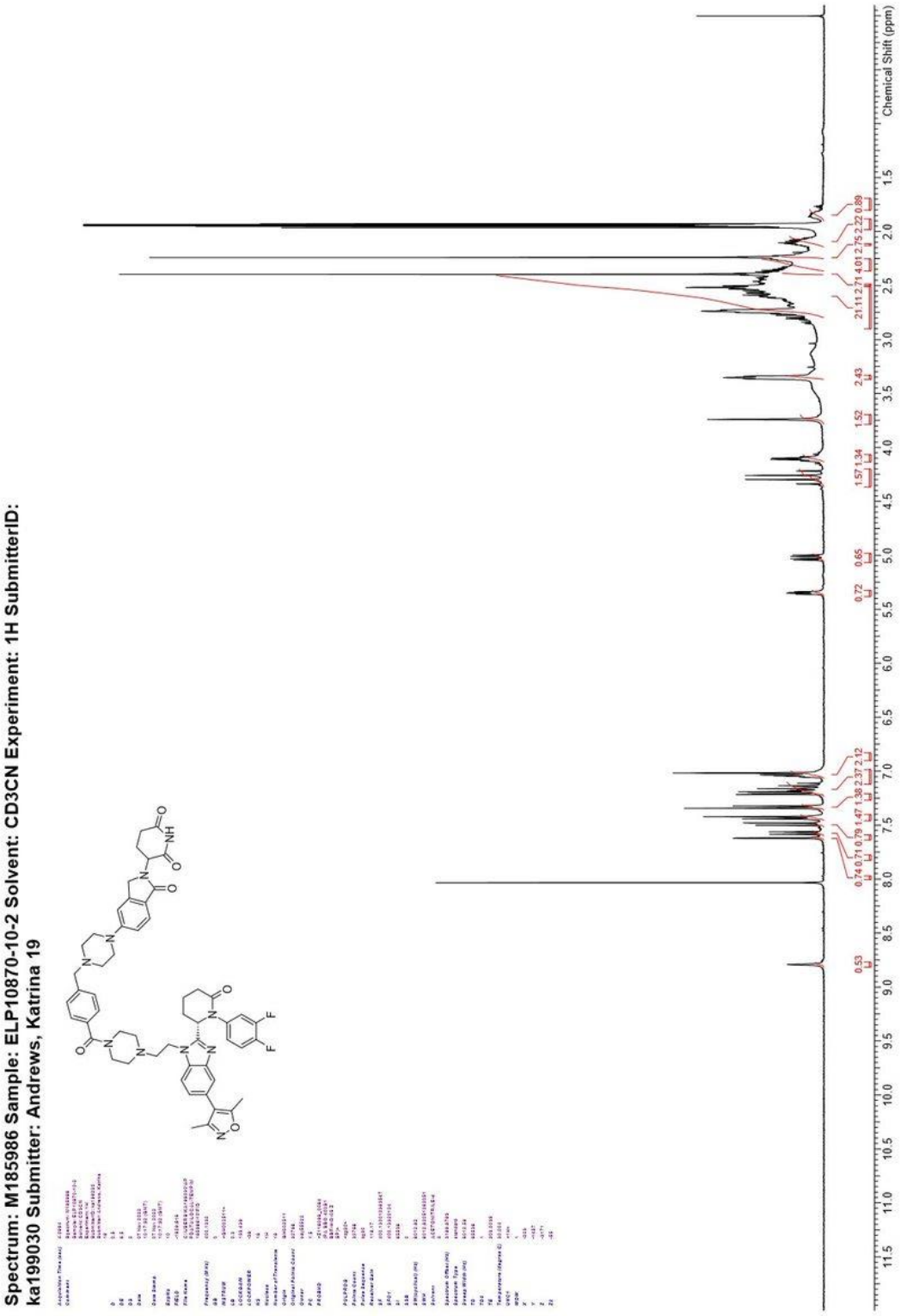

3-{5-[4-({4-[4-(2-{2-[(2*S*)-1-(3,4-Difluorophenyl)-6-oxopiperidin-2-yl]-5-(3,5-dimethyl-1,2-oxazol-4-yl)-1*H*-1,3-benzodiazol-1-yl}ethyl)piperazine-1-carbonyl]phenyl}methyl)piperazin-1-yl]-1-oxo-2,3-dihydro-1*H*-isoindol-2-yl}piperidine-2,6-dione (157)

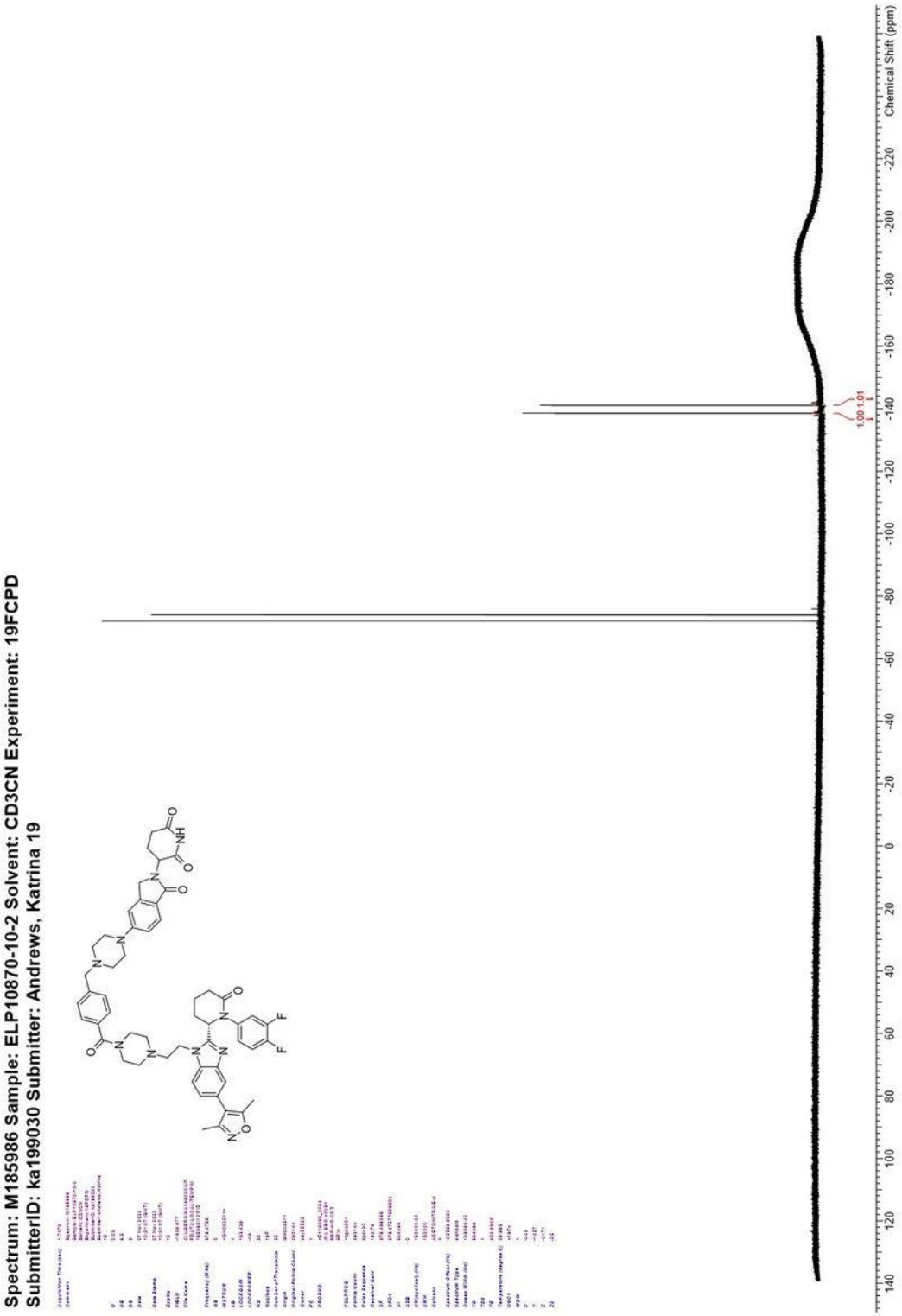

(2*S*,4*R*)-*N*-({2-[2-(2-{2-[4-(2-{2-[(2*S*)-1-(3,4-Difluorophenyl)-6-oxopiperidin-2-yl]-5-(3,5-dimethyl-1,2-oxazol-4-yl)-1*H*-1,3-benzodiazol-1-yl}ethyl)piperazin-1-yl]-2-oxoethoxy}ethoxy)ethoxy]-4-(4-methyl-1,3-thiazol-5-yl)phenyl}methyl)-1-[(2*S*)-2-[(1-fluorocyclopropyl)formamido]-3,3-dimethylbutanoyl]-4-hydroxypyrrolidine-2-carboxamide (160)

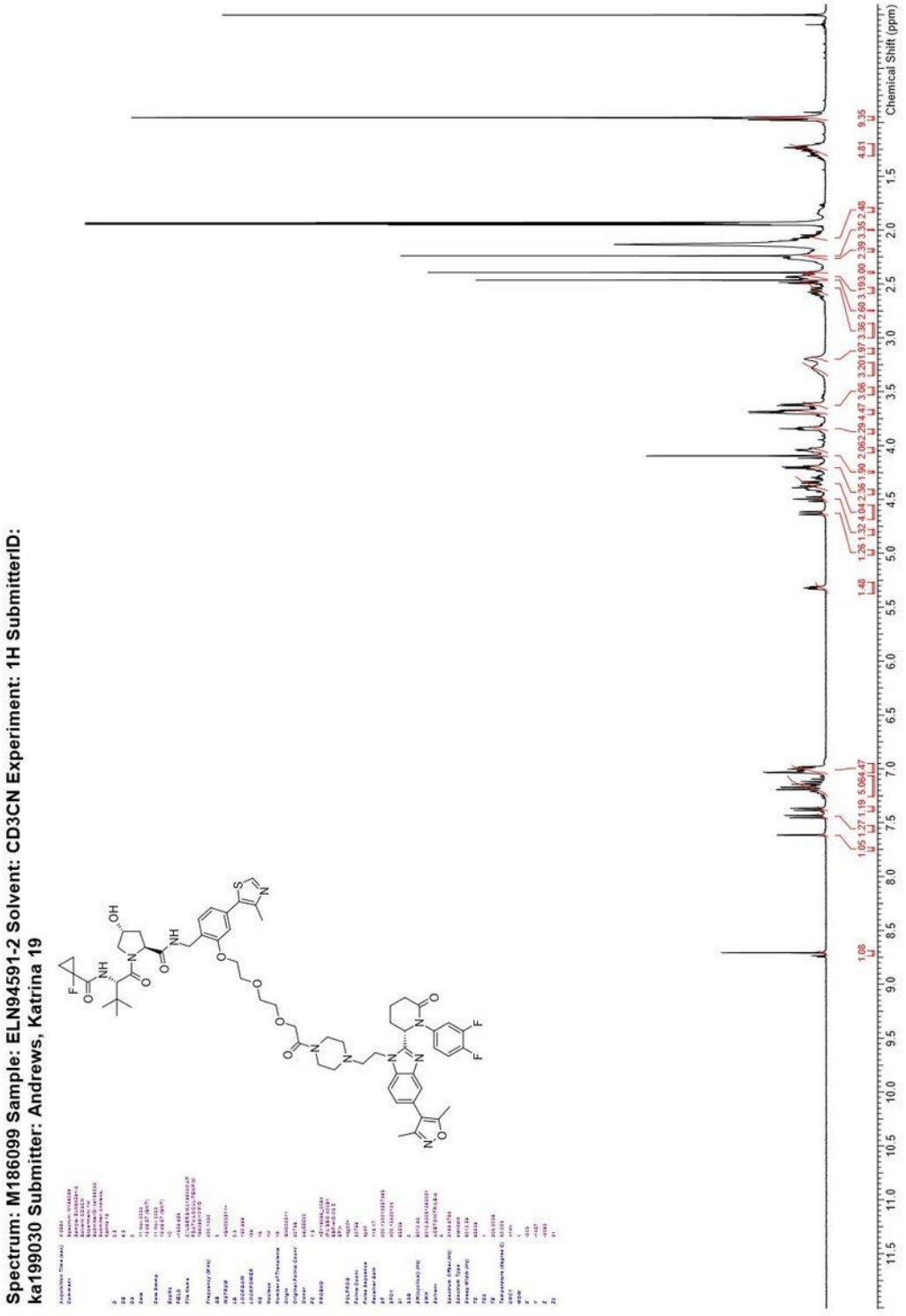

(2*S*,4*R*)-*N*-({2-[2-(2-{2-[4-(2-{2-[(2*S*)-1-(3,4-Difluorophenyl)-6-oxopiperidin-2-yl]-5-(3,5-dimethyl-1,2-oxazol-4-yl)-1*H*-1,3-benzodiazol-1-yl}ethyl)piperazin-1-yl]-2-oxoethoxy}ethoxy)ethoxy]-4-(4-methyl-1,3-thiazol-5-yl)phenyl}methyl)-1-[(2*S*)-2-[(1-fluorocyclopropyl)formamido]-3,3-dimethylbutanoyl]-4-hydroxypyrrolidine-2-carboxamide (160)

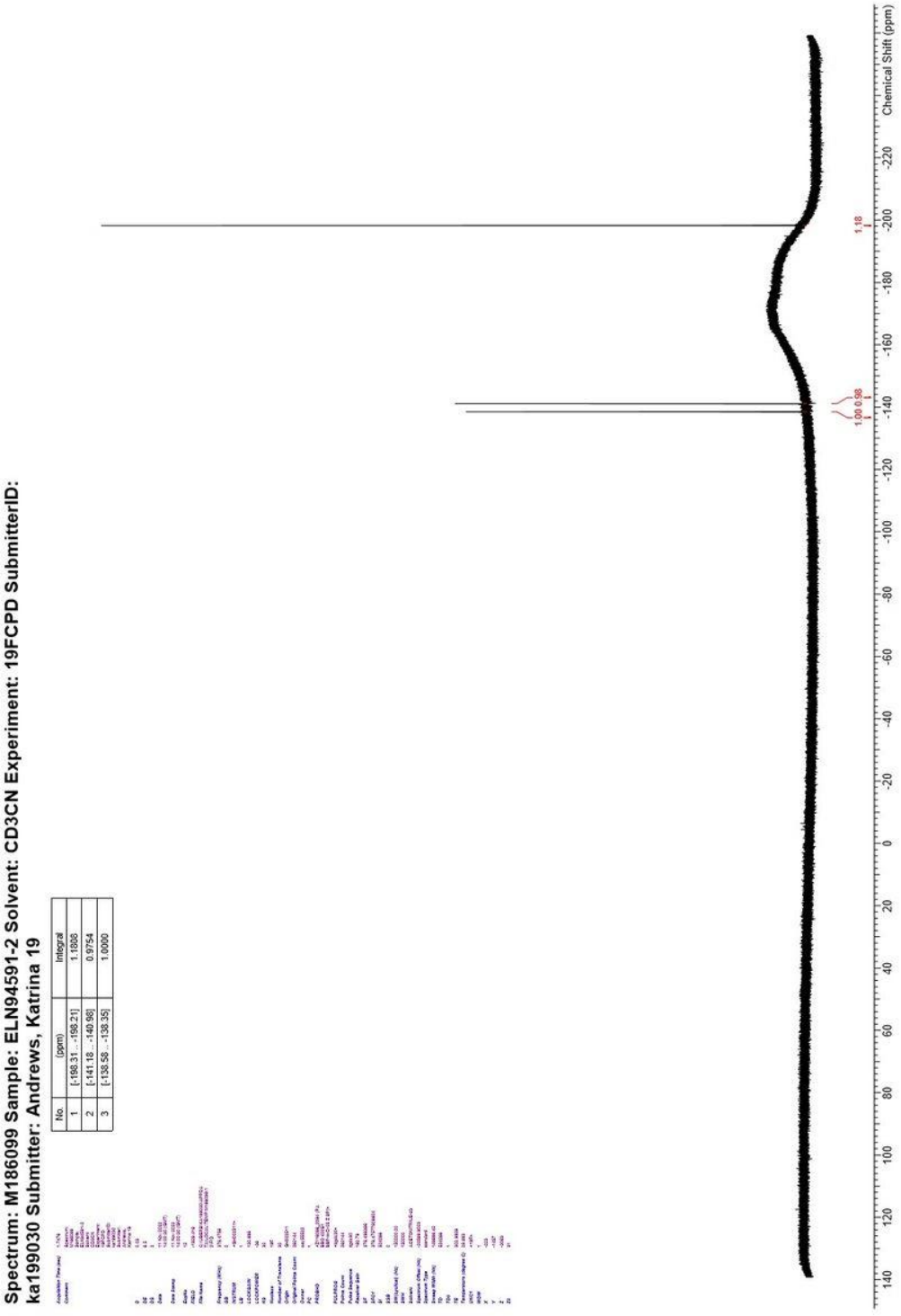

(2*S*,4*R*)-*N*-[(2-{2-[2-(2-{2-[4-(2-{2-[(2*S*)-1-(3,4-Difluorophenyl)-6-oxopiperidin-2-yl]-5-(3,5-dimethyl-1,2-oxazol-4-yl)-1*H*-1,3-benzodiazol-1-yl}ethyl)piperazin-1-yl]-2-oxoethoxy}ethoxy)ethoxy]ethoxy}-4-(4-methyl-1,3-thiazol-5-yl)phenyl)methyl]-1-[(2*S*)-2-[(1-fluorocyclopropyl)formamido]-3,3-dimethylbutanoyl]-4-hydroxypyrrolidine-2-carboxamide (161)

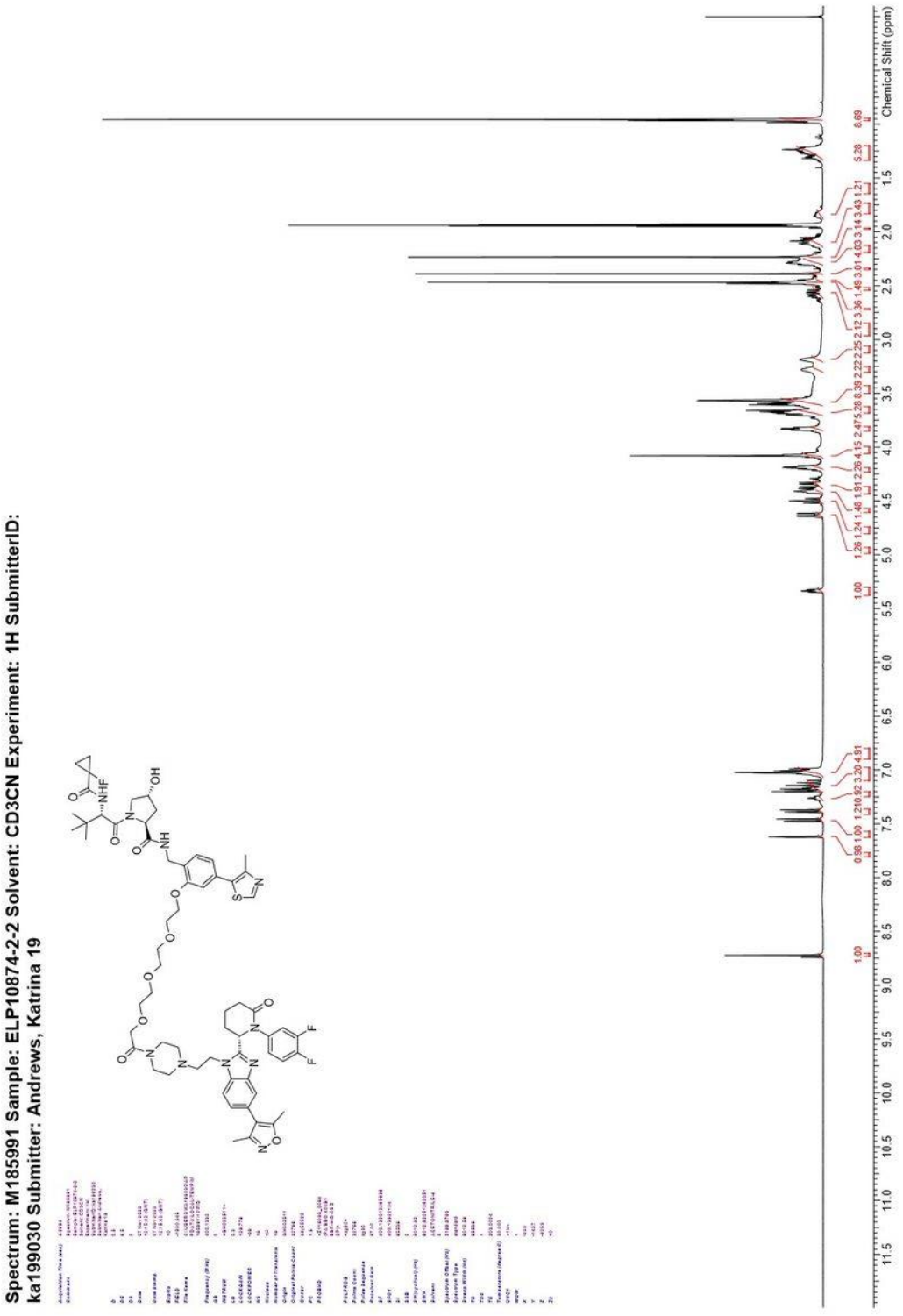

(2*S*,4*R*)-*N*-[(2-{2-[2-(2-{2-[4-(2-{2-[(2*S*)-1-(3,4-Difluorophenyl)-6-oxopiperidin-2-yl]-5-(3,5-dimethyl-1,2-oxazol-4-yl)-1*H*-1,3-benzodiazol-1-yl}ethyl)piperazin-1-yl]-2-oxoethoxy}ethoxy)ethoxy]ethoxy}-4-(4-methyl-1,3-thiazol-5-yl)phenyl)methyl]-1-[(2*S*)-2-[(1-fluorocyclopropyl)formamido]-3,3-dimethylbutanoyl]-4-hydroxypyrrolidine-2-carboxamide (161)

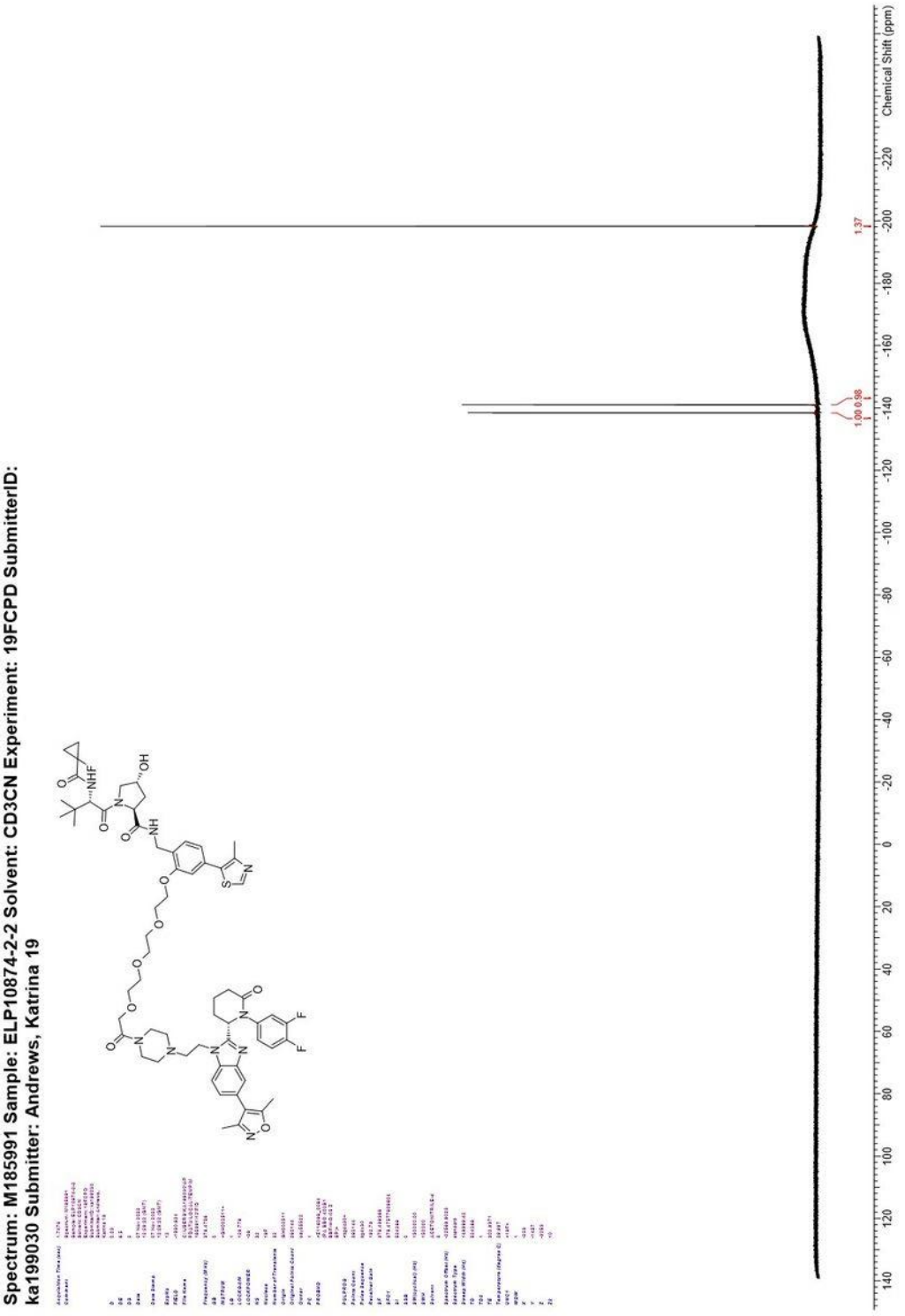

(2*S*,4*R*)-*N*-{[2-({14-[4-(2-{2-[(2*S*)-1-(3,4-Difluorophenyl)-6-oxopiperidin-2-yl]-5-(3,5-dimethyl-1,2-oxazol-4-yl)-1*H*-1,3-benzodiazol-1-yl}ethyl)piperazin-1-yl]-14-oxo-3,6,9,12-tetraoxatetradecan-1-yl}oxy)-4-(4-methyl-1,3-thiazol-5-yl)phenyl]methyl}-1-[(2*S*)-2-[(1-fluorocyclopropyl)formamido]-3,3-dimethylbutanoyl]-4-hydroxypyrrolidine-2-carboxamide (162)

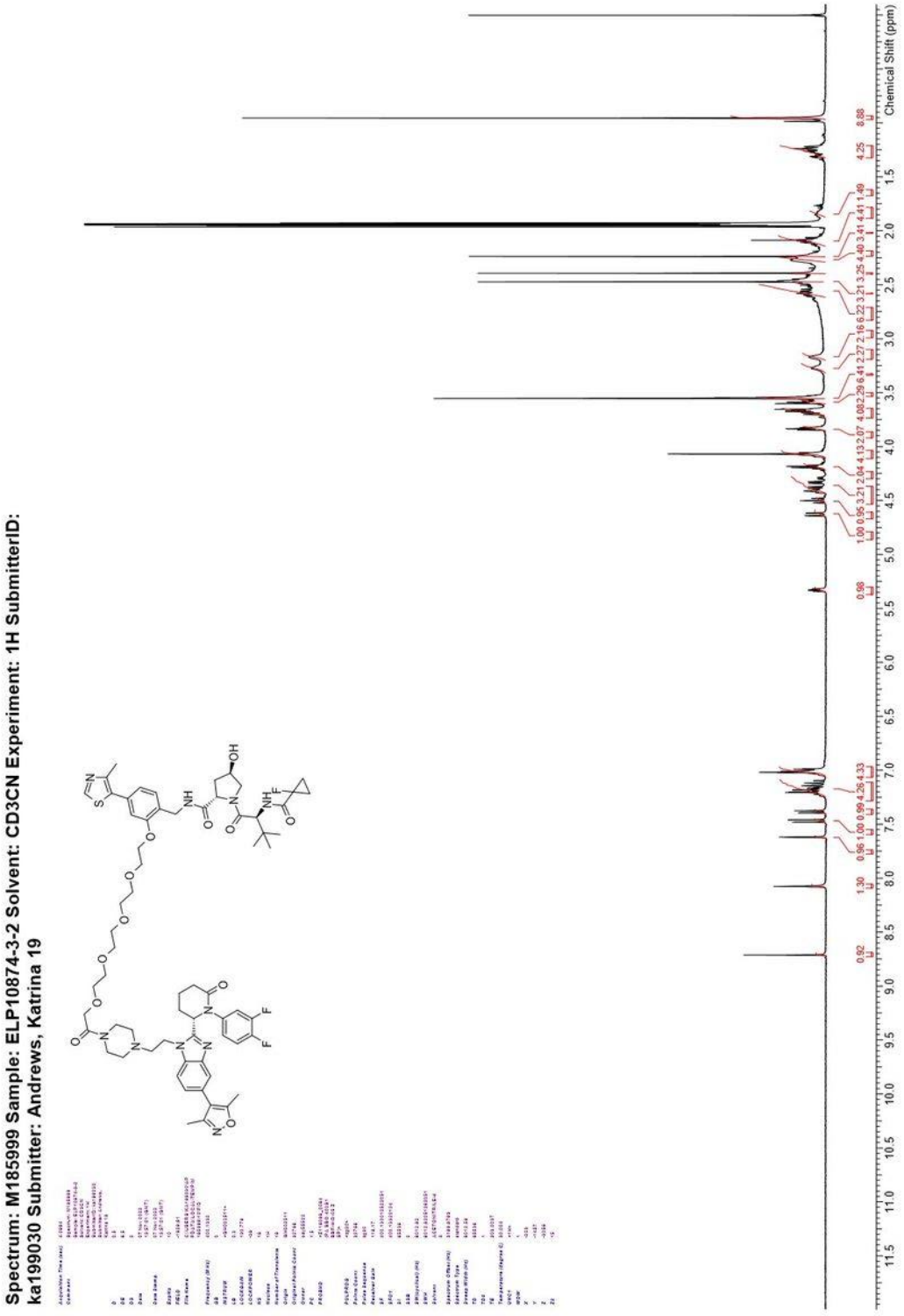

(2*S*,4*R*)-*N*-{[2-({14-[4-(2-{2-[(2*S*)-1-(3,4-Difluorophenyl)-6-oxopiperidin-2-yl]-5-(3,5-dimethyl-1,2-oxazol-4-yl)-1*H*-1,3-benzodiazol-1-yl}ethyl)piperazin-1-yl]-14-oxo-3,6,9,12-tetraoxatetradecan-1-yl}oxy)-4-(4-methyl-1,3-thiazol-5-yl)phenyl]methyl}-1-[(2*S*)-2-[(1-fluorocyclopropyl)formamido]-3,3-dimethylbutanoyl]-4-hydroxypyrrolidine-2-carboxamide (162)

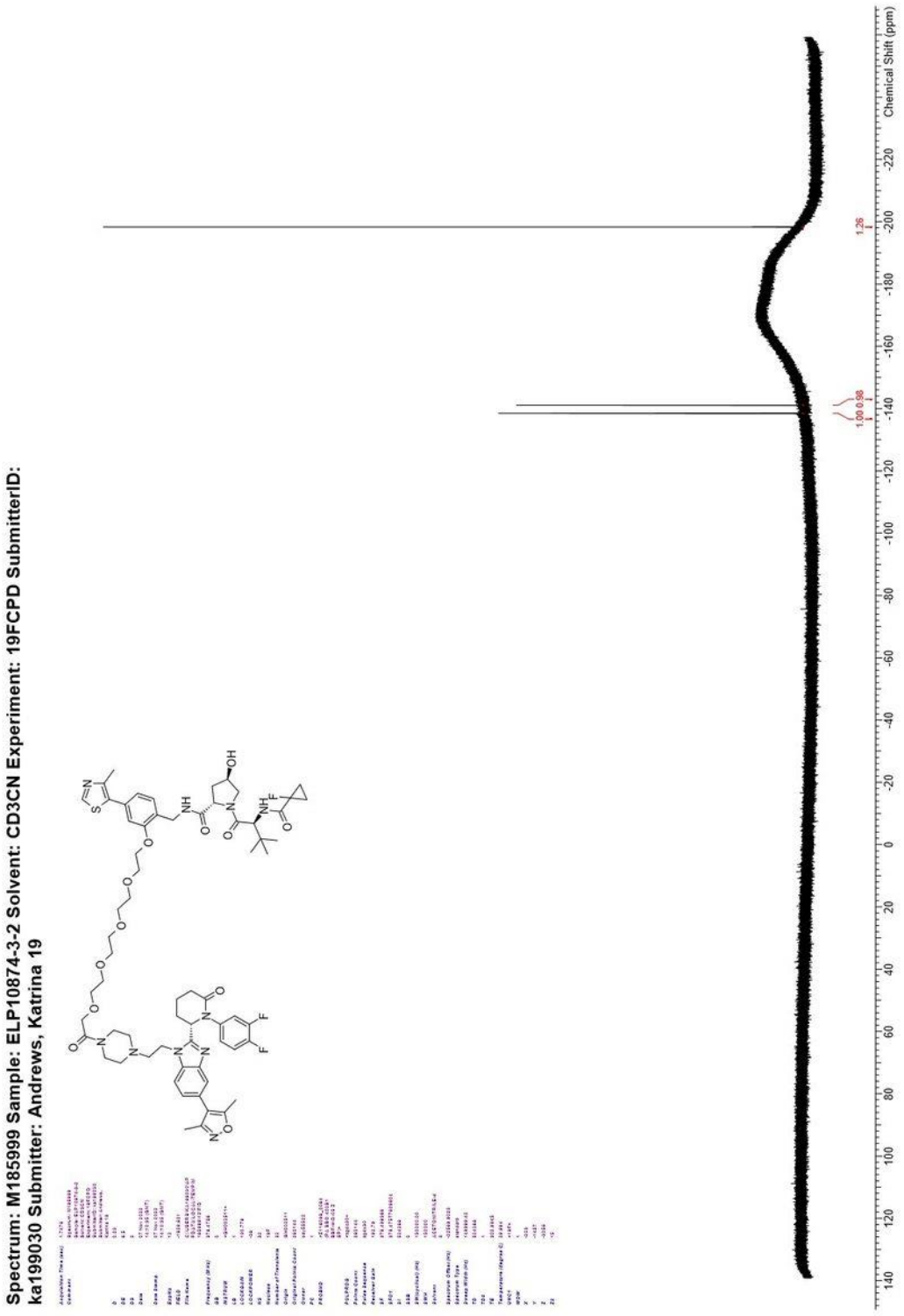

(2*S*,4*R*)-*N*-{[2-({9-[4-(2-{2-[(2*S*)-1-(3,4-Difluorophenyl)-6-oxopiperidin-2-yl]-5-(3,5-dimethyl-1,2-oxazol-4-yl)-1*H*-1,3-benzodiazol-1-yl}ethyl)piperazin-1-yl]-9-oxononyl}oxy)-4-(4-methyl-1,3-thiazol-5-yl)phenyl]methyl}-1-[(2*S*)-2-[(1-fluorocyclopropyl)formamido]-3,3-dimethylbutanoyl]-4-hydroxypyrrolidine-2-carboxamide (163)

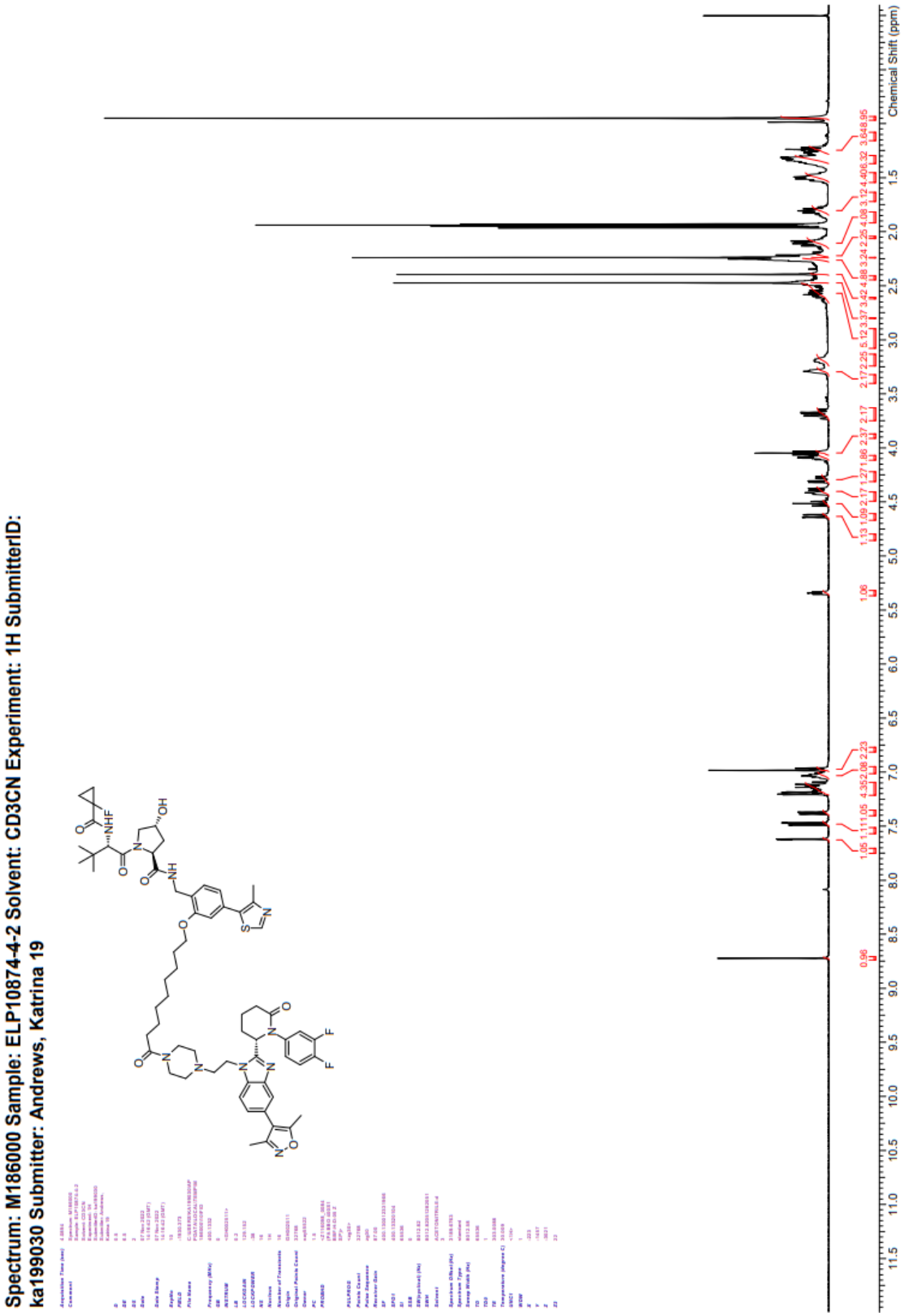

(2*S*,4*R*)-*N*-{[2-({9-[4-(2-{2-[(2*S*)-1-(3,4-Difluorophenyl)-6-oxopiperidin-2-yl]-5-(3,5-dimethyl-1,2-oxazol-4-yl)-1*H*-1,3-benzodiazol-1-yl}ethyl)piperazin-1-yl]-9-oxononyl}oxy)-4-(4-methyl-1,3-thiazol-5-yl)phenyl]methyl}-1-[(2*S*)-2-[(1-fluorocyclopropyl)formamido]-3,3-dimethylbutanoyl]-4-hydroxypyrrolidine-2-carboxamide (163)

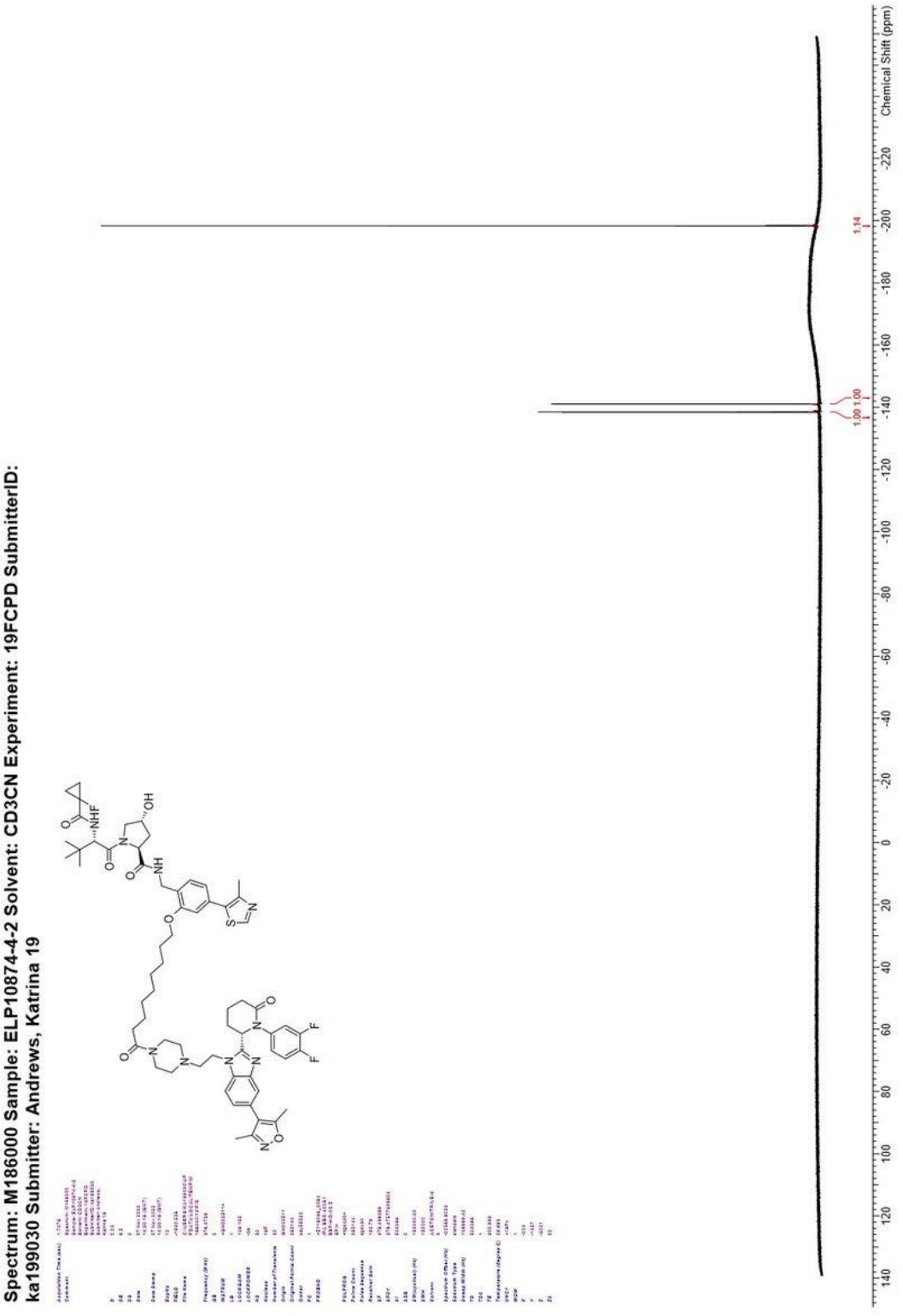

(2*S*,4*R*)-*N*-{[2-({12-[4-(2-{2-[(2*S*)-1-(3,4-Difluorophenyl)-6-oxopiperidin-2-yl]-5-(3,5-dimethyl-1,2-oxazol-4-yl)-1*H*-1,3-benzodiazol-1-yl}ethyl)piperazin-1-yl]-12-oxododecyl}oxy)-4-(4-methyl-1,3-thiazol-5-yl)phenyl]methyl}-1-[(2*S*)-2-[(1-fluorocyclopropyl)formamido]-3,3-dimethylbutanoyl]-4-hydroxypyrrolidine-2-carboxamide (164)

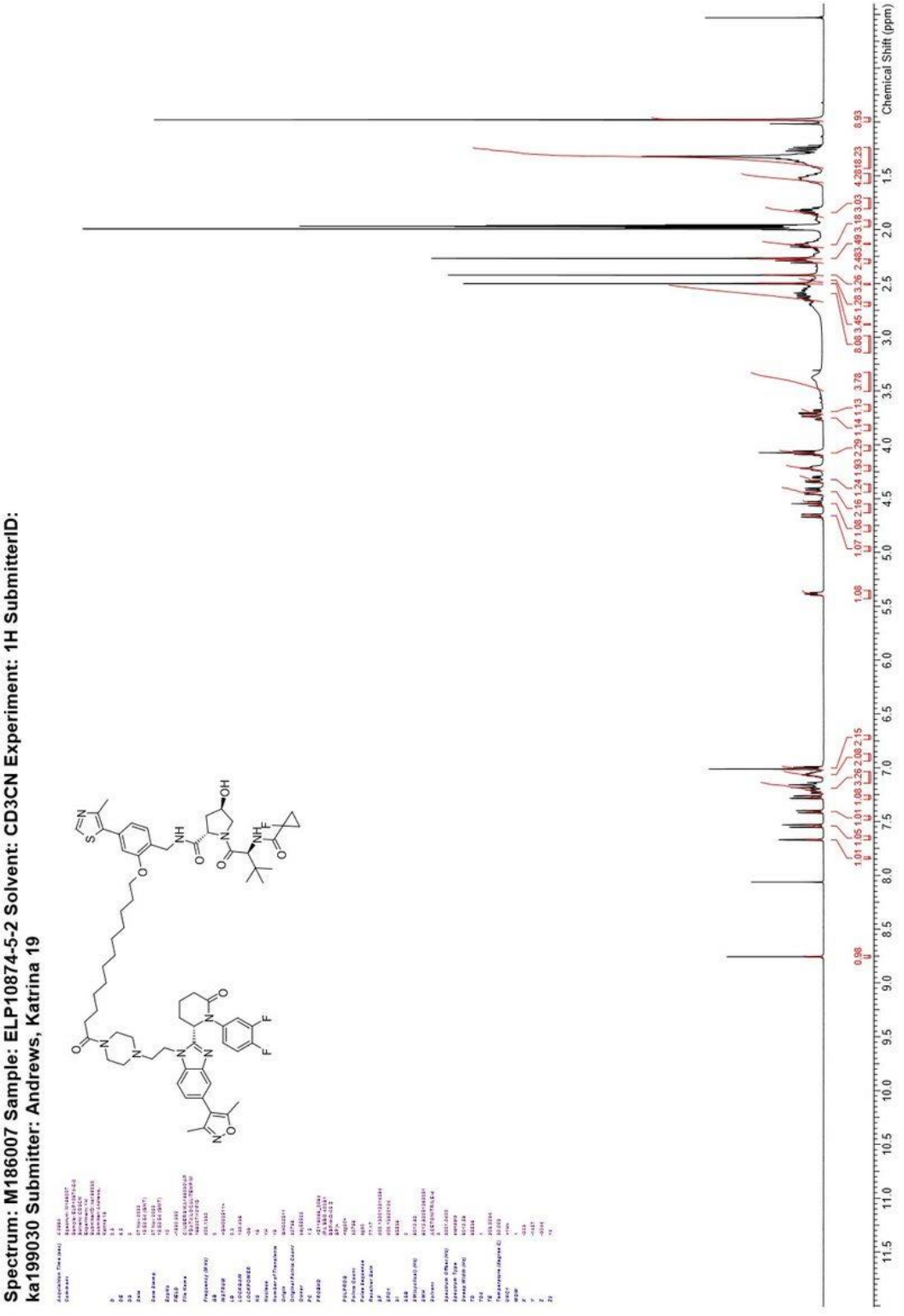

(2*S*,4*R*)-*N*-{[2-({12-[4-(2-{2-[(2*S*)-1-(3,4-Difluorophenyl)-6-oxopiperidin-2-yl]-5-(3,5-dimethyl-1,2-oxazol-4-yl)-1*H*-1,3-benzodiazol-1-yl}ethyl)piperazin-1-yl]-12-oxododecyl}oxy)-4-(4-methyl-1,3-thiazol-5-yl)phenyl]methyl}-1-[(2*S*)-2-[(1-fluorocyclopropyl)formamido]-3,3-dimethylbutanoyl]-4-hydroxypyrrolidine-2-carboxamide (164)

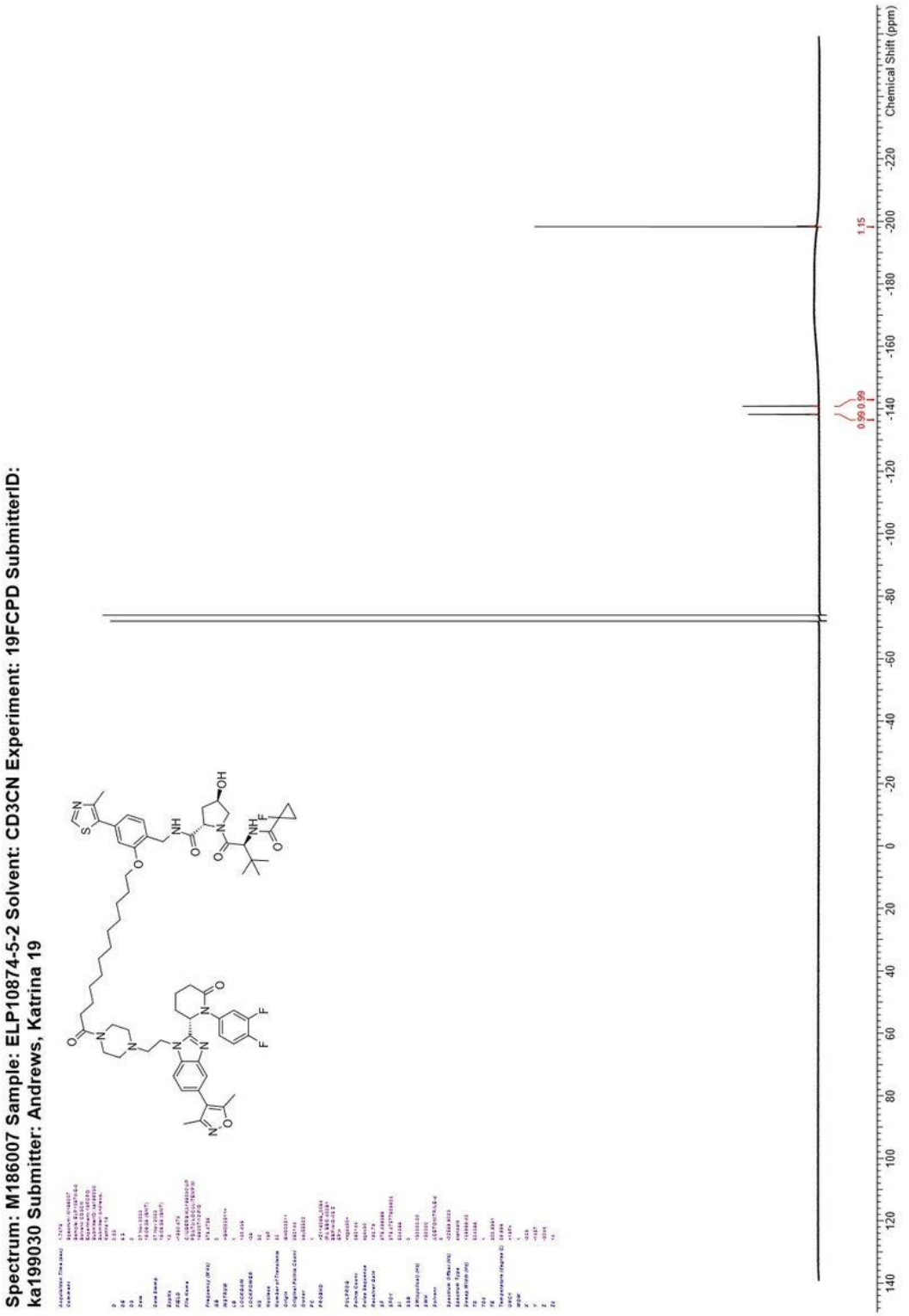

(2*S*,4*R*)-1-[(2*S*)-2-{14-[4-(2-{2-[(2*S*)-1-(3,4-Difluorophenyl)-6-oxopiperidin-2-yl]-5-(3,5-dimethyl-1,2-oxazol-4-yl)-1*H*-1,3-benzodiazol-1-yl}ethyl)piperazin-1-yl]-14-oxo-3,6,9,12-tetraoxatetradecanamido}-3,3-dimethylbutanoyl]-4-hydroxy-*N*-[(1*S*)-1-[4-(4-methyl-1,3-thiazol-5-yl)phenyl]ethyl]pyrrolidine-2-carboxamide (168)

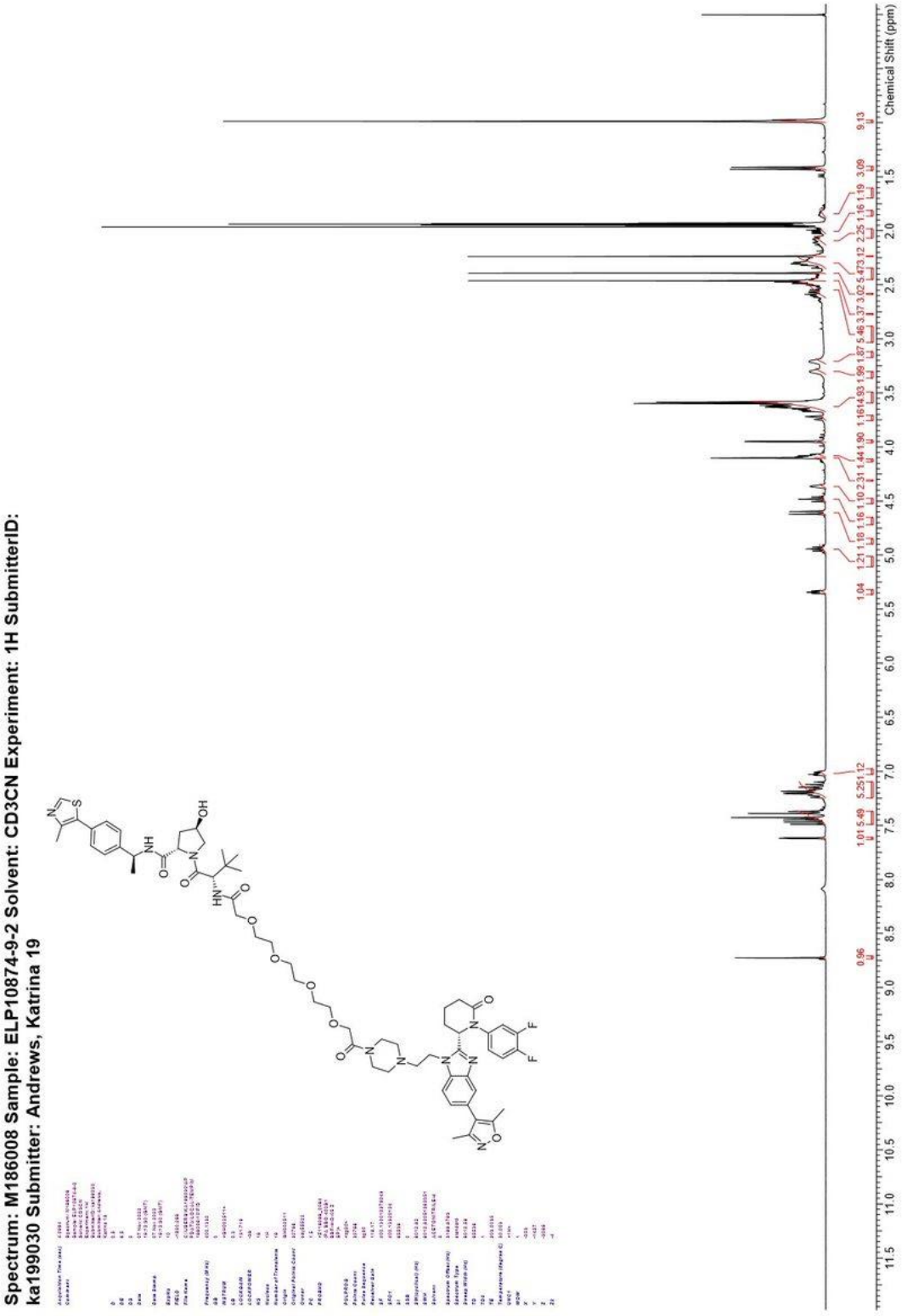

(2*S*,4*R*)-1-[(2*S*)-2-{14-[4-(2-{2-[(2*S*)-1-(3,4-Difluorophenyl)-6-oxopiperidin-2-yl]-5-(3,5-dimethyl-1,2-oxazol-4-yl)-1*H*-1,3-benzodiazol-1-yl}ethyl)piperazin-1-yl]-14-oxo-3,6,9,12-tetraoxatetradecanamido}-3,3-dimethylbutanoyl]-4-hydroxy-*N*-[(1*S*)-1-[4-(4-methyl-1,3-thiazol-5-yl)phenyl]ethyl]pyrrolidine-2-carboxamide (168)

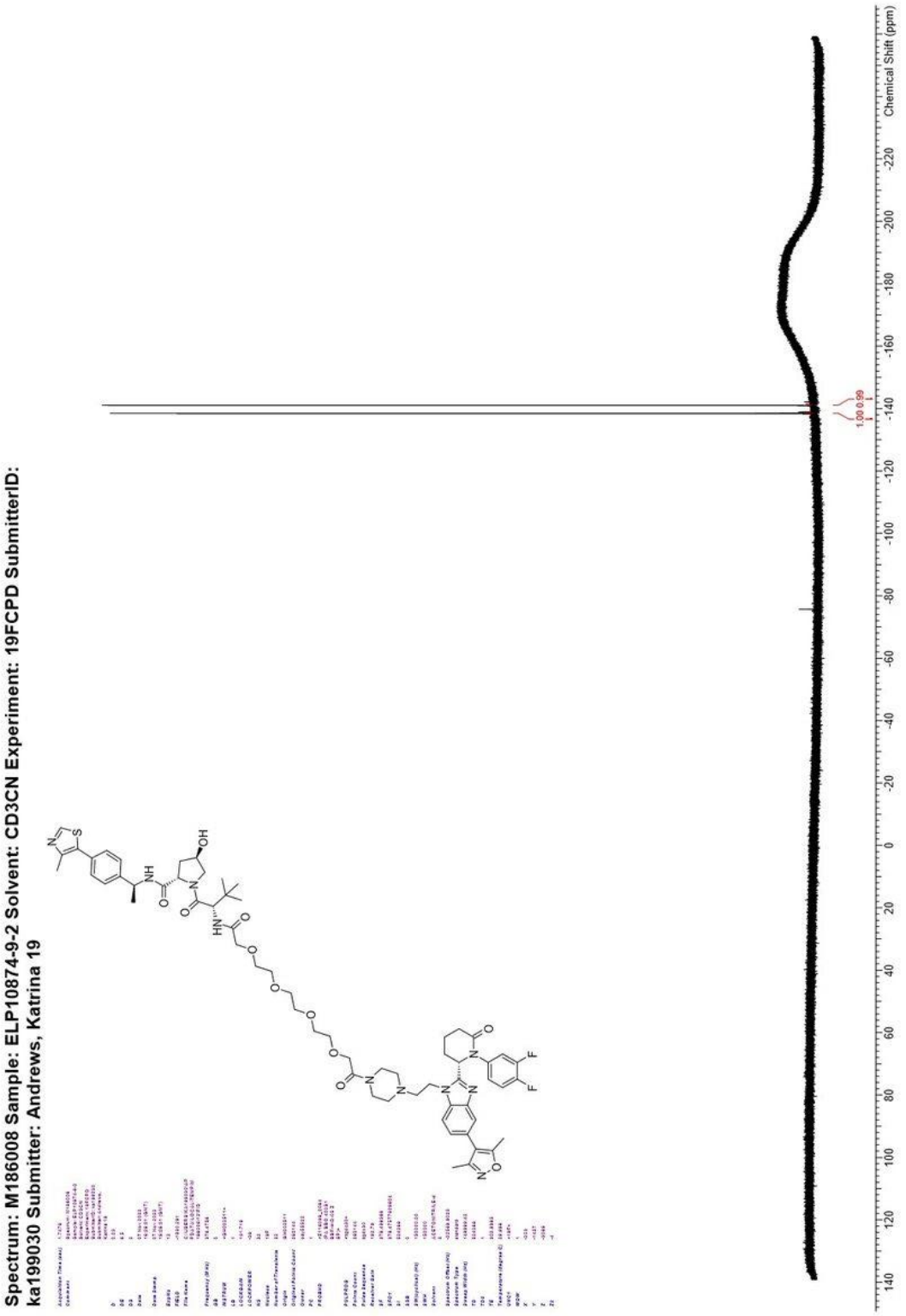

(2*S*,4*R*)-1-[(2*S*)-2-{7-[4-(2-{2-[(2*S*)-1-(3,4-Difluorophenyl)-6-oxopiperidin-2-yl]-5-(3,5-dimethyl-1,2-oxazol-4-yl)-1*H*-1,3-benzodiazol-1-yl}ethyl)piperazin-1-yl]-7-oxoheptanamido}-3,3-dimethylbutanoyl]-4-hydroxy-*N*-[(1*S*)-1-[4-(4-methyl-1,3-thiazol-5-yl)phenyl]ethyl]pyrrolidine-2-carboxamide (169)

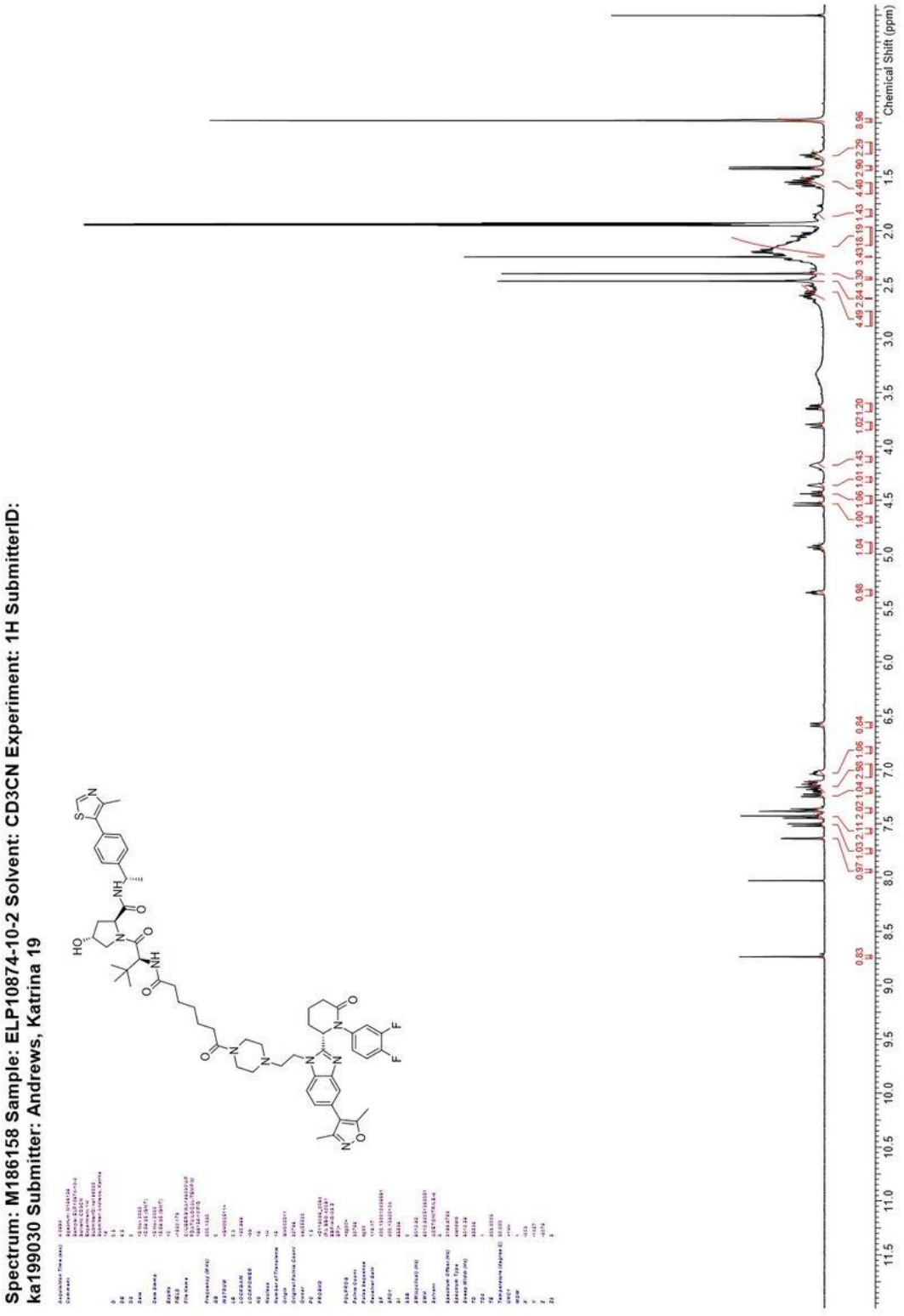

(2*S*,4*R*)-1-[(2*S*)-2-{7-[4-(2-{2-[(2*S*)-1-(3,4-Difluorophenyl)-6-oxopiperidin-2-yl]-5-(3,5-dimethyl-1,2-oxazol-4-yl)-1*H*-1,3-benzodiazol-1-yl}ethyl)piperazin-1-yl]-7-oxoheptanamido}-3,3-dimethylbutanoyl]-4-hydroxy-*N*-[(1*S*)-1-[4-(4-methyl-1,3-thiazol-5-yl)phenyl]ethyl]pyrrolidine-2-carboxamide (169)

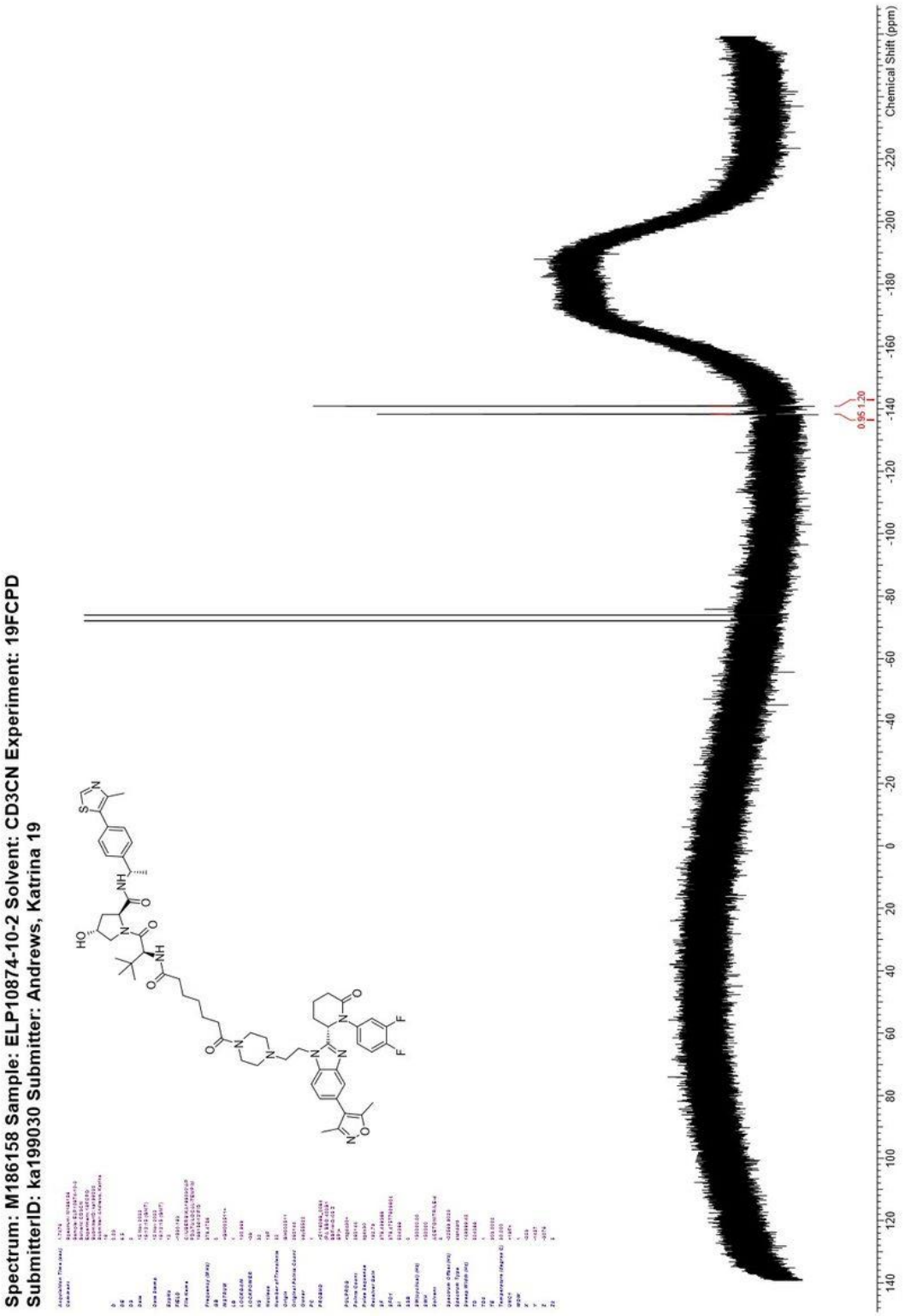

(2*S*,4*R*)-1-[(2*S*)-2-{10-[4-(2-{2-[(2*S*)-1-(3,4-Difluorophenyl)-6-oxopiperidin-2-yl]-5-(3,5-dimethyl-1,2-oxazol-4-yl)-1*H*-1,3-benzodiazol-1-yl}ethyl)piperazin-1-yl]-10-oxodecanamido}-3,3-dimethylbutanoyl]-4-hydroxy-*N*-[(1*S*)-1-[4-(4-methyl-1,3-thiazol-5-yl)phenyl]ethyl]pyrrolidine-2-carboxamide (170)

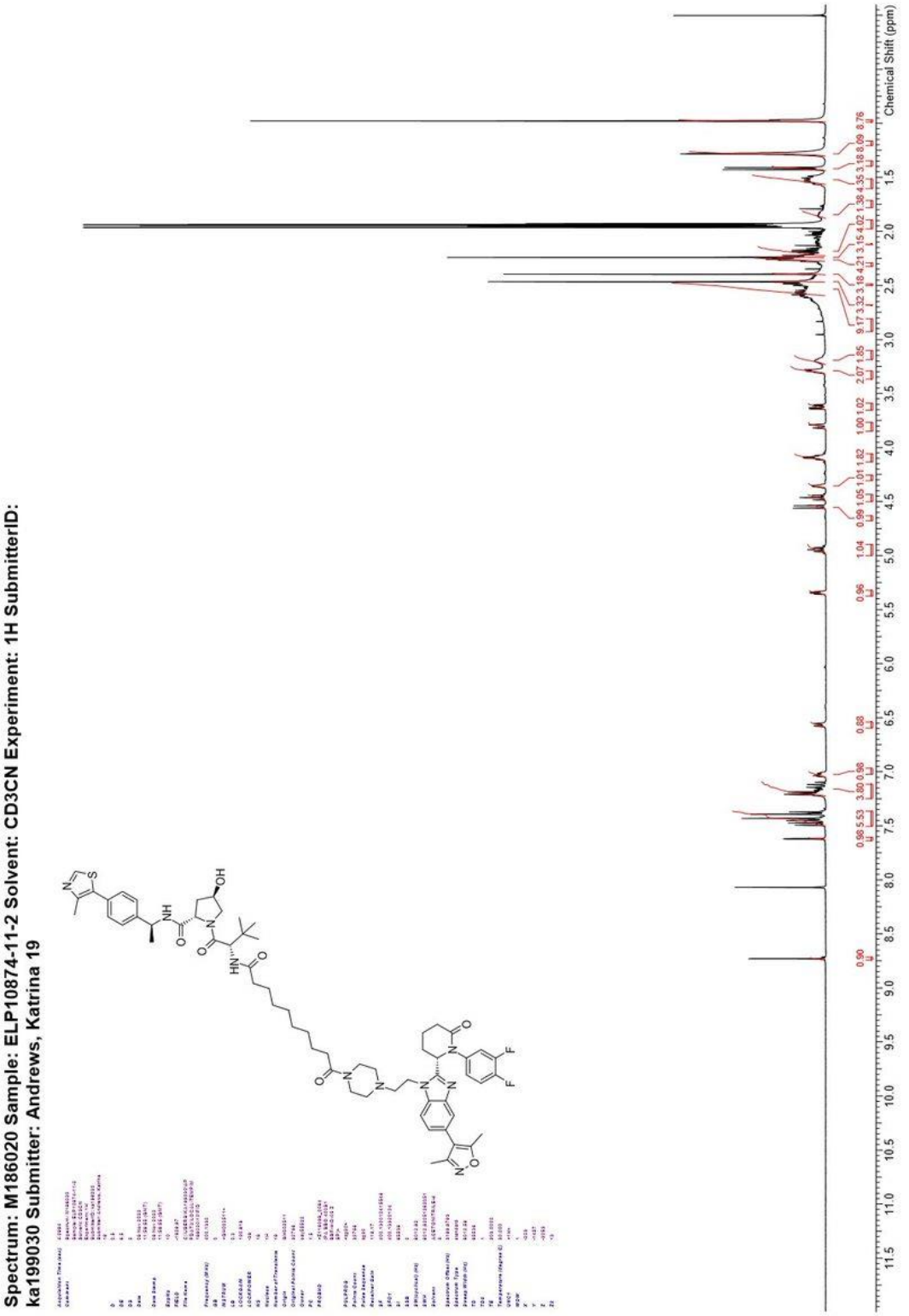

(2*S*,4*R*)-1-[(2*S*)-2-{10-[4-(2-{2-[(2*S*)-1-(3,4-Difluorophenyl)-6-oxopiperidin-2-yl]-5-(3,5-dimethyl-1,2-oxazol-4-yl)-1*H*-1,3-benzodiazol-1-yl}ethyl)piperazin-1-yl]-10-oxodecanamido}-3,3-dimethylbutanoyl]-4-hydroxy-*N*-[(1*S*)-1-[4-(4-methyl-1,3-thiazol-5-yl)phenyl]ethyl]pyrrolidine-2-carboxamide (170)

